

frontiers

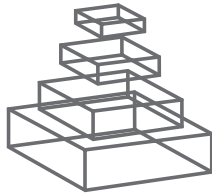
RESEARCH TOPICS

BASAL GANGLIA X - PROCEEDINGS OF THE 10TH TRIENNIAL MEETING OF THE INTERNATIONAL BASAL GANGLIA SOCIETY

Hosted by
Charles J. Wilson, Jose Bargas, James M.
Tepper and Elizabeth Abercrombie



frontiers in
SYSTEMS NEUROSCIENCE



frontiers

FRONTIERS COPYRIGHT STATEMENT

© Copyright 2007-2012
Frontiers Media SA.
All rights reserved.

All content included on this site, such as text, graphics, logos, button icons, images, video/audio clips, downloads, data compilations and software, is the property of or is licensed to Frontiers Media SA ("Frontiers") or its licensees and/or subcontractors. The copyright in the text of individual articles is the property of their respective authors, subject to a license granted to Frontiers.

The compilation of articles constituting this e-book, as well as all content on this site is the exclusive property of Frontiers. Images and graphics not forming part of user-contributed materials may not be downloaded or copied without permission.

Articles and other user-contributed materials may be downloaded and reproduced subject to any copyright or other notices. No financial payment or reward may be given for any such reproduction except to the author(s) of the article concerned.

As author or other contributor you grant permission to others to reproduce your articles, including any graphics and third-party materials supplied by you, in accordance with the Conditions for Website Use and subject to any copyright notices which you include in connection with your articles and materials.

All copyright, and all rights therein, are protected by national and international copyright laws.

The above represents a summary only. For the full conditions see the Conditions for Authors and the Conditions for Website Use.

Cover image provided by Ibbl sarl, Lausanne CH

ISSN 1664-8714

ISBN 978-2-88919-036-2

DOI 10.3389/978-2-88919-036-2

ABOUT FRONTIERS

Frontiers is more than just an open-access publisher of scholarly articles: it is a pioneering approach to the world of academia, radically improving the way scholarly research is managed. The grand vision of Frontiers is a world where all people have an equal opportunity to seek, share and generate knowledge. Frontiers provides immediate and permanent online open access to all its publications, but this alone is not enough to realize our grand goals.

FRONTIERS JOURNAL SERIES

The Frontiers Journal Series is a multi-tier and interdisciplinary set of open-access, online journals, promising a paradigm shift from the current review, selection and dissemination processes in academic publishing.

All Frontiers journals are driven by researchers for researchers; therefore, they constitute a service to the scholarly community. At the same time, the Frontiers Journal Series operates on a revolutionary invention, the tiered publishing system, initially addressing specific communities of scholars, and gradually climbing up to broader public understanding, thus serving the interests of the lay society, too.

DEDICATION TO QUALITY

Each Frontiers article is a landmark of the highest quality, thanks to genuinely collaborative interactions between authors and review editors, who include some of the world's best academicians. Research must be certified by peers before entering a stream of knowledge that may eventually reach the public - and shape society; therefore, Frontiers only applies the most rigorous and unbiased reviews.

Frontiers revolutionizes research publishing by freely delivering the most outstanding research, evaluated with no bias from both the academic and social point of view.

By applying the most advanced information technologies, Frontiers is catapulting scholarly publishing into a new generation.

WHAT ARE FRONTIERS RESEARCH TOPICS?

Frontiers Research Topics are very popular trademarks of the Frontiers Journals Series: they are collections of at least ten articles, all centered on a particular subject. With their unique mix of varied contributions from Original Research to Review Articles, Frontiers Research Topics unify the most influential researchers, the latest key findings and historical advances in a hot research area!

Find out more on how to host your own Frontiers Research Topic or contribute to one as an author by contacting the Frontiers Editorial Office: researchtopics@frontiersin.org

BASAL GANGLIA X - PROCEEDINGS OF THE 10TH TRIENNIAL MEETING OF THE INTERNATIONAL BASAL GANGLIA SOCIETY

Hosted By

Charles J. Wilson, University of Texas at San Antonio, USA

Jose Bargas, Universidad Nacional Autónoma de México, Mexico

James M. Tepper, Rutgers, The State University of NJ, USA

Elizabeth Abercrombie, Rutgers-Newark: The State University of New Jersey, USA



This volume contains articles describing research on the basic, pre-clinical and clinical neuroscience of the basal ganglia written by attendees of the 10th Triennial Meeting of the International Basal Ganglia Society (IBAGS) that was held June 20-24th, 2010 at the Ocean Place Resort in Long Branch, New Jersey, USA. For each of the preceding 9 IBAGS meetings, the meeting proceedings were published conventionally as a volume in the Advances in Behavioral Biology series.

These volumes were expensive, were published only in very small quantities, had very limited availability to both basal ganglia researchers and the general neuroscience community, were not available on-line and the articles contained in each were not indexed in online searchable databases. Now, for the first time, IBAGS is taking full advantage of modern innovations in scientific publication and publishing IBAGS X as a Research Topics issue of Frontiers in Systems Neuroscience. The issue will be available on-line and is fully indexed by searchable databases including PubMed. Articles will include reports on the latest research on the anatomy and neurophysiology of single neurons and functional circuitry in the striatum, globus pallidus, subthalamic nucleus and substantia nigra as well as the latest data on animal models of basal ganglia dysfunction as well as behavioral and clinical studies in human patients.

Table of Contents

07 Introduction to Basal Ganglia X – proceedings of the 10th Triennial Meeting of the International Basal Ganglia Society

James M. Tepper

Basal Ganglia Electrophysiology

09 Dopaminergic Presynaptic Modulation of Nigral Afferents: Its Role in the Generation of Recurrent Bursting in SubstantiaNigra Pars Reticulata Neurons

José de JesúsAceves, Pavel E. Rueda-Orozco, Ricardo Hernández, Víctor Plata, Osvaldo Ibañez-Sandoval, Elvira Galarraga and José Bargas

19 Dopaminergic Modulation of Corticostriatal Responses in Medium Spiny Projection Neurons from Direct and Indirect Pathways

Edén Flores-Barrera, Bianca J. Vizcarra-Chacón, José Bargas, Dagoberto Tapia and Elvira Galarraga

25 The Impact of Stimulation Induced Short-Term Synaptic Plasticity on Firing Patterns in the Globus Pallidus of the Rat

Jenia Bugaysen, Izhar Bar-Gad and Alon Korngreen

33 Disinhibition Bursting of Dopaminergic Neurons

Collin J. Lobb, Todd W. Troyer, Charles J. Wilson and Carlos A. Paladini

41 Regulation of SubstantiaNigra Pars ReticulataGABAergic Neuron Activity by H2O2 via Flufenamic Acid-Sensitive Channels and KATP Channels

Christian R. Lee, Paul Witkovsky and Margaret E. Rice

53 Dissecting the Contribution of Individual Receptor Subunits to the Enhancement of N-methyl-D-Aspartate Currents by Dopamine D1 Receptor Activation in Striatum

Emily L. Jocoy, Véronique M. André, Damian M. Cummings, Shilpa P. Rao, Nanping Wu, Amy J. Ramsey, Marc G. Caron, Carlos Cepeda and Michael S. Levine

69 Role of Striatum in the Pause and Burst Generation in the Globus Pallidus of 6-OHDA-Treated Rats

Hitoshi Kita and Takako Kita

80 Functional Properties of Striatal Fast-Spiking Interneurons

Joshua D. Berke

87 Striatal Fast-Spiking Interneurons: From Firing Patterns to Postsynaptic Impact

Andreas Klaus, Henrike Planert, J. J. Johannes Hjorth, Joshua D. Berke, Gilad Silberberg and Jeanette Hellgren Kotaleski

104 TheSubthalamic Nucleus becomes a Generator of Bursts in the Dopamine-Depleted State. Its High Frequency Stimulation Dramatically Weakens Transmission to the Globus Pallidus

Rachida Ammari, Bernard Bioulac, Liliana Garcia and Constance Hammond

- 114** *Cortical Potentials Evoked by Deep Brain Stimulation in the Subthalamic Area*
Annaelle Devergnas and Thomas Wichmann
- 122** *The Corticostriatal System in Dissociated Cell Culture*
Fiona E. Randall, Marianela Garcia-Munoz, Catherine Vickers, Sarah C. Schock, William A. Staines and Gordon W. Arbuthnott

Basal Ganglia Pharmacology

- 129** *Widespread Increases in Malondialdehyde Immunoreactivity in Dopamine-Rich and Dopamine-Poor Regions of Rat Brain Following Multiple, High Doses of Methamphetamine*
Kristen A. Horner, Yamiece E. Gilbert and Susan D. Cline
- 140** *Nitric Oxide–Soluble Guanylyl Cyclase–Cyclic GMP Signaling in the Striatum: New Targets for the Treatment of Parkinson’s Disease?*
Anthony R. West and Kuei Y. Tseng
- 149** *Dopamine Signaling in Dorsal Versus Ventral Striatum: The Dynamic Role of Cholinergic Interneurons*
Sarah Threlfell and Stephanie Jane Cragg
- 159** *Differential Calcium Dependence of Axonal Versus Somatodendritic Dopamine Release, with Characteristics of Both in the Ventral Tegmental Area*
Billy T. Chen, Jyoti C. Patel, Kimberly A. Moran and Margaret E. Rice
- 167** *Electrophysiological Effects of Trace Amines on Mesencephalic Dopaminergic Neurons*
Ada Ledonne, Nicola Berretta, Alessandro Davoli, Giada Ricciardo Rizzo, Giorgio Bernardi and Nicola Biagio Mercuri
- 172** *The Role of BDNF/TrkB Signaling in Acute Amphetamine-Induced Locomotor Activity and Opioid Peptide Gene Expression in the Rat Dorsal Striatum*
Jacqueline F. McGinty, Alexandra J. Bache, Nortorious T. Coleman and Wei-Lun Sun
- 180** *The 5-HT_{2A} Receptor Antagonist M100907 Produces Antiparkinsonian Effects and Decreases Striatal Glutamate*
Twum A. Ansah, Marcus C. Ferguson and Tultul Nayyar
- 186** *Nitric Oxide Synthase Inhibitor Improves De Novo and Long-Term L-DOPA-Induced Dyskinesia in Hemiparkinsonian Rats*
Fernando Eduardo Padovan-Neto, Marcela Bermúdez Echeverry, Silvana Chiavegatto and Elaine Del-Bel

Basal Ganglia Anatomy

- 197** *Distribution of Tyrosine Hydroxylase-Expressing Interneurons with Respect to Anatomical Organization of the Neostriatum*
Bengi Ünal, Osvaldo Ibáñez-Sandoval, Fulva Shah, Elizabeth D. Abercrombie and James M. Tepper
- 208** *An Improved BAC Transgenic Fluorescent Reporter Line for Sensitive and Specific Identification of Striatonigral Medium Spiny Neurons*
Kristen K. Ade, Yehong Wan, Meng Chen, Bernd Gloss and Nicole Calakos
- 217** *The Corticostriatal and Corticosubthalamic Pathways: Two Entries, One Target. So What?*
Abraham Mathai and Yoland Smith

- 227 Localization and Function of GABA Transporters GAT-1 and GAT-3 in the Basal Ganglia**
Xiao-Tao Jin, Adriana Galvan, Thomas Wichmann and Yolanda Smith
- 237 Neuroglial Plasticity at Striatal Glutamatergic Synapses in Parkinson's Disease**
Rosa M. Villalba and Yolanda Smith

Genetic Models of Basal Ganglia Disorders

- 246 Dysregulated Neuronal Activity Patterns Implicate Corticostriatal Circuit Dysfunction in Multiple Rodent Models of Huntington's Disease**
Benjamin R. Miller, Adam G. Walker, Scott J. Barton and George V. Rebec
- 256 Functional Changes in Neocortical Activity in Huntington's Disease Model Mice: An in vivo Intracellular Study**
Edward A. Stern
- 263 Altered Balance of Activity in the Striatal Direct and Indirect Pathways in Mouse Models of Huntington's Disease**
Véronique M. André, Yvette E. Fisher and Michael S. Levine
- 274 In vivo Dopamine Efflux is Decreased in Striatum of both Fragment (R6/2) and Full-Length (YAC128) Transgenic Mouse Models of Huntington's Disease**
Joshua W. Callahan and Elizabeth D. Abercrombie
- 284 Multi-Neuronal Recordings in the Basal Ganglia in Normal and Dystonic Rats**
Mark S. Baron, Kunal D. Chaniary, Ann C. Rice and Steven M. Shapiro

Basal Ganglia Function in Health and Disease

- 294 Dopaminergic balance between reward maximization and policy complexity**
Naama Parush, Naftali Tishby and Hagai Bergman
- 305 Reduced GABA Content in the Motor Thalamus during Effective Deep Brain Stimulation of the Subthalamic Nucleus**
Alessandro Stefani, Ernesto Fedele, Mariangela Pierantozzi, Salvatore Galati, Francesco Marzetti, Antonella Peppe, Francesco Saverio Pastore, Giorgio Bernardi and Paolo Stanzione
- 313 Dynamic Stereotypic Responses of Basal Ganglia Neurons to Subthalamic Nucleus High-Frequency Stimulation in the Parkinsonian Primate**
Anan Moran, Edward Stein, Hadass Tischler, Katya Bebelovsky and Izhar Bar-Gad
- 324 Neighboring Pallidal Neurons Do Not Exhibit more Synchronous Oscillations than Remote Ones in the MPTP Primate Model of Parkinson's Disease**
Rea Mitelman, Boris Rosin, Hila Zadka, Maya Slovik, Gali Heimer, Ya'akov Ritov, Hagai Bergman and Shlomo Elias
- 336 Reduced Pallidal Output Causes Dystonia**
Atsushi Nambu, Satomi Chiken, Pullanipally Shashidharan, Hiroki Nishibayashi, Mitsuhiro Ogura, Koji Kakishita, Satoshi Tanaka, Yoshihisa Tachibana, Hitoshi Kita and Toru Itakura
- 342 Inter-hemispheric asymmetry of nigrostriatal dopaminergic lesion: a possible compensatory mechanism in Parkinson's disease**
Javier Blesa, Carlos Juri, Miguel Á. García-Cabezas, Rebeca Adánez, Miguel Á. Sánchez-González, Carmen Cavada and José A. Obeso

349 *Loss of Specificity in Basal Ganglia Related Movement Disorders*

Maya Bronfeld and Izhar Bar-Gad

362 *Frontal Cortex-Like Functions of the Subthalamic Nucleus*

Christelle Baunez and Sylvie Lardeux

370 *Noradrenaline and Parkinson's Disease*

Claire Delaville, Philippe De Deurwaerdère and Abdelhamid Benazzouz

382 *Pharmacological and Physiological Characterization of the Tremulous Jaw Movement Model of Parkinsonian Tremor: Potential Insights into the Pathophysiology of Tremor*

Lyndsey E. Collins-Praino, Nicholas E. Paul, Kristen L. Rychalsky, James R. Hinman, James J. Chrobak, Patrick B. Senatus and John D. Salamone

Learning in the Basal Ganglia

396 *Putative Cholinergic Interneurons in the Ventral and Dorsal Regions of the Striatum Have Distinct Roles in a Two Choice Alternative Association Task*

Orli Yarom and Dana Cohen

405 *A critical review of habit learning and the basal ganglia*

Carol A Seger and Brian J Spiering

414 *Basal Ganglia Preferentially Encode Context Dependent Choice in a Two-Armed Bandit Task*

André Garenne, Benjamin Pasquereau, Martin Guthrie, Bernard Bioulac and Thomas Boraud

Computational Approaches to the Study of the Basal Ganglia

423 *Input dependent cell assembly dynamics in a model of the striatal medium spiny neuron network*

Adam Ponzi and Jeffery R Wickens

437 *Creation of Computerized 3D MRI-Integrated Atlases of the Human Basal Ganglia and Thalamus*

Abbas F. Sadikot, M. Mallar Chakravarty, Gilles Bertrand, Vladimir V. Rymar, Fahd Al-Subaie and D. Louis Collins

445 *Chaotic desynchronization as the therapeutic mechanism of deep brain stimulation*

Charles J Wilson, Bryce Beverlin and Theoden I Netoff



Introduction to Basal Ganglia X – proceedings of the 10th Triennial Meeting of the International Basal Ganglia Society

James M. Tepper*

Rutgers, The State University of New Jersey, Newark, NJ, USA

**Correspondence: jtepper@andromeda.rutgers.edu*

INTRODUCTION

The International Basal Ganglia Society (IBAGS) had its origins in 1983 at a Satellite Meeting of the International Union of Physiological Sciences held at Lorne, Australia. At that meeting Professor John McKenzie organized a symposium devoted to the structure and function of the basal ganglia that attracted some 50 attendees from 12 countries. Thirty years later, IBAGS has grown into international organization with over 400 members from over 30 countries spanning the entire world. More information about the history of IBAGS and its previous triennial meetings can be found at www.ibags.info.

The present volume consists of contributions from attendees of the Tenth Triennial Meeting of IBAGS, held June 20th–24th, 2010, at the Ocean Place Resort in Long Branch, NJ, USA, on the Jersey shore. The meeting attracted 278 scientific attendees representing over 30 different countries. The program included 50 invited speakers and over 180 poster presentations. The scientific sessions comprised a broad range of themes including “New Insights Into Basal Ganglia Diseases From Genetic Models,” “Novel and Understudied Basal Ganglia Circuits and Pathways,” “What Do the Basal Ganglia Really Do,” “Cognitive Functions of The Basal Ganglia,” “Non-Motor Sequela of Basal Ganglia Diseases,” “Dysfunction of the Basal Ganglia in Dystonia And Dyskinesia,” “Atypical Neuromodulators in the Basal Ganglia – Beyond Acetylcholine and Dopamine,” and “Basal Ganglia Function: Novel Insights From Computational Modeling.” Other highlights of the meeting included the Keynote Lecture on optogenetics by Karl Diesseroth, the Special Lecture by Charlie Wilson who was inducted as the 6th IBAGS Lifetime Member, and the lobster cook-out and bonfire on the beach. And of course, the welcome attendance and energetic participation of John McKenzie, some 30 years after he organized the meeting that gave birth to IBAGS.

After all previous IBAGS meetings, contributions were solicited from attendees that were published as a single, hardcover volume. This volume, and the contributions in it, were not-peer reviewed nor indexed by PubMed or other commonly used databases. Thus the articles written were principally available only to IBAGS members or others who had purchased the (usually expensive) volume. For IBAGS X, we elected to take advantage of modern technology and publish the proceedings electronically, as a Special Topics Issue of *Frontiers in Systems Neuroscience*. All submissions were subject to the normal Frontiers journals’ peer review system, and virtually all of the accepted submissions were published on-line within 2 weeks of final acceptance. For the first time, the IBAGS proceedings articles are all indexed and searchable in PubMed and other scientific indexing services, and freely available to anyone with an internet connection.

Now, that the last of the submissions have been reviewed and accepted for publication, the 46 articles resulting from IBAGS X have been sorted into 7 topics (Basal Ganglia Electrophysiology, Basal Ganglia Pharmacology, Basal Ganglia Anatomy, Genetic Models of Basal Ganglia Disorders, Basal Ganglia Function in Health and Disease, Learning in the Basal Ganglia and Computational Approaches to the study of the Basal Ganglia) and compiled into this e-book. We hope you find the collection interesting and valuable.

We all look forward to IBAGS XI, which is scheduled to take place in Eilat, Israel, in March 2013, under the direction of Hagai Bergman and Izhar Bar-Gad.

IBAGS X OFFICERS AND COMMITTEES

OFFICERS

- President
 - James M. Tepper, USA
- Past President
 - Henk Groenewegen, Netherlands
- President-elect
 - Hagai Bergman, Israel
- Secretary
 - Elizabeth. D. Abercrombie, USA
- Secretary-elect
 - Izhar Bar-Gad, Israel
- Treasurer
 - Yoland Smith, USA

LOCAL ORGANIZING COMMITTEE

- James M. Tepper, USA
- Elizabeth D. Abercrombie, USA
- Mark Bevan, USA/UK
- Savio Chan, USA
- Carlos Cepeda, USA
- Kristin Keefe, USA
- Carlos Paladini, USA

PROGRAM COMMITTEE

- Mike Levine, Chair, USA
- Thomas Boraud, France
- Micaela Morelli, Italy
- Lynn Raymond, Canada
- Margaret Rice, USA
- Jochen Roeper, Germany
- Ed Stern, Israel
- Kuei-Yan Tseng, USA

- Tom Wichmann, USA
- Jeff Wickens, New Zealand

TRAVEL FELLOWSHIP COMMITTEE

- Tony West, Chair, USA
- Stephanie Cragg, UK
- Atsushi Nambu, Japan

IBAGS X COUNCIL

- Erwan Bezard, France
- Angela Cenci-Nilsson, Sweden
- David Finkelstein, Australia
- Pete Magill, UK
- Micaela Morelli, Italy
- Atsushi Nambu, Japan
- José Obeso, Spain

- Jochen Roeper, Germany
- Abbas Sadikot, Canada
- Henk Berendse, Netherlands

ACKNOWLEDGMENTS

The National Institute of Neurological Disorders and Stroke (NINDS), Pfizer, The Kenneth Audekman Family Foundation, and Eli Lilly and Company are gratefully acknowledged for their financial support of IBAGS X.

Received: 05 April 2012; accepted: 05 April 2012; published online: 01 May 2012.

Citation: Tepper JM (2012) Introduction to Basal Ganglia X – proceedings of the 10th Triennial Meeting of the International Basal Ganglia Society. Front. Syst. Neurosci. 6:29. doi: 10.3389/fnsys.2012.00029

Copyright © 2012 Tepper. This is an open-access article distributed under the terms of the Creative Commons Attribution Non Commercial License, which permits non-commercial use, distribution, and reproduction in other forums, provided the original authors and source are credited.



Dopaminergic presynaptic modulation of nigral afferents: its role in the generation of recurrent bursting in substantia nigra pars reticulata neurons

José de Jesús Aceves, Pavel E. Rueda-Orozco, Ricardo Hernández, Víctor Plata, Osvaldo Ibañez-Sandoval, Elvira Galarraga and José Bargas*

División de Neurociencias, Instituto de Fisiología Celular, Universidad Nacional Autónoma de México, Distrito Federal México, México

Edited by:

James M. Tepper, Rutgers, The State University of New Jersey, USA

Reviewed by:

Christian Lee, New York University School of Medicine, USA

Carlos A. Paladini, University of Texas at San Antonio, USA

*Correspondence:

José Bargas, Division of Neuroscience, Institute of Cell Physiology, Universidad Nacional Autónoma de México, PO Box: 70-253, Distrito Federal México 04510, México.
e-mail: jlbargas@ifc.unam.mx

Previous work has shown the functions associated with activation of dopamine presynaptic receptors in some substantia nigra pars reticulata (SNr) afferents: (i) striatonigral terminals (direct pathway) possess presynaptic dopamine D_1 -class receptors whose action is to enhance inhibitory postsynaptic currents (IPSCs) and GABA transmission. (ii) Subthalamonigral terminals possess D_1 - and D_2 -class receptors where D_1 -class receptor activation enhances and D_2 -class receptor activation decreases excitatory postsynaptic currents. Here we report that pallidonigral afferents possess D_2 -class receptors (D_3 and D_4 types) that decrease inhibitory synaptic transmission via presynaptic modulation. No action of D_1 -class agonists was found on pallidonigral synapses. In contrast, administration of D_1 -receptor antagonists greatly decreased striatonigral IPSCs in the same preparation, suggesting that tonic dopamine levels help in maintaining the function of the striatonigral (direct) pathway. When both D_3 and D_4 type receptors were blocked, pallidonigral IPSCs increased in amplitude while striatonigral connections had no significant change, suggesting that tonic dopamine levels are repressing a powerful inhibition conveyed by pallidonigral synapses (a branch of the indirect pathway). We then blocked both D_1 - and D_2 -class receptors to acutely decrease direct pathway (striatonigral) and enhance indirect pathways (subthalamonigral and pallidonigral) synaptic force. The result was that most SNr projection neurons entered a recurrent bursting firing mode similar to that observed during Parkinsonism in both patients and animal models. These results raise the question as to whether the lack of dopamine in basal ganglia output nuclei is enough to generate some pathological signs of Parkinsonism.

Keywords: basal ganglia, striatum, substantia nigra pars reticulata, dopamine function, striatonigral synapses, pallidonigral synapses, D_1 -receptors, D_2 -receptors

INTRODUCTION

The internal globus pallidus (GPi) and substantia nigra pars reticulata (SNr) are the basal ganglia (BG) output nuclei. Besides projecting to the thalamus to form the cortico-BG loops (Chevalier et al., 1985; Albin et al., 1989; Smith and Bolam, 1989; Alexander and Crutcher, 1990; DeLong, 1990; Smith et al., 1998; Haber, 2003), output nuclei also project to pons and brain stem to control descending pathways and central pattern generators (CPGs) that regulate muscular tone and automatic or rhythmic motor responses (Takakusaki et al., 2003, 2004; Grillner et al., 2008). In birds, reptiles, and lower vertebrates in which the cortex is not well developed, the control of brain stem nuclei is a main function of the BG (Reiner et al., 1998; Grillner et al., 2005, 2008; Gale and Perkel, 2010). In the SNr, inhibitory postsynaptic currents (IPSCs) are in part provided by striatonigral direct pathway terminals (Grofová and Rinwick, 1970; Chevalier et al., 1985; Smith and Bolam, 1991; Deniau et al., 1996; Matuszewich and Yamamoto, 1999), which possess functional presynaptic dopamine D_1 -receptors whose activation increases direct pathway inhibition (Porceddu et al., 1986; Altar and Hauser, 1987; Floran et al., 1990; Radnikow and Misgeld, 1998; Chuhma et al., 2011). Enhancement of direct pathway inhibition facilitates movements while its reduction represses them (Albin

et al., 1989; Bateup et al., 2010; Kravitz et al., 2010; Redgrave et al., 2010). In contrast, subthalamonigral afferents compose the last step of the indirect pathway (Nakanishi et al., 1987; Bevan et al., 1994). Presynaptic modulation of subthalamonigral terminals by dopamine uses both classes of dopamine receptors: D_1 and D_2 (Ibañez-Sandoval et al., 2006). Activation of D_1 enhances while activation of D_2 depresses subthalamonigral excitatory postsynaptic currents (EPSCs). Interestingly, simultaneous blockade of both receptors induced larger evoked EPSCs, suggesting that D_2 -receptors have more influence than D_1 -receptors in the modulation of transmission (Ibañez-Sandoval et al., 2006).

In parallel, the external globus pallidus (GPe) also sends an inhibitory input to SNr (Bevan et al., 1996; Kita, 2007; Connelly et al., 2010). In the present work we investigated dopaminergic presynaptic modulation of inhibitory pallidonigral afferents. We found that D_2 -class receptors regulate these terminals with no sign of D_1 -receptor modulation as compared to striatonigral D_1 -mediated modulation in the same preparation. Interestingly, and as shown before for subthalamonigral afferents (Ibañez-Sandoval et al., 2006), we found that addition of selective receptor antagonists disclose a tonic action of ambient dopamine levels on both, striatonigral and pallidonigral afferents, supporting the notion that dopamine

receptors are sensing extracellular dopamine continuously (Yanovsky et al., 2003). Furthermore, the blockade of all dopamine receptor types altogether induced a recurrent bursting firing pattern in SNr projection neurons, a mode of firing typically seen in both Parkinsonian humans and animals (e.g., Magill et al., 2001; Walters et al., 2007; Walters and Bergstrom, 2009; Zold et al., 2009). This finding indicates that it is enough to acutely block dopamine receptors to induce a Parkinsonian firing pattern in SNr neurons. Given the direct projection of SNr to brain stem nuclei controlling muscular tone and CPGs activation, a question as to whether dopamine dysfunction in the output nuclei is enough to produce some Parkinsonian signs (Morris et al., 1994; Hemsley and Crocker, 1998; Hikosaka et al., 2000; Takakusaki et al., 2003) is set forth.

MATERIALS AND METHODS

Procedures were carried out in accordance with the National Institutes of Health Guide for Care and Use of Laboratory Animals (NIH Publications No. 8023, revised 1996) and were approved by the Institutional Animal Care Committee of UNAM. Methods have been reported elsewhere (Beurrier et al., 2006; Ibáñez-Sandoval et al., 2006). Briefly, Wistar rats (15–40 postnatal day), were anesthetized with isoflurane, decapitated, and their brains removed. Parasagittal or parahorizontal slices (300 μ m) containing the neostriatum (NSt), globus pallidus (GP), and substantia nigra pars reticulata (SNr) were obtained with a vibratome in saline of the following composition (in millimolar): 124 choline chloride, 2.5 KCl, 1.0 $MgCl_2$, 1.2 NaH_2PO_4 , 2.0 $CaCl_2$, and 10 glucose ($-4^\circ C$ 95% O_2 , 5% CO_2). Whole-cell patch-clamp recordings were performed on rat SNr neurons (Ibáñez-Sandoval et al., 2006, 2007). Neurons within the SNr were visualized with infrared differential interference videomicroscopy using a X60 water-immersion objective. For voltage-clamp recordings micropipettes 2–5 $M\Omega$ resistance were filled with internal saline containing high Cl^- (in millimolar): 70 KH_2PO_4 , 36 KCl, 2 $MgCl_2$, 10 HEPES, 1.1 EGTA, 0.2 Na_2ATP , 0.2 Na_3GTP , 5 mM QX-314, 5 mM CsCl, and 0.1% biocytin (pH 7.2; 275 mOsm/l) that allowed to record inward IPSCs from SNr neurons after field stimulation in the internal capsule (IC) 0.5–1.0 mm outside the SNr border (Radnikow and Misgeld, 1998; Wallmichrath and Szabo, 2002). Bipolar pencil shaped concentric tungsten electrodes, 11.5 μ m at the tip, and 1 $k\Omega$ DC resistance were used. For current-clamp recordings we used internal saline of the following composition (in millimolar): 120 KSO_3CH_3 , 10 NaCl, 10 EGTA, 10 HEPES, 1 $CaCl_2$, 2 $MgCl_2$, 2 ATP-Mg, 0.3 GTP-Na (pH 7.3, 290 mOsm/l). Superfusion saline contained antagonists for glutamatergic receptors: 10 μ M 6-cyano-7-nitroquinoxaline-2,3-dione (CNQX) and 50 μ M D-(–)-2-amino-5-phosphopentanoic acid (APV) to isolate IPSCs. In parasagittal slices, 3 out of 10 recordings evoked pallidonigral IPSCs and the rest evoked striatonigral IPSCs (Figure 1). In parahorizontal slices 6 out of 10 recordings evoked pallidonigral IPSCs and the rest evoked striatonigral IPSCs. IPSCs from each source were easily discernible with electrophysiological techniques (Figure 1; Connelly et al., 2010) so that when an obvious mixture of IPSCs from both sources was obtained, it was discarded from the present analysis. Holding potential was -80 mV. A paired-pulse protocol was employed with inter-pulse intervals of 50 ms to evaluate changes in the paired-pulse ratio (PPR) of evoked IPSCs (PPR = 2nd IPSC/1st IPSC) to verify presynaptic actions of

transmitters (Ibáñez-Sandoval et al., 2006). Amplitude of first IPSC was used to build time courses of dopaminergic actions. Because striatonigral fibers pass through the GPe, D_2 -class selective agonists were tested in slices taken from animals with a stereotaxic lesion (ibotenic acid) of the GPe (1.4 mm AP, 3.4 L, and 4.7 mm V) and compared to recordings obtained without a lesion. The lesion further confirmed the differences of IPSCs from both sources. Ibotenic acid solution (dissolved in PBS adjusted to pH 7.4 with NaOH 3.0 μ g/0.4 μ l) was used to lesion the GPe. These values closely followed Paxinos and Watson (1982) coordinates system.

Drugs were stored as dry aliquots and stock solutions were prepared prior to each experiment and added to the perfusion solution in the final concentration indicated. SKF 81297: (\pm)-6-Chloro-2,3,4,5-tetrahydro-1-phenyl-1H-3-benzazepine hydrobromide (10 nM–50 μ M); SCH 23390: 7-chloro-8-hydroxy-3-methyl-1-phenyl-2,3,4,5-tetrahydro-1H-3-benzazepine (50 nM and 1 μ M); CNQX: 6-cyano-7-nitroquinoxaline-2,3-dione (10 μ M), D-AP-5: D-(–)-2-amino-5-phosphopentanoic acid (50 μ M), bicuculline methiodide or methchloride (10 μ M), and QX-314 (5 mM inside the recording pipette), all were obtained from Sigma-Aldrich (St. Louis MO, USA). The neurons in the present work were SNr projection neurons ($n = 250$; see: Ibáñez-Sandoval et al., 2006). IPSCs parameters from different afferents, i.e., striatonigral and pallidonigral were compared with Mann–Whitney's U -tests. IPSCs parameters in the same synapses before and after adding a given drug were compared with Wilcoxon's t -tests. At least 10 min of stable recordings before and after administering the drugs were used to reach stable average IPSCs amplitudes. Each symbol represents mean and SEM of quantal variation in a single representative experiment. Sample averages are given in the text. Differences in parameters of fitted functions were compared by using their estimation error and Student's t -tests.

RESULTS

Figure 1 shows that striatonigral and pallidonigral synaptic inputs cannot be confused (Connelly et al., 2010). For similar stimulus, evoked striatonigral IPSCs were significantly smaller than pallidonigral IPSCs (mean \pm SEM for the first IPSC of a paired response): 235 ± 50 pA ($n = 32$) vs. 1399 ± 152 pA ($n = 20$; $P < 0.0001$), respectively. Responses to paired-pulse stimulation were also different: striatonigral IPSCs showed paired-pulse facilitation: PPR = 1.41 ± 0.07 (Figures 1A,G; $n = 30$) whereas pallidonigral IPSCs always exhibited paired-pulse depression: PPR = 0.4 ± 0.06 (Figures 1B,G; $n = 19$; $P < 0.0001$), although not always as strong as that depicted in Figure 1D. Short-term plasticity (10 pulses at 20 Hz) exhibited facilitation without failures in striatonigral connections (Figure 1C; $n = 8$), whereas it exhibited depression with intermittent failures in pallidonigral synapses (Figure 1D; $n = 4$). The decay time constant/rise time ratio was also different: 4.5 ± 0.5 ($n = 30$) in striatonigral synapses and 12.6 ± 0.8 in pallidonigral synapses ($n = 19$; $P < 0.0001$) showing that pallidonigral IPSCs are briefer than striatonigral ones (Connelly et al., 2010). Intensity–Amplitude (I–A) relationships were also constructed and fitted to a three parameter sigmoidal function (Tecuapetla et al., 2005):

$$A(I) = \frac{A_{\max}}{1 + e^{-k(I-I_h)}}$$

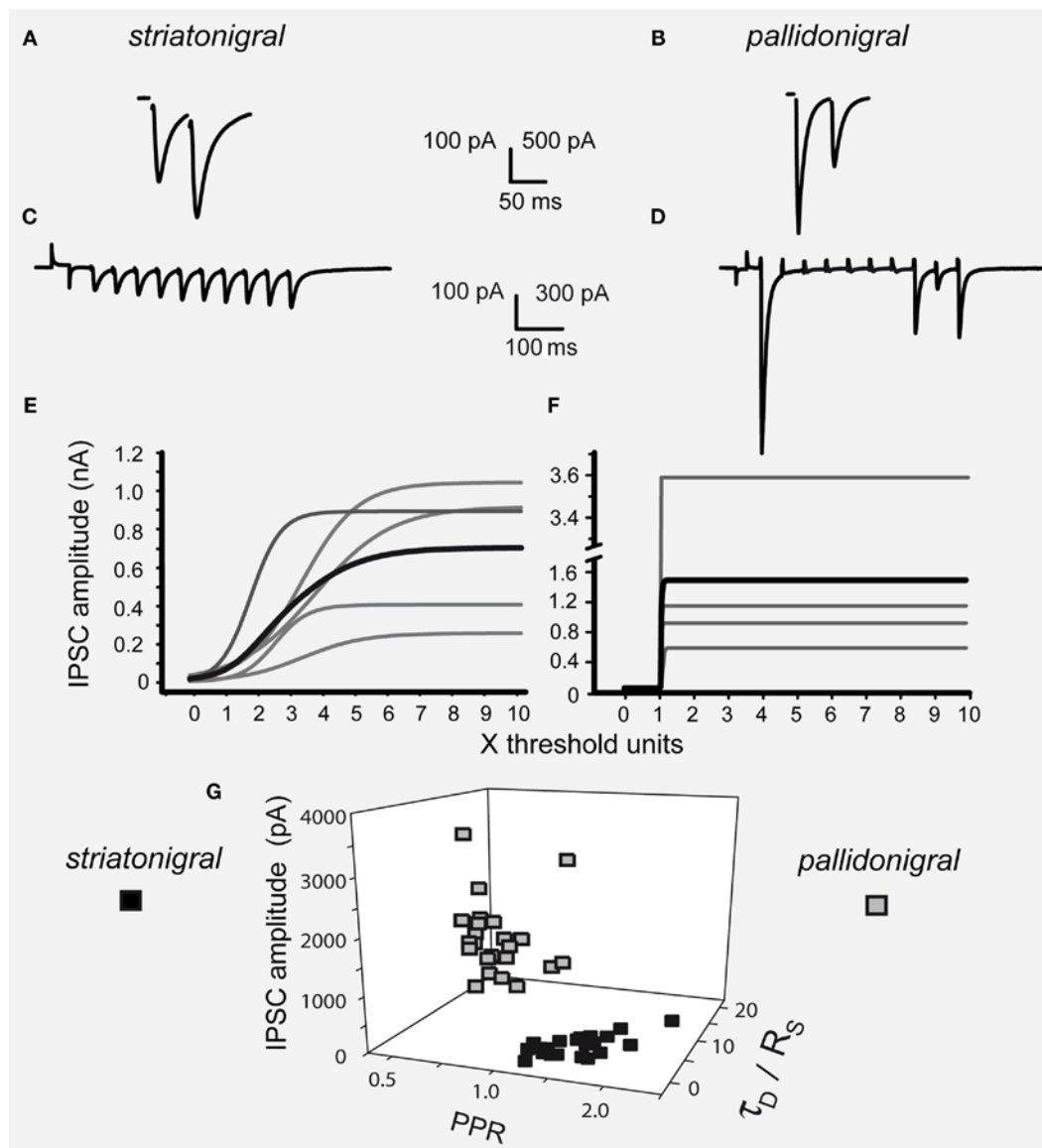


FIGURE 1 | Differences between striatonigral and pallidonigral inhibitory postsynaptic currents. (A) Striatonigral inhibitory postsynaptic currents (IPSCs) exhibited paired-pulse facilitation. (B) Pallidonigral IPSCs exhibit paired-pulse depression. (C) Short-term synaptic plasticity (STP) from striatonigral afferents is facilitation. (D) STP from pallidonigral afferents is depression with numerous failures. (E) Intensity–amplitude plots (I–A plots) from striatonigral IPSCs exhibit a sigmoidal shape. (F) I–A plots from pallidonigral IPSCs exhibit a jump to

maximal amplitude after reaching threshold. I–A plots were fitted to: $A(I) = A_{\max} / (1 + e^{-k(I-I_h)})$ where $A(I)$ = IPSC amplitude as a function of stimulus intensity, A_{\max} = maximal amplitude reached, k = slope factor, and I_h = stimulus intensity necessary to reach IPSC amplitude equal to half maximal amplitude. All parameters were significantly different. (G) Cluster plot showing that IPSCs from these sources can be separated. PPR = paired-pulse ratio. τ_D = decay time constant of IPSCs. R_s = rise time of IPSCs.

where $A(I)$ = IPSC amplitude as a function of stimulus intensity, A_{\max} = maximal amplitude reached, k = slope factor, and I_h = stimulus intensity necessary to reach IPSC amplitude equal to half maximal amplitude. All three parameters were significantly different when comparing IPSCs from striatonigral vs. pallidonigral afferents: A_{\max} : 430 ± 3 pA vs. 1512 ± 10 pA ($n = 8$; $P < 0.0001$); k : 3.6 ± 0.3 vs. 14 ± 5 ($n = 8$; $P < 0.0001$) and I_h : 2.3 ± 0.2 vs. 1.1 ± 0.1 ($n = 8$; $P < 0.005$).

These features coincide with a previous report (Connelly et al., 2010) and were verified qualitatively by evoking IPSCs from either the subthalamic nucleus (NST) or the GPe, however, in these

occasions IPSCs were considerably smaller and amplitude could not be compared by itself given the different distances from stimulating and recording electrodes (not shown). Striatonigral IPSCs features have been well described (Radnikow and Misgeld, 1998; Wallmichrath and Szabo, 2002; Beurrier et al., 2006; Chuhma et al., 2011) as well as IPSCs from pallidal origin making synapses into the SNr and other nuclei (Tecuapetla et al., 2005; Baufreton et al., 2009; Connelly et al., 2010). Finally, three of these variables were used to build a cluster plot (Figure 1G) which confirmed the easiness to separate IPSCs from each source.

The actions of selective dopamine receptor agonists for D_1 - and D_2 -receptor classes were tested. As it has been repeatedly demonstrated, the action of dopaminergic D_1 -class selective agonists at nanomolar concentrations was that of enhancing striatonigral IPSCs (Floran et al., 1990; Radnikow and Misgeld, 1998; Chuhma et al., 2011): striatonigral IPSC increased $153 \pm 10\%$ after 300 nM SKF 81297 ($n = 15$; $P < 0.001$) and the paired-pulse ratio (PPR = IPSC2/IPSC1) decreased from 1.4 ± 0.13 in the control to 1.0 ± 0.12 during SKF 81297 ($P < 0.001$), confirming a presynaptic modulation. These actions were reversible and blocked by 100 nM of the D_1 -antagonist SCH 23390 ($n = 5$; not shown here but see below) indicating that at these concentrations the action is specific. In addition, here we show that the agonists have no significant action on pallidonigral IPSCs (cf., **Figures 2A,B**).

Contrasting results were obtained when a selective D_2 -class receptor agonist, 500 nM quinorolane, was employed: striatonigral IPSCs suffered no significant alteration (**Figure 2C**; $n = 5$ NS; Chuhma et al., 2011) whereas pallidonigral IPSCs were significantly inhibited (**Figure 2D**) by $73 \pm 18\%$ (**Figure 2D**; $n = 19$; $P < 0.0001$). PPR increased from 0.76 ± 0.1 to 1.83 ± 0.2 ($P < 0.001$), suggesting a presynaptic action. These actions were reversible and blocked by 500 nM sulpiride, a D_2 -antagonist ($n = 5$; not shown but see below).

Summarizing, physiological action of D_1 -receptor agonists on striatonigral terminals is that of IPSC enhancement as previously shown (Floran et al., 1990; Radnikow and Misgeld, 1998; Chuhma

et al., 2011) with no action on pallidonigral terminals. On the other hand, physiological action of D_2 -receptor agonists on pallidonigral IPSCs is that of depression with no significant action on striatonigral terminals.

Therefore we were forced to infer that reports about D_1 -mediated inhibition of striatonigral terminals (Miyazaki and Lacey, 1998) were either involving a non-specific action, a pallidal contamination, or both. To test this hypothesis we used larger micromolar concentrations of the D_1 -agonist while evoking IPSCs from both pathways. **Figures 3A,B** show that 5 μ M SKF 81297 decreased IPSCs evoked from both set of terminals. Striatonigral IPSC decreased $82 \pm 13\%$ ($n = 18$; $P < 0.001$) and pallidonigral responses decreased by $35 \pm 15\%$ ($n = 6$; $P < 0.005$). These actions could not be blocked by micromolar concentrations of SCH 23390 (not shown), suggesting that they were not specific. In view of these results we built a concentration–response relationship (C–R plot) using a wide range of SKF 81297 concentrations while stimulating striatonigral afferents. This C–R plot can be seen in **Figure 3C**: it is biphasic. When the Hill equation was fitted to the ascending (specific part) EC_{50} was 440 ± 60 nM and the Hill coefficient 1.6 ± 0.2 , suggesting cooperativity and a specific action at submicromolar concentrations. Moreover, the fact that pallidonigral inputs are also affected when they do not respond when submicromolar concentrations of agonists are used confirmed non-specific actions.

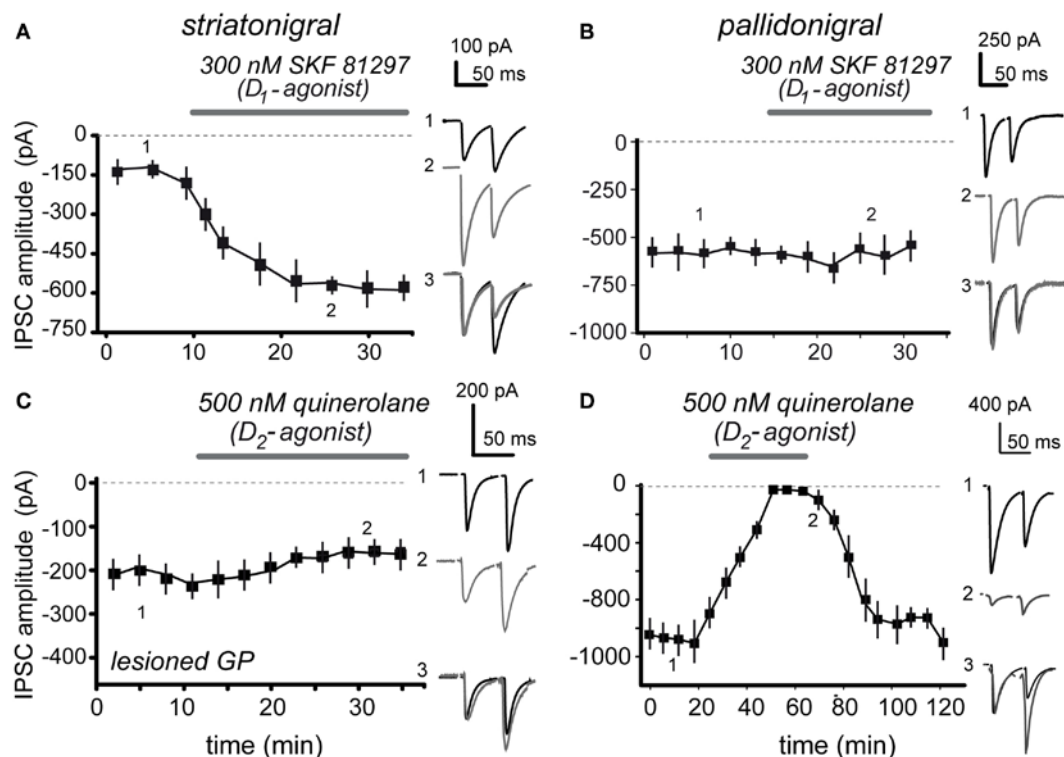


FIGURE 2 | Contrasting actions of D_1 - and D_2 -receptor agonists on striatonigral and pallidonigral IPSCs. (A) 100 nM of the selective D_1 -class receptor agonist, SKF 81297, enhanced striatonigral IPSCs. **(B)** 100 nM SKF 81297, had no action on pallidonigral IPSCs. **(C)** 500 nM of the selective D_2 -class receptor agonist, quinorolane, had no significant action on striatonigral IPSCs. In

some cases the GPe was lesioned to better avoid contamination from pallidonigral afferents. **(D)** 500 nM quinorolane greatly reduced pallidonigral IPSCs. Note changes in PPR accompanying significant effects. Record 3 in each frame is the superimposition of records 1 and 2 after normalization of the first IPSC to better appreciate the PPR change when it is present.

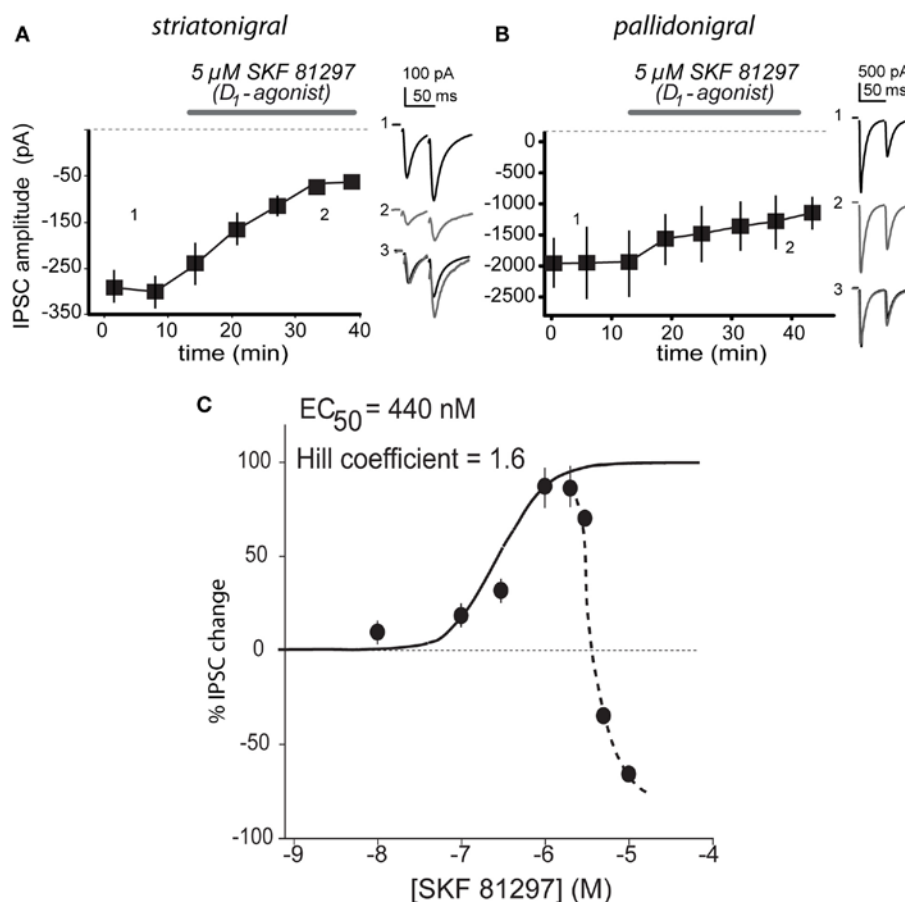


FIGURE 3 | Biphasic concentration–response relationship of D_1 -agonist. (A) 5 μ M SKF 81297 decreased IPSCs evoked from striatonigral terminals. **(B)** 5 μ M SKF 81297 decreased IPSCs evoked from pallidonigral terminals. Record 3 in each frame is the superimposition of representative records 1 and 2 after normalization of the

first IPSC to better appreciate the PPR change when it is present. **(C)** Concentration–response relationship (C–R plot) showed a biphasic response on striatonigral responses: once 3 μ M are surpassed, IPSCs decay with increasing concentrations. Ascending C–R plot was fitted with the Hill equation finding a submicromolar EC_{50} .

Given the low concentrations of agonists needed to activate D_1 - and D_2 -class receptors in their respective terminals (striatonigral and pallidonigral) we inferred that, perhaps, endogenous extracellular dopamine exerts a tonic action on these receptors. **Figure 4** shows that this hypothesis is correct. **Figures 4A,B** show that 50 nM of a D_1 -class receptor selective antagonist, SCH 23390, are enough to inhibit striatonigral IPSCs with no significant action on pallidonigral IPSC. Striatonigral IPSC decreased from 319 ± 75 in the control to 150 ± 11 pA after 50 nM SCH 23390 ($n = 12$; $P < 0.02$). **Figures 4C,D** confirm these findings and further show that potency and speediness of D_1 -action is concentration dependent. Striatonigral IPSC is greatly reduced – almost abolished – when a low micromolar antagonist concentration is maintained in the superfusion (**Figure 4C**). The effect is reversible (not shown). Traces chosen at different times during the time course, superimposed, and normalized to the amplitude of the first IPSC, show that the PPR is greatly increased from 1.9 ± 0.4 in the control to 2.4 ± 0.6 after SCH 23390 ($n = 21$; $P < 0.001$; when the IPSC is abolished PPR cannot be measured); confirming a presynaptic site of action. On the other hand, SCH 23390 did not produce any action on pallidonigral IPSC at any concentration (**Figure 4D**). In summary,

D_1 -receptors in direct pathway striatonigral terminals are sensitive detectors of extracellular dopamine. Moreover, blockade of dopaminergic action can reduce striatonigral synaptic reliability to a minimum.

In addition, **Figures 4E,F** illustrate the actions of selective antagonists for D_3 - and D_4 -type dopamine receptors: 500 nM U-9914A, a selective D_3 -type receptor antagonist enhanced pallidonigral IPSCs by $262 \pm 16\%$ after ($n = 12$; $P < 0.001$) while the PPR decreased from 0.87 ± 0.08 in the control to 0.51 ± 0.1 during the antagonist. On the other hand, 500 nM LY7550, a selective D_4 -type receptor antagonist increased pallidonigral IPSCs by $170 \pm 20\%$ ($n = 7$; $P < 0.001$) while PPR decreased from 0.78 ± 0.07 in the control to 0.57 ± 0.09 during the blockade. Sulpiride a generic D_2 -class receptor antagonist had similar actions (not shown): pallidonigral IPSCs increased by $150 \pm 14\%$ ($n = 3$) while PPR decreased from 0.77 ± 0.03 in the control to 0.35 ± 0.01 during blockade. To summarize, $D_{3/4}$ -receptors in pallidonigral terminals (Murray et al., 1994; Bevan et al., 1996; Marshall et al., 2001; Rivera et al., 2003; Seeman et al., 2006; Acosta-García et al., 2009; Gasca-Martínez et al., 2010) are sensitive to extracellular dopamine, which has the role of tonically repressing the force

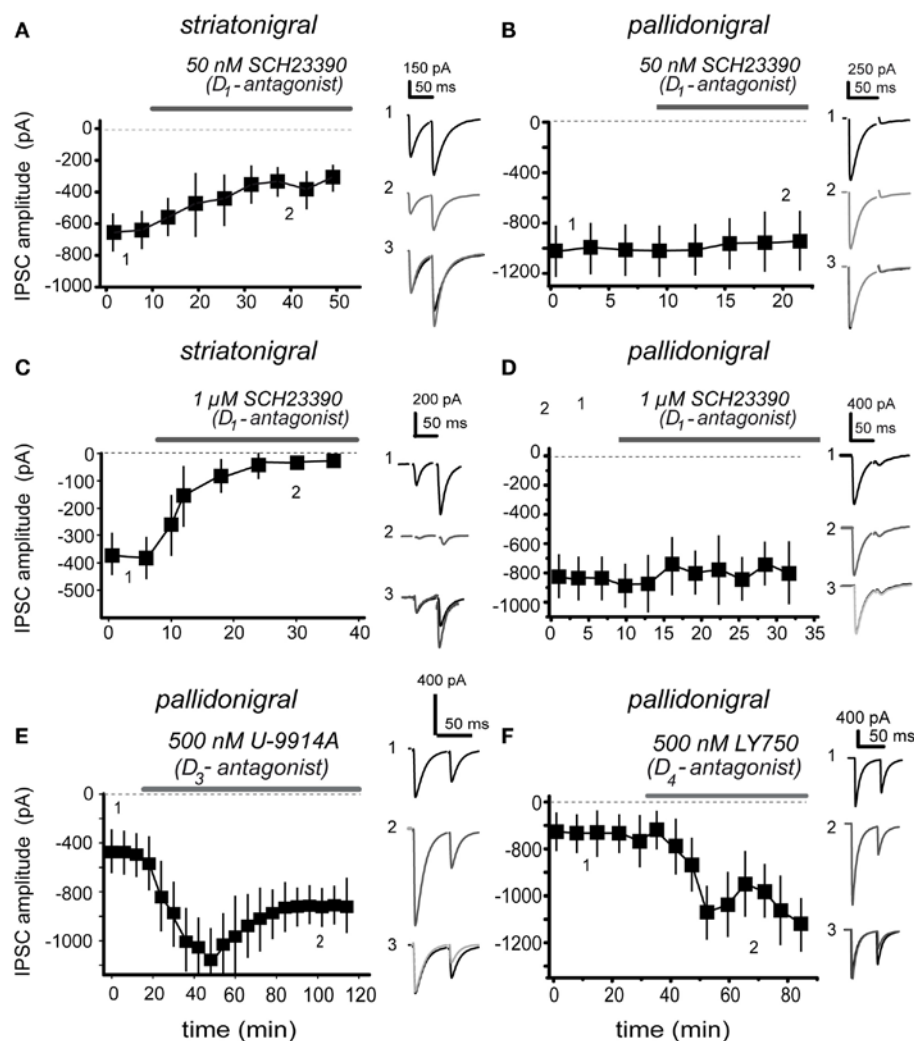


FIGURE 4 | Presynaptic dopamine receptors sense endogenous extracellular dopamine. (A) 50 nM of selective dopamine D_1 -receptor antagonist, SCH 3390, are enough to reduce striatonigral IPSC amplitude. (B) The same antagonist concentration has no action on pallidonigral IPSC. (C) Increasing D_1 -antagonist concentration (1 μ M) greatly reduced IPSC while speeding up dopamine actions on striatonigral IPSC, suggesting a concentration dependent mechanism. (D) The same antagonist

concentration has no action on pallidonigral IPSC. (E) 500 nM U-9914A, a selective D_3 -type receptor antagonist, significantly enhanced pallidonigral IPSC. Note a partial reversion. (F) 500 nM LY750, a selective D_4 -type receptor antagonist, significantly increased pallidonigral IPSC. Record 3 in each frame is the superimposition of representative records 1 and 2 after normalization of the first IPSC to better appreciate the PPR change when it is present.

of these synapses. Some functional differences in the actions of these receptor types perhaps deserve further investigation (cf., Figures 4E,F).

Finally, because subthalamonigral terminals are also tonically controlled by presynaptic dopamine receptors (D_1 - and D_2 -class; Ibáñez-Sandoval et al., 2006) and because blockade of these receptors enhance subthalamonigral EPSCs (Ibáñez-Sandoval et al., 2006), we propose the following hypothesis based in the present and previous results (Radnikow and Misgeld, 1998; Acosta-García et al., 2009; Chuhma et al., 2011): that acute blockade of both D_1 - and D_2 -class (including $D_{3/4}$ -types) receptors (by 1 μ M SCH 23390 plus 1 μ M sulpiride) altogether may decrease direct pathway synapses (striatonigral) and, at the same time, enhance indirect pathway synapses (subthalamonigral and pallidonigral), both actions being required in physiopathological

models of Parkinsonism to elicit the signs of the disease. The result can be seen in Figure 5: SNr neurons shifted from a tonic firing pattern in the control to a bursting firing pattern after blockade of dopamine receptors ($n = 7$ neurons; Ibáñez-Sandoval et al., 2007).

One of the most supported neuronal correlates of Parkinsonism: recurrent bursting in SNr neurons, was similar to that previously reported *in vivo* and *in vitro* (Hammond et al., 2007; Ibáñez-Sandoval et al., 2007; Walters et al., 2007; Walters and Bergstrom, 2009; Zold et al., 2009). Transitions from tonic to bursting firing mode can rarely be seen spontaneously in control preparations (Ibáñez-Sandoval et al., 2007).

To see whether excitatory subthalamonigral afferents, that is, the STN-GP circuit, was participating in this firing behavior, we added the NMDA-receptor antagonist APV (50 μ M) to provoke a partial

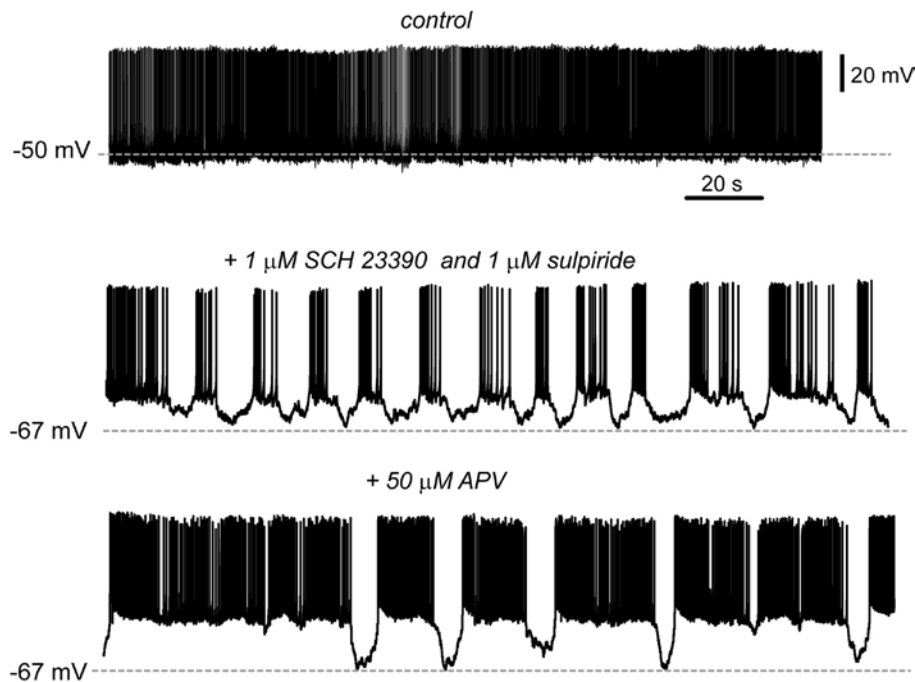


FIGURE 5 | Blockade of dopamine receptors changes the firing pattern of SNr neurons. Spontaneous tonic firing was the usual firing pattern recorded in SNr neurons in control conditions (top). During acute blockade of dopamine D_1 - and D_2 -class receptors ($1 \mu\text{M}$ SCH 23390 plus $1 \mu\text{M}$ sulpiride) SNr firing pattern shifted from tonic to a bursting pattern in $n = 7$ cells; two cells exhibited bursting

before adding the blockers. To see whether besides striatonigral and pallidonigral afferents, subthalamonigral afferents were also contributing to this firing mode, the glutamate NMDA-receptor antagonist, $50 \mu\text{M}$ APV was added to the bath saline (bottom). The firing tended to return to a tonic firing pattern but it was frequently interrupted by sudden hyperpolarizations.

block of STN influence. The result was that the firing pattern became less bursty and more tonic (Ibáñez-Sandoval et al., 2007), however, firing was still abruptly interrupted by sudden hyperpolarizations, probably coming from enhanced pallidonigral inputs.

DISCUSSION

The present work shows that extracellular dopamine concentrations are tonically being sensed by the synaptic terminals of inhibitory inputs to the SNr in opposite ways. Thus, blockade of D_1 -type receptors in striatonigral (direct pathway) afferents decreased striatonigral inhibition while blockade of $D_{3/4}$ -types receptors in pallidonigral terminals enhanced pallidonigral inhibition. Pallidonigral afferents are presynaptically controlled by D_2 -class but not D_1 -class receptors. Still other inputs to the SNr have to be studied to see whether they are presynaptically modulated.

STRIATONIGRAL AND PALLIDONIGRAL IPSCs ARE DIFFERENT

Striatonigral IPSCs are smaller but last longer than pallidonigral IPSCs. In addition, they exhibit short-term facilitation and are positively regulated by D_1 -receptors (Floran et al., 1990; Radnikow and Misgeld, 1998; Connelly et al., 2010). Strong evidence for the last property has been obtained with optogenetic techniques (Chuhma et al., 2011), supporting the present and previous reports. In comparison, pallidonigral IPSCs are larger and exhibit different degrees of short-term depression (Connelly et al., 2010). The two classes of inhibition are so different that cannot be confused. Pallidonigral IPSCs are negatively regulated by D_2 -class receptors and have no

D_1 -modulation. Notably, short-term facilitation works as a high pass filter of incoming inputs whereas short-term depression works as a low pass filter (Abbott and Regehr, 2004). In contrast, subthalamonigral excitatory synapses are controlled by both D_1 - and D_2 -class receptors (Ibáñez-Sandoval et al., 2006).

Selective dopamine receptor agonists exert their specific actions at nanomolar or low micromolar concentrations but higher concentrations become non-specific, thus explaining previous contradictions (cf., Miyazaki and Lacey, 1998; Radnikow and Misgeld, 1998) and probably similar discrepancies within the striatal/accumbinal circuitry (Guzman et al., 2003; Taverna et al., 2005). To summarize: D_1 -receptor activation enhances GABA release in terminals from medium spiny neurons of the direct pathway whereas $D_{3/4}$ -receptor activation represses GABA release from pallidonigral terminals.

STRIATONIGRAL AND PALLIDONIGRAL DOPAMINE RECEPTORS SENSE EXTRACELLULAR AMBIENT ENDOGENOUS DOPAMINE

Because nanomolar concentrations of selective receptor agonist are needed to modify transmission, we hypothesized that administrations of selective dopamine receptor antagonist would disclose the actions of endogenous dopamine present in the extracellular space. Therefore, to disclose the action of ambient endogenous dopamine we applied selective D_1 - and $D_{3/4}$ -receptor antagonists. Our findings were that according to the concentration, suppression of endogenous dopamine action greatly reduced striatonigral transmission while it enhanced pallidonigral transmission. These results indicated that extracellular dopamine concentrations are

regulating synaptic release probability in both types of connections, increasing release probability in striatonigral synapses and decreasing release probability in pallidonigral synapses.

Therefore, the following working hypothesis resulted from the present experiments: tonic levels of dopamine in SNr are necessary to maintain the normal function of direct pathway connections and maintain in check indirect pathway synapses from both pallidonigral terminals (present work) and subthalamonigral terminals (Ibáñez-Sandoval et al., 2007). The logical functional consequence of this hypothesis was tested: blockade of tonic dopamine action would enhance indirect pathway transmission and reduce direct pathway input thus yielding a previously observed neuronal correlate of Parkinsonism: SNr neurons shifted their tonic firing pattern to a bursting firing pattern typical of subjects with the disease (Takakusaki et al., 2004; Rivlin-Etzion et al., 2006; Hammond et al., 2007; Ibáñez-Sandoval et al., 2007; Walters et al., 2007; Zold et al., 2009).

Tonic spontaneous firing is preserved in the slice preparation in both GPe and STN (e.g., Beurrier et al., 1999; Chan et al., 2011). Calcium imaging techniques recording dozens of cells simultaneously within the striatal circuit show that there is always some spontaneous activity in striatal spiny neurons in control conditions (Carrillo-Reid et al., 2008). Moreover, there is a great amount of convergence between the striatum and the substantia nigra and inhibitory striatonigral events are of large amplitude (e.g., Chuhma et al., 2011). Thus, for a SNr neuron there always may be some striatal cell firing. Therefore, the lost balance between direct and indirect pathways by the acute blockade of dopamine receptors is the most probable cause of bursting in SNr neurons during the present experiments.

Postsynaptic dopamine receptors on SNr neurons cannot explain bursting because their function is to increase tonic firing frequency via a cation current; their blockade resulting in lower tonic frequency with irregularities, but not continuous bursting behavior (Lee and Tepper, 2007; Zhou et al., 2009).

FUNCTIONAL CONSEQUENCES

Because the change in firing pattern of SNr neurons was achieved acutely by blocking dopamine receptors one can speculate what would happen during a chronic absence of dopamine in the output

nuclei of the BG. The absence of dopamine (e.g., Parkinsonism) may reduce the function of direct pathway synapses in such a way that maintaining this state of affairs in the long-time would lead to loss of direct pathway synapses due to long-term synaptic plasticity. In contrast, maintaining a high function in pallidonigral and subthalamonigral synapses would produce long-term potentiation of these synapses. These events taken together may tend to change the circuitry permanently, making not only L-DOPA inefficient but, perhaps, making the chronic diseased circuitry radically different than the control or healthy circuit: that is, more dependent on the subthalamopallidal loop (Magill et al., 2001; Baufreton et al., 2009).

Bursting in SNr neurons leads to tremor and rigidity (Hemsley and Crocker, 1998; Takakusaki et al., 2004). Moreover, this configuration of synaptic weights would lead to the loss of high pass filtering of SNr inputs (direct pathway's short-term facilitation) and an increase in low pass filtering of SNr inputs (pallidonigral short-term depression; Abbott and Regehr, 2004) setting the stage to favor the entrance to an akinetic frequency lock (Hutchison et al., 2004; Avila et al., 2010). Consequently, therapeutic ways of activating the direct pathway in the chronic patient may be fundamental to avoid irreversible plastic changes in the network (Hammond et al., 2007; Walters et al., 2007; Walters and Bergstrom, 2009; Zold et al., 2009; Bateup et al., 2010; Kravitz et al., 2010).

ACKNOWLEDGMENTS

We thank A. Laville, D. Tapia and G. X. Ayala for helpful comments and technical support. This work was funded by Investigacion Multidisciplinaria de Proyectos Universitarios de Liderazgo y Superacion Academica (IMPULSA)-Universidad Nacional Autónoma de México (UNAM) 03, Dirección General de Asuntos del Personal Académico-UNAM Grants IN-205610 to José Bargas, and IN-206010 to Elvira Galarraga. Fundación Miguel Alemán AC to José Bargas. Pavel E. Rueda-Orozco was postdoctoral fellow at UNAM. Osvaldo Ibañez-Sandoval Ricardo Hernandez, José de Jesús Aceves, and Víctor Plata had or have CONACyT-Mexico doctoral fellowships.

REFERENCES

- Abbott, L. F., and Regehr, W. G. (2004). Synaptic computation. *Nature* 431, 796–803.
- Acosta-García, J., Hernández-Chan, N., Paz-Bermúdez, F., Sierra, A., Erlij, D., Aceves, J., and Florán, B. (2009). D4 and D1 dopamine receptors modulate [3H] GABA release in the substantia nigra pars reticulata of the rat. *Neuropharmacology* 57, 725–730.
- Albin, R. L., Young, A. B., and Penney, J. B. (1989). The functional anatomy of basal ganglia disorders. *Trends Neurosci.* 12, 366–375.
- Alexander, G. E., and Crutcher, M. D. (1990). Functional architecture of basal ganglia circuits: neural substrates of parallel processing. *Trends Neurosci.* 13, 266–271.
- Altar, C. A., and Hauser, K. (1987). Topography of substantia nigra innervation by D1 receptor-containing striatal neurons. *Brain Res.* 410, 1–11.
- Avila, I., Parr-Brownlie, L. C., Brazhnik, E., Castaneda, E., Bergstrom, D. A., and Walters, J. R. (2010). Beta frequency synchronization in basal ganglia output during rest and walk in a hemiparkinsonian rat. *Exp. Neurol.* 221, 307–319.
- Bateup, H. S., Santini, E., Shen, W., Birnbaum, S., Valjent, E., Surmeier, D. J., Fisone, G., Nestler, E. J., and Greengard, P. (2010). Distinct subclasses of medium spiny neurons differentially regulate striatal motor behaviors. *Proc. Natl. Acad. Sci. U.S.A.* 107, 14845–14850.
- Baufreton, J., Kirkham, E., Atherton, J. F., Menard, A., Magill, P. J., Bolam, J. P., and Bevan, M. D. (2009). Sparse but selective and potent synaptic transmission from the globus pallidus to the subthalamic nucleus. *J. Neurophysiol.* 102, 532–545.
- Beurrier, C., Ben-Ari, Y., and Hammond, C. (2006). Preservation of the direct and indirect pathways in an in vitro preparation of the mouse basal ganglia. *Neuroscience* 140, 77–86.
- Beurrier, C., Congar, P., Bioulac, B., and Hammond, C. (1999). Subthalamic nucleus neurons switch from single-spike activity to burst-firing mode. *J. Neurosci.* 19, 599–609.
- Bevan, M. D., Bolam, J. P., and Crossman, A. R. (1994). Convergent synaptic input from the neostriatum and the subthalamus onto identified nigrothalamic neurons in the rat. *Eur. J. Neurosci.* 16, 320–334.
- Bevan, M. D., Smith, A. D., and Bolam, J. P. (1996). The substantia nigra as a site of synaptic integration of functionally diverse information arising from the ventral pallidum and the globus pallidus in the rat. *Neuroscience* 75, 5–12.
- Carrillo-Reid, L., Tecuapetla, F., Tapia, D., Hernández-Cruz, A., Galarraga, E., Drucker-Colin, R., and Bargas, J. (2008). Encoding network states by striatal cell assemblies. *J. Neurophysiol.* 99, 1435–1450.
- Chan, C. S., Glajch, K. E., Gertler, T. S., Guzman, J. N., Mercer, J. N., Lewis, A. S., Goldberg, A. B., Tkatch, T., Shigemoto, R., Fleming, S. M., Chetkovich, D. M., Osten, P., Kita, H., and Surmeier, D. J. (2011). HCN channelopathy in external globus pallidus neurons in models

- of Parkinson's disease. *Nat. Neurosci.* 14, 85–92.
- Chevalier, G., Vacher, S., Deniau, J. M., and Desban, M. (1985). Disinhibition as a basic process in the expression of striatal function. I. The striato-nigral influence on tecto-spinal/tecto-diencephalic neurons. *Brain Res.* 334, 215–226.
- Chuhma, N., Tanaka, K. F., Hen, R., and Rayport, S. (2011). Functional connectome of the striatal medium-spiny neuron. *J. Neurosci.* 31, 1183–1192.
- Connelly, W. M., Schulz, J. M., Lees, G., and Reynolds, J. N. (2010). Differential short-term plasticity at convergent inhibitory synapses to the substantia nigra pars reticulata. *J. Neurosci.* 30, 14854–14861.
- DeLong, M. R. (1990). Primate models of movement disorders of basal ganglia origin. *Trends Neurosci.* 13, 281–285.
- Deniau, J. M., Menetrey, A., and Charpier, S. (1996). The lamellar organization of the rat substantia nigra pars reticulata: segregated patterns of striatal afferents and relationship to the topography of corticostriatal projections. *J. Neurosci.* 16, 761–781.
- Floran, B., Aceves, J., Sierra, A., and Martinez-Fong, D. (1990). Activation of D1 dopamine receptors stimulates the release of GABA in the basal ganglia of the rat. *Neurosci. Lett.* 116, 136–140.
- Gale, S. D., and Perkel, D. J. (2010). Anatomy of a songbird basal ganglia circuit essential for vocal learning and plasticity. *J. Chem. Neuroanat.* 39, 124–131.
- Gasca-Martinez, D., Hernandez, A., Sierra, A., Valdiosera, R., Anaya-Martinez, V., Floran, B., Erlij, D., and Aceves, J. (2010). Dopamine inhibits GABA transmission from the globus pallidus to the thalamic reticular nucleus via presynaptic D4 receptors. *Neuroscience* 169, 1672–1681.
- Grillner, S., Markram, H., De Schutter, E., Silberberg, G., and LeBeau, F. E. (2005). Microcircuits in action from CPGs to neocortex. *Trends Neurosci.* 28, 525–533.
- Grillner, S., Wallén, P., Saitoh, K., and Kozlov, A. B. (2008). Robertson neural bases of goal-directed locomotion in vertebrates: an overview. *Brain Res. Rev.* 57, 2–12.
- Grofová, I., and Rinvik, E. (1970). An experimental electron microscopic study on the striatonigral projection in the cat. *Exp. Brain Res.* 11, 249–262.
- Guzman, J. N., Hernandez, A., Galarraga, E., Tapia, D., Laville, A., Vergara, R., Aceves, J., and Bargas, J. (2003). Dopaminergic modulation of axon collaterals interconnecting spiny neurons of the rat striatum. *J. Neurosci.* 23, 8931–8940.
- Haber, S. N. (2003). The primate basal ganglia: parallel and integrative networks. *J. Chem. Neuroanat.* 26, 317–330.
- Hammond, C., Bergman, H., and Brown, P. (2007). Pathological synchronization in Parkinson's disease: networks, models and treatments. *Trends Neurosci.* 30, 357–364.
- Hemsley, K. M., and Crocker, A. D. (1998). The effects of an irreversible dopamine receptor antagonist, N-ethoxycarbonyl-2-ethoxy-1,2-dihydroquinoline (EEDQ), on the regulation of muscle tone in the rat: the role of the substantia nigra. *Neurosci. Lett.* 251, 77–80.
- Hikosaka, O., Takikawa, Y., and Kawagoe, R. (2000). Role of the basal ganglia in the control of purposive saccadic eye movements. *Physiol. Rev.* 80, 953–978.
- Hutchinson, W. D., Dostrovsky, J. O., Walters, J. R., Courtemanche, R., Boraud, T., Goldberg, J., and Brown, P. (2004). Neuronal oscillations in the basal ganglia and movement disorders: evidence from whole animal and human recordings. *J. Neurosci.* 24, 9240–9243.
- Ibáñez-Sandoval, O., Carrillo-Reid, L., Galarraga, E., Tapia, D., Mendoza, E., Gomora, J. C., Aceves, J., and Bargas, J. (2007). Bursting in substantia nigra pars reticulata neurons in vitro: possible relevance for Parkinson disease. *J. Neurophysiol.* 98, 2311–2323.
- Ibáñez-Sandoval, O., Hernandez, A., Floran, B., Galarraga, E., Tapia, D., Valdiosera, R., Erlij, D., Aceves, J., and Bargas, J. (2006). Control of the subthalamic innervation of substantia nigra pars reticulata by D1 and D2 dopamine receptors. *J. Neurophysiol.* 95, 1800–1811.
- Kita, H. (2007). Globus pallidus external segment. *Prog. Brain Res.* 160, 111–133.
- Kravitz, A. V., Freeze, B. S., Parker, P. R., Kay, K., Thwin, M. T., Deisseroth, K., and Kreitzer, A. C. (2010). Regulation of parkinsonian motor behaviours by optogenetic control of basal ganglia circuitry. *Nature* 466, 622–626.
- Lee, C. R., and Tepper, J. M. (2007). A calcium-activated nonselective cation conductance underlies the plateau potential in rat substantia nigra GABAergic neurons. *J. Neurosci.* 27, 6531–6541.
- Magill, P. J., Bolam, J. P., and Bevan, M. D. (2001). Dopamine regulates the impact of the cerebral cortex on the subthalamic nucleus-globus pallidus network. *Neuroscience* 106, 313–330.
- Marshall, J. F., Henry, B. L., Billings, L. M., and Hoover, B. R. (2001). The role of the globus pallidus D2 subfamily of dopamine receptors in pallidal immediate early gene expression. *Neuroscience* 105, 365–378.
- Matuszewich, L., and Yamamoto, B. K. (1999). Modulation of GABA release by dopamine in the substantia nigra. *Synapse* 32, 29–36.
- Miyazaki, T., and Lacey, M. G. (1998). Presynaptic inhibition by dopamine of a discrete component of GABA release in rat substantia nigra pars reticulata. *J. Physiol.* 513, 805–817.
- Morris, M. E., Jansek, R., Matyas, T. A., and Summers, J. J. (1994). The pathogenesis of gait hypokinesia in Parkinson's disease. *Brain* 117, 1169–1181.
- Murray, A. M., Ryoo, H. L., Gurevich, E., and Joyce, J. N. (1994). Localization of dopamine D3 receptors to mesolimbic and D2 receptors to mesostriatal regions of human forebrain. *Proc. Natl. Acad. Sci. U.S.A.* 91, 11271–11275.
- Nakanishi, H., Kita, H., and Kitai, S. T. (1987). Intracellular study of rat substantia nigra pars reticulata neurons in an in vitro slice preparation: electrical membrane properties and response characteristics to subthalamic stimulation. *Brain Res.* 437, 45–55.
- Paxinos, G., and Watson, C. (1982). *The Rat Brain in Stereotaxic Coordinates*. New York: Academic Press.
- Porceddu, M. L., Giorgi, O., Ongini, E., Mele, S., and Biggio, G. (1986). 3H-SCH 23390 binding sites in the rat substantia nigra: evidence for a presynaptic localization and innervation by dopamine. *Life Sci.* 39, 321–328.
- Radnikow, G., and Miggelid, U. (1998). Dopamine D1 receptors facilitate GABA synaptic currents in the rat substantia nigra pars reticulata. *J. Neurosci.* 18, 2009–2016.
- Redgrave, P., Rodriguez, M., Smith, Y., Rodriguez-Oroz, M. C., Lehericy, S., Bergman, H., Agid, Y., DeLong, M. R., and Obeso, J. A. (2010). Goal-directed and habitual control in the basal ganglia: implications for Parkinson's disease. *Nat. Rev. Neurosci.* 11, 760–772.
- Reiner, A., Medina, L., and Veenman, C. L. (1998). Structural and functional evolution of the basal ganglia in vertebrates. *Brain Res. Rev.* 28, 235–285.
- Rivera, A., Trías, S., Peñafiel, A., Angel Narváez, J., Díaz-Cabiale, Z., Moratalla, R., and de la Calle, A. (2003). Expression of D4 dopamine receptors in striatonigral and striatopallidal neurons in the rat striatum. *Brain Res.* 989, 35–41.
- Rivlin-Etzion, M., Marmor, O., Heimer, G., Raz, A., Nini, A., and Bergman, H. (2006). Basal ganglia oscillations and pathophysiology of movement disorders. *Curr. Opin. Neurobiol.* 16, 629–637.
- Seeman, P., Wilson, A., Gmeiner, P., and Kapur, S. (2006). Dopamine D2 and D3 receptors in human putamen, caudate nucleus, and globus pallidus. *Synapse* 60, 205–211.
- Smith, Y., Bevan, M. D., Shink, E., and Bolam, J. P. (1998). Microcircuitry of the direct and indirect pathways of the basal ganglia. *Neuroscience* 86, 353–387.
- Smith, Y., and Bolam, J. P. (1989). Neurons of the substantia nigra pars reticulata receive a dense GABA-containing input from the globus pallidus in the rat. *Brain Res.* 493, 160–167.
- Smith, Y., and Bolam, J. P. (1991). Convergence of synaptic inputs from the striatum and the globus pallidus onto identified nigrocollicular cells in the rat: a double anterograde labelling study. *Neuroscience* 44, 45–73.
- Takakusaki, K., Habaguchi, T., Ohtinata-Sugimoto, J., Saitoh, K., and Sakamoto, T. (2003). Basal ganglia efferents to the brainstem centers controlling postural muscle tone and locomotion: a new concept for understanding motor disorders in basal ganglia dysfunction. *Neuroscience* 119, 293–308.
- Takakusaki, K., Saitoh, K., Harada, H., and Kashiwayanagi, M. (2004). Role of basal ganglia-brainstem pathways in the control of motor behaviors. *Neurosci. Res.* 50, 137–151.
- Taverna, S., Canciani, B., and Pennartz, C. M. (2005). Dopamine D1-receptors modulate lateral inhibition between principal cells of the nucleus accumbens. *J. Neurophysiol.* 93, 1816–1819.
- Tecuapetla, F., Carrillo-Reid, L., Guzmán, J. N., Galarraga, E., and Bargas, J. (2005). Different inhibitory inputs onto neostriatal projection neurons as revealed by field stimulation. *J. Neurophysiol.* 93, 1119–1126.
- Wallmichrath, I., and Szabo, B. (2002). Cannabinoids inhibit striatonigral GABAergic neurotransmission in the mouse. *Neuroscience* 113, 671–682.
- Walters, J. R., and Bergstrom, D. A. (2009). “Basal ganglia network synchronization in animal models of Parkinson's disease,” in *Cortico-Subcortical Dynamics in Parkinson's Disease Contemporary Neuroscience*, ed. K.-Y. Tseng (New York: Humana Press), 117–142.
- Walters, J. R., Hu, D., Itoga, C. A., Parr-Brownlie, L. C., and Bergstrom, D. A. (2007). Phase relationships support a role for coordinated activity in the indirect pathway in organizing slow oscillations in basal ganglia output after loss of dopamine. *Neuroscience* 149, 762–776.

- Yanovsky, Y., Mades, S., and Misgeld, U. (2003). Retrograde signaling changes the venue of postsynaptic inhibition in rat substantia nigra. *Neuroscience* 122, 317–328.
- Zhou, F. W., Jin, Y., Matta, S. G., Xu, M., and Zhou, F. M. (2009). An ultra-short dopamine pathway regulates basal ganglia output. *J. Neurosci.* 29, 10424–10435.
- Zold, C. L., Belluscio, M., Kasanetz, F., Pomata, P. E., Riquelme, L. A., Gonon, F., and Murer, M. G. (2009). “Converging into a unified model of Parkinson’s disease pathophysiology,” in *Cortico-Subcortical Dynamics in Parkinson’s Disease Contemporary Neuroscience*, ed. K.-Y. Tseng (New York: Humana Press), 252–259.
- Conflict of Interest Statement:** The authors declare that the research was conducted in the absence of any commercial or financial relationships that could be construed as a potential conflict of interest.
- Received: 15 December 2010; paper pending published: 04 January 2011; accepted: 23 January 2011; published online: 10 February 2011.
- Citation: Aceves JJ, Rueda-Orozco PE, Hernández R, Plata V, Ibañez-Sandoval O, Galarraga E and Bargas J (2011) Dopaminergic presynaptic modulation of nigral afferents: its role in the generation of recurrent bursting in substantia nigra pars reticulata neurons. *Front. Syst. Neurosci.* 5:6. doi: 10.3389/fnsys.2011.00006
- Copyright © 2011 Aceves, Rueda-Orozco, Hernández, Plata, Ibañez-Sandoval, Galarraga and Bargas. This is an open-access article subject to an exclusive license agreement between the authors and Frontiers Media SA, which permits unrestricted use, distribution, and reproduction in any medium, provided the original authors and source are credited.



Dopaminergic modulation of corticostriatal responses in medium spiny projection neurons from direct and indirect pathways

Edén Flores-Barrera, Bianca J. Vizcarra-Chacón, José Bargas, Dagoberto Tapia and Elvira Galarraga*

División de Neurociencias, Instituto de Fisiología Celular, Universidad Nacional Autónoma de México, México City, Federal District, México

Edited by:

James M. Tepper, Rutgers, The State University of New Jersey, USA

Reviewed by:

Michael S. Levine, Brain Research Institute, USA

Jeffery R. Wickens, Okinawa Institute of Science and Technology, Japan

*Correspondence:

Elvira Galarraga, División de Neurociencias, Instituto de Fisiología Celular, Universidad Nacional Autónoma de México, PO Box: 70-253, México City, Federal District 04510, México.
e-mail: egalarraga@ifc.unam.mx

Suprathreshold corticostriatal responses recorded from medium spiny neurons (MSNs) from the direct and indirect pathways of the basal ganglia are different. Their differences readily distinguish D_1 - and D_2 -type receptor expressing MSNs in both bacterial artificial chromosome-transgenic mice and their control littermates as well as in rats: indirect pathway neurons are more excitable than direct pathway neurons revealing autoregenerative spikes underlying their spike trains, whereas direct pathway neurons exhibit more prolonged plateau potentials and spike trains. SKF 81297, a selective agonist for D_1 -class receptors enhanced corticostriatal responses in direct pathway neurons, while quinlorane, a selective agonist for D_2 -class receptors reduced orthodromic and autoregenerative responses in indirect pathway neurons thus making both neuron classes similarly excitable. Because dopaminergic postsynaptic actions target Ca_v1 (L) class voltage-gated calcium channels in MSNs, we hypothesized that these channels are involved and can explain a part of the dopaminergic actions on corticostriatal integration. Both 2.5 μ M nifedipine and 400 nM flunarizine, selective Ca_v1 channel blockers, reduced corticostriatal responses in both D_1 - and D_2 -receptor expressing neurons, respectively. A previous blockade of Ca_v1 channels occluded the actions of dopamine agonists in both neuronal classes. In contrast, a Ca_v1 (L) channel activator, 2.5 μ M Bay K 8644, enhanced corticostriatal responses in neurons from both pathways. It is concluded that Ca_v1 intrinsic currents mediate a part of the dopaminergic modulation during orthodromic synaptic integration of cortical inputs in both classes of MSNs.

Keywords: Ca_v1 channels, strionigral pathway, striopallidal pathway, medium spiny neurons, dopamine receptors, corticostriatal pathway

INTRODUCTION

Striatal dopamine (DA) is involved in initiation of learned procedures (Schultz, 2007). Localization of different DA receptors in medium spiny neurons (MSNs) belonging to direct and indirect pathways of the basal ganglia (Gerfen, 2000) has led to the idea that balanced activity in these two pathways is regulated by opposite actions of DA in each of them: the “two pathways hypothesis” (Albin et al., 1989; Mink, 2003; Redgrave et al., 2010). Both voltage- and current-clamp data in single cells have partially confirmed these assumptions: D_1 -class receptor (D_1R) activation facilitates firing in MSNs of the direct pathway by enhancing Ca_v1 (L) calcium current, whereas D_2 -class receptor (D_2R) activation represses firing in MSNs of the indirect pathway by decreasing the same current (Surmeier et al., 1995; Hernández-López et al., 1997, 2000). Supposedly, facilitating the direct pathway and preventing activity in the indirect pathway are DA roles when promoting movement (Bateup et al., 2010; Kravitz et al., 2010). These DA receptors use different signaling cascades to target Ca_v1 (L) calcium channels (Surmeier et al., 1995; Hernández-López et al., 1997, 2000).

Nonetheless, although clear differences in DA actions can be recorded during direct stimulation experiments (Surmeier et al., 1995, 2007; Galarraga et al., 1997; Hernández-López et al., 1997, 2000; Salgado et al., 2005), these differences have

not been observed during more physiological corticostriatal synaptic responses (Flores-Barrera et al., 2010), when neurons are embedded in their rich polysynaptic network where indirect effects can ensue (Albin et al., 1989; Mink, 2003; Flores-Barrera et al., 2009; Bateup et al., 2010; Kravitz et al., 2010; Redgrave et al., 2010). Two questions need to be answered: First, if indirect pathway D_2 -expressing neurons are more excitable than direct pathway neurons (Day et al., 2006; Flores-Barrera et al., 2010) then, it is important to know whether activation of D_1 -class receptors is strong enough to make direct pathway neurons more excitable, perhaps as excitable as indirect pathway neurons. Secondly, it is also important to know whether D_2 -class receptor activation is strong enough to decrease significantly the corticostriatal response of indirect pathway neurons. In other words, to test the robustness of dopaminergic actions on corticostriatal responses it is necessary to observe whether DA actions do in fact produce a balance in excitability as the “two pathway hypothesis” postulates. If this is so, it is necessary to know how much margin is available to the system in order to achieve the supposed balance. To answer these questions, we used selective agonists and antagonists of D_1 - and D_2 -class receptors, bacterial artificial chromosome (BAC) transgenic mice to identify the recorded neurons, and

evoked suprathreshold synaptic responses in which both polysynaptic and intrinsic currents are involved (Flores-Barrera et al., 2009, 2010).

Because both DA receptors and Ca_v1 channels are found in dendrites of MSNs where most cortical inputs arrive (Freund et al., 1984; Carter and Sabatini, 2004; Kreitzer and Malenka, 2005; Day et al., 2006), and because DA modulation particularly targets Ca_v1 channels in MSNs (Surmeier et al., 1995; Hernández-López et al., 1997, 2000), the present study focuses in the involvement of this intrinsic current on corticostriatal synaptic integration and its role during dopaminergic modulation. However, the present work was not intended to exclude other possible contributors. It was found that dopaminergic actions expected by the two pathways hypothesis are robust and readily observed upon corticostriatal responses, provided the recorded cells from both pathways are identified and selective pharmacological tools are employed.

MATERIALS AND METHODS

All experiments were carried out in accordance with the National Institutes of Health Guide for Care and Use of Laboratory Animals and were approved by the Institutional Animal Care Committee of the Universidad Nacional Autónoma de México. BAC-transgenic mice for D_1 - and D_2 -receptors expressing MSNs (D_1 - and D_2 -MSNs) of 60- to 90-day-old mice were anesthetized, decapitated, and their brains removed and submerged in an iced saline solution containing (in mM): 120 NaCl, 3 KCl, 25 NaHCO_3 , 2 CaCl_2 , 1 MgCl_2 , and 11 glucose (33–35°C, 300 mOsm/l with glucose, pH 7.4, after bubbling with 95% O_2 plus 5% CO_2). Briefly, and as previously described in detail, 350 μm thick parasagittal slices were cut (Flores-Barrera et al., 2010) on a vibratome and left to equilibrate for at least 1 h at room temperature in the same saline. Thereafter, slices were transferred to a recording chamber and continuously superfused with the same saline at 33–35°C. Intracellular recordings were performed from spiny neurons of the dorsal neostriatum using sharp electrodes filled with potassium-acetate 3 M and 1% biocytin (d.c. resistance 80–120 $\text{M}\Omega$). Records were obtained with an active bridge electrometer (Neuro Data, Cygnus Technology, Inc., Delaware Water Gap, PA, USA), digitized, and saved for off-line analysis with a personal computer. After recordings, neurons were injected with biocytin for its anatomical identification. Biocytin injected neurons were identified as D_1 - or D_2 -type receptors expressing MSNs. D_1 - and D_2 -type dopaminergic agonists: SKF 81297 and quinlorane, as well as antagonists: SCH 23390 and sulpiride were used. Ca_v1 (L) type calcium agonist Bay K 8644 and L-type calcium channel blockers, nifedipine (Sigma, St. Louis, MO, USA), and calciseptine (Alomone Labs, Jerusalem, Israel) were dissolved and applied to the bath saline. Most experiments were paired, so that recordings in the presence and absence of bath-applied drugs were compared in the same neuron with non-parametric statistics (Systat v.7., SPSS Inc., Chicago, IL, USA): When D_1 and D_2 -MSNs parameters were compared Mann–Whitney's U test was employed. Statistical significance was set at $P < 0.05$.

RESULTS

DOPAMINERGIC MODULATION OF CORTICOSTRIATAL RESPONSES IN MSNs FROM DIRECT AND INDIRECT PATHWAYS

Medium spiny neurons were identified as belonging to the direct or indirect pathways by double labeling the biocytin-filled and green fluorescent protein positive (GFP+) recorded cells.

Figure 1A shows a suprathreshold corticostriatal response (red) from a BAC D_1 -receptor expressing neuron. Photomicrograph at right shows the double labeled recorded neuron (superimposed eGFP-green and biocytin-red). **Figure 1B** shows a suprathreshold corticostriatal response (green) from a BAC D_2 -receptor expressing neuron. Photomicrograph at right shows the double labeled neuron. Corticostriatal responses in D_1 -receptor expressing MSN (D_1 -MSN) show action potentials of increasing amplitude and a slowly decaying plateau potentials, whereas D_2 -receptor expressing MSN (D_2 -MSN) shows a larger but briefer depolarization with firing of inactivating action potentials followed by a quasi exponential decay. Inset in **Figure 1A** shows superimposition of both recordings to emphasize their differences (Flores-Barrera et al., 2010): area under D_1 -MSNs response is $10,568 \pm 523 \text{ mV}\cdot\text{ms}$ and area under D_2 -MSNs response, without including the autoregenerative response, is $8,204 \pm 697 \text{ mV}\cdot\text{ms}$, respectively ($n = 36$; $P < 0.001$).

Corticostriatal responses evoked with increasing stimulation strength were tested in D_1 -MSNs with 1 μM SKF 81297, a selective D_1 -class receptor agonist (**Figures 2A–C**, black traces: control; red traces: plus SKF 81297). In all direct pathway neurons recorded, D_1 -receptor activation enhanced the response, augmenting the depolarization, and the number of action potentials fired. Surprisingly, responses exhibited inactivation of action potentials during synaptic depolarization, a phenomenon more commonly seen in D_2 -MSNs but rarely seen in D_1 -MSNs in control conditions (Flores-Barrera et al., 2010). That is, D_1 -receptor activation could render direct pathway neurons as excitable as

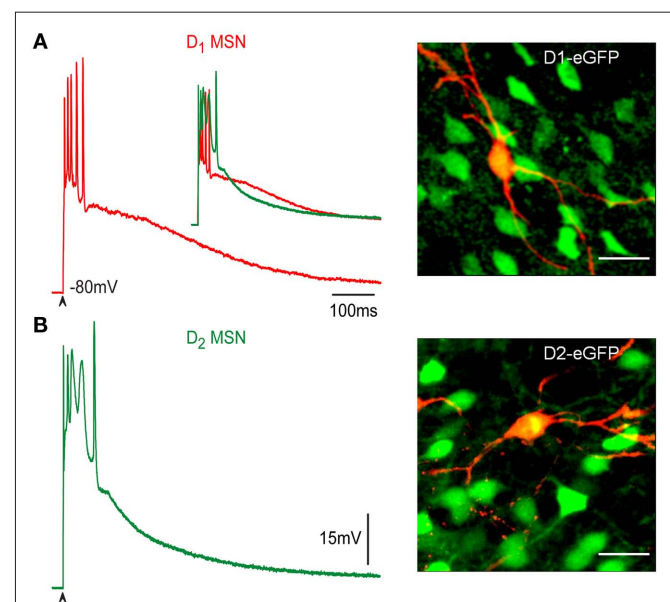


FIGURE 1 | Corticostriatal response in D_1 - and D_2 -MSNs. (A,B)

Suprathreshold corticostriatal responses in direct (red) and indirect (green) pathway MSNs are different (inset in **A**, superimposed records) and can serve to identify the neurons during physiological experiments: intrinsic autoregenerative response underlies spikes in D_2 -MSNs, a more sustained plateau potential is characteristic of D_1 -MSNs. At right, superimposition of biocytin-filled recorded cells in red with green fluorescent protein positive (GFP+) neurons from BAC mice. Recorded cells are double labeled (yellow). Calibration: 20 μm .

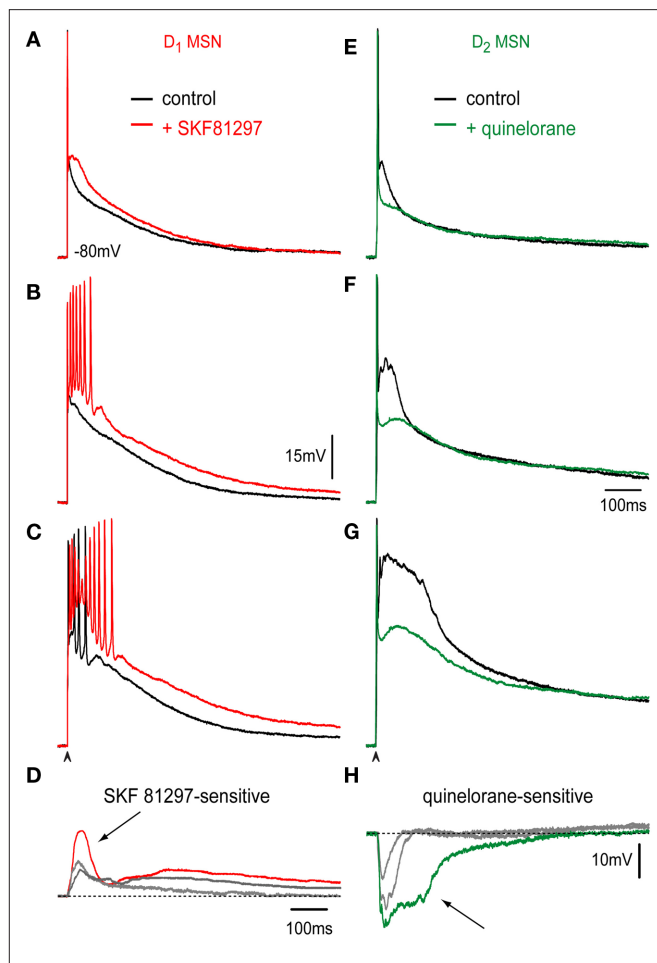


FIGURE 2 | Dopaminergic modulation of corticostriatal responses in D₁- and D₂-MSNs. (A–C) Orthodromic corticostriatal responses to a single stimulus of increasing stimulation intensity in a D₁-MSN. Controls: black and after addition of 1 μ M of the D₁R selective agonist SKF 81297 (red); superimposed in each frame. Note increasing firing and depolarization due to D₁R activation including action potential inactivation (C). (E–G) Orthodromic corticostriatal responses to a single stimulus of increasing stimulation intensity in a D₂-MSN. Controls: black and after addition of 1 μ M of the D₂R selective agonist quinolorane (green); superimposed in each frame. Underlying autoregenerative response is shown instead of the action potential train. Note a decrease in synaptically evoked depolarizations due to D₂R activation in each frame. (D,H) Subtraction of superimposed recordings above: D₁R action facilitated both initial and sustained plateau depolarizations. Note a possible autoregenerative response (arrow, D). D₂R action decreased depolarizations at all stimulus intensities, including autoregenerative responses (arrow, H).

indirect pathway neurons. Action of SKF 81297 was completely blocked by the D₁-receptor antagonist 1 μ M SCH 23390 ($n = 3$; not shown). Percentages of depolarization enhancement induced by D₁-agonist in the maximal corticostriatal response were $29 \pm 8\%$ ($n = 8$; $P < 0.03$). **Figure 2D** shows subtractions from the records above. Note that D₁-receptor activation enhances the corticostriatal response both by prolonging and increasing the plateau potential in a gradual manner and, most importantly, by disclosing an initial underlying autoregenerative response at the initial depolarization during the highest stimulus strength (**Figure 2D**, arrow).

Corticostriatal responses evoked with increasing stimulation strength were tested in D₂-MSNs with 1 μ M quinolorane, a selective D₂-class receptor agonist (**Figures 2E–G**, black traces: control; green traces: plus quinolorane). In all indirect pathway neurons D₂-receptor activation reduced the response, decreasing the depolarization. In these traces, it was preferred to illustrate the autoregenerative response that commonly underlies the train of action potentials in indirect pathway neurons (Flores-Barrera et al., 2010) to show that D₂R action decreases that response. Action of quinolorane was completely blocked by the D₂-receptor antagonist 1 μ M sulpiride ($n = 3$; not shown). Percentages of depolarization reduction induced by D₂-agonist in the maximal corticostriatal response without including the autoregenerative response were $23 \pm 6\%$ ($n = 10$; $P < 0.03$). That is, D₂-receptor activation significantly decreased the synaptic response of indirect pathway neurons. **Figure 2H** shows subtractions from the records above. Note that D₂-receptor activation decreases the corticostriatal response including the autoregenerative response (**Figure 2H**, arrow; Bargas et al., 1991; Flores-Barrera et al., 2010).

Taking all the results together it appears that DA actions can balance the excitability of direct and indirect pathway neurons of the basal ganglia by both enhancing the excitability of direct and repressing the excitability of indirect pathway neurons (Galarraga et al., 1997; Carter and Sabatini, 2004; Liu et al., 2004; Day et al., 2008) as the “two pathways hypothesis” requires. Areas under synaptic responses for each cell type after DA receptors activation and with respect to their own controls are $9,124 \pm 609$ mV·ms vs. $11,810 \pm 1,264$ mV·ms for D₁-MSNs ($n = 8$, $P < 0.03$) and $8,950 \pm 1,006$ mV·ms vs. $7,173 \pm 687$ mV·ms for D₂-MSNs ($n = 10$; $P < 0.03$).

Ca_v1 CALCIUM CURRENT CONTRIBUTION DURING CORTICOSTRIATAL RESPONSES

Both DA receptors and Ca_v1 (L) calcium channels are found in dendrites of MSNs where cortical inputs arrive to generate corticostriatal responses (Freund et al., 1984; Carter and Sabatini, 2004; Kreitzer and Malenka, 2005; Day et al., 2006). Ca_v1 channels are activated during corticostriatal responses in non-identified MSNs (Galarraga et al., 1997; Adermark and Lovinger, 2007; Flores-Barrera et al., 2009). These channels are also a main target for D₁- and D₂-receptors signaling during direct somatic stimulation (Hernández-López et al., 1997, 2000). Finally, Ca_v1 channels have also been shown to participate in the generation of down- to up-state voltage transitions in MSNs (Vergara et al., 2003). Therefore, it is logical to infer that they may be involved in the evoked corticostriatal responses in both direct and indirect MSNs, however, this last point has not been proved.

Figures 3A,B show that the Ca_v1 channel blocker, 400 nM calciseptine, reduces corticostriatal responses in both D₁- and D₂-MSNs. Superimposed records in control (black) and in the presence of calciseptine (blue) confirm that intrinsic calcium currents are activated by corticostriatal transmission in both classes of projection neurons. Blockade of Ca_v1 channels in D₁-MSNs decreased the corticostriatal response by $29 \pm 2\%$ ($n = 7$; $P < 0.05$), while it decreased the response by $29 \pm 2\%$ ($n = 8$; $P < 0.007$) in D₂-MSNs. Similar reductions were observed after 2.5 μ M nica-dipine (see **Figure 4**). Note two rising components in D₁-MSNs:

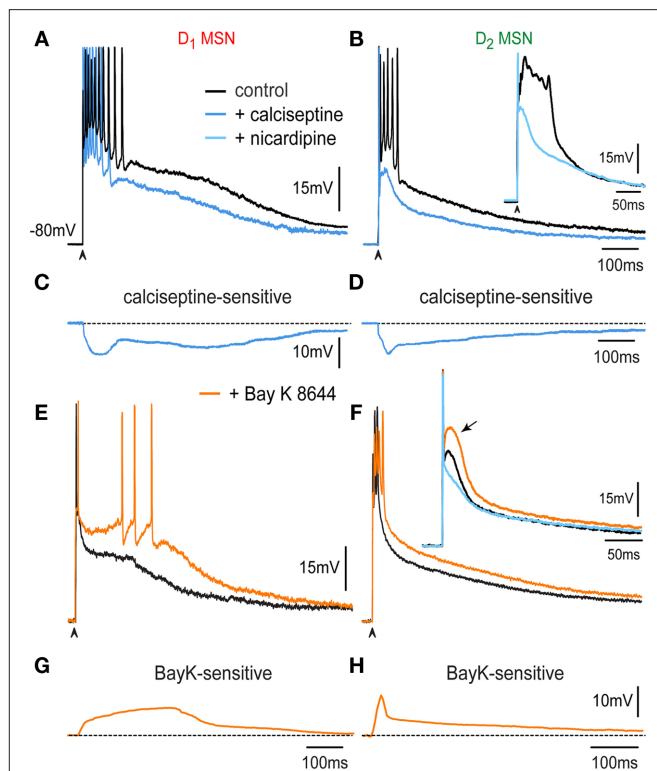


FIGURE 3 | Contribution of Ca_v1 calcium current during the corticostriatal response in D_1 - and D_2 -MSNs. (A) Superimposed records: in control (black) and in the presence of 400 nM calciseptine (blue) in a D_1 -MSN. (B) Superimposed records: in control (black) and in the presence of 400 nM calciseptine (blue) in a D_2 -MSN. Note briefer train of action potentials in D_2 -MSNs as compared to D_1 -MSNs (cf. A,B). Inset: shows the autoregenerative response that underlies the train of action potentials in D_2 -MSNs (cf. Figure 2), before (black trace) and during 2.5 μM nicardipine (light blue). (C,D) Subtractions of superimposed records above disclose the calciseptine-sensitive component in D_1 - and D_2 -MSNs. Note initial and late rising components in D_1 -MSNs, and only the initial followed by continuous decay in D_2 -MSNs. (E) Superimposed records: in control (black) and in the presence of 2.5 μM Bay K 8644 (orange) in a D_1 -MSN. (F) Superimposed records: in control (black) and in the presence of 2.5 μM Bay K 8644 (orange) in a D_2 -MSN. Ca_v1 agonist prolonged the plateau potential and induced the firing of more action potentials in D_1 -MSNs, whereas it depolarized the response of D_2 -MSNs along its decay. Inset in (F) shows that Bay K 8644 helps in eliciting an autoregenerative response in D_2 -MSNs. (G,H) Subtraction of Bay K 8644 actions: Note an increasing and sustained depolarization in D_1 -MSNs, and a decaying depolarization after the initial peak in D_2 -MSNs.

initial and late, and only an initial component plus a prolonged decay in D_2 -MSNs. Subtractions of superimposed records disclose the calciseptine-sensitive component (Figures 3C,D; Flores-Barrera et al., 2010). Areas under responses for each cell type after blockers of Ca_v1 channels with respect to their own controls are $11,646 \pm 750$ mV·ms vs. $8,212 \pm 462$ mV·ms for D_1 -MSNs ($n = 7$; $P < 0.03$) and $7,876 \pm 864$ mV·ms vs. $5,611 \pm 675$ mV·ms for D_2 -MSNs ($n = 8$; $P < 0.007$). Inset in Figure 3B shows in other indirect pathway neuron, a reduction in the orthodromic autoregenerative response after 2.5 μM nicardipine.

We next tested the effects of the Ca_v1 (L) calcium agonist Bay K 8644 (2.5–5 μM) on the corticostriatal response. Superimposed records: in control (black) and in the presence of 2.5 μM Bay K 8644 (orange) in

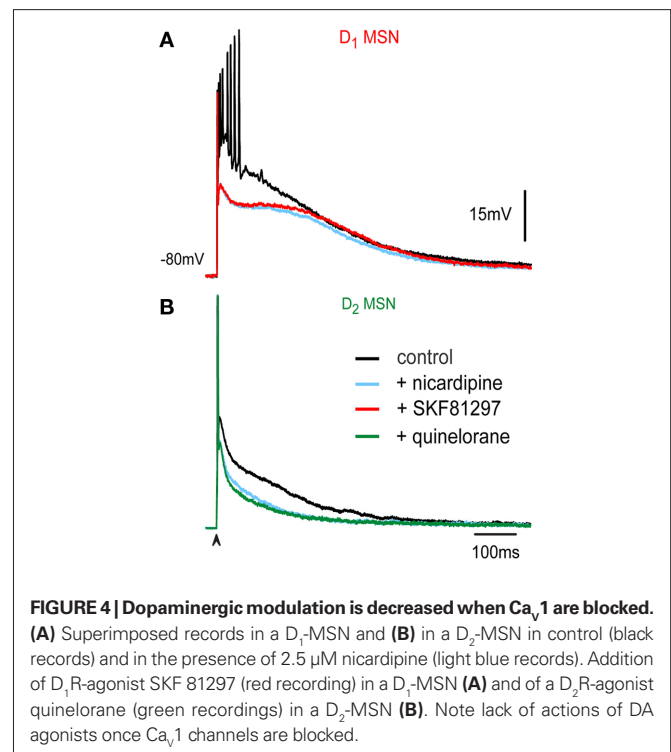


FIGURE 4 | Dopaminergic modulation is decreased when Ca_v1 are blocked. (A) Superimposed records in a D_1 -MSN and (B) in a D_2 -MSN in control (black records) and in the presence of 2.5 μM nicardipine (light blue records). Addition of D_1 -agonist SKF 81297 (red recording) in a D_1 -MSN (A) and of a D_2 -agonist quinolorane (green recordings) in a D_2 -MSN (B). Note lack of actions of DA agonists once Ca_v1 channels are blocked.

a D_1 -MSN (Figure 3E) and in a D_2 -MSN (Figure 3F) show that the Ca_v1 agonist prolongs the plateau potential and induces the firing of more action potentials in D_1 -MSNs, whereas it depolarized the response of D_2 -MSNs along its entire decay. Bay K 8644 helps in eliciting an autoregenerative response in D_2 -MSNs (inset in Figure 3F). Bay K 8644 actions show increasing and sustained depolarizations in D_1 -MSNs (Figure 3G), and a decaying depolarization after the initial peak in D_2 -MSNs (Figure 3H). Inset in Figure 3F shows in another indirect pathway neuron, after 2.5 μM nicardipine in the presence of Bay K 8644 a reduction in orthodromic autoregenerative response.

Because the actions of calcium blockers was so similar in both neuronal classes, the different roles that Ca_v1 channels accomplish in each response, as disclosed by Bay K 8644, suggests that other synaptic or intrinsic currents are in charge of Ca_v1 channels regulation, perhaps at dendritic sites.

Areas under synaptic responses for each cell type after Ca_v1 agonist Bay K 8644 with respect to their own controls are $11,821 \pm 1,324$ mV·ms vs. $15,306 \pm 1,600$ mV·ms for D_1 -MSNs ($n = 4$; $P < 0.05$) and $7,919 \pm 2,178$ mV·ms vs. $11,308 \pm 2,600$ mV·ms for D_2 -MSNs ($n = 4$; $P < 0.05$).

DOPAMINERGIC MODULATION IS OCCLUDED WHEN Ca_v1 CHANNELS ARE BLOCKED

Figure 4A shows superimposed corticostriatal responses in a representative D_1 -MSN in control (black), in the presence of 2.5 μM nicardipine (light blue) and after application of the D_1 -class receptor agonist 1 μM SKF 81297 (red). Note absence of action of D_1 -agonist after blockade of Ca_v1 channels. Figure 4B shows superimposed corticostriatal responses in a representative D_2 -MSN in control (black), in the presence of 2.5 μM nicardipine (light blue) and after application of the D_2 -class receptor agonist 1 μM quinolorane

(green). Note absence of action of D_2 -agonist after blockade of Ca_v1 channels. These experiments suggest that Ca_v1 channels are a major target of DA modulation during corticostriatal integration.

DISCUSSION

Corticostriatal responses of D_1 - and D_2 -MSNs constitute an “electrophysiological footprint” that readily distinguishes between direct and indirect pathway neurons (Flores-Barrera et al., 2010) because dendritic excitability, and therefore, corticostriatal integration is different in D_1 - and D_2 -MSNs when all synaptic and intrinsic currents are in place (Day et al., 2008; Flores-Barrera et al., 2010). The present work demonstrated: (1) A selective dopaminergic D_1 -class receptor mediated increase in firing and depolarization of the corticostriatal response in D_1 -MSNs in such a way as to approach the level of excitability found in D_2 -MSNs. (2) A selective dopaminergic D_2 -class receptor mediated a significant decrease in firing and depolarization of the corticostriatal response in D_2 -MSNs. (3) Ca_v1 (L) calcium currents contribute to corticostriatal integration in both D_1 - and D_2 -MSNs; including the autoregenerative response underlying the train of spikes characteristic of D_2 -MSNs. (4) Blockade of Ca_v1 channels occluded the actions of selective DA receptor agonists in their respective responsive neurons from the direct and indirect pathways. (5) By acting in both pathways simultaneously DA may balance the excitability of the neurons from both basal ganglia pathways to make D_2 -MSNs less excitable than D_1 -MSNs, if necessary, thus reversing their responsiveness to cortical commands. These findings show that there is enough margin to tune up the excitability of the neurons from both pathways, upon demand. This tuning capability is very probably lost during Parkinsonism (Flores-Barrera et al., 2010).

The present work did not exclude, however, the possible participation of other calcium channels (Carter and Sabatini, 2004; Salgado et al., 2005; Higley and Sabatini, 2010) in corticostriatal integration and only underlines the importance of Ca_v1 channels.

Ca_v1 channels are positioned near cortical glutamatergic synapses in MSNs dendrites (Freund et al., 1984; Carter and Sabatini, 2004; Higley and Sabatini, 2010), a strategic location to participate in corticostriatal integration. However, in spite of voltage- and current-clamp recordings during direct stimulation experiments in single cells agree with the assumptions of the “two pathways hypothesis,” that are, first, D_1 -class receptor activation facilitates firing in D_1 -MSNs during direct somatic stimulation of single cells (Hernández-López et al., 1997) and enhances Ca_v1 calcium current in isolated neurons (Surmeier et al., 1995), and secondly, D_2 -class receptor activation represses firing in MSNs of the indirect pathway by decreasing the same current (Hernández-López et al., 1997, 2000; Day et al., 2008), the fact is that in trying to find these differences during striatal network activity, *in vivo*, the expectations of the two pathways hypothesis become very variable and even contradictory (Liang et al., 2008; Kravitz et al., 2010).

It is argued that an undisputed electrophysiological evidence of the two pathways hypothesis is lacking during more physiological conditions because indirect circuit influences distort or increase the variability of the responses (e.g., Kravitz et al., 2010). Therefore, in this work we wanted to observe whether dopaminergic actions expected by the “two pathways hypothesis” is robust enough to be preserved during corticostriatal suprathreshold dendritic integration which is known to activate polysynaptic pathways as well

as several intrinsic inward and outward currents (Flores-Barrera et al., 2009, 2010). This implies to test DA actions during more physiological responses.

The present experimental work demonstrates the main postulate of the “two pathways hypothesis,” that is, that the excitability of neurons from both basal ganglia pathways can reach a dynamic balance due to both D_1 - and D_2 -class receptors activation which enhance and decrease, respectively, the corticostriatal responses of direct and indirect pathway neurons. DA actions have a wide range of operation since D_1 -MSNs can become more excitable than D_2 -MSNs if necessary. Therefore, the present data support DA role as that of balancing both basal ganglia pathways. Targeting of Ca_v1 channels was somehow expected since the gating of voltage-dependent and ligand-gated (ionotropic) ion channels in the dendritic membrane, as well as long-term synaptic plasticity, depend on calcium entry through these channels (Snyder et al., 2000; Hallett et al., 2006; Adermark and Lovinger, 2007).

Variable results and randomness in firing found *in vivo* more physiological situations (Kostal et al., 2007) are attributed to a population or vectorial neural coding (Wu et al., 2002), evidence of which, has been obtained for the striatal microcircuit (Carrillo-Reid et al., 2008, 2009). Thus, although the present work supports potent and robust DA postsynaptic actions in a more physiological situation, several groups have also reported potent presynaptic actions on terminals making contact with each class of projection neuron (Flores-Hernández et al., 1997; Guzmán et al., 2003; Bamford et al., 2004; Tecuapetla et al., 2007) and following determined connections rules (Taverna et al., 2008), suggesting the possibility of a concomitant dynamic regulation of synaptic weights as well as dopaminergic regulation of striatal interneurons (Tepper et al., 2004).

CONCLUSION

Dopamine plays a fundamental role in normal basal ganglia function, the deficits arising from reductions in the sustained stimulation of DA receptors show a rather wide involvement in behavioral processes (Schultz, 2007). After DA depletion, a reduction in the corticostriatal response was reported in substance P expressing MSNs whereas an enhancement in the response was observed in enkephalin expressing MSNs, partially explained by a decrease of synaptic GABAergic connections among MSNs (Flores-Barrera et al., 2010). In contrast, the present study shows that the dopaminergic D_1 R activation increased the corticostriatal response in D_1 -MSN up to the point of action potential inactivation as that observed in D_2 -MSNs whereas D_2 R activation depressed the corticostriatal response in D_2 -MSNs and decreases duration and amplitude of calcium autoregenerative responses recorded in these neurons. Therefore, dopaminergic DA receptors actions tend to equalize the excitability of MSNs from both pathways.

Because modulation of Ca_v1 channels is lost in the absence of DA, the changes observed in the corticostriatal response after DA depletion: a decrease in the depolarizing plateau of SP+ expressing MSNs, and a greater intrinsic excitability of ENK+ expressing MSNs can be readily explained. The end result is that both classes of MSNs lose their ability to balance their activity during Parkinsonism (Flores-Barrera et al., 2010), being, perhaps, a main cause of movement impairment.

It is concluded that strong cortical stimulation can overcome all these indirect network effects so that the present results support the DA role expected by the “two pathways hypothesis.”

ACKNOWLEDGMENTS

We thank Antonio Laville and Gabriela X Ayala for technical support and advice. This work was supported by grants from a Project Program grant IMPULSA 03 from UNAM, by Consejo Nacional

de Ciencia y Tecnología (Mexico) Grant 98004, and by grants from Dirección General de Asuntos del Personal Académico, Universidad Nacional Autónoma de México: IN205610 and IN206010 to José Bargas and Elvira Galarraga.

REFERENCES

- Adermark, L., and Lovinger, D. M. (2007). Combined activation of L-type Ca^{2+} channels and synaptic transmission is sufficient to induce striatal long-term depression. *J. Neurosci.* 27, 6781–6787.
- Albin, R. L., Young, A. B., and Penney, J. B. (1989). The functional anatomy of basal ganglia disorders. *Trends Neurosci.* 12, 366–375.
- Bamford, N. S., Zhang, H., Schmitz, Y., Wu, N. P., Cepeda, C., Levine, M. S., Schmauss, C., Zakharenko, S. S., Zablow, L., and Sulzer, D. (2004). Heterosynaptic dopamine neurotransmission selects sets of corticostriatal terminals. *Neuron* 42, 653–663.
- Bargas, J., Galarraga, E., and Aceves, J. (1991). Dendritic activity on neostriatal neurons as inferred from somatic intracellular recordings. *Brain Res.* 539, 159–163.
- Bateup, H. S., Santini, E., Shen, W., Birnbaum, S., Valjent, E., Surmeier, D. J., Fisone, G., Nestler, E. J., and Greengard, P. (2010). Distinct subclasses of medium spiny neurons differentially regulate striatal motor behaviors. *Proc. Natl. Acad. Sci. U.S.A.* 107, 14845–14850.
- Carrillo-Reid, L., Tecuapetla, F., Tapia, D., Hernandez-Cruz, A., Galarraga, E., Drucker-Colin, R., and Bargas, J. (2008). Encoding network states by striatal cell assemblies. *J. Neurophysiol.* 99, 1435–1450.
- Carrillo-Reid, L., Tecuapetla, F., Vautrelle, N., Hernandez, A., Vergara, R., Galarraga, E., and Bargas, J. (2009). Muscarinic enhancement of persistent sodium current synchronizes striatal medium spiny neurons. *J. Neurophysiol.* 102, 682–690.
- Carter, A. G., and Sabatini, B. L. (2004). State-dependent calcium signaling in dendritic spines of striatal medium spiny neurons. *Neuron* 44, 483–493.
- Day, M., Wang, Z., Ding, J., An, X., Ingham, C. A., Shering, A. F., Wokosin, D., Ilijic, E., Sun, Z., Sampson, A. R., Mugnaini, E., Deutch, A. Y., Sesack, S. R., Arbuthnott, G. W., and Surmeier, D. J. (2006). Selective elimination of glutamatergic synapses on striatopallidal neurons in Parkinson disease models. *Nat. Neurosci.* 9, 251–259.
- Day, M., Wokosin, D., Plotkin, J. L., Tian, X., and Surmeier, D. J. (2008). Differential excitability and modulation of striatal medium spiny neuron dendrites. *J. Neurosci.* 28, 11603–11614.
- Flores-Barrera, E., Laville, A., Plata, V., Tapia, D., Bargas, J., and Galarraga, E. (2009). Inhibitory contribution to suprathreshold corticostriatal responses: an experimental and modeling study. *Cell. Mol. Neurobiol.* 29, 719–731.
- Flores-Barrera, E., Vizcarra-Chacón, B. J., Tapia, D., Bargas, J., and Galarraga, E. (2010). Different corticostriatal integration in spiny projection neurons from direct and indirect pathways. *Front. Syst. Neurosci.* 4:15. doi: 10.3389/fnsys.2010.00015
- Flores-Hernández, J., Galarraga, E., and Bargas, J. (1997). Dopamine selects glutamatergic excitatory inputs to the neostriatum. *Synapse* 25, 185–195.
- Freund, T. F., Powell, J. F., and Smith, A. D. (1984). Tyrosine hydroxylase-immunoreactive boutons in synaptic contact with identified striatonigral neurons, with particular reference to dendritic spines. *Neuroscience* 13, 1189–1215.
- Galarraga, E., Hernández-López, S., Reyes, A., Barral, J., and Bargas, J. (1997). Dopamine facilitates EPSPs through an L-type Ca^{2+} -conductance. *Neuroreport* 8, 2183–2186.
- Gerfen, C. R. (2000). Molecular effects of dopamine on striatal-projection pathways. *Trends Neurosci.* 23, S64–S70.
- Guzmán, J. N., Hernandez, A., Galarraga, E., Tapia, D., Laville, A., Vergara, R., Aceves, J., and Bargas, J. (2003). Dopaminergic modulation of axon collaterals interconnecting spiny neurons of the rat striatum. *J. Neurosci.* 23, 8931–8940.
- Hallett, P. J., Spoelgen, R., Hyman, B. T., Standaert, D. G., and Dunah, A. W. (2006). Dopamine D1 activation potentiates striatal NMDA receptors by tyrosine phosphorylation-dependent subunit trafficking. *J. Neurosci.* 26, 4690–4700.
- Hernández-López, S., Bargas, J., Surmeier, D. J., Reyes, A., and Galarraga, E. (1997). D1 receptor activation enhances evoked discharge in neostriatal medium spiny neurons by modulating an L-type Ca^{2+} -conductance. *J. Neurosci.* 17, 3334–3342.
- Hernández-López, S., Tkatch, T., Pérez-García, E., Galarraga, E., Bargas, J., Hamm, H., and Surmeier, D. J. (2000). D2 dopamine receptors in striatal medium spiny neurons reduce L-type Ca^{2+} currents and excitability through a novel PLCB1/IP3/calcineurin signaling cascade. *J. Neurosci.* 20, 8987–8995.
- Higley, M. J., and Sabatini, B. L. (2010). Competitive regulation of synaptic Ca^{2+} influx by D2 dopamine and A2A adenosine receptors. *Nat. Neurosci.* 13, 958–967.
- Kostal, L., Lansky, P., and Rospars, J. P. (2007). Neuronal coding and spiking randomness. *Eur. J. Neurosci.* 26, 2693–2701.
- Kravitz, A. V., Freeze, B. S., Parker, P. R., Kay, K., Thwin, M. T., Deisseroth, K., and Kreitzer, A. C. (2010). Regulation of parkinsonian motor behaviours by optogenetic control of basal ganglia circuitry. *Nature* 466, 622–626.
- Kreitzer, A. C., and Malenka, R. C. (2005). Dopamine modulation of state dependent endocannabinoid release and long-term depression in the striatum. *J. Neurosci.* 25, 10537–10545.
- Liang, L., DeLong, M. R., and Papa, S. M. (2008). Inversion of dopamine responses in striatal medium spiny neurons and involuntary movements. *J. Neurosci.* 28, 7537–7547.
- Liu, J. C., DeFazio, R. A., Espinosa-Jeffrey, A., Cepeda, C., de Vellis, J., and Levine, M. S. (2004). Calcium modulates dopamine potentiation of N-methyl-D-aspartate responses: electrophysiological and imaging evidence. *J. Neurosci. Res.* 76, 315–322.
- Mink, J. W. (2003). The basal ganglia and involuntary movements: impaired inhibition of competing motor patterns. *Arch. Neurol.* 60, 1365–1368.
- Redgrave, P., Rodriguez, M., Smith, Y., Rodriguez-Oroz, M. C., Lehericy, S., Bergman, H., Agid, Y., DeLong, M. R., and Obeso, J. A. (2010). Goal-directed and habitual control in the basal ganglia: implications for Parkinson's disease. *Nat. Rev. Neurosci.* 11, 760–772.
- Salgado, H., Tecuapetla, F., Perez-Rosello, T., Perez-Burgos, A., Perez-Garci, E., Galarraga, E., and Bargas, J. (2005). A reconfiguration of $\text{CaV}2 \text{ Ca}^{2+}$ channels current and its dopaminergic D2 modulation in developing neostriatal neurons. *J. Neurophysiol.* 94, 3771–3787.
- Schultz, W. (2007). Multiple dopamine functions at different time courses. *Annu. Rev. Neurosci.* 30, 259–288.
- Snyder, G. L., Allen, P. B., Fienberg, A. A., Valle, C. G., Hagan, R. L., Nairn, A. C., and Greengard, P. (2000). Regulation of phosphorylation of the GluR1 AMPA receptor in the neostriatum by dopamine and psychostimulants in vivo. *J. Neurosci.* 20, 4480–4488.
- Surmeier, D. J., Bargas, J., Hemmings, H. C. Jr., Nairn, A. C., and Greengard, P. (1995). Modulation of calcium currents by a D1 dopaminergic protein kinase/phosphatase cascade in rat neostriatal neurons. *Neuron* 14, 385–397.
- Surmeier, D. J., Ding, J., Day, M., Wang, Z., and Shen, W. (2007). D1 and D2 dopamine-receptor modulation of striatal glutamatergic signaling in striatal medium spiny neurons. *Trends Neurosci.* 30, 228–235.
- Taverna, S., Ilijic, E., and Surmeier, D. J. (2008). Recurrent collateral connections of striatal medium spiny neurons are disrupted in models of Parkinson's disease. *J. Neurosci.* 28, 5504–5512.
- Tecuapetla, F., Carrillo-Reid, L., Bargas, J., and Galarraga, E. (2007). Dopaminergic modulation of short term synaptic plasticity at striatal inhibitory synapses. *Proc. Natl. Acad. Sci. U.S.A.* 104, 10258–10263.
- Tepper, J. M., Koós, T., and Wilson, C. J. (2004). GABAergic microcircuits in the neostriatum. *Trends Neurosci.* 27, 662–669.
- Vergara, R., Rick, C., Hernández-López, S., Laville, J. A., Guzmán, J. N., Galarraga, E., Surmeier, D. J., and Bargas, J. (2003). Membrane potential oscillations of striatal medium spiny neurons in a corticostriatal slice. *J. Physiol.* 553, 169–182.
- Wu, S., Amari, S., and Nakahara, H. (2002). Population coding and decoding in a neural field: a computational study. *Neural Comput.* 14, 999–1026.

Conflict of Interest Statement: The authors declare that the research was conducted in the absence of any commercial or financial relationships that could be construed as a potential conflict of interest.

Received: 17 December 2010; paper pending published: 06 March 2011; accepted: 15 March 2011; published online: 29 March 2011.

Citation: Flores-Barrera E, Vizcarra-Chacón BJ, Bargas J, Tapia D and Galarraga E (2011) Dopaminergic modulation of corticostriatal responses in medium spiny projection neurons from direct and indirect pathways. *Front. Syst. Neurosci.* 5:15. doi: 10.3389/fnsys.2011.00015
Copyright © 2011 Flores-Barrera, Vizcarra-Chacón, Bargas, Tapia and Galarraga. This is an open-access article subject to an exclusive license agreement between the authors and Frontiers Media SA, which permits unrestricted use, distribution, and reproduction in any medium, provided the original authors and source are credited.



The impact of stimulation induced short-term synaptic plasticity on firing patterns in the globus pallidus of the rat

Jenia Bugaysen^{1,2}, Izhar Bar-Gad^{1,2} and Alon Korngreen^{1,2*}

¹ The Leslie and Susan Gonda Multidisciplinary Brain Research Center, Bar-Ilan University, Ramat Gan, Israel

² The Mina and Everard Goodman Faculty of Life Sciences, Bar-Ilan University, Ramat Gan, Israel

Edited by:

James M. Tepper, Rutgers, The State University of New Jersey, USA

Reviewed by:

Atsushi Nambu, National Institute for Physiological Sciences, Japan

Hitoshi Kita, The University of Tennessee Health Science Center, USA

*Correspondence:

Alon Korngreen, Mina and Everard Goodman Faculty of Life Sciences, Leslie and Susan Gonda Multidisciplinary Brain Research Center, Bar-Ilan University, Ramat Gan 52900, Israel.
e-mail: korngra@mail.biu.ac.il

Electrical stimulation in the globus pallidus (GP) leads to complex modulations of neuronal activity in the stimulated nucleus. Multiple *in vivo* studies have demonstrated the modulation of both firing rates and patterns during and immediately following the GP stimulation. Previous *in vitro* studies, together with computational studies, have suggested the involvement of short-term synaptic plasticity (STP) during the stimulation. The aim of the current study was to explore *in vitro* the effects of STP on neuronal activity of GP neurons during local repetitive stimulation. We recorded synaptic potentials and assessed the modulations of spontaneous firing in a postsynaptic neuron in acute brain slices via a whole-cell pipette. Low-frequency repetitive stimulation locked the firing of the neuron to the stimulus. However, high-frequency repetitive stimulation in the GP generated a biphasic modulation of the firing frequency consisting of inhibitory and excitatory phases. Using blockers of synaptic transmission, we show that GABAergic synapses mediated the inhibitory and glutamatergic synapses the excitatory part of the response. Furthermore, we report that at high stimulation frequencies both types of synapses undergo short-term depression leading to a time dependent modulation of the neuronal firing. These findings indicate that STP modulates the dynamic responses of pallidal activity during electrical stimulation, and may contribute to a better understanding of the mechanism underlying deep brain stimulation like protocols.

Keywords: globus pallidus, rat, extracellular potential, action potential, patch-clamp, short-term plasticity, synaptic plasticity, extracellular stimulation

INTRODUCTION

High-frequency deep brain stimulation (HF-DBS) in the globus pallidus internus (GPi) and subthalamic nucleus (STN) is a widely employed method for treating Parkinson's disease (PD; Benabid, 2003) and other disorders associated with the basal ganglia (BG). However, despite its proven therapeutic success, the physiological effects of DBS in the BG are still unclear. Some electrophysiological recordings performed on humans intra-operatively (Dostrovsky et al., 2000; Wu et al., 2001; Filali et al., 2004) have reinforced the view of full inhibition of neuronal firing in the stimulated nucleus. However, other experimental (Hashimoto et al., 2003; Bar-Gad et al., 2004; Meissner et al., 2005; Montgomery and Gale, 2008; McCairn and Turner, 2009) and theoretical (McIntyre et al., 2004; Johnson and McIntyre, 2008) studies have reported that stimulation leads to complex activation of the stimulated nucleus or its targets. Furthermore, HF-DBS has been shown to affect other firing pattern properties including oscillatory and bursty activity (Meissner et al., 2005; Montgomery, 2006; Hahn et al., 2008; Xu et al., 2008; McCairn and Turner, 2009). Thus, the accumulating evidence highlights the importance of both firing rate and pattern changes during stimulation.

While studies of therapeutic stimulation have focused on the static effects of DBS, other dynamic aspects have been studied in response to stimulation *in vitro*. Specifically, the firing dynamics of the BG has been shown to be highly responsive to short-term

synaptic plasticity (STP; Hammond et al., 2008; Gubellini et al., 2009). For example, the globus pallidus [GP – the rodent homolog of the primate globus pallidus externus (GPe)] function is controlled by GABAergic input from the striatum (Francois et al., 1984; Percheron et al., 1984; Yelnik et al., 1984; Kita and Kitai, 1994), collaterals of neighboring GP neurons (Parent et al., 2000), and additional glutamatergic inputs from the STN (Smith and Parent, 1988). Several studies have shown that STP can affect firing dynamics in GP neurons *in vitro* (Rav-Acha et al., 2005; Sims et al., 2008). It has been suggested that GABA may induce GP synchronization by affecting the timing of GP spiking, and that the GP GABAergic synapse displays short-term depression (Rav-Acha et al., 2005; Sims et al., 2008). Moreover, excitatory inputs reaching the GP from the STN are also shaped by STP (Hanson and Jaeger, 2002). In addition to these short-term dynamics, both excitatory and inhibitory synapses in the GP have been reported to express metabotropic receptors that further modulate the plasticity of the circuit and its response to prolonged stimulation (Kaneda and Kita, 2005; Kaneda et al., 2005, 2007; Hashimoto and Kita, 2008). Other examples demonstrating the effect of STP on neuronal firing have been observed in the STN, and the entopeduncular nucleus (EP – the rodent homolog of the GPi; Hammond et al., 2008; Gubellini et al., 2009). However, while STP has thus been found to affect the firing of BG neurons, the role of these STP rules during prolonged, DBS-like stimulation has yet to be investigated.

Recent computational and experimental studies have suggested the existence of STP during HF-DBS (McIntyre et al., 2004b; McCairn and Turner, 2009). These findings led us to hypothesize that STP is involved in altering the information transmission which underlies the effects of HF-DBS on PD. We have recently shown that high-frequency microstimulation in either segment of the GP in the Parkinsonian primate results in short-term modulations (Erez et al., 2009). In particular, we suggested that the efficacy of the synapses is reduced over a time course of a few seconds and is restored within a short time frame after the cessation of the stimulation. This efficacy determines both the changes in the response timing (firing rate) and response pattern (timing). Defining the nature of these dynamic processes and the characterization of their cellular and network properties can shed light on the use of DBS in PD and other BG-related disorders. Here we used the whole-cell configuration of the patch-clamp technique to follow the synaptic and firing dynamics of GP neurons in response to repetitive stimulation.

MATERIALS AND METHODS

IN VITRO SLICE PREPARATION AND SOLUTIONS

Thick sagittal slices of 300 μm were obtained from rat somatosensory cortex, striatum, and GP using previously described techniques (Stuart et al., 1993; Bugaysen et al., 2010). Wistar rats, 16–22 days old, were killed by rapid decapitation according to the guidelines of the Bar-Ilan University animal welfare committee. This procedure was approved by the national committee for experiments on laboratory animals at the Israeli Ministry of Health (permit number BIU281206). The brain was quickly removed and placed in ice-cold artificial cerebrospinal fluid (ACSF) containing (in mM): 125 NaCl, 4 KCl, 25 NaHCO_3 , 1.25 Na_2HPO_4 , 2 CaCl_2 , 2 MgCl_2 , 25 glucose, and 0.5 Na-ascorbate (pH 7.4 with 95% O_2 /5% CO_2). Slices were cut using an HR2 Slicer (Sigman Electronic, Germany) and transferred to a submersion-type chamber, where they were maintained for the remainder of the day. In several experiments the following drugs were added to ACSF: bicuculline (BCC) methiodide to block GABA_A receptors (final concentration 50 μM), APV (50 μM), and CNQX (15 μM) to block NMDA and AMPA receptors, respectively.

The experiments reported here were carried out at 34°C. The GP nucleus and individual GP neurons were visualized using infrared differential interference contrast (IR-DIC) microscopy. The recording chamber was constantly perfused with oxygenated ACSF. The standard pipette solution contained (in mM): 140 K-gluconate, 10 NaCl, 10 HEPES, 4 MgATP, 0.05 SPERMIN, 5 L-Glutathione, 0.2 EGTA, and 0.4 GTP (Sigma, pH 7.2 with KOH). The reference electrode was an Ag–AgCl pellet placed in the bath. The 10-mV liquid junction potential measured under the ionic conditions reported here was not corrected for.

IN VITRO ELECTROPHYSIOLOGY

Cell-attached and whole-cell recordings were obtained from the soma of GP neurons with an Axopatch-200B amplifier (Axon Instruments). Voltage was filtered at 10 kHz and sampled at 20 kHz, unless stated otherwise, using patch pipettes (4–8 M Ω) pulled from thick-walled borosilicate glass capillaries (2.0 mm outer diameter, 0.5 mm wall thickness, Hilgenberg, Malsfeld, Germany). Electrical stimulation was performed using monopolar 0.2–0.7 M Ω glass-coated tungsten microelectrodes. The stimulation pulses consisted

of 50 μA biphasic currents (200 μs cathodal followed by 200 μs anodal phase). The anode was an Ag–AgCl pellet placed in the bath. The stimulating electrode was positioned at the dorsal side of the GP. The recording electrodes were positioned 0.5 mm toward the center of the GP away from the stimulating electrode. The interval between consecutive pulses was 100, 50, and 25 ms, over 30 s leading to stimulation frequencies of 10 Hz (300 stimuli), 20 Hz (600 stimuli), and 40 Hz (1200 stimuli), respectively.

DATA ANALYSIS

All off-line analyses were carried out using Offline Sorter 2.8.6 (Plexon), NeuroExplorer 4.007 (Nex Technologies), Matlab R2007b (Mathworks), and IgorPro 6.0 (WaveMetrics) on a personal computer. The pre-stimulus average extracellular and intracellular firing rate was calculated from spikes extracted from 30 s of continuous recording. Throughout the manuscript the firing rate is the time dependent average firing rate aligned to the stimulation onset. The maximal inhibition of firing rate was calculated as the difference between the minimal firing rate during the stimulus and the pre-stimulus average firing rate. The latency to maximal inhibition was calculated as the time from the onset of the stimulus to the minimal firing rate. Experimental results were consistently obtained from cells from at least seven rats. All the results for a particular experiment were pooled and displayed as mean \pm SD, unless otherwise stated. Significant changes in measured parameters before and after application of the drugs during stimulation were tested using a *t*-test (* < 0.05 and ** < 0.01).

RESULTS

We applied the whole-cell configuration of the patch-clamp technique to evaluate the impact of short-term STP on the firing pattern of GP neurons during repetitive stimulation. A possible drawback of the whole-cell configuration is the washout of important cellular components by the pipette solution. We have previously shown that the whole-cell configuration did not alter significantly the spontaneous firing rate of GP neurons (Bugaysen et al., 2010). To evaluate the impact of this configuration during repetitive stimulation we first performed a control experiment in the cell-attached mode of the patch-clamp technique. Following the onset of a 40-Hz stimulation sequence, the cells responded with a period in which no APs were observed (**Figure 1A**, top). This inhibitory effect lasted 3 s after which APs were once again observed. A similar response to stimulation was observed when the recordings were performed on the whole-cell configuration (**Figure 1A**, bottom). We quantified the pre-stimulus firing rate, the maximal inhibition of the average firing rate during stimulation, and the latency to maximal inhibition (**Figure 1B**). All these parameters did not differ significantly between cell-attached recordings and whole-cell recordings ($p > 0.05$, $n = 12$).

It has been previously reported that GABAergic synapses in the GP display short-term depression (Rav-Acha et al., 2005). That study showed that a short 10 Hz stimulation burst generates a 50% depression of the GABAergic synapse while stimulation bursts above 20 Hz cause almost complete depression of the synapse. We have previously reported that in acute brain slices the average spontaneous firing rate was 13 Hz (Bugaysen et al., 2010). These findings prompted us to select two stimulation frequencies

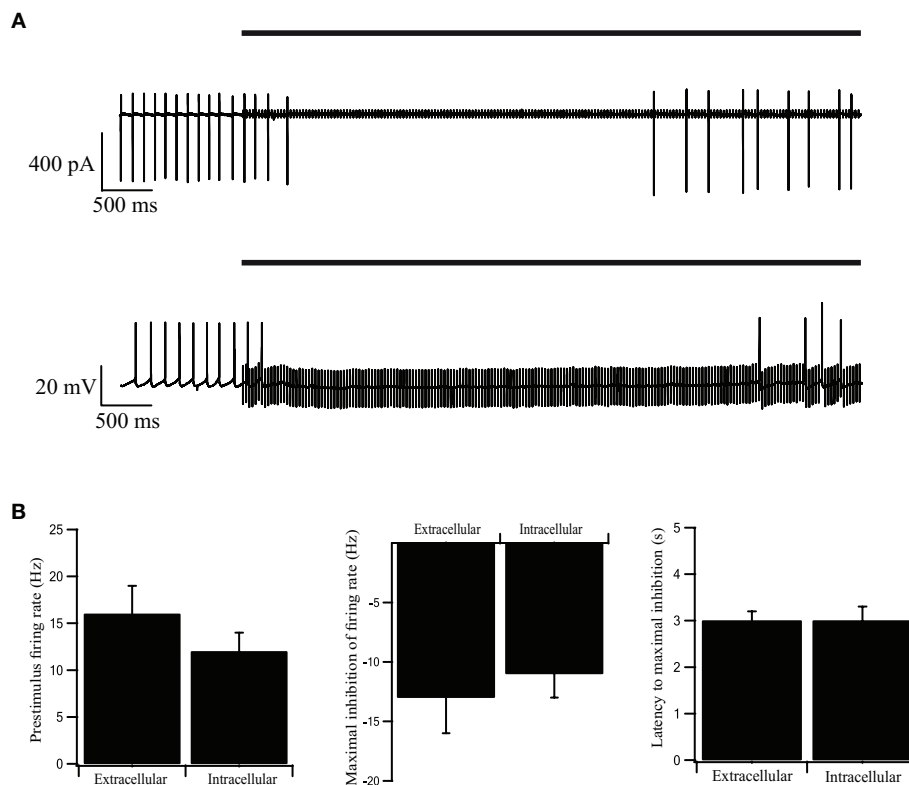


FIGURE 1 | Intracellular and extracellular recordings from stimulated GP neurons in acute rat brain slices. (A) Continuous recording of the extracellular potential (top trace) recorded in the cell-attached mode of the patch-clamp technique and the membrane potential (bottom trace) recorded in the whole-cell mode, during an extracellular stimulation in the GP. The stimulation artifact of the cell-attached recording was scaled down by a factor

of 20 to enable a clearer view of the extracellular spikes. The bold horizontal lines indicate the period of repetitive stimulation. **(B)** Extracellular and intracellular average pre-stimulus firing rate, inhibition of firing rate, and latency to maximal inhibition, recorded in the cell-attached, and whole-cell modes across the population of neurons in GP ($n = 12$). Error bars are expressed as mean \pm SEM.

for the current study. To investigate the effect of low-frequency stimulation we used a repetitive stimulation at 10 Hz. To investigate the effect of high-frequency stimulation we applied a repetitive stimulation of 40 Hz.

Visual inspection of the recordings during a 10-Hz stimulation protocol did not reveal any change in the spontaneous firing frequency, although apparent IPSPs could be clearly discerned following each stimulus (**Figure 2A**, top). To verify that the stimulation pulses excited GABAergic synapses we bath applied the GABA_A blocker BCC. Following application of BCC the spontaneous firing frequency appeared to increase (**Figure 2A**, bottom). To quantify the effect of BCC we calculated the stimulus-triggered average (STA) of the membrane potential (**Figure 2B**). A clear IPSP could be observed following the stimulus (**Figure 2B**, top trace). This average IPSP was abolished following the application of BCC (**Figure 2B**, bottom trace). In some of the cases, a small depolarization could be discerned in the STA following BCC application. This suggested that the stimulus additionally activated excitatory fibers. To test this suggestion we repeated the 10-Hz stimulation experiment while blocking glutamatergic synaptic transmission. Following the bath application of APV and CNQX the firing frequency appeared to decrease (**Figure 2C**). In the example (**Figure 2D**), the STA under control conditions displayed a shallow IPSP that increased following

the application of APV and CNQX. Thus, microstimulation of the GP in acute brain slices from the rat excited both GABAergic and glutamatergic synapses.

To quantify the effects that were observed visually we calculated the population average firing rate ($n = 41$ cells) and normalized it to the pre-stimulus population average firing rate. During a 30-s stimulation at 10 Hz the firing rate decreased slightly (**Figure 3A**). Following the application of BCC the pre-stimulus population average firing rate increased almost 3-fold (**Figure 3B**). During the 10-Hz stimuli train the population average firing rate increased slightly (**Figure 3B**). In a different experiment, bath application of APV and CNQX reduced the pre-stimulus population average firing rate (**Figure 3C**). No effect on the population average firing rate was observed during the 10-Hz stimuli train (**Figure 3C**). Next we calculated the population average post-stimulus time histograms (PSTHs) for the experiments in which a 10-Hz stimuli train was applied (**Figure 4**). Under control conditions, the firing rate increased slightly and then decreased substantially immediately following the stimulus (**Figure 4A**). This post-stimulus inhibition was eliminated by the application of BCC leaving only the immediate excitation (**Figure 4B**). Inversely, application of APV and CNQX left the inhibition almost intact while abolishing the initial post-stimulus excitation (**Figure 4C**). Thus, as predicted by short burst

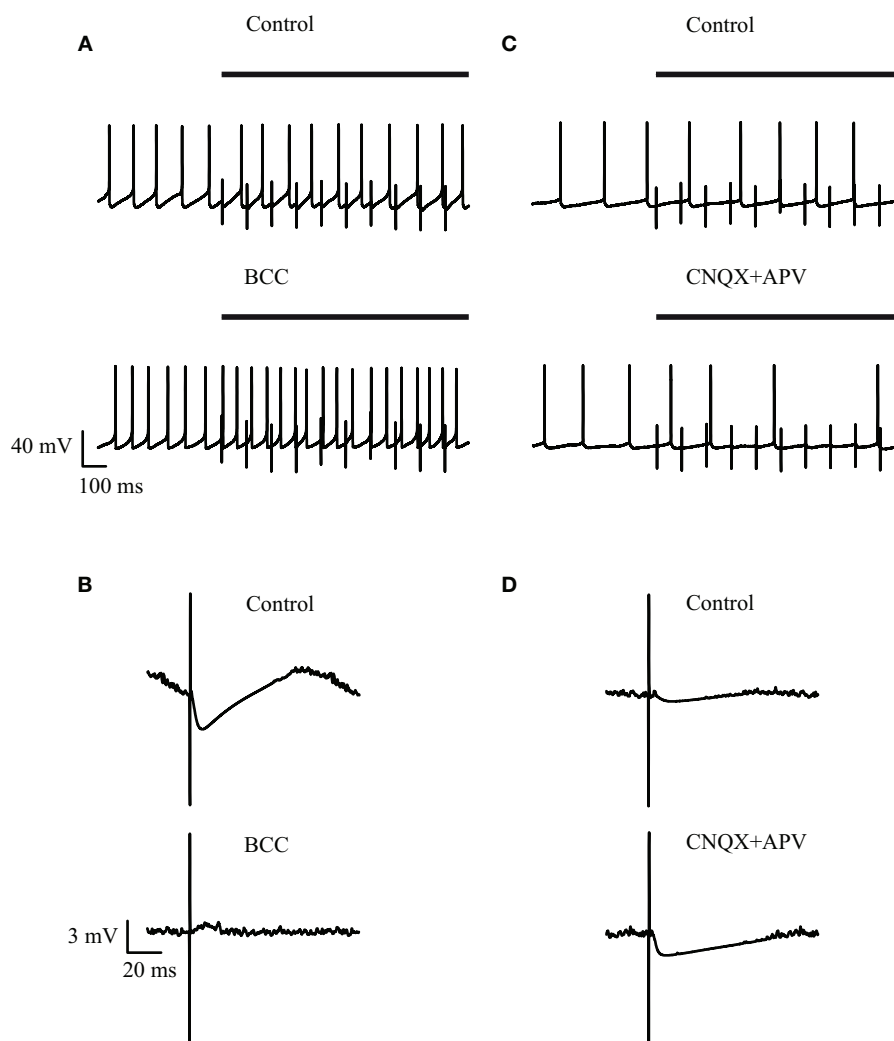


FIGURE 2 | Effect of GABAergic and glutamatergic antagonists on the membrane potential during low-frequency (10 Hz) stimulation. (A,C) Continuous recording of the membrane potential before (top trace) and after (bottom trace) application of (A) 50 μ M bicuculline or (C) 15 μ M CNQX and

50 μ M APV, during the stimulation. The bold horizontal lines indicate the period of repetitive stimulation. (B,D) Stimulus-triggered average of membrane potential before (top) and after (bottom) application of (B) 50 μ M bicuculline or (D) 15 μ M CNQX and 50 μ M APV, during the stimulation.

stimulation studies (Rav-Acha et al., 2005), repetitive stimulation at 10 Hz appeared to synchronize the firing of GP neurons by generating common delays from the stimulation pulses.

Next, we investigated the influence of 40 Hz repetitive stimulation on the firing of GP neurons. Following the onset of stimulation the cells responded with a period in which no APs were observed (Figures 5A,C, top traces). Application of BCC increased the pre-stimulus firing rate and eliminated the inhibitory period (Figure 5A, bottom trace). Conversely, application of APV and CNQX did not appear to alter the inhibitory period but reduced the firing rate following this period (Figure 5C). Since the 10-Hz stimulation did not change the firing frequency we were able to calculate a STA and get an average synaptic response (Figure 2). At higher stimulation frequencies the firing frequency was not stationary. Therefore it was not possible to calculate the STA. To offer a qualitative display of the synaptic potentials during the stimulation

we added to Figure 5 membrane potential responses to a single stimulus. Figures 5B,D display a single, apparently inhibitory, synaptic response 100 ms following the onset of the 40-Hz stimulation. As predicted by voltage-clamp experiments (Rav-Acha et al., 2005; Sims et al., 2008) the amplitude of the synaptic potential was considerably reduced 1 s into the stimulus train (Figures 5B,D, gray line). The IPSP observed immediately following the onset of the stimulation was abolished following the application of BCC (Figure 5B, bottom trace) but not by the application of APV and CNQX (Figure 5D, bottom trace).

To quantify the effects that were observed visually we calculated the population average firing rate ($n = 43$ cells) and normalized it to the pre-stimulus population average firing rate. During a 30-s stimulation at 40 Hz the firing rate first decreased and then increased (Figure 6A). Following the application of BCC the pre-stimulus population average firing rate increased 2.5-fold

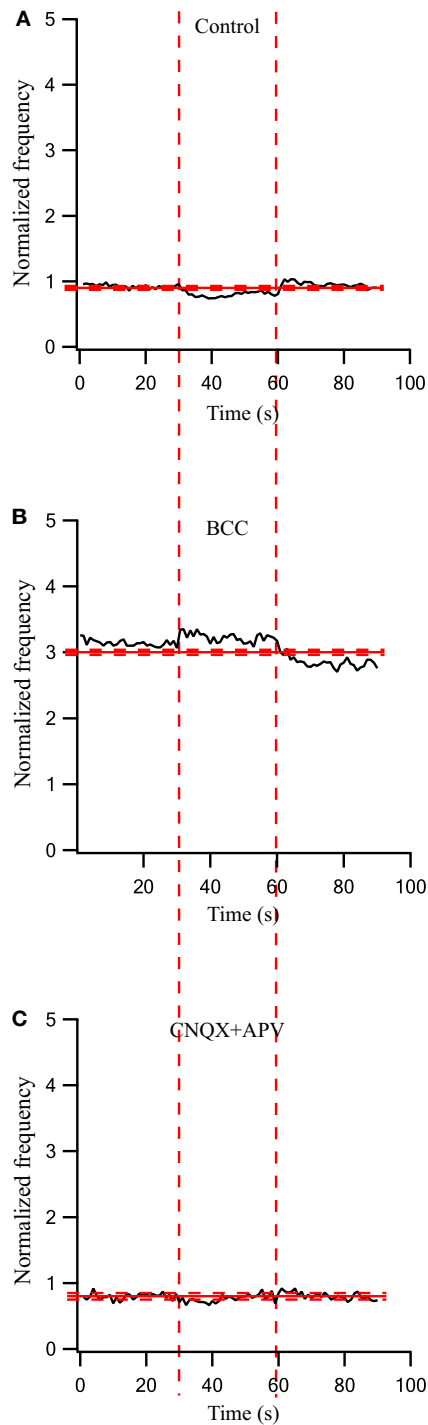


FIGURE 3 | Firing rate changes during stimulation at 10 Hz before and after application of GABAergic and glutamatergic antagonists. (A) Population firing rate of GP neurons in normal extracellular solution ($n = 41$). **(B)** Population frequency of GP neurons after applying 50 μM bicuculline to the extracellular solution ($n = 17$). **(C)** Population frequency of GP neurons after applying 15 μM CNQX and 50 μM APV to the extracellular solution ($n = 14$). The thick and dashed horizontal lines indicate the average and SD of the pre-stimulus frequency, respectively. The dashed vertical lines mark the beginning and the end of the stimulus.

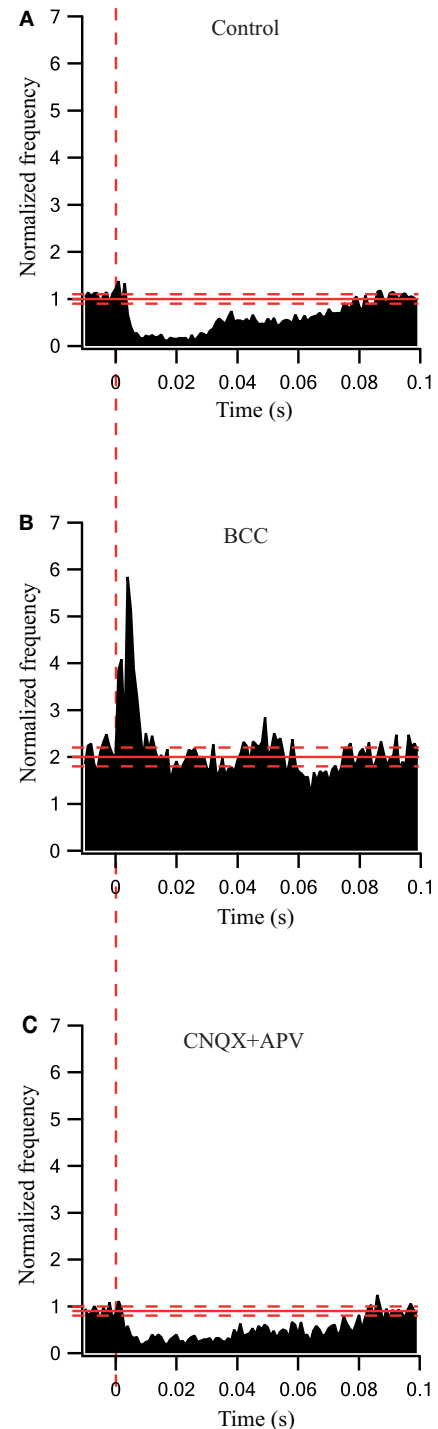
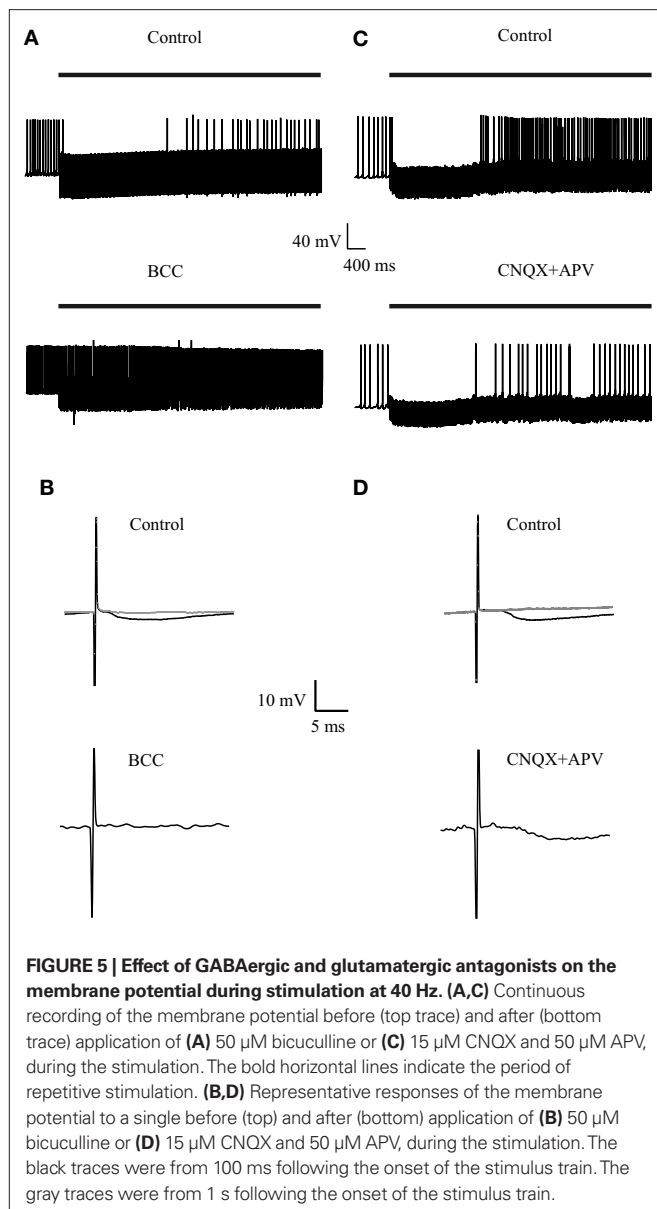


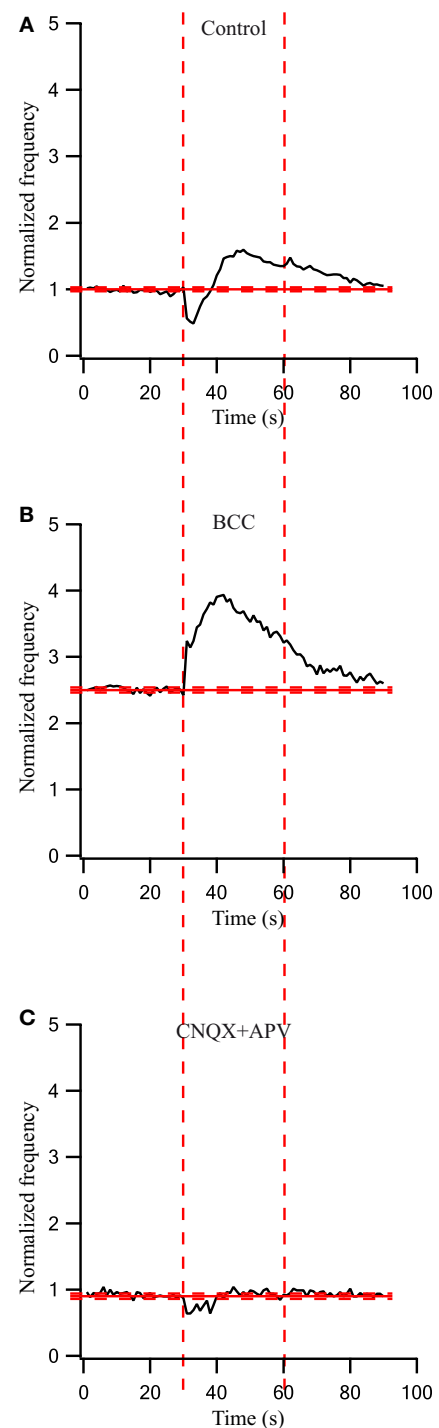
FIGURE 4 | Synaptically locked response changes during stimulation at 10 Hz before and after application of GABAergic and glutamatergic antagonists. (A) Population PSTH of GP neurons in normal extracellular solution ($n = 38$). **(B)** Population PSTH of GP neurons after applying 50 μM bicuculline to the extracellular solution ($n = 17$). **(C)** Population PSTH of GP neurons after applying 15 μM CNQX and 50 μM APV to the extracellular solution ($n = 14$). The thick and dashed horizontal lines indicate the average and SD of pre-stimulus frequency, respectively. The dashed vertical line marks the beginning of the stimulation pulse.



(Figure 6B). During the 40-Hz stimuli train the population average firing rate increased to almost 4-fold of the control values and then started to decrease (Figure 6B). Bath application of APV and CNQX eliminated the excitatory phase of the cellular response and decreased the inhibitory response (Figure 6C). Since these effects were not stationary in time we did not calculate the PSTHs under these conditions.

DISCUSSION

In the current work we described the dynamic changes to the firing rate and pattern of GP neurons during repetitive stimulation. We showed that at a low rate of stimulation the firing of the neurons is locked to the stimulus due to the combined activation of excitatory and inhibitory synapses. At higher stimulation frequencies, the firing rate of the neurons displayed a biphasic response consisting



of an initial inhibition followed by excitation. The dynamics of the response suggest that both GABAergic and glutamatergic synapses in the GP undergo short-term depression during the stimulation.

Several elegant studies have shown that both GABAergic and glutamatergic synapses in the GP undergo short-term depression (Hanson and Jaeger, 2002; Rav-Acha et al., 2005; Sims et al., 2008; Erez et al., 2009). It has been shown that when blocking inhibition with picrotoxin, the excitatory synapses from the STN display both short-term facilitation and depression (Hanson and Jaeger, 2002). This complex short-term plasticity most likely accounts for the initial increase and later decrease in the firing of GP neurons during HFS (Figure 6B). In addition, GABAergic synapses in the GP have been shown to display short-term depression (Rav-Acha et al., 2005; Sims et al., 2008). Activation of these synapses and their subsequent depression provides an explanation for the initial inhibition of the firing rate during HFS (Figures 1, 5, and 6). As HFS increases the depression of the GABAergic synapse in the GP the IPSPs will decrease. This leads to a reduction in the locking to the stimulation induced by the inhibitory input. Thus, prolonged HFS in the GP will lead to a drastic depression of both inhibitory and excitatory synapses. This in turn will reduce the coupling of the GP to its input and the synchronization within the GP. Moreover, depression of the GABAergic synapses may reduce the overall inhibitory drive in the GP leading to an increase in the spontaneous firing rate of GP neurons. Application of BCC demonstrated that reduction in this drive may result in a substantial increase in the spontaneous firing rate (Figures 3 and 6).

Contrary to HFS, it is tempting to speculate that low-frequency stimulation may increase synchrony in the GP. It has been shown (Rav-Acha et al., 2005) that a 10-Hz stimulation will depress GABAergic synapses in the GP to a steady state level of ~50%. Thus, low-frequency stimulation stimulates a network with active

inhibitory and excitatory synapses. This leads to the locking observed in this study (Figures 3 and 4). The firing rate of GP neurons *in vivo* ranges from 5 to 80 Hz (Gardiner and Kitai, 1992; Kelland et al., 1995). This may suggest that in the rat GP synaptic depression is constantly modulated by network activity.

It is interesting to compare the current *in vitro* findings in acute brain slices in the rat to the extracellular recordings obtained from behaving primates. A dynamic process affecting the synaptic transmission has been reported in the Parkinsonian (MPTP treated) primate (Erez et al., 2009). The stimulation rate in the primate was higher (135 Hz) than the one tested in this study (40 Hz). This is in line with previous studies that have shown slower processes in the rat compared to the primate. The baseline firing rate in the normal primate is 50–75 spikes/s (DeLong, 1971) which is higher than the average frequency found in *in vivo* rat studies (Gardiner and Kitai, 1992; Kelland et al., 1995). In the primate study, a dynamic process was observed during both the excitatory and inhibitory responses to the stimulation. This may have been due to the dominance of the fibers stimulated: excitatory axons from the STN in one case versus the inhibitory axons from the striatum and GP in the other. This difference in dominance in different recording sessions may have arisen from the inhomogeneous distribution of the incoming fibers and the change in the stimulating electrode and recording electrode locations. Thus, it is tempting to speculate, based on the results presented here, that short-term plasticity in the GP contributes differentially to the activity of the network depending on the stimulation frequency.

ACKNOWLEDGMENTS

This research was supported by the Legacy Heritage Bio-Medical Program of the Israeli Science Foundation to Alon Korngreen and Izhar Bar-Gad (Grant no. 981/10).

REFERENCES

- Bar-Gad, I., Elias, S., Vaadia, E., and Bergman, H. (2004). Complex locking rather than complete cessation of neuronal activity in the globus pallidus of a 1-methyl-4-phenyl-1,2,3,6-tetrahydropyridine-treated primate in response to pallidal microstimulation. *J. Neurosci.* 24, 7410–7419.
- Benabid, A. L. (2003). Deep brain stimulation for Parkinson's disease. *Curr. Opin. Neurobiol.* 13, 696–706.
- Bugaysen, J., Bronfeld, M., Tischler, H., Bar-Gad, I., and Korngreen, A. (2010). Electrophysiological characteristics of globus pallidus neurons. *PLoS ONE* 5, e12001. doi: 10.1371/journal.pone.0012001
- DeLong, M. R. (1971). Activity of pallidal neurons during movement. *J. Neurophysiol.* 34, 414–427.
- Dostrovsky, J. O., Levy, R., Wu, J. P., Hutchison, W. D., Tasker, R. R., and Lozano, A. M. (2000). Microstimulation-induced inhibition of neuronal firing in human globus pallidus. *J. Neurophysiol.* 84, 570–574.
- Erez, Y., Czitron, H., McCairn, K., Belevsky, K., and Bar-Gad, I. (2009). Short-term depression of synaptic transmission during stimulation in the globus pallidus of 1-methyl-4-phenyl-1,2,3,6-tetrahydropyridine-treated primates. *J. Neurosci.* 29, 7797–7802.
- Filali, M., Hutchison, W. D., Palter, V. N., Lozano, A. M., and Dostrovsky, J. O. (2004). Stimulation-induced inhibition of neuronal firing in human subthalamic nucleus. *Exp. Brain Res.* 156, 274–281.
- Francois, C., Percheron, G., Yelnik, J., and Heyner, S. (1984). A Golgi analysis of the primate globus pallidus. I. Inconstant processes of large neurons, other neuronal types, and afferent axons. *J. Comp. Neurol.* 227, 182–199.
- Gardiner, T. W., and Kitai, S. T. (1992). Single-unit activity in the globus pallidus and neostriatum of the rat during performance of a trained head movement. *Exp. Brain Res.* 88, 517–530.
- Gubellini, P., Salin, P., Kerkerian-Le Goff, L., and Baunez, C. (2009). Deep brain stimulation in neurological diseases and experimental models: from molecule to complex behavior. *Prog. Neurobiol.* 89, 79–123.
- Hahn, P. J., Russo, G. S., Hashimoto, T., Miciocinovic, S., Xu, W., McIntyre, C. C., and Vitek, J. L. (2008). Pallidal burst activity during therapeutic deep brain stimulation. *Exp. Neurol.* 211, 243–251.
- Hammond, C., Ammari, R., Bioulac, B., and Garcia, L. (2008). Latest view on the mechanism of action of deep brain stimulation. *Mov. Disord.* 23, 2111–2121.
- Hanson, J. E., and Jaeger, D. (2002). Short-term plasticity shapes the response to simulated normal and Parkinsonian input patterns in the globus pallidus. *J. Neurosci.* 22, 5164–5172.
- Hashimoto, K., and Kita, H. (2008). Serotonin activates presynaptic and postsynaptic receptors in rat globus pallidus. *J. Neurophysiol.* 99, 1723–1732.
- Hashimoto, T., Elder, C. M., Okun, M. S., Patrick, S. K., and Vitek, J. L. (2003). Stimulation of the subthalamic nucleus changes the firing pattern of pallidal neurons. *J. Neurosci.* 23, 1916–1923.
- Johnson, M. D., and McIntyre, C. C. (2008). Quantifying the neural elements activated and inhibited by globus pallidus deep brain stimulation. *J. Neurophysiol.* 100, 2549–2563.
- Kaneda, K., and Kita, H. (2005). Synaptically released GABA activates both pre- and postsynaptic GABA(B) receptors in the rat globus pallidus. *J. Neurophysiol.* 94, 1104–1114.
- Kaneda, K., Kita, T., and Kita, H. (2007). Repetitive activation of glutamatergic inputs evokes a long-lasting excitation in rat globus pallidus neurons *in vitro*. *J. Neurophysiol.* 97, 121–133.
- Kaneda, K., Tachibana, Y., Imanishi, M., Kita, H., Shigemoto, R., Nambu, A., and Takada, M. (2005). Down-regulation of metabotropic glutamate receptor 1 alpha in globus pallidus and substantia nigra of Parkinsonian monkeys. *Eur. J. Neurosci.* 22, 3241–3254.
- Kelland, M. D., Soltis, R. P., Anderson, L. A., Bergstrom, D. A., and Walters, J.

- R. (1995). *In vivo* characterization of two cell types in the rat globus pallidus which have opposite responses to dopamine receptor stimulation: comparison of electrophysiological properties and responses to apomorphine, dizocilpine, and ketamine anesthesia. *Synapse* 20, 338–350.
- Kita, H., and Kitai, S. T. (1994). The morphology of globus pallidus projection neurons in the rat: an intracellular staining study. *Brain Res.* 636, 308–319.
- McCaig, K. W., and Turner, R. S. (2009). Deep brain stimulation of the globus pallidus internus in the Parkinsonian primate: local entrainment and suppression of low-frequency oscillations. *J. Neurophysiol.* 101, 1941–1960.
- McIntyre, C. C., Grill, W. M., Sherman, D. L., and Thakor, N. V. (2004a). Cellular effects of deep brain stimulation: model-based analysis of activation and inhibition. *J. Neurophysiol.* 91, 1457–1469.
- McIntyre, C. C., Savasta, M., Kerkerian-Le Goff, L., and Vitek, J. L. (2004b). Uncovering the mechanism(s) of action of deep brain stimulation: activation, inhibition, or both. *Clin. Neurophysiol.* 115, 1239–1248.
- Meissner, W., Leblois, A., Hansel, D., Bioulac, B., Gross, C. E., Benazzouz, A., and Boraud, T. (2005). Subthalamic high frequency stimulation resets subthalamic firing and reduces abnormal oscillations. *Brain* 128, 2372–2382.
- Montgomery, E. B. Jr. (2006). Effects of GPi stimulation on human thalamic neuronal activity. *Clin. Neurophysiol.* 117, 2691–2702.
- Montgomery, E. B. Jr., and Gale, J. T. (2008). Mechanisms of action of deep brain stimulation (DBS). *Neurosci. Biobehav. Rev.* 32, 388–407.
- Parent, A., Sato, F., Wu, Y., Gauthier, J., Levesque, M., and Parent, M. (2000). Organization of the basal ganglia: the importance of axonal collateralization. *Trends Neurosci.* 23, S20–S27.
- Percheron, G., Yelnik, J., and Francois, C. (1984). A Golgi analysis of the primate globus pallidus. III. Spatial organization of the striato-pallidal complex. *J. Comp. Neurol.* 227, 214–227.
- Rav-Acha, M., Sagiv, N., Segev, I., Bergman, H., and Yarom, Y. (2005). Dynamic and spatial features of the inhibitory pallidal GABAergic synapses. *Neuroscience* 135, 791–802.
- Sims, R. E., Woodhall, G. L., Wilson, C. L., and Stanford, I. M. (2008). Functional characterization of GABAergic pallidopallidal and striatopallidal synapses in the rat globus pallidus in vitro. *Eur. J. Neurosci.* 28, 2401–2408.
- Smith, Y., and Parent, A. (1988). Neurons of the subthalamic nucleus in primates display glutamate but not GABA immunoreactivity. *Brain Res.* 453, 353–356.
- Stuart, G. J., Dodt, H. U., and Sakmann, B. (1993). Patch-clamp recordings from the soma and dendrites of neurons in brain slices using infrared video microscopy. *Pflügers Arch.* 423, 511–518.
- Wu, Y. R., Levy, R., Ashby, P., Tasker, R. R., and Dostrovsky, J. O. (2001). Does stimulation of the GPi control dyskinesia by activating inhibitory axons? *Mov. Disord.* 16, 208–216.
- Xu, W., Russo, G. S., Hashimoto, T., Zhang, J., and Vitek, J. L. (2008). Subthalamic nucleus stimulation modulates thalamic neuronal activity. *J. Neurosci.* 28, 11916–11924.
- Yelnik, J., Percheron, G., and Francois, C. (1984). A Golgi analysis of the primate globus pallidus. II. Quantitative morphology and spatial orientation of dendritic arborizations. *J. Comp. Neurol.* 227, 200–213.

Conflict of Interest Statement: The authors declare that the research was conducted in the absence of any commercial or financial relationships that could be construed as a potential conflict of interest.

Received: 29 December 2010; paper pending published: 17 February 2011; accepted: 21 March 2011; published online: 30 March 2011.

Citation: Bugaysen J, Bar-Gad I and Korngreen A (2011) The impact of stimulation induced short-term synaptic plasticity on firing patterns in the globus pallidus of the rat. *Front. Syst. Neurosci.* 5:16. doi: 10.3389/fnsys.2011.00016

Copyright © 2011 Bugaysen, Bar-Gad and Korngreen. This is an open-access article subject to a non-exclusive license between the authors and Frontiers Media SA, which permits use, distribution and reproduction in other forums, provided the original authors and source are credited and other Frontiers conditions are complied with.



Disinhibition bursting of dopaminergic neurons

Collin J. Lobb, Todd W. Troyer, Charles J. Wilson and Carlos A. Paladini*

Neurosciences Institute, University of Texas at San Antonio, San Antonio, TX, USA

Edited by:

James M. Tepper, Rutgers, The State University of New Jersey, USA

Reviewed by:

Mark Bevan, Northwestern University, USA

Mark D. Humphries, University of Sheffield, UK

*Correspondence:

Carlos A. Paladini, Neurosciences Institute, University of Texas at San Antonio, One UTSA Circle, San Antonio, TX 78249, USA.
e-mail: carlos.paladini@utsa.edu

Substantia nigra pars compacta (SNpc) dopaminergic neurons receive strong tonic inputs from GABAergic neurons in the substantia nigra pars reticulata (SNpr) and globus pallidus (GP), and glutamatergic neurons in the subthalamic nucleus. The presence of these tonic inputs raises the possibility that phasic disinhibition may trigger phasic bursts in dopaminergic neurons. We first applied constant NMDA and GABA_A conductances onto a two-compartment single cell model of the dopaminergic neuron (Kuznetsov et al., 2006). The model exhibited disinhibition bursting upon stepwise removal of inhibition. A further bifurcation analysis suggests that disinhibition may be more robust than excitation alone in that for most levels of NMDA conductance, the cell remains capable of bursting even after a complete removal of inhibition, whereas too much excitatory input will drive the cell into depolarization block. To investigate the network dynamics of disinhibition, we used a modified version of an integrate-and-fire based model of the basal ganglia (Humphries et al., 2006). Synaptic activity generated in the network was delivered to the two-compartment single cell dopaminergic neuron. Phasic activation of the D1-expressing medium spiny neurons in the striatum (D1STR) produced disinhibition bursts in dopaminergic neurons through the direct pathway (D1STR to SNpr to SNpc). Anatomical studies have shown that D1STR neurons have collaterals that terminate in GP. Adding these collaterals to the model, we found that striatal activation increased the intra-burst firing frequency of the disinhibition burst as the weight of this connection was increased. Our studies suggest that striatal activation is a robust means by which disinhibition bursts can be generated by SNpc dopaminergic neurons, and that recruitment of the indirect pathway via collaterals may enhance disinhibition bursting.

Keywords: dopamine, GABA, burst, model, network

INTRODUCTION

In behaving animals, midbrain dopaminergic neurons fire bursts of action potentials in response to salient stimuli (Redgrave et al., 1990; Horvitz et al., 1997; Schultz, 1998), when a greater than expected reward is received (Schultz et al., 1997), or during sequence learning (Jin and Costa, 2010). The mechanisms by which dopaminergic neurons generate bursts are an area of intense study. The absence of burst firing in slices (e.g., Kita et al., 1986; Grace and Onn, 1989) suggests that bursts are generated in response to afferent input. One view of the dopaminergic neuron *in vivo* is that single-spiking is generated by an *in vitro*-like calcium – (Kita et al., 1986; Grace and Onn, 1989; Wilson and Callaway, 2000) or sodium-based (Guzman et al., 2009; Khaliq and Bean, 2010) pacemaking mechanism in which spikes can be advanced or delayed due to afferent input. Under such a scheme, bursts are caused by phasic excitatory inputs, e.g., inputs activating AMPA, NMDA, or nicotinic acetylcholine receptors (Grace and Bunney, 1984; Grenhoff et al., 1986; Chergui et al., 1993; Morikawa et al., 2003; Blythe et al., 2007, 2009; Deister et al., 2009; Lobb et al., 2010). However, dopaminergic neurons *in vivo* are subject to strong tonic synaptic inputs, suggesting that an alternative but complementary mechanism by which dopaminergic neurons may fire bursts is through disinhibition.

Dopaminergic neurons receive strong synaptic activation from spontaneously active inputs *in vivo* (e.g., Grace and Bunney, 1985; Tepper and Lee, 2007). The effect of these tonic inputs can be seen by subtraction. Local application of NMDA, but not AMPA, receptor antagonists significantly reduce spontaneous burst firing

in vivo (Charley et al., 1991; Overton and Clark, 1992; Chergui et al., 1993; Christoffersen and Meltzer, 1995). Paladini and Tepper (1999), and Brazhnik et al. (2008) found that local application of a variety of GABA_A antagonists by pressure ejection onto the recorded neuron shifted the firing pattern of the dopaminergic neuron from a single-spiking mode to a bursting one, indicating that tonic GABA_A receptor activation was strong enough to suppress burst firing. These experiments suggest that dopaminergic neurons are subject to at least two types of tonic inputs *in vivo*: an NMDA-mediated excitatory input and a GABA_A-mediated inhibitory input. We have recently demonstrated that dopaminergic neurons that receive tonic NMDA and GABA_A inputs can maintain their spontaneous activity and are capable of generating bursts through disinhibition (Lobb et al., 2010). Using a combination of network and compartmental computational modeling, we explore how disinhibition bursting of dopaminergic neurons might arise from striatal activation.

MATERIALS AND METHODS

This study investigated conditions under which disinhibition in the basal ganglia network leads to bursting in midbrain dopaminergic neurons. Our model was based on a combination of two previously published models. The first is the current-based, integrate-and-fire type network model of the basal ganglia described in Humphries et al. (2006). This network model was used to generate the synaptic input onto a two-compartment model of a substantia nigra pars compacta (SNpc) dopaminergic neuron (Kuznetsov et al., 2006).

The network model contained five collections of neurons: D1STR (D1-expressing striatum, $N = 64$ neurons, threshold $\theta = 30$ mV, time constant $\tau_m = 25$ ms), globus pallidus (GP; $N = 64$, $\theta = 30$ mV, $\tau_m = 14$ ms), STN ($N = 64$, $\theta = 20$ mV, $\tau_m = 6$ ms), substantia nigra pars reticulata (SNpr; $N = 64$, $\theta = 30$ mV, $\tau_m = 8$ ms), and SNpc ($N = 64$, see single cell model below). See Humphries et al. (2006) for the full specification of the model.

The original Humphries et al. (2006) model consists of multiple anatomically based microchannels to allow for a mechanism of action selection. For simplicity, we employed only a single microchannel. Connections were added between nuclei as shown in **Figure 1**. The D1STR–SNpc connection arises from neurons in striatal patches whereas the D1STR–SNpr connection arises from neurons in the striatal matrix (Gerfen, 1984). It is unclear if both would be activated during a rewarding scenario and thus the D1STR–SNpc connection is disregarded in this study. All connections were given a weight of -1 , 0 , or $+1$, where a negative value represents an inhibitory connection and a positive value represents an excitatory connection. Connections could be removed or disabled in the network by setting the connection weight to zero. An afferent neuron made a synaptic connection onto each neuron in a target nucleus with a probability of 0.25 . As described in Humphries et al. (2006), inhibitory connections were modeled as exponentially decaying negative currents with a decay time $\tau_{\text{GABA}} = 3$ ms. Excitatory connections had both AMPA and NMDA components, each modeled as a simple decaying exponential with decay times $\tau_{\text{AMPA}} = 2$ ms and $\tau_{\text{NMDA}} = 100$ ms. The peak amplitude of individual AMPA and GABA_A postsynaptic potentials were 3 mV; individual NMDA potentials peaked at 0.1 mV. Dopamine levels were set to the “normal” condition in Humphries et al. (2006; $\lambda_{\text{D1}} = \lambda_{\text{D2}} = 0.3$). Background pacemaking activity seen in basal ganglia neurons (STN: 12 Hz, GP: 26 Hz, SNpr: 32 Hz) was induced by inject-

ing a suprathreshold fixed current. The level of this current was adjusted to maintain background firing rates for the reduced model described in **Figures 3–5** (STN: 66.1 pA, GP: 17 pA, SNpr: 14 pA) and the full model described in **Figures 6 and 7** (STN: 100.5 pA, GP: 17 pA, SNpr: 26 pA). As described in Humphries et al. (2006), each neuron model contained a noise term with a mean \pm SD of 0 ± 0.0008 mV.

Disinhibition bursts were initiated by modeling bursts of cortical inputs as step pulses of current delivered to D1STR neurons ($+2$ nA, 150 ms). Simulations were run for 1 s before these current injections to mitigate any effect of onset transients. Simulations were implemented in MATLAB (Mathworks, Natick, MA, USA) as described in Humphries et al. (2006).

Inputs to the single cell SNpc model arose from the SNpr, GP, and STN. The SNpr and GP inputs made synapses onto both somatic and dendritic compartments of the two-compartment model and activated postsynaptic GABA_A receptors on dopaminergic neurons (Paladini and Tepper, 1999). STN inputs made synapses onto the burst-generating, dendritic compartment of the two-compartment model and activated postsynaptic NMDA receptors. Postsynaptic activation of AMPA receptors was excluded because local application of an AMPA receptor antagonist *in vivo* does not change the activity of dopaminergic neurons (Chergui et al., 1994). In contrast, tonic STN input contributes to spontaneous bursting *in vivo* (Smith and Grace, 1992; Chergui et al., 1994) that is strongly affected by local application of NMDA receptor antagonists (Chergui et al., 1994). GABA_A-mediated currents were added to both somatic and dendritic compartments of the two-compartment dopaminergic neuron model.

The synaptic conductances waveforms were described as a difference of exponentials: $G_{\text{syn}}(t) = \delta * [e^{-(t/\tau_{\text{fall}})} - e^{-(t/\tau_{\text{rise}})}]$. Spike times were drawn from activation in the network model and each triggered a step increase of size δ . For GABA_A receptors (input from GP and SNr), $\tau_{\text{rise}} = 1$ ms, $\tau_{\text{fall}} = 6$ ms, and $\delta_{\text{GABA}} = 0.043$ ms/cm². For NMDA receptors (input from STN), $\tau_{\text{rise}} = 3$ ms, $\tau_{\text{fall}} = 40$ ms, and $\delta_{\text{NMDA}} = 0.030$ ms/cm².

Single cell simulations were run in XPPAUT (Ermentrout, 2002) using the RUNGE–KUTTA method with $dt = 0.01$ or 0.005 ms. Bifurcation diagrams were made with the XPPAUT implementation of AUTO. Equations were implemented as described in the original model and are not reproduced here. The full set of parameters used here is given in **Table 1**. Calcium buffering parameters are identical to the original model with the exception of the calcium pump density, which was increased from 2500 to $10,000$ $\mu\text{m/s}$ to increase the frequency of dopaminergic neuron bursting produced in the model.

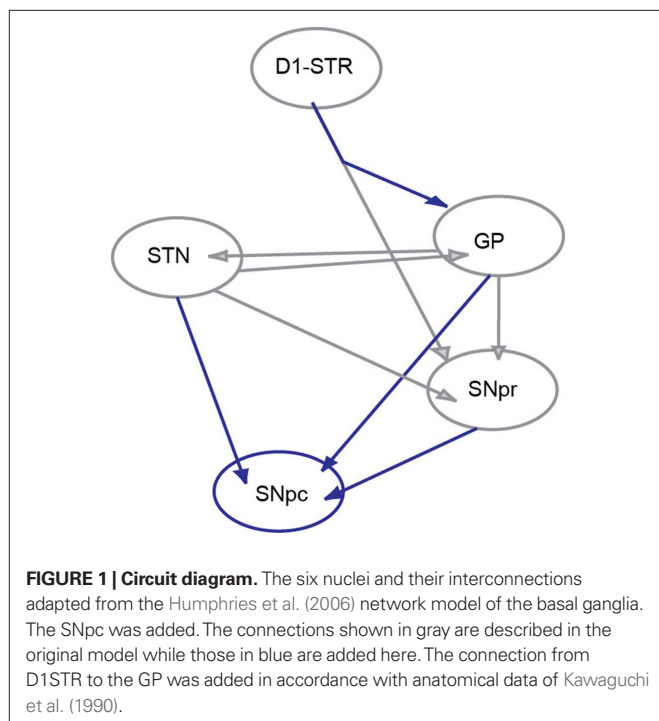


Table 1 | Parameters used in the compartmental model.

Parameter	Value	Parameter	Value	Parameter	Value
g_{Leak}	0.095	g_{NMDA}	See text	E_{Leak}	-50 mV
g_{KCa}	0.3	g_{GABAA}	See text	r_1	10 μm
g_{K2}	10	E_{Na}	55 mV	r_2	0.5 μm
g_{Na}	150	E_{Ca}	100 mV	n_d	10
g_{K1}	0.0	E_{K}	-90 mV	Mg	0.5 mM
g_c	0.25	E_{NMDA}	0 mV	v_{SK}	7
g_{Ca}	0.15	E_{GABAA}	-60 mV	V_{HK}	-10 mV

RESULTS

SINGLE CELL

We first investigated the range of synaptic parameters that can give rise to bursting in our single cell model of the midbrain dopaminergic neuron. When all the synaptic conductances are set to 0, the dopaminergic neuron shows a very regular pattern of spiking at a frequency of approximately 4–5 Hz (**Figure 2A**). The model can generate a sustained burst in response to a phasic NMDA conductance (**Figure 2B**, $g_{\text{NMDA}} = 0.28 \text{ mS/cm}^2$ at 1100 ms). Bursts could also be generated through disinhibition. Constant NMDA and GABA_A conductances were applied to the model to maintain balanced spiking (**Figure 2C**; $g_{\text{GABA}_A} = 0.14 \text{ mS/cm}^2$, $g_{\text{NMDA}} = 0.28 \text{ mS/cm}^2$). At $t = 1100 \text{ ms}$ the GABA_A conductance was set to 0 and the cell fired a sustained burst of action potentials (intra-burst frequency in **Figure 2B,C** are both 47 Hz).

Given that dopamine neuron bursting can result from either an increase in excitation or a removal of inhibition, we determined which combinations of GABA_A and NMDA conductance values permitted repetitive spiking. In particular, we calculated a two-parameter bifurcation diagram that separated oscillatory (repetitive spiking) behavior from fixed-point (non-spiking) behavior (**Figure 2D**). The hatched region represents combinations of syn-

aptic conductances for which the cell fires trains of action potentials. Parameters below to the right of this hatched region correspond to situations in which firing is prevented by too much inhibition. Note that firing is also absent above and to the left of the hatched region. For these parameters, the model enters depolarization block and ceases to fire, a problem that is even more severe for AMPA-mediated, vs. NMDA-mediated, excitation (Deister et al., 2009).

The shape of the firing region suggests that disinhibition may be more robust than excitation as a mechanism for burst generation. This is because for most starting conditions, the system will remain in the firing regime even after a complete removal of inhibition. In contrast, NMDA conductance values must stay within a bounded region to support burst firing. Too much excitation and the system will move vertically outside the oscillating region and cease firing due to depolarization block.

This firing region was $[\text{Mg}^{2+}]$ dependent (**Figure 2E**). Increasing Mg^{2+} RUNGE–KUTTA method concentrations reduces the negative slope conductance of the NMDA conductance, and the firing region becomes elongated. Under these conditions, the action of disinhibition and excitation are more similar in that removing too much inhibition will also drive the model into depolarization block and shut off bursting.

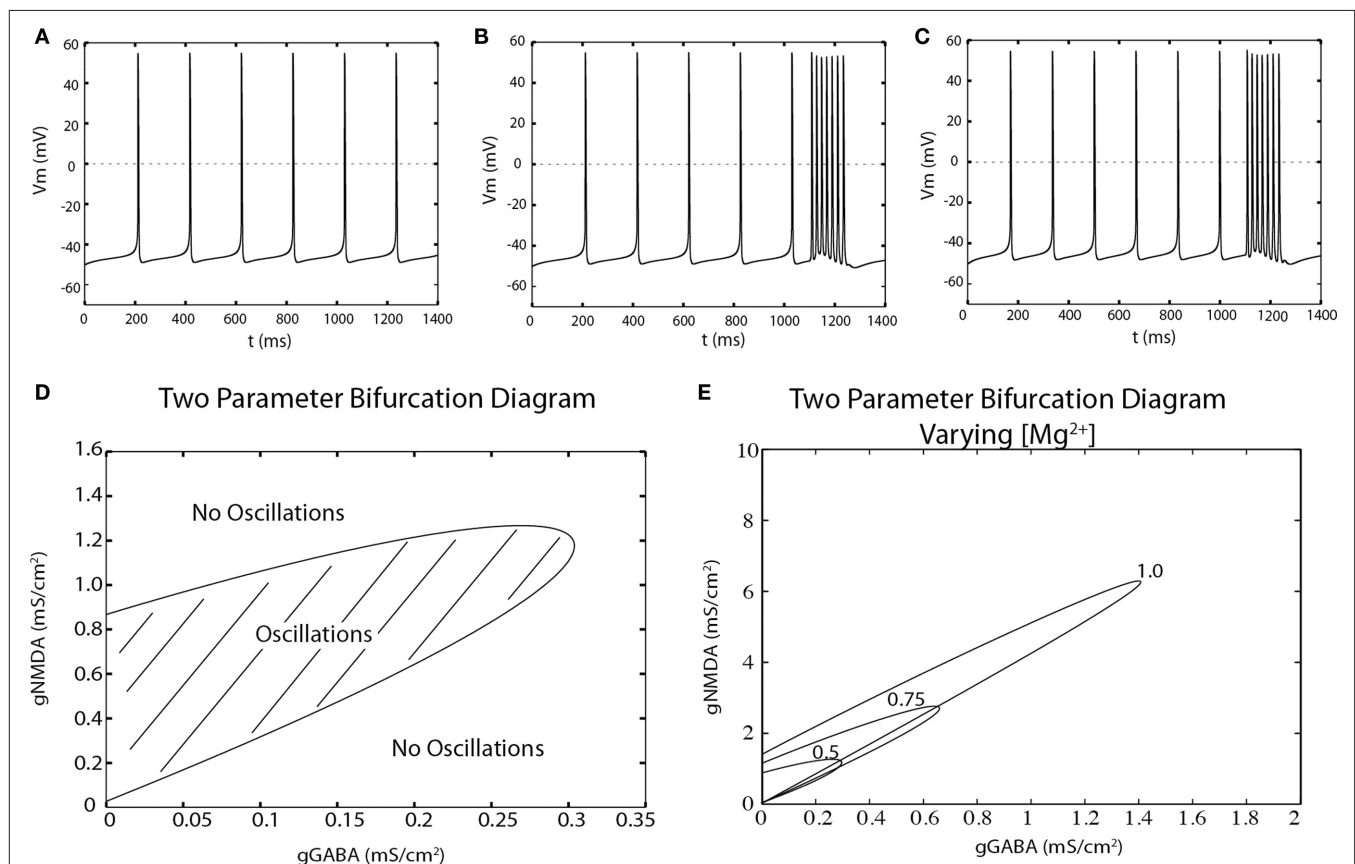


FIGURE 2 | The dopaminergic neuron can fire disinhibition bursts.

(A) Spontaneous, single-spiking in the absence of tonic input in a two-compartment model of the dopaminergic neuron. (B) Phasic activation of NMDA receptors (at $t = 1100, 150 \text{ ms}$) produces a burst of action potentials. (C) The model exhibits single-spiking at similar frequencies as in (A) and can

produces bursts by disinhibition upon complete removal of tonic inhibition at $t = 1100 \text{ ms}$ for 150 ms. (D) The NMDA and GABA_A conductances at which repetitive spiking can be generated (hatched region) is computed by a two-point bifurcation diagram in AUTO (XPPAUT). (E) Magnesium dependence of the oscillatory region.

DIRECT PATHWAY

After considering the single cell model in isolation, we investigated how disinhibition bursts could be driven by synaptic input patterns resulting from a network model of the basal ganglia based on the model of Humphries et al. (2006; see Materials and Methods). We first considered the influence of the D1STR–SNpr–SNpc (“direct”) pathway. All connections other than the D1STR–SNpr, SNpr–SNpc, STN–SNpr, and STN–SNpc were disabled. Neurons in D1STR received direct current injection intended to model a burst

of cortical input. Outputs from the network model were read into XPPaut and incremented their respective conductance equations by δ . These values were estimated such that the mean conductance was approximately $g_{\text{GABAA}} = 0.14 \text{ mS/cm}^2$ and $g_{\text{NMDA}} = 0.28 \text{ mS/cm}^2$. An example is shown in **Figure 3**. Stimulation of the striatum evoked a burst in the dopaminergic neuron. The number of spikes in that burst was dependent on the length of time in which the striatum was stimulated (**Figures 4B,C**; 30–150 ms). The intra-burst firing frequency, however, was unaffected (**Figure 4A**).

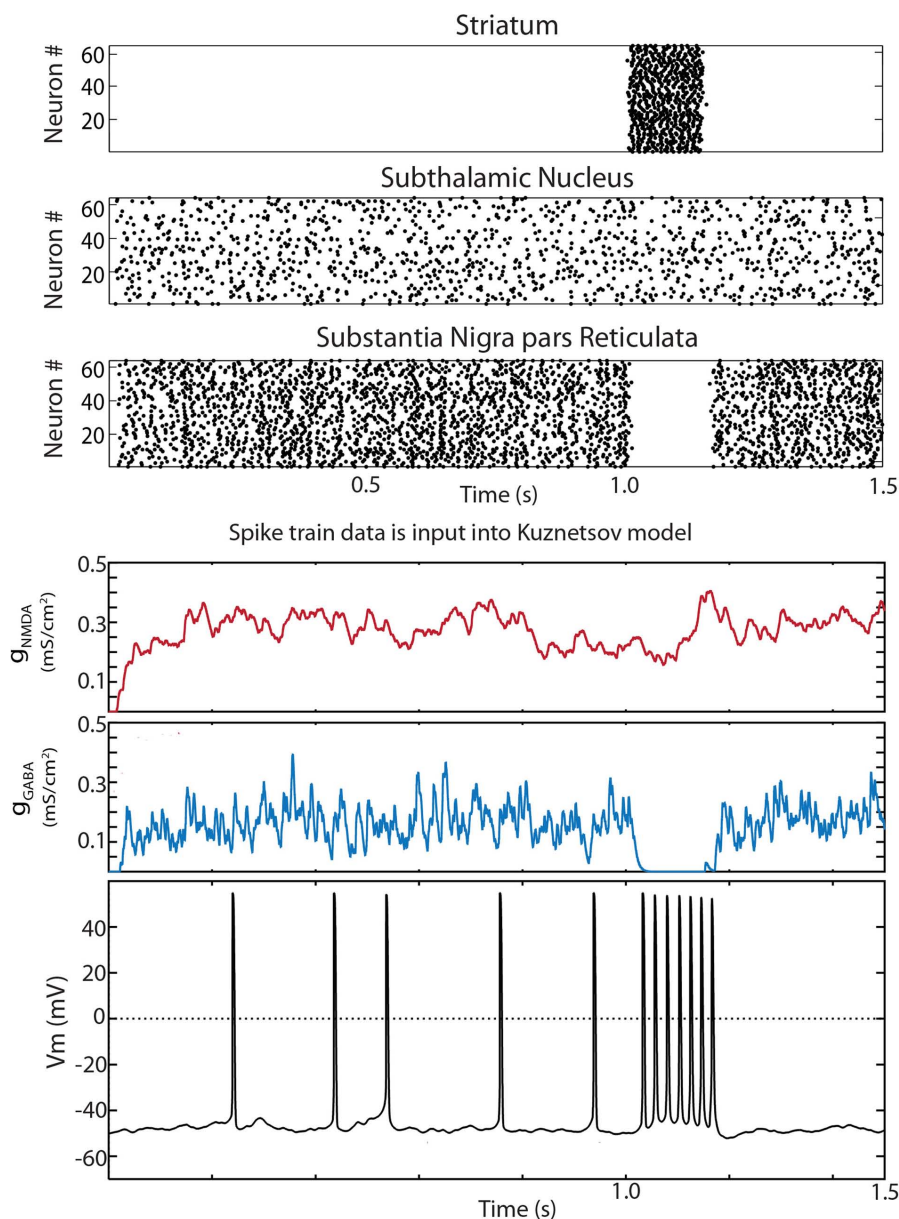


FIGURE 3 | Disinhibition bursts can be evoked by striatal stimulation in the reduced Humphries et al. (2006) model. Raster plots for the 64 neurons in the D1 striatum, STN and SNpr. The only connections present in the reduced model were D1 striatum to SNpr, STN–SNpc, STN–SNpr, and SNpr–SNpc. At 1 s all 64 D1 striatal projection neurons were activated by current injection for a period of 150 ms. The simulation was run for a total of

10 s. The input to a random SNpc neuron was captured, saved to a file, and read in by the modified Kuznetsov et al. (2006) model. The synaptic conductances and resulting trace are shown below. Conductances were initially set at zero. The dopaminergic neuron model fired single spikes at approximately 5 Hz and exhibited a burst of action potentials during the period of striatal stimulation.

What percentage of the medium spiny neurons must become activated to sufficiently inhibit the SNpr neurons to cause disinhibition bursting in the SNpc? In the previous simulations, all of the medium spiny neurons in the D1STR were stimulated at $t = 1000$ ms. Changing the probability that a D1STR neuron was stimulated had a large effect on the intra-burst firing frequency and

the number of spikes in the burst (**Figure 5**). The probability for which an individual D1STR neuron was stimulated was set to 0.03 (1 of 64 cells activated), 0.1, 0.25, 0.4, 0.6, 0.8, or 1.0. A high frequency burst of a significant number of spikes was generated in response to a stimulation of only a few neurons (**Figure 5**). Thus, even weak striatal stimulation can evoke bursts in dopaminergic neurons.

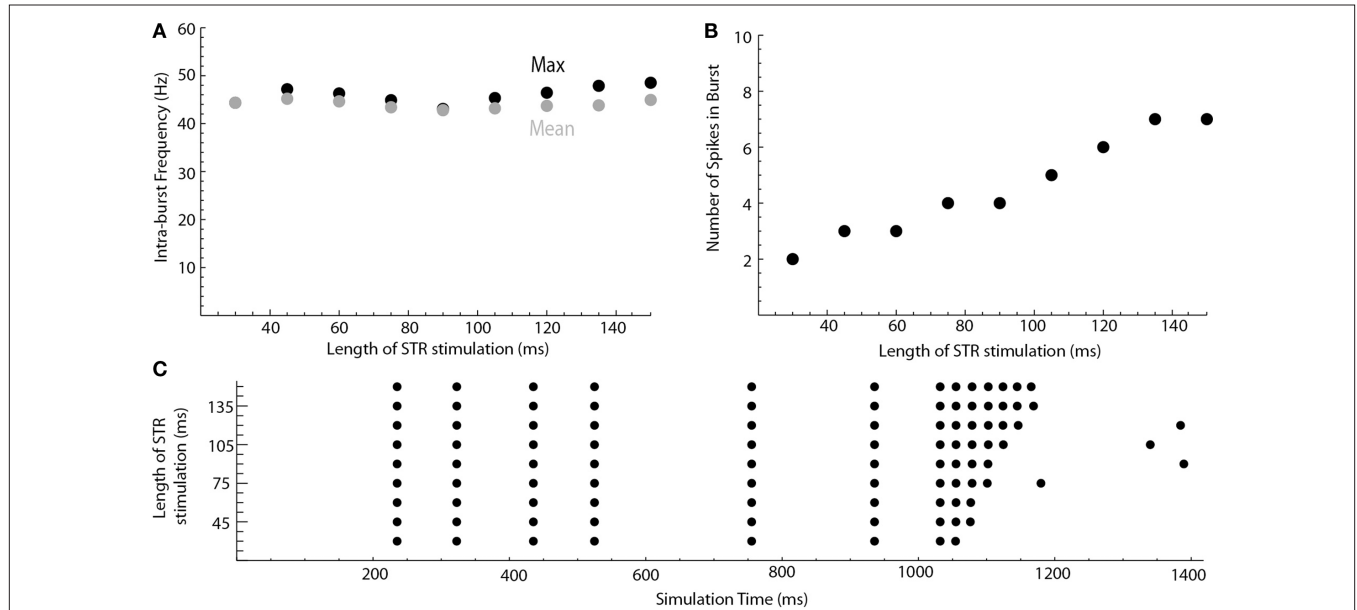


FIGURE 4 | Length of striatal stimulation controls the number of spikes in the disinhibition burst but not the intra-burst firing frequency. (A) Shows the intra-burst firing frequency of the disinhibition burst (max. black, mean gray). **(B)** Shows the number of spikes in the burst. A raster plot of the results is shown in **(C)**.

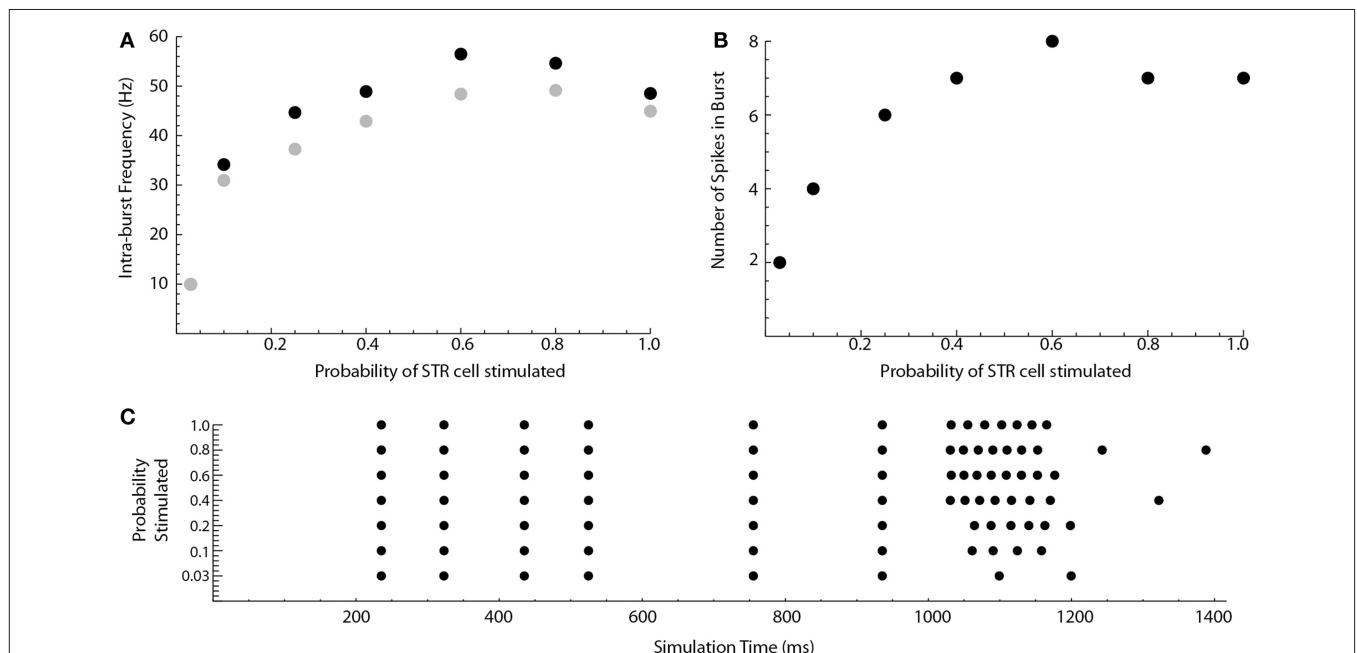


FIGURE 5 | Weak striatal stimulation can cause disinhibition bursts. The probability that a striatal cell will be stimulated at $t = 1000$ ms in the reduced Humphries model is varied. **(A)** Shows the intra-burst firing frequency of the disinhibition burst (max. black, mean gray). **(B)** Shows the number of spikes in the burst. A raster plot of the results is shown in **(C)**.

INDIRECT AND DIRECT PATHWAYS

Do dopaminergic neurons still evoke a burst when the indirect pathway is included in the model? The connections between GP–SNpc, GP–STN, STN–GP, GP–SNpr, and STN–SNpr were enabled. The constant current parameter for each cell type was modified such that the firing rates of the STN and SNpr were similar to the simulations presented in the previous section. Bursts were still evoked upon stimulation of all striatal neurons (**Figure 6**). Note that the inhibition is not completely removed during striatal stimulation. When the above indirect pathway connections were enabled in the network model, SNpc dopaminergic neurons received tonic inhibitory input from two sources: SNpr and GP. In the simulations shown in **Figure 6**, only SNpr neurons were inhibited upon D1STR stimulation. Thus, disinhibition need not be an all-or-none phenomenon (e.g., Lobb et al., 2011).

D1STR neurons projecting to the SNpr give off collaterals that terminate in the GP (Kawaguchi et al., 1990; Parent et al., 1995). This connection was added to the network model. Disinhibition bursting was enhanced by inclusion of the D1STR–GP connection (**Figure 7**). An example is shown in **Figure 7A** for a D1STR–GP weight of -1.0 . Near-maximal frequency bursting could be obtained with a connection strength of only 0.2 (in comparison with other connections, which have a weight of ± 1.0). The enhancement in SNpc activity is due to an inhibition of both GP and SNpr neurons (disinhibiting SNpc neurons) and a disinhibition of the STN through the GP (strongly exciting SNpc neurons). This suggests that striatal activation is a robust means by which bursts can be generated by SNpc dopaminergic neurons.

DISCUSSION

In this paper, we used computer simulations with network-generated time-varying conductances to explore disinhibition bursting in the basal ganglia. We first showed that the two-compartment

single cell model of the dopaminergic neuron maintained its ability to fire trains of action potentials when tonic NMDA and GABA_A conductances were applied. We then used a bifurcation analysis to map out the combinations of NMDA and GABA_A conductances for which the model was able to produce sustained trains of action potentials. As expected, increasing inhibition or lowering excitation shifts the dopaminergic neuron into the non-oscillatory region, resulting in a pause in spiking (as seen in Figure 3A of Lobb et al., 2010). The bifurcation analysis revealed that large increases in excitation can also cause the dopaminergic neuron to cross into the non-oscillatory region, with the cessation of spiking due to a depolarization block of sodium mediated action potentials. In contrast, for moderate levels of the NMDA conductance, spiking was maintained even after complete removal of inhibition.

Disinhibition bursts could be evoked through the D1STR–SNpr–SNpc pathway by phasic activation of the D1STR. The duration of the striatal stimulation is an important determinant of the number of spikes in the burst, but has little effect on its intra-burst firing frequency. Striatal inhibition of the SNpr is powerful and thus only a small percentage of striatal cells need to be activated to evoke a burst in dopaminergic neurons.

Tonic inhibition onto dopaminergic neurons is a combination of inputs from GP and SNpr. In our simulations, the firing rate of the GP and SNpr were similar, and thus silencing of the SNpr would only remove that percentage of the tonic inhibition. The burst in SNpc neurons is affected by the percentage of tonic inhibition that is removed by a disinhibitory stimulus such as striatal activation; specifically, increased removal of inhibition increases the intra-burst firing frequency of the disinhibition burst (Lobb et al., 2011).

Disinhibition of the SNpc was enhanced by including a collateral from D1STR to the GP. This was due to an inhibition of the GP (thereby disinhibiting SNpc) and subsequent disinhibition of the subthalamic nucleus (thereby exciting the SNpc). Another interesting question that

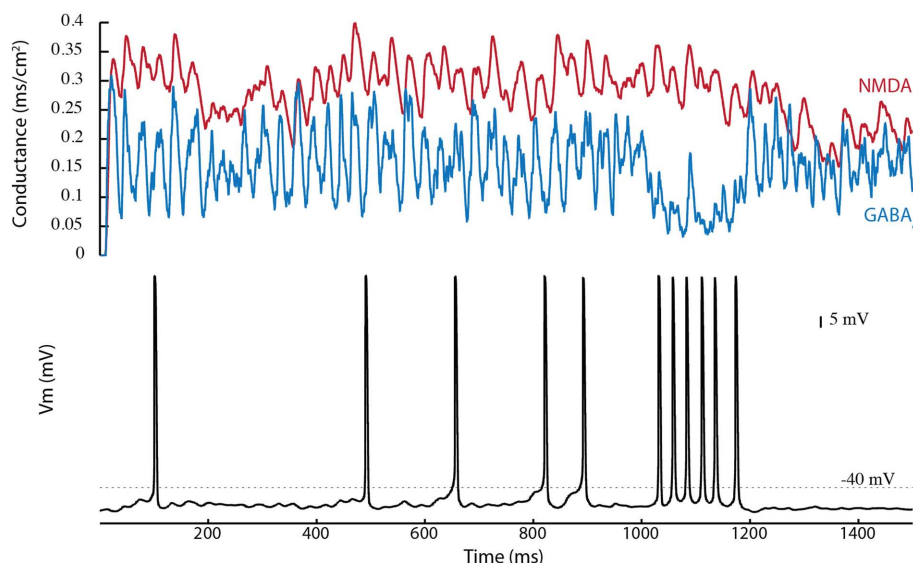


FIGURE 6 | Tonic inhibition by GP reduces direct pathway mediated disinhibition bursting in the Humphries et al. (2006) model. In the Humphries model, tonic inhibition is provided by both the GP and SNpr. All connections are added except the D1STR–GP connection. Since GP and SNpr have similar firing rates, silencing of the SNpr by striatal stimulation removes approximately half of the inhibition at $t = 1000$ ms. Disinhibition bursts can still be produced.

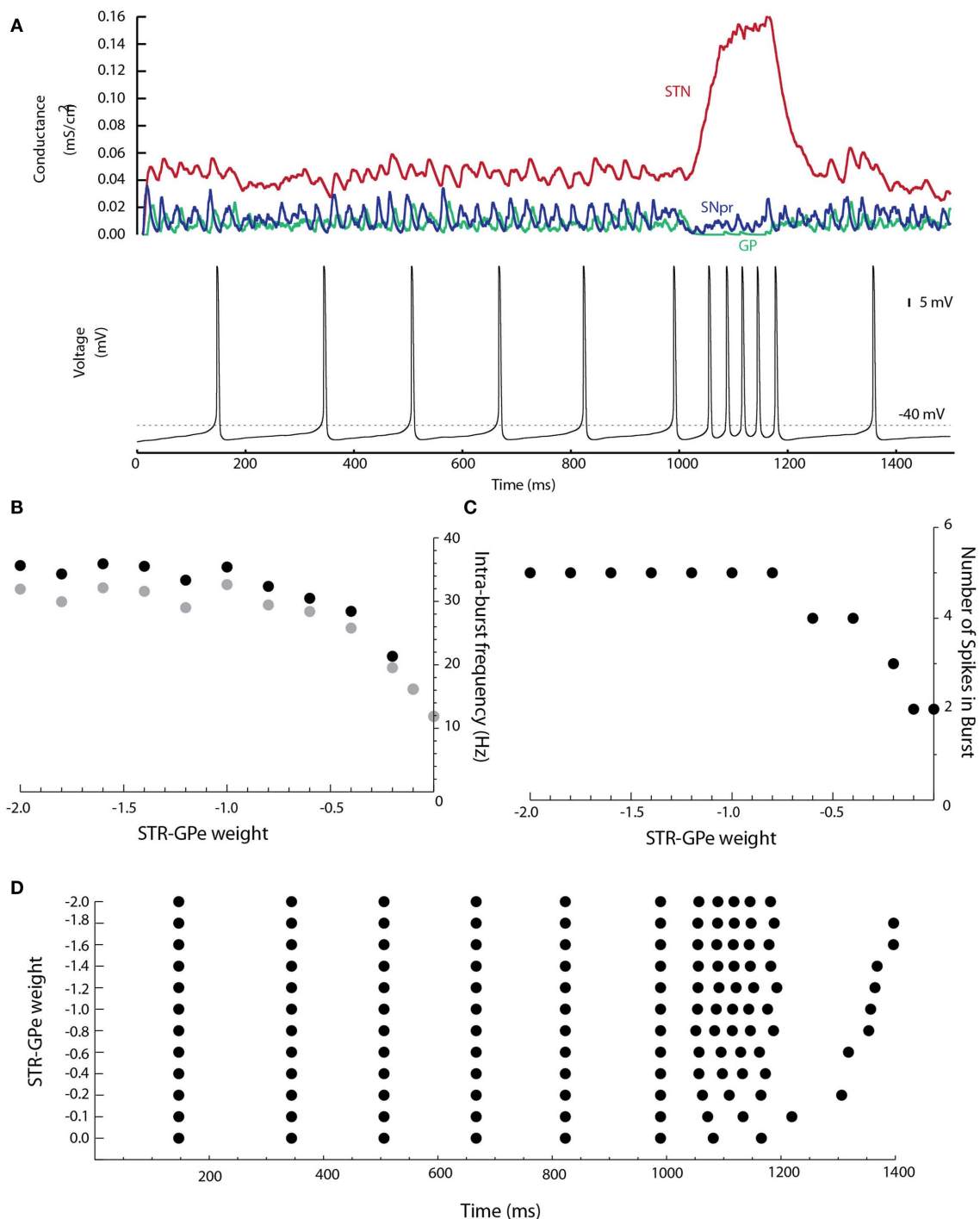


FIGURE 7 | The D1STR-GP connection promotes burst firing. (A) The D1STR-GP connection was added with a weight of -1.0 . The synaptic conductances generated in the network model from the STN (red), GP (green), and SNpr (blue) are shown on the top. The resulting voltage trace is shown below. **(B)** Shows the intra-burst firing frequency of the disinhibition burst (max

black, mean gray) as a function of the D1STR-GP weight. **(C)** Shows the number of spikes in the burst. A raster plot of the results is shown in **(D)**. To avoid ceiling effects, in these simulations δ was reduced to $\delta_{\text{GABA}} = 0.0043 \text{ ms/cm}^2$ and $\delta_{\text{NMDA}} = 0.0030 \text{ ms/cm}^2$ so that the mean tonic conductances were approximately $g_{\text{GABA}} = 0.02 \text{ ms/cm}^2$ and $g_{\text{NMDA}} = 0.04 \text{ ms/cm}^2$.

arises from these simulations is what the net effect of striatal stimulation will be on the SNpr and its disinhibition. The SNpr is inhibited by striatal activation but excited through the STN. The GP may also disinhibit the SNpr depending on whether striatopallidal inhibition is

stronger than recurrent pallidosubthalamic excitation. In these simulations, the net effect on the SNpr is an inhibition. To achieve effective disinhibition, the SNpr excitation through the indirect pathway should be minimized, e.g., by increasing the weight of D1STR-SNpr synapses.

In this model, only some of the basic features of these connections are implemented. Many features, such as a high degree of convergence from one nucleus onto another, the action of neuromodulators, synaptic enhancement or depression, and the presence of correlated activity within different nuclei are not included. We anticipate that factors such as these may play a large role in determining the weights of each connection and thus could have a major impact on bursting. Similarly, we have focused on stimulation of the D1-containing medium spiny neurons. Cortical activation of D2-containing medium spiny neurons may also evoke bursting in dopaminergic neurons similar to our results above. Finally, cortical activation may also evoke strong excitation in subthalamic neurons via the hyperdirect pathway. However, unlike striatal stimulation, activity in the GP and SNpr would be increased, thereby counteracting the

STN-mediated excitation, and reducing the frequency of the ensuing burst.

CONCLUSION

In summary, we investigated the high conductance state of the dopaminergic neuron and show that disinhibition bursts can be produced through the D1STR–SNpr–SNpc circuit. Inclusion of the indirect pathway actually promotes disinhibition bursting. Together, these results suggest that striatal activation of the SNpc is not just a feasible mechanism for evoking disinhibition bursts. Instead, it may provide a reliable and robust means of evoking bursts in dopaminergic neurons.

ACKNOWLEDGMENTS

This work was supported by NIH grants MH079276 to Carlos A. Paladini, and MH084494 to Collin J. Lobb.

REFERENCES

- Blythe, S. N., Atherton, J. E., and Bevan, M. D. (2007). Synaptic activation of dendritic AMPA and NMDA receptors generates transient high-frequency firing in substantia nigra dopamine neurons in vitro. *J. Neurophysiol.* 97, 2837–2850.
- Blythe, S. N., Wokosin, D., Atherton, J. E., and Bevan, M. D. (2009). Cellular mechanisms underlying burst firing in substantia nigra dopamine neurons. *J. Neurosci.* 29, 15531–15541.
- Brazhnik, E., Shah, F., and Tepper, J. M. (2008). GABAergic afferents activate both GABAA and GABAB receptors in mouse substantia nigra dopaminergic neurons in vivo. *J. Neurosci.* 28, 10386–10398.
- Charlley, P. J., Grenhoff, J., Chergui, K., De la Chapelle, B., Buda, M., Svensson, T. H., and Chouvet, G. (1991). Burst firing of mesencephalic dopamine neurons is inhibited by somatodendritic application of kynurenic acid. *Acta Physiol. Scand.* 142, 105–112.
- Chergui, K., Akaoka, H., Charlley, P. J., Saunier, C. F., Buda, M., and Chouvet, G. (1994). Subthalamic nucleus modulates burst firing of nigra dopamine neurons via NMDA receptors. *Neuroreport* 5, 1185–1188.
- Chergui, K., Charlley, P. J., Akaoka, H., Saunier, C. F., Brunet, J. L., Buda, M., Svensson, T. H., and Chouvet, G. (1993). Tonic activation of NMDA receptors causes spontaneous burst discharge of rat midbrain dopamine neurons in vivo. *Eur. J. Neurosci.* 5, 137–144.
- Christoffersen, C. L., and Meltzer, L. T. (1995). Evidence for N-methyl-D-aspartate and AMPA subtypes of the glutamate receptor on substantia nigra dopamine neurons: possible preferential role for N-methyl-D-aspartate receptors. *Neuroscience* 67, 373–381.
- Deister, C. A., Teagarden, M., Wilson, C. J., and Paladini, C. A. (2009). An intrinsic neuronal oscillator underlies dopaminergic neuron bursting. *J. Neurosci.* 29, 15888–15897.
- Ermentrout, B. (2002). *Simulating, Analyzing, and Animating Dynamical Systems: A Guide to Xppaut for Researchers and Students*. Philadelphia, PA: Society for Industrial and Applied Mathematics.
- Gerfen, C. R. (1984). The neostriatal mosaic: compartmentalization of corticostriatal input and striatonigral output systems. *Nature* 311, 461–464.
- Grace, A. A., and Bunney, B. S. (1984). The control of firing pattern in nigral dopamine neurons: burst firing. *J. Neurosci.* 4, 2877–2890.
- Grace, A. A., and Bunney, B. S. (1985). Opposing effects of striatonigral feedback pathways on midbrain dopamine cell activity. *Brain Res.* 333, 271–284.
- Grace, A. A., and Onn, S. P. (1989). Morphology and electrophysiological properties of immunocytochemically identified rat dopamine neurons recorded in vitro. *J. Neurosci.* 9, 3463–3481.
- Grenhoff, J., Aston-Jones, G., and Svensson, T. H. (1986). Nicotinic effects on the firing pattern of midbrain dopamine neurons. *Acta Physiol. Scand.* 128, 351–358.
- Guzman, J. N., Sánchez-Padilla, J., Chan, C. S., and Surmeier, D. J. (2009). Robust pacemaking in substantia nigra dopaminergic neurons. *J. Neurosci.* 29, 11011–11019.
- Horvitz, J. C., Stewart, T., and Jacobs, B. L. (1997). Burst activity of ventral tegmental dopamine neurons is elicited by sensory stimuli in the awake cat. *Brain Res.* 759, 251–258.
- Humphries, M. D., Stewart, R. D., and Gurney, K. N. (2006). A physiologically plausible model of action selection and oscillatory activity in the basal ganglia. *J. Neurosci.* 26, 12921–12942.
- Jin, X., and Costa, R. M. (2010). Start/stop signals emerge in nigrostriatal circuits during sequence learning. *Nature* 466, 457–462.
- Kawaguchi, Y., Wilson, C. J., and Emson, P. C. (1990). Projection subtypes of rat neostriatal matrix cells revealed by intracellular injection of biocytin. *J. Neurosci.* 10, 3421–3438.
- Khaliq, Z. M., and Bean, B. P. (2010). Pacemaking in dopaminergic ventral tegmental area neurons: depolarizing drive from background and voltage-dependent sodium conductances. *J. Neurosci.* 30, 7401–7413.
- Kita, T., Kita, H., and Kitai, S. T. (1986). Electrical membrane properties of rat substantia nigra compacta neurons in an in vitro slice preparation. *Brain Res.* 372, 21–30.
- Kuznetsov, A. S., Kopell, N. J., and Wilson, C. J. (2006). Transient high-frequency firing in a coupled-oscillator model of the mesencephalic dopaminergic neuron. *J. Neurophysiol.* 95, 932–947.
- Lobb, C. J., Wilson, C. J., and Paladini, C. A. (2010). A dynamic role for GABA receptors on the firing pattern of midbrain dopaminergic neurons. *J. Neurophysiol.* 104, 403–413.
- Lobb, C. J., Wilson, C. J., and Paladini, C. A. (2011). High frequency, short latency disinhibition bursting of midbrain dopaminergic neurons. *J. Neurophysiol.* doi: 10.1152/jn.01076.2010. [Epub ahead of print].
- Morikawa, H., Khodakhah, K., and Williams, J. T. (2003). Two intracellular pathways mediate metabotropic glutamate receptor-induced Ca²⁺ mobilization in dopamine neurons. *J. Neurosci.* 23, 149–157.
- Overton, P., and Clark, D. (1992). Ionophoretically administered drugs acting at the N-methyl-D-aspartate receptor modulate burst firing in A9 dopamine neurons in the rat. *Synapse* 10, 131–140.
- Paladini, C. A., and Tepper, J. M. (1999). GABA(A) and GABA(B) antagonists differentially affect the firing pattern of substantia nigra dopaminergic neurons in vivo. *Synapse* 32, 165–176.
- Parent, A., Charara, A., and Pinault, D. (1995). Single striatofugal axons arborizing in both pallidal segments and in the substantia nigra in primates. *Brain Res.* 698, 280–284.
- Redgrave, P., Prescott, T. J., and Gurney, K. (1990). Is the short-latency dopamine response too short to signal reward error? *Trends Neurosci.* 22, 146–161.
- Schultz, W. (1998). Predictive reward signal of dopamine neurons. *J. Neurophysiol.* 80, 1–27.
- Schultz, W., Dayan, P., and Montague, P. R. (1997). A neural substrate of prediction and reward. *Science* 275, 1593–1599.
- Smith, I. D., and Grace, A. A. (1992). Role of the subthalamic nucleus in the regulation of nigral dopamine neuron activity. *Synapse* 12, 287–303.
- Tepper, J. M., and Lee, C. R. (2007). GABAergic control of substantia nigra dopaminergic neurons. *Prog. Brain Res.* 160, 189–208.
- Wilson, C. J., and Callaway, J. C. (2000). Coupled oscillator model of the dopaminergic neuron of the substantia nigra. *J. Neurophysiol.* 83, 3084–3100.

Conflict of Interest Statement: The authors declare that the research was conducted in the absence of any commercial or financial relationships that could be construed as a potential conflict of interest.

Received: 26 January 2011; accepted: 26 April 2011; published online: 10 May 2011.
Citation: Lobb CJ, Troyer TW, Wilson CJ and Paladini CA (2011) Disinhibition bursting of dopaminergic neurons. *Front. Syst. Neurosci.* 5:25. doi: 10.3389/fnsys.2011.00025
Copyright © 2011 Lobb, Troyer, Wilson and Paladini. This is an open-access article subject to a non-exclusive license between the authors and Frontiers Media SA, which permits use, distribution and reproduction in other forums, provided the original authors and source are credited and other Frontiers conditions are complied with.



Regulation of substantia nigra pars reticulata GABAergic neuron activity by H_2O_2 via flufenamic acid-sensitive channels and K_{ATP} channels

Christian R. Lee¹, Paul Witkovsky² and Margaret E. Rice^{1,3*}

¹ Department of Neurosurgery, New York University School of Medicine, New York, NY, USA

² Department of Ophthalmology, New York University School of Medicine, New York, NY, USA

³ Department of Physiology and Neuroscience, New York University School of Medicine, New York, NY, USA

Edited by:

James M. Tepper, Rutgers, The State University of New Jersey, USA

Reviewed by:

Mark D. Bevan, Northwestern University, USA

José Vargas, National Autonomous University of Mexico, Mexico

*Correspondence:

Margaret E. Rice, Department of Physiology and Neuroscience, New York University School of Medicine, 550 First Avenue, New York, NY 10016, USA.

e-mail: margaret.rice@nyu.edu

Substantia nigra pars reticulata (SNr) GABAergic neurons are key output neurons of the basal ganglia. Given the role of these neurons in motor control, it is important to understand factors that regulate their firing rate and pattern. One potential regulator is hydrogen peroxide (H_2O_2), a reactive oxygen species that is increasingly recognized as a neuromodulator. We used whole-cell current clamp recordings of SNr GABAergic neurons in guinea-pig midbrain slices to determine how H_2O_2 affects the activity of these neurons and to explore the classes of ion channels underlying those effects. Elevation of H_2O_2 levels caused an increase in the spontaneous firing rate of SNr GABAergic neurons, whether by application of exogenous H_2O_2 or amplification of endogenous H_2O_2 through inhibition of glutathione peroxidase with mercaptosuccinate. This effect was reversed by flufenamic acid (FFA), implicating transient receptor potential (TRP) channels. Conversely, depletion of endogenous H_2O_2 by catalase, a peroxidase enzyme, decreased spontaneous firing rate and firing precision of SNr neurons, demonstrating tonic control of firing rate by H_2O_2 . Elevation of H_2O_2 in the presence of FFA revealed an inhibition of tonic firing that was prevented by blockade of ATP-sensitive K^+ (K_{ATP}) channels with glibenclamide. In contrast to guinea-pig SNr neurons, the dominant effect of H_2O_2 elevation in mouse SNr GABAergic neurons was hyperpolarization, indicating a species difference in H_2O_2 -dependent regulation. Thus, H_2O_2 is an endogenous modulator of SNr GABAergic neurons, acting primarily through presumed TRP channels in guinea-pig SNr, with additional modulation via K_{ATP} channels to regulate SNr output.

Keywords: basal ganglia, diffusible messenger, GABA, hydrogen peroxide, reactive oxygen species, TRP channels

INTRODUCTION

The GABAergic neurons of the substantia nigra pars reticulata (SNr) comprise one of the major output nuclei of the basal ganglia, and convey information from the basal ganglia network through projections that target the thalamus and superior colliculus, as well as other nuclei including the pedunculopontine nucleus and the mesencephalic locomotor region (Beckstead and Frankfurter, 1982; Deniau and Chevalier, 1992; Redgrave et al., 1992; Mana and Chevalier, 2001; Takakusaki et al., 2003; Cebrián et al., 2005; Lee and Tepper, 2007a; Nambu, 2007). Identifying intrinsic membrane conductances and extrinsic factors that influence the excitability of these neurons is therefore important for understanding regulation of movement by the basal ganglia.

Substantia nigra pars reticulata GABAergic neurons are spontaneously active *in vivo* and *in vitro* (Wilson et al., 1977; Deniau et al., 1978; Guyenet and Aghajanian, 1978; Nakanishi et al., 1987; Lacey et al., 1989; Yung et al., 1991; Stanford and Lacey, 1996; Richards et al., 1997; Atherton and Bevan, 2005; Lee and Tepper, 2007b; Zhou et al., 2008). A variety of conductances contribute to this tonic firing, and spontaneous activity persists in the absence of synaptic input indicating that it is intrinsically generated (Atherton and

Bevan, 2005). Tonic firing can be modulated, however, by synaptic input as well as by activation of membrane conductances that cause changes in firing rate and pattern (Rick and Lacey, 1994; Stanford and Lacey, 1996; Shen and Johnson, 2006; Zhou et al., 2006, 2008; Ibáñez-Sandoval et al., 2007). Among the important membrane conductances in SNr GABAergic neurons are those mediated by transient receptor potential (TRP) channels (Lee and Tepper, 2007b; Zhou et al., 2008). A number of TRP channel subfamilies are expressed in the CNS (Clapham et al., 2003, 2005), and the canonical TRP type-3 (TRPC3) channel has been identified as a regulator of SNr GABAergic neuron excitability in neonatal mice (Zhou et al., 2008). Activation of TRPC3 channels in SNr neurons increases the firing rate of these cells and contributes to the tonic depolarization that maintains their spontaneous firing (Zhou et al., 2008, 2009). In addition, TRP channel activation may underlie a depolarizing plateau potential observed in these neurons (Lee and Tepper, 2007b). A potential opponent of TRP channel activity is ATP-sensitive K^+ (K_{ATP}) channels, which can cause membrane hyperpolarization and suppress firing in SNr GABAergic neurons (Schwanstecher and Panten, 1993; Stanford and Lacey, 1996; Dunn-Meynell et al., 1998).

The emerging neuromodulator hydrogen peroxide (H₂O₂) can activate both some TRP channels and K_{ATP} channels (Ichinari et al., 1996; Herson and Ashford, 1997; Tokube et al., 1998; Hara et al., 2002; Avshalumov and Rice, 2003; Avshalumov et al., 2005; Bao et al., 2005; Freestone et al., 2009). Through these effects, H₂O₂ has been shown to be an important neuromodulator in basal ganglia neurons, including striatal medium spiny neurons (MSNs), which are depolarized by H₂O₂ through a TRP channel-dependent mechanism (Bao et al., 2005), and dopaminergic (DAergic) neurons of the substantia nigra pars compacta (SNc), which are hyperpolarized by activation of K_{ATP} channels (Avshalumov et al., 2005). Whether H₂O₂ has a neuromodulatory action on SNr GABAergic neurons is unknown. Here, we investigated regulation of SNr GABAergic neuron activity by H₂O₂ using whole-cell current clamp recordings of visualized SNr GABAergic neurons in guinea-pig and mouse midbrain slices. In marked contrast to the inhibitory effect of H₂O₂ on SNc DAergic neurons, we found that SNr GABAergic neurons in guinea pig are excited by H₂O₂. Pharmacological methods implicated TRP channels as probable targets of H₂O₂ signaling in these neurons. However, SNr GABAergic neurons recorded from mouse are inhibited by H₂O₂. These results reveal a new mechanism regulating basal ganglia output via H₂O₂-dependent modulation of SNr neuron firing.

MATERIALS AND METHODS

SLICE PREPARATION

Whole-cell recordings were obtained in midbrain slices containing the substantia nigra (SN) from adult male guinea pigs (Hartley, 150–250 g) or mice (C57BL/6, 120 days). All procedures were performed in accordance with the National Institutes of Health *Guide for the Care and Use of Laboratory Animals* and with the approval of the New York University School of Medicine Institutional Animal Care and Use Committee. Procedures for preparation of midbrain slices were similar to those described previously (Avshalumov et al., 2005; Lee and Tepper, 2007a,b). Briefly, animals were deeply anesthetized with 50 mg/kg pentobarbital administered i.p., then transcardially perfused with ice-cold solution containing (in mM): 225 sucrose; 2.5 KCl; 0.5 CaCl₂; 7 MgCl₂; 28 NaHCO₃; 1.25 NaH₂PO₄; 7 glucose; 1 ascorbate; and 3 pyruvate, equilibrated with 95% O₂/5% CO₂. The brain was quickly removed, trimmed to a block containing the midbrain, and sectioned at 300 μm in the same medium using a Leica VT1200S vibrating blade microtome (Leica Microsystems, Bannockburn, IL, USA). Slices were immediately transferred to warmed (34°C) recovery medium containing (in mM): 125 NaCl; 2.5 KCl; 1.25 NaH₂PO₄; 25 NaHCO₃; 1 MgCl₂; 2 CaCl₂; 25 glucose; 1 ascorbate; 3 pyruvate; and 0.4 myo-inositol, equilibrated with 95% O₂/5% CO₂, which gradually cooled to room temperature over the next hour; slices were maintained in this medium until use. Physiological recording was conducted in a submersion recording chamber, with slices continuously superfused at 1.4 mL/min with artificial cerebrospinal fluid (aCSF) at 32°C containing (in mM): 124 NaCl; 3.7 KCl; 26 NaHCO₃; 2.4 CaCl₂; 1.3 MgSO₄; 1.3 KH₂PO₄; and 10 glucose, equilibrated with 95% O₂/5% CO₂.

VISUALIZED WHOLE-CELL RECORDING

Neurons were visualized at 40× using a water-immersion objective on an Olympus BX51WI microscope equipped with infrared differential interference contrast (IR-DIC) optics (Olympus America,

Center Valley, PA, USA). Pipettes were constructed from 1.5 mm o.d. borosilicate capillary tubing (World Precision Instruments, Sarasota, FL, USA) using a Sutter P-97 Flaming/Brown micropipette puller (Sutter Instrument Company, Novato, CA, USA) and filled with a solution containing (in mM): 129 potassium gluconate, 11 KCl, 10 HEPES, 2 MgCl₂, 10 EGTA, 3 Na₂-ATP, and 0.3 Na₃-GTP, which was titrated to a pH of 7.3 with KOH. In some experiments, the pipette backfill also included an H₂O₂-sensitive fluorescent probe as described below. Pipettes had resistances of 3–6 MΩ. Recordings were obtained using an Axopatch 200B amplifier, low pass filtered at 2 kHz, and digitized by a Digidata 1322A connected to a personal computer running Clampex 9 (Molecular Devices, Sunnyvale, CA, USA). In the present experiments, we used visualized whole-cell current clamp recordings to allow for control of the intracellular and extracellular environments in neurons while monitoring how H₂O₂ affects the spontaneous activity of these cells. Previous studies found no differences in the firing rate and regularity of firing between whole-cell and perforated-patch recordings in SNr GABAergic neurons (Atherton and Bevan, 2005).

The SN contains both DAergic and GABAergic neurons which can be distinguished by their electrophysiological characteristics. When compared to DAergic neurons, nigral GABAergic neurons recorded in guinea-pig slices *in vitro* have a higher spontaneous firing rate, narrower action potential, shorter duration after hyperpolarization (AHP), and a less pronounced sag in response to hyperpolarizing current pulses (Hainsworth et al., 1991; Yung et al., 1991; Hajós and Greenfield, 1994), characteristics that are indistinguishable from those observed in rat SNr GABAergic neurons (Matsuda et al., 1987; Nakanishi et al., 1987; Grace and Onn, 1989; Lacey et al., 1989; Richards et al., 1997; Gulácsi et al., 2003; Lee and Tepper, 2007a,b). Data presented are from neurons determined to be GABAergic based on these characteristics.

FLUORESCENT IMAGING OF H₂O₂

Fluorescent imaging of H₂O₂ was carried out using methods similar to those described previously (Avshalumov et al., 2005, 2007, 2008; Bao et al., 2005). The H₂O₂-sensitive indicator 5-(and-6)-chloromethyl-2',7'-dichlorodihydrofluorescein diacetate, acetyl ester (CM-H₂DCF-DA, Invitrogen, Carlsbad, CA, USA) was loaded into individual neurons via the pipette backfill solution. For these experiments, stock solutions of CM-H₂DCF-DA were made in ethanol with 10% v/v KOH (8 N); the final concentration of indicator in the pipette solution was 8 μM. Following electrophysiological identification of SNr GABAergic neurons, cells were held for 20 min before imaging to allow the indicator to infiltrate the recorded cell (Avshalumov et al., 2005). After diacetate cleavage, the parent molecule H₂DCF becomes fluorescent DCF when oxidized by H₂O₂ or other reactive oxygen species. Excitation wavelength (488 nm) was controlled by a DeltaRam monochromator (Photon Technology International, Birmingham, NJ, USA) and emission at 535 nm detected using an IC-200 CCD camera (Photon Technology International). Images were acquired at 1 Hz with 30 ms exposure and eight frame averaging using ImageMaster 5.0 (Photon Technology International).

DRUGS AND CHEMICALS

All components of physiological solutions, as well as H₂O₂, mercaptosuccinate (MCS), flufenamic acid (FFA), and glibenclamide were purchased from Sigma-Aldrich (St. Louis, MO, USA). Tetrodotoxin

(TTX) citrate and 2-aminoethoxydiphenyl borate (2-APB) were purchased from Tocris Bioscience (Ellisville, MO, USA). Catalase (bovine liver) was purchased from Calbiochem (San Diego, CA, USA). Solutions of H₂O₂, MCS, and catalase were made fresh daily. Solutions of FFA, 2-APB, and glibenclamide were prepared in DMSO (Sigma-Aldrich) before dilution in aCSF; final concentrations of DMSO did not exceed 0.05%, which was also present in control aCSF for studies with these agents. All other agents were added directly to aCSF; application of all agents to slices via the superfusing aCSF did not exceed 20 min.

DATA ANALYSIS

Electrophysiological data were analyzed using Clampfit 9 (Molecular Devices). Spontaneous firing rates were determined from 60 s of spontaneous activity with zero holding current under control conditions and during the period of maximal effect following drug or enzyme application. Maximal effects were observed within 10 min of application. Neurons that did not exhibit a steady baseline firing rate under control conditions were excluded from analysis. Regularity of firing was assessed from the coefficient of variation (CV) which was calculated as the standard deviation of the interspike interval divided by the mean interspike interval (Atherton and Bevan, 2005). Action potential parameters were measured from spike threshold, which was determined manually. Membrane potential between action potentials was measured from a region just after repolarization of the AHP and just prior to depolarization preceding the next action potential. Voltages were corrected for the liquid junction potential which was estimated to be 13 mV using JPCalc (Barry, 1994).

Fluorescence imaging data were analyzed using ImageMaster 5.0 (Photon Technology International) to determine the fluorescence intensity (FI) for a region of interest in each frame drawn around the cell body. Background fluorescence was measured from an area within the same field of view but outside of the region of interest and subtracted from the region of interest. The resulting FI was normalized and data are presented as [(intensity – basal)/ (basal)] × 100%.

All data are presented as mean ± SEM. Statistical evaluation of the data was conducted using paired *t*-tests or repeated measures ANOVA followed by pairwise contrasts to assess significance between groups using SAS (SAS Institute, Cary, NC, USA). Differences were considered significant with *p* < 0.05.

RESULTS

H₂O₂ INCREASES THE SPONTANEOUS FIRING RATE OF GUINEA-PIG SNr GABAergic NEURONS

To assess the sensitivity of SNr GABAergic neurons to H₂O₂, we first examined the effect of exogenous H₂O₂ (1.5 mM, Chen et al., 2001; Avshalumov et al., 2005). In contrast to the suppression of firing seen in a large proportion of SNc DAergic neurons (Avshalumov et al., 2005), exogenous H₂O₂ augmented the spontaneous firing rate of SNr GABAergic neurons from 15.9 ± 1.2 Hz in control conditions to 21.6 ± 1.5 Hz in H₂O₂ (Figures 1A–C; *n* = 23; *t* = 6.53; *p* < 0.001). Firing rate increased in all SNr neurons tested, with an average increase of 39 ± 6%. The H₂O₂-induced increase reached a maximum after an average latency of 4.2 ± 0.5 min following H₂O₂ entry into the recording chamber. Previous studies demonstrated an

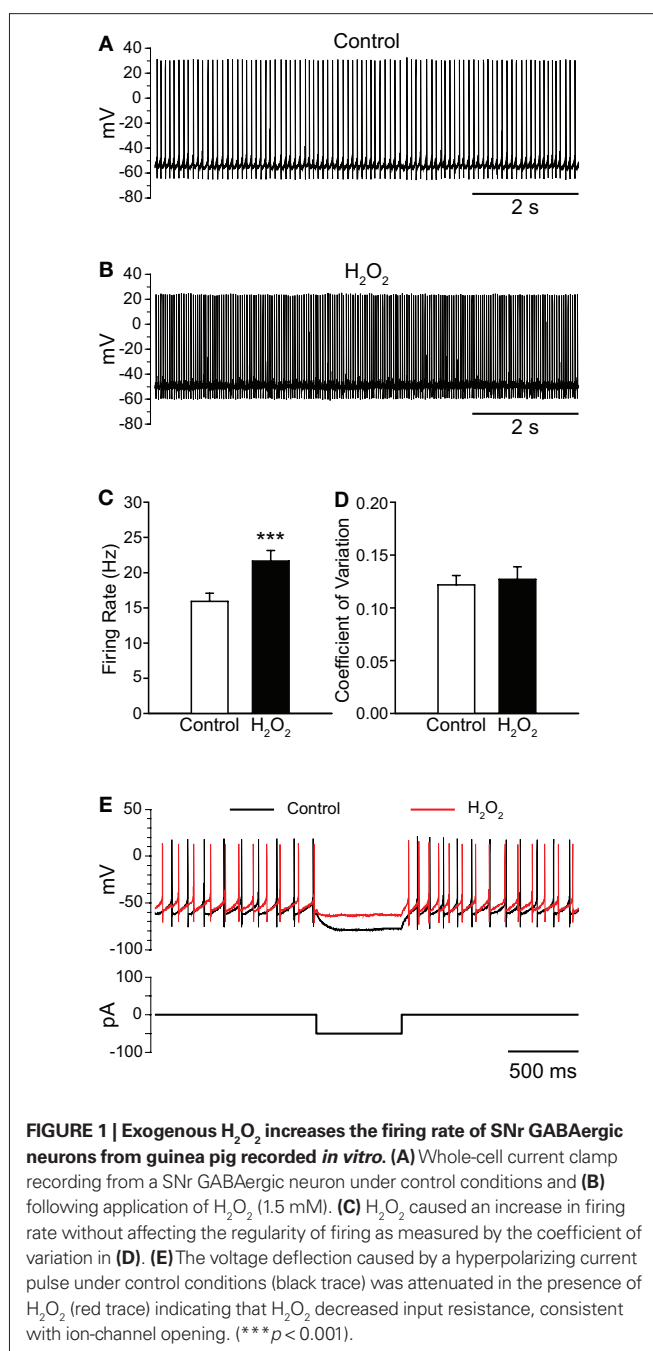


FIGURE 1 | Exogenous H₂O₂ increases the firing rate of SNr GABAergic neurons from guinea pig recorded *in vitro*. (A) Whole-cell current clamp recording from a SNr GABAergic neuron under control conditions and (B) following application of H₂O₂ (1.5 mM). (C) H₂O₂ caused an increase in firing rate without affecting the regularity of firing as measured by the coefficient of variation in (D). (E) The voltage deflection caused by a hyperpolarizing current pulse under control conditions (black trace) was attenuated in the presence of H₂O₂ (red trace) indicating that H₂O₂ decreased input resistance, consistent with ion-channel opening. (***) *p* < 0.001.

absence of oxidative damage in brain slices with this concentration of H₂O₂ under similar conditions (Chen et al., 2001). Importantly, the effect of H₂O₂ on SNr neurons was reversible, providing evidence for the absence of toxicity in the present studies (control 14.2 ± 2.1 Hz; H₂O₂ 18.4 ± 3.2 Hz; washout 14.0 ± 2.3 Hz; *n* = 5; *F*_(2,8) = 13.68; *p* < 0.01; control vs. washout *p* > 0.05).

The increase in firing rate elicited by H₂O₂ elevation was not accompanied by a change in the regularity of firing, as measured by the CV of interspike intervals, which was 0.122 ± 0.009 in control conditions and 0.127 ± 0.012 in the presence of H₂O₂ (Figure 1D; *p* > 0.05). Additionally, when a hyperpolarizing current pulse was delivered to SNr neurons from rest, the voltage deflection observed

in the presence of H₂O₂ was strongly attenuated relative to that elicited under control conditions (**Figure 1E**), indicating decreased input resistance, consistent with ion-channel opening in the presence of H₂O₂.

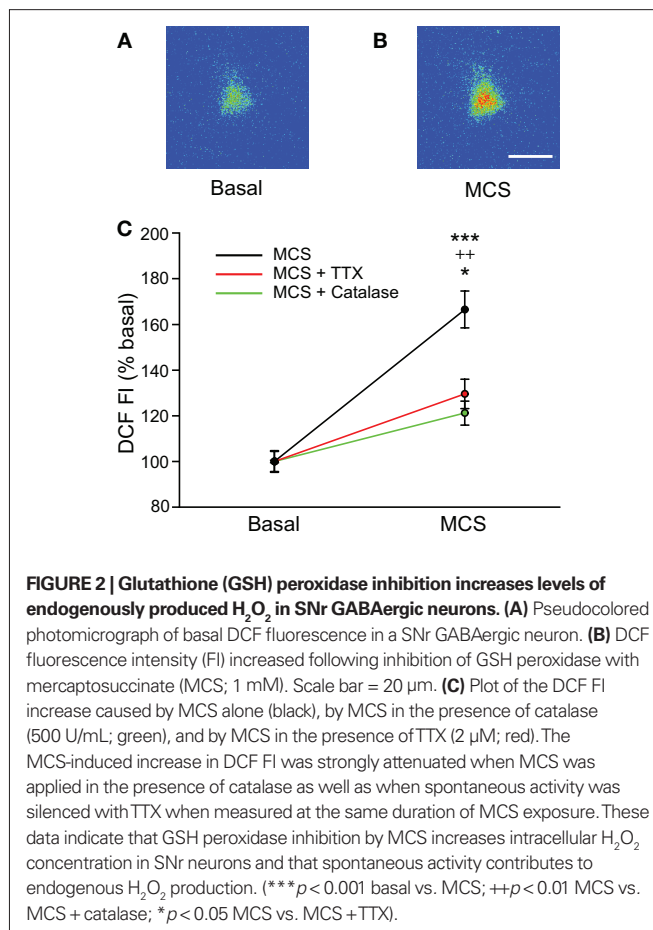
Elevation of H₂O₂ also caused slight, but significant changes to several action potential parameters, including depolarization of action potential threshold from -48.0 ± 0.9 to -46.7 ± 0.9 mV in H₂O₂ ($n = 23$; $t = 3.08$; $p < 0.01$) and attenuation of spike amplitude from 67.1 ± 1.8 to 61.7 ± 1.7 mV ($n = 23$; $t = -4.32$; $p < 0.001$). The amplitude of spike AHP was also attenuated from -28.2 ± 0.6 to -26.2 ± 0.8 mV in the presence of H₂O₂ ($n = 23$; $t = 4.55$; $p < 0.001$). Lastly, membrane potential measured between action potentials was depolarized from -60.2 ± 0.9 to -58.2 ± 1.0 mV in the presence of H₂O₂ ($n = 23$; $t = 4.39$; $p < 0.001$).

SNr GABAergic NEURONS ARE EXCITED BY ELEVATED LEVELS OF ENDOGENOUS H₂O₂

The use of exogenous H₂O₂ established that this potential modulator can affect the spontaneous firing rate of SNr GABAergic neurons. We next examined whether elevation of *endogenously* produced H₂O₂ also alters the activity of these cells. For these experiments, basal levels of H₂O₂ were enhanced by inhibiting glutathione (GSH) peroxidase, an H₂O₂ metabolizing enzyme, with MCS (1 mM; Avshalumov et al., 2005). The ability of MCS to enhance endogenous H₂O₂ levels was verified by monitoring H₂O₂-sensitive DCF fluorescence. Application of MCS led to an increase in DCF FI in guinea-pig SNr GABAergic neurons that reached a plateau 8.3 \pm 0.7 min after MCS entered the recording chamber, with an average increase to $166 \pm 8\%$ of basal FI (**Figures 2A–C**; $n = 12$; $t = 11.45$; $p < 0.001$). It should be noted that oxidation of H₂DCF to fluorescent DCF is irreversible, precluding washout measurements. The increase in DCF FI induced by MCS was strongly attenuated when applied simultaneously with the H₂O₂ metabolizing enzyme, catalase (500 U/mL; Avshalumov et al., 2003; $n = 7$; $F_{(1,17)} = 27.01$; $p < 0.001$ two-way repeated measures ANOVA), confirming that the DCF signal was largely H₂O₂ dependent (**Figure 2C**).

We hypothesized that tonic H₂O₂ generation in SNr GABAergic neurons was activity dependent, given the spontaneous activity of these cells in slice preparations (Richards et al., 1997; Gulácsi et al., 2003; Atherton and Bevan, 2005; Lee and Tepper, 2007a,b). To test this, we examined the effect of MCS on DCF FI after blocking spontaneous activity with TTX (2 μ M). Under these conditions, the increase in DCF FI measured at the time of maximal increase in DCF FI in MCS alone was significantly attenuated compared to that seen with normal activity (**Figure 2C**; $n = 5$; $F_{(1,15)} = 15.85$; $p < 0.01$ two-way repeated measures ANOVA). The attenuated increase in DCF FI in TTX was still significant compared to basal DCF FI ($t = 13.38$; $p < 0.001$), likely reflecting the small amount of H₂O₂ produced during basal metabolism. These data indicate that the MCS-induced increase in DCF FI in SNr GABAergic neurons largely reflects amplification of activity-dependent H₂O₂ levels.

As with exogenous H₂O₂, elevation of endogenous H₂O₂ by MCS caused a significant increase in the spontaneous firing rate of guinea-pig SNr GABAergic neurons from 13.6 ± 0.8 to 17.6 ± 1.2 Hz (**Figures 3A–C**; $n = 29$; $t = 6.00$; $p < 0.001$), with an average increase of $30 \pm 4\%$. Maximal effects were seen 7.8 \pm 0.6 min after MCS application. This was slightly longer than that seen with exogenous H₂O₂,

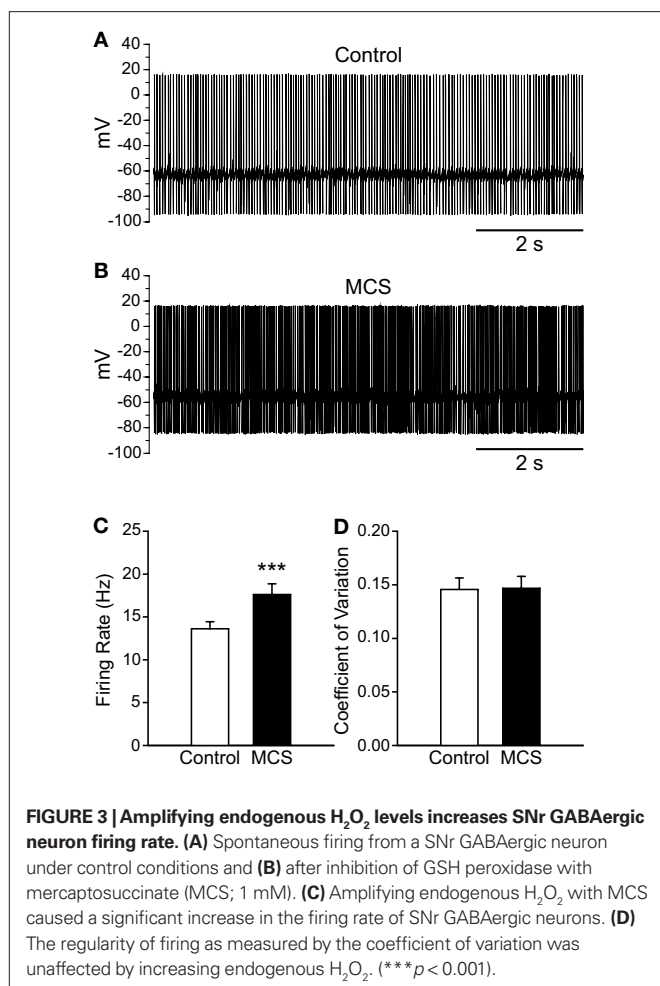


presumably reflecting the time required for enzyme inhibition and endogenous H₂O₂ accumulation. Most neurons (28/29) responded to MCS with an increase in firing rate, though one exhibited a decrease. The increase was reversible upon washout of MCS with aCSF (control 12.3 ± 1.2 Hz; MCS 14.6 ± 1.6 Hz; washout 11.8 ± 1.3 Hz; $n = 5$; $F_{(2,8)} = 9.16$; $p < 0.01$; control vs. washout $p > 0.05$), again indicating that the effect of H₂O₂ on cell firing is not a consequence of irreversible oxidative damage. The regularity of firing was unaffected by MCS, as reflected in the CV which was 0.146 ± 0.011 under control conditions and 0.147 ± 0.011 in MCS (**Figure 3D**; $p > 0.05$).

Several small changes in action potential parameters were seen when endogenous H₂O₂ levels were enhanced with MCS, including depolarization of action potential threshold from -48.5 ± 1.6 to -44.6 ± 1.7 mV in MCS ($n = 21$; $t = 4.62$; $p < 0.001$) and attenuation of spike amplitude from 75.1 ± 1.7 to 70.4 ± 1.6 mV ($n = 21$; $t = -6.83$; $p < 0.001$). Action potential AHP was attenuated from -27.8 ± 1.1 to -25.3 ± 1.1 mV in MCS ($n = 21$; $t = 5.46$; $p < 0.001$). Finally, the membrane potential measured between action potentials was depolarized in the presence of MCS from -58.8 ± 1.5 to -54.0 ± 1.5 mV ($n = 21$; $t = 7.90$; $p < 0.001$).

H₂O₂ PRODUCED DURING SPONTANEOUS ACTIVITY MAINTAINS FIRING RATE AND REGULARITY OF FIRING

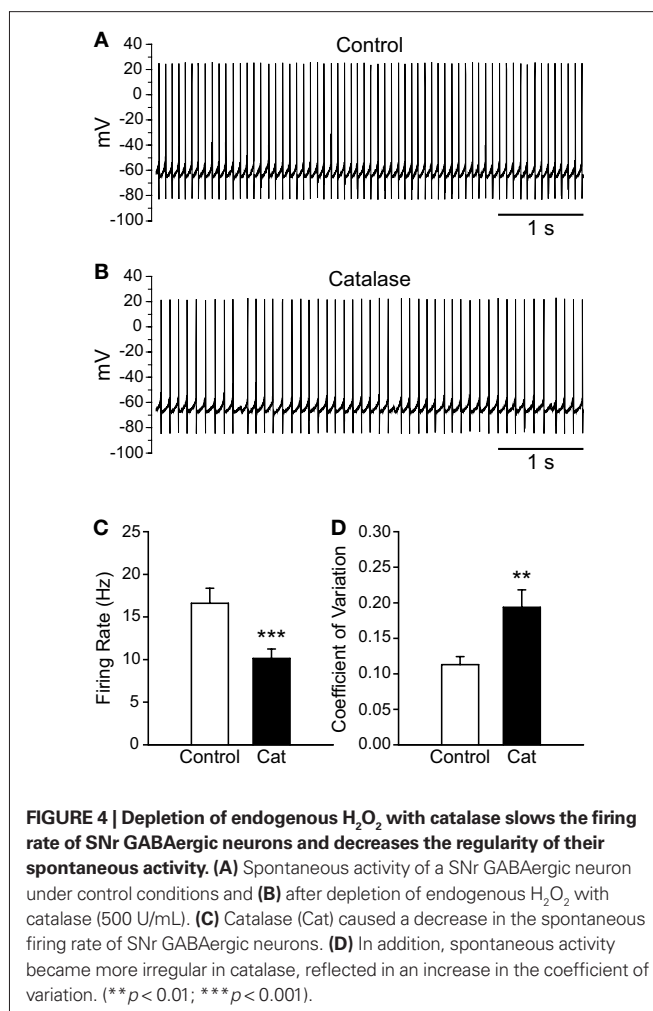
To determine whether basal levels of endogenous H₂O₂ generated in SNr GABAergic neurons during spontaneous activity also influence firing rate, we depleted endogenous H₂O₂ using



catalase (500 U/mL; Avshalumov et al., 2003). Catalase caused a ~40% decrease in the spontaneous firing rate of SNr GABAergic neurons from 16.6 ± 1.8 to 10.1 ± 1.1 Hz (Figures 4A–C; $n = 11$; $t = -6.33$; $p < 0.001$). Additionally, the precision of action potential discharge was decreased, as indicated by an increase in the CV from 0.113 ± 0.011 under control conditions to 0.194 ± 0.024 after catalase (Figure 4D; $n = 11$; $t = 4.06$; $p < 0.01$). These data show that basal H₂O₂ levels modulate the rate and regularity of spontaneous activity in SNr GABAergic neurons.

H₂O₂-INDUCED INCREASES IN SNr GABAergic NEURON FIRING RATE ARE REVERSED BY FFA

Having shown that H₂O₂ elevation increases the firing rate of SNr GABAergic neurons and that H₂O₂ depletion decreases it, we next sought to determine whether putative TRP channels had a role in these effects. We first tested FFA (20–40 μ M; Bao et al., 2005; Lee and Tepper, 2007b; Zhou et al., 2008), which can block a number of TRP channel subtypes, including H₂O₂-activated TRPM2 channels (Hill et al., 2004; Clapham, 2007). The concentrations of FFA found to be effective in the present experiments are lower than those associated with non-specific effects on ion channels other than TRP channels (Takahira et al., 2005; Wang et al., 2006; Gardam et al., 2008; Yau et al., 2010). Consistent with a role for H₂O₂-sensitive TRP channels, FFA reversed the increase in firing



rate caused by either exogenous or endogenous H₂O₂ elevation. In these experiments, exogenous H₂O₂ caused an increase in firing rate from 15.3 ± 1.3 to 21.5 ± 1.9 Hz, which was reversed by FFA (Figures 5A–D; $n = 11$; $F_{(2,20)} = 30.85$; $p < 0.001$; all pairwise contrasts $p < 0.01$). In fact, when TRP channels were blocked, firing rate during H₂O₂ exposure fell below control to 7.3 ± 2.4 Hz (Figure 5D). The suppression of firing rate below control levels could reflect the blockade of a tonic depolarizing current mediated by TRP channels (Zhou et al., 2008) and/or the unmasking of an additional effect of H₂O₂ on channels mediating a hyperpolarizing conductance. We explored these possibilities in separate experiments described in the following section.

As with exogenous H₂O₂, MCS-enhanced endogenous H₂O₂ levels caused an increase in firing rate from 14.0 ± 1.3 to 19.2 ± 2.3 Hz, which was reversed by FFA to 10.3 ± 2.5 Hz (Figures 5E–H; $n = 11$; $F_{(2,20)} = 18.35$; $p < 0.001$; all pairwise contrasts $p < 0.05$). Again, in the presence of FFA, MCS caused a suppression of firing rate below control (Figure 5H). We then tested the efficacy of another TRP channel blocker, 2-APB (Xu et al., 2005; Clapham, 2007; Togashi et al., 2008; not illustrated). Results with 2-APB (100 μ M) were similar with H₂O₂ or MCS, so that data were pooled for analysis. As with FFA, 2-APB reversed the increase in firing rate seen with H₂O₂ or MCS (control 14.1 ± 2.1 Hz; H₂O₂ or MCS 17.9 ± 2.5 Hz; H₂O₂ or

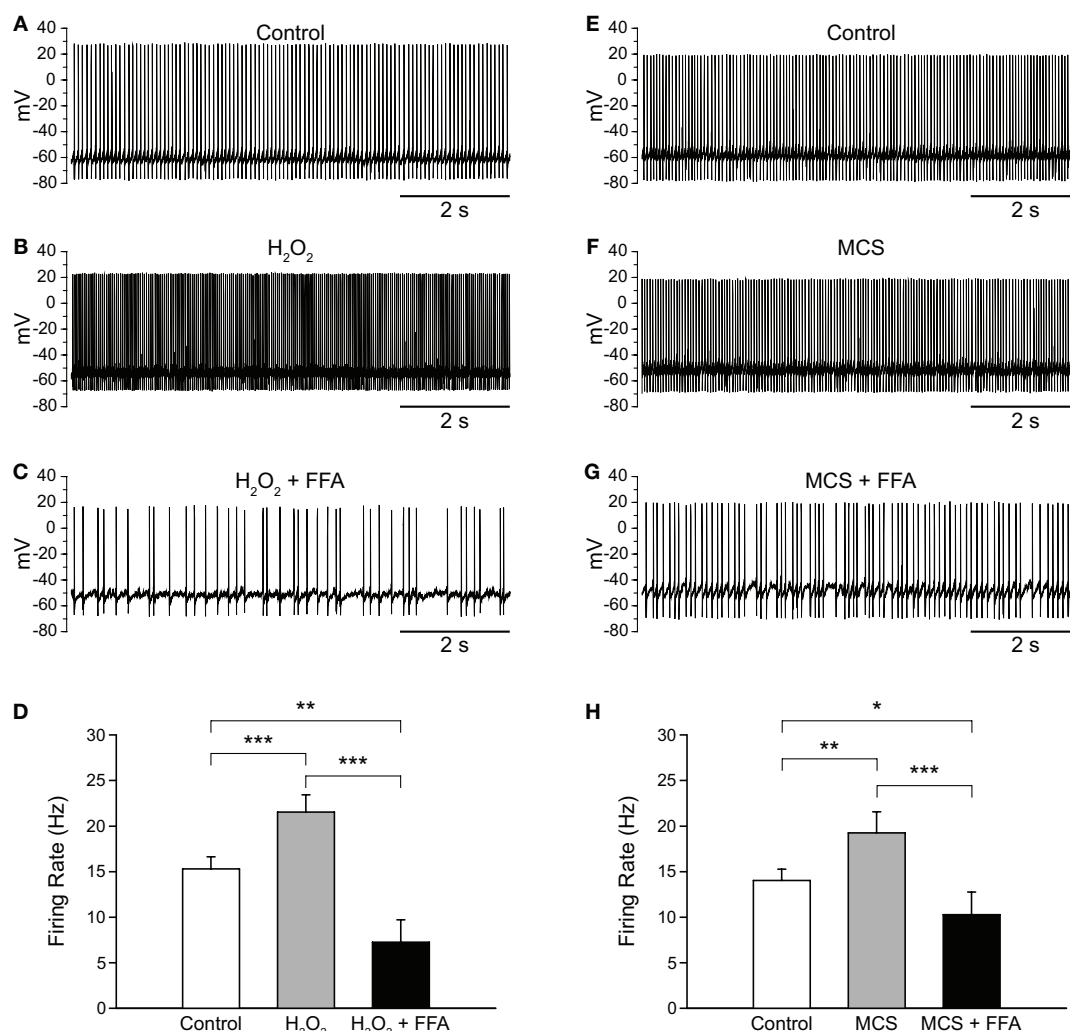


FIGURE 5 | Flufenamic acid (FFA) reverses H₂O₂-induced increases in firing rate. (A) Spontaneous activity of a SNr GABAergic neuron under control conditions, (B) following H₂O₂ (1.5 mM) application, and (C) with FFA (20 μM) applied in the continued presence of H₂O₂. (D) The H₂O₂-induced increase in firing rate was reversed by FFA and the resulting firing rate suppressed below

control. (E) Activity of another SNr GABAergic neuron under control conditions, (F) following amplification of endogenous H₂O₂ with MCS (1 mM), and (G) in FFA (20 μM) in the continued presence of MCS. (H) Increases in firing rate induced by amplified endogenous H₂O₂ were similarly reversed and suppressed below control levels by FFA. (**p* < 0.05; ***p* < 0.01; ****p* < 0.001).

MCS + 2-APB 11.4 ± 2.8 Hz; *n* = 6; $F_{(2,10)} = 23.67$; *p* < 0.001; control vs. H₂O₂ or MCS *p* < 0.01; H₂O₂ or MCS vs. H₂O₂ or MCS + 2-APB *p* < 0.01).

Previous experiments have shown that tonic activation of TRP channels maintains basal firing rate, as well as the regularity of firing, in SNr GABAergic neurons (Zhou et al., 2008), with consequences of TRP channel blockade that appear much like the consequences of H₂O₂ depletion by catalase reported here (Figure 4). To determine whether endogenous H₂O₂ contributes to the tonic activation of putative TRP channels in SNr GABAergic neurons, we tested whether the decrease in firing rate caused by FFA (Zhou et al., 2008) would persist following catalase-induced H₂O₂ depletion. Catalase alone caused a decrease in firing rate from 16.4 ± 2.0 to 10.0 ± 0.9 Hz (Figures 6A,B; *n* = 4; $F_{(2,6)} = 22.93$; *p* < 0.01; control vs. catalase *p* < 0.05). However, when FFA (20 μM) was applied in the continued presence of catalase, the effect

of FFA on firing rate was abolished, resulting in no change in firing rate from that observed with catalase alone (Figures 6C,D; 9.4 ± 0.8 Hz; *p* > 0.05). These data indicate that basal H₂O₂ is an important factor underlying the tonic activation of TRP channels in SNr neurons.

H₂O₂ SUPPRESSES FIRING VIA K_{ATP} CHANNEL ACTIVATION IN THE PRESENCE OF FFA

As described in the previous section, blocking TRP channels with FFA in the presence of elevated H₂O₂ not only reversed the excitatory effect seen, but led to a decrease in firing rate below control. Initially, we assumed that this decrease below control reflected blockade of TRP channel contributions to the tonic activity of SNr GABAergic neurons reported previously (Zhou et al., 2008). To test this assumption, we first applied FFA, then applied H₂O₂ or MCS in the continued presence of FFA.

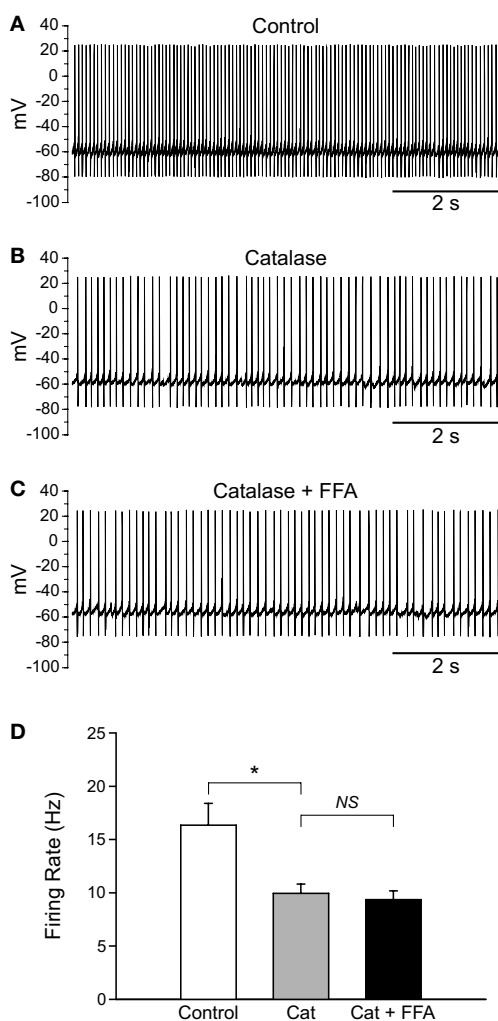


FIGURE 6 | FFA-sensitive channels are tonically activated by H₂O₂ in SNr GABAergic neurons. (A) Spontaneous firing of a SNr GABAergic neuron under control conditions, (B) following depletion of basal H₂O₂ with catalase (500 U/mL), and (C) in FFA (20 μ M) in the continued presence of catalase. (D) Catalase (Cat) caused a significant decrease in firing rate which was unchanged when FFA was added in the continued presence of catalase. (NS not significant; * $p < 0.05$).

Application of FFA (20 μ M) caused a decrease in firing rate from 16.2 ± 1.1 to 10.8 ± 1.7 Hz ($p < 0.05$) and an increase in the CV from 0.092 ± 0.007 to 0.154 ± 0.022 ($n = 5$; $t = 3.48$; $p < 0.05$), consistent with tonic excitation and maintenance of firing regularity mediated by TRP channels (Zhou et al., 2008). Addition of exogenous H₂O₂ in the continued presence of FFA caused a further decrease in firing rate to 0.7 ± 0.7 Hz (Figures 7A–D; $n = 5$; $F_{(2,8)} = 82.49$; $p < 0.001$; FFA vs. FFA + H₂O₂ $p < 0.01$). In 4/5 neurons, H₂O₂ caused a complete suppression of firing when applied in the presence of FFA. The same pattern was seen when endogenous H₂O₂ levels were elevated while TRP channels were blocked. Again, FFA alone caused a decrease in firing rate from 15.5 ± 3.4 to 8.6 ± 1.9 Hz ($p < 0.05$). Addition of MCS caused a further decrease in firing rate to 2.3 ± 1.2 Hz (Figures 7F–I; $n = 7$; $F_{(2,12)} = 10.30$; $p < 0.01$; FFA vs. FFA + MCS $p < 0.05$).

The finding that elevated H₂O₂ caused a further decrease in firing rate when TRP channels were blocked led us to investigate whether this effect was due to unopposed activation of K_{ATP} channels. To test this hypothesis we applied FFA followed by H₂O₂ or MCS along with a K_{ATP}-channel blocker, glibenclamide (3 μ M). Glibenclamide was co-applied with H₂O₂ or MCS to minimize total recording time. As before, FFA (20–40 μ M) caused a decrease in firing rate from 14.9 ± 1.7 to 10.8 ± 1.7 Hz ($p < 0.01$). However, in contrast to the suppression of activity when H₂O₂ alone was applied in the presence of FFA, co-application of H₂O₂ plus glibenclamide in the continued presence of FFA produced a slight increase in firing rate to 13.4 ± 1.7 Hz (Figure 7E; $n = 8$; $F_{(2,14)} = 8.33$; $p < 0.01$; FFA vs. FFA + glibenclamide + H₂O₂ $p < 0.05$). Similarly, in experiments with MCS plus glibenclamide, FFA caused a decrease in firing rate from 16.4 ± 2.7 Hz under control conditions to 11.8 ± 2.2 Hz ($p < 0.01$), which did not change when MCS was applied with glibenclamide in the continued presence of FFA (12.3 ± 2.2 Hz; Figure 7J; $n = 7$; $F_{(2,12)} = 13.82$; $p < 0.001$; FFA vs. FFA + glibenclamide + MCS $p > 0.05$). Thus, the suppression of SNr neuron firing caused by H₂O₂ when TRP channels are blocked is mediated by K_{ATP}-channel activation.

Next, we tested whether K_{ATP} channel activation attenuated the increase in firing rate caused by H₂O₂ when TRP channels were functioning. In these experiments, glibenclamide (3 μ M) alone did not alter the firing rate of SNr GABAergic neurons (control 15.6 ± 0.8 Hz; glibenclamide 14.9 ± 0.9 Hz; $n = 15$; $p > 0.05$); in the presence of glibenclamide, exogenous H₂O₂ caused an increase in firing rate of $52 \pm 17\%$ ($n = 6$) and MCS caused an increase of $46 \pm 13\%$ ($n = 9$). Although the increases in firing rate caused by H₂O₂ or MCS in the presence of glibenclamide tended to be greater than those in the absence of K_{ATP} channel blockade (see preceding sections), these increases were not significantly greater than with H₂O₂ or MCS alone ($p > 0.05$ two-way repeated measures ANOVA in both cases). Therefore, it would appear that H₂O₂-induced activation of K_{ATP} channels only modestly attenuates the excitation caused by TRP channel activation. Overall, these data indicate that the primary effect of H₂O₂ elevation is to increase the activity of guinea-pig SNr GABAergic neurons by activating one or more FFA-sensitive channel.

H₂O₂ SUPPRESSES FIRING IN GABAergic NEURONS RECORDED IN MOUSE SNr

To provide mechanistic insight into the regulation of TRP channels by H₂O₂ we investigated the effects of H₂O₂ on SNr neurons in mouse midbrain slices where a specific subtype of TRP channel, namely TRPC3, is selectively expressed (Zhou et al., 2008). In contrast to our results in guinea-pig SNr, exogenous H₂O₂ (150 μ M to 1.5 mM) inhibited the firing of these neurons (Figures 8A,B). Mouse SNr GABAergic neurons exhibited a spontaneous firing rate of 16.1 ± 2.1 Hz under control conditions which fell to 1.0 ± 0.7 Hz in the presence of exogenous H₂O₂ (Figure 8C; $n = 6$; $t = -6.23$; $p < 0.01$). This inhibition of firing was surprisingly strong and resulted in 4/6 neurons falling silent. In a subset of neurons where washout was assessed, H₂O₂ caused complete silencing of firing from an average control firing rate of 14.9 ± 2.4 Hz ($n = 3$; $p < 0.05$). The firing rate returned to 7.2 ± 1.2 Hz following washout

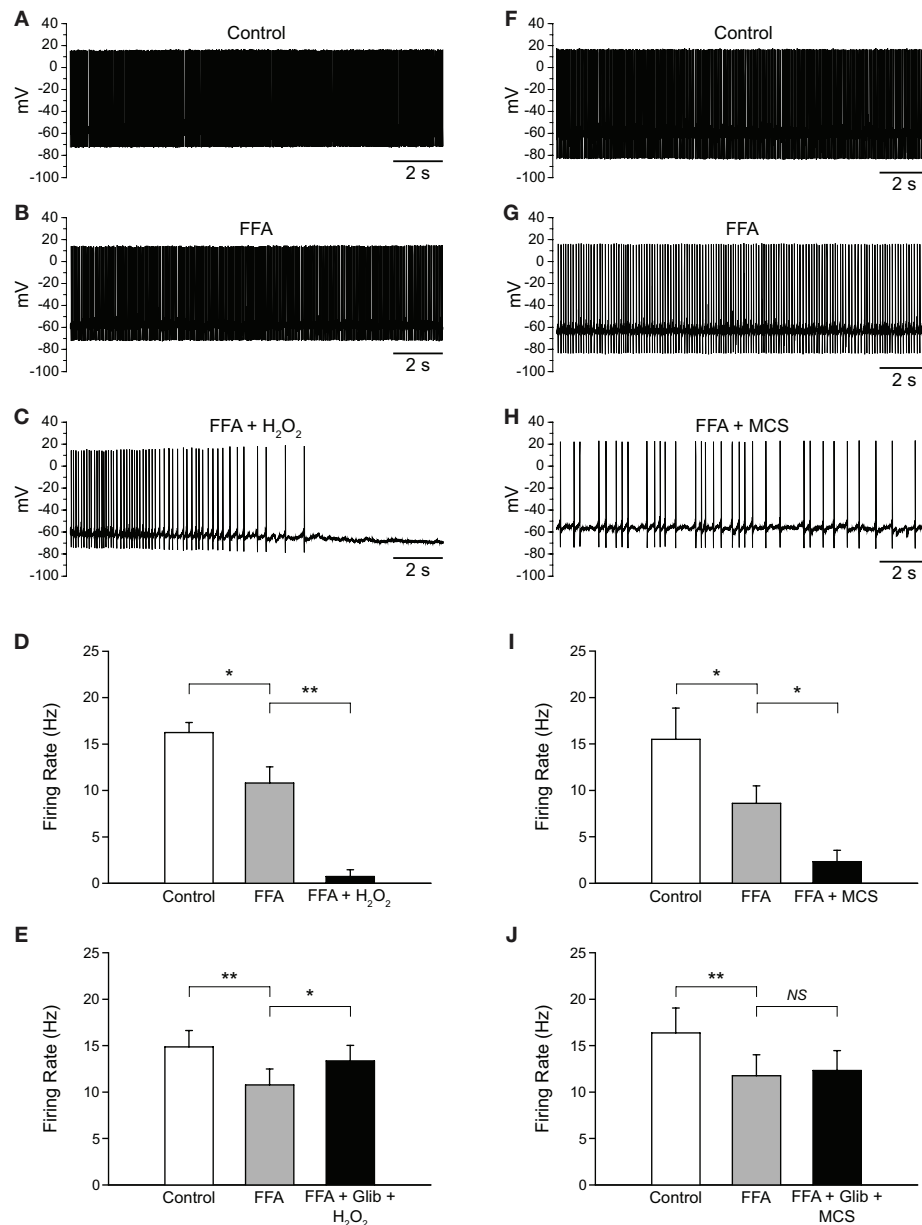


FIGURE 7 | H₂O₂ can alter SNr GABAergic neuron activity via both TRP and K_{ATP} channels. (A) Spontaneous firing of a SNr GABAergic neuron under control conditions, **(B)** with TRP channels blocked by FFA (20 μ M), and **(C)** with H₂O₂ (1.5 mM) in the continued presence of FFA. **(D)** Following blockade of TRP channels, exogenous H₂O₂ suppressed SNr neuron firing. In some cases [as in **(C)**] a marked hyperpolarization was seen that was sufficient to silence the neuron. **(E)** This suppression of firing was prevented by the K_{ATP}

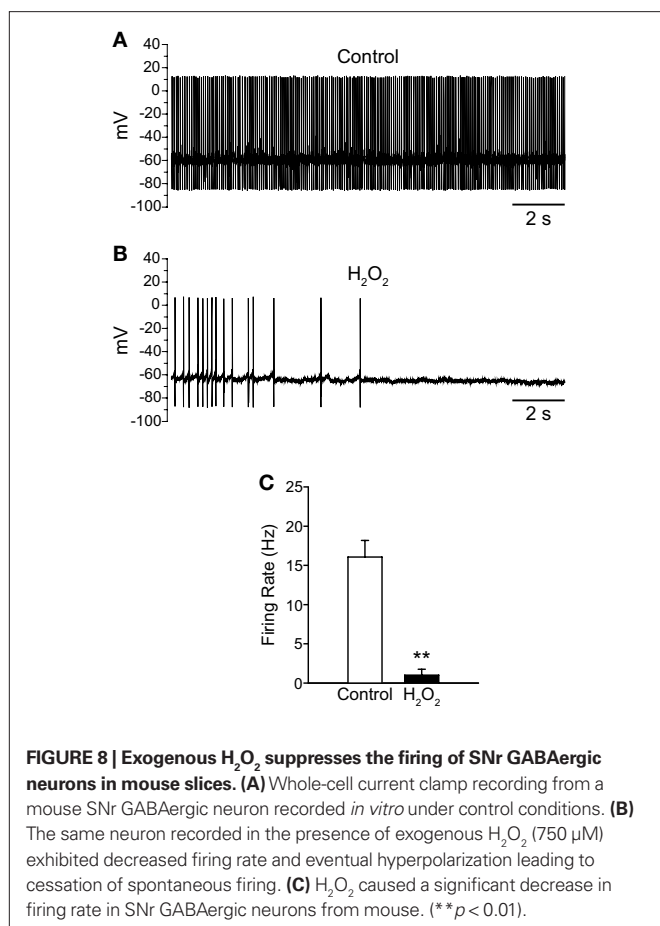
channel blocker glibenclamide (Glib; 3 μ M). **(F)** Recording from another SNr GABAergic neuron under control conditions, **(G)** with FFA (20 μ M), and **(H)** with MCS (1 mM) in the continued presence of FFA. **(I)** Amplifying endogenous H₂O₂ levels with MCS caused a suppression of firing rate when TRP channels were blocked with FFA. **(J)** The MCS-induced suppression of neuronal activity was also prevented by glibenclamide. (NS not significant; * p < 0.05; ** p < 0.01).

in control aCSF, which was not significantly different from the control firing rate in this sample ($F_{(2,4)} = 17.43$; p < 0.05; control vs. washout p > 0.05).

DISCUSSION

Here we report regulation of SNr GABAergic neuron activity by the emerging neuromodulator H₂O₂. Elevation of endogenous H₂O₂ increased the spontaneous firing rate of SNr GABAergic

neurons recorded *in vitro* from guinea-pig slices whereas depletion of H₂O₂ decreased firing rate and regularity. We also found a minor inhibitory role for H₂O₂-sensitive K_{ATP} channels that was magnified in the presence of TRP-channel blockers. Further, we found that the firing of SNr GABAergic neurons recorded *in vitro* from slices obtained from mouse was suppressed by H₂O₂, indicating that the mode of H₂O₂ regulation of these neurons may be species specific. Overall, our results provide the first evidence



that H₂O₂ fine-tunes the firing rate and regularity of basal ganglia output neurons through TRP channels, which appear to be the primary targets of H₂O₂-dependent modulation in guinea-pig SNr GABAergic neurons.

H₂O₂ SIGNALING VIA ION-CHANNEL ACTIVATION

A key source of cellular H₂O₂ production is the mitochondrial electron transport chain, in which H₂O₂ is formed from O₂ during the process of oxidative phosphorylation to produce ATP (Boveris and Chance, 1973; Peuchen et al., 1997; Liu et al., 2002). Mitochondria are the primary source of H₂O₂ for rapid neuronal signaling via ion-channel activation (Bao et al., 2009), although other sources of H₂O₂ contribute to slower signaling processes, including downstream effects of growth factors (Rhee et al., 2005; Miller et al., 2007). As shown here, the metabolic demand of neurons in the SNr during spontaneous activity governs H₂O₂ generation, as seen in the marked attenuation of MCS-enhanced DCF FI in SNr GABAergic neurons when neuronal activity was silenced by TTX relative to that seen during spontaneous firing. These findings are consistent with the previously reported link between neuronal activity and mitochondrial metabolism (Kann et al., 2003).

The present findings complement earlier studies of the effects of H₂O₂ on neuronal excitability, in which both inhibitory and excitatory effects have been observed. For example, an H₂O₂-dependent hyperpolarization of CA1 pyramidal neurons has been reported that is mediated by an unidentified K⁺ channel(s)

(Seutin et al., 1995). Similarly, a predominantly inhibitory effect of H₂O₂ has been reported for guinea-pig and rat SNc DAergic neurons and guinea-pig striatal DAergic axons that is mediated by K_{ATP} channels (Avshalumov and Rice, 2003; Avshalumov et al., 2003, 2005; Freestone et al., 2009). However, there is also evidence for excitatory effects of H₂O₂ in guinea-pig and rat GABAergic striatal MSNs, mediated by an FFA-sensitive channel (Smith et al., 2003; Bao et al., 2005). Moreover, rat SNr GABAergic neurons have been shown to exhibit both inward and outward currents in response to rotenone, with the majority of neurons exhibiting a presumed TRP-channel mediated inward current (Freestone et al., 2009).

The studies of neuronal TRP channel activation by H₂O₂ noted above used exogenous peroxide or rotenone, a mitochondrial inhibitor, to elevate H₂O₂ levels and activate a FFA-sensitive conductance (Smith et al., 2003; Bao et al., 2005; Freestone et al., 2009). We show here not only that milder H₂O₂ elevation by GSH peroxidase inhibition activates TRP channels in SNr GABAergic neurons, but also that the activity of these cells is regulated by tonically produced H₂O₂. The predominantly excitatory effect of H₂O₂ on guinea-pig SNr GABAergic neurons, despite the presence of functional H₂O₂-sensitive K_{ATP} channels, may reflect the relative density of TRP channels to K_{ATP} channels in these cells. Overall, these results suggest that differential responsiveness of basal ganglia neurons to H₂O₂ may be based largely on the ratio of TRP to K_{ATP} channels.

Evidence for presumed TRP channel involvement in H₂O₂-dependent regulation of SNr GABAergic neurons comes from several complementary results reported here. First, two distinct agents that block TRP channels, FFA and 2-APB, similarly reversed the increase in firing rate induced by H₂O₂. Second, although blocking tonically active TRP channels alone which decreases the firing rate of SNr GABAergic neurons (Zhou et al., 2008; results here) could contribute to these results, we also showed that when TRP channels were first blocked by FFA, resulting in a decrease in firing rate, application of H₂O₂ with FFA causes a further suppression of firing rate. If H₂O₂ and FFA were acting at separate conductances, it is unlikely that a suppression of firing rate would have been observed; rather an increase in firing rate would be expected. Third, application of FFA following a decrease in firing rate induced by catalase did not result in a further decrease in firing rate. If FFA were acting on a non-H₂O₂-sensitive channel, a further change in firing rate would have been expected. It should be noted that in all experiments, we limited off-target actions of FFA by using low concentrations: concentrations used were similar or lower than those used previously to examine the role of TRP channels in modulating SNr neuron firing (Zhou et al., 2008), and lower than concentrations shown to cause non-specific effects (Takahira et al., 2005; Wang et al., 2006; Gardam et al., 2008; Yau et al., 2010). Given this strong and consistent pharmacological evidence, we are pursuing additional approaches to identify the precise TRP-channel subtype(s) mediating H₂O₂-induced increases in firing rate in these neurons, with the caveat that we cannot rule out the possibility that H₂O₂ is acting on another channel class with similar pharmacological properties.

Mechanisms of H₂O₂-dependent ion-channel activation are not completely understood. There is evidence for direct action at some TRP channels, namely TRPM2 (Wehage et al., 2002; Eisfeld and Lückhoff, 2007), and K_{ATP} channels (Ichinari et al., 1996; Tokube

et al., 1998). However, recent studies argue against direct TRP channel activation by H₂O₂ (Toth and Csanady, 2010) and suggest that activation may be mediated by H₂O₂-dependent elevation of an intracellular signaling molecule (Kolisek et al., 2005; Perraud et al., 2005; Lange et al., 2008; Hecquet and Malik, 2009). Intracellular calcium can also be elevated by H₂O₂ (Freestone et al., 2009). This could lead to activation of a calcium-activated conductance such as that mediated by the TRPC3 channel (Zitt et al., 1997), which is reported to be the sole TRP channel in neonatal mouse SNr neurons (Zhou et al., 2008). Our finding that young adult mouse SNr neurons are inhibited rather than excited by H₂O₂ suggests that the nature of H₂O₂-dependent modulation of SNr neurons may be species- and/or developmentally determined, possibly reflecting different complements of H₂O₂-sensitive channels.

IMPLICATIONS OF MODULATION OF SNr NEURON ACTIVITY BY ENDOGENOUS H₂O₂

Basal activity-dependent H₂O₂ generation in SNr GABAergic neurons contributes to the maintenance of tonic firing rate in these cells, with a decrease in firing rate and regularity after H₂O₂ depletion by catalase that is similar to the effect of blocking TRP channels reported previously (Zhou et al., 2008). These results suggest that TRP-channels are tonically active, at least in part through a mechanism involving H₂O₂. However, these channels are not maximally active at rest as evidenced by the ability of H₂O₂, as reported here, as well as other neuromodulators, including dopamine, to increase the firing rate of these neurons via further TRP-channel activation (Zhou et al., 2009). The decrease in firing rate and increase in CV observed when TRP channels are blocked by FFA (Zhou et al., 2008; results here) or when tonic H₂O₂-dependent activation is lost in the presence of catalase reflects the removal of a tonic depolarizing influence on these neurons. Indeed, a slight hyperpolarization of these neurons by direct current injection causes a similar decrease in firing rate and decrease in regularity of firing (Zhou et al., 2006). Further, the slight changes in spike parameters observed in the presence of H₂O₂ or MCS are consistent with those observed in response to injection of a slight depolarizing current in SNr GABAergic neurons (Lee et al., unpublished observations).

The ability of H₂O₂ to modulate the firing rate of SNr neurons raises the possibility that H₂O₂ might influence network interactions in the SNr. As a neutral, membrane-permeable molecule, H₂O₂ is not confined to the cell in which it is produced, but rather leaves cells by diffusing through the lipid membrane or through membrane aquaporins (Bienert et al., 2007). Thus, increased activity in one SNr neuron might lead to increased H₂O₂ production and subsequent excitation of neighboring cells, resulting in feed-forward excitation. Such local effects could be even more far reaching through circuit interactions. For example, much of the inhibitory input to SNc DAergic neurons is from axon collaterals of SNr GABAergic neurons (Tepper and Lee, 2007; Lee and Tepper, 2009). Previous studies have shown that H₂O₂ elevation inhibits somatodendritic release of DA in the SNc (Chen et al., 2002); one contributing factor could be increased inhibitory input to those neurons from H₂O₂-enhanced excitation of SNr GABAergic neurons.

In addition to these possible physiological functions of endogenous H₂O₂, aberrant H₂O₂ signaling could contribute to the pathological changes in firing of SNr GABAergic neurons that is seen in Parkinson's disease (PD). In human PD and in PD animal models, increased SNr output causes abnormal inhibition of thalamocortical neurons (Albin et al., 1989; DeLong, 1990; MacLeod et al., 1990; Wichmann and DeLong, 1996, 2006; Murer et al., 1997; Bergman et al., 1998; Hurtado et al., 1999; Hutchison et al., 2004). Linking these observations to the present findings, PD is associated with impaired activity of mitochondrial complex I and increased oxidative stress possibly including elevated H₂O₂ production in the SN (Parker et al., 1989; Schapira et al., 1990; Greenamyre et al., 2001; Turnbull et al., 2001; Dauer and Przedborski, 2003; Dawson and Dawson, 2003; Lin and Beal, 2006). Most studies of the contribution of H₂O₂ and other reactive oxygen species to the pathogenesis of PD have focused on the contribution of these molecules to DAergic neurodegeneration through oxidative damage (Jenner and Olanow, 1998; Zhang et al., 2000). The present findings suggest a more dynamic role for H₂O₂ as a contributing factor to the pathological changes in the activity of SNr GABAergic output neurons in PD by increasing the excitability of these cells via TRP-channel activation.

CONCLUSION

Overall, the present results from SNr GABAergic neurons build on a growing body of evidence supporting a role for H₂O₂ as a neuromodulator. The primary effect of H₂O₂ on guinea-pig SNr GABAergic neurons is to maintain and regulate their firing rate through presumed TRP-channel activation. An inhibitory effect of H₂O₂ resulting from K_{ATP}-channel activation predominates when TRP-channel activity is blocked in guinea-pig SNr, or under control conditions in mouse SNr. However, K_{ATP}-channel blockade alone has no effect on tonic firing rate in guinea-pig SNr GABAergic neurons, in contrast to the tonic, inhibitory effect of H₂O₂ acting via K_{ATP} channels in SNc DAergic neurons in the same species (Avshalumov et al., 2005). Activation of inhibitory K_{ATP} channels during H₂O₂ elevation is also less effective in SNr GABAergic neurons than in striatal MSNs, in which the net depolarizing effect of elevated H₂O₂ or other reactive oxygen species is attenuated significantly by concurrent activation of H₂O₂-sensitive K_{ATP} channels (Calabresi et al., 1999; Bao et al., 2005). Together with the present data, these findings indicate that H₂O₂ is an important signaling molecule throughout the basal ganglia, with effects determined by the relative responsiveness of H₂O₂-sensitive excitatory TRP channels and inhibitory K_{ATP} channels that defines the specificity of signaling by this diffusible messenger.

ACKNOWLEDGMENTS

The authors thank Dr. Jyoti C. Patel for helpful comments on this manuscript. This work was supported by National Institutes of Health, National Institute of Neurological Disorders and Stroke grants NS063656 (Christian R. Lee) and NS036362 (Margaret E. Rice), the Richard H. Chartrand Foundation (Paul Witkovsky), and the Edmond J. Safra Philanthropic Foundation (Margaret E. Rice).

REFERENCES

- Albin, R. L., Young, A. B., and Penney, J. B. (1989). The functional anatomy of basal ganglia disorders. *Trends Neurosci.* 12, 366–375.
- Atherton, J. F., and Bevan, M. D. (2005). Ionic mechanisms underlying autonomous action potential generation in the somata and dendrites of GABAergic substantia nigra pars reticulata neurons *in vitro*. *J. Neurosci.* 25, 8272–8281.
- Avshalumov, M. V., Bao, L., Patel, J. C., and Rice, M. E. (2007). H₂O₂ signaling in the nigrostriatal dopamine pathway via ATP-sensitive potassium channels: issues and answers. *Antioxid. Redox Signal.* 9, 219–231.
- Avshalumov, M. V., Chen, B. T., Koós, T., Tepper, J. M., and Rice, M. E. (2005). Endogenous hydrogen peroxide regulates the excitability of midbrain dopamine neurons via ATP-sensitive potassium channels. *J. Neurosci.* 25, 4222–4231.
- Avshalumov, M. V., Chen, B. T., Marshall, S. P., Peña, D. M., and Rice, M. E. (2003). Glutamate-dependent inhibition of dopamine release in striatum is mediated by a new diffusible messenger, H₂O₂. *J. Neurosci.* 23, 2744–2750.
- Avshalumov, M. V., Patel, J. C., and Rice, M. E. (2008). AMPA receptor-dependent H₂O₂ generation in striatal medium spiny neurons, but not dopamine axons: one source of a retrograde signal that can inhibit dopamine release. *J. Neurophysiol.* 100, 1590–1601.
- Avshalumov, M. V., and Rice, M. E. (2003). Activation of ATP-sensitive K⁺ (K_{ATP}) channels by H₂O₂ underlies glutamate-dependent inhibition of striatal dopamine release. *Proc. Natl. Acad. Sci. U.S.A.* 100, 11729–11734.
- Bao, L., Avshalumov, M. V., Patel, J. C., Lee, C. R., Miller, E. W., Chang, C. J., and Rice, M. E. (2009). Mitochondria are the source of hydrogen peroxide for dynamic brain-cell signaling. *J. Neurosci.* 29, 9002–9010.
- Bao, L., Avshalumov, M. V., and Rice, M. E. (2005). Partial mitochondrial inhibition causes striatal dopamine release suppression and medium spiny neuron depolarization via H₂O₂ elevation, not ATP depletion. *J. Neurosci.* 25, 10029–10040.
- Barry, P. H. (1994). JPCalc, a software package for calculating liquid junction potential corrections in patch-clamp, intracellular, epithelial and bilayer measurements and for correcting junction potential measurements. *J. Neurosci. Methods* 51, 107–116.
- Beckstead, R. M., and Frankfurter, A. (1982). The distribution and some morphological features of substantia nigra neurons that project to the thalamus, superior colliculus and pedunculopontine nucleus in the monkey. *Neuroscience* 7, 2377–2388.
- Bergman, H., Raz, A., Feingold, A., Nini, A., Nelken, I., Hansel, D., Ben-Pazi, H., and Reches, A. (1998). Physiology of MPTP tremor. *Mov. Disord.* 13, 29–34.
- Bienert, G. P., Möller, A. L., Kristiansen, K. A., Schulz, A., Möller, I. M., Schjoerring, J. K., and Jahn, T. P. (2007). Specific aquaporins facilitate the diffusion of hydrogen peroxide across membranes. *J. Biol. Chem.* 282, 1183–1192.
- Boveris, A., and Chance, B. (1973). The mitochondrial generation of hydrogen peroxide. General properties and effect of hyperbaric oxygen. *Biochem. J.* 134, 707–716.
- Calabresi, P., Marfia, G. A., Centonze, D., Pisani, A., and Bernardi, G. (1999). Sodium influx plays a major role in the membrane depolarization induced by oxygen and glucose deprivation in rat striatal spiny neurons. *Stroke* 30, 171–179.
- Cebrián, C., Parent, A., and Prensa, L. (2005). Patterns of axonal branching of neurons of the substantia nigra pars reticulata and pars lateralis in the rat. *J. Comp. Neurol.* 492, 349–369.
- Chen, B. T., Avshalumov, M. V., and Rice, M. E. (2001). H₂O₂ is a novel, endogenous modulator of synaptic dopamine release. *J. Neurophysiol.* 85, 2468–2476.
- Chen, B. T., Avshalumov, M. V., and Rice, M. E. (2002). Modulation of somatodendritic dopamine release by endogenous H₂O₂: susceptibility in substantia nigra but resistance in VTA. *J. Neurophysiol.* 87, 1155–1158.
- Clapham, D. E. (2007). SnapShot: mammalian TRP channels. *Cell* 129, 220.
- Clapham, D. E., Julius, D., Montell, C., and Schultz, G. (2005). International Union of Pharmacology. XLIX. Nomenclature and structure-function relationships of transient receptor potential channels. *Pharmacol. Rev.* 57, 427–450.
- Clapham, D. E., Montell, C., Schultz, G., and Julius, D. (2003). International Union of Pharmacology. XLIII. Compendium of voltage-gated ion channels: transient receptor potential channels. *Pharmacol. Rev.* 55, 591–596.
- Dauer, W., and Przedborski, S. (2003). Parkinson's disease: mechanisms and models. *Neuron* 39, 889–909.
- Dawson, T. M., and Dawson, V. L. (2003). Molecular pathways of neurodegeneration in Parkinson's disease. *Science* 302, 819–822.
- DeLong, M. R. (1990). Primate models of movement disorders of basal ganglia origin. *Trends Neurosci.* 13, 281–285.
- Deniau, J. M., and Chevalier, G. (1992). The lamellar organization of the rat substantia nigra pars reticulata: distribution of projection neurons. *Neuroscience* 46, 361–377.
- Deniau, J. M., Hammond, C., Riszk, A., and Feger, J. (1978). Electrophysiological properties of identified output neurons of the rat substantia nigra (pars compacta and pars reticulata): evidences for the existence of branched neurons. *Exp. Brain Res.* 32, 409–422.
- Dunn-Meynell, A. A., Rawson, N. E., and Levin, B. E. (1998). Distribution and phenotype of neurons containing the ATP-sensitive K⁺ channel in rat brain. *Brain Res.* 814, 41–54.
- Eisfeld, J., and Lückhoff, A. (2007). TRPM2. *Handb. Exp. Pharmacol.* 179, 237–252.
- Freestone, P. S., Chung, K. K., Guatteo, E., Mercuri, N. B., Nicholson, L. F., and Lipski, J. (2009). Acute action of rotenone on nigral dopaminergic neurons – involvement of reactive oxygen species and disruption of Ca²⁺ homeostasis. *Eur. J. Neurosci.* 30, 1849–1859.
- Gardam, K. E., Geiger, J. E., Hickey, C. M., Hung, A. Y., and Magoski, N. S. (2008). Flufenamic acid affects multiple currents and causes intracellular Ca²⁺ release in *Aplysia* bag cell neurons. *J. Neurophysiol.* 100, 38–49.
- Grace, A. A., and Onn, S. P. (1989). Morphology and electrophysiological properties of immunocytochemically identified rat dopamine neurons recorded *in vitro*. *J. Neurosci.* 9, 3463–3481.
- Greenamyre, J. T., Sherer, T. B., Betarbet, R., and Panov, A. V. (2001). Complex I and Parkinson's disease. *IUBMB Life* 52, 135–141.
- Gulácsi, A., Lee, C. R., Sikk, A., Viitanen, T., Kaila, K., Tepper, J. M., and Freund, T. F. (2003). Cell type-specific differences in chloride-regulatory mechanisms and GABA_A receptor-mediated inhibition in rat substantia nigra. *J. Neurosci.* 23, 8237–8246.
- Guyenet, P. G., and Aghajanian, G. K. (1978). Antidromic identification of dopaminergic and other output neurons of the rat substantia nigra. *Brain Res.* 150, 69–84.
- Hainsworth, A. H., Röper, J., Kapoor, R., and Ashcroft, F. M. (1991). Identification and electrophysiology of isolated pars compacta neurons from guinea-pig substantia nigra. *Neuroscience* 43, 81–93.
- Hajós, M., and Greenfield, S. A. (1994). Synaptic connections between pars compacta and pars reticulata neurons: electrophysiological evidence for functional modules within the substantia nigra. *Brain Res.* 660, 216–224.
- Hara, Y., Wakamori, M., Ishii, M., Maeno, E., Nishida, M., Yoshida, T., Yamada, H., Shimizu, S., Mori, E., Kudoh, J., Shimizu, N., Kurose, H., Okada, Y., Imoto, K., and Mori, Y. (2002). LTRPC2 Ca²⁺-permeable channel activated by changes in redox status confers susceptibility to cell death. *Mol. Cell* 9, 163–173.
- Hecquet, C. M., and Malik, A. B. (2009). Role of H₂O₂-activated TRPM2 calcium channel in oxidant-induced endothelial injury. *Thromb. Haemost.* 101, 619–625.
- Herson, P. S., and Ashford, M. L. (1997). Activation of a novel non-selective cation channel by alloxan and H₂O₂ in the rat insulin-secreting cell line CRI-G1. *J. Physiol.* 501, 59–66.
- Hill, K., Benham, C. D., McNulty, S., and Randall, A. D. (2004). Flufenamic acid is a pH-dependent antagonist of TRPM2 channels. *Neuropharmacology* 47, 450–460.
- Hurtado, J. M., Gray, C. M., Tamas, L. B., and Sigvardt, K. A. (1999). Dynamics of tremor-related oscillations in the human globus pallidus: a single case study. *Proc. Natl. Acad. Sci. U.S.A.* 96, 1674–1679.
- Hutchison, W. D., Dostrovsky, J. O., Walters, J. R., Courtemanche, R., Borad, T., Goldberg, J., and Brown P. (2004). Neuronal oscillations in the basal ganglia and movement disorders: evidence from whole animal and human recordings. *J. Neurosci.* 24, 9240–9243.
- Ibáñez-Sandoval, O., Carrillo-Reid, L., Galarraga, E., Tapia, D., Mendoza, E., Gomora, J. C., Aceves, J., and Bargas, J. (2007). Bursting in substantia nigra pars reticulata neurons *in vitro*: possible relevance for Parkinson disease. *J. Neurophysiol.* 98, 2311–2323.
- Ichinari, K., Kakei, M., Matsuoka, T., Nakashima, H., and Tanaka, H. (1996). Direct activation of the ATP-sensitive potassium channel by oxygen free radicals in guinea-pig ventricular cells: its potentiation by MgADP. *J. Mol. Cell. Cardiol.* 28, 1867–1877.
- Jenner, P., and Olanow, C. W. (1998). Understanding cell death in Parkinson's disease. *Ann. Neurol.* 44, S72–S84.
- Kann, O., Schuchmann, S., Buchheim, K., and Heinemann, U. (2003). Coupling of neuronal activity and mitochondrial metabolism as revealed by NAD(P)H fluorescence signals in organotypic hippocampal slice cultures of the rat. *Neuroscience* 119, 87–100.
- Kolisek, M., Beck, A., Fleig, A., and Penner, R. (2005). Cyclic ADP-ribose and hydrogen peroxide synergize with ADP-ribose in the activation of TRPM2 channels. *Mol. Cell* 18, 61–69.
- Lacey, M. G., Mercuri, N. B., and North, R. A. (1989). Two cell types in rat substantia nigra zona compacta distinguished by membrane properties and the actions of dopamine and opioids. *J. Neurosci.* 9, 1233–1241.

- Lange, I., Penner, R., Fleig, A., and Beck, A. (2008). Synergistic regulation of endogenous TRPM2 channels by adenine dinucleotides in primary human neutrophils. *Cell Calcium* 44, 604–615.
- Lee, C. R., and Tepper, J. M. (2007a). Morphological and physiological properties of parvalbumin- and calretinin-containing gamma-aminobutyric acidergic neurons in the substantia nigra. *J. Comp. Neurol.* 500, 958–972.
- Lee, C. R., and Tepper, J. M. (2007b). A calcium-activated nonselective cation conductance underlies the plateau potential in rat substantia nigra GABAergic neurons. *J. Neurosci.* 27, 6531–6541.
- Lee, C. R., and Tepper, J. M. (2009). Basal ganglia control of substantia nigra dopaminergic neurons. *J. Neural Transm. Suppl.* 73, 71–90.
- Lin, M. T., and Beal, M. F. (2006). Mitochondrial dysfunction and oxidative stress in neurodegenerative diseases. *Nature* 443, 787–795.
- Liu, Y., Fiskum, G., and Schubert, D. (2002). Generation of reactive oxygen species by the mitochondrial electron transport chain. *J. Neurochem.* 80, 780–787.
- MacLeod, N. K., Ryman, A., and Arbuthnott, G. W. (1990). Electrophysiological properties of nigrothalamic neurons after 6-hydroxydopamine lesions in the rat. *Neuroscience* 38, 447–456.
- Mana, S., and Chevalier, G. (2001). The fine organization of nigro-collicular channels with additional observations of their relationships with acetylcholinesterase in the rat. *Neuroscience* 106, 357–374.
- Matsuda, Y., Fujimura, K., and Yoshida, S. (1987). Two types of neurons in the substantia nigra pars compacta studied in a slice preparation. *Neurosci. Res.* 5, 172–179.
- Miller, E. W., Tulyathan, O., Isacoff, E. Y., and Chang, C. J. (2007). Molecular imaging of hydrogen peroxide produced for cell signaling. *Nat. Chem. Biol.* 3, 263–267.
- Murer, M. G., Riquelme, L. A., Tseng, K. Y., and Pazo, J. H. (1997). Substantia nigra pars reticulata single unit activity in normal and 6OHDA-lesioned rats: effects of intrastriatal apomorphine and subthalamic lesions. *Synapse* 27, 278–293.
- Nakanishi, H., Kita, H., and Kitai, S. T. (1987). Intracellular study of rat substantia nigra pars reticulata neurons in an *in vitro* slice preparation: electrical membrane properties and response characteristics to subthalamic stimulation. *Brain Res.* 437, 45–55.
- Nambu, A. (2007). Globus pallidus internal segment. *Prog. Brain Res.* 160, 135–150.
- Parker, W. D., Boyson, S. J., and Parks, J. K. (1989). Abnormalities of the electron transport chain in idiopathic Parkinson's disease. *Ann. Neurol.* 26, 719–723.
- Perraud, A. L., Takanishi, C. L., Shen, B., Kang, S., Smith, M. K., Schmitz, C., Knowles, H. M., Ferraris, D., Li, W., Zhang, J., Stoddard, B. L., and Scharenberg, A. M. (2005). Accumulation of free ADP-ribose from mitochondria mediates oxidative stress-induced gating of TRPM2 cation channels. *J. Biol. Chem.* 280, 6138–6148.
- Peuchen, S., Bolaños, J. P., Heales, S. J., Almeida, A., Duchon, M. R., and Clark, J. B. (1997). Interrelationships between astrocyte function, oxidative stress and antioxidant status within the central nervous system. *Prog. Neurobiol.* 52, 261–281.
- Redgrave, P., Marrow, L., and Dean, P. (1992). Topographical organization of the nigroreticular projection in rat: evidence for segregated channels. *Neuroscience* 50, 571–595.
- Rhee, S. G., Kang, S. W., Jeong, W., Chang, T. S., Yang, K. S., and Woo, H. A. (2005). Intracellular messenger function of hydrogen peroxide and its regulation by peroxiredoxins. *Curr. Opin. Cell Biol.* 17, 183–189.
- Richards, C. D., Shiroyama, T., and Kitai, S. T. (1997). Electrophysiological and immunocytochemical characterization of GABA and dopamine neurons in the substantia nigra of the rat. *Neuroscience* 80, 545–557.
- Rick, C. E., and Lacey, M. G. (1994). Rat substantia nigra pars reticulata neurons are tonically inhibited via GABA_A, but not GABA_B, receptors *in vitro*. *Brain Res.* 659, 133–137.
- Schapira, A. H., Cooper, J. M., Dexter, D., Clark, J. B., Jenner, P., and Marsden, C. D. (1990). Mitochondrial complex I deficiency in Parkinson's disease. *J. Neurochem.* 54, 823–827.
- Schwanstecher, C., and Panten, U. (1993). Tolbutamide- and diazoxide-sensitive K⁺ channel in neurons of substantia nigra pars reticulata. *Naunyn Schmiedeberg Arch. Pharmacol.* 348, 113–117.
- Seutin, V., Scuvée-Moreau, J., Massotte, L., and Dresse, A. (1995). Hydrogen peroxide hyperpolarizes rat CA1 pyramidal neurons by inducing an increase in potassium conductance. *Brain Res.* 683, 275–278.
- Shen, K. Z., and Johnson, S. W. (2006). Subthalamic stimulation evokes complex EPSCs in the rat substantia nigra pars reticulata *in vitro*. *J. Physiol.* 573, 697–709.
- Smith, M. A., Herson, P. S., Lee, K., Pinnock, R. D., and Ashford, M. L. (2003). Hydrogen-peroxide-induced toxicity of rat striatal neurones involves activation of a non-selective cation channel. *J. Physiol.* 547, 417–425.
- Stanford, I. M., and Lacey, M. G. (1996). Electrophysiological investigation of adenosine triphosphate-sensitive potassium channels in the rat substantia nigra pars reticulata. *Neuroscience* 74, 499–509.
- Takahira, M., Sakurai, M., Sakurada, N., and Sugiyama, K. (2005). Fenamates and diltiazem modulate lipid-sensitive mechano-gated 2P domain K⁺ channels. *Pflügers Arch.* 451, 474–478.
- Takakusaki, K., Habaguchi, T., Ohtinata-Sugimoto, J., Saitoh, K., and Sakamoto, T. (2003). Basal ganglia efferents to the brainstem centers controlling postural muscle tone and locomotion: a new concept for understanding motor disorders in basal ganglia dysfunction. *Neuroscience* 119, 293–308.
- Tepper, J. M., and Lee, C. R. (2007). GABAergic control of substantia nigra dopaminergic neurons. *Prog. Brain Res.* 160, 189–208.
- Togashi, K., Inada, H., and Tominaga, M. (2008). Inhibition of the transient receptor potential cation channel TRPM2 by 2-aminoethoxydiphenyl borate (2-APB). *Br. J. Pharmacol.* 153, 1324–1330.
- Tokube, K., Kiyosue, T., and Arita, M. (1998). Effects of hydroxyl radicals on K_{ATP} channels in guinea-pig ventricular myocytes. *Pflügers Arch.* 437, 155–157.
- Toth, B., and Csanady, L. (2010). Identification of direct and indirect effectors of the transient receptor potential melastatin 2 (TRPM2) cation channel. *J. Biol. Chem.* 285, 30091–30102.
- Turnbull, S., Tabner, B. J., El-Agnaf, O. M., Moore, S., Davies, Y., and Allsop, D. (2001). alpha-Synuclein implicated in Parkinson's disease catalyses the formation of hydrogen peroxide *in vitro*. *Free Radic. Biol. Med.* 30, 1163–1170.
- Wang, D., Grillner, S., and Wallén, P. (2006). Effects of flufenamic acid on fictive locomotion, plateau potentials, calcium channels and NMDA receptors in the lamprey spinal cord. *Neuropharmacology* 51, 1038–1046.
- Wehage, E., Eisfeld, J., Heiner, I., Jüngling, E., Zitt, C., and Lückhoff, A. (2002). Activation of the cation channel long transient receptor potential channel 2 (LTTRPC2) by hydrogen peroxide. A splice variant reveals a mode of activation independent of ADP-ribose. *J. Biol. Chem.* 277, 23150–23156.
- Wichmann, T., and DeLong, M. R. (1996). Functional and pathophysiological models of the basal ganglia. *Curr. Opin. Neurobiol.* 6, 751–758.
- Wichmann, T., and DeLong, M. R. (2006). Basal ganglia discharge abnormalities in Parkinson's disease. *J. Neural Transm. Suppl.* 70, 21–25.
- Wilson, C. J., Young, S. J., and Groves, P. M. (1977). Statistical properties of neuronal spike trains in the substantia nigra: cell types and their interactions. *Brain Res.* 136, 243–260.
- Xu, S. Z., Zeng, F., Boulay, G., Grimm, C., Harteneck, C., and Beech, D. J. (2005). Block of TRPC5 channels by 2-aminoethoxydiphenyl borate: a differential, extracellular and voltage-dependent effect. *Br. J. Pharmacol.* 145, 405–414.
- Yau, H. J., Baranauskas, G., and Martina, M. (2010). Flufenamic acid decreases neuronal excitability through modulation of voltage-gated sodium channel gating. *J. Physiol.* 588, 3869–3882.
- Yung, W. H., Häusser, M. A., and Jack, J. J. (1991). Electrophysiology of dopaminergic and non-dopaminergic neurons of the guinea-pig substantia nigra pars compacta *in vitro*. *J. Physiol.* 436, 643–667.
- Zhang, Y., Dawson, V. L., and Dawson, T. M. (2000). Oxidative stress and genetics in the pathogenesis of Parkinson's disease. *Neurobiol. Dis.* 7, 240–250.
- Zhou, F. W., Jin, Y., Matta, S. G., Xu, M., and Zhou, F. M. (2009). An ultra-short dopamine pathway regulates basal ganglia output. *J. Neurosci.* 29, 10424–10435.
- Zhou, F. W., Matta, S. G., and Zhou, F. M. (2008). Constitutively active TRPC3 channels regulate basal ganglia output neurons. *J. Neurosci.* 28, 473–482.
- Zhou, F. W., Xu, J. J., Zhao, Y., LeDoux, M. S., and Zhou, F. M. (2006). Opposite functions of histamine H₁ and H₂ receptors and H₁ receptor in substantia nigra pars reticulata. *J. Neurophysiol.* 96, 1581–1591.
- Zitt, C., Obukhov, A. G., Strübing, C., Zobel, A., Kalkbrenner, F., Lückhoff, A., and Schultz, G. (1997). Expression of TRPC3 in Chinese hamster ovary cells results in calcium-activated cation currents not related to store depletion. *J. Cell Biol.* 138, 1333–1341.

Conflict of Interest Statement: The authors declare that the research was conducted in the absence of any commercial or financial relationships that could be construed as a potential conflict of interest.

Received: 01 January 2011; accepted: 05 March 2011; published online: 04 April 2011.

Citation: Lee CR, Witkovsky P and Rice ME (2011) Regulation of substantia nigra pars reticulata GABAergic neuron activity by H₂O₂ via flufenamic acid-sensitive channels and K_{ATP} channels. *Front. Syst. Neurosci.* 5:14. doi: 10.3389/fnsys.2011.00014 Copyright © 2011 Lee, Witkovsky and Rice. This is an open-access article subject to a non-exclusive license between the authors and Frontiers Media SA, which permits use, distribution and reproduction in other forums, provided the original authors and source are credited and other Frontiers conditions are complied with.



Dissecting the contribution of individual receptor subunits to the enhancement of *N*-methyl-D-aspartate currents by dopamine D1 receptor activation in striatum

Emily L. Jocoy¹, Véronique M. André¹, Damian M. Cummings¹, Shilpa P. Rao¹, Nanping Wu¹, Amy J. Ramsey², Marc G. Caron², Carlos Cepeda¹ and Michael S. Levine^{1*}

¹ Intellectual and Developmental Disabilities Research Center, Semel Institute, David Geffen School of Medicine, University of California Los Angeles, Los Angeles, CA, USA

² Department of Cell Biology, Duke University, Durham, NC, USA

Edited by:

Elizabeth Abercrombie, Rutgers-Newark: The State University of New Jersey, USA

Reviewed by:

Kuei Y. Tseng, Rosalind Franklin University of Medicine and Science, USA
Stephen Rayport, Columbia University, USA

*Correspondence:

Michael S. Levine, Intellectual and Developmental Disabilities Research Center, Semel Institute, Room 58-258, David Geffen School of Medicine, University of California Los Angeles, 760 Westwood Plaza, Los Angeles, CA 90024, USA.
e-mail: mlevine@mednet.ucla.edu

Dopamine, via activation of D1 receptors, enhances *N*-methyl-D-aspartate (NMDA) receptor-mediated responses in striatal medium-sized spiny neurons. However, the role of specific NMDA receptor subunits in this enhancement remains unknown. Here we used genetic and pharmacological tools to dissect the contribution of NR1 and NR2A/B subunits to NMDA responses and their modulation by dopamine receptors. We demonstrate that D1 enhancement of NMDA responses does not occur or is significantly reduced in mice with genetic knock-down of NR1 subunits, indicating a critical role of these subunits. Interestingly, spontaneous and evoked α -amino-3-hydroxyl-5-methyl-4-isoxazole-propionic acid (AMPA) receptor-mediated responses were significantly enhanced in NR1 knock-down animals, probably as a compensatory mechanism for the marked reduction in NMDA receptor function. The NMDA receptor subunits NR2A and NR2B played differential roles in D1 modulation. Whereas genetic deletion or pharmacological blockade of NR2A subunits enhanced D1 potentiation of NMDA responses, blockade of NR2B subunits reduced this potentiation, suggesting that these regulatory subunits of the NMDA receptor counterbalance their respective functions. In addition, using D1 and D2 receptor EGFP-expressing mice, we demonstrate that NR2A subunits contribute more to NMDA responses in D1-MSSNs, whereas NR2B subunits contribute more to NMDA responses in D2 cells. The differential contribution of discrete receptor subunits to NMDA responses and dopamine modulation in the striatum has important implications for synaptic plasticity and selective neuronal vulnerability in disease states.

Keywords: NMDA, dopamine, receptor subunits, modulation, striatum

INTRODUCTION

Glutamate and dopamine (DA) receptor interactions are vital to numerous functions including learning and memory, motor coordination, and reward mechanisms (Calabresi et al., 2000; Surmeier et al., 2007; Schultz, 2010). When dysfunctional, these receptor interactions contribute to the manifestation of psychiatric and neurodegenerative disorders (Andre et al., 2010b). Glutamatergic and DA inputs converge on the spines of striatal medium-sized spiny neurons (MSSNs) to regulate neuronal excitability (Bouyer et al., 1984; Freund et al., 1984). DA differentially modulates excitatory inputs. Specifically, *N*-methyl-D-aspartate receptor (NMDAR)-mediated responses are potentiated by D1 receptor (D1R) and attenuated by D2R activation (Cepeda et al., 1993; Snyder et al., 1998; Chergui and Lacey, 1999; Levine et al., 1996b; Brady and O'Donnell, 2004; Tseng and O'Donnell, 2004). Modulation can occur through a variety of mechanisms including multiple transduction pathways, voltage-gated Ca^{2+} channels, receptor subunit phosphorylation and mobilization, changes in receptor surface expression, and direct protein–protein coupling (Cepeda et al., 1998; Snyder et al., 1998; Lee et al., 2002; Surmeier et al., 2007; Pascoli et al., 2011).

NMDA receptors are heteromers constituted by different NR1, NR2, and/or NR3 subunits. The most common receptor combination consists of two NR1 subunits, which are obligatory for a functional receptor, and two NR2 subunits which confer different physiological properties (Laube et al., 1998). NMDA receptors expressed by MSSNs consist of NR1, NR2A, and/or NR2B subunits, thus allowing for diheteromeric (NR1/NR2A or NR1/NR2B) and triheteromeric (NR1/NR2A/NR2B) receptors (Dunah and Standaert, 2003).

Mice with genetic deletion of specific NMDA receptor subunits have been created (Ikeda et al., 1995; Sakimura et al., 1995; Kutsuwada et al., 1996; Mohn et al., 1999). Although deletion of some subunits (e.g., NR1 or NR2B) can be lethal, other genetic strategies can be used to examine the role of these subunits. This, in conjunction with the availability of relatively selective pharmacological antagonists, constitutes a powerful tool to begin dissecting the role of NMDA receptor subunits. The present study examined how specific NMDA receptor subunits sculpt NMDAR-mediated responses and how they affect DA modulation in MSSNs, particularly the enhancement of NMDA currents by D1 receptor activation. In addition, we used mice expressing the reporter gene, enhanced

green fluorescent protein (EGFP) in direct (D1R-containing) and indirect (D2R-containing) pathway MSSNs to examine the relative contribution of NR2A/B subunits to NMDA responses and their modulation by dopamine receptor agonists.

MATERIALS AND METHODS

All experimental procedures were performed in accordance with the United States Public Health Service *Guide for Care and Use of Laboratory Animals* and were approved by the Institutional Animal Care and Use Committee at the University of California, Los Angeles. Every effort was made to minimize pain and discomfort. Experiments were conducted on four groups of mice: (1) NR1 knock-down (KD; WT $n = 4$, age 98 ± 7 days; KD $n = 6$, age 100 ± 6 days), generated using homologous recombination in embryonic stem cells (Mohn et al., 1999). This mouse line expresses only 5% of the subunit and is viable. (2) Mice with the NR2A subunit genetically removed (NR2AKO; slice: WT $n = 31$, age 37 ± 3 days; NR2AKO $n = 28$, 36 ± 3 days; acute dissociation: WT $n = 34$, age 37 ± 3 days; NR2AKO $n = 44$, age 37 ± 2 days). (3) Mice with the NR2A subunit genetically removed and expressing EGFP under the control of the D1R promoter (D1 WT $n = 21$, age 38 ± 3 days; D1 NR2AKO $n = 15$, age 38 ± 2 days), and (4) Mice with the NR2A subunit genetically removed and expressing EGFP under the control of the D2R promoter (D2 WT $n = 15$, age 38 ± 4 days; D2 NR2AKO $n = 21$, age 38 ± 2 days). EGFP mice were heterozygous. This is important as it was recently shown that D2-EGFP homozygous mice have significant increases in D2R expression (Kramer et al., 2011). Electrophysiological properties were examined in slices and acutely isolated MSSNs using whole-cell patch clamp recordings in voltage clamp mode.

BRAIN SLICE PREPARATION

Mice were deeply anesthetized with halothane, killed by decapitation, and the brains dissected and immediately placed in oxygenated ice cold low Ca^{2+} and high Mg^{2+} artificial cerebrospinal fluid (ACSF) containing (in mM) NaCl, 130; NaH_2PO_4 , 1.25; KCl, 3; NaHCO_3 , 26; MgCl_2 , 5; CaCl_2 , 1, and glucose, 10. Coronal slices (350 μm) were cut and transferred to an incubating chamber containing ACSF (with 2 mM CaCl_2 and 2 mM MgCl_2) oxygenated with 95% O_2 –5% CO_2 (pH 7.2–7.4, 290–310 mOsm, $25 \pm 2^\circ\text{C}$). Following recovery, slices were placed on the stage of an upright microscope (Olympus BX51), submerged in continuously flowing ACSF (4 ml/min). All experiments were performed at room temperature.

Whole-cell patch clamp recordings in voltage clamp mode were obtained from MSSNs in the dorsolateral striatum visualized with the aid of infrared videomicroscopy (Cepeda et al., 1998). MSSNs were identified by somatic size and typical basic membrane properties (input resistance, membrane capacitance, and time constant). Series resistance was $<25 \text{ M}\Omega$. The patch pipette (4–6 $\text{M}\Omega$) contained the following solution (in mM): Cs–methanesulfonate 125, KCl 3, NaCl 4, MgCl_2 1, MgATP 5, EGTA 9, HEPES 8, GTP 1, phosphocreatine 10, leupeptin 0.1, QX-314 4 (pH 7.25–7.3, osmolarity 280–290 mOsm). Passive membrane properties of MSSNs were determined by applying a depolarizing step voltage command (10 mV) and using the membrane test function integrated in the pClamp8 software (Axon Instruments, Foster City, CA, USA). This function reports membrane capacitance (in pF), input resistance (in $\text{M}\Omega$) and time constant (in ms or μs).

Spontaneous EPSCs were isolated by holding the membrane at -70 mV and blocking GABA_A receptors with bicuculline methiodide (BIC, 20 μM). The amplitude, frequency, and kinetic properties of spontaneous EPSCs were measured using MiniAnalysis software (Synaptosoft Inc, Fort Lee, NJ, USA). Evoked EPSCs were recorded by stimulating the corpus callosum (0.01–1 mA square pulses, 0.1 ms duration) using a monopolar glass electrode placed 150–250 μm dorsal from the recording pipette. To isolate synaptic responses mediated by non-NMDA receptors, the GABA_A receptor blockers BIC (20 μM) or picrotoxin (100 μM) were applied, while CNQX or NBQX (10 μM) was applied to block non-NMDARs and isolate NMDAR responses. NMDAR–EPSCs were recorded either at $+40$ or -70 mV depending on the presence or absence of Mg^{2+} in the ACSF solution. Three responses (15 s between stimulations) were recorded and averaged at each intensity to construct input-output relationships.

ACUTELY ISOLATED NEURONS

Detailed procedures have been published (Flores-Hernandez et al., 2002; Cepeda et al., 2008b). Briefly, slices were obtained as described above. After at least 1 h of incubation in oxygenated ACSF, the dorsal striatum was dissected, placed in an oxygenated cell-stir chamber (Wheaton, Millville, NJ, USA) and enzymatically treated for 20 min with papain (0.5 mg/ml, Calbiochem) at 35°C in a N -[2-hydroxyethyl] piperazine- N' -[2-ethanesulfonic acid] (HEPES)-buffered Hank's balanced salts solution (HBSS, Sigma Chemical) supplemented with (in mM) 1 pyruvic acid, 0.005 glutathione, 0.1 N^G -nitro-L-arginine, and 1 kynurenic acid (pH 7.4, 300–310 mOsm). After enzymatic digestion, the tissue was rinsed with a low Ca^{2+} HEPES-buffered Na-isethionate solution containing (in mM) 140 Na-isethionate, 2 KCl, 2 MgCl_2 , 0.1 CaCl_2 , 23 glucose, and 15 HEPES (pH 7.4, 300–310 mOsm/l). Striatal slices were mechanically dissociated with fire-polished Pasteur pipettes. The cell suspension was then plated into a 35-mm nunclon Petri dish mounted on the stage of an upright microscope (Zeiss Axioscope, Thornwood, NY, USA) containing a HEPES-buffered salt solution.

Standard whole-cell patch clamp techniques were used to obtain voltage clamp recordings (Bargas et al., 1994). The internal solution consisted of (in mM) 175 N -methyl-D-glucamine (NMDG), 40 HEPES, 2 MgCl_2 , 10 ethylene glycol-bis (β -aminoethyl ether)- N,N,N',N' -tetraacetic acid (EGTA), 12 phosphocreatine, 2 Na_2ATP , 0.2 Na_2GTP , and 0.1 leupeptin (pH 7.25, 265–270 mOsm/l). The external solution consisted of (in mM) 135 NaCl, 20 CsCl, 3 BaCl_2 , 2 CaCl_2 , 10 glucose, 10 HEPES, and 0.0003 tetrodotoxin (TTX; pH 7.4, 300–310 mOsm/l). Recordings were obtained with an Axon Instruments 200A patch clamp amplifier and controlled by a computer running pClamp (v. 8.1; Axon Instruments, Foster City, CA, USA).

Drugs were applied through a pressure-driven fast perfusion system (SF-77B, Warner Instruments, Hamden, CT) synchronized by pClamp. Values for peak currents and peak current densities were calculated for all neurons. NMDA currents (3 s duration every 20 s) were evoked by applying different concentrations of the agonist while holding the cell at -70 mV .

DRUGS

The selective NR2A antagonist NVP-AAM077 (NVP, 0.001–1 μM) was a gift from Novartis; zinc (10–300 nM), another NR2A antagonist, was applied in the presence of 10 mM tricine to remove

ambient zinc. NR2B antagonists Ifenprodil (0.01–20 μ M) was from Sigma; and Conantokin G (1 μ M) from Peptides International. Stocks of NMDA (100 mM), NVP (1 mM), Ifenprodil (1 mM), 6-Chloro PB (SKF 81297, 1 mM), and quinpirole (10 mM) were all dissolved in H₂O and stored in the freezer until use.

DATA ANALYSIS AND STATISTICS

In the text, values are presented as means \pm SEMs. Group means for all measures were compared using Student's *t*-tests (for two group comparisons) and appropriately designed ANOVAs followed by suitable *post hoc* comparison tests (for multiple group comparisons) using SigmaStat software (SPSS, Chicago, IL, USA). Differences were considered statistically significant when $p < 0.05$.

RESULTS

ROLE OF NR1 SUBUNITS

As deletion of NR1 subunits is lethal, the contribution of these subunits to NMDAR-mediated responses was examined in NR1-KD mice (Mohn et al., 1999). MSSNs in slices from WT and NR1-KD mice displayed similar passive membrane properties including capacitance, input resistance and time constant (Table 1). As expected, NMDAR-mediated currents evoked by electrical stimulation of cortical inputs were severely reduced in NR1-KD MSSNs (Figure 1A, left). Interestingly, evoked AMPAR-mediated currents were significantly increased, suggesting compensatory mechanisms (Figure 1A right). Similarly, the frequency of spontaneous EPSCs at a holding potential of -70 mV in the presence of BIC was significantly increased in MSSNs from NR1-KD mice (Figure 1B). In addition, the kinetics of spontaneous synaptic events was changed. EPSCs displayed significantly faster rise and decay times, as well as reduced half-amplitude durations in cells from NR1-KD compared to control mice (Table 2).

In acutely isolated MSSNs, passive membrane properties were also similar (Table 1). Bath application of increasing concentrations of NMDA-induced inward currents but the amplitudes of these responses were significantly smaller in cells from NR1-KD mice (Figure 2A). The peak and current density amplitudes of AMPAR-induced currents were also significantly increased in NR1-KD mice (Figure 2B), suggesting changes in postsynaptic AMPA receptors.

DOPAMINE D1 RECEPTOR MODULATION OF NMDA CURRENTS IS ALTERED IN NR1-KD MICE

We have shown previously that activation of D1 receptors enhances synaptically evoked NMDA responses (Levine et al., 1996a). In cells from WT mice the D1 agonist SKF 81297 (1 μ M) increased

peak current amplitude whereas in cells from NR1-KD mice the agonist produced little effects or even decreased peak current amplitude (Figure 3A).

There also was decreased modulation of NMDAR-mediated responses by the dopamine D1 receptor agonist in isolated MSSNs (Figure 3B). The percent increase in NMDA responses was significantly reduced in NR1-KD animals. No differences were found in D2 receptor modulation (Figure 3B, right bar graph).

ROLE OF NR2A SUBUNITS

The membrane properties of MSSNs in slice or after acute dissociation were practically identical in control and NR2AKO mice. NMDAR-mediated EPSCs evoked by electrical stimulation were compared in slices. The membrane potential was held at $+40$ mV to remove the Mg²⁺ block of NMDARs and GABA_A and non-NMDA glutamate receptors were blocked with picrotoxin and CNQX, respectively. Responses from NR2AKOs ($n = 18$) had smaller peak amplitudes than those of WT ($n = 14$) and statistically significant differences occurred at stimulation intensities between 0.8 and 1.0 mA ($p < 0.05$; Figure 4A). Decay times were slower in cells from NR2AKOs than those of WT at higher intensities as well ($p < 0.05$; Figure 4A right graph).

To isolate AMPAR-mediated responses, EPSCs were evoked at a holding potential of -70 mV in the presence of picrotoxin. Peak amplitudes were similar between cells from NR2AKOs ($n = 18$) and WT ($n = 14$; Figure 4B). Moreover, ratios of NMDAR- to AMPAR-mediated currents were consistently smaller ($p < 0.01$) in NR2AKOs, indicating that smaller NMDAR-EPSC amplitudes were due to alterations in NMDARs and not due to differences in activation of excitatory inputs to MSSNs.

The effects of acutely blocking NR2A-containing NMDARs were also examined using a pharmacological approach. Following 5 min perfusion of NVP (0.1 μ M), peak amplitudes of evoked NMDAR-mediated EPSCs in WT were decreased significantly compared to baseline responses ($34.6 \pm 3.8\%$, $n = 12$, $p < 0.01$) and decay times were increased ($31.1 \pm 13.9\%$, $p < 0.05$). In contrast, NVP had practically no effect on the amplitude of evoked responses in cells from NR2AKO mice (Figure 5). Taken together, these findings suggest that the NR2A subunit contributes significantly to synaptic NMDAR-mediated responses. Genetic deletion or acute pharmacological block of NR2A-containing NMDARs caused a reduction in peak amplitudes and prolonged the decay time of the response.

In dissociated WT cells increasing concentrations of NVP (0.001, 0.01, 0.1, and 1 μ M) or zinc (10, 30, 100, 300 nM) attenuated both peak and steady-state currents in a dose-dependent manner (Figures 6A,B). The peak component of the current was attenuated by NVP more than the steady-state component ($p < 0.05$) whereas zinc attenuated steady-state currents more than peak currents ($p < 0.05$; Figure 6A graphs). This demonstrates that NR2A subunits contribute not only to synaptic NMDA responses but also to responses induced in the soma and proximal dendrites, where excitatory synaptic inputs are less abundant.

The effect of genetic deletion of NR2A subunits on NMDA responses induced by activation of mostly extrasynaptic receptors located at or near the soma was then studied in dissociated MSSNs from WT and NR2AKO mice. Peak current and current density amplitudes evoked by increasing concentrations of NMDA

Table 1 | NR1-KD cells in slices: passive membrane properties.

	Cm (pF)	Rm (M Ω)	Tau (ms)
WT ($n = 12$)	78.8 \pm 5.9	115.9 \pm 14	2.3 \pm 0.13
NR1-KD ($n = 9$)	80.4 \pm 6.2	129.4 \pm 11	2.1 \pm 0.13
NR1-KD DISSOCIATED CELLS: PASSIVE MEMBRANE PROPERTIES			
	Cm (pF)	Rm (G Ω)	Tau (μ s)
WT ($n = 23$)	13.7 \pm 0.4	2.2 \pm 0.2	152 \pm 11
NR1-KD ($n = 24$)	14.2 \pm 0.6	1.9 \pm 0.2	168 \pm 19

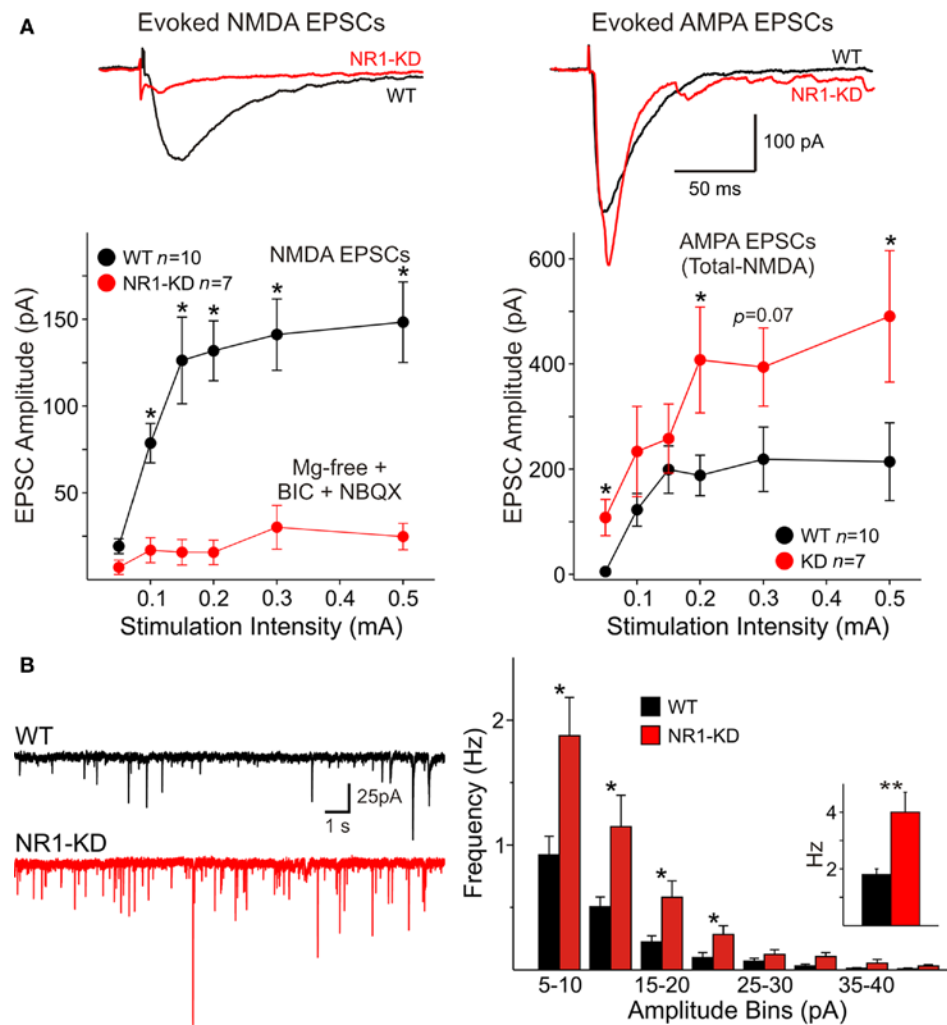


FIGURE 1 | (A) Traces show average NMDA and AMPAR-mediated responses evoked by cortical stimulation in Mg^{2+} -free conditions and in the presence of non-NMDA (NBQX) and $GABA_A$ receptor blockers (BIC). Currents evoked by activation of NMDA receptors (left) were severely reduced in MSSNs from NR1-KD mice. In contrast, AMPA responses (right) were significantly increased. Cells were voltage clamped at -70 mV. Graphs indicate that at different stimulation intensities the NMDA currents were almost non-existent in NR1-KD cells (left), whereas the amplitude of AMPA currents was increased (right).

Amplitude of AMPA currents was determined by subtraction of NMDA currents from the total current in the absence of glutamatergic antagonists. **(B)** Spontaneous excitatory postsynaptic currents (sEPSCs) recorded in MSSNs of ~ 3 month-old NR1-KD and control mice. Traces show sEPSCs recorded in the presence of a $GABA_A$ receptor antagonist (BIC, $20 \mu M$) with membranes voltage clamped at -70 mV. Amplitude-frequency histograms for sEPSCs. Mean frequency of sEPSCs is indicated in the inset. $*p < 0.05$; $**p < 0.01$; $***p < 0.001$ in this and subsequent figures.

Table 2 | Kinetics of sEPSCs in NR1-KD.

	Rise time (ms)	Decay time (ms)	Half-width (ms)
WT ($n = 12$)	2.9 ± 0.2	11.8 ± 0.9	13.8 ± 1.0
NR1-KD ($n = 9$)	$2.1 \pm 0.2^{**}$	$7.8 \pm 0.6^{***}$	$10.9 \pm 0.7^{**}$

$^{**}p = 0.002$; $^{***}p = 0.0001$.

(1, 10, 100, and 1000 μM) were similar in NR2AKO and WT mice (not shown). Moreover, EC_{50} values for mean peak current amplitudes and current densities were also similar [$45.3 \pm 8.4 \mu M$ for WTs ($n = 8$) and $39.1 \pm 3.4 \mu M$ for NR2AKOs ($n = 16$)]. However, in the presence of increasing concentrations of NVP or zinc, the

attenuation of NMDAR-mediated currents was significantly reduced in NR2AKOs (**Figures 7A,B**). Because synaptic inputs are mostly eliminated in dissociated MSSNs, these results suggest that either the NR2A subunit does not contribute significantly to mostly extra-synaptic NMDA receptors, or that compensatory effects result from genetic ablation of this subunit. In support of the second alternative, application of Ifenprodil (1 and 10 μM), a NR2B antagonist, attenuated peak currents from NR2AKOs significantly more in MSSNs from NR2AKO compared to WT mice ($p < 0.05$; **Figure 7C**).

To examine if there is a differential contribution of NR2A subunits in D1R- and D2R-expressing MSSNs, D1R-, or D2R EGFP mice were crossed to the NR2AKO mice, thereby creating double transgenic mice with EGFP labeling of D1R- or D2R-expressing cells with and without NR2A. In acutely isolated D1R-expressing MSSNs,

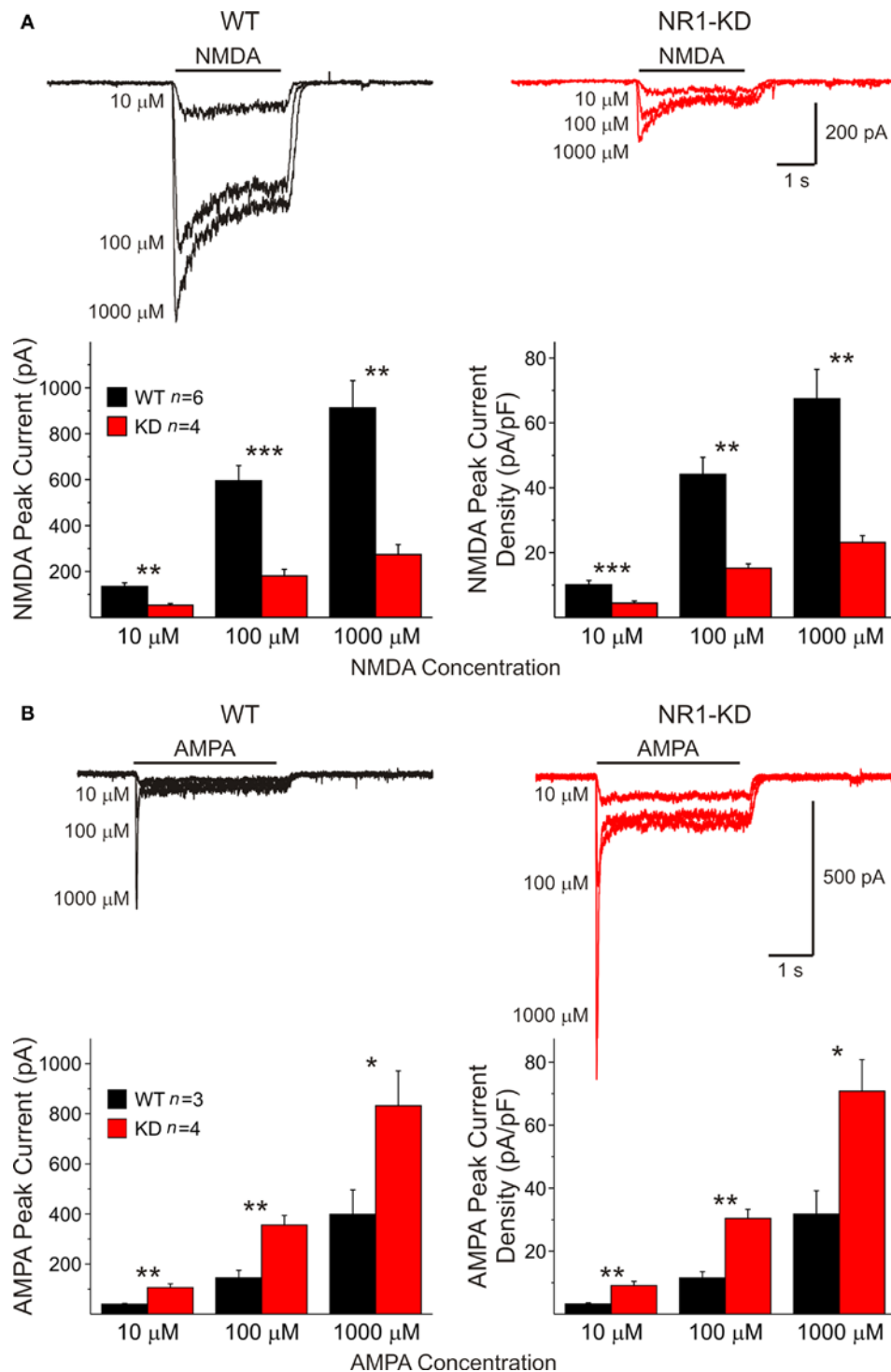


FIGURE 2 | (A) In isolated MSSNs, bath application of increasing concentrations of NMDA-induced inward currents. As shown in the graphs, the amplitude of NMDAR-mediated peak and current densities was significantly smaller in cells from NR1-KD mice. **(B)** In contrast, peak and current densities induced by AMPA were significantly increased, suggesting compensatory mechanisms.

NMDAR-mediated peak current densities were consistently smaller in NR2AKOs than WTs across all concentrations (100, 500, and 1000 μM NMDA, $p < 0.05$; **Figure 8A**). In contrast, NMDAR-mediated current

densities were similar between D2-NR2AKO and D2-WT MSSNs at all NMDA concentrations (**Figure 8B**). These data suggest a greater contribution of NR2A to D1R- compared to D2R-expressing MSSNs.

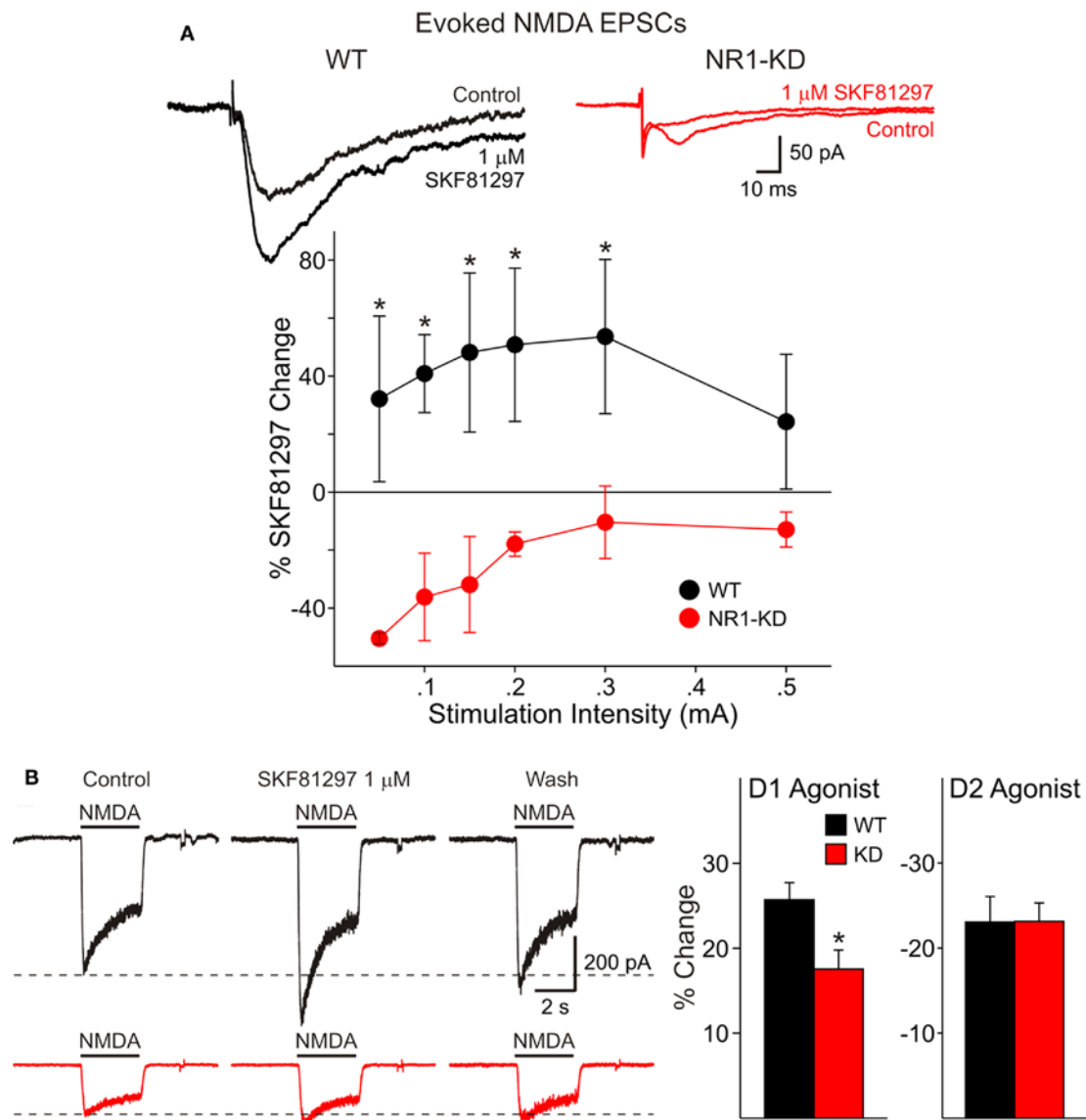


FIGURE 3 | (A) In cells from WT mice (left) the D1 agonist SKF 81297 increased peak current amplitude of evoked NMDA responses, whereas in cells from NR1-KD mice (right) the agonist produced no change or decreased peak current amplitude. **(B)** There also was decreased modulation of NMDA

responses by the dopamine D1 receptor agonist in isolated MSSNs. The percent increase in NMDA responses was significantly reduced in NR1-KD animals (left bar graph) whereas the decrease by a D2 agonist was unaffected (right bar graph).

GENETIC DELETION OF NR2A ENHANCES D1R POTENTIATION OF NMDA RESPONSES

The selective D1R agonist SKF 81297 (1 μ M) was used to examine the potentiation of NMDAR-mediated responses in isolated MSSNs from NR2AKO and control animals. In the entire population of MSSNs, without distinction of DA receptor-subtype expression, the percent increase was greater in NR2AKO mice than in WT mice but the difference was not statistically significant (Figure 9A graph). However, after separating MSSNs by subtype using EGFP, NMDA currents in D1R-expressing neurons ($n = 24$) from NR2AKO mice displayed significant increases in potentiation compared to D1R-expressing cells ($n = 21$) from WT mice ($p < 0.05$; Figure 9A traces and

Figure 9B left). In contrast, no significant differences in D2R attenuation of NMDAR-mediated currents occurred between D2-WT ($n = 13$) and D2-NR2AKO ($n = 10$) MSSNs (Figure 10 left). This indicates that D1R potentiation of NMDA responses is enhanced in the absence of NR2A subunits in D1R-expressing MSSNs.

ROLE OF NR2B SUBUNITS

As NR2BKO mice do not survive postnatally (Tovar et al., 2000), two NR2B subunit antagonists, Ifenprodil and Conantokin G were used to examine the contribution of NR2B subunits to NMDA responses and DA receptor modulation: NMDAR-EPSCs were isolated pharmacologically (Mg^{2+} -free ACSF in the presence of

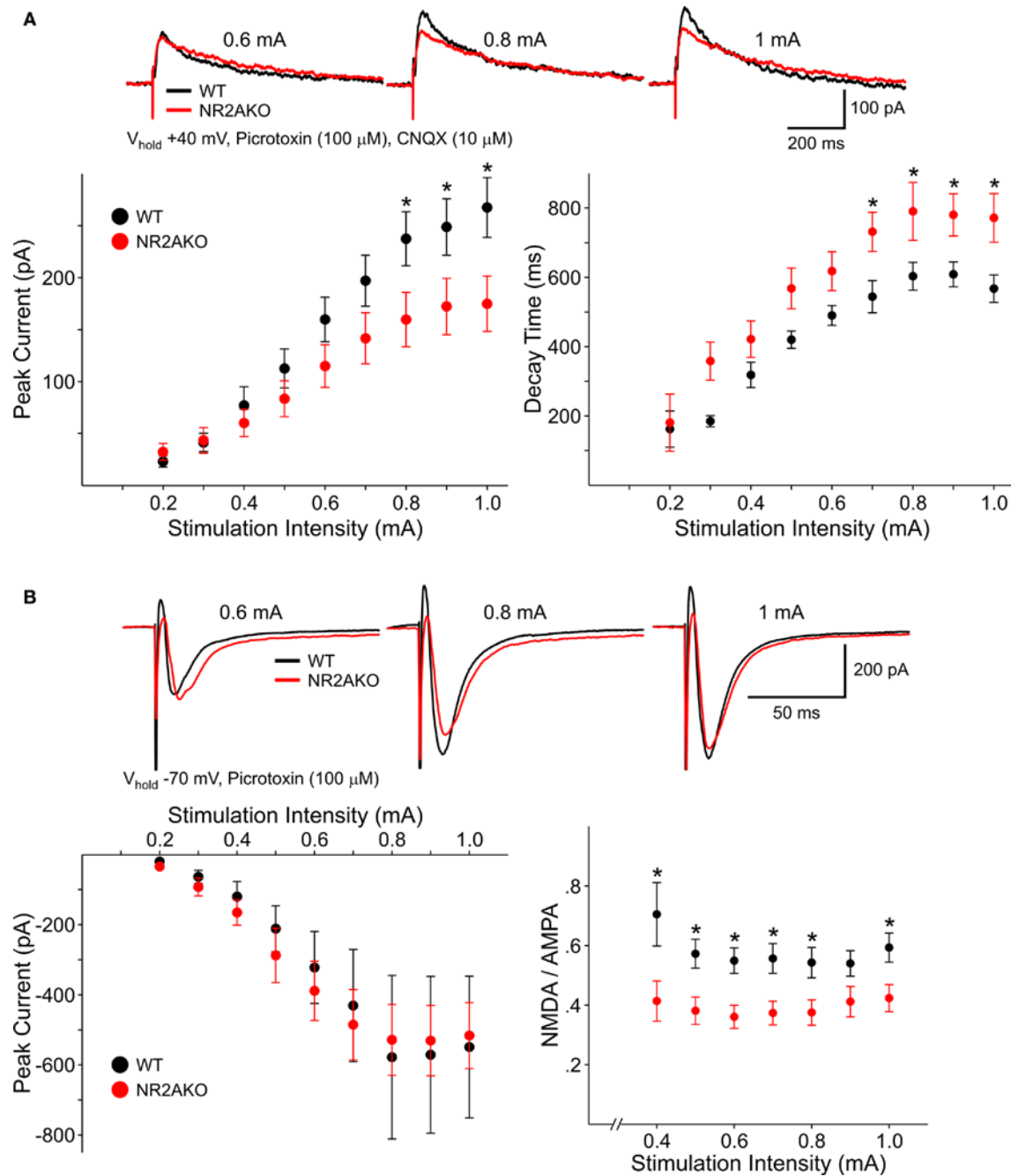


FIGURE 4 | (A) Representative traces of NMDAR-mediated evoked EPSCs from WT and NR2AKO MSSNs at different stimulation current intensities. Graphs are summary data illustrating that mean peak amplitudes of NMDAR-EPSCs are significantly smaller in MSSNs from NR2AKOs compared to those of WT at higher stimulation intensities. In addition, deletion of NR2A results in slower mean decay times. **(B)** In contrast, genetic deletion of

NR2A does not alter AMPAR-mediated EPSCs. Representative traces of evoked AMPAR-EPSCs from WT and NR2AKO MSSNs at different stimulation current intensities. Mean peak amplitudes of AMPAR-EPSCs are similar between genotypes at all intensities. Ratios of mean peak amplitudes of NMDAR- to AMPAR-EPSCs are significantly smaller in NR2AKOs than WTs.

BIC and CNQX). Ifenprodil (5 μ M), a non-competitive NR2B antagonist, only slightly decreased peak NMDAR-EPSC amplitudes $14.2 \pm 4.2\%$ ($p < 0.05$; **Figure 11A**). The competitive antagonist, Conantokin G (1 μ M) significantly decreased peak NMDAR-mediated EPSCs in MSSNs ($36.9 \pm 8.1\%$, $p < 0.05$;

Figure 11B). Faster decay times tended to occur after either Ifenprodil or Conantokin application, although the difference did not reach statistical significance. Taken together, these findings indicate that the NR2B subunit also contributes to synaptic NMDA responses.

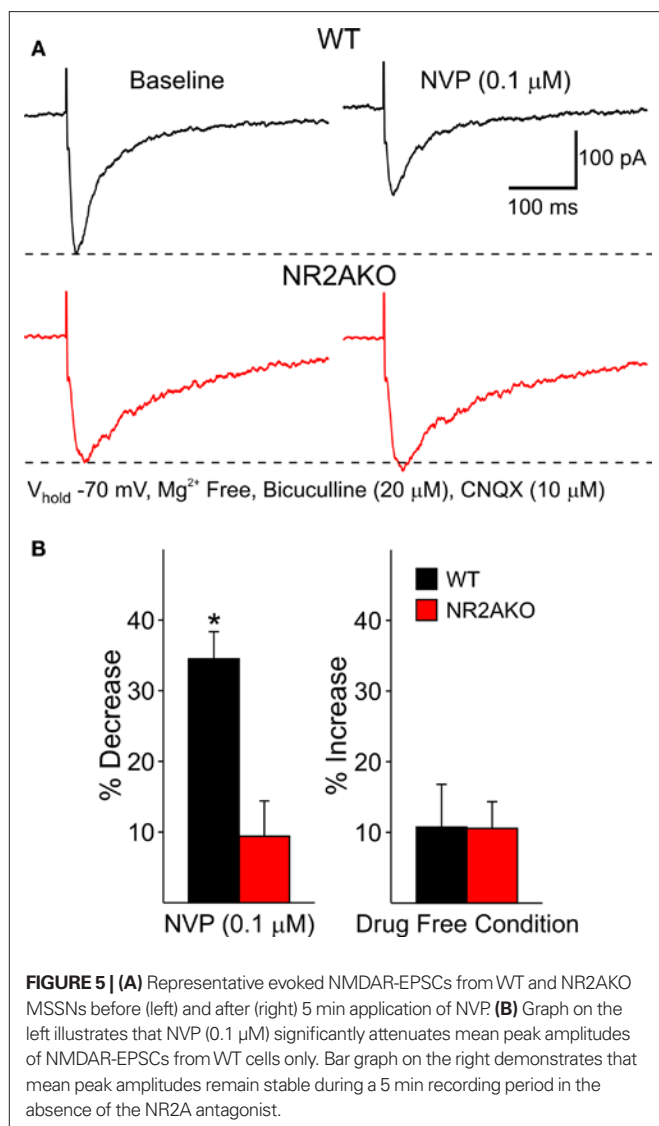


FIGURE 5 | (A) Representative evoked NMDAR-EPSCs from WT and NR2AKO MSSNs before (left) and after (right) 5 min application of NVP. **(B)** Graph on the left illustrates that NVP (0.1 μM) significantly attenuates mean peak amplitudes of NMDAR-EPSCs from WT cells only. Bar graph on the right demonstrates that mean peak amplitudes remain stable during a 5 min recording period in the absence of the NR2A antagonist.

In isolated MSSNs increasing concentrations of Ifenprodil (0.1, 1, and 10 μM) significantly attenuated both peak and steady-state NMDA currents. Steady-state currents were attenuated more than peak currents ($p < 0.05$; **Figure 12A**). The role of NR2B within MSSN subpopulations was examined by applying Ifenprodil to D1-WT and D2-WT cells. NMDAR-mediated peak current densities were blocked in both groups, however current densities from D2-WTs ($n = 8$) were slightly, but consistently, more sensitive to Ifenprodil than D1-WTs ($n = 8$, $p < 0.05$; **Figure 12B**). This difference in Ifenprodil sensitivity suggests that, functionally, levels of NR2B-containing NMDARs are greater in D2-WT than D1-WT cells.

PHARMACOLOGICAL BLOCKADE OF NR2B SUBUNITS REDUCES D1R POTENTIATION OF NMDA RESPONSES

To determine if D1R modulation of NMDAR-mediated currents is affected by the NR2B subunit, recordings from D1-WT MSSNs were made with and without Ifenprodil (1 μM). NMDAR-mediated

currents were potentiated regardless of the presence or absence of Ifenprodil. However, a significant decrease in potentiation by SKF 81297 (1 μM) was observed when Ifenprodil was present ($20.8 \pm 1.8\%$, $n = 28$ in the absence, and $14.1 \pm 1.6\%$, $n = 23$ in the presence of Ifenprodil, $p = 0.01$; **Figure 9B** middle). These data suggest that the NR2B subunit finely tunes D1R modulation; without NR2B, D1R modulation of NMDAR-mediated currents is dampened. In contrast, pharmacological blockade of NR2B subunits did not significantly affect D2R-mediated attenuation of NMDAR-mediated responses with quinpirole (10 μM; **Figure 10** middle).

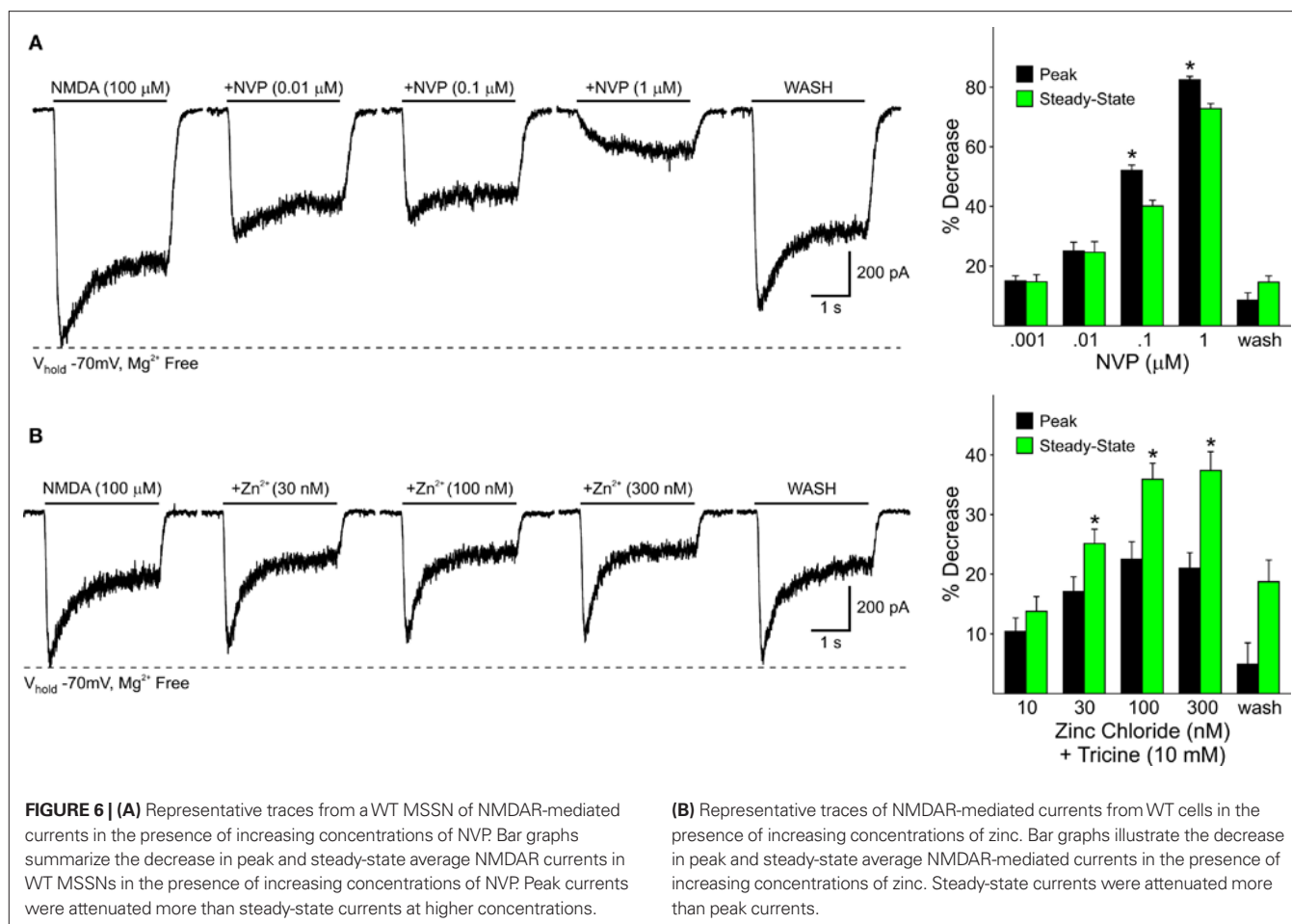
EFFECTS OF COMBINED GENETIC AND PHARMACOLOGICAL BLOCK OF NR2A AND NR2B SUBUNITS ON D1R MODULATION

The combined effect of NR2A and NR2B subunits on D1R modulation was analyzed by genetically deleting NR2A and pharmacologically blocking NR2B-expressing NMDARs. Modulation was compared between D1R-expressing WT cells ($n = 24$), in which NR2A and NR2B subunits remained intact, and D1R-expressing cells in which NR2A was genetically deleted and NR2B subunits were blocked by Ifenprodil ($n = 11$). Interestingly, potentiation levels of NMDAR-mediated currents were similar for both groups (**Figure 9B** right). These data suggest that in the absence of NR2 subunits, the presence of NR1 is enough to maintain normal D1R potentiation levels.

The combined role of NR2 subunits in D2R attenuation of NMDAR-mediated currents also was examined. D2R modulation was compared between MSSNs with NR2 subunits intact (D2-WTs, $n = 9$) and MSSNs in which NR2A was genetically deleted and NR2B was blocked by Ifenprodil (D2-NR2AKO + Ifenprodil, $n = 9$). NMDAR-mediated currents from both groups were attenuated similarly by quinpirole, suggesting that the combined presence or absence of NR2A and NR2B subunits does not play a significant role in D2R modulation of NMDA currents (**Figure 10** right).

DISCUSSION

The major findings of this study are that NR1, NR2A, and NR2B subunits differentially sculpt and modulate glutamatergic inputs in striatal MSSNs. Down-regulation of NR1 subunits in NR1-KD mice produces a significant reduction of NMDAR-mediated responses and removes the ability of D1 receptors to enhance these responses. Associated with these changes, AMPA receptor function is increased in striatal slices and dissociated neurons. Absence or pharmacological blockade of NR2A and NR2B subunits affect the amplitude and kinetics of NMDA responses and produce contrasting effects on D1 modulation. Whereas absence of NR2A subunits enhances NMDAR-mediated potentiation, pharmacological blockade of NR2B subunits decreases this potentiation, suggesting that these subunits have different roles and counterbalance each other. In contrast, D2R modulation of NMDA responses is largely unaffected by NR2A/B subunits. Finally, we also demonstrate that the relative proportion of NR2 subunits is different in subpopulations of MSSNs, with D1 cells (direct pathway) functionally expressing relatively more NR2A-containing NMDARs and D2 cells (indirect pathway) functionally expressing more NR2B-containing NMDARs. The



fact that many of the findings could be demonstrated in slices and in isolated cell preparations is one of the strengths of the present study.

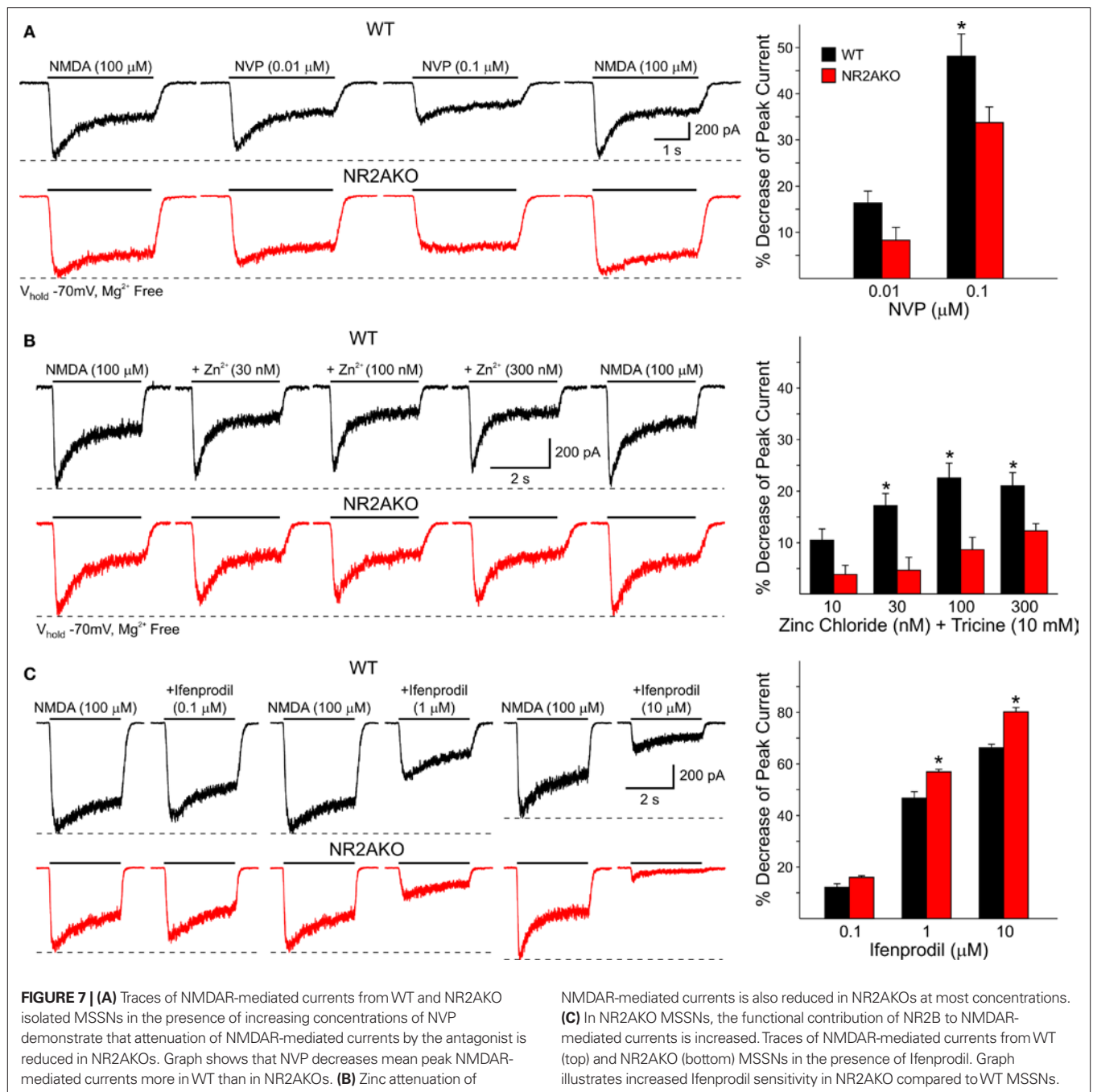
The NR1 subunit is obligatory for a functional NMDA receptor. Thus, the reduction in NMDA receptor-mediated currents in MSSNs from NR1-KD mice was expected. However, the increase in AMPAR-mediated responses was unexpected and suggested compensatory mechanisms to counter deficits in NMDA receptor function. While this effect could be the result of homeostatic mechanisms to balance such deficits, it could also reflect a limitation of the use of genetic knock-out or knock-down animals to examine the function of specific receptor subunits. The very low expression of NR1 subunits during development could have contributed to the changes in AMPA receptor function observed in the present study.

Spontaneous EPSCs displayed faster kinetics indicating that AMPA receptor subunit composition or glutamate transporters may also have changed. However, it cannot be ruled out that the near absence of NR1 subunits contributed to faster EPSCs as NMDAR-mediated responses have slower kinetics than AMPA responses. Finally, in dissociated MSSNs responses to AMPA were increased in NR1-KD animals. Alterations in frequency and kinetics of spontaneous EPSCs, as well as increased responsiveness to AMPA, suggest changes at both the circuit and receptor levels after knock-down of NR1 subunits.

Dopamine D1 receptor modulation of NMDAR-mediated currents in NR1-KD mice showed significant deficits. Enhancement of NMDAR-mediated responses by D1 receptors in striatum is enacted through a number of intracellular signaling cascades including cAMP–PKA–DARPP32, Ca^{2+} conductances, and phosphorylation of NMDA receptor subunits (Snyder et al., 1998; Fiorentini and Missale, 2004; Cepeda et al., 2008a). Reduced expression of NR1 subunits completely obliterated D1 receptor modulation, suggesting that this subunit may represent a final common path for these signaling cascades.

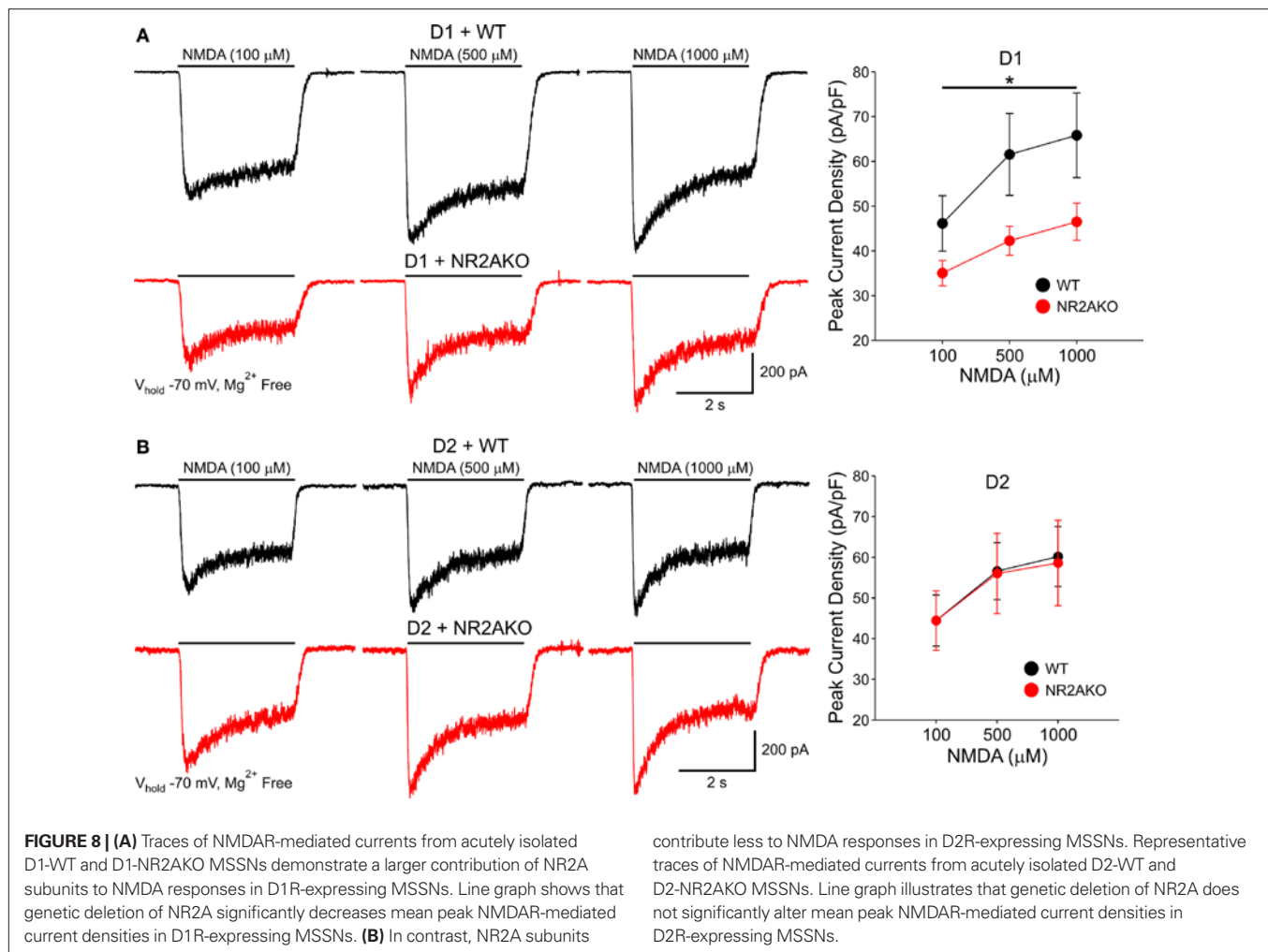
The NR2A/B regulatory subunits confer different sensitivity to zinc and polyamines, open probability, deactivation time, and channel conductance, to name a few (Kohr, 2006). Although still controversial, it appears that NR2 subunit expression differs depending on receptor location with the most prominent contribution of NR2A-containing NMDARs at synaptic sites and NR2B-containing NMDARs at both synaptic and extrasynaptic receptor locations. The present study provides some support for this idea, as genetic KO of NR2A subunits changed the kinetics of evoked synaptic responses.

D1 receptor potentiation of NMDA currents is altered by NR2 subunit composition, but D2R attenuation of these currents is not. Genetic deletion of the NR2A subunit leads to enhanced D1R potentiation of NMDAR-mediated currents, suggesting



that the presence of the NR2A subunit normally counters D1R potentiation. Direct protein coupling is known to occur between the C-terminus of the D1R and the C-terminus of the NR2A subunit, and in the presence of PKA and PKC antagonists, this direct coupling causes a decrease in NMDAR-mediated currents (Lee et al., 2002; Lee and Liu, 2004). This attenuation of currents occurs because fewer NMDARs are expressed on the membrane. In NR2AKO mice, the NR2A subunit is missing, thus direct coupling between D1Rs and NR2A-containing NMDARs cannot occur.

In contrast, the presence of the NR2B subunit enhances D1R potentiation. Genetic deletion of the NR2A subunit at NMDARs located at the soma and proximal dendrites leads to increased Ifenprodil sensitivity and pharmacological blockade of NR2B-containing NMDARs reduces D1R potentiation. Interestingly, studies in the striatum and prefrontal cortex have demonstrated that activation of D1Rs leads to increased surface expression of the NR2B subunit, potentially explaining the observed enhancement of NMDAR-mediated currents (Dunah and Standaert, 2001; Hallett et al., 2006). The mechanism



responsible for this transfer of NMDARs from the intracellular membrane to the plasma membrane surface involves phosphorylation of NR2B subunits by tyrosine kinases (Dunah and Standaert, 2001; Dunah et al., 2004; Hallett et al., 2006; Gao and Wolf, 2008; Pascoli et al., 2011). Therefore, pharmacological blockade of the NR2B subunit will prevent increased surface expression by D1R activation and the level of potentiation of NMDAR-mediated currents will decrease. Heteromeric complexes consisting of NMDA and D1Rs are known to exist and these complexes increase the density of D1Rs at the postsynaptic density (Fiorentini and Missale, 2004).

It appears that NR2A and NR2B subunits maintain a balance, and when one of these subunits is missing or antagonized, the other predominates and the degree of D1R modulation becomes affected. However, when both NR2A and NR2B subunits are blocked, D1R modulation levels of NMDAR-mediated currents are similar to WT levels. Perhaps phosphorylation of NR1 subunits is sufficient to allow renormalization of D1R potentiation (Snyder et al., 1998).

Interestingly, changes in NR2 subunit composition do not alter D2R modulation of NMDA currents. Direct protein–protein coupling does occur between NMDARs and D2Rs, although only in

the presence of cocaine (Liu et al., 2006). It is striking that despite the existence of D2-NR2B heteroreceptors, pharmacological block of NR2B-expressing receptors does not alter D2R modulation. Because these heteroreceptors appear to occur only under particular conditions, they may not play an important role in normal D2R modulation of NMDAR-mediated currents.

Prior studies examining NR2 subunit expression in striatum observed the presence of NR2A and NR2B subunits in MSSNs. However, conclusive data regarding the preferred expression of NR2 subunits between MSSNs of the direct (D1) and indirect (D2) pathways was not observed (Landwehrmeyer et al., 1995; Standaert et al., 1999). In the present study, significant functional differences in NR2 subunit composition of NMDARs were observed with D1R-containing cells expressing relatively greater NR2A subunit levels while D2R-containing cells express relatively greater NR2B subunit levels. Opposite results were observed by Fantin et al. (2007), concluding that NR2A subunits regulate D2 while NR2B subunits regulate D1 MSSNs. Differences in methodology could explain these opposing findings. One caveat of the present study is that only acutely isolated MSSNs were used for the NR2 subunit experiments. Thus, observed differences in NR2 subunit expression between D1R- and D2R-expressing MSSNs are applicable

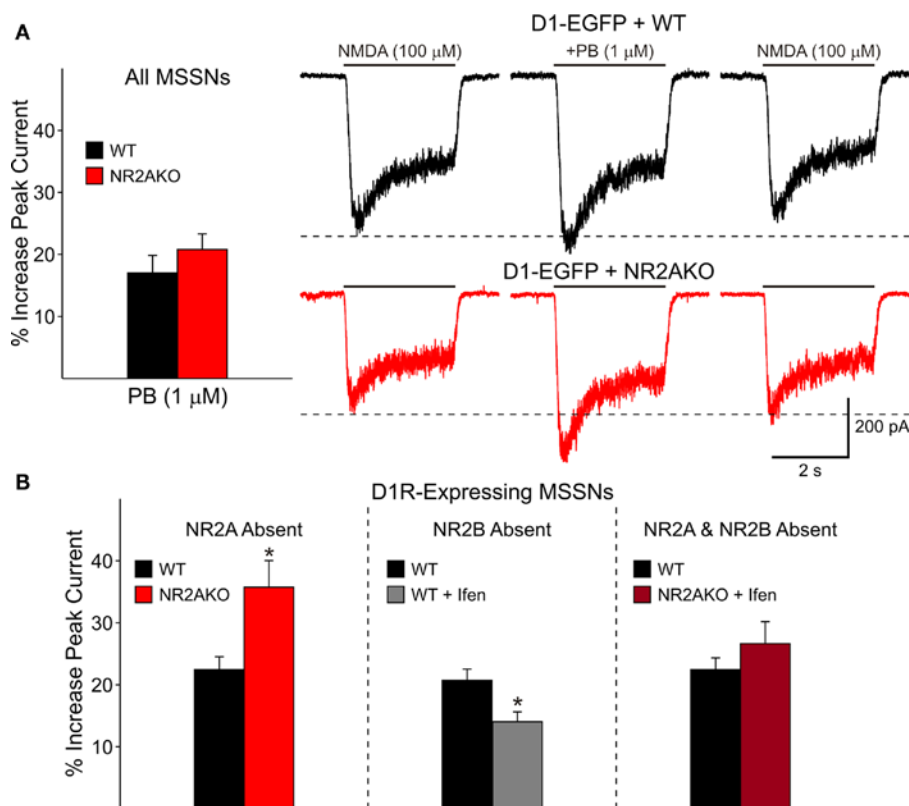


FIGURE 9 | (A) Bar graph shows that genetic deletion of NR2A does not significantly alter D1R-modulation of NMDAR-mediated currents in both D1R- and D2R-expressing cells. Traces on the right illustrate NMDAR-mediated currents in D1-WT and D1-NR2AKO MSSNs. The D1 agonist (PB) significantly potentiates NMDAR-mediated currents more in D1R-expressing cells from NR2AKOs. **(B)** The bar graph on the left illustrates that genetic deletion of NR2A

significantly increases D1R potentiation of NMDA currents. The bar graph in the middle demonstrates that pharmacological block of NR2B-expressing NMDARs results in a significant decrease in D1R potentiation. The bar graph on the right illustrates that the combined genetic deletion of NR2A and pharmacological block of NR2B-expressing NMDARs does not significantly alter D1R modulation.

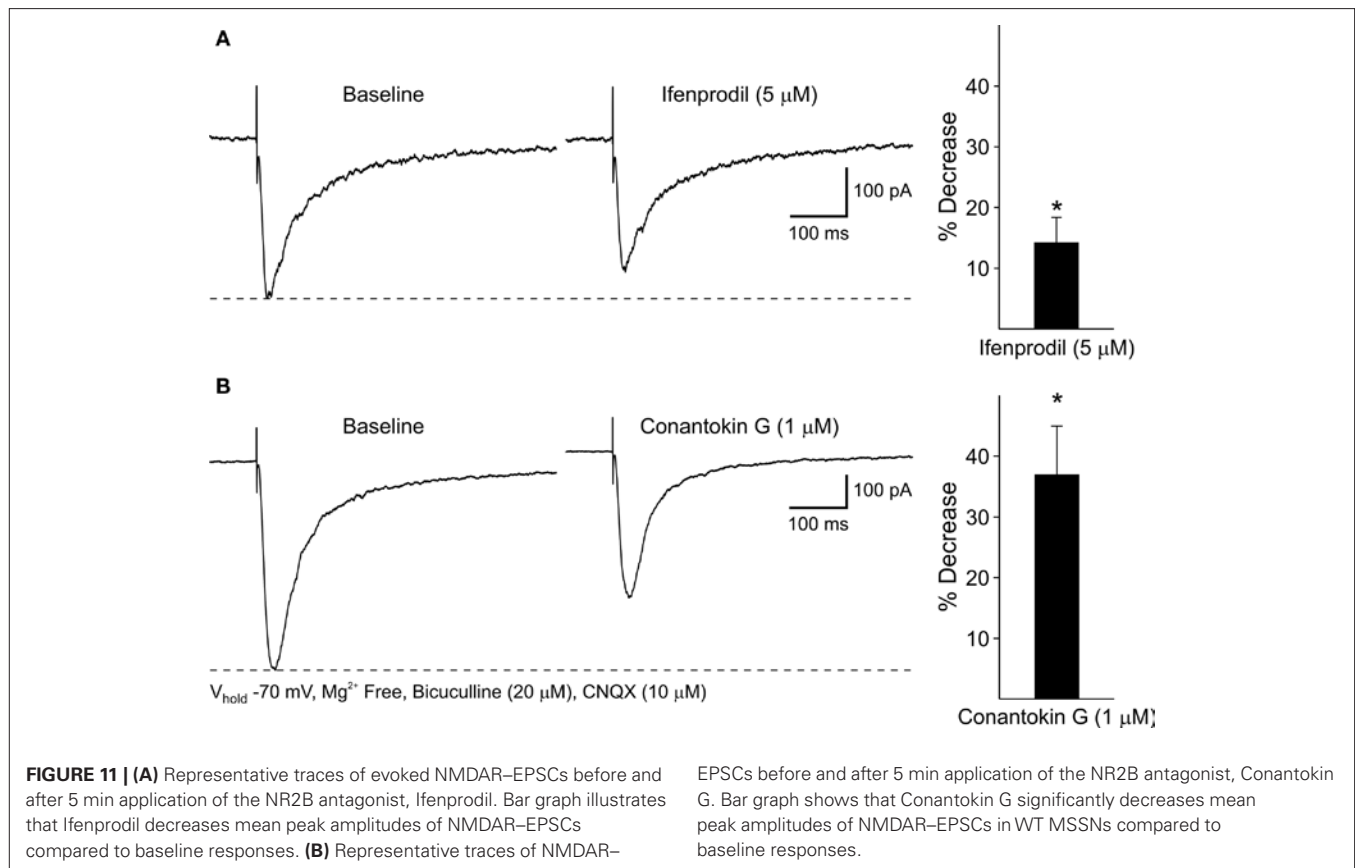
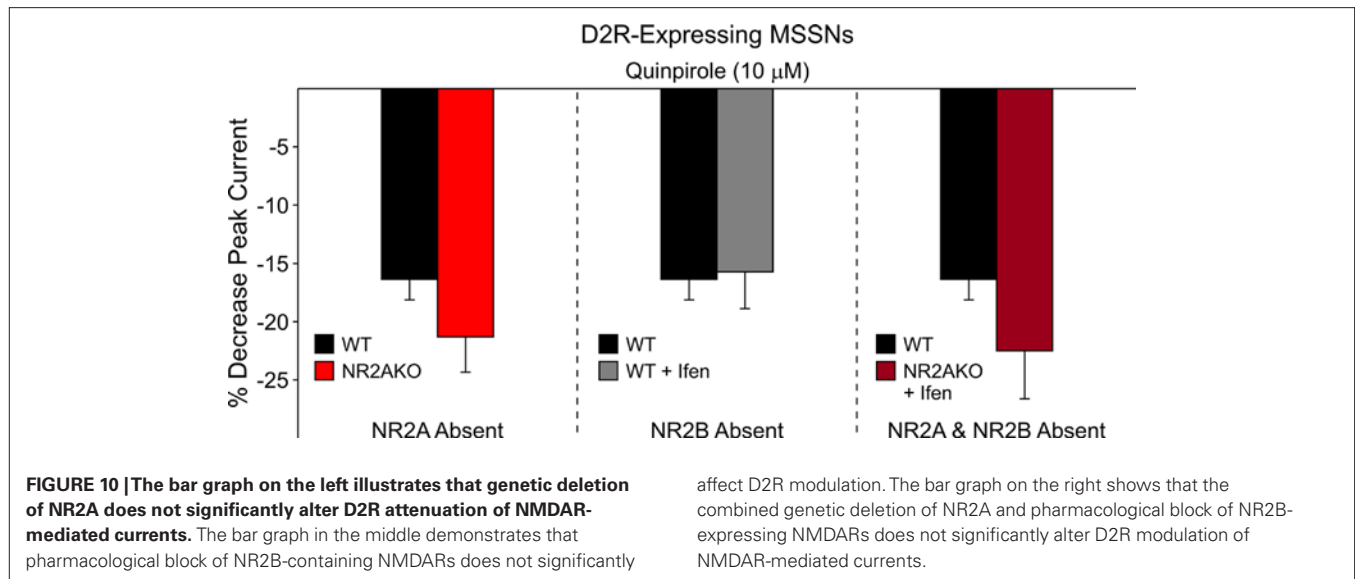
only to NMDARs located at the soma and proximal dendrites. These data do not provide information about the distribution of NR2A- and NR2B-containing NMDARs at distal dendrite locations on MSSN subpopulations.

Differences in NR2 subunit expression may play a key role in excitotoxicity and, therefore, could increase the overall vulnerability of subpopulations of MSSNs. Several pieces of evidence suggest that D1 MSSNs are less vulnerable to excitotoxicity than D2 MSSNs. D1 cells express greater levels of NR2A-containing NMDARs than D2 cells and these NMDARs have faster decay times (Monyer et al., 1994; Flint et al., 1997). As a result, Ca^{2+} flux is more restricted in D1 cells, potentially providing more protection for these cells. The combination of increased excitability (Kreitzer and Malenka, 2007; Cepeda et al., 2008b; Gertler et al., 2008) and greater functional expression of NR2B-containing NMDARs in D2 cells may increase their vulnerability to excitotoxicity.

The functional importance of NR2 subunit composition of NMDARs is highlighted by pathological conditions in which changes in subunit composition occur, including Huntington's disease (HD). Alterations in NR2 subunit composition are observed in a mouse model of HD (Ali and Levine, 2006). Additionally, shifts

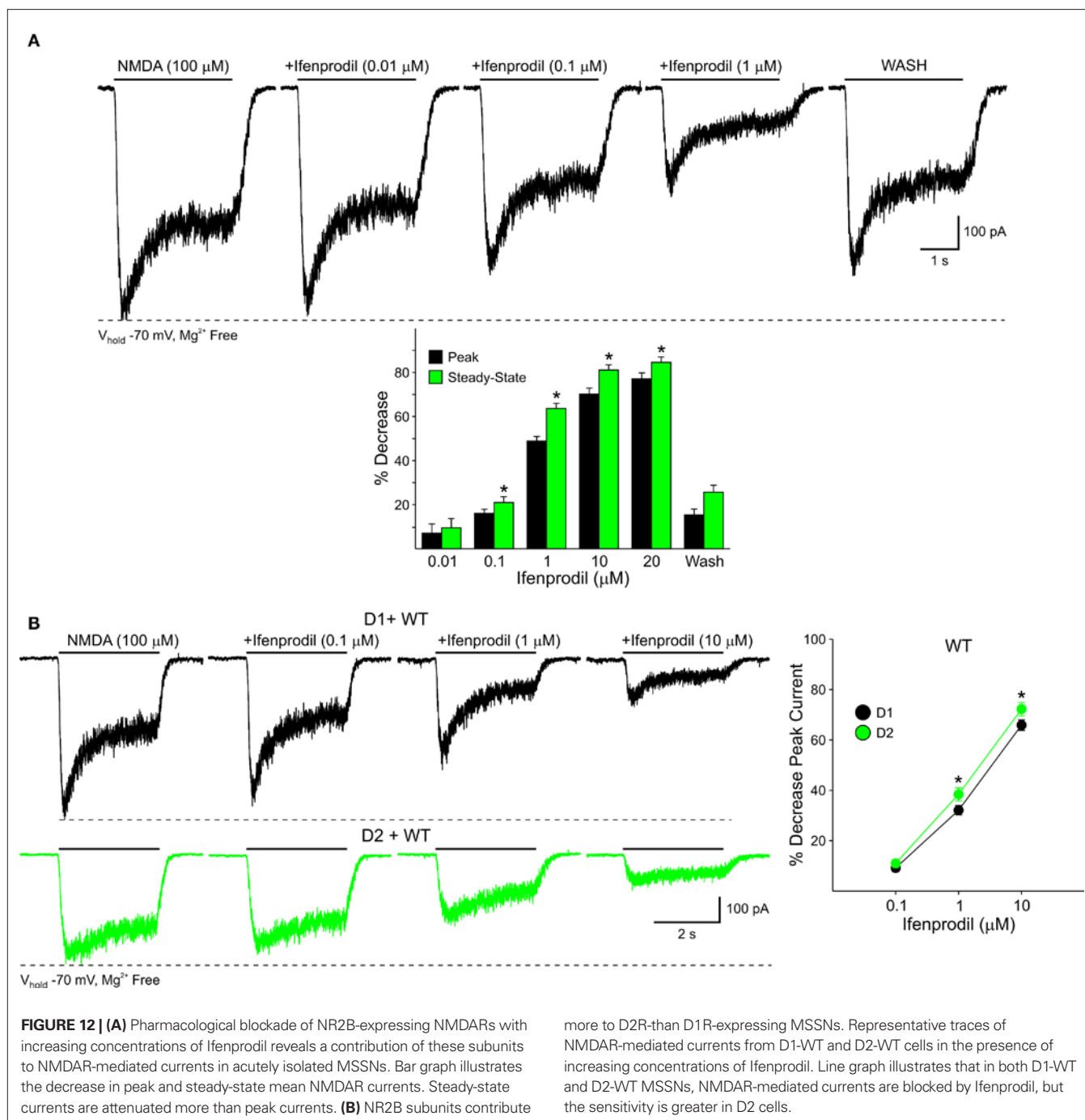
in the NR2 subunit ratio of another HD model leads to increased striatal neurodegeneration by overexpression of NR2B subunits, further emphasizing that changes in NR2 composition can exacerbate pathological conditions (Heng et al., 2009). The location of NR2 subunits also plays an important role. NR2A subunits are predominantly found at the synapse, whereas NR2B subunits occur at both synaptic and extrasynaptic sites. It has been shown that stimulation of synaptic NMDA receptors confers cell protection in mouse models of HD, whereas stimulation of NR2B-containing NMDA receptors at extrasynaptic locations is pro-apoptotic and detrimental for cell survival (Okamoto et al., 2009; Milnerwood et al., 2010).

NMDA receptors play an essential role in cognition and mood regulation. Blockade or deficits in NMDA receptor-function have been associated with the negative symptoms of schizophrenia (Olney et al., 1999). However, individual subunits appear to play different roles. In the NR1-KD mouse used in the present study, behavioral alterations similar to those observed in pharmacologically induced animal models of schizophrenia have been reported (Mohn et al., 1999; Ramsey, 2009). Cognitive deficits in NR1-KD mice could be compounded by the lack of D1 receptor potentiation of NMDA responses. In contrast, NR2A subunit KO mice



demonstrate a selective reduction in anxiety and depression, supporting a role of NR2A subunits in the modulation of emotional behaviors (Boyce-Rustay and Holmes, 2006). Absence of the NR2A subunits in mice also leads to deficits in discrimination learning (Brigman et al., 2008), suggesting this subunit plays a role in synaptic plasticity. In contrast, NR2B antagonists appear

to improve cognitive performance in attentional tasks (Kos et al., 2011). The idea that NR2A and NR2B subunits play differential roles in synaptic plasticity remains controversial, and most studies indicate that both are required for long-term synaptic changes (Erreger et al., 2005; Fox et al., 2006; Schotanus and Chergui, 2008; Muller et al., 2009). The fact that their interactions



with D1 receptors are bidirectional lends support to the idea of specific functions of each subunit in synaptic plasticity, at least in striatum.

CONCLUSION

In conclusion, using genetic and pharmacological tools we provide evidence that NMDA receptor subunits differentially contribute to the sculpting of NMDA responses and their modulation by D1 dopamine receptors in striatal MSSNs. The NR1 subunit is critical for both functions as down-regulation of this subunit almost

completely eliminates NMDA responses and their modulation. NR2A/B subunits can affect amplitude and kinetics of the response and play contrasting roles in D1 receptor modulation. In addition, we demonstrate that in D1 receptor-containing MSSNs the NR2A subunit has a more prominent functional role, whereas in D2 receptor-containing MSSNs the NR2B subunit predominates. This could have important implications for differential synaptic plasticity and neuronal vulnerability of MSSNs of the direct and indirect pathways. We have demonstrated that D1 receptor activation enhances NMDA responses (Cepeda et al., 1993; Andre et al., 2010a). If NR2A

subunits are more concentrated around synapses, it is possible that D1 receptor enhancement of synaptic NMDA responses would support plasticity in direct pathway MSSNs. In contrast, the presence of NR2B subunits at both synaptic and extrasynaptic loci, could make neurons of the indirect pathway more vulnerable to excess glutamate release and would be detrimental for cell survival (Hardingham et al., 2002). Additional studies will be necessary to unravel the role of second messenger cascades and protein–protein interactions in these contrasting roles of NR2A/B subunits.

REFERENCES

- Ali, N. J., and Levine, M. S. (2006). Changes in expression of N-methyl-D-aspartate receptor subunits occur early in the R6/2 mouse model of Huntington's disease. *Dev. Neurosci.* 28, 230–238.
- Andre, V. M., Cepeda, C., Cummings, D. M., Jocoy, E. L., Fisher, Y. E., William Yang, X., and Levine, M. S. (2010a). Dopamine modulation of excitatory currents in the striatum is dictated by the expression of D1 or D2 receptors and modified by endocannabinoids. *Eur. J. Neurosci.* 31, 14–28.
- Andre, V. M., Cepeda, C., and Levine, M. S. (2010b). Dopamine and glutamate in Huntington's disease: a balancing act. *CNS Neurosci. Ther.* 16, 163–178.
- Bargas, J., Howe, A., Eberwine, J., Cao, Y., and Surmeier, D. J. (1994). Cellular and molecular characterization of Ca^{2+} currents in acutely isolated, adult rat neostriatal neurons. *J. Neurosci.* 14, 6667–6686.
- Bouyer, J. J., Park, D. H., Joh, T. H., and Pickel, V. M. (1984). Chemical and structural analysis of the relation between cortical inputs and tyrosine hydroxylase-containing terminals in rat neostriatum. *Brain Res.* 302, 267–275.
- Boyce-Rustay, J. M., and Holmes, A. (2006). Genetic inactivation of the NMDA receptor NR2A subunit has anxiolytic- and antidepressant-like effects in mice. *Neuropsychopharmacology* 31, 2405–2414.
- Brady, A. M., and O'Donnell, P. (2004). Dopaminergic modulation of prefrontal cortical input to nucleus accumbens neurons in vivo. *J. Neurosci.* 24, 1040–1049.
- Brigman, J. L., Feyder, M., Saksida, L. M., Bussey, T. J., Mishina, M., and Holmes, A. (2008). Impaired discrimination learning in mice lacking the NMDA receptor NR2A subunit. *Learn. Mem.* 15, 50–54.
- Calabresi, P., Gubellini, P., Centonze, D., Picconi, B., Bernardi, G., Chergui, K., Svenningsson, P., Fienberg, A. A., and Greengard, P. (2000). Dopamine and cAMP-regulated phosphoprotein 32 kDa controls both striatal long-term depression and long-term potentiation, opposing forms of synaptic plasticity. *J. Neurosci.* 20, 8443–8451.
- Cepeda, C., Andre, V. M., Jocoy, E. L., and Levine, M. S. (2008a). "NMDA and dopamine: diverse mechanisms applied to interacting receptor systems," in *The Biology of the NMDA Receptor*, ed. A. M. Vandongen (Boca Raton, FL: Taylor & Francis Group, LLC), 41–57.
- Cepeda, C., André, V. M., Yamazaki, I., Wu, N., Kleiman-Weiner, M., and Levine, M. S. (2008b). Differential electrophysiological properties of dopamine D1 and D2 receptor-containing striatal medium-sized spiny neurons. *Eur. J. Neurosci.* 27, 671–682.
- Cepeda, C., Buchwald, N. A., and Levine, M. S. (1993). Neuromodulatory actions of dopamine in the neostriatum are dependent upon the excitatory amino acid receptor subtypes activated. *Proc. Natl. Acad. Sci. U.S.A.* 90, 9576–9580.
- Cepeda, C., Colwell, C. S., Itri, J. N., Chandler, S. H., and Levine, M. S. (1998). Dopaminergic modulation of NMDA-induced whole cell currents in neostriatal neurons in slices: contribution of calcium conductances. *J. Neurophysiol.* 79, 82–94.
- Chergui, K., and Lacey, M. G. (1999). Modulation by dopamine D1-like receptors of synaptic transmission and NMDA receptors in rat nucleus accumbens is attenuated by the protein kinase C inhibitor Ro 32-0432. *Neuropharmacology* 38, 223–231.
- Dunah, A. W., Sirianni, A. C., Fienberg, A. A., Bastia, E., Schwarzschild, M. A., and Standaert, D. G. (2004). Dopamine D1-dependent trafficking of striatal N-methyl-D-aspartate glutamate receptors requires Fyn protein tyrosine kinase but not DARPP-32. *Mol. Pharmacol.* 65, 121–129.
- Dunah, A. W., and Standaert, D. G. (2001). Dopamine D1 receptor-dependent trafficking of striatal NMDA glutamate receptors to the postsynaptic membrane. *J. Neurosci.* 21, 5546–5558.
- Dunah, A. W., and Standaert, D. G. (2003). Subcellular segregation of distinct heteromeric NMDA glutamate receptors in the striatum. *J. Neurochem.* 85, 935–943.
- Erreger, K., Dravid, S. M., Banke, T. G., Wyllie, D. J., and Traynelis, S. F. (2005). Subunit-specific gating controls rat NR1/NR2A and NR1/NR2B NMDA channel kinetics and synaptic signalling profiles. *J. Physiol.* 563, 345–358.
- Fantin, M., Marti, M., Auberson, Y. P., and Morari, M. (2007). NR2A and NR2B subunit containing NMDA receptors differentially regulate striatal output pathways. *J. Neurochem.* 103, 2200–2211.
- Fiorentini, C., and Missale, C. (2004). Oligomeric assembly of dopamine D1 and glutamate NMDA receptors: molecular mechanisms and functional implications. *Biochem. Soc. Trans.* 32, 1025–1028.
- Flint, A. C., Maisch, U. S., Weishaupt, J. H., Kriegstein, A. R., and Monyer, H. (1997). NR2A subunit expression shortens NMDA receptor synaptic currents in developing neocortex. *J. Neurosci.* 17, 2469–2476.
- Flores-Hernandez, J., Cepeda, C., Hernandez-Echeagaray, E., Calvert, C. R., Jokel, E. S., Fienberg, A. A., Greengard, P., and Levine, M. S. (2002). Dopamine enhancement of NMDA currents in dissociated medium-sized striatal neurons: role of D1 receptors and DARPP-32. *J. Neurophysiol.* 88, 3010–3020.
- Fox, C. J., Russell, K. I., Wang, Y. T., and Christie, B. R. (2006). Contribution of NR2A and NR2B NMDA subunits to bidirectional synaptic plasticity in the hippocampus in vivo. *Hippocampus* 16, 907–915.
- Freund, T. F., Powell, J. F., and Smith, A. D. (1984). Tyrosine hydroxylase-immunoreactive boutons in synaptic contact with identified striatonigral neurons, with particular reference to dendritic spines. *Neuroscience* 13, 1189–1215.
- Gao, C., and Wolf, M. E. (2008). Dopamine receptors regulate NMDA receptor surface expression in prefrontal cortex neurons. *J. Neurochem.* 106, 2489–2501.
- Gertler, T. S., Chan, C. S., and Surmeier, D. J. (2008). Dichotomous anatomical properties of adult striatal medium spiny neurons. *J. Neurosci.* 28, 10814–10824.
- Hallett, P. J., Spoelgen, R., Hyman, B. T., Standaert, D. G., and Dunah, A. W. (2006). Dopamine D1 activation potentiates striatal NMDA receptors by tyrosine phosphorylation-dependent subunit trafficking. *J. Neurosci.* 26, 4690–4700.
- Hardingham, G. E., Fukunaga, Y., and Bading, H. (2002). Extrasynaptic NMDARs oppose synaptic NMDARs by triggering CREB shut-off and cell death pathways. *Nat. Neurosci.* 5, 405–414.
- Heng, M. Y., Detloff, P. J., Wang, P. L., Tsien, J. Z., and Albin, R. L. (2009). In vivo evidence for NMDA receptor-mediated excitotoxicity in a murine genetic model of Huntington disease. *J. Neurosci.* 29, 3200–3205.
- Ikeda, K., Araki, K., Takayama, C., Inoue, Y., Yagi, T., Aizawa, S., and Mishina, M. (1995). Reduced spontaneous activity of mice defective in the epsilon 4 subunit of the NMDA receptor channel. *Brain Res. Mol. Brain Res.* 33, 61–71.
- Kohr, G. (2006). NMDA receptor function: subunit composition versus spatial distribution. *Cell Tissue Res.* 326, 439–446.
- Kos, T., Nikiforuk, A., Rafa, D., and Popik, P. (2011). The effects of NMDA receptor antagonists on attentional set-shifting task performance in mice. *Psychopharmacology (Berl)* 214, 911–921.
- Kramer, P. F., Christensen, C. H., Hazelwood, L. A., Dobi, A., Bock, R., Sibley, D. R., Mateo, Y., and Alvarez, V. A. (2011). Dopamine D2 receptor overexpression alters behavior and physiology in Drd2-EGFP mice. *J. Neurosci.* 31, 126–132.
- Kreitzer, A. C., and Malenka, R. C. (2007). Endocannabinoid-mediated rescue of striatal LTD and motor deficits in Parkinson's disease models. *Nature* 445, 643–647.
- Kutsuwada, T., Sakimura, K., Manabe, T., Takayama, C., Katakura, N., Kushiya, E., Natsume, R., Watanabe, M., Inoue, Y., Yagi, T., Aizawa, S., Arakawa, M., Takahashi, T., Nakamura, Y., Mori, H., and Mishina, M. (1996). Impairment of suckling response, trigeminal neuronal pattern formation, and

- hippocampal LTD in NMDA receptor epsilon 2 subunit mutant mice. *Neuron* 16, 333–344.
- Landwehrmeyer, G. B., Standaert, D. G., Testa, C. M., Penney, J. B. Jr., and Young, A. B. (1995). NMDA receptor subunit mRNA expression by projection neurons and interneurons in rat striatum. *J. Neurosci.* 15, 5297–5307.
- Laube, B., Kuhse, J., and Betz, H. (1998). Evidence for a tetrameric structure of recombinant NMDA receptors. *J. Neurosci.* 18, 2954–2961.
- Lee, F. J., and Liu, F. (2004). Direct interactions between NMDA and D1 receptors: a tale of tails. *Biochem. Soc. Trans.* 32, 1032–1036.
- Lee, F. J., Xue, S., Pei, L., Vukusic, B., Chery, N., Wang, Y., Wang, Y. T., Niznik, H. B., Yu, X. M., and Liu, F. (2002). Dual regulation of NMDA receptor functions by direct protein-protein interactions with the dopamine D1 receptor. *Cell* 111, 219–230.
- Levine, M. S., Altemus, K. L., Cepeda, C., Cromwell, H. C., Crawford, C., Ariano, M. A., Drago, J., Sibley, D. R., and Westphal, H. (1996a). Modulatory actions of dopamine on NMDA receptor-mediated responses are reduced in D1A-deficient mutant mice. *J. Neurosci.* 16, 5870–5882.
- Levine, M. S., Li, Z., Cepeda, C., Cromwell, H. C., and Altemus, K. L. (1996b). Neuromodulatory actions of dopamine on synaptically-evoked neostriatal responses in slices. *Synapse* 24, 65–78.
- Liu, X. Y., Chu, X. P., Mao, L. M., Wang, M., Lan, H. X., Li, M. H., Zhang, G. C., Parekar, N. K., Fibuch, E. E., Haines, M., Neve, K. A., Liu, F., Xiong, Z. G., and Wang, J. Q. (2006). Modulation of D2R-NR2B interactions in response to cocaine. *Neuron* 52, 897–909.
- Milnerwood, A. J., Gladding, C. M., Pouladi, M. A., Kaufman, A. M., Hines, R. M., Boyd, J. D., Ko, R. W., Vasuta, O. C., Graham, R. K., Hayden, M. R., Murphy, T. H., and Raymond, L. A. (2010). Early increase in extrasynaptic NMDA receptor signaling and expression contributes to phenotype onset in Huntington's disease mice. *Neuron* 65, 178–190.
- Mohn, A. R., Gainetdinov, R. R., Caron, M. G., and Koller, B. H. (1999). Mice with reduced NMDA receptor expression display behaviors related to schizophrenia. *Cell* 98, 427–436.
- Monyer, H., Burnashev, N., Laurie, D. J., Sakmann, B., and Seeburg, P. H. (1994). Developmental and regional expression in the rat brain and functional properties of four NMDA receptors. *Neuron* 12, 529–540.
- Muller, T., Albrecht, D., and Gebhardt, C. (2009). Both NR2A and NR2B subunits of the NMDA receptor are critical for long-term potentiation and long-term depression in the lateral amygdala of horizontal slices of adult mice. *Learn Mem.* 16, 395–405.
- Okamoto, S., Pouladi, M. A., Talantova, M., Yao, D., Xia, P., Ehrnhoefer, D. E., Zaidi, R., Clemente, A., Kaul, M., Graham, R. K., Zhang, D., Vincent Chen, H. S., Tong, G., Hayden, M. R., and Lipton, S. A. (2009). Balance between synaptic versus extrasynaptic NMDA receptor activity influences inclusions and neurotoxicity of mutant huntingtin. *Nat. Med.* 15, 1407–1413.
- Olney, J. W., Newcomer, J. W., and Farber, N. B. (1999). NMDA receptor hypofunction model of schizophrenia. *J. Psychiatr. Res.* 33, 523–533.
- Pascoli, V., Besnard, A., Herve, D., Pages, C., Heck, N., Girault, J. A., Caboche, J., and Vanhoutte, P. (2011). Cyclic adenosine monophosphate-independent tyrosine phosphorylation of NR2B mediates cocaine-induced extracellular signal-regulated kinase activation. *Biol. Psychiatry* 69, 218–227.
- Ramsey, A. J. (2009). NR1 knockdown mice as a representative model of the glutamate hypothesis of schizophrenia. *Prog. Brain Res.* 179, 51–58.
- Sakimura, K., Kutsuwada, T., Ito, I., Manabe, T., Takayama, C., Kushiya, E., Yagi, T., Aizawa, S., Inoue, Y., Sugiyama, H., and Mishina, M. (1995). Reduced hippocampal LTP and spatial learning in mice lacking NMDA receptor epsilon 1 subunit. *Nature* 373, 151–155.
- Schotanus, S. M., and Chergui, K. (2008). NR2A-containing NMDA receptors depress glutamatergic synaptic transmission and evoked-dopamine release in the mouse striatum. *J. Neurochem.* 106, 1758–1765.
- Schultz, W. (2010). Dopamine signals for reward value and risk: basic and recent data. *Behav. Brain Funct.* 6, 24.
- Snyder, G. L., Fienberg, A. A., Huganir, R. L., and Greengard, P. (1998). A dopamine/D1 receptor/protein kinase A/dopamine- and cAMP-regulated phosphoprotein (Mr 32 kDa)/protein phosphatase-1 pathway regulates dephosphorylation of the NMDA receptor. *J. Neurosci.* 18, 10297–10303.
- Standaert, D. G., Friberg, I. K., Landwehrmeyer, G. B., Young, A. B., and Penney, J. B. Jr. (1999). Expression of NMDA glutamate receptor subunit mRNAs in neurochemically identified projection and interneurons in the striatum of the rat. *Brain Res. Mol. Brain Res.* 64, 11–23.
- Surmeier, D. J., Ding, J., Day, M., Wang, Z., and Shen, W. (2007). D1 and D2 dopamine-receptor modulation of striatal glutamatergic signaling in striatal medium spiny neurons. *Trends Neurosci.* 30, 228–235.
- Tovar, K. R., Sprouffske, K., and Westbrook, G. L. (2000). Fast NMDA receptor-mediated synaptic currents in neurons from mice lacking the epsilon2 (NR2B) subunit. *J. Neurophysiol.* 83, 616–620.
- Tseng, K. Y., and O'Donnell, P. (2004). Dopamine-glutamate interactions controlling prefrontal cortical pyramidal cell excitability involve multiple signaling mechanisms. *J. Neurosci.* 24, 5131–5139.

Conflict of Interest Statement: The authors declare that the research was conducted in the absence of any commercial or financial relationships that could be construed as a potential conflict of interest.

Received: 26 January 2011; paper pending published: 26 March 2011; accepted: 28 April 2011; published online: 11 May 2011.

Citation: Jocoy EL, André VM, Cummings DM, Rao SP, Wu N, Ramsey AJ, Caron MG, Cepeda C and Levine MS (2011) Dissecting the contribution of individual receptor subunits to the enhancement of N-methyl-D-aspartate currents by dopamine D1 receptor activation in striatum. *Front. Syst. Neurosci.* 5:28. doi: 10.3389/fnsys.2011.00028
Copyright © 2011 Jocoy, André, Cummings, Rao, Wu, Ramsey, Caron, Cepeda and Levine. This is an open-access article subject to a non-exclusive license between the authors and Frontiers Media SA, which permits use, distribution and reproduction in other forums, provided the original authors and source are credited and other Frontiers conditions are complied with.



Role of striatum in the pause and burst generation in the globus pallidus of 6-OHDA-treated rats

Hitoshi Kita* and Takako Kita

Department of Anatomy and Neurobiology, College of Medicine, The University of Tennessee Health Science Center, Memphis, TN, USA

Edited by:

James M. Tepper, Rutgers, The State University of New Jersey, USA

Reviewed by:

Alessandro Stefani, University of Rome, Italy

Judith Walters, National Institute of Neurological Disease and Stroke, National Institutes of Medicine, USA

*Correspondence:

Hitoshi Kita, Department of Anatomy and Neurobiology, College of Medicine, The University of Tennessee Health Science Center, 855 Monroe Avenue, Memphis, TN 38163, USA.
e-mail: hkita@uthsc.edu

Electrophysiological studies in patients and animal models of Parkinson's disease (PD) often reported increased burst activity of neurons in the basal ganglia. Neurons in the globus pallidus external (GPe) segment in 6-hydroxydopamine (6-OHDA)-treated hemi-parkinsonian rats fire with strong bursts interrupted by pauses. The goal of this study was to evaluate the hypothesis that dopamine (DA)-depletion increases burst firings of striatal (Str) neurons projecting to the GPe and that the increased Str-GPe burst inputs play a significant role in the generation of pauses and bursts in GPe and its projection sites. To evaluate this hypothesis, the unitary activity of Str and GPe was recorded from control and 6-OHDA-treated rats anesthetized with 0.5–1 % isoflurane. The occurrence of pauses and bursts in the firings of GPe neurons was significantly higher in 6-OHDA than in normal rats. Muscimol injection into the Str of 6-OHDA rats increased average firing rate and greatly reduced the pauses and bursts in GPe. Recordings from Str revealed that most of the presumed projection neurons in control rats have very low spontaneous activity, and even the occasional neurons that did exhibit spontaneous burst firings did so with an average rate of less than 2 Hz. In DA-depleted Str, neurons having stronger bursts and a higher average firing rate were encountered more frequently. Juxtacellular labeling revealed that most of these neurons were medium spiny neurons projecting only to GPe. Injection of a behaviorally effective dose of methyl-L-DOPA into the Str of 6-OHDA rats significantly increased the average firing rate and decreased the number of pauses of GPe neurons. These data validate the hypothesis that DA-depletion increases burst firings of Str neurons projecting to the GPe and that the increased Str-GPe burst inputs play a significant role in the generation of pauses and bursts in GPe. These results suggest that treatment to reduce burst Str-GPe inhibitory inputs may help to restore some PD disabilities.

Keywords: dopamine depletion, pauses, burst, firing pattern, unitary activity, globus pallidus, striatum, basal ganglia

INTRODUCTION

Electrophysiological observations made in patients and animal models of basal ganglia diseases reported various changes in the activity of basal ganglia neurons including abnormal firing patterns, increased bursts and pauses, and abnormal synchronized oscillations (Pan and Walters, 1988; Filion and Tremblay, 1991; Bergman et al., 1994; Ni et al., 2000; Soares et al., 2004; Wichmann and DeLong, 2006; Stefani et al., 2011). Among these, the most often observed changes are increased burst and pause activity of neurons in the basal ganglia, particularly in the pallidum and the subthalamic nucleus (STN; Pan and Walters, 1988; Filion and Tremblay, 1991; Bergman et al., 1994; Ni et al., 2000; Soares et al., 2004; Wichmann and DeLong, 2006). The increased bursts and pauses alone may not directly lead to the manifestation of basal ganglia diseases, but they do interfere with the processing of information required to execute coordinated movements and thus may indirectly influence the development of various basal ganglia diseases.

Because DA-depletion has been shown to increase the firing activity of striatal-globus pallidus external (Str-GPe) projection neurons by changing their synaptic activity and membrane properties (Hernandez-Lopez et al., 2000; West and Grace, 2002;

Mallet et al., 2006; Shen et al., 2008; Flores-Barrera et al., 2010; Surmeier et al., 2010) and because *in vivo* studies have shown that the firing activity of Str projection neurons greatly increases after DA-depletion (Pang et al., 2001; Tseng et al., 2001; West and Grace, 2002; Mallet et al., 2006), it seems possible that increased Str activity plays substantial roles in the generation of abnormal firings in the basal ganglia (Walters et al., 2007; Walters and Bergstrom, 2010). Thus, our hypothesis is that DA-depletion increases burst firings of Str neurons projecting to the GPe and that these increased Str burst inputs contribute significantly to the generation of pauses and bursts in GPe neurons. DA-depletion may also increase the irregular activity of GPe neurons by other mechanisms such as increasing synchronous activity in the cortico-STN-GPe projection and removing DA suppression of N-type calcium channels in GPe neurons (Stefani et al., 2002; Galati et al., 2009). We hypothesize that the strong, irregular burst, and pause activity of GPe contributes greatly to the generation of irregular activity in neurons of the basal ganglia output nuclei, the internal segment of the globus pallidus (GPI), and the substantia nigra pars reticulata (SNr), which then disables information processing capability at their projection sites in the thalamus and brainstem (Stefani et al., 2011).

To test this hypothesis, unit recordings of Str and GPe neurons were performed in isoflurane anesthetized control and 6-hydroxydopamine (6-OHDA)-treated rats (6-OHDA rats), the rodent model of Parkinson's disease (PD). The results indicate that DA-depletion increases burst firings of Str–GPe projection neurons, and the intra-Str injection of the GABA_A agonist muscimol to block Str activity reduced the pauses and bursts in GPe firing. This report also provides evidence that intra-Str injection of a behaviorally effective dose of the DA precursor methyl-L-DOPA can decrease the pauses and the bursts. These results support the hypothesis that increased burst firings of Str–GPe projection neurons play substantial roles in the generation of abnormal firing patterns in the GPe and that this increased abnormal GPe activity may then induce abnormal activity in the entire basal ganglia and be a cause of psychomotor disabilities in PD. It can be further suggested that treatment to reduce burst Str–GPe inhibitory inputs may help to restore some of these disabilities.

MATERIALS AND METHODS

The experiments were performed on adult male Sprague Dawley rats (300–380 g) in compliance with the National Institutes of Health Guide for Care and Use of Laboratory Animals and the University of Tennessee Health Science Center Guide for the Use and Care of Laboratory Animals in Research.

BEHAVIORAL TESTS

All rats received 2 kinds of behavioral tests 2 times before and 2–4 times after the DA-depletion surgery described below. The rotational asymmetry test monitored the ambulatory movements of rats in a 1-m diameter chamber for 15 min using a video monitor system (Viewer, Bioobserve, Konigswinter, Germany), which could identify and track the rats' head, body, and tail positions frame by frame (30 frames/s). The body location data were used to calculate the distance and direction of the body movement between frames. For the limb use asymmetry test, rats were placed in a 28-cm diameter acrylic cylinder and videotaped for 10 min. The number of times the left and right forelimbs touched the wall of the cylinder were counted.

DA-DEPLETION AND HEAD HOLDER INSTALLATION

After the behavioral tests, 10 rats were anesthetized with a mixture of Ketamine (85 mg/kg, i.p.) and Xylazine (15 mg/kg, i.p.), treated with desmethyylimipramine (25 mg/kg, i.p.) and pargyline (5 mg/kg, i.p.), and placed in a stereotaxic apparatus. A craniotomy was performed on the skull, and 6-OHDA (8 µg in 4 µl of saline containing 0.1% ascorbic acid) in six rats or the vehicle in four rats was injected into the left ascending mesotelencephalic DA-bundle. The 6-OHDA or vehicle was delivered slowly over a period of 10 min through a glass micropipette (tip diameter of about 50 µm) glued to the needle of a 10-µl Hamilton syringe. The syringe plunger was advanced by a pulse motor-driven actuator. After 2 weeks of recovery, the behavioral tests were performed again. Four of the six rats injected with 6-OHDA developed a strong left turn preference in the rotational asymmetry test and a strong left forelimb use preference (<0.2 right/left touches in the cylinder test). The two 6-OHDA rats that failed to meet these behavioral criteria developed akinesia. These two rats

were rejected for the unit recording study in order to constrain the experimental group to one set of behavioral changes. None of the four rats injected with the vehicle developed behavioral asymmetries.

After the behavioral tests, a second surgery was performed on the control and 6-OHDA rats. The rats were anesthetized with a mixture of Ketamine (85 mg/kg, i.p.) and Xylazine (15 mg/kg, i.p.) and mounted on a stereotaxic apparatus. To fix the rats' heads painlessly to a stereotaxic frame, a plastic head holder made with polycarbonate and stainless steel pipes was placed on the dorsal surface of the skull and secured with dental acrylic. Also, a craniotomy was performed over the lateral agranular cortex, which is the motor cortex (MC) of rodents, and a parallel bipolar stimulus electrode (100 µm insulated stainless steel wires with tip separation of 0.6–0.7 mm) was implanted. For two control and one 6-OHDA rats, a pair of silver ball electrodes was also placed on the dura matter, one covering the right frontal agranular cortex and another covering the cerebellum to monitor the electrocorticogram. Another craniotomy was performed over the pallidum for recording electrode penetration. A thin layer of dental acrylic was used to cover the recording hole until the hole was needed for the recording sessions. After the surgery, the rats were monitored every hour until they recovered from anesthesia. If the rats showed any sign of pain, buprenorphine (0.01–0.05 mg/kg, i.p.) was administered.

UNIT RECORDINGS

Unit recordings began 5–7 days after installation of the head holder and stimulus electrodes, during which some gain in body weight and normal behavior was observed in the rats. For the recordings, the rats were anesthetized with 2.5% isoflurane in oxygen and mounted on the stereotaxic device using the head holder. During the recording, the rats were maintained with 0.5–1.0% isoflurane that was adjusted to eliminate spontaneous whisker movements as well as any body movement to MC stimulation. Each rat was recorded 2–3 times a week for 3–4 weeks. After 4 weeks, the accurate placement of the recording electrode became difficult due to the progressive increase in the thickness of the dura matter, and therefore, the recordings were stopped.

Single-unit recordings of Str and GPe neurons were made with insulated tungsten or Elgiloy alloy microelectrodes with an AC resistance of 1–2.5 MΩ. For Juxtacellular labeling of Str neurons, glass micropipettes filled with 1 M NaCl and 2% Neurobiotin were used, and recorded neurons were labeled by a method described elsewhere (Pinault, 1996). This report includes only the neurons that responded to MC stimulation (300 µs duration single pulse, strength 80 µA), which ensures that the neurons were in the same functional territories of Str and GPe that receive projections from the stimulus site. Unitary activity was amplified, passed through a 0.7 to 2-KHz band-pass filter (A-M Systems Model 1800, home modified), and converted into digital data by a homemade window discriminator. Digitized units and electrocorticograms were recorded using a computer. The Str and GPe neurons were identified by their firing patterns and by x-ray images of the skull and the electrode. The locations were also identified histologically at the end of the experiments as described below.

ANALYSIS OF UNIT ACTIVITY

Globus pallidus external neurons were recorded from four control and four 6-OHDA rats, and Str neurons were recorded from two rats from each group. The data obtained from the rats were pooled into control and 6-OHDA groups because the firing property obtained from anesthetized rats within each group were similar enough to combine. The existence of the refractory period in the single-unit recordings was tested by calculating an autocorrelogram of digitized spikes for 50 s of for GPe and 120 s for Str. The digitized data were also used calculate the rate and the burst index of firing of neurons. Bursts were detected by the “surprise” method of Legendy and Salcman (1985) using a surprise value ≥ 3 and with the number of spikes ≥ 3 defining a burst. These values were adopted from an extensive study of burst activity in monkey pallidum and STN (Wichmann and Soares, 2006). The proportion of spikes in bursts (%) was chosen as the index because this method has been used frequently in other studies. To detect pauses in GPe firing, gaps in the spike trains were filled with phantom spikes with an inter-spike-interval equal to the mean inter-spike-interval of real spikes, and the Legendy and Salcman method with the same criteria used for burst detection were applied to the phantom spikes to identify

pauses (Figure 1A). For the frequency component analysis, the spike trains were transformed using a moving average filter into a signal containing the density of the spikes versus time. The width of the moving average filter was 20 ms to ensure that the cut off of the filter was 50 Hz. In the power histograms, the values express the fraction of the total power in the 0 to 50-Hz band.

INTRA-STRIATAL INJECTIONS

The intra-Str injection of muscimol (0.04 μg in 0.2 μl saline) or methyl-L-DOPA (4 μg in 0.2 μl saline) was performed in a similar manner to the 6-OHDA injection described above. The injection site in Str was first determined by observing the MC-induced unit responses that were recorded through the injection micropipette, and then the drugs were injected slowly (0.04 $\mu\text{l}/\text{min}$) with an electric actuator on the microsyringe plunger. The drug injection was performed with at least a 3-day interval between injections. The dose of methyl-L-DOPA was determined by the ambulatory direction and distance tests on 2 of the 6-OHDA rats (Kita and Kita, 2011). The dose of muscimol was based on previous observations that 0.04 μg of muscimol blocked MC-induced excitation in an approximately 0.5 mm radius of the injection area (data not shown).

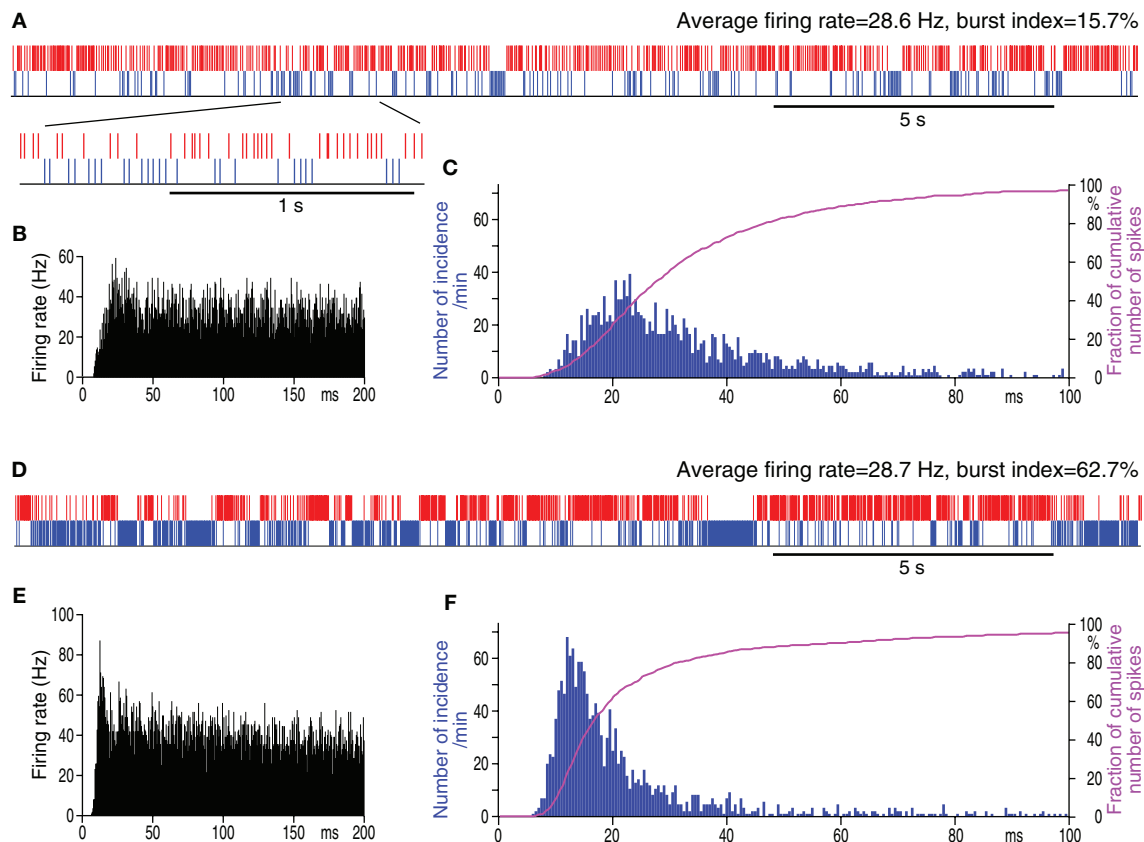


FIGURE 1 | Spontaneous firing patterns of a GPe neuron from a control (A–C) and from a 6-OHDA rat (D–F) having similar average firing rates. In (A,D), actual digitized spikes are shown in red. Blue phantom spikes occupying pauses have an inter-spike-interval equal to the mean inter-spike-intervals of

actual spikes. The phantom spikes were used for the detection of pauses (details in the section Materials and Methods). Autocorrelograms (B,E) and spike interval histograms (C,F) show that the neuron from the 6-OHDA rat has a larger peak at shorter inter-spike-intervals.

HISTOLOGY

For the final experiment, 2–3 recording sites were marked by passing a cathodal current (10 μ A for 5 s) through metal recording electrodes. About 1–2 days after the lesion, the rats were deeply anesthetized with a mixture of Ketamine (100 mg/Kg) and Xylazine (20 mg/Kg) and were perfused through the heart with 10–20 ml of isotonic saline followed by a fixative. The fixative was a mixture of 4% formaldehyde and 0.2% picric acid in a 0.12-M sodium phosphate buffer (200–300 ml, pH 7.4). After perfusion, the brains were removed and postfixed overnight at 4°C and then equilibrated in a 10%, followed by a 30%, phosphate buffered (pH 7.4) sucrose solution. The brains were cut into 40 μ m sagittal sections on a freezing microtome. Sections from Neurobiotin injected brains were incubated for 5 h in phosphate buffered saline (PBS) containing 0.5% skim milk, 0.05% Triton X-100, and ABC Elite (1:150 dilution; Vector). After several washes with PBS, the sections were incubated for 10–20 min in 0.05 M Tris-HCl buffered saline (pH 7.6) containing 0.04% diaminobenzidine tetrahydrochloride, 0.04% NiCl_2 , and 0.001% H_2O_2 to reveal the biotin containing neurons. Some of the sections were immunostained for tyrosine hydroxylase (TH), and others were stained with 1% cresyl violet to verify the recording sites. The sections for TH staining were incubated first for 5 h in PBS containing 0.5% skim milk and 0.05% Triton X-100 and then for 48 h in PBS containing a monoclonal mouse anti-TH antibody (Sigma, 1:4,000), 0.5% skim milk, and 0.05% Triton X-100. Subsequently, the sections were incubated with biotinylated goat anti-mouse IgG antibody (1:200 dilution; Vector, Burlingame, CA, USA) in the PBS incubation medium for 2 h. The sections were treated with ABC and diaminobenzidine tetrahydrochloride as described in the Neurobiotin sections. The sections were mounted on gelatin-coated slides, air-dried, dehydrated in graded alcohols to xylene, and coverslipped. All of the chemicals used for making the fixative, buffers, and other histological solutions were obtained from Sigma-Aldrich (St. Louis, MO, USA). Neurobiotin labeled axons were traced using a light microscope with a $\times 20$ or a $\times 40$ objective and a camera lucida (Olympus BX50).

RESULTS

DA-DEPLETION INCREASES PAUSES AND BURSTS IN GPe FIRINGS

Many previous observations of GPe neurons in patients or animal models of PD focused on the changes in the average firing rate and the generation of burst firings (Pan and Walters, 1988; Fillion and Tremblay, 1991; Bergman et al., 1994; Ni et al., 2000; Soares et al., 2004; Wichmann and DeLong, 2006). Many of these observations were performed under local anesthesia or unanesthetized animals. The aims of the present analysis of GPe neurons were first, to evaluate whether or not increased burst firings of GPe neurons in 6-OHDA rats can be seen under isoflurane anesthesia, thus validating experimental conditions, and second, to evaluate whether any increased bursts were accompanied by an increased occurrence of pauses in the firings.

The spontaneous activity of 52 GPe neurons recorded from control and 54 from 6-OHDA rats was analyzed. The GPe neurons included in this report were of the high frequency firing with pause type, which are the most common type found in GPe (DeLong, 1971). The neurons with a slow, less than 10 Hz, rhythmic firing of large, broad spikes were encountered mainly in the caudomedial

and ventral regions of the nucleus and were excluded from the present analysis. The analysis of the spontaneous firing patterns revealed that the mean firing rate was similar in the control and 6-OHDA rats, but the burst index was significantly higher in GPe of 6-OHDA rats (Table 1). This result indicates that the increase in burst activity can be seen in 0.5–1% isoflurane anesthetized 6-OHDA rats. The analysis also revealed that both the number of pauses and the fraction of total time occupied by the pauses were significantly higher in 6-OHDA rats (Table 1). Figure 1 shows an example of a control and a 6-OHDA GPe neuron with similar average firing rates. The neuron from a 6-OHDA rat has a higher burst index that was associated with an occurrence of a large number of longer pauses. The autocorrelograms and inter-spike-interval histograms show that the neuron from the 6-OHDA rat has a larger peak at shorter inter-spike-interval distributions compared with the neuron from the control rat.

MUSCIMOL INJECTION INTO Str

It can be assumed that if Str–GPe projections play a role in the generation of pauses and bursts in the firings of GPe neurons, silencing the activity of Str projection neurons by a local injection of the GABA_A receptor agonist muscimol should decrease the pauses and bursts in GPe. In the experiment, MC-induced multi-unit excitatory responses were recorded using a micropipette containing muscimol to place the tip of the pipette to the middle of the MC-responsive area of the Str. Then, a neuron in the sensorimotor territory of GPe was recorded before and 10–20 min after muscimol injection (0.04 μ g in 0.2 μ l saline, 0.04 μ l/min).

A total of 8 GPe neurons in 6-OHDA rats was tested by intra-Str injection of muscimol (Table 2). Muscimol significantly increased the average firing rate of GPe neurons, which indicated that Str provides substantial inhibition to GPe and that the muscimol did not spread into the GPe recording sites. Muscimol also significantly decreased the number of pauses, the fraction of time occupied by pauses, the burst index, and the <3 Hz components of the firing frequency distribution of the firings in GPe neurons (Table 2; Figure 2). However, the autocorrelograms and inter-spike-interval distributions show that muscimol did not abolish the high frequency firing components having a peak at inter-spike-interval distributions ≈ 18 ms. These results provide strong support for the hypothesis that Str–GPe inputs provide the driving force for the generation of pauses and bursts in GPe firings. The data also suggest that other excitatory driving forces such as STN glutamatergic inputs drive high frequency firings of GPe neurons.

Table 1 | Properties of spontaneous firings of GPe neurons in control and 6-OHDA rats.

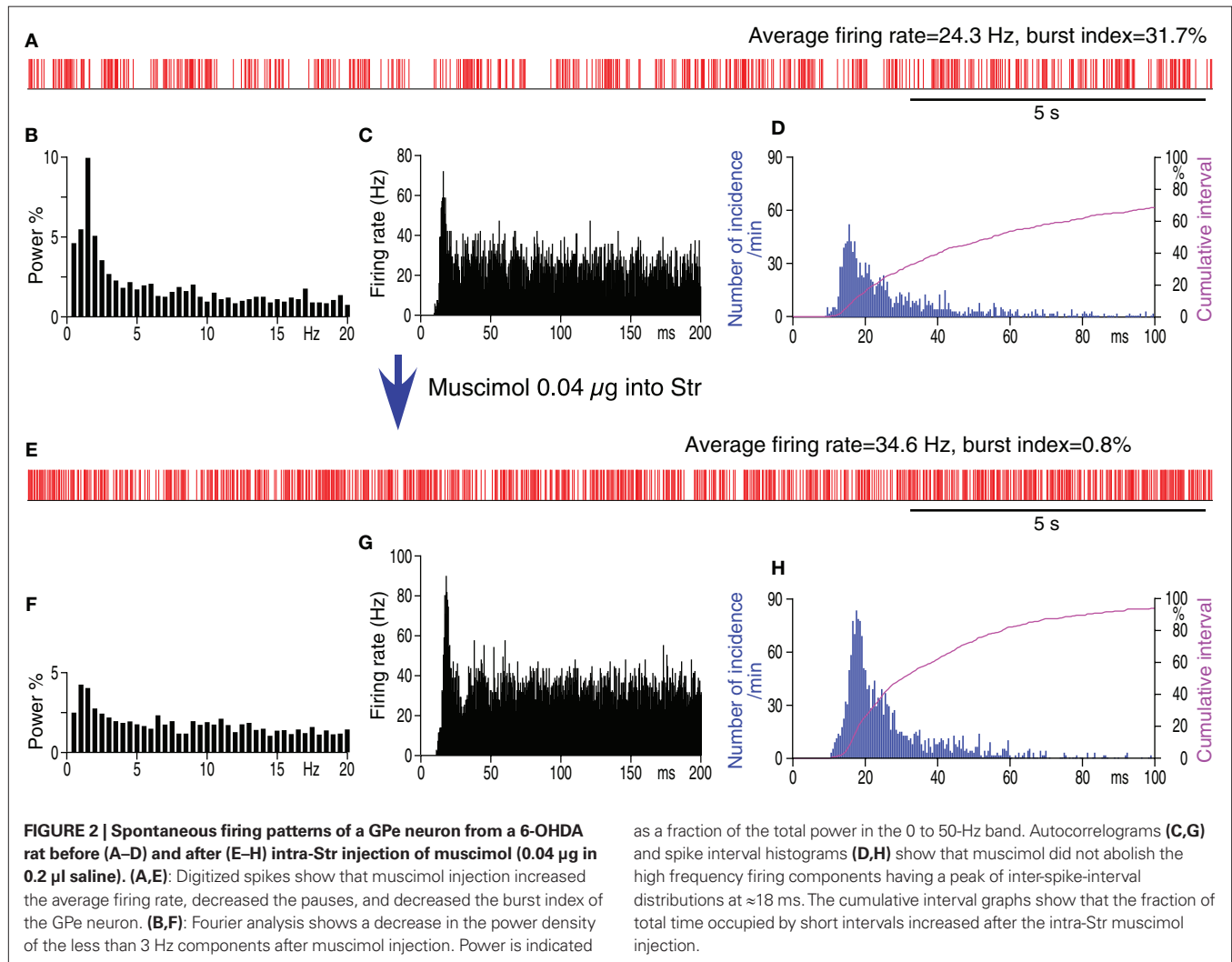
	Control, <i>n</i> = 52		6-OHDA, <i>n</i> = 54
Firing rate	29.3 \pm 12.2	ns	26.2 \pm 10.2
Burst index (%)	13.1 \pm 14.2	<i>p</i> < 0.0001	44.3 \pm 15.6
Pause fraction (%)	11.9 \pm 4.1	<i>p</i> < 0.0001	23.2 \pm 5.2
Number of pauses/min	26.8 \pm 17.3	<i>p</i> < 0.0001	55.6 \pm 14.8

Data: mean \pm SD; statistics: Mann–Whitney U-test; ns: not significant; pause fraction: fraction of total time occupied by pauses.

Table 2 | Effects of intra-Str injections of methyl-L-DOPA and muscimol on firing properties of GPe neurons in 6-OHDA rats.

	Muscimol, <i>n</i> = 8			Methyl-L-DOPA, <i>n</i> = 8		
	Before		After	Before		After
Firing rate	29.4 ± 4.7	<i>p</i> < 0.02	39.6 ± 8.5	31.7 ± 6.6	<i>p</i> < 0.01	41.1 ± 9.9
Burst index (%)	36.0 ± 14.6	<i>p</i> < 0.0005	1.7 ± 2.1	43.1 ± 8.2	<i>p</i> < 0.005	27.2 ± 10.7
Pause fraction (%)	25.5 ± 6.8	<i>p</i> < 0.005	13.5 ± 5.4	26.9 ± 6.8	<i>p</i> < 0.005	16.8 ± 4.6
Number of pauses/min	63.8 ± 19.3	<i>p</i> < 0.01	36.5 ± 8.6	68.0 ± 15.4	<i>p</i> < 0.01	40.4 ± 14.5

Data: mean ± SD; statistics: paired *t*-test; pause fraction: fraction of total time occupied by pauses longer than 100 ms.



FIRING PATTERN OF Str NEURONS

Striatal projection neurons in anesthetized normal rats show spontaneous membrane potential shifts between hyperpolarized and depolarized states, and spike firings occur in groups during the depolarized states (Wilson and Groves, 1981). Thus, the firing pattern of Str projection neurons differs from both the tonic firing with large single or doublet spikes of putative cholinergic interneurons and the high frequency firing with sharp spikes of putative parvalbumin-containing interneurons. Intracellular

recordings in halothane or urethane-anesthetized rats reported that DA-depletion significantly increased the number of spikes during the depolarized states (Pang et al., 2001; Tseng et al., 2001). These previous findings together with the results of the present intra-Str muscimol injection experiments suggest that Str–GPe inputs increase the pauses and bursts in firings of GPe neurons. To study changes in the activity pattern of Str neurons after DA-depletion in more detail, the spontaneous activity of possible projection neurons was recorded.

Under the present experimental conditions, spontaneously active putative projection neurons were only occasionally found in the Str of control rats, although MC stimulation disclosed numerous silent or only occasionally firing neurons when these neurons responded with an excitation to the stimulation. We recorded 11 spontaneously active neurons with an average firing rate of 0.5–3.8 Hz in the sensorimotor territory of the Str of control rats (**Figure 3A**; **Table 3**). **Figure 3A** shows that burst firings of Str neurons tend to occur in groups with an inter burst interval of approximately 1 Hz, as seen in the frequency distribution histogram (**Figure 3B**). The spontaneously active putative projection neurons were more frequently encountered in the Str of 6-OHDA than in normal rats. In 6-OHDA rats, 22 neurons with irregular spontaneous activity of 1.1–11.6 Hz were recorded from the sensorimotor territory of the Str (**Figure 3D**; **Table 3**). The frequency distribution histograms (**Figures 3B,E**) and **Table 3** show that burst firings occur more frequently with shorter inter burst intervals in the Str of 6-OHDA than in control rats. The burst index was slightly but significantly lower in the neurons from 6-OHDA rats. **Figures 3C,F** show population inter-spike-interval distributions calculated from all recorded neurons. Both histograms show that short range, >100 ms, inter-spike-interval distributions are similar and have a peak at about 10 ms.

Table 4 compares the characteristics of the 121 and 442 bursts detected in the 11 neurons from control and the 22 neurons from 6-OHDA rats, respectively. The duration and the surprise value of bursts were slightly but significantly decreased in the 6-OHDA group. However, the number of spikes per burst increased in this group. These observations are consistent with the report that DA-depletion made up- and down-state transitions more distinct and that a larger proportion of up-states, even short ones,

triggered spikes (Tseng et al., 2001). Eight of the 22 Str neurons from 6-OHDA rats were juxtacellularly labeled with Neurobiotin. They were all medium spiny neurons, and the main axons of five of the neurons were determined to have terminal fields confined to GPe (**Figure 4**), but the other three faded out before entering GPe. These data suggest that DA-depletion increased the spontaneous activity of Str–GPe projection neurons, and the increase is accompanied with an increased occurrence of stronger burst firings.

Table 3 | Properties of spontaneous firings of Str neurons in control and 6-OHDA rats.

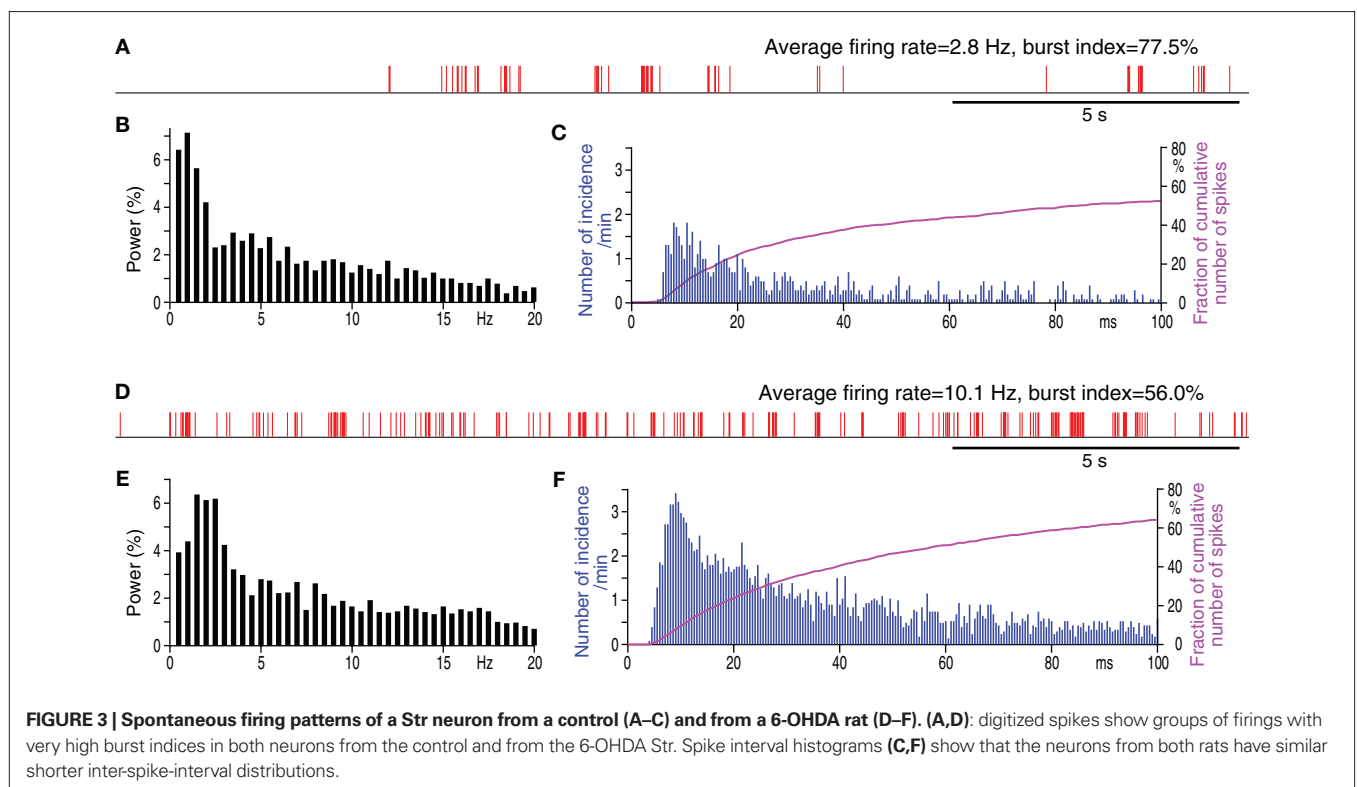
	Normal, <i>n</i> = 11		6-OHDA, <i>n</i> = 22
Firing rate (Hz)	2.1 ± 1.2	<0.0001	6.4 ± 2.7
Burst index (%)	73.5 ± 9.1	<0.02	61.8 ± 13.1
Burst interval (s)	4.6 ± 2.6	<0.01	2.4 ± 1.0

Burst index: fraction of spikes in bursts over a total number of spikes. Data: mean ± SD; Statistics: Mann–Whitney U-test.

Table 4 | Properties of bursts of Str neurons in control and 6-OHDA rats.

	Normal, <i>n</i> = 121		6-OHDA, <i>n</i> = 442
Burst duration (ms)	340 ± 339	<0.02	264 ± 334
Surprise value	9.2 ± 5.3	<0.05	8.5 ± 8.5
Number of spikes/burst	6.9 ± 4.2	<0.0001	9.0 ± 8.6

Data: mean ± SD; statistics: Mann–Whitney U-test.



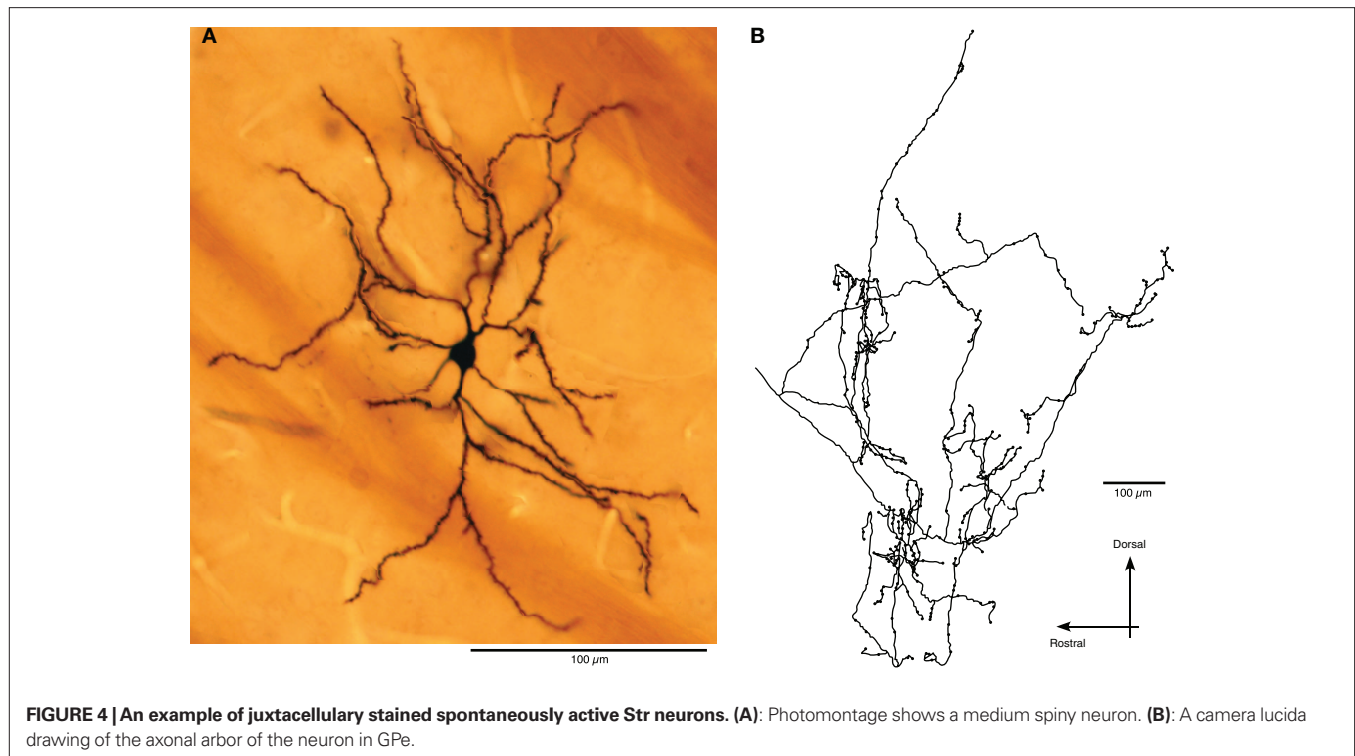


FIGURE 4 | An example of juxtacellularly stained spontaneously active Str neurons. (A): Photomontage shows a medium spiny neuron. **(B):** A camera lucida drawing of the axonal arbor of the neuron in GPe.

METHYL-L-DOPA INJECTION INTO Str

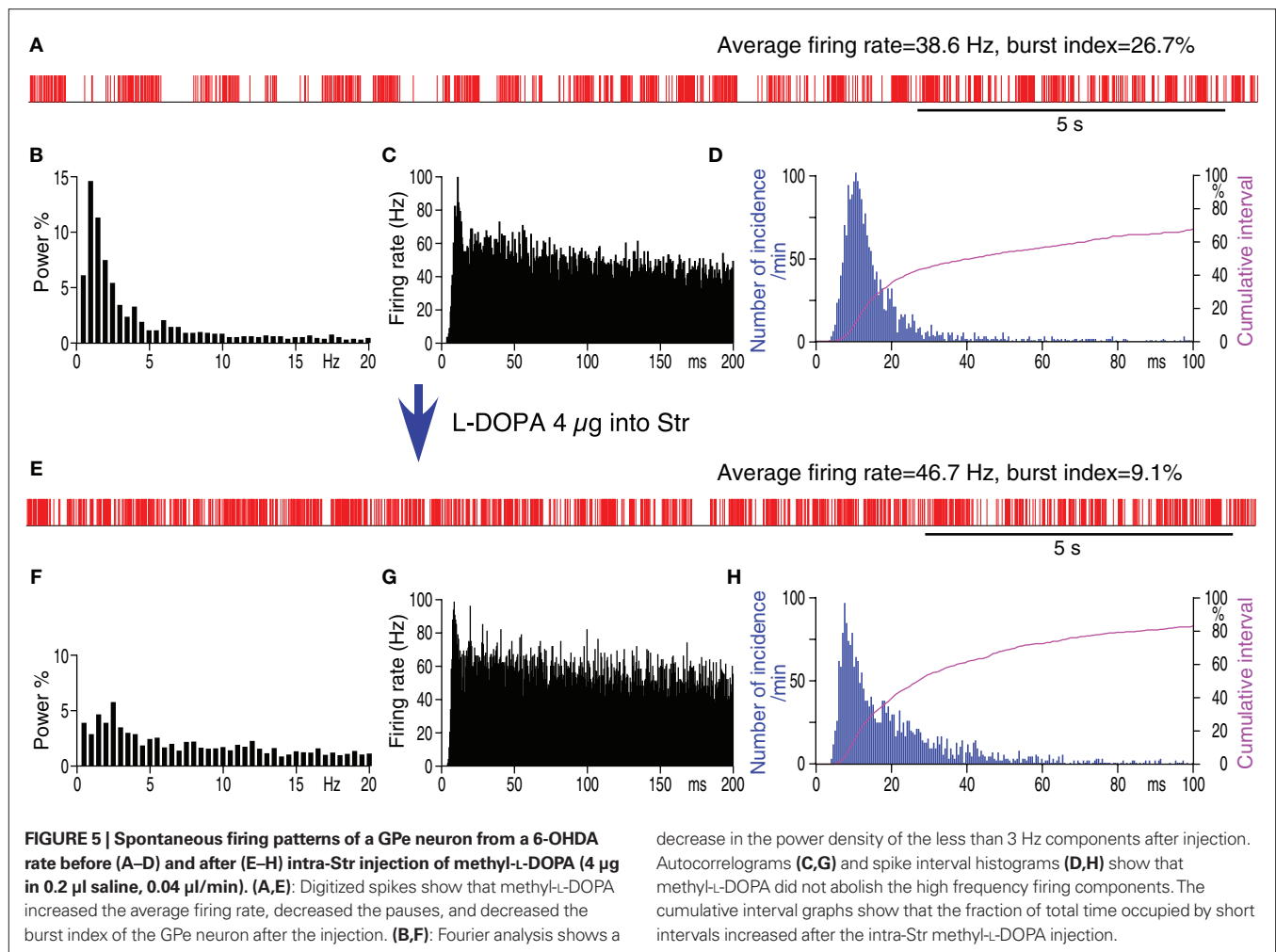
To evaluate to what degree the increased pauses and bursts of GPe neurons could be attributed to DA-depletion in Str, the acute effects of intra-Str injection of the DA precursor methyl-L-DOPA on the firing of GPe neurons in 6-OHDA rats were examined. The tip of the methyl-L-DOPA injection pipette was placed in the sensorimotor territory of the Str, in a similar manner to the muscimol injection described above. The neurons in the sensorimotor territory of GPe were recorded before and 10–20 min after the methyl-L-DOPA injections (4 µg in 0.2 µl saline, 0.04 µl/min). This dose of methyl-L-DOPA was based on behavioral tests that determined the amount that changed the preferred turning direction from left to right and also increased the total distance moved during the test period (Kita and Kita, 2011). **Figure 5** and **Table 2** show that methyl-L-DOPA significantly increased the average firing rate and decreased the fraction of spikes in bursts and the fraction of time occupied by pauses. Methyl-L-DOPA also decreased the <3 Hz components of the frequency distribution. The autocorrelograms and inter-spike-interval distributions show that methyl-L-DOPA shifted the peak of the inter-spike-interval distribution to the left and did not abolish the high frequency component of firings with short inter-spike-intervals. These changes were very similar to those resulting from intra-Str muscimol injections. These results indicate that acute replacement of DA in Str can reduce burst and pause generation in GPe.

DISCUSSION

RECORDING CONDITIONS

The present unit recordings were performed under 0.5–1% isoflurane anesthesia. We believe that the anesthetized rats offer more homogenous conditions for unit activity recording than

awake rats because monitoring the movements and finding quietly resting periods that are long enough for data acquisition is very difficult with awake rats. For instance, even after acclimating the awake rats to 2–3 h of restraint, they often move their whiskers; this whisking related unit activity, probably including both movement initiation and movement evoked sensory afferent inputs, could be often found in Str and GPe (Kita, unpublished observation). During unit recordings, taking advantage of the quick adjustment capability of gas inhalation anesthesia, the anesthesia level was adjusted to eliminate spontaneous whisker movements as well as any other body movement to MC stimulation. Under these conditions, the rats did not show movement responses to light touch but responded to painful stimuli such as a foot pinch. The level of anesthesia judged by electrocorticogram observation was stage two or three sleep but not slow wave sleep (data not shown). These levels were chosen to avoid the induction of strong, synchronized, slow oscillations during slow wave sleep that is induced by higher isoflurane doses. Under slow wave sleep, cortical, Str neurons, and probably thalamic neurons undergo synchronized, slow oscillation, also known as up- and down-state or depolarized- and hyperpolarized-state (Stern et al., 1997). Probably because of this wide cortical synchrony, many Str projection neurons fire during the up-state. It has also been shown that the slow oscillation changes after DA-depletion (Pang et al., 2001; Mallet et al., 2006). However, Str projection neurons are almost silent in normal quietly resting awake rats and monkeys. Our recording conditions were set to create the Str activity resembling that of quietly resting awake animals. The present data show that a significant increase in burst firing can be observed in GPe of 6-OHDA rats anesthetized with isoflurane.



INCREASED Str INPUTS SIGNIFICANTLY INCREASE PAUSES AND BURSTS OF GPe NEURONS AFTER DA-DEPLETION

The most common firing type of GPe neurons is high frequency firing with pauses (DeLong, 1971). The pauses are most likely triggered by GABAergic inputs based on the following reported observations: a local injection of the GABA_A antagonist gabazine eliminates most of pauses (Kita et al., 2004), a burst activation of Str inputs can induce a long inhibition in GPe (Kaneda and Kita, 2005), burst firings of Str neurons are synchronous with pauses of GPe firings (Walters et al., 2007), and pauses are not preceded by bursts rejecting involvement of calcium-activated potassium current (Elias et al., 2007). Also, a number of studies have shown an increased activity of Str neurons after DA-depletion (Pang et al., 2001; Tseng et al., 2001). Based on these data, we formed the hypothesis that DA-depletion increases burst firings of Str neurons projecting to the GPe, which then generate pauses in the firing of GPe neurons, which then finally contribute to the generation of burst firing in the GPe itself and in the projection sites of GPe. This study provides key supportive data for the hypothesis that silencing Str by local injection of muscimol significantly decreased pauses and bursts of GPe firings.

The membrane potential of Str projection neurons in normal rats is periodically shifted between hyperpolarized and depolarized states by cortical inputs, with spike firings occurring only during the depolarized states (Wilson and Groves, 1981; Stern et al., 1998). In control rats, the depolarized states are mostly subthreshold, with only occasional firings during these states. After DA-depletion, the depolarized states reach the threshold more frequently due to altered glutamatergic and GABAergic inputs and altered membrane properties of the neurons; thus firing increases during DA-depleted depolarized states (Chen et al., 2001; Pang et al., 2001; Tseng et al., 2001; West and Grace, 2002; Mallet et al., 2006). The present data are consistent with the previous observations that the occurrence of bursts in Str neurons and the average number of spikes per burst significantly increased after DA-depletion. Juxtacellular labeling results suggest that most of the burst firing of Str neurons are from those that project only to GPe. The present data also revealed two new aspects: One is that bursts tend to occur in groups in both normal and DA-depleted Str, suggesting a very low, ≈ 0.1 Hz, oscillation that can be seen in the both conditions. Similar, very slow oscillations were reported in other nuclei of basal ganglia and other brain areas (Walters and Bergstrom, 2010). The second is that distributions of short inter-spike-intervals are similar in control and DA-depleted Str, suggesting that bursts

with short inter-spike-intervals occur in normal Str. Str-GPe synapses should be significantly augmented during the burst activation and evoke strong GABA_A and GABA_B receptor mediated IPSPs (Kaneda and Kita, 2005; Sims et al., 2008) and alter opioid receptor mediated modulations of ionic currents in GPe neurons (Ogura and Kita, 2000; Spadoni et al., 2004). The Str-GPe inhibition may also be increased by removal of pre- and postsynaptic DA suppression of Str-GPe synapses (Florin et al., 1997; Cooper and Stanford, 2001; Shin et al., 2003; Watanabe et al., 2009). Thus, Str burst firings will effectively inhibit GPe neurons. However, it has to be noted that these observations do not provide strong evidence that the GABAergic Str burst inputs always directly cause the hyperpolarizations for pauses. It has been documented that GPe neurons in slice preparations generated pauses when they were hyperpolarized by a continuous somatic current injection (Hashimoto and Kita, 2006; Deister et al., 2009). The increased GABAergic inputs from Str and the increased glutamatergic inputs from STN can create a condition such that timely arrival of GABAergic or glutamatergic inputs can flip the membrane of GPe neurons between hyperpolarized and depolarized states (Hashimoto and Kita, 2006). These pauses could contribute to the increase in burst activity of GPe neurons commonly observed in patients and animal models of PD. Pauses can intensify burst firings of GPe itself by the rebound excitation mechanism (i.e., deinactivation of Na-channels during hyperpolarization) and by the GPe-STN-GPe negative feedback inputs. Our data suggest that the pauses in GPe firing can generate strong disinhibition bursts in the STN and GPi in 6-OHDA rats (Kita, unpublished observation), though this may not be the significant factor in normal animals (Elias et al., 2008).

CONTRIBUTION OF STN INPUTS IN THE BURST GENERATION IN GPe

The GPe receives a major excitatory input from STN, and the burst activity and mean firing rate of STN increase significantly after DA-depletion (Magill et al., 2001; Bevan et al., 2002; Sharott et al., 2005; Galvan and Wichmann, 2008; Israel and Bergman, 2008; Galati et al., 2009). It has also been shown in urethane-anesthetized rats that acute DA-depletion by chemical blockade of the medial forebrain bundle significantly increased acute pathological synchronization of the cortico-STN-GPe pathway (Galati et al., 2009). The increased burst activity in STN may be in part due to the increased burst activity of GPe as well as to the increased cortico-STN synchronous inputs, changes in pedunculopontine inputs, and altered membrane properties of STN neurons (Shen and Johnson, 2000, 2005; Baufreton and Bevan, 2008; Dejean et al., 2008; Galati et al., 2009). This study shows that intra-Str injection of muscimol in 6-OHDA rats did not abolish a high frequency (inter-spike-interval peak ≈ 18 ms) component of firing, though it significantly decreased bursts, pauses, and the <3 Hz components of the firing frequency distribution of the firings in GPe neurons. A study in normal monkey GPe showed that a combined local injection of GABA_A and glutamate antagonists is required to regularize firings of GPe neurons (Kita et al., 2004). Thus, both Str and STN inputs contribute to the generation of burst activity in GPe.

AVERAGE FIRING RATE OF GPe NEURONS

Studies in animal models of PD reported either no change or a significant decrease in the average firing rate of GPe neurons (Filion, 1979; Pan and Walters, 1988; Albin et al., 1989; DeLong, 1990; Filion and Tremblay, 1991; Ni et al., 2000; Magill et al., 2001; Soares et al., 2004; Mallet et al., 2008). In the present recording conditions, the average firing rate of GPe neurons did not decrease significantly in spite of the increased Str inhibition. It has also been shown that DA-depletion down regulates HCN2 channel expressions in GPe neurons, though it normally enhances autonomous firing of neurons (Chan et al., 2011). This unchanged average firing rate suggests that these increased inhibitory forces were counter-balanced by increased excitatory inputs from STN, because a significant increase in the firing rate of STN neurons after DA-depletion is a commonly reported observation (Hollerman and Grace, 1992; Bergman et al., 1994; Magill et al., 2001; Pelled et al., 2002; Wichmann and DeLong, 2006).

EFFECTS OF INTRA-Str METHYL-L-DOPA INJECTION

Injection of a behaviorally effective dose of methyl-L-DOPA into the Str of 6-OHDA rats decreased the pauses and bursts of GPe neurons. These changes were attributed to the decreased spontaneous burst activity of Str-GPe neurons. DA-depletion increases D2-R expression in Str-GPe neurons (Gerfen et al., 1990) and also sensitizes D2-Rs on cortico-Str terminals (Bamford et al., 2004). Thus, the changes may be due to activation of these D2-Rs by DA converted from L-DOPA in Str (Xu and Dluzen, 1996; Tanaka et al., 1999). The elucidation of the L-DOPA effects on spontaneous firing and the cortical and thalamic stimulation-induced responses of Str neurons will be the subjects of future investigations.

FUNCTIONAL IMPLICATIONS

This report documents that DA-depletion increases the spontaneous activity of some Str-GPe projection neurons and that the increased Str-GPe inputs play significant roles in the generation of pauses and bursts of firings in GPe neurons. This study also shows that intra-Str injection of a behaviorally effective dose of methyl-L-DOPA reduces these pauses and bursts. We infer from these observations that DA-depleted Str generates abnormal signals in GPe that can be transmitted to the basal ganglia output nuclei GPi/SNr, which then disables information processing capability at their projection sites in the thalamus and brainstem that may lead to the manifestation of psychomotor disabilities in PD (Stefani et al., 2011). It can be further suggested that treatment to reduce burst Str-GPe inhibitory inputs may help to restore some of these disabilities.

ACKNOWLEDGMENTS

This work was supported by the National Institute of Neurological Disorders and Stroke Grants NS-47085 and NS-57236. We thank R. Kita for editing the manuscript and J. Butler for technical assistance.

REFERENCES

- | | | | |
|--|--|---|--|
| <p>Albin, R. L., Young, A. B., and Penney, J. B. (1989). The functional anatomy of basal ganglia disorders. <i>Trends Neurosci.</i> 12, 366–375.</p> | <p>Bamford, N. S., Zhang, H., Schmitz, Y., Wu, N. P., Cepeda, C., Levine, M. S., Schmauss, C., Zakharenko, S. S., Zablow, L., and Sulzer, D. (2004). Heterosynaptic dopamine neurotransmission selects</p> | <p>sets of corticostriatal terminals. <i>Neuron</i> 42, 653–663.</p> <p>Baufreton, J., and Bevan, M. D. (2008). D2-like dopamine receptor-mediated modulation of activity-dependent</p> | <p>plasticity at GABAergic synapses in the subthalamic nucleus. <i>J. Physiol. (Lond.)</i> 586, 2121–2142.</p> <p>Bergman, H., Wichmann, T., Karmon, B., and DeLong, M. R. (1994). The primate</p> |
|--|--|---|--|

- subthalamic nucleus. II. Neuronal activity in the MPTP model of parkinsonism. *J. Neurophysiol.* 72, 507–520.
- Bevan, M. D., Magill, P. J., Terman, D., Bolam, J. P., and Wilson, C. J. (2002). Move to the rhythm: oscillations in the subthalamic nucleus-external globus pallidus network. *Trends Neurosci.* 25, 525–531.
- Chan, C. S., Glajch, K. E., Gertler, T. S., Guzman, J. N., Mercer, J. N., Lewis, A. S., Goldberg, A. B., Tkatch, T., Shigemoto, R., Fleming, S. M., Chetkovich, D. M., Osten, P., Kita, H., and Surmeier, D. J. (2011). HCN channelopathy in external globus pallidus neurons in models of Parkinson's disease. *Nat. Neurosci.* 14, 85–92.
- Chen, M. T., Morales, M., Woodward, D. J., Hoffer, B. J., and Janak, P. H. (2001). In vivo extracellular recording of striatal neurons in the awake rat following unilateral 6-hydroxydopamine lesions. *Exp. Neurol.* 171, 72–83.
- Cooper, A. J., and Stanford, I. M. (2001). Dopamine D2 receptor mediated presynaptic inhibition of striatopallidal GABA(A) IPSCs in vitro. *Neuropharmacology* 41, 62–71.
- Deister, C. A., Chan, C. S., Surmeier, D. J., and Wilson, C. J. (2009). Calcium-activated SK channels influence voltage-gated ion channels to determine the precision of firing in globus pallidus neurons. *J. Neurosci.* 29, 8452–8461.
- Dejean, C., Gross, C. E., Bioulac, B., and Boraud, T. (2008). Dynamic changes in the cortex-basal ganglia network after dopamine depletion in the rat. *J. Neurophysiol.* 100, 385–396.
- DeLong, M. R. (1971). Activity of pallidal neurons during movement. *J. Neurophysiol.* 34, 414–427.
- DeLong, M. R. (1990). Primate models of movement disorders of basal ganglia origin. *Trends Neurosci.* 13, 281–285.
- Elias, S., Joshua, M., Goldberg, J. A., Heimer, G., Arkadir, D., Morris, G., and Bergman, H. (2007). Statistical properties of pauses of the high-frequency discharge neurons in the external segment of the globus pallidus. *J. Neurosci.* 27, 2525–2538.
- Elias, S., Ritov, Y., and Bergman, H. (2008). Balance of increases and decreases in firing rate of the spontaneous activity of basal ganglia high-frequency discharge neurons. *J. Neurophysiol.* 100, 3086–3104.
- Filion, M. (1979). Effects of interruption of the nigrostriatal pathway and of dopaminergic agents on the spontaneous activity of globus pallidus neurons in the awake monkey. *Brain Res.* 178, 425–441.
- Filion, M., and Tremblay, L. (1991). Abnormal spontaneous activity of globus pallidus neurons in monkeys with MPTP-induced parkinsonism. *Brain Res.* 547, 142–151.
- Floran, B., Floran, L., Sierra, A., and Aceves, J. (1997). D2 receptor-mediated inhibition of GABA release by endogenous dopamine in the rat globus pallidus. *Neurosci. Lett.* 237, 1–4.
- Flores-Barrera, E., Vizcarra-Chacon, B. J., Tapia, D., Bargas, J., and Galarraga, E. (2010). Different corticostriatal integration in spiny projection neurons from direct and indirect pathways. *Front. Syst. Neurosci.* 4:15. doi: 10.3389/fnsys.2010.00015
- Galati, S., Stanzione, P., D'Angelo, V., Fedele, E., Marzetti, F., Sancesario, G., Procopio, T., and Stefani, A. (2009). The pharmacological blockade of medial forebrain bundle induces an acute pathological synchronization of the cortico-subthalamic nucleus-globus pallidus pathway. *J. Physiol. (Lond.)* 587, 4405–4423.
- Galvan, A., and Wichmann, T. (2008). Pathophysiology of parkinsonism. *Clin. Neurophysiol.* 119, 1459–1474.
- Gerfen, C. R., Engber, T. M., Mahan, L. C., Susel, Z., Chase, T. N., Monsma, F. J. Jr., and Sibley, D. R. (1990). D1 and D2 dopamine receptor-regulated gene expression of striatonigral and striatopallidal neurons. *Science* 250, 1429–1432.
- Hashimoto, K., and Kita, H. (2006). Slow oscillatory activity of rat globus pallidus neurons in vitro. *Eur. J. Neurosci.* 23, 443–453.
- Hernandez-Lopez, S., Tkatch, T., Perez-Garci, E., Galarraga, E., Bargas, J., Hamm, H., and Surmeier, D. J. (2000). D2 dopamine receptors in striatal medium spiny neurons reduce L-type Ca^{2+} currents and excitability via a novel PLC[β 1]-IP3-calcineurin-signaling cascade. *J. Neurosci.* 20, 8987–8995.
- Hollerman, J. R., and Grace, A. A. (1992). Subthalamic nucleus cell firing in the 6-OHDA-treated rat: basal activity and response to haloperidol. *Brain Res.* 590, 291–299.
- Israel, Z., and Bergman, H. (2008). Pathophysiology of the basal ganglia and movement disorders: from animal models to human clinical applications. *Neurosci. Biobehav. Rev.* 32, 367–377.
- Kaneda, K., and Kita, H. (2005). Synaptically released GABA activates both pre- and postsynaptic GABA(B) receptors in the rat globus pallidus. *J. Neurophysiol.* 94, 1104–1114.
- Kita, H., and Kita, T. (2011). Cortical stimulation evokes abnormal responses in the dopamine-depleted rat basal ganglia. *J. Neurosci.* in press.
- Kita, H., Nambu, A., Kaneda, K., Tachibana, Y., and Takada, M. (2004). Role of ionotropic glutamatergic and GABAergic inputs on the firing activity of neurons in the external pallidum in awake monkeys. *J. Neurophysiol.* 92, 3069–3084.
- Legendy, C. R., and Salzman, M. (1985). Bursts and recurrences of bursts in the spike trains of spontaneously active striate cortex neurons. *J. Neurophysiol.* 53, 926–939.
- Magill, P. J., Bolam, J. P., and Bevan, M. D. (2001). Dopamine regulates the impact of the cerebral cortex on the subthalamic nucleus-globus pallidus network. *Neuroscience* 106, 313–330.
- Mallet, N., Ballion, B., Le Moine, C., and Gonon, F. (2006). Cortical inputs and GABA interneurons imbalance projection neurons in the striatum of parkinsonian rats. *J. Neurosci.* 26, 3875–3884.
- Mallet, N., Pogossyan, A., Marton, L. F., Bolam, J. P., Brown, P., and Magill, P. J. (2008). Parkinsonian beta oscillations in the external globus pallidus and their relationship with subthalamic nucleus activity. *J. Neurosci.* 28, 14245–14258.
- Ni, Z., Bouali-Benazzouz, R., Gao, D., Benabid, A. L., and Benazzouz, A. (2000). Changes in the firing pattern of globus pallidus neurons after the degeneration of nigrostriatal pathway are mediated by the subthalamic nucleus in the rat. *Eur. J. Neurosci.* 12, 4338–4344.
- Ogura, M., and Kita, H. (2000). Dynorphin exerts both postsynaptic and presynaptic effects in the globus pallidus of the rat. *J. Neurophysiol.* 83, 3366–3376.
- Pan, H. S., and Walters, J. R. (1988). Unilateral lesion of the nigrostriatal pathway decreases the firing rate and alters the firing pattern of globus pallidus neurons in the rat. *Synapse* 2, 650–656.
- Pang, Z., Ling, G. Y., Gajendran, M., and Xu, Z. C. (2001). Enhanced excitatory synaptic transmission in spiny neurons of rat striatum after unilateral dopamine denervation. *Neurosci. Lett.* 308, 201–205.
- Pelled, G., Bergman, H., and Goelman, G. (2002). Bilateral overactivation of the sensorimotor cortex in the unilateral rodent model of Parkinson's disease—a functional magnetic resonance imaging study. *Eur. J. Neurosci.* 15, 389–394.
- Pinaut, D. (1996). A novel single-cell staining procedure performed in vivo under electrophysiological control: morpho-functional features of juxtacellularly labeled thalamic cells and other central neurons with biocytin or neurobiotin. *J. Neurosci. Methods* 65, 113–136.
- Sharott, A., Magill, P. J., Harnack, D., Kupsch, A., Meissner, W., and Brown, P. (2005). Dopamine depletion increases the power and coherence of beta-oscillations in the cerebral cortex and subthalamic nucleus of the awake rat. *Eur. J. Neurosci.* 21, 1413–1422.
- Shen, K. Z., and Johnson, S. W. (2000). Presynaptic dopamine D2 and muscarinic M3 receptors inhibit excitatory and inhibitory transmission to rat subthalamic neurones in vitro. *J. Physiol. (Lond.)* 525(Pt 2), 331–341.
- Shen, K. Z., and Johnson, S. W. (2005). Dopamine depletion alters responses to glutamate and GABA in the rat subthalamic nucleus. *Neuroreport* 16, 171–174.
- Shen, W., Flajolet, M., Greengard, P., and Surmeier, D. J. (2008). Dichotomous dopaminergic control of striatal synaptic plasticity. *Science* 321, 848–851.
- Shin, R. M., Masuda, M., Miura, M., Sano, H., Shirasawa, T., Song, W. J., Kobayashi, K., and Aosaki, T. (2003). Dopamine D4 receptor-induced postsynaptic inhibition of GABAergic currents in mouse globus pallidus neurons. *J. Neurosci.* 23, 11662–11672.
- Sims, R. E., Woodhall, G. L., Wilson, C. L., and Stanford, I. M. (2008). Functional characterization of GABAergic pallidopallidal and striatopallidal synapses in the rat globus pallidus in vitro. *Eur. J. Neurosci.* 28, 2401–2408.
- Soares, J., Kliem, M. A., Betarbet, R., Greenamyre, J. T., Yamamoto, B., and Wichmann, T. (2004). Role of external pallidal segment in primate parkinsonism: comparison of the effects of 1-methyl-4-phenyl-1,2,3,6-tetrahydropyridine-induced parkinsonism and lesions of the external pallidal segment. *J. Neurosci.* 24, 6417–6426.
- Spadoni, F., Martella, G., Martorana, A., Lavaroni, F., D'Angelo, V., Bernardi, G., and Stefani, A. (2004). Opioid-mediated modulation of calcium currents in striatal and pallidal neurons following reserpine treatment: focus on kappa response. *Synapse* 51, 194–205.
- Stefani, A., Fedele, E., Pierantozzi, M., Galati, S., Marzetti, F., Peppe, A., Pastore, F. S., Bernardi, G., and Stanzione, P. (2011). Reduced GABA content in the motor thalamus during effective deep brain stimulation of the subthalamic nucleus. *Front. Syst. Neurosci.* 5:17. doi: 10.3389/fnsys.2011.00017
- Stefani, A., Spadoni, F., Martorana, A., Lavaroni, F., Martella, G., Sancesario, G., and Bernardi, G. (2002). D2-mediated modulation of N-type calcium currents in rat globus pallidus neurons following dopamine denervation. *Eur. J. Neurosci.* 15, 815–825.
- Stern, E. A., Jaeger, D., and Wilson, C. J. (1998). Membrane potential syn-

- chrony of simultaneously recorded striatal spiny neurons in vivo. *Nature* 394, 475–478.
- Stern, E. A., Kincaid, A. E., and Wilson, C. J. (1997). Spontaneous subthreshold membrane potential fluctuations and action potential variability of rat corticostriatal and striatal neurons in vivo. *J. Neurophysiol.* 77, 1697–1715.
- Surmeier, D. J., Shen, W., Day, M., Gertler, T., Chan, S., Tian, X., and Plotkin, J. L. (2010). The role of dopamine in modulating the structure and function of striatal circuits. *Prog. Brain Res.* 183, 149–167.
- Tanaka, H., Kannari, K., Maeda, T., Tomiyama, M., Suda, T., and Matsunaga, M. (1999). Role of serotonergic neurons in L-DOPA-derived extracellular dopamine in the striatum of 6-OHDA-lesioned rats. *Neuroreport* 10, 631–634.
- Tseng, K. Y., Kasanetz, F., Kargieman, L., Riquelme, L. A., and Murer, M. G. (2001). Cortical slow oscillatory activity is reflected in the membrane potential and spike trains of striatal neurons in rats with chronic nigrostriatal lesions. *J. Neurosci.* 21, 6430–6439.
- Walters, J. R., and Bergstrom, D. A. (2010). “Synchronous activity in basal ganglia circuits,” in *Handbook of Basal Ganglia Structure and Function*, eds S. Heinz Steiner and K. Y. Tseng (Philadelphia, PA: Elsevier), 429–443.
- Walters, J. R., Hu, D., Itoga, C. A., Parr-Brownlie, L. C., and Bergstrom, D. A. (2007). Phase relationships support a role for coordinated activity in the indirect pathway in organizing slow oscillations in basal ganglia output after loss of dopamine. *Neuroscience* 144, 762–776.
- Watanabe, K., Kita, T., and Kita, H. (2009). Presynaptic actions of d2-like receptors in the rat cortico-striato-globus pallidus disynaptic connection in vitro. *J. Neurophysiol.* 101, 665–671.
- West, A. R., and Grace, A. A. (2002). Opposite influences of endogenous dopamine D1 and D2 receptor activation on activity states and electrophysiological properties of striatal neurons: studies combining in vivo intracellular recordings and reverse microdialysis. *J. Neurosci.* 22, 294–304.
- Wichmann, T., and DeLong, M. R. (2006). Basal ganglia discharge abnormalities in Parkinson's disease. *J. Neural Transm. Suppl.* 21–25.
- Wichmann, T., and Soares, J. (2006). Neuronal firing before and after burst discharges in the monkey basal ganglia is predictably patterned in the normal state and altered in parkinsonism. *J. Neurophysiol.* 95, 2120–2133.
- Wilson, C. J., and Groves, P. M. (1981). Spontaneous firing patterns of identified spiny neurons in the rat neostriatum. *Brain Res.* 220, 67–80.
- Xu, K., and Dluzen, D. E. (1996). L-DOPA modulation of corpus striatal dopamine and dihydroxyphenylacetic acid output from intact and 6-OHDA lesioned rats. *J. Neural Transm.* 103, 1295–1305.

Conflict of Interest Statement: The authors declare that the research was conducted in the absence of any commercial or financial relationships that could be construed as a potential conflict of interest.

Received: 07 April 2011; paper pending published: 03 May 2011; accepted: 27 May 2011; published online: 08 June 2011.

Citation: Kita H and Kita T (2011) Role of striatum in the pause and burst generation in the globus pallidus of 6-OHDA-treated rats. *Front. Syst. Neurosci.* 5:42. doi: 10.3389/fnsys.2011.00042

Copyright © 2011 Kita and Kita. This is an open-access article subject to a non-exclusive license between the authors and Frontiers Media SA, which permits use, distribution and reproduction in other forums, provided the original authors and source are credited and other Frontiers conditions are complied with.



Functional properties of striatal fast-spiking interneurons

Joshua D. Berke*

Neuroscience Program, Department of Psychology, University of Michigan, Ann Arbor, MI, USA

Edited by:

Charles J. Wilson, University of Texas at San Antonio, USA

Reviewed by:

Enrico Bracci, University of Manchester, UK

Giuseppe Sciamanna, Santa Lucia Foundation, Italy

***Correspondence:**

Joshua D. Berke, Department of Psychology, University of Michigan, 530 Church Street, Ann Arbor, MI 48109, USA.
e-mail: jdberke@umich.edu

Striatal fast-spiking interneurons (FSIs) have a major influence over behavioral output, and a deficit in these cells has been observed in dystonia and Tourette syndrome. FSIs receive cortical input, are coupled together by gap junctions, and make perisomatic GABAergic synapses onto many nearby projection neurons. Despite being critical components of striatal microcircuits, until recently little was known about FSI activity in behaving animals. Striatal FSIs are near-continuously active in awake rodents, but even neighboring FSIs show uncorrelated activity most of the time. A coordinated “pulse” of increased FSI firing occurs throughout striatum when rats initiate one chosen action while suppressing a highly trained alternative. This pulse coincides with a drop in globus pallidus population activity, suggesting that pallido-striatal disinhibition may have an important role in timing or coordinating action execution. In addition to changes in firing rate, FSIs show behavior-linked modulation of spike timing. The variability of inter-spike intervals decreases markedly following instruction cues, and FSIs also participate in fast striatal oscillations that are linked to rewarding events and dopaminergic drugs. These studies have revealed novel and unexpected properties of FSIs, that should help inform new models of striatal information processing in both normal and aberrant conditions.

Keywords: striatum, interneuron, GABA, basal ganglia, gamma oscillations, dopamine, amphetamine, antipsychotic

INTRODUCTION

The striatum is the largest component of basal ganglia circuitry, and the primary location at which information is passed into those circuits from cortex and thalamus. Alterations in striatal physiology are implicated in a wide range of neurological and psychiatric disorders from Parkinson's Disease to drug addiction. Although controversies continue concerning the precise normal behavioral functions of striatum (and basal ganglia more generally; Turner and Desmurget, 2010), most investigators think that it is critical for adaptive decision-making: the refinement, selection, and energization of behaviors through trial-and-error learning (Berke, 2009b). Understanding exactly what computational algorithms are achieved by striatum – and how – is a major ongoing challenge in systems neuroscience. Fast-spiking interneurons (FSIs) are relatively sparse elements of striatal networks that nonetheless seem to be critical nodes governing and orchestrating striatal output. In this brief review I first summarize key anatomical and physiological properties of these cells that are thought to be key to their functional properties, before considering some of the quite surprising observations from a series of recent studies examining their firing patterns in awake, behaving animals.

FSI ANATOMY AND CONNECTIVITY

Striatal FSIs are GABAergic cells that express the calcium-binding protein parvalbumin, and in most respects are similar to FSIs in other structures such as cortex. They comprise roughly 1% of striatal neurons (Luk and Sadikot, 2001), scattered throughout the structure but with a strong lateral > medial gradient (Gerfen et al., 1985). This distribution is not found for other interneuron types and may indicate a particularly important role for FSIs in sensorimotor (lateral) striatum. Compared to nearby medium-spiny projection neurons (MSNs), FSIs receive convergent inputs from a wider range of distinct cortical regions, suggestive of a role

in sensorimotor integration (Ramanathan et al., 2002). However, while MSNs receive very few synapses from each of a large number of different corticostriatal axons (Kincaid et al., 1998), FSIs receive more numerous inputs from each of a smaller number of afferents (Bennett and Bolam, 1994). An important unresolved question is whether the cortical cells that project to FSIs are somehow distinct to other corticostriatal neurons. FSIs appear to be more sensitive to cortical inputs than MSNs – for example, focal stimulation of cortex provokes an immediate-early gene response in FSIs over a broader expanse of striatum than MSNs (Parthasarathy and Graybiel, 1997). FSIs connect to each other via both chemical synapses and gap junctions on their dendrites (Kita et al., 1990; Fukuda, 2009), with the resulting electrical meshwork presumably coordinating FSI activity in some fashion. FSIs each make GABA_A-mediated synapses onto hundreds of surrounding MSNs, largely onto the somatic region where they can have a powerful influence over MSN spike initiation. By contrast, MSN–MSN GABAergic synapses tend to be distal to the cell body and individually weaker (Koos et al., 2004; Gustafson et al., 2006), albeit larger in number, and MSNs do not provide reciprocal connections onto FSIs (Chuhma et al., 2011). These anatomical features quite reasonably led to the view that FSIs serve a broad, coordinated function, rather than participating in the rich details of striatal information processing (e.g., Plenz, 2003). Finally, FSIs receive an unusual back-projection from globus pallidus (GP; Bevan et al., 1998), that is quite divergent – i.e., small portions of pallidum can affect large areas of striatum (Rajakumar et al., 1994; Spooren et al., 1996).

FSI PHYSIOLOGY IN CULTURE AND SLICE PREPARATIONS

Fast-spiking interneurons have similar properties throughout striatum, including nucleus accumbens (Taverna et al., 2007). As is the case for cortical FSIs, striatal FSIs have distinctive very brief

waveforms (Kawaguchi, 1993) and can fire spikes at substantially higher rates than MSNs (e.g., Plenz and Kitai, 1998). Even with steady input they can fire in a variety of patterns, including both single spiking and irregular high-frequency bursts (“stuttering”). Such bursts are typically preceded by gamma-band fluctuations in membrane potential, and reflect intrinsic resonance of FSIs at gamma frequencies (Bracci et al., 2003). This is potentially important, as in neocortical and hippocampal circuits FSI-mediated gamma frequency inhibition is critical for organizing projection cells into functional cell assemblies (Buzsáki, 2006). Although it is not yet clear if similar mechanisms operate in striatum (see below), *in vitro* FSIs seem to be especially likely to participate in striatal cell assemblies (Carrillo-Reid et al., 2008), that arise even without patterned afferent input.

Important advances by Koos and colleagues verified that FSIs form functional electrical connections with each other, and that even single FSI spikes can potentially delay or abolish MSN spiking evoked by current injection (Koos and Tepper, 1999). FSIs appear to influence somewhere between 25 and 75% of MSNs within several hundred microns of their cell body, and to preferentially contact striatonigral (D1+) MSNs (Gittis et al., 2010), although striatopallidal (D2+) MSNs are also targets (Planert et al., 2010). Based on a detailed examination of MSN membrane voltage, Wilson (2009) has argued that FSI inputs are likely responsible for rapid fluctuations that determine the precise time course of MSN spiking.

FSI activity in slices is affected by major neuromodulatory systems, acting through both pre- and post-synaptic receptors. Dopamine increases FSI activity by depolarization (mediated via D5 receptors) while also reducing GABAergic input onto these cells (via pre-synaptic D2 receptors; Centonze et al., 2003). Serotonin also appears to excite FSIs (Blomeley and Bracci, 2009). Acetylcholine seems to exert a more mixed effect, directly depolarizing FSIs (via nicotinic receptors) while reducing their influence on MSNs (via pre-synaptic muscarinic receptors on FSI terminals; Koos and Tepper, 2002). FSIs can show synaptic plasticity at multiple time scales, including strong short-term depression of their synapses onto MSNs (Plenz and Kitai, 1998; Koos et al., 2004; Gittis et al., 2010; Planert et al., 2010) and spike-timing-dependent LTP/LTD at their own inputs (e.g., Fino et al., 2008). FSI-mediated control of MSN spike timing likely also has a strong influence over synaptic change at MSN inputs – differences in GABAergic transmission may be a key factor behind discrepant observations of Hebbian and anti-Hebbian corticostriatal plasticity (Fino et al., 2005; Shen et al., 2008).

FSI PHYSIOLOGY IN ANESTHETIZED ANIMALS

Studies in urethane-anesthetized rats have provided an important bridge between *in vitro* investigations of FSIs and behavioral experiments. Using a juxtacellular labeling approach, Mallet et al. (2005, 2006) confirmed that all extracellularly recorded neurons with very brief waveforms are parvalbumin-positive, and that these cells can readily respond to cortical stimulation by firing bursts with very short inter-spike intervals (2–3 ms). This FSI response appears to mediate powerful feed-forward inhibition, that can constrain the temporal response of MSNs to cortical input. For reasons that are not yet fully clear, such shaping of MSN spike timing was altered following dopamine depletion – even

though the spontaneous firing rate of FSIs was not altered, striatopallidal MSNs tended to have less precise evoked responses. In both normal and dopamine-depleted animals, MSNs were more spontaneously active when the cortex was undergoing slow-wave oscillations compared to tail pinch-induced cortical desynchronization, while FSIs showed the opposite pattern – evidence of a broadly reciprocal relationship between MSN and FSI activity, at least on relatively slow timescales.

IDENTIFYING FSIS IN FREELY MOVING ANIMALS

There are inherent uncertainties in trying to distinguish different (chemically defined) subpopulations of neurons using extracellular recording alone, and historically studies of striatum in behaving animals have not attempted to do so. The main exception has been monkey studies that contrast “phasically active” (presumed MSNs) with “tonically active” neurons (TANs). TANs are thought to be cholinergic interneurons as they show regular firing and long-duration waveforms, which are properties of rat cholinergic interneurons studied under anesthesia (Wilson et al., 1990). Beginning in 2004 my colleagues and I reported (Berke et al., 2004) that there are also clearly distinguishable subgroups of rat striatal neurons, including a set of neurons that are near-continuously (i.e., tonically) active. However, rather than resembling TANs these active cells had very *brief* waveforms, fired high-frequency bursts during natural sleep or high-voltage spindle oscillations, and showed a graded distribution, being more prevalent in lateral striatum. Taken together these properties provide strong evidence that these cells are the parvalbumin-positive FSIs. The basic distinction between a larger population of presumed MSNs that are typically silent most of the time, and a smaller population of presumed FSIs that have very brief waveforms and are near-continuously active is also clear in our subsequent studies using different data sets in rats (e.g., Gage et al., 2010; Wiltshcko et al., 2010), or mice (Gittis et al., submitted) and in the work of other groups (e.g., Schmitzer-Torbert and Redish, 2008; Lansink et al., 2010; Morra et al., 2010). Not all rodent striatal cells easily fall into these two classes – for example, some active cells seem to have a characteristic intermediate-duration waveform and consistent behavioral responses (Berke, 2008) and may be another class of GABAergic interneuron (perhaps the somatostatin-positive cells). Also, a somewhat puzzling observation is that a *very* low proportion of rat striatal cells resemble monkey TANs based on waveform and firing pattern. The actual proportion of cholinergic neurons is not known to be substantially different between the two species, although there are differences in cholinergic cell shape (Yelnick et al., 1993). Conversely there have been no descriptions as yet of FSIs in primate extracellular recordings, and this seems to reflect experimental methods more than real species differences (Wu and Parent, 2000). Nonetheless, the results of recent investigations lead to some recommendations. Firstly, given that FSIs are tonically active in awake animals, the term “TANs” in monkeys is a confusing misnomer (as has been pointed out before, for other reasons – Bennett and Wilson, 2003) and should perhaps be dropped in favor of “presumed cholinergic interneurons.” Secondly, the strong tendency of presumed FSIs to transition to high-frequency bursting during natural slow-wave sleep seems to be a particularly useful criterion for distinguishing them (Berke, 2008), and so routinely

recording during sleep is highly valuable. These FSI bursts, which resemble the intrinsic stuttering mode of FSIs (Golomb et al. 2007, Klaus et al. 2011), do not occur on every cycle of cortical slow-waves, and are not usually synchronized between neighboring cells (Berke et al. 2004).

FSI ACTIVITY DURING AWAKE AND DRUG-INDUCED BEHAVIORAL STATES

Overall, FSIs tend to have higher firing rates in awake animals (typically 10–30 Hz) than during natural slow-wave sleep, while the reverse tends to be true for MSNs (unpublished observations). This crude FSI/MSN reciprocity corresponds well to the prior studies under anesthesia discussed above. By contrast, at least two major FSI properties expected from the prior literature were not observed. Despite their gap-junction connectivity FSIs do not seem to show millisecond-scale synchronization in awake animals (Berke, 2008) – even when neighboring FSIs are recorded from the same tetrode. A subsequent modeling study of the striatal FSI network (Hjorth et al., 2009) found that the dominant effect of gap junctions is to lower firing rates by shunting current between cells, and it is only under conditions of very high input synchrony that gap junctions promote synchrony of spike outputs. It appears that FSI inputs are not normally sufficiently synchronous in awake animals, with the possible exception of intermittent states like high-voltage spindles. In addition, we found no evidence for rapid FSI inhibition of MSNs, using cross-correlograms to plot MSN spike probability around FSI spike times (Gage et al., 2010). Although cross-correlograms are not an highly sensitive tool, especially with low spike counts, in the same experiments we were readily able to see rapid FSI inhibition of nearby projection cells in motor cortex. This difference was unexpected given the strong brain slice evidence that striatal FSIs control MSN spike times, and clearly needs to be investigated further. As it stands, it appears that not to be the case that each FSI spike provokes synchronous moments of silence in the surrounding volume of MSNs. One factor that is likely relevant is that in awake animals MSNs usually have relatively depolarized membrane potentials (Mahon et al., 2006) that are close to the chloride reversal potential – although FSI GABA release should still tend to reduce MSN spike probability under these conditions. Another potential factor is that the recent spiking history of MSNs and FSIs can alter synaptic actions – for example through short-term depression – leading to strong interactions only under specific behavioral conditions (Fujisawa et al., 2008). Certainly it was anticipated that FSI action on MSNs would be more complex than simple inhibition (Plenz, 2003; Bracci and Panzeri, 2006), and this has now been observed in large-scale striatal network simulations in which removing FSIs actually results in lowered overall MSN firing (Humphries et al., 2009).

Some major classes of psychoactive drugs achieve their behavioral effects largely through actions in striatum, and so administering these drugs in striatal recording studies offers both a means of manipulating striatal circuitry, and possible insights into how such drugs operate at the circuit level. Wiltschko et al. (2010) gave rats systemic injections of either the stimulant amphetamine or a D2 antagonist (an antipsychotic), and compared the effects on MSNs and FSIs. As seen in previous investigations in behaving animals

(Rebec, 2006) the effects on MSNs were highly variable. Even though the two drugs respectively stimulated, and suppressed, psychomotor activation, in each case many MSNs increased firing rate compared to control saline injections, and many decreased. The story for FSIs was very different – all FSIs were suppressed by the D2 antagonist, while following amphetamine most FSIs increased firing rate (and none decreased activity). This far more uniform response confirms that the presumed FSIs are a functionally distinct population of striatal neurons, and shows that their influence over striatal output is not reflected simply by reciprocal firing to the overall MSN population. Interestingly, FSIs also have distinct drug responses to MSNs at the level of nuclear signaling – amphetamine causes phosphorylation of the transcriptional regulation MeCP2 selectively in ventral striatal FSIs, and the level of phosphorylation correlates with behavioral sensitization (Deng et al., 2010). The specific mechanisms leading to drug-altered FSI activity are not trivial to determine (see discussion in Wiltschko et al., 2010). Perhaps the most straightforward possibilities are that amphetamine-induced dopamine increases produce depolarization of FSIs via D1-type receptors, while the D2 antagonist reduces FSI spiking by increasing GABAergic transmission onto FSIs, due to a combination of enhanced pallidostriatal activity (Billings and Marshall, 2003) and reduced autoreceptor function at the corresponding GABAergic terminals in striatum. In a related pharmacological/recording study Morra et al. (2010) gave the stimulant methamphetamine, in combination with cannabinoid CB1 receptors antagonists in the nucleus accumbens. Once again they found that FSIs (in this case in ventral striatum) were more likely than MSNs to have firing rates positively correlated with drug-induced changes in locomotor activity. Taken together these results indicate that FSIs tend to act in a similar way on slow time scales, and may be very important for mediating psychoactive drug actions on behavior, yet do so without producing dramatic changes in overall striatal output.

FSI ACTIVITY DURING BEHAVIORAL TASKS

So far only a few studies have examined the correlations between FSI firing and more specific behaviors, so some interpretations remain preliminary. Nonetheless there are some clear initial conclusions that can be drawn. Given that FSI firing rates show quite consistent positive correlations with simple measures of locomotor activity, one might expect that these cells would also show consistent activity patterns relative to behavioral events. In general, this is not the case. In rats performing maze tasks FSIs were shown to have strong event-related changes in firing rate, but with complex time courses that were highly idiosyncratic (Berke, 2008; Schmitzer-Torbert and Redish, 2008). There was little sign of an overall FSI population response – even at times when MSN population activity was changing – and simultaneously recorded, neighboring FSIs that would be expected to contact highly overlapping sets of MSNs had apparently unrelated time courses. This was quite surprising, and not readily compatible with the idea that FSIs simply provide a coordinated broad inhibition of MSNs. If it is indeed the case that individual MSNs are receiving very distinct patterns of perisomatic input from each of a handful of FSIs (~4–27; Koos and Tepper, 1999), this could be responsible for the “noisy” high-frequency component of MSN membrane voltage (Mahon et al., 2006; Wilson, 2009)

but it is not clear what functional role this could achieve. It may be that a network-level, rather than single-cell, perspective will be informative here (see below).

In a subsequent study we examined single units in striatum, GP, and motor cortex in an operant task designed to help separate out processes of movement inhibition, preparation, and execution (Gage et al., 2010). Rats had to maintain their noses in a central hole before receiving first an instruction tone indicating that a left or right movement would be required, then after a delay another sound telling them to proceed. Once again we observed that FSIs had highly idiosyncratic firing rate time courses, with (for example) no systematic preference for contralateral or ipsilateral movements. However, in this task we found that FSI firing rates *did* show a specific moment of transient coordination, with FSIs throughout striatum increasing firing rate just as the rat initiated his chosen left or right movement. We suggested that the need to engage one action while suppressing another highly trained alternative might be responsible for this brief yet broad FSI “pulse,” which was not seen around other movements in the task. This is an interesting possibility in light of observations that humans with Tourette Syndrome – characterized by difficulties in suppressing overtrained “tics” – have a deficit in striatal FSIs (Kalanithi et al., 2005; Kataoka et al., 2010).

The coordinated FSI population activity increase was accompanied by a matching decrease in overall GP activity, a striking finding that suggests that disinhibition in the pallidostriatal pathway is driving the FSI pulse. The pallidostriatal pathway allows for a wide range of influences over striatal processing, since GP is a central hub receiving input from all over the basal ganglia. It is also a particularly good candidate for driving distributed, coordinated changes in FSI firing given that the pallidostriatal pathway is more divergent than striatopallidal projections. This idea is quite different to previous concepts of broadly coordinated FSI activity conveying feed-forward inhibition from cortex (see above). Although FSIs obviously get cortical inputs and certainly can provide rapid feed-forward inhibition to MSNs, it has so far proven hard to observe evidence of this process occurring under natural conditions. In part this is likely because normal information processing generally involves much weaker, less abrupt signals than electrical cortical stimulation. But it is also because cortical inputs appear to actually drive complex, idiosyncratic activity patterns in FSIs that are usually uncoordinated and cause subtle shifts in MSN spike timing rather than broad changes in firing rate.

FSIs AND THE DYNAMIC ORGANIZATION OF STRIATAL MICROCIRCUITS

So far I have focused on changes in FSI firing rate, but there is intriguing evidence that behavior-linked changes in FSI spike timing may be just as, or even more, important. Firstly, FSIs can change their pattern of firing even without marked shifts in rate. For example, the cell shown in **Figure 1** (recorded during the operant left/right task described above) shows erratic bursting during the early part of each trial. Once the instruction tone is played, however, firing becomes far more regular, and this regularity persists throughout the delay period until the rat executes his chosen movement, at which point the erratic bursting resumes. In a

quantitative analysis (Lau et al., 2010) we found that the instruction tone leads to broad regularization of FSI firing, that was similar to that observed in artificial networks of coupled FSIs following a shift from uniformly random to heterogeneously patterned inputs. In the simulations we found that the gap-junction coupling between FSIs was essential for this phenomenon, which we suggested reflects the transition from a “searching” to a “selected” network state. More direct manipulations of gap-junction connectivity will certainly be needed to test this idea.

Secondly, FSIs participate in multiple forms of local field potential oscillation in the awake striatum (Berke et al., 2004; Berke, 2005), and can modulate their entrainment even without changes in firing rate (Berke, 2009a). Although the contributions of specific frequencies to striatal information processing

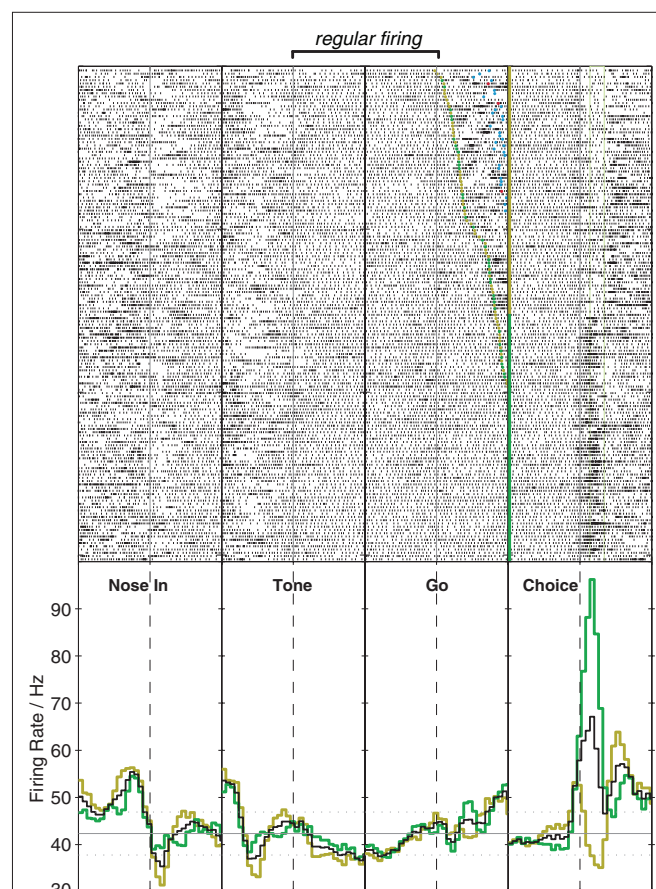


FIGURE 1 | Stabilization of FSI firing pattern with action programming.

This example shows activity of a single striatal FSI during performance of an instructed left/right choice task (Gage et al., 2010). Upper panels show raster plots (151 trials total), lower panels show peri-event histograms of firing rate (time range: -0.5 to 0.5 s in each case). The rat begins the trial by inserting his nose into an illuminated port (Nose In) and waits for an instruction cue (Tone) that indicates whether a subsequent left or right movement will be rewarded, provided the rat waits for a second cue (Go) before initiating his movement (Choice). For the raster aligned on the Go cue, trials are ordered by reaction time. The FSI shows a sharp increase in firing rate beginning shortly before movement onset, that in this case is stronger for ipsilateral (green) than contralateral movements (gold). The onset of the tone is not associated with a substantial firing rate change, but causes the cell to spike far more regularly until the action is executed (for quantitative analysis, see Lau et al., 2010).

remain unclear, LFPs (especially in ventral striatum) show frequent spontaneous transitions between one state involving beta (~20 Hz) and low-gamma (~50 Hz), and another state involving theta (~8 Hz) and high-gamma (~80 Hz). Dopaminergic drugs such as amphetamine or apomorphine push the network into the theta/high-gamma state, and the same transition is seen around reward receipt (Berke, 2009a) or cues predictive of rewards (unpublished observations). FSIs are much more likely to show clear locking to gamma oscillations than MSNs, and it appears that distinct subpopulations of FSI participate in theta/high-gamma and beta/low-gamma respectively (Berke, 2009a). Other groups investigating striatal LFPs have also reported similar gamma state transitions and FSI involvement (van der Meer et al., 2010). Such phenomena need to be interpreted with caution, given uncertainties about how LFP oscillations are generated in non-laminar structures such as striatum (Berke, 2005). Nonetheless, oscillations are an important potential mechanism by which FSIs might contribute to the dynamic gating of distinct afferent input streams (Akam and Kullmann, 2010) and the formation of projection cell ensembles (Harris et al., 2003), and need to be investigated further in striatum.

CONCLUSION

WHAT HAVE WE LEARNED ABOUT FSIS, AND NEXT STEPS

The advent of striatal FSI monitoring in behaving animals offers an opportunity to move beyond examining “coding” by single neurons to explore how cellular interactions within local micro-circuits help achieve behavioral functions. Perhaps the most striking finding so far is how unexpectedly FSIs seem to behave in the context of awake circuit dynamics, compared to brain slices, anesthesia, or sleep. Whereas FSIs in slices are quiescent but strongly inhibit MSNs when artificially stimulated, awake FSIs usually emit a near-continuous stream of single spikes whose influence on nearby MSNs is not readily detectable. FSIs are coupled together by functional gap junctions, yet we have so far seen no clear evidence for precise spike synchronization. Although broad feed-forward inhibition of cortical signals is thought to be an important aspect of FSI function, we have instead found evidence for their transient coordination by a pallidostriatal “feedback” pathway. Putting together many results, our working hypothesis is that three distinct types of inputs to FSIs control three distinct aspects of FSI firing: (1) heterogeneous cortical inputs produce idiosyncratic patterns of behavior-linked FSI firing, that influence cell assembly formation within local striatal modules; (2) gap junctions between FSIs help stabilize their activity as actions are firmly selected; and (3) the pallidostriatal pathway helps coordinate FSI firing rates across wide areas of striatum, perhaps helping to provide timed suppression of unwanted, incompatible actions.

REFERENCES

- Akam, T., and Kullmann, D. M. (2010). Oscillations and filtering networks support flexible routing of information. *Neuron* 67, 308–320.
- Bennett, B. D., and Bolam, J. P. (1994). Synaptic input and output of parvalbumin-immunoreactive neurons in the neostriatum of the rat. *Neuroscience* 62, 707–719.
- Bennett, B. D., and Wilson, C. J. (2003). “TANs, PANs and STANs,” in *The Basal Ganglia VI*, eds A. M. Graybiel, M. R. DeLong, and S. T. Kitai (New York: Plenum Press), 225–236.
- Berke, J. D. (2005). “Participation of striatal neurons in large-scale oscillatory networks,” in *The Basal Ganglia VIII*, eds J. P. Bolam, C. A. Ingham, and P. J. Magill (New York: Springer), 25–35.
- Berke, J. D. (2008). Uncoordinated firing rate changes of striatal fast-spiking interneurons during behavioral task performance. *J. Neurosci.* 28, 10075–10080.
- Berke, J. D. (2009a). Fast oscillations in cortical-striatal networks switch frequency following rewarding events and stimulant drugs. *Eur. J. Neurosci.* 30, 848–859.
- Exactly how FSIs sculpt MSN activity in behaving animals remains mysterious. Perhaps the most likely possibility is that an inhibitory response of MSNs to FSI spikes is highly contingent upon additional factors that change at specific moments during behavioral tasks, such as short-term synaptic depression, simultaneous spiking of multiple FSIs, or the status of cholinergic modulation. In part such hypotheses can be tested using standard methods, but two further types of approach are highly promising for exploring the behavioral functions of FSIs. The first is based on novel tools for manipulating select cell types in awake animals. For example, although it is well established that local interference with striatal GABA transmission can produce dyskinesias including dystonia, the specific contributions of distinct GABAergic elements in striatum has been unclear. Using drugs that interfere with glutamatergic input to FSIs but not MSNs, we have recently found that a selective reduction in FSI activity within sensorimotor striatum is sufficient to produce dystonic symptoms (Gittis et al., submitted), without substantial changes to mean firing rates of nearby MSNs. In addition to confirming the importance of FSIs for avoiding aberrant action selection, this observation supports our previous suggestion (Wiltschko et al., 2010) that FSI suppression is a promising candidate mechanism by which antipsychotics often result in acute dystonic side effects (Kamin et al., 2000). To test ideas about FSI function during normal behaviors it will be useful to perform more precisely timed selective suppression of FSIs (e.g., using optogenetic methods), and assess – as one example – if and when this interferes with the normal behavioral inhibition of unwanted choices during action selection.
- A complementary second promising approach is simultaneous monitoring of large (30–100+) numbers of cells within small striatal subregions, using either electrodes with large numbers of nearby contacts or optical recording methods. The spontaneous formation and switching between assemblies of synchronous striatal neurons has been observed both *in vitro* and in large-scale simulations (Ponzi and Wickens, 2010). FSIs seem to have a vital role controlling assembly formation (Humphries et al., 2009; Humphries, 2011), via processes that may not be easily captured when considering pairwise interactions alone. Yet there has been little network-level examination of striatum in behaving animals, and in combination with selective manipulations this is an exciting frontier for future investigation of FSIs, neuromodulation, and other aspects of striatal function.

ACKNOWLEDGMENTS

For the experiments described here that were performed in my laboratory, primary funding came from the Tourette Syndrome Foundation, the Whitehall Foundation, the National Institute on Drug Abuse, and the National Institute of Mental Health, together with the University of Michigan.

- Berke, J. D. (2009b). "Procedural learning: striatum," in *Encyclopedia of Neuroscience*, eds L. R. Squire, T. Albright, F. E. Bloom, F. H. Gage, and N. Spitzer (Oxford: Elsevier).
- Berke, J. D., Okatan, M., Skurski, J., and Eichenbaum, H. B. (2004). Oscillatory entrainment of striatal neurons in freely moving rats. *Neuron* 43, 883–896.
- Bevan, M. D., Booth, P. A., Eaton, S. A., and Bolam, J. P. (1998). Selective innervation of neostriatal interneurons by a subclass of neuron in the globus pallidus of the rat. *J. Neurosci.* 18, 9438–9452.
- Billings, L. M., and Marshall, J. F. (2003). D2 antagonist-induced c-fos in an identified subpopulation of globus pallidus neurons by a direct intrapallidal action. *Brain Res.* 964, 237–243.
- Blomeley, C. P., and Bracci, E. (2009). Serotonin excites fast-spiking interneurons in the striatum. *Eur. J. Neurosci.* 29, 1604–1614.
- Bracci, E., Centonze, D., Bernardi, G., and Calabresi, P. (2003). Voltage-dependent membrane potential oscillations of rat striatal fast-spiking interneurons. *J. Physiol. (Lond.)* 549, 121–130.
- Bracci, E., and Panzeri, S. (2006). Excitatory GABAergic effects in striatal projection neurons. *J. Neurophysiol.* 95, 1285–1290.
- Buzsáki, G. (2006). *Rhythms of the Brain*. New York: Oxford University Press.
- Carrillo-Reid, L., Tecuapetla, F., Tapia, D., Hernandez-Cruz, A., Galarraga, E., Drucker-Colin, R., and Bargas, J. (2008). Encoding network states by striatal cell assemblies. *J. Neurophysiol.* 99, 1435–1450.
- Centonze, D., Grande, C., Usiello, A., Gubellini, P., Erbs, E., Martin, A. B., Pisani, A., Tognazzi, N., Bernardi, G., Moratalla, R., Borrelli, E., and Calabresi, P. (2003). Receptor subtypes involved in the presynaptic and postsynaptic actions of dopamine on striatal interneurons. *J. Neurosci.* 23, 6245–6254.
- Chuhma, N., Tanaka, K. F., Hen, R., and Rayport, S. (2011). Functional connectome of the striatal medium spiny neuron. *J. Neurosci.* 31, 1183–1192.
- Deng, J. V., Rodriguez, R. M., Hutchinson, A. N., Kim, I. H., Wetsel, W. C., and West, A. E. (2010). MeCP2 in the nucleus accumbens contributes to neural and behavioral responses to psychostimulants. *Nat. Neurosci.* 13, 1128–1136.
- Fino, E., Deniau, J. M., and Venance, L. (2008). Cell-specific spike-timing-dependent plasticity in GABAergic and cholinergic interneurons in corticostriatal rat brain slices. *J. Physiol. (Lond.)* 586, 265–282.
- Fino, E., Glowinski, J., and Venance, L. (2005). Bidirectional activity-dependent plasticity at corticostriatal synapses. *J. Neurosci.* 25, 11279–11287.
- Fujisawa, S., Amarasingham, A., Harrison, M. T., and Buzsáki, G. (2008). Behavior-dependent short-term assembly dynamics in the medial prefrontal cortex. *Nat. Neurosci.* 11, 823–833.
- Fukuda, T. (2009). Network architecture of gap junction-coupled neuronal linkage in the striatum. *J. Neurosci.* 29, 1235–1243.
- Gage, G. J., Stoetznner, C. R., Wiltshko, A. B., and Berke, J. D. (2010). Selective activation of striatal fast-spiking interneurons during choice execution. *Neuron* 67, 466–479.
- Gerfen, C. R., Baimbridge, K. G., and Miller, J. J. (1985). The neostriatal mosaic: compartmental distribution of calcium-binding protein and parvalbumin in the basal ganglia of the rat and monkey. *Proc. Natl. Acad. Sci. U.S.A.* 82, 8780–8784.
- Gittis, A. H., Leventhal, D. K., Fensterheim, B. A., Pettibone, J. R., Berke, J. D., and Kreitzer, A. C. (submitted). Selective inhibition of striatal fast-spiking interneurons elicits dystonia.
- Gittis, A. H., Nelson, A. B., Thwin, M. T., Palop, J. J., and Kreitzer, A. C. (2010). Distinct roles of GABAergic interneurons in the regulation of striatal output pathways. *J. Neurosci.* 30, 2223–2234.
- Golomb, D., Donner, K., Shacham, L., Shlosberg, D., Amitai, Y., and Hansel, D. (2007). Mechanisms of firing patterns in fast-spiking cortical interneurons. *PLoS Comput. Biol.* 3, e156. doi: 10.1371/journal.pcbi.0030156
- Gustafson, N., Gireesh-Dharmaraj, E., Czubyko, U., Blackwell, K. T., and Plenz, D. (2006). A comparative voltage and current-clamp analysis of feedback and feedforward synaptic transmission in the striatal microcircuit in vitro. *J. Neurophysiol.* 95, 737–752.
- Harris, K. D., Csicsvari, J., Hirase, H., Dragoi, G., and Buzsáki, G. (2003). Organization of cell assemblies in the hippocampus. *Nature* 424, 552–556.
- Hjorth, J., Blackwell, K. T., and Hellgren Kotaleski, J. (2009). Gap junctions between striatal fast-spiking interneurons regulate spiking activity and synchronization as a function of cortical activity. *J. Neurosci.* 29, 5276–5286.
- Humphries, M. D. (2011). Spike-train communities: finding groups of similar spike trains. *J. Neurosci.* 31, 2321–2336.
- Humphries, M. D., Wood, R., and Gurney, K. (2009). Dopamine-modulated dynamic cell assemblies generated by the GABAergic striatal microcircuit. *Neural Netw.* 22, 1174–1188.
- Kalanithi, P. S., Zheng, W., Kataoka, Y., DiFiglia, M., Grantz, H., Saper, C. B., Schwartz, M. L., Leckman, J. F., and Vaccarino, F. M. (2005). Altered parvalbumin-positive neuron distribution in basal ganglia of individuals with Tourette syndrome. *Proc. Natl. Acad. Sci. U.S.A.* 102, 13307–13312.
- Kamin, J., Manwani, S., and Hughes, D. (2000). Emergency psychiatry: extrapyramidal side effects in the psychiatric emergency service. *Psychiatr. Serv.* 51, 287–289.
- Kataoka, Y., Kalanithi, P. S., Grantz, H., Schwartz, M. L., Saper, C., Leckman, J. F., and Vaccarino, F. M. (2010). Decreased number of parvalbumin and cholinergic interneurons in the striatum of individuals with Tourette syndrome. *J. Comp. Neurol.* 518, 277–291.
- Kawaguchi, Y. (1993). Physiological, morphological, and histochemical characterization of three classes of interneurons in rat neostriatum. *J. Neurosci.* 13, 4908–4923.
- Kincaid, A. E., Zheng, T., and Wilson, C. J. (1998). Connectivity and convergence of single corticostriatal axons. *J. Neurosci.* 18, 4722–4731.
- Kita, H., Kosaka, T., and Heizmann, C. W. (1990). Parvalbumin-immunoreactive neurons in the rat neostriatum: a light and electron microscopic study. *Brain Res.* 536, 1–15.
- Klaus, A., Planert, H., Hjorth, J., Berke, J. D., Silberberg, G., and Kotaleski, J. H. (2011). Striatal fast-spiking interneurons: from firing patterns to postsynaptic impact. *Front. Syst. Neurosci.* 5:57. doi: 10.3389/fnsys.2011.00057
- Koos, T., and Tepper, J. M. (1999). Inhibitory control of neostriatal projection neurons by GABAergic interneurons. *Nat. Neurosci.* 2, 467–472.
- Koos, T., and Tepper, J. M. (2002). Dual cholinergic control of fast-spiking interneurons in the neostriatum. *J. Neurosci.* 22, 529–535.
- Koos, T., Tepper, J. M., and Wilson, C. J. (2004). Comparison of IPSCs evoked by spiny and fast-spiking neurons in the neostriatum. *J. Neurosci.* 24, 7916–7922.
- Lansink, C. S., Goltstein, P. M., Lankelma, J. V., and Pennartz, C. M. (2010). Fast-spiking interneurons of the rat ventral striatum: temporal coordination of activity with principal cells and responsiveness to reward. *Eur. J. Neurosci.* 32, 494–508.
- Lau, T., Gage, G. J., Berke, J. D., and Zochowski, M. (2010). Local dynamics of gap-junction-coupled interneuron networks. *Phys. Biol.* 7, 16015.
- Luk, K. C., and Sadikot, A. F. (2001). GABA promotes survival but not proliferation of parvalbumin-immunoreactive interneurons in rodent neostriatum: an in vivo study with stereology. *Neuroscience* 104, 93–103.
- Mahon, S., Vautrelle, N., Pezard, L., Slaght, S. J., Deniau, J. M., Chouvet, G., and Charpier, S. (2006). Distinct patterns of striatal medium spiny neuron activity during the natural sleep-wake cycle. *J. Neurosci.* 26, 12587–12595.
- Mallet, N., Ballion, B., Le Moine, C., and Gonon, F. (2006). Cortical inputs and GABA interneurons imbalance projection neurons in the striatum of parkinsonian rats. *J. Neurosci.* 26, 3875–3884.
- Mallet, N., Le Moine, C., Charpier, S., and Gonon, F. (2005). Feedforward inhibition of projection neurons by fast-spiking GABA interneurons in the rat striatum in vivo. *J. Neurosci.* 25, 3857–3869.
- Morra, J. T., Glick, S. D., and Cheer, J. F. (2010). Neural encoding of psychomotor activation in the nucleus accumbens core, but not the shell, requires cannabinoid receptor signaling. *J. Neurosci.* 30, 5102–5107.
- Parthasarathy, H. B., and Graybiel, A. M. (1997). Cortically driven immediate-early gene expression reflects modular influence of sensorimotor cortex on identified striatal neurons in the squirrel monkey. *J. Neurosci.* 17, 2477–2491.
- Planert, H., Szydlowski, S. N., Hjorth, J. J., Grillner, S., and Silberberg, G. (2010). Dynamics of synaptic transmission between fast-spiking interneurons and striatal projection neurons of the direct and indirect pathways. *J. Neurosci.* 30, 3499–3507.
- Plenz, D. (2003). When inhibition goes incognito: feedback interaction between spiny projection neurons in striatal function. *Trends Neurosci.* 26, 436–443.
- Plenz, D., and Kitai, S. T. (1998). Up and down states in striatal medium spiny neurons simultaneously recorded with spontaneous activity in fast-spiking interneurons studied in cortex-striatum-substantia nigra organotypic cultures. *J. Neurosci.* 18, 266–283.
- Ponzi, A., and Wickens, J. (2010). Sequentially switching cell assemblies in random inhibitory networks of spiking neurons in the striatum. *J. Neurosci.* 30, 5894–5911.
- Rajakumar, N., Elisevich, K., and Flumerfelt, B. A. (1994). The pallidostriatal projection in the rat: a recurrent inhibitory loop? *Brain Res.* 651, 332–336.

- Ramanathan, S., Hanley, J. J., Deniau, J. M., and Bolam, J. P. (2002). Synaptic convergence of motor and somatosensory cortical afferents onto GABAergic interneurons in the rat striatum. *J. Neurosci.* 22, 8158–8169.
- Rebec, G. V. (2006). Behavioral electrophysiology of psychostimulants. *Neuropsychopharmacology* 31, 2341–2348.
- Schmitzer-Torbert, N. C., and Redish, A. D. (2008). Task-dependent encoding of space and events by striatal neurons is dependent on neural subtype. *Neuroscience* 153, 349–360.
- Shen, W., Flajolet, M., Greengard, P., and Surmeier, D. J. (2008). Dichotomous dopaminergic control of striatal synaptic plasticity. *Science* 321, 848–851.
- Spooren, W. P., Lynd-Balta, E., Mitchell, S., and Haber, S. N. (1996). Ventral pallidostriatal pathway in the monkey: evidence for modulation of basal ganglia circuits. *J. Comp. Neurol.* 370, 295–312.
- Taverna, S., Canciani, B., and Pennartz, C. M. (2007). Membrane properties and synaptic connectivity of fast-spiking interneurons in rat ventral striatum. *Brain Res.* 1152, 49–56.
- Turner, R. S., and Desmurget, M. (2010). Basal ganglia contributions to motor control: a vigorous tutor. *Curr. Opin. Neurobiol.* 20, 704–716.
- van der Meer, M. A., Kalenscher, T., Lansink, C. S., Pennartz, C. M., Berke, J. D., and Redish, A. D. (2010). Integrating early results on ventral striatal gamma oscillations in the rat. *Front. Neurosci.* 4:300. doi: 10.3389/fnins.2010.00300
- Wilson, C. (2009). “What controls the timing of striatal spiny cell action potentials?” in *The Basal Ganglia IX*, eds H. J. Groenewegen, P. Voorn, H. W. Berendse, A. B. Mulder, and A. R. Cools (Heidelberg: Springer Dordrecht), 49–61.
- Wilson, C. J., Chang, H. T., and Kitai, S. T. (1990). Firing patterns and synaptic potentials of identified giant aspiny interneurons in the rat neostriatum. *J. Neurosci.* 10, 508–519.
- Wiltchko, A. B., Pettibone, J. R., and Berke, J. D. (2010). Opposite effects of stimulant and antipsychotic drugs on striatal fast-spiking interneurons. *Neuropsychopharmacology* 35, 1261–1270.
- Wu, Y., and Parent, A. (2000). Striatal interneurons expressing calretinin, parvalbumin or NADPH-diaphorase: a comparative study in the rat, monkey and human. *Brain Res.* 863, 182–191.
- Yelnick, J., Percheron, G., Francois, C., and Garnier, A. (1993). Cholinergic neurons of the rat and primate striatum are morphologically different. *Prog. Brain Res.* 99, 25–34.
- Conflict of Interest Statement:** The author declares that the research was conducted in the absence of any commercial or financial relationships that could be construed as a potential conflict of interest.

Received: 12 April 2011; paper pending published: 10 May 2011; accepted: 03 June 2011; published online: 20 June 2011.

Citation: Berke JD (2011) Functional properties of striatal fast-spiking interneurons. *Front. Syst. Neurosci.* 5:45. doi: 10.3389/fnsys.2011.00045

Copyright © 2011 Berke. This is an open-access article subject to a non-exclusive license between the authors and Frontiers Media SA, which permits use, distribution and reproduction in other forums, provided the original authors and source are credited and other Frontiers conditions are complied with.



Striatal fast-spiking interneurons: from firing patterns to postsynaptic impact

Andreas Klaus^{1,2,3*}, Henrike Planert^{1,3}, J. J. Johannes Hjorth^{3,4}, Joshua D. Berke⁵, Gilad Silberberg^{1,3} and Jeanette Hellgren Kotaleski^{1,3,4}

¹ Nobel Institute for Neurophysiology, Department of Neuroscience, Karolinska Institute, Stockholm, Sweden

² Laboratory of Systems Neuroscience, National Institute of Mental Health, Bethesda, MD, USA

³ Stockholm Brain Institute, Research School, Stockholm, Sweden

⁴ School of Computer Science and Communication, Royal Institute of Technology, AlbaNova University Centre, Stockholm, Sweden

⁵ Department of Psychology and Neuroscience Program, University of Michigan, Ann Arbor, MI, USA

Edited by:

Charles J. Wilson, University of Texas at San Antonio, USA

Reviewed by:

Dieter Jaeger, Emory University, USA

Kim Avrama Blackwell, George Mason University Krasnow Institute, USA

*Correspondence:

Andreas Klaus, Department of Neuroscience, Karolinska Institute, Retzius väg 8, S-171 77 Stockholm, Sweden.
e-mail: andreas.klaus@nih.gov

In the striatal microcircuit, fast-spiking (FS) interneurons have an important role in mediating inhibition onto neighboring medium spiny (MS) projection neurons. In this study, we combined computational modeling with *in vitro* and *in vivo* electrophysiological measurements to investigate FS cells in terms of their discharge properties and their synaptic efficacies onto MS neurons. *In vivo* firing of striatal FS interneurons is characterized by a high firing variability. It is not known, however, if this variability results from the input that FS cells receive, or if it is promoted by the stuttering spike behavior of these neurons. Both our model and measurements *in vitro* show that FS neurons that exhibit random stuttering discharge in response to steady depolarization do not show the typical stuttering behavior when they receive fluctuating input. Importantly, our model predicts that electrically coupled FS cells show substantial spike synchronization only when they are in the stuttering regime. Therefore, together with the lack of synchronized firing of striatal FS interneurons that has been reported *in vivo*, these results suggest that neighboring FS neurons are not in the stuttering regime simultaneously and that *in vivo* FS firing variability is more likely determined by the input fluctuations. Furthermore, the variability in FS firing is translated to variability in the postsynaptic amplitudes in MS neurons due to the strong synaptic depression of the FS-to-MS synapse. Our results support the idea that these synapses operate over a wide range from strongly depressed to almost fully recovered. The strong inhibitory effects that FS cells can impose on their postsynaptic targets, and the fact that the FS-to-MS synapse model showed substantial depression over extended periods of time might indicate the importance of cooperative effects of multiple presynaptic FS interneurons and the precise orchestration of their activity.

Keywords: stuttering discharge, parvalbumin-positive interneuron, medium spiny projection neuron, synaptic depression, cortex

1 INTRODUCTION

Striatal fast-spiking (FS) interneurons provide strong inhibitory input to medium-sized spiny (MS) projection neurons (Koós and Tepper, 1999; Tepper et al., 2004, 2008; Mallet et al., 2005; Gustafson et al., 2006). The proximal location of FS-to-MS synapses enables FS neurons to influence MS activity – either by delaying or by totally suppressing spike generation in MS cells (Tepper et al., 2004, 2008). Despite their small number in the striatum (~1%; Kita et al., 1990; Luk and Sadikot, 2001), FS interneurons are therefore able to shape the output of the striatum to the downstream nuclei of the basal ganglia.

The discharge of striatal FS neurons in awake, behaving animals is characterized by irregular fluctuations of the instantaneous firing rate with numerous high-frequency bursts, single spikes, and

periods of silence (Berke et al., 2004; Berke, 2008; Gage et al., 2010). It is currently not known if and to which extent FS firing variability is determined by the input that these neurons receive under natural conditions. An additional source of the firing variability could originate from intrinsic cellular mechanisms that underlie the irregular, random bursting (“stuttering”) in FS neurons. Stuttering spike behavior is characterized by a variable number of spikes per burst and a variable interburst interval (**Figure 1B**). Since stuttering discharge has only been reported *in vitro* in response to somatic step currents (Kawaguchi, 1993; Gupta et al., 2000; Koós and Tepper, 2002; Bracci et al., 2003; Tepper et al., 2004; La Camera et al., 2006; Druckmann et al., 2007; Taverna et al., 2007), we in this study systematically investigated the effect of fluctuating and steady input on FS firing patterns in a model and *in vitro*. Indeed, we observed random stuttering only in response to steady input. In this regime, however, our model predicts a significant amount of spike synchronization among electrically coupled FS cells, which is in contrast to the lack of synchronized spiking among striatal FS interneurons *in vivo* (Berke, 2008). Conversely, when driven by fluctuating input, FS model neurons showed reliable spike timing

Abbreviations: f_{AMPA} , Total input frequency for AMPA synapses in the model; f_{GABA} , Total input frequency for GABAergic synapses in the model; ISI, Interspike interval; PSP, Postsynaptic potential; q_{DC} , Fraction of steady current injection in the input. For synaptic input, q_{DC} is zero whereas a step current corresponds to q_{DC} equal to unity; V_m , Average subthreshold membrane potential between the action potentials in a firing neuron. The membrane potential from 10 ms before to 2 minimum interspike intervals after each spike was excluded for the estimation of V_m .

and no spike synchronization. Therefore, these results suggest that in the awake, behaving animal, neighboring striatal FS interneurons are not in the stuttering regime simultaneously and that the high *in vivo* FS firing variability is more likely determined by the input fluctuations.

High firing rates of striatal FS interneurons *in vivo* (Berke, 2008, 2011) and the synaptic depression in FS-to-MS synapses (Plenz and Kitai, 1998; Koós et al., 2004; Gittis et al., 2010; Planert et al., 2010) cause changes in FS firing patterns to affect the synaptic strength of these synapses. This will ultimately modify the impact that FS cells have over MS firing, and thus, over striatal output. We therefore investigated how *in vivo* firing patterns in striatal FS interneurons influence the amplitude distribution of PSPs in MS cells. Our FS-to-MS synapse model predicted that these synapses are strongly depressed over extended periods of time. Despite the lack of general FS spike synchronization *in vivo*, this result suggests that the combined inhibition mediated by multiple presynaptic FS cells might be required to effectively shape the activity of MS projection neurons.

2 MATERIALS AND METHODS

2.1 THE NEURON MODEL

Parvalbumin-positive FS interneurons have been characterized by their immunochemical, morphological, and electrophysiological properties in both striatum (Kawaguchi, 1993, 1997; Taverna et al., 2007) and cortex (Kawaguchi and Kubota, 1997; Markram et al., 2004). Despite some striking differences in the organization of the cortical and striatal microcircuits, in which they are embedded, these neurons show many similarities in both areas, including a similar electrophysiological signature (see references above), a common developmental origin (Marín et al., 2000) and the coupling via gap junctions (Galarreta and Hestrin, 1999; Koós and Tepper, 1999; Beierlein et al., 2000; Amitai et al., 2002; Fukuda, 2009). Therefore, to model the stuttering in striatal FS interneurons, we used the channel descriptions of a previously published cortical one-compartment model (Golomb et al., 2007). This model contained the following voltage-dependent ionic channels, which have also been reported to be expressed in the rat striatum (Lenz et al., 1994; Weiser et al., 1994; Chung et al., 2000; Kotaleski et al., 2006): a fast Na^+ window current (I_{Na}), a fast delayed rectifier K^+ current (I_{Kdr}), and a slowly inactivating (d-type) K^+ current (I_{Kd}). The d-type current has been shown to delay spike initiation (Goldberg et al., 2008), which is also observed in many striatal FS interneurons (Plenz and Kitai, 1998). With a small Na^+ window current and a sufficiently large d-type K^+ current, the model was able to generate the typical subthreshold oscillations (40–50 Hz) and stuttering episodes in response to somatic current injections as observed in striatal FS interneurons (Figure 1). In the current study, the half-maximum potential for the sodium current was $\theta_m = -22$ mV and the d-type conductance was $g_{\text{KD}} = 1.6$ mS/cm² (Table 1, see also Golomb et al., 2007). Some experiments were also performed with a model neuron that produced tonic discharge ($\theta_m = -28$ mV, $g_{\text{KD}} = 0.39$ mS/cm², see Figures A2 and A3 in Appendix). To induce oscillatory fluctuations in the subthreshold membrane potential during the interburst episodes, a Gaussian white noise current with zero mean and 15 pA SD (0.1 ms time step) was applied to the model neuron (Golomb et al., 2007).

In order to model distal synaptic input and dendritic gap junctions, we extended the original one-compartment model of Golomb et al. (2007) by a dendritic tree consisting of three identical subtrees (cf. Kotaleski et al., 2006). Each subtree comprised one primary, two secondary, and four tertiary dendrites (i.e., each of the primary and secondary dendrites branched into two daughter arms). To allow for the same high firing rates as in the original one-compartment model, we increased the active conductances by a factor of 2 in the morphologically extended model, and in addition assumed active primary dendrites. Detailed model cell parameters are shown in Table 1.

We used a single FS model neuron for the simulation of the responses to fluctuating input, and a pair of FS model cells for the study of electrical coupling in these neurons. To be able to use parallel computing for the simulation of the FS cell pair, we implemented the FS model in Parallel GENESIS (Bower and Beeman, 1998) with a fixed step size of 10 μ s. The model implementation can be obtained from <http://senselab.med.yale.edu/modeldb/showmodel.asp?model=140254>

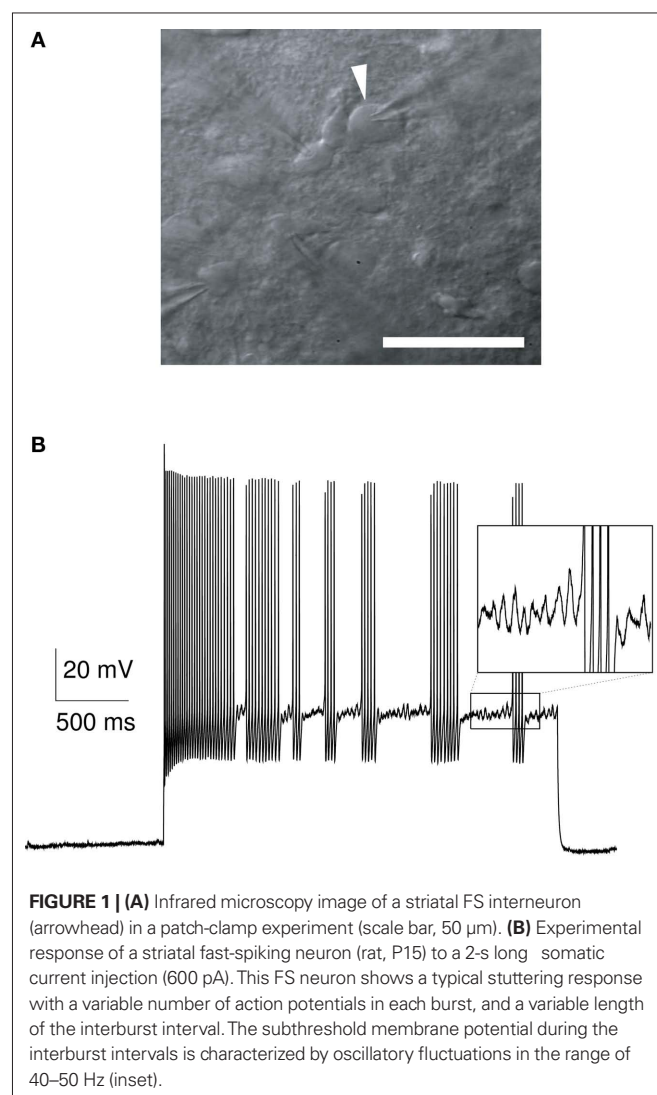


Table 1 | Parameters for the FS model neuron.

	Morphology and channel conductances			
	Soma	Primary dendrites	Secondary dendrites	Tertiary dendrites
$n \times n_{\text{comp}}$	1 × 1	3 × 2	6 × 4	12 × 8
$l \times d$	15 × 15 μm	90 × 1 μm	148 × 0.75 μm	240 × 0.5 μm
g_{Na}	225 mS/cm ²	22.5 mS/cm ²	–	–
g_{KDR}	450 mS/cm ²	45.0 mS/cm ²	–	–
g_{KD}	1.6 mS/cm ²	0.16 mS/cm ²	–	–
g_{AMPA}	✓	✓	✓	✓
g_{GABA}	✓	✓	✓	–

The model cell consisted of a soma and three identical subtrees (one primary, two secondary, and four tertiary dendrites each). The soma and dendritic sections were specified by their total number n , their number of subcompartments n_{comp} , their sectional length l and their diameter d . The total number of compartments was 127 (Kotaleski et al., 2006). Specific membrane resistance, specific axial resistance, and specific membrane capacitance were set to $R_M = 12 \text{ k}\Omega \text{ cm}^2$, $R_A = 200 \text{ }\Omega \text{ cm}$, and $C_M = 0.7 \text{ }\mu\text{F/cm}^2$, respectively. The resting membrane potential was varied from -65 to -70 mV. The reversal potentials for Na^+ , K^+ , GABA, and AMPA were 50, -90 , -60 , and 0 mV, respectively. The half-maximum potential for the Na^+ window current, θ_{nr} , was set to -22 mV (Golomb et al., 2007).

2.2 SYNAPTIC INPUT AND ELECTRICAL COUPLING IN THE MODEL

The FS neuron model included α -amino-3-hydroxyl-5-methyl-4-isoxazole-propionate (AMPA) and fast γ -aminobutyric acid (GABA) synapses. Some tests were performed with additional N -methyl-D-aspartate (NMDA) synapses (not shown). The presented results did not depend on the presence or absence of NMDA synapses. All synapses received independent input in the form of random Poisson spike trains. AMPA synapses were distributed over all 127 compartments (Kotaleski et al., 2006). If NMDA synapses were present, they were located in the same compartments and received the same input as the AMPA synapses. GABA synapses were located more proximally, resulting in a total number of 31 inhibitory synapses (Table 1). *In vitro* measurements of spontaneous activity have shown that FS neurons receive a similar ratio between inhibitory and excitatory currents during an up-state (Blackwell et al., 2003). Therefore, to compensate for the smaller number of inhibitory synapses, the activation rate per GABA synapse was approximately threefold higher than for AMPA synapses. This was equivalent to using three GABA synapses per proximal compartment and activating them at the same rate as AMPA since we used the non-saturating synapse model *synchan* in GENESIS. The time constants of the double-exponential function, which described the evolution of the synaptic conductances in this model, were $\tau_1 = 0.7$, $\tau_2 = 2$ ms for AMPA, $\tau_1 = 1.3$, $\tau_2 = 4$ ms for GABA, and $\tau_1 = 3.6$, $\tau_2 = 116$ ms for NMDA synapses, respectively (Hjorth et al., 2009).

Gap junctions between two FS neurons were modeled as conductive elements between the soma, the outer proximal dendrites, or the outer secondary dendrites. The conductance of a single gap junction was set to 0.5 nS, a value within the range of gap junction conductances in cortical FS neurons (Galarreta and Hestrin, 2002). A single soma-somatic gap junction resulted in a coupling coefficient of $\sim 11\%$ in our model, which was within the range of coupling coefficients reported in the striatum (Galarreta and Hestrin, 2001;

Koós et al., 2004). In order to obtain the same coefficient for the dendro-dendritic coupling, we increased the number of gap junctions on the primary and secondary dendrites to two and three, respectively.

2.3 MODELING OF THE FS-TO-MS SYNAPTIC DYNAMICS

For the FS-to-MS connections we used data from rat that was recently published by Planert et al. (2010). In short, synaptic connections were identified and characterized by stimulation of a presynaptic FS cell with a train (10, 20, or 40 Hz) of 8 strong and brief current pulses (0.5–2 nA, 3 ms), followed by a so-called recovery test pulse approximately 550 ms after the end of the train, all reliably eliciting action potentials (APs). Postsynaptic neurons were held near -80 mV to ensure strongly depolarizing responses to GABAergic input. For the analysis of synaptic properties, average postsynaptic traces over multiple repetitions were examined for the existence of synaptic responses (Planert et al., 2010).

The depressing synapse was modeled using a scheme described by Markram et al. (1998), where the synapse is assumed to have a limited amount of resources which are slowly restored over time (see also Tsodyks et al., 1998). The amplitude of a postsynaptic potential, PSP_n , in response to the n th AP in a spike train is a product of the fraction of available resources, R_n , and a facilitating utilization factor, u_n , scaled by the absolute synaptic efficacy, A_{se} :

$$\text{PSP}_n = A_{se} R_n u_n. \quad (1)$$

The utilization factor is increased by each AP and decays back toward U in the time between APs:

$$u_{n+1} = u_n \exp\left(-\frac{t_{\text{ISI}}}{\tau_F}\right) + U \left[1 - u_n \exp\left(-\frac{t_{\text{ISI}}}{\tau_F}\right)\right] \quad (2)$$

with $u_1 = U$. t_{ISI} denotes the time between the n th and $(n+1)$ th AP. Each AP utilizes the fraction u_n from the synaptic resources, R_n , which then recovers to a value of 1 at a rate of τ_D :

$$R_{n+1} = R_n (1 - u_n) \exp\left(-\frac{t_{\text{ISI}}}{\tau_D}\right) + 1 - \exp\left(-\frac{t_{\text{ISI}}}{\tau_D}\right), \quad (3)$$

with $R_1 = 1$. The parameters U , τ_D , and τ_F were fitted to the experimental traces using a two-step process. First, the amplitudes were extracted by fitting an exponential decay to the previous response and subtracting it from the new response. The second step in the parameter fitting performed a grid search (range 0–5 s for $\tau_{D,F}$ and 0–1 for U). The error was defined as the weighted sum of the absolute values of the amplitude difference at each peak between the reference trace and the modeled trace. The initial response and the recovery test response (RTR) were weighted five times stronger, and the second response was weighted by two. This was done to prevent the first set of inputs from dominating over the RTR. The parameters were fitted to a train of spikes at 20 Hz and verified for some synapses at 10 and 40 Hz (see Figure A1 in Appendix).

2.4 SLICE PREPARATION AND EXPERIMENTAL RECORDINGS

All animal experiments were carried out according to the guidelines of the Stockholm municipal committee for animal experiments. Slices (300 μm thick) were obtained from rats on postnatal days

14 to 23, cut in ice-cold extracellular solution, kept at 35°C for 30 minutes, and then moved to room temperature before the recording. Whole-cell patch recordings were obtained at a temperature of $35 \pm 0.5^\circ\text{C}$. Neurons were visualized using IR-DIC microscopy (Zeiss FS Axioskop, Oberkochen, Germany) as shown in **Figure 1A**. Recorded neurons were selected visually in cortex and striatum. In the striatum, neighboring cells with lateral somatic distances less than 100 μm were recorded simultaneously. MS neurons and fast-spiking interneurons were classified according to their typical membrane properties. The extracellular solution (both for cutting and recording) contained (in mM) 125 NaCl, 25 glucose, 25 NaHCO_3 , 2.5 KCl, 2 CaCl_2 , 1.25 NaH_2PO_4 , 1 MgCl_2 . Recordings were amplified using Axoclamp 2B or Multiclamp 700B amplifiers (Molecular Devices, CA, USA), filtered at 2 kHz, digitized (5–20 kHz) using ITC-18 (Instrutech, Port Washington, NY, USA), and acquired using Igor Pro (Wavemetrics, Lake Oswego, OR, USA). Patch pipettes were pulled with a Flaming/Brown micropipette puller P-97 (Sutter Instruments, Novato, CA, USA) and had an initial resistance of 5–10 $\text{M}\Omega$, containing (in mM) 10 HEPES, 0.3 GTP-Na, and 10 Na_2 -phosphocreatine. The intracellular solution furthermore contained either 110 K-gluconate, 10 KCl, and 4 ATP-Mg, or 110 K-gluconate, 10 KCl, 4 ATP-Na, and 4 MgCl_2 , or 105 K-gluconate, 30 KCl, and 4 ATP-Mg. Chloride concentrations were increased for some connectivity experiments, as increasing internal chloride increases absolute synaptic current amplitudes. We did not observe differences in parameters describing the synaptic dynamics (not shown). All striatal FS responses reported in **Figure 3** were recorded with the last mentioned concentrations. In a subset of neurons, 0.2–0.5% biocytin was added. Liquid junction potential was not corrected for. Recordings were performed in current-clamp mode, with access resistance compensated throughout the experiments. Data was discarded when access resistance exceeded 35 $\text{M}\Omega$.

2.5 STIMULATION PROTOCOL (GENERATION OF FLUCTUATING CURRENT INPUT)

We investigated the spiking pattern of the model neuron and of stuttering striatal and cortical (layer 2/3 and 5) FS cells in response to fluctuating versus steady input. Current input with varying degree of fluctuations was generated as follows. We used the FS model neuron to simulate somatic, subthreshold membrane potential fluctuations in response to random synaptic input ($f_{\text{AMPA}} = 760$, $f_{\text{GABA}} = 560$ Hz, firing rate was ~ 11 Hz). To avoid the influence of any suprathreshold activity, the model neuron was prevented from firing by removing the active sodium conductance. The resulting membrane potential was used as a measure of the synaptic input fluctuations, and a current proportional to the membrane potential was used for subsequent somatic injection (the time course of the fastest fluctuations in the resulting trace matched therefore the membrane time constant of the model neuron, which was ~ 8 ms). The scaling of the current was chosen such that the firing rate in the model (now with sodium conductance) matched the synaptically driven case. In most cases, generated current traces induced the same spikes as the synaptic input had done originally (not shown). This indicates that somatic current injection was able to mimic to a high degree the synaptic input of dendritic origin in the FS model. Next, we determined the amount of steady current injection that resulted in the same firing rate as in the case of synaptic

input (10–12 Hz). We denote this input by $q_{\text{DC}} = 1$ (fraction of steady current equal to unity, no synaptic input). Conversely, we denote the current trace that was entirely derived from the synaptic activation by $q_{\text{DC}} = 0$ (fraction of steady current equal to zero). To control the amount of input fluctuations, we varied the level of steady input, q_{DC} , between zero and one. The firing rate of the model neuron was held constant by reducing the synaptic AMPA and GABA conductances accordingly.

2.6 IN VIVO RECORDINGS

Samples (>12 min duration) of awake *in vivo* rat FS spike trains were taken from a previously described data set (Berke et al., 2004; Berke, 2008). Interspike intervals (ISIs) smaller than 1.5 ms (<0.8%) were excluded from the analysis.

2.7 DATA ANALYSIS

Correlation analysis

Sub- and suprathreshold synchronization and spike train similarity was measured by Pearson's correlation coefficient

$$C(t) = \frac{\sum_{i=1}^n x_i y_{i+t}}{\sqrt{\sum_{i=1}^n x_i^2 \sum_{i=1}^n y_i^2}}, \quad (4)$$

where t denotes the time lag between the two zero-mean vectors of data samples, x_i and y_i ($i = 1, \dots, n+t$). For a time lag $t = 0$ and for identical vectors x_i and y_i , the correlation, $C(0)$, is equal to unity. Since we were interested in millisecond synchronization, the bin size for the suprathreshold activity was 1 or 2 ms. Synchronization was either shown as a function of time lag or reported as a single number, the latter referring to the correlation value at time lag zero.

Measurement of stuttering onset

The time of stuttering onset was measured as the time of the first spike peak in the first stuttering episode for each model neuron. The onset time difference for a pair of FS neurons was defined as the absolute value of the time difference of stuttering onset in the two neurons. To avoid stimulus-driven correlation in the stuttering discharge of two neurons, the begin of step current input was randomly shifted by ± 25 ms for each cell.

Measurement of the phase lag of the subthreshold oscillations

The phase lag of the subthreshold oscillations between two FS model neurons was defined as the phase difference for frequencies 40–48 Hz, i.e., for frequencies for which the power spectrum showed a peak (see **Figure A5** in Appendix). The phase difference was mapped from $0 - 2\pi$ ($0 - 360^\circ$) to $0 - \pi$ by mirroring the phase angles in the polar coordinate system along the horizontal axis. This is equivalent to using the absolute value if the phase difference would have been defined in the range $\pm\pi$.

Measurement of spike clustering

For the analysis of clustered spikes in the model and *in vitro*, we used the minimal interspike interval, ISI_{min} , for each individual trace and considered two spikes to be member of the same spike group if their ISI was less than $2 \text{ ISI}_{\text{min}}$. To exclude the possibility that ISI_{min} was affected by ISI outliers, which were sometimes observed for

short, strong depolarizations in the case of fluctuating input, ISI_{\min} was obtained by using the second percentile of the ISIs. However, the results did not depend on this particular choice, i.e., similar results were obtained when using the smallest ISI or the first percentile. ISI_{\min} varied between individual FS neurons and was also dependent on the stimulus strength; for the striatal FS cells it was 14.7 ± 8.8 ms (mean \pm SD, average over various input scalings, $n = 450$ traces). The shortest ISI for each cell was 3–5 ms (second percentile). Clusters were defined as groups with 3 or more spikes. For the simulated traces in the stuttering and the tonically firing FS model neuron, we also used the coefficient of variation of the ISI, CV_{ISI} , as an indicator for spike clustering (see **Figures A2 and A3** in Appendix).

Spike shuffling

For an *in vivo* spike train with mean firing frequency, f , we obtained shuffled, Poisson-distributed ISIs from an exponential distribution with rate parameter $\lambda = 1/f$, and uniformly distributed ISIs from a continuous uniform distribution on the interval $(0, 2/f)$. To account for the refractory period, random numbers were discarded and repeatedly drawn if an ISI was shorter than 1.5 ms. The resulting spike trains had the same spike rate, f , as the original *in vivo* trace.

Statistical analysis

Values are expressed as mean \pm SD if not noted otherwise. For the regression analysis between sub- and suprathreshold activity we used the *F*-test, for the multiple comparison between control and electrical coupling the one-way ANOVA test (significance level 0.01), and for comparison of the mean percentage of clustered spikes the unequal variance *t*-test. Data was analyzed in MATLAB (Mathworks, MA, USA) and R¹ and visualized with GNUPLLOT².

3 RESULTS

3.1 STUTTERING DISCHARGE REQUIRES STEADY DEPOLARIZATION

Many fast-spiking (FS) interneurons show random stuttering in response to somatic current steps (**Figure 1B**). However, the response to such an artificial step current can only reveal specific features of the electrophysiological signature of neuronal cells (see, e.g., Mainen and Sejnowski, 1995). Two hallmarks of the stuttering in FS interneurons are the clustered spiking and the stochastic nature of firing discharge (Englitz et al., 2008). To study if these features contribute to FS firing under more physiological conditions, we investigated the influence of input fluctuations on the spike activity in FS interneurons. This was first done in a morphologically extended version of the one-compartment model by Golomb et al. (2007), which allowed the conductance-based modeling of proximal and distal synaptic input (**Table 1**).

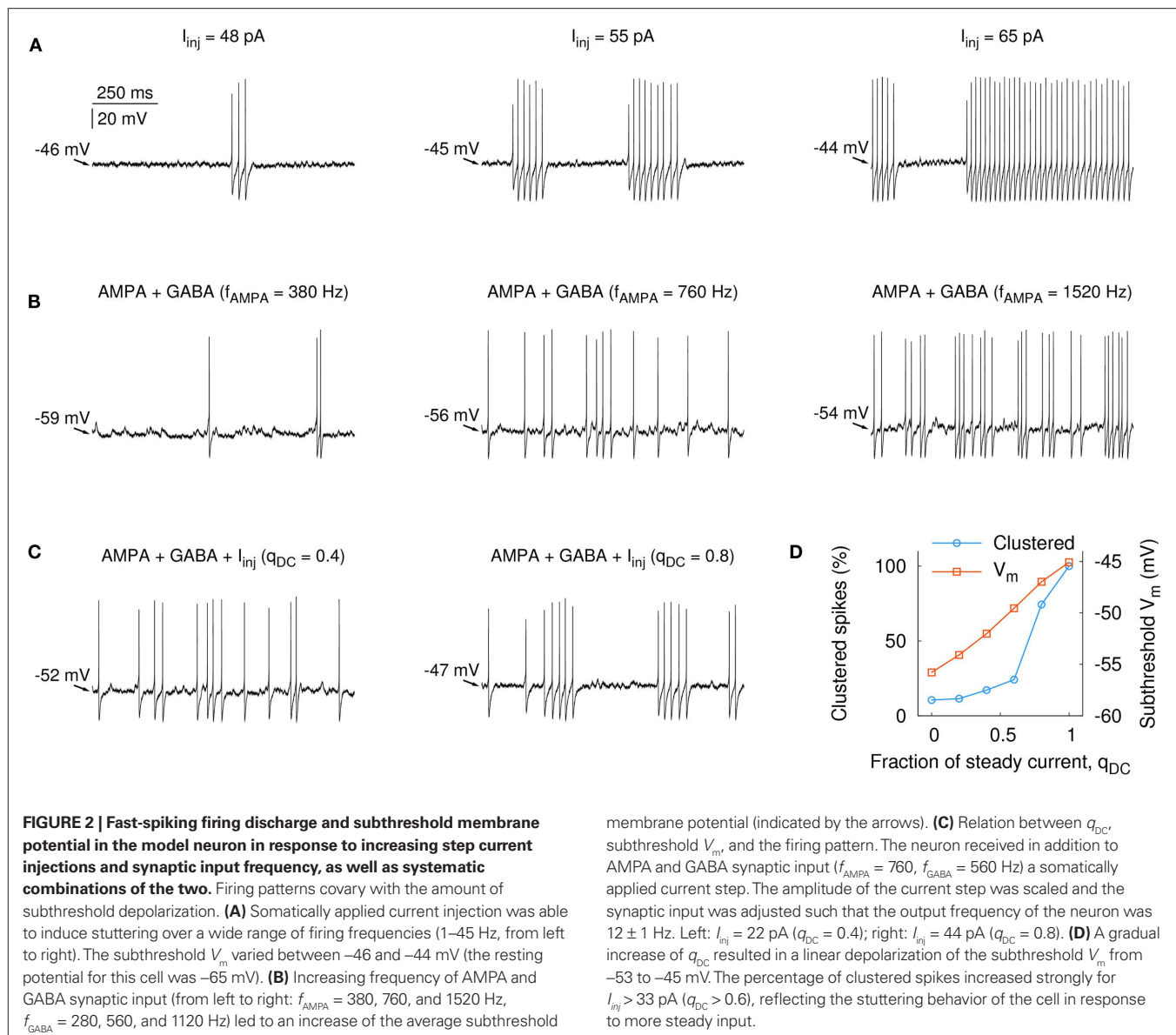
In the FS model, stuttering in response to somatic step currents could be observed over a wide range of firing frequencies, where both the spike rate and the average length of the stuttering episodes increased with larger input amplitudes (**Figure 2A**, firing rates ranged from 1 to 45 Hz from left to right). The amplitude of the somatic current step also had an influence on the subthreshold membrane potential, V_m . In the model, V_m was about -46 mV when

the first spikes were elicited (i.e., 19 mV above the resting potential, left panel in **Figure 2A**) and depolarized by an additional 2 mV at firing rates > 40 Hz (**Figure 2A**, right panel). When the FS model was activated by synaptic AMPA input, the spike discharge was characterized by many single spikes and spike doublets, without showing the characteristic stuttering behavior (**Figure 2B**, increasing synaptic input frequency from left to right). Interestingly, even though V_m depolarized with increasing input frequency, it remained far below -46 mV, which was the subthreshold membrane potential above which stuttering was readily observed for step current injections (**Figure 2A**). At a firing rate of 25 Hz, for example, the subthreshold V_m was -54 mV (**Figure 2B**, right panel). To study the effect of the input type on the subthreshold depolarization and on the stuttering discharge in more detail, we systematically varied the fraction of steady input, q_{DC} . For each level of q_{DC} , the firing rate of the FS model was held constant by simultaneously reducing the synaptic conductances (see Section 2). Thus, larger values of q_{DC} resulted in smaller input fluctuations at the same FS spike rate. **Figure 2C** shows the responses of the FS model for two levels of q_{DC} . To obtain the same firing rate (~ 12 Hz) for $q_{DC} = 0.4$ and 0.8 , the synaptic conductances were reduced to 50 and 14% compared to $q_{DC} = 0$, respectively. The synaptic input train in **Figure 2C** is the same as in the middle trace of **Figure 2B** ($f_{AMPA} = 760$, $f_{GABA} = 560$ Hz, only synaptic amplitudes were reduced). This can be seen in the spike signature, which is hardly affected by the reduction of the synaptic conductances at $q_{DC} = 0.4$, despite the fact that the subthreshold V_m depolarized from -56 mV (synaptic input only, $q_{DC} = 0$) to -52 mV ($q_{DC} = 0.4$). At $q_{DC} = 0.8$, however, the spike signature changed to more stuttering-like firing ($V_m = -47$ mV, right panel in **Figure 2C**). In summary, increasing levels of q_{DC} led to a linear depolarization of the subthreshold V_m and an abrupt (non-linear) change from more regular firing to stuttering discharge at the same firing rate (**Figure 2D**).

The opening of synaptic channels decreases the input resistance of a neuron. Was the smaller amount of subthreshold depolarization a result of the synaptic activation alone (the GABA synapses had a reversal potential of -60 mV), or was it also attributable to the input fluctuations? To answer this question, we created traces of fluctuating current that resembled somatic potential fluctuations in the case of synaptic input. The current traces were derived from the model for different amounts of q_{DC} (see Section 2). This allowed us to study the response of the model neuron by an entirely current-driven approach, that is, without the activation of synaptic conductances. Furthermore, the current traces enabled us to measure the response of striatal FS interneurons to changing levels of input fluctuations in whole-cell patch-clamp recordings *in vitro*. The traces in **Figure 3A** show the resulting discharge for the model and a striatal FS cell for different levels of steady input, q_{DC} . As for the case with synaptic conductances (**Figures 2C,D**), V_m increased in a linear manner, and with decreasing input fluctuations the firing pattern changed from regular spiking to stuttering discharge with a high percentage of clustered spikes (**Figures 3B,C**; black traces: $n = 5$ striatal neurons, firing rate ranged from 2.2 to 64 Hz; red trace: model neuron). The mean percentage of clustered spikes was significantly different between fluctuating and steady input (4.7 and 82.9%, respectively; $p = 0.0002$, $n = 5$ striatal FS neurons, unequal variance *t*-test, right panel in **Figure 3C**). These

¹<http://www.r-project.org/>

²<http://gnuplot.info>



results indicate that steady input leads to a more depolarized subthreshold membrane potential and induces stuttering discharge in FS interneurons (compare **Figures A2 and A3** in Appendix for a tonically firing FS model).

Importantly, the responses to steady input ($q_{\text{DC}} = 1$) in the model and *in vitro* showed a large variability between trials, whereas spike trains in response to fluctuating input ($q_{\text{DC}} = 0$) were more repeatable from trial to trial (cf. Mainen and Sejnowski, 1995). For striatal FS neurons, this can be seen in the elevated trial-to-trial correlation for $q_{\text{DC}} = 0$ compared to $q_{\text{DC}} = 1$ (**Figure 3D**, $p < 10^{-5}$, $n = 4$ cells, unequal variance *t*-test, bin size 2 ms). The trial-to-trial correlation at $q_{\text{DC}} = 1$ was not significantly different from zero ($p = 0.92$, one-sample *t*-test) as was the trial-to-trial correlation for shuffled traces (random permutation of 2 ms bins, not shown). Taken together, these results show that the amount of input fluctuations strongly influences the firing pattern and the spike time reliability in striatal FS interneurons.

3.2 SPIKE SYNCHRONY IN ELECTRICALLY COUPLED FS INTERNEURONS

Fast-spiking interneurons in the striatum are coupled by gap junctions (Kita et al., 1990; Galarreta and Hestrin, 2001; Fukuda, 2009) and electrical connections between these neurons have been confirmed *in vitro* (Koós and Tepper, 1999). In cortical FS cells, such electrical coupling contributes to synchronized spiking (Gibson et al., 2005; Mancilla et al., 2007). However, in awake, behaving animals, neighboring FS cells in the striatum do not show any sign of broadly synchronized firing (Berke, 2008). The lack of spike synchrony among striatal FS cells *in vivo* might give an indication of the input regime in which these cells operate, i.e., fluctuating versus steady input (Hjorth et al., 2009). We therefore used the stuttering FS model neuron to explore how the amount of input fluctuations influences the spike synchronization in a pair of electrically connected cells.

In the model, electrical coupling through gap junctions had a strong ability to synchronize periods of stuttering activity in neurons that received steady current input. **Figure 4A** shows an

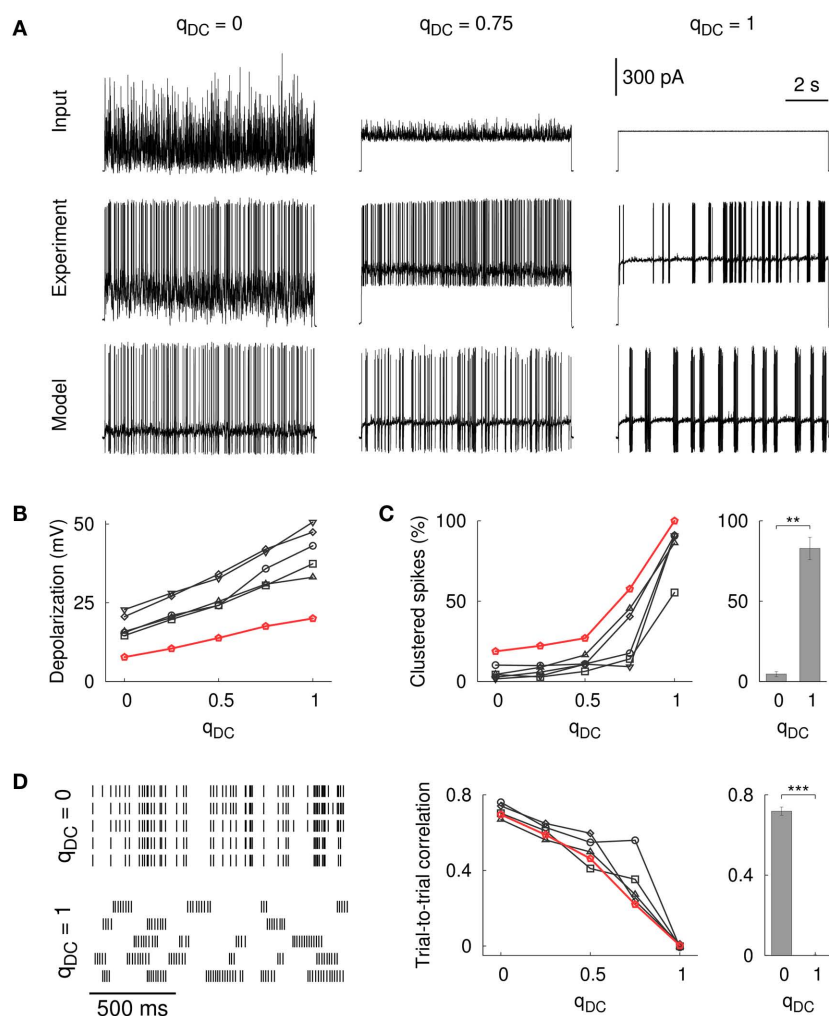


FIGURE 3 | Influence of input fluctuations on FS firing patterns in the model and *in vitro*. (A) The spike pattern of the model neuron and of a striatal FS neuron following a somatically applied current injection with varying degree of fluctuations. Responses are shown for $q_{DC} = 0$, 0.75, and 1.0 (from left to right). The scale bars for the voltage traces correspond to 30 mV. The scale bar for the current traces corresponds to the *in vitro* experiment. (B) Depolarization of the subthreshold membrane potential (measured from the resting baseline). The membrane potential depolarized continuously as the input fluctuations diminish, that is, with increasing levels of steady input (black lines: $n = 5$ striatal FS neurons, red line: model cell). Two random input traces and different scalings were tested (450 traces in total, firing rate ranged from 2.2 to 64.4 Hz, the average firing rate was 18.9 ± 11.5 Hz). (C) Steady current input resulted in

stuttering seen as an increase in the percentage of clustered spikes. The number of clustered spikes was significantly different between fluctuating and steady input [$n = 5$ striatal FS cells, $t(4.4) = -11.0$, $p = 0.0002$, unequal variance t -test]. (D) Left: example rastergram for a striatal FS neuron that repeatedly receives the same input (5 trials). Spike trains were more reliable for FS cells that were not in the stuttering regime ($q_{DC} = 0$). Variability was high for stuttering cells ($q_{DC} = 1$) resulting in zero trial-to-trial correlation [$t(3) = 0.11$, $p = 0.92$, one-sample t -test]. Middle: trial-to-trial correlation as a function of q_{DC} (black lines: $n = 5$ striatal FS neurons, red line: model cell). Right: The difference between $q_{DC} = 0$ and $q_{DC} = 1$ was statistically significant [$n = 5$ striatal FS neurons, $t(3.2) = 34.7$, $p < 10^{-4}$, unequal variance t -test]. The bin size for the spike detection was 2 ms.

example of two unconnected FS neurons (upper traces) and the same pair of cells electrically coupled at the distal part of the primary dendrites (lower traces, $\sim 11\%$ steady-state coupling). Although the cross-correlation, which measures the spike synchronization between the two neurons, decreased substantially with increasing distance between the location of the gap junctions and the soma (Figure 4B), the time difference of stuttering onset in both cells was in the majority of cell pairs smaller than 50 ms for proximal coupling (i.e., soma and primary dendrites, Figure 4C). In the model, proximal electrical coupling was also

able to synchronize subthreshold oscillations in the connected FS neurons, although this effect was not very strong (Figures A4 and A5 in Appendix). Importantly, the fast entrainment of spiking activity in two connected neurons did not require a small phase lag between the preceding subthreshold oscillations, which is apparent in the missing correlation between the phase lag of the subthreshold oscillations and the time difference of the stuttering onset in both cells (Figure 4C). Furthermore, proximal coupling via gap junctions did not significantly change the number of spikes per burst but it resulted in a delayed stuttering discharge after stimulus

onset (**Figure 4D**). The reason for this firing delay, which was only seen for proximal coupling, is most likely the shunting of charge across the gap junctions.

In the case of steady current injection, a small number of spikes in one FS neuron was sufficient to induce a stuttering episode in an electrically connected cell (**Figures 4A,C**). We next analyzed the spike synchronization in two electrically connected FS cells over a wide range of input fluctuations, i.e., from $q_{DC} = 0$ to 1 (**Figure 4E**). The voltage traces in **Figure 4F** show an example of two cells that were not in the stuttering regime. The neurons received a small amount of somatic current input ($q_{DC} = 0.4$) and in addition AMPA and GABA synaptic input. Although gap junctions at the primary dendrites were able to induce and suppress single APs in connected neurons (**Figure 4F**, arrows), spike synchronization as measured by the cross-correlation between FS 1 and FS 2 was low (**Figure 4E**). With increasing levels of q_{DC} , FS firing tended to be more clustered and more variable (increasing CV_{ISI} , upper panel in **Figure 4E**, see also **Figure A2** in Appendix), and spike correlation between the two connected cells increased (lower panel in **Figure 4E**). To test if this spike synchronization required steady input in both FS model neurons, we repeated the simulation with one of the FS cells, FS 1, being permanently in the stuttering regime, and by varying q_{DC} for FS 2 only (**Figures 4G,H**). **Figure 4H** shows an example of two model cells that receive different levels of q_{DC} as it can be seen in the different levels of V_m and different firing patterns in the two cells. While the stuttering cell, FS 1, showed strong changes in the spike signature (i.e., low values of spike time reliability) as a result of electrical coupling, the neighboring neuron, FS 2, showed a high spike time reliability when driven by fluctuating input (**Figure 4G**, lower panel), thus, resulting in little spike synchronization among the two cells (**Figure 4G**, upper panel). Therefore, stuttering in a single FS model neuron was not sufficient to broadly induce synchronized spikes in electrically connected neighbor cells. These

results and the lack of spike synchrony *in vivo* (Berke, 2008) suggest that in awake, behaving animals, striatal FS cells are not in the stuttering regime simultaneously.

3.3 FS FIRING PATTERNS INFLUENCE THE DISTRIBUTION OF POSTSYNAPTIC POTENTIALS IN MEDIUM SPINY NEURONS

The discharge of striatal FS neurons in awake, behaving animals is characterized by large fluctuations of the instantaneous firing rate with numerous high-frequency bursts, single spikes, and periods of silence (Berke et al., 2004; Berke, 2008). Given the strong depressive component in the dynamics of striatal FS-to-MS synapses (Plenz and Kitai, 1998; Koós et al., 2004; Gittis et al., 2010; Planert et al., 2010), differences in the firing patterns of FS interneurons might affect the influence on the postsynaptic MS cells (cf. Abbott et al., 1997). We used the firing patterns of three FS neurons from the prior *in vivo* studies by Berke et al. (2004) and Berke (2008), and simulated the resulting train of synaptic potentials in postsynaptic MS neurons. The measurement of the FS-to-MS synaptic parameters was done *in vitro* (Planert et al., 2010). **Figure 5A** shows an example of the averaged postsynaptic MS response to a train of presynaptic FS spikes *in vitro* (8 spikes plus one test pulse). From these averaged responses we extracted the PSPs and used their amplitude values for the parameter fitting in the FS-to-MS model synapse (see Section 2). The model synapse was able to replicate the PSP amplitudes for different FS firing frequencies (**Figure A1** in Appendix). **Figure 5B** shows the normalized PSP amplitude for a typical FS-to-MS synapse as a function of spike number for different ISIs (1.5–20 ms). A fully recovered synapse responded with a sequence of decreasing PSP amplitudes to the first few spikes independent of input frequency. Differences in the PSP amplitudes and their steady-state values became, however, evident for larger numbers of APs. Lower spike frequencies allowed more synaptic recovery between the arrival of spikes, resulting in larger steady-state amplitudes (compare, e.g., ISI = 6 and 20 ms in

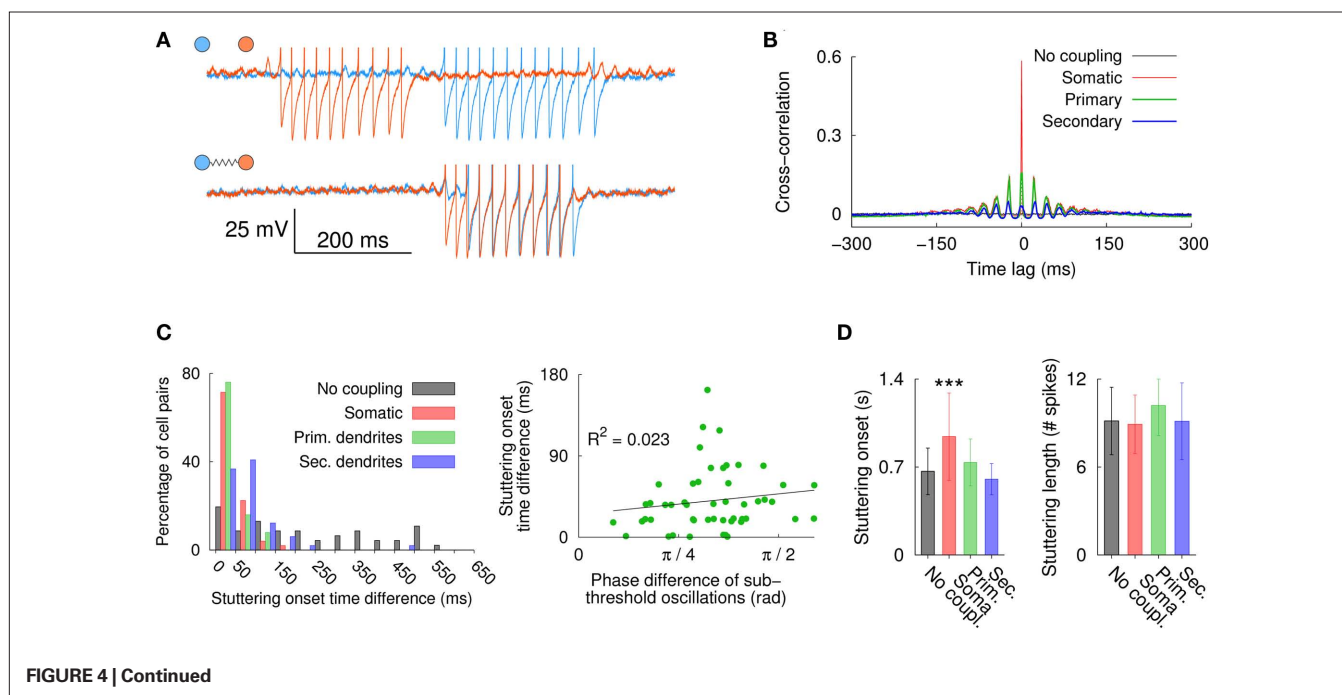


FIGURE 4 | Continued

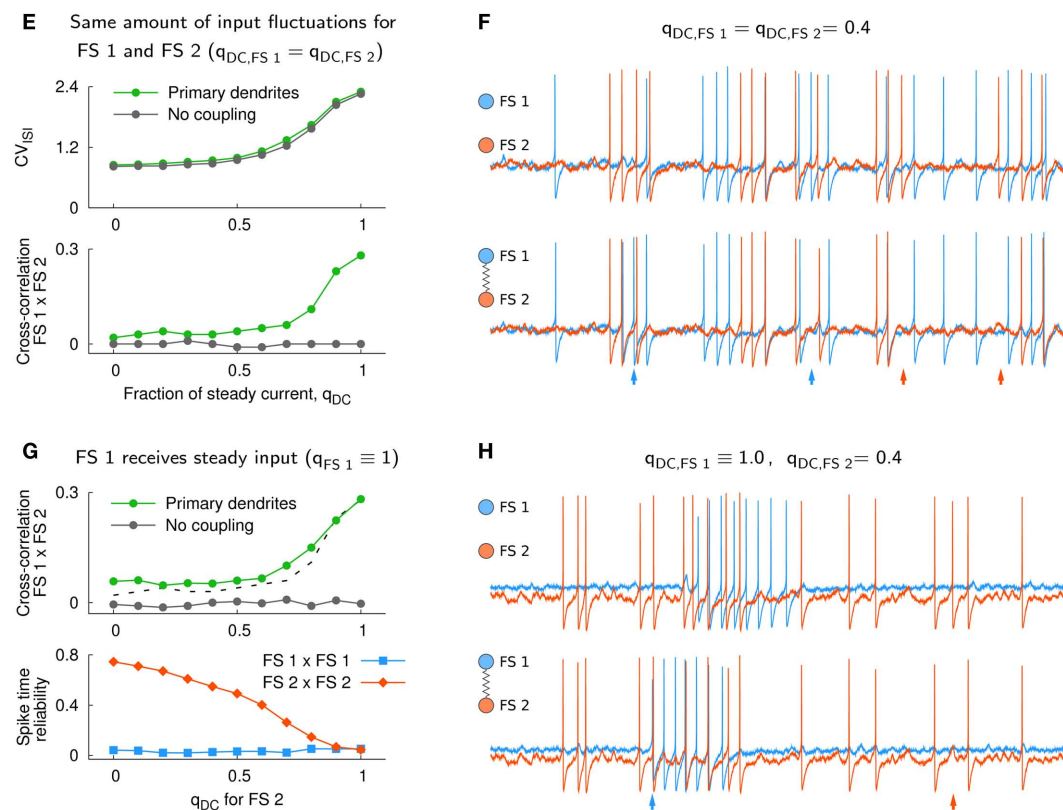


FIGURE 4 | Synchronization of suprathreshold spiking activity in the

neuron model. (A) Section of the voltage traces for a pair of uncoupled and electrically coupled FS cells (upper and lower traces, respectively). Each neuron received the same steady somatic input and only electrical coupling was added to the primary dendrites (2×0.5 nS total). The onset of the somatic current step input was random for each neuron (onset at 50 ± 25 ms). Spikes were truncated at -30 mV for better visualization. **(B)** Average cross-correlogram of spiking activity in the two neurons ($n = 10$; somatic current injection 74 pA, 60 s duration; bin size 1 ms). **(C)** Absolute onset time difference of the first stuttering episode in the two neurons ($n = 49$, left panel). The bars between 0 and 50 ms, for example, indicate the percentage of cell pairs with a time difference in the range 0 – 50 ms. There was no significant relation between the phase difference of the subthreshold oscillations and the stuttering onset time difference for electrically coupled FS neurons [right panel, $R^2 = 0.023$, $F(1,98) = 1.106$, $p = 0.298$, $n = 50$; gap junctions located at primary dendrites, see also **Figures A4 and A5** in Appendix]. **(D)** The average delay of the first stuttering episode after stimulus onset increased significantly in somatically coupled neurons, i.e., from 665 ms under the control condition without electrical coupling to 942 ms for somatically coupled neurons [$n = 49$; one-way ANOVA, $F(3,192) = 20.65$, $p < 10^{-6}$, Tukey–Kramer multiple comparison]. Electrical coupling did not have a strong effect on the average stuttering length, which was measured as the average number of action potentials within the first burst and

ranged from 8.9 to 10.2 spikes for all conditions. The comparison of the average stuttering lengths gave a p -value of 0.024 ($n = 49$; one-way ANOVA, $F(3,192) = 3.23$). Error bars denote the SD. **(E)** CV_{ISI} (upper panel) and spike synchronization as measured by the cross-correlation at time lag zero (lower panel, bin size 2 ms) for two FS model neurons that received the same amount of input fluctuations. The spike synchronization was almost absent in electrically coupled neurons that received fluctuating (synaptic) input and it increased in a similar manner as the CV_{ISI} for increasing levels of steady input, q_{DC} . **(F)** The traces show an example for $q_{DC} = 0.4$. The two neurons received the following input: $f_{AMPA} = 1900$, $f_{GABA} = 1400$ Hz, $g_{AMPA} = g_{GABA} = 200$ pA, somatic current injection $I_{inj} = 22$ pA; upper traces: uncoupled, lower traces: gap junctions at the distal part of the primary dendrites (2×0.5 nS total). **(G)** Spike synchronization (upper panel, bin size 2 ms) and spike time reliability (lower panel) in two FS model neurons that received different levels of q_{DC} . High spike synchronization between the FS model neurons required steady input in both neurons [the cross-correlation from **(E)** is plotted as a dashed line for comparison]. Electrical coupling did not affect the spike signature in FS 2 if it received fluctuating input, which can be seen by the high spike time reliability at $q_{DC} = 0$. However, in the stuttering cell, FS 1, the temporal spike occurrence was dramatically altered by electrical coupling (low spike time reliability). **(H)** Example traces for two neurons that received different levels of steady input ($q_{DC} = 1$ and 0.4 for FS 1 and FS 2, respectively).

Figure 5B). Full recovery of the synaptic resources required longer firing pauses. **Figure 5C** shows the normalized values of recovered PSP amplitudes as a function of pause duration, which is measured from the end of a preceding spike train that caused a steady-state depression of the synapse (same synapse as in **Figure 5B**, in black). The time course for the synaptic recovery, τ_p , ranged from 230 ms to almost 5 s (1.03 ± 1.34 s, $n = 11$ synapses from rat). Thus, depressing FS-to-MS synapses particularly emphasize the onset of FS firing after prolonged pauses. Taken together, these results sug-

gest that differences in the FS firing pattern have an influence on the amount of synaptic depression and/or recovery and therefore on PSP amplitudes. We determined the distribution of PSP amplitudes in the FS-to-MS synapse model in response to FS firing patterns that were recorded *in vivo* and compared it to PSP distributions that resulted from random, shuffled spike activity.

The upper rastergram in **Figure 5D** shows a 5 -s long section and a 500 -ms detail (black bar) from an extracellular *in vivo* recording in a freely moving rat (“awake”). This “awake” spike activity was

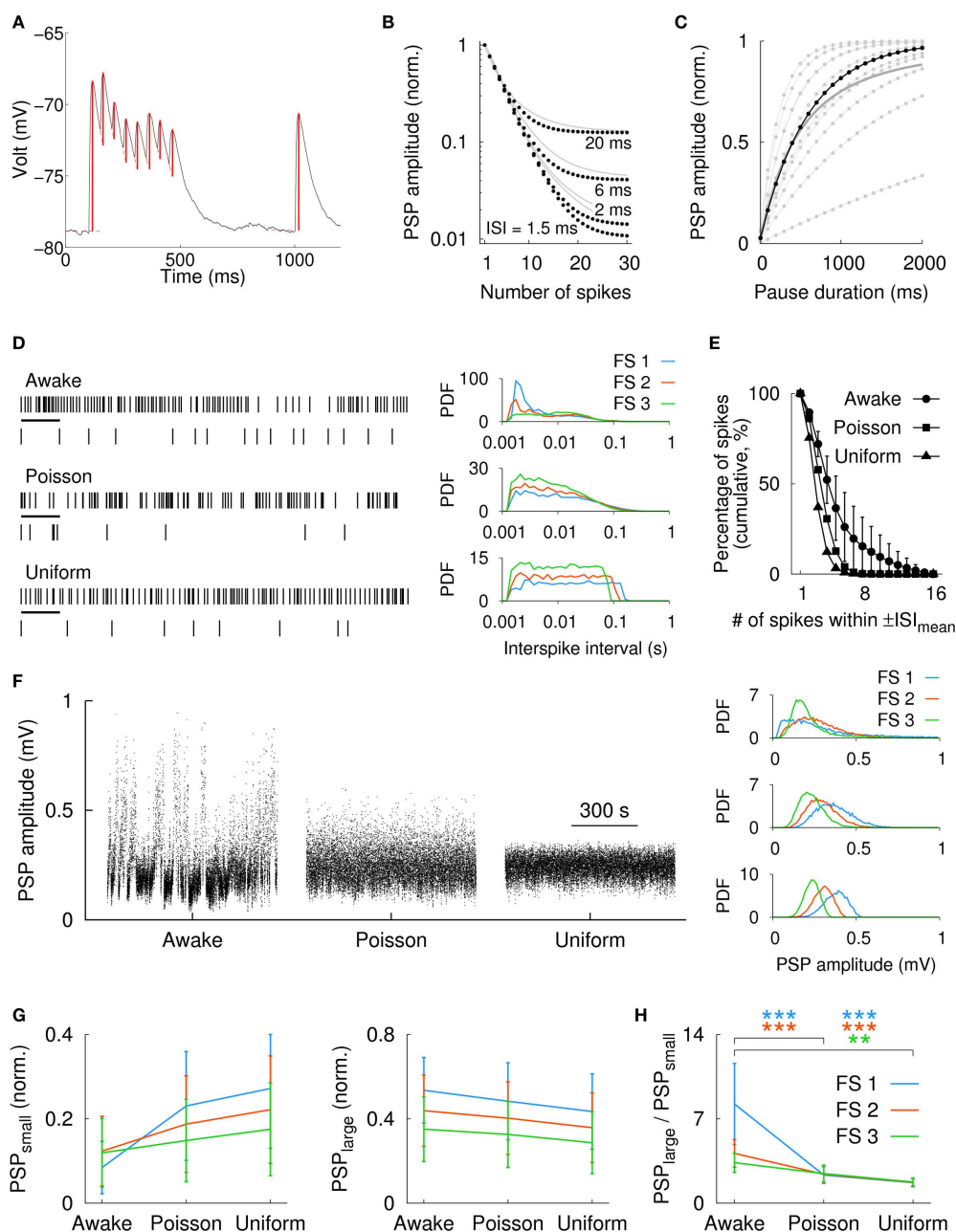


FIGURE 5 | Influence of natural FS firing discharge on the PSP distribution in MS neurons. (A) Averaged experimental postsynaptic response of an FS-to-MS connection. Synaptic activation amplitudes (red vertical lines) for the model fitting were extracted by subtracting the baseline or the residual of the exponential decay of preceding PSPs. **(B)** Simulated synaptic depression in a typical FS-to-MS synapse (black dots) for synthetic spike traces at different frequencies (gray lines: average over $n = 11$ synapses, rat). A cluster of 4 spikes resulted in more than 50% depression. **(C)** Recovery from synaptic depression for the same synapse (black) as a function of time. Gray/dots: individual synapses, gray/solid: average over all synapses ($n = 11$). **(D)** Left: spike raster of an extracellularly recorded striatal FS cell in an awake, behaving rat, and for two modes of shuffling (Poisson distributed and uniformly distributed). Shown is a 5-s long fragment of a 760-s recording. In addition, a more detailed view of 500 ms length (corresponding to the black horizontal bars in the upper traces) is shown below each raster. Right: probability density functions (PDFs) of the interspike intervals in three FS cells for the awake and spike shuffled data (same vertical order as in the left panel). Firing

rates were 12 Hz (FS 1), 17 Hz (FS 2), and 23 Hz (FS 3). The awake spike raster in the left panel corresponds to FS 3. **(E)** Average *in vivo* spike clustering in the FS cells ($n = 3$) for the awake condition and for the two modes of spike shuffling. In the awake data, more than 10% of all spikes were part of spike clusters with 9 or more spikes (cluster duration was defined as $\pm \text{ISI}_{\text{mean}}$). **(F)** Left: distribution of the simulated postsynaptic potentials for a typical FS-to-MS synapse in response to the spike train of FS 3. For the original spike train (awake), the distribution of PSPs covered the widest range, i.e., from very small (depressed synapse) to almost maximum (fully recovered; maximum possible PSP for this synapse was ~ 1 mV). Right: PDFs of the simulated PSPs for the same synapse and the spike trains in all three FS cells [same vertical order as in **(D)**]. **(G)** Average value of the 25% smallest ($\text{PSP}_{\text{small}}$, left panel) and largest ($\text{PSP}_{\text{large}}$, right panel) PSPs for all three FS cells. **(H)** The rank of the ratio $\text{PSP}_{\text{large}}/\text{PSP}_{\text{small}}$ was for the awake data always larger than for the corresponding Poisson or uniformly distributed spike times ($n = 11$ synapses). Statistical significance: $**p < 0.001$, $***p < 0.0001$ (Kruskal-Wallis test with Tukey-Kramer multiple comparison).

used to derive Poisson distributed and uniformly distributed spike rasters with the same average spike rate. **Figure 5D** (right panel) shows the ISI distributions in three FS cells for the *in vivo* and the corresponding shuffled spike trains. The graph in **Figure 5E** visualizes the clustering of spikes; it shows the percentage of spikes that contain at least a given number of APs within a period of $\pm \text{ISI}_{\text{mean}}$ ms around each spike. Here, we analyzed the clustering in terms of the mean interspike interval, ISI_{mean} , which was more comparable to the time constant of synaptic depression than ISI_{min} was (see above). ISI_{mean} ranged from 43 to 82 ms for the three neurons. In the awake spike train, more than 10% of the spikes were organized in groups of at least nine spikes (**Figure 5E**). For Poisson and uniformly shuffled spike trains, the percentage of spikes that were member of large spike clusters was comparatively smaller (**Figure 5E**). High-frequency clusters and intermittent firing pauses in the *in vivo* spike train furthermore resulted in a wide range of simulated PSP amplitudes. **Figure 5F** shows the PSP amplitude distribution for the model of a typical FS-to-MS synapse for *in vivo* as well as Poisson and uniformly shuffled spike activity (from left to right). The PSP distributions for the *in vivo* input and the shuffled data for this synapse are shown in the right panels of **Figure 5F** for the three FS cells (same vertical order as in **Figure 5D**). The relative large number of extended spike cluster in the awake data, as it can be seen in **Figure 5E**, resulted in a reduction of the small PSP amplitudes as shown in **Figure 5G** for all three FS cells (left panel, $n = 11$ synapses). Here, $\text{PSP}_{\text{small}}$ was defined as the average normalized amplitude of the 25% smallest PSPs. Importantly, pauses in the awake FS activity allowed also for the recovery of synaptic amplitudes as evident from the average normalized amplitude of the 25% largest PSPs, $\text{PSP}_{\text{large}}$, which was largest for the awake data (**Figure 5G**, right panel). Consequently, the ratio $\text{PSP}_{\text{large}}/\text{PSP}_{\text{small}}$ was largest for the awake spike train, and shuffling of the data as described above destroyed the structure of the *in vivo* firing and resulted in a smaller range of observed PSP amplitudes (**Figure 5H**). Therefore, these results suggest that FS-to-MS synapses utilize a large fraction of their possible amplitude spectrum in response to *in vivo*-like input, i.e., from strongly depressed to entirely recovered.

4 DISCUSSION

4.1 MODELING OF FS FIRING

Fast-spiking interneurons can be characterized electrophysiologically by their firing discharge in response to somatic current steps (Markram et al., 2004; Taverna et al., 2007). Based on the model of a cortical FS neuron, it was suggested that the size of the Na^+ window current influences minimal firing rate and firing patterns (Golomb et al., 2007). In the present study, we used a morphologically extended version of the FS model by Golomb et al. (2007) with a small Na^+ window current, which together with “intrinsic” (white) noise induced the characteristic stuttering behavior and subthreshold oscillations observed in many FS cells of the cortex and the striatum. Indeed, although the precise origin of the stuttering discharge is not known, intrinsic stochastic mechanisms are the most likely source for the irregular bursting in these cells (Englitz et al., 2008).

The FS model parameters in the present study were not additionally adjusted to match the FS cell properties recorded *in vitro*. Consequently, the FS model showed some differences compared to

the *in vitro* measurements, that is, the model had a stronger afterhyperpolarization (Golomb et al., 2007) and a longer minimal ISI. While the strong afterhyperpolarization was not a critical issue for the present study, the larger ISI in the model cell (~ 10 ms compared to less than 4 ms *in vitro* and *in vivo*) prevented the use of simulated spike trains for the depressing synapse model because synaptic depression was strongly dependent on the ISI. However, instead of adjusting the model parameters in order to achieve a shorter minimal ISI, we used spike trains from striatal FS interneurons recorded *in vivo* (Berke et al., 2004; Berke, 2008) for the simulation of the postsynaptic FS-to-MS response. Importantly, despite the above differences, the model captured and predicted key features of striatal and cortical FS interneurons *in vitro* (**Figure 3** and **Figure A6** in Appendix, respectively). For increasing levels of steady input, both the model and *in vitro* measurements showed: (i) a linear rise of the subthreshold V_m , (ii) a non-linear onset of stuttering discharge, and (iii) an increase of the trial-to-trial variability. Therefore, the broad agreement between the model and the measurements *in vitro* provides strong support for the validity of the results from the simulation of electrically coupled FS cells (see below).

4.2 FS FIRING AND THE INFLUENCE OF STEADY AND FLUCTUATING INPUT

In the present study, we investigated the influence of steady and fluctuating input on FS firing. As shown previously, steady input resulted in random stuttering activity in the model (Golomb et al., 2007) as well as *in vitro* (Kawaguchi, 1993; Markram et al., 2004), while the response to fluctuating (synaptic) input was characterized by reliable spiking (Mainen and Sejnowski, 1995; Schneidman et al., 1998) without showing the characteristic stuttering discharge (La Camera et al., 2006). The profound difference in the spike reliability for different input was also reflected in the amount of spike synchronization among electrically coupled FS cells in the model. Although the steady-state coupling in electrically connected FS neurons is not sufficient to induce APs in neighboring FS cells in the striatum (Koós and Tepper, 1999) and in the model, our simulations indicate that spikes are easily synchronized when the neurons receive suprathreshold, steady input. This finding is consistent with previous reports from *in vitro* and modeling studies in the striatum (Tepper et al., 2004; Hjorth et al., 2009) and the cortex (Galarreta and Hestrin, 1999; Nomura et al., 2003; Mancilla et al., 2007; Zahid and Skinner, 2009). In contrast, spike synchronization was drastically reduced when the FS cells received fluctuating input (see Hjorth et al., 2009, who showed a similar behavior in a model of tonically firing FS cells).

In our experiments, additional (steady) depolarization was achieved by somatic current injection. In the striatum, similar effects might result from the excitatory effects of various neuromodulators, such as serotonin (Blomeley and Bracci, 2009), acetylcholine (Koós and Tepper, 2002), and dopamine (Bracci et al., 2002) – many of them showing task-related regulation (see, e.g., Hyland et al., 2002). Membrane depolarization can also be induced by the metabotropic glutamate receptor mGluR1 (Bonsi et al., 2007) or by NMDA receptor mediated currents, although a recent study reports a lack of NMDA receptor mediated synaptic currents (Gittis et al., 2010). Thus, whether the reported amounts of depolarization occur *in vivo* and if they would be sufficient for

FS neurons to enter the stuttering regime at least transiently is not known. Our modeling results for a pair of electrically connected FS cells and the lack of evident spike synchronization *in vivo* (Berke, 2008) rather suggest that in awake, behaving animals neighboring FS interneurons are not in the stuttering regime simultaneously. Therefore, the FS firing variability *in vivo* with short periods of high firing (reminiscent of stuttering) is likely to represent temporally precise activity, which is driven by the fluctuations in the input (Softky and Koch, 1993; van Vreeswijk and Sompolinsky, 1996). Importantly, inhibitory connections between striatal FS neurons can not fully explain the lack of *in vivo* spike synchronization since only about half of the pairs of FS cells are connected (Gittis et al., 2010). It should be noted, however, that although gap junction coupling between striatal FS interneurons has been demonstrated in electrophysiological recordings *in vitro* (Tepper et al., 2004) and immunohistochemical stainings (Fukuda, 2009), another possible explanation for the absence of spike synchronization might be the lack of functional electrical coupling *in vivo*. Indeed, gap junctions have been shown to be regulated by various factors (Harris, 2001; Urschel et al., 2006; Gonzalez-Nieto et al., 2008) and *in vivo* patch-clamp recordings, in which subthreshold activity can be recorded, would allow the investigation of this question directly.

4.3 FS FIRING VARIABILITY IS TRANSLATED INTO VARIABILITY OF POSTSYNAPTIC RESPONSES IN MS PROJECTION NEURONS

Fast-spiking interneurons of the striatum form symmetrical synapses on MS projection neurons. Similar to cortical FS to principal neuron connections (Galarreta and Hestrin, 1998), these synapses show depressing dynamics *in vitro* (Plenz and Kitai, 1998; Gittis et al., 2010; Planert et al., 2010). The *in vivo* FS discharge in behaving rats is characterized by numerous large clusters of high-frequency spikes, which resulted in strong depression in the synapse model. Importantly, pauses in the FS firing allowed for the recovery of synaptic resources. Together this suggests that striatal FS-to-MS synapses might operate over a wide range of PSP amplitudes in which the depressive nature of the synapses contributes to the variability of PSP sizes. However, if synaptic depression in FS-to-MS connections is dominating the synaptic dynamics also *in vivo* is currently not known. In fact, recent evidence from cortical neurons suggests that synaptic depression observed *in vitro* can be diminished by ongoing activity *in vivo* (Reig et al., 2006; Reig and Sanchez-Vives, 2007). Nevertheless, the impact of FS synapses on postsynaptic MS neurons also depends on the timing of the PSPs, which directly reflects the firing variability observed in FS cells. Striatal FS neurons receive

excitatory afferents from cortex and thalamus, and inhibitory input along the pallidostriatal pathway and from intrastriatal sources (as well as various modulatory projections, see above; Wilson, 2004). These inputs are most likely the main source for the observed firing variability in the FS cells.

Striatal FS neurons have been shown to prevent or delay spiking in postsynaptic MS cells (Koós and Tepper, 1999). However, our results indicate that FS cells *in vivo* communicate via substantially depressed synapses over extended periods of time. The summative effect of several converging FS cells (Tepper et al., 2004) as well as temporal summation might compensate for the depletion in individual synapses. In order to study the combined effect of all presynaptic FS cells onto a single MS neuron, knowledge about the spike times in the presynaptic FS population would be required. Similarly, to predict how postsynaptic currents (which are proportional to our PSPs in the current-clamp measurements) influence an MS neuron *in vivo* requires knowledge about the membrane potential of the MS cell, since these neurons are known to show strong inward rectification (Kawaguchi, 1993). These points were not addressed in this study and could be a question for future research.

5 CONCLUSION

Our results indicate that FS firing variability observed *in vivo* is most likely due to the input that these neurons receive, and that this variability is translated into variability of the postsynaptic responses in MS projection neurons. The fact that the FS-to-MS synapse model showed substantial depression over extended periods of time in response to natural FS firing patterns might indicate the importance of cooperative effects of multiple presynaptic FS interneurons and the precise orchestration of their activity in shaping the activity of the MS projection neuron.

ACKNOWLEDGMENTS

Andreas Klaus, Henrike Planert, J. J. Johannes Hjorth, Gilad Silberberg and Jeanette Hellgren Kotaleski are grateful for support from the Swedish Research Council and the Parkinson's Foundation. Andreas Klaus was in addition supported by the NIH–Karolinska Institute joint PhD program. Henrike Planert and Gilad Silberberg received additional support from the European Commission Coordination Action ENINET (contract number LSHM-CT-2005-19063), the Human Frontier Science Program, and the European Union Seventh Framework Programme (Cortex and Select and Act). Joshua D. Berke is grateful for support from the Tourette Syndrome Association, the Whitehall Foundation, and the US National Institute on Drug Abuse.

REFERENCES

- Abbott, L. F., Varela, J. A., Sen, K., and Nelson, S. B. (1997). Synaptic depression and cortical gain control. *Science* 275, 221–224.
- Amitai, Y., Gibson, J., Beierlein, M., Patrick, S., Ho, A., Connors, B., and Golomb, D. (2002). The spatial dimensions of electrically coupled networks of interneurons in the neocortex. *J. Neurosci.* 22, 4142.
- Beierlein, M., Gibson, J., and Connors, B. (2000). A network of electrically coupled interneurons drives synchronized inhibition in neocortex. *Nat. Neurosci.* 3, 904–910.
- Berke, J. (2008). Uncoordinated firing rate changes of striatal fast-spiking interneurons during behavioral task performance. *J. Neurosci.* 28, 10075.
- Berke, J. (2011). Functional properties of striatal fast-spiking interneurons. *Front. Syst. Neurosci.* 5:45. doi: 10.3389/fnsys.2011.00045
- Berke, J., Okatan, M., Skurski, J., and Eichenbaum, H. (2004). Oscillatory entrainment of striatal neurons in freely moving rats. *Neuron* 43, 883–896.
- Blackwell, K., Czubyko, U., and Plenz, D. (2003). Quantitative estimate of synaptic inputs to striatal neurons during up and down states *in vitro*. *J. Neurosci.* 23, 9123–9132.
- Blomeley, C. P., and Bracci, E. (2009). Serotonin excites fast-spiking interneurons in the striatum. *Eur. J. Neurosci.* 29, 1604–1614.
- Bonsi, P., Sciamanna, G., Mitrano, D. A., Cuomo, D., Bernardi, G., Platania, P., Smith, Y., and Pisani, A. (2007). Functional and ultrastructural analysis of group I mGluR in striatal fast-spiking interneurons. *Eur. J. Neurosci.* 25, 1319–1331.

- Bower, J., and Beeman, D. (1998). *The Book of GENESIS: Exploring Realistic Neural Models with the General NEural Simulation System*. New York, NY: Springer-Verlag.
- Bracci, E., Centonze, D., Bernardi, G., and Calabresi, P. (2002). Dopamine excites fast-spiking interneurons in the striatum. *J. Neurophysiol.* 87, 2190–2194.
- Bracci, E., Centonze, D., Bernardi, G., and Calabresi, P. (2003). Voltage-dependent membrane potential oscillations of rat striatal fast-spiking interneurons. *J. Physiol. (Lond.)* 549, 121–130.
- Chung, Y., Shin, C., Kim, M., and Cha, C. (2000). Immunohistochemical study on the distribution of six members of the Kv1 channel subunits in the rat basal ganglia. *Brain Res.* 875, 164–170.
- Druckmann, S., Banitt, Y., Gidon, A., Schürmann, F., Markram, H., and Segev, I. (2007). A novel multiple objective optimization framework for constraining conductance-based neuron models by experimental data. *Front. Neurosci.* 1:7–18. doi: 10.3389/neuro.01.1.001.2007
- Englitz, B., Stiefel, K. M., and Sejnowski, T. J. (2008). Irregular firing of isolated cortical interneurons in vitro driven by intrinsic stochastic mechanisms. *Neural Comput.* 20, 44–64.
- Fukuda, T. (2009). Network architecture of gap junction-coupled neuronal linkage in the striatum. *J. Neurosci.* 29, 1235–1243.
- Gage, G. J., Stoetznner, C. R., Wiltshcko, A. B., and Berke, J. D. (2010). Selective activation of striatal fast-spiking interneurons during choice execution. *Neuron* 67, 466–479.
- Galarreta, M., and Hestrin, S. (1998). Frequency-dependent synaptic depression and the balance of excitation and inhibition in the neocortex. *Nat. Neurosci.* 1, 587–594.
- Galarreta, M., and Hestrin, S. (1999). A network of fast-spiking cells in the neocortex connected by electrical synapses. *Nature* 402, 72–75.
- Galarreta, M., and Hestrin, S. (2001). Electrical synapses between GABA-releasing interneurons. *Nat. Rev. Neurosci.* 2, 425–433.
- Galarreta, M., and Hestrin, S. (2002). Electrical and chemical synapses among parvalbumin fast-spiking GABAergic interneurons in adult mouse neocortex. *Proc. Natl. Acad. Sci. U.S.A.* 99, 12438–12443.
- Gibson, J. R., Beierlein, M., and Connors, B. W. (2005). Functional properties of electrical synapses between inhibitory interneurons of neocortical layer 4. *J. Neurophysiol.* 93, 467–480.
- Gittis, A. H., Nelson, A. B., Thwin, M. T., Palop, J. J., and Kreitzer, A. C. (2010). Distinct roles of GABAergic interneurons in the regulation of striatal output pathways. *J. Neurosci.* 30, 2223–2234.
- Goldberg, E., Clark, B., Zagha, E., Nahmani, M., Erisir, A., and B. R. (2008). K⁺ channels at the axon initial segment dampen near-threshold excitability of neocortical fast-spiking GABAergic interneurons. *Neuron* 58, 387–400.
- Golomb, D., Donner, K., Shacham, L., Shlosberg, D., Amitai, Y., and Hansel, D. (2007). Mechanisms of firing patterns in fast-spiking cortical interneurons. *PLoS Comput. Biol.* 3, e156. doi: 10.1371/journal.pcbi.0030156
- Gonzalez-Nieto, D., Gmez-Hernandez, J. M., Larrosa, B., Gutierrez, C., Muoz, M. D., Fasciani, I., O'Brien, J., Zappal, A., Cicirata, F., and Barrio, L. C. (2008). Regulation of neuronal connexin-36 channels by pH. *Proc. Natl. Acad. Sci.* 105, 17169–17174.
- Gupta, A., Wang, Y., and Markram, H. (2000). Organizing principles for a diversity of GABAergic interneurons and synapses in the neocortex. *Science* 287, 273.
- Gustafson, N., Gireesh-Dharmaraj, E., Czubyko, U., Blackwell, K., and Plenz, D. (2006). A comparative voltage and current-clamp analysis of feedback and feedforward synaptic transmission in the striatal microcircuit in vitro. *J. Neurophysiol.* 95, 737–752.
- Harris, A. L. (2001). Emerging issues of connexin channels: biophysics fills the gap. *Q. Rev. Biophys.* 34, 325–472.
- Hjorth, J., Blackwell, K., and Hellgren Kotaleski, J. (2009). Gap junctions between striatal fast-spiking interneurons regulate spiking activity and synchronization as a function of cortical activity. *J. Neurosci.* 29, 5276–5286.
- Hyland, B., Reynolds, J., Hay, J., Perk, C., and Miller, R. (2002). Firing modes of midbrain dopamine cells in the freely moving rat. *Neuroscience* 114, 475–492.
- Kawaguchi, Y. (1993). Physiological, morphological, and histochemical characterization of three classes of interneurons in rat neostriatum. *J. Neurosci.* 13, 4908–4923.
- Kawaguchi, Y. (1997). Neostriatal cell subtypes and their functional roles. *Neurosci. Res.* 27, 1–8.
- Kawaguchi, Y., and Kubota, Y. (1997). GABAergic cell subtypes and their synaptic connections in rat frontal cortex. *Cereb. Cortex* 7, 476–486.
- Kita, H., Kosaka, T., and Heizmann, C. (1990). Parvalbumin-immunoreactive neurons in the rat neostriatum: a light and electron microscopic study. *Brain Res.* 536, 1–15.
- Koós, T., and Tepper, J. (1999). Inhibitory control of neostriatal projection neurons by GABAergic interneurons. *Nat. Neurosci.* 2, 467–472.
- Koós, T., Tepper, J., and Wilson, C. (2004). Comparison of IPSCs evoked by spiny and fast-spiking neurons in the neostriatum. *J. Neurosci.* 24, 7916–7922.
- Koós, T., and Tepper, J. M. (2002). Dual cholinergic control of fast-spiking interneurons in the neostriatum. *J. Neurosci.* 22, 529–535.
- Kotaleski, J., Plenz, D., and Blackwell, K. (2006). Using potassium currents to solve signal-to-noise problems in inhibitory feedforward networks of the striatum. *J. Neurophysiol.* 95, 331–341.
- La Camera, G., Rauch, A., Thurbon, D., Lüscher, H., Senn, W., and Fusi, S. (2006). Multiple time scales of temporal response in pyramidal and fast spiking cortical neurons. *J. Neurophysiol.* 96, 3448–3464.
- Lenz, S., Perney, T., Qin, Y., Robbins, E., and Chesselet, M. (1994). GABA-ergic interneurons of the striatum express the shaw-like potassium channel Kv3.1. *Synapse* 18, 55–66.
- Luk, K. C., and Sadikot, A. F. (2001). GABA promotes survival but not proliferation of parvalbumin-immunoreactive interneurons in rodent neostriatum: an in vivo study with stereology. *Neuroscience* 104, 93–103.
- Mainen, Z., and Sejnowski, T. (1995). Reliability of spike timing in neocortical neurons. *Science* 268, 1503–1506.
- Mallet, N., Le Moine, C., Charpier, S., and Gonon, F. (2005). Feedforward inhibition of projection neurons by fast-spiking GABA interneurons in the rat striatum in vivo. *J. Neurosci.* 25, 3857–3869.
- Mancilla, J., Lewis, T., Pinto, D., Rinzel, J., and Connors, B. (2007). Synchronization of electrically coupled pairs of inhibitory interneurons in neocortex. *J. Neurosci.* 27, 2058.
- Marín, O., Anderson, S. A., and Rubenstein, J. L. R. (2000). Origin and molecular specification of striatal interneurons. *J. Neurosci.* 20, 6063–6076.
- Markram, H., Toledo-Rodriguez, M., Wang, Y., Gupta, A., Silberberg, G., and Wu, C. (2004). Interneurons of the neocortical inhibitory system. *Nat. Rev. Neurosci.* 5, 793–807.
- Markram, H., Wang, Y., and Tsodyks, M. (1998). Differential signaling via the same axon of neocortical pyramidal neurons. *Proc. Natl. Acad. Sci. U.S.A.* 95, 5323–5328.
- Nomura, M., Fukai, T., and Aoyagi, T. (2003). Synchrony of fast-spiking interneurons interconnected by GABAergic and electrical synapses. *Neural Comput.* 15, 2179–2198.
- Planert, H., Szydlowski, S. N., Hjorth, J. J., Grillner, S., and Silberberg, G. (2010). Dynamics of synaptic transmission between fast-spiking interneurons and striatal projection neurons of the direct and indirect pathways. *J. Neurosci.* 30, 3499–3507.
- Plenz, D., and Kitai, S. T. (1998). Up and down states in striatal medium spiny neurons simultaneously recorded with spontaneous activity in fast-spiking interneurons studied in cortex-striatum-substantia nigra organotypic cultures. *J. Neurosci.* 18, 266–283.
- Reig, R., Gallego, R., Nowak, L. G., and Sanchez-Vives, M. V. (2006). Impact of cortical network activity on short-term synaptic depression. *Cereb. Cortex* 16, 688–695.
- Reig, R., and Sanchez-Vives, M. V. (2007). Synaptic transmission and plasticity in an active cortical network. *PLoS ONE* 2, e670. doi: 10.1371/journal.pone.0000670
- Schneidman, E., Freedman, B., and Segev, I. (1998). Ion channel stochasticity may be critical in determining the reliability and precision of spike timing. *Neural Comput.* 10, 1679–1703.
- Softky, W., and Koch, C. (1993). The highly irregular firing of cortical cells is inconsistent with temporal integration of random EPSPs. *J. Neurosci.* 13, 334–350.
- Taverna, S., Canciani, B., and Pennartz, C. (2007). Membrane properties and synaptic connectivity of fast-spiking interneurons in rat ventral striatum. *Brain Res.* 1152, 49–56.
- Tepper, J., Koós, T., and Wilson, C. (2004). GABAergic microcircuits in the neostriatum. *Trends Neurosci.* 27, 662–669.
- Tepper, J., Wilson, C., and Koós, T. (2008). Feedforward and feedback inhibition in neostriatal GABAergic spiny neurons. *Brain Res. Rev.* 58, 272–281.
- Tsodyks, M., Pawelzik, K., and Markram, H. (1998). Neural networks with dynamic synapses. *Neural Comput.* 10, 821–835.
- Urschel, S., Hher, T., Schubert, T., Alev, C., Shl, G., Wrsdrfer, P., Asahara, T., Dermietzel, R., Weiler, R., and Willecke, K. (2006). Protein kinase a-mediated phosphorylation of connexin36 in mouse retina results in decreased gap junctional communication between AII amacrine cells. *J. Biol. Chem.* 281, 33163–33171.
- van Vreeswijk, C., and Sompolinsky, H. (1996). Chaos in neuronal networks with balanced excitatory and inhibitory activity. *Science* 274, 1724–1726.
- Weiser, M., Vega-Saenz de Miera, E., Kentros, C., Moreno, H., Franzen, L., Hillman, D., Baker, H., and B. R.

- (1994). Differential expression of shaw-related K⁺ channels in the rat central nervous system. *J. Neurosci.* 14, 949–972.
- Wilson, C. (2004). “Basal Ganglia,” in *The synaptic organization of the brain*, 5th Edn, Chapter 9, ed. G. Shepherd (New York: Oxford University Press), 361–413.
- Zahid, T., and Skinner, F. K. (2009). Predicting synchronous and asynchronous network groupings of hippocampal interneurons coupled with dendritic gap junctions. *Brain Res.* 1262, 115–129.
- Conflict of Interest Statement:** The authors declare that the research was conducted in the absence of any commercial or financial relationships that could be construed as a potential conflict of interest.
- Received: 24 March 2011; paper pending published: 02 May 2011; accepted: 17 June 2011; published online: 13 July 2011.
- Citation: Klaus A, Planert H, Hjorth JJJ, Berke JD, Silberberg G and Hellgren Kotaleski J (2011) Striatal fast-spiking interneurons: from firing patterns to post-synaptic impact. *Front. Syst. Neurosci.* 5:57. doi: 10.3389/fnsys.2011.00057
- Copyright © 2011 Klaus, Planert, Hjorth, Berke, Silberberg and Hellgren Kotaleski. This is an open-access article subject to a non-exclusive license between the authors and Frontiers Media SA, which permits use, distribution and reproduction in other forums, provided the original authors and source are credited and other Frontiers conditions are complied with.

APPENDIX

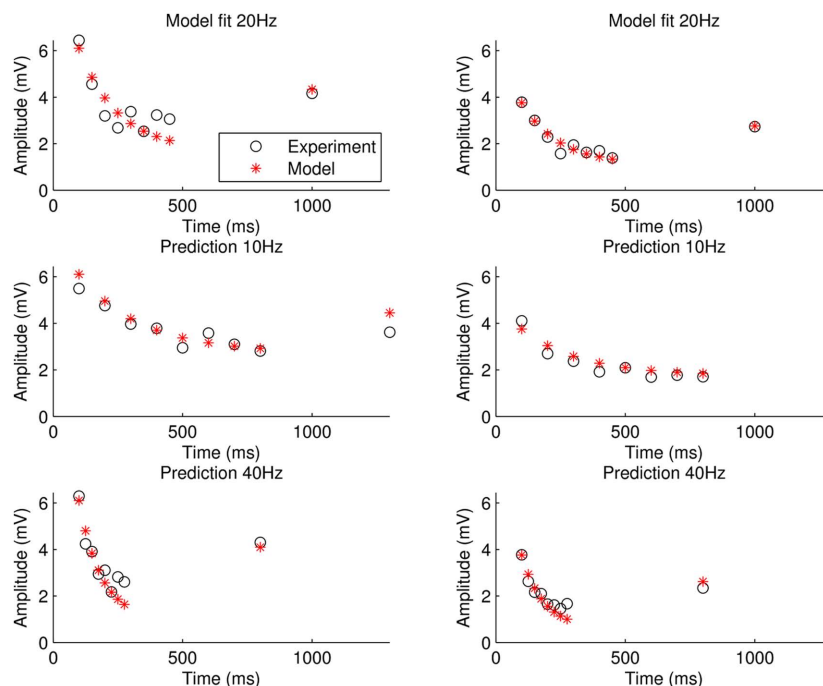


FIGURE A1 | The synaptic dynamics were modeled using the scheme described by Tsodyks et al. (1998). Example fitting of synaptic parameters (U , τ_D , τ_P and A_{syn}) for extracted amplitudes from experimental responses at 20 Hz, and verification of the fitting on experimental responses at 10 and

40 Hz for two synapses (left and right column, respectively). For the parameter fitting, see Section 2 in the main text. Black circles indicate experimental amplitudes and red asterisks the amplitudes generated by the model.

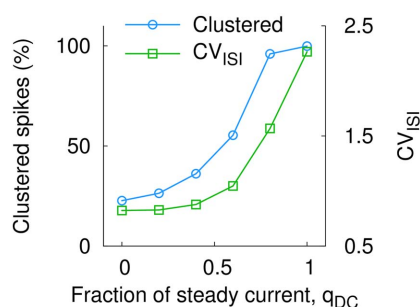


FIGURE A2 | Comparison between the percentage of clustered spikes and the CV_{ISI} in the stuttering FS model. Stuttering increased both the percentage of spikes that were member of a spike cluster and the variability of the interspike intervals. For a tonically firing FS cell, the percentage of clustered spikes would be close to 100%, whereas the CV_{ISI} would be close to zero (not shown, cf. Figure A3 in Appendix).

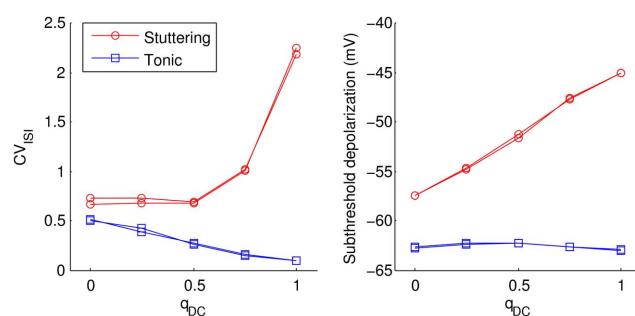


FIGURE A3 | Steady input increased the firing variability in the stuttering FS model as can be seen in an increase of the CV_{ISI} . In an FS model neuron that showed tonic discharge, as opposed to stuttering, the firing variability diminished as the fraction of steady input, q_{DC} , increased. Two responses are shown for each neuron. For the stuttering cell, we used for the sodium current a half-maximum potential of $\theta_m = -22$ mV and for the conductance of the d-type current $g_{KD} = 1.6$ mS/cm² (see Section 2, main text). The parameters for the model neuron that produced tonic discharge were $\theta_m = -28$ mV and $g_{KD} = 0.39$ mS/cm² (Golomb et al., 2007).

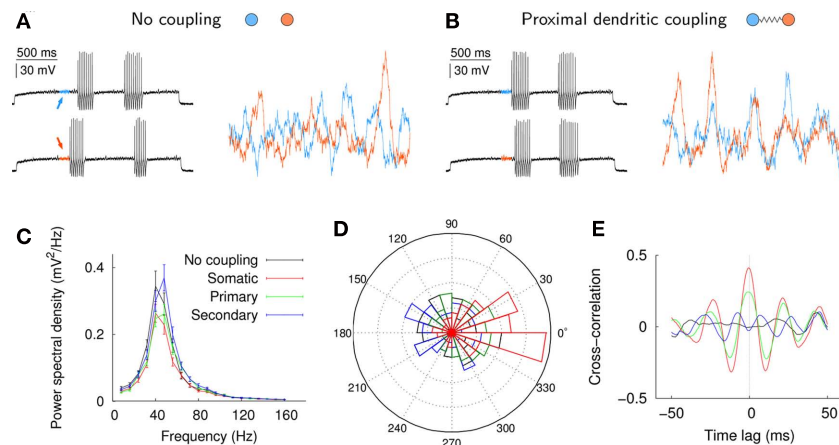
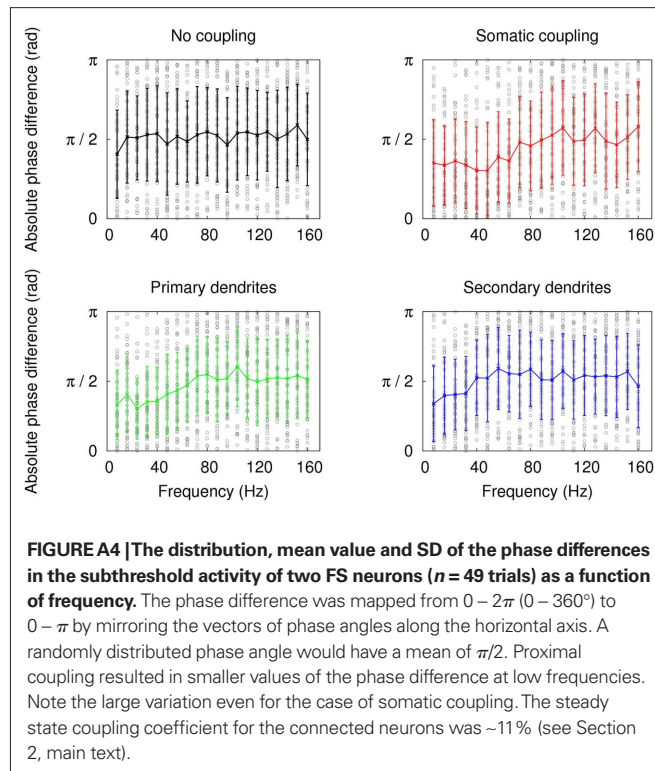


FIGURE A5 | Subthreshold oscillations in response to somatic current injection (2 s, 74 pA) in the neuron model. The input current was adjusted such that 50% of the cells fired within 1 s after stimulus onset (stimulus onset was at 50 ± 25 ms). **(A)** Voltage traces and 125 ms of subthreshold activity before the first stuttering episode for two cells without electrical coupling. **(B)** Example trace for the same cells coupled by two proximally located dendritic gap junctions (2×0.5 nS, electrical coupling coefficient 11%). **(C)** Average power spectral density of the 125-ms subthreshold membrane potential section as depicted in **(A,B)** ($n = 49$). The subthreshold activity was characterized by a peak in the power spectral density at 30–60 Hz. Neurons were either coupled at the

soma (red), at the distal part of the primary dendrites (green) or at the distal part of the secondary dendrites (blue). The single gap junction conductance was 0.5 nS. The number of gap junctions was adjusted such that the electrical coupling coefficient (steady state) at the soma was $\sim 11\%$ for each case. **(D)** Histogram of the phase difference ($0-360^\circ$, 20 bins) between subthreshold oscillations for the different coupling conditions at the peak power frequency 40–48 Hz. The phase difference in this range is reduced for somatically coupled cells (cf. Figure A4 in Appendix). **(E)** Average cross-correlogram of the subthreshold voltage traces showed a maximum at time lag zero for proximal, and antiphase behavior for distal coupling.

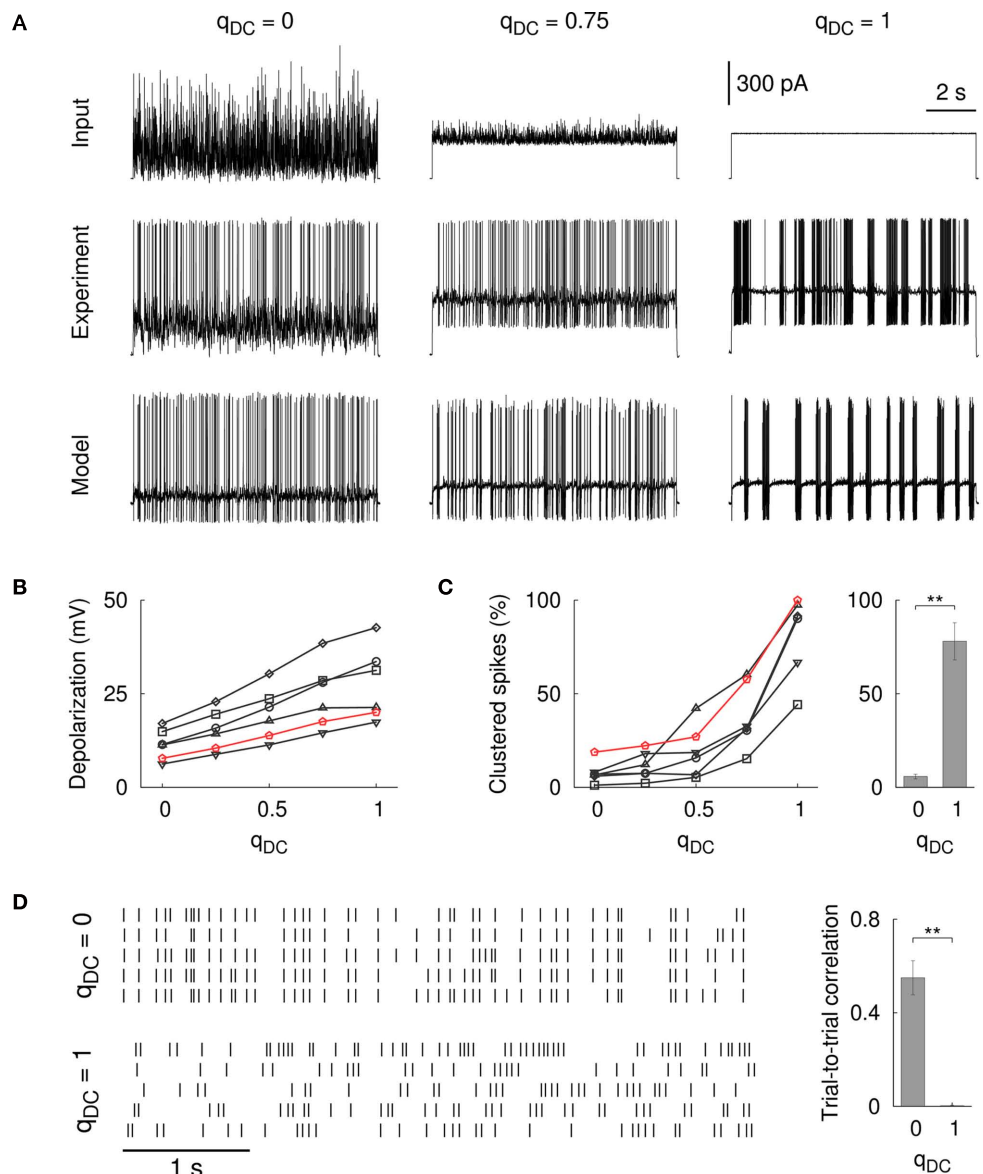


FIGURE A6 | Influence of input fluctuations in cortical FS interneurons. (A)

The spike pattern of the model neuron and of a cortical FS cell for $q_{DC} = 0, 0.75$, and 1.0 (left to right; scale bar for voltage traces, 30 mV). **(B)** Depolarization of the subthreshold membrane potential (measured from the resting baseline). Black lines: $n = 5$ cortical FS neurons, red line: model cell. Two random input traces and different scalings were tested (81 traces in total, 10 s each). Firing rate was 15.8 ± 7.6 Hz and ranged from 2.5 to 31 Hz. **(C)** Steady current input resulted in stuttering seen as an increase in the percentage of clustered spikes. The number of clustered spikes was significantly different between fluctuating and steady input [$n = 5$ cortical FS cells, $t(4, 1) = -7.2$, $p = 0.0017$, unequal variance t -test]. **(D)** Trial-to-trial variability of spiking was low in cortical FS

neurons that were driven by fluctuating input ($q_{DC} = 0$, spike rasters in the left panel are shown for one FS cell). In contrast, a high variability was observed in response to steady input ($q_{DC} = 1$, spike rasters for the same neuron). The difference of the trial-to-trial correlation between $q_{DC} = 0$ and $q_{DC} = 1$ was statistically significant [right panel, $n = 4$ cortical FS neurons, $t(4, 0) = 7.5$, $p = 0.0017$, unequal variance t -test]. The trial-to-trial correlation for the stuttering neurons was not different from zero [$n = 4$ cells, $t(2) = 0.92$, $p = 0.45$, one-sample t -test]. Five trials (10 s each) were tested per condition and neuron. It should be noted that one cortical FS cell was recorded with a low intracellular chloride concentration (8 mM). All other neurons were recorded with the same intracellular concentrations as for the striatal FS neurons (**Figure 3**, main text).



The subthalamic nucleus becomes a generator of bursts in the dopamine-depleted state. Its high frequency stimulation dramatically weakens transmission to the globus pallidus

Rachida Ammari^{1,2,3†}, Bernard Bioulac^{3,4}, Liliana Garcia^{3,4‡} and Constance Hammond^{1,2**}

¹ Inserm UMR 901 INMED, Marseille, France

² Aix Marseille Université Faculté des Sciences, Marseille, France

³ Institut des Maladies Neurodégénératives, UMR 5293, CNRS, Bordeaux, France

⁴ Institut des Maladies Neurodégénératives, UMR 5293, Université de Bordeaux, Bordeaux, France

Edited by:

James M. Tepper, Rutgers, The State University of New Jersey, USA

Reviewed by:

Steven W. Johnson, Oregon Health & Science University, USA

Hagai Bergman, The Hebrew University of Jerusalem, Israel

*Correspondence:

Constance Hammond, INMED UMR 901 Inserm, 163 route de Luminy, BP 13, 13273 Marseille Cédex 09, France.
e-mail: hammond@inmed.univ-mrs.fr

†Present address:

Rachida Ammari, Department of Neuroscience, Physiology and Pharmacology, Medical Sciences Building, UCL, Gower Street, London, WC1E 6BT, UK.

‡Liliana Garcia and Constance Hammond are equivalent last authors.

Excessive burst firing in the dopamine-depleted basal ganglia correlates with severe motor symptoms of Parkinson's disease that are attenuated by high frequency electrical stimulation of the subthalamic nucleus (STN). Here we test the hypothesis that pathological bursts in dopamine-depleted basal ganglia are generated within the STN and transmitted to globus pallidus neurons. To answer this question we recorded excitatory synaptic currents and potentials from subthalamic and pallidal neurons in the basal ganglia slice (BGS) from dopamine-depleted mice while continuously blocking GABA_A receptors. In control mice, a single electrical stimulus delivered to the internal capsule or the rostral pole of the STN evoked a short duration, small amplitude, monosynaptic EPSC in subthalamic neurons. In contrast, in the dopamine-depleted BGS, this monosynaptic EPSC was amplified and followed by a burst of polysynaptic EPSCs that eventually reverberated three to seven times, providing a long lasting response that gave rise to bursts of EPSCs and spikes in GP neurons. Repetitive (10–120 Hz) stimulation delivered to the STN in the dopamine-depleted BGS attenuated STN-evoked bursts of EPSCs in pallidal neurons after several minutes of stimulation but only high frequency (90–120 Hz) stimulation replaced them with small amplitude EPSCs at 20 Hz. We propose that the polysynaptic pathway within the STN amplifies subthalamic responses to incoming excitation in the dopamine-depleted basal ganglia, thereby transforming the STN into a burst generator and entraining pallidal neurons in pathogenic bursting activities. High frequency stimulation of the STN prevents the transmission of this pathological activity to globus pallidus and imposes a new glutamatergic synaptic noise on pallidal neurons.

Keywords: basal ganglia, subthalamic nucleus, Parkinson, high frequency stimulation, burst firing, basal ganglia slice

INTRODUCTION

Patients suffering from Parkinson's disease, as well as animal models of Parkinson's, exhibit abnormally synchronized neuronal oscillatory activity at multiple levels of the basal ganglia–cortical loop, particularly within the subthalamic nucleus (STN; Bergman et al., 1994; for review (Hammond et al., 2007)). *In vitro*, these pathological oscillations have been observed in organotypic co-cultures of globus pallidus (GP, the rodent equivalent of the external segment of the globus pallidus in primates) and STN with frontomedial cortex and dorsolateral striatum (Plenz and Kitaï, 1999), but have so far been absent from *ex vivo* preparations (Wilson et al., 2006). In this co-culture preparation which lacked dopaminergic neurons of the substantia nigra (SN), STN, and GP neurons spontaneously produced synchronized oscillating bursts. Disconnection of the STN from the cortex and the striatum did not abolish synchronized oscillatory bursting, whereas interruption of the STN from GP suppressed bursting in both STN and GP. This led to the conclusion that GP bursts, although weaker than STN bursts, were required for synchronized oscillatory burst generation (Plenz and Kitaï, 1999), probably via STN rebound excitation (Baufreton et al., 2005; Bevan et al., 2006, 2007). Bursting activity was attributed to a central

pacemaker system consisting of the interconnected GABAergic GP and glutamatergic STN neurons. Interestingly, 1 h after disconnection of the STN from the GP, long lasting and uncorrelated burst activity built up in the STN, although spontaneous activity was almost absent in the isolated GP (Plenz and Kitaï, 1999).

These observations can be explained by an alternative hypothesis, namely that abnormal bursts are generated by STN neurons alone (Ryan and Sanders, 1993; Murer et al., 1997). We and others have suggested that a polysynaptic glutamatergic network inside the STN amplifies the STN excitatory drive onto GP (Ammari et al., 2010), entopeduncular nucleus (Ammari et al., 2010) and substantia nigra reticulata (SNr; Shen and Johnson, 2006; Ammari et al., 2010) neurons under certain conditions. In the present paper we have blocked GABA_A synaptic transmission to decrease the impact of the reciprocal GP–STN pathway, while recording synaptic currents from patch-clamped STN and GP neurons in the basal ganglia slice (BGS; Beurrier et al., 2006) from control or reserpine-treated mice.

We now report that dopamine deprivation causes the STN to generate large bursts of EPSCs (compound EPSCs) in response to a single stimulation of its afferents in the internal capsule (IC). These bursts consist of a series of polysynaptic EPSCs, and

may reverberate several times without further stimulation. Both the primary and reverberating bursts propagate to GP neurons. High frequency stimulation of the STN (STN-HFS) dramatically weakens transmission of compound EPSCs to GP neurons and replaces them with small amplitude EPSCs at 20 Hz. We propose that the polysynaptic glutamatergic network within the STN would normally be partly under the inhibitory control of dopaminergic signaling (Shen and Johnson, 2000) and therefore relatively difficult to activate (Shen and Johnson, 2006; Ammari et al., 2010). In contrast, when dopamine-deprived, the polysynaptic STN network becomes the central generator of bursts in the basal ganglia, in particular when activated by afferent excitations. We show that the transmission of bursts from STN to GP neurons and probably to the other target neurons of the STN as well, is dramatically weakened by continuous stimulation of STN neurons at approximately 100 Hz, causing depression of glutamatergic synaptic transmission.

MATERIALS AND METHODS

RESERPINE TREATMENT

Experiments were performed in slices obtained from naive or reserpine-treated 13- to 28-day-old C57Bl6 mice. Experiments were carried out in accordance with European Communities Council Directive of 24 November 1986 (86/609/EEC) for care of laboratory animals. Reserpine (5 mg/kg, i.p.) and α -methyl-*p*-tyrosine (a tyrosine hydroxylase inhibitor; 250 mg/kg, i.p.) were injected at 20 and 4 h, respectively, before preparation of slices to deplete dopaminergic terminals and prevent new synthesis of dopamine (Moody and Spear, 1992). In their cages, the injected mice showed a complete lack of spontaneous activity and when placed on the grid they were unable to grasp it.

SLICING PROCEDURE

Mice were killed by decapitation under isoflurane anesthesia and 400- μ m-thick oblique parasagittal slices were cut with an angle of $10 \pm 2^\circ$ to obtain BGS as previously described (Beurrier et al., 2006). For the slicing procedure, the solution contained (in mM) 110 choline, 2.5 KCl, 1.25 NaH_2PO_4 , 7 MgCl_2 , 0.5 CaCl_2 , 25 NaHCO_3 , 7 glucose. After a recovery period, the slices were recorded in a submersion-type chamber at room temperature with standard ACSF saturated with 95% O_2 /5% CO_2 and containing (in mM) 126 NaCl, 3.5 KCl, 1.2 NaH_2PO_4 , 1.3 MgCl_2 , 2.4 CaCl_2 , 25 NaHCO_3 , 12 glucose.

ELECTROPHYSIOLOGICAL RECORDINGS

Cells were visualized with infrared-differential interference optics (BMX Olympus). We performed patch-clamp recordings in the whole-cell or cell-attached configuration using the Multiclamp 700A amplifier, the Digidata 1344A interface and PClamp9 software (Axon Instruments, Foster City, CA, USA). For voltage and current clamp recordings, patch electrodes (6–10 M Ω) contained (in mM): 120 K-gluconate, 5 KCl, 1 CaCl_2 , 10 HEPES, 10 EGTA, 2.5 MgATP, 0.5 NaGTP and 2 QX-314, pH 7.2–7.4 (275–285 mOsm). Biocytin (5 mg/ml) was added to the pipette solution and osmolarity corrected when necessary so that the recorded neurons were filled with biocytin (0.4%) for post hoc morphological analysis. We identified STN neurons by their localization, GP neurons by their localization, I–V curves, and morphology (Ammari et al., 2010).

STIMULATION

Synaptic currents were evoked in the STN and GP neurons using a bipolar stimulating electrode (33 k Ω impedance in response to 1 V at 1000 Hz, separation of the two electrodes: 100 μ m, Phymep NEX). Rectangular pulses (100 μ s duration) of constant current (50–800 μ A) were delivered every 30 s unless otherwise stated. For 10–120 Hz STN stimulation we used a stimulator made in the laboratory (UMR CNRS, 5293) to deliver constant-current pulses, as previously described (Garcia et al., 2003). Stimulation was applied between the two poles of the electrode. It consisted of negative current pulses of fixed duration (100 μ s), fixed frequency (10–120 Hz), and intensity adjusted between 100 and 300 μ A (0.5–1.5 V). Stimulation was applied over periods of several minutes. To remove artifacts, a sample and hold electronic device was built in the laboratory as previously described (Garcia et al., 2003). Synchronized with the stimulator, the artifact suppressor allowed the recorded signal to be held at the level before the current pulse and to restore the signal a few microseconds later. Comparison of recording traces before and after artifact suppression allowed checking that the sample-and-hold procedure did not consistently affect EPSCs recordings.

DRUGS

Drugs were prepared as concentrated stock solutions and diluted in ACSF for bath application immediately prior to use. Gabazine, a selective GABA_A receptor antagonist; (\pm)-2-amino-5-phosphonopentanoic acid (AP5, a selective NMDA receptor antagonist), 6-cyano-7-nitroquinoxaline 2, 3-dione (CNQX, an AMPA-KA receptors antagonist), were all purchased from Sigma Aldrich (France).

DATA ANALYSIS AND STATISTICS

Evoked and spontaneous EPSCs were quantified using pClamp 9 software (Axon Instruments, Foster City, CA, USA). We quantified the total charge (in nA.ms), latency (ms), duration (ms), peak amplitude (pA), and time to peak (ms) of EPSCs. Spontaneous and HFS-evoked EPSCs were analyzed off-line with Mini Analysis program (Synaptosoft 6.0), to determine their frequency, amplitude, and pattern. All detected currents were then visually inspected to reject artifactual events.

Average values are presented as means \pm SEM and we performed statistical comparisons with Mann–Whitney rank sum test (SigmaStat 3.1). We set the level of significance as $P < 0.05$ (*); (**) for $P < 0.01$; (***) for $P < 0.001$.

RESULTS

All recordings were performed in the continuous presence of Gabazine (10 μ M) in order to block GABA_A synaptic transmission in the BGS.

DA-DEPLETED STN NEURONS GENERATE REPETITIVE BURSTS OF GLUTAMATERGIC EPSCs

In control BGS, IC or rostral STN stimulation (100–500 μ A, 100 μ s) evoked in STN neurons small amplitude (peak amplitude: -105 ± 5 pA, time to peak 10.3 ± 0.7 ms) and short duration (35 ± 2 ms) EPSCs with a mean latency of 2.9 ± 0.1 ms (total charge: 0.80 ± 0.05 nA.ms) in whole-cell recorded STN neurons ($V_H = -70$ mV, $n = 7$). The corresponding EPSP recorded in current

clamp mode, was of longer duration (116 ± 6 ms at $V_m = -70$ mV, range 58–225 ms, $n = 7$), due to the activation of depolarizing voltage-gated currents in the STN neuronal membrane. It gave rise to only one or two spikes ($V_m = -60$ mV; **Figure 1A**, left).

After reserpine treatment, the IC or STN-evoked EPSC in STN neurons had a lower threshold (60–100 μ A instead of 200–300 μ A), was intensity-dependent and strikingly amplified (**Figure 1A**, right). It had a higher amplitude (-166 ± 11 pA) and a longer duration (109 ± 18 ms) than the EPSC recorded in control STN ($n = 11$; $P < 0.001$ for both). Overall, DA depletion increased the total charge approximately fourfold (3.5 ± 0.5 nA.ms; **Figure 1A**, bottom histograms). In corresponding current clamp recordings, the IC or STN-evoked EPSP was also largely increased in duration (543 ± 14 ms at $V_m = -70$ mV, range 360–730 ms) and gave rise to trains of spikes (4–14 spikes) at 35 ± 1 Hz ($n = 7$). Sometimes, the evoked EPSCs reverberated in STN neurons up to seven times after

a single, brief IC stimulation (**Figure 1B**). The total mean duration of the reverberations after a single shock delivered to the IC was 1117 ± 103 ms and their mean frequency was 4.5 ± 0.5 Hz (total charge: 20 ± 1 nA.ms, $n = 5$). Interestingly, spontaneous, repetitive bursts of EPSCs were also recorded from STN neurons in cell-attached (not shown) or whole-cell (**Figure 1C**) configuration in the absence of any stimulation. Evoked and spontaneous bursts of EPSCs were totally abolished by the application of glutamatergic antagonists (APV 50 μ M + CNQX 10 μ M; data not shown). We next tested whether STN bursts propagate to GP neurons.

STN-GENERATED BURSTS OF EPSCs PROPAGATE TO GP NEURONS

Previous studies showed that brief high intensity STN stimulation evoked long lasting compound EPSCs in target neurons of the STN (GP, EP, and SNr neurons) in sagittal or horizontal slices from control mice (Shen and Johnson, 2006; Ammari et al., 2010).

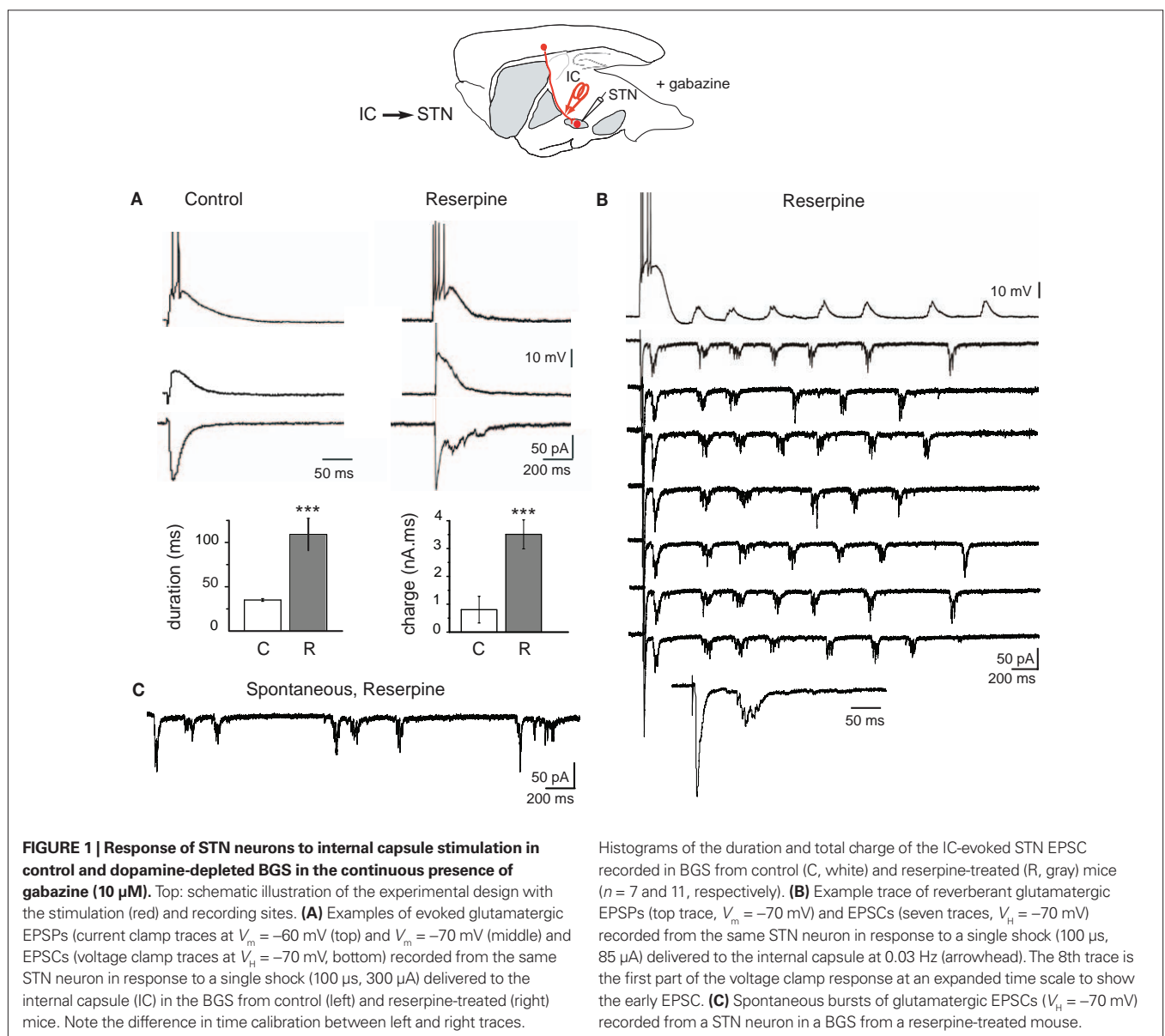


FIGURE 1 | Response of STN neurons to internal capsule stimulation in control and dopamine-depleted BGS in the continuous presence of gabazine (10 μ M). Top: schematic illustration of the experimental design with the stimulation (red) and recording sites. **(A)** Examples of evoked glutamatergic EPSPs (current clamp traces at $V_m = -60$ mV (top) and $V_m = -70$ mV (middle) and EPSCs (voltage clamp traces at $V_H = -70$ mV, bottom) recorded from the same STN neuron in response to a single shock (100 μ s, 300 μ A) delivered to the internal capsule (IC) in the BGS from control (left) and reserpine-treated (right) mice. Note the difference in time calibration between left and right traces.

Histograms of the duration and total charge of the IC-evoked STN EPSC recorded in BGS from control (C, white) and reserpine-treated (R, gray) mice ($n = 7$ and 11, respectively). **(B)** Example trace of reverberant glutamatergic EPSPs (top trace, $V_m = -70$ mV) and EPSCs (seven traces, $V_H = -70$ mV) recorded from the same STN neuron in response to a single shock (100 μ s, 85 μ A) delivered to the internal capsule at 0.03 Hz (arrowhead). The 8th trace is the first part of the voltage clamp response at an expanded time scale to show the early EPSC. **(C)** Spontaneous bursts of glutamatergic EPSCs ($V_H = -70$ mV) recorded from a STN neuron in a BGS from a reserpine-treated mouse.

These responses consisted of an early monosynaptic EPSC followed by a barrage of polysynaptic EPSCs which dramatically prolonged the response up to several hundreds of milliseconds. The late polysynaptic glutamatergic component depended on the presence of the STN cell bodies in the slice. When the same experiment was performed in DA-depleted BGS we observed that the threshold STN stimulation for the generation of the late barrage of polysynaptic EPSCs in GP neurons was lowered by a factor of two to three (from 200 to 60–100 μ A, single pulse, 100 μ s duration). At intensities 1.5 times the threshold of the late component, the duration, and total charge of the late component in reserpine slices were increased compared to control slices (non-significant change from 510 ± 141 ms to 739 ± 150 ms for the duration and significant increase from 5.3 ± 1.0 to 19.4 ± 1.2 nA.ms for the charge, $P < 0.001$; $n = 12$ GP control and $n = 5$ GP reserpine; **Figures 2A,C**). In cell-attached and whole-cell current clamp recordings, compound EPSCs gave rise to long lasting bursts of spikes in GP neurons (**Figure 2B**).

The late polysynaptic component of the compound EPSC could reverberate three to five times at a mean frequency of 4.8 ± 0.6 Hz in response to a single and brief (100 μ s) STN stimulation (total duration of the reverberations: 1480 ± 194 ms, total charge 31 ± 2.8 nA.ms, $n = 5$; **Figure 2D**). These reverberating bursts of EPSCs gave rise to reverberant bursts of spikes in cell-attached recordings (**Figure 2E**). Finally, spontaneous, APV/CNQX-sensitive bursts of EPSCs were sometimes recorded in the absence of any stimulation in DA-depleted GP neurons (not shown). We next tested the role of high frequency STN stimulation (STN-HFS) on the activity of the STN-GP glutamatergic synapses in the DA-depleted BGS.

STN-HFS REPLACED LONG LASTING BURSTS OF EPSCs IN GP NEURONS BY SMALL AMPLITUDE EPSCs

We recorded the glutamatergic activity of GP neurons during stimulation of the STN at 8–10 or 90–120 Hz. We used the voltage clamp mode ($V_H = -70$ mV) to analyze the STN-GP synaptic glutamatergic transmission without participation of depolarization-gated membrane currents. The same parameters of STN stimulation (100 μ s, 300 μ A) that at 0.03 Hz reliably evoked long lasting compound EPSCs in GP neurons in the DA-depleted BGS (mean amplitude -176.7 ± 8.7 pA, $n = 5$), only evoked short duration EPSCs after 3–5 min of 8–10 Hz stimulation (steady state; **Figure 3A**). In the 100-ms interval between the 8–10 Hz stimuli, we observed several small amplitude EPSCs (**Figures 3A bottom,C**). They had a mean amplitude of 20.1 ± 0.5 pA and a mean frequency of 42 ± 2 Hz ($n = 1087$ events). STN-HFS at 90–120 Hz for 3–5 min evoked significantly smaller EPSCs (12.9 ± 0.2 pA) at a significantly lower mean frequency (19.6 ± 3.0 Hz, $n = 1010$ events; **Figures 3B–D**). The dramatic weakening of the STN-GP synaptic transmission by STN-HFS is also supported by the dramatic reduction of mean charge of the evoked EPSCs: from 3500 ± 500 pA.ms (reserpine, see above) to 78 ± 2 pA.ms (10 Hz) and 49 ± 1 pA.ms (100 Hz).

We also compared these EPSCs evoked by STN-HFS ($_{HFS}$ EPSCs) to spontaneous EPSCs (sEPSCs) recorded before the stimulation from the same GP neurons (**Figures 4A,B**). Spontaneous EPSCs from DA-depleted GP neurons had a mean amplitude of 17.9 ± 1.5 pA (range: 2.8–48.2 pA) with a mean frequency of 5.5 ± 1.2 Hz (range inter sEPSC intervals: 1.5–1653 ms, $n = 1085$

events; **Figures 4A,C**). STN-HFS at 100 Hz evoked $_{HFS}$ EPSCs of significantly smaller amplitude than that of sEPSCs (0 Hz) and of $_{HFS}$ EPSCs recorded during 10 Hz (notice that the mean amplitudes of EPSCs were not significantly different between 0 and 10 Hz, $P = 0.1$; **Figure 4C**). Finally, 100 Hz STN-HFS narrowed the distribution of $_{HFS}$ EPSCs amplitude since it suppressed the occurrence of $_{HFS}$ EPSCs over 40 pA (range 2.2–38 pA) compared to 10 Hz STN-HFS (2.1–92 pA; **Figure 4D**). But both 10 and 100 Hz STN-HFS strikingly narrowed the distribution of $_{HFS}$ EPSCs frequency compared to that of sEPSCs (inter $_{HFS}$ EPSC intervals: 1.2–181 ms for 10 Hz and 2.7–273 ms for 100 Hz; **Figure 4E**). We could not analyze the pattern (bursty or not) of the $_{HFS}$ EPSCs due to the small amplitude of many of these events.

DISCUSSION

We show that DA-depleted STN neurons without GABA_A synaptic feedback from GP and EP neurons generate bursts of EPSCs lasting several hundreds of milliseconds in response to a single and brief activation of their glutamatergic afferents in the IC. These EPSCs, together with depolarizing voltage-gated currents, give rise to bursts of propagating spikes and activate GP neurons that in turn generate bursts of spikes. Moreover, a single stimulus produced repetitive bursts along the STN-GP pathway due to the reverberation of IC-evoked bursts in STN neurons, suggesting that the STN alone becomes responsible for the well-known bursting pattern recorded *in vivo* in the parkinsonian state. Feedback IPSCs from GP neurons may synchronize and amplify cortically evoked bursts in STN neurons (Baufreton and Bevan, 2008) but are not instrumental for repetitive bursting.

We propose that the dopaminergic synapses afferent to STN neurons control the afferent glutamatergic synapses to the STN and the glutamatergic polysynaptic network within the STN. As previously shown in control condition (Ammari et al., 2010), this dopaminergic control can be counterbalanced by a strong excitatory input to the STN, allowing the STN polysynaptic network generating a long lasting excitation of its target neurons. Likewise, STN neurons can provide, when needed, a widespread and time-locked reset of target neurons activity (Frank, 2006). In the chronic absence of dopaminergic control, this reset would become repetitive and out of control. This would explain why HFS at the level of the STN remains an efficient way to ameliorate parkinsonian symptoms (Benabid et al., 2009).

There are two sequential amplifications of incoming excitation in the STN: one occurs at the level of synaptic connections to and/or between STN neurons, and the other is intrinsic to the STN neuronal membrane. The STN is innervated by dopamine-containing pathways that arise from the substantia nigra compacta (SNc) and the ventral tegmental area (Brown et al., 1979; Meibach and Katzman, 1979; Hassani et al., 1997). Tyrosine hydroxylase positive axons form asymmetric synapses and release DA in a Ca²⁺-dependent manner in the STN (Cragg et al., 2004). Dopamine D₁- and D₂-like receptor subtypes are both expressed in the STN (Mansour et al., 1990; Flores et al., 1999). Dopamine reduces the amplitude of evoked glutamate EPSCs of control STN neurons by over 30% *in vitro* (Shen and Johnson, 2000). Although the precise site of action of dopamine is unknown, removal of this inhibition could explain the increased STN response to incoming excitation in DA-depleted state.

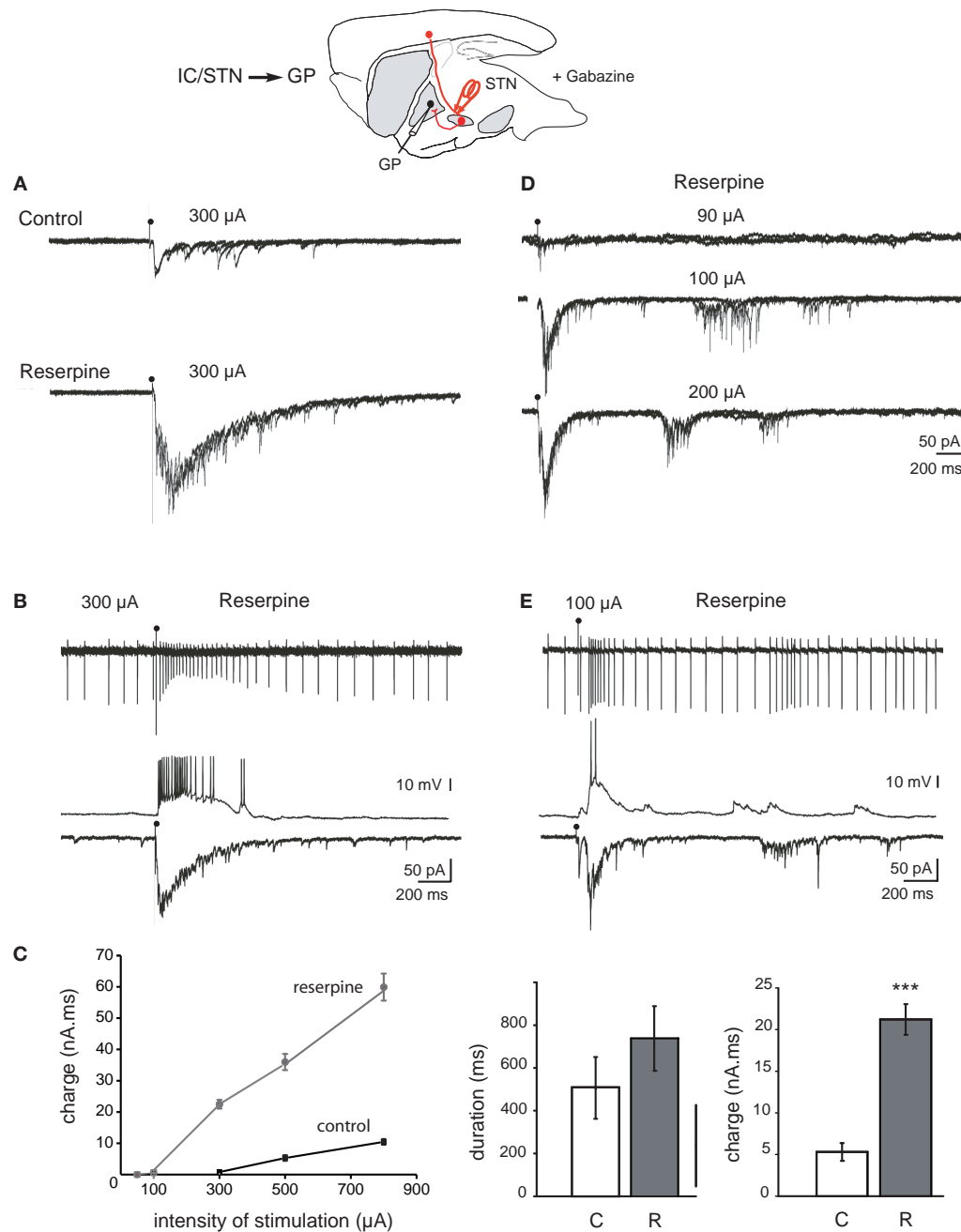


FIGURE 2 | Response of GP neurons to stimulation of the internal capsule or rostral STN in control and dopamine-depleted BGS. Top: Schematic illustration of the experimental design with the stimulation (red) and recording sites. **(A)** Example traces from GP cells recorded from control BGS (top) and BGS from a reserpinized mouse (bottom). A single shock (100 μ s, 300 μ A) was delivered with the same stimulating electrode to the rostral pole of the STN at the time of the artifact. It evoked compound glutamatergic EPSCs ($V_H = -70$ mV, three superimposed traces). **(B)** Recordings from the same GP neuron in cell-attached current clamp mode (top), whole-cell current clamp mode (middle, $V_m = -60$ mV) and whole-cell voltage clamp mode (bottom, $V_H = -70$ mV) in a BGS from a reserpinized mouse. A single shock delivered to the rostral pole of the STN (100 μ s, 300 μ A) evoked a long lasting train of spikes, an EPSP giving rise to a long lasting train of spikes and a compound

EPSC. **(C)** Total charge (nA.ms) of the compound EPSCs recorded in **(A)** as a function of the intensity of stimulation (μ A; black circles: control, gray circles: reserpine). Histograms of the duration (left), and charge (right) of the compound EPSCs evoked in control (white, C) and reserpine (gray, R) conditions with the same stimulating electrode and at the same intensity of stimulation (300 μ A). **(D)** Reverberating bursts of EPSCs recorded from the same GP neuron in a BGS from a reserpinized mouse. A single shock (100 μ s, arrow head) was delivered to the rostral pole of the STN at the indicated intensities. **(E)** Example trace of a reverberant glutamatergic train of spikes (cell-attached, top), EPSPs (whole-cell, $V_m = -60$ mV, middle) and bursts of EPSCs (whole-cell, $V_H = -70$ mV, bottom) recorded from the same GP neuron in a BGS from a reserpinized mouse, in response to a single shock (100 μ s, 85 μ A) delivered to the rostral pole of the STN.

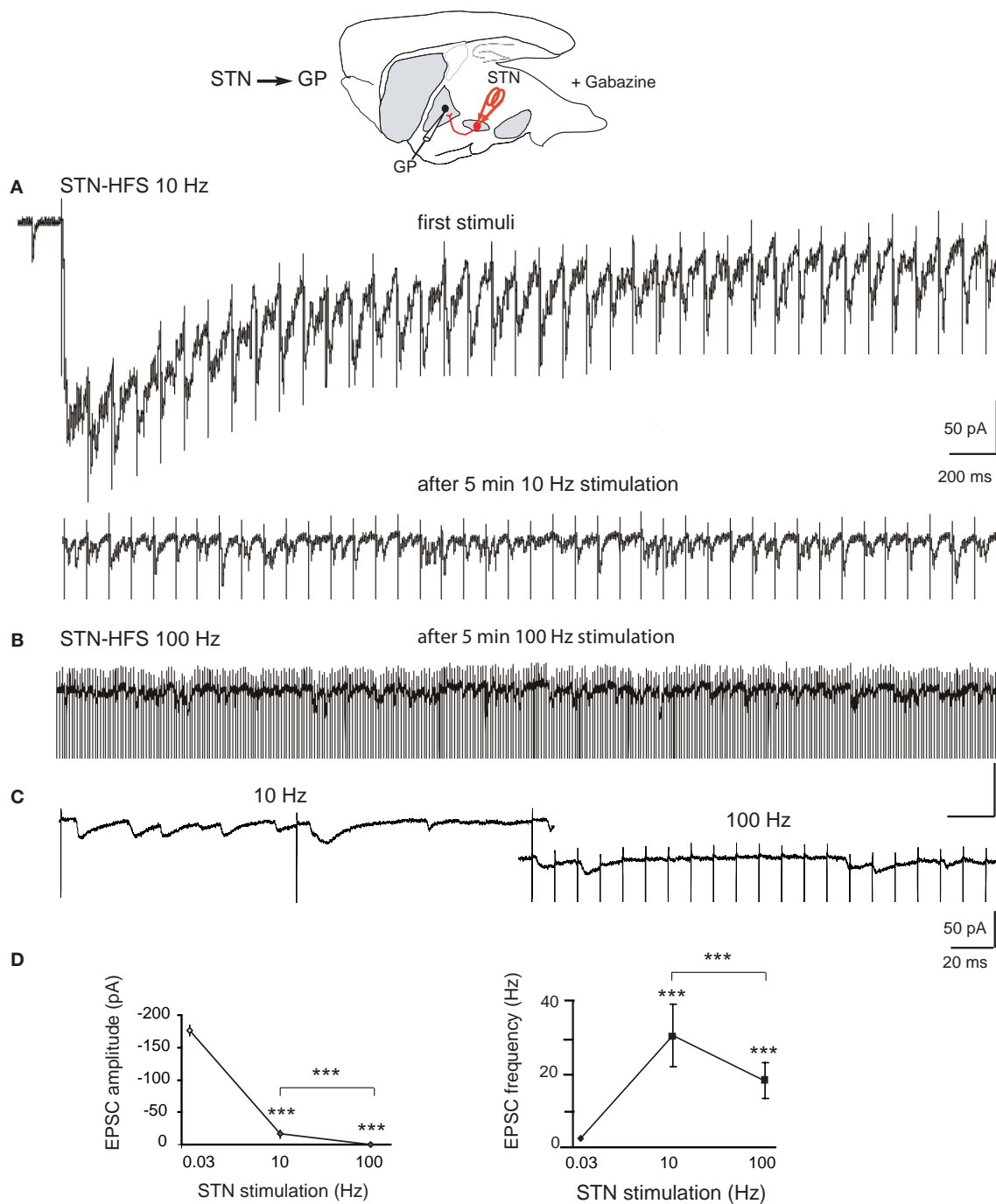


FIGURE 3 | Effects of STN-HFS on the EPSCs evoked in GP neurons in dopamine-depleted BGS. Top: Schematic illustration of the experimental design with the stimulation (red) and recording sites. **(A)** STN-HFS at 10 Hz evoked EPSCs at 10 Hz. Note that HFS causes an initial shift in holding current that is caused by time-dependent summation of the late components of compound EPSCs. After 5 min of 10 Hz stimulation, the EPSCs evoked in the same GP neuron had a lower amplitude. **(B)** STN-evoked glutamatergic EPSCs

recorded in the same GP neuron as in **(A)** during STN-HFS at 100 Hz. **(C)**: Close up of traces under 10 and 100 Hz STN-HFS. **(D)** Averaged data showing the effects of 10 and 100 Hz STN stimulation compared to 0.03 Hz (control) on the amplitude and frequency of the EPSCs evoked in DA-depleted GP neurons. Each data point is the mean \pm SEM. For the response at 0.03 Hz we considered the complex response as a whole and plotted its peak amplitude and frequency as if it were a single EPSC.

The second amplification is achieved by the depolarizing voltage-dependent currents of the STN membrane activated by EPSPs. These include the NMDA (Standaert et al., 1994), Ca^{2+} (Beurrier et al., 1999; Song et al., 2000), persistent Na^+ (Bevan and

Wilson, 1999; Beurrier et al., 2000) and Ca^{2+} -activated depolarizing cationic (Beurrier et al., 1999; Zhu et al., 2004) currents which all prolong the STN firing period in response to the stimulation of glutamatergic afferents (Otsuka et al., 2001; Kass and Mintz, 2006).

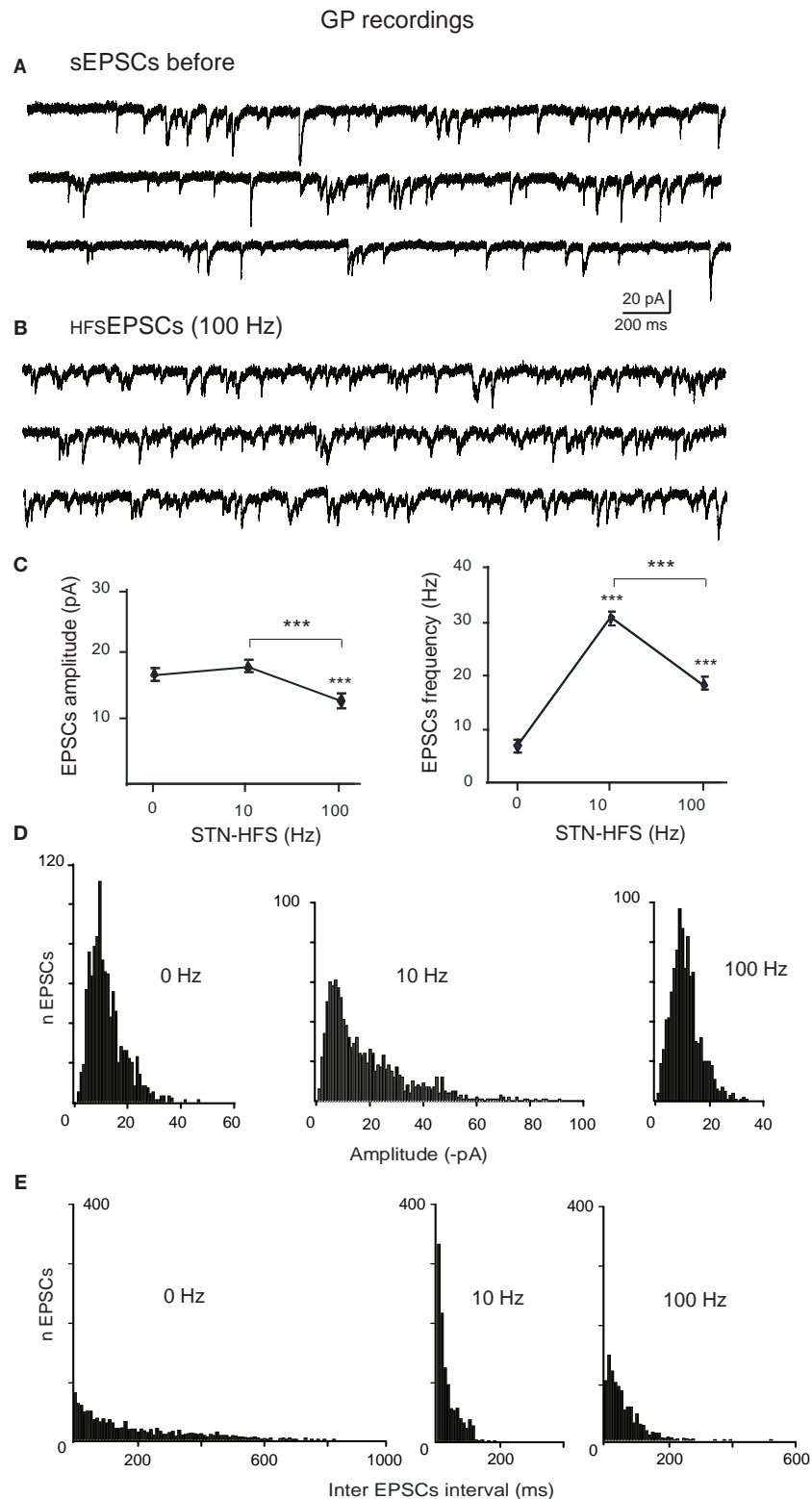


FIGURE 4 | Comparison of spontaneous glutamatergic EPSCs recorded before and during STN-HFS. (A) Three example traces showing the spontaneous EPSCs (sEPSCs) recorded in voltage clamp mode ($V_H = -70$ mV) from a GP neuron in a BGS from a reserpinized mouse. **(B)** Three example traces from the same GP neuron as in **(A)** showing the EPSCs recorded during STN-HFS at 100 Hz (I_{HFS} EPSCs, filtered traces without stimulation artifacts). **(C)**

Average data showing the effects of 10 and 100 Hz STN stimulation compared to before HFS (0 Hz) on the amplitude and frequency of the EPSCs recorded in DA-depleted GP neurons. Each data point is the mean \pm SEM. Histograms of the amplitudes [bin 1 pA, **(D)**] and inter EPSCs intervals [bin 10 ms, **(E)**] for the spontaneous EPSCs (0 Hz) and the I_{HFS} EPSCs recorded during 10 or 100 Hz STN stimulation in the same GP neuron, as indicated.

Kass and Mintz (2006) showed that STN neurons produce various patterns of activity when synaptically activated: silence, classical tonic firing, plateau potentials, burst responses, and rhythmic bursts. This allows STN neurons to adapt their pattern of activity to the environmental context. How these intrinsic membrane currents are affected by the chronic reduction of dopaminergic synaptic transmission is largely unknown (Baufreton and Bevan, 2008). Overall, the resultant effect of dopamine depletion is an increased impact of cortical afferents on neuronal activity in the STN (Magill et al., 2001).

In vivo studies also suggest that the cortico-STN pathway malfunctions in the chronic absence of dopamine. The coherent oscillations between cortical regions and STN neurons recorded from anaesthetized, chronically 6-OHDA-lesioned rats (Sharott et al., 2005; Mallet et al., 2008) and un-medicated parkinsonian patients (Eusebio et al., 2009) are predominantly led by activity in the cortex (Magill et al., 2001; Litvak et al., 2011). The glutamatergic hyperdirect pathway is the likely candidate, but *in vivo* trans-striatal influences via the external globus pallidus (Bevan et al., 2002) cannot be excluded. Malfunction of the cortico-STN pathway, possibly reinforced by the feedback STN-cortex (Degos et al., 2008) and local STN-STN (Shen and Johnson, 2006; Ammari et al., 2010) glutamatergic pathways, in the absence of dopamine, is also supported by the beneficial effect of high frequency stimulation of motor cortical areas on parkinsonian motor symptoms (Drouot et al., 2004; Fregni et al., 2006; Gradinaru et al., 2009; Lefaucheur, 2009).

In their dynamic model of STN neurons, Gillies and Willshaw (2004) predicted that when recurrent glutamatergic synapses between STN neurons are rare (3% of connectivity among STN neurons; Kita et al., 1983) and/or of low synaptic weight, direct cortical drive can push large interconnected regions of the STN into a uniform high state as observed *in vivo* (Magill et al., 2004). As a consequence, glutamatergic STN neurons may therefore not only provide a drive to target neurons in their resting low state (Robledo and Feger, 1990), but also a widespread reset when stimulated into the high activity state. This situation has been experimentally described *in vitro* in all target neurons of the STN (SNr, GP, and EP neurons) in response to high intensity STN stimulation (Ammari et al., 2010). When the synaptic weight of recurrent collaterals is increased, the model predicts that oscillatory behavior can emerge. If we hypothesize that dopamine controls the weight of recurrent collateral synapses in the STN, this model explains the present results in the dopamine-depleted state.

The mechanisms of action of STN-HFS on the activity of STN target neurons have been rarely analyzed from *in vivo* or *ex vivo* preparations from animal models of Parkinson's disease.

REFERENCES

- Ammari, R., Lopez, C., Bioulac, B., Garcia, L., and Hammond, C. (2010). Subthalamic nucleus evokes similar long lasting glutamatergic excitations in pallidal, entopeduncular and nigral neurons in the basal ganglia slice. *Neuroscience* 166, 808–818.
- Baufreton, J., Atherton, J. F., Surmeier, D. J., and Bevan, M. D. (2005). Enhancement of excitatory synaptic integration by GABAergic inhibition in the subthalamic nucleus. *J. Neurosci.* 25, 8505–8517.
- Baufreton, J., and Bevan, M. D. (2008). D-2-like dopamine receptor-mediated modulation of activity-dependent plasticity at GABAergic synapses in the subthalamic nucleus. *J. Physiol. (Lond.)* 586, 2121–2142.
- Benabid, A. L., Chabardes, S., Torres, N., Piallat, B., Krack, P., Fraix, V., and Pollak, P. (2009). Functional neurosurgery for movement disorders: a historical perspective. *Prog. Brain Res.* 175, 379–391.
- Benazzouz, A., Gao, D. M., Ni, Z. G., Piallat, B., Bouali-Benazzouz, R., and Benabid, A. L. (2000). Effect of high-frequency stimulation of the subthalamic nucleus on the neuronal activities of the substantia nigra pars reticulata and ventrolateral nucleus of the thalamus in the rat. *Neuroscience* 99, 289–295.
- Bergman, H., Wichmann, T., Karmon, B., and DeLong, M. R. (1994). The primate subthalamic nucleus. II. Neuronal activity in the MPTP model of parkinsonism. *J. Neurophysiol.* 72, 507–520.
- Beurrier, C., Ben-Ari, Y., and Hammond, C. (2006). Preservation of the direct and indirect pathways in an *in vitro*

In MPTP-treated monkeys, STN-HFS drives the activity of GP (Hashimoto et al., 2003) and SNr (Galati et al., 2006) neurons, whereas it inhibits SNr neurons in 6-hydroxydopamine lesioned rats (Benazzouz et al., 2000). In neuroleptic-treated rats, STN-HFS, at parameters that reverse catalepsy in freely moving animals, either excited or inhibited the firing of SNr neurons. However, the net resultant effect was a reshaping of their firing into a tonic and regular mode (Degos et al., 2005; Deniau et al., 2010). We have previously shown that the polysynaptic late component of the STN-evoked compound EPSC in GP neurons is suppressed by 10 Hz stimulation (Ammari et al., 2010) as in SNr neurons (Shen and Johnson, 2008) in control slices. The present results show that 10 Hz stimulation depresses the late component of the compound EPSC in DA-depleted GP neurons, but leaves some late EPSCs during the interstimulus interval. STN-HFS at 100 Hz is more efficient at weakening the transmission along the STN-GP pathway because it reduces the amplitude of all EPSCs. This form of depression could result from desensitization (Jones and Westbrook, 1996), internalization (Carroll et al., 1999) and surface trafficking (Choquet, 2010) of AMPA receptors.

In previous studies we showed that STN-HFS suppresses endogenous firing of STN somas and drives their activity probably via antidromic activation of their efferent axons (Garcia et al., 2003, 2005). The present study shows that orthodromically, STN-HFS not only suppresses the transmission of cortically evoked, pathological oscillations from STN to GP neurons but also introduces small amplitude HFS-evoked, postsynaptic EPSCs, that could be considered as a “stimulated resting” glutamatergic noise. This new regular synaptic noise under HFS could serve to regularize GP neuronal firing and re-establish synaptic integrative properties of GP neurons.

CONCLUSION

We propose that dopamine depletion transforms the STN into a central generator of bursts in which glutamatergic, rather than GABAergic, inputs to the STN play a central role. Transmission of these pathological oscillations to target neurons of the STN is readily interrupted by STN-HFS.

ACKNOWLEDGMENTS

Supported by Institut National de la Santé et de la Recherche Médicale (Inserm), Centre National de la Recherche Scientifique (CNRS), and grant from ERA-Net Neuron (PhysDBS). Rachida Ammari was supported by a PhD grant from the Ministère de la Recherche et de la technologie (MRT) and Fondation pour la Recherche Médicale (FRM).

- preparation of the mouse basal ganglia. *Neuroscience*. 140, 77–86.
- Beurrier, C., Bioulac, B., and Hammond, C. (2000). Slowly inactivating sodium current (INap) underlies single-spike activity in rat subthalamic neurons. *J. Neurophysiol.* 83, 1951–1957.
- Beurrier, C., Congar, P., Bioulac, B., and Hammond, C. (1999). Subthalamic nucleus neurons switch from single-spike activity to burst-firing mode. *J. Neurosci.* 19, 599–609.
- Bevan, M. D., Atherton, J. F., and Baufreton, J. (2006). Cellular principles underlying normal and pathological activity in the subthalamic nucleus. *Curr. Opin. Neurobiol.* 16, 621–628.
- Bevan, M. D., Hallworth, N. E., and Baufreton, J. (2007). GABAergic control of the subthalamic nucleus. *Prog. Brain Res.* 160, 173–188.
- Bevan, M. D., Magill, P. J., Terman, D., Bolam, J. P., and Wilson, C. J. (2002). Move to the rhythm: oscillations in the subthalamic nucleus-external globus pallidus network. *Trends Neurosci.* 25, 525–531.
- Bevan, M. D., and Wilson, C. J. (1999). Mechanisms underlying spontaneous oscillation and rhythmic firing in rat subthalamic neurons. *J. Neurosci.* 19, 7617–7628.
- Brown, L. L., Markman, M. H., Wolfson, L. I., Dvorkin, B., Warner, C., and Katzman, R. (1979). A direct role of dopamine in the rat subthalamic nucleus and an adjacent intrapeduncular area. *Science* 206, 1416–1418.
- Carroll, R. C., Lissin, D. V., von, Z. M., Nicoll, R. A., and Malenka, R. C. (1999). Rapid redistribution of glutamate receptors contributes to long-term depression in hippocampal cultures. *Nat. Neurosci.* 2, 454–460.
- Choquet, D. (2010). Fast AMPAR trafficking for a high-frequency synaptic transmission. *Eur. J. Neurosci.* 32, 250–260.
- Cragg, S. J., Baufreton, J., Xue, Y., Bolam, J. P., and Bevan, M. D. (2004). Synaptic release of dopamine in the subthalamic nucleus. *Eur. J. Neurosci.* 20, 1788–1802.
- Degos, B., Deniau, J. M., Le, C. J., Mailly, P., and Maurice, N. (2008). Evidence for a direct subthalamo-cortical loop circuit in the rat. *Eur. J. Neurosci.* 27, 2599–2610.
- Degos, B., Deniau, J. M., Thierry, A. M., Glowinski, J., Pezard, L., and Maurice, N. (2005). Neuroleptic-induced catalepsy: electrophysiological mechanisms of functional recovery induced by high-frequency stimulation of the subthalamic nucleus. *J. Neurosci.* 25, 7687–7696.
- Deniau, J. M., Degos, B., Bosch, C., and Maurice, N. (2010). Deep brain stimulation mechanisms: beyond the concept of local functional inhibition. *Eur. J. Neurosci.* 32, 1080–1091.
- Drouot, X., Oshino, S., Jarraya, B., Besret, L., Kishima, H., Remy, P., Dauguet, J., Lefaucheur, J. P., Dolle, F., Conde, F., Bottlaender, M., Peschanski, M., Keravel, Y., Hantraye, P., and Palfi, S. (2004). Functional recovery in a primate model of Parkinson's disease following motor cortex stimulation. *Neuron* 44, 769–778.
- Eusebio, A., Pogossyan, A., Wang, S., Averbach, B., Gaynor, L. D., Cantiniaux, S., Witjas, T., Limousin, P., Azulay, J. P., and Brown, P. (2009). Resonance in subthalamo-cortical circuits in Parkinson's disease. *Brain* 132, 2139–2150.
- Flores, G., Liang, J. J., Sierra, A., Martinez-Fong, D., Quirion, R., Aceves, J., and Srivastava, L. K. (1999). Expression of dopamine receptors in the subthalamic nucleus of the rat: characterization using reverse transcriptase-polymerase chain reaction and autoradiography. *Neuroscience* 91, 549–556.
- Frank, M. J. (2006). Hold your horses: a dynamic computational role for the subthalamic nucleus in decision making. *Neural Netw.* 19, 1120–1136.
- Fregni, F., Boggio, P. S., Santos, M. C., Lima, M., Vieira, A. L., Rigonatti, S. P., Silva, M. T., Barbosa, E. R., Nitsche, M. A., and Pascual-Leone, A. (2006). Noninvasive cortical stimulation with transcranial direct current stimulation in Parkinson's disease. *Mov. Disord.* 21, 1693–1702.
- Galati, S., Mazzone, P., Fedele, E., Pisani, A., Peppe, A., Pierantozzi, M., Brusa, L., Tropepi, D., Moschella, V., Raiteri, M., Stanzione, P., Bernardi, G., and Stefani, A. (2006). Biochemical and electrophysiological changes of substantia nigra pars reticulata driven by subthalamic stimulation in patients with Parkinson's disease. *Eur. J. Neurosci.* 23, 2923–2928.
- Garcia, L., Audin, J., D'Alessandro, G., Bioulac, B., and Hammond, C. (2003). Dual effect of high-frequency stimulation on subthalamic neuron activity. *J. Neurosci.* 23, 8743–8751.
- Garcia, L., D'Alessandro, G., Fernagut, P. O., Bioulac, B., and Hammond, C. (2005). The impact of high frequency stimulation parameters on the pattern of discharge of subthalamic neurons. *J. Neurophysiol.* 94, 3362–3369.
- Gillies, A., and Willshaw, D. (2004). Models of the subthalamic nucleus. The importance of intranuclear connectivity. *Med. Eng. Phys.* 26, 723–732.
- Gradinaru, V., Mogri, M., Thompson, K. R., Henderson, J. M., and Deisseroth, K. (2009). Optical deconstruction of parkinsonian neural circuitry. *Science* 324, 354–359.
- Hammond, C., Bergman, H., and Brown, P. (2007). Pathological synchronization in Parkinson's disease: networks, models and treatments. *Trends Neurosci.* 30, 357–364.
- Hashimoto, T., Elder, C. M., Okun, M. S., Patrick, S. K., and Vitek, J. L. (2003). Stimulation of the subthalamic nucleus changes the firing pattern of pallidal neurons. *J. Neurosci.* 23, 1916–1923.
- Hassani, O. K., Francois, C., Yelnik, J., and Feger, J. (1997). Evidence for a dopaminergic innervation of the subthalamic nucleus in the rat. *Brain Res.* 749, 88–94.
- Jones, M. V., and Westbrook, G. L. (1996). The impact of receptor desensitization on fast synaptic transmission. *Trends Neurosci.* 19, 96–101.
- Kass, J. I., and Mintz, I. M. (2006). Silent plateau potentials, rhythmic bursts, and pacemaker firing: three patterns of activity that coexist in quadrastable subthalamic neurons. *Proc. Natl. Acad. Sci. U.S.A.* 103, 183–188.
- Kita, H., Chang, H. T., and Kitai, S. T. (1983). The morphology of intracellularly labeled rat subthalamic neurons: a light microscopic analysis. *J. Comp. Neurol.* 215, 245–257.
- Lefaucheur, J. P. (2009). Treatment of Parkinson's disease by cortical stimulation. *Expert Rev. Neurother.* 9, 1755–1771.
- Litvak, V., Jha, A., Eusebio, A., Oostenveld, R., Foltynie, T., Limousin, P., Zrinzo, L., Hariz, M. I., Friston, K., and Brown, P. (2011). Resting oscillatory cortico-subthalamic connectivity in patients with Parkinson's disease. *Brain* 134, 359–374.
- Magill, P. J., Bolam, J. P., and Bevan, M. D. (2001). Dopamine regulates the impact of the cerebral cortex on the subthalamic nucleus-globus pallidus network. *Neuroscience* 106, 313–330.
- Magill, P. J., Sharott, A., Bevan, M. D., Brown, P., and Bolam, J. P. (2004). Synchronous unit activity and local field potentials evoked in the subthalamic nucleus by cortical stimulation. *J. Neurophysiol.* 92, 700–714.
- Mallet, N., Pogossyan, A., Sharott, A., Csicsvari, J., Bolam, J. P., Brown, P., and Magill, P. J. (2008). Disrupted dopamine transmission and the emergence of exaggerated beta oscillations in subthalamic nucleus and cerebral cortex. *J. Neurosci.* 28, 4795–4806.
- Mansour, A., Meador-Woodruff, J. H., Bunzow, J. R., Civelli, O., Akil, H., and Watson, S. J. (1990). Localization of dopamine D2 receptor mRNA and D1 and D2 receptor binding in the rat brain and pituitary: an in situ hybridization-receptor autoradiographic analysis. *J. Neurosci.* 10, 2587–2600.
- Meibach, R. C., and Katzman, R. (1979). Catecholaminergic innervation of the subthalamic nucleus: evidence for a rostral continuation of the A9 (substantia nigra) dopaminergic cell group. *Brain Res.* 173, 364–368.
- Moody, C. A., and Spear, L. P. (1992). Effects of acute dopamine depletion on responsiveness to D1 and D2 receptor agonists in infant and weanling rat pups. *Psychopharmacology (Berl.)* 107, 39–49.
- Murer, M. G., Riquelme, L. A., Tseng, K. Y., and Pazo, J. H. (1997). Substantia nigra pars reticulata single unit activity in normal and 60HDA-lesioned rats: effects of intrastriatal apomorphine and subthalamic lesions. *Synapse* 27, 278–293.
- Otsuka, T., Murakami, F., and Song, W. J. (2001). Excitatory postsynaptic potentials trigger a plateau potential in rat subthalamic neurons at hyperpolarized states. *J. Neurophysiol.* 86, 1816–1825.
- Plenz, D., and Kitai, S. T. (1999). A basal ganglia pacemaker formed by the subthalamic nucleus and external globus pallidus. *Nature* 400, 677–682.
- Robledo, P., and Feger, J. (1990). Excitatory influence of rat subthalamic nucleus to substantia nigra pars reticulata and the pallidal complex: electrophysiological data. *Brain Res.* 518, 47–54.
- Ryan, L. J., and Sanders, D. J. (1993). Subthalamic nucleus lesion regularizes firing patterns in globus pallidus and substantia nigra pars reticulata neurons in rats. *Brain Res.* 626, 327–331.
- Sharott, A., Magill, P. J., Harnack, D., Kupsch, A., Meissner, W., and Brown, P. (2005). Dopamine depletion increases the power and coherence of beta-oscillations in the cerebral cortex and subthalamic nucleus of the awake rat. *Eur. J. Neurosci.* 21, 1413–1422.
- Shen, K. Z., and Johnson, S. W. (2000). Presynaptic dopamine D2 and muscarinic M3 receptors inhibit excitatory and inhibitory transmission to rat subthalamic neurons in vitro. *J. Physiol.* 525(Pt 2), 331–341.
- Shen, K. Z., and Johnson, S. W. (2006). Subthalamic stimulation evokes complex EPSCs in the rat substantia nigra pars reticulata in vitro. *J. Physiol.* 573, 697–709.
- Shen, K. Z., and Johnson, S. W. (2008). Complex EPSCs evoked in substantia nigra reticulata neurons are disrupted by repetitive stimulation of the subthalamic nucleus. *Synapse* 62, 237–242.
- Song, W. J., Baba, Y., Otsuka, T., and Murakami, F. (2000). Characterization

- of Ca(2+) channels in rat subthalamic nucleus neurons. *J. Neurophysiol.* 84, 2630–2637.
- Standaert, D. G., Testa, C. M., Young, A. B., and Penney, J. B. Jr. (1994). Organization of N-methyl-D-aspartate glutamate receptor gene expression in the basal ganglia of the rat. *J. Comp. Neurol.* 343, 1–16.
- Wilson, C. L., Cash, D., Galley, K., Chapman, H., Lacey, M. G., and Stanford, I. M. (2006). Subthalamic nucleus neurones in slices from 1-methyl-4-phenyl-1,2,3,6-tetrahydropyridine-lesioned mice show irregular, dopamine-reversible firing pattern changes, but without synchronous activity. *Neuroscience* 143, 565–572.
- Zhu, Z. T., Munhall, A., Shen, K. Z., and Johnson, S. W. (2004). Calcium-dependent subthreshold oscillations determine bursting activity induced by N-methyl-D-aspartate in rat subthalamic neurons in vitro. *Eur. J. Neurosci.* 19, 1296–1304.
- Conflict of Interest Statement:** The authors declare that the research was conducted in the absence of any commercial or financial relationships that could be construed as a potential conflict of interest.
- Received: 29 March 2011; accepted: 01 June 2011; published online: 13 June 2011.
- Citation: Ammari R, Bioulac B, Garcia L and Hammond C (2011) The subthalamic nucleus becomes a generator of bursts in the dopamine-depleted state. Its high frequency stimulation dramatically weakens transmission to the globus pallidus. *Front. Syst. Neurosci.* 5:43. doi: 10.3389/fnys.2011.00043
- Copyright © 2011 Ammari, Bioulac, Garcia and Hammond. This is an open-access article subject to a non-exclusive license between the authors and Frontiers Media SA, which permits use, distribution and reproduction in other forums, provided the original authors and source are credited and other Frontiers conditions are complied with.



Cortical potentials evoked by deep brain stimulation in the subthalamic area

Annaelle Devergnas^{1*} and Thomas Wichmann^{1,2}

¹ Wichmann Lab, Division of Neuropharmacology and Neurologic Diseases, Yerkes National Primate Research Center, Emory University, Atlanta, GA, USA

² Department Neurology, School of Medicine, Emory University, Atlanta, GA, USA

Edited by:

James M. Tepper, Rutgers, The State University of New Jersey, USA

Reviewed by:

Gordon Arbutnot, Okinawa Institute of Science and Technology, Japan
Philip Starr, University of California San Francisco, USA

*Correspondence:

Annaelle Devergnas, Yerkes National Primate Research Center, Emory University, 954 Gatewood Road NE, Atlanta, GA 30329, USA.
e-mail: adevergnas@emory.edu

Deep brain stimulation (DBS) of the subthalamic nucleus (STN) has been used since the mid-1990s as a treatment for patients with Parkinson's disease, and more recently also in other conditions, such as dystonia or obsessive compulsive disorder. Non-invasive studies of cortical evoked potentials (EPs) that follow individual STN-DBS stimuli has provided us with insights about the conduction of the DBS pulses to the cortex. Such EPs have multiple components of different latencies, making it possible to distinguish short-latency and long-latency responses (3–8 ms and 18–25 ms latency, respectively). The available evidence indicates that these short- and long-latency EPs correspond to conduction from the STN stimulation site to the cortical recording location via anti- and orthodromic pathways, respectively. In this review we survey the literature from recording studies in human patients treated with STN-DBS for Parkinson's disease and other conditions, as well as recent animal studies (including our own) that have begun to elucidate details of the pathways, frequency dependencies, and other features of EPs. In addition, we comment on the possible clinical utility of this knowledge.

Keywords: cortical evoked potential, deep brain stimulation, subthalamic nucleus

INTRODUCTION

High-frequency stimulation of subcortical brain targets (deep brain stimulation, DBS), specifically of the subthalamic nucleus (STN) is an effective clinical treatment for patients with advanced Parkinson's disease. The effectiveness of DBS is currently under evaluation in other disorders as well, including intractable dystonia (Coubes et al., 2000; Vercueil et al., 2001; Yianni et al., 2003; Vidailhet et al., 2005), obsessive compulsive disorder (Cosyns et al., 2003; Gabriels et al., 2003; Nuttin et al., 2003), or epilepsy (Chabardes et al., 2002, 2008; Hodaie et al., 2002). While the mechanism of action of STN-DBS remains unclear and may differ across functional domains and disease states, authors agree that many of the effects of STN stimulation ultimately involve the modulation of the activities or excitability of the frontal cortex. This belief has prompted a large number of studies of stimulation-related changes in cortical activity patterns. Thus, imaging studies of the effects of STN-DBS have provided unique insight into slow, large-scale changes in cortical activity (Carbon and Eidelberg, 2002), while studies of electrophysiological changes induced by STN-DBS have provided data with higher spatial and temporal resolution. In this review, we review the literature on cortical evoked potentials (EPs) induced by STN-DBS, and supplement this material with some of our own primate recording studies.

RELEVANT CIRCUIT ANATOMY

Knowledge of the anatomy of the circuit elements by which the basal ganglia are connected to regions of the thalamus and cortex is important for an understanding of the mechanisms that are involved in EP generation after electrical stimulation of the STN. As shown in **Figure 1**, the STN is located in a very crowded region of the brain. Only some of the major pathways that may contribute to the generation of EPs are shown in **Figure 1**.

The STN is part of the "indirect" pathway of the basal ganglia. This pathway links the principal input structure of the basal ganglia, the striatum, to the output structures, the internal segment of the globus pallidus (GPi), and the substantia nigra pars reticulata (SNr), via the external segment of the globus pallidus (GPe) and the STN. As part of this pathway, the STN receives GPe inputs, and sends glutamatergic (excitatory) projections to both segments of the globus pallidus and to the SNr. Projections from GPi and SNr are directed to the thalamus (ventral anterior, ventral lateral, and intralaminar nuclei). Thalamic efferents are then directed back to the frontal cortex.

In addition to the indirect pathway connections from the GPe, the STN receives direct cortical inputs. The existence of this projection has been documented several decades ago in rats and monkeys (Monakow et al., 1978; Bevan et al., 1995; Nambu et al., 2000), but the exact anatomical origin(s) of this projection are still debated. Anatomical and electrophysiological studies in rats have indicated that cortical afferents to the STN originate principally from neurons in layer V of the cerebral cortex, with at least some arising as collaterals of corticospinal projections (Donoghue and Kitai, 1981; Kitai and Deniau, 1981; Giuffrida et al., 1985). Cortical stimulation studies in rats have suggested that the cortico-subthalamic projection arises from both the ipsilateral and contralateral cortex (Rouzaire-Dubois and Scarnati, 1985), and that responses of STN neurons to stimulation of the contralateral cortex can be eliminated by sectioning the corpus callosum (Fujimoto and Kita, 1993). Primate studies, in contrast, have indicated that the cortico-subthalamic projection is ipsilateral, and arises from more circumscribed cortical areas (Monakow et al., 1978; Carpenter et al., 1981; Jurgens, 1984; Matsumura et al., 1992; Nambu et al., 1996). In monkeys, projections from the primary motor cortex were shown to terminate in the dorsolateral motor portion of the STN. The

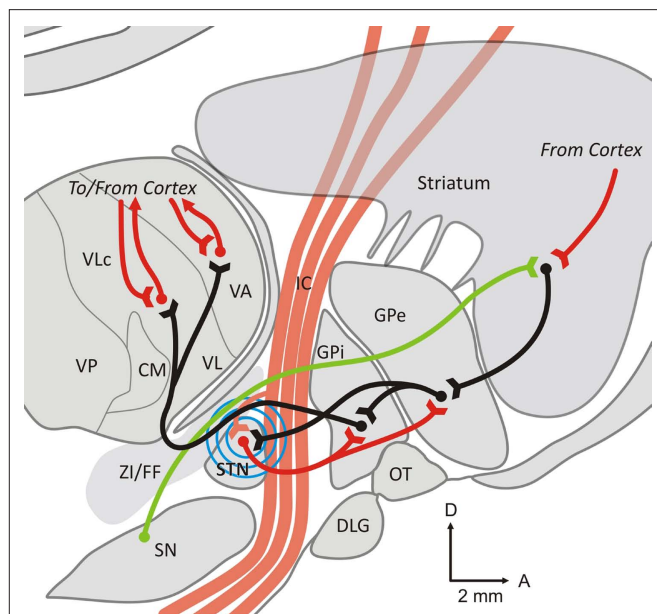


FIGURE 1 | Parasagittal slice through the monkey brain at the L7 level.

The figure shows some of the major anatomical pathways that are affected by STN stimulation, and may contribute to the generation of cortical evoked potentials. Excitatory (glutamatergic) pathways are shown as red lines, inhibitory (GABAergic) connections are shown as black lines, and modulatory dopaminergic fibers as green lines. The blue circles symbolize the spread of the electrical stimulation of the STN. See text for further details.

Abbreviations: CM, centromedian nucleus of the thalamus; DLG, lateral geniculate body; FF, Fields of Forel; IC, internal capsule; GPe, external pallidal segment; GPi, internal pallidal segment; OT, optic tract; Put, putamen; SN, substantia nigra; STN, subthalamic nucleus; VA, ventral anterior nucleus of the thalamus; VL, ventrolateral nucleus of the thalamus; ZI, zona incerta.

premotor and supplementary motor areas project also to the STN but target principally the ventromedial part (partly overlapping with the projection from the primary motor cortex); Region more concerned by oculomotor and associative aspects of the motor behavior (Parent and Hazrati, 1995; Nambu et al., 1996). Although this has not been examined in as much detail, non-motor areas of the frontal cortex are also likely to project to the STN (Monakow et al., 1978; Canteras et al., 1990; Maurice et al., 1998).

Because STN-DBS may not entirely respect nuclear boundaries, it is important to consider the anatomic proximity of the STN to nearby fiber tracts. Only a subset of these fiber tracts are shown in **Figure 1**. The STN abuts and is traversed by medial components of the internal capsule, and is in immediate proximity to the zona incerta (ZI) and the fields of Forel (dorsal to the STN), which contain a variety of fiber tracts, particularly pallido-thalamic fibers (Baron et al., 2001), as well as dopaminergic, serotonergic, and other projections from the brainstem to the striatum and other areas. In addition, cerebello-thalamic fibers travel close to the medial and posterior part of the STN (Yelnik and Percheron, 1979; Chang et al., 1983; Kita et al., 1983; Parent and Hazrati, 1995; Hamani et al., 2004).

MECHANISM OF ACTION OF STN-DBS

The currently used DBS electrodes are bundles of four macroelectrodes whose exposed tips are separated by 0.5–1.5 mm. During DBS procedures, these electrodes are implanted into brain regions

like the STN. Typically, STN-DBS electrodes are implanted into the central STN. The most ventral electrode tends to be implanted at the ventral border of the STN, or may extend into the dorsal SNr. Depending on the contact separation of the specific electrode used, the top contact is either located in the ZI or in the central thalamus. Subsequently, continuous high-frequency stimulation is delivered via an implanted pulse generator which can be externally programmed.

The exact mechanisms of action of DBS remain uncertain. Modeling studies have suggested that the electrical parameter used in clinically effective monopolar stimulation (for instance, stimulation with 130 Hz, and a 90- μ s pulse width) affects axons within a 2.5-mm radius around the contact center (Wu et al., 2001; McIntyre et al., 2004). Depending on the implantation location, this volume of activation includes areas beyond the borders of the STN.

Early explanations of the mechanisms by which STN-DBS produces its antiparkinsonian effects were strongly influenced by the observation that lesions of the basal ganglia output nuclei and DBS of the STN produce roughly similar clinical outcomes in patients with Parkinson's disease (Benabid, 2003), suggesting that both may act to inhibit basal ganglia output. Support for this view came from studies of neuronal activity in the STN neurons during stimulation and from recordings of the neuronal activity in the rodent SNr (Benazzouz et al., 1995, 2000). However, in these studies electrical stimulation artifacts prevented the analysis of recordings during the stimulation, so that only post-stimulation activities could be tested. Several of the more recent studies have used digital stimulus artifact removal techniques (Wichmann, 2000; Hashimoto et al., 2002; Montgomery et al., 2005; Erez et al., 2010), and have either confirmed that basal ganglia output is reduced by STN stimulation (Tai et al., 2003; Meissner et al., 2005; Ma et al., 2007) or shown that it is increased (Hashimoto et al., 2003; Maurice et al., 2003; Montgomery, 2006; Xu et al., 2008; Moran et al., 2010). The conclusion that STN output to the basal ganglia output nuclei may be increased is also supported by microdialysis (Windels et al., 2000, 2003, 2005) and imaging studies (fMRI and PET, see, e.g., Jech et al., 2001; Perlmutter et al., 2002; Hershey et al., 2003).

While there is no agreement on the effects of STN stimulation on the overall firing rates in the basal ganglia, the effects of STN stimulation on activity patterns in the basal ganglia are less controversial. One of the prominent findings in the available studies is that the stimulation appears to entrain basal ganglia output, thus replacing disruptive basal ganglia output with potentially less disruptive rhythmic activities which may act like a “functional lesion” (Hashimoto et al., 2003; Ma et al., 2007; Erez et al., 2009). It is important to realize that the different rate and pattern changes with STN-DBS may not be exclusive of one another. In fact, it has been proposed that STN-DBS may act by several concurrent mechanisms on different various parkinsonian signs (Temperli et al., 2003).

GENERAL FEATURES OF EPs RELATED TO STN-DBS IN CLINICAL STUDIES

Stimulation of the STN with single stimuli or with trains of stimuli produces potentials that can be detected with stimulus-triggered averaging of electroencephalographic (EEG) or electrocorticographic (ECoG) signals in frontal and central cortical

regions. Several studies have reported the presence of such cortical EPs during low-frequency STN stimulation in patients with Parkinson's disease (Limousin et al., 1998; Ashby et al., 2001; Baker et al., 2002; Mackinnon et al., 2005; Eusebio et al., 2009; Kuriakose et al., 2009).

With low-frequency stimulation of the STN, cortical EPs with short (3–8 ms) or long latencies (18–25 ms) can be distinguished. Thus, Ashby et al. (2001) reported the presence of short-latency EPs in almost all of their parkinsonian patients, while a later study found that short-latency EPs were more variable across subjects, occurring in less than half of the electrodes tested (Mackinnon et al., 2005), but that EPs at longer latency (average of 23 ms) occurred more reliably (Mackinnon et al., 2005). Long-latency EPs were also described by other authors in studies which examined EPs in response to stimulation of the contact that yielded the best clinical response (Limousin et al., 1998; Eusebio et al., 2009). In these human studies, the amplitude of EPs strongly depended on the location of the DBS contact(s) used for stimulation, likely reflecting the topography of the STN and of the fiber tracts around it. In contrast, the anatomical distribution and polarity of the potentials were found to be relatively constant across cortical regions, regardless of contact choice. Short- and long-latency EPs were found as positive potentials in the ipsilateral frontal cortex and as negative potentials over the parietal cortex (Mackinnon et al., 2005). Other authors confirmed that the largest short- or long-latency EPs are found in the ipsilateral frontal and central areas (Eusebio et al., 2009; Kuriakose et al., 2009). EPs of short latency were found to be smaller than those of longer latency.

Studies of EPs evoked by STN-area stimulation at clinically used frequencies (80–130 Hz) are limited because the inter-stimulus interval is shorter than the latency of the long-latency EPs. Several studies have, however, examined EPs evoked by stimulation at frequencies between 5 and 30 Hz. Using such stimulation of the electrode contact that gave the best clinical response, the amplitude of the EP was found to be frequency-dependent, with a peak at 20 Hz stimulation, while the latency remained constant, regardless of the stimulation frequency (Eusebio et al., 2009). A more limited comparison of the EPs evoked by STN–DBS of 3 or 30 Hz in parkinsonian patients did not find significant changes in EPs (Kuriakose et al., 2009).

MECHANISMS OF EP GENERATION IN STN–DBS

SHORT-LATENCY EPs

Ashby et al. (2001) found that short-latency frontal cortical EPs have a short chronaxie, a short refractory period, and follow trains of stimuli up to 100 Hz without change in amplitude. These characteristics suggest that the short-latency EPs arise from the activation of low-threshold neuronal elements, such as myelinated axons, rather than from the activation of cell bodies. Given the short latencies, it is likely that such responses are produced by antidromic stimulation of fibers in the vicinity of the STN. The aforementioned high-frequency following is one of the features traditionally used to verify the antidromic spread of neuronal stimulation (Degos et al., 2008), and thus, consistent with the notion that short-latency responses are antidromically mediated. Antidromic transmission from a stimulation site in the STN-area to the cortex has been documented with intracellular recordings of neurons in deep cortical layers in rodents (Li et al., 2007; Gradinaru et al., 2009).

The time needed for *orthodromic* conduction between motor cortex and STN in non-human primates was found to be 5.8 ± 4.5 ms (Nambu et al., 2000). Because of the absence of synaptic delays, *antidromic* conduction can be expected to be at least 1–2 ms faster in these animals, and may be slightly longer in patients. Thus, the latency found for short-latency EPs (3–8 ms in humans) is in the range of antidromically mediated potentials.

Short-latency cortical EPs induced by STN stimulation have been found in anesthetized (Li et al., 2007) and conscious rats (Dejean et al., 2009), consistent with antidromic activation of corticofugal fibers. A detailed current-source density analysis established the source of the recorded waves as layer V (Li et al., 2007). Recent optogenetic experiments in dopamine-depleted rodents also support the concept that STN stimulation has antidromically mediated effects on the cerebral cortex (Gradinaru et al., 2009). In these studies, activation of corticofugal fibers was found to be a prerequisite for the beneficial effects of STN stimulation.

The discussion of antidromic cortical activation focuses on the cortico-subthalamic and corticospinal pathways. It remains unclear whether these pathways are separate or whether the cortico-subthalamic projection is a collateral of the corticospinal projection. If the fiber tract(s) responsible for short-latency EPs terminate in the spinal cord, suprathreshold stimulation would be expected to result not only in the generation of EPs, but also in EMG activation which would be expected to be time-locked to the stimulus. This hypothesis has been tested in several studies. Ashby et al. (1999) found in 14 parkinsonian patients undergoing STN–DBS a short-latency facilitation of EMG in the distal and proximal upper limb muscles, with latencies shorter than those seen in transcortical magnetic stimulation induced in the same subjects. This result was interpreted as suggesting that the activation of the peripheral muscles was not dependent on transcortical transmission, but was directly transmitted from the STN stimulation site to the peripheral muscles (Ashby et al., 1999). The same conclusion was reached in a subsequent study in which the facilitation peaks in the EMG (like short-latency EPs) occurred most consistently with stimulation of ventral contacts of the electrode (Ashby et al., 2001). However, more recent studies have failed to identify EMG activation patterns that are time-locked with STN stimulation (Hanajima et al., 2004; Mackinnon et al., 2005; Kuriakose et al., 2009). The discrepancies between these studies are most easily explained by differences in the location of the stimulating electrodes, the strength of stimulation and other technical differences. The negative outcome of the more recent studies obviously suggests that STN stimulation does not always antidromically activate the corticospinal tract to the extent of activation of peripheral muscles.

In our recent electrophysiologic recording studies in monkeys (Figure 2), we compared the effects of stimulation of the STN on cortical activities with those of stimulation of the GPi. The animals were chronically implanted with EEG recording electrodes, and stimulation electrodes were acutely placed in the center of the STN or into the lateral GPi. We found that only stimulation in the STN produced short-latency cortical EPs, while stimulation at either site produced long-latency EPs (see below), suggesting that only STN stimulation, but not GPi stimulation, antidromically activated fibers related to the motor cortical recording site.

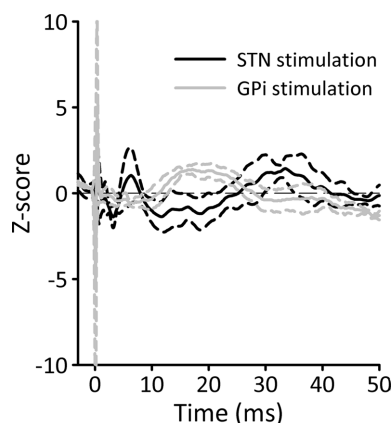


FIGURE 2 | Cortical potentials evoked by STN or GPi stimulation,

recorded in an awake MPTP-treated primate. The animal was chronically implanted with two epidural EEG recording electrodes over the primary motor cortex. Single STN or GPi stimuli were delivered via a constant current source [SNEX-100 bipolar stimulation electrode (Rhodes Medical), biphasic stimulation, 10 Hz, 100 μ s/phase, contact separation, 0.5 mm]. The figure shows EEG potential changes, averaged across 100 stimulation trials. The EEG was recorded with a differential montage between the two electrodes (filter settings 0.5–100 Hz). Prior to averaging, peri-stimulation EEG segments were aligned to the onset of stimulation (Time 0 ms). The solid lines represent the average response (black for STN and gray for GPi) and the dashed lines correspond to the SD.

It remains to be studied whether antidromic activation of fibers of passage is restricted to the motor system, or whether non-motor afferents to the STN are also antidromically activated. Recent anatomical studies have confirmed that the STN receives non-motor inputs (see above). It is possible that STN stimulation produces some of its non-motor side effects on mood, verbal fluency or response inhibition (Aron and Poldrack, 2006; Ballanger et al., 2009; Hershey et al., 2010) via antidromic activation of these non-motor pathways. Differences between GPi and STN stimulation as seen for motor cortex stimulation may also hold for the stimulation of non-motor areas of cortex, which may, in turn, be related to the different non-motor side effect profile of the two procedures (Bronstein et al., 2011). The amplitude of short-latency EPs is typically larger with stimulation via the ventral contacts than with stimulation via the dorsal contacts (Ashby et al., 2001; Mackinnon et al., 2005). It was proposed that the most ventral contacts of the DBS electrode may be closest to myelinated passing fibers in the internal capsule which could be reached by current spread. However, this argument needs to be revisited, because modeling studies have suggested that myelinated fibers are also easily reached with stimulation of the dorsal STN (Mcintyre et al., 2004) and because the density of myelinated fibers within the lateral and rostral STN does not change significantly with the ventral or dorsal location.

Finally, it needs to be recognized that short-latency EPs after STN stimulation may also arise from antidromic transmission of the ZI. The ZI is immediately dorsal to the STN (Parent and Hazrati, 1995) and very likely to be within the area of stimulation during STN-DBS. It receives cortical input from layer V from large frontal areas (Bartho et al., 2002; Bartho et al., 2007). In rats, the heaviest projection to the ZI comes from the cingular cortex, with lesser

contributions from the frontal and parietal cortex (Mitrofanis and Mikuletic, 1999). Most of the downstream projections from the ZI are bilateral, particularly with the brainstem and thalamus (Power and Mitrofanis, 2001).

LONG-LATENCY EPs

The origin of long-latency EPs is likely different from that of the short-latency EPs. The length of these latencies is not compatible with antidromic transmission from the STN to the cerebral cortex, making it likely that they are produced instead by orthodromic transmission (Limousin et al., 1998). EPs of long latency are predominately produced by dorsal STN stimulation (Mackinnon et al., 2005).

Stimulation of either GPi or STN in parkinsonian patients generates long-latency EPs at similar cortical locations in the ipsilateral fronto-central cortex (Limousin et al., 1998; Tisch et al., 2008). This supports the notion that long-latency EPs involve the activation of pallido-thalamic fibers, a feature that would be common to both stimulation sites. The pallido-thalamic pathway passes through the internal capsule, and runs through the fields of Forel, in proximity to the dorsal and rostral part STN (Hamani et al., 2004). STN-DBS could trigger the activation of these fibers either through activation of the excitatory STN efferents to the GPi, which would then secondarily activate pallido-thalamic fibers, or via direct activation of pallido-thalamic projections through current spread from the STN to the Fields of Forel (Mcintyre et al., 2004; Miocinovic et al., 2006). A contribution of the subthalamo-pallido-thalamic route is supported by studies of STN-DBS-related EPs in patients with prior pallidotomies. In some of these patients, cortical EPs were found to be smaller than expected (Baker et al., 2002). The finding of relatively slow cortical responses to GPi stimulation (10 Hz, 3.5–4 V, 60–90 μ s) in dystonic patients (Tisch et al., 2008) also supports the hypothesis that at least a portion of the long-latency EPs are mediated via stimulation of pallido-thalamic fibers. However, in a study by Limousin et al. (1998) EPs evoked by STN-DBS had a shorter latency (18–20 ms) than EPs evoked by GPi stimulation (25.0–25.8 ms). In our comparisons of EPs recorded from fixed location in the motor cortex, and induced by STN or GPi stimulation (gray lines in Figure 2), the long-latency responses evoked by GPi stimulation occurred earlier than those evoked by STN stimulation (black lines in Figure 2), suggesting that STN stimulation produced its long-latency effects not via direct activation of pallido-thalamic fibers, but through activation of STN efferents to the pallidum.

Because the largest amplitude of long-latency STN-DBS-evoked EPs is found in the same cortical areas that show the largest potentials evoked by stimulation of the contralateral median nerve, the DBS-induced EP may be generated by activity in the region of the ipsilateral primary motor and sensorimotor cortex, in line with the known anatomical afferent and efferent patterns of the basal ganglia (Mackinnon et al., 2005).

Because EP characteristics seem to be relatively unaffected by dopaminergic medications, it has been suggested that the generation or propagation the EPs is (relatively) independent of dopaminergic circuit (Eusebio et al., 2009). Eusebio et al. (2009) observed that oscillatory activity following EPs may be reduced by the medication, perhaps reflecting reduced resonance of the

cortico-basal ganglia-thalamocortical loops. A suppressing effect of STN stimulation on oscillatory cortical activities is also supported by experiments in rodents, where the amplitude of evoked cortical LFPs inversely correlated with slow oscillatory activity (Li et al., 2007). The relative independence of EPs from dopaminergic effects may only apply to parkinsonian individuals, however. STN-DBS is now carried out in an increasing number of non-parkinsonian conditions (see above). In patients with these conditions, en-passant activation of dopaminergic or serotonergic fibers could be involved in the generation of long-latency EPs. However, in a small comparative study of EPs in parkinsonian or epilepsy patients (Baker et al., 2002) there were no significant differences between the two groups. This study would be worth repeating with additional patients or other disease conditions. Moreover, it had been suggested that this long-latency EP could also be independent of basal ganglia involvement. This long-latency EP could be either attributed to a cortico-cortical pathway driven from the intracortical projections of the pyramids that are antidromically stimulated, or either attributed to the pyramidal branches to the thalamus, those feed back to cortex and so could drive the late response (Phillips, 1959).

Stimulation of the ZI may also have orthodromic effects on cortex, via its GABAergic projection to the ventral anterior thalamus (Bartho et al., 2002). Similar to the activation of pallido-thalamic projection, activation of ZI output induces hyperpolarization of thalamocortical neurons followed by rebound bursts (Kuriakose et al., 2009).

Finally, rodent studies have shown that projections exist between the STN and the prefrontal cortex, providing yet another potential orthodromic route of transmission (Jackson and Crossman, 1981; Kita and Kitai, 1987; Degos et al., 2008). However, it is not clear whether this projection exists in primates.

ACTIVITY OF CIRCUITS DOWNSTREAM FROM THE STIMULATION SITE

Activation of the pallido-thalamic pathway by STN-DBS may alter the neuronal activity in the nuclei of the ventral and intralaminar thalamus that receive basal ganglia input (Anderson et al., 2003; Xu et al., 2008). As an example, Mackinnon et al. (2005) have proposed that low-frequency stimulation of the STN may lead to an inhibitory volley along pallido-thalamic pathways that may hyperpolarize ventral thalamic neurons and de-inactivate somatic calcium conductances which would then result in rebound bursting activity of thalamocortical neurons. The excitatory rebound activity may lead to the production of a cortical evoked potential in related cortical areas (Sherman, 2001; Mackinnon et al., 2005). Due to the slow kinetics of low-threshold calcium bursting activities, clinically effective high-frequency stimulation of the STN would simply lead to suppression of thalamocortical activities by inducing a hyperpolarization state during the stimulation, resulting in a net suppression of the activity of cortical neurons. In support of this idea, thalamic activity was found to be reduced during high-frequency stimulation of the GPi (Anderson et al., 2003), and a decrease in cerebral blood flow was found in the primary motor cortex of parkinsonian patients, during STN stimulation (Ceballos-Baumann et al., 1999; Payoux et al., 2004). However, modeling studies have suggested that high-frequency STN stimulation may induce more complex changes in thalamic firing activities (Guo et al., 2008). Of course, the low-pass filter characteristics of the

recording conditions, dictated by the size of the electrodes and the dielectric properties of the scalp and other tissue elements, further contribute to the temporal dynamics of the recordings (similar to its contribution to the frequency of EEG responses).

The thalamus, finally, projects to the frontal cortex. Layer IV is the main target of thalamocortical afferents, and would, thus, be the primary cortical layer affected by orthodromically mediated effects of STN-DBS. Large pyramidal cells in layer V are the principal sources of subcortical efferents, and would be considered the primary cortical elements activated via antidromic stimulation effects, as has been shown in cats (Phillips, 1959; Giuffrida et al., 1985) and in rats (Li et al., 2007).

In addition to the latency, the durations of EPs are an interesting feature of these potentials. In our primate recording study, short-latency potential after STN-DBS stimulation lasted 7.2 ± 0.4 ms while long-latency potentials had a total duration of 30.5 ± 3.5 ms (Figure 2). The temporal spread after short stimuli goes beyond the variability of transmission delays at single synapses, suggesting that the stimulation may involve more than one pathway of origin, or that it may affect thalamic or cortical networks of connections which may eventually contribute to the temporally spread-out cortical response.

POTENTIAL CLINICAL RELEVANCE

It remains an open question whether EPs evoked by STN-DBS are related to clinically relevant phenomena. One possibility is that cortical EPs may reflect changes in cortical excitability. In support of this idea, Ashby et al. (1999) found that short-latency EPs were facilitated by paired stimuli at inter-stimulus intervals between 2 and 10 ms, suggesting a cortical summation of postsynaptically generated EPs with short individual refractory periods (Ashby et al., 2001). Such cortical facilitation could also be partially reflected in increases in cerebral blood flow as have been detected in functional imaging studies (Limousin et al., 1997; Ceballos-Baumann et al., 1999; Hershey et al., 2003).

Experiments using transcranial magnetic stimulation (TMS) to probe cortical excitability have also detected changes in motor cortical excitability with multi-pulse STN-DBS in parkinsonian patients. In these experiments, the short-interval intracortical inhibition was normalized by STN stimulation, but the stimulation did not affect motor EP amplitudes or excitability thresholds (Cunic et al., 2002; Pierantozzi et al., 2002). These summation effect may not be the only mechanism by which STN-DBS may alter cortical activation, because short-latency facilitation of motor cortex excitability can also be seen with single-pulse STN stimulation in patients with Parkinson's disease, specifically with TMS protocols that activate corticospinal neurons through cortical interneurons (Hanajima et al., 2004; Kuriakose et al., 2009). One of the key differences between these studies and the earlier paired-pulse experiments is that the TMS stimuli and the STN-DBS were not time-locked in the paired-pulse studies, so that the temporal evolution of facilitation after each STN stimulus could not be examined. In recent studies Kuriakose et al. (2009) noted changes in motor cortex excitability only at specific time intervals after STN stimulation, corresponding to the duration of short and medium EP peaks. These findings suggest that the cortical facilitation found by TMS was linked to the occurrence of the EP induced by STN stimulation.

Although the antiparkinsonian effects of TMS are generally considered to be moderate compared to those of DBS (Fregni et al., 2005). Similar to the DBS effects (Benabid, 2003; Benabid et al., 2005), the frequency-dependence of the two treatments appears to be similar: low-frequency TMS does not produce beneficial effects (Arias et al., 2010), while high frequency TMS may produce motor benefits (Elahi and Chen, 2009).

Several authors have studied whether the presence or amplitude of EPs could be used as an intraoperative guide to optimize placement of DBS electrode. This would be beneficial, particularly in cases in whom the therapeutic effects of STN–DBS are not immediately apparent (such as in patients with dystonia, epilepsy, depression, or OCD). This approach appears to work in cases of GPi–DBS in dystonic patients (Tisch et al., 2008), but in the case of STN–DBS, the short- or long-latency components of EPs do not appear to strongly correlate with the clinical outcome of the surgery (Ashby et al., 1999; Mackinnon et al., 2005). A principal problem with these studies is that EP testing was done with stimulation at frequencies below 30 Hz (see above) to examine long-latency EPs. At least in Parkinson's disease patients, these stimulation conditions are not optimal from a clinical perspective (Benabid, 2003) and may, in fact, limit the usefulness of intraoperative EP testing as a targeting tool to identify clinical useful stimulation sites. Interestingly, a recent study has indicated that the clinically effective contacts may correspond to those that produce long-latency EPs when tested at a stimulation frequency of 10 Hz (Kuriakose et al., 2009). The utility of short-latency EPs has not been fully evaluated in this context, but studies in awake rodents treated with dopamine receptor blockers documented a correlation between the amplitude of short-latency cortical activation and the degree of improvement in akinesia (Dejean et al., 2009).

CONCLUSION

Measuring cortical EPs provides us with a unique opportunity to non-invasively monitor with high temporal resolution the effects of DBS on the cerebral cortex. However, the mechanisms that are involved in generating these potential changes remain relatively poorly understood. The available information suggests that STN–DBS affects multiple anatomical routes which alter cortical activities with different latencies from the stimulation.

Cortical potentials evoked by STN–DBS may not simply be epiphenomena of the stimulation, but may reflect the temporal progression of changes in cortical excitability which may be related to the clinical effects of DBS therapy in Parkinson's disease patients. However, the details of the relationship between the EPs and the clinical effects are not clear. For instance, if these potentials reflect specific activity changes at the cortical level, it is conceivable that the apparent need for high-frequency stimulation for a beneficial effects in patients with Parkinson's disease may arise from the need to optimize the interplay between short- and long-latency effects of the stimulation (or avoid long-latency potentials altogether through rapidly resetting the cortical response through short-latency responses).

We have yet to learn how to utilize the EP results to optimize the clinical outcome of patients who are being treated with STN–DBS. More study of the utility of intraoperative EP recordings to verify electrode placement, or of postoperative EP recordings as an aide to more rapid programming of the STN stimulator is needed to fully examine the potential of this technique. Animal experiments combining pharmacological or lesioning techniques to study the contribution of different anatomical routes to the stimulation response would be useful to further our understanding of the generation of EPs, and of the processes they reflect, both at the cortical and subcortical levels.

REFERENCES

- Anderson, M. E., Postupna, N., and Ruffo, M. (2003). Effects of high-frequency stimulation in the internal globus pallidus on the activity of thalamic neurons in the awake monkey. *J. Neurophysiol.* 89, 1150–1160.
- Arias, P., Vivas, J., Grieve, K. L., and Cudeiro, J. (2010). Controlled trial on the effect of 10 days low-frequency repetitive transcranial magnetic stimulation (rTMS) on motor signs in Parkinson's disease. *Mov. Disord.* 25, 1830–1838.
- Aron, A. R., and Poldrack, R. A. (2006). Cortical and subcortical contributions to Stop signal response inhibition: role of the subthalamic nucleus. *J. Neurosci.* 26, 2424–2433.
- Ashby, P., Kim, Y. J., Kumar, R., Lang, A. E., and Lozano, A. M. (1999). Neurophysiological effects of stimulation through electrodes in the human subthalamic nucleus. *Brain* 122(Pt 10), 1919–1931.
- Ashby, P., Paradiso, G., Saint-Cyr, J. A., Chen, R., Lang, A. E., and Lozano, A. M. (2001). Potentials recorded at the scalp by stimulation near the human subthalamic nucleus. *Clin. Neurophysiol.* 112, 431–437.
- Baker, K. B., Montgomery, E. B. Jr., Rezai, A. R., Burgess, R., and Luders, H. O. (2002). Subthalamic nucleus deep brain stimulus evoked potentials: physiological and therapeutic implications. *Mov. Disord.* 17, 969–983.
- Ballanger, B., Van Eimeren, T., Moro, E., Lozano, A. M., Hamani, C., Boulinguez, P., Pelliccia, G., Houle, S., Poon, Y. Y., Lang, A. E., and Strafella, A. P. (2009). Stimulation of the subthalamic nucleus and impulsivity: release your horses. *Ann. Neurol.* 66, 817–824.
- Baron, M. S., Sidibe, M., Delong, M. R., and Smith, Y. (2001). Course of motor and associative pallidothalamic projections in monkeys. *J. Comp. Neurol.* 429, 490–501.
- Bartho, P., Freund, T. F., and Acsady, L. (2002). Selective GABAergic innervation of thalamic nuclei from zona incerta. *Eur. J. Neurosci.* 16, 999–1014.
- Bartho, P., Slezia, A., Varga, V., Bokor, H., Pinault, D., Buzsaki, G., and Acsady, L. (2007). Cortical control of zona incerta. *J. Neurosci.* 27, 1670–1681.
- Benabid, A. L. (2003). Deep brain stimulation for Parkinson's disease. *Curr. Opin. Neurobiol.* 13, 696–706.
- Benabid, A. L., Chabardes, S., and Seigneuret, E. (2005). Deep-brain stimulation in Parkinson's disease: long-term efficacy and safety – What happened this year? *Curr. Opin. Neurol.* 18, 623–630.
- Benazzouz, A., Gao, D. M., Ni, Z. G., Piallat, B., Bouali-Benazzouz, R., and Benabid, A. L. (2000). Effect of high-frequency stimulation of the subthalamic nucleus on the neuronal activities of the substantia nigra pars reticulata and ventrolateral nucleus of the thalamus in the rat. *Neuroscience* 99, 289–295.
- Benazzouz, A., Piallat, B., Pollak, P., and Benabid, A. L. (1995). Responses of substantia nigra pars reticulata and globus pallidus complex to high frequency stimulation of the subthalamic nucleus in rats: electrophysiological data. *Neurosci. Lett.* 189, 77–80.
- Bevan, M. D., Francis, C. M., and Bolam, J. P. (1995). The glutamate-enriched cortical and thalamic input to neurons in the subthalamic nucleus of the rat: convergence with GABA-positive terminals. *J. Comp. Neurol.* 361, 491–511.
- Bronstein, J. M., Tagliati, M., Alterman, R. L., Lozano, A. M., Volkmann, J., Stefani, A., Horak, F. B., Okun, M. S., Foote, K. D., Krack, P., Pahwa, R., Henderson, J. M., Hariz, M. I., Bakay, R. A., Rezai, A., Marks, W. J., Jr., Moro, E., Vitek, J. L., Weaver, F. M., Gross, R. E., and Delong, M. R. (2011). Deep brain stimulation for Parkinson disease: an expert consensus and review of key issues. *Arch. Neurol.* 68, 165.
- Canteras, N. S., Shammah-Lagnado, S. J., Silva, B. A., and Ricardo, J. A. (1990). Afferent connections of the subthalamic nucleus: a combined retrograde and anterograde horseradish peroxidase study in the rat. *Brain Res.* 513, 43–59.
- Carbon, M., and Eidelberg, D. (2002). Modulation of regional brain function by deep brain stimulation: studies with positron emission tomography. *Curr. Opin. Neurol.* 15, 451–455.
- Carpenter, M. B., Carleton, S. C., Keller, J. T., and Conte, P. (1981). Connections of the subthalamic nucleus in the monkey. *Brain Res.* 224, 1–29.

- Ceballos-Baumann, A. O., Boecker, H., Bartenstein, P., Von Falkenhayn, I., Riescher, H., Conrad, B., Moringlane, J. R., and Alesch, F. (1999). A positron emission tomographic study of subthalamic nucleus stimulation in Parkinson disease: enhanced movement-related activity of motor-association cortex and decreased motor cortex resting activity. *Arch. Neurol.* 56, 997–1003.
- Chabardes, S., Kahane, P., Minotti, L., Koudsie, A., Hirsch, E., and Benabid, A. L. (2002). Deep brain stimulation in epilepsy with particular reference to the subthalamic nucleus. *Epileptic Disord.* 4(Suppl. 3), S83–S93.
- Chabardes, S., Minotti, L., Chassagnon, S., Piallat, B., Torres, N., Seigneuret, E., Vercueil, L., Carron, R., Hirsch, E., Kahane, P., and Benabid, A. L. (2008). Basal ganglia deep-brain stimulation for treatment of drug-resistant epilepsy: review and current data. *Neurochirurgie* 54, 436–440.
- Chang, H. T., Kita, H., and Kitai, S. T. (1983). The fine structure of the rat subthalamic nucleus: an electron microscopic study. *J. Comp. Neurol.* 221, 113–123.
- Cosyns, P., Gabriels, L., and Nuttin, B. (2003). Deep brain stimulation in treatment refractory obsessive compulsive disorder. *Verh. K. Acad. Geneesk. Belg.* 65, 385–399; discussion 399–400.
- Coubes, P., Roubertie, A., Vayssiere, N., Hemm, S., and Echenne, B. (2000). Treatment of DYT1-generalised dystonia by stimulation of the internal globus pallidus. *Lancet* 355, 2220–2221.
- Cunic, D., Roshan, L., Khan, F. I., Lozano, A. M., Lang, A. E., and Chen, R. (2002). Effects of subthalamic nucleus stimulation on motor cortex excitability in Parkinson's disease. *Neurology* 58, 1665–1672.
- Degos, B., Deniau, J. M., Le Cam, J., Mailly, P., and Maurice, N. (2008). Evidence for a direct subthalamo-cortical loop circuit in the rat. *Eur. J. Neurosci.* 27, 2599–2610.
- Dejean, C., Hyland, B., and Arbutnot, G. (2009). Cortical effects of subthalamic stimulation correlate with behavioral recovery from dopamine antagonist induced akinesia. *Cereb. Cortex* 19, 1055–1063.
- Donoghue, J. P., and Kitai, S. T. (1981). A collateral pathway to the neostriatum from corticofugal neurons of the rat sensory-motor cortex: an intracellular HRP study. *J. Comp. Neurol.* 201, 1–13.
- Elahi, B., and Chen, R. (2009). Effect of transcranial magnetic stimulation on Parkinson motor function – systematic review of controlled clinical trials. *Mov. Disord.* 24, 357–363.
- Erez, Y., Czitron, H., Mccairn, K., Belevsky, K., and Bar-Gad, I. (2009). Short-term depression of synaptic transmission during stimulation in the globus pallidus of 1-methyl-4-phenyl-1,2,3,6-tetrahydropyridine-treated primates. *J. Neurosci.* 29, 7797–7802.
- Erez, Y., Tischler, H., Moran, A., and Bar-Gad, I. (2010). Generalized framework for stimulus artifact removal. *J. Neurosci. Methods* 191, 45–59.
- Eusebio, A., Pogossyan, A., Wang, S., Averbach, B., Gaynor, L. D., Cantiniaux, S., Witjas, T., Limousin, P., Azulay, J. P., and Brown, P. (2009). Resonance in subthalamo-cortical circuits in Parkinson's disease. *Brain* 132, 2139–2150.
- Fregni, F., Simon, D. K., Wu, A., and Pascual-Leone, A. (2005). Non-invasive brain stimulation for Parkinson's disease: a systematic review and meta-analysis of the literature. *J. Neurol. Neurosurg. Psychiatr.* 76, 1614–1623.
- Fujimoto, K., and Kita, H. (1993). Response characteristics of subthalamic neurons to the stimulation of the sensorimotor cortex in the rat. *Brain Res.* 609, 185–192.
- Gabriels, L., Cosyns, P., Nuttin, B., Demeulemeester, H., and Gybels, J. (2003). Deep brain stimulation for treatment-refractory obsessive-compulsive disorder: psychopathological and neuropsychological outcome in three cases. *Acta Psychiatr. Scand.* 107, 275–282.
- Giuffrida, R., Li Volsi, G., Maugeri, G., and Perciavalle, V. (1985). Influences of pyramidal tract on the subthalamic nucleus in the cat. *Neurosci. Lett.* 54, 231–235.
- Gradinaru, V., Mogri, M., Thompson, K. R., Henderson, J. M., and Deisseroth, K. (2009). Optical deconstruction of parkinsonian neural circuitry. *Science* 324, 354–359.
- Guo, Y., Rubin, J. E., McIntyre, C. C., Vitek, J. L., and Terman, D. (2008). Thalamocortical relay fidelity varies across subthalamic nucleus deep brain stimulation protocols in a data-driven computational model. *J. Neurophysiol.* 99, 1477–1492.
- Hamani, C., Saint-Cyr, J. A., Fraser, J., Kaplitt, M., and Lozano, A. M. (2004). The subthalamic nucleus in the context of movement disorders. *Brain* 127, 4–20.
- Hanajima, R., Ashby, P., Lozano, A. M., Lang, A. E., and Chen, R. (2004). Single pulse stimulation of the human subthalamic nucleus facilitates the motor cortex at short intervals. *J. Neurophysiol.* 92, 1937–1943.
- Hashimoto, T., Elder, C. M., Okun, M. S., Patrick, S. K., and Vitek, J. L. (2003). Stimulation of the subthalamic nucleus changes the firing pattern of pallidal neurons. *J. Neurosci.* 23, 1916–1923.
- Hashimoto, T., Elder, C. M., and Vitek, J. L. (2002). A template subtraction method for stimulus artifact removal in high-frequency deep brain stimulation. *J. Neurosci. Methods* 113, 181–186.
- Hershey, T., Campbell, M. C., Videen, T. O., Lugar, H. M., Weaver, P. M., Hartlein, J., Karimi, M., Tabbal, S. D., and Perlmuter, J. S. (2010). Mapping Go-No-Go performance within the subthalamic nucleus region. *Brain* 133, 3625–3634.
- Hershey, T., Revilla, F. J., Wernle, A. R., McGeer-Minnich, L., Antenor, J. V., Videen, T. O., Dowling, J. L., Mink, J. W., and Perlmuter, J. S. (2003). Cortical and subcortical blood flow effects of subthalamic nucleus stimulation in PD. *Neurology* 61, 816–821.
- Hodaie, M., Wennberg, R. A., Dostrovsky, J. O., and Lozano, A. M. (2002). Chronic anterior thalamus stimulation for intractable epilepsy. *Epilepsia* 43, 603–608.
- Jackson, A., and Crossman, A. R. (1981). Subthalamic nucleus efferent projection to the cerebral cortex. *Neuroscience* 6, 2367–2377.
- Jech, R., Urgosik, D., Tintera, J., Nebuzelsky, A., Krasensky, J., Liscak, R., Roth, J., and Ruzicka, E. (2001). Functional magnetic resonance imaging during deep brain stimulation: a pilot study in four patients with Parkinson's disease. *Mov. Disord.* 16, 1126–1132.
- Jurgens, U. (1984). The efferent and afferent connections of the supplementary motor area. *Brain Res.* 300, 63–81.
- Kita, H., Chang, H. T., and Kitai, S. T. (1983). The morphology of intracellularly labeled rat subthalamic neurons: a light microscopic analysis. *J. Comp. Neurol.* 215, 245–257.
- Kita, H., and Kitai, S. T. (1987). Efferent projections of the subthalamic nucleus in the rat: light and electron microscopic analysis with the PHA-L method. *J. Comp. Neurol.* 260, 435–452.
- Kitai, S. T., and Deniau, J. M. (1981). Cortical inputs to the subthalamus: intracellular analysis. *Brain Res.* 214, 411–415.
- Kuriakose, R., Saha, U., Castillo, G., Udupa, K., Ni, Z., Gunraj, C., Mazzella, F., Hamani, C., Lang, A. E., Moro, E., Lozano, A. M., Hodaie, M., and Chen, R. (2009). The nature and time course of cortical activation following subthalamic stimulation in Parkinson's disease. *Cereb. Cortex* 20, 1926–1936.
- Li, S., Arbutnot, G. W., Jutras, M. J., Goldberg, J. A., and Jaeger, D. (2007). Resonant antidromic cortical circuit activation as a consequence of high-frequency subthalamic deep-brain stimulation. *J. Neurophysiol.* 98, 3525–3537.
- Limousin, P., Brown, P., Marsden, L., Defebvre, L., and Rothwell, J. (1998). Evoked potentials from subthalamic nucleus, internal pallidum and thalamic stimulation in parkinsonian and postural tremor patients. *J. Physiol.* 509P, 176P–177P.
- Limousin, P., Greene, J., Pollak, P., Rothwell, J., Benabid, A. L., and Frackowiak, R. (1997). Changes in cerebral activity pattern due to subthalamic nucleus or internal pallidum stimulation in Parkinson's disease. *Ann. Neurol.* 42, 283–291.
- Ma, Y., Bevan, M. D., and Wichmann, T. (2007). Effects of subthalamic nucleus stimulation on neuronal activity in the internal pallidal segment in monkeys. *Soc. Neurosci. Abstr.*
- Mackinnon, C. D., Webb, R. M., Silberstein, P., Tisch, S., Asselman, P., Limousin, P., and Rothwell, J. C. (2005). Stimulation through electrodes implanted near the subthalamic nucleus activates projections to motor areas of cerebral cortex in patients with Parkinson's disease. *Eur. J. Neurosci.* 21, 1394–1402.
- Matsumura, M., Kojima, J., Gardiner, T. W., and Hikosaka, O. (1992). Visual and oculomotor functions of monkey subthalamic nucleus. *J. Neurophysiol.* 67, 1615–1632.
- Maurice, N., Deniau, J. M., Menetrey, A., Glowinski, J., and Thierry, A. M. (1998). Prefrontal cortex-basal ganglia circuits in the rat: involvement of ventral pallidum and subthalamic nucleus. *Synapse* 29, 363–370.
- Maurice, N., Thierry, A. M., Glowinski, J., and Deniau, J. M. (2003). Spontaneous and evoked activity of substantia nigra pars reticulata neurons during high-frequency stimulation of the subthalamic nucleus. *J. Neurosci.* 23, 9929–9936.
- McIntyre, C. C., Mori, S., Sherman, D. L., Thakor, N. V., and Vitek, J. L. (2004). Electric field and stimulating influence generated by deep brain stimulation of the subthalamic nucleus. *Clin. Neurophysiol.* 115, 589–595.
- Meissner, W., Leblois, A., Hansel, D., Bioulac, B., Gross, C. E., Benazzouz, A., and Boraud, T. (2005). Subthalamic high frequency stimulation resets subthalamic firing and reduces abnormal oscillations. *Brain* 128, 2372–2382.
- Micicovic, S., Parent, M., Butson, C. R., Hahn, P. J., Russo, G. S., Vitek, J. L., and McIntyre, C. C. (2006). Computational analysis of subthalamic nucleus and lenticular fasciculus activation during therapeutic deep brain stimulation. *J. Neurophysiol.* 96, 1569–1580.

- Mitrofanis, J., and Mikuletic, L. (1999). Organisation of the cortical projection to the zona incerta of the thalamus. *J. Comp. Neurol.* 412, 173–185.
- Monakow, K. H., Akert, K., and Kunzle, H. (1978). Projections of the precentral motor cortex and other cortical areas of the frontal lobe to the subthalamic nucleus in the monkey. *Exp. Brain Res.* 33, 395–403.
- Montgomery, E. B. Jr. (2006). Effects of GPi stimulation on human thalamic neuronal activity. *Clin. Neurophysiol.* 117, 2691–2702.
- Montgomery, E. B. Jr., Gale, J. T., and Huang, H. (2005). Methods for isolating extracellular action potentials and removing stimulus artifacts from microelectrode recordings of neurons requiring minimal operator intervention. *J. Neurosci. Methods* 144, 107–125.
- Moran, A., Stein, E., Tischler, H., Belevsky, K., and Bar-Gad, I. (2010). “Decoupling of intra-neuron oscillations and inter-neuron synchronization during high frequency stimulation of the subthalamic nucleus,” in *IBAGS X*.
- Nambu, A., Takada, M., Inase, M., and Tokuno, H. (1996). Dual somatotopic representations in the primate subthalamic nucleus: evidence for ordered but reversed body-map transformations from the primary motor cortex and the supplementary motor area. *J. Neurosci.* 16, 2671–2683.
- Nambu, A., Tokuno, H., Hamada, I., Kita, H., Imanishi, M., Akazawa, T., Ikeuchi, Y., and Hasegawa, N. (2000). Excitatory cortical inputs to pallidal neurons via the subthalamic nucleus in the monkey. *J. Neurophysiol.* 84, 289–300.
- Nuttin, B. J., Gabriels, L., Van Kuyck, K., and Cosyns, P. (2003). Electrical stimulation of the anterior limbs of the internal capsules in patients with severe obsessive-compulsive disorder: anecdotal reports. *Neurosurg. Clin. N. Am.* 14, 267–274.
- Parent, A., and Hazrati, L. N. (1995). Functional anatomy of the basal ganglia. II. The place of subthalamic nucleus and external pallidum in basal ganglia circuitry. *Brain Res. Brain Res. Rev.* 20, 128–154.
- Payoux, P., Remy, P., Damier, P., Miloudi, M., Loubinoux, I., Pidoux, B., Gaura, V., Rascol, O., Samson, Y., and Agid, Y. (2004). Subthalamic nucleus stimulation reduces abnormal motor cortical overactivity in Parkinson disease. *Arch. Neurol.* 61, 1307–1313.
- Perlmuter, J. S., Mink, J. W., Bastian, A. J., Zackowski, K., Hershey, T., Miyawaki, E., Koller, W., and Videen, T. O. (2002). Blood flow responses to deep brain stimulation of the thalamus. *Neurology* 58, 1388–1394.
- Phillips, C. G. (1959). Actions of antidromic pyramidal volleys on single Betz cells in the cat. *Q. J. Exp. Physiol. Cogn. Med. Sci.* 44, 1–25.
- Pierantozzi, M., Palmieri, M. G., Mazzone, P., Mariani, M. G., Rossini, P. M., Stefani, A., Giacomini, P., Peppe, A., and Stanzione, P. (2002). Deep brain stimulation of both subthalamic nucleus and internal globus pallidus restores intracortical inhibition in Parkinson's disease paralleling apomorphine effects: a paired magnetic stimulation study. *Clin. Neurophysiol.* 113, 108–113.
- Power, B. D., and Mitrofanis, J. (2001). Zona incerta: Substrate for contralateral interconnectivity in the thalamus of rats. *J. Comp. Neurol.* 436, 52–63.
- Rouzaire-Dubois, B., and Scarnati, E. (1985). Bilateral corticosubthalamic nucleus projections: an electrophysiological study in rats with chronic cerebral lesions. *Neuroscience* 15, 69–79.
- Sherman, S. M. (2001). Tonic and burst firing: dual modes of thalamocortical relay. *Trends Neurosci.* 24, 122–126.
- Tai, C. H., Borau, T., Bezard, E., Bioulac, B., Gross, C., and Benazzouz, A. (2003). Electrophysiological and metabolic evidence that high-frequency stimulation of the subthalamic nucleus bridges neuronal activity in the subthalamic nucleus and the substantia nigra reticulata. *FASEB J.* 17, 1820–1830.
- Temperli, P., Ghika, J., Villemure, J. G., Burkhard, P. R., Bogousslavsky, J., and Vingerhoets, F. J. (2003). How do parkinsonian signs return after discontinuation of subthalamic DBS? *Neurology* 60, 78–81.
- Tisch, S., Rothwell, J. C., Zrinzo, L., Bhatia, K. P., Hariz, M., and Limousin, P. (2008). Cortical evoked potentials from pallidal stimulation in patients with primary generalized dystonia. *Mov. Disord.* 23, 265–273.
- Vercueil, L., Pollak, P., Fraix, V., Caputo, E., Moro, E., Benazzouz, A., Xie, J., Koudsie, A., and Benabid, A. L. (2001). Deep brain stimulation in the treatment of severe dystonia. *J. Neurol.* 248, 695–700.
- Vidalhet, M., Vercueil, L., Houeto, J. L., Krystkowiak, P., Benabid, A. L., Cornu, P., Lagrange, C., Tezenas Du Montcel, S., Dormont, D., Grand, S., Blond, S., Detante, O., Pillon, B., Ardouin, C., Agid, Y., Destee, A., and Pollak, P. (2005). Bilateral deep-brain stimulation of the globus pallidus in primary generalized dystonia. *N. Engl. J. Med.* 352, 459–467.
- Wichmann, T. (2000). A digital averaging method for removal of stimulus artifacts in neurophysiologic experiments. *J. Neurosci. Methods* 98, 57–62.
- Windels, F., Bruet, N., Poupard, A., Feuerstein, C., Bertrand, A., and Savasta, M. (2003). Influence of the frequency parameter on extracellular glutamate and gamma-aminobutyric acid in substantia nigra and globus pallidus during electrical stimulation of subthalamic nucleus in rats. *J. Neurosci. Res.* 72, 259–267.
- Windels, F., Bruet, N., Poupard, A., Urbain, N., Chouvet, G., Feuerstein, C., and Savasta, M. (2000). Effects of high frequency stimulation of subthalamic nucleus on extracellular glutamate and GABA in substantia nigra and globus pallidus in the normal rat. *Eur. J. Neurosci.* 12, 4141–4146.
- Windels, F., Carcenac, C., Poupard, A., and Savasta, M. (2005). Pallidal origin of GABA release within the substantia nigra pars reticulata during high-frequency stimulation of the subthalamic nucleus. *J. Neurosci.* 25, 5079–5086.
- Wu, Y. R., Levy, R., Ashby, P., Tasker, R. R., and Dostrovsky, J. O. (2001). Does stimulation of the GPi control dyskinesia by activating inhibitory axons? *Mov. Disord.* 16, 208–216.
- Xu, W., Russo, G. S., Hashimoto, T., Zhang, J., and Vitek, J. L. (2008). Subthalamic nucleus stimulation modulates thalamic neuronal activity. *J. Neurosci.* 28, 11916–11924.
- Yelnik, J., and Percheron, G. (1979). Subthalamic neurons in primates: a quantitative and comparative analysis. *Neuroscience* 4, 1717–1743.
- Yianni, J., Bain, P., Giladi, N., Auca, M., Gregory, R., Joint, C., Nandi, D., Stein, J., Scott, R., and Aziz, T. (2003). Globus pallidus internus deep brain stimulation for dystonic conditions: a prospective audit. *Mov. Disord.* 18, 436–442.

Conflict of Interest Statement: The authors declare that the research was conducted in the absence of any commercial or financial relationships that could be construed as a potential conflict of interest.

Received: 01 March 2011; paper pending published: 20 March 2011; accepted: 29 April 2011; published online: 13 May 2011.
Citation: Devergnas A and Wichmann T (2011) Cortical potentials evoked by deep brain stimulation in the subthalamic area. *Front. Syst. Neurosci.* 5:30. doi: 10.3389/fnsys.2011.00030
Copyright © 2011 Devergnas and Wichmann. This is an open-access article subject to a non-exclusive license between the authors and Frontiers Media SA, which permits use, distribution and reproduction in other forums, provided the original authors and source are credited and other Frontiers conditions are complied with.



The corticostriatal system in dissociated cell culture

Fiona E. Randall¹, Marianela Garcia-Munoz¹, Catherine Vickers¹, Sarah C. Schock², William A. Staines² and Gordon W. Arbuthnott^{1*}

¹ Brain Mechanisms for Behaviour Unit, Okinawa Institute of Science and Technology, Okinawa, Japan

² Department of Cellular and Molecular Medicine, University of Ottawa, Ottawa, ON, Canada

Edited by:

Jose Vargas, Universidad Nacional Autónoma de México, Mexico

Reviewed by:

Enrico Bracci, University of Manchester, UK

M. Gustavo Murer, Universidad de Buenos Aires, Argentina

Paul Bolam, University of Oxford, UK

*Correspondence:

Gordon W. Arbuthnott, Brain Mechanisms for Behaviour Unit, Okinawa Institute of Science and Technology, 1919-1 Tancha, Kunigami-gun 904-0412, Okinawa, Japan.

e-mail: gordon@oist.jp

The sparse connectivity within the striatum *in vivo* makes the investigation of individual corticostriatal synapses very difficult. Most studies of the corticostriatal input have been done using electrical stimulation under conditions where it is hard to identify the precise origin of the cortical input. We have employed an *in vitro* dissociated cell culture system that allows the identification of individual corticostriatal pairs and have been developing methods to study individual neuron inputs to striatal neurons. In mixed corticostriatal cultures, neurons had resting activity similar to the system *in vivo*. Up/down states were obvious and seemed to encompass the entire culture. Mixed cultures of cortical neurons from transgenic mice expressing green fluorescent protein with striatal neurons from wild-type mice of the same developmental stage allowed visual identification of individual candidate corticostriatal pairs. Recordings were performed between 12 and 37 days *in vitro* (DIV). To investigate synaptic connections we recorded from 69 corticostriatal pairs of which 44 were connected in one direction and 25 reciprocally. Of these connections 41 were corticostriatal (nine inhibitory) and 53 striatocortical (all inhibitory). The observed excitatory responses were of variable amplitude (−10 to −370 pA, $n = 32$). We found the connections very secure – with negligible failures on repeated stimulation (approximately 1 Hz) of the cortical neuron. Inhibitory corticostriatal responses were also observed (−13 to −314 pA, $n = 9$). Possibly due to the mixed type of culture we found an inhibitory striatocortical response (−14 to −598 pA, $n = 53$). We are now recording from neurons in separate compartments to more closely emulate neuroanatomical conditions but still with the possibility of the easier identification of the connectivity.

Keywords: dissociated neuronal culture, cryopreserved neurons, corticostriatal, basal ganglia, synaptic physiology

INTRODUCTION

The striatum is the primary gateway for cortical inputs to the basal ganglia, in order to understand how inputs from the cortex to the basal ganglia influence behavior the characteristics of the corticostriatal projections must be understood.

Anatomical considerations suggest massive cortical convergence on striatal neurons. Both Kincaid et al. (1998) and ourselves (Wickens and Arbuthnott, 2010) estimate that about 5,000 cortical neurons might have synaptic contact with a single striatal neuron. Surprisingly, each cortical neuron of the 5,000 might only make one synapse on the striatal target neuron. Even more surprising is the statistic that the likelihood of overlap between cortical inputs to adjacent striatal neurons is less than 10%. Of course, if 10% of the inputs are enough to fire the neurons, the overlap will allow the formation of adjacent groups of striatal neurons relaying common information from the cortex. However, the estimates of the number of cortical neurons likely to be needed to drive one striatal neuron suggest each input is so weak that almost 1,000 synapses must be co-activated to cause firing of a medium spiny neuron. That estimate derives from calculations on corticostriatal organotypic cultures (Blackwell et al., 2003) but up to one-half of the depolarization might derive from GABA inputs rather than from cortical synapses.

There are other ways to approach this question. We know from our own (Wright et al., 2001) and Wilson's (Sachdev et al., 2004) work that a single striatal neuron can fire in response to the

movement of one whisker. That implies that the cortical neurons of one whisker barrel can fire a single striatal neuron; and cortical barrels have well known numerical anatomy (Helmstaedter et al., 2007). Of the 1,500 neurons in layer V of a single barrel about 225 might be inhibitory interneurons and of the rest, about 1/3 are likely to project to the striatum. So a barrel might have about 425 layer V corticostriatal neurons of which about 20% fire on any individual whisker deflection (Higley and Contreras, 2005). Therefore, it might take only 85 neurons to fire a single striatal neuron.

Others have estimated the size of one cortical input to a striatal neuron from stimuli small enough to cause failures of transmission (so called “minimal stimulation”) in slices of the corticostriatal system. That estimate ranges from 12 to 26 pA (Mori, 1994a,b,c; Ding et al., 2008). Assuming an input resistance of about 100 M Ω and the need of 30–40 mV depolarization to fire the neuron from a −80 mV resting potential, about 15–30 simultaneous inputs would be required to reach threshold. Of course the duration of the synaptic responses and the non-linearity of the membrane responses will modify that estimate. One objective of our study of corticostriatal cultures was to get a direct estimate of the strength of the excitatory connection between a single cortical neuron and a single striatal neuron.

We have established an *in vitro* dissociated cell culture method that allows identification of anatomically connected cortical and striatal neurons. Electrophysiological recording of connected

neurons is a versatile tool allowing the study of many basic properties of neuronal communication in brain circuits (Debanne et al., 2008). Here we describe the electrophysiological characteristics of cortical and striatal neurons in the dissociated culture, as well as the functional synapses between pairs of neurons. We show that dissociated neurons of the cortex and striatum in culture have comparable electrophysiological characteristics to neurons recorded both in slices and *in vivo*. We also show that functional synaptic connections form in culture.

This experimental system provides a useful platform for in-depth investigation of the corticostriatal system in an *in vitro* preparation. In particular the spontaneous activity in striatal neurons has been unavailable to study in corticostriatal slices without pharmacological manipulation (Wilson and Groves, 1980, 1981; Wilson, 1993; Wilson and Kawaguchi, 1996; Vergara et al., 2003). However, spontaneous firing characteristics have been studied in organotypic cultures (Plenz and Kitai, 1998) and they are visible in mixed cultures of dissociated primary cortical and striatal cells (Arbuthnott et al., 2005). We took advantage of recordings in this culture system to study some of the properties of this spontaneous activity, and to look for the connectivity between cortical and striatal neurons. Cortical and striatal neurons were readily distinguishable in culture as one type was always prepared from a green fluorescent protein (GFP) transgenic mouse (Tsirigotis et al., 2001).

Striatal neurons probably receive input from thousands of cortical neurons *in vivo* (Kincaid et al., 1998; Wickens and Arbuthnott, 2010) and therefore studying individual pairs of connected cortical and striatal neurons is almost impossible. This multiplicity of connections does not occur in mixed cultures and patching neighboring neurons has often allowed us to identify corticostriatal synaptic pairs for study.

MATERIALS AND METHODS

Cryopreserved mouse neurons were obtained from QBM Cell Science Ottawa and defrosted and cultured on 35 mm IBIDI plates (Martinsried, Germany) with a marked grid on the base. The dishes were pre-coated with poly-D-lysine. Cells were restricted to the area in the center of the plates with a silicon flexiPERM ring (Greiner Bio-One). The cultures were plated at a cell density of ≈ 700 cells/ μ l with mixtures of cortical cells from a UBC driven 6 his-ubiquitin/GFP mouse (Tsirigotis et al., 2001) and striatal cells from wild-type mouse of the same age and strain. For the first 18 h in culture, the medium (Brain Bits LLC, Springfield) was supplemented with 5% heat-inactivated horse serum (Invitrogen, Carlsbad, CA, USA). The cultures were maintained in a humidified incubator (Forma Stericycle, Thermo Scientific) at 37°C, 5% CO₂/95% O₂. Half of the culture medium was exchanged twice-a-week with new medium including 1% penicillin/streptomycin (Invitrogen).

Neurons were typically recorded at 15–20 DIV (range 12–37 DIV). On the day of recording the dish was placed on the stage of an inverted microscope (Olympus IX81) with two Sutter micro-manipulators on the stage. The dish was perfused with artificial CSF (NaCl 136; KCl 5; MgCl 1; CaCl 2.5; Hepes buffer 10; glucose 10 – all mM) at a rate of about 2 ml/min. Neurons were patched with microelectrodes (6–12 M Ω) filled with potassium gluconate internal solution (NaCl 8; potassium gluconate 132;

MgATP 2; NaGTP 0.4; KCl 6; HEPES buffer 10 – all mM). Alexa 594 (2 μ g/ml) was added to the striatal electrode and Alexa 488 (2 μ g/ml, Invitrogen) to the cortical one. In later experiments both pipettes had 0.2% biocytin (Invitrogen) also in the internal solution. The electrodes were placed close to the relevant neuron and whole cell patch clamp recordings were made with a two-channel amplifier (Axon 700b) and pCLAMP software (Molecular Devices Inc.). Because of the arrangement of the extended stage of the microscope the neurons needed to be close together – within the field of view of the 20 \times objective that was used to visualize the cells (<300 μ m). Initially, the properties of each neuron were characterized in voltage clamp. Neuron membrane potential was manipulated from -90 to -20 mV using current steps to look at the membrane properties of the neurons. For pairs of neurons in voltage clamp, we stimulated one with depolarizing voltage pulses sufficient to elicit one action potential every 1.2 s and recorded the response in the other neuron while manipulating the resting potential of the postsynaptic neuron from -80 to -30 mV. Further protocols to study spontaneous activity and the responses of the neurons to trains of stimuli were recorded as time permitted. In earlier experiments we simply studied the spontaneous activity in striatal or cortical neurons one at a time and in those experiments we applied 8 μ M DNQX (6,7-dinitroquinoxaline-2,3-dione, Sigma-Aldrich) for 2 min before returning to artificial CSF flow.

Filled pairs were fixed with 4% paraformaldehyde, washed and stored in 10% phosphate buffered saline. They were imaged using a fluorescent microscope. Following imaging, neurons were treated with VECTASTAIN Elite ABC kit (Vector Labs) and then stained with 3,3'-diaminobenzidine (DAB) substrate kit (Vector labs) to reveal the biocytin staining.

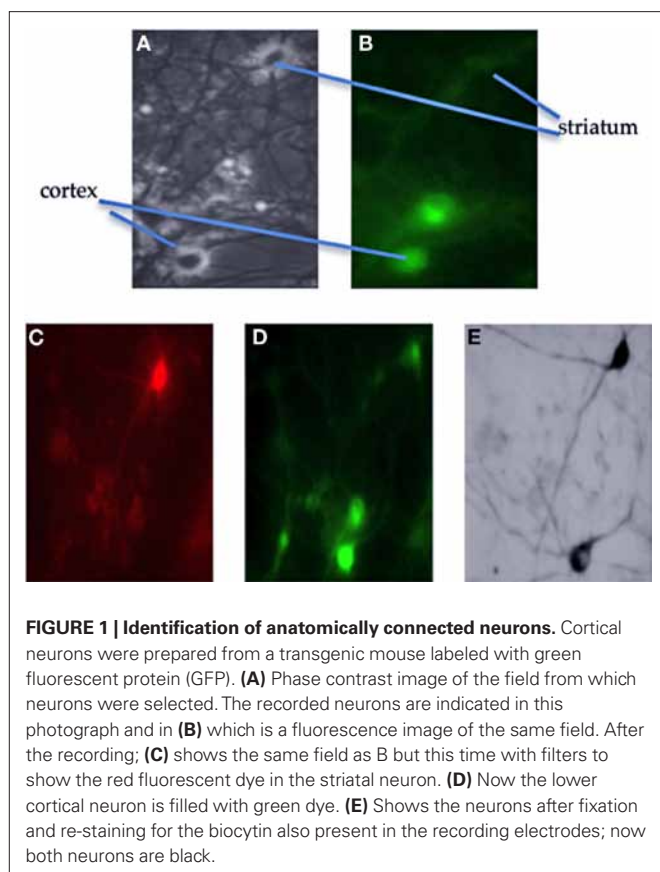
RESULTS

IDENTIFICATION OF CORTICOSTRIATAL PAIRS IN CULTURE

Cortical and striatal neurons in a mixed culture are very difficult to discern based on their cytological differences alone. For example, neurons with what looked like apical dendrites were visible in both cortical and striatal cells. The use of GFP-expressing cells from a transgenic mouse allowed for clear differential identification of cortical neurons in mixed cultures, since striatal cells were from a wild-type mouse (Figure 1). We designated any two neurons (one GFP-positive and one GFP-negative) recorded at the same time as a pair. Slightly more than 50% of recorded pairs showed synaptic activity between them (69). Of those 44 pairs were connected only in one direction (16 corticostriatal and 28 striatocortical) the rest (25) were reciprocally connected. We analyzed all the connections independently which gave a total of 41 corticostriatal and 53 striatocortical connections.

STIMULATION OF CORTICAL NEURONS

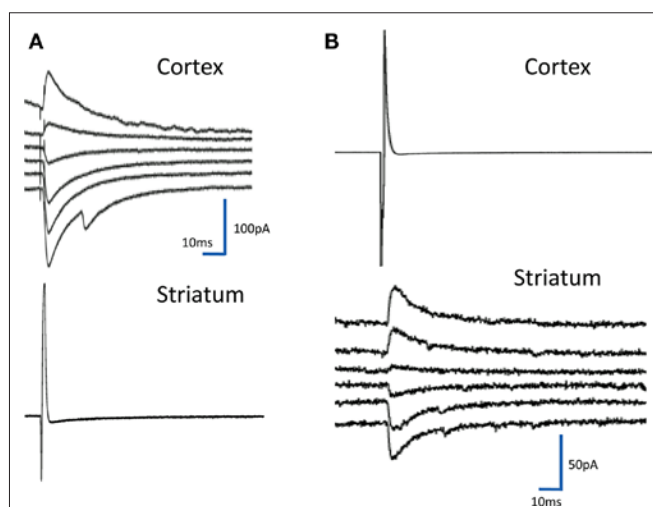
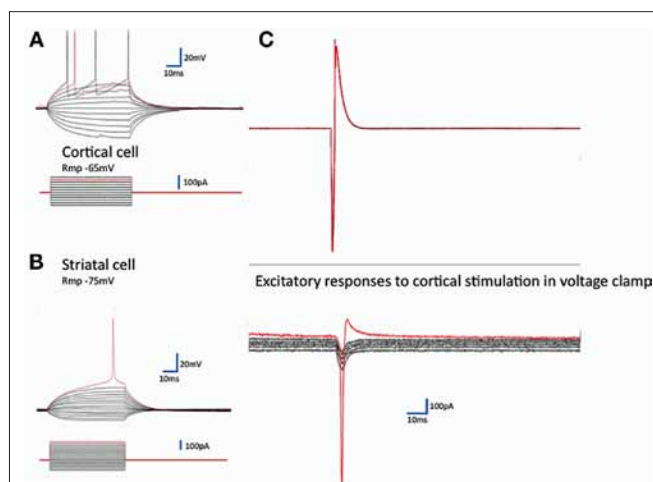
The expected cortical EPSCs in striatal neurons evoked by stimulation of a single cortical neuron in the culture were seen (Figure 2) in 32/41 corticostriatal connections (though of course some spread of activity among the cortical cells in the dish was expected – and seen sometimes in synaptic responses with multiple phases). The excitatory responses were of variable amplitude (-10 to -370 pA, $n = 32$).



Other cortical neurons identified by the GFP (9) produced an inhibitory response on striatal neurons as shown in **Figure 3B**. Since the GFP tag is driven by the ubiquitin promoter, it is present in all cells and in separate experiments we have looked for and not found any GFP-negative cells in cultures from these mice.

Inhibitory responses are assumed to arise from activation of an inhibitory neuron by the stimulus. All but three of the inhibitory responses had latencies of less than 2 ms. In two cases the response was mixed with a reversing and non-reversing component. Given the number of reciprocally connected neurons this small number is surprising but not all the striatal neurons fired action potentials in response to the cortical neuron input.

In 53 connections the activity was in the opposite direction to what was expected; stimulation of a striatal neuron induced an IPSC in the cortical neuron (**Figure 3A**). Inhibition was defined by looking at the reversal potential of the response. Since chloride reversal potential in our neurons is about -45 mV we assumed that these reversing potentials were driven by GABA that is known to be the major transmitter in striatal neurons. Most of the responses had latencies compatible with monosynaptic connections (mean 1.92 ± 0.92 ms, $N = 94$) but there were some longer ones that may have been polysynaptic. There was no obvious relationship between size and latency in the current set therefore we cannot assume that the larger post synaptic currents are polysynaptic.



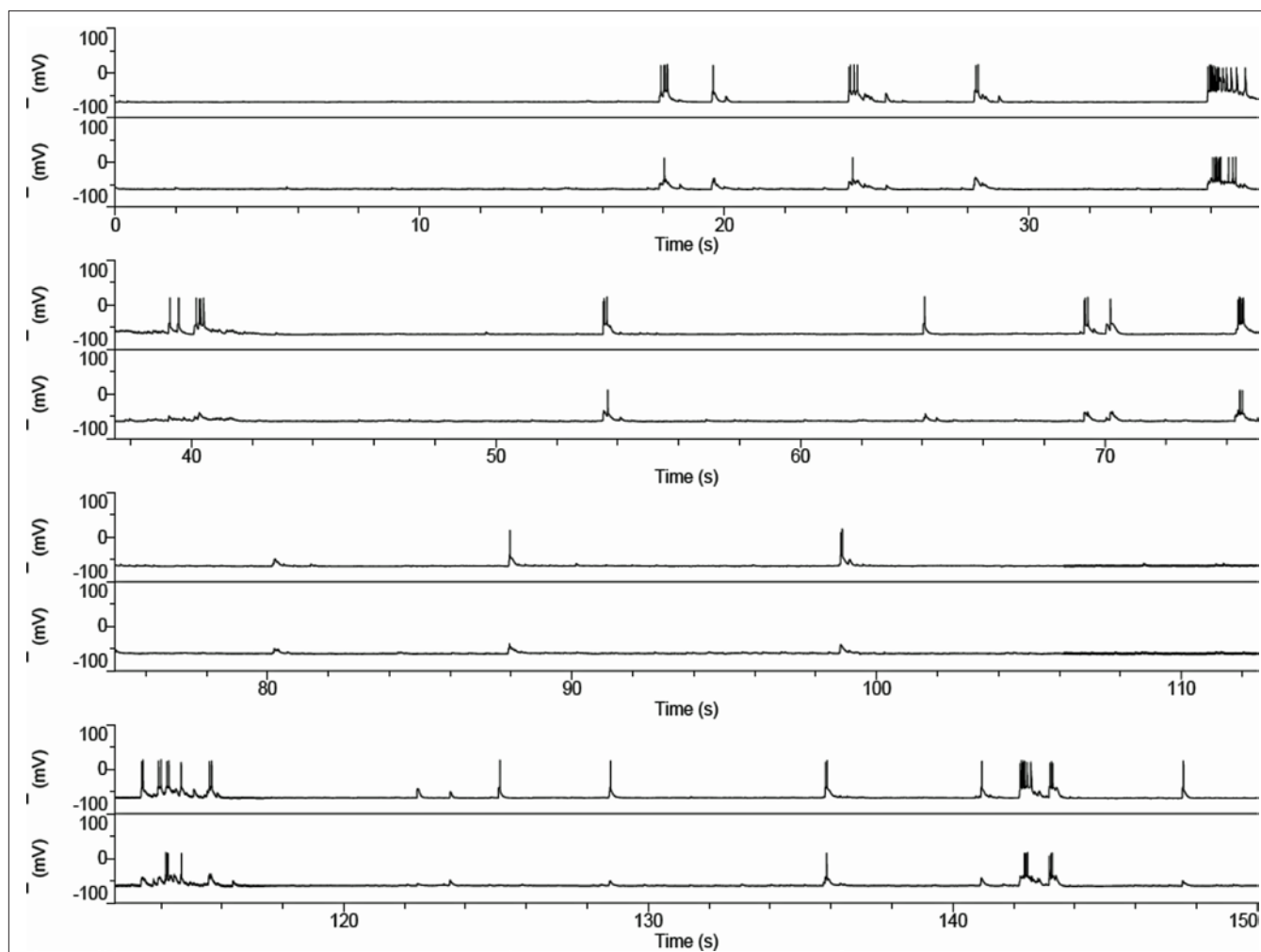


FIGURE 4 | Spontaneous activity in corticostriatal cultures. Current clamp records of a pair of cortical (upper trace) and striatal neuron firing patterns in culture show occasional bursts at about 0.1 Hz with “UP” states that last approximately 0.5 s. Although slower than the typical pattern *in vivo* the pattern is very reminiscent of that seen in the anesthetized rat (Wilson and Groves, 1981; Wilson et al., 1983). The records shown are continuously recorded in time.

RESTING SPONTANEOUS CONDITIONS

The resting spontaneous firing is illustrated in **Figure 4**. The firing is typically in bursts of action potentials (**Figure 4**) sitting on long depolarizations typical of “UP” states as seen in striatal neurons *in vivo*. These “UP” states (**Figure 5**) are variable between cultures but have several properties in common. They are markedly synchronous. The rate of responding is modified by membrane polarization. Neurons fire less often from more hyperpolarized potentials although subthreshold depolarizations are larger in the more hyperpolarized states.

Cortical neurons also show similar “UP/DOWN” states (Cowan and Wilson, 1994) and they do so in cultures even in the absence of striatal neurons.

Pharmacological blockade

Previous work on cortical cultures (Corner et al., 2002) exploring the response of burst firing to blockade of glutamate receptors showed that bursts were extremely sensitive to DNQX applied to the bath. Our cortical neurons, and striatal neurons in mixed cortex and

striatal cultures, generated bursts that were also extremely sensitive to DNQX. The effect was rapid and returned the striatal neurons to resting “DOWN” state membrane potential with complete reversal after only 2 min in normal perfusion medium (**Figure 6**).

DISCUSSION

SPONTANEOUS ACTIVITY

Isolated cortical neurons have been shown to support burst-like activity even when isolated in the cat’s skull from surrounding tissue (Burns, 1950, 1951; Timofeev et al., 2000). In cortical slices (Boakes et al., 1988; Allene et al., 2008) as well as in dissociated cell culture (Potter and DeMarse, 2001; Wagenaar et al., 2005; Rolston et al., 2007) and slice culture (Plenz and Kitai, 1998; Johnson and Buonomano, 2007; Plenz and Thiagarajan, 2007) cortical neurons exhibit bursts of activity associated with depolarized membrane potentials. These intermittent bursts are maintained even in the absence of the thalamic input to the cortex (Burns, 1950, 1951), though *in vivo* and in slices in which thalamocortical fibers are preserved these UP states in cortex are driven by thalamic input and inhibited by synchronous activity

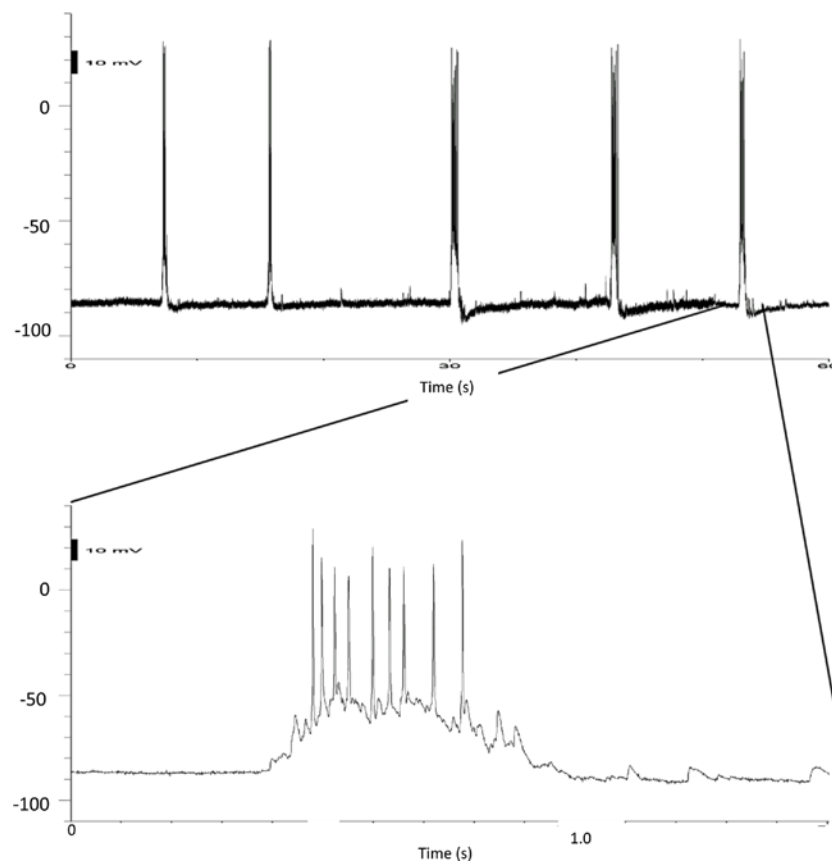


FIGURE 5 | Details of UP states. Current clamp recordings of a striatal neuron in a mixed culture. The upper record on a slower timescale shows the rate of the bursts, while the final burst on the record is shown at a faster timescale below.

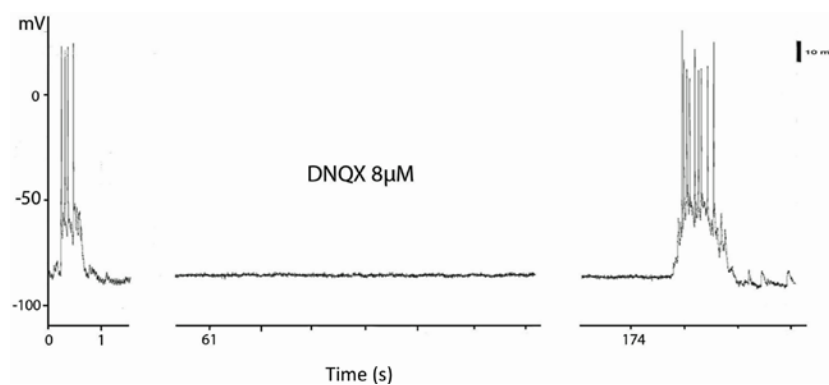


FIGURE 6 | Blockade of UP states by blockade of AMPA receptors The current clamp records are taken from a continuous record of a striatal neuron in a mixed corticostriatal culture. The culture was treated with artificial CSF containing 8 μ M DNQX for 1 min and the bursts were abolished for the next 2 min. The first burst of the recovery is shown at 174 s after DNQX application.

resulting from cortical stimulation (Rigas and Castro-Alamancos, 2007; Gibson et al., 2008; Haider and McCormick, 2009). Clearly in the organotypic cultures they must have another origin and intrinsic cortical activity seems the likeliest explanation. Viewed in multielectrode arrays the bursts are synchronous over many of the electrodes suggesting that the property is one of the assembly rather than a

single neuron property (Wagenaar et al., 2005; Rolston et al., 2007) especially since timed stimuli to the cortical network can influence activity in all of the culture (Wagenaar et al., 2005).

Furthermore the bursts in cortex influence strongly the following of striatal neurons *in vivo* and *in vitro* (Schlosser et al., 1999). Evidence from other situations suggests that striatal neurons will follow such

cortical activity in a fairly stereotyped fashion. In anesthetized rats, for instance, the cortex fires synchronous bursts that underlie the dominant voltage changes in the EEG (Stern et al., 1997, 1998; Mahon et al., 2001; Kasanetz et al., 2002). Although Blackwell et al. (2003) suggest that at least half of the depolarization that forms the UP states in striatal neurons in organotypic culture is contributed through GABA mediated chloride channel opening, it is not thought that the inhibition comes directly from cortex, but that it may result from the cortical driving of fast-spiking striatal interneurons. These neurons are certainly present in our cultures (Schock et al., 2010) and so the UP states we record may have a similar mixture of synaptic origins. We have not knowingly recorded from “fast-spiking interneurons” they can be a little hard to recognize in cultures where the morphology of the neurons is less obviously diagnostic of cell types, we certainly have not filled any with the well described physiology and anatomical characteristics. They are also relatively rare even *in vivo* though their importance in supporting the striatal firing patterns are a consequence of their powerful synaptic inputs on to the striatal output neurons, rather than their numbers (Koos and Tepper, 1999; Koos et al., 2004).

Our dissociated cell cultures with identifiable cortical neurons in close association with striatal neurons show that this “minimal” system will support the kind of UP/DOWN activity typical of their behavior *in vivo*. That already suggests that although dopamine may modulate the behavior it is not necessary for its expression in this system since no dopamine neurons from substantia nigra are present in the cultures. We have seen occasional tyrosine hydroxylase positive interneurons but they do not heavily innervate the cultures (Schock et al., 2010). Although no dopamine is present in our cultures we have not encountered giant spontaneous postsynaptic GABAergic currents either. We have explored the electrophysiological characteristics of striatal neurons in a series of different neuronal culture systems that have both cortical and striatal neurons harvested from rat or mouse embryos. In these preparations too the cortex produces bursts of activity nearly synchronously across the cultures (Arbuthnott et al., 2005). The striatal neurons follow those bursts (Garcia-Munoz et al., 2010). Bursting in cortical and striatal neurons is blocked by application of glutamate antagonists of the AMPA type.

SINGLE NEURON INTERACTIONS

Synaptic activity between pairs of neurons was seen in 55% of recorded pairs, slightly less than the proportion found in cortical slices by Debanne et al. (2008). Corticostriatal EPSCs varied in size in individual pairs; sometimes they were large enough to trigger action potentials. We stimulated only one cortical neuron enough to fire an action potential but we have no control over how many neurons were connected to the stimulated neuron and then synapsed with the striatal neuron from which we were recording. We have developed electron-microscopic methods that will allow us to measure how many synapses are made by the stimulated neuron on the recorded one but have not so far been able to use them on a connected pair of neurons. However, if there is spread from the activated neuron to many cortical neurons the rise time of the subsequent EPSP on the striatal neuron ought to be slower—even if the effects of different inputs to the neurons cannot be distinguished. In many cases we can see clearly discontinuous rise times on the EPSPs, but the relationship between time to peak and size was not straightforward, therefore there is no obvious correlation between the two measures. The answer to the question with which we started

“How big is the response to a single corticostriatal synapse?” is not at all obvious. The average size of the EPSCs with short enough latencies to be supposed monosynaptic is 100 pA, but the range includes currents smaller (10 pA) and larger (371 pA) than the estimates from previous work (e.g., Mori et al., 1994a,b,c; Blackwell et al., 2003; Ding et al., 2008) quoted in the introduction.

Some nine of the corticostriatal responses were inhibitory in nature. This abnormal connectivity is easy to explain if the cortical interneurons that we know are in the cultures (Schock et al., 2010), make synapses with the striatal neurons nearby. This seems indeed to be the case for many of the corticostriatal inhibitory pairs since there are clear cases of “intermittent bursting” responses in the records from the cortical neurons involved. This is not true in every case, however. In a few cases (two pairs so far) we have clear evidence for both excitatory and inhibitory input evoked by cortical neuron firing. Such cases make it likely that at least some of the responses are polysynaptic and may involve either inhibitory cortical or striatal neurons if our interpretation is correct. A more detailed analysis awaits more recorded pairs so that latencies can be separated and the input neurons characterized in more detail.

The other class of pairwise interactions is also not seen *in vivo*. An inhibitory action of striatal neurons on cortical neurons was observed. These synaptic actions have latencies compatible with monosynaptic activation and are often large at -80 mV (-14 to -598 pA peak; median 120; mean 168 ± 148 ; $N = 53$). They were not seen in the organotypic cultures described by Plenz and Aertsen (1996). Striatal neurons, having many of the characteristics of spiny output neurons, produce IPSCs considerably larger than those seen between pairs of striatal neurons in acute slices (Koos and Tepper, 1999; Koos et al., 2004). There may be several reasons for this, not only because the synapses are unusually numerous or otherwise abnormal, but also that the neurons at the striatal electrode might not be MSNs. Although unlikely, some of the activity we record might be from pallidal neurons (since globus pallidus is also formed from the ganglionic eminence that is the source of our neurons). It is, however, hard to believe that all of these pairs are of that nature since parvalbumin and calretinin immunopositive neurons are not much more common in the cultures than they are in the striatum *in vivo* (Schock et al., 2010) and there they are interneurons, not pallidal in origin. Similarly the typical spontaneous activity and whole neuron physiology of pallidal neurons are not obvious in the neurons from which we recorded. We looked for a bimodal distribution of the sizes of the inhibitory synaptic currents in striatocortical pairs we recorded but did not find it, although there is a long tail of very large currents that may suggest that there was a subgroup of synaptic currents of a different source.

CONCLUSION

We have developed a co-culture of dissociated cells from cortex and striatum in which pairs of neurons that are interconnected can be recorded. In such cultures we observed excitatory corticostriatal pairs, a few inhibitory pairs and a recurrent connectivity in the opposite direction with striatal neurons powerfully inhibiting cortical ones. In spite of this complex synaptology the cultures have a robust spontaneous activity pattern that is very like that observed in the corticostriatal system *in vivo*. Quantitative comparisons between this set of data and those from *in vivo* recordings may perhaps be misleading, in spite of the qualitative similarity of activity in the cultures to *in vivo* patterns of activity.

REFERENCES

- Allene, C., Cattani, A., Ackman, J. B., Bonifazi, P., Aniksztejn, L., Ben-Ari, Y., and Cossart, R. (2008). Sequential generation of two distinct synapse-driven network patterns in developing neocortex. *J. Neurosci.* 28, 12851–12863.
- Arbuthnott, G. W., Poulter, M. O., and Staines, W. A. (2005). "Corticostratial co-cultures; a minimal system for "up" states in striatal cells?" in *British Neuroscience Association Annual Meeting*, Brighton.
- Blackwell, K. T., Czubyko, U., and Pleniz, D. (2003). Quantitative estimate of synaptic inputs to striatal neurons during up and down states in vitro. *J. Neurosci.* 23, 9123–9132.
- Boakes, R. J., Burns, B. D., and Webb, A. C. (1988). Transmission of burst responses through slices of rat cerebral cortex. *J. Physiol. (Lond.)* 404, 467–478.
- Burns, B. D. (1950). Some properties of the cat's isolated cerebral cortex. *J. Physiol. (Lond.)* 111, 50–68.
- Burns, B. D. (1951). Some properties of the isolated cerebral cortex in the unanaesthetized cat. *J. Physiol. (Lond.)* 112, 156–175.
- Corner, M. A., van Pelt, J., Wolters, P. S., Baker, R. E., and Nuytinc, R. H. (2002). Physiological effects of sustained blockade of excitatory synaptic transmission on spontaneously active developing neuronal networks – an inquiry into the reciprocal linkage between intrinsic biorhythms and neuroplasticity in early ontogeny. *Neurosci. Biobehav. Rev.* 26, 127–185.
- Cowan, R. L., and Wilson, C. J. (1994). Spontaneous firing patterns and axonal projections of single corticostratial neurons in the rat medial agranular cortex. *J. Neurophysiol.* 71, 17–32.
- Debanne, D., Boudkazi, S., Campanac, E., Cudmore, R. H., Giraud, P., Fronzaroli-Molinieres, L., Carlier, E., and Caillard, O. (2008). Paired-recordings from synaptically coupled cortical and hippocampal neurons in acute and cultured brain slices. *Nat. Protoc.* 3, 1559–1568.
- Ding, J., Peterson, J. D., and Surmeier, D. J. (2008). Corticostratial and thalamostriatal synapses have distinctive properties. *J. Neurosci.* 28, 6483–6492.
- Garcia-Munoz, M., Carrillo-Reid, L., and Arbuthnott, G. W. (2010). Functional anatomy: dynamic states in basal ganglia circuits. *Front. Neuroanat.* 4:144. doi: 10.3389/fnana.2010.00144
- Gibson, J. R., Bartley, A. F., Hays, S. A., and Huber, K. M. (2008). Imbalance of neocortical excitation and inhibition and altered up states reflect network hyperexcitability in the mouse model of fragile x syndrome. *J. Neurophysiol.* 100, 2615–2626.
- Haider, B., and McCormick, D. A. (2009). Rapid neocortical dynamics: cellular and network mechanisms. *Neuron* 62, 171–189.
- Helmstaedter, M., de Kock, C. P. J., Feldmeyer, D., Bruno, R. M., and Sakmann, B. (2007). Reconstruction of an average cortical column in silico. *Brain Res. Rev.* 55, 193–203.
- Higley, M. J., and Contreras, D. (2005). Integration of synaptic responses to neighboring whiskers in rat barrel cortex in vivo. *J. Neurophysiol.* 93, 1920–1934.
- Johnson, H. A., and Buonomano, D. V. (2007). Development and plasticity of spontaneous activity and up states in cortical organotypic slices. *J. Neurosci.* 27, 5915–5925.
- Kasanetz, F., Riquelme, L. A., and Murer, M. G. (2002). Disruption of the two-state membrane potential of striatal neurones during cortical desynchronization in anaesthetized rats. *J. Physiol. (Lond.)* 543, 577–589.
- Kincaid, A. E., Zheng, T., and Wilson, C. J. (1998). Connectivity and convergence of single corticostratial axons. *J. Neurosci.* 18, 4722–4731.
- Koos, T., and Tepper, J. M. (1999). Inhibitory control of neostriatal projection neurons by GABAergic interneurons. *Nat. Neurosci.* 2, 467–472.
- Koos, T., Tepper, J. M., and Wilson, C. J. (2004). Comparison of IPSCs evoked by spiny and fast-spiking neurons in the neostriatum. *J. Neurosci.* 24, 7916–7922.
- Mahon, S., Deniau, J. M., and Charpier, S. (2001). Relationship between EEG potentials and intracellular activity of striatal and cortico-striatal neurons: an in vivo study under different anesthetics. *Cereb. Cortex* 11, 360–373.
- Mori, A., Takahashi, T., Miyashita, Y., and Kasai, H. (1994a). Quantal properties of H-type glutamatergic synaptic input to the striatal medium spiny neurons. *Brain Res.* 654, 177–179.
- Mori, A., Takahashi, T., Miyashita, Y., and Kasai, H. (1994b). Quantal properties of S-type glutamatergic synaptic input to the striatal medium spiny neuron from neonate rat. *Neurosci. Lett.* 169, 199–202.
- Mori, A., Takahashi, T., Miyashita, Y., and Kasai, H. (1994c). Two distinct glutamatergic synaptic inputs to the striatal medium spiny neurones of neonatal rats and paired-pulse depression. *J. Physiol.* 476, 217–228.
- Pleniz, D., and Aertsen, A. (1996). Neural dynamics in cortex-striatum co-cultures. I. Anatomy and electrophysiology of neuronal cell types. *Neuroscience* 70, 861–891.
- Pleniz, D., and Kitai, S. T. (1998). Up and down states in striatal medium spiny neurons simultaneously recorded with spontaneous activity in fast-spiking interneurons studied in cortex-striatum-substantia nigra organotypic cultures. *J. Neurosci.* 18, 266–283.
- Pleniz, D., and Thiagarajan, T. C. (2007). The organizing principles of neuronal avalanches: cell assemblies in the cortex? *Trends Neurosci.* 30, 101–110.
- Potter, S. M., and DeMarse, T. B. (2001). A new approach to neural cell culture for long-term studies. *J. Neurosci. Methods* 110, 17–24.
- Rigas, P., and Castro-Alamancos, M. A. (2007). Thalamocortical up states: differential effects of intrinsic and extrinsic cortical inputs on persistent activity. *J. Neurosci.* 27, 4261–4272.
- Rolston, J. D., Wagenaar, D. A., and Potter, S. M. (2007). Precisely timed spatiotemporal patterns of neural activity in dissociated cortical cultures. *Neuroscience* 148, 294–303.
- Sachdev, R. N. S., Ebner, F. F., and Wilson, C. J. (2004). Effect of subthreshold up and down states on the whisker-evoked response in somatosensory cortex. *J. Neurophysiol.* 92, 3511–3521.
- Schlosser, B., ten Bruggencate, G., and Sutor, B. (1999). Local disinhibition of neocortical neuronal circuits causes augmentation of glutamatergic and GABAergic synaptic transmission in the rat neostriatum in vitro. *Exp. Neurol.* 157, 180–193.
- Schock, S., Jolin-Dahel, K., Schock, P., Staines, W., Garcia-Munoz, M., and Arbuthnott, G. (2010). Striatal interneurons in dissociated cell culture. *Histochem. Cell Biol.* 134, 1–12.
- Stern, E. A., Jaeger, D., and Wilson, C. J. (1998). Membrane potential synchrony of simultaneously recorded striatal spiny neurons in vivo. *Nature* 394, 475–478.
- Stern, E. A., Kincaid, A. E., and Wilson, C. J. (1997). Spontaneous subthreshold membrane potential fluctuations and action potential variability of rat corticostratial neurons in vivo. *J. Neurophysiol.* 77, 1697–1715.
- Timofeev, I., Grenier, F., Bazhenov, M., Sejnowski, T. J., and Steriade, M. (2000). Origin of slow cortical oscillations in deafferented cortical slabs. *Cereb. Cortex* 10, 1185–1199.
- Tsirigotis, M., Thurig, S., Dube, M., Vanderhyden, B. C., Zhang, M., and Gray, D. A. (2001). Analysis of ubiquitination in vivo using a transgenic mouse model. *Biotechniques* 31, 120–130.
- Vergara, R., Rick, C., Hernandez-López, S., Laville, J. A., Guzman, J. N., Galarraga, E., Surmeier, D. J., and Vargas, J. (2003). Spontaneous voltage oscillations in striatal projection neurons in a rat corticostratial slice. *J. Physiol. (Lond.)* 553, 169–182.
- Wagenaar, D. A., Madhavan, R., Pine, J., and Potter, S. M. (2005). Controlling bursting in cortical cultures with closed-loop multi-electrode stimulation. *J. Neurosci.* 25, 680–688.
- Wickens, J. R., and Arbuthnott, G. W. (2010). "Gating of cortical input to the striatum," in *Handbook of Basal Ganglia Structure and Function, a Decade of Progress*, eds H. Steiner and K. Y. Tseng (Amsterdam: Elsevier), 341–352.
- Wilson, C. J. (1993). The generation of natural firing patterns in neostriatal neurons. *Prog. Brain Res.* 99, 277–297.
- Wilson, C. J., Chang, H. T., and Kitai, S. T. (1983). Disfacilitation and long-lasting inhibition of neostriatal neurons in the rat. *Exp. Br. Res.* 51, 227–235.
- Wilson, C. J., and Groves, P. M. (1980). Fine structure and synaptic connections of the common spiny neuron in the rat neostriatum. A study employing intracellular injection of horseradish peroxidase. *J. Comp. Neurology* 194, 599–615.
- Wilson, C. J., and Groves, P. M. (1981). Spontaneous firing patterns of identified spiny neurons in the rat neostriatum. *Brain Res.* 220, 67–80.
- Wilson, C. J., and Kawaguchi, Y. (1996). The origins of two-state spontaneous membrane potential fluctuations of neostriatal spiny neurons. *J. Neurosci.* 16, 2397–2410.
- Wright, A. K., Ramanathan, S., and Arbuthnott, G. W. (2001). Identification of the source of the bilateral projection system from cortex to somatosensory neostriatum and an exploration of its physiological actions. *Neuroscience* 103, 87–96.

Conflict of Interest Statement: The authors declare that the research was conducted in the absence of any commercial or financial relationships that could be construed as a potential conflict of interest.

Received: 31 January 2011; paper pending published: 08 March 2011; accepted: 08 June 2011; published online: 28 June 2011.
Citation: Randall FE, Garcia-Munoz M, Vickers C, Schock SC, Staines WA and Arbuthnott GW (2011) The corticostratial system in dissociated cell culture. *Front. Syst. Neurosci.* 5:52. doi: 10.3389/fnsys.2011.00052
Copyright © 2011 Randall, Garcia-Munoz, Vickers, Schock, Staines and Arbuthnott. This is an open-access article subject to a non-exclusive license between the authors and Frontiers Media SA, which permits use, distribution and reproduction in other forums, provided the original authors and source are credited and other Frontiers conditions are complied with.



Widespread increases in malondialdehyde immunoreactivity in dopamine-rich and dopamine-poor regions of rat brain following multiple, high doses of methamphetamine

Kristen A. Horner^{1*}, Yamiece E. Gilbert^{1,2} and Susan D. Cline¹

¹ Division of Basic Medical Sciences, Mercer University School of Medicine, Macon, GA, USA

² Master of Public Health Program, Department of Community Medicine, Mercer University School of Medicine, Macon, GA, USA

Edited by:

Elizabeth Abercrombie, Rutgers-Newark: The State University of New Jersey, USA

Reviewed by:

Christine E. Collins, Vanderbilt University, USA
Preston E. Garrahy, Indiana University, USA

*Correspondence:

Kristen A. Horner, Division of Basic Medical Sciences, Mercer University School of Medicine, 1550 College Street, Macon, GA 31207, USA.
e-mail: horner_ka@mercer.edu

Treatment with multiple high doses of methamphetamine (METH) can induce oxidative damage, including dopamine (DA)-mediated reactive oxygen species (ROS) formation, which may contribute to the neurotoxic damage of monoamine neurons and long-term depletion of DA in the caudate putamen (CPu) and substantia nigra pars compacta (SNpc). Malondialdehyde (MDA), a product of lipid peroxidation by ROS, is commonly used as a marker of oxidative damage and treatment with multiple high doses of METH increases MDA reactivity in the CPu of humans and experimental animals. Recent data indicate that MDA itself may contribute to the destruction of DA neurons, as MDA causes the accumulation of toxic intermediates of DA metabolism via its chemical modification of the enzymes necessary for the breakdown of DA. However, it has been shown that in human METH abusers there is also increased MDA reactivity in the frontal cortex, which receives relatively fewer DA afferents than the CPu. These data suggest that METH may induce neuronal damage regardless of the regional density of DA or origin of DA input. The goal of the current study was to examine the modification of proteins by MDA in the DA-rich nigrostriatal and mesoaccumbal systems, as well as the less DA-dense cortex and hippocampus following a neurotoxic regimen of METH treatment. Animals were treated with METH (10 mg/kg) every 2 h for 6 h, sacrificed 1 week later, and examined using immunocytochemistry for changes in MDA-adducted proteins. Multiple, high doses of METH significantly increased MDA immunoreactivity (MDA-ir) in the CPu, SNpc, cortex, and hippocampus. Multiple METH administration also increased MDA-ir in the ventral tegmental area and nucleus accumbens. Our data indicate that multiple METH treatment can induce persistent and widespread neuronal damage that may not necessarily be limited to the nigrostriatal DA system.

Keywords: neurotoxicity, lipid peroxidation, striatum, substantia nigra, psychostimulant, dopamine

INTRODUCTION

Methamphetamine (METH) is a widely abused psychostimulant whose use has dire social and medical consequences. Over 60 million people world-wide report abusing amphetamine-type stimulants, especially METH (Maxwell, 2005). In the United States, METH use is endemic in the Western states, while the epidemic of METH use and abuse is growing notably in the Midwestern and Southern states (Substance Abuse and Mental Health Services Administration, Office of Applied Studies, 2010). The short-term effects of METH use include euphoria, increased locomotor activity, and hyperthermia, whereas long-term use can lead to dependence, addiction, paranoia, and psychosis. Repeated high doses of METH can lead to neurotoxic insults within the basal ganglia of both rodents and humans, which may underlie some of the symptoms of long-term abuse (Hotchkiss and Gibb, 1980; Volkow et al., 2001; Johnson-Davis et al., 2002). In particular, treatment with multiple high doses of METH results in damage to dopamine (DA) neurons of the substantia nigra pars compacta (SNpc), which project heavily to the caudate putamen (CPu), while the DA neurons in the adjacent ventral tegmental area (VTA), which project to the nucleus accumbens (NAc) are less severely affected (Ricaurte et al.,

1980). The damage to the DA neurons in the SNpc is evidenced by long-term losses in several prototypical markers of dopaminergic neurons, including a loss of DA uptake sites, decreased tyrosine hydroxylase (TH) activity and severely reduced DA tissue levels in the CPu (Kogan et al., 1976; Hotchkiss and Gibb, 1980; Ricaurte et al., 1980; Seiden and Ricaurte, 1987).

The exact mechanism(s) that mediate the enhanced and relatively selective neurotoxicity of nigrostriatal neurons in response to repeated METH treatment are not entirely understood. Several studies have identified oxidative stress as a contributing factor in METH-induced neurotoxicity (Yamamoto and Zhu, 1998; Lavoie and Hastings, 1999; Yamamoto and Bankson, 2005; Krasnova and Cadet, 2009). One of the most common markers of oxidative stress is the lipid peroxidation product malondialdehyde (MDA; Aldini et al., 2007). METH can increase the oxidation of DA, resulting in the formation of reactive DA quinones and superoxide radicals within the terminals of dopaminergic neurons (Lavoie and Hastings, 1999; Krasnova and Cadet, 2009). These reactive oxygen species (ROS) can attack polyunsaturated fatty acids, which are enriched in neuronal membranes, resulting in the generation of MDA (Brown and Yamamoto, 2003; Brown et al., 2005; Del Rio et al., 2005; Krasnova

and Cadet, 2009; Lieberman and Marks, 2009). Accordingly, enhanced levels of MDA or MDA-like reactivity have been found in the brains of METH addicts and METH-treated experimental animals (Acikgoz et al., 1998; Yamamoto and Zhu, 1998; Kim et al., 1999; Kita et al., 2000; Gluck et al., 2001; Fitzmaurice et al., 2006). However, recent data raises the possibility that MDA is not just the result of oxidative stress and cellular damage, but can act on its own to induce neuronal toxicity (Jinsmaa et al., 2009; Long et al., 2009).

For example, MDA is a reactive electrophile that can modify amino groups in proteins, rendering enzymes non-functional (Del Rio et al., 2005; Aldini et al., 2007). MDA inhibits mitochondrial electron transport proteins, which may lead to ROS generation and mitochondrial dysfunction in neurons (Long et al., 2009). Furthermore, it has been shown that MDA can increase levels of toxic intermediates of DA catabolism (Jinsmaa et al., 2009) and repeated treatment with METH can increase MDA and other reactive aldehydes in the DA-rich nigrostriatal pathway (Yamamoto and Zhu, 1998; Gluck et al., 2001; Fitzmaurice et al., 2006; Horner et al., 2010). However, recent data show that in human abusers of METH, reactive aldehyde levels are also increased in the frontal cortex, a region that has relatively fewer DA afferents from the SNpc and contains lower tissue levels of DA than the CPu (Emson et al., 1977; Scatton et al., 1983; Johnson-Davis et al., 2002; Fitzmaurice et al., 2006). Together, these data suggest that METH can induce significant oxidative damage regardless of the regional density of DA or origin of DA input. Furthermore, it is possible that the formation of MDA-protein adducts could lead to DA-related cellular damage, as well as non-DA-related damage to neurons via direct interactions of MDA with essential proteins and amino acids.

The purpose of the current study was to examine and compare the effect of multiple high doses of METH on the generation of MDA-adducted protein in the DA-rich nigrostriatal and mesoaccumbal systems. We also examined the generation of MDA-adducted proteins by multiple METH treatment in the hippocampus and cortex, two areas that are less intensely innervated by DA afferents than the CPu and NAc. While previous studies have examined MDA reactivity following METH administration in experimental animals and in human METH addicts, many of these studies used the thiobarbituric acid reactive substances (TBARS) assay to detect changes in MDA levels (Acikgoz et al., 1998; Jayanthi et al., 1998; Kim et al., 1999; Kita et al., 2000; Gluck et al., 2001; Fitzmaurice et al., 2006). While a standard approach for MDA measurement in body fluids and tissues, the TBARS assay is not specific for MDA and detects free, non-adducted MDA, including MDA that has been released from its adducts with biomolecules as well as unreacted, diffusible MDA that may not impair cellular function (Moore and Roberts, 1998). The current study employed immunocytochemistry with specificity for MDA-adducted proteins, which allowed us to detect MDA-induced neuronal damage, while maintaining anatomical and cellular resolution. We also examined levels of TH immunoreactivity (TH-ir) in the CPu and the NAc, in order to confirm that repeated METH treatment resulted in a severe depletion of DA in the nigrostriatal pathway as compared to the mesoaccumbal pathway. Finally, we determined whether the levels of MDA-adducted protein induced by multiple METH treatment correlated significantly with the severity of TH depletion in the CPu, as compared to the NAc.

MATERIALS AND METHODS

ANIMALS

Male Sprague-Dawley rats (Harlan Laboratories, Indianapolis, IN, USA), weighing 250–350 g were used in all experiments. Rats were housed in groups of four in plastic cages in a temperature-controlled room. Rats were on a 14:10 h light/dark cycle and had free access to food and water. All animal care and experimental manipulations were approved by the Institutional Animal Care and Use Committee of Mercer University School of Medicine and were in accordance with the National Institutes of Health *Guide for the Care and Use of Laboratory Animals*.

PHARMACOLOGICAL PROCEDURES

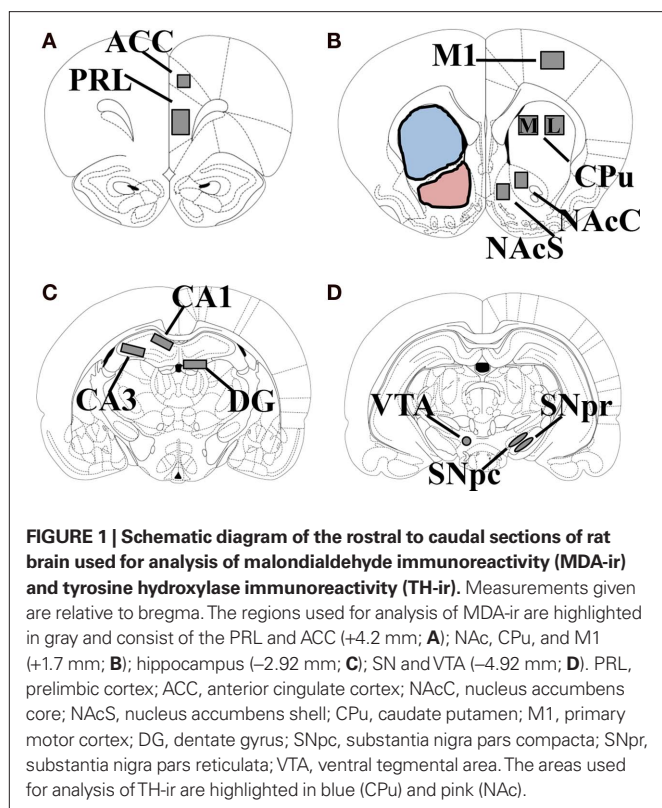
(±) Methamphetamine hydrochloride was obtained from the National Institute on Drug Abuse (Bethesda, MD, USA). The drug doses were calculated as the free base, diluted in saline, and administered subcutaneously. On the day of the experiment, the rats were weighed, housed in plastic tub cages (eight rats per cage), and transferred to the laboratory. Animals received a total of four injections of either METH (10 mg/kg, s.c.) or saline with a 2 h-interval between each injection. This dosing regimen has been shown to result in significant depletion of DA in the nigrostriatal system (Hotchkiss and Gibb, 1980; Johnson-Davis et al., 2002).

TISSUE SECTIONING

One week after exposure to multiple doses of METH, rats were sacrificed by exposure to CO₂, followed by decapitation. The brains were rapidly harvested, quick frozen in isopentane on dry ice and stored at −80°C. The brains were then cut into 12-μm sections on a cryostat (Minotome Plus, Triangle Biomedical Sciences, Durham, NC, USA). Coronal sections were taken through the anterior cingulate cortex (ACC)/prelimbic cortex (PRL; +4.2 mm anterior to bregma), CPu/NAc/primary motor cortex (M1; +1.7 mm anterior to bregma), hippocampus (−2.92 mm posterior to bregma), and SN/VTA (−4.92 mm posterior to bregma; **Figure 1**). Sections were thaw-mounted onto Superfrost Plus slides (VWR, Radnor, PA, USA) and stored at −20°C until their use in immunocytochemical assays.

TH IMMUNOCYTOCHEMISTRY

A modified peroxidase anti-peroxidase method was used to detect changes in TH-ir in the CPu and NAc (Sternberger, 1979; Johnson-Davis et al., 2002). Slides were thawed, washed in 0.1 M phosphate-buffered saline (PBS) and post-fixed in 4% paraformaldehyde/0.9% NaCl for 10 min. Slides were rinsed three times for 5 min in PBS and the sections circled with a PAP pen. Non-specific binding was blocked with 10% normal horse serum/0.3% Triton-X for 2 h at room temperature. The blocking solution was then removed, and the sections were incubated overnight in humid chambers at 4°C with a monoclonal mouse-anti TH antibody (1:300; Immunostar, Hudson, WI, USA) diluted in 0.3% Triton-X/PBS. The next day, the slides were rinsed three times for 5 min in PBS, and incubated for 1.5 h at room temperature with anti-mouse (H + L) peroxidase generated in horse (1:150; Vector Laboratories, Burlingame, CA, USA) diluted in PBS/0.3% Triton-X. The slides were rinsed three times in PBS, and incubated with 0.1% DAB/0.005% H₂O₂ in PBS for 4–8 min. The slides were rinsed briefly in deionized H₂O, dehydrated in a series of alcohols, and coverslipped out of xylene.



MDA IMMUNOCYTOCHEMISTRY

Sections through PRL/ACC, CPu/NAc/M1, hippocampus, and SN/VTA were examined for changes in MDA-adducted proteins. Briefly, slides were washed three times in PBS, and fixed in 4% paraformaldehyde/0.9% NaCl for 10 min. The sections were then outlined with a PAP pen, followed by three washes in PBS and blocked with 10% normal horse serum in 0.3% Triton-X for 2 h at room temperature. The blocking solution was then removed, and the sections were incubated with a polyclonal rabbit anti-MDA antibody (1:200; Abcam, Cambridge, MA, USA), overnight at 4°C in humidified chambers. The sections were then washed with PBS, and incubated for 2 h at room temperature with a biotinylated goat anti-rabbit IgG antiserum (1:200; Vector Laboratories) diluted in 5% horse serum/PBS. Slides were then washed three times in PBS, incubated 1 h at room temperature in ABC solution (Elite ABC Kit, Vector Laboratories) and washed three more times in PBS. Bound antibody was detected by incubating the sections in a 3,3'-diaminobenzidine/Ni²⁺ solution (Vector Laboratories) for 4–8 min. Slides were washed with deionized H₂O, dehydrated in a series of alcohols and coverslipped out of xylene.

IMAGE ANALYSIS

Slides from TH immunocytochemistry were analyzed using Image J (National Institutes of Health; <http://rsb.info.nih.gov/ij/>), as previously described (Johnson-Davis et al., 2002) and the images captured with a video camera (CCD IEEE-1394, Scion Corporation, Frederick, MD, USA). Basic densitometric analysis yielded average density (gray) values over the region of interest. Before the measurement of sections, the linearity of the video camera to increasing

signal intensity was determined using the average gray values of signals of known optical density from a photographic step tablet (Eastman Kodak Company, Rochester, NY, USA). The intensity of the light was adjusted such that the values measured from the slides of TH-ir brain sections fell within the linear portion of the system's response. Lighting and camera conditions remained constant during the process of capturing and collection of density measurements. Mean gray values were measured in the left hemisphere for the whole CPu, which was designated as the area below the corpus callosum and above the anterior commissure, ending approximately at the ventral tip of the lateral ventricle (see **Figure 1B**, blue highlighted area). The whole NAc was designated as the area just dorsal to the anterior commissure, ending at the ventral tip of the lateral ventricle (in order to capture the entire core) and dorsal to the medial forebrain bundle/ventral pallidum on the ventral border (see **Figure 1B**, pink highlighted area). In order to correct for background labeling, the mean gray value of the white matter was subtracted from the mean gray value of the CPu or NAc, for each animal in the study.

For the analysis of MDA immunoreactivity (MDA-ir), sections were captured from a VistaVision microscope (VWR, Radnor, PA, USA) with a video camera (CCD Moticam 2300, Motic, Richmond, BC, Canada), using a 10× objective. Immunoreactivity was measured in the left hemisphere of each brain in the following pixel areas: 300 × 500 for PRL, 200 × 200 for ACC, 500 × 300 for M1, 400 × 400 for medial and lateral CPu, 200 × 300 for nucleus accumbens core, 150 × 300 for nucleus accumbens shell, 300 × 100 for CA1, 400 × 100 for CA3 and dentate gyrus (DG), a 500 × 150 oval for SNpc and substantia nigra pars reticulata (SNpr), and a circle with a diameter of 152 pixels for the VTA (**Figure 1**). The areas analyzed for semi-quantification were held constant for all experiments and was based on modified procedures from (Simpson et al., 1995; Choe et al., 2002; Horner et al., 2006). The number of MDA-labeled particles that exceeded the threshold density in each region of interest was determined using the particle analysis option in Image J. The pixel range for particle size was determined before analysis by outlining positively labeled cells from several randomly selected sections and determining the average size of the labeled cells in terms of pixel area. The lower limit for a “labeled cell” on the particle analysis setting was then set to the smallest number of pixels measured for any cell, whereas the upper limit was set at the maximal particle size on the particle analysis option on Image J. The threshold density was adjusted such that background staining was eliminated and the number of immunoreactive pixels per the selected area in each region of interest was measured above this threshold.

STATISTICAL ANALYSIS

The effect of multiple METH treatment on TH-ir and MDA-ir was analyzed using a two-tailed unpaired *t*-test for each region of interest. Differences in MDA-ir between the sub-regions of cortex or hippocampus following multiple METH treatment were analyzed using a one-way analysis of variance followed by Tukey's multiple comparisons *post hoc* test. Correlation between the number of MDA-ir particles and TH-ir mean gray values for the CPu and NAc were calculated according to the Pearson method. The alpha level for all analyses was set at 0.05.

RESULTS

EFFECTS OF MULTIPLE HIGH DOSES OF METH ON MDA-IR IN THE CPU AND NAC

Exposure to multiple, high doses of METH resulted in an increase in MDA-ir particles in both the lateral and medial regions of CPu (**Figure 2A**). Semi-quantitative analysis revealed that multiple METH treatment significantly increased MDA-ir in the lateral ($t = 5.03$, $p = 0.0001$) and medial ($t = 5.04$, $p = 0.0001$) CPu (**Figure 2B**). There was not a significant difference in the level of MDA-ir between the lateral and medial regions of CPu in METH-treated animals ($t = 1.39$, $p = 0.172$). Exposure to multiple METH treatment also increased MDA-ir particles in the core and shell of NAc (**Figure 3A**). Semi-quantitative analysis showed that multiple METH treatment significantly increased MDA-ir in the core ($t = 5.68$, $p < 0.0001$) and shell ($t = 4.68$, $p = 0.0004$) of NAc (**Figure 3B**). There was not a significant difference between the level of MDA-ir induced by multiple METH treatment for the core vs. shell sub-regions of NAc ($t = 2.04$, $p = 0.06$). However, multiple METH treatment induced significantly higher levels of MDA-ir in the CPu as compared to the NAc ($t = 5.35$, $p < 0.0001$).

EFFECTS OF MULTIPLE HIGH DOSES OF METH ON MDA-IR IN THE SN AND VTA

Exposure to multiple, high doses of METH resulted in an increase in MDA-ir particles in the SNpc, but did not alter the amount of MDA-ir staining in the SNpr (**Figure 4A**). Exposure to multiple METH treatment also increased MDA-ir particles in the VTA (**Figure 4A**). Semi-quantitative analysis revealed that multiple METH treatment significantly increased MDA-ir in the SNpc ($t = 6.62$, $p < 0.0001$), but not the SNpr ($t = 0.65$, $p = 0.949$). Multiple METH treatment also significantly increased the number of MDA-ir particles in the VTA ($t = 5.00$, $p = 0.0002$; **Figure 4B**). Additional analysis revealed that multiple METH treatment resulted in a greater increase in MDA-ir in the SNpc as compared to the VTA ($t = 11.17$, $p < 0.0001$).

EFFECTS OF MULTIPLE HIGH DOSES OF METH ON MDA-IR IN THE CORTEX

Exposure to multiple, high doses of METH resulted in an increase in MDA-ir particles all regions of cortex examined (**Figure 5A**). Semi-quantitative analysis revealed that multiple METH treatment significantly increased MDA-ir in the PRL ($t = 5.29$, $p = 0.0003$), ACC ($t = 7.20$, $p < 0.0001$), and M1 ($t = 8.41$, $p < 0.0001$; **Figure 5B**). Additional analysis revealed that the level of MDA-ir was

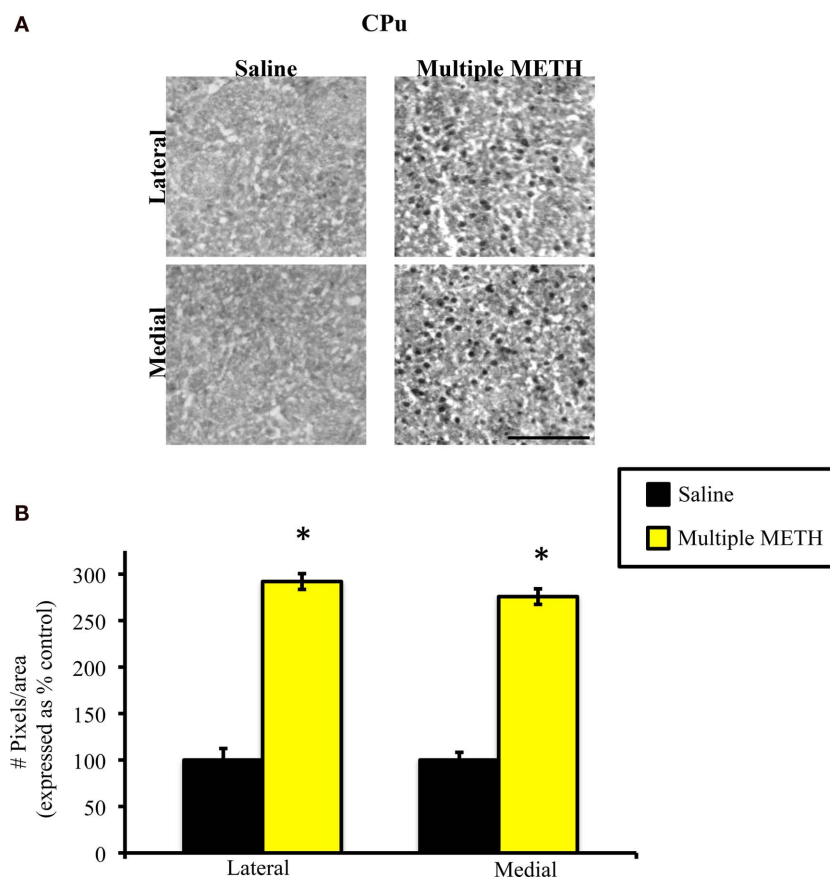


FIGURE 2 | Photomicrographs of MDA immunoreactivity (MDA-ir) in the lateral and medial CPu (A), 1 week after saline or multiple METH treatment (4×10 mg/kg, s.c.). Scale bar represents 100 μ M. Data are presented as the percentage of MDA-ir particles in saline-treated control

animals (\pm SEM, $n = 7$ –14 animals/group). Semi-quantitative analysis showed that treatment with multiple doses of METH significantly increased MDA-ir in both the lateral and medial CPu (**B**). * $p < 0.05$ as compared to saline-treated animals.

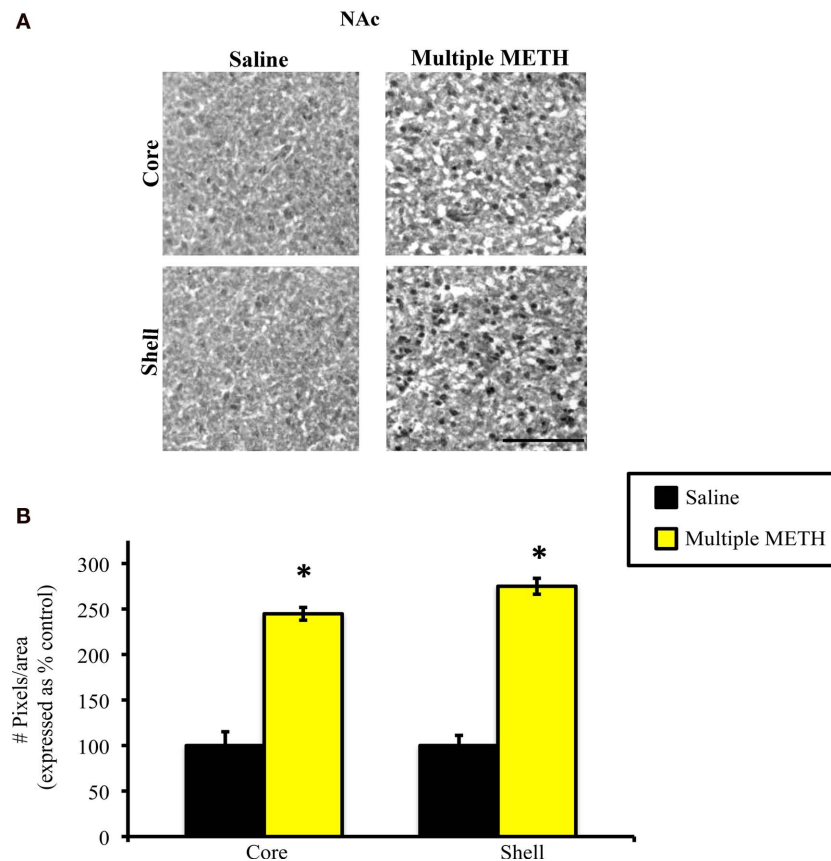


FIGURE 3 | Photomicrographs of MDA-ir in the core and shell of the NAc (A), 1 week after saline or multiple METH treatment (4×10 mg/kg, s.c.). Scale bar represents 100 μ m. Data are presented as the percentage of MDA-ir particles in saline-treated control animals (\pm SEM, $n = 7$ –14 animals/group). Semi-quantitative analysis showed that treatment with multiple doses of METH significantly increased MDA-ir in both the core and shell of the NAc (B). * $p < 0.05$ as compared to saline-treated animals.

significantly greater in the ACC sub-region of cortex as compared to the PRL ($p < 0.01$) and M1 ($p < 0.001$) cortical sub-regions following multiple METH treatment.

EFFECTS OF MULTIPLE HIGH DOSES OF METH ON MDA-IR IN THE HIPPOCAMPUS

Exposure to multiple, high doses of METH resulted in an increase in MDA-ir particles in all regions of hippocampus examined (Figure 6A). Semi-quantitative analysis revealed that multiple METH treatment significantly increased MDA-ir in CA1 ($t = 5.00$, $p = 0.0001$), CA3 ($t = 6.46$, $p < 0.0001$), and DG ($t = 4.01$, $p = 0.002$; Figure 6B). Additional analysis revealed that the level of MDA-ir was significantly greater in the CA3 sub-region of hippocampus as compared to the CA1 ($p < 0.001$) and DG ($p < 0.001$) hippocampal sub-regions following multiple METH treatment.

EFFECTS OF MULTIPLE HIGH DOSES OF METH ON TH-IR IN THE CPU AND NAC

Treatment with multiple, high doses of METH decreased the amount of TH-ir in the CPu, as well as the NAc (Figures 7A,B). Densitometric analysis revealed that exposure to multiple doses of METH significantly reduced staining for TH in the CPu ($t = 6.02$, $p < 0.0001$) and NAc ($t = 2.98$, $p = 0.009$; Figure 7C). However,

the decrease in TH-ir induced by multiple METH treatment was significantly greater in the CPu, as compared to the NAc ($t = 6.25$, $p < 0.0001$), with TH-ir being reduced to approximately 60 and 20% of control, respectively. In order to examine whether a relationship might exist between the degree of MDA-protein adducts induced by multiple METH treatment and the depletion of TH, we determined whether a correlation existed between the number of MDA-ir particles and the average gray values for TH-ir. In the CPu, a significant negative correlation existed between the number of MDA-ir particles (medial plus lateral regions) and the average gray values for TH-ir ($r = -0.82$, $p < 0.0001$; Figure 7D). In the whole NAc, there was not a significant correlation between the number of MDA-ir particles (core plus shell regions) and the average gray values for TH-ir ($r = -0.40$, $p = 0.10$; Figure 7E). There was not a significant correlation between the number of MDA-ir particles and the average gray values for TH-ir when the core ($r = -0.40$, $p = 0.15$) and shell ($r = -0.47$, $p = 0.09$) were each analyzed separately (data not shown).

DISCUSSION

The purpose of the present study was to examine the effects of multiple high doses of METH on the modification of proteins by MDA in the nigrostriatal and mesoaccumbal systems, as well as

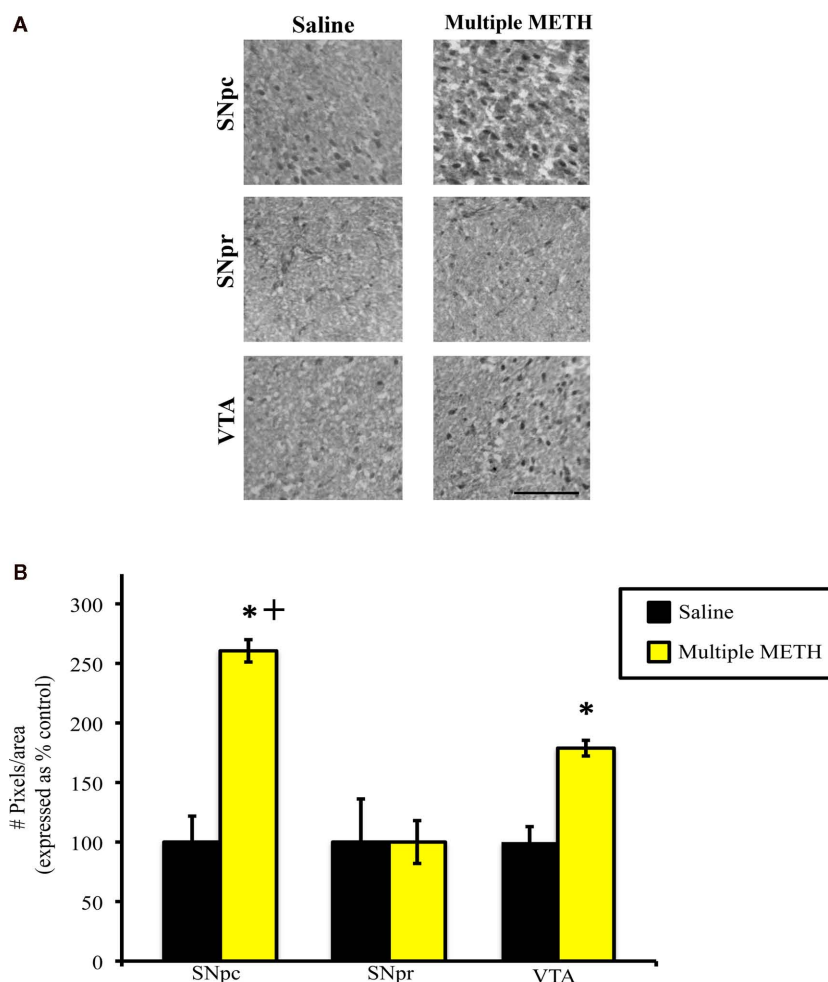


FIGURE 4 | Photomicrographs of MDA-ir in the SNpc, SNpr, and VTA (A) 1 week after saline or multiple METH treatment (4×10 mg/kg, s.c.). Scale bar represents 100 μ m. Data are presented as the percentage of MDA-ir particles in saline-treated control animals (\pm SEM, $n = 7$ –14 animals/group). Semi-quantitative analysis showed that treatment with multiple

doses of METH significantly increased MDA-ir in the SNpc and VTA, but not in the SNpr (B). Multiple METH treatment also resulted in significantly greater MDA-ir in the SNpc, as compared to the VTA. * $p < 0.05$ as compared to saline-treated animals. + $p < 0.05$ as compared to the VTA in METH-treated animals.

in cortex and hippocampus. We have shown that repeated METH administration results in increases in MDA-modified proteins in several regions of brain that persisted for 1 week after treatment, raising the possibility that long-term METH-induced neuronal damage could arise, in part, from the MDA-induced inactivation of essential protein functions. MDA-ir was significantly increased in the SNpc and CPu after multiple METH administration, which is in line with the toxic effects of multiple METH treatment on the dopaminergic neurons in this pathway. Multiple METH administration also significantly increased MDA-ir in the VTA and NAc, which was unexpected, as the dopaminergic neurons of the mesoaccumbal pathway are less severely affected by this treatment regimen. Furthermore, multiple METH treatment MDA-ir was significantly increased in the cortex and hippocampus, two regions that contain relatively lower levels of DA, indicating that MDA can induce significant protein adduction independent of the DA system. The data from the current study illustrate that there is widespread adduction of proteins by MDA following repeated treatment with

METH. Furthermore, our data show that MDA-protein adducts can occur in areas that receive less dense DA input, as well as in areas that are DA-dense and sensitive to the neurotoxic effects of METH treatment.

Our study focused on the accumulation of MDA-adducted proteins after exposure to a neurotoxic regimen of METH treatment as an indication of biomolecular damage by MDA that may impair cellular function. While we have yet to characterize the specific targets of MDA, it is important, nevertheless, to speculate about the potential mechanisms by which MDA production may contribute to METH-induced neurotoxicity, as these hypotheses will guide future research on METH-induced MDA neuronal damage. As mentioned above, MDA can induce cellular damage via DA-related mechanisms, or through the inhibition of mitochondrial function (Jinsmaa et al., 2009; Long et al., 2009). It is possible that in regions where there is a dense concentration of DA, such as the nigrostriatal pathway, DA-related mechanisms of MDA-induced damage may predominate and contribute to the destruction of

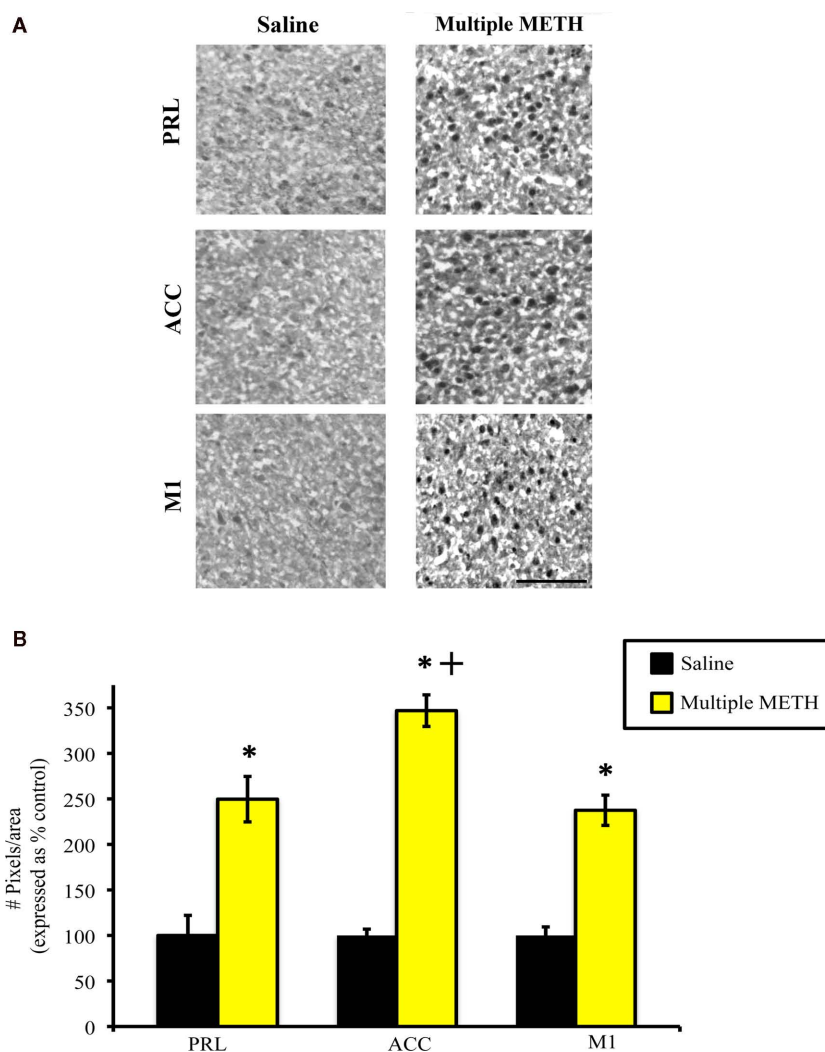


FIGURE 5 | Photomicrographs of MDA-ir in the PRL, ACC, and M1 (A), 1 week after saline or multiple METH treatment (4×10 mg/kg, s.c.). Scale bar represents 100 μ M. Data are presented as the percentage of MDA-ir particles in saline-treated control animals (\pm SEM, $n = 7$ –14 animals/group). Semi-quantitative analysis showed that treatment with multiple doses of METH

significantly increased MDA-ir in all three regions of cortex examined (B). Multiple METH treatment also resulted in significantly greater MDA-ir in the ACC sub-region of cortex, as compared to the PRL and M1 cortical sub-regions. * $p < 0.05$ as compared to saline-treated animals; † $p < 0.05$ as compared to the PRL and M1 sub-regions of cortex in METH-treated animals.

these neurons. DA is metabolized by monoamine oxidase (MAO) to produce 3,4-dihydroxyphenylacetaldehyde (DOPAL), which is then oxidized by aldehyde dehydrogenase-2 (ALDH-2) to produce 3,4-dihydroxyphenylacetic acid (DOPAC; Marchitti et al., 2007). Metabolism of DA by MAO and ALDH-2 prevents its cytoplasmic accumulation and its conversion to a neurotoxic quinone that conduces the eventual destruction of dopaminergic neurons (Lavoie and Hastings, 1999; Yamamoto and Bankson, 2005; Marchitti et al., 2007; Krasnova and Cadet, 2009). However, recent data indicates that MDA can lead to accumulation of DOPAL via irreversible inhibition of ALDH-2 activity (Jinsmaa et al., 2009). DOPAL is an aldehyde that is chemically reactive with proteins and has been shown to be several times more toxic to dopaminergic neurons than the DA-derived quinone (Rooke et al., 2000; Burke et al., 2003, 2004; Jinsmaa et al., 2009). In addition, the infusion of DOPAL into

the SNpc or VTA results in higher levels of toxicity in the SNpc as compared to the VTA (Burke et al., 2003). Interestingly, the VTA has been shown to express higher levels of factors involved in cell survival and protection than the SNpc, suggesting that the SNpc may be more vulnerable to toxic insults than the VTA (Grimm et al., 2004). Thus, repeated exposure to METH may result in MDA-mediated increases in DOPAL in both the SNpc and VTA, but the increase in DOPAL may have less of a toxic impact in the VTA, whereas the neurons of the SNpc may be more severely affected.

Interestingly, very little MDA-ir was found in the SNpr after multiple METH treatment, as compared to all other regions examined. The lack of MDA-ir induced by multiple METH treatment could be due to the fact that the SNpr is comprised of γ -aminobutyric acid (GABA)-containing neurons and also contains relatively low levels of DA (Gerfen and Bolam, 2010). However, somatodendritic release

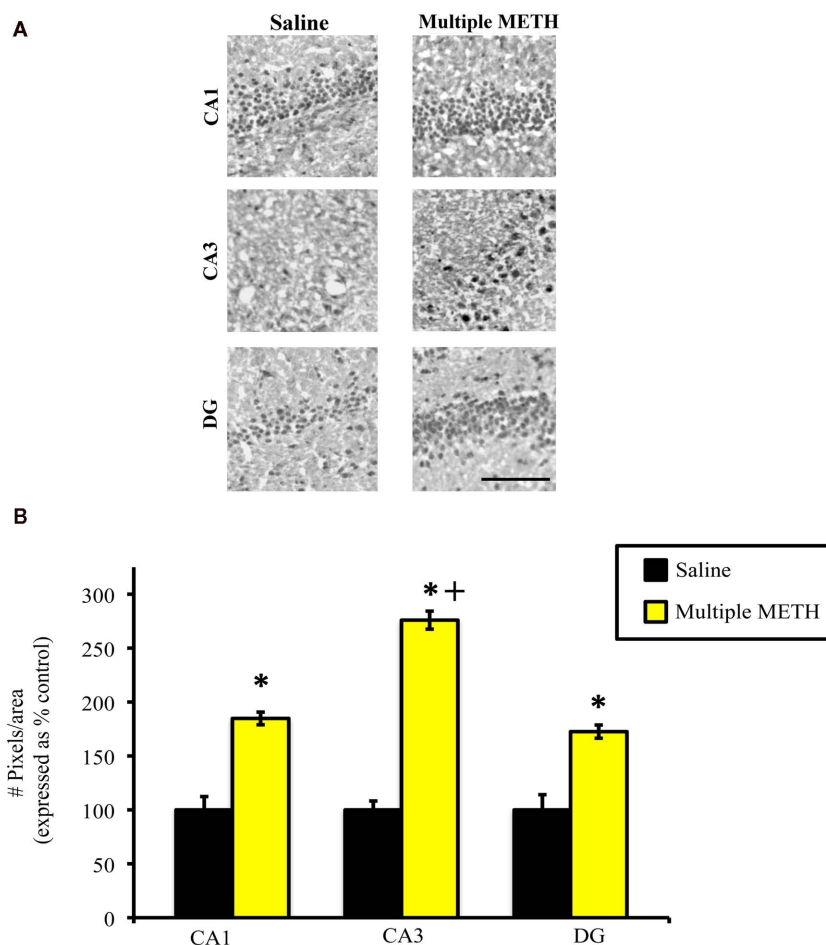


FIGURE 6 | Photomicrographs of MDA-ir in CA1, CA3, and DG (A) 1 week after saline or multiple METH treatment (4 × 10 mg/kg, s.c.). Scale bar represents 100 μ M. Data are presented as the percentage of MDA-ir particles in saline-treated control animals (\pm SEM, $n = 7$ –14 animals/group). Semi-quantitative analysis showed that treatment with multiple doses of METH significantly

increased MDA-ir in all regions of hippocampus examined (B). Multiple METH treatment also resulted in significantly greater MDA-ir in the CA3 sub-region of hippocampus, as compared to the CA1 and DG hippocampal sub-regions. * $p < 0.05$ as compared to saline-treated animals; + $p < 0.05$ as compared to the CA1 and DG sub-regions of hippocampus in METH-treated animals.

of DA into the SNpr from the dopaminergic neurons of the adjacent SNpc has been well-documented (Korf et al., 1976; Chéramy et al., 1981; Robertson et al., 1991; Heeringa and Abercrombie, 1995; Windels and Kiyatkin, 2006) and METH has been shown to increase extracellular levels of DA in the substantia nigra (Bustamante et al., 2002). Thus, DA levels may increase in the SNpr during METH treatment, setting the stage for DA-related increases in MDA-ir within this region, aside from any non-DA-related increases in MDA-ir that might also occur. At this point, however, it is not clear what factors might contribute to the relative resistance of the SNpr to the development METH-induced MDA-protein adducts following multiple METH treatment. Additional studies are needed in order to address the potential mechanisms that might underlie the resistance of the SNpr to the development of METH-induced MDA-protein adducts.

It is important to note, however, that our data indicate that repeated METH treatment results in significantly greater levels of MDA-ir in the nigrostriatal system vs. the mesoaccumbal system, raising the possibility that the enhanced neurotoxicity of the

nigrostriatal system could simply be the result of relatively higher levels MDA-adducted proteins within this region. Interestingly, our data also show that there is a significant negative correlation between the loss of TH-ir and the increase in MDA-adducted proteins in the CPU, indicating a relationship exists between increased MDA accumulation and depletion of TH in the nigrostriatal system. This inverse relationship between MDA-ir and TH-ir was not observed in the NAc. It is possible that in the nigrostriatal system, where TH levels decrease as levels of MDA-modified proteins increase, MDA-mediated inhibition of ALDH-2 and accumulation of DOPAL (which is structurally similar to DA) may lead to feedback inhibit on the production of TH, due to cellular sensing of high DA-like compound levels (Burke et al., 2003). On the other hand, in the mesoaccumbal system, where TH levels do not appear to be related to levels of MDA-modified proteins, ALDH enzymes may be able to effectively eliminate DOPAL and avoid feedback inhibition of TH synthesis. Indeed, other ALDH isoforms, such as ALDH-1, can compensate for DOPAL oxidation in the event of ALDH-2 blockade (Manzer et al., 2003; Marchitti et al., 2007; Jinsmaa et al.,

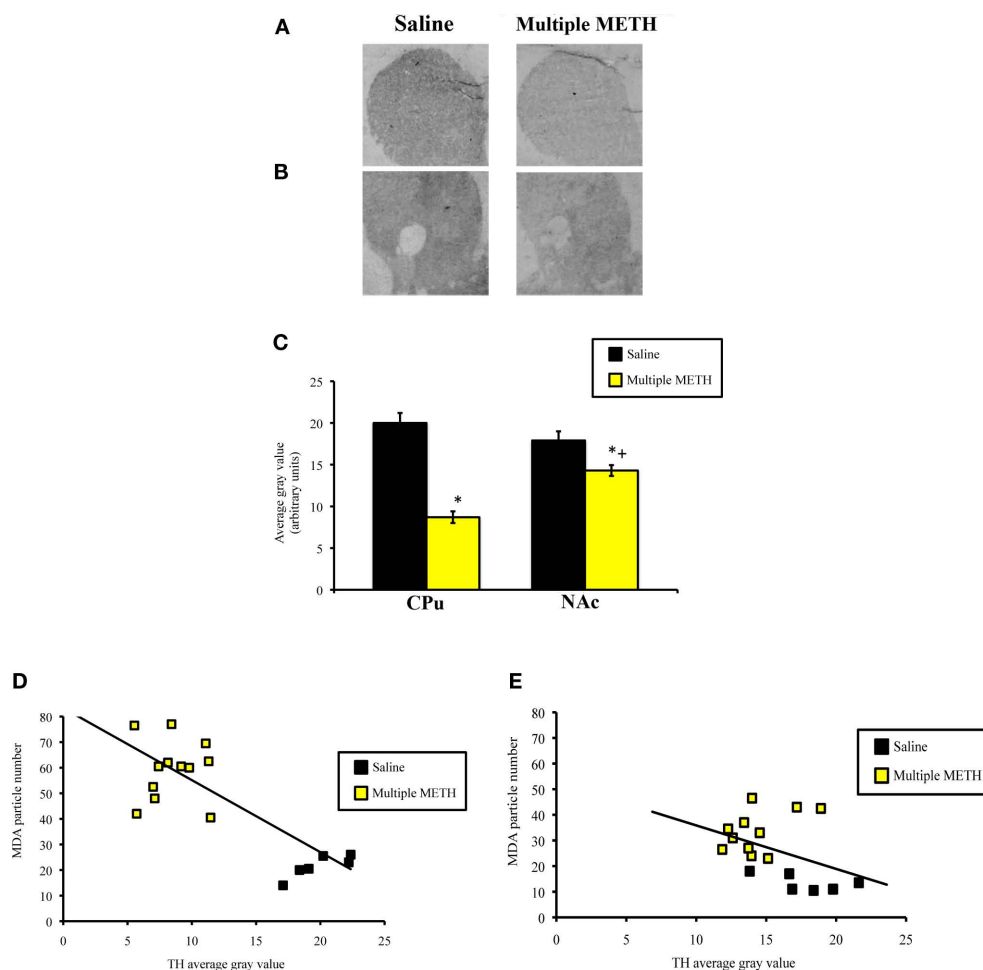


FIGURE 7 | Photomicrographs of TH-ir in the CPu (A) and NAc (B), 1 week after multiple METH treatment (4×10 mg/kg, s.c.) and quantitative analysis of the effects of multiple METH treatment on TH-ir in the whole CPu and whole NAc (C). Values are average gray values (arbitrary units, \pm SEM, $n = 7-14$ animals/group). Treatment with multiple doses of METH significantly decreased

TH-ir in the CPu and NAc, with a significantly greater reduction in TH-ir observed in the CPu vs. NAc of METH-treated animals. There was a significant negative correlation between the total number of MDA-ir particles and the average gray values for TH-ir in the CPu (D), but not NAc (E). * $p < 0.05$ vs. respective saline-treated animals; *+ $p < 0.05$ vs. TH-ir in the CPu of METH-treated animals.

2009). It is possible that in the mesoaccumbal system, inhibition of ALDH-2 by MDA may be ameliorated by ALDH-1-mediated oxidation of DOPAL to DOPAC. However, it is important to point out that ALDH-1 is expressed to a higher degree in the SNpc as compared to the VTA (McCaffery and Drager, 1994; Jinsmaa et al., 2009). Clearly, additional studies are needed to further examine the relative contribution of ALDH isoforms to the clearance of MDA-mediated increases in DOPAL within the SNpc and VTA.

Multiple METH treatment also increased the levels of MDA-modified proteins in the prefrontal cortex, as MDA-ir was increased in both the PRL and ACC. The frontal cortex contains relatively lower levels of DA than the CPu, but exposure to multiple high doses of METH has been shown to result in depletion of DA levels and TH hydroxylase activity in the frontal cortex (Hotchkiss and Gibb, 1980; Ricaurte et al., 1980). Therefore, it is possible that increased levels of MDA in the frontal cortex contribute to the loss of DA levels and markers in this region, through the accumulation

of toxic DA metabolites as a result of the inhibition of ALDH-2, as described above. However, the increases in MDA-adducted proteins observed in the sub-regions of prefrontal cortex after multiple METH treatment were similar in magnitude to what was observed in the CPu (data not shown), despite the relative differences in DA levels between these two regions, suggesting that MDA-protein modifications may occur in non-DA neurons, leading to widespread neuronal damage. In support of this observation is the finding that multiple METH treatment can induce apoptosis in non-DA neurons in the cortex (Pu et al., 1996; Cadet et al., 2003). Thus, following multiple METH treatment, MDA may also lead to damage of non-DA neurons in the cortex via direct adduction of proteins and nucleic acids or disruption of mitochondrial function. This non-DA-related mechanism of cellular damage could be responsible for a relatively larger portion of METH-induced neuronal damage than the DA-mediated mechanism of neuronal damage, given the lower levels of DA input in the cortex. Future

studies examining which proteins are specifically adducted by MDA within the cortex, and their relative contribution to the depletion of DA markers and apoptosis of non-DA neurons in the cortex will shed light on this issue.

Our data also indicate that multiple high doses of METH increase MDA-modified proteins in the hippocampus, as MDA-ir was significantly increased in the CA1, CA3, and DG. The hippocampus receives sparse input from DA afferents, but receives dense inputs from serotonergic afferents (Rau et al., 2006). Thus, it is likely in this region, the toxic effects of MDA adduction have little to do with the DA system and inhibition of ALDH-2 activity. Treatment with multiple high doses of METH depletes serotonin (5-HT) concentrations in the hippocampus, as well as the rate-limiting enzyme in 5-HT synthesis, tryptophan hydroxylase (TPH; Hotchkiss and Gibb, 1980; Ricaurte et al., 1980, 1983; Bakhit et al., 1981; Green et al., 1992). In this instance, it is possible that MDA contributes to METH-induced damage of 5-HT neurons through direct modification of proteins essential for the function and survival of these neurons. Multiple METH treatment also results in severe depletion of 5-HT and TPH in the CPU and frontal cortex (Hotchkiss and Gibb, 1980; Ricaurte et al., 1980), and it is possible that direct MDA adduction of proteins necessary for the viability of serotonergic input to these regions contribute to this phenomenon. Alternatively, MDA-induced ROS generation could lead to oxidation of 5-HT, producing the metabolite tryptamine-4,5-dione, which may contribute to serotonergic neurotoxicity following METH treatment (Wrona and Dryhurst, 2001). However, a relationship between MDA-induced ROS generation and production of 5-HT-derived toxic metabolites has not been established. Additional studies are needed to investigate the potential role that MDA accumulation might play in the destruction of 5-HT neurons by METH.

Interestingly, there was a greater degree of MDA-ir induced by multiple METH treatment in the CA3 sub-region, as compared to the CA1 and DG sub-regions of hippocampus and a greater degree of MDA-ir induced by multiple METH in the ACC, as compared to

the PRL and M1 sub-regions of cortex. It is unclear what potential mechanism(s) might underlie the enhanced induction of MDA-ir in the CA3 sub-region of hippocampus or ACC sub-region of cortex. However, damage to the CA3 could explain the deficits in short-term memory and spatial learning that has been observed in human METH abusers and in animals exposed to repeated, high doses of METH (McEwen, 1999; Chapman et al., 2001; Thompson et al., 2004), while damage to the ACC could explain the deficits in cognition and emotional processing often observed in METH addicts (Baxter et al., 1989; Clow and Hammer, 1991; Bush et al., 2000). Clearly, additional studies are needed in order to determine the factors that might underlie the relative enhancement of METH-induced MDA-protein adducts within these sub-regions of cortex and hippocampus.

In summary, treatment with multiple high doses of METH increases MDA-adducted proteins in the nigrostriatal system, which is the system that is the most vulnerable to the neurotoxic effects this treatment regimen. Multiple METH treatment also increased levels of MDA-modified proteins in the mesoaccumbal system, yet this system suffers comparatively less neurotoxic damage than the nigrostriatal system. It is possible that the neurotoxic damage to the nigrostriatal system by multiple METH treatment is due to inhibition of ALDH-2 by MDA, resulting in accumulation of DOPAL. It is possible that MDA also inhibits ALDH-2 activity in the mesoaccumbal system, but due to relative differences in ALDH enzymes and cell survival molecules expressed in this system, the neurotoxic effects of multiple METH treatment may be less deleterious. Studies are currently underway in our laboratory to determine whether multiple METH treatment alters ALDH-2 expression and levels of DOPAL in the nigrostriatal vs. mesoaccumbal systems. In addition, multiple METH treatment also increased MDA-modified proteins in the cortex and hippocampus, two regions that are less densely innervated by DA afferents, but nonetheless suffer significant damage as a result of METH treatment, suggesting that MDA may directly contribute to the damage of non-DA neurons within these regions.

REFERENCES

- Acikgoz, O., Gonenc, S., Kayatekin, B. M., Uysal, N., Pekcetin, C., Semin, I., and Gure, A. (1998). Methamphetamine causes lipid peroxidation and an increase in superoxide dismutase activity in the rat striatum. *Brain Res.* 813, 200–202.
- Aldini, G., Dalle-Donne, I., Facino, R. M., Milzani, A., and Carini, M. (2007). Intervention strategies to inhibit protein carboxylation by lipoxidation-derived reactive carbonyls. *Med. Res. Rev.* 27, 817–868.
- Bakhit, C., Morgan, M. E., Peat, M. A., and Gibb, J. W. (1981). Long-term effects of methamphetamine on synthesis and metabolism of 5-hydroxytryptamine in various regions of the rat brain. *Neuropharmacology* 20, 1135–1140.
- Baxter, L. R. Jr., Schwartz, J. M., Phelps, M. E., Mazziotto, J. C., Guze, B. H., Selin, C. E., Gerner, R. H., and Sumida, R. M. (1989). Reduction of prefrontal cortex glucose metabolism common to three types of depression. *Arch. Gen. Psychiatry* 46, 243–250.
- Brown, J. M., Quinton, M. S., and Yamamoto, B. K. (2005). Methamphetamine-induced inhibition of mitochondrial complex II: roles of glutamate and peroxynitrate. *J. Neurochem.* 95, 429–436.
- Brown, J. M., and Yamamoto, B. K. (2003). Effects of amphetamine on mitochondrial function: role of free radicals and oxidative stress. *Pharmacol. Ther.* 99, 45–53.
- Burke, W. J., Li, S. W., Chung, H. D., Ruggiero, D. A., Kristal, B. S., Johnson, E. M., Lampe, P., Kumar, V. B., Franko, M., Williams, E. A., and Zahm, D. S. (2004). Neurotoxicity of MAO metabolites of catecholamine neurotransmitters: role in neurodegenerative diseases. *Neurotoxicology* 25, 101–115.
- Burke, W. J., Li, S. W., Williams, E. A., Nonneman, R., and Zahm, D. S. (2003). 3,4-Dihydroxyphenylacetaldehyde is the toxic dopamine metabolite in vivo: implications for Parkinson's disease pathogenesis. *Brain Res.* 989, 205–213.
- Bush, G., Luu, P., and Posner, M. I. (2000). Cognitive and emotional influences in anterior cingulate cortex. *Trends Cogn. Sci.* 4, 215–222.
- Bustamante, D., You, Z. B., Castel, M. N., Johansson, S., Gojny, M., Terenius, L., Hokfelt, T., and Herrera-Marschitz, M. (2002). Effect of single and repeated methamphetamine treatment on neurotransmitter release in substantia nigra and neostriatum of the rat. *J. Neurochem.* 83, 645–654.
- Cadet, J. L., Subramaniam, J., and Deng, X. (2003). Speed kills: cellular and molecular bases of methamphetamine-induced nerve terminal degeneration and neuronal apoptosis. *FASEB J.* 17, 1775–1788.
- Chapman, D. E., Hanson, G. R., Kessner, R. P., and Keefe, K. A. (2001). Long-term changes in basal ganglia function after a neurotoxic regimen of methamphetamine. *J. Pharmacol. Exp. Ther.* 296, 520–527.
- Chéramy, A., Leviel, V., and Glowinski, J. (1981). Dendritic release of dopamine in the substantia nigra. *Nature* 289, 537–542.
- Choe, E. S., Chung, K. T., Mao, L., and Wang, J. Q. (2002). Amphetamine increases phosphorylation of extracellular signal-regulated kinase and transcription factors in the rat striatum via group I metabotropic glutamate receptors. *Neuropsychopharmacology* 27, 565–575.
- Clow, D. W., and Hammer, R. P. Jr. (1991). Cocaine abstinence following chronic treatment alters cerebral metabolism in dopaminergic reward regions; bromocriptine enhances recovery. *Neuropsychopharmacology* 4, 71–75.
- Del Rio, D., Stewart, A. J., and Pellegrini, N. (2005). A review of recent studies on malondialdehyde as a toxic molecule and biological marker of oxidative stress. *Nutr. Metab. Cardiovasc. Res.* 15, 316–328.
- Emson, P. C., Koob, G., and Iversen, L. L. (1977). Origin of dopaminergic affer-

- ents to the rat frontal cortex [proceedings]. *Br. J. Pharmacol.* 60, 270P–271P.
- Fitzmaurice, P. S., Tong, J., Yazdanpanah, M., Liu, P. P., Kalasinsky, K. S., and Kish, S. J. (2006). Levels of 4-hydroxynonenal and malondialdehyde are increased in brain of human chronic users of methamphetamine. *J. Pharmacol. Exp. Ther.* 319, 703–709.
- Gerfen, C. R., and Bolam, J. P. (2010). “The neuroanatomical organization of the basal ganglia,” in *Handbook of Basal Ganglia Structure and Function*, eds H. Steiner and K. Y. Tseng (New York, NY: Academic Press), 3–23.
- Gluck, M. R., Moy, L. Y., Jayatilake, E., Hogan, K. A., Manzano, L., and Sonsalla, P. K. (2001). Parallel increases in lipid and protein oxidative markers in several mouse brain regions after methamphetamine treatment. *J. Neurochem.* 79, 152–160.
- Green, A. R., De Souza, R. J., Williams, J. L., Murray, T. K., and Cross, A. J. (1992). The neurotoxic effects of methamphetamine on 5-hydroxytryptamine and dopamine in brain: evidence for the protective effect of chlormethiazole. *Neuropharmacology* 31, 315–321.
- Grimm, J., Mueller, A., Hefti, F., and Rosenthal, A. (2004). Molecular basis for catecholaminergic neuron diversity. *Proc. Natl. Acad. Sci. U.S.A.* 101, 13891–13896.
- Heeringa, M. J., and Abercrombie, E. D. (1995). Biochemistry of somatodendritic dopamine release in substantia nigra: an in vivo comparison with striatal dopamine release. *J. Neurochem.* 65, 192–200.
- Horner, K. A., Gilbert, Y. E., and Cline, S. D. (2010). “Multiple high doses of methamphetamine increase malondialdehyde immunoreactivity in the nigrostriatal and mesolimbic systems of rat brain,” in *Paper Presented at the Triennial International Basal Ganglia Society Meeting*, Long Branch.
- Horner, K. A., Westwood, S. C., Hanson, G. R., and Keefe, K. A. (2006). Multiple high doses of methamphetamine increase the number of preneuropeptide Y mRNA-expressing neurons in the striatum of rat via a dopamine D1 receptor-dependent mechanism. *J. Pharmacol. Exp. Ther.* 319, 414–421.
- Hotchkiss, A. J., and Gibb, J. W. (1980). Long-term effects of multiple doses of methamphetamine on tryptophan hydroxylase and tyrosine hydroxylase activity in rat brain. *J. Pharmacol. Exp. Ther.* 214, 257–262.
- Jayanthi, S., Ladenheim, B., and Cadet, J. L. (1998). Methamphetamine-induced changes in antioxidant enzymes and lipid peroxidation in copper/zinc-superoxide dismutase transgenic mice. *Ann. N. Y. Acad. Sci.* 844, 92–102.
- Jinsmaa, Y., Florang, V. R., Rees, J. N., Anderson, D. G., Strack, S., and Doorn, J. A. (2009). Products of oxidative stress inhibit aldehyde oxidation and reduction pathways in dopamine catabolism yielding elevated levels of a reactive intermediate. *Chem. Res. Toxicol.* 22, 835–841.
- Johnson-Davis, K. L., Hanson, G. R., and Keefe, K. A. (2002). Long-term post-synaptic consequences of methamphetamine on preprotachykinin mRNA expression. *J. Neurochem.* 82, 1472–1479.
- Kim, H.-C., Jhoo, W.-K., Choi, D.-Y., Im, D.-H., Shin, E.-J., Suh, J.-H., Floyd, R. A., and Bing, G. (1999). Protection of methamphetamine nigrostriatal toxicity by dietary selenium. *Brain Res.* 851, 76–86.
- Kita, T., Shimada, K., Mastunari, Y., Wagner, G. C., Kubo, K., and Nakashima, T. (2000). Methamphetamine-induced striatal dopamine neurotoxicity and cyclooxygenase-2 protein expression in BALB/c mice. *Neuropharmacology* 39, 399–406.
- Kogan, F. J., Nichols, W. K., and Gibb, J. W. (1976). Influence of methamphetamine on nigral and striatal tyrosine hydroxylase activity and on striatal dopamine levels. *Eur. J. Pharmacol.* 36, 363–371.
- Korf, J., Zielesman, M., and Westerink, B. H. C. (1976). Dopamine release in the substantia nigra? *Nature* 260, 257–258.
- Krasnova, I. N., and Cadet, J. L. (2009). Methamphetamine toxicity and the messengers of death. *Brain Res. Rev.* 60, 397–407.
- Lavoie, M. J., and Hastings, T. G. (1999). Dopamine quinone formation and protein modification associated with the striatal neurotoxicity of methamphetamine: evidence against a role for extracellular dopamine. *J. Neurosci.* 19, 1484–1491.
- Lieberman, M., and Marks, A. D. (2009). *Marks' Basic Medical Biochemistry: A Clinical Approach*, Baltimore, MD: Lippincott Williams & Wilkins.
- Long, J., Liu, C., Sun, L., Gao, H., and Liu, J. (2009). Neuronal mitochondrial toxicity of malondialdehyde: inhibitory effects on respiratory function and enzyme activities in rat brain mitochondria. *Neurochem. Res.* 34, 786–794.
- Manzer, R., Qamar, L., Estey, T., Pappa, A., Petersen, D. R., and Vasilou, V. (2003). Molecular cloning and baculovirus expression of the rabbit corneal aldehyde dehydrogenase (ALDH1A1) cDNA. *DNA Cell Biol.* 22, 329–338.
- Marchitti, S. A., Deitrich, R. A., and Vasilou, V. (2007). Neurotoxicity and metabolism of the catecholamine-derived 3,4-dihydroxyphenylacetaldehyde, a reactive intermediate of dopamine metabolism by 4-hydroxy-2-nonenal. *Pharmacol. Rev.* 59, 125–150.
- Maxwell, J. C. (2005). Emerging research on methamphetamine. *Curr. Opin. Psychiatry* 18, 235–242.
- McCaffery, P., and Drager, U. C. (1994). High levels of a retinoic acid-generating dehydrogenase in the mesotelencephalic dopamine system. *Proc. Natl. Acad. Sci. U.S.A.* 91, 7772–7776.
- McEwen, B. (1999). Stress and hippocampal plasticity. *Annu. Rev. Neurosci.* 22, 105–122.
- Moore, K., and Roberts, L. J. II. (1998). Measurement of lipid peroxidation. *Free Radic. Res.* 28, 659–671.
- Pu, C., Broening, H. W., and Vorhees, C. V. (1996). Effect of methamphetamine on glutamate-positive neurons in the adult and developing rat somatosensory cortex. *Synapse* 23, 328–334.
- Rau, K. S., Birdsall, E., Volz, T. J., Riordan, J. A., Baucum, A. J. I., Adair, B. P., Bitter, R., Gibb, J. W., Hanson, G. R., and Fleckenstein, A. E. (2006). Methamphetamine administration reduces hippocampal vesicular monoamine transporter-2 uptake. *J. Pharmacol. Exp. Ther.* 318, 676–682.
- Ricaurte, G. A., Fuller, R. W., Perry, K. W., Seiden, L. S., and Schuster, C. R. (1983). Fluoxetine increases long-lasting neostriatal dopamine depletion after administration of d-methamphetamine and d-amphetamine. *Neuropharmacology* 22, 1165–1169.
- Ricaurte, G. A., Schuster, C. R., and Seiden, L. S. (1980). Long-term effects of repeated methylamphetamine administration on dopamine and serotonin neurons in the rat brain: a regional study. *Brain Res.* 193, 153–163.
- Robertson, G. S., Damsma, G., and Fibiger, H. C. (1991). Characterization of dopamine release in the substantia nigra by in vivo microdialysis in freely moving rats. *J. Neurosci.* 11, 2209–2216.
- Rooke, N., Li, D.-J., Li, J., and Keung, W. M. (2000). The mitochondrial monoamine oxidase-aldehyde dehydrogenase pathway: a potential site of action of daidzin. *J. Med. Chem.* 43, 4169–4179.
- Scatton, B., Javoy-Agid, F., Rouquier, L., Dubois, B., and Agid, Y. (1983). Reduction of cortical dopamine, noradrenaline, serotonin and their metabolites in Parkinson's disease. *Brain Res.* 275, 321–328.
- Seiden, L. S., and Ricaurte, G. A. (1987). “Neurotoxicity of methamphetamine and related drugs,” in *Psychopharmacology: The Third Generation of Progress*, ed. H. Meltzer (New York: Raven Press), 359–366.
- Simpson, J. N., Wang, J. Q., and McGinty, J. F. (1995). Repeated amphetamine administration induces a prolonged augmentation of phosphorylated cyclase response element-binding protein and fos-related antigen immunoreactivity in rat striatum. *Neuroscience* 69, 441–457.
- Sternberger, L. (1979). The unlabeled antibody (PAP) method, introduction. *J. Histochem. Cytochem.* 27, 1657.
- Substance Abuse and Mental Health Services Administration, Office of Applied Studies. (2010). *The DAWN Report: Emergency Department Visits Involving Methamphetamine: 2004 to 2008*. Rockville, MD: Drug Abuse Warning Network.
- Thompson, P. M., Hayashi, K. M., Simon, S. L., Geaga, J. A., Hong, M. S., Sui, Y., Lee, J. Y., Toga, A. W., Ling, W., and London, E. D. (2004). Structural abnormalities in the brains of human subjects who use methamphetamine. *J. Neurosci.* 24, 6028–6036.
- Volkow, N. D., Chang, L., Wang, G. J., Fowler, J. S., Franceschi, D., Sedler, M. J., Gatley, S. J., Hintzemann, R., Ding, Y. S., and Wong, C. (2001). Higher cortical and lower subcortical metabolism in detoxified methamphetamine abusers. *Am. J. Psychiatry* 158, 383–389.
- Windels, F., and Kiyatkin, E. A. (2006). Dopamine action in the substantia nigra reticulata: iontophoretic studies in awake, unrestrained rats. *Eur. J. Neurosci.* 24, 1385–1394.
- Wrona, M. A., and Dryhurst, G. (2001). A putative metabolite of serotonin, tryptamine-4,5-dione, is an irreversible inhibitor of tryptophan hydroxylase: possible relevance to the serotonergic neurotoxicity of methamphetamine. *Chem. Res. Toxicol.* 14, 1184–1192.
- Yamamoto, B. K., and Bankson, M. G. (2005). Amphetamine neurotoxicity: cause and consequence of oxidative stress. *Crit. Rev. Neurobiol.* 17, 87–117.
- Yamamoto, B. K., and Zhu, W. (1998). The effects of methamphetamine on the production of free radicals and oxidative stress. *J. Pharmacol. Exp. Ther.* 287, 107–114.

Conflict of Interest Statement: The authors declare that the research was conducted in the absence of any commercial or financial relationships that could be construed as a potential conflict of interest.

Received: 21 December 2010; accepted: 27 April 2011; published online: 09 May 2011.
Citation: Horner KA, Gilbert YE and Cline SD (2011) Widespread increases in malondialdehyde immunoreactivity in dopamine-rich and dopamine-poor regions of rat brain following multiple, high doses of methamphetamine. *Front. Syst. Neurosci.* 5:27. doi: 10.3389/fnsys.2011.00027
Copyright © 2011 Horner, Gilbert and Cline. This is an open-access article subject to a non-exclusive license between the authors and Frontiers Media SA, which permits use, distribution and reproduction in other forums, provided the original authors and source are credited and other Frontiers conditions are complied with.



Nitric oxide–soluble guanylyl cyclase–cyclic GMP signaling in the striatum: new targets for the treatment of Parkinson’s disease?

Anthony R. West^{1*} and Kuei Y. Tseng^{2*}

¹ Department of Neuroscience, The Chicago Medical School, Rosalind Franklin University of Medicine and Science, North Chicago, IL, USA

² Department of Cellular and Molecular Pharmacology, The Chicago Medical School, Rosalind Franklin University of Medicine and Science, North Chicago, IL, USA

Edited by:

Elizabeth Abercrombie, Rutgers-Newark: The State University of New Jersey, USA

Reviewed by:

Dalton J. Surmeier, Northwestern University, USA

Alessandro Stefani, University of Rome, Italy

M. Gustavo Murer, Universidad de Buenos Aires, Argentina

*Correspondence:

Anthony R. West, Department of Neuroscience, Rosalind Franklin University of Medicine and Science, 3333 Green Bay Road, North Chicago, IL 60064, USA.
e-mail: Anthony.West@rosalindfranklin.edu;

Kuei Y. Tseng, Department of Cellular and Molecular Pharmacology, The Chicago Medical School, Rosalind Franklin University of Medicine and Science, North Chicago, IL, USA.
e-mail: kuei-yuan.tseng@rosalindfranklin.edu

Striatal nitric oxide (NO)-producing interneurons play an important role in the regulation of corticostriatal synaptic transmission and motor behavior. Striatal NO synthesis is driven by concurrent activation of NMDA and dopamine (DA) D1 receptors. NO diffuses into the dendrites of medium-sized spiny neurons which contain high levels of NO receptors called soluble guanylyl cyclases (sGC). NO-mediated activation of sGC leads to the synthesis of the second messenger cGMP. In the intact striatum, transient elevations in intracellular cGMP primarily act to increase neuronal excitability and to facilitate glutamatergic corticostriatal transmission. NO–cGMP signaling also functionally opposes the inhibitory effects of DA D2 receptor activation on corticostriatal transmission. Not surprisingly, abnormal striatal NO–sGC–cGMP signaling becomes apparent following striatal DA depletion, an alteration thought to contribute to pathophysiological changes observed in basal ganglia circuits in Parkinson’s disease (PD). Here, we discuss recent developments in the field which have shed light on the role of NO–sGC–cGMP signaling pathways in basal ganglia dysfunction and motor symptoms associated with PD and L-DOPA-induced dyskinesias.

Keywords: basal ganglia, striatum, dopamine, nitric oxide, Parkinson’s disease

NO SIGNALING IN THE STRIATUM

Nitric oxide (NO) is a gaseous neuromodulator and is implicated in the regulation of numerous physiological and pathophysiological processes in both the peripheral and central nervous system (Boehning and Snyder, 2003; Bredt, 2003; Garthwaite, 2008). Since its discovery in 1987 as the “endothelial derived relaxation factor” (EDRF) in peripheral blood vessels (Palmer et al., 1987), three distinct isoforms of the NO-producing enzyme nitric oxide synthase (NOS; brain/neuronal NOS, inducible NOS, endothelial NOS) have been described (Alderton et al., 2001; Garthwaite, 2008). Of particular interest is the neuronal NOS (nNOS), which is ubiquitously distributed throughout the brain and relatively abundant in the dorsal striatum and nucleus accumbens (Bredt et al., 1990; Vincent, 1994). Striatal NO is synthesized primarily in nNOS-containing interneurons, which are readily revealed using NADPH-diaphorase histochemical staining (Figures 1A,B) as well as nNOS immunohistochemical labeling (Hope et al., 1991; Kawaguchi, 1993; Gracy and Pickel, 1997). The remainder of this review will focus in detail on how NO synthesis is regulated by DA D1- and D2-like receptors and their interactions with glutamate inputs/receptors, and how nitrgic signaling then affects striatal output in normal and parkinsonian animals.

MODULATION OF STRIATAL NOS ACTIVITY BY DOPAMINE D1 AND D2 RECEPTOR ACTIVATION

Remarkably consistent outcomes have been reported in studies examining the impact of DA D1- and D2-like receptor agonists/antagonists on striatal NOS activity and cGMP production (Altar et al., 1990; Morris et al., 1997; Di Stefano et al., 2005; Sammut et al., 2006, 2007b; Siuciak et al., 2006; Park and West, 2009; Hoque et al., 2010). Early studies by Altar et al. (1990) were the first to show that D1-like receptor activation induced by SKF 38393 increases striatal tissue levels of cGMP, whereas antagonism of this receptor with SCH 23390 decreases similar measures of cGMP. In the same study these authors reported that the D2 receptor antagonists haloperidol and sulpiride robustly elevated striatal tissue levels of cGMP. These findings have been confirmed and extended in more recent studies (Di Stefano et al., 2005; Siuciak et al., 2006). Thus, consistent with the above work, D2-like receptor agonism was shown to decrease striatal tissue levels of cGMP (Di Stefano et al., 2005). Moreover, work by Schmidt and colleagues showed that the facilitatory effects of D1-like receptor agonist and D2 receptor antagonist on striatal tissue levels of cGMP are abolished in nNOS^{-/-} (i.e., knockout) mice (Siuciak et al., 2006). Together, the above studies confirm that both D1- and D2-like receptor activation strongly regulates

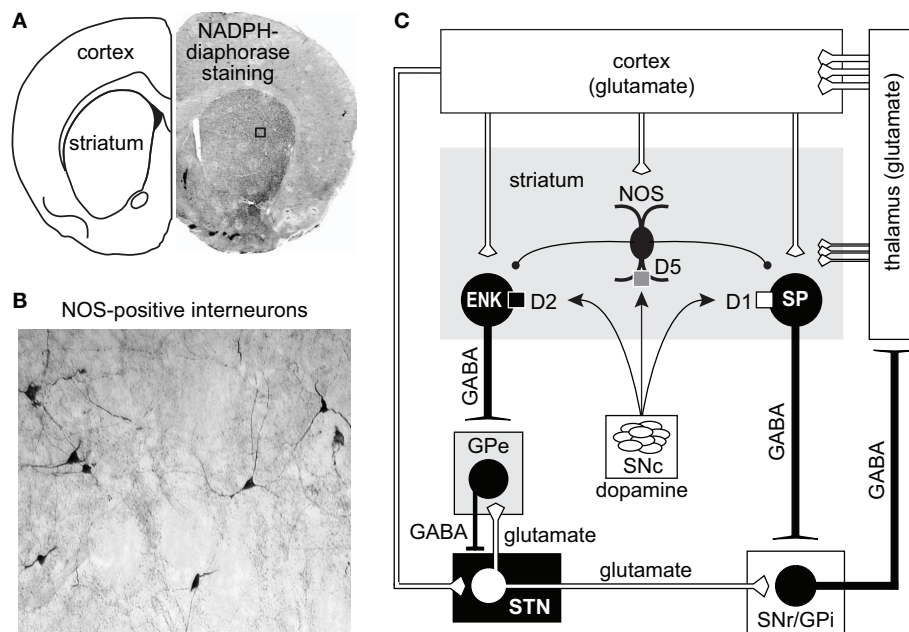


FIGURE 1 | (A,B) Coronal section of the forebrain revealing the presence of NADPH-diaphorase staining and NOS-positive interneurons in cortex and striatum. **(C)** Diagram illustrating the major connections of the basal ganglia. The cerebral cortex provides the major inputs to the striatum. Both direct (D1/substance P-SP-) and indirect (D2/enkephalin-ENK-) striatal output neurons receive modulatory input arising from local NOS interneurons. Direct projecting neurons provide axon

collaterals to the output nuclei of the basal ganglia: internal segment of the globus pallidus (GPi) and to the substantia nigra pars reticulata (SNr). Indirect striatal output neurons are indirectly connected to the GPi and SNr through connections that involve the external segment of the globus pallidus (GPe) and the subthalamic nucleus (STN). Feedback pathways to the cortex arise from GABAergic output neurons in the GPi and the SNr via the thalamo-cortical circuit.

striatal nNOS activity, albeit in opposing manners (i.e., D1 receptor activation is facilitatory, D2 receptor activation is inhibitory), and identify a critical role of nNOS–NO signaling in the generation of striatal cGMP.

Consistent with the above studies of striatal cGMP synthesis, our laboratory has reported that electrical and chemical stimulation of the substantia nigra and systemic administration of the D1 receptor agonist SKF 81297 all robustly increase amperometric measures of striatal NO efflux via nNOS and D1-like receptor-dependent mechanisms (Sammur et al., 2006, 2007a; Park and West, 2009). Interestingly, the facilitatory effects of nigrostriatal DA cell activation and SKF 81297 on striatal NO efflux were both attenuated by systemic administration of the D2-like receptor agonist quinpirole, whereas administration of the D2-like receptor antagonist eticlopride augmented evoked NO efflux (Sammur et al., 2007a).

Other work has examined the impact of D1 and D2 receptor interactions using histochemical measures of striatal NOS activity (NADPH-d staining). Reports from leading laboratories have demonstrated that the catalytic activity of the nNOS enzyme is responsible for producing NADPH-d staining (Dawson et al., 1991; Hope et al., 1991) and that measurements of staining in striatal interneurons accurately reflect enzyme activity (Morris et al., 1997; Sancesario et al., 2004). Moreover, quantification of NADPH-d staining using optical density is a valuable index of striatal nNOS activity which can be observed in identified interneurons across striatal subregions (Kuo et al., 1994; Morris et al., 1997; Sancesario et al., 2004; Hoque et al., 2010). Studies using NADPH-diaphorase staining as an indirect measure of striatal nNOS activity have also shown that admin-

istration of D1-like receptor antagonist decreases enzyme activity, whereas D2-like receptor antagonists have the opposite effect (Morris et al., 1997; Hoque et al., 2010). Similar to our above studies using NO microsensor recordings, pretreatment with the D2 receptor agonist quinpirole abolished the facilitatory effect of SKF 81297 on NADPH-diaphorase staining/nNOS activity (Hoque et al., 2010). These studies indicate that D1- and D2-like receptor activation has opposing effects on striatal nNOS activity (reviewed in West, 2010).

IMPACT OF DOPAMINE–GLUTAMATE INTERACTIONS ON NEURONAL NOS ACTIVITY

Reciprocal functional interactions between D1 and NMDA receptors are believed to occur in a variety of neurons in the CNS via direct physical interactions and following activation of second messengers (Cepeda and Levine, 2006). In the striatum, DA–glutamate interactions involved in the regulation of nNOS activity are likely to be complex as these transmitter systems converge both at the level of the NOS interneurons (Fujiyama and Masuko, 1996; Hidaka and Totterdell, 2001) and the principle medium-sized spiny neurons (MSNs; Morello et al., 1997; Sancesario et al., 2000; Hidaka and Totterdell, 2001). We have recently begun to study the interaction between DA and glutamate as it pertains to striatal NOS activity using NO microsensor recordings combined with local reverse microdialysis for intra-striatal drug delivery (Park and West, 2009). These studies found that local infusion of D1 agonist potentiates nNOS activity elicited via electrical stimulation of cortical afferents (Park and West, 2009). Interestingly, both the effects of electrical stimulation and D1 agonist were blocked by local D1 antagonist

infusion, suggesting that D1 receptor co-activation is required for NOS stimulation by cortical inputs (Park and West, 2009). Further studies revealed that the increase in striatal NO efflux elicited by systemic administration of D1 agonist is blocked by intrastratial infusion of the selective nNOS inhibitor 7-nitroindazole, the DA D1 receptor antagonist SCH 23390, and NMDA receptor antagonists (CPP and kynurenic acid), indicating that D1 receptor-mediated NO efflux is dependent on concurrent D1 and NMDA receptor activation (see **Figure 2**). Our studies using NADPH-diaphorase staining as a complementary measure of striatal nNOS activity have also shown that systemic administration of the NMDA receptor antagonist CPP attenuated staining in the dorsal striatum (Hoque et al., 2010). As expected NOS activity stimulated by systemic administration of D1 receptor agonist or D2 receptor antagonist was attenuated by D1 antagonism and D2 agonism, respectively. Moreover, pretreatment with an NMDA receptor antagonist blocked the facilitatory effects of D1 receptor agonist and D2 receptor antagonist on NOS activity. Importantly, in all studies statistical interactions were observed between drug pretreatments and D1 agonist/D2 antagonist treatments, indicating that the drug pretreatments were acting to block the effect of the DA modulation, and not by simply lowering overall basal levels of NOS activity in a manner independent of a DA receptor-mediated mechanism (Hoque et al., 2010).

Taken together, these findings are consistent with the multitude of studies reporting that D1 receptor activation potentiates NMDA-induced responses in cortical and striatal neurons (Cepeda

and Levine, 1998). Moreover, these novel observations indicate that reciprocal D1–NMDA and D2–NMDA receptor interactions play critical and opposing roles in regulating striatal NOS activity. Future studies will need to determine which specific modes of DA transmission favor D1–NMDA facilitation and which lead to D2–NMDA suppression of NOS activity. However, based on the above discussion of the effects of D1 and D2 antagonism on nNOS activity, we predict that tonic levels of DA act to suppress NMDA receptor-mediated nNOS stimulation by activation of D2-like receptors. During robust phasic activation of DA transmission occurring during burst firing (mimicked by stimulation of the substantia nigra and D1 receptor agonist treatment), D1–NMDA receptor interactions would facilitate nNOS activity and NO transmission. In the DA-depleted parkinsonian striatum or following D1 receptor blockade, we predict that loss of D1 tone would prohibit activation of nNOS and suppress NO signaling (Park and West, 2009). As discussed below in our summary of work performed in animal models of Parkinson's disease (PD), currently there is evidence in support of and against this model.

ROLE OF NOS INTERNEURONS IN THE REGULATION OF CORTICOSTRIATAL TRANSMISSION

Corticostratial afferents target two functionally distinct groups of MSNs that form the “direct” (striatonigral MSNs) and the “indirect” (striatopallidal MSNs) pathways (Albin et al., 1989; Alexander and Crutcher, 1990; Parent, 1990; DeLong and Wichmann, 2007; **Figure 1C**). Corticostratial projections also provide excitatory input to striatal interneurons (Kawaguchi, 1993) which are involved in the feed-forward regulation of MSNs by GABA (Tepper et al., 2004; Mallet et al., 2005) and NO (Sammur et al., 2007a, 2010; Ondracek et al., 2008). While GABA binds to receptors on the surface of the plasma membrane, newly synthesized NO diffuses past the plasma membrane into the dendrites of striatal MSNs, which contain high levels of NO receptors called soluble guanylyl cyclases (sGC; **Figure 3**; Ariano, 1983; Ding et al., 2004). In fact, sGC expression and activity are reportedly higher in the striatum than in any other brain region (Hofmann et al., 1977; Matsuoka et al., 1992). Once generated, NO has been reported to induce or modulate various forms of short and long-term corticostratial synaptic plasticity (Calabresi et al., 1999, 2000; Doreulee et al., 2003; West and Grace, 2004; Ondracek et al., 2008; Sammur et al., 2010), and alter synchrony within neuronal networks (O'Donnell and Grace, 1997; Sammur et al., 2007a; Chepkova et al., 2009). Most of these studies indicate that this NO signal is derived from nNOS localized to striatal interneurons. However, evidence that LTP of corticostratial transmission is blocked in slices following administration of a non-selective NOS inhibitor and in mutant mice lacking the endothelial NOS gene (Doreulee et al., 2003) indicates that NO derived from the vasculature is also capable of modulating corticostratial transmission.

Our studies have shown that in both chloral hydrate and urethane anesthetized rats, tonic, and phasic NO–sGC–cGMP signaling acts to promote short-term excitatory influences on corticostratial synaptic activity recorded in identified MSNs (**Figure 3**; West and Grace, 2004; Ondracek et al., 2008; Sammur et al., 2010). Our initial studies examined the impact of tonic NO signaling on short-term plasticity induced across corticostratial synapses during

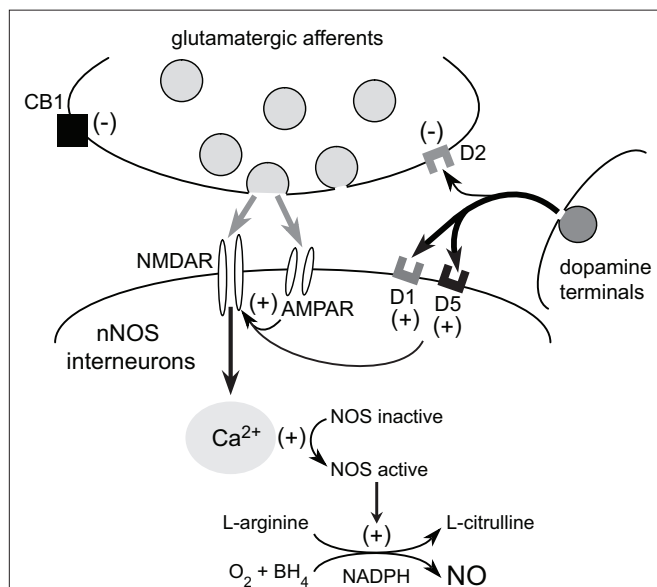


FIGURE 2 | Glutamatergic modulation of striatal NOS interneurons by cortical inputs. Corticostratial activation exerts direct excitatory effects on NOS interneurons via AMPA and NMDA receptor activation. NMDA receptor-dependent calcium influx activates nNOS and facilitates the conversion of L-arginine into L-citrulline and NO production. Dopamine release from the nigrostriatal pathway facilitates nNOS activity via D1/5 receptor stimulation. Furthermore, striatal NMDA receptor activation plays a critical role in the facilitatory effects of D1/5 receptor activation on striatal NO synthesis. Given that D1/5 receptor tone is also necessary for NMDA receptor activation of NOS, it is likely that reciprocal DA and glutamate interactions are crucial for the activation of striatal nNOS and NO transmission.

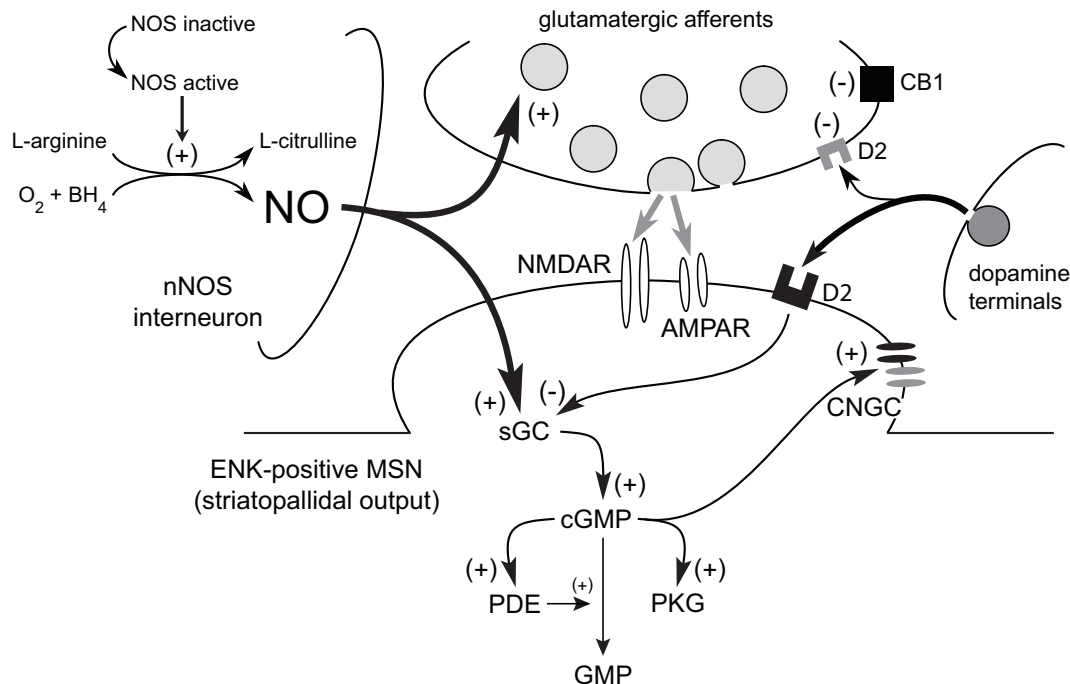


FIGURE 3 | Model of the role of NO signaling in the short-term facilitation of corticostriatal transmission. Tonic NO signaling increases glutamatergic transmission across corticostriatal synapses via a sGC–cGMP-dependent mechanism. Similarly, phasic NO–sGC–cGMP signaling also increases corticostriatal synaptic transmission and the responsiveness of MSNs to this input. Transient increases in intracellular cGMP levels can

affect MSN activity via activation of PKG and downstream targets (e.g., cyclic nucleotide gated channels; CNGC). Numerous phosphodiesterases (PDEs), which metabolize cyclic nucleotides, limit the effects of cGMP on MSN function. In striatopallidal output neurons (ENK-positive MSN), the facilitatory action of cGMP may be directly opposed via D2 receptor activation.

paired-pulse stimulation of the frontal cortex (West and Grace, 2004). In these studies, MSNs were monitored using *in vivo* intracellular recordings during intrastratial infusion of either vehicle or the NO scavenger CPT-IO. Interestingly, MSNs recorded in the presence of the NO scavenger were less responsive to the paired-pulse stimulation protocol and exhibited lower levels of synaptic facilitation during stimulation of corticostriatal pathways (West and Grace, 2004). More recently, we have examined the impact of high frequency train stimulation of the frontal cortex on evoked spike activity in striatal MSNs (Ondracek et al., 2008; Sammut et al., 2010). Importantly, the stimulation protocol used in our studies (train duration = 1 s, pulse frequency = 30 Hz, inter-train interval = 2 s) was designed to approximate the natural burst firing (spikes per burst, intra-burst frequency, and bursts per second) and up and down state activity of corticostriatal pyramidal neurons recorded in anesthetized rats (Cowan & Wilson, 1994). As we have discussed above, we have found that this protocol consistently produces an intensity-dependent and transient increase in striatal NO efflux (Sammut et al., 2007a; Ondracek et al., 2008; Park and West, 2009). Inhibition of this evoked NO efflux was shown to eliminate excitatory responses to stimulation and increase the short-term depression (STD) of cortically evoked spike activity (Ondracek et al., 2008).

Our laboratory has also examined the impact of phasic NO signaling on the spontaneous generation of local field potentials recorded in the intact rat striatum (Sammut et al., 2007a).

These studies demonstrated that systemic administration of a non-specific NOS and sGC inhibitor (methylene blue) simultaneously decreased: (1) NO efflux evoked via cortical stimulation, and (2) the peak oscillation frequency (observed within the delta band) of local striatal field potential oscillations. These observations are consistent with studies using local application of NO–sGC inhibitors which were found to decrease the amplitude of spontaneous glutamate-driven up states (West and Grace, 2004). Additionally, stimulation of corticostriatal pathways facilitates electrotonic coupling between MSNs in rat striatal slices in a manner which is blocked by NOS inhibitors and mimicked by bath application of an NO generator (O'Donnell and Grace, 1997). NO signaling may therefore induce a functional coupling between MSNs and act to synchronize the oscillatory activity of related neuronal ensembles. When examined *in vivo*, disruption of nNOS activity increases the magnitude of D2 receptor-mediated STD of cortically evoked spike activity induced during phasic stimulation of frontal cortical afferents (Ondracek et al., 2008). Thus, in the intact striatum, corticostriatal transmission may be preferentially detected and amplified by nNOS interneurons in a feed-forward manner which may facilitate the synchronization of local network activity with glutamate-driven events. Interruption of NO neuromodulation, therefore, is likely to disrupt the integration of corticostriatal transmission, short-term plasticity, and functional coupling of MSNs in striatal networks (West and Grace, 2004; Sammut et al., 2007b; Ondracek et al., 2008). Consistent with this, it is

clear that pharmacological or genetic downregulation of striatal NOS activity has profound effects on striatal output as measured in electrophysiological (West and Grace, 2000; West et al., 2002) and behavioral studies (Del Bel et al., 2005).

Interestingly, studies performed in brain slice preparations from both rats and mice have frequently reported inhibitory effects (i.e., LTD) of NO-sGC-cGMP signaling on excitatory corticostriatal transmission (reviewed in Calabresi et al., 2007). A parsimonious explanation for this apparent flip flop of the impact of NO on corticostriatal plasticity observed between *in vivo* and *in vitro* preparations is that corticostriatal pathway stimulation can be processed differently in the intact versus reduced striatum, and that in both preparations, NO may promote this differential processing. Indeed, similar mechanisms are implicated in studies using *in vivo* and *in vitro* preparations (e.g., sGC and PDEs play a key role in NO-mediated effects in all of these studies). Furthermore, the former tenet is supported by studies showing that stimulation protocols known to produce LTD of corticostriatal neurotransmission *in vitro*, produce LTP *in vivo* (Charpier and Deniau, 1997). A similar switch from LTD to LTP is observed *in vitro* following removal of magnesium from the bath perfusate (Calabresi et al., 1992). Thus, it is likely that with most common protocols cortical stimulation delivered *in vivo* results in greater activation of glutamatergic drive onto postsynaptic AMPA receptors and more effective removal of the voltage-dependent magnesium block of NMDA receptors, leading to a state that generally favors LTP. In contrast, similar stimulation of corticostriatal signaling *in vitro* favors LTD in the absence of the removal of magnesium block of NMDA receptors. In support of this, most studies show that LTD-induction in the mature striatum is not NMDA receptor dependent, whereas LTP requires activation of these channels (Reviewed in Surmeier et al., 2009). Like LTP, stimulation of striatal NOS activity also requires NMDA receptor activation in both *in vivo* and *in vitro* preparations (Nishi et al., 2005; Sammut et al., 2007a; Park and West, 2009). Given this, it is more readily understandable how corticostriatal pathway activation could lead to NO-dependent facilitation of synaptic efficacy (i.e., an LTP-like phenomenon). However, studies by Calabresi et al. (2007) have produced compelling evidence that facilitation of signaling at any number of key sites in the NO-sGC-cGMP-PKG cascade mediates LTD and occludes further LTD induced via corticostriatal stimulation. Because these studies stimulated cortical areas close to the recording electrode or white matter between cortex and striatum (Calabresi et al., 1999), it is possible that NMDA receptor stimulation was not required for NOS activation in this preparation as these interneurons may have been activated by direct current spread within striatum. In any event, the information available at this time suggests that, in addition to promoting short-term increases in excitatory synaptic transmission, NO signaling may act to facilitate and stabilize the dominant state of long-term synaptic plasticity occurring across corticostriatal synapses (i.e., primarily potentiation when postsynaptic NMDA receptors are activated, or depression in the absence of this activation). Because NO is a potent vasodilator, it may also function to couple changes in synaptic plasticity and blood flow in striatal microcircuits. Future studies using new genetic and optical approaches will have to determine the role of NO in LTP and LTD of synaptic transmission (i.e., bidirectional plasticity) at both excitatory and inhibitory synapses onto identified striatonigral and striatopallidal MSNs.

STRIATAL PATHOPHYSIOLOGY IN PARKINSON'S DISEASE: INVOLVEMENT OF NO-sGC-cGMP SIGNALING PATHWAYS

Parkinson's disease is associated with a preferential degeneration of the nigrostriatal DA pathway (Hornykiewicz, 1975). The loss of DA modulation triggers a complex series of neurochemical, anatomical, and electrophysiological alterations that lead to persistent changes in striatal neurons and their signaling pathways. For instance, striatonigral MSNs develop D1 receptor supersensitivity and reduced expression of D1 receptors (Gerfen et al., 1990). Elevations in D2 receptor protein and mRNA are also observed together with increases in enkephalin expression in striatopallidal MSNs (Gerfen et al., 1990). A substantial population of corticostriatal terminals also expresses D2 receptors (Wang and Pickel, 2002) which become hypersensitive in the absence of DA innervation (Calabresi et al., 1993; Bamford et al., 2004; Picconi et al., 2004). The loss of DA tone on these D2 heteroreceptors is likely to result in enhanced glutamatergic transmission and altered NMDA receptor function (Meshul et al., 1999; Nash et al., 1999; Betarbet et al., 2004). Alterations in dendritic spine morphology and complexity have also been described in both DA-depleted rats and patients with PD (Ingham et al., 1989; Stephens et al., 2005) which may occur preferentially in striatopallidal MSNs (Day et al., 2006).

Most pathophysiological models and metabolic studies of PD predict that the net effect of these alterations is an imbalance in striatal output in which the indirect pathway becomes functionally hyperactive and the direct pathway is hypoactive (Marsden, 1982; Albin et al., 1989; Alexander et al., 1990; Hirsch et al., 2000; see Figure 1C). Recent studies using optogenetic control of striatonigral and striatopallidal MSNs have provided substantial evidence supporting the validity of this pioneering basal ganglia model (Kravitz et al., 2010). These studies by Kravitz and colleagues showed that bilateral activation of striatopallidal MSNs elicits a parkinsonian state characterized by freezing, bradykinesia, and decreased locomotion. Stimulation of striatonigral MSNs reduced freezing and facilitated locomotion. Additionally, stimulation of striatonigral MSNs reversed motor deficits observed in parkinsonian mice (Kravitz et al., 2010).

The above model has also served as the framework for recent studies aimed at understanding how changes in striatal DA transmission impact the temporal dynamics and plasticity of corticobasal ganglia transmission. For instance, recent studies have suggested that striatopallidal neurons in DA-depleted animals become more responsive to corticostriatal inputs and as a result, exhibit bursts of spike activity which correlates with cortical oscillations (Tseng et al., 2001; Mallet et al., 2006; Walters et al., 2007). Thus, loss of D2 receptor-mediated inhibition of striatopallidal neurons and their corticostriatal inputs results in the unfiltered spreading of cortical rhythms to the GP and other components of the basal ganglia and some of the modifications in neuron activity that may underlie the pathophysiology of PD (Murer et al., 2002). In addition to increased spike activity (Mallet et al., 2006), striatopallidal neurons recorded in DA-depleted mice also exhibit a selective loss of endocannabinoid-dependent LTD (Kreitzer and Malenka, 2007). Further studies by Surmeier et al. (2009) have shown that following DA depletion, the pairing of presynaptic and postsynaptic activity, in any order, induced LTD in D1 receptor-expressing MSNs and LTP in D2 receptor-expressing MSNs in an

exclusive manner which prohibited bidirectional plasticity (Shen et al., 2008). These observations indicate that, following striatal DA depletion, activity-dependent changes in the strength of corticostriatal synaptic transmission occur in parallel with alterations in intrinsic excitability (Surmeier et al., 2009).

While the role of NO–sGC–cGMP signaling in the above pathological changes induced in the parkinsonian striatum remains to be fully characterized, it is clear that disruption of striatal NO–sGC–cGMP signaling cascades results in profound changes in behavioral, electrophysiological, and molecular responses to pharmacological manipulations of DA and glutamate transmission (Morris, 1995; Greengard, 2001; West et al., 2002; Del Bel et al., 2005; Ondracek et al., 2008; Threlfell et al., 2009; Sammut et al., 2010; West et al., 2009). For example, studies by Del Bel et al. (2005) have shown that striatal nNOS interneurons play a critical role in the generation of motor behavior. Systemic and intrastriatal exposure to NOS and sGC inhibitors has been shown to depress basal locomotion and induce catalepsy (Stewart et al., 1994; Del Bel et al., 2004; Echeverry et al., 2007). Pharmacological disruption of NO function also potentiates catalepsy induced via D2-class receptor antagonists (Del Bel and Guimaraes, 2000; Cavas and Navarro, 2002). Furthermore, motor activation stimulated by substance P (Mancuso et al., 1994), NMDA receptor antagonists (Deutsch et al., 1996), and DA receptor agonists (Starr and Starr, 1995) is suppressed following systemic administration of NOS inhibitors.

The above behavioral studies demonstrate that in animals with an intact DA system, striatal NO–sGC–cGMP transmission is likely to play an important role in facilitating locomotor activity. It is less clear how this role for NO–sGC–cGMP signaling may change in the parkinsonian striatum. Various measures of striatal NOS activity have indicated that NO signaling may be disrupted in patients with PD (Bockelmann et al., 1994; Eve et al., 1998) and DA-depleted rats (De Vente et al., 2000; Sahach et al., 2000; Barthwal et al., 2001; Sancesario et al., 2004). With regard to NOS activity measured in DA-depleted rodents, however, conflicting outcomes have been reported between the above studies performed in rats and studies of mouse models (see Chalimoniuk and Langfort, 2007; Chalimoniuk et al., 2004). Moreover, conflicting results have been reported in studies measuring cGMP levels in striatal tissue from DA-depleted rodents (De Vente et al., 2000; Chalimoniuk et al., 2004; Sancesario et al., 2004; Chalimoniuk and Langfort, 2007; Giorgi et al., 2008). Interestingly, PDE mRNA, protein, and activity are elevated in DA-depleted rats (Sancesario et al., 2004; Giorgi et al., 2008), indicating that cyclic nucleotide metabolism is elevated in PD. While speculative, this may be a compensatory homeostatic change induced in MSNs in response to overactivity resulting from striatal DA depletion (i.e., an attempt by the MSNs to reverse cyclic nucleotide over-production). In support of this, a subpopulation of MSNs (40%) has been reported to be hyper-responsive to NO generators (Galati et al., 2008). Therefore, upregulation of PDE activity would be expected to compensate for this abnormal responsivity of these MSNs to NO. A parallel down-regulation of nNOS activity and NO signaling would also facilitate the normalization of cyclic nucleotide levels following DA depletion. As indicated above, there is strong evidence for this in both DA-depleted rats (De Vente et al., 2000; Sahach et al., 2000; Barthwal et al., 2001; Sancesario et al., 2004)

and post-mortem tissue from patients with PD (Bockelmann et al., 1994; Eve et al., 1998). However, studies examining how parallel measures of nNOS, sGC, cGMP, PKG, and various PDEs change across time following DA depletion are needed to clarify the complex pathophysiological and homeostatic changes in this signaling pathway in PD.

Given the above findings, it is likely that striatal DA denervation results in transient and dynamic alterations in the synthesis (NOS and sGC dependent) and degradation (PDE dependent) of striatal cyclic nucleotides. These complex changes are likely to be complicated further by L-DOPA treatment. Indeed, in patients with PD, serum levels of cGMP are reportedly increased following L-DOPA therapy (Chalimoniuk and Stepien, 2004). However, studies in DA-depleted rats have shown that L-DOPA-induced dyskinesias are associated with decreased striatal cyclic nucleotide levels (Giorgi et al., 2008; Picconi et al., 2011). Moreover, the non-selective PDE inhibitor zaprinast was shown to reverse decreases in striatal cyclic nucleotide levels and abnormal involuntary movements induced by L-DOPA administration (Giorgi et al., 2008; Picconi et al., 2011). Calabresi and colleagues also showed that PDE inhibition can rescue abnormal synaptic plasticity observed in dyskinetic rats (Picconi et al., 2011). On the other hand, studies aimed at decreasing NO signaling (and presumably cGMP levels) have shown that co-administration of NOS inhibitors with L-DOPA attenuates L-DOPA-induced dyskinesias (Padovan-Neto et al., 2009). NOS inhibition also improved the motor performance of the same animals on a rotorod test (Padovan-Neto et al., 2009). Taken together, the above studies suggest that under some circumstances, drugs with opposite pharmacological profiles (PDE inhibitors increase cGMP, nNOS inhibitors decrease cGMP) may both be beneficial for reversing L-DOPA-induced dyskinesias. Further studies determining the time course of L-DOPA-induced changes in cyclic nucleotide levels in the absence and presence of these inhibitors should open new avenues which will be essential for understanding and treating PD and side effects associated with L-DOPA therapy.

CONCLUSION

Studies reported to date indicate that it will be important to clarify how NO–sGC–cGMP signaling is dysregulated in hypo- and hyperdopaminergic states and how this can be normalized to restore function within striatal output pathways. Taken together, the above studies indicate that cGMP synthesis and catabolism, as well as the temporal and spatial patterning of NO–sGC–cGMP signaling may be perturbed in MSNs in the parkinsonian striatum. Moreover, these signaling abnormalities are likely to be a reflection of functional disturbances in DA and glutamate interactions and iatrogenic effects of chronic L-DOPA treatment. Definitive characterization of the impact of NO–sGC–cGMP signaling and downstream targets in animal models of parkinsonism and L-DOPA-induced dyskinesia should provide key information on how cyclic nucleotide signaling cascades can be modulated as an approach for treating motor symptoms in PD and other neurological disorders.

ACKNOWLEDGMENTS

This work is supported by United States Public Health grants NS047452 and NS047452-S1 to Anthony R. West, and DA004093 and Rosalind Franklin University Start-up funds to Kuei Y. Tseng.

REFERENCES

- Albin, R. L., Young, A. B., and Penney, J. B. (1989). The functional anatomy of basal ganglia disorders. *Trends Neurosci.* 12, 366–375.
- Alderton, W. K., Cooper, C. E., and Knowles, R. G. (2001). Nitric oxide synthases: structure, function and inhibition. *Biochem. J.* 357, 593–615.
- Alexander, G. E., and Crutcher, M. D. (1990). Functional architecture of basal ganglia circuits: neural substrates of parallel processing. *Trends Neurosci.* 13, 266–271.
- Alexander, G. E., Crutcher, M. D., and DeLong, M. R. (1990). Basal ganglia-thalamocortical circuits: parallel substrates for motor, oculomotor, “prefrontal” and “limbic” functions. *Prog. Brain Res.* 85, 119–146.
- Altar, C. A., Boyar, W. C., and Kim, H. S. (1990). Discriminatory roles for D1 and D2 dopamine receptor subtypes in the in vivo control of neostriatal cyclic GMP. *Eur. J. Pharmacol.* 181, 17–21.
- Ariano, M. A. (1983). Distribution of components of the guanosine 3',5'-phosphate system in rat caudate-putamen. *Neuroscience* 10, 707–723.
- Bamford, N. S., Robinson, S., Palmiter, R. D., Joyce, J. A., Moore, C., and Meshul, C. K. (2004). Dopamine modulates release from corticostriatal terminals. *J. Neurosci.* 24, 9541–9552.
- Barthwal, M. K., Srivastava, N., and Dikshit, M. (2001). Role of nitric oxide in a progressive neurodegeneration model of Parkinson's disease in the rat. *Redox Rep.* 6, 297–302.
- Betarbet, R., Poisik, O., Sherer, T. B., and Greenamyre, J. T. (2004). Differential expression and ser897 phosphorylation of striatal N-methyl-D-aspartate receptor subunit NR1 in animal models of Parkinson's disease. *Exp. Neurol.* 187, 76–85.
- Bockelmann, R., Wolf, G., Ransmayr, G., and Riederer, P. (1994). NADPH-diaphorase/nitric oxide synthase containing neurons in normal and Parkinson's disease putamen. *J. Neural Transm.* 7, 115–121.
- Boehning, D., and Snyder, S. H. (2003). Novel neural modulators. *Annu. Rev. Neurosci.* 26, 105–131.
- Bredt, D. S. (2003). Nitric oxide signaling in brain: potentiating the gain with YC-1. *Mol. Pharmacol.* 63, 1206–1208.
- Bredt, D. S., Hwang, P. M., and Snyder, S. H. (1990). Localization of nitric oxide synthase indicating a neural role for nitric oxide. *Nature* 347, 768–770.
- Calabresi, P., Centonze, D., Gubellini, P., Marfia, G. A., Pisani, A., Sancesario, G., and Bernardi, G. (2000). Synaptic transmission in the striatum: from plasticity to neurodegeneration. *Prog. Neurobiol.* 61, 231–265.
- Calabresi, P., Gubellini, P., Centonze, D., Sancesario, G., Morello, M., Giorgi, M., Pisani, A., and Bernardi, G. (1999). A critical role of the nitric oxide/cGMP pathway in corticostriatal long-term depression. *J. Neurosci.* 19, 2489–2499.
- Calabresi, P., Mercuri, N. B., Sancesario, G., and Bernardi, G. (1993). Electrophysiology of dopamine-denervated striatal neurons. Implications for Parkinson's disease. *Brain* 116, 433–452.
- Calabresi, P., Picconi, B., Tozzi, A., and Di Filippo, M. (2007). Dopamine-mediated regulation of corticostriatal synaptic plasticity. *Trends Neurosci.* 30, 211–219.
- Calabresi, P., Pisani, A., Mercuri, N. B., and Bernardi, G. (1992). Long-term potentiation in the striatum is unmasked by removing the voltage-dependent magnesium block of NMDA receptor channels. *Eur. J. Neurosci.* 4, 929–935.
- Cavas, M., and Navarro, J. F. (2002). Coadministration of L-NOARG and tiapride: effects on catalepsy in male mice. *Prog. Neuropsychopharmacol. Biol. Psychiatry* 26, 69–73.
- Cepeda, C., and Levine, M. S. (1998). Dopamine and N-methyl-D-aspartate receptor interactions in the neostriatum. *Dev. Neurosci.* 20, 1–18.
- Cepeda, C., and Levine, M. S. (2006). Where do you think you are going? The NMDA-D1 receptor trap. *Sci. STKE* 2006, pe20.
- Chalimoniuk, M., and Langfort, J. (2007). The effect of subchronic, intermittent L-DOPA treatment on neuronal nitric oxide synthase and soluble guanylyl cyclase expression and activity in the striatum and midbrain of normal and MPTP-treated mice. *Neurochem. Int.* 50, 821–833.
- Chalimoniuk, M., and Stepien, A. (2004). Influence of the therapy with pergolide mesylate plus L-DOPA and with L-DOPA alone on serum cGMP level in PD patients. *Pol. J. Pharmacol.* 56, 647–650.
- Chalimoniuk, M., Langfort, J., Lukacova, N., and Marsala, J. (2004). Upregulation of guanylyl cyclase expression and activity in striatum of MPTP-induced parkinsonism in mice. *Biochem. Biophys. Res. Commun.* 324, 118–126.
- Charpier, S., and Deniau, J. M. (1997). In vivo activity-dependent plasticity at cortico-striatal connections: evidence for physiological long-term potentiation. *Proc. Natl. Acad. Sci. U.S.A.* 94, 7036–7040.
- Chepkova, A. N., Fleischer, W., Kazmierczak, T., Doreulee, N., Haas, H. L., and Sergeeva, O. A. (2009). Developmental alterations of DHPG-induced long-term depression of corticostriatal synaptic transmission: switch from NMDA receptor-dependent towards CB1 receptor-dependent plasticity. *Pflugers Arch.* 459, 131–141.
- Cowan, R. L., and Wilson, C. J. (1994). Spontaneous firing patterns and axonal projections of single corticostriatal neurons in the rat medial agranular cortex. *J. Neurophysiol.* 71, 17–32.
- Dawson, T. M., Bredt, D. S., Fotuhi, M., Hwang, P. M., and Snyder, S. H. (1991). Nitric oxide synthase and neuronal NADPH diaphorase are identical in brain and peripheral tissues. *Proc. Natl. Acad. Sci. U.S.A.* 88, 7797–7801.
- Day, M., Wang, Z., Ding, J., An, Z., Ingham, C. A., Shering, A. F., Wokosin, D., Ilijic, E., Sun, Z., Sampson, A. R., Mugnaini, E., Deutch, A. Y., Sesack, S. R., Arbuthnott, G. W., and Surmeier, D. J. (2006). Selective elimination of glutamatergic synapses on striato-pallidal neurons in Parkinson disease models. *Nat. Neurosci.* 9, 251–259.
- De Vente, J., Markerink-van Ittersum, M., Van Abeelen, J., Emson, P. C., Axer, H., and Steinbusch, H. W. M. (2000). NO-mediated cGMP synthesis in cholinergic neurons in the rat forebrain: effects of lesioning dopaminergic or serotonergic pathways on nNOS and cGMP synthesis. *Eur. J. Neurosci.* 12, 507–519.
- Del Bel, E. A., da Silva, C. A., Guimaraes, F. S., and Bermudez-Echeverry, M. (2004). Catalepsy induced by intrastriatal administration of nitric oxide synthase inhibitors in rats. *Eur. J. Pharmacol.* 485, 175–181.
- Del Bel, E. A., and Guimaraes, F. S. (2000). Sub-chronic inhibition of nitric-oxide synthesis modifies haloperidol-induced catalepsy and the number of NADPH-diaphorase neurons in mice. *Psychopharmacology (Berl.)* 147, 356–361.
- Del Bel, E. A., Guimaraes, F. S., Bermudez-Echeverry, M., Gomes, M. Z., Schiaveto-de-souza, A., Padovan-Neto, F. E., Tumas, V., Barion-Cavalcanti, A. P., Lazzarini, M., Nucci-da-Silva, L. P., and de Paula-Souza, D. (2005). Role of nitric oxide on motor behavior. *Cell. Mol. Neurobiol.* 25, 371–392.
- DeLong, M. R., and Wichmann, T. (2007). Circuits and circuit disorders of the basal ganglia. *Arch. Neurol.* 64, 20–24.
- Deutsch, S. I., Rosse, R. B., Paul, S. M., Tomasino, V., Koetzner, L., Morn, C. B., and Mastropaolo, J. (1996). 7-Nitroindazole and methylene blue, inhibitors of neuronal nitric oxide synthase and NO-stimulated guanylate cyclase, block MK-801-elicited behaviors in mice. *Neuropsychopharmacology* 15, 37–43.
- Di Stefano, A., Sozio, P., Cacciatore, I., Cocco, A., Giorgioni, G., Costa, B., Montali, M., Lucacchini, A., Martini, C., Spoto, G., Di Pietrantonio, F., Di Matteo, E., and Pinnen, F. (2005). Preparation and pharmacological characterization of trans-2-amino-5(6)-fluoro-6(5)-hydroxy-1-phenyl-2,3-dihydro-1H-indenes as D2-like dopamine receptor agonists. *J. Med. Chem.* 48, 2646–2654.
- Ding, J. D., Burette, A., Nedvetsky, P. I., Schmidt, H. H., and Weinberg, R. J. (2004). Distribution of soluble guanylyl cyclase in the rat brain. *J. Comp. Neurol.* 472, 437–448.
- Doreulee, N., Sergeeva, O. A., Yanovsky, Y., Chepkova, A. N., Selbach, O., Godecke, A., Schrader, J., and Haas, H. L. (2003). Cortico-striatal synaptic plasticity in endothelial nitric oxide synthase deficient mice. *Brain Res.* 964, 159–163.
- Echeverry, M. B., Salgado, M. L., Ferreira, F. R., da-Silva, C. A., and Del Bel, E. A. (2007). Intracerebroventricular administration of nitric oxide-sensitive guanylyl cyclase inhibitors induces catalepsy in mice. *Psychopharmacology (Berl.)* 194, 271–278.
- Eve, D. J., Nisbet, A. P., Kingsbury, A. E., Hewson, E. L., Daniel, S. E., Lees, A. J., Marsden, C. D., and Foster, O. J. (1998). Basal ganglia neuronal nitric oxide synthase mRNA expression in Parkinson's disease. *Mol. Brain Res.* 63, 62–71.
- Fujiyama, F., and Masuko, S. (1996). Association of dopaminergic terminals and neurons releasing nitric oxide in the rat striatum: an electron microscopic study using NADPH-diaphorase histochemistry and tyrosine hydroxylase immunohistochemistry. *Brain Res. Bull.* 40, 121–127.
- Galati, S., D'Angelo, V., Scarnati, E., Stanzione, P., Martorana, A., Procopio, T., Sancesario, G., and Stefani, A. (2008). In vivo electrophysiology of dopamine-denervated striatum: focus on the nitric oxide/cGMP signaling pathway. *Synapse* 62, 409–420.
- Garthwaite, J. (2008). Concepts of neural nitric oxide-mediated transmission. *Eur. J. Neurosci.* 27, 2783–2802.
- Gerfen, C. R., Engber, T. M., Mathan, L. C., Susel, Z., Chase, T. N., Monsma, F. J., and Sibley, D. R. (1990). D1 and D2 dopamine receptor-regulated gene expression of striatonigral and striatopallidal neurons. *Science* 250, 1429–1432.
- Giorgi, M., D'Angelo, V., Esposito, Z., Nuccetelli, V., Sorge, R., Martorana, A., Stefani, A., Bernardi, G., and Sancesario, G. (2008). Lowered cAMP and cGMP signalling in the brain during levodopa-induced dyskinesias in hemiparkinsonian rats: new aspects in the pathogenetic mechanisms. *Eur. J. Neurosci.* 28, 941–950.

- Gracy, K. N., and Pickel, V. M. (1997). Ultrastructural localization and comparative distribution of nitric oxide synthase and N-methyl-D-aspartate receptors in the shell of the rat nucleus accumbens. *Brain Res.* 747, 259–272.
- Greengard, P. (2001). The neurobiology of slow synaptic transmission. *Science* 294, 1024–1030.
- Hidaka, S., and Totterdell, S. (2001). Ultrastructural features of the nitric oxide synthase-containing interneurons in the nucleus accumbens and their relationship with tyrosine hydroxylase-containing terminals. *J. Comp. Neurol.* 431, 139–154.
- Hirsch, E. C., Perier, C., Orioux, G., Francois, C., Feger, J., Yelnik, J., Vila, M., Levy, R., Tolosa, E. S., Marin, C., Trinidad Herrero, M., Obeso, J. A., and Agid, Y. (2000). Metabolic effects of nigrostriatal denervation in basal ganglia. *Trends Neurosci.* 23, S78–S85.
- Hofmann, M., Spano, P. F., Trabucchi, M., and Kumakura, K. (1977). Guanylate cyclase activity in various rat brain areas. *J. Neurochem.* 29, 395–396.
- Hope, B. T., Michael, G. J., Knigge, K. M., and Vincent, S. R. (1991). Neuronal NADPH diaphorase is a nitric oxide synthase. *Proc. Natl. Acad. Sci. U.S.A.* 88, 2811–2814.
- Hoque, K. E., Indorkar, R. P., Sammut, S., and West, A. R. (2010). Impact of dopamine-glutamate interactions on striatal neuronal nitric oxide synthase activity. *Psychopharmacology (Berl.)* 207, 571–581.
- Hornykiewicz, O. (1975). Brain monoamines and parkinsonism. *Natl. Inst. Drug Abuse Res. Monogr. Ser.* 00, 13–21.
- Ingham, C. A., Hood, S. H., and Arbuthnott, G. W. (1989). Spine density on neostriatal neurons changes with 6-hydroxydopamine lesions and with age. *Brain Res.* 503, 334–338.
- Kawaguchi, Y. (1993). Physiological, morphological, and histochemical characterization of three classes of interneurons in rat neostriatum. *J. Neurosci.* 13, 4908–4923.
- Kravitz, A. V., Freeze, B. S., Parker, P. R. L., Kay, K., Thwin, M. T., Deisseroth, K., and Kreitzer, A. C. (2010). Regulation of parkinsonian motor behaviours by optogenetic control of basal ganglia circuitry. *Nature* 466, 622–626.
- Kreitzer, A. C., and Malenka, R. C. (2007). Endocannabinoid-mediated rescue of striatal LTD and motor deficits in Parkinson's disease models. *Nature* 445, 643–647.
- Kuo, H., Grant, S., Muth, N., Hengemihle, J., and Ingram, D. K. (1994). The correlation between neuron counts and optical density of NADPH-diaphorase histochemistry in the rat striatum: a quantitative study. *Brain Res.* 660, 57–65.
- Mallet, N., Ballion, B., Le Moine, C., and Gonon, F. (2006). Cortical inputs and GABA interneurons imbalance projection neurons in the striatum of parkinsonian rats. *J. Neurosci.* 26, 3875–3884.
- Mallet, N., Le Moine, C., Charpier, S., and Gonon, F. (2005). Feedforward inhibition of projection neurons by fast-spiking GABA interneurons in the rat striatum in vivo. *J. Neurosci.* 25, 3857–3869.
- Mancuso, F., Calignano, A., and Sorrentino, L. (1994). Endogenous nitric oxide modulates behavioural effects elicited by substance P in rat. *Eur. J. Pharmacol.* 271, 329–333.
- Marsden, C. D. (1982). The mysterious motor function of the basal ganglia: the Robert Wartenberg Lecture. *Neurology* 32, 514–539.
- Matsuoka, I., Giulli, G., Poyard, M., Stengel, D., Parma, J., Guellaen, G., and Hanoune, J. (1992). Localization of adenylyl and guanylyl cyclase in rat brain by in situ hybridization: comparison with calmodulin mRNA distribution. *J. Neurosci.* 12, 3350–3360.
- Meshul, C. K., Emre, N., Nakamura, C. M., Allen, C., Donohue, M. K., and Buckman, J. F. (1999). Time-dependent changes in striatal glutamate synapses following a 6-hydroxydopamine lesion. *Neuroscience* 88, 1–16.
- Morello, M., Reiner, A., Sancesario, G., Karle, E. J., and Bernardi, G. (1997). Ultrastructural study of nitric oxide synthase-containing striatal neurons and their relationship with parvalbumin-containing neurons in rats. *Brain Res.* 776, 30–39.
- Morris, B. J. (1995). Stimulation of immediate-early gene expression in striatal neurones by nitric oxide. *J. Biol. Chem.* 270, 24740–24744.
- Morris, B. J., Simpson, C. S., Mundell, S., Maceachern, K., Johnston, H. M., and Nolan, A. M. (1997). Dynamic changes in NADPH-diaphorase staining reflect activity of nitric oxide synthase: evidence for a dopaminergic regulation of striatal nitric oxide release. *Neuropharmacology* 36, 1589–1599.
- Murer, M. G., Tseng, K. Y., Kasantz, F., Belluscio, M., and Riquelme, L. A. (2002). Brain oscillations, medium spiny neurons, and dopamine. *Cell. Mol. Neurobiol.* 22, 611–632.
- Nash, J. E., Hill, M. P., and Brothchie, J. M. (1999). Antiparkinsonian actions of blockade of NR2B-containing NMDA receptors in the reserpine-treated rat. *Exp. Neurol.* 155, 42–48.
- Nishi, A., Watanabe, Y., Higashi, H., Tanaka, M., Nairn, A. C., and Greengard, P. (2005). Glutamate regulation of DARPP-32 phosphorylation in neostriatal neurons involves activation of multiple signaling cascades. *Proc. Natl. Acad. Sci. U.S.A.* 102, 1199–1204.
- O'Donnell, P., and Grace, A. A. (1997). Cortical afferents modulate striatal gap junction permeability via nitric oxide. *Neuroscience* 76, 1–5.
- Ondracek, J. M., Dec, A., Hoque, K. E., Lim, S. A., Rasouli, G., Indorkar, R. P., Linardakis, J., Klika, B., Mukherji, S. J., Burnazi, M., Threlfell, S., Sammut, S., and West, A. R. (2008). Feed-forward excitation of striatal neuron activity by frontal cortical activation of nitric oxide signaling in vivo. *Eur. J. Neurosci.* 27, 1739–1754.
- Padovan-Neto, F. E., Echeverry, M. B., Tumas, V., and Del-Bel, E. A. (2009). Nitric oxide synthase inhibition attenuates L-DOPA-induced dyskinesias in a rodent model of Parkinson's disease. *Neuroscience* 159, 927–935.
- Palmer, R. M., Ferrige, A. G., and Moncada, S. (1987). Nitric oxide release accounts for the biological activity of endothelium-derived relaxing factor. *Nature* 327, 524–526.
- Parent, A. (1990). Extrinsic connections of the basal ganglia. *Trends Neurosci.* 13, 254–258.
- Park, D. J., and West, A. R. (2009). Regulation of striatal nitric oxide synthesis by local dopamine and glutamate interactions. *J. Neurochem.* 111, 1457–1465.
- Picconi, B., Bagetta, V., Ghiglieri, V., Paille, V., Di Filippo, M., Pendolino, M., Tozzi, A., Giampa, C., Fusco, F. R., Sgobio, C., and Calabresi, P. (2011). Inhibition of phosphodiesterases rescues striatal long-term depression and reduces levodopa-induced dyskinesia. *Brain* 134, 375–387.
- Picconi, B., Centonze, D., Rossi, S., Bernardi, G., and Calabresi, P. (2004). Therapeutic doses of L-dopa reverse hypersensitivity of corticostriatal D2-dopamine receptors and glutamatergic overactivity in experimental parkinsonism. *Brain* 127, 1661–1669.
- Sahach, V. F., Baziliuk, O. V., Oleshko, M. M., Kotsiuruba, O. V., Bukhanevych, O. M., and Appenzeller, O. (2000). The nitric oxide system in a chronic deficiency of mesostriatal dopamine: the action of nitroglycerin. *Fiziol. Zh.* 46, 55–63.
- Sammut, S., Dec, A., Mitchell, D., Linardakis, J., Ortiguela, M., and West, A. R. (2006). Phasic dopaminergic transmission increases NO efflux in the rat dorsal striatum via a neuronal NOS and a dopamine D(1/5) receptor-dependent mechanism. *Neuropsychopharmacology* 31, 493–505.
- Sammut, S., Park, D. J., and West, A. R. (2007a). Frontal cortical afferents facilitate striatal nitric oxide transmission in vivo via a NMDA receptor and neuronal NOS-dependent mechanism. *J. Neurochem.* 103, 1145–1156.
- Sammut, S., Bray, K. E., and West, A. R. (2007b). Dopamine D2 receptor-dependent modulation of striatal NO synthase activity. *Psychopharmacology (Berl.)* 191, 793–803.
- Sammut, S., Threlfell, S., and West, A. R. (2010). Nitric oxide-soluble guanylyl cyclase signaling regulates corticostriatal transmission and short-term synaptic plasticity of striatal projection neurons recorded in vivo. *Neuropharmacology* 58, 624–631.
- Sancesario, G., Giorgi, M., D'Angelo, V., Modica, A., Martorana, A., Morello, M., Bengtson, C. P., and Bernardi, G. (2004). Down-regulation of nitrergic transmission in the rat striatum after chronic nigrostriatal deafferentation. *Eur. J. Neurosci.* 20, 989–1000.
- Sancesario, G., Morello, M., Reiner, A., Giacomini, P., Massa, R., Schoen, S., and Bernardi, G. (2000). Nitrergic neurons make synapses on dual-input dendritic spines of neurons in the cerebral cortex and the striatum of the rat: implication for a postsynaptic action of nitric oxide. *Neuroscience* 99, 627–642.
- Shen, W., Flajolet, M., Greengard, P., and Surmeier, D. J. (2008). Dichotomous dopaminergic control of striatal synaptic plasticity. *Science* 321, 848–851.
- Siuciak, J. A., McCarthy, S. A., Chapin, D. S., Fujiwara, R. A., James, L. C., Williams, R. D., Stock, J. L., McNeish, J. D., Strick, C. A., Menniti, F. S., and Schmidt, C. J. (2006). Genetic deletion of the striatum-enriched phosphodiesterase PDE10A: evidence for altered striatal function. *Neuropharmacology* 51, 374–385.
- Starr, M. S., and Starr, B. S. (1995). Do NMDA receptor-mediated changes in motor behaviour involve nitric oxide? *Eur. J. Pharmacol.* 272, 211–217.
- Stephens, B., Mueller, A. J., Shering, A. F., Hood, S. H., Taggart, P., Arbuthnott, G. W., Bell, J. E., Kilford, L., Kingsbury, A. E., Daniel, S. E., and Ingham, C. A. (2005). Evidence of a breakdown of corticostriatal connections in Parkinson's disease. *Neuroscience* 132, 741–754.
- Stewart, J., Deschamps, S. E., and Amir, S. (1994). Inhibition of nitric oxide synthase does not block the development of sensitization to the behavioral activating effects of amphetamine. *Brain Res.* 641, 141–144.
- Surmeier, D. J., Plotkin, J., and Shen, W. (2009). Dopamine and synaptic

- plasticity in dorsal striatal circuits controlling action selection. *Curr. Opin. Neurobiol.* 19, 621–628.
- Tepper, J. M., Koos, T., and Wilson, C. J. (2004). GABAergic microcircuits in the neostriatum. *Trends Neurosci.* 27, 662–669.
- Threlfell, S., Sammut, S., Menniti, F. S., Schmidt, C. J., and West, A. R. (2009). Inhibition of phosphodiesterase 10A increases the responsiveness of striatal projection neurons to stimulation of frontal cortical afferents. *J. Pharm. Exp. Ther.* 328, 785–795.
- Tseng, K. Y., Kasanetz, F., Kargieman, L., Riquelme, L. A., and Murer, M. G. (2001). Cortical slow oscillatory activity is reflected in the membrane potential and spike trains of striatal neurons in rats with chronic nigrostriatal lesions. *J. Neurosci.* 21, 6430–6439.
- Vincent, S. R. (1994). Nitric oxide: a radical neurotransmitter in the central nervous system. *Prog. Neurobiol.* 42, 129–160.
- Walters, J. R., Hu, D., Itoga, C. A., Parr-Brownlie, L. C., and Bergstrom, D. A. (2007). Phase relationships support a role for coordinated activity the indirect pathway in organizing slow oscillations in basal ganglia output after loss of dopamine. *Neuroscience* 144, 762–776.
- Wang, H., and Pickel, V. M. (2002). Dopamine D2 receptors are present in prefrontal cortical afferents and their targets in patches of the rat caudate-putamen nucleus. *J. Comp. Neurol.* 442, 392–404.
- West, A. R. (2010). “Nitric oxide signaling in the striatum,” in *Handbook of Basal Ganglia Structure and Function*, eds H. Steiner and K. Y. Tseng (New York, NY: Academic Press/Elsevier), 187–200.
- West, A. R., Galloway, M. P., and Grace, A. A. (2002). Regulation of striatal dopamine neurotransmission by nitric oxide: effector pathways and signaling mechanisms. *Synapse* 44, 227–245.
- West, A. R., and Grace, A. A. (2000). Striatal nitric oxide signaling regulates the neuronal activity of mid-brain dopamine neurons in vivo. *J. Neurophysiol.* 83, 1796–1808.
- West, A. R., and Grace, A. A. (2004). The nitric oxide-guanylyl cyclase signaling pathway modulates membrane activity States and electrophysiological properties of striatal medium spiny neurons recorded in vivo. *J. Neurosci.* 24, 1924–1935.
- West, A. R., Sammut, S., and Ariano, M. A. (2009). “Striatal nitric oxide–cGMP signaling in an animal model of parkinson’s disease,” Chapter 11. *Contemporary Neuroscience*, Humana Press, Springer.
- West, A. R., Sammut, S., and Ariano, M. A. (2009). “Chapter 11: Striatal nitric oxide–cGMP signaling in an animal model of Parkinson’s disease,” in *Cortico-subcortical dynamics in Parkinson’s disease*, ed. K. Y. Tseng (New York, NY: Humana Press, Springer), 171–184.
- Conflict of Interest Statement:** The authors declare that the research was conducted in the absence of any commercial or financial relationships that could be construed as a potential conflict of interest.

Received: 24 December 2010; paper pending published: 27 March 2011; accepted: 16 June 2011; published online: 30 June 2011.

Citation: West AR and Tseng KY (2011) Nitric oxide–soluble guanylyl cyclase–cyclic GMP signaling in the striatum: new targets for the treatment of Parkinson’s disease? *Front. Syst. Neurosci.* 5:55. doi: 10.3389/fnsys.2011.00055

Copyright © 2011 West and Tseng. This is an open-access article subject to a non-exclusive license between the authors and Frontiers Media SA, which permits use, distribution and reproduction in other forums, provided the original authors and source are credited and other Frontiers conditions are complied with.



Dopamine signaling in dorsal versus ventral striatum: the dynamic role of cholinergic interneurons

Sarah Threlfell^{1,2} and Stephanie Jane Cragg^{1,2*}

¹ Department of Physiology, Anatomy and Genetics, University of Oxford, Oxford, UK

² Oxford Parkinson's Disease Centre, University of Oxford, Oxford, UK

Edited by:

James M. Tepper, Rutgers, The State University of New Jersey, USA

Reviewed by:

Ingo Willuhn, University of Washington, USA

Michelle E. Ehrlich, Mount Sinai School of Medicine, USA

*Correspondence:

Stephanie Jane Cragg, Oxford Parkinson's Disease Centre, University of Oxford, Parks Road, Oxford OX1 3PT, UK.
e-mail: stephanie.cragg@dpag.ox.ac.uk

Mesostriatal dopaminergic neurons and striatal cholinergic interneurons participate in signaling the motivational significance of environmental stimuli and regulate striatal plasticity. Dopamine (DA) and acetylcholine (ACh) have potent interactions within the striatum at multiple levels that include presynaptic regulation of neurotransmitter release and postsynaptic effects in target cells (including ACh neurons). These interactions may be highly variable given the dynamic changes in the firing activities of parent DA and ACh neurons. Here, we consider how striatal ACh released from cholinergic interneurons acting at both nicotinic and muscarinic ACh receptors powerfully modulates DA transmission. This ACh–DA interaction varies in a manner that depends on the frequency of presynaptic activation, and will thus strongly influence how DA synapses convey discrete changes in DA neuron activity that are known to signal events of motivational salience. Furthermore, this ACh modulation of DA transmission within striatum occurs via different profiles of nicotinic and muscarinic receptors in caudate–putamen compared to nucleus accumbens, which may ultimately enable region-specific targeting of striatal function.

Keywords: dopamine, striatal territories, acetylcholine receptors, release probability, cholinergic interneuron

INTRODUCTION

The striatum is a large subcortical nucleus involved in motor coordination and cognition, as well as disorders such as Parkinson's disease, Tourette's syndrome, Huntington's disease, schizophrenia, and drug addiction (Wilson, 2004). The principal neurons of the striatum are the medium spiny neurons (MSNs) which constitute ~90% of the striatal neuron population and form the striatal output (Bolam et al., 2000). The remaining striatal neurons are comprised of at least three types of interneuron, including the large, aspiny, tonically active cholinergic interneuron (Kawaguchi, 1993). As the input nucleus of the basal ganglia, the striatum receives, and gates massive convergent innervation via the MSNs to generate appropriate behaviors. Among this convergent innervation, striatal projection neurons receive dopaminergic inputs from the midbrain alongside excitatory inputs from both cortex and thalamus. Nigrostriatal dopaminergic afferents and corticostriatal/thalamostriatal glutamatergic afferents commonly synapse onto the same MSN dendritic spine (Moss and Bolam, 2008). Dopamine (DA) is therefore well positioned within this synaptic triad to shape striatal output.

In order to appreciate the significance of discrete activity in DA neurons to striatal function it is important to consider factors controlling the availability of DA from axon terminals in the striatum. Acetylcholine (ACh) and DA have dense overlapping axonal arborizations and a potent reciprocal relationship within the striatum. Mesostriatal DA neurons and striatal cholinergic interneurons participate in signaling the motivational significance of environmental stimuli and regulate striatal plasticity (Schultz, 1998, 2002; Calabresi et al., 2000; Partridge et al., 2002; Morris et al., 2004). Interactions between these neurotransmitters in the striatum occur at presynaptic and postsynaptic levels, through synchronous

changes in their parent neuron activities and reciprocal presynaptic regulation of release (Calabresi et al., 2000; Zhou et al., 2002; Centonze et al., 2003; Pisani et al., 2003; Morris et al., 2004; Cragg, 2006). In addition, it is essential to consider that the striatum is a heterogeneous nucleus, and is organized into different (albeit overlapping) territories, anatomically, biochemically, functionally, and also neurochemically in terms of neurotransmitter interactions (Haber et al., 2000; Nakano et al., 2000; Cragg, 2003; Voorn et al., 2004; Belin et al., 2009).

A primary focus of our work is to understand how ACh regulates striatal DA neurotransmission across different striatal regions and under conditions representing the physiological repertoire of activity patterns of DA neurons. We use the real time electrochemical detection technique, fast-scan cyclic voltammetry at carbon fiber-microelectrodes to be able to explore subsecond DA transmission. This work will help us to understand how striatal DA availability varies with DA neuron activity. In this *Perspective*, we will draw from recent findings to summarize our current understanding of how ACh modulates DA transmission via actions at both nicotinic and muscarinic receptors. This regulation occurs in a variable manner dependent on DA neuron activity, and moreover, involves different receptor subtypes/subunits in sensorimotor- versus limbic-associated striatum.

DOPAMINE AND ACETYLCHOLINE SYSTEMS IN THE STRIATUM

STRIATAL SUBTERRITORIES

Collectively, the striatum participates in a wide variety of motivational, associative, and sensorimotor-related brain functions (Albin et al., 1995; Haber et al., 2000; Gerdeman et al., 2003;

Voorn et al., 2004; Everitt and Robbins, 2005; Schultz, 2006). The striatum is a highly heterogeneous structure where the principal neurons, the MSNs, are intermingled in an irregular fashion with at least three different types of interneuron as well as a variety of inputs from cortex, thalamus, and midbrain. Within this heterogeneous structure, subterritories exist which differ according to their functional roles as well as their afferent inputs from, and projections to other nuclei. For example, dorsal striatal regions are classically associated with sensorimotor function, with glutamatergic afferents from motor cortex and dopaminergic afferents from substantia nigra pars compacta (SNc; McGeorge and Faull, 1989; Haber et al., 2000; Reep et al., 2003). Ventral striatal regions are associated with limbic function with glutamatergic afferents from prefrontal cortex, amygdala and hippocampus, and dopaminergic afferents from ventral tegmental area (VTA; Kelley and Domesick, 1982; McGeorge and Faull, 1989; Sesack et al., 1989; Brog et al., 1993; Pennartz et al., 1994; O'Donnell and Grace, 1995; Haber et al., 2000). When exploring factors which regulate striatal DA availability, it is therefore important to consider different striatal subterritories, especially when considering potential therapeutic targets for which a regional specificity of action may be ideal. And yet, while these regions are delineated in many respects, they also interact through interconnections and other crosstalk (Haber et al., 2000; Belin and Everitt, 2008; Belin et al., 2009). Therefore, factors which have distinct regulatory functions within one striatal region may also have important consequences for function in other regions.

DOPAMINE AND ACETYLCHOLINE DISTRIBUTION IN STRIATUM

A high density of dopaminergic and cholinergic terminals exists in the striatum and they are often only about 1 μm apart (Descarries et al., 1997). DA inputs to the striatum arise predominantly from the “A9”–“A10” DA neurons in the midbrain. Neurons in the VTA and SNc project in a topographic pattern to differentially innervate the ventral striatum (nucleus accumbens, NAc) and the dorsal striatum (caudate–putamen, CPu) respectively (Bjorklund and Lindvall, 1984; Gerfen et al., 1987; McFarland and Haber, 2000; Voorn et al., 2004). Mesostriatal DA neurons exhibit two broad and well-defined firing modes *in vivo*; single-spike firing in regular or irregular patterns (~1–10 Hz) and burst firing of 3–5 spikes at a frequency of ~15–100 Hz (Grace and Bunney, 1984a,b; Hyland et al., 2002), and there are also periods when DA neurons are in a hyperpolarized, quiescent state. The switch in firing mode of mesostriatal DA neurons, from low to higher firing frequencies, is thought to encode information about the prediction and receipt of reward or behaviorally salient stimuli (Schultz, 1986, 2002; Morris et al., 2004; Matsumoto and Hikosaka, 2009). Despite DA neurons forming a relatively small population of neurons, a single DA neuron projecting to the striatum forms a very dense arbor, occupying up to 5.7% of the volume of the striatum, with a high density of axonal varicosities forming a synapse approximately every 10–20 μm^3 (Descarries et al., 1996; Arbuthnott and Wickens, 2007; Matsuda et al., 2009; Moss and Bolam, 2010). Furthermore, an individual DA neuron is thought to make several hundred thousand synapses – at least an order of magnitude higher than most other CNS neurons (Matsuda et al., 2009). Although DA neurons make a huge number of structurally defined synapses, DA receptors and uptake transporters exist extrasynaptically (Nirenberg

et al., 1996, 1997; Pickel, 2000) and DA is able to spillover from the synapse to participate in extrasynaptic or “volume” transmission (Fuxe and Agnati, 1991; Garriss et al., 1994; Gonon, 1997; Cragg and Rice, 2004; Rice and Cragg, 2008). DA is therefore extremely well positioned to modulate striatal function: DA synapses are situated on the necks of spines of MSNs adjacent to corticostriatal or thalamostriatal glutamatergic inputs (Freund et al., 1984; Smith and Bolam, 1990; Groves et al., 1994; Moss and Bolam, 2008). DA receptors are present throughout the striatum, with D1-like receptors on striatonigral MSNs (Hersch et al., 1995; Matamalas et al., 2009) and D2-like receptors on striatopallidal MSNs, cholinergic interneurons as well as DA axons (Sesack et al., 1994; Alcantara et al., 2003; Matamalas et al., 2009).

In the striatum, cholinergic innervation arises solely from cholinergic interneurons (Woolf, 1991; Contant et al., 1996; Calabresi et al., 2000), which despite representing only 1–2% of all striatal neurons, provide an extensive axonal arborization throughout the striatum in a manner similar to dopaminergic axons. Quantitative electron microscopy studies indicate approximately 2×10^8 ACh varicosities/ mm^3 in the striatum, and each striatal cholinergic interneuron has 500,000 axon varicosities. Similar to dopaminergic axon terminals, a 10- μm -radius sphere of striatal neuropil contains about 400 cholinergic axon terminals (Contant et al., 1996; Descarries and Mechawar, 2000). These cholinergic interneurons are spontaneously active in the striatum (Bennett and Wilson, 1999; Zhou et al., 2001, 2003). Similar to dopaminergic neurons, cholinergic interneurons are also critically involved in signaling learning associated with events of unexpected high salience (Calabresi et al., 2000; Schultz, 2002; Berridge and Robinson, 2003; Centonze et al., 2003; Wickens et al., 2003; Wise, 2004). Whilst DA neurons signal these events by switching from low to higher frequency, burst firing modes (Schultz, 1986, 2002; Morris et al., 2004; Matsumoto and Hikosaka, 2009), cholinergic interneurons respond simultaneously with a pause in firing which can also be flanked by a preceding and succeeding brief high frequency firing in a “burst-pause-burst” pattern (Morris et al., 2004; Joshua et al., 2008). The coincident timing of activity changes in DA and ACh neurons associated with events of unexpected salience highlights the synchronous interaction between these transmitters in the striatum.

Both DA and ACh are able to participate in extrasynaptic signaling (i.e., volume transmission; Descarries et al., 1996, 1997; Zoli et al., 1998), but the close proximity of striatal dopaminergic and cholinergic terminals ensures interactions between the dopaminergic and cholinergic systems. Indeed, the co-operative interactions of the dopaminergic and cholinergic systems are very important for the proper functioning of the striatum (Calabresi et al., 2000; Centonze et al., 2003; Rice and Cragg, 2004; Zhang and Sulzer, 2004; Cragg et al., 2005). There is a longstanding hypothesis of an antagonistic balance between DA and ACh in normal striatal function (Calabresi et al., 2000; Zhou et al., 2002; Centonze et al., 2003; Pisani et al., 2003). This hypothesis arose from studies which found that both DA replacement treatments and anti-cholinergic treatments were able to alleviate the debilitating motor symptoms of Parkinson's disease (Barbeau, 1962; Pisani et al., 2003), and at the postsynaptic level, DA and ACh can have opposing effects on the excitability of striatal output neurons and on corticostriatal plasticity (Calabresi et al., 2000, 2007; Centonze et al., 2003;

Pisani et al., 2003; Morris et al., 2004). Their interactions *in situ* may however be co-operative (Morris et al., 2004; Cragg, 2006), since the direction of physiological changes in activities of DA and ACh neurons during behavior is opposite.

Striatal ACh acts at two classes of cholinergic receptors, nicotinic acetylcholine receptors (nAChRs), and muscarinic acetylcholine receptors (mAChRs). Nicotinic receptors are ligand-gated ion channels composed of five subunits arranged symmetrically around a central pore. Muscarinic receptors are seven transmembrane domain, G-protein-coupled receptors. ACh via actions at both mAChRs and nAChRs is able to powerfully regulate striatal DA availability in a manner which differs according to the striatal subregion and DA neuron activity. In addition, the subtypes of both mAChRs and nAChRs responsible differ between dorsal and ventral striatal territories.

FREQUENCY-DEPENDENT REGULATION OF DOPAMINE RELEASE PROBABILITY BY PRESYNAPTIC NICOTINIC RECEPTORS (nAChRs)

Striatal DA release may not correlate directly with the activity of DA neurons in midbrain due to mechanisms that may include use-dependent changes or “plasticity” in DA release probability (Chergui et al., 1994; Cragg, 2003; Montague et al., 2004) as seen at other CNS synapses. Within the striatum, DA release probability following a single action potential is relatively high, with subsequent short-term depression limiting further release by subsequent action potentials within a burst of action potentials (Schmitz et al., 2002; Cragg, 2003).

Ligands for nAChRs have long been known to have a powerful control over striatal DA release (Di Chiara and Imperato, 1988; Dajas-Bailador and Wonnacott, 2004). However, we now appreciate that the control of DA release probability by ACh and presynaptic nAChRs is dynamic and complex depending on the activity of DA neurons and multiple nAChR subunits (Zhou et al., 2001; Rice and Cragg, 2004; Zhang and Sulzer, 2004; Exley et al., 2008; Drenan et al., 2010; Threlfell et al., 2010). Typically, striatal DA release is associated with a use-dependent, short-term depression of release probability at short inter-pulse intervals (Abeliovich et al., 2000; Cragg, 2003; Montague et al., 2004). Studies using real time electrochemical detection of DA in striatal slices indicate that ACh released from tonically active cholinergic interneurons (Bennett and Wilson, 1999; Zhou et al., 2001, 2003) acts at $\beta 2^*$ -nAChRs on striatal DA axons contributing to the high probability of DA release evoked by a single pulse (Zhou et al., 2001; Rice and Cragg, 2004). Reducing ACh actions at nAChRs by application of nAChR antagonists, or by desensitization of nAChRs using nicotine, reduces initial DA release probability and subsequently relieves short-term depression (Figure 1; Rice and Cragg, 2004; Zhang and Sulzer, 2004). ACh therefore contributes to the initial probability that DA is released, and in turn, the subsequent short-term depression of DA release.

One of the key consequences of ACh activation of nAChRs on dopaminergic axons is a limit placed on how subsequent action potentials in a train, or burst, can evoke further DA release. In other words, ACh action at nAChRs promotes how DA axons release in response to single or low frequency action potentials, but at the

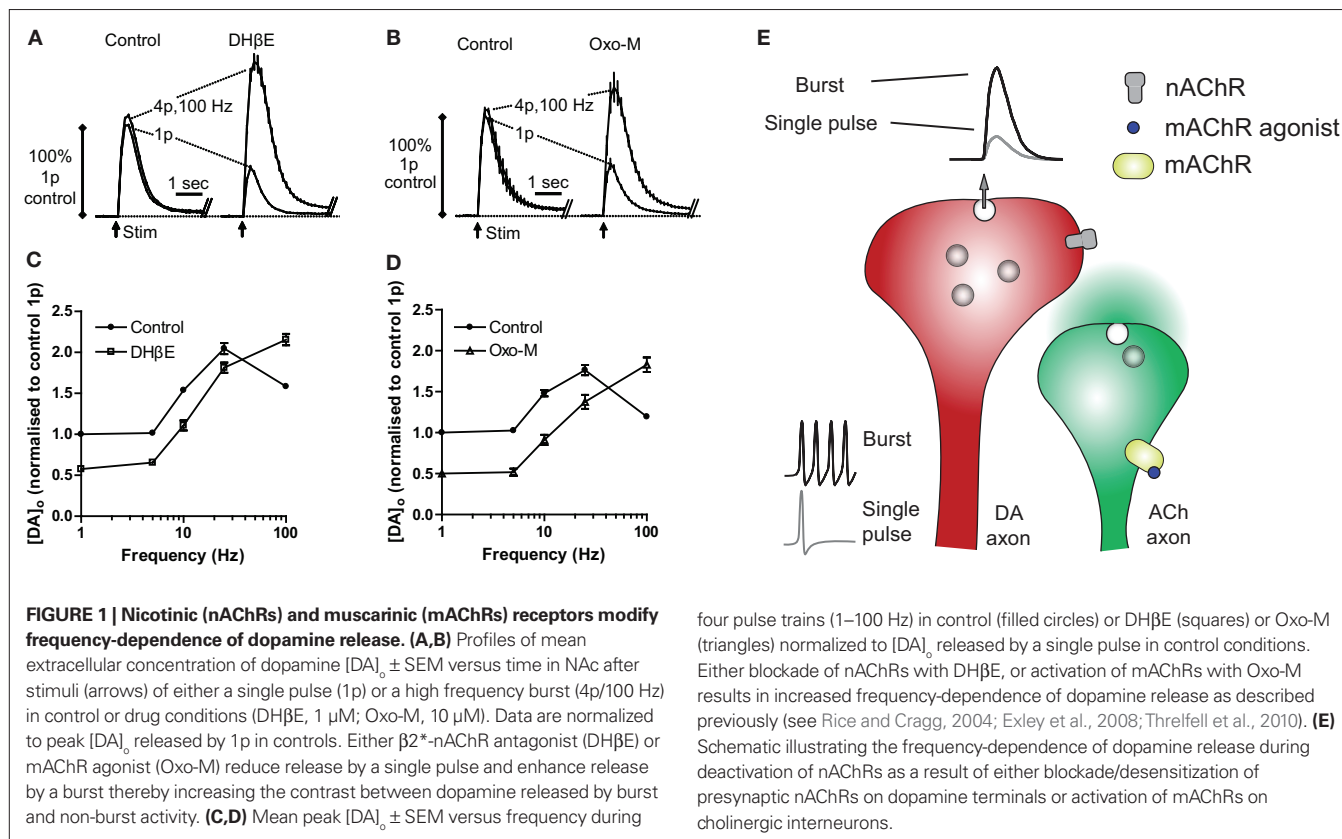


FIGURE 1 | Nicotinic (nAChRs) and muscarinic (mAChRs) receptors modify frequency-dependence of dopamine release. (A,B) Profiles of mean extracellular concentration of dopamine $[DA]_0 \pm SEM$ versus time in NAC after stimuli (arrows) of either a single pulse (1p) or a high frequency burst (4p/100 Hz) in control or drug conditions (DHβE, 1 μM ; Oxo-M, 10 μM). Data are normalized to peak $[DA]_0$ released by 1p in controls. Either $\beta 2^*$ -nAChR antagonist (DHβE) or mAChR agonist (Oxo-M) reduce release by a single pulse and enhance release by a burst thereby increasing the contrast between dopamine released by burst and non-burst activity. **(C,D)** Mean peak $[DA]_0 \pm SEM$ versus frequency during

four pulse trains (1–100 Hz) in control (filled circles) or DHβE (squares) or Oxo-M (triangles) normalized to $[DA]_0$ released by a single pulse in control conditions. Either blockade of nAChRs with DHβE, or activation of mAChRs with Oxo-M results in increased frequency-dependence of dopamine release as described previously (see Rice and Cragg, 2004; Exley et al., 2008; Threlfell et al., 2010). **(E)** Schematic illustrating the frequency-dependence of dopamine release during deactivation of nAChRs as a result of either blockade/desensitization of presynaptic nAChRs on dopamine terminals or activation of mAChRs on cholinergic interneurons.

expense of greater release during high frequency action potentials, e.g., in a burst. Thus, nAChRs *limit* how well striatal DA release correlates with the frequency of activity of DA neurons in midbrain; nAChR activity promotes a “low frequency pass” filter. Conversely, when nAChRs are turned off, and short-term depression of DA release probability is relieved, striatal DA release becomes highly sensitive to the frequency of activity of DA neurons. It can be viewed that nAChR blockade suppresses initial DA release but permits a “high frequency pass” filter as seen at many CNS synapses (Rice and Cragg, 2004; Cragg, 2006). Consequently, reduced nAChR activity can (a) *augment* DA release following *bursts* of DA neuron activity (>20 Hz) such as those that accompany presentation of unexpected reward or conditioned salient stimuli (Mireniewicz and Schultz, 1996; Hyland et al., 2002) and (b) *reduce* DA release during low DA neuron activity such as that seen following omission of an expected reward (Tobler et al., 2003). This enhanced sensitivity of DA release to activity in DA neurons during low nAChR activity may occur during pauses in activity in ACh interneurons.

This ability of ACh via nAChRs to regulate DA availability in a manner that is dependent on frequency of DA neurons suggests that changes in ACh interneuron activity, e.g., pauses, will have key consequences on DA signaling when DA neurons concurrently switch from firing at low frequencies to bursts of high frequency activity, such as during events of high salience. A pause in the nAChR filtering mechanism will increase the contrast in DA signaling during different modes of activity of DA neurons and ultimately enhance DA function at the level of the MSN by modulating DA action at D1 or D2 receptors on discrete MSN populations as well as other DA receptor-expressing interneurons/axons.

nAChR SUBUNITS ON STRIATAL DOPAMINE AXONS

Dopamine neurons express a range of nAChR subunits, and several different stoichiometric configurations are proposed to exist in DA axons and regulate striatal DA transmission. Currently, 14 mammalian nAChR subunits $\alpha 1$ – $\alpha 10$ and $\beta 1$ – $\beta 4$ have been identified. These subunits are organized into subfamilies I–IV, according to gene sequence and structure (Corringer et al., 2000; Le Novere et al., 2002). To date, only nine nAChR subunits from subfamilies II ($\alpha 7$) and III ($\alpha 2$ – $\alpha 6$, $\beta 2$ – $\beta 4$) have been identified in mammalian brain (Corringer et al., 2000; Le Novere et al., 2002). These subunits can form homomeric pentamers (all of one type of subunit, e.g., $\alpha 7$) or heteromeric pentamers, consisting of combinations of various α - and β -type subunits. In rodents, DA neurons in VTA and SNc express mRNAs for the nAChR subunits $\alpha 4$, $\alpha 5$, $\alpha 6$, $\beta 2$, and $\beta 3$, as well as lower levels of $\alpha 3$, $\alpha 7$, and $\beta 4$ (Azam et al., 2002). This diversity of subunit expression has the potential to give rise to multiple types of pentameric receptors in somatodendritic and axon terminal regions of DA neurons with a corresponding multitude of potential functions.

Differences in the nAChR subunits present in axon terminals versus somatodendritic regions of DA neurons exist. Whereas $\alpha 7$ - and $\beta 4$ -subunits are present in VTA and SNc, they are not present in DA axon terminals in striatum (Champtiaux et al., 2003; Quik et al., 2005). Furthermore, despite existing in the primate striatum, there is no $\alpha 3$ -subunit in rodent striatum (Wonnacott et al., 2000; Zoli et al., 2002; Champtiaux et al., 2003; Gotti et al., 2005; Quik et al., 2005). The $\alpha 4$, $\alpha 5$, $\alpha 6$, $\beta 2$, and $\beta 3$ subunits are however found

at high density in DA axon terminals in rodent striatum, where they can assemble as functional heteromeric nicotinic receptors. As heteromeric receptors, nicotinic subunits arrange to form two α/β pairs, and a fifth subunit, α or β . The boundary of each α/β pair is one of two ACh-binding sites at each nAChR (Gotti and Clementi, 2004) which must be occupied for the receptor to function. In striatal DA axons, the two α/β pairs are the $\alpha 4/\beta 2$ and/or $\alpha 6/\beta 2$ and/or $\alpha 4/\beta 4$ (Luetje, 2004; Salminen et al., 2004; Quik et al., 2005). The fifth subunit in the nAChR pentamer may consist of any other subunit, including $\alpha 5$ or $\beta 3$.

All nAChRs on striatal DA axon terminals are thought to contain the $\beta 2$ subunit (Champtiaux et al., 2003; Salminen et al., 2004). Deduction of the other subunits present within these $\beta 2$ -nAChRs has been aided by use of a selective $\alpha 6$ -/ $\alpha 3$ -nAChR antagonist α -conotoxin MII (α -CtxMII; Cartier et al., 1996; Whiteaker et al., 2000; McIntosh et al., 2004). The majority of striatal nAChRs located on DA terminals can therefore be separated into two groups according to their sensitivity to α -CtxMII. Studies using α -CtxMII to determine which nAChR subunits are responsible for nicotine-evoked striatal DA release from synaptosomes have revealed that up to 60% of nicotine-evoked DA is not prevented by α -CtxMII and therefore results from non- $\alpha 6$ -nAChRs (Kulak et al., 1997; Kaiser et al., 1998; Salminen et al., 2007). Therefore both $\alpha 6$ -nAChRs (comprising $\alpha 6\alpha 4\beta 2\beta 3$ and $\alpha 6/\beta 2$) and non- $\alpha 6$ -nAChRs (comprising $\alpha 4\beta 2$ and $\alpha 4\alpha 5\beta 2$) exist on striatal DA axons (Zoli et al., 2002; Champtiaux et al., 2003; Salminen et al., 2004; Quik et al., 2005; Exley and Cragg, 2008; Gotti et al., 2009; Jennings et al., 2009). However as emerging data is beginning to indicate, expression does not necessarily indicate function.

nAChR SUBUNITS RESPONSIBLE FOR REGULATION OF STRIATAL DOPAMINE TRANSMISSION IN DORSAL VERSUS VENTRAL STRIATUM

Previous studies identifying the subunits responsible for nicotinic regulation of striatal DA release from synaptosomes have typically not differentiated between striatal subterritories. It is important to distinguish factors (such as nAChR subunits) regulating DA availability across different striatal subregions due to different the behaviors associated with distinct striatal subterritories. For example, DA neurons innervating more dorsal striatal regions are those most vulnerable in Parkinson's disease, therefore understanding mechanisms regulating availability of DA within such territories will help to unveil future therapeutic targets/neuroprotective strategies in such diseases.

Recent work from our own lab using the $\alpha 6$ -selective nAChR antagonist α -CtxMII has revealed that $\alpha 6$ -nAChRs dominate activity-dependent regulation of DA transmission in ventral striatum, whereas in dorsal striatum $\alpha 6$ -nAChRs play a minor role (Exley and Cragg, 2008; Exley et al., 2008). Due to a lack of other subunit-specific pharmacological nAChR ligands, further delineation of the nAChR subunits necessary for activity-dependent regulation of DA transmission requires the use of subunit-null and transgenic mice expressing mutant nAChR subunits. A recent study using mice expressing a non-native hypersensitive $\alpha 6$ subunit ($\alpha 6'$) revealed activity-dependent DA release in central CPu in the absence of any nAChR ligand. This activity-dependence was absent in $\alpha 6'$ mice lacking $\alpha 4$ subunits ($\alpha 6'\alpha 4$ KO), which the authors

suggested might indicate a role for $\alpha 6 \alpha 4 \beta 2^*$ nAChRs in regulation of DA release in the central CPu region (Drenan et al., 2010). However, this role remains to be established for native $\alpha 6$ subunits in CPu, and moreover, unpublished data from our own lab in knockout mice continues to suggest that $\alpha 6 \beta 2^*$ -nAChRs in dorsal striatum play only a limited role compared to $\alpha 4 \beta 2^*$ -nAChRs, whereas $\alpha 4 \alpha 6 \beta 2^*$ -nAChRs may dominate $\beta 2^*$ -nAChR function in NAc (Exley et al., 2011).

FREQUENCY-DEPENDENT REGULATION OF DOPAMINE RELEASE PROBABILITY BY MUSCARINIC AUTORECEPTORS (mAChRs) ON CHOLINERGIC INTERNEURONS

Like nAChRs, muscarinic receptors (mAChRs) are also able to regulate striatal DA availability. Until recently, data within the literature was conflicting, with some reports suggesting that mAChRs enhance DA release (Lehmann and Langer, 1982; Raiteri et al., 1984; Schoffelemeier et al., 1986; Xu et al., 1989; De Klippel et al., 1993; Zhang et al., 2002b; Grilli et al., 2008), and others reporting the opposite (Schoffelemeier et al., 1986; Kemel et al., 1989; Xu et al., 1989; De Klippel et al., 1993; Kudernatsch and Sutor, 1994; Zhang et al., 2002b; Tzavara et al., 2004). Recent data from our lab has revealed that mAChRs can in fact regulate DA bidirectionally depending on activity of DA neurons (Threlfell et al., 2010). This activity-dependent regulation of DA by mAChRs is reminiscent of that shown by nicotinic receptors (Rice and Cragg, 2004; Zhang and Sulzer, 2004; Exley et al., 2008).

Activation of striatal mAChRs inhibits DA release by single pulses or low frequencies of presynaptic activity, but enhances the sensitivity of DA release to frequency, increasing DA released by higher frequencies (Threlfell et al., 2010). Thus, either activation of mAChRs, or inhibition/desensitization of nAChRs enhances the sensitivity of DA release to frequency, and as such restores release to exhibit classical, dynamic probability of neurotransmitter release as seen at other synapses (Thomson, 2000a,b). However, unlike for striatal nAChRs, there is no anatomical evidence for the presence of striatal mAChRs on dopaminergic axon terminals to influence DA release directly (Jones et al., 2001; Zhang et al., 2002b; Zhou et al., 2003). Many other striatal neurons by contrast, express and are regulated by mAChRs, including striatal cholinergic interneurons (Bernard et al., 1992, 1998; Yan and Surmeier, 1996; Alcantara et al., 2001; Bonsi et al., 2008), GABAergic interneurons (Koos and Tepper, 2002), MSNs (Weiner et al., 1990; Levey et al., 1991; Calabresi et al., 2000; Yan et al., 2001), and glutamatergic afferents (Sugita et al., 1991; Calabresi et al., 2000; Pakhotin and Bracci, 2007). Previous studies have identified regulation of DA release by mAChRs on a variety of striatal neurons/inputs. For example, mAChR regulation of GABA acting at GABA_A receptors has been implicated in the control of DA in protocols using high [K⁺] to evoke [³H] DA release (Zhang et al., 2002b), but the mAChR modulation of dynamic DA release probability that we have described during discrete electrical stimuli persists in the presence of synaptic blockers for GABA/glutamate (Threlfell et al., 2010). Rather, this dynamic regulation of striatal DA by mAChRs requires cholinergic tone at nAChRs on DA axons, since blockade of ACh input from cholinergic interneurons to nAChRs precludes effects of mAChR activation and vice versa. Striatal cholinergic interneurons express somatodendritic and axonal mAChRs (Bernard et al., 1992, 1998;

Alcantara et al., 2001; Zhang et al., 2002a), which are autoreceptors. When these autoreceptors are activated cholinergic interneurons become silenced and ACh release is inhibited (via inhibition of Ca_v2-type Ca²⁺ conductances and/or K_v⁺ channel opening; Raiteri et al., 1984; Schoffelemeier et al., 1986; Yan and Surmeier, 1996; Calabresi et al., 1998, 2000; Zhang et al., 2002a; Zhou et al., 2003; Ding et al., 2006; Bonsi et al., 2008). The reduction in ACh release following mAChR autoreceptor activation consequently deactivates nAChRs on dopaminergic axons, and in turn, increases the sensitivity of DA release to presynaptic depolarization frequency as seen following inhibition/desensitization of nicotinic receptors (see Figure 1).

These data revise our understanding of striatal mAChR–DA interactions in several ways. Firstly, striatal mAChRs offer variable, bidirectional control of DA release probability depending on presynaptic activity. This reconciles previous contradictory findings since striatal mAChRs do not simply suppress or enhance DA release but can do both depending on the frequency of depolarization. Secondly, this variable mAChR control of DA release is not via multiple striatal neuron types but via the control of ACh release from striatal cholinergic interneurons. These mAChRs, by modifying ACh release, powerfully gate the nAChR regulation of DA release. Finally, we also show important differences in the mAChR subtypes regulating DA (and cholinergic interneurons) in sensorimotor- versus limbic-associated striatum.

mAChR SUBTYPES AND LOCATIONS WITHIN STRIATUM

Five different types of mAChRs exist in the striatum, M₁–M₅, these G-protein-coupled mAChRs are present throughout the striatum on a variety of neurons and axon terminals. Like DA receptors, these mAChRs are commonly divided into two families, M₁-like (M₁, M₃, and M₅) and M₂-like (M₂ and M₄) according to the G-protein the receptor is coupled to. M₁-like receptors are coupled to the G_s class of G_o proteins, whereas M₂-like receptors are coupled to G_i proteins, thereby modulating different intracellular signaling pathways. The muscarinic receptor subtypes M₁, M₂, and M₄ are the dominant striatal subtypes (Zhang et al., 2002b; Zhou et al., 2003). There is now considerable evidence that discrete expression and function of M₁, M₂, and M₄ receptors can be partitioned to different striatal neurons and neurotransmitter interactions. For example, MSNs express primarily M₁ and M₄, with M₄ receptors dominant on striatonigral MSNs with very low or undetectable levels of M₂, M₃, and M₅ (Weiner et al., 1990; Levey et al., 1991; Santiago and Potter, 2001; Yan et al., 2001; Shen et al., 2005; Wang et al., 2006). Striatal cholinergic interneurons by contrast have dominant expression and function of M₂ and M₄ mAChRs (Yan and Surmeier, 1996; Bernard et al., 1998; Alcantara et al., 2001; Ding et al., 2006). M₃ receptors are expressed by midbrain DA neurons where they mediate midbrain actions of ACh inputs (Forster et al., 2002; Lester et al., 2010), but current anatomical evidence does not suggest that they are transported to DA axon terminals in the striatum (Weiner et al., 1990).

DIFFERENT mAChR SUBTYPES ARE RESPONSIBLE FOR REGULATION OF STRIATAL DOPAMINE IN DORSAL VERSUS VENTRAL STRIATUM

The mAChRs regulating striatal DA release differ between dorsal and ventral striatal subterritories. Due to the poor pharmacological selectivity of drug ligands for specific distinct muscarinic receptor

subtypes (ligands are subtype-preferring but not selective), we have made use of transgenic mice lacking individual mAChR subtypes (Wess et al., 2003) to study the receptor subtypes that are responsible for regulation of DA in specific striatal subregions. The use of knockout mice as tools to study normal receptor function is not always free from caveats as such mice can often display significant compensation for gene deletions. However, there appears to be little or no compensation in remaining mAChRs for the subtype-specific null mice used here (Gomez et al., 1999a,b). Given that cholinergic interneurons are responsible for a powerful modulation of striatal DA, we studied mice lacking the receptors those interneurons usually express as autoreceptors: M_2 - and M_4 -mAChRs. We also explored mAChR control of DA release in M_5 -mAChR null mice. Although there is a lack of anatomical evidence that these receptors can be found on striatal DA axons, midbrain DA neurons express M_5 receptors for midbrain ACh function (Forster et al., 2002; Lester et al., 2010) and there is some limited evidence that striatal M_5 Rs might regulate DA transmission (Zhang et al., 2002b; Bendor et al., 2010).

In dorsal striatum, a region classically associated with motor function, both M_2 - and M_4 -mAChRs are necessary for muscarinic regulation of DA release. Deletion of either M_2 - or M_4 -mAChRs prevents muscarinic receptor modulation of DA (Threlfell et al., 2010). By contrast in more limbic striatal regions, in the NAc core or shell, only the M_4 -mAChR is necessary for muscarinic receptor control (Threlfell et al., 2010). Deletion of M_2 -mAChRs in the NAc core or shell does not prevent muscarinic control of DA; only deletion of the M_4 -mAChR eliminates muscarinic control. In both dorsal striatum and NAc, elimination of the M_5 -mAChR has no effect on the activity-dependent regulation of DA by muscarinic receptors therefore they do not participate in activity-dependent regulation of DA by mAChR agonists. However, muscarinic-mediated suppression of DA release following single pulse stimulation in mice lacking the M_5 R does appear to be more pronounced in both dorsal and ventral striatum suggesting that if presynaptic M_5 Rs do exist on a subset of DA terminals, they function to enhance DA release, as suggested by others (Zhang et al., 2002b; Bendor et al., 2010).

At present, it is unclear why such differences in mAChR control of DA release by M_2/M_4 mAChRs would exist between dorsal and ventral striatum. It is currently unknown whether these differences are attributable to different expression/role of M_4 Rs versus M_2 Rs in cholinergic interneurons that innervate each territory, or a different basal ACh tone at nAChRs, or whether there are other intrinsic regional differences in cholinergic interneurons including compensatory adaptations that can accommodate loss of M_2 Rs in NAc but not in dorsal striatum. There is no comparative study of expression/function of mAChRs in regulation of cholinergic activity in dorsal versus ventral striatum and no evidence for a difference in the levels of ACh reaching nAChRs (Exley et al., 2008). There are however, reports that mAChRs are found at higher levels in ventral than dorsal striatum in rats (Tayebati et al., 2004) and that cholinergic interneurons in limbic/prefrontal versus sensorimotor territories can be differentiated by different expression levels of other types of receptors (μ -opioid; Jabourian et al., 2005). Thus, distinct muscarinic mechanisms/receptors in subpopulations of cholinergic interneurons may explain the

differing mAChR control of DA release in dorsal striatum and NAc. These regional differences in M_2/M_4 function could ultimately be exploited for discrete modulation of DA/ACh. For example, ACh/DA function might be modified selectively in NAc by activation of M_4 Rs, and in dorsal striatum by M_2 R inhibition. It is possible that regional differences may exist due to differential intracellular coupling of M_2 - and M_4 -mAChRs on cholinergic interneurons in different striatal regions, or perhaps differential expression of M_2 - and M_4 -mAChRs on cholinergic interneurons in these two regions. Further electrophysiological characterization of cholinergic interneurons in mice lacking M_2 - or M_4 -mAChRs may shed light on potential differences between dorsal and ventral striatum, and is currently underway.

SUMMARY AND PERSPECTIVE

Striatal nAChRs and mAChRs powerfully modulate DA transmission in a manner that varies with presynaptic activity in DA neurons. This regulation can strongly influence how DA synapses transmit discrete bursts in neuronal activity that signal events of motivational salience, and in turn will influence all DA-dependent functions of the striatum. Intriguingly, cholinergic modulation of DA transmission within striatum is via regionally specific portfolios of nicotinic (Exley et al., 2008, 2011) and muscarinic (Threlfell et al., 2010) receptors (**Figure 2**), which may ultimately enable region-specific targeting of striatal function. For example, ACh/DA function within striatum could be modified selectively in NAc by activation of M_4 Rs, and in dorsal striatum by M_2 R inhibition. A specific nAChR such as the $\alpha 4\alpha 6\beta 2^*$ -nAChR in NAc might be a target to exploit in the treatment of nicotine addiction. There are longstanding notions that there is a postsynaptic antagonistic balance between striatal ACh and DA and that antimuscarinic therapies are useful in diseases like Parkinson's and dystonia (e.g., see Pisani et al., 2007). The suppression of striatal ACh release by M_2/M_4 autoreceptors together with the effects of M_2/M_4 receptor activation on DA transmission reviewed here give support to the notion that enhancers of muscarinic M_2/M_4 receptor function might be a useful therapy in such disorders (Pisani et al., 2007). More generally, these data also highlight that regulation of DA neurotransmission by a given neuromodulator is not fixed, or unidirectional; it can be variable and bidirectional in an activity-dependent manner, a principle which may apply equally to other neuromodulators and neurotransmitters.

With increasing availability of new molecular biological tools facilitating neuron-specific elimination/expression of proteins, we are in a better position than ever to advance our appreciation of how receptors in the basal ganglia are able to regulate striatal function. The advancing field of optogenetics which exploits genetics to incorporate light activated ion channels (rhodopsins) into genetically defined populations of neurons to allow activation or inhibition of these neurons with high temporal precision, will undoubtedly facilitate future studies of the complex interplay of a multitude of neurotransmitters and neuromodulators within the highly heterogeneous striatum. When considering how striatal output governs different behaviors, it is imperative to assess the role played by interactions between many striatal neurotransmitters and neuromodulators and the ACh–DA interaction is one powerful interaction that should be given appropriate consideration.

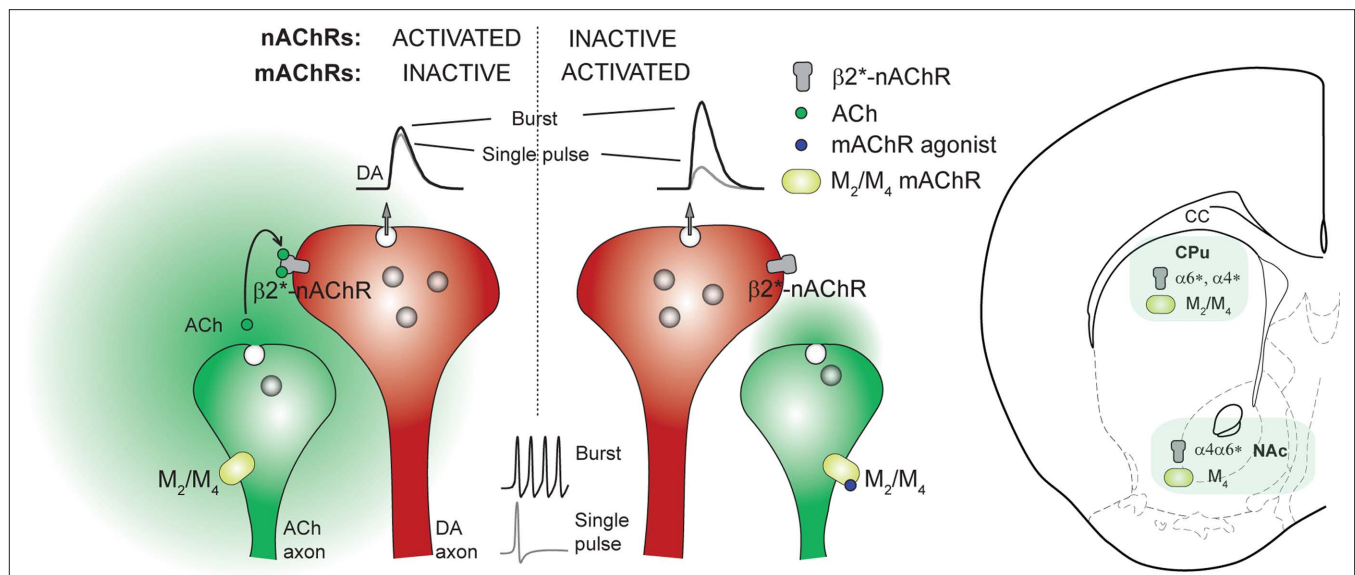


FIGURE 2 | Scheme illustrating cholinergic regulation of dopamine (DA) release during burst and non-burst activity in DA axons and nAChR/mAChR subtypes responsible in CPu and NAc. *Left*, When mAChRs are inactive under control conditions, endogenous acetylcholine (ACh) released from tonically active striatal cholinergic interneurons (ChIs) maintains ACh tone at $\beta 2^*$ -nAChRs on dopaminergic axons. This tonic $\beta 2^*$ -nAChR activity ensures that DA release has a high probability of occurring in response to a single stimulus pulse. Short-term synaptic depression follows such DA release and limits re-release by successive pulses within bursts, i.e., DA release is insensitive to frequency. *Center*, Activation of mAChR autoreceptors on ChIs (e.g., with mAChR agonist Oxo-M) reduces ACh tone at $\beta 2^*$ -nAChRs on DA

axon terminals, thereby reducing DA release probability by a single stimulus, relieving short-term depression and increasing the relative probability of release at subsequent action potentials. After reduction of ACh tone at $\beta 2^*$ -nAChRs by activation of mAChR autoreceptors on ChIs, or blockade/desensitization of nAChRs, DA release becomes more sensitive to frequency of presynaptic activity (see Rice and Cragg, 2004; Exley and Cragg, 2008). *Right*, mAChR subtypes and nAChR subunits that regulate DA availability differ between dorsal and ventral striatal subterritories. In dorsal striatum (CPu), M_2 and M_4 populations of mAChRs, and $\alpha 6^*$ - and $\alpha 4^*$ -nAChRs appear to modulate DA release. In ventral striatum (NAc), only M_4 mAChRs and $\alpha 4\alpha 6^*$ -nAChRs appear to modulate DA release.

REFERENCES

- Abeliovich, A., Schmitz, Y., Farinas, I., Choi-Lundberg, D., Ho, W. H., Castillo, P. E., Shinsky, N., Verdugo, J. M., Armanini, M., Ryan, A., Hynes, M., Phillips, H., Sulzer, D., and Rosenthal, A. (2000). Mice lacking alpha-synuclein display functional deficits in the nigrostriatal dopamine system. *Neuron* 25, 239–252.
- Albin, R. L., Young, A. B., and Penney, J. B. (1995). The functional anatomy of disorders of the basal ganglia. *Trends Neurosci.* 18, 63–64.
- Alcantara, A. A., Chen, V., Herring, B. E., Mendenhall, J. M., and Berlanga, M. L. (2003). Localization of dopamine D2 receptors on cholinergic interneurons of the dorsal striatum and nucleus accumbens of the rat. *Brain Res.* 986, 22–29.
- Alcantara, A. A., Mrzljak, L., Jakab, R. L., Levey, A. I., Hersch, S. M., and Goldman-Rakic, P. S. (2001). Muscarinic m1 and m2 receptor proteins in local circuit and projection neurons of the primate striatum: anatomical evidence for cholinergic modulation of glutamatergic prefronto-striatal pathways. *J. Comp. Neurol.* 434, 445–460.
- Arbuthnott, G. W., and Wickers, J. (2007). Space, time and dopamine. *Trends Neurosci.* 30, 62–69.
- Azam, L., Winzer-Serhan, U. H., Chen, Y., and Leslie, F. M. (2002). Expression of neuronal nicotinic acetylcholine receptor subunit mRNAs within midbrain dopamine neurons. *J. Comp. Neurol.* 444, 260–274.
- Barbeau, A. (1962). The pathogenesis of Parkinson's disease: a new hypothesis. *Can. Med. Assoc. J.* 87, 802–807.
- Belin, D., and Everitt, B. J. (2008). Cocaine seeking habits depend upon dopamine-dependent serial connectivity linking the ventral with the dorsal striatum. *Neuron* 57, 432–441.
- Belin, D., Jonkman, S., Dickinson, A., Robbins, T. W., and Everitt, B. J. (2009). Parallel and interactive learning processes within the basal ganglia: relevance for the understanding of addiction. *Behav. Brain Res.* 199, 89–102.
- Bendor, J., Lizardi-Ortiz, J. E., Westphalen, R. I., Brandstetter, M., Hemmings, H. C. Jr., Sulzer, D., Flajolet, M., and Greengard, P. (2010). AGAP1/AP-3-dependent endocytic recycling of M(5) muscarinic receptors promotes dopamine release. *EMBO J.* 29, 2813–2826.
- Bennett, B. D., and Wilson, C. J. (1999). Spontaneous activity of neostriatal cholinergic interneurons in vitro. *J. Neurosci.* 19, 5586–5596.
- Bernard, V., Laribi, O., Levey, A. I., and Bloch, B. (1998). Subcellular redistribution of m2 muscarinic acetylcholine receptors in striatal interneurons in vivo after acute cholinergic stimulation. *J. Neurosci.* 18, 10207–10218.
- Bernard, V., Normand, E., and Bloch, B. (1992). Phenotypical characterization of the rat striatal neurons expressing muscarinic receptor genes. *J. Neurosci.* 12, 3591–3600.
- Berridge, K. C., and Robinson, T. E. (2003). Parsing reward. *Trends Neurosci.* 26, 507–513.
- Bjorklund, A., and Lindvall, O. (1984). "Dopamine-containing systems in the CNS," in *Handbook of Chemical Neuroanatomy*, eds T. Hokfelt and A. Bjorklund (New York: Elsevier), 55–122.
- Bolam, J. P., Hanley, J. J., Booth, P. A., and Bevan, M. D. (2000). Synaptic organisation of the basal ganglia. *J. Anat.* 196(Pt 4), 527–542.
- Bonsi, P., Martella, G., Cuomo, D., Platania, P., Sciamanna, G., Bernardi, G., Wess, J., and Pisani, A. (2008). Loss of muscarinic autoreceptor function impairs long-term depression but not long-term potentiation in the striatum. *J. Neurosci.* 28, 6258–6263.
- Brog, J. S., Salyapongse, A., Deutch, A. Y., and Zahm, D. S. (1993). The patterns of afferent innervation of the core and shell in the "accumbens" part of the rat ventral striatum: immunohistochemical detection of retrogradely transported fluoro-gold. *J. Comp. Neurol.* 338, 255–278.
- Calabresi, P., Centonze, D., Gubellini, P., Pisani, A., and Bernardi, G. (2000). Acetylcholine-mediated modulation of striatal function. *Trends Neurosci.* 23, 120–126.
- Calabresi, P., Centonze, D., Pisani, A., Sancesario, G., North, R. A., and Bernardi, G. (1998). Muscarinic IPSPs in rat striatal cholinergic interneurons. *J. Physiol.* 510(Pt 2), 421–427.
- Calabresi, P., Picconi, B., Tozzi, A., and Di Filippo, M. (2007). Dopamine-mediated regulation of corticostriatal synaptic plasticity. *Trends Neurosci.* 30, 211–219.
- Cartier, G. E., Yoshikami, D., Gray, W. R., Luo, S., Olivera, B. M., and McIntosh, J. M. (1996). A new alpha-conotoxin which targets alpha3beta2 nicotinic

- acetylcholine receptors. *J. Biol. Chem.* 271, 7522–7528.
- Centonze, D., Gubellini, P., Pisani, A., Bernardi, G., and Calabresi, P. (2003). Dopamine, acetylcholine and nitric oxide systems interact to induce corticostriatal synaptic plasticity. *Rev. Neurosci.* 14, 207–216.
- Champitoux, N., Gotti, C., Cordero-Erasquin, M., David, D. J., Przybylski, C., Lena, C., Clementi, F., Moretti, M., Rossi, F. M., Le Novère, N., McIntosh, J. M., Gardier, A. M., and Changeux, J. P. (2003). Subunit composition of functional nicotinic receptors in dopaminergic neurons investigated with knock-out mice. *J. Neurosci.* 23, 7820–7829.
- Chergui, K., Saud-Chagny, M. F., and Gonon, F. (1994). Nonlinear relationship between impulse flow, dopamine release and dopamine elimination in the rat brain in vivo. *Neuroscience* 62, 641–645.
- Contant, C., Umbriaco, D., Garcia, S., Watkins, K. C., and Descarries, L. (1996). Ultrastructural characterization of the acetylcholine innervation in adult rat neostriatum. *Neuroscience* 71, 937–947.
- Corringer, P. J., Le Novère, N., and Changeux, J. P. (2000). Nicotinic receptors at the amino acid level. *Annu. Rev. Pharmacol. Toxicol.* 40, 431–458.
- Cragg, S. J. (2003). Variable dopamine release probability and short-term plasticity between functional domains of the primate striatum. *J. Neurosci.* 23, 4378–4385.
- Cragg, S. J. (2006). Meaningful silences: how dopamine listens to the ACh pause. *Trends Neurosci.* 29, 125–131.
- Cragg, S. J., Exley, R., and Clements, M. A. (2005). "Striatal acetylcholine control of reward-related dopamine signaling," in *The Basal Ganglia VIII*, eds J. P. Bolam, C. A. Ingham, and P. J. Magill (New York: Springer), 99–108.
- Cragg, S. J., and Rice, M. E. (2004). DANCING past the DAT at a DA synapse. *Trends Neurosci.* 27, 270–277.
- Dajas-Bailador, F., and Wonnacott, S. (2004). Nicotinic acetylcholine receptors and the regulation of neuronal signalling. *Trends Pharmacol. Sci.* 25, 317–324.
- De Klippel, N., Sarre, S., Ebinger, G., and Michotte, Y. (1993). Effect of M1- and M2-muscarinic drugs on striatal dopamine release and metabolism: an in vivo microdialysis study comparing normal and 6-hydroxydopamine-lesioned rats. *Brain Res.* 630, 57–64.
- Descarries, L., Gisiger, V., and Steriade, M. (1997). Diffuse transmission by acetylcholine in the CNS. *Prog. Neurobiol.* 53, 603–625.
- Descarries, L., and Mechawar, N. (2000). Ultrastructural evidence for diffuse transmission by monoamine and acetylcholine neurons of the central nervous system. *Prog. Brain Res.* 125, 27–47.
- Descarries, L., Watkins, K. C., Garcia, S., Bosler, O., and Doucet, G. (1996). Dual character, asynaptic and synaptic, of the dopamine innervation in adult rat neostriatum: a quantitative autoradiographic and immunocytochemical analysis. *J. Comp. Neurol.* 375, 167–186.
- Di Chiara, G., and Imperato, A. (1988). Drugs abused by humans preferentially increase synaptic dopamine concentrations in the mesolimbic system of freely moving rats. *Proc. Natl. Acad. Sci. U.S.A.* 85, 5274–5278.
- Ding, J., Guzman, J. N., Tkatch, T., Chen, S., Goldberg, J. A., Ebert, P. J., Levitt, P., Wilson, C. J., Hamm, H. E., and Surmeier, D. J. (2006). RGS4-dependent attenuation of M4 autoreceptor function in striatal cholinergic interneurons following dopamine depletion. *Nat. Neurosci.* 9, 832–842.
- Drenan, R. M., Grady, S. R., Steele, A. D., McKinney, S., Patzlaff, N. E., McIntosh, J. M., Marks, M. J., Miwa, J. M., and Lester, H. A. (2010). Cholinergic modulation of locomotion and striatal dopamine release is mediated by $\alpha 6 \alpha 4$ nicotinic acetylcholine receptors. *J. Neurosci.* 30, 9877–9889.
- Everitt, B. J., and Robbins, T. W. (2005). Neural systems of reinforcement for drug addiction: from actions to habits to compulsion. *Nat. Neurosci.* 8, 1481–1489.
- Exley, R., Clements, M. A., Hartung, H., McIntosh, J. M., and Cragg, S. J. (2008). $\alpha 6$ -containing nicotinic acetylcholine receptors dominate the nicotine control of dopamine neurotransmission in nucleus accumbens. *Neuropsychopharmacology* 33, 2158–2166.
- Exley, R., and Cragg, S. J. (2008). Presynaptic nicotinic receptors: a dynamic and diverse cholinergic filter of striatal dopamine neurotransmission. *Br. J. Pharmacol.* 153(Suppl. 1), S283–S297.
- Exley, R., Maubourguet, N., David, V., Eddine, R., Evrard, A., Pons, S., Marti, F., Threlfell, S., Cazala, P., McIntosh, J. M., Changeux, J. P., Maskos, U., Cragg, S. J., and Faure, P. (2011). Distinct contributions of $\alpha 4$ and $\alpha 6$ nAChR subunits in the reinforcing effects of nicotine. *Proc. Natl. Acad. Sci. U.S.A.* (in press).
- Forster, G. L., Yeomans, J. S., Takeuchi, J., and Blaha, C. D. (2002). M5 muscarinic receptors are required for prolonged accumbal dopamine release after electrical stimulation of the pons in mice. *J. Neurosci.* 22, RC190.
- Freund, T. F., Powell, J. E., and Smith, A. D. (1984). Tyrosine hydroxylase-immunoreactive boutons in synaptic contact with identified striatonigral neurons, with particular reference to dendritic spines. *Neuroscience* 13, 1189–1215.
- Fuxe, K., and Agnati, L. F. (1991). *Volume Transmission in the Brain*. New York: Raven Press.
- Garris, P. A., Ciolkowski, E. L., Pastore, P., and Wightman, R. M. (1994). Efflux of dopamine from the synaptic cleft in the nucleus accumbens of the rat brain. *J. Neurosci.* 14, 6084–6093.
- Gerdeman, G. L., Partridge, J. G., Lupica, C. R., and Lovinger, D. M. (2003). It could be habit forming: drugs of abuse and striatal synaptic plasticity. *Trends Neurosci.* 26, 184–192.
- Gerfen, C. R., Herkenham, M., and Thibault, J. (1987). The neostriatal mosaic: II. Patch- and matrix-directed mesostriatal dopaminergic and non-dopaminergic systems. *J. Neurosci.* 7, 3915–3934.
- Gomeza, J., Shannon, H., Kostenis, E., Felder, C., Zhang, L., Brodtkin, J., Grinberg, A., Sheng, H., and Wess, J. (1999a). Pronounced pharmacologic deficits in M2 muscarinic acetylcholine receptor knockout mice. *Proc. Natl. Acad. Sci. U.S.A.* 96, 1692–1697.
- Gomeza, J., Zhang, L., Kostenis, E., Felder, C., Byrmaster, F., Brodtkin, J., Shannon, H., Xia, B., Deng, C., and Wess, J. (1999b). Enhancement of D1 dopamine receptor-mediated locomotor stimulation in M(4) muscarinic acetylcholine receptor knockout mice. *Proc. Natl. Acad. Sci. U.S.A.* 96, 10483–10488.
- Gonon, F. (1997). Prolonged and extrasynaptic excitatory action of dopamine mediated by D1 receptors in the rat striatum in vivo. *J. Neurosci.* 17, 5972–5978.
- Gotti, C., and Clementi, F. (2004). Neuronal nicotinic receptors: from structure to pathology. *Prog. Neurobiol.* 74, 363–396.
- Gotti, C., Clementi, F., Fornari, A., Gaimarri, A., Guiducci, S., Manfredi, I., Moretti, M., Pedrazzi, P., Pucci, L., and Zoli, M. (2009). Structural and functional diversity of native brain neuronal nicotinic receptors. *Biochem. Pharmacol.* 78, 703–711.
- Gotti, C., Moretti, M., Clementi, F., Riganti, L., McIntosh, J. M., Collins, A. C., Marks, M. J., and Whiteaker, P. (2005). Expression of nigrostriatal $\alpha 6$ -containing nicotinic acetylcholine receptors is selectively reduced, but not eliminated, by beta 3 subunit gene deletion. *Mol. Pharmacol.* 67, 2007–2015.
- Grace, A. A., and Bunney, B. S. (1984a). The control of firing pattern in nigral dopamine neurons: burst firing. *J. Neurosci.* 4, 2877–2890.
- Grace, A. A., and Bunney, B. S. (1984b). The control of firing pattern in nigral dopamine neurons: single spike firing. *J. Neurosci.* 4, 2866–2876.
- Grilli, M., Patti, L., Robino, E., Zappettini, S., Raiteri, M., and Marchi, M. (2008). Release-enhancing pre-synaptic muscarinic and nicotinic receptors co-exist and interact on dopaminergic nerve endings of rat nucleus accumbens. *J. Neurochem.* 105, 2205–2213.
- Groves, P. M., Linder, J. C., and Young, S. J. (1994). 5-Hydroxydopamine-labeled dopaminergic axons: three-dimensional reconstructions of axons, synapses and postsynaptic targets in rat neostriatum. *Neuroscience* 58, 593–604.
- Haber, S. N., Fudge, J. L., and McFarland, N. R. (2000). Striatonigrostriatal pathways in primates form an ascending spiral from the shell to the dorsolateral striatum. *J. Neurosci.* 20, 2369–2382.
- Hersch, S. M., Ciliax, B. J., Gutekunst, C. A., Rees, H. D., Heilman, C. J., Yung, K. K., Bolam, J. P., Ince, E., Yi, H., and Levey, A. I. (1995). Electron microscopic analysis of D1 and D2 dopamine receptor proteins in the dorsal striatum and their synaptic relationships with motor corticostriatal afferents. *J. Neurosci.* 15(Pt 2), 5222–5237.
- Hyland, B. I., Reynolds, J. N., Hay, J., Perk, C. G., and Miller, R. (2002). Firing modes of midbrain dopamine cells in the freely moving rat. *Neuroscience* 114, 475–492.
- Jabourian, M., Venance, L., Bourgoin, S., Ozon, S., Perez, S., Godeheu, G., Glowinski, J., and Kemel, M. L. (2005). Functional mu opioid receptors are expressed in cholinergic interneurons of the rat dorsal striatum: territorial specificity and diurnal variation. *Eur. J. Neurosci.* 21, 3301–3309.
- Jennings, K. A., Threlfell, S., Exley, R., and Cragg, S. J. (2009). Unmasking the role of nicotine receptors in nicotine addiction: recent advances in understanding nicotine action on dopamine systems. *Cell Sci. Rev.* 5, 82–112.
- Jones, I. W., Bolam, J. P., and Wonnacott, S. (2001). Presynaptic localisation of the nicotinic acetylcholine receptor beta2 subunit immunoreactivity in rat nigrostriatal dopaminergic neurones. *J. Comp. Neurol.* 439, 235–247.
- Joshua, M., Adler, A., Mitelman, R., Vaadia, E., and Bergman, H. (2008). Midbrain dopaminergic neurons and striatal cholinergic interneurons encode the difference between reward and aversive events at different epochs

- of probabilistic classical conditioning trials. *J. Neurosci.* 28, 11673–11684.
- Kaiser, S. A., Soliakov, L., Harvey, S. C., Luetje, C. W., and Wonnacott, S. (1998). Differential inhibition by alpha-conotoxin-MII of the nicotinic stimulation of [3H]dopamine release from rat striatal synaptosomes and slices. *J. Neurochem.* 70, 1069–1076.
- Kawaguchi, Y. (1993). Physiological, morphological, and histochemical characterization of three classes of interneurons in rat neostriatum. *J. Neurosci.* 13, 4908–4923.
- Kelley, A. E., and Domesick, V. B. (1982). The distribution of the projection from the hippocampal formation to the nucleus accumbens in the rat: an anterograde- and retrograde-horseradish peroxidase study. *Neuroscience* 7, 2321–2335.
- Kemel, M. L., Desban, M., Glowinski, J., and Gauchy, C. (1989). Distinct presynaptic control of dopamine release in striosomal and matrix areas of the cat caudate nucleus. *Proc. Natl. Acad. Sci. U.S.A.* 86, 9006–9010.
- Koos, T., and Tepper, J. M. (2002). Dual cholinergic control of fast-spiking interneurons in the neostriatum. *J. Neurosci.* 22, 529–535.
- Kudernatsch, M., and Sutor, B. (1994). Cholinergic modulation of dopamine overflow in the rat neostriatum: a fast cyclic voltammetric study in vitro. *Neurosci. Lett.* 181, 107–112.
- Kulak, J. M., Nguyen, T. A., Olivera, B. M., and McIntosh, J. M. (1997). Alpha-conotoxin MII blocks nicotine-stimulated dopamine release in rat striatal synaptosomes. *J. Neurosci.* 17, 5263–5270.
- Le Novere, N., Corringier, P. J., and Changeux, J. P. (2002). The diversity of subunit composition in nAChRs: evolutionary origins, physiologic and pharmacologic consequences. *J. Neurobiol.* 53, 447–456.
- Lehmann, J., and Langer, S. Z. (1982). Muscarinic receptors on dopamine terminals in the cat caudate nucleus: neuromodulation of [3H]dopamine release in vitro by endogenous acetylcholine. *Brain Res.* 248, 61–69.
- Lester, D. B., Miller, A. D., and Blaha, C. D. (2010). Muscarinic receptor blockade in the ventral tegmental area attenuates cocaine enhancement of laterodorsal tegmentum stimulation-evoked accumbens dopamine efflux in the mouse. *Synapse* 64, 216–223.
- Levey, A. I., Kitt, C. A., Simonds, W. F., Price, D. L., and Brann, M. R. (1991). Identification and localization of muscarinic acetylcholine receptor proteins in brain with subtype-specific antibodies. *J. Neurosci.* 11, 3218–3226.
- Luetje, C. W. (2004). Getting past the asterisk: the subunit composition of presynaptic nicotinic receptors that modulate striatal dopamine release. *Mol. Pharmacol.* 65, 1333–1335.
- Matamalas, M., Bertran-Gonzalez, J., Salomon, L., Degos, B., Deniau, J. M., Valjent, E., Herve, D., and Girault, J. A. (2009). Striatal medium-sized spiny neurons: identification by nuclear staining and study of neuronal subpopulations in BAC transgenic mice. *PLoS ONE* 4, e4770. doi: 10.1371/journal.pone.0004770
- Matsuda, W., Furuta, T., Nakamura, K. C., Hioki, H., Fujiyama, F., Arai, R., and Kaneko, T. (2009). Single nigrostriatal dopaminergic neurons form widely spread and highly dense axonal arborizations in the neostriatum. *J. Neurosci.* 29, 444–453.
- Matsumoto, M., and Hikosaka, O. (2009). Two types of dopamine neuron distinctly convey positive and negative motivational signals. *Nature* 459, 837–841.
- McFarland, N. R., and Haber, S. N. (2000). Convergent inputs from thalamic motor nuclei and frontal cortical areas to the dorsal striatum in the primate. *J. Neurosci.* 20, 3798–3813.
- McGeorge, A. J., and Faull, R. L. (1989). The organization of the projection from the cerebral cortex to the striatum in the rat. *Neuroscience* 29, 503–537.
- McIntosh, J. M., Azam, L., Staheli, S., Dowell, C., Lindstrom, J. M., Kuryatov, A., Garrett, J. E., Marks, M. J., and Whiteaker, P. (2004). Analogs of alpha-conotoxin MII are selective for alpha6-containing nicotinic acetylcholine receptors. *Mol. Pharmacol.* 65, 944–952.
- Mirenowicz, J., and Schultz, W. (1996). Preferential activation of midbrain dopamine neurons by appetitive rather than aversive stimuli. *Nature* 379, 449–451.
- Montague, P. R., McClure, S. M., Baldwin, P. R., Phillips, P. E., Budygin, E. A., Stuber, G. D., Kilpatrick, M. R., and Wightman, R. M. (2004). Dynamic gain control of dopamine delivery in freely moving animals. *J. Neurosci.* 24, 1754–1759.
- Morris, G., Arkadir, D., Nevet, A., Vaadia, E., and Bergman, H. (2004). Coincident but distinct messages of midbrain dopamine and striatal tonically active neurons. *Neuron* 43, 133–143.
- Moss, J., and Bolam, J. P. (2008). A dopaminergic axon lattice in the striatum and its relationship with cortical and thalamic terminals. *J. Neurosci.* 28, 11221–11230.
- Moss, J., and Bolam, J. P. (2010). “The relationship between dopaminergic axons and glutamatergic synapses in the striatum: structural considerations,” in *Dopamine Handbook*, eds L. L. Iversen, S. D. Iversen, S. B. Dunnett, and A. Bjorklund (Oxford: Oxford University Press), 49–59.
- Nakano, K., Kayahara, T., Tsutsumi, T., and Ushiro, H. (2000). Neural circuits and functional organization of the striatum. *J. Neurol.* 247(Suppl. 5), V1–V15.
- Nirenberg, M. J., Chan, J., Vaughan, R. A., Uhl, G. R., Kuhar, M. J., and Pickel, V. M. (1997). Immunogold localization of the dopamine transporter: an ultrastructural study of the rat ventral tegmental area. *J. Neurosci.* 17, 4037–4044.
- Nirenberg, M. J., Vaughan, R. A., Uhl, G. R., Kuhar, M. J., and Pickel, V. M. (1996). The dopamine transporter is localized to dendritic and axonal plasma membranes of nigrostriatal dopaminergic neurons. *J. Neurosci.* 16, 436–447.
- O'Donnell, P., and Grace, A. A. (1995). Synaptic interactions among excitatory afferents to nucleus accumbens neurons: hippocampal gating of prefrontal cortical input. *J. Neurosci.* 15(Pt 1), 3622–3639.
- Pakhotin, P., and Bracci, E. (2007). Cholinergic interneurons control the excitatory input to the striatum. *J. Neurosci.* 27, 391–400.
- Partridge, J. G., Apparsundaram, S., Gerhardt, G. A., Ronesi, J., and Lovinger, D. M. (2002). Nicotinic acetylcholine receptors interact with dopamine in induction of striatal long-term depression. *J. Neurosci.* 22, 2541–2549.
- Pennartz, C. M., Groenewegen, H. J., and Lopes da Silva, F. H. (1994). The nucleus accumbens as a complex of functionally distinct neuronal ensembles: an integration of behavioural, electrophysiological and anatomical data. *Prog. Neurobiol.* 42, 719–761.
- Pickel, V. M. (2000). Extrasynaptic distribution of monoamine transporters and receptors. *Prog. Brain Res.* 125, 267–276.
- Pisani, A., Bernardi, G., Ding, J., and Surmeier, D. J. (2007). Re-emergence of striatal cholinergic interneurons in movement disorders. *Trends Neurosci.* 30, 545–553.
- Pisani, A., Bonsi, P., Centonze, D., Gubellini, P., Bernardi, G., and Calabresi, P. (2003). Targeting striatal cholinergic interneurons in Parkinson's disease: focus on metabotropic glutamate receptors. *Neuropharmacology* 45, 45–56.
- Quik, M., Vailati, S., Bordia, T., Kulak, J. M., Fan, H., McIntosh, J. M., Clementi, F., and Gotti, C. (2005). Subunit composition of nicotinic receptors in monkey striatum: effect of treatments with 1-methyl-4-phenyl-1,2,3,6-tetrahydropyridine or L-DOPA. *Mol. Pharmacol.* 67, 32–41.
- Raiteri, M., Leardi, R., and Marchi, M. (1984). Heterogeneity of presynaptic muscarinic receptors regulating neurotransmitter release in the rat brain. *J. Pharmacol. Exp. Ther.* 228, 209–214.
- Reep, R. L., Cheatwood, J. L., and Corwin, J. V. (2003). The associative striatum: organization of cortical projections to the dorsocentral striatum in rats. *J. Comp. Neurol.* 467, 271–292.
- Rice, M. E., and Cragg, S. J. (2004). Nicotine amplifies reward-related dopamine signals in striatum. *Nat. Neurosci.* 7, 583–584.
- Rice, M. E., and Cragg, S. J. (2008). Dopamine spillover after quantal release: rethinking dopamine transmission in the nigrostriatal pathway. *Brain Res. Rev.* 58, 303–313.
- Salminen, O., Drapeau, J. A., McIntosh, J. M., Collins, A. C., Marks, M. J., and Grady, S. R. (2007). Pharmacology of alpha-conotoxin MII-sensitive subtypes of nicotinic acetylcholine receptors isolated by breeding of null mutant mice. *Mol. Pharmacol.* 71, 1563–1571.
- Salminen, O., Murphy, K. L., McIntosh, J. M., Drago, J., Marks, M. J., Collins, A. C., and Grady, S. R. (2004). Subunit composition and pharmacology of two classes of striatal presynaptic nicotinic acetylcholine receptors mediating dopamine release in mice. *Mol. Pharmacol.* 65, 1526–1535.
- Santiago, M. P., and Potter, L. T. (2001). Biotinylated m4-toxin demonstrates more M4 muscarinic receptor protein on direct than indirect striatal projection neurons. *Brain Res.* 894, 12–20.
- Schmitz, Y., Schmauss, C., and Sulzer, D. (2002). Altered dopamine release and uptake kinetics in mice lacking D2 receptors. *J. Neurosci.* 22, 8002–8009.
- Schoffelemeier, A. N., Van Vliet, B. J., Wardeh, G., and Mulder, A. H. (1986). Muscarine receptor-mediated modulation of [3H]dopamine and [14C]acetylcholine release from rat neostriatal slices: selective antagonism by gallamine but not pirenzepine. *Eur. J. Pharmacol.* 128, 291–294.
- Schultz, W. (1986). Responses of midbrain dopamine neurons to behavioral trigger stimuli in the monkey. *J. Neurophysiol.* 56, 1439–1461.
- Schultz, W. (1998). Predictive reward signal of dopamine neurons. *J. Neurophysiol.* 80, 1–27.
- Schultz, W. (2002). Getting formal with dopamine and reward. *Neuron* 36, 241–263.

- Schultz, W. (2006). Behavioral theories and the neurophysiology of reward. *Annu. Rev. Psychol.* 57, 87–115.
- Sesack, S. R., Aoki, C., and Pickel, V. M. (1994). Ultrastructural localization of D2 receptor-like immunoreactivity in midbrain dopamine neurons and their striatal targets. *J. Neurosci.* 14, 88–106.
- Sesack, S. R., Deutch, A. Y., Roth, R. H., and Bunney, B. S. (1989). Topographical organization of the efferent projections of the medial prefrontal cortex in the rat: an anterograde tract-tracing study with *Phaseolus vulgaris* leucoagglutinin. *J. Comp. Neurol.* 290, 213–242.
- Shen, W., Hamilton, S. E., Nathanson, N. M., and Surmeier, D. J. (2005). Cholinergic suppression of KCNQ channel currents enhances excitability of striatal medium spiny neurons. *J. Neurosci.* 25, 7449–7458.
- Smith, A. D., and Bolam, J. P. (1990). The neural network of the basal ganglia as revealed by the study of synaptic connections of identified neurones. *Trends Neurosci.* 13, 259–265.
- Sugita, S., Uchimura, N., Jiang, Z. G., and North, R. A. (1991). Distinct muscarinic receptors inhibit release of gamma-aminobutyric acid and excitatory amino acids in mammalian brain. *Proc. Natl. Acad. Sci. U.S.A.* 88, 2608–2611.
- Tayebati, S. K., Di Tullio, M. A., and Amenta, F. (2004). Age-related changes of muscarinic cholinergic receptor subtypes in the striatum of Fisher 344 rats. *Exp. Gerontol.* 39, 217–223.
- Thomson, A. M. (2000a). Facilitation, augmentation and potentiation at central synapses. *Trends Neurosci.* 23, 305–312.
- Thomson, A. M. (2000b). Molecular frequency filters at central synapses. *Prog. Neurobiol.* 62, 159–196.
- Threlfell, S., Clements, M. A., Khodai, T., Pienaar, I. S., Exley, R., Wess, J., and Cragg, S. J. (2010). Striatal muscarinic receptors promote activity dependence of dopamine transmission via distinct receptor subtypes on cholinergic interneurons in ventral versus dorsal striatum. *J. Neurosci.* 30, 3398–3408.
- Tobler, P. N., Dickinson, A., and Schultz, W. (2003). Coding of predicted reward omission by dopamine neurons in a conditioned inhibition paradigm. *J. Neurosci.* 23, 10402–10410.
- Tzavara, E. T., Bymaster, F. P., Davis, R. J., Wade, M. R., Perry, K. W., Wess, J., McKinzie, D. L., Felder, C., and Nomikos, G. G. (2004). M4 muscarinic receptors regulate the dynamics of cholinergic and dopaminergic neurotransmission: relevance to the pathophysiology and treatment of related CNS pathologies. *FASEB J.* 18, 1410–1412.
- Voorn, P., Vanderschuren, L. J., Groenewegen, H. J., Robbins, T. W., and Pennartz, C. M. (2004). Putting a spin on the dorsal-ventral divide of the striatum. *Trends Neurosci.* 27, 468–474.
- Wang, Z., Kai, L., Day, M., Ronesi, J., Yin, H. H., Ding, J., Tkatch, T., Lovinger, D. M., and Surmeier, D. J. (2006). Dopaminergic control of corticostriatal long-term synaptic depression in medium spiny neurons is mediated by cholinergic interneurons. *Neuron* 50, 443–452.
- Weiner, D. M., Levey, A. I., and Brann, M. R. (1990). Expression of muscarinic acetylcholine and dopamine receptor mRNAs in rat basal ganglia. *Proc. Natl. Acad. Sci. U.S.A.* 87, 7050–7054.
- Wess, J., Duttaroy, A., Zhang, W., Gomeza, J., Cui, Y., Miyakawa, T., Bymaster, F. P., McKinzie, L., Felder, C. C., Lamping, K. G., Faraci, F. M., Deng, C., and Yamada, M. (2003). M1-M5 muscarinic receptor knockout mice as novel tools to study the physiological roles of the muscarinic cholinergic system. *Recept. Channels* 9, 279–290.
- Whiteaker, P., McIntosh, J. M., Luo, S., Collins, A. C., and Marks, M. J. (2000). 125I-alpha-conotoxin MII identifies a novel nicotinic acetylcholine receptor population in mouse brain. *Mol. Pharmacol.* 57, 913–925.
- Wickens, J. R., Reynolds, J. N., and Hyland, B. I. (2003). Neural mechanisms of reward-related motor learning. *Curr. Opin. Neurobiol.* 13, 685–690.
- Wilson, C. J. (2004). “Basal ganglia,” in *The Synaptic Organization of the Brain*, ed. G. M. Shepherd (Oxford: Oxford University Press), 361–414.
- Wise, R. A. (2004). Dopamine, learning and motivation. *Nat. Rev. Neurosci.* 5, 483–494.
- Wonnacott, S., Kaiser, S., Mogg, A., Soliakov, L., and Jones, I. W. (2000). Presynaptic nicotinic receptors modulating dopamine release in the rat striatum. *Eur. J. Pharmacol.* 393, 51–58.
- Woolf, N. J. (1991). Cholinergic systems in mammalian brain and spinal cord. *Prog. Neurobiol.* 37, 475–524.
- Xu, M., Mizobe, F., Yamamoto, T., and Kato, T. (1989). Differential effects of M1- and M2-muscarinic drugs on striatal dopamine release and metabolism in freely moving rats. *Brain Res.* 495, 232–242.
- Yan, Z., Flores-Hernandez, J., and Surmeier, D. J. (2001). Coordinated expression of muscarinic receptor messenger RNAs in striatal medium spiny neurons. *Neuroscience* 103, 1017–1024.
- Yan, Z., and Surmeier, D. J. (1996). Muscarinic (m2/m4) receptors reduce N- and P-type Ca²⁺ currents in rat neostriatal cholinergic interneurons through a fast, membrane-delimited, G-protein pathway. *J. Neurosci.* 16, 2592–2604.
- Zhang, H., and Sulzer, D. (2004). Frequency-dependent modulation of dopamine release by nicotine. *Nat. Neurosci.* 7, 581–582.
- Zhang, W., Basile, A. S., Gomeza, J., Volpicelli, L. A., Levey, A. I., and Wess, J. (2002a). Characterization of central inhibitory muscarinic autoreceptors by the use of muscarinic acetylcholine receptor knock-out mice. *J. Neurosci.* 22, 1709–1717.
- Zhang, W., Yamada, M., Gomeza, J., Basile, A. S., and Wess, J. (2002b). Multiple muscarinic acetylcholine receptor subtypes modulate striatal dopamine release, as studied with M1-M5 muscarinic receptor knock-out mice. *J. Neurosci.* 22, 6347–6352.
- Zhou, F. M., Liang, Y., and Dani, J. A. (2001). Endogenous nicotinic cholinergic activity regulates dopamine release in the striatum. *Nat. Neurosci.* 4, 1224–1229.
- Zhou, F. M., Wilson, C., and Dani, J. A. (2003). Muscarinic and nicotinic cholinergic mechanisms in the mesostriatal dopamine systems. *Neuroscientist* 9, 23–36.
- Zhou, F. M., Wilson, C. J., and Dani, J. A. (2002). Cholinergic interneuron characteristics and nicotinic properties in the striatum. *J. Neurobiol.* 53, 590–605.
- Zoli, M., Moretti, M., Zanardi, A., McIntosh, J. M., Clementi, F., and Gotti, C. (2002). Identification of the nicotinic receptor subtypes expressed on dopaminergic terminals in the rat striatum. *J. Neurosci.* 22, 8785–8789.
- Zoli, M., Torri, C., Ferrari, R., Jansson, A., Zini, I., Fuxe, K., and Agnati, L. F. (1998). The emergence of the volume transmission concept. *Brain Res. Brain Res. Rev.* 26, 136–147.

Conflict of Interest Statement: The authors declare that the research was conducted in the absence of any commercial or financial relationships that could be construed as a potential conflict of interest.

Received: 30 December 2010; paper pending published: 26 January 2011; accepted: 17 February 2011; published online: 03 March 2011.

Citation: Threlfell S and Cragg SJ (2011) Dopamine signaling in dorsal versus ventral striatum: the dynamic role of cholinergic interneurons. *Front. Syst. Neurosci.* 5:11. doi: 10.3389/fnsys.2011.00011

Copyright © 2011 Threlfell and Cragg. This is an open-access article subject to an exclusive license agreement between the authors and Frontiers Media SA, which permits unrestricted use, distribution, and reproduction in any medium, provided the original authors and source are credited.



Differential calcium dependence of axonal versus somatodendritic dopamine release, with characteristics of both in the ventral tegmental area

Billy T. Chen^{1,†}, Jyoti C. Patel², Kimberly A. Moran¹ and Margaret E. Rice^{1,2*}

¹ Department of Physiology and Neuroscience, New York University School of Medicine, New York, NY, USA

² Department of Neurosurgery, New York University School of Medicine, New York, NY, USA

Edited by:

Elizabeth D. Abercrombie,
Rutgers-Newark: The State University
of New Jersey, USA

Reviewed by:

Alessandro Stefani, University of
Rome, Italy
Constance Hammond, Université de la
Méditerranée, France
R. Mark Wightman, University of North
Carolina at Chapel Hill, USA

*Correspondence:

Margaret E. Rice, Department of
Physiology and Neuroscience,
New York University School of
Medicine, 550 First Avenue, New York,
NY 10016, USA.
e-mail: margaret.rice@nyu.edu

†Present address:

Billy T. Chen, Biomedical Research
Center, National Institute on Drug
Abuse, Baltimore, MD, USA.

Midbrain dopamine (DA) neurons in the substantia nigra pars compacta (SNc) and ventral tegmental area (VTA) exhibit somatodendritic release of DA. Previous studies indicate a difference between the Ca^{2+} dependence of somatodendritic DA release in the SNc and that of axonal DA release in dorsal striatum. Here, we evaluated the Ca^{2+} dependence of DA release in the VTA and nucleus accumbens (NAc) shell for comparison with that in the SNc and dorsal striatum. Release of DA was elicited by single-pulse stimulation in guinea-pig brain slices and monitored with subsecond resolution using carbon-fiber microelectrodes and fast-scan cyclic voltammetry. In dorsal striatum and NAc, DA release was not detectable at extracellular Ca^{2+} concentrations ($[\text{Ca}^{2+}]_o$) below 1 mM; however, a progressive increase in evoked extracellular DA concentration ($[\text{DA}]_o$) was seen with $[\text{Ca}^{2+}]_o \geq 1.5$ mM. By contrast, in SNc and VTA, robust increases in $[\text{DA}]_o$ could be elicited in 0.25 mM $[\text{Ca}^{2+}]_o$ that were ~60% of those seen in 1.5 mM $[\text{Ca}^{2+}]_o$. In SNc, a plateau in single-pulse evoked $[\text{DA}]_o$ was seen at $[\text{Ca}^{2+}]_o \geq 1.5$ mM, mirroring the release plateau reported previously for pulse-train stimulation in SNc. In VTA, however, evoked $[\text{DA}]_o$ increased progressively throughout the range of $[\text{Ca}^{2+}]_o$ tested (up to 3.0 mM). These functional data are consistent with the microanatomy of the VTA, which includes DA axon collaterals as well as DA somata and dendrites. Differences between axonal and somatodendritic release data were quantified using Hill analysis, which showed that the Ca^{2+} dependence of axonal DA release is low affinity with high Ca^{2+} cooperativity, whereas somatodendritic release is high affinity with low cooperativity. Moreover, this analysis revealed the dual nature of DA release in the VTA, with both somatodendritic and axonal contributions.

Keywords: Ca^{2+} , dopamine, nucleus accumbens, somatodendritic release, striatum, substantia nigra, synaptic transmission, voltammetry

INTRODUCTION

Brain dopamine (DA) arises primarily from two midbrain cell groups, the substantia nigra pars compacta (SNc; A9) and the ventral tegmental area (VTA; A10; Dahlström and Fuxe, 1964), both of which project ipsilaterally via the median forebrain bundle to forebrain regions (Ungerstedt, 1971; Fallon and Moore, 1978). Dopaminergic neurons of the SNc project to dorsal striatum and facilitate movement mediated by the basal ganglia, whereas dopaminergic neurons of the VTA project to the nucleus accumbens (NAc), prefrontal cortex, and other mesolimbic structures that underlie emotion, reward, and cognition.

Release of DA occurs in both SNc and VTA (Björklund and Lindvall, 1975; Geffen et al., 1976; Nieoullon et al., 1977; Rice et al., 1994, 1997; Iravani et al., 1996; Jaffe et al., 1998; Chen and Rice, 2001, 2002; Patel et al., 2009). However, in SNc, DA release sites are exclusively somatodendritic (Juraska et al., 1977; Wassef et al., 1981), whereas the VTA receives synaptic DA input from its own axon collaterals and those from the SNc (Deutch et al., 1988; Bayer and Pickel, 1990). In the SNc, the release mechanism appears to be exocytotic (Jaffe et al., 1998; Fortin et al., 2006), requiring depolarization and Ca^{2+} entry (Geffen et al., 1976; Chéramy et al., 1981;

Rice et al., 1994, 1997; Chen and Rice, 2001; Patel et al., 2009), albeit with a minimal dependence on extracellular Ca^{2+} concentration ($[\text{Ca}^{2+}]_o$), which distinguishes it from axonal DA release (Rice et al., 1997; Hoffman and Gerhardt, 1999; Chen and Rice, 2001; Chen et al., 2006; Fortin et al., 2006).

Previous comparison of somatodendritic DA release in the SNc vs. axonal DA release in dorsal striatum revealed a strikingly lower Ca^{2+} dependence of somatodendritic DA release (Chen and Rice, 2001). That study had two limitations, however: first, the low Ca^{2+} levels tested were undefined; second, DA release was evoked by pulse-train stimulation, which elicits the concurrent release of glutamate and GABA that can modulate DA release in both the dorsal striatum and SNc (Chen and Rice, 2002; Avshalumov et al., 2003; Patel et al., 2009). Moreover, the Ca^{2+} dependence of DA release in NAc or VTA was not examined in that study.

In the present work, we used single stimulation pulses, which mimic single action potentials, to evoke DA release that is free from modulation by concurrently released glutamate and GABA (Chen et al., 2006). Release was examined in SNc, VTA, dorsal striatum, and NAc shell in a series of defined $[\text{Ca}^{2+}]_o$. With this refined paradigm, we demonstrate the validity of previous work

suggesting limited Ca²⁺ dependence of somatodendritic vs. axonal DA release. Strikingly, the data from VTA showed a unique Ca²⁺ dependence, with readily detectable evoked extracellular DA concentration ([DA]_o) in low [Ca²⁺]_o, as seen in SNc, but an exponential Ca²⁺ dependence with increasing [Ca²⁺]_o (>1 mM), as seen in NAc and dorsal striatum.

MATERIALS AND METHODS

SLICE PREPARATION AND SOLUTIONS

Male Hartley guinea pigs (150–250 g) were deeply anesthetized with 50 mg/kg pentobarbital (intraperitoneally) and decapitated. All animal handling procedures were in accordance with NIH guidelines and were approved by the New York University School of Medicine Animal Care and Use Committee. Methods for brain slice preparation were as described previously (Chen and Rice, 2001; Chen et al., 2006). Briefly, coronal striatal and midbrain slices (400 μm) were prepared using a Vibratome (Ted Pella, Inc., St. Louis, MO). Slices were cut in ice-cold HEPES-buffered artificial cerebrospinal fluid (aCSF), containing (in mM): NaCl (120); KCl (5); NaHCO₃ (20); HEPES acid (6.7); HEPES salt (3.3); CaCl₂ (2); MgSO₄ (2); and glucose (10) saturated with 95% O₂/5% CO₂, then allowed to recover in HEPES-buffered aCSF for at least 1 h at room temperature before transfer to a submersion recording chamber (Warner Instrument Corp., Hamden, CT). Once in the recording chamber, slices were equilibrated for an additional 30 min in aCSF, which contained (in mM): NaCl (124); KCl (3.7); NaHCO₃ (26); CaCl₂ (0.0–3.0); MgSO₄ (1.3); KH₂PO₄ (1.3); and glucose (10) saturated with 95% O₂/5% CO₂ and maintained at 32°C with a flow rate of 1.2 mL/min.

To assess the Ca²⁺ dependence of DA release as a function of defined [Ca²⁺]_o, Ca²⁺ added to normal aCSF was titrated with the Ca²⁺ chelator EGTA, according to Bers (1982), with all media containing 1 mM EGTA. In all experiments, D₂ autoreceptors were blocked by sulpiride (1 μM) and the DA transporter (DAT) inhibited by GBR-12909 (2 μM) to eliminate the influence of autoreceptor-mediated inhibition and DA uptake (Chen and Rice, 2001), both of which are more pronounced in striatum than SNc (Cragg and Greenfield, 1997; Cragg et al., 1997a).

FAST-SCAN CYCLIC VOLTAMMETRY AND EXPERIMENTAL DESIGN

Evoked DA release was monitored in real time using fast-scan cyclic voltammetry (FCV) with carbon-fiber electrodes made from 7 μm carbon fibers (type HM, unsized, Courtaulds), which were spark-etched to a tip diameter of 2–4 μm (MPB Electrodes; St. Bartholomew's and the Royal London School of Medicine and Dentistry, University of London, UK). Instrumentation for FCV was a Millar Voltammeter (available from J. Millar, St. Bartholomew's and the Royal London School of Medicine and Dentistry), with data acquisition controlled by Clampex 7.0 software (Molecular Devices, Foster City, CA), which imported voltammograms to a PC via a DigiData 1200B A/D board (Molecular Devices). Scan rate for FCV was 800 V/s, with a sampling interval of 100 ms; scan range was −0.7 to +1.3 V (vs. Ag/AgCl). Because the sensitivity of carbon-fiber microelectrodes can change with changes in divalent cation concentration (Kume-Kick and Rice, 1998; Chen et al., 1999), electrodes were calibrated in the recording chamber at 32°C after each experiment with DA in aCSF

with each Ca²⁺ concentration tested. The DA calibration factor for each Ca²⁺ concentration was used to calculate evoked [DA]_o in that medium.

Single-pulse stimulation was used to evoke DA release. Although the stimulus pulse would be expected to elicit release of other transmitters, initial DA release is unaffected by subsequent receptor activation by these transmitters. Previous studies have confirmed the independence of single-pulse evoked [DA]_o from regulation by glutamate and GABA by the lack of effect on signal amplitude and time course in striatum and SNc by a cocktail of receptor antagonists: AP5 (NMDA), GYKI-52466 (AMPA), picrotoxin (GABA_A), and saclofen (GABA_B) (Chen et al., 2006). Indeed, evaluation of the effect of a concurrently released transmitter on evoked DA release requires multiple-pulse stimulation (e.g., Chen and Rice, 2002; Avshalumov et al., 2003). The lack of effect of receptor antagonists on single-pulse evoked [DA]_o also implies the absence of tonic glutamatergic or GABAergic regulation of DA in our slice preparations. Consequently, these antagonists were not added to the aCSF in the present studies. Stimulus pulse duration was 1 ms with amplitudes of 0.7–1.0 mA. In dorsal striatum and NAc, consistent evoked [DA]_o can be elicited with repetitive local stimulation (Bull et al., 1990; Patel et al., 1995; Chen and Rice, 2001). Here, axonal DA release in dorsal striatum and NAc shell was evoked at 10-min intervals; the third of three consistent evoked increases in [DA]_o was included in the data average for each [Ca²⁺]_o. In SNc and VTA, maximal release is often seen with the first stimulus, then decreases with repetition (Rice et al., 1997). Thus, DA release obtained from two sites in medial SNc and in VTA were averaged for inclusion in the data set for a given [Ca²⁺]_o, then the procedure repeated with a different [Ca²⁺]_o on the contralateral side.

DRUGS AND CHEMICALS

Sulpiride, DA, EGTA, and components of aCSF and HEPES-aCSF were obtained from Sigma-Aldrich Chemical Co. (St. Louis, MO); GBR-12909 was from Tocris Bioscience (Ellisville, MO). All solutions were made immediately before use.

STATISTICAL ANALYSIS

Data are given as normalized means ± SEM, where *n* = number of slices. Maximum evoked [DA]_o in 1.5 mM [Ca²⁺]_o for each region was considered to be 100%. Differences in evoked [DA]_o in varying [Ca²⁺]_o vs. control were assessed using one-way ANOVA followed by Kruskal–Wallis *post-hoc* analysis. Normalized peak [DA]_o data in each [Ca²⁺]_o were also analyzed using the Hill equation to determine Ca²⁺ cooperativity for each region (Schneggenburger and Neher, 2000).

RESULTS

Ca²⁺ DEPENDENCE OF SINGLE-PULSE EVOKED DA RELEASE IN DORSAL STRIATUM AND SNc

In dorsal striatum, axonal DA release elicited by a single-pulse showed a marked dependence on [Ca²⁺]_o (Figures 1A,B). Evoked [DA]_o was below the detection limit at 0 and 0.5 mM [Ca²⁺]_o, was detectable at 1 mM [Ca²⁺]_o, then increased progressively with further increases in [Ca²⁺]_o. Peak evoked [DA]_o was 1.32 ± 0.18 μM (*n* = 6) in 1.5 mM [Ca²⁺]_o. This [Ca²⁺]_o (1.5 mM) is roughly physiological and therefore was used as the reference (control) level, and considered

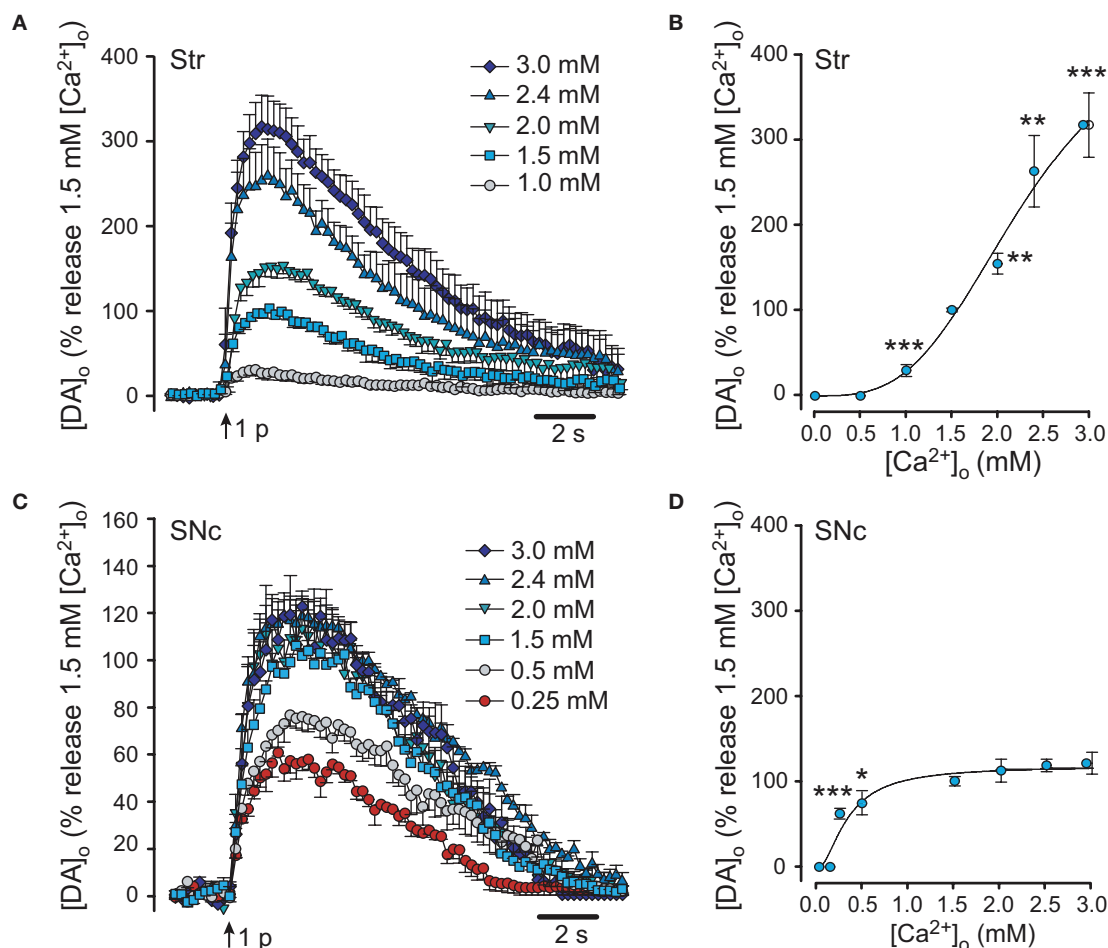


FIGURE 1 | Ca²⁺ dependence of evoked synaptic DA release in dorsal striatum and SNc. (A) Average single-pulse evoked [DA]_o in dorsal striatum in varying [Ca²⁺]_o. Maximum [DA]_o in 1.5 mM [Ca²⁺]_o in dorsal striatum was taken as 100%. Release could not be evoked in [Ca²⁺]_o ≤ 0.5 mM, but increased progressively as [Ca²⁺]_o was increased from 1.0 to 3.0 mM. **(B)** Ca²⁺-dependence of DA release in dorsal striatum. Significance of difference from peak [DA]_o in 1.5 mM [Ca²⁺]_o is indicated by ***p* < 0.01 or ****p* < 0.001 (*n* = 5–6). **(C)** Average single-pulse evoked [DA]_o in SNc in varying [Ca²⁺]_o.

Maximum [DA]_o in 1.5 mM [Ca²⁺]_o in SNc was taken as 100%. Somatodendritic release of DA could be seen at [Ca²⁺]_o ≥ 0.25 mM. Release was maximal in 1.5 mM [Ca²⁺]_o. **(D)** Ca²⁺ dependence of evoked DA release in SNc. In contrast to the Ca²⁺-dependence of axonal DA release in dorsal striatum, somatodendritic release was already more than half-maximal in 0.25 mM [Ca²⁺]_o, but then reached a plateau at [Ca²⁺]_o ≥ 1.5 mM. Significance of difference from peak [DA]_o in 1.5 mM [Ca²⁺]_o is indicated by **p* < 0.01 or ****p* < 0.001 (*n* = 6–12).

to be 100%. Demonstrating the marked Ca²⁺-dependence of axonal DA release, peak evoked [DA]_o in 1.0 mM Ca²⁺ was 30 ± 7% of control (**Figures 1A,B**). Increasing [Ca²⁺]_o to 2.0, 2.4, and 3.0 mM increased evoked [DA]_o to 154 ± 12%, 261 ± 42%, and 315 ± 37% of control, respectively. Each increase in evoked [DA]_o differed significantly from control in 1.5 mM Ca²⁺ (*n* = 5–6; *p* < 0.01–0.001 vs. control). The Ca²⁺-dependence of single-pulse evoked DA release in dorsal striatum was roughly sigmoidal (**Figure 1B**).

In the SNc, evoked [DA]_o was not detected in 0 mM [Ca²⁺]_o (0 added Ca²⁺ plus 1 mM EGTA) affirming that somatodendritic DA release requires Ca²⁺ influx (Patel et al., 2009). The lowest [Ca²⁺]_o at which there was detectable evoked [DA]_o in the SNc was 0.25 mM (**Figures 1C,D**). Peak evoked [DA]_o in SNc in 1.5 mM [Ca²⁺]_o was again considered to be 100%. Evoked [DA]_o was 0.70 ± 0.04 μM in 1.5 mM Ca²⁺ (*n* = 12). In 0.25 mM [Ca²⁺]_o, evoked DA release was

62 ± 5% of that in 1.5 mM [Ca²⁺]_o (*n* = 6; *p* < 0.001; **Figures 1C,D**). This level of stimulated [DA]_o was further elevated in 0.5 mM [Ca²⁺]_o, to 74 ± 13%, however it remained significantly lower than control (*n* = 6; *p* < 0.05). Similar to pulse-train evoked [DA]_o (Chen and Rice, 2001), single-pulse evoked [DA]_o reached a plateau at higher levels of [Ca²⁺]_o, with no significant difference seen between release in 1.5 mM [Ca²⁺]_o and that in 2.0 mM (112 ± 13%; *n* = 7), 2.4 mM (118 ± 7%; *n* = 10), or 3.0 mM [Ca²⁺]_o (121 ± 13%; *n* = 6; *p* > 0.05 for each vs. control; **Figure 1D**).

Ca²⁺ DEPENDENCE OF SINGLE-PULSE EVOKED DA RELEASE IN NAC AND VTA

Single-pulse evoked DA release in the NAc shell showed a strong Ca²⁺ dependence (**Figures 2A,B**), which was similar to that seen in dorsal striatum (**Figures 1A,B**). In the NAc, evoked [DA]_o was

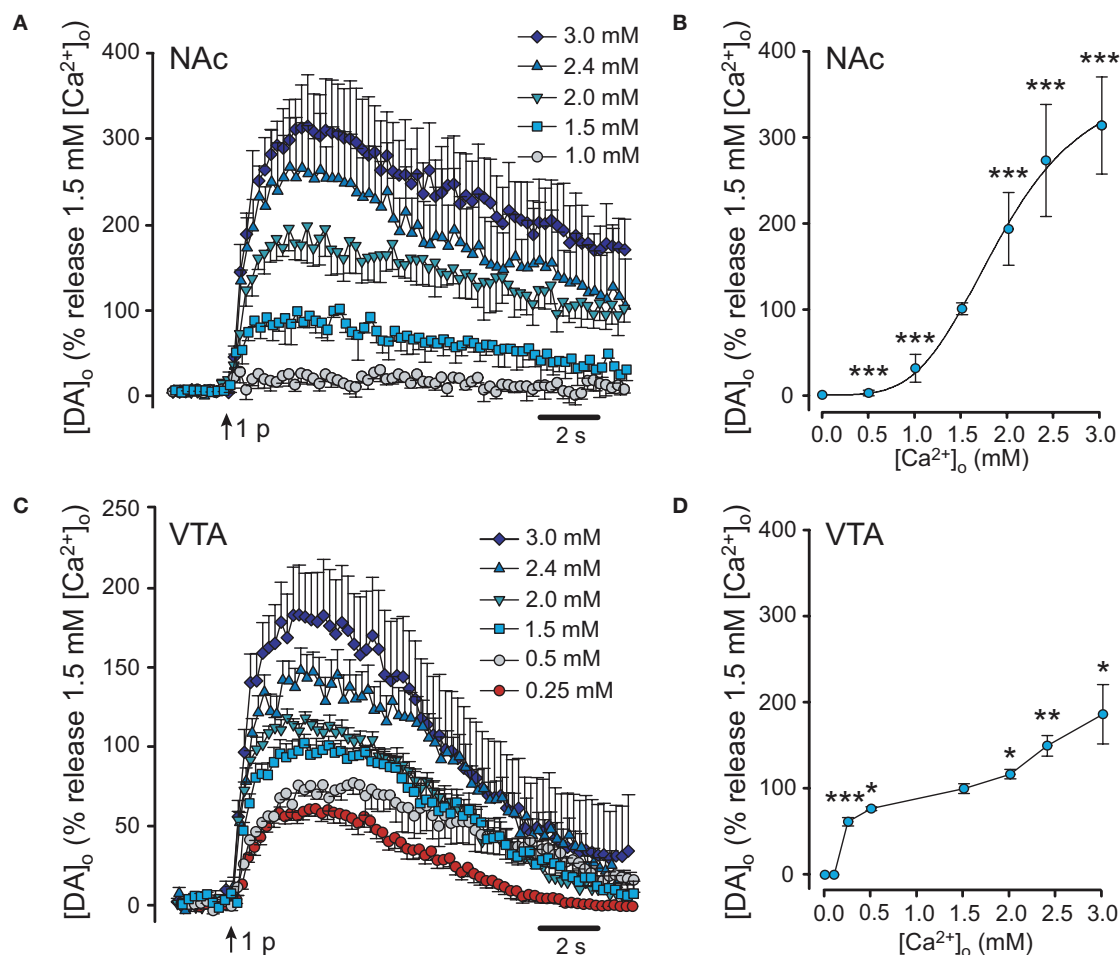


FIGURE 2 | The Ca²⁺ dependence of DA release in NAc and VTA.

(A) Average evoked [DA]_o in the presence of varying [Ca²⁺]_o in NAc shell. Maximum [DA]_o in 1.5 mM [Ca²⁺]_o in NAc was taken as 100%. As in dorsal striatum, synaptic DA release in NAc could not be evoked in [Ca²⁺]_o ≤ 0.5 mM, but increased progressively as [Ca²⁺]_o was increased from 1.0 to 3.0 mM. **(B)** Ca²⁺ dependence of evoked DA release in NAc. Significance of difference from peak [DA]_o in 1.5 mM [Ca²⁺]_o is indicated by ****p* < 0.001 (*n* = 7). **(C)** Average evoked [DA]_o in the VTA the presence of varying [Ca²⁺]_o. Maximum [DA]_o in 1.5 mM [Ca²⁺]_o in VTA was taken as 100%.

Somatodendritic release characteristics were evident in the robust DA release seen in 0.25 mM [Ca²⁺]_o. Unlike pure somatodendritic release in the SNc, however, evoked [DA]_o in the VTA continued to increase as [Ca²⁺]_o was increased beyond 1.5 mM. **(D)** Ca²⁺ dependence of evoked DA release in the VTA. In low [Ca²⁺]_o (<1 mM), the pattern of evoked release in the VTA resembled that seen in SNc. However, release in the VTA did not plateau at [Ca²⁺]_o ≥ 1.5 mM, as it did in SNc (**Figure 1D**). Significance of difference from peak [DA]_o in 1.5 mM [Ca²⁺]_o is indicated by **p* < 0.05, ***p* < 0.01, or ****p* < 0.001 (*n* = 6–16).

also undetectable in 0 and 0.5 mM [Ca²⁺]_o, then increased progressively with increasing [Ca²⁺]_o. Peak evoked [DA]_o was $0.46 \pm 0.10 \mu\text{M}$ (*n* = 7) in 1.5 mM [Ca²⁺]_o and was taken as the control level. Peak evoked [DA]_o in 1.0 mM [Ca²⁺]_o was $31 \pm 16\%$ of control (**Figures 2A,B**). Increasing [Ca²⁺]_o to 2.0, 2.4, and 3.0 mM increased evoked [DA]_o to $193 \pm 42\%$, $271 \pm 42\%$, and $313 \pm 57\%$ of control, respectively. Each increase in [DA]_o differed significantly from control evoked [DA]_o in 1.5 mM [Ca²⁺]_o (*n* = 7; *p* < 0.001 for each vs. control).

In the VTA, the lowest [Ca²⁺]_o at which a response was seen was again 0.25 mM (**Figures 2C,D**), with undetectably low release in 0 mM [Ca²⁺]_o. Peak evoked [DA]_o in 1.5 mM [Ca²⁺]_o was $0.68 \pm 0.06 \mu\text{M}$ (*n* = 9) and was considered to be control release for the VTA. Peak evoked [DA]_o in 0.25 mM [Ca²⁺]_o was $62 \pm 5\%$ of that in 1.5 mM [Ca²⁺]_o (*n* = 9; *p* < 0.001 vs. control). Stimulated [DA]_o was further

elevated in 0.5 mM [Ca²⁺]_o to $77 \pm 2\%$ (*n* = 3; *p* < 0.05 vs. control). Unlike evoked [DA]_o in SNc, however, single-pulse evoked [DA]_o in the VTA did not plateau at [Ca²⁺]_o ≥ 1.5 mM, but continued to increase with increasing [Ca²⁺]_o. Evoked [DA]_o in 2.0 mM [Ca²⁺]_o was $117 \pm 5\%$ of control (*n* = 9; *p* < 0.05 vs. control), $150 \pm 12\%$ in 2.4 mM (*n* = 16; *p* < 0.01 vs. control), and $186 \pm 34\%$ in 3.0 mM [Ca²⁺]_o (*n* = 8; *p* < 0.05 vs. control; **Figures 2C,D**). Thus, DA release in the VTA shows characteristics of axonal, as well as somatodendritic release.

HILL ANALYSIS OF THE Ca²⁺ DEPENDENCE OF SINGLE-PULSE EVOKED DA RELEASE

The Ca²⁺-dependence data from each region was evaluated further using a three-parameter Hill analysis, in which the slope determined indicates the power of the Ca²⁺ dependence (**Figure 3**).

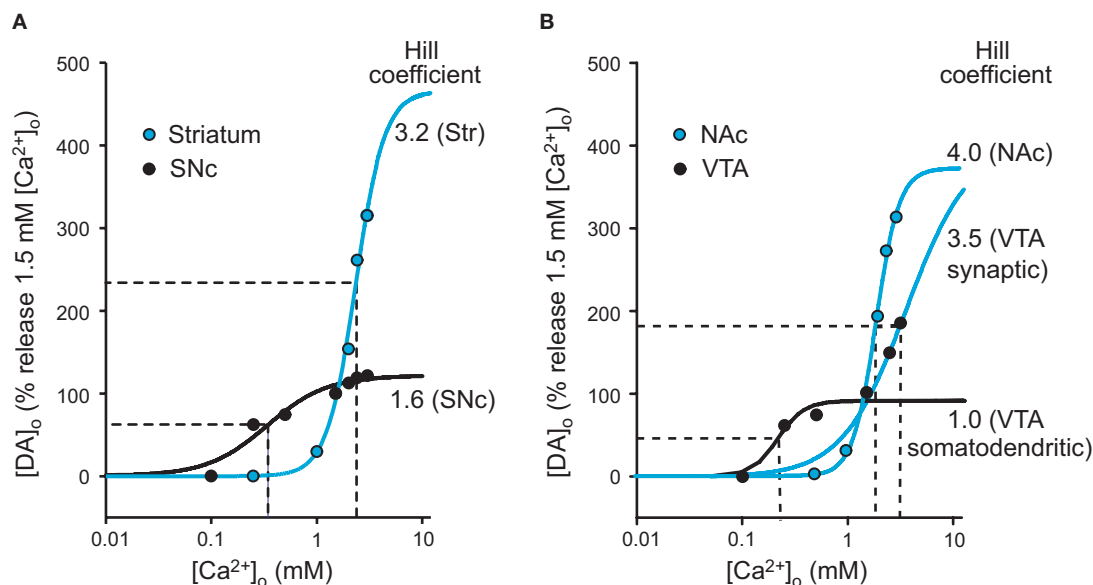


FIGURE 3 | Hill analysis of the Ca²⁺-dependence of nigrostriatal and mesolimbic DA release. Single-pulse evoked [DA]_o data normalized to peak evoked [DA]_o in 1.5 mM [Ca²⁺]_o as 100% for each region for (A) dorsal striatum and SNc and (B) NAc and VTA. Blue lines indicate Hill fit for axonal release, black lines for somatodendritic release. The Hill coefficient for each fit indicates the exponential dependence of DA release on [Ca²⁺]_o. Both axonal and somatodendritic were needed to fit data from the VTA ([Ca²⁺]_o < 1.5 mM vs.

[Ca²⁺]_o > 1.0 mM) (B). The x-axis for each Hill plot was extended to 10 mM [Ca²⁺]_o to permit extrapolation of the Ca²⁺ dependence to a roughly maximal level for each region. These expanded plots permitted calculation of an EC₅₀ (the [Ca²⁺]_o at which DA release is half-maximal) for each region (dashed lines). The EC₅₀ for dorsal striatum was 2.3 mM [Ca²⁺]_o and that for SNc was 0.3 mM. In NAc, EC₅₀ was 1.9 mM, with 0.3 mM for somatodendritic release in VTA. Data points (taken from Figures 1B,D and 2B,D) are given as means without error bars for clarity.

Fitting the normalized points for dorsal striatum to Hill's function (Schneggenburger and Neher, 2000) gave a slope of 3.2, which indicates an approximately third-power dependence on [Ca²⁺]_o (Figure 3A). By contrast, Hill analysis of the Ca²⁺ dependence of DA release in the SNc gave a slope of only 1.6 (Figure 3A), confirming a more shallow dependence on [Ca²⁺]_o for somatodendritic DA release in the SNc than for axonal DA release in dorsal striatum. The slope for the NAc shell was 4.0 (Figure 3B), which did not differ significantly from that determined for dorsal striatum ($p > 0.05$). Differing from all these regions, however, two distinct Hill fits were required for the VTA: the slope for evoked [DA]_o in [Ca²⁺]_o ≤ 1.5 mM was 1.0, whereas that for [Ca²⁺]_o ≥ 1.0 mM was 3.5 (Figure 3B). These data are consistent with dual characteristics of somatodendritic and axonal DA release in the VTA.

The [Ca²⁺]_o at which evoked [DA]_o was half-maximal, the EC₅₀, was also determined from the Hill plots to indicate the relative Ca²⁺ sensitivity for DA release in each region. The EC₅₀ for dorsal striatum was 2.3 mM [Ca²⁺]_o, but only 0.3 mM [Ca²⁺]_o in SNc. Similarly, the EC₅₀ for NAc was 1.9 mM [Ca²⁺]_o, but only 0.3 mM [Ca²⁺]_o for somatodendritic DA release in the VTA (Figure 3).

DISCUSSION

We determined the Ca²⁺ dependence of single-pulse axonal and somatodendritic DA release in the nigrostriatal and mesolimbic pathways using a defined series of [Ca²⁺]_o in brain slices. We show that DA release in the SNc and VTA has a lower [Ca²⁺]_o threshold and exhibits lower Ca²⁺ cooperativity than seen with axonal DA release in the dorsal striatum and NAc shell. Moreover, somato-

dendritic DA release in the SNc is maximal at near physiological [Ca²⁺]_o, whereas axonal release shows an exponential increase with increasing [Ca²⁺]_o. In contrast to the SNc, however, DA release in the VTA exhibits a low affinity, high cooperativity axonal component, as well as a high affinity, low cooperativity somatodendritic component. These data are the first to reveal functional somatodendritic and axonal DA release in VTA, consistent with predictions from VTA microanatomy.

COMPARISON WITH PULSE-TRAIN EVOKED DA RELEASE

Patterns of DA release evoked by single-pulse stimulation in dorsal striatum and SNc in defined [Ca²⁺]_o (Figure 1) paralleled those seen with pulse-train stimulation reported previously (Chen and Rice, 2001). Given the absence of regulation of single-pulse evoked release by concurrently released glutamate and GABA acting at ionotropic receptors (Chen et al., 2006), this indicates that the basic patterns are not influenced significantly by the Ca²⁺-dependence of other transmitters. This is important because somatodendritic DA release in the SNc can be strongly inhibited by GABAergic input (Chen and Rice, 2002), which would be expected to increase progressively with increasing [Ca²⁺]_o. Consequently, increasing suppression of DA release from Ca²⁺-dependent GABA release with increasing [Ca²⁺]_o might have contributed to the plateau in [DA]_o evoked by multiple-pulse stimulation reported previously (Chen and Rice, 2001). However, the new single-pulse DA release data in the present report demonstrate that the predominant contributing factor to the plateau is the Ca²⁺ dependence of the DA release process itself.

What might contribute to the plateau in evoked $[DA]_o$ in SNc? Possible factors include saturation of Ca²⁺ influx and depletion of the readily releasable pool (RRP) of DA (e.g., Südhof, 2000). Given that the relationship between $[Ca^{2+}]_o$ and $[Ca^{2+}]_i$ is usually assumed to be linear (Dodge and Rahamimoff, 1967; Reid et al., 1998), with saturation of Ca²⁺ influx only at $[Ca^{2+}]_o \gg 10$ mM (see Church and Stanley, 1996), this leaves depletion of the RRP as the more likely explanation, as seen at the calyx of Held synapse (Schneggenburger et al., 1999). The observation that evoked $[DA]_o$ in the SNc plateaued at a ~10-fold lower $[Ca^{2+}]_o$ than that predicted for dorsal striatum or NAc (Figures 3A,C) is consistent with the limited number of vesicles and presence of alternative DA storage sites in SNc DA somata and dendrites (Wilson et al., 1977; Wassef et al., 1981; Groves and Linder, 1983; Nirenberg et al., 1996), as well as the ~10-fold lower DA content of SNc and VTA compared to striatum (Rice et al., 1997).

DIFFERENCES IN THE Ca²⁺-DEPENDENCE OF DA RELEASE BETWEEN STRIATUM AND MIDBRAIN

In dorsal striatum and NAc shell, evoked $[DA]_o$ was detectable from 1.0 mM $[Ca^{2+}]_o$ and increased exponentially as $[Ca^{2+}]_o$ was increased to 3.0 mM. The similarity of $[Ca^{2+}]_o$ threshold and the exponential dependence of DA release in these regions suggest that basic Ca²⁺-dependent release mechanisms are homogenous throughout the striatal complex. In SNc and VTA, however, evoked $[DA]_o$ was detectable in 0.25 mM $[Ca^{2+}]_o$, at which evoked $[DA]_o$ was already at 60% of control levels in both midbrain regions. In contrast to the plateau seen in SNc, however, single-pulse evoked DA release in the VTA continued to rise with increasing $[Ca^{2+}]_o$.

Hill analysis of the Ca²⁺-dependence data for striatum and SNc, as well as for NAc and the somatodendritic component of DA release in the VTA, revealed an approximately two-fold greater dependence on $[Ca^{2+}]_o$ for axonal vs. somatodendritic release (Figure 3). Axonal DA release in dorsal striatum was dependent on the third-power of $[Ca^{2+}]_o$, indicating that DA release in this region requires the cooperative action of three Ca²⁺ ions. These data are strikingly consistent with the third-power dependence for DA release from striatal synaptosomes reported by Nachshen and Sanchez-Armass (1987), who used completely different methods of DA detection and data analysis than those used here. Similarly, axonal DA release in the NAc shell showed a fourth-power dependence in the present studies. The Ca²⁺ dependence of axonal DA release in both regions was within range of other well-examined synaptic systems that use glutamate as their transmitter, with a second-power dependence on $[Ca^{2+}]_o$ at the squid giant synapse (Katz and Miledi, 1970), the cerebellar parallel fiber-Purkinje cell synapse (Mintz et al., 1995), and the hippocampal Schaeffer collateral synapses (Qian et al., 1997), but a fourth-power at the neuromuscular junction (Dodge and Rahamimoff, 1967) and a fifth-power dependence at the calyx of Held synapse (Bollmann et al., 2000; Schneggenburger and Neher, 2000; Sun et al., 2007). By contrast, the dependence of somatodendritic release was less than to the second-power, and thus lower than the dependence for these established synaptic systems.

These differences between axonal and somatodendritic DA release, although consistent with previous studies in guinea-pig brain slices (Chen and Rice, 2001), contrast with recent findings from mouse brain slices, in which no difference in the Ca²⁺ depend-

ence of DA release between dorsal striatum and either SNc or VTA was observed (Ford et al., 2010). Given that both sets of studies used similar methods, the simplest explanation for the discrepancy in SNc responsiveness may be a species difference. Mouse (and rat) SNc show a marked contribution from axonal serotonin (5-HT) input to the voltammetric signal (Cragg et al., 1997b; John et al., 2006; Ford et al., 2010). However, in the guinea-pig SNc, pure DA release is observed (Cragg et al., 1997b; Rice et al., 1997). Thus, the axonal-like Ca²⁺ dependence of the release signal in mouse SNc (Ford et al., 2010) is likely to include a significant component of axonal 5-HT release, which could mask the $[DA]_o$ plateau reported here. Contributions from 5-HT would be amplified by the higher sensitivity of carbon-fiber electrodes for 5-HT vs. DA (O'Connor and Kruk, 1991; Patel et al., 1992). Interestingly, the Ca²⁺ dependence reported for mouse VTA over a range of 0.5–2.5 mM $[Ca^{2+}]_o$ (Ford et al., 2010) is similar to that reported here for guinea-pig VTA (Figure 2D). Given that the somatodendritic characteristics of DA release in the VTA are discerned only at $[Ca^{2+}]_o \leq 0.5$ mM, the evoked $[DA]_o$ response at $[Ca^{2+}]_o \geq 0.5$ mM would reflect primarily axonal contributions, as reported here for the first time, and therefore would not be expected to differ from that in striatum.

DIFFERENTIAL Ca²⁺ SENSITIVITY OF SOMATODENDRITIC VERSUS AXONAL DA RELEASE

Comparison of EC₅₀ values for the Ca²⁺ dependence of DA release in each region revealed that the Ca²⁺ sensitivity for somatodendritic DA release is six- to seven-fold higher than for axonal release, supporting our earlier hypothesis that a minimal level of Ca²⁺ entry is enough to trigger pure somatodendritic DA release (Chen and Rice, 2001; Chen et al., 2006; Patel et al., 2009). The reasons for the greater sensitivity of somatodendritic DA release to $[Ca^{2+}]_o$ are not yet clear, but could reflect a combination of several contributing factors. One known factor is the involvement of intracellular Ca²⁺ store activation in amplifying somatodendritic DA release in the SNc (Patel et al., 2009). This amplification can involve store activation by either ryanodine receptors, which are localized near the plasma membrane in SNc DA neurons, or IP₃ (inositol-1,4,5-triphosphate) receptors. Notably, facilitation of DA release in the SNc by activation of ryanodine receptors is enhanced in low vs. high $[Ca^{2+}]_o$ (Patel et al., 2009), which may contribute to the pattern of Ca²⁺ sensitivity of DA release reported here.

In addition, although the difference in the Ca²⁺ sensitivity of somatodendritic and axonal DA release might suggest a difference in release mechanism, the goodness-of-fit of the Hill plots for midbrain and striatum (Figure 3) suggests a common Ca²⁺-dependent exocytotic process in both. Indeed, there is an absolute requirement for Ca²⁺-influx to trigger somatodendritic release, as release is abolished in Ca²⁺-free aCSF (Figures 1D and 2D) and in the presence of the Ca²⁺ channel blocker Cd²⁺ (Patel et al., 2009). Moreover, DA release from primary cultures is suppressed by disruption of SNARE proteins (Fortin et al., 2006), consistent with an exocytotic mechanism underlying somatodendritic DA release.

On the other hand, the higher Ca²⁺ sensitivity and lower Ca²⁺ cooperativity of somatodendritic vs. axonal DA release support the idea that exocytotic machinery may differ between these release sites (Bergquist et al., 2002; Fortin et al., 2006; Witkovsky et al., 2009). For example, the Ca²⁺-sensing protein primarily responsible for triggering

exocytotic transmitter release is synaptotagmin (Südhof and Rizo, 1996; Südhof, 2000, 2002; Chapman, 2002) of which there are at least eight different isoforms with differing Ca²⁺ affinities in vertebrate brain (Südhof, 2002). For example, synaptotagmin 1 and 2, which are the predominant isoforms found on vesicles involved in fast synaptic transmission (Xu et al., 2007), have a 10–20-fold lower Ca²⁺ affinity than those of synaptotagmin 7 and 3 (Südhof, 2002; Sugita et al., 2002a,b). Notably, DA neurons in the SNc lack synaptotagmin 1 and 2 (Witkovsky et al., 2009), but express synaptotagmin 7 (Mendez et al., 2011), which may contribute to the higher Ca²⁺ sensitivity of somatodendritic release. Thus, the presence of different synaptotagmin isoforms in different neurons or different compartments of the same neuron could alter the Ca²⁺ sensitivity and kinetics of transmitter release. The somatodendritic compartment of DA neurons also expresses different complements of SNARE proteins than found at axon terminals (Bergquist et al., 2002; Witkovsky et al., 2009).

AXONAL AS WELL AS SOMATODENDRITIC DA RELEASE CHARACTERISTICS OF THE VTA

In the VTA, DA release showed high Ca²⁺ sensitivity like that in SNc, consistent with somatodendritic release. However, the exponential increase in evoked [DA]_o with increasing [Ca²⁺]_o indicated an axonal component, as well. Thus, the Ca²⁺ dependence of somatodendritic DA release differentiates this process from axonal release. These distinctions reveal that the VTA exhibits both somatodendritic and axonal DA release, consistent with the microanatomy of this region, which includes DA axons, as well as DA somata and dendrites. Indeed, the VTA has DA synapses arising from its own axon collaterals, as well as minor synaptic input from the SNc (Deutch et al., 1988; Bayer and Pickel, 1990). Although sparse, the axonal component of VTA DA release reported here is robust, and is likely to be a contributing factor in the ability of the VTA to sustain DA release with repetitive stimulation (e.g., Iravani et al., 1996). Indeed, because of this potential confounding factor, mechanistic studies of somatodendritic DA release have often focused on the SNc (e.g., Chen

and Rice, 2001; Patel et al., 2009; Witkovsky et al., 2009), because the SNc is devoid of dopaminergic collaterals and axonal synapses (Juraska et al., 1977; Wassef et al., 1981). The dual nature of DA release in the VTA also implies that factors in addition to Ca²⁺ may differentially affect the two components. For example, DA neuron firing rate might be a key regulator of the somatodendritic component, whereas local presynaptic regulation might independently suppress or enhance axonal release consequent to neuronal activity.

CONCLUSION

The present studies demonstrate two key differences between axonal and somatodendritic DA release: low sensitivity, but high cooperativity of axonal release throughout striatum; and high sensitivity and low cooperativity in the midbrain. Based on these distinct features, we conclude that the VTA exhibits both somatodendritic and axonal DA release, providing new insight into DA signaling in this region. Additionally, these findings suggest that disease states that affect vesicle release or calcium entry could have differential consequences among the brain regions examined here. Conditions in which DA levels were depleted, but not eliminated, would not be expected to alter the Ca²⁺ dependence patterns reported, assuming the only change was in the size of the releasable pool of DA. However, this might not be the case in disease states that affect transmitter release machinery, for example deletion or mutation of proteins that associate with synaptic vesicles. In support of this hypothesis, altered Ca²⁺ dependence of axonal DA release in dorsal striatum has been reported following knockout of α -synuclein in a model of Parkinson's disease (Abeliovich et al., 2000) and with over-expression of mutant torsinA, the product of the *DYT1* gene underlying early onset dystonia (Bao et al., 2010).

ACKNOWLEDGMENTS

Supported by NIH/NINDS Grant NS036362 (MER) and NIH-NIDCD Training Grant 5T32 DC000063 (KAM). We are grateful to Dr Paul Witkovsky for a critical reading of the manuscript.

REFERENCES

- Abeliovich, A., Schmitz, Y., Fariñas, I., Choi-Lundberg, D., Ho, W. H., Castillo, P. E., Shinsky, N., Verdugo, J. M., Armanini, M., Ryan, A., Hynes, M., Phillips, H., Sulzer, D., and Rosenthal, A. (2000). Mice lacking α -synuclein display functional deficits in the nigrostriatal dopamine system. *Neuron* 25, 239–252.
- Avshalumov, M. V., Chen, B. T., Marshall, S. P., Pena, D. M., and Rice, M. E. (2003). Glutamate-dependent inhibition of dopamine release in striatum is mediated by a new diffusible messenger, H₂O₂. *J. Neurosci.* 23, 2744–2750.
- Bao, L., Patel, J. C., Walker, R. H., Shashidharan, P., and Rice, M. E. (2010). Dysregulation of striatal dopamine release in a mouse model of dystonia. *J. Neurochem.* 114, 1781–1791.
- Bayer, V. E., Pickel, V. M. (1990). Ultrastructural localization of tyrosine hydroxylase in the rat ventral tegmental area: relationship between immunolabeling density and neuronal associations. *J. Neurosci.* 10, 2996–3013.
- Bergquist, F., Niaz, H. S., and Nissbrant, H. (2002). Evidence for different exocytosis pathways in dendritic and terminal dopamine release in vivo. *Brain Res.* 950, 245–253.
- Bers, D. M. (1982). A simple method for the accurate determination of free [Ca] in Ca-EGTA solutions. *Am. J. Physiol.* 242, C404–C408.
- Björklund, O., and Lindvall, O. (1975). Dopamine in dendrites of substantia nigra neurons: suggestions for a role in dendritic terminals. *Brain Res.* 83, 531–537.
- Bollmann, J. H., Sakmann, B., and Borst, J. G. (2000). Calcium sensitivity of glutamate release in a calyx-type terminal. *Science* 289, 953–957.
- Bull, D. R., Palij, P., Sheehan, M. J., Millar, J., Stamford, J. A., Kruk, Z. L., and Humphrey, P. P. (1990). Application of fast cyclic voltammetry to measurement of electrically evoked dopamine overflow from brain slices *in vitro*. *J. Neurosci. Meth.* 32, 37–44.
- Chapman, E. R. (2002). Synaptotagmin: Ca²⁺ sensor that triggers exocytosis? *Nat. Rev. Mol. Cell Biol.* 3, 498–508.
- Chen, B. T., Kume-Kick, J., and Rice, M. E. (1999). Calibration factors for cationic and anionic neurochemicals at carbon-fiber microelectrodes are oppositely affected by the presence of Ca²⁺ and Mg²⁺. *Electroanalysis* 11, 344–348.
- Chen, B. T., Moran, K. A., Avshalumov, M. V., and Rice, M. E. (2006). Limited regulation of somatodendritic dopamine release by voltage-sensitive Ca²⁺ channels contrasted with strong regulation of axonal dopamine release. *J. Neurochem.* 96, 645–655.
- Chen, B. T., and Rice, M. E. (2001). Novel Ca²⁺ dependence and time course of somatodendritic dopamine release: substantia nigra vs. striatum. *J. Neurosci.* 21, 7841–7847.
- Chen, B. T., and Rice, M. E. (2002). Synaptic regulation of somatodendritic dopamine release by glutamate and GABA differs between substantia nigra and ventral tegmental area. *J. Neurochem.* 81, 158–169.
- Chéramy, A., Leviel, V., and Glowinski, J. (1981). Dendritic release of dopamine in the substantia nigra. *Nature* 289, 537–542.
- Church, P. J., and Stanley, E. F. (1996). Single L-type calcium channel conductance with physiological levels of calcium in chick ciliary ganglion neurons. *J. Physiol.* 496, 59–68.
- Cragg, S. J., and Greenfield, S. A. (1997). Differential autoreceptor control of somatodendritic and axon terminal dopamine release in substantia nigra, ventral tegmental area, and striatum. *J. Neurosci.* 17, 5738–5746.

- Cragg, S. J., Rice, M. E., and Greenfield, S. A. (1997a). Heterogeneity of electrically evoked dopamine release and reuptake in substantia nigra, ventral tegmental area, and striatum. *J. Neurophysiol.* 77, 863–873.
- Cragg, S. J., Hawkey, C. R., and Greenfield, S. A. (1997b). Comparison of serotonin and dopamine release in substantia nigra and ventral tegmental area: region and species differences. *J. Neurochem.* 69, 2378–2386.
- Dahlström, A., and Fuxe, K. (1964). Evidence for the existence of monoamine-containing neurons in the central nervous system. Demonstration of monoamines in the cell bodies of brain stem neurons. *Acta Physiol. Scand.* 62, 1–55.
- Deutch, A. Y., Goldstein, M., Baldino, F. Jr., and Roth, R. H. (1988). Telencephalic projections of the A8 dopamine cell group. *Ann. N. Y. Acad. Sci.* 537, 27–50.
- Dodge, F. A. Jr., and Rahamimoff, R. (1967). Cooperative action of calcium ions in transmitter release at the neuromuscular junction. *J. Physiol. (Lond.)* 193, 419–432.
- Fallon, J. H., and Moore, R. Y. (1978). Catecholamine innervation of the basal forebrain. IV. Topography of the dopamine projection to the basal forebrain and neostriatum. *J. Comp. Neurol.* 180, 545–580.
- Ford, C. P., Gantz, S. C., Phillips, P. E., and Williams, J. T. (2010). Control of extracellular dopamine at dendrite and axon terminals. *J. Neurosci.* 30, 6975–6983.
- Fortin, G. D., Desrosiers, C. C., Yamaguchi, N., and Trudeau, L.-E. (2006). Basal somatodendritic dopamine release requires snare proteins. *J. Neurochem.* 96, 1740–1749.
- Geffen, L. B., Jessell, T. M., Cuello, A. C., and Iversen, L. L. (1976). Release of dopamine from dendrites in rat substantia nigra. *Nature* 260, 258–260.
- Groves, P. M., and Linder, J. C. (1983). Dendro-dendritic synapses in substantia nigra: descriptions based on analysis of serial sections. *Exp. Brain Res.* 49, 209–217.
- Hoffman, A. F., and Gerhardt, G. A. (1999). Differences in pharmacological properties of dopamine release between the substantia nigra and striatum: an in vivo electrochemical study. *J. Pharmacol. Exp. Ther.* 289, 455–463.
- Iravani, M. M., Muscat, R., and Kruk, Z. L. (1996). Comparison of somatodendritic and axon terminal dopamine release in the ventral tegmental area and the nucleus accumbens. *Neuroscience* 70, 1025–1037.
- Jaffe, E. H., Marty, A., Schulte, A., and Chow, R. H. (1998). Extrasynaptic vesicular transmitter release from the somata of substantia nigra neurons in rat midbrain slices. *J. Neurosci.* 18, 3548–3553.
- John, C. E., Budygin, E. A., Mateo, Y., and Jones, S. R. (2006). Neurochemical characterization of the release and uptake of dopamine in ventral tegmental area and serotonin in substantia nigra of the mouse. *J. Neurochem.* 9, 267–282.
- Juraska, J. M., Wilson, C. J., and Groves, P. M. (1977). The substantia nigra of the rat: a Golgi study. *J. Comp. Neurol.* 172, 585–600.
- Katz, B., and Miledi, R. (1970). Further study of the role of calcium in synaptic transmission. *J. Physiol.* 207, 789–801.
- Kume-Kick, J., and Rice, M. E. (1998). Dependence of dopamine calibration factors on media Ca²⁺ and Mg²⁺ at carbon-fiber microelectrodes used with fast-scan cyclic voltammetry. *J. Neurosci. Meth.* 84, 55–62.
- Mendez, J. A., Bourque, M. J., Fasano, C., Kortleven, C., and Trudeau, L. E. (2011). Somatodendritic dopamine release requires synaptotagmin 4 and 7 and the participation of voltage-gated calcium channels. *J. Biol. Chem.* (in press).
- Mintz, I. M., Sabatini, B. L., and Regehr, W. G. (1995). Calcium control of transmitter release at a cerebellar synapse. *Neuron* 15, 675–688.
- Nachshen, D. A., and Sanchez-Armass, S. (1987). Co-operative action of calcium ions in dopamine release from rat brain synaptosomes. *J. Physiol. (Lond.)* 387, 415–423.
- Nieoullon, A., Cheramy, A., and Glowinski, J. (1977). Release of DA in vivo from cat substantia nigra. *Nature* 266, 375–377.
- Nirenberg, M. J., Chan, J., Liu, Y., Edwards, R. H., and Pickel, V. M. (1996). Ultrastructural localization of the vesicular monoamine transporter-2 in midbrain dopaminergic neurons: potential sites for somatodendritic storage and release of dopamine. *J. Neurosci.* 16, 4135–4145.
- O'Connor, J. J., and Kruk, Z. L. (1991). Fast cyclic voltammetry can be used to measure stimulated endogenous 5-hydroxytryptamine release in untreated rat brain slices. *J. Neurosci. Meth.* 38, 25–33.
- Patel, J., Trout, S. J., and Kruk, Z. L. (1992). Regional differences in evoked dopamine efflux in brain slices of rat anterior and posterior caudate putamen. *Naunyn Schmiedebergs Arch. Pharmacol.* 346, 267–276.
- Patel, J., Trout, S. J., Palij, P., Whelpton, R., and Kruk, Z. L. (1995). Biphasic inhibition of stimulated endogenous dopamine release by 7-OH-DPAT in slices of rat nucleus accumbens. *Br. J. Pharmacol.* 115, 421–426.
- Patel, J. C., Witkovsky, P., Avshalumov, M. V., and Rice, M. E. (2009). Mobilization of calcium from intracellular stores facilitates somatodendritic dopamine release. *J. Neurosci.* 20, 6568–6579.
- Qian, J., Colmers, W. F., and Saggau, P. (1997). Inhibition of synaptic transmission by neuropeptide Y in rat hippocampal area CA1: modulation of presynaptic Ca²⁺ entry. *J. Neurosci.* 17, 8169–8177.
- Reid, C. A., Bekkers, J. M., and Clements, J. D. (1998). N- and P/Q-type Ca²⁺ channels mediate transmitter release with a similar cooperativity at rat hippocampal autapses. *J. Neurosci.* 18, 2849–2855.
- Rice, M. E., Cragg, S. J., and Greenfield, S. A. (1997). Characteristics of electrically evoked somatodendritic dopamine release in substantia nigra and ventral tegmental area in vitro. *J. Neurophysiol.* 77, 853–862.
- Rice, M. E., Richards, C. D., Nedergaard, S., Hounsgaard, J., Nicholson, C., and Greenfield, S. A. (1994). Direct monitoring of dopamine and 5-HT release in substantia nigra and ventral tegmental area in vitro. *Exp. Brain Res.* 100, 395–406.
- Schneggenburger, R., Meyer, A. C., and Neher, E. (1999). Release fraction and total size of a pool of immediately available transmitter quanta at a calyx synapse. *Neuron* 23, 399–409.
- Schneggenburger, R., and Neher, E. (2000). Intracellular calcium dependence of transmitter release rates at a fast central synapse. *Nature* 406, 889–893.
- Südhof, T. C. (2000). The synaptic vesicle cycle revisited. *Neuron* 28, 317–320.
- Südhof, T. C. (2002). Synaptotagmins: why so many? *J. Biol. Chem.* 277, 7629–7632.
- Südhof, T. C., and Rizo, J. (1996). Synaptotagmins: C2-domain proteins that regulate membrane traffic. *Neuron* 17, 379–388.
- Sugita, S., Shin, O.-H., Han, W., Lao, Y., and Südhof, T. C. (2002a). Synaptotagmins form a hierarchy of exocytotic Ca²⁺ sensors with distinct Ca²⁺ affinities. *EMBO J.* 21, 270–280.
- Sugita, S., Han, W., Butz, S., Liu, X., Fernández-Chacón, R., Lao, Y., and Südhof, T. C. (2002b). Synaptotagmin VII as a plasma membrane Ca²⁺ sensor in exocytosis. *Neuron* 30, 459–473.
- Sun, J., Pang, Z. P., Qin, D., Fahim, A. T., Adachi, R., and Südhof, T. C. (2007). A dual-Ca²⁺-sensor model for neurotransmitter release in a central synapse. *Nature* 450, 676–683.
- Ungerstedt, U. (1971). Stereotaxic mapping of the monoaminergic pathways in the rat brain. *Acta Physiol. Scand. Suppl.* 367, 1–48.
- Wassaf, M., Berod, A., and Sotelo, C. (1981). Dopaminergic dendrites in the pars reticulata of the rat substantia nigra and their striatal input. Combined immunocytochemical localization of tyrosine hydroxylase and anterograde degeneration. *Neuroscience* 6, 2125–2139.
- Wilson, C. J., Groves, P. M., and Fiková, E. (1977). Monoaminergic synapses, including dendro-dendritic synapses in the rat substantia nigra. *Exp. Brain Res.* 30, 161–174.
- Witkovsky, P., Patel, J. C., Lee, C. R., and Rice, M. E. (2009). Immunocytochemical identification of proteins involved in dopamine release from the somatodendritic compartment of nigral dopaminergic neurons. *Neuroscience* 164, 488–496.
- Xu, J., Mashimo, T., and Südhof, T. C. (2007). Synaptotagmin-1, -2, and -9: Ca²⁺-sensors for fast release that specify distinct presynaptic properties in subsets of neurons. *Neuron* 54, 567–581.

Conflict of Interest Statement: The authors declare that the research was conducted in the absence of any commercial or financial relationships that could be construed as a potential conflict of interest.

Received: 15 January 2011; accepted: 23 May 2011; published online: 13 June 2011.
Citation: Chen BT, Patel JC, Moran KA and Rice ME (2011) Differential calcium dependence of axonal versus somatodendritic dopamine release, with characteristics of both in the ventral tegmental area. *Front. Syst. Neurosci.* 5:39. doi: 10.3389/fnsys.2011.00039

Copyright © 2011 Chen, Patel, Moran and Rice. This is an open-access article subject to a non-exclusive license between the authors and Frontiers Media SA, which permits use, distribution and reproduction in other forums, provided the original authors and source are credited and other Frontiers conditions are complied with.



Electrophysiological effects of trace amines on mesencephalic dopaminergic neurons

Ada Ledonne^{1,2}, Nicola Berretta², Alessandro Davoli^{1,2}, Giada Ricciardo Rizzo^{1,2}, Giorgio Bernardi^{1,2} and Nicola Biagio Mercuri^{1,2*}

¹ Università degli Studi di Roma "Tor Vergata," Rome, Italy

² Experimental Neurology Laboratory, Istituto Di Ricovero e Cura a Carattere Scientifico Fondazione Santa Lucia, Rome, Italy

Edited by:

Elizabeth Abercrombie,
Rutgers-Newark The State University
of New Jersey, USA

Reviewed by:

Kuei Y. Tseng, Rosalind Franklin
University of Medicine and Science,
USA
James M. Tepper, Rutgers, The State
University of New Jersey, USA

*Correspondence:

Nicola Biagio Mercuri, Centro Europeo
Ricerca sul Cervello, Via del Fosso di
Fiorano 64 00143, Rome, Italy.
e-mail: mercurin@med.uniroma2.it

Trace amines (TAs) are a class of endogenous compounds strictly related to classic monoamine neurotransmitters with regard to their structure, metabolism, and tissue distribution. Although the presence of TAs in mammalian brain has been recognized for decades, until recently they were considered to be by-products of amino acid metabolism or as "false" neurotransmitters. The discovery in 2001 of a new family of G-protein-coupled receptors (GPCRs), namely trace amine receptors, has re-ignited interest in TAs. In particular, two members of the family, trace amine receptor 1 (TA₁) and trace amine receptor 2 (TA₂), were shown to be highly sensitive to these endogenous compounds. Experimental evidence suggests that TAs modulate the activity of catecholaminergic neurons and that TA dysregulation may contribute to neuropsychiatric disorders, including schizophrenia, attention deficit hyperactivity disorder, depression and Parkinson's disease, all of which are characterized by altered monoaminergic networks. Here we review recent data concerning the electrophysiological effects of TAs on the activity of mesencephalic dopaminergic neurons. In the context of recent data obtained with TA₁ receptor knockout mice, we also discuss the mechanisms by which the activation of these receptors modulates the activity of these neurons. Three important new aspects of TAs action have recently emerged: (a) inhibition of firing due to increased release of dopamine; (b) reduction of D2 and GABA_B receptor-mediated inhibitory responses (excitatory effects due to disinhibition); and (c) a direct TA₁ receptor-mediated activation of GIRK channels which produce cell membrane hyperpolarization. While the first two effects have been well documented in our laboratory, the direct activation of GIRK channels by TA₁ receptors has been reported by others, but has not been seen in our laboratory (Geracitano et al., 2004). Further research is needed to address this point, and to further characterize the mechanism of action of TAs on dopaminergic neurons.

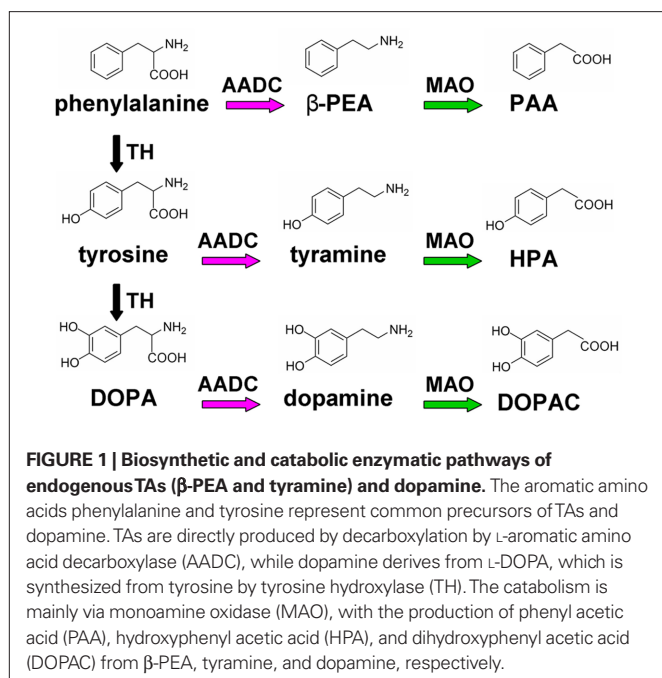
Keywords: dopaminergic neurons, tyramine, β -phenylethylamine, trace amine receptor 1, neuropsychiatric disorders

Trace amines (TAs) are a class of endogenous compounds strictly related to classic monoaminergic neurotransmitters, regarding the structure, metabolic pathways, cellular localization, and tissue distribution (Berry, 2004; Grandy, 2007). The group includes β -phenylethylamine (β -PEA), tyramine (TYR), octopamine (OCT), synephrine (SYN), and tryptamine (TRP). TAs have been identified in several prokaryotic and eukaryotic organisms and in all investigated vertebrate and invertebrate species, including humans (Grandy, 2007). Their distribution in the mammalian brain strictly corresponds to the location of the main monoaminergic nuclei and their projecting areas.

Trace amines and biogenic amines share the same biosynthetic and metabolic pathways (Figure 1). They are produced in monoaminergic neurons from aromatic amino acids L-phenylalanine and tyrosine by amino acid decarboxylase (AADC), and are mainly catabolized by monoamine oxidase (MAO). Although the rates of synthesis are similar, TAs levels in the brain are two orders of magnitude lower than of classic monoaminergic neurotransmitters, most likely due to a rapid turnover, with a half-life of approximately 30 s. Although synaptosomal localization of TAs has been reported (Baldessarini and Vogt, 1972; Boulton and Baker,

1975), the evidence for the existence of specific mechanisms for vesicular storage is still controversial. Recently, both vesicular and non-vesicular release of TAs has been described (Kosa et al., 2000; Grandy, 2007). Due to their highly lipophilic nature (particularly of β -PEA) it is possible that TAs are mainly released from axon terminals by diffusion across the cell membrane, and that their levels reflect an equilibrium between synthesis and catabolism (Berry, 2004).

In invertebrates, TAs act as neurotransmitters to control a variety of physiological functions, including locomotion, feeding, and learning-associated behaviors (Roeder, 2005; Sotnikova et al., 2008). In contrast, in the mammalian brain the physiological role and the mechanisms of action of TAs remain poorly understood. They have been often regarded as by-products of amino acid metabolism with no clear functional relevance. TAs have also been considered to act as "false" neurotransmitters, due to their ability to release catecholamines in amphetamine-like manner, *via* their displacement from synaptic vesicles and a reversal of plasma membrane transporters. It could be possible that by emptying synaptic vesicles (but with no affinity to monoaminergic receptors), TAs could produce, in the long run, a weakening of monoaminergic transmission.



Recently, altered brain TAs levels have been reported in several neuropsychiatric disorders, including schizophrenia, attention deficit hyperactivity disorder (ADHD), depression, and Parkinson's disease (PD), suggesting the involvement of these amines in pathophysiology of monoaminergic systems (Branchek and Blackburn, 2003; Burchett and Hicks, 2006).

Interest in TAs has been re-ignited following the discovery, in 2001, of a novel class of G-protein-coupled receptors (GPCRs) that can be activated by these amines (Borowsky et al., 2001; Bunzow et al., 2001). The family of these "trace amine-associated receptors" (TAARs) consists of 15 members. However, only two, "trace amine receptor 1" (TA₁) and "trace amine receptor 2" (TA₂) (Maguire et al., 2009) were shown to be sensitive to TAs. TA₁, the best characterized receptor subtype, is coupled to G_s protein and exerts its intracellular effect by activation of the adenylyl cyclase (Borowsky et al., 2001; Bunzow et al., 2001).

Trace amine receptor 1 receptors are distributed in the CNS mainly in the monoaminergic systems, including mesencephalic dopaminergic (DAergic) neurons, where they are co-localized with dopamine (DA) transporter, DAT (Xie et al., 2007). However, the physiological role of TA₁ receptors in the CNS in general, and in mesencephalic DAergic neurons in particular, is still not known. Recent studies suggest that these receptors modulate monoaminergic transmission (Sotnikova et al., 2008; Xie and Miller, 2009) by acting on monoamine transporters (e.g., DAT) and/or by directly affecting neuronal firing (Lindemann et al., 2008; Bradaia et al., 2009; Revel et al., 2011).

In addition to the TA₁ receptor-mediated effects, other cellular mechanisms by which TAs affect the activity of monoaminergic neurons have been described. It has been reported that TAs can activate sigma (σ) receptors which inhibit K⁺ and Ca²⁺ ion channels (Nguyen et al., 1998; Zhang and Cuevas, 2002). In addition, in invertebrates TAs activate ligand-gated chloride channels (Pirri

et al., 2009; Ringstad et al., 2009), suggesting that these endogenous compounds may modulate neuronal activity by triggering rapid ionic events also in vertebrates (Branicky and Schafer, 2009).

The first electrophysiological investigation of the effects of TAs on DAergic neuronal activity was an extracellular study conducted in midbrain slices by Pinnock (1983). He demonstrated an inhibitory effect of TYR and OCT on firing of DAergic neurons in the *Substantia nigra* pars compacta (SNpc). A similar inhibitory effect was demonstrated for β-PEA in extracellular recordings conducted from the same group of neurons *in vivo* (Rodriguez and Barroso, 1995). Intravenous applications of this amine (0.4–3.4 mg/kg) evoked a rapid but short-lasting (2–4 min) reduction in the firing frequency and in the occurrence of bursting.

Trace amines-induced inhibitory effect on firing of SNpc DAergic neurons has been further characterized in our laboratory (Geracitano et al., 2004). Using intracellular recordings with sharp microelectrodes in rat midbrain slices, we have demonstrated that TAs reduce the spontaneous firing rate of these neurons in a reversible and concentration-dependent manner (Figure 2A). The inhibitory effect was mediated by indirect activation of somatodendritic D2 autoreceptors (D2 receptors located on DAergic neurons), consequent to increased DA release (Figure 2B). In particular, TAs-induced efflux of newly synthesized DA from reserpine-insensitive pools, through a mechanism involving both the membrane transporter-dependent and -independent mechanisms (Geracitano et al., 2004). More recent electrophysiological data demonstrated that TYR releases DA and indirectly activates D2 receptors also in subthalamic neurons (Zhu et al., 2007).

Trace amines can also modulate the activity of DAergic mesencephalic neurons by a direct action on TA₁ receptors. Patch-clamp recordings of ventral tegmental area (VTA) DAergic neurons in mice with a knockout of TA₁ receptors (TA₁ KO mice) have demonstrated that these neurons have a higher spontaneous firing rate than in wild-type littermates (Lindemann et al., 2008; Bradaia et al., 2009). The increased firing rate of VTA neurons in TA₁ KO mice supports the contention that, under normal conditions, there is a tonic inhibitory effect of TAs on DAergic neuron activity exerted through TA₁ receptors. The inhibitory effect of TYR was not present in TA₁ KO mice, further indicating that the slower firing in wild-type animals is mediated by constitutive activation of TA₁ receptors by TAs (Lindemann et al., 2008). This was confirmed by using a selective TA₁ receptor antagonist, *N*-(3-Ethoxyphenyl)-4-pyrrolidin-1-yl-3-trifluoromethyl-benzamide (EPPTB) that increased firing frequency of DAergic neurons in the VTA of wild-type mice, but not in TA₁ KO mice (Bradaia et al., 2009). The latter study also demonstrated that TYR inhibits firing of these neurons by activation of TA₁ receptors linked to G-protein-gated inwardly rectifying K⁺ channels (GIRK channels; also known as Kir3) and additional experiments performed with heterologously expressed receptor and channel proteins in *Xenopus* oocytes showed that the TA₁-induced GIRK channel activation involves a PTX-insensitive, G-protein-dependent mechanism (most likely G_s; Bradaia et al., 2009).

Trace amines modify neuronal responses to classic neurotransmitters, and thus exert neuromodulatory effects. Electrophysiological recordings conducted in our laboratory with sharp microelectrodes from SNpc DAergic neurons in midbrain slices revealed

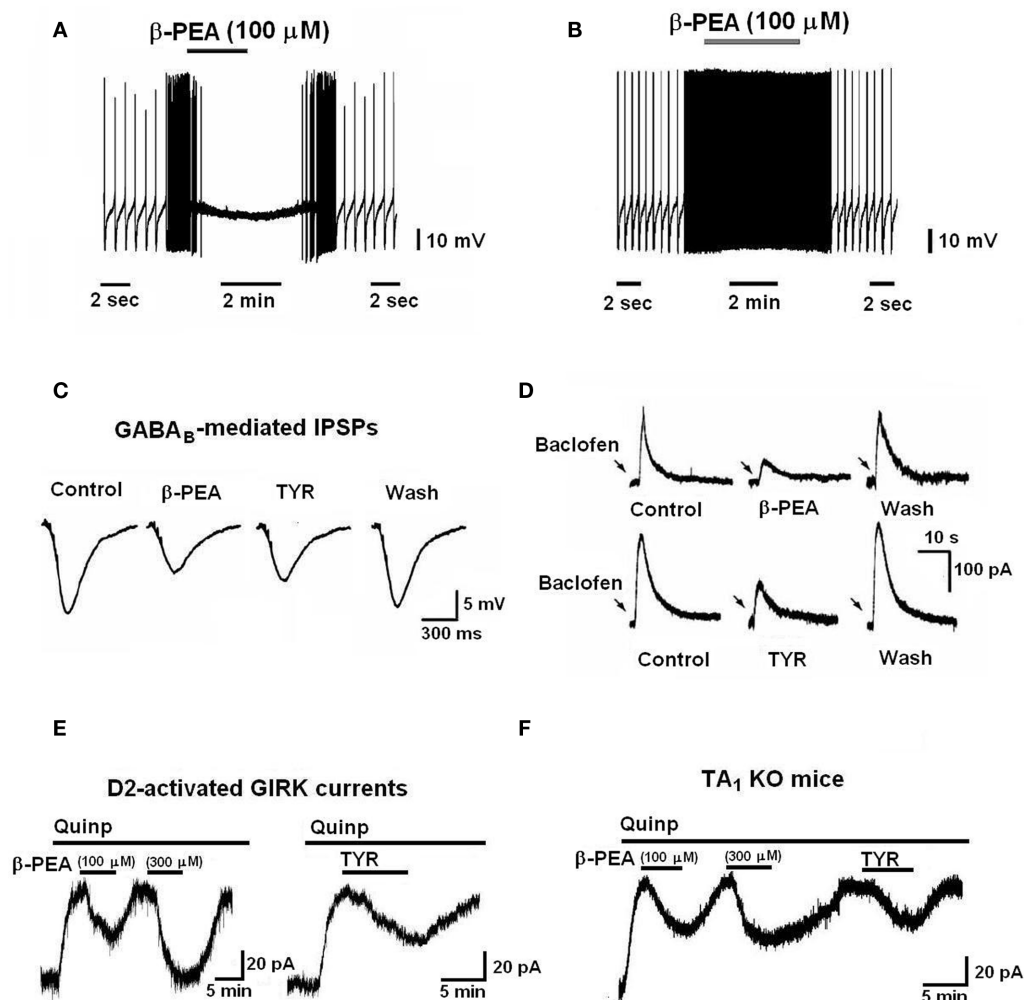


FIGURE 2 | Electrophysiological effects of TAs on mesencephalic dopaminergic neurons. (A) β -PEA produces a reversible hyperpolarization and inhibition of spontaneous firing in mesencephalic dopaminergic neurons. (B) The TAs-induced inhibition of firing is mediated by indirect activation of D2 autoreceptors, subsequent to the release of newly synthesized dopamine. The effect was absent in dopaminergic neurons treated with an inhibitor of DA synthesis (carbidopa, 300 μ M for 30 min) and was blocked by a D2 receptor antagonist, sulpiride (1 μ M; data not shown). (C) The amplitude of electrically evoked inhibitory postsynaptic potentials (IPSPs) mediated by

GABA_B receptors is reduced by bath application of β -PEA (100 μ M) and TYR (100 μ M). (D) TAs reduce the outward currents produced by pressure application of the GABA_B agonist, baclofen (arrows) in a reversible manner. (E) Negative modulatory effects of TAs on the D2-autoreceptors-mediated responses. The quinpirole-induced GIRK channel activation is reduced by both β -PEA and TYR in a reversible and concentration-dependent manner. (F) The D2/GIRK-mediated outward current evoked by TAs is not mediated by the activation of TA₁ receptors, since it was present in TA₁ receptor knockout mice.

that TAs reduce GABAergic inhibitory neurotransmission to these neurons (Federici et al., 2005). In particular, both β -PEA and TYR, in micromolar concentrations, depressed the amplitude of electrically evoked inhibitory postsynaptic potentials (IPSPs) mediated by GABA_B receptors (Figure 2C), without modifying the GABA_A-evoked synaptic responses (Federici et al., 2005). Moreover, the cellular responses (hyperpolarization/outward current) evoked by the stimulation of postsynaptic GABA_B receptors with a GABA_B agonist baclofen were reduced by both β -PEA and TYR (Figure 2D). The TAs-induced depression of GABA_B-mediated outward currents (involving GIRK channels) was neither dependent on protein kinases activity, nor on changes in the intracellular Ca²⁺ levels (Federici et al., 2005).

Trace amines also reduce GABA_B-mediated responses at the presynaptic level. It is known that the inhibitory synaptic input to midbrain DAergic neurons mediated by GABA involves not only activation of postsynaptic GABA_A receptors, but also presynaptic GABA_B receptors which reduce GABA release (Giustizieri et al., 2005). We have reported that both β -PEA and TYR antagonize the GABA_B-dependent presynaptic inhibition of GABAergic inputs to SNpc DAergic neurons, by limiting the inhibitory effect of baclofen on the frequency of the spontaneous inhibitory postsynaptic currents (GABA_A-induced sIPSCs; Berretta et al., 2005).

In addition, TAs have a neuromodulatory effect on the postsynaptic responses mediated by D2 receptors in DAergic neurons. Using conventional intracellular and single-electrode voltage-clamp

recordings from SNpc DAergic neurons, we have demonstrated that cell membrane hyperpolarization/outward current induced by quinpirole (a D2 receptor agonist) is reduced by concomitant application of β -PEA and TYR (Ledonne et al., 2010). The effect was reversible and concentration-dependent (Figure 2E). In an attempt to characterize the mechanisms underlying the inhibition of quinpirole-induced responses, we found that TAs effects were not mediated by TA_1 (Figure 2F) and sigma (σ) receptors, nor were dependent on G-protein activation. Furthermore, inhibitory effects of TAs on D2 receptor-mediated responses could not be demonstrated in *Xenopus* oocytes expressing both D2 receptors and GIRK channel (Ledonne et al., 2010). The latter results suggest that the inhibitory effect of TAs on DAergic neurons depends on the activation of not yet identified neuron-specific sites.

All these results indicate that TAs control the activity of DAergic mesencephalic neurons through a complex mechanism that involves both indirect and direct inhibitory effects. Indirect effects are due to DA release through a reversal of DAT function, and possibly by a non-DAT-mediated mechanism. This causes an strengthening of DAergic inhibition mediated by somatodendritic D2 receptors (Geracitano et al., 2004). Direct inhibitory effects depend on activation of TA_1 receptors. The results obtained by others in TA_1 KO mice and using specific antagonists of these receptors indicated that TAs tonically inhibit the activity of DAergic VTA neurons (Bradaia et al., 2009; Revel et al., 2011). However, we could not see a direct inhibitory effect of TA in SNpc and VTA neurons in our experiments. A part the technical differences in recording the dopaminergic cells (intracellular versus patch-clamp) we do not have a suitable explanation to account for the discrepancy between these and our results.

REFERENCES

- Baldessarini, R. J., and Vogt, M. (1972). Regional release of aromatic amines from tissues of the rat brain in vitro. *J. Neurochem.* 19, 755–761.
- Berretta, N., Giustizieri, M., Bernardi, G., and Mercuri, N. B. (2005). Trace amines reduce GABA_B receptor-mediated presynaptic inhibition at GABAergic synapses of the rat substantia nigra pars compacta. *Brain Res.* 1062, 175–178.
- Berry, M. D. (2004). Mammalian central nervous system trace amines. Pharmacological amphetamines, physiological neuromodulators. *J. Neurochem.* 90, 257–271.
- Borowsky, B., Adham, N., Jones, K. A., Raddatz, R., Artyushyn, R., Ogozalek, K. L., Durkin, M. M., Lakhlani, P. P., Bonini, J. A., Pathirana, S., Boyle, N., Pu, X., Kouranova, E., Lichtblau, H., Ochoa, F. Y., Branchek, T. A., and Gerald, C. (2001). Trace amines: identification of a family of mammalian G protein-coupled receptors. *Proc. Natl. Acad. Sci. U.S.A.* 98, 8966–8971.
- Boulton, A. A., and Baker, G. B. (1975). The subcellular distribution of β -phenylethylamine, p-tyramine and tryptamine in rat brain. *J. Neurochem.* 25, 477–481.
- Bradaia, A., Trube, G., Stalder, H., Norcross, R. D., Ozmen, L., Wettstein, J. G., Pinard, A., Buchy, D., Gassmann, M., Hoener, M. C., and Bettler, B. (2009). The selective antagonist EPPTB reveals TAAR1-mediated regulatory mechanisms in dopaminergic neurons of the mesolimbic system. *Proc. Natl. Acad. Sci. U.S.A.* 106, 20081–20086.
- Branchek, T. A., and Blackburn, T. P. (2003). Trace amines receptors as target for novel therapeutics: legend, myth and fact. *Curr. Opin. Pharmacol.* 3, 90–97.
- Branicky, R., and Schafer, W. R. (2009). Tyramine: a new receptor and a new role at the synapse. *Neuron* 62, 458–460.
- Bunzow, J. R., Sonders, M. S., Arttamangkul, S., Harrison, L. M., Zhang, G., and Quigley, D. I., Darland, T., Suchland, K. L., Pasumamula, S., Kennedy, J. L., Olson, S. B., Magenis, R. E., Amara, S. G., and Grandy, D. K. (2001). Amphetamine, 3,4-methylenedioxymethamphetamine, lysergic acid diethylamide, and metabolites of the catecholamine neurotransmitters are agonists of a rat trace amine receptor. *Mol. Pharmacol.* 60, 1181–1188.
- Burchett, S. A., and Hicks, T. P. (2006). The mysterious trace amines: protean neuromodulators of synaptic transmission in mammalian brain. *Prog. Neurobiol.* 79, 223–246.
- Calabresi, P., Picconi, B., Tozzi, A., and Di Filippo, M. (2007). Dopamine-mediated regulation of corticostriatal synaptic plasticity. *Trends Neurosci.* 30, 211–219.
- Federici, M., Geracitano, R., Tozzi, A., Longone, P., Di Angelantonio, S., Bengtson, C. P., Bernardi, G., and Mercuri, N. B. (2005). Trace amines depress GABA_B response in dopaminergic neurons by inhibiting G $\beta\gamma$ -gated inwardly rectifying potassium channels. *Mol. Pharmacol.* 67, 1283–1290.
- Geracitano, R., Federici, M., Prisco, S., Bernardi, G., and Mercuri, N. B. (2004). Inhibitory effects of trace amines on rat midbrain dopaminergic neurons. *Neuropharmacology* 46, 807–814.
- Giustizieri, M., Bernardi, G., Mercuri, N. B., and Berretta, N. (2005). Distinct mechanisms of presynaptic inhibition at GABAergic synapses of the rat substantia nigra pars compacta. *J. Neurophysiol.* 94, 1992–2003.
- Grandy, D. K. (2007). Trace amine-associated receptor 1-Family arche-type or iconoclast? *Pharmacol. Ther.* 116, 355–390.
- Kosa, E., Marcilhac-Flouriot, A., Fache, M. P., and Siaud, P. (2000). Effects of beta phenylethylamine on the hypothalamo-pituitary-adrenal axis in the male rat. *Pharmacol. Biochem. Behav.* 67, 527–535.
- Kreitzer, A. C., and Malenka, R. C. (2008). Striatal plasticity and basal ganglia circuit function. *Neuron* 60, 543–554.
- Ledonne, A., Federici, M., Giustizieri, M., Pessia, M., Imbrici, P., Millan, M. J., Bernardi, G., and Mercuri, N. B. (2010). Trace amines depress D2-autoreceptor-mediated responses on midbrain dopaminergic cells. *Br. J. Pharmacol.* 160, 1509–1520.
- Lindemann, L., Meyer, C. A., Jeanneau, K., Bradaia, A., Ozmen, L., Bluethmann, H., Bettler, B., Wettstein, J. G., Borroni, E., Moreau, J. L., and Hoener, M. C. (2008). Trace amine-associated receptor 1 modulates dopaminergic activity. *J. Pharmacol. Exp. Ther.* 324, 948–956.
- Maguire, J. J., Parker, W. A., Foord, S. M., Bonner, T. A., Neubig, R. R., and Davenport, A. P. (2009). International Union of Pharmacology. LXXII. Recommendations for trace amine receptor nomenclature. *Pharmacol. Rev.* 61, 1–8.

ACKNOWLEDGMENT

The authors are grateful to Dr. Janusz Lipsky for the advices in correcting and modifying the manuscript.

- Nguyen, V. H., Ingram, S. L., Kassiou, M., and Christie, M. J. (1998). σ -Binding sites ligands inhibit K^+ currents in rat locus coeruleus neurons in vitro. *Eur. J. Pharmacol.* 361, 157–163.
- Pinnock, R. D. (1983). Sensitivity of compacta neurones in the rat substantia nigra slice to dopamine agonists. *Eur. J. Pharmacol.* 96, 269–276.
- Pirri, J. K., McPherson, A. D., Donnelly, J. M., Francis, M. M., and Alkema, M. J. (2009). A tyramine-gated chloride channel coordinates distinct motor programs of a *Caenorhabditis elegans* escape response. *Neuron* 62, 526–538.
- Revel, F. G., Moreau, J. L., Gainetdinov, R. R., Bradaia, A., Sotnikova, T. D., Mory, R., Durkin, S., Zbinden, K. G., Norcross, R., Meyer, C. A., Metzler, V., Chaboz, S., Ozmen, L., Trube, G., Pouzet, B., Bettler, B., Caron, M. G., Wettstein, J. G., and Hoener, M. C. (2011). TAAR1 activation modulates monoaminergic neurotransmission, preventing hyperdopaminergic and hypoglutamatergic activity. *Proc. Natl. Acad. Sci. U.S.A.* 108, 8485–8490.
- Ringstad, N., Abe, N., and Horvitz, R. (2009). Ligand gated chloride channels are receptors for biogenic amines in *C. elegans*. *Science* 325, 96–100.
- Rodriguez, M., and Barroso, N. (1995). β -Phenylethylamine regulation of dopaminergic nigrostriatal cell activity. *Brain Res.* 703, 201–204.
- Roeder, T. (2005). Tyramine and octopamine: ruling behaviour and metabolism. *Annu. Rev. Entomol.* 50, 447–477.
- Sotnikova, T. D., Zorina, O. I., Ghisi, V., Caron, M. G., and Gainetdinov, R. R. (2008). Trace amine associated receptor 1 and movement control. *Parkinsonism. Relat. Disord.* 14, 99–102.
- Xie, Z., and Miller, G. M. (2009). Trace amine-associated receptor 1 as a monoaminergic modulator in brain. *Biochem. Pharmacol.* 78, 1095–1104.
- Xie, Z., Westmoreland, S. V., Bahn, M. E., Chen, G., Yang, H., Vallender, E., Yao, W. D., Madras, B. K., and Miller, G. M. (2007). Rhesus monkey trace amine-associated receptor 1 signaling: enhancement by monoamine transporters and attenuation by D2 autoreceptor in vitro. *J. Pharmacol. Exp. Ther.* 321, 116–127.
- Zhang, H., and Cuevas, J. (2002). Sigma receptors inhibit high-voltage activated calcium channels in rat sympathetic and parasympathetic neurons. *J. Neurophysiol.* 87, 2867–2879.
- Zhu, Z. T., Munhall, A. C., and Johnson, S. W. (2007). Tyramine excites rat subthalamic neurons in vitro by a dopamine-dependent mechanism. *Neuropharmacology* 52, 1169–1178.
- conducted in the absence of any commercial or financial relationships that could be construed as a potential conflict of interest.

Received: 31 January 2011; paper pending published: 27 March 2011; accepted: 16 June 2011; published online: 04 July 2011.

Citation: Ledonne A, Berretta N, Davoli A, Rizzo GR, Bernardi G and Mercuri NB (2011) Electrophysiological effects of trace amines on mesencephalic dopaminergic neurons. *Front. Syst. Neurosci.* 5:56. doi: 10.3389/fnsys.2011.00056

Copyright © 2011 Ledonne, Berretta, Davoli, Rizzo, Bernardi and Mercuri. This is an open-access article subject to a non-exclusive license between the authors and Frontiers Media SA, which permits use, distribution and reproduction in other forums, provided the original authors and source are credited and other Frontiers conditions are complied with.

Conflict of Interest Statement: The authors declare that the research was



The role of BDNF/TrkB signaling in acute amphetamine-induced locomotor activity and opioid peptide gene expression in the rat dorsal striatum

Jacqueline F. McGinty^{1*}, Alexandra J. Bache², Nortorious T. Coleman¹ and Wei-Lun Sun¹

¹ Department of Neurosciences, Medical University of South Carolina, Charleston, SC, USA

² Department of Psychology, College of Charleston, Charleston, SC, USA

Edited by:

Elizabeth Abercrombie, Rutgers – Newark: The State University of New Jersey, USA

Reviewed by:

Kristen Ashley Horner, Mercer University School of Medicine, USA
Kristen Keefe, University of Utah, USA

*Correspondence:

Jacqueline F. McGinty, Department of Neurosciences, Medical University of South Carolina, 173 Ashley Avenue MSC 510, Charleston, SC 29425, USA.
e-mail: mcginty@musc.edu

Exposure to psychostimulants increases brain-derived neurotrophic factor (BDNF) mRNA and protein levels in the cerebral cortex and subcortical structures. Because BDNF is co-localized with dopamine and glutamate in afferents to the striatum of rats, it may be co-released with those neurotransmitters upon stimulation. Further, there may be an interaction between the intracellular signaling cascades activated by dopamine, glutamate, and TrkB receptors in medium spiny striatal neurons. In the present study, the effect of acute amphetamine administration on TrkB phosphorylation, as an indirect indicator of activation, and striatal gene expression, was evaluated. In Experiment 1, 15 min or 2 h after a single saline or amphetamine (2.5 mg/kg, i.p.) injection, the caudate-putamen (CPU), nucleus accumbens (NAc), and dorsomedial prefrontal cortex (dmPFC) were extracted and processed for phospho (p)-TrkB immunoreactivity. Immunoprecipitation analyses indicated that neither the tyrosine phosphorylation (p-Tyr) or autophosphorylation sites of TrkB (706) were changed in NAc, CPU, or dmPFC 15 min after amphetamine administration. In contrast, p-Tyr and the PLC γ phosphorylation site of TrkB (816) were increased in the NAc and CPU 2 h after amphetamine. In Experiment 2, intra-striatal infusion of the tyrosine kinase inhibitor, K252a, increased amphetamine-induced vertical activity but not total distance traveled. In addition, K252a inhibited amphetamine-induced preprodynorphin, but not preproenkephalin, mRNA expression in the striatum. These data indicate that acute amphetamine administration induces p-TrkB activation and signaling in a time- and brain region-dependent manner and that TrkB/BDNF signaling plays an important role in amphetamine-induced behavior and striatal gene expression.

Keywords: dynorphin, enkephalin, neurotrophic factors, phosphorylation, psychostimulants, striatum, TrkB receptors

INTRODUCTION

Amphetamine (AMPH) triggers behavioral activation and gene expression in the striatum by integrating dopamine and glutamate inputs to medium spiny neurons (MSNs) that project to the dorsal and ventral pallidum and ventral midbrain. Activation of genes/proteins that mediate or temper the psychomotor response to stimulants is triggered primarily by D1 dopamine–Gs-coupled-PKA signaling (McGinty et al., 2008). However, dopamine and glutamatergic afferents to the striatum also express brain-derived neurotrophic factor (BDNF) that activates TrkB receptors present on all MSNs (Freeman et al., 2003). Thus, there is a potential interaction between dopamine, glutamate, and BDNF/TrkB signaling in the behavioral and neurochemical response to AMPH. Overlapping signaling cascades activated by these MSN inputs suggest that the striatum responds to an initial, moderate dose of AMPH with a complex repertoire that both mediates psychomotor effects and simultaneously functions to bring the network back to homeostasis. Thus, we investigated the regulation and function of TrkB activation in the response of MSNs to acute AMPH.

AMPH activates the extracellular signal-regulated kinase (ERK)/mitogen-activated protein kinase (ERK MAPK) cascade that leads to CREB phosphorylation and striatal opioid peptide expression

(McGinty et al., 2008). Because D1 receptors are positively coupled to adenylate cyclase, it had been assumed that the cAMP/PKA cascade is sufficient for CaCRE-mediated gene expression subsequent to CREB phosphorylation by dopaminergic agonists. In MSNs, CREB is phosphorylated in response to dopaminergic (Cole et al., 1995; Simpson et al., 1995) and glutamatergic signals (Vanhoutte et al., 1999). In dissociated striatal cultures, CREB phosphorylation and Fos immunoreactivity induced by dopamine, the D1 dopamine agonist, SKF82958, or forskolin, is blocked by NMDA receptor antagonists (Konradi et al., 1996; Valjent et al., 2005). Therefore, phospho-CREB is thought to integrate dopaminergic and glutamatergic signals that modulate the cAMP response element (CRE)-mediated expression of target genes, such as c-fos and opioid peptides, in these neurons. CREB is also a common phosphorylation target of all three pathways activated by neurotrophins: the ERK MAPK, phosphoinositol-3 kinase (PI-3K), and phospholipase C γ (PLC γ) signaling cascades (Patapoutian and Reichardt, 2001).

Brain-derived neurotrophic factor/TrkB signaling is critical for activity-dependent synaptic plasticity, the cellular basis of learning and memory, and neuroadaptations underlying drug seeking (Rattiner et al., 2004; Ou and Gean, 2006; Russo et al.,

2008; McGinty et al., 2010). The normal striatum contains little BDNF mRNA; instead it receives extensive projections from the substantia nigra and cortical pyramidal neurons that synthesize BDNF and transport the protein anterogradely to be released in an action potential and calcium-dependent manner (Sauer et al., 1994; Seroogy et al., 1994; Altar et al., 1997). The biological effects of BDNF are primarily mediated by the tropomyosin kinase receptor, TrkB (Chao, 2003), which is abundantly expressed in cortical pyramidal neurons, ventral midbrain dopamine neurons, and GABAergic striatal MSNs (Numan and Seroogy, 1999; Freeman et al., 2003). Furthermore, BDNF directly stimulates opioid peptide gene expression, as exogenous BDNF infused into the striatum (Sauer et al., 1994) or substantia nigra (Arenas et al., 1996) increases the expression of striatal MSN peptides. Conversely, BDNF deficient mice express less opioid peptide mRNA in the striatum (Saylor et al., 2006) and exhibit more prolonged hyperlocomotor activity following acute amphetamine exposure (Saylor and McGinty, 2008).

Because AMPH stimulates dopamine and glutamate transmission in these pathways, BDNF is also likely to be released and may contribute to AMPH-induced changes in striatal signaling. Direct measurement of BDNF release is problematic; however, evidence of BDNF binding to and activation of TrkB receptors can be indirectly measured by the degree of TrkB phosphorylation (Poo, 2001). Further, BDNF mRNA levels positively correlate with activity in the cerebral cortex (Rocamora, et al., 1996; Poo, 2001) and BDNF mRNA increases in many cortical areas after injection of acute cocaine or amphetamines (Le Foll, et al., 2005; Saylor and McGinty, 2008). Since BDNF regulates the constitutive expression of MSN opioid peptides, AMPH-induced opioid gene expression is dependent on ERK activation, and BDNF modifies reward-related behaviors, we have begun to investigate whether or not BDNF/TrkB signaling contributes to AMPH-induced behavioral activity and striatal signaling.

MATERIALS AND METHODS

ANIMALS AND DESIGN

All procedures were carried out in accordance with the National Institutes of Health Guide for Care and Use of Laboratory Animals (NIH Publications No. 8023, revised 1996) and were approved by the Institutional Animal Care Committee of MUSC. Adult male Sprague-Dawley rats (250–275 g; Charles River, Raleigh, NC, USA) were individually housed under standard conditions (12 h light–dark cycle; food and water *ad libitum*). All animals were handled daily for 5 days. On day 6, the rats were randomly assigned to treatment groups. In Experiment 1, the rats were injected i.p. with 2.5 mg/kg D-amphetamine sulfate (NIDA Res Triangle Institute, NC, USA) or saline. Fifteen minutes or 2 h after injection, the rats were decapitated and the PFC, nucleus accumbens (NAc), and caudate–putamen (CPu) were dissected out for immunoblotting procedures.

In Experiment 2, on the sixth day, rats were anesthetized with an equithesin/ketamine cocktail and intracranial guide cannulae were implanted bilaterally into the dorsal striatum as described (Shi and McGinty, 2006). Rats recovered and were handled for 5 days following surgery. On the test day, rats were habituated to photocell chambers (Accuscan Instruments, Inc., Columbus, OH,

USA). At the end of 1 h habituation, the striatum was infused bilaterally with 1 μ l of 35.7 mM K252a (a non-selective kinase inhibitor with high affinity for Trk receptors-Biomol) or 50% DMSO vehicle (veh) at a rate of 0.25 μ l/min. The dose of K252a was based on effective intracranial infusions in published studies (Ou and Gean, 2006; Whitfield, et al., 2011). After the infusions, rats were put back into the photocell chambers until they received an i.p. injection of AMPH (2.5 mg/kg) or 1 ml/kg saline (sal) 20 min later. Behavioral activity was recorded for 3 h (based on peak opioid peptide mRNA response to AMPH; Wang et al., 1995) after the i.p. injections. Immediately after behavioral testing, the rats were anesthetized with equithesin and decapitated. Brains were dissected and frozen for *in situ* hybridization histochemistry.

WESTERN BLOTTING

Tissue was homogenized in lysis buffer with protein phosphatase inhibitor mixtures. The protein concentration was measured with BCA assay. Equal amount of proteins (15 μ g) were resolved using 6% SDS-PAGE and transferred to a nitrocellulose membrane. The membrane was blocked with 5% milk/TBST and probed with rabbit primary antiserum against TrkB, phospho-tyrosine (p-Tyr), p-TrkB 706 (Cell Signaling Technology, Inc.), or p-TrkB 816 (gift of Dr. Moses Chao, NYU) overnight at 4°C. For total TrkB, the intensity of each protein sample was normalized by calnexin (Stressgen Bioreagents). After a series of washing, membranes were incubated with HRP-conjugated anti-goat secondary antibody, the immunoreactive bands on the membrane were detected by ECL+ chemiluminescence reagents on a X-ray film. Membranes were re-probed with calnexin after stripping. Integrated density values were measured for individual bands using Image J software.

IMMUNOPRECIPITATION

The procedure for immunoprecipitation has been described previously (Sun et al., 2009). Briefly, 200 μ g of sample was incubated with TrkB antibody and protein A agarose beads. After washing with lysis buffer, Laemmli sample buffer was added to the collected beads and boiled for 5 min. Equal amount of samples was loaded and subjected to western blotting. Membranes were probed with p-Tyr, p-TrkB 706, p-TrkB 816, or TrkB antisera. Five percent of total homogenates was used as input to normalize band intensities.

MOTOR ACTIVITY RECORDING

Horizontal activity (total distance traveled) and vertical activity (rearing) were monitored for 3 h in photocell chambers (Accuscan Instruments, USA). Beam breaks were recorded continuously and clustered in 5 min bins by a PC running VersaMax/Digiscan System Software (Accuscan Instruments, Inc.).

IN SITU HYBRIDIZATION HISTOCHEMISTRY

Brains were cut at 12 μ m through the striatum and mounted on slides. Adjacent sections were processed for Nissl-staining to detect cannula tracks and *in situ* hybridization histochemistry as previously described (Shi and McGinty, 2006). Briefly, the sections were fixed in buffered 4% paraformaldehyde and pre-hybridized to minimize non-specific binding. Sections were hybridized with a 48-mer ³⁵S-dATP- or ³³P-dATP-labeled oligonucleotide encoding preprodynorphin (PPD) or preproenkephalin (PPE), washed,

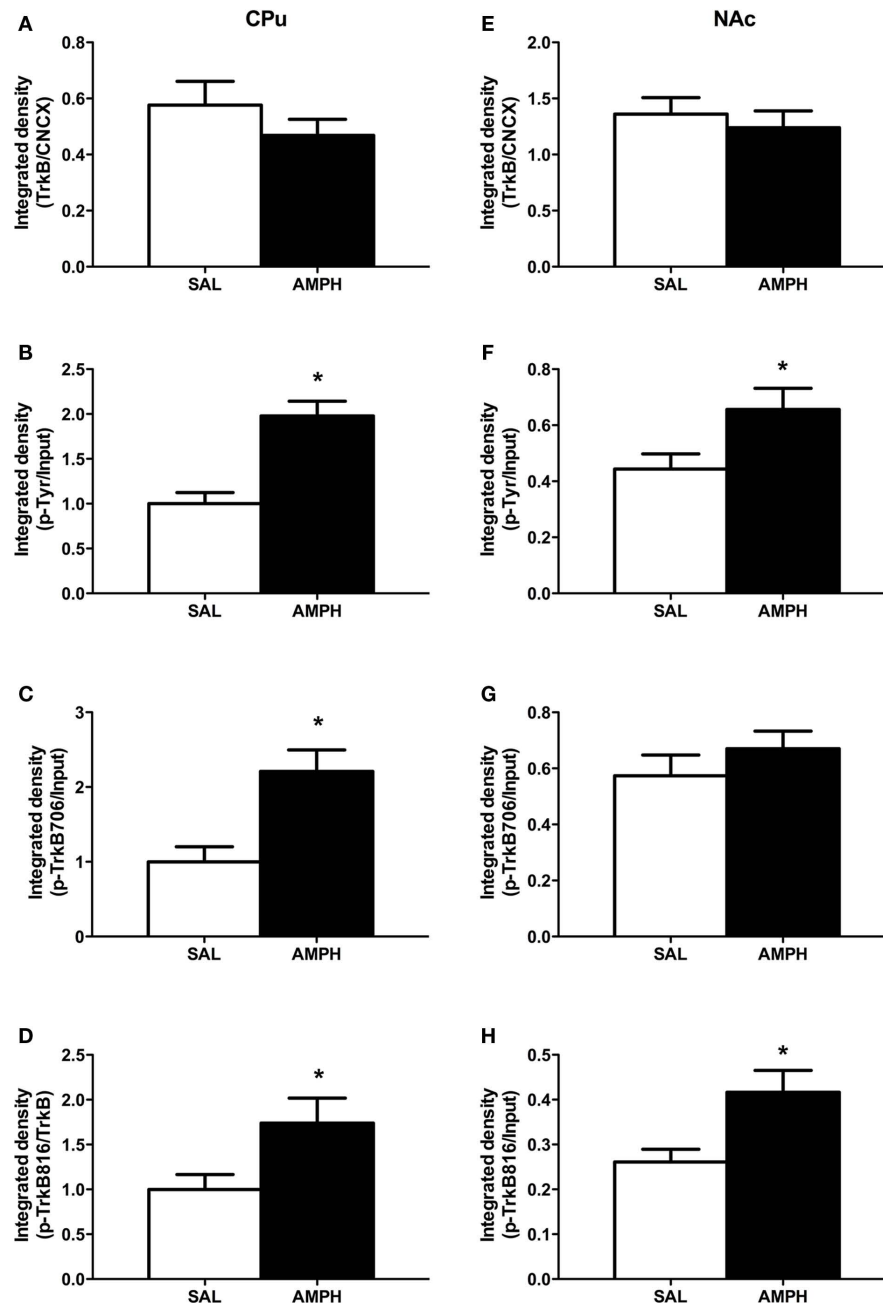


FIGURE 1 | Two hours after a single AMPH injection, TrkB phosphorylation is increased. (A) Total TrkB receptor protein level in the CPU was not altered, **(B)** tyrosine phosphorylation of TrkB (p-Tyr) was increased in the CPU, **(C)** autophosphorylation of TrkB (p-TrkB 706) was increased in the CPU, **(D)** PLC γ phosphorylation site of TrkB (p-TrkB 816) was increased in the CPU, **(E)** total TrkB

receptor protein level in the NAc was not altered, **(F)** tyrosine phosphorylation of TrkB (p-Tyr) was increased in the NAc, **(G)** autophosphorylation of TrkB (p-TrkB 706) was not increased in the NAc, **(H)** PLC γ phosphorylation site of TrkB (p-TrkB 816) was increased in the NAc, * $p < 0.05$ when compared to saline-treated group indicated by mean \pm SEM. $N = 6/\text{group}$.

and dried before putting the slides on X-ray film and exposing for 1–4 weeks. The integrated density of the hybridization signals on three adjacent sections per brain was quantified by NIH Image analysis after subtracting white matter background. Under the density slice option, the hybridization signal in the entire dorsal striatum in the injected side was measured using a circle (200 pixel diameter) as described (Wang and McGinty, 1995).

STATISTICAL ANALYSIS

Behavioral data were analyzed by calculating the area under the curve (AUC) for the activity counts plotted against time followed by a mixed factor analysis of variance (ANOVA). For the hybridization data, a mixed factor nested ANOVA was performed on the integrated density values collected from three adjacent sections per rat. For Western blot data (Experiment 1), a two-tailed t -test was performed on

integrated density values. When an ANOVA *F*-ratio was significant, multiple comparisons were made using a Student-Newman-Keuls test. Independent *t*-tests were used to analyze the difference between groups. Results were determined to be significant when $p < 0.05$.

RESULTS

EXPERIMENT 1: AMPH INCREASED TRKB PHOSPHORYLATION IN THE STRIATUM IN A DELAYED MANNER

Fifteen minutes after a single AMPH injection, neither total or phospho-TrkB receptor protein levels in the dorsomedial prefrontal cortex (dmPFC), NAc, and CPu were altered (data not shown). In contrast, p-Tyr (tyrosine phosphorylation of TrkB), p-TrkB 706 (autophosphorylation site), and p-TrkB 816 (PLC γ phosphorylation site) immunoreactivities were significantly increased in the CPu 2 h after amphetamine (**Figures 1A–D**). In the NAc at 2 h, amphetamine significantly increased p-Tyr and p-TrkB 816, but not p-TrkB 706, immunoreactivity (**Figures 1E–H**). No differences were detected in the dmPFC 2 h after AMPH injection (data not shown).

EXPERIMENT 2: K252A AUGMENTED AMPH-INDUCED VERTICAL ACTIVITY AND SUPPRESSED AMPH-INDUCED PPD MRNA

AMPH-stimulated horizontal movement measured as total distance traveled and vertical activity as previously described (Shi and McGinty, 2006). Intra-striatal infusion of K252a did not alter

AMPH-induced total distance traveled but augmented AMPH-induced vertical activity (**Figure 2**). *In situ* hybridization revealed that AMPH-stimulated PPD and PPE mRNA levels in the CPu as previously described (Smith and McGinty, 1994; Shi and McGinty, 2006). Intra-striatal infusion of K252a suppressed AMPH-induced PPD, but not PPE, mRNA levels in the CPu (**Figure 3**). A representative cannula placement for this experiment is illustrated in **Figure 4**.

DISCUSSION

Two hours, but not 15 min, after a single AMPH injection, p-TrkB protein expression was increased in the CPu and NAc, but not in the dmPFC. Similar to a previous study (Meredith et al., 2002), total TrkB immunoreactivity was not increased 2 h after acute AMPH. However, in that study repeated daily AMPH injections (5 mg/kg) caused an increased in TrkB mRNA and/or immunoreactivity in several brain structures, including the striatum. In the present study, AMPH induces TrkB phosphorylation, a marker of TrkB receptor activation (Chao, 2003; Reichardt, 2006), in a time- and region-specific manner. Although trans-activation and non-neurotrophin-mediated activation of growth factor receptors has been reported (Huang et al., 2008; Jeanneteau et al., 2008), TrkB dimerization and phosphorylation most commonly occurs subsequent to BDNF binding (Chao, 2003). In the striatum, although the nigrostriatal track also contains BDNF, the majority of BDNF is synthesized,

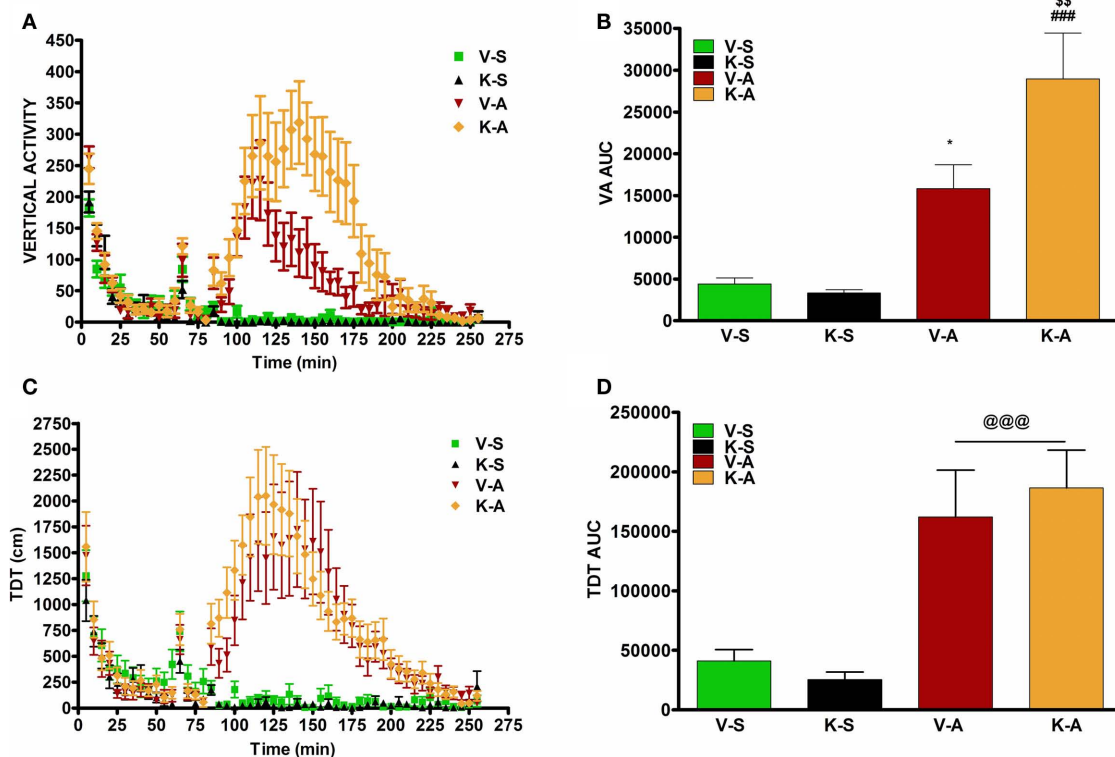


FIGURE 2 | AMPH-induced vertical activity (VA), but not total distance traveled (TDT), is augmented by K252a. (A) Vertical activity recorded for 1 h before intra-striatal K252a or vehicle infusion and for 3 h after AMPH or saline injection. (B) Area under the curve (AUC) analysis for 3 h after i.p. injections indicated by mean \pm SEM. * $p < 0.05$ K-A vs. V-A; $^{ss}p < 0.01$ K-A vs. K-S;

$p < 0.001$ V-A vs. V-S. **(C)** Activity recorded for 1 h before intra-striatal K252a or vehicle infusion and for 3 h after AMPH or saline injection. **(D)** Area under the curve (AUC) analysis for 3 h after i.p. injections indicated by mean \pm SEM. @@@ = $p < 0.001$ vs. V-S and K-S. V-S, vehicle saline; K-S, K252a-saline; V-A, vehicle-AMPH; K-A, K252a-AMPH. $N = 6-8/\text{group}$.

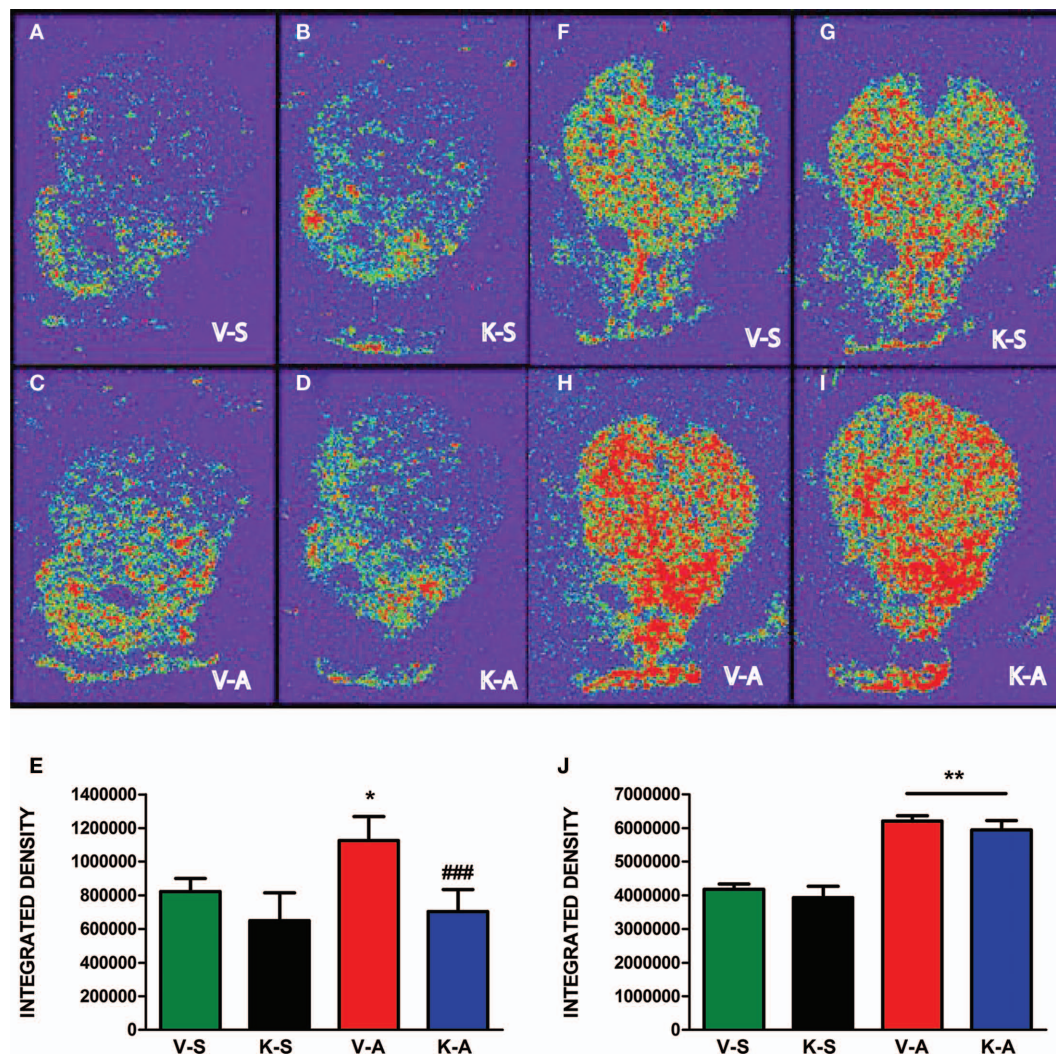


FIGURE 3 | AMPH-induced increase in PPD mRNA, but not PPE mRNA, is blocked by K252a. (A–D) PPD mRNA. **(E)** Integrated density measurements for PPD mRNA indicated as mean \pm SEM * p < 0.05 vs. V-S; ### p < 0.001 vs. V-A. **(F–I)** PPE mRNA. **(J)** Integrated density measurements for PPE mRNA indicated as mean \pm SEM ** p < 0.01 vs. V-S and K-S. V-S, vehicle saline; K-S, K252a-saline; V-A, vehicle-AMPH; K-A, K252a-AMPH (n = 6–8/group).

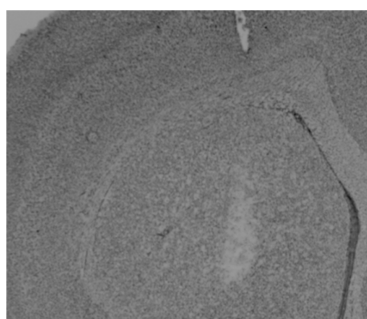


FIGURE 4 | Image captured with a CCD camera of a thionin-stained section illustrating a cannula track in the dorsocentral striatum illuminated on a light box. Note the lack of necrosis surrounding the injector track.

stored, and released from corticostriatal neurons (Altar et al., 1997). As for other neuropeptides, BDNF is stored and released from dense core vesicles in an action potential-dependent manner (Kohara et al., 2001; Balkowiec and Katz, 2002) that requires more intense stimulation than that of glutamate from small clear vesicles (Lessman, 1998; Carvalho et al., 2008). Thus, it is reasonable that TrkB phosphorylation was not evident 15 min after AMPH but was detected 2 h later if BDNF release occurred in a delayed, stimulus-dependent manner. This time course is consistent with the peak in motor activity and extracellular glutamate levels in the striatum that occurs between 30 and 90 min, in contrast to extracellular dopamine levels that peak between 15 and 30 min after this dose of AMPH (Gray et al., 1999; Rawls and McGinty, 2000).

The elevation of p-TrkB in the NAc and CPU 2 h after acute AMPH contrasts with a recent study indicating that pan-Tyr-TrkB was induced by a single cocaine injection in the NAc of mice

(Crooks et al., 2010). However, in their report, the increase of p-TrkB immunoreactivity was observed 9–12 h, but not 10 min or 3 h, after cocaine. The discrepant timepoint for TrkB activation in the two studies may be due to the different species and/or psychostimulants used. In addition to the pan-activation of TrkB on tyrosine sites in this study, the induction of p-TrkB 816 was detected in the NAc and CPu after acute AMPH administration. p-TrkB 816 triggers PLC γ -mediated signaling (Chao, 2003; Reichardt, 2006). Thus, it is plausible that the TrkB–PLC γ pathway in part mediates the BDNF-regulated intracellular transduction in response to acute AMPH. However, other TrkB-related signaling (e.g., Akt and ERK) should be further investigated.

K252a enhanced AMPH-induced vertical activity without altering horizontal ambulation (measured as total distance traveled). Vertical activity is part of a rat's exploratory repertoire that is thought to be mediated predominantly by the CPu and predominates after high doses or repeated administration of AMPH that produce stereotypical rearing behavior (Kelly et al., 1975; Lyon and Robbins, 1975). Thus, augmentation of vertical activity by K252a may represent a disinhibition of rearing in response to a moderate dose of AMPH that normally is tempered by activation of Trk receptor tyrosine kinase, or possibly another kinases inhibited by K252a. Since total distance traveled was not altered, overall exploratory locomotion was increased by the combination of K252a and AMPH. Of the many different receptor antagonists and agonists we have investigated in this paradigm over the years (Wang and McGinty, 1999; McGinty et al., 2010), K252a is the first one that has yielded this behavioral profile in combination with acute AMPH. As for intracellular kinases, PKA and MEK inhibitors upstream of ERK

MAPK both reduce AMPH-induced horizontal and vertical activity (Sutton et al., 2000; Shi and McGinty, 2006) whereas the PI-3 kinase inhibitor, wortmannin, decreases AMPH-induced vertical activity and increases horizontal activity (Shi et al., in preparation). However, although K252a has a higher affinity for tyrosine kinases, particularly Trk family receptors, than ser/thr kinases *in vitro* (Berg et al., 1992; Tapley et al., 1992; Martin et al., 2011), conclusions about the effects of K252a in this *in vivo* study should be drawn with caution and considered preliminary until confirmed by other Trk inhibitors or BDNF scavengers.

K252a suppressed AMPH-induced PPD, but not PPE, mRNA expression in the striatum. Since PPD is expressed only in the D1-regulated, direct pathway, and PPE mRNA only in the indirect pathway in the CPu (Gerfen, 1992), the data suggest that K252a acts predominantly via kinase cascades in direct pathway MSNs. It is less likely that inhibition of kinase cascades in indirect pathway MSNs leads to suppression of AMPH-induced PPD mRNA in direct pathway neurons. The selective effect of K252a on PPD vs. PPE gene expression also diminishes the likelihood that the K252a effects are mediated by ser/thr kinases stimulated by the major striatal regulators like D1, group I metabotropic glutamate, or muscarinic receptors because antagonists of these pathways block AMPH-induced PPD and PPE gene expression (Wang and McGinty, 1996a,b, 1999; McGinty et al., 2010). Alternatively, consideration must be given to the possibility that tyrosine kinase inhibition mediated by TrkB receptors underlies these K252a effects. However, since all MSNs in the striatum express TrkB receptors (Freeman et al., 2003; Lobo et al., 2010), it is unclear how selectivity of TrkB receptor stimulation would be accomplished unless it enhanced activity in one pathway

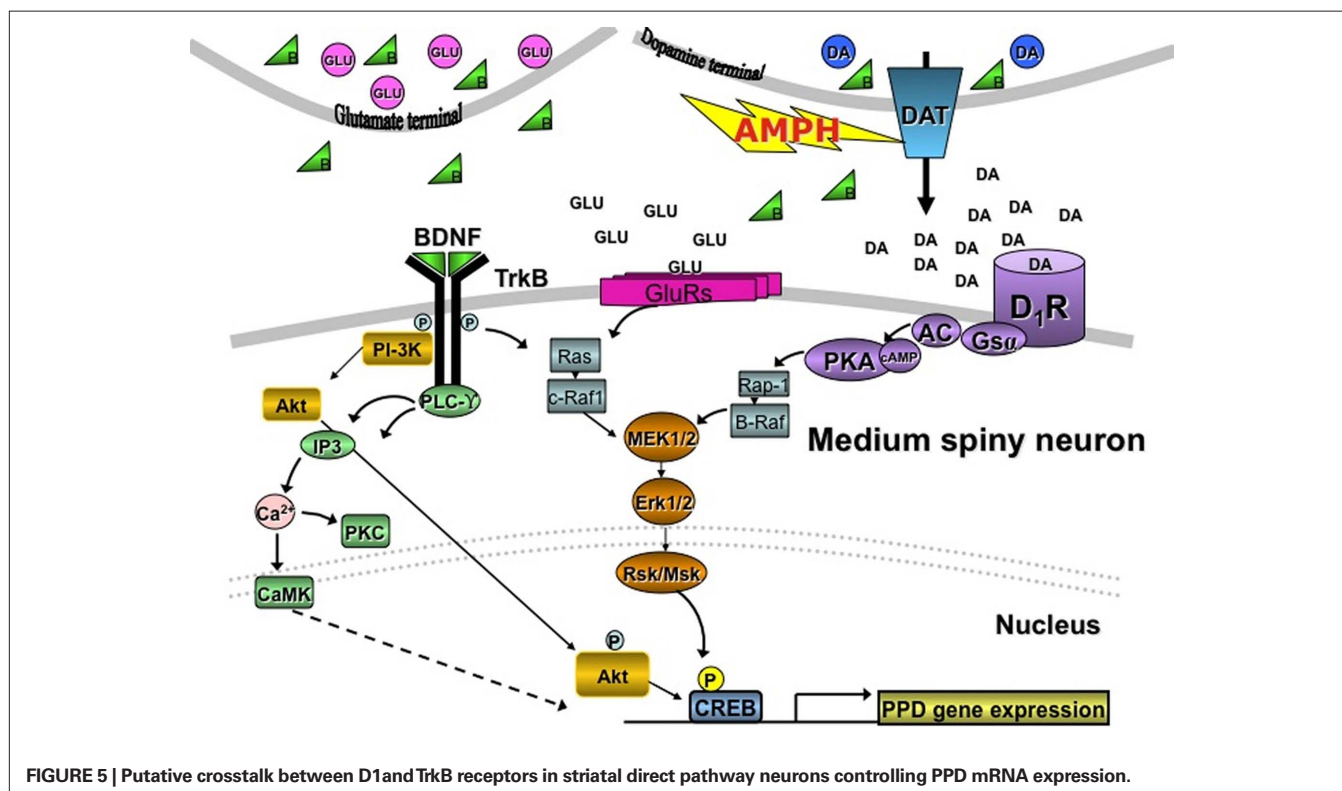


FIGURE 5 | Putative crosstalk between D1 and TrkB receptors in striatal direct pathway neurons controlling PPD mRNA expression.

and dampened activity in the other. Support for this idea stems from evidence that a TrkB receptor knockout exclusively in the direct pathway enhances, whereas a TrkB receptor knockout in indirect pathway neurons dampens, cocaine-induced behavioral sensitization and conditioned place preference in mice despite greater abundance of TrkB receptors on indirect pathway neurons (Lobo et al., 2010). Further, the expression of D1 and D3, but not D2, receptors is decreased in TrkB knockout mice (Guillin et al., 2001; Do et al., 2007; Saylor and McGinty, 2010), suggesting a dominant positive tone exerted by TrkB receptors on dorsal and ventral striatal neurons bearing these receptors. Thus, it is possible that by increasing BDNF release from dopamine and glutamate terminals in the striatum that TrkB receptors contribute to the behavioral and neurochemical sequelae in direct pathway neurons as depicted in **Figure 5**.

REFERENCES

- Altar, C. A., Cai, N., Bliven, T., Juhasz, M., Conner, J. M., Acheson, A. L., Lindsay, R. M., and Wiegand, S. J. (1997). Anterograde transport of brain-derived neurotrophic factor and its role in the brain. *Nature* 393, 856–860.
- Arenas, E., Akkerud, P., Wong, V., Boylan, C., Persson, H., Lindsay, R. M., and Altar, C. A. (1996). Effects of BDNF and NT-4/5 on striatonigral neuropeptides or nigral GABA neurons in vivo. *Eur. J. Neurosci.* 8, 1707–1717.
- Balkowiec, A., and Katz, D. (2002). Cellular mechanisms regulating activity-dependent release of native brain-derived neurotrophic factor from hippocampal neurons. *J. Neurosci.* 22, 10399–10407.
- Berg, M. M., Sternberg, D. W., Parada, L. F., and Chao, M. V. (1992). K-252a inhibits nerve growth factor-induced *trk* proto-oncogene tyrosine phosphorylation and kinase activity. *J. Biol. Chem.* 267, 13–16.
- Carvalho, A. L., Caldeira, M. V., Santos, S. D., and Duarte, C. B. (2008). Role of brain-derived neurotrophic factor at glutamatergic synapses. *Br. J. Pharmacol.* 153, S310–S324.
- Chao, M. V. (2003). Neurotrophins and their receptors: a convergent point for many signalling pathways. *Nat. Rev. Neurosci.* 4, 299–309.
- Cole, R. L., Konradi, C., Douglass, J., and Hyman, S. E. (1995). Neuronal adaptation to amphetamine and dopamine: molecular mechanisms of prodynorphin gene regulation in rat striatum. *Neuron* 14, 813–823.
- Crooks, K. R., Kleven, D. T., Rodriguez, R. M., Wetsel, W. C., and McNamara, J. O. (2010). TrkB signaling is required for behavioral sensitization and conditioned place preference induced by a single injection of cocaine. *Neuropharmacology* 58, 1067–1077.
- Do, T., Kerr, B., and Kuzhikandathil, E. V. (2007). Brain-derived neurotrophic factor regulates the expression of D1 dopamine receptors. *J. Neurochem.* 100, 416–428.
- Freeman, A. Y., Soghomonian, J.-J., and Pierce, R. C. (2003). Tyrosine kinase B and C receptors in the neostriatum and nucleus accumbens are co-localized in enkephalin-positive and enkephalin-negative neuronal profiles and their expression is influenced by cocaine. *Neuroscience* 117, 147–156.
- Gerfen, C. R. (1992). The neostriatal mosaic: multiple levels of compartmental organization. *Trends Neurosci.* 15, 133–139.
- Gray, A. M., Rawls, S. M., Shippenberg, T. S., and McGinty, J. F. (1999). The kappa opioid agonist, U-69593, decreases acute amphetamine-evoked behaviors and calcium-dependent dialysate levels of dopamine and glutamate in the ventral striatum. *J. Neurochem.* 73, 1066–1074.
- Guillin, O., Diaz, J., Carroll, P., Griffon, N., Schwartz, J. C., and Sokoloff, P. (2001). BDNF controls dopamine D3 receptor expression and triggers behavioural sensitization. *Nature* 411, 86–89.
- Huang, Y. Z., Pan, E., Xiong, Z. Q., and McNamara, J. O. (2008). Zinc-mediated trans-activation of TrkB potentiates the hippocampal mossy fiber-CA3 pyramidal synapse. *Neuron* 57, 546–558.
- Jeanneteau, F., Garabedian, M. J., and Chao, M. V. (2008). Activation of Trk neurotrophin receptors by glucocorticoids provides a neuroprotective effect. *Proc. Natl. Acad. Sci. U.S.A.* 105, 4862–4867.
- Kelly, P. H., Seviour, P. W., and Iversen, S. D. (1975). Amphetamine and apomorphine responses in the rat following 6-OHDA lesions of the nucleus accumbens septi and corpus striatum. *Brain Res.* 94, 507–522.
- Kohara, K., Kitamura, A., Morishima, M., and Tsumoto, T. (2001). Activity-dependent transfer of brain-derived neurotrophic factor to postsynaptic neurons. *Science* 291, 2419–2423.
- Konradi, C., Leveque, J. C., and Hyman, S. E. (1996). Amphetamine and dopamine-induced immediate early gene expression in striatal neurons depends on postsynaptic NMDA receptors and calcium. *J. Neurosci.* 16, 4231–4239.
- Le Foll, B., Diaz, J., and Sokoloff, P. (2005). A single cocaine exposure increases BDNF and D3 receptor expression: implications for drug-conditioning. *Neuroreport* 16, 175–178.
- Lessman, V. (1998). Neurotrophin-dependent modulation of glutamatergic synaptic transmission in the mammalian CNS. *Gen. Pharmacol.* 31, 667–674.
- Lobo, M. K., Covington, H. E. III, Chaudhury, D., Friedman, A. K., Sun, H., Dietz, D. M., Zaman, S., Koo, J. W., Kennedy, P. J., Mouzon, E., Mogri, M., Neve, R. L., Deisseroth, K., Han, M.-H., and Nestler, E. J. (2010). Cell type specific loss of BDNF signaling mimics optogenetic control of cocaine reward. *Science* 330, 385–390.
- Lyon, M., and Robbins, T. (1975). The action of central nervous system stimulant drugs: a general theory concerning amphetamine effects. *Curr. Dev. Psychopharmacol.* 2, 70–63.
- Martin, K. J., Shapiro, N., Traynor, R., Elliott, M., and Arthur, S. C. (2011). Comparison of the specificity of Trk inhibitors in recombinant and neuronal assays. *Neuropharmacology* 61, 148–155.
- McGinty, J. F., Shi, X. D., Schwendt, M., Saylor, A., and Toda, S. (2008). Regulation of psychostimulant-induced signaling and gene expression in the striatum. *J. Neurochem.* 104, 1440–1449.
- McGinty, J. F., Whitfield, T. W., and Berglind, W. J. (2010). Brain-derived neurotrophic factor and cocaine addiction. *Brain Res.* 1314, 183–193.
- Meredith, G. E., Callon, S., and Scheuer, D. A. (2002). Brain-derived neurotrophic factor expression is increased in the rat amygdala, piriform cortex and hypothalamus following repeated amphetamine administration. *Brain Res.* 949, 218–227.
- Numan, S., and Seroogy, K. B. (1999). Expression of *trkB* and *trkC* mRNAs by adult midbrain dopamine neurons: a double label in situ hybridization study. *J. Comp. Neurol.* 403, 295–308.
- Ou, L. C., and Gean, P. W. (2006). Regulation of amygdala-dependent learning by brain-derived neurotrophic factor is mediated by extracellular signal regulated kinase and phosphatidylinositol-3-kinase. *Neuropsychopharmacology* 31, 287–296.
- Patapoutian, A., and Reichardt, L. F. (2001). Trk receptors: mediators of neurotrophin action. *Curr. Opin. Neurobiol.* 11, 272–280.
- Poo, M. (2001). Neurotrophins as synaptic modulators. *Nat. Rev. Neurosci.* 2, 24–32.
- Rattiner, L. M., Davis, M., French, C. T., and Ressler, K. J. (2004). Brain-derived neurotrophic factor and tyrosine kinase receptor B involvement in amygdala-dependent fear conditioning. *J. Neurosci.* 24, 4796–4806.
- Rawls, S. M., and McGinty, J. F. (2000). Delta opioid receptors regulate calcium-dependent, amphetamine-evoked glutamate levels in the striatum: an in vivo microdialysis study. *Brain Res.* 861, 296–304.
- Reichardt, L. F. (2006). Neurotrophin-regulated signaling pathways. *Philos. Trans. R. Soc. Lond. B Biol. Sci.* 361, 1545–1564.
- Rocamora, N., Welker, E., Pascual, M., and Soriano, E. (1996). Upregulation of BDNF mRNA expression in the barrel cortex of adult mice after sensory stimulation. *J. Neurosci.* 16, 4411–4419.
- Russo, S. J., Mazei-Robison, M. S., Ables, J. L., and Nestler, E. J. (2008). Neurotrophic factors and structural plasticity in addiction. *Neuropharmacology* 56, 73–82.

CONCLUSION

Taken together, these data suggest that AMPH indirectly stimulates BDNF/TrkB receptors and that K252a augments acute AMPH-induced vertical activity and inhibits PPD gene expression via an undefined kinase cascade, possibly TrkB-coupled, in the D1-regulated, direct pathway. The possibility that this AMPH-stimulated kinase cascade involves BDNF/TrkB, dopamine, and glutamate interactions in the striatum requires further exploration.

ACKNOWLEDGMENTS

The authors thank Moses Chao, Ph.D. for p806-TrkB antiserum and Matthew C. Hearing, Ph.D., Sarah A. Eisenstein, Ph.D., and Stacey Sigmon for advice and technical assistance. Supported by RO1 DA03982.

- Sauer, H., Campbell, K., Wiegand, S. J., Lindsay, R. M., and Bjorklund, A. (1994). Brain-derived neurotrophic factor enhances striatal neuropeptide expression in both the intact and the dopamine-depleted rat striatum. *Neuroreport* 5, 609–612.
- Saylor, A. J., and McGinty, J. F. (2008). Amphetamine-induced locomotion and gene expression are altered in BDNF heterozygous mice. *Genes Brain Behav.* 7, 906–914.
- Saylor, A. J., and McGinty, J. F. (2010). An intra-striatal brain-derived neurotrophic factor infusion restores striatal gene expression in Bdnf heterozygous mice. *Brain Struct. Funct.* 215, 97–104.
- Saylor, A. J., Meredith, G. E., Vercillo, M. S., Zahm, D. S., and McGinty, J. F. (2006). BDNF heterozygous mice demonstrate age-related changes in striatal and nigral gene expression. *Exp. Neurol.* 199, 362–372.
- Seroogy, K. B., Lundgren, K. H., Tran, T. M., Guthrie, K. M., Isackson, P. J., and Gall, C. M. (1994). Dopaminergic neurons in rat ventral midbrain express brain-derived neurotrophic factor and neurotrophin-3 mRNAs. *J. Comp. Neurol.* 342, 321–334.
- Shi, X., and McGinty, J. F. (2006). ERK MAP kinase inhibitors decrease amphetamine-induced behavior and neuropeptide gene expression in the striatum. *Neuroscience* 138, 1289–1298.
- Simpson, J. N., Wang, J. Q., and McGinty, J. F. (1995). Repeated amphetamine administration induces a prolonged augmentation of phosphorylated-CREB and Fos-related antigen immunoreactivity in rat striatum. *Neuroscience* 69, 441–457.
- Smith, A. J. W., and McGinty, J. F. (1994). Acute amphetamine and methamphetamine alter opioid peptide mRNA expression in the rat striatum. *Brain Res. Mol. Brain Res.* 21, 359–362.
- Sun, W. L., Zhou, L., Quinones-Jenab, V., and Jenab, S. (2009). Cocaine effects on dopamine and NMDA receptors interactions in the striatum of Fischer rats. *Brain Res. Bull.* 80, 377–381.
- Sutton, M. A., McGibney, K., and Beninger, R. J. (2000). Conditioned locomotion in rats following amphetamine infusion into the nucleus accumbens: blockade by coincident inhibition of protein kinase. *Behav. Pharmacol.* 11, 365–376.
- Tapley, P., Lamballe, F., and Barbacid, M. (1992). K252a is a selective inhibitor of the tyrosine protein kinase activity of the trk receptor family of oncogenes and neurotrophin receptors. *Oncogene* 7, 371–381.
- Valjent, E., Pascoli, V., Svenningsson, P., Paul, S., Enslen, H., Corvol, J. C., Stipanovich, A., Caboche, J., Lombroso, P. J., Nairn, A. C., Greengard, P., Herve, D., and Girault, J. A. (2005). Regulation of a protein phosphatase cascade allows convergent dopamine and glutamate signals to activate ERK in the striatum. *Proc. Natl. Acad. Sci. U.S.A.* 102, 491–496.
- Vanhoutte, P., Barnier, J. V., Guibert, B., Pages, C., Besson, M. J., Hipskind, P. A., and Caboche, J. (1999). Glutamate induces phosphorylation of Elk-1 and CREB, along with c-fos activation, via an extracellular signal-regulated kinase-dependent pathway in brain slices. *Mol. Cell. Biol.* 19, 136–146.
- Wang, J. Q., and McGinty, J. F. (1995). Dose-dependent alterations in zif/268 and preprodynorphin mRNA expression induced by amphetamine or methamphetamine in rat brain. *J. Pharmacol. Exp. Ther.* 273, 909–917.
- Wang, J. Q., and McGinty, J. F. (1996a). D1 and D2 receptor regulation of preproenkephalin and preprodynorphin mRNA in rat striatum following acute injection of amphetamine or methamphetamine. *Synapse* 22, 114–122.
- Wang, J. Q., and McGinty, J. F. (1996b). Intra-striatal injection of the metabotropic glutamate receptor antagonist MCPG attenuates acute amphetamine-stimulated neuropeptide mRNA expression in rat striatum. *Neurosci. Lett.* 218, 13–16.
- Wang, J. Q., and McGinty, J. F. (1999). Glutamate-dopamine interactions mediate the effects of psychostimulant drugs. *Addict. Biol.* 4, 143–152.
- Wang, J. Q., Smith, A. W. S., and McGinty, J. F. (1995). A single injection of amphetamine or methamphetamine induces dynamic alterations in c-fos, zif/268 and preprodynorphin mRNA expression in rat forebrain. *Neuroscience* 68, 83–95.
- Whitfield, T. W., Shi, X., Sun, W.-L., and McGinty, J. F. (2011). The suppressive effect of an intra-prefrontal cortical infusion of BDNF on cocaine-seeking is Trk receptor and extracellular signal-regulated protein kinase mitogen-activated protein kinase dependent. *J. Neurosci.* 32, 834–842.

Conflict of Interest Statement: The authors declare that the research was conducted in the absence of any commercial or financial relationships that could be construed as a potential conflict of interest.

Received: 28 February 2011; paper pending published: 27 April 2011; accepted: 27 June 2011; published online: 21 July 2011.

Citation: McGinty JF, Bache AJ, Coleman NT and Sun W-L (2011) The role of BDNF/TrkB signaling in acute amphetamine-induced locomotor activity and opioid peptide gene expression in the rat dorsal striatum. *Front. Syst. Neurosci.* 5:60. doi: 10.3389/fnsys.2011.00060

Copyright © 2011 McGinty, Bache, Coleman and Sun. This is an open-access article subject to a non-exclusive license between the authors and Frontiers Media SA, which permits use, distribution and reproduction in other forums, provided the original authors and source are credited and other Frontiers conditions are complied with.



The 5-HT_{2A} receptor antagonist M100907 produces antiparkinsonian effects and decreases striatal glutamate

Twum A. Ansah*, Marcus C. Ferguson and Tultul Nayyar

Department of Neuroscience and Pharmacology, Meharry Medical College, Nashville, TN, USA

Edited by:

Elizabeth Abercrombie, Rutgers-Newark:
The State University of New Jersey,
USA

Reviewed by:

John D. Salamone, University of
Connecticut, USA

Sheila Fleming, University of
Cincinnati, USA

Giselle Petzinger, University of
Southern California, USA

*Correspondence:

Twum A. Ansah, Department of
Neuroscience and Pharmacology,
Meharry Medical College, 1005 D.B.
Todd Blvd, Nashville, TN 37208, USA.
e-mail: tansah@mmc.edu

5-HT plays a regulatory role in voluntary movements of the basal ganglia and has a major impact on disorders of the basal ganglia such as Parkinson's disease (PD). Clinical studies have suggested that 5-HT₂ receptor antagonists may be useful in the treatment of the motor symptoms of PD. We hypothesized that 5-HT_{2A} receptor antagonists may restore motor function by regulating glutamatergic activity in the striatum. Mice treated with 1-methyl-4-phenyl-1,2,3,6-tetrahydropyridine (MPTP) exhibited decreased performance on the beam-walking apparatus. Peripheral administration of the 5-HT_{2A} receptor antagonist M100907 improved performance of MPTP-treated mice on the beam-walking apparatus. *In vivo* microdialysis revealed an increase in striatal extracellular glutamate in MPTP-treated mice and local perfusion of M100907 into the dorsal striatum significantly decreased extracellular glutamate levels in saline and MPTP-treated mice. Our studies suggest that blockade of 5-HT_{2A} receptors may represent a novel therapeutic target for the motor symptoms of PD.

Keywords: dopamine, glutamate, M100907, microdialysis, motor deficits, MPTP, parkinsonism, serotonin

INTRODUCTION

Serotonin (5-HT) projections from the dorsal raphe nucleus innervate all components of the basal ganglia circuitry (Lavoie and Parent, 1990). 5-HT has been shown to modulate not only dopamine (DA) neurotransmission in the striatum, but also GABA and glutamate transmission in the output regions of the basal ganglia via a number of 5-HT receptors (Nicholson and Brotchie, 2002). Thus, 5-HT may play a regulatory role in voluntary movements of the basal ganglia and have a major impact on disorders of the basal ganglia such as Parkinson's disease (PD; Di Matteo et al., 2008). Clinical studies have suggested that 5-HT₂ receptor antagonists may be beneficial in the treatment of the motor symptoms of PD. For example, ritanserin, a 5-HT_{2A/C} receptor antagonist, has been shown to reduce akinesia and improve gait in PD patients (Henderson et al., 1992) as well as ameliorate neuroleptic-induced parkinsonism (Bersani et al., 1990). It was reported that ritanserin reduces extrapyramidal side effects when added to typical antipsychotics (Miller et al., 1990, 1992). Whereas typical antipsychotic drugs (APD), which are potent DA D2 antagonists (such as haloperidol), cause parkinsonian side effects, atypical APD with relatively high 5-HT_{2A}: DA D2 receptor affinities ratio (such as clozapine) are less prone to induce these extrapyramidal parkinsonian-like side effects (Altar et al., 1986; Meltzer et al., 1989; Matsubara et al., 1993; Nyberg et al., 1993). Furthermore, animal studies have shown that haloperidol-induced catalepsy is reduced by 5-HT_{2A} receptor antagonists (Balsara et al., 1979; Neal-Beliveau et al., 1993; Bartoszyk et al., 1996; Lucas et al., 1997; Young et al., 1999). Lucas et al. (1997) showed in rats that the reduction of neuroleptic-induced catalepsy by ritanserin was independent of changes in DA dynamics suggesting that the anti-cataleptic effects of ritanserin may involve non-dopaminergic targets, possibly glutamatergic. Whereas 5-HT_{2A} receptors are widely distributed in the brain (Pompeiano et al.,

1994; Ward and Dorsa, 1996; Mijster et al., 1997; Bubser et al., 2001), anatomical studies have suggested that cortico-striatal and pallidostriatal neurons are the major source of 5-HT_{2A} receptor binding in the striatum (Bubser et al., 2001). As such, 5-HT_{2A}-containing afferents to the striatum offer an anatomical substrate for the ability of 5-HT_{2A} receptor antagonists to modulate basal ganglia circuitry that may be dysfunctional in PD. Recently, we have shown that the 5-HT_{2A} receptor antagonist M100907 but not the selective 5-HT_{2C} receptor antagonist SB 206553 improved motor impairments in mice treated with 1-methyl-4-phenyl-1,2,3,6-tetrahydropyridine (MPTP; Ferguson et al., 2010). A number of studies in the literature are consistent with the interpretation that the 5-HT_{2A} receptor regulates glutamatergic transmission in the cortex (Aghajanian and Marek, 1997, 1999; Scruggs et al., 2000, 2003). Whether 5-HT_{2A} receptor regulates glutamatergic transmission in the striatum has not been adequately studied. We hypothesized that 5-HT_{2A} receptors localized on cortico-striatal axons regulate glutamatergic activity in the striatum and that 5-HT_{2A} receptor antagonists may restore motor function by normalizing the overactive glutamatergic drive resulting from DA depletion.

We assessed the effect of the 5-HT_{2A} receptor antagonist M100907 on motor impairments in MPTP-treated mice. Using *in vivo* microdialysis, we also determined whether intrastriatal M100907 administration will alter extracellular glutamate concentrations.

MATERIALS AND METHODS

ANIMALS

Male C57BL/6J mice, 70–77 days of age at the start of experiments, were obtained from Jackson Labs (Bar Harbor, ME, USA). Animals were group housed in a temperature and humidity controlled room and maintained on a 12L:12D light–dark cycle (lights off at 1900 h). Food and water were provided *ad libitum*. All studies were

performed in accordance with the National Institutes of Health Guide for Care and Use of Laboratory Animals and under the oversight of the Meharry Medical College Animal Care and Use Committee.

DRUG TREATMENTS

Mice were injected with 20 mg/kg (ip) MPTP (Sigma-Aldrich, St. Louis, MO, USA) or saline every 2 h for a total of four injections, resulting in a cumulative dose of 80 mg/kg. All experiments were done 3 weeks after MPTP administration. The selective 5-HT_{2A} receptor antagonist, M100907 [(R-(+)-alpha-(2,3-dimethoxyphenyl)-1-[2-(4-fluorophenethyl)]-4-piperidinemethanol]; Kehne et al., 1996], was dissolved in 0.1 M tartaric acid solution and adjusted to pH 6.5–7.0 with NaOH. All injection volumes were 10 ml/kg. M100907 was injected intraperitoneally 30 min before behavioral testing. All mice received a single dose of either vehicle or M100907. Thus, all comparisons were between subjects. The doses of M100907 (0.0001–0.01 mg/kg) used in the motor function test were based on the available literature as well as our previous studies (Ferguson et al., 2010) which showed that the selected doses did not alter general locomotor behavior.

BEAM-WALKING APPARATUS

The apparatus used in this experiment was as described previously (Ferguson et al., 2010). It consisted of a 1 cm square stainless steel beam of 105 cm in length. The beam was suspended 49 cm above the floor of the test chamber. Mice were habituated to the goal box for 3 min, then placed a distance of 10 cm from goal box. They were allowed to traverse the beam to the goal box. Upon successful traversal of the beam to the goal box at the 10 cm distance, mice were placed at increasing distances of 30, 50, and 80 cm from the goal box and trained to traverse the beam for one trial at each distance for two consecutive days. Mice able to traverse the full 80 cm length of the beam to the goal box within 60 s were considered to reach criterion. Three weeks post-MPTP or saline treatment, mice were subjected to three consecutive trials on the beam during which time they were videotaped. The number of footslips off the beam in each trial, and the mean number of hindlimb footslips during a three-trial session, were recorded (Dluzen et al., 2001; Fernagut et al., 2004; Strome et al., 2006; Allbutt and Henderson 2007; Quinn et al., 2007; Urakawa et al., 2007) by persons unaware of the treatment condition of the animals. A total of 104 mice were trained for studies using the beam-walking task. Separate groups of animals were used for assessment of baseline beam-walking performance of saline-treated ($n = 31$), MPTP-treated ($n = 31$) and MPTP-treated mice receiving three doses of M100907 ($n = 14$ /dose). This approach reduces the possible confound of motor learning which can occur with multiple testing of the same animals.

REGIONAL MONOAMINE CONCENTRATIONS

Separate groups of animals were used to determine the effects of MPTP treatment on regional monoamine concentrations. Animals (saline, $n = 15$; MPTP, $n = 18$) were sacrificed 3 weeks after saline or MPTP administration, which is the same time point that the behavioral studies and *in vivo* microdialysis were performed. These animals did not receive pharmacological agents. The tissues harvested for monoamine determination included the striatum, nucleus accumbens, substantia nigra, and cerebellum. The tissues

were dissected from 1.0 mm thick coronal slices (Deutch et al., 1985) and samples stored at -80°C until assayed. Regional concentrations of dopamine and serotonin were determined by HPLC-EC as previously described (Deutch and Cameron, 1992), with protein concentrations determined by the method of Lowry et al. (1951).

IN VIVO MICRODIALYSIS

Two weeks after MPTP or saline treatment, mice (saline, $n = 11$; MPTP, $n = 11$) were implanted with a chronic indwelling guide cannula; 5–7 days later the mice were used in dialysis sessions examining the ability of the 5-HT_{2A} antagonist M100907 to modify glutamate release in the striatum. One day prior to use, the efficiency of transmitter recovery by the probe was determined by collecting three 10-min samples (perfusing flow rate of 2.0 $\mu\text{L}/\text{min}$) after placing the probe in a solution of glutamate (200 pg/ μL) in artificial cerebrospinal fluid (aCSF; 140 mM NaCl, 3.4 mM KCl, 1.5 mM CaCl_2 , 1.0 mM MgCl_2 , 1.4 mM NaH_2PO_4 , and 4.85 mM NaHPO_4 , pH 7.4). Mice were anesthetized with isoflurane for stereotaxic surgery to place guide cannula (Plastics One; Roanoke, VA, USA) into the right striatum (anterior–posterior, +0.6 mm; dorso–ventral, -4.2 mm; and lateral, 2.0 mm relative to bregma; Franklin and Paxinos, 2008). A dual dental adhesive (Plastics One; Roanoke, VA, USA) was applied to the skull surface and base of the cannula, and then built up with a small amount of dental acrylic compound. Four to five days post-operatively, the dialysis probe (1.5 mm active exchange surface) was inserted and the animal was placed in a small Plexiglas chamber (9' round) that is placed in the dialysis chamber. The swivel assembly and attached tubing was carefully counterbalanced to allow free movement of the mouse. The dialysis probe was perfused overnight at 0.2 $\mu\text{L}/\text{min}$ with aCSF. The following morning, the flow rate was increased to 2.0 $\mu\text{L}/\text{min}$. Five 20-min baseline samples were collected, after which M100907 (100 nM) was administered through the dialysis probe and an additional seven fractions were collected. At the end of the experiment mice were deeply anesthetized with sodium pentobarbital (60 mg/kg, i.p.), perfused intracardially with 4% paraformaldehyde and serial coronal sections (40 μm) were cut through the striatum and stained with cresyl violet. If the probe placement was not correct (i.e., outside the striatum), the data from that animal were discarded. The levels of amino acids in the dialysate were determined using reverse phase HPLC-EC and fluorescent detection. Aminobutyric acid was added to dialysis samples as an internal standard. Samples were derivatized using o-phthalaldehyde and loaded into an autosampler for injection onto a 1.5 micron C18 column (Alltech Associates; Deerfield, IL, USA). The mobile phase was 100 mM sodium phosphate buffer containing 10% methanol (pH 3.70) and flow rate was set at 1.2 ml/min with the column temperature maintained at 40°C . The glutamate derivatization products were detected with a RF-10Axl fluorescence detector (Shimadzu Corp; Kyoto, Japan) and an electrochemical detector (ESA; Chelmsford, MA, USA) placed in series. Mean baseline levels of glutamate were calculated by averaging the concentrations of the five basal dialysate samples. If any baseline sample from an animal varies by more than 30% of the mean, it was eliminated; data from animals with less than three basal samples were not included in the analysis.

DATA ANALYSIS

Data were expressed as means \pm SEM and analyzed by one-way analysis of variance (ANOVA) or two-way ANOVA (microdialysis data). When appropriate, comparisons were carried out with Tukey's *post hoc* tests. Alpha levels were set at 0.05.

RESULTS

REGIONAL MONOAMINE CONCENTRATIONS

To evaluate the extent of dopaminergic lesion, the levels of DA in the striatum, substantia nigra, nucleus accumbens and cerebellum were measured by HPLC. MPTP treatment had significant main effect on DA in subcortical regions [$F_{(7,107)} = 4.542$; $p < 0.001$; **Figure 1**]. *Post hoc* analysis revealed that DA was significantly decreased in the striatum ($p < 0.01$), substantia nigra and nucleus accumbens ($p < 0.05$) but not in the cerebellum. The 5-HT content in these brain regions of MPTP-treated mice remained generally unchanged except for a small but insignificant decrease in the substantia nigra (data not shown).

EFFECTS OF 5-HT_{2A} RECEPTOR ANTAGONIST M100907 ON PERFORMANCE ON THE BEAM-WALKING APPARATUS

1-Methyl-4-phenyl-1,2,3,6-tetrahydropyridine produced more than 10-fold increase in the number of footslips during beam traversal (number of footslips/subject: Control 0.42 ± 0.12 ; MPTP 5.97 ± 0.58 ; $n = 31$ /group). We (Ferguson et al., 2010) and others (Fredriksson et al., 1990; Tillerson et al., 2002; Tillerson and Miller, 2003) have shown that levodopa can reverse the MPTP-induced motor deficits suggesting that the motor function test employed is sensitive to deficits in the nigrostriatal system, believed to underlie motor impairments in PD. There was significant main effect of M100907 on motor performance of MPTP-treated mice on the beam-walking apparatus [$F_{(3,76)} = 14.183$; $p < 0.0001$; **Figure 2**]. *Post hoc* analysis showed that M100907 produced dose-dependent decreases ($p < 0.001$) in the number of footslips produced by

MPTP treatment (**Figure 2**). The doses of M100907 used did not have any effects on the performance of beam-traversal task of control mice (Ferguson et al., 2010).

EFFECTS OF 5-HT_{2A} RECEPTOR ANTAGONIST M100907 ON EXTRACELLULAR GLUTAMATE IN THE STRIATUM

We hypothesized that 5-HT_{2A} receptor antagonists may restore motor function by normalizing the overactive glutamatergic drive resulting from DA depletion. We have used *in vivo* microdialysis to determine whether extracellular striatal glutamate is increased in mice treated with MPTP and whether local administration of the 5-HT_{2A} receptor antagonist M100907 will decrease striatal glutamate. The mean basal striatal extracellular glutamate levels in the dialysates obtained from saline-treated mice used in these studies were $3.41 \pm .24$ pmol/ μ L (mean \pm SEM; $n = 11$; **Figure 3**). Local application of 1 μ M tetrodotoxin resulted in a dramatic fall in basal glutamate output reaching 25% of baseline (data not shown). This suggests that a significant fraction of the resting level of striatal glutamate is of neuronal origin. **Figure 3A** depicts the time course of the effects of M100907 on basal glutamate levels (expressed as percentage of values of saline-injected controls) of saline and MPTP-treated mice. MPTP-treated mice exhibited increased basal extracellular glutamate levels compared to the saline-treated mice (**Figure 3A**). Local perfusion of 100 nM M100907 into the dorsal striatum decreased basal glutamate levels in saline- and MPTP-treated mice. Two-way ANOVA of the time course data revealed significant main effects for treatment [$F_{(1,28)} = 230.7$; $p < 0.0001$, drug effect, $F_{(1,28)} = 305$, $p < 0.0001$, and treatment \times drug interaction $F_{(1,28)} = 65.67$; $p < 0.0001$; **Figure 3A**]. The significant treatment \times drug interaction suggests that despite elevated basal glutamate levels in the MPTP-treated mice, M100907 was capable of significantly suppressing glutamate output. **Figure 3B** compares the effects of M100907 on extracellular glutamate values of saline and MPTP-treated mice. The baseline data were obtained from the average of five time points and data for drug treatment were obtained from average of seven time points from **Figure 3A**. One-way ANOVA revealed significant main effects [$F_{(3,28)} = 49.20$;

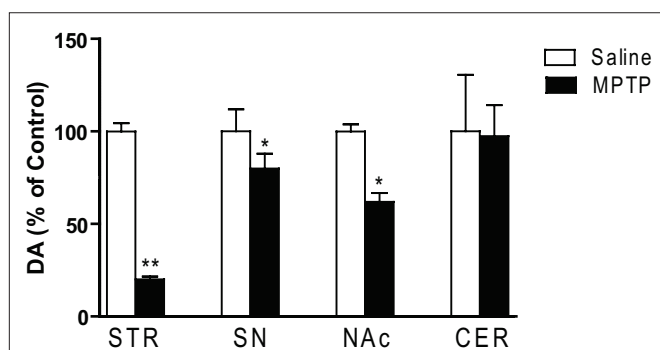


FIGURE 1 | Dopamine concentrations in subcortical regions of saline and MPTP-treated mice. Dopamine concentrations were determined 3 weeks after the last MPTP injection. In addition to changes in the striatal complex, a significant decrease in dopamine in the substantia nigra was seen ($n = 10$ /group). Abbreviations: CER, cerebellar cortex; NAc, nucleus accumbens; SN, substantia nigra; STR, striatum. Data are expressed as percent of saline-injected control mice. Dopamine concentrations (mean ng/mg protein \pm SEM) in control mice: STR: 144.7 ± 9.3 ; NAc: 14.1 ± 0.54 ; SN: 6.8 ± 0.5 ; CER: 0.17 ± 0.05 . * $p < 0.05$, ** $p < 0.01$; relative to saline-injected controls.

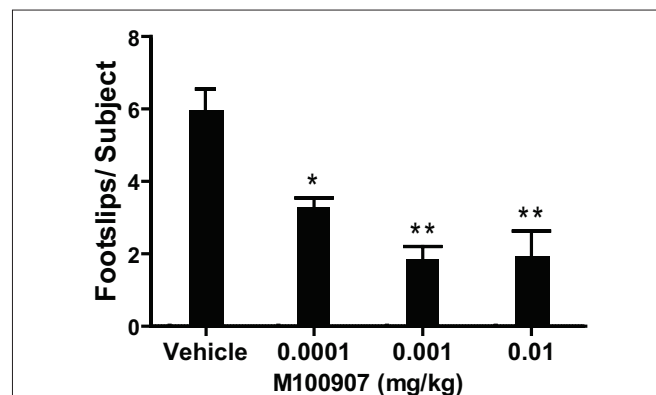


FIGURE 2 | M100907 relieved motor deficits in MPTP-treated mice.

MPTP-treated mice received vehicle or various doses of M100907. Data are presented as mean \pm SEM. M100907 dose-dependently reduced the number of footslips in MPTP-treated mice. * $p < 0.05$, ** $p < 0.01$; relative to saline-injected controls; in one-way ANOVA with Tukey's *post hoc* comparison.

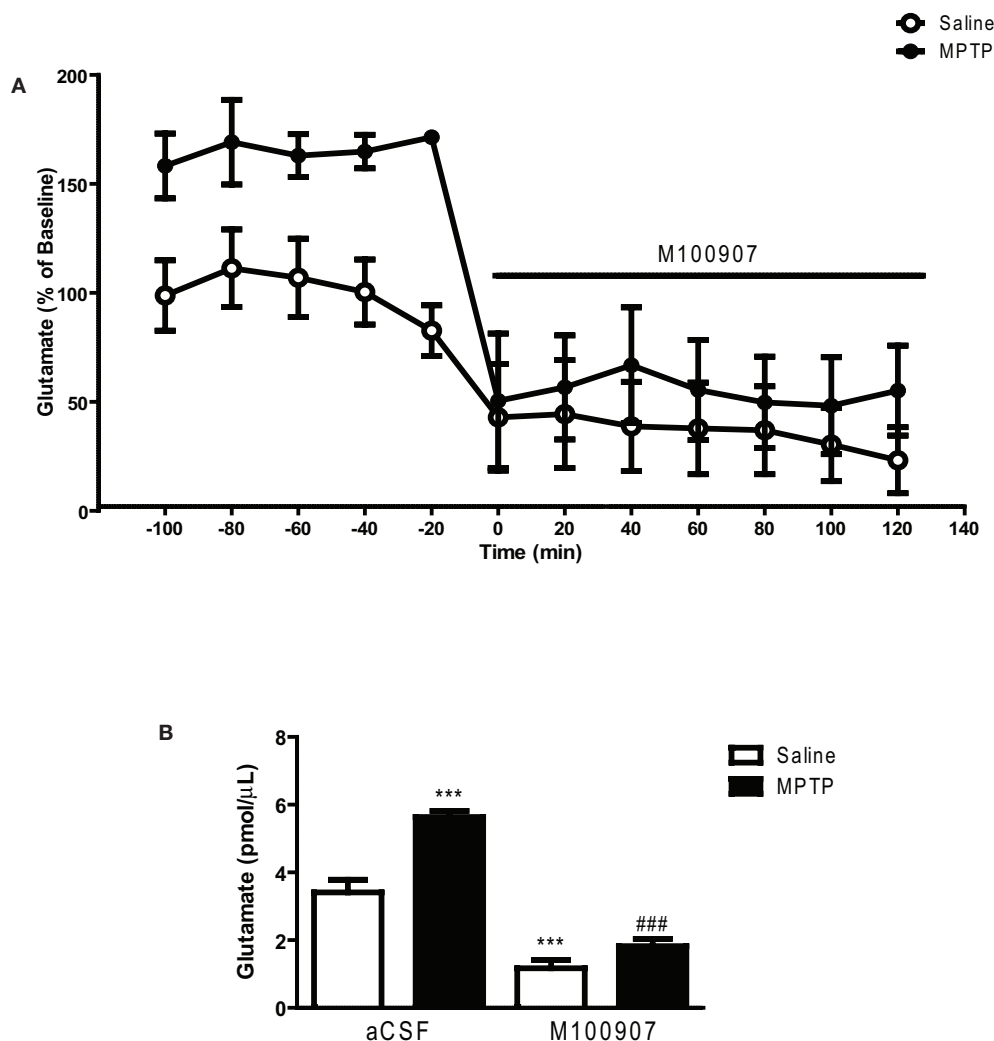


FIGURE 3 | M100907 decreased glutamate levels in the dorsal striatum in saline and MPTP-treated mice. Data are expressed as percentages of values in saline-injected control mice. Dialysis was carried out 3 weeks after MPTP or saline treatment and 7 days after the cannula implantation. **(A)** Five baseline samples were first collected and then a challenge dose of M100907 (100 nM)

and an additional seven samples were collected. **(B)** The effects of M100907 on extracellular glutamate values of saline and MPTP-treated mice. *** $p < 0.001$ compared with saline-injected control mice; ### $p < 0.001$ when compared with MPTP-treated mice. The line segment on time course graphs indicate duration of drug administration.

$p < 0.0001$; **Figure 3B**]. *Post hoc* analysis using the Tukey's multiple comparison test revealed a significant increase ($p < 0.001$) in basal extracellular glutamate values in MPTP-treated mice (**Figure 3B**). Local perfusion of 100 nM M100907 into the dorsal striatum significantly decreased basal glutamate levels in saline ($p < 0.001$) and MPTP ($p < 0.001$)-treated mice (**Figure 3B**).

DISCUSSION

5-HT may play a role in voluntary movements regulated by the basal ganglia and have a major impact on disorders of the basal ganglia such as PD (Di Matteo et al., 2008). Clinical studies have suggested that 5-HT₂ receptor antagonists may be useful in the treatment of the motor symptoms of PD (Bersani et al., 1990; Henderson et al., 1992). We hypothesized that 5-HT_{2A} receptor antagonists may restore motor function by regulating glutamater-

gic activity in the striatum. We have shown that the 5-HT_{2A} receptor antagonist M100907 improved performance of MPTP-treated mice on the beam-walking apparatus. *In vivo* microdialysis studies revealed an increase in striatal extracellular glutamate in MPTP-treated mice and local perfusion of M100907 into the dorsal striatum significantly decreased basal glutamate levels in saline and MPTP-treated mice.

Recently, it has been shown that ACP-103 (pimavancerin), a potent 5-HT_{2A} receptor inverse agonist that blocks 5-HT agonists at 5-HT_{2A} receptors (Vanover et al., 2006) can suppress tacrine-induced tremulous jaw movements in rats (Vanover et al., 2008). Mianserin, a 5-HT_{2A/C} receptor antagonist produced similar anti-tremor effects in rats (Carlson et al., 2003). These data and our studies point to the potential beneficial effects of blockade to 5-HT_{2A} receptors in motor symptoms of PD.

A possible mechanism of regulation of striatal function by 5-HT_{2A} receptors comes from studies showing that following DA depletion, the hyperactive locomotor behaviors induced by intra-striatal infusion of the D1 agonist SKF82958 can be reduced by the 5-HT_{2A} receptor antagonist M100907 (Bishop et al., 2005). It appears the direct striatal output pathway plays a major role in these effects of 5-HT_{2A} receptors (Gresch and Walker, 1999). A more plausible mechanism to explain our findings is an indirect action occurring through regulation of glutamate release. There are a number of studies that support our hypothesis. For example, *in situ* hybridization and immunohistochemical studies have revealed widespread distribution of 5-HT_{2A} receptors in the striatum (Pompeiano et al., 1994; Ward and Dorsa, 1996; Mijster et al., 1997; Bubser et al., 2001), however the major source of 5-HT_{2A} receptors appears to be the heteroreceptors located on the terminals of the cortico-striatal glutamatergic axons (Bubser et al., 2001). It has been postulated that the loss of striatal DA removes a tonic inhibitory constraint on cortico-striatal glutamatergic axons (DeLong, 1990). Thus, anatomical studies in the 6-hydroxydopamine (6-OHDA)-lesioned rat, MPTP-treated primates, and PD patients reveal adaptive changes at cortico-striatal synapses suggestive of hyperactivity at these glutamatergic synapses (Anglade et al., 1996; Meshul et al., 1999, 2002; Raju et al., 2008). Consistent with the anatomical studies, we (this study) and

others (Robinson et al., 2003) using *in vivo* microdialysis studies and proton magnetic resonance spectroscopy (Chassain et al., 2008) have demonstrated increased glutamate concentrations in the striatum of MPTP-treated mice. Activation of 5-HT_{2A} heteroreceptors in several brain areas has been shown to evoke glutamate release (Aghajanian and Marek, 1997; Scruggs et al., 2000, 2003). Thus, it is conceivable that 5-HT_{2A} receptor antagonists may restore motor function by normalizing the overactive glutamatergic drive resulting from DA depletion. Indeed we have shown that local perfusion of M100907 into the dorsal striatum significantly decreased basal glutamate levels in MPTP-treated mice. A more direct approach will be to demonstrate improvement in motor performance following local application of M100907 into the dorsal striatum. These experiments will be the subject of future studies.

In conclusion we have shown that the antiparkinsonian effects of 5-HT_{2A} receptor antagonists may be mediated by regulation of striatal glutamate and that antagonism of striatal 5-HT_{2A} receptors may offer non-dopaminergic therapeutic target for the motor symptoms of PD.

ACKNOWLEDGMENTS

We are indebted to Dr. Elaine Sanders-Bush, Vanderbilt University for the generous gift of M100907. This work was supported by U54 NS041071.

REFERENCES

- Aghajanian, G. K., and Marek, G. J. (1997). Serotonin induces excitatory postsynaptic potentials in apical dendrites of neocortical pyramidal cells. *Neuropharmacology* 36, 589–599.
- Aghajanian, G. K., and Marek, G. J. (1999). Serotonin and hallucinogens. *Neuropsychopharmacology* 21, 16S–23S.
- Allbutt, H. N., and Henderson, J. M. (2007). Use of the narrow beam test in the rat, 6-hydroxydopamine model of Parkinson's disease. *J. Neurosci. Methods* 159, 195–202.
- Altar, C. A., Wasley, A. M., Neale, R. F., and Stone, G. A. (1986). Typical and atypical antipsychotic occupancy of D2 and S2 receptors: an autoradiographic analysis in rat brain. *Brain Res. Bull.* 16, 517–525.
- Anglade, P., Mouatt-Prigent, A., Agid, Y., and Hirsch, E. (1996). Synaptic plasticity in the caudate nucleus of patients with Parkinson's disease. *Neurodegeneration* 5, 121–128.
- Balsara, J. J., Jadhav, J. H., and Chandorkar, A. G. (1979). Effect of drugs influencing central serotonergic mechanisms on haloperidol-induced catalepsy. *Psychopharmacology (Berl.)* 62, 67–69.
- Bartoszyk, G. D., Roos, C., and Ziegler, H. (1996). 5-HT_{1A} receptors are not involved in clozapine's lack of cataleptogenic potential. *Neuropharmacology* 35, 1645–1646.
- Bersani, G., Grispi, A., Marini, S., Pasini, A., Valducci, M., and Ciani, N. (1990). 5-HT₂ antagonist ritanserin in neuroleptic-induced Parkinsonism: a double-blind comparison with orphenadrine and placebo. *Clin. Neuropharmacol.* 13, 500–506.
- Bishop, C., Daut, G. S., and Walker, P. D. (2005). Serotonin 5-HT_{2A} but not 5-HT_{2C} receptor antagonism reduces hyperlocomotor activity induced in dopamine-depleted rats by striatal administration of the D1 agonist SKF 82958. *Neuropharmacology* 49, 350–358.
- Bubser, M., Backstrom, J. R., Sanders-Bush, E., Roth, B. L., and Deutch, A. Y. (2001). Distribution of serotonin 5-HT_{2A} receptors in afferents of the rat striatum. *Synapse* 39, 297–304.
- Carlson, B. B., Wisniecki, A., and Salamone, J. D. (2003). Local injections of the 5-hydroxytryptamine antagonist mianserin into substantia nigra pars reticulata block tremulous jaw movements in rats: studies with a putative model of Parkinsonian tremor. *Psychopharmacology* 165, 229–237.
- Chassain, C., Bielicki, G., Durand, E., Lollignier, S., Essafi, F., Traore, A., and Durif, F. (2008). Metabolic changes detected by proton magnetic resonance spectroscopy *in vivo* and *in vitro* in a murine model of Parkinson's disease, the MPTP-intoxicated mouse. *J. Neurochem.* 105, 874–882.
- DeLong, M. R. (1990). Primate models of movement disorders of basal ganglia origin. *Trends Neurosci.* 13, 281–285.
- Deutch, A. Y., and Cameron, D. S. (1992). Pharmacological characterization of dopamine systems in the nucleus accumbens core and shell. *Neuroscience* 46, 49–56.
- Deutch, A. Y., Tam, S. Y., and Roth, R. H. (1985). Footshock and conditioned stress increase 3,4-dihydroxyphenylacetic acid (DOPAC) in the ventral tegmental area but not substantia nigra. *Brain Res.* 333, 143–146.
- Di Matteo, V., Pierucci, M., Esposito, E., Crescimanno, G., Benigno, A., and Di Giovanni, G. (2008). Serotonin modulation of the basal ganglia circuitry: therapeutic implication for Parkinson's disease and other motor disorders. *Prog. Brain Res.* 172, 423–463.
- Dluzen, D. E., Gao, X., Story, G. M., Anderson, L. I., Kucera, J., and Walro, J. M. (2001). Evaluation of nigrostriatal dopaminergic function in adult +/- and +/- BDNF mutant mice. *Exp. Neurol.* 170, 121–128.
- Ferguson, M. C., Nayyar, T., Deutch, A. Y., and Ansah, T. A. (2010). 5-HT_{2A} receptor antagonists improve motor impairments in the MPTP mouse model of Parkinson's disease. *Neuropharmacology* 59, 31–36.
- Fernagut, P. O., Digué, E., Bioulac, B., and Tison, F. (2004). MPTP potentiates 3-nitropropionic acid-induced striatal damage in mice: reference to striatonigral degeneration. *Exp. Neurol.* 185, 47–62.
- Franklin, K. B. J., and Paxinos, G. (2008). *The Mouse Brain in Stereotaxic Coordinates*, 3rd Edn. San Diego: Academic Press.
- Fredriksson, A., Plaznik, A., Sundstrom, E., Jonsson, G., and Archer, T. (1990). MPTP-induced hypoactivity in mice: reversal by L-dopa. *Pharmacol. Toxicol.* 67, 295–301.
- Gresch, P. J., and Walker, P. D. (1999). Synergistic interaction between serotonin-2 receptor and dopamine D1 receptor stimulation on striatal preprotachykinin mRNA expression in the 6-hydroxydopamine lesioned rat. *Brain Res. Mol. Brain Res.* 70, 125–134.
- Henderson, J., Yiannikas, C., and Graham, J. S. (1992). Effect of ritanserin, a highly selective 5-HT₂ receptor antagonist, on Parkinson's disease. *Clin. Exp. Neurol.* 29, 277–282.
- Kehne, J. H., Baron, B. M., Carr, A. A., Chaney, S. F., Elands, J., Feldman, D. J., Frank, R. A., van Giersbergen, P. L., McCloskey, T. C., Johnson, M. P., McCarty, D. R., Poirot, M., Senyah, Y., Siegel, B. W., and Widmaier, C. (1996). Preclinical characterization of the potential of the putative atypical antipsychotic MDL 100,907 as a potent 5-HT_{2A} antagonist with a favorable CNS safety profile. *J. Pharmacol. Exp. Ther.* 277, 968–981.

- Lavoie, B., and Parent, A. (1990). Immunohistochemical study of the serotonergic innervation of the basal ganglia in the squirrel monkey. *J. Comp. Neurol.* 299, 1–16.
- Lowry, O. H., Rosebrough, N. J., Farr, A. L., and Randall, R. J. (1951). Protein measurement with the Folin phenol reagent. *J. Biol. Chem.* 193, 265–275.
- Lucas, G., Bonhomme, N., De Deurwaerdere, P., Le Moal, M., and Spampinato, U. (1997). 8-OH-DPAT, a 5-HT_{1A} agonist and ritanserin, a 5-HT_{2A/C} antagonist, reverse haloperidol-induced catalepsy in rats independently of striatal dopamine release. *Psychopharmacology (Berl.)* 131, 57–63.
- Matsubara, S., Matsubara, R., Kusumi, I., Koyama, T., and Yamashita, I. (1993). Dopamine D₁, D₂ and serotonin₂ receptor occupation by typical and atypical antipsychotic drugs in vivo. *J. Pharmacol. Exp. Ther.* 265, 498–508.
- Meltzer, H. Y., Matsubara, S., and Lee, J. C. (1989). The ratios of serotonin₂ and dopamine₂ affinities differentiate atypical and typical antipsychotic drugs. *Psychopharmacol. Bull.* 25, 390–392.
- Meshul, C. K., Emre, N., Nakamura, C. M., Allen, C., Donohue, M. K., and Buckman, J. F. (1999). Time-dependent changes in striatal glutamate synapses following a 6-hydroxydopamine lesion. *Neuroscience* 88, 1–16.
- Meshul, C. K., Kamel, D., Moore, C., Kay, T. S., and Krentz, L. (2002). Nicotine alters striatal glutamate function and decreases the apomorphine-induced contralateral rotations in 6-OHDA-lesioned rats. *Exp. Neurol.* 175, 257–274.
- Mijnster, M. J., Raimundo, A. G., Koskuba, K., Klop, H., Docter, G. J., Groenewegen, H. J., and Voorn, P. (1997). Regional and cellular distribution of serotonin 5-hydroxytryptamine_{2A} receptor mRNA in the nucleus accumbens, olfactory tubercle, and caudate putamen of the rat. *J. Comp. Neurol.* 389, 1–11.
- Miller, C. H., Fleischacker, W. W., Ehrmann, H., and Kane, J. M. (1990). Treatment of neuroleptic induced akathisia with the 5-HT₂ antagonist ritanserin. *Psychopharmacol. Bull.* 26, 373–376.
- Miller, C. H., Hummer, M., Pycha, R., and Fleischacker, W. W. (1992). The effect of ritanserin on treatment-resistant neuroleptic induced akathisia: case reports. *Prog. Neuropsychopharmacol. Biol. Psychiatry* 16, 247–251.
- Neal-Beliveau, B. S., Joyce, J. N., and Lucki, I. (1993). Serotonergic involvement in haloperidol-induced catalepsy. *J. Pharmacol. Exp. Ther.* 265, 207–217.
- Nicholson, S. L., and Brotchie, J. M. (2002). 5-hydroxytryptamine (5-HT, serotonin) and Parkinson's disease – opportunities for novel therapeutics to reduce the problems of levodopa therapy. *Eur. J. Neurol.* 9(Suppl. 3), 1–6.
- Nyberg, S., Farde, L., Eriksson, L., Halldin, C., and Eriksson, B. (1993). 5-HT₂ and D₂ dopamine receptor occupancy in the living human brain. A PET study with risperidone. *Psychopharmacology (Berl.)* 110, 265–272.
- Pompeiano, M., Palacios, J. M., and Mengod, G. (1994). Distribution of the serotonin 5-HT₂ receptor family mRNAs: comparison between 5-HT_{2A} and 5-HT_{2C} receptors. *Brain Res. Mol. Brain Res.* 23, 163–178.
- Quinn, L. P., Perren, M. J., Brackenborough, K. T., Woodhams, P. L., Vidgeon-Hart, M., Chapman, H., Pangalos, M. N., Upton, N., and Virley, D. J. (2007). A beam-walking apparatus to assess behavioural impairments in MPTP-treated mice: pharmacological validation with R(-)-deprenyl. *J. Neurosci. Methods* 164, 43–49.
- Raju, D. V., Ahern, T. H., Shah, D. J., Wright, T. M., Standaert, D. G., Hall, R. A., and Smith, Y. (2008). Differential synaptic plasticity of the corticostriatal and thalamostriatal systems in an MPTP-treated monkey model of Parkinsonism. *Eur. J. Neurosci.* 27, 1647–1658.
- Robinson, S., Freeman, P., Moore, C., Touchon, J. C., Krentz, L., and Meshul, C. K. (2003). Acute and subchronic MPTP administration differentially affects striatal glutamate synaptic function. *Exp. Neurol.* 180, 74–87.
- Scruggs, J. L., Patel, S., Bubser, M., and Deutch, A. Y. (2000). DOI-Induced activation of the cortex: dependence on 5-HT_{2A} heteroreceptors on thalamocortical glutamatergic neurons. *J. Neurosci.* 20, 8846–8852.
- Scruggs, J. L., Schmidt, D., and Deutch, A. Y. (2003). The hallucinogen 1-[2,5-dimethoxy-4-iodophenyl]-2-aminopropane (DOI) increases cortical extracellular glutamate levels in rats. *Neurosci. Lett.* 346, 137–140.
- Strome, E. M., Cepeda, I. L., Sossi, V., and Doudet, D. J. (2006). Evaluation of the integrity of the dopamine system in a rodent model of Parkinson's disease: small animal positron emission tomography compared to behavioral assessment and autoradiography. *Mol. Imaging Biol.* 8, 292–299.
- Tillerson, J. L., Caudle, W. M., Revereon, M. E., and Miller, G. W. (2002). Detection of behavioral impairments correlated to neurochemical deficits in mice treated with moderate doses of 1-methyl-4-phenyl-1,2,3,6-tetrahydropyridine. *Exp. Neurol.* 178, 80–90.
- Tillerson, J. L., and Miller, G. W. (2003). Grid performance test to measure behavioral impairment in the MPTP-treated-mouse model of Parkinsonism. *J. Neurosci. Methods* 123, 189–200.
- Urakawa, S., Hida, H., Masuda, T., Misumi, S., Kim, T. S., and Nishino, H. (2007). Environmental enrichment brings a beneficial effect on beam walking and enhances the migration of doublecortin-positive cells following striatal lesions in rats. *Neuroscience* 144, 920–933.
- Vanover, K. E., Betz, A. J., Weber, S. M., Bibbiani, F., Kielaite, A., Weiner, D. M., Davis, R. E., Chase, T. N., and Salamone, J. D. (2008). A 5-HT_{2A} receptor inverse agonist, ACP-103, reduces tremor in a rat model and levodopa-induced dyskinesias in a monkey model. *Pharmacol. Biochem. Behav.* 90, 540–544.
- Vanover, K. E., Weiner, D. M., Makhay, M., Veinbergs, I., Gardell, L. R., Lameh, J., Del Tredici, A. L., Piu, F., Schiffer, H. H., Ott, T. R., Burstein, E. S., Uldam, A. K., Thygesen, M. B., Schlienger, N., Andersson, C. M., Son, T. Y., Harvey, S. C., Powell, S. B., Geyer, M. A., Tolf, B. R., Brann, M. R., and Davis, R. E. (2006). Pharmacological and behavioral profile of N-(4-fluorophenylmethyl)-N-(1-methylpiperidin-4-yl)-N'-(4-(2-methylpropyl)oxy)phenylmethyl carbamide (2R,3R)-dihydroxybutanedioate (2:1) (ACP-103), a novel 5-hydroxytryptamine(2A) receptor inverse agonist. *J. Pharmacol. Exp. Ther.* 317, 910–918.
- Ward, R. P., and Dorsa, D. M. (1996). Colocalization of serotonin receptor subtypes 5-HT_{2A}, 5-HT_{2C}, and 5-HT₆ with neuropeptides in rat striatum. *J. Comp. Neurol.* 370, 405–414.
- Young, C. D., Bubser, M., Meltzer, H. Y., and Deutch, A. Y. (1999). Clozapine pretreatment modifies haloperidol-elicited forebrain Fos induction: a regionally-specific double dissociation. *Psychopharmacology (Berl.)* 144, 255–263.

Conflict of Interest Statement: The authors declare that the research was conducted in the absence of any commercial or financial relationships that could be construed as a potential conflict of interest.

Received: 25 February 2011; paper pending published: 18 April 2011; accepted: 03 June 2011; published online: 14 June 2011.

Citation: Ansah TA, Ferguson MC and Nayyar T (2011) The 5-HT_{2A} receptor antagonist M100907 produces antiparkinsonian effects and decreases striatal glutamate. *Front. Syst. Neurosci.* 5:48. doi: 10.3389/fnsys.2011.00048

Copyright © 2011 Ansah, Ferguson and Nayyar. This is an open-access article subject to a non-exclusive license between the authors and Frontiers Media SA, which permits use, distribution and reproduction in other forums, provided the original authors and source are credited and other Frontiers conditions are complied with.



Nitric oxide synthase inhibitor improves de novo and long-term L-DOPA-induced dyskinesia in hemiparkinsonian rats

Fernando Eduardo Padovan-Neto^{1,2}, Marcela Bermúdez Echeverry^{2,3}, Silvana Chiavegatto⁴ and Elaine Del-Bel^{1,2*}

¹ Department of Behavioral Neuroscience, Medical School, University of São Paulo, Ribeirão Preto, São Paulo, Brazil

² Department of Physiology, Dentistry School, University of São Paulo, Ribeirão Preto, São Paulo, Brazil

³ Department of Morphophysiology, School of Medicine, University of Santander, Campus Bucaramanga, Santander, Colombia

⁴ Department of Pharmacology, Biomedical Sciences Institute, University of São Paulo, Ribeirão Preto, SP, Brazil

Edited by:

Elizabeth Abercrombie, Rutgers-Newark: The State University of New Jersey, USA

Reviewed by:

Kuei Y. Tseng, Rosalind Franklin University of Medicine and Science, USA

Jorge Aceves Ruiz, Centro de Investigación y Estudios Avanzados del IPN, Mexico

*Correspondence:

Elaine Del-Bel, Departamento MEF – Fisiologia, Faculdade de Odontologia de Ribeirão Preto, Universidade de São Paulo, Av. Café S/N, Ribeirão Preto, SP 14040-904, Brazil.
e-mail: eadelbel@forp.usp.br

Inhibitors of neuronal and endothelial nitric oxide synthase decrease L-3,4-dihydroxyphenylalanine (L-DOPA)-induced dyskinesias in rodents. The mechanism of nitric oxide inhibitor action is unknown. The aims of the present study were to investigate the decrease of L-DOPA-induced abnormal involuntary movements (AIMs) in 6-hydroxydopamine (6-OHDA)-lesioned rats by nitric oxide inhibitors following either acute or chronic treatment. The primary findings of this study were that NG-nitro-L-Arginine, an inhibitor of endothelial and neuronal nitric oxide synthase, attenuated AIMs induced by chronic and acute L-DOPA. In contrast, rotational behavior was attenuated only after chronic L-DOPA. The 6-OHDA lesion and the L-DOPA treatment induced a bilateral increase (1.5 times) in the neuronal nitric oxide synthase (nNOS) protein and nNOS mRNA in the striatum and in the frontal cortex. There was a parallel increase, bilaterally, of the FosB/ Δ FosB, primarily in the ipsilateral striatum. The exception was in the contralateral striatum and the ipsilateral frontal cortex, where chronic L-DOPA treatment induced an increase of approximately 10 times the nNOS mRNA. Our results provided further evidence of an anti-dyskinetic effect of NOS inhibitor. The effect appeared under L-DOPA acute and chronic treatment. The L-DOPA treatment also revealed an over-expression of the neuronal NOS in the frontal cortex and striatum. Our results corroborated findings that L-DOPA-induced rotation differs between acute and chronic treatment. The effect of the NOS inhibitor conceivably relied on the L-DOPA structural modifications in the Parkinsonian brain. Taken together, these data provided a rationale for further evaluation of NOS inhibitors in the treatment of L-DOPA-induced dyskinesia.

Keywords: nitric oxide, nitric oxide synthase, Parkinson's disease, L-DOPA-induced dyskinesia, nitric oxide synthase inhibitors, FosB/ Δ FosB, abnormal involuntary movements, striatum

INTRODUCTION

The impairments of Parkinson's disease (PD) can be controlled by treatment with the dopamine precursor L-DOPA (L-3,4-dihydroxyphenylalanine). Regardless of treatment, the disease continues to progress (Tuite and Riss, 2003). Chronic treatment with L-DOPA causes abnormal involuntary movements (AIMs/dyskinesia) in both animals and humans (Marsden and Parkes, 1977; Iancu et al., 2005, for review see Jenner, 2008). The emergence of AIMs with repeated L-DOPA treatment of 6-hydroxydopamine (6-OHDA) lesion rats has allowed for the examination of the mechanisms responsible for treatment-related dyskinesia in PD and the detection of molecules that are able to prevent or reverse their appearance (Cenci et al., 1998). Despite intensely investigated, long-term

adaptations contributing to the development of L-DOPA-induced dyskinesia, virtually nothing is known about the acute expression of dyskinetic movements after a single dose of L-DOPA.

Parkinson's disease is also a disorder marked by an imbalance of non-dopaminergic transmitters (Jenner, 2008; Barone, 2010). Nitric oxide (NO) is a neurotransmitter formed from L-arginine and molecular oxygen by the action of three highly homologous isoforms of nitric oxide synthase (NOS): neuronal (nNOS), endothelial (eNOS), and inducible (iNOS; for review see Guix et al., 2005; Garthwaite, 2008). Within the striatum, endogenous NO is produced by a subclass of aspiny interneurons containing nNOS (Kubota et al., 1993; Morello et al., 1997; Kawaguchi, 1997; Tepper and Bolam, 2004) partly controlled by dopaminergic input (Kawaguchi, 1997; Calabresi et al., 2000; Centonze et al., 2001; West and Grace, 2002, 2004).

The production of NO and superoxide have been implicated in neurodegenerative disorders such as PD (Ebadi and Sharma, 2003). For example, in the striatum in Parkinsonian animal models and humans, NOS has been described as either depressed (rodents – De-Vente et al., 2000; Barthwal et al., 2001; Sancesario et al., 2004; humans – Böckelmann et al., 1994; Eve et al., 1998) or increased (rodents – Ponzoni et al., 2000; Gomes and Del Bel, 2003; Gomes et al., 2008; humans – Hunot et al., 1996; Eve et al., 1998). Additionally,

Abbreviations: 6-OHDA, 6-hydroxydopamine; 7-NI, 7-nitroindazole; AIMs, abnormal involuntary movements; cGMP, cyclic guanosine monophosphate; eNOS, endothelial nitric oxide synthase; iNOS, inducible nitric oxide synthase; L-DOPA, L-3,4-dihydroxyphenylalanine; L-NAME, N(G)-nitro-L-arginine methylester; L-NOARG, NG-nitro-L-Arginine; MFB, medial forebrain bundle; MPTP, 1-methyl-4-phenyl-1,2,3,6-tetrahydropyridine; nNOS, neuronal nitric oxide synthase; NO, nitric oxide; NOS, nitric oxide synthase; PD, Parkinson's disease; sGC, soluble guanylyl cyclase; SIN-1, 3-morpholinosydnonimine; SNc, substantia nigra pars compacta; SNL, lateral substantia nigra; SNV, ventral substantia nigra; TH, tyrosine hydroxylase.

in the 6-OHDA-lesioned striatum, a considerable population of medium spiny neurons presented an excitatory response induced by the NO donor 3-morpholinosydnonimine (SIN-1; Di Giovanni et al., 2003; Galati et al., 2008) instead of the inhibition observed in non-lesioned animals. Because NO may worsen PD symptoms (Gomes et al., 2008), several NOS inhibitors have been suggested for pharmacological treatment (Calabrese et al., 2000; Del-Bel et al., 2005; Aquilano et al., 2008; Jenner, 2008; Kavya et al., 2008).

Nitergic mechanisms could contribute to L-DOPA-induced dyskinesia (Monville et al., 2006; Lane et al., 2008). In PD patients, L-DOPA therapy has been shown to cause a marked increase in the production of the NO second messenger cyclic guanosine monophosphate (cGMP) within the cerebellum and in the serum (Chalimoniuk et al., 2004). Sanchez et al. (2002) showed that NO stimulated L-DOPA release in the striatum in a time- and concentration-dependent manner. In mice, L-DOPA therapy has been shown to induce striatal NO production (Itokawa et al., 2006). Additionally, Chalimoniuk and Langfort (2007) showed that L-DOPA up-regulated the NO/soluble guanylyl cyclase (sGC)/cGMP pathway to levels found in MPTP (1-methyl-4-phenyl-1,2,3,6-tetrahydropyridine)-injected mice. Our group had recently shown that 7-nitroindazole (7-NI) and N(G)-nitro-L-Arginine (L-NOARG), nNOS and nNOS/eNOS inhibitors, respectively, can reduce the severity of L-DOPA-induced dyskinesia generated in the 6-OHDA-lesioned rats (Padovan-Neto et al., 2009; Novaretti et al., 2010) and mice (Del-Bel et al., 2011). Nevertheless, the mechanism of how NOS inhibition decreases L-DOPA-dyskinesias is unknown.

The aim of the present study was to investigate, in hemiparkinsonian rats, the effect of NOS inhibition in the L-DOPA-induced AIMs achieved following either single or chronic treatment. The expression of the nNOS protein and mRNA was analyzed in the reactive 6-OHDA-lesioned and contralateral striatum.

MATERIALS AND METHODS

DRUGS

Apomorphine hydrochloride (Sigma-Aldrich, St. Louis, MO, USA); L-DOPA (Prolopa dispersive, Hoffman-LaRoche, Rio de Janeiro, RJ, Brazil) plus benserazide-HCl; NG-nitro-L-arginine (L-NOARG; Sigma-Aldrich, St. Louis, MO, USA). All drugs were dissolved in physiological saline and administered in a volume of 2 ml/kg.

ANIMALS AND 6-HYDROXYDOPAMINE (6-OHDA) TREATMENT

Adult male *Wistar* rats (200–250 g) were housed in groups of five per cage in a temperature-controlled room (23°C), under 12-h light/dark cycle with free access to food and water. Behavioral test was performed from 2:00 to 6:00 PM. All experiments were conducted according to the principles and procedures described by the Guidelines for the Care and Use of Mammals in Neuroscience and Behavioral Research (ILAR, USA). The Institution's housing conditions and experimental procedures were previously approved by the local Animal Ethics Committee (protocol number: 101/2009).

Rats were submitted to stereotaxic surgery as described by Padovan-Neto et al. (2009). Briefly, rats were anesthetized with tribromoethanol (0.25 mg/kg i.p., Sigma-Aldrich, St. Louis, MO, USA) and received a single injection of either saline or 6-OHDA (16 µg in 3 µl of saline containing 0.05% ascorbic acid Sigma-Aldrich, St. Louis, MO, USA) into the right medial forebrain bundle (MFB), coordinates in mm relative

to bregma: antero-posterior (AP): −4.4; lateral (L): −1.2; dorso-ventral (DV): −8.2 (Paxinos and Watson, 1998). The infusion was at the rate of 1 µl/min and the cannula was left in the place for 3 min before withdrawal. To limit the damage in noradrenergic neurons, desipramine hydrochloride (25 mg/kg i.p., Sigma-Aldrich, St. Louis, MO, USA) and pargyline (40 mg/kg, Sigma-Aldrich, St. Louis, MO, USA) were administered 30 min before 6-OHDA injection. Brain was removed from the animals for western blot, RT-PCR and histopathological analyses. Two separate experimental groups of rats each were used for behavioral and pathological analyses. Behavioral experiments were performed on a separate group of animals.

BEHAVIORAL TESTS

Stepping test

This is a modified version of the stepping test originally proposed by Chang et al. (1999) and Olsson et al. (1995). Rats were held at the rear part of the torso by one hand with their hind limbs lifted and one forepaw held steady along its trunk by the hand of the experimenter. Then, the animal was moved ahead across a table for a distance of 90 cm in 12 s (Novaretti et al., 2010). During this interval the numbers of adjusting steps of the weight-bearing forepaw to compensate for the straight ahead movement of the body were counted. For each animal the test was begun randomly with the right or left forepaw. The animal performance was measures pre-drug, 1 and 2 h after L-DOPA intake (post-drug). The experimenter was blind to the treatment.

Open field test

The procedure was described by Cools (1980). The rats were placed in an open arena which consisted of a circular enclosure (72 cm diameter) surrounded by a 49 cm Plexiglas wall with the floor divided into 12 sections. Rats were placed in the center of the arena and allowed to explore it for 5 min. The following behaviors were recorded by observation: number of crossings (i.e., number of floor sections traversed, meaning horizontal exploration), the number of edge and center squares entered (Sullivan et al., 1994), the number of rearing (standing with the forepaws raised in the middle of the arena or against the walls, denoting the vertical exploration) and grooming.

Rotational behavior test

Rotational behavior was measured after either apomorphine or L-DOPA injection by placing the animals in a 40-cm-diameter bowl surrounded by a 16-cm wall. The rats were allowed to acclimate to the environment for 5–10 min before drug treatment. Contralateral rotations, defined as complete 360° turns away from the lesioned side of the brain, were counted. For apomorphine (0.5 mg/kg, s.c.) the total number of full contralateral turns was counted during 45 min. Only rats showing >2 turns/min (>90 turns/45 min) were included in the study. After L-DOPA treatment (100 mg/kg, gavage), the number of contralateral turns was counted for 2 h in periods of 5 min at 0, 25, 55, 85, and 115 min after injection.

Abnormal Involuntary Movements (AIMs)

A trained observer blind to treatment assessed each rat for the presence of AIMs at 1 and 2 h after saline or L-DOPA accordingly to the rat dyskinesia scale (Cenci et al., 1998; Winkler et al., 2002). Briefly, rats were videotaped for 1 min and scores ranging from 0 to

4 were given for topographical distribution of axial, limb, orofacial and locomotor AIMs. To obtain a more accurate scale, additional scores also ranging from 0 to 4 were attributed to the amplitude of axial and limb AIMs (Winkler et al., 2002). Each AIM was presented separately at 1 and 2 h after L-DOPA.

TYROSINE HYDROXYLASE (TH) IMMUNOREACTIVITY

Dopaminergic depletion was confirmed with TH immunohistochemistry.

Tissue processing

Twenty-four hours after last test, rats were deeply anesthetized with urethane (25 mg/kg, Sigma-Aldrich, St. Louis, MO, USA) and then rapidly perfused transcardially with 250 ml of cold saline and 400 ml of 4% paraformaldehyde (Sigma-Aldrich, St. Louis, MO, USA) in 0.1 M phosphate buffer (pH 7.4). The tissues were cut at 25 μ m on a freezing microtome. Sections through the striatum and SNc were collected in 0.01 M phosphate-buffered saline solution containing 0.02% sodium azide and stored at 4°C until use.

Immunohistochemistry reaction

Tyrosine hydroxylase-immunohistochemistry was performed using a standard peroxidase based method (Gomes et al., 2008). Briefly, the sections were incubated with primary TH antibody (1:2000, Pel Freez, Rogers, AR, USA) overnight at 4°C followed by biotinylated secondary antibody (Vectastain ABC Kit, Vector Laboratories, Southfield, MI, USA) and horseradish peroxidase (HRP)-conjugated streptavidin (Vectastain ABC Kit, Vector Laboratories, Southfield, MI, USA). The sections were developed using diaminobenzidine (Sigma-Aldrich, St. Louis, MO, USA) as the chromogen.

Image analysis

The AP localizations (from Bregma in mm) of the analyzed areas were: AP: -5.2 for SNc and AP: -6.03 for ventral and lateral substantia nigra (SNV and SNL respectively, **Figure 1**). Labeling of TH positive cells/fibers in SNc were assessed by measuring optical density of the entire area of the structure. Background (corpus callosum) was subtracted from all subsequent measurements. Results are presented the percentage of the optical density over the area (in mm²) of the ipsilateral side compared to the contralateral one. The number of TH positive neurons in the SNL and SNV were counted manually and results are expressed as the number of positive stained neurons per mm² of the structure. For each selected area, quantifications were carried out using four sections per animal, separated by 125 μ m approximately. Quantifications were performed blindly, bilaterally, using a light microscope (Leica DMRB) equipped with a video camera (Leica DFC420). Neuroanatomical sites were identified using the atlas of Paxinos and Watson (1998). The analysis was done using the software ImageJ¹.

WESTERN BLOT ANALYSIS

The animals were decapitated, the lesion-reactive (right) and the contralateral (left-control) striatum were microdissected on an ice-cooled dissection cover, with the help of magnifying lens (Leica Zoom 2000), and immediately frozen in liquid nitrogen (-196°C). Tissue samples were stored at -80°C until use. Left and right striatum

was processed separately. The homogenates were centrifuged at 10000 rpm for 25 min at 4°C. The supernatants were recovered for protein concentration measurements using Bradford assay (Bio-Rad Protein assay, Bio-Rad, Germany). Proteins (30 μ g) were resolved by sodium dodecyl sulfate polyacrylamide gel electrophoresis (8% SDS-PAGE) and semi-dry transferred to a nitrocellulose membrane.

Because the FosB primary antibody recognizes both full-length FosB and Δ FosB-related proteins, the staining obtained with this antibody is referred to as FosB/ Δ FosB. Nitrocellulose membranes were incubated at 4°C overnight using the following antibodies: mouse monoclonal anti-nNOS (1:1000, BD Biosciences, USA), rabbit polyclonal anti-FosB/ Δ FosB (1:1000, Santa Cruz Biotechnology, USA), mouse monoclonal anti- β -actin (1:5000, Santa Cruz Biotechnology, USA). Bound antibodies were detected with HRP-conjugated secondary anti-mouse or anti-rabbit antibodies (1:5000, Jackson Immuno Research Laboratories, USA). Bands were visualized by enhanced chemiluminescence (ECL, Amersham, UK) and quantified with the software ImageJ². The integrated density (product of the area and mean gray value) of each band of the proteins of interest was normalized to the integrated density of β -actin and used to compare relative levels of the proteins of interest. Each experiment was performed at least three times with similar results.

REAL-TIME QUANTITATIVE PCR

For RT-PCR (see Bibancos et al., 2007), the brain regions dissected were the prefrontal cortex, the striatum, and the hippocampus (contralateral and lesion-reactive), in a similar way described for the western blot. Frozen samples were immersed in TRIzol (Invitrogen™ Cat. No. 15596-026) and homogenized (Polytron PT10/35-Brinkmann, Westbury, NY, USA) by 30 s using maximum speed. Total RNA was isolated according to the manufacturer's guidelines and quantified by a spectrophotometer. The integrity of RNA was verified on ethidium bromide-stained 1% agarose gel, and the fluorescence intensity ratio of 28S/18S rRNA was determined (Eagle Eye; Stratagene, La Jolla, CA, USA). Only samples that met our criteria of quality (both 260/280 nm and 28S/18S > 1.8) were included in the experiments. The DNA was removed from RNA samples before reverse transcription with a RQ1 RNase-Free DNase (Promega® Cat. No. M6101) at 37°C for 30 min and the enzyme inactivated at 65°C for 10 min, maintaining the integrity of the RNA.

Total RNA (2 μ g) was reverse transcribed at the same time using a master mix containing oligo (dT; Invitrogen™ Cat. No. 18418-012) primer and SuperScript™ III Reverse Transcriptase (Invitrogen™ Cat. No. 18080-093) in a final volume of 20 μ l. Specific primers (*Rattus norvegicus*) for the nNOS enzyme, and the control genes cyclophilin A (peptidylprolyl isomerase A: Ppia), glyceraldehyde-3-phosphate dehydrogenase (Gapd) and beta-actin (Actb) were designed using the Primer3 software³. The following criteria were followed: primer size (18–20 nucleotides), G/C content (~50%), annealing temperature (58–60°C), amplicon size (93–221 nucleotides) and proximity of 3' end, when possible. Forward and reverse primers were designed in different exons (with the exception of the intron less genes: *Drd1a*) and specificity was confirmed by a Basic

²<http://rsb.info.nih.gov>

³http://frodo.wi.mit.edu/cgi-bin/primer3/primer3_www.cgi

⁴<http://www.ncbi.nlm.nih.gov/BLAST>

¹<http://rsb.info.nih.gov>

Local Alignment Search Tool (BLAST)⁴ software-assisted search of a non-redundant nucleotide sequence database for rat, and electrophoresis on an ethidium bromide-stained 3% agarose gel. Real-time PCR analysis of gene expression was carried out in an ABI Prism 7700 sequence detection system (Applied Biosystems). The optimal concentration of cDNA and primers as well as the maximum efficiency of amplification were obtained through five-point, twofold dilution curve analysis for each gene. Each PCR contained 12.5 ng of reverse-transcribed RNA, 200 nm of each specific primer, SYBR® GREEN PCR Master Mix (Applied Biosystems Cat. No. 4309155), and RNase free water to a 20 µl final volume. cDNA samples from each area for all treatments and strain were processed at the same time in triplicate for each gene and the negative controls included for each brain area/primer. The PCR conditions were 10 min at 95°C, followed by 40 cycles at 95°C for 15 s and 60°C for 60 s, and a melting step (dissociation curve) was performed after each run to further confirm the specificity of the products and the absence of primer dimers. Real-time data were analyzed using Sequence Detector System 1.7 (Applied Biosystems). The relative expression in all brain areas was calculated according to a previous study (geNorm v 3.4, Vandesompele et al., 2002).

The following pairs of primers for cDNA, from genes available at the NCBI-NIH GeneBank, were used to nNOS (NM 052799; product of 202 bp): sense 5'-ATT CAA CAG CGT CTC CTC CT-3' and antisense 5'-AAT CCT CTC CCC TCC CAG T-3'. Reference genes: Ppia (NM 017101; product of 101 bp): sense 5'-AAT GCT GGA CCA AAC ACA AA-3' and antisense 5'-CCT TCT TTC ACC TTC CCA AA-3'; Gapd (NM 017008; product of 162 bp): sense 5'-ATG GTG AAG GTC GGT GTG-3' and antisense 5'-GAA CTT GCC GTG GGT AGA G-3'; Actb (NM 031144; product of 174 bp): sense 5'-CGT TGA CAT CCG TAA AGA CC-3' and antisense 5'-GCC ACC AAT CCA CAC AGA-3'.

STATISTICAL ANALYSIS

The effects of L-NOARG on acute and chronic L-DOPA-induced AIMs were evaluated, respectively, by Mann–Whitney and Wilcoxon non-parametric tests. L-NOARG effects on rotational behavior were evaluated by one way repeated measure ANOVA (rANOVA), Student's *t*-test or Student's paired *t*-test as indicated. L-NOARG effects on stepping test were obtained on each side (ipsi- and contralateral) with two way ANOVA or one way rANOVA as indicated. Stepping test was analyzed on each side by two way rANOVA being test session (pre-test and test) and time (day 1 and day 15) the repeated measures. When significant interactions were found on time, one way rANOVA were performed for each day. Western blot and data RT-PCR data was compared by using one and two way rANOVA as indicated. Data are presented as mean ± SEM. *Post hoc* analysis was performed by Sidak or Student *t*-test as indicated. Statistical significance level was set at $p < 0.05$.

EXPERIMENTAL DESIGN

Unilaterally 6-OHDA-lesioned rats were assigned to treatment groups according to apomorphine-rotational behavior test performance (day 21 following surgery), to ensure that these measures were matched between groups. No ipsilateral rotation (complete 360° turns toward the lesion-reactive striatum) was observed. 6-OHDA-lesioned rats

presenting more than two rotations in 1 min were included in the study. L-DOPA or vehicle treatment started approximately 1 week after apomorphine test. The study consisted of four different experiments.

Experiment 1

Experiment 1 was a behavioral evaluation of control, 6-OHDA lesioned and dyskinetic rats to assess spontaneous locomotor activity, horizontal activity, and forelimb use asymmetry by the open field and the stepping tests. Approximately 2 days after the apomorphine-rotational behavior test (wash-out time), independent groups of 6-OHDA-lesioned ($n = 7$) and controls ($n = 6-7$) were submitted to the stepping test or the open field test. 6-OHDA-lesioned rats treated with L-DOPA ($n = 6-9$) were also tested at the 15th day of L-DOPA treatment. The open field test was completed before L-DOPA intake. The stepping test was performed before (pre-test) and after L-DOPA treatment.

Experiment 2

Experiment 2 aimed to compare the molecular effects in the striatum (bilaterally), estimating the nNOS expression (mRNA and protein) and FosB/ΔFosB (protein). Rats were sacrificed 24 h after the last behavioral test for immunohistochemistry, western blot or RT-PCR analysis. The RT-PCR analysis was prepared in controls (control/saline, $n = 7$) and 6-OHDA-lesioned rats ($n = 13$). 6-OHDA-lesioned rats matched for the apomorphine-rotational behavior score were divided into two groups: 6-OHDA/sal (saline 15 days, once a day, gavage, $n = 7$) and 6-OHDA/L-DOPA (L-DOPA + benserazide, 100 and 25 mg/kg, respectively, 15 days, once a day, gavage, $n = 6$). The western blot protein analysis was prepared in control/sal ($n = 5$), 6-OHDA/sal ($n = 5$) and 6-OHDA/L-DOPA + benserazide (100 and 25 mg/kg) after either 1 day (acute; $n = 5$) or 15 days (chronic; $n = 5$) of treatment.

Experiment 3

Experiment 3 was designed to compare the behavioral effects of acute L-NOARG on established L-DOPA-induced AIMs. Rats received daily administration (for 15 days) of either vehicle (groups: control/sal, $n = 10$ and 6-OHDA/sal, $n = 10$) or L-DOPA + benserazide (groups: control/L-DOPA, $n = 11$ and 6-OHDA/L-DOPA, $n = 17$). Rats were matched for the AIM scores on day 15 of L-DOPA treatment. On day 16, animals were divided into subgroups: control/sal, $n = 5$; 6-OHDA/sal, $n = 5$; control/L-DOPA, $n = 5-6$; or 6-OHDA/L-DOPA, $n = 8-9$. Animals received (intraperitoneal (i.p.), 30 min before L-DOPA) either 50 mg/kg of L-NOARG or saline. The L-NOARG effect was calculated by comparing AIM scores, rotational behavior and the results of the stepping-test, between days 15 and 16.

Experiment 4

Experiment 4 was designed to compare the behavioral effects of acute L-NOARG on acute L-DOPA-induced AIMs. Rats were divided into subgroups (control/sal, $n = 5$; 6-OHDA/sal, $n = 5-6$; control/L-DOPA, $n = 5$; or 6-OHDA/L-DOPA, $n = 10-11$) and received either 50 mg/kg of L-NOARG or saline 30 min before L-DOPA. AIMs, rotational behavior and the stepping test were evaluated. The L-NOARG effect was calculated by comparing behavioral data between the groups.

RESULTS

6-OHDA-lesioned rats presented apomorphine-induced rotation contralateral to the lesion (317 ± 44 turns/45 min). No rotation was observed in the control animals. Quantification of striatal TH-positive cells and fibers by optical density was measured in the substantia nigra compacta (SNc) and in the SNL and SNV (Figure 1). TH-immunostaining (Figure 1A) indicated a dopaminergic cell loss >95% in the SNc (Figure 1C), ipsilateral to the 6-OHDA injection (Figures 1A,B). SNL and SNV also presented a reduction in the number of cells and fibers (Figures 1A,B,D). No change was observed in control rats (data not shown).

BEHAVIORAL EVALUATION OF 6-OHDA-INDUCED LESION AND L-DOPA-INDUCED AIMS IN RATS

Due to the lack of statistical difference between tests performed at 1 and 2 h ($p > 0.05$, paired *t*-test) with the stepping test, data were presented as the mean of values collected at these times. 6-OHDA-lesioned rats, but not controls, presented an impairment of the contralateral forehand paw when compared to the ipsilateral paw

(approximately 70%, Figure 2A). L-DOPA treatment on day 1 improved stepping performance (Figure 2B, group: $F_{(1,26)} = 112.35$, $p < 0.05$; test: $F_{(1,26)} = 56.82$, $p < 0.05$; interaction: $F_{(1,26)} = 26.15$, $p < 0.05$). The effect was maintained through the last day of treatment (Figure 2B, day 15), with no differences between groups (pre-test and test, $p > 0.05$). The ipsilateral paw adjusting steps were not changed by lesion or drug treatment (Figure 2A). Finally, there was a significant correlation ($r = 0.56$, $p = 0.02$, Figure 2C) between apomorphine induction of the rotational behavior and forehand paw test impairment.

The open field test revealed a decrease in the motor activity after 6-OHDA-lesion (rearing and the number of squares crossed in comparison with controls, Table 1; $p < 0.05$). The lesioned rats demonstrated a noticeable preference for exploration of the right side of the field, but there was no significant difference in grooming. L-DOPA treatment did not change these parameters ($p > 0.05$; Table 1).

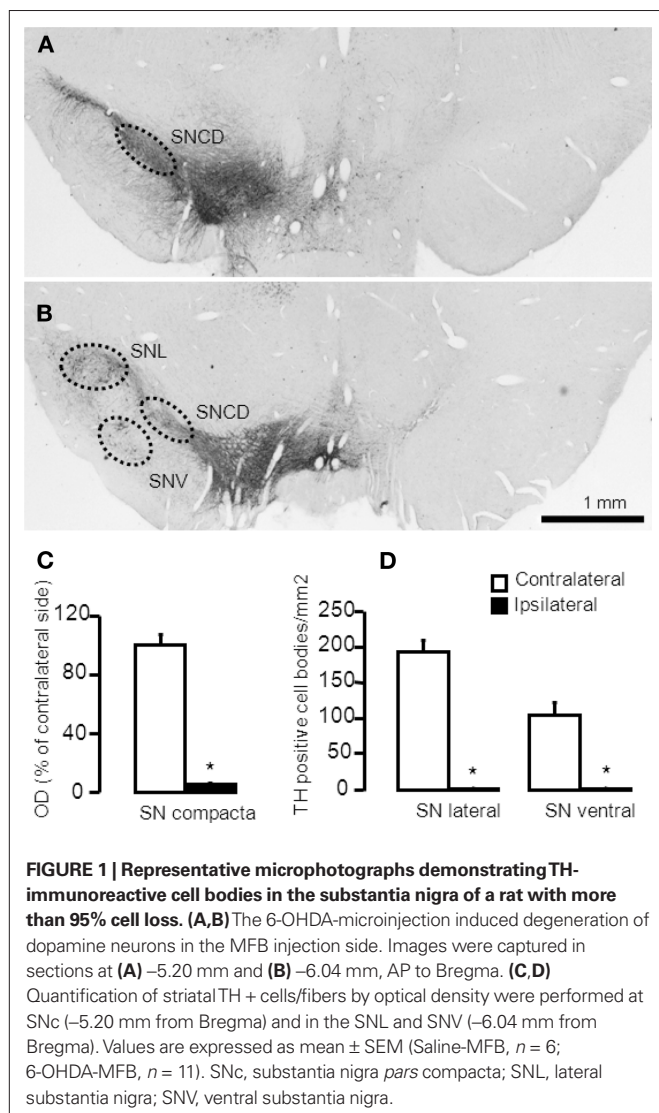
NEURONAL NOS EXPRESSION IN THE STRIATUM OF CONTROL, 6-OHDA-LESIONED AND L-DOPA-TREATED (DYSKINETIC) RATS

In the striatum, the expression of nNOS transcript in both hemispheres differed significantly among the groups (Figure 3B; side-treatment interaction: $F_{(2,17)} = 5.06$, $p < 0.05$). There was a modest increase (1.5 times) in the ipsilateral striatum of both 6-OHDA-lesioned and dyskinetic rats. However, in the striatum contralateral to the lesion in the L-DOPA-treated rats, there was a greater (10 times) increase in nNOS mRNA expression. A similar result was observed in the prefrontal cortex, but the greatest increase in nNOS mRNA was observed in the ipsilateral frontal cortex (Figure 3A; side-treatment interaction: $F_{(2,16)} = 14.91$, $p < 0.05$, Figure 3A). No changes were observed in the hippocampus (Figure 3C, $p > 0.05$).

The western blot analysis (Figure 4) indicated a bilateral increase in the nNOS protein content in the striatum (treatment: $F_{(2,6)} = 82.56$, $p < 0.05$, side: $F_{(1,6)} = 17.22$, $p < 0.05$; interaction: $F_{(1,6)} = 0.57$; $p < 0.05$). In the striatum of 6-OHDA-lesioned and L-DOPA-induced AIMS rats, there was an increase of nNOS protein between 19 and 24% (Figure 4; $p < 0.05$). Additionally, FosB/ Δ FosB protein was visualized bilaterally in the striatum of lesioned rats (Figure 5A). Acute and chronic L-DOPA administration to 6-OHDA-lesioned rats induced a bilateral increase in the expression of FosB/ Δ FosB protein (side: $F_{(1,4)} = 757.77$, $p < 0.05$; treatment: $F_{(1,4)} = 314.46$, $p < 0.05$; interaction: $F_{(1,4)} = 201.30$, $p < 0.05$). The increase was larger in the striatum ipsilateral to the lesion. Chronic L-DOPA treatment induced a more pronounced FosB/ Δ FosB expression in the ipsilateral striatum when compared to the ipsilateral striatum in the acute L-DOPA-treated rats ($p < 0.05$; Figure 5B).

BEHAVIORAL EFFECTS OF ACUTE L-NOARG TREATMENT ON ESTABLISHED L-DOPA-INDUCED AIMS

L-DOPA chronic treatment, in general, induced an increase in the number of turns (time: $F_{(2,32)} = 78.27$, $p < 0.05$) and AIMS ($p < 0.05$). L-DOPA treatment in the control rats induced no AIMS and no turns. L-NOARG reduced locomotor AIMS (Figure 6A, 1 h; $p < 0.05$), limb/orofacial AIMS (Figure 6B; 2 h; $p < 0.05$) and contralateral turns (Figures 6C,D; $p < 0.05$). L-DOPA treatment



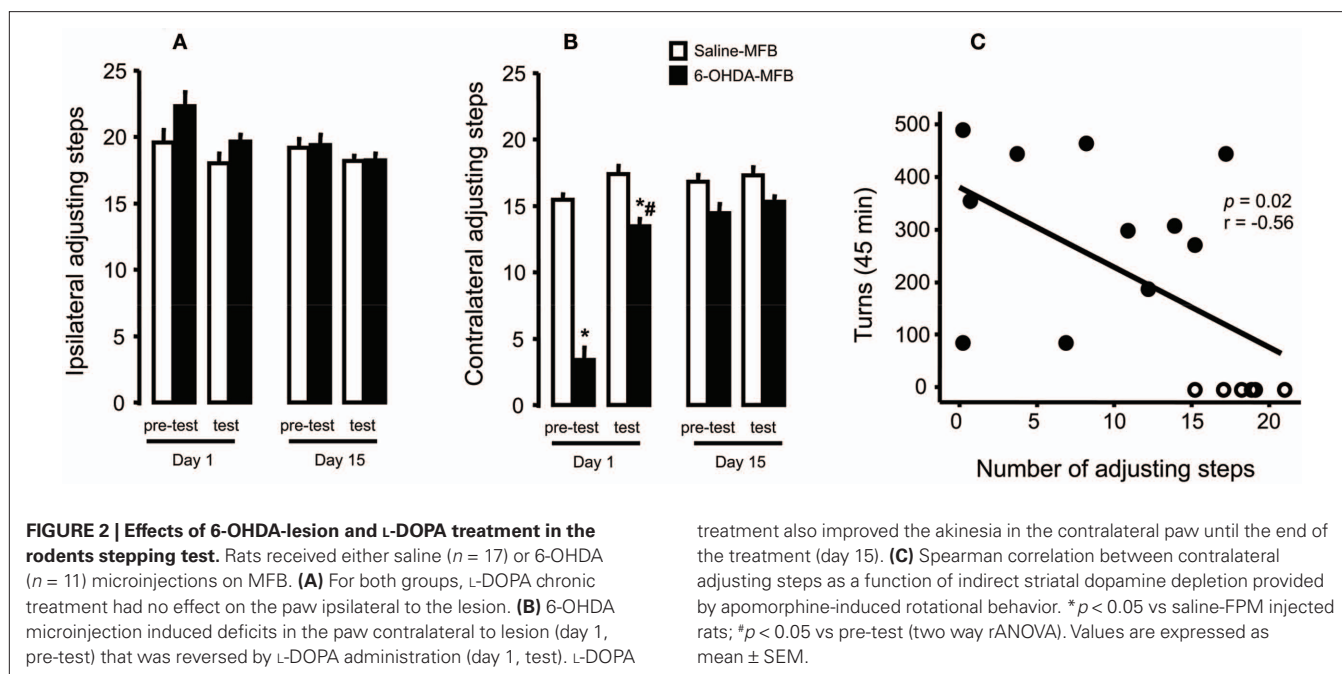


Table 1 | Exploratory behavior of rats in open field arena.

	Rearings	Squares crossed	Grooming	Preference (%)
Control ($n = 7$)	26 \pm 2.58	31.29 \pm 2.81	5 \pm 0.62	Left: 100
6-OHDA ($n = 7$)	15.14 \pm 3.82*	17.43 \pm 2.22*	4.29 \pm 1.02	Right: 85.7
6-OHDA/L-DOPA ($n = 6$)/day 1	10 \pm 2.50	14.83 \pm 1.89	3 \pm 0.58	Left: 14.3
6-OHDA/L-DOPA ($n = 6$)/day 15	5.83 \pm 1.74	10.33 \pm 1.38	2.67 \pm 0.56	Right: 83.3
				Left: 16.6
				Right: 100

Numbers are mean \pm SEM. * $p < 0.05$ vs control (paired *t*-test).

improved stepping test performance in the contralateral paw, as demonstrated in **Figure 2**. The adjusting step in the ipsilateral paw did not change. L-NOARG before L-DOPA induced no effect in the ipsilateral paw (**Figure 6E**; $p > 0.05$) but did result in a small reduction ($< 20\%$) in the contralateral paw (**Figure 6F**; treatment: $F_{(1,11)} = 3.02$, $p > 0.05$; group: $F_{(1,11)} = 1.57$, $p > 0.05$; interaction: $F_{(1,11)} = 9.01$, $p < 0.05$).

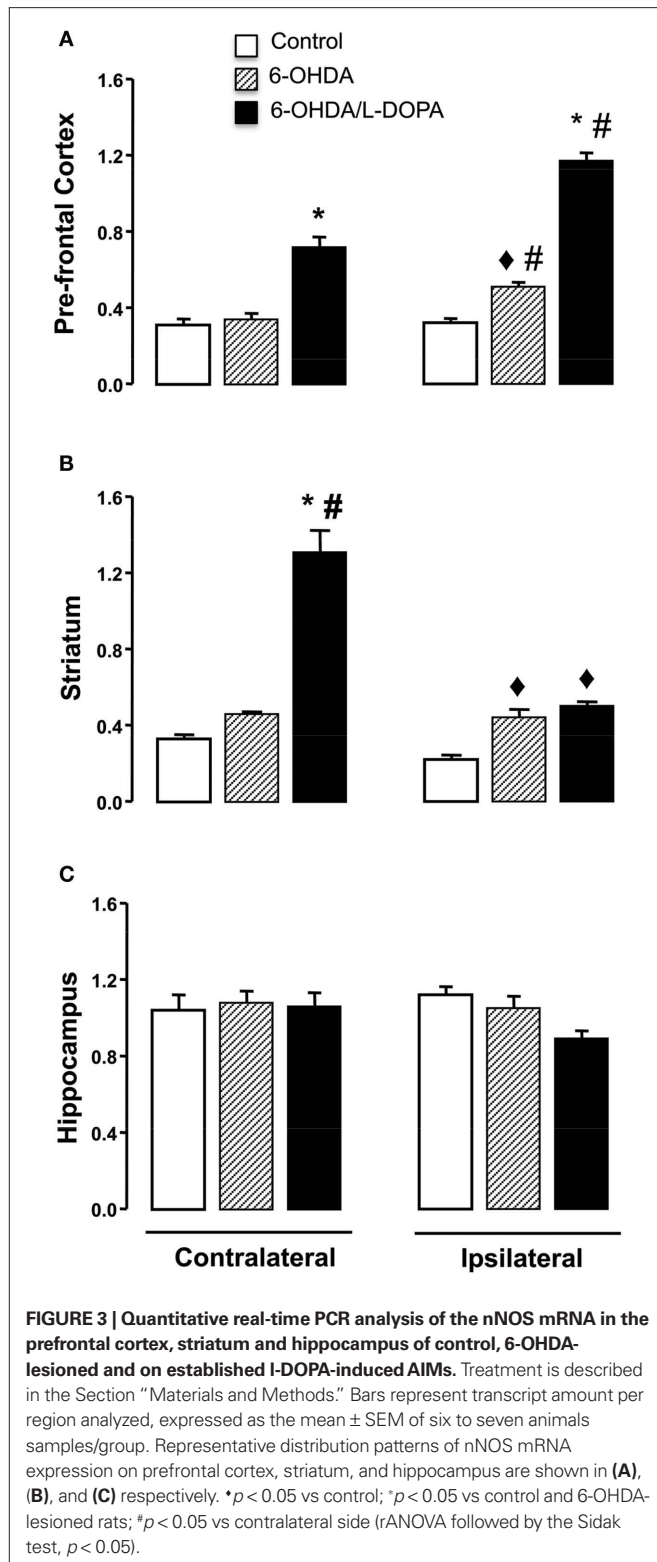
BEHAVIORAL EFFECTS OF L-NOARG ON ACUTE L-DOPA-INDUCED AIMS

All subtypes of AIMS were observed 1 and 2 h after the administration of acute L-DOPA to 6-OHDA-lesioned rats (**Figures 7A,B**). Pre-treatment with L-NOARG reduced AIMS (limb, limb amplitude, and orofacial) at the first hour (**Figures 7A,B**, $p < 0.05$) and locomotor AIMS after 2 h of L-DOPA treatment (**Figure 7B**; $p < 0.05$). In contrast, L-NOARG did not change L-DOPA-induced rotation (**Figures 7C,D**). Administration of a single L-DOPA treatment to 6-OHDA-lesioned rats induced a slight increase in the stepping test performance of the ipsilateral paw, with no difference in the contralateral paw (**Figure 7E**; group: $F_{(1,27)} = 0.38$, $p > 0.05$; treatment: $F_{(1,27)} = 2.26$, $p > 0.05$; interaction: $F_{(1,27)} = 6.94$, $p < 0.05$).

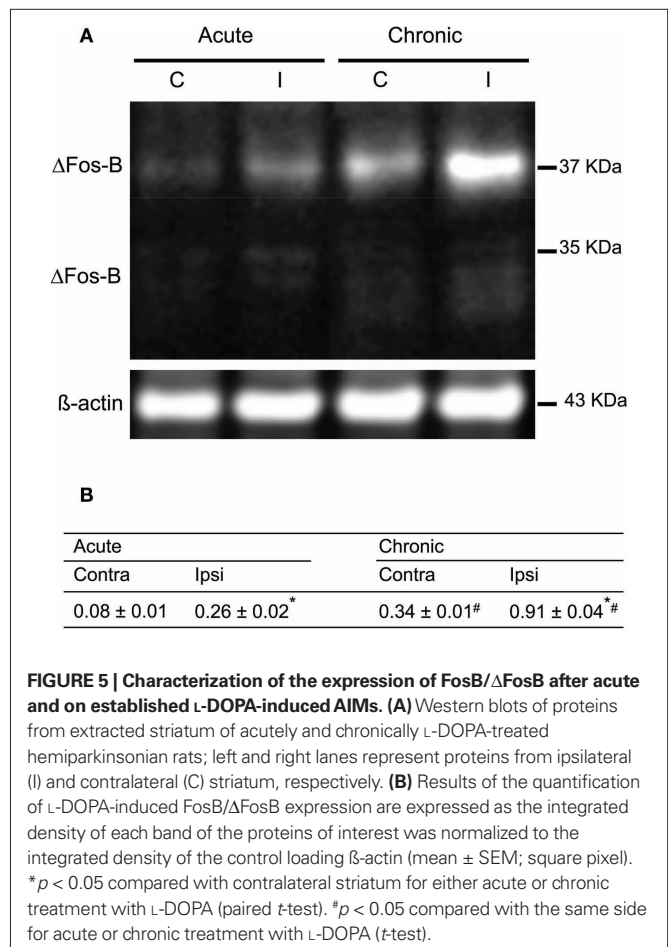
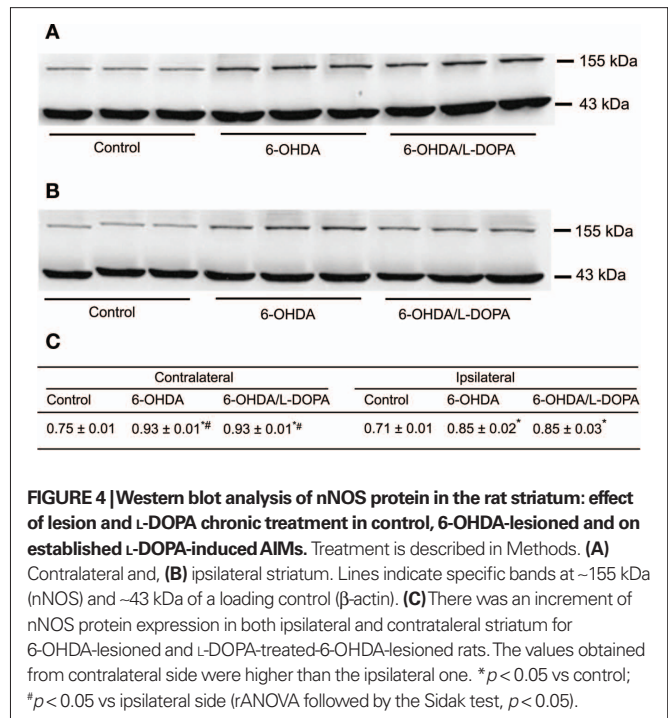
Pre-treatment with L-NOARG decreased stepping test in the contralateral paw performance (**Figure 7F**; group, $F_{(1,27)} = 16.23$, $p < 0.05$; treatment: $F_{(1,27)} = 5.21$, $p < 0.05$; interaction: $F_{(1,27)} = 11.37$, $p < 0.05$) with no effect in the ipsilateral paw.

DISCUSSION

The main findings of this study were that L-NOARG attenuated AIMS induced by acute and chronic L-DOPA treatment. Rotational behavior was attenuated only after chronic L-DOPA administration. L-DOPA improved stepping test performance, and its chronic administration did not alter open field behavior. Our results indicated a correlation between apomorphine-induced rotation and the decrease in the number of adjusting steps performed with the contralateral forepaw in the 6-OHDA-lesioned rats. In the striatum and the frontal cortex, the 6-OHDA lesion and the L-DOPA treatment induced a bilateral increase in the nNOS protein, nNOS mRNA and the FosB/ Δ FosB, the FosB/ Δ FosB being greatest in the ipsilateral striatum. In contrast, there was an increase of 10 times in the nNOS mRNA in the contralateral striatum and in the ipsilateral frontal cortex with L-DOPA-chronic treatment.



Individual AIM categories are highly interrelated, but this does not imply that each AIM category represents the same phenomena. Moreover, there is currently no consensus on the



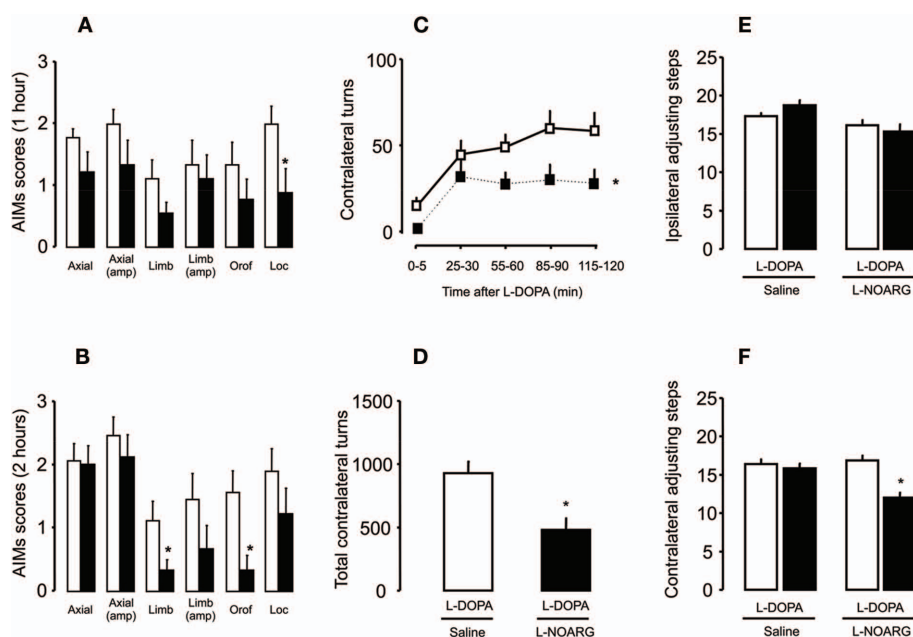


FIGURE 6 | Effects of L-NOARG pre-treatment on AIMs, rotational behavior and stepping test on established L-DOPA-induced AIMs. (A) L-NOARG pre-treatment significantly reduced locomotor AIM scores at 1 h after L-DOPA. **(B)** Limb and orofacial AIMs scores were significantly reduced by L-NOARG at 2 h after L-DOPA. * $p < 0.05$ (Wilcoxon). **(C)** L-NOARG pre-treatment reduced contralateral turns measured during 5 min at 0, 25, 55, 85, and 115 min after L-DOPA treatment.

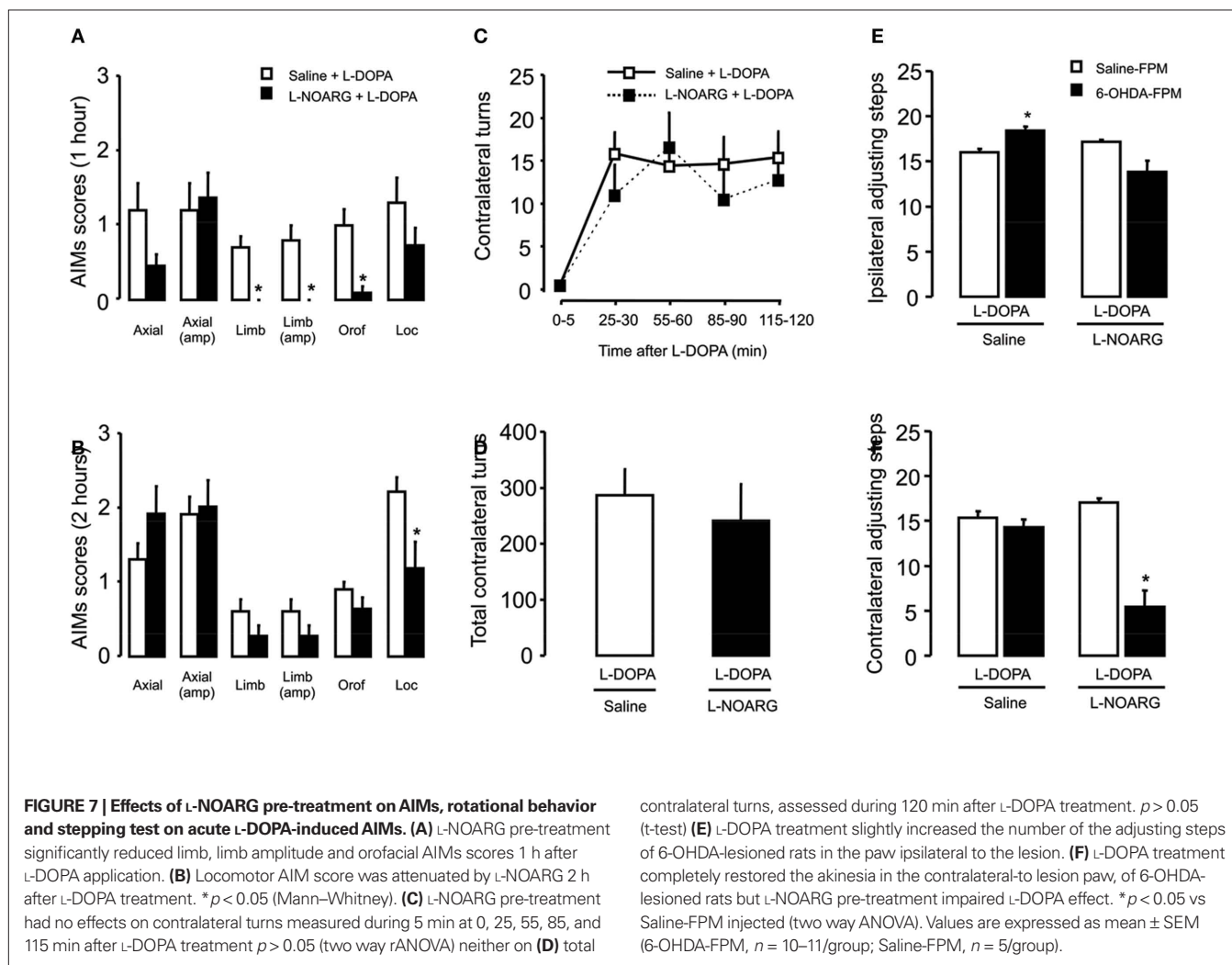
* $p < 0.05$ (one way rANOVA). **(D)** L-NOARG reduced total contralateral turns measured during 120 min after L-DOPA. $p < 0.05$ (paired t-test). After chronic L-DOPA treatment L-NOARG pre-treatment did not affect **(E)** ipsilateral adjusting steps and **(F)** slight reduced adjusting steps performed with contralateral paw. * $p < 0.05$ vs Saline-FPM (one way rANOVA). Values are expressed as mean \pm SEM (6-OHDA-FPM, $n = 8-9$ /group; Saline-FPM, $n = 5-6$ /group).

behavioral components underlying turning. The interpretation of circling behavior has been greatly debated with the introduction of a rodent rating scale for dyskinesia (Henry et al., 1998; Lundblad et al., 2002; Konitsiotis and Tsironis, 2006; Lane et al., 2006; Cenci and Konradi, 2010). The phenomenon of rotation was first described by Ungerstedt and Arbuthnott (1970). The administration of post-synaptic dopamine agonists, such as L-DOPA, induced contraversive rotation through asymmetric striatal receptor stimulation (Zetterstrom et al., 1986; Schwarting et al., 1991). The mechanisms by which asymmetry in central dopaminergic systems translated into the motor response of turning remains unclear (for a review, see Miller and Beninger, 1991; Dunnett and Robbins, 1992). Turning has been interpreted as either a lateralized expression of sensory hyperattention or as the result of asymmetries in the dopaminergic control of posture or locomotion (for review see Miller and Beninger, 1991; Schwarting and Huston, 1996; Lundblad et al., 2002). Early reports suggested that the amplitude enhancement of the contralateral rotational response was caused by basal ganglia sensitization similar to that thought to underlie the development of dyskinesias (Papa et al., 1994; Henry et al., 1998; Mura et al., 2002). Our results corroborated findings of L-DOPA-induced rotation differences between acute and chronic treatment. It reflected a difference in the underlying neural mechanisms revealed by the distinct NO system interference.

The adjusting steps task is used as an index of severe dopaminergic depletion (Olsson et al., 1995; Schwarting and Huston, 1996; Chang et al., 1999). In corroboration, adjusting steps correlated with apomorphine-induced rotations. L-NOARG *per se* slightly

decreased adjusting steps of the contralateral paw, an effect that disappeared with chronic L-DOPA treatment. The impairment in the stepping test could be interpreted as motor behavior impairment in the unprimed L-DOPA rats. However, previous results (Novaretti et al., 2010) have shown no interference of 7-NI in the stepping test performance following either acute or chronic L-DOPA treatment. The open field test, a test that evaluates exploratory behavior as an index of motor activity, was not modified by either acute or chronic L-DOPA treatment. Therefore, given that L-NOARG did not interfere with acute L-DOPA rotational behavior, our results suggested that the effect of the NOS inhibitor could conceivably rely on the L-DOPA structural modifications in the Parkinsonian brain (Cenci et al., 1998, 2002; Lundblad et al., 2002).

The implications of NO in the response to anti-dyskinetic therapy are poorly understood. Substantial evidence has demonstrated the involvement of NO in the degeneration of dopaminergic neurons of the nigrostriatal pathway (Duncan and Heales, 2005). There are several possible mechanisms through which NOS inhibitors may influence L-DOPA-induced dyskinesias. NO modulates L-DOPA release from the striatum (Sanchez et al., 2002; Abreu-González et al., 2006). Additionally, in the rat striatum and medial preoptic area, NO increased both dopamine and serotonin release in a cGMP-dependent manner (Trabace et al., 2004). The development of abnormal movements has been associated with changes in gene and protein expression in dopamine-denervated striatal neurons (Cenci et al., 1998; Andersson et al., 1999; Pavón et al., 2006). In response to L-DOPA, FosB/ Δ FosB expression appeared to be selectively induced in the nitroergic neurons in the striatum,



where it facilitates the expression of histone acetyltransferase, resulting in enhanced local phosphorylated histone and further changes in gene expression (Darmopil et al., 2009; Santini et al., 2009). NO may be involved either in the neurodegeneration/death or neuroprotection of dopaminergic neurons (Przedborski et al., 1996; Dehmer et al., 2000; Zhang et al., 2000; Gomes and Del-Bel, 2003; Gomes et al., 2008).

L-DOPA-induced dyskinesia has been linked to pathological cortico-striatal synaptic plasticity, which is mediated by long-lasting molecular changes (for review see Cenci and Konradi, 2010). In PD, there is an increase in NADPH-diaphorase-positive glial cells in the substantia nigra suggesting up-regulation of iNOS (Hunot et al., 1996), but there is also elevated expression of nNOS mRNA in other areas of basal ganglia (Eve et al., 1998) and increased nitrite levels in the cerebrospinal fluid (Qureshi et al., 1995), all suggesting increased NO production. Nevertheless, De-Vente et al. (2000) and Sancesario et al. (2004) reported that lesions of the dopaminergic innervation also using 6-OHDA resulted in a 50% decrease in NOS activity in the injured striatum and frontal cortex. We could not explain why NOS mRNA was increased 10 times (approximately) in the contralateral striatum and frontal cortex and why it did

not result in protein increase. It is possible that nNOS expression increase is associated with neurodegenerative rearrangements of the remaining neurocircuitries, preserving and/or further impairing the affected functions.

CONCLUSION

Our study provided further evidence of the anti-dyskinetic effects of a NOS inhibitor under acute and chronic L-DOPA treatment. Our results revealed an over-expression of the neuronal NOS in the frontal cortex and striatum in Parkinsonian and dyskinetic rats probably associated with rearrangements of the remaining neurocircuitries. Taken together, these data provide a rationale for further evaluation of NOS inhibitors in the treatment of L-DOPA-induced dyskinesia.

ACKNOWLEDGMENTS

This research was supported by grants from CAPES/COFECUB, FAPESP/INSERM, FAPESP, and CNPq. We would like to acknowledge the Célia A. da-Silva excellent technical assistance. This work would not be realized without the assistance and kindness of Professor José Eduardo Krieger – INCOR-USP.

REFERENCES

- Abreu-González, P., González-Hernández, T., Afonso-Oramas, D., Cruz-Muros, I., Barroso-Chinea, P., González, M., and C. (2006). Tetrahydrobiopterin stimulates L-DOPA release from striatal tissue. *Eur. J. Pharmacol.* 541, 33–37.
- Andersson, M., Hilbertson, A., and Cenci, M. A. (1999). Striatal fosB expression is causally linked with L-DOPA-induced abnormal involuntary movements and the associated upregulation of striatal prodynorphin mRNA in a rat model of Parkinson's disease. *Neurobiol. Dis.* 6, 461–474.
- Aquilano, K., Baldelli S. Rotilio G, and CirioloMR. (2008). Role of nitric oxide synthases in Parkinson's disease: a review on the antioxidant and anti-inflammatory activity of polyphenols. *Neurochem. Res.* 33, 2416–2426.
- Barone, P. (2010). Neurotransmission in Parkinson's disease: beyond dopamine. *Eur. J. Neurol.* 17, 364–376.
- Barthwal, M. K., Srivastava, N., and Dikshit, M. (2001). Role of nitric oxide in a progressive neurodegeneration model of Parkinson's disease in the rat. *Redox Rep.* 6, 297–302.
- Bibancos, T., Jardim, D. L., Aneas, I., and Chiavegatto, S. (2007). Social isolation and expression of serotonergic neurotransmission-related genes in several brain areas of male mice. *Genes Brain Behav.* 6, 529–539.
- Böckelmann, R., Wolf, G., Ransmayr, G., and Riederer, P. (1994). NADPH-diaphorase/nitric oxide synthase containing neurons in normal and Parkinson's disease putamen. *J. Neural Transm. Park. Dis. Dement. Sect. 7*, 115–121.
- Calabrese, V., Bates, T. E., and Stella, A. M. (2000). NO synthase and NO-dependent signal pathways in brain aging and neurodegenerative disorders: the role of oxidant/antioxidant balance. *Neurochem. Res.* 25, 1315–1341.
- Calabresi, P., Centonze, D., Gubellini, P., Marfia, G. A., Pisani, A., Sancesario, G., and Bernardi, G. (2000). Synaptic transmission in the striatum: from plasticity to neurodegeneration. *Prog. Neurobiol.* 61, 231–265.
- Cenci, M. A., and Konradi, C. (2010). Maladaptive striatal plasticity in L-DOPA-induced dyskinesia. *Prog. Brain Res.* 183, 209–233.
- Cenci, M. A., Lee, C. S., and Bjorklund, A. (1998). L-DOPA-induced dyskinesia in the rat is associated with striatal overexpression of prodynorphin- and glutamic acid decarboxylase mRNA. *Eur. J. Neurosci.* 10, 2694–2706.
- Cenci, M. A., Whishaw, I. Q., and Schallert, T. (2002). Animal models of neurological deficits: how relevant is the rat? *Nat. Rev. Neurosci.* 3, 574–579.
- Centonze, D., Picconi, B., Gubellini, P., Bernardi, G., and Calabresi, P. (2001). Dopaminergic control of synaptic plasticity in the dorsal striatum. *Eur. J. Neurosci.* 13, 1071–1077.
- Chalimoniuk, M., and Langfort, J. (2007). The effect of subchronic, intermittent L-DOPA treatment on neuronal nitric oxide synthase and soluble guanylyl-cyclase expression and activity in the striatum and midbrain of normal and MPTP-treated mice. *Neurochem. Int.* 50, 821–833.
- Chalimoniuk, M., Stepie, A., and Strosznajder, J. B. (2004). Pergolidesmesylate, a dopaminergic receptor agonist, applied with L-DOPA enhances serum antioxidant enzyme activity in Parkinson disease. *Clin. Neuropharmacol.* 27, 223–229.
- Chang, J. W., Wachtel, S. R., Young, D., and Kang, U. J. (1999). Biochemical and anatomical characterization of forepaw adjusting steps in rat models of Parkinson's disease: studies on medial forebrain bundle and striatal lesions. *Neuroscience* 88, 617–628.
- Cools, A. R. (1980). Role of the neostriatal dopaminergic activity in sequencing and selecting behavioural strategies: facilitation of processes involved in selecting the best strategy in a stressful situation. *Behav. Brain Res.* 1, 361–378.
- Darmopil, S., Martin, A. B., De Diego, I. R., Ares, S., and Moratalla, R. (2009). Genetic inactivation of dopamine D1 but not D2 receptors inhibits L-DOPA-induced dyskinesia and histone activation. *Biol. Psychiatry* 66, 603–613.
- Dehmer, T., Lindenau, J., Haid, S., Dichgans, J., and Schulz, J. B. (2000). Deficiency of inducible nitric oxide synthase protects against MPTP toxicity in vivo. *J. Neurochem.* 74, 2213–2216.
- Del-Bel, E., Padovan-Neto, F. E., Raisman-Vozari, R., and Lazzarini, M. (2011). Role of nitric oxide in motor control: implications for Parkinson's disease pathophysiology and treatment. *Curr. Pharm. Des.* 17, 471–488.
- Del-Bel, E. A., Guimarães, F. S., Bermudez-Echeverry, M., Gomes, M. Z., Schiaveto-De-Souza, A., Padovan-Neto, F., Tumas, V., Barion-Cavalcanti, A. P., Lazzarini, M., Nucci-Da-Silva, L. P., and De Paula-Souza, D. (2005). Role of nitric oxide on motor behavior. *Cell. Mol. Neurobiol.* 25, 371–392.
- De-Vente, J., Van Ittersum, M., Van Abeelen, J., Emsen, P. C., Axer, H., and Steinbusch, H. W. M. (2000). NO-mediated cGMP synthesis in cholinergic neurons in the rat forebrain: effects of lesioning dopaminergic or serotonergic pathways on nNOS and cGMP synthesis. *Eur. J. Neurosci.* 12, 507–519.
- Di Giovanni, G., Ferraro, G., Sardo, P., Galati, S., Esposito, E., and La Grutta, V. (2003). Nitric oxide modulates striatal neuronal activity via soluble guanylylcyclase: an in vivo microiontophoretic study in rats. *Synapse* 48, 100–107.
- Duncan, A. J., and Heales, S. J. (2005). Nitric oxide and neurological disorders. *Mol. Aspects Med.* 26, 67–96.
- Dunnett, S. B., and Robbins, T. W. (1992). The functional role of mesotelencephalic dopamine systems. *Biol. Rev. Camb. Philos. Soc.* 67, 491–518.
- Ebadi, M., and Sharma, S. K. (2003). Peroxynitrite and mitochondrial dysfunction in the pathogenesis of Parkinson's disease. *Antioxid. Redox Signal.* 5, 319–335.
- Eve, D., Nisbet, A., Kingsbury, A., Hewson, E., Daniel, S., Lees, A., Marsden, C., and Foster, O. (1998). Basal ganglia neuronal nitric oxide synthase mRNA expression in Parkinson's disease. *Brain Res. Mol. Brain Res.* 63, 62–71.
- Galati, S., D'Angelo, V., Scarnati, E., Stanzione, P., Martorana, A., Procopio, T., Sancesario, G., and Stefani, A. (2008). In vivo electrophysiology of dopamine-denervated striatum: focus on the nitric oxide/cGMP signaling pathway. *Synapse* 62, 409–420.
- Garthwaite, J. (2008). Concepts of neural nitric oxide-mediated transmission. *Eur. J. Neurosci.* 27, 2783–2802.
- Gomes, M. Z., and Del Bel, E. A. (2003). Effects of electrolytic and 6-hydroxydopamine lesions of rat nigrostriatal pathway on nitric oxide synthase and nicotinamide adenine dinucleotide phosphate diaphorase. *Brain Res. Bull.* 62, 107–115.
- Gomes, M. Z., Raisman-Vozari, R., and Del Bel, E. A. (2008). A nitric oxide synthase inhibitor decreases 6-hydroxydopamine effects on tyrosine hydroxylase and neuronal nitric oxide synthase in the rat nigrostriatal pathway. *Brain Res.* 1203, 160–169.
- Guix, F. X., Uribealago, I., Coma, M., and Munoz, F. J. (2005). The physiology and pathophysiology of nitric oxide in the brain. *Prog. Neurobiol.* 76, 126–152.
- Henry, B., Crossman, A. R., and Brothie, J. M. (1998). Characterization of enhanced behavioral responses to L-DOPA following repeated administration in the 6-OHDA-lesioned rat model of Parkinson's disease. *Exp. Neurol.* 151, 334–342.
- Hunot, S., Boissière, F., Faucheux, B., Brugg, B., Mouatt-Prigent, A., Agid, Y., and Hirsch, E. (1996). Nitric oxide synthase and neuronal vulnerability in Parkinson's disease. *Neuroscience* 72, 355–363.
- Iancu, R., Mohapel, P., Brundin, P., and Paul, G. (2005). Behavioral characterization of a unilateral 6-OHDA-lesion model of Parkinson's disease in mice. *Behav. Brain Res.* 162, 1–10.
- Itokawa, K., Ohkuma, A., Araki, N., Tamura, N., and Shimazu, K. (2006). Effect of L-DOPA on nitric oxide production in striatum of freely mobile mice. *Neurosci. Lett.* 402, 142–144.
- Jenner, P. (2008). Molecular mechanisms of L-DOPA-induced dyskinesia. *Nat. Rev. Neurosci.* 9, 665–677.
- Kavya, R., Saluja, R., Singh, S., and Dikshit, M. (2008). Nitric oxide synthase regulation and diversity: implications in Parkinson's disease. *Nitric Oxide* 15, 280–294.
- Kawaguchi, Y. (1997). Neostriatal cell subtypes and their functional roles. *Neurosci. Res.* 27, 1–8.
- Konitsiotis, S., and Tsironis, C. (2006). Levodopa-induced dyskinesia and rotational behavior in hemiparkinsonian rats: independent features or components of the same phenomenon? *Behav. Brain Res.* 170, 337–341.
- Kubota, Y., Mikawa, S., and Kawaguchi, Y. (1993). Neostriatal GABAergic interneurons contain NOS, calretinin or parvalbumin. *Neuroreport* 5, 205–208.
- Lane, E. L., Cheetham, S. C., and Jenner, P. (2006). Does contraversive circling in the 6-OHDA-lesioned rat indicate an ability to induce motor complications as well as therapeutic effects in Parkinson's disease? *Exp. Neurol.* 197, 284–290.
- Lane, E. L., Soulet, D., Vercammen, L., Cenci, M. A., and Brundin, P. (2008). Neuroinflammation in the generation of post-transplantation dyskinesia in Parkinson's disease. *Neurobiol. Dis.* 32, 220–228.
- Lundblad, M., Andersson, M., Winkler, C., Kirik, D., Wierup, N., and Cenci, M. (2002). Pharmacological validation of behavioural measures of akinesia and dyskinesia in a rat model of Parkinson's disease. *Eur. J. Neurosci.* 15, 120–132.
- Marsden, C. D., and Parkes, J. D. (1977). Success and problems of long-term levodopa therapy in Parkinson's disease. *Lancet* 1, 345–349.
- Miller, R., and Beninger, R. J. (1991). On the interpretation of asymmetries of posture and locomotion produced with dopamine agonists in animals with unilateral depletion of striatal dopamine. *Prog. Neurobiol.* 36, 229–256.
- Monville, C., Torres, E. M., and Dunnett, S. B. (2006). Comparison of incremental and accelerating protocols of

- the rotarod test for the assessment of motor deficits in the 6-OHDA model. *J. Neurosci. Methods* 158, 219–223.
- Morello, M., Reiner, A., Sancesario, G., Karle, E. J., and Bernardi, G. (1997). Ultrastructural study of nitric oxide synthase-containing striatal neurons and their relationship with parvalbumin-containing neurons in rats. *Brain Res.* 776, 30–39.
- Mura, A., Mintz, M., and Feldon, J. (2002). Behavioral and anatomical effects of long-term L-dihydroxyphenylalanine (L-DOPA) administration in rats with unilateral lesions of the nigrostriatal system. *Exp. Neurol.* 177, 252–264.
- Novaretti, N., Padovan-Neto, F. E., Tumas, V., Da-Silva, C. A., and Del Bel, E. A. (2010). Lack of tolerance for the anti-dyskinetic effects of 7-nitroindazole, a neuronal nitric oxide synthase inhibitor, in rats. *Braz. J. Med. Biol. Res.* 43, 1047–1053.
- Olsson, M., Nikkiah, G., Bentlage, C., and Björklund, A. (1995). Forelimb akinesia in the rat Parkinson model: differential effects of dopamine agonists and nigral transplants as assessed by a new stepping test. *J. Neurosci.* 15, 3863–3875.
- Padovan-Neto, F. E., Echeverry, M. B., Tumas, V., and Del-Bel, E. A. (2009). Nitric oxide synthase inhibition attenuates L-DOPA-induced dyskinesias in a rodent model of Parkinson's disease. *Neuroscience* 159, 927–935.
- Papa, S. M., Engber, T. M., Kask, A. M., and Chase, T. N. (1994). Motor fluctuations in levodopa treated Parkinsonian rats: relation to lesion extent and treatment duration. *Brain Res.* 662, 69–74.
- Pavón, N., Martín, A., Mendiádua, A., and Moratalla, R. (2006). ERK phosphorylation and FosB expression are associated with L-DOPA-induced dyskinesia in hemiparkinsonian mice. *Biol. Psychiatry* 59, 64–74.
- Paxinos, G., and Watson, C. (1998). *The Rat Brain in Stereotaxic Coordinates*. New York: Academic Press.
- Ponzoni, S., Guimarães, F. S., Del Bel, E. A., and García-Cairasco, N. (2000). Behavioral effects of intra-nigral microinjections of manganese chloride: interaction with nitric oxide. *Prog. Neuropsychopharmacol. Biol. Psychiatry* 24, 307–325.
- Przedborski, S., Jackson-Lewis, V., Yokoyama, R., Shibata, T., Dawson, V. L., and Dawson, T. M. (1996). Role of neuronal nitric oxide in 1-methyl-4-phenyl-1,2,3,6-tetrahydropyridine (MPTP)-induced dopaminergic neurotoxicity. *Proc. Natl. Acad. Sci. U.S.A.* 93, 4565–4571.
- Qureshi, G. A., Baig, S., Bednar, I., Sodersten, P., Forsberg, G., and Siden, A. (1995). Increased cerebrospinal fluid concentration of nitrite in Parkinson's disease. *Neuroreport* 6, 1642–1644.
- Sancesario, G., Giorgi, M., D'angelo, V., Modica, A., Martorana, A., Morello, M., Bengtson, C. P., and Bernardi, G. (2004). Down-regulation of nitric transmission in the rat striatum after chronic nigrostriatal deafferentation. *Eur. J. Neurosci.* 20, 989–1000.
- Sanchez, J. J., Abreu, P., and Gonzalez, M. C. (2002). Sodium nitroprusside stimulates L-DOPA release from striatal tissue through nitric oxide and cGMP. *Eur. J. Pharmacol.* 438, 79–83.
- Santini, E., Alcacer, C., Cacciatore, S., Heiman, M., Hervé, D., Greengard, P., Girault, J. A., Valjent, E., and Fisone, G. (2009). L-DOPA activates ERK signaling and phosphorylates histone H3 in the striatonigral medium spiny neurons of hemiparkinsonian mice. *J. Neurochem.* 108, 621–633.
- Schwartz, R. K., Bonatz, A. E., Carey, R. J., and Huston, J. P. (1991). Relationships between indices of behavioral asymmetries and neurochemical changes following mesencephalic 6-hydroxy-dopamine injections. *Brain Res.* 554, 46–55.
- Schwartz, R. K., and Huston, J. P. (1996). Unilateral 6-OHDA lesions of meso-striatal dopamine neurons and their physiological sequelae. *Prog. Neurobiol.* 49, 215–266.
- Sullivan, R. M., Fraser, A., and Szechtman, H. (1994). Asymmetrical orientation to edges of an openfield: modulation by striatal dopamine and relationship to motor asymmetries in the rat. *Brain Res.* 637, 114–118.
- Tepper, J. M., and Bolam, J. P. (2004). Functional diversity and specificity of neostriatal interneurons. *Curr. Opin. Neurobiol.* 14, 685–692.
- Trabace, L., Cassano, T., Tucci, P., Steardo, L., Kendrick, K. M., and Cuomo, V. (2004). The effects of nitric oxide on striatal serotonergic transmission involve multiple targets: an in vivo microdialysis study in the awake rat. *Brain Res.* 2008, 293–298.
- Tuite, P., and Riss, J. (2003). Recent developments in the pharmacological treatment of Parkinson's disease. *Expert. Opin. Investig. Drugs* 12, 1335–1352.
- Ungerstedt, U., and Arbuthnott, G. W. (1970). Quantitative recording of rotational behavior in rats after 6-hydroxy-dopamine lesions of the nigrostriatal dopamine system. *Brain Res.* 24, 485–493.
- Vandesompele, J., De Preter, K., Pattyn, F., Poppe, B., Van Roy, N., De Paepe, A., and Speleman, F. (2002). Accurate normalization of real-time quantitative RT-PCR data by geometric averaging of multiple internal control genes. *Genome Biol.* 3, research0034.1–research0034.11.
- West, A. R., and Grace, A. A. (2002). Opposite influences of endogenous dopamine D1 and D2 receptor activation on activity states and electrophysiological properties of striatal neurons: studies combining in vivo intracellular recordings and reverse microdialysis. *J. Neurosci.* 22, 294–304.
- West, A. R., and Grace, A. A. (2004). The nitric oxide-guanylylcyclase signaling pathway modulates membrane activity states and electrophysiological properties of striatal medium spiny neurons recorded in vivo. *J. Neurosci.* 24, 1924–1935.
- Winkler, C., Kirik, D., Björklund, A., and Cenci, M. A. (2002). L-DOPA-induced dyskinesia in the intrastratial 6-OHDA model of Parkinson's disease: relation to motor and cellular parameters of nigrostriatal function. *Neurobiol. Dis.* 10, 165–186.
- Zetterström, T., Herrera-Marschitz, M., and Ungerstedt, U. (1986). Simultaneous measurement of dopamine release and rotational behaviour in 6-hydroxydopamine denervated rats using intracerebral dialysis. *Brain Res.* 376, 1–7.
- Zhang, J., Graham, D. G., Montine, T. J., and Ho, Y. S. (2000). Enhanced N-methyl-4-phenyl-1,2,3,6-tetrahydropyridine toxicity in mice deficient in CuZn-superoxide dismutase or glutathione peroxidase. *J. Neuropathol. Exp. Neurol.* 59, 53–61.

Conflict of Interest Statement: The authors declare that the research was conducted in the absence of any commercial or financial relationships that could be construed as a potential conflict of interest.

Received: 23 February 2011; accepted: 23 May 2011; published online: 10 June 2011.

Citation: Padovan-Neto FE, Echeverry MB, Chiavegatto S and Del-Bel E (2011) Nitric oxide synthase inhibitor improves *de novo* and long-term L-DOPA-induced dyskinesia in hemiparkinsonian rats. *Front. Syst. Neurosci.* 5:40. doi: 10.3389/fnsys.2011.00040

Copyright © 2011 Padovan-Neto, Echeverry, Chiavegatto and Del-Bel. This is an open-access article subject to a non-exclusive license between the authors and Frontiers Media SA, which permits use, distribution and reproduction in other forums, provided the original authors and source are credited and other Frontiers conditions are complied with.



Distribution of tyrosine hydroxylase-expressing interneurons with respect to anatomical organization of the neostriatum

Bengi Ünal, Osvaldo Ibáñez-Sandoval, Fulva Shah, Elizabeth D. Abercrombie and James M. Tepper*

Center for Molecular and Behavioral Neuroscience, Rutgers, The State University of New Jersey, Newark, NJ, USA

Edited by:

Jose Bargas, Universidad Nacional Autónoma de México, Mexico

Reviewed by:

Abbas F. Sadikot, McGill University, Canada

Lucía Prensa Sepúlveda, Universidad Autónoma de Madrid, Spain

*Correspondence:

James M. Tepper, Center for Molecular and Behavioral Neuroscience, Rutgers University, 197 University Avenue, Newark, NJ 07102, USA.
e-mail: jtepper@andromeda.rutgers.edu

We have recently shown *in vitro* that striatal tyrosine hydroxylase-expressing interneurons identified in transgenic mice by expression of enhanced green fluorescent protein (TH-eGFP) display electrophysiological profiles that are distinct from those of other striatal interneurons. Furthermore, striatal TH-eGFP interneurons show marked diversity in their electrophysiological properties and have been divided into four distinct subtypes. One question that arises from these observations is whether striatal TH-eGFP interneurons are distributed randomly, or obey some sort of organizational plan as has been shown to be the case with other striatal interneurons. An understanding of the striatal TH-eGFP interneuronal patterning is a vital step in understanding the role of these neurons in striatal functioning. Therefore, in the present set of studies the location of electrophysiologically identified striatal TH-eGFP interneurons was mapped. In addition, the distribution of TH-eGFP interneurons with respect to the striatal striosome–matrix compartmental organization was determined using μ -opioid receptor (MOR) immunofluorescence or intrinsic TH-eGFP fluorescence to delineate striosome and matrix compartments. Overall, the distribution of the different TH-eGFP interneuronal subtypes did not differ in dorsal versus ventral striatum. However, striatal TH-eGFP interneurons were found to be mostly in the matrix in the dorsal striatum whereas a significantly higher proportion of these neurons was located in MOR-enriched domains of the ventral striatum. Further, the majority of striatal TH-eGFP interneurons was found to be located within 100 μ m of a striosome–matrix boundary. Taken together, the current results suggest that TH-eGFP interneurons obey different organizational principles in dorsal versus ventral striatum, and may play a role in communication between striatal striosome and matrix compartments.

Keywords: GABAergic, striatum, striosome, matrix, dopamine island

INTRODUCTION

Acquisition of motor learning and volitional initiation of behavior critically depend on faithful transfer of information among the components of the basal ganglia. The neostriatum is the largest structure and the major input nucleus of the basal ganglia. Furthermore, the striatum plays a pivotal role in the shaping of the ongoing activity of the tonically active basal ganglia nuclei, the substantia nigra pars reticulata and globus pallidus external segment, via different dopamine receptor expressing spiny projection neurons (SPNs) that give rise to the direct and indirect striatofugal pathways, respectively (Albin et al., 1989; Gerfen et al., 1990; Kawaguchi et al., 1990; Kita, 2001; Kita et al., 2006).

Spiny projection neurons account for about 95% of the striatal neuronal population (Oorschot, 2010). The remaining neurons are all local interneurons. The latter display a remarkable degree of neurochemical and electrophysiological diversity (Kawaguchi et al., 1995; Rymar et al., 2004; Oorschot, 2010). Striatal interneurons can be grouped into two main groups, cholinergic interneurons and GABAergic interneurons. The GABAergic interneurons are comprised of parvalbumin (PV)-expressing fast-spiking, neuropeptide Y (NPY)–somatostatin (SOM)–nitric oxide synthase (NOS) co-expressing, calretinin (CR)-expressing (Kawaguchi, 1993; Kawaguchi et al., 1995; Wu and Parent, 2000; Tepper, 2010),

and tyrosine hydroxylase (TH)-expressing (Dubach et al., 1987; Tashiro et al., 1989a; Meredith et al., 1999; Mazloom and Smith, 2006; Tande et al., 2006; Huot et al., 2007) cells.

We recently used brain slices from transgenic mice engineered to express enhanced green fluorescent protein under the control of TH-promoter (TH-eGFP) to characterize the anatomy and physiology of striatal TH neurons, and established that they are a novel class of GABAergic interneurons. We showed not only that striatal TH-eGFP neurons were markedly distinct from SPNs as well as other from other striatal interneurons but also that these neurons exhibited a striking heterogeneity in terms of their electrophysiological characteristics and could be subdivided into four distinct subtypes termed Types I–IV (Ibáñez-Sandoval et al., 2010).

Why is there such a level of electrophysiological diversity in this small group of neurons and how may it affect striatal functioning? In order to address these questions, previous findings regarding TH-eGFP interneurons should be considered within the context of the anatomical and functional heterogeneity in the striatum. The neostriatum can be subdivided into dorsal and ventral divisions, comprising the caudate nucleus and putamen, and the nucleus accumbens, respectively (Gerfen and Wilson, 1996). The nucleus accumbens can be further divided into core and shell regions, each

with distinct inputs and outputs (Zaborszky et al., 1985; Berendse et al., 1988; Ragsdale and Graybiel, 1981; Heimer et al., 1997; Voorn et al., 2004; Ikemoto, 2007).

In addition to dorsal and ventral divisions, the striatum can be further subdivided into patch or striosome, and matrix domains, which also reflect another layer of differential afferent and efferent connectivity (Graybiel et al., 1981, 1987; Gerfen et al., 1990; Gerfen, 1992). These interdigitating compartments are neurochemically distinct. The matrix shows strong immunoreactivity for acetylcholinesterase and calbindin whereas striosomes are characterized by strong(er) expression of substance P, enkephalin, and limbic associated membrane protein (Graybiel et al., 1981; Gerfen et al., 1985; Bolam et al., 1988; Voorn et al., 1989; Holt et al., 1997). Additional striosome/matrix differences exist in terms of enhanced expression of other signaling molecules in the striosomes such as: μ -opioid receptor (MOR), AMPA receptor subunit 1 (GluR1), voltage-gated potassium channel interacting protein 1 (Mikula et al., 2009), dopamine receptor subtypes (Rivera et al., 2002), and olfactory-type G-protein alpha subunit expression (Sako et al., 2010).

Although the function of this mosaic organization remains elusive, it has a critical organizing effect in striatal cytoarchitecture. The orientation and trajectory of SPN dendritic and axonal arborization obey compartmental boundaries (Kawaguchi et al., 1990), whereas processes of cholinergic and GABAergic do not (Chesselet and Graybiel, 1986; Cowan et al., 1990; Kawaguchi, 1992). Furthermore, the somata of cholinergic and NPY interneurons have been noted to be preferentially situated at the compartmental boundaries (Kubota and Kawaguchi, 1993; Martone et al., 1994; Saka et al., 2002; Bernácer et al., 2005, 2007). These data collectively suggest the existence of important differences in signal processing in striosome and matrix domains in which certain classes of striatal interneurons may play a crucial role (Saka et al., 2002).

In the current set of studies, we mapped the location of TH-eGFP cells with respect to multiple levels of the anatomical organization of the striatum. First, the locations of different electrophysiologically defined TH-eGFP subtypes within the striatal volume were determined. Second, striatal TH-eGFP neurons were mapped with respect to striosome and matrix compartments defined on the basis of MOR immunofluorescence. Finally, a small subset of TH-eGFP neurons was recorded in different compartments identified by the intensity of TH-eGFP-TH fluorescence in young mice. Our results show that electrophysiologically identified subtypes are equally prevalent in all regions of the striatum. However, when the finer level anatomical organization of the striatum is taken into account, a different pattern emerged in terms of TH-eGFP neuron distribution. In the dorsal striatum, TH-eGFP neurons are diffusely spread out with most of them residing in the matrix compartment as expected from area distribution whereas, in the ventral striatum, there is a disproportionately higher presence of TH-eGFP neurons in MOR-enriched regions.

MATERIALS AND METHODS

SUBJECTS

The progeny of hemizygous Tg(Th-EGFP)DJ76Gsat/Mmnc (GENSAT) mice (Gong et al., 2003) obtained from the Mutant Mouse Regional Resource Centers at University of California at

Los Angeles and backcrossed to FVB mice were used in the experiments. Mice were bred and kept in the temperature and humidity controlled AAALAC-accredited animal facility and maintained on a 12/12 dark light cycle with light onset at 7 a.m. After weaning on postnatal day 21, animals were genotyped from tail snips to confirm that they were TH-eGFP positive. All experimental protocols were in accordance with Rutgers University Institutional Animal Care and Use Committee and the NIH Guide to the Care and Use of Laboratory Animals. Utmost effort was exercised to minimize the number of mice used and the discomfort and/or pain the mice underwent.

IN VITRO ELECTROPHYSIOLOGY

Following intraperitoneal (i.p.) injection of ketamine (100 mg/kg; Ketaject, Henry Schein, Melville, NY, USA), TH-eGFP mice were transcardially perfused with ice-cold modified Ringer's solution that contained (in millimolar) 124 Choline Cl, 2.5 KCl, 26 NaHCO₃, 3.3 MgCl₂, 1.2 NaH₂PO₄, 10 glucose or 248 sucrose, 2.5 KCl, 7 MgCl₂, 23 NaHCO₃, 1.2 NaH₂PO₄, 7 glucose, 1 ascorbate, and 3 pyruvate. Subsequently, 250–350 μ m coronal or 10° parahorizontal striatal sections were obtained using a vibrating microtome (Vibratome™ 3000, St Louis, MO, USA). Slices were transferred initially into a slice chamber that contained Ringer's Solution (in millimolar: 124 NaCl, 2.5 KCl, 26 NaHCO₃, 1.3 MgCl₂, 1.2 NaH₂PO₄, 10 glucose, 2 CaCl₂, 1 ascorbic acid, 3 pyruvate, 0.4 myoinositol) maintained at 33°C and later kept at room temperature until the time of recording. During the recordings slices were continuously perfused with normal Ringer's solution at a flow rate of 2 ml/min, which was maintained at 33°C via TC-324B inline heater system (Warner Instruments, Hamden, CT, USA). TH-eGFP neurons were identified by infrared DIC and epifluorescence visualization with a 40 \times objective using a BX50-WI Olympus microscope. Whole-cell patch clamp recordings in current clamp mode were obtained using glass pipettes (3–7 M Ω) filled with (in millimolar): 130 KMeSO₃, 10 NaCl, 10 HEPES, 1 EGTA, 0.1 CaCl₂, 2 MgCl₂, 3 ATP, 0.3 GTP, pH adjusted to 7.3. Biocytin (0.2%) was added to the intracellular solution in order to label the recorded neuron for later identification and anatomical investigation of recorded striatal TH-eGFP neurons.

Recordings were acquired with a Neurodata IR-283 current clamp amplifier and digitized at 10–40 kHz via a Micro 1401 Mk II data acquisition unit and transferred to a PC using Signal™ v.4 software (CED, Cambridge, UK) for offline analysis. To examine the basic membrane properties of the TH-eGFP neurons, a sequence of hyperpolarizing and depolarizing current steps from –200 to +200 pA were injected for 500 ms. Current–voltage (I–V) curves were constructed by averaging 10 ms epochs within the last 100 ms of the 500-ms current injection that was devoid of action potentials (APs) or spontaneous synaptic potentials. Membrane input resistance was estimated from calculating the slope of the I–V relation at 0 pA current injection (resting membrane potential). AP measurements were taken from the first AP evoked by injection of threshold depolarizing current. AP half-width was determined by measuring the time between points of half-maximal AP amplitude. The spike after hyperpolarization amplitude was computed by subtracting the trough value of the 200-ms time window following the AP from the AP threshold value. Finally, the membrane time constant (τ)

was defined as the time it takes the membrane to fall to 63% of the steady state value by fitting an exponential to the initial phase of the membrane response to a -20 pA current injection.

BIOCYTIN CYTOCHEMISTRY

Following electrophysiological characterization, sections containing biocytin-filled neurons were fixed in 4% paraformaldehyde in 0.1 M phosphate buffer (PB) overnight at 4°C and transferred next day into 0.1 M PB. Sections were then washed for 3×10 min in 0.1 M PB followed by 10% methanol and 3% H_2O_2 for 15 min, and incubated with avidin–biotin–peroxidase complex (Vector Laboratories; 1:200) and 0.1% Triton X-100 overnight at 4°C . After washing 6×10 min in 0.1 M PB the sections were reacted with 3,3'-diaminobenzidine (0.025%) and H_2O_2 (0.0008%) in PB with nickel intensification (2.5 mM nickel ammonium sulfate and 7 mM ammonium chloride) to visualize the biocytin-stained neuron for later reconstruction using NeuroLucida™ (MBF Bioscience, VT, USA). Slices were later postfixed in osmium tetroxide (0.1% in PB) for 30 min, dehydrated through a graded series of ethanol, followed by wash with xylene. Air-dried sections were then mounted in Depex (Electron Microscopy Sciences, PA, USA) and coverslipped.

In a subset of sections, instead of DAB, biocytin was visualized by a Texas Red streptavidin conjugate (1:200, overnight at 4°C). This allowed visualization of the intrinsic fluorescent TH-eGFP signal (from somata and proximal neurites) along with detection of the biocytin fill by Texas Red.

MU-OPIOID RECEPTOR IMMUNOCYTOCHEMISTRY

Adult TH-eGFP mice were sacrificed following deep anesthesia with i.p. Ketamine (200 mg/kg). Mice were then transcardially perfused with chilled Ringer's solution followed by fixation with freshly prepared 4% paraformaldehyde added to 15% saturated picric acid in 0.1 M PB. After decapitation, brains were stored in the same fixative for overnight fixation. On the next day, following several washes with PBS, $60\text{ }\mu\text{m}$ free-floating sections were obtained using a Vibratome™ 1200. Sections were pretreated with 1% sodium borohydride followed by 10% methanol and 3% H_2O_2 in PBS prior to incubation in 10% normal donkey serum, 2% bovine serum albumin, and 0.5% Triton X-100 for 1 h. Next, sections were incubated in a solution containing 1:1000 rabbit anti-MOR monoclonal antibody (Immunostar Inc., Hudson, WI, USA #24216) along with 10% normal donkey serum, 2% bovine serum albumin, and 0.5% Triton X-100 (Sigma-Aldrich Co., St. Louis, MO, USA) in PBS for 24 h at room temperature. After washing three times for 10 min each in PBS, sections were transferred to a solution containing 1:500 Texas Red donkey anti-rabbit secondary (Molecular Probes, Inc., Eugene, OR, USA), 10% normal donkey serum, and 2% bovine serum albumin in PBS at 4°C overnight. After three 10 min washes in PBS, sections were wet mounted in Vectashield (Vector Laboratories, Burlingame, CA, USA), coverslipped and sealed with nail polish.

STEREOLOGY AND ANATOMICAL MAPPING

For sections containing biocytin-filled neurons, the slices were outlined using NeuroLucida™. Briefly, section outlines, borders of the corpus callosum, anterior commissure and striatum were traced at $10\times$ and a marker was placed at the location of recorded

TH-eGFP somata. In order to account for variability in section condition (i.e., differential shrinkage), two sets of reference sections were cut at $100\text{ }\mu\text{m}$ in the coronal or 10° parahorizontal plane and Nissl-stained. Sections containing the biocytin-filled TH-eGFP somata were matched to the Nissl-stained reference sections at the closest z-depth and any deviations in dorso-ventral or medio-lateral aspects of the tissue were compensated for using the built-in shrinkage correction of the software. Registration to Nissl-stained reference sections thus enabled assigning individual z-depth values to recorded sections. A 45° line spanning from the most ventral end of the lateral ventricle to the most ventral end of the external capsule was drawn to parse the striatum into dorsal and ventral divisions.

In MOR-immunolabeled sections from TH-eGFP mice, every fifth section containing the striatum was traced at $4\times$ following random determination of the initial section by the default workflow of the Optical Fractionator probe in StereoInvestigator™ v.9 (MBF Biosciences, Williston, VT, USA). The outlines of the entire section, the corpus callosum, the anterior commissure and the striatum were traced and visualized by different color contours. Additionally, the striatum was parsed into dorsal and ventral divisions based on the cell packing density and direction of fiber fascicles piercing the striatum, and with reference to the mouse brain atlas of Franklin and Paxinos (2001). The border between dorsal and ventral striatum was further adjusted on the basis of strong MOR staining around the nucleus accumbens core segment.

Under epifluorescence illumination at 530 nm, patch/striosome and matrix compartments were outlined based on differential MOR immunoreactivity as it has been established that striosomes express stronger MOR-enkephalin immunoreactivity than the surrounding matrix in the dorsal striatum (Herkenham and Pert, 1981; Gerfen, 1989; Voorn et al., 1989). However, in the ventral striatum the afferent organization of MOR-rich domains resemble the dorsal striatal matrix (Jongen-Relo et al., 1993, 1994).

The methodology for stereological cell-counting procedure under epifluorescent illumination was adapted from previous reports using a similar approach (Henny and Jones, 2008; Prasad and Richfield, 2010). After virtual overlay of a $544\text{-}\mu\text{m} \times 380\text{-}\mu\text{m}$ grid on the contoured serial sections, cell counting was performed at $40\times$ under epifluorescence illumination at 380 nm to detect striatal TH-eGFP expressing somata. At each counting site, section thickness was measured, which yielded an average tissue thickness of $50.7 \pm 1.14\text{ }\mu\text{m}$ indicating that there was $\sim 16\%$ shrinkage from the original cut thickness. Optical disector frame dimensions were set to $180\text{ }\mu\text{m} \times 180\text{ }\mu\text{m}$ with $30\text{ }\mu\text{m}$ z-depth and 5% guard zones on top and at the bottom. Only those TH-eGFP somata falling entirely within the borders, i.e., falling in between and coming in contact with inclusion borders but not touching the exclusion borders were counted. The loci of the counted TH-eGFP somata with respect to MOR intensely immunoreactive regions were also noted during counting to determine the compartmental distribution of the cells. Since section thickness was measured at every site, the numbers reported here are the stereological estimates weighed by section thickness. Raw data from biocytin-filled cells and stereologically sampled TH-eGFP neurons were aligned and overlaid using NeuroLucida™ Explorer and the Solid Modeling extension module (MBF Biosciences, Williston, VT, USA).

DATA ANALYSIS

Data were analyzed using CED Signal™, Origin 7.0, Microsoft Excel™ and PAWS v. 18 software. Subtypes of TH-eGFP neurons were determined based on the electrophysiological criteria described in Ibáñez-Sandoval et al. (2010). For statistical comparisons, multivariate ANOVA and Bonferroni *post hoc* tests performed in electrophysiological recordings. Independent samples *t*-test, Pearson's chi-square test and Pearson's correlation were performed on anatomical data sets. *P* values <0.05 were accepted as statistically significant.

RESULTS

LOCALIZATION OF DIFFERENT TH-eGFP CELL TYPES

Sixty-three electrophysiologically identified and biocytin-stained TH-eGFP neurons ($n = 31$ in coronal and $n = 32$ in parahorizontal orientations) were mapped as shown in Figure 1. As each of the recorded slices were assigned a unique z-depth value on the basis of the reference sections, the data from coronal and parahorizontal slices could be merged with each other by NeuroLucida Explorer. In order to obtain a combined image and data set, parahorizontally mapped TH-eGFP cells were virtually rotated 90° along the anterior–posterior and 10° along the dorsal–ventral axes and merged with the cluster of TH-eGFP cells obtained in the coronal orientation (Figure 1C).

Quantitative assessment of the distribution of electrophysiologically identified TH-eGFP neuron subtypes was analyzed in three dimensions (Figure 1C). In the cumulative distribution for the coronal orientation, a 45° horizontal line was drawn dorsal to the anterior commissure extending from the ventral most point of the lateral ventricle to the ventral-most point of the external

capsule (Voorn et al., 2004) in order to mark the division between dorsal and ventral striatum. On the basis of this division, it was estimated that 81% (51/63) of the recorded and filled neurons were in the dorsal striatum with the remaining 19% (12/63) within the territory of the ventral striatum. Pearson's Chi-square analysis was performed in order to see whether any of the electrophysiologically distinct subtypes were disproportionately present in dorsal or ventral striatum. The results indicated that distribution of TH-eGFP interneuron subtypes did not differ in dorsal and ventral striatum [Pearson's $\chi^2(3) = 6.088, p > 0.05$]. In both dorsal and ventral striatum, Type I TH-eGFP neurons constituted the majority of recorded neurons (Figure 1C), consistent with our previous observations (Ibáñez-Sandoval et al., 2010). Sixty percent of the Type IV neurons in our sample were located in ventral striatum but this observation did not reach statistical significance, most likely because only a few of the mapped neurons belonged to this category ($n = 5$).

STEREOLOGICAL CELL COUNTING AND MAPPING WITH RELATION TO MOR STAINING DENSITY

Striatal TH interneurons in a different set of sections were identified on the basis of their eGFP fluorescence irrespective of their electrophysiological profile and sampled using optical fractionator methodology and localized with regard to striatal MOR patches (Figures 2A–E). In the dorsal striatum, dark areas of weaker TH-eGFP fiber fluorescence were observed to show a strong overlap with intensely MOR-labeled domains (Figures 2A–C). The overall stereological estimates yielded an average of 2756 ± 192.4 (mean Gundersen's coefficient of error = 0.11) TH-eGFP neurons per striatum per hemisphere ($n = 10$ hemispheres), in good agreement with values previously reported for striatal TH-eGFP interneurons (Ibáñez-Sandoval et al., 2010). Of the TH-eGFP neurons, 723.2 ± 44.9 were found to be located in MOR-enriched domains corresponding to different compartments of striatal striosome–matrix organization in dorsal and ventral striatum combined. In addition, proximity to the nearest striosome–matrix boundary was measured among 332 matrix-bound TH-eGFP somata. Slightly more than half of the entire population resided within 100 μm or less from the perimeter of the MOR-enriched regions in both dorsal and ventral striatum (Figure 2F).

The numbers obtained from the stereological mapping were used in regression analyses in order to understand the relationship between the TH-eGFP neurons in MOR-enriched domains and the fraction of MOR-enriched domains with respect to the entire striatum. The regression analysis indicated that the fraction of TH-eGFP neurons falling within MOR-enriched islands was dramatically different in dorsal versus ventral striatum (Figures 3A,B). Although the TH-eGFP neurons were present in MOR-enriched striosomes of the dorsal striatum at a chance level ($r^2 = 0.069$; Figure 3C), in the ventral striatum significantly more TH-eGFP neurons were located in MOR-enriched domains than what would be expected by chance ($r^2 = 0.662$; Figure 4D). Indeed, the regression between these parameters was found to be statistically significant, as the coefficients predicting the relationship in dorsal and ventral striatum ($B = -0.332$ on dorsal striatum versus $B = 0.914$ in ventral striatum) were found to differ significantly by *t*-test [$t(1) = 3.935, p = 0.001$; Figures 3C,D]. The proportion of striatal area comprised of MOR-enriched domains did not differ between dorsal

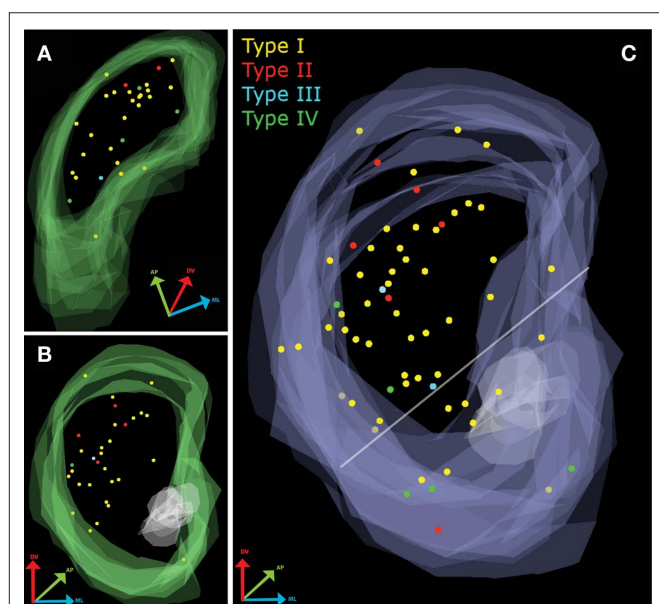
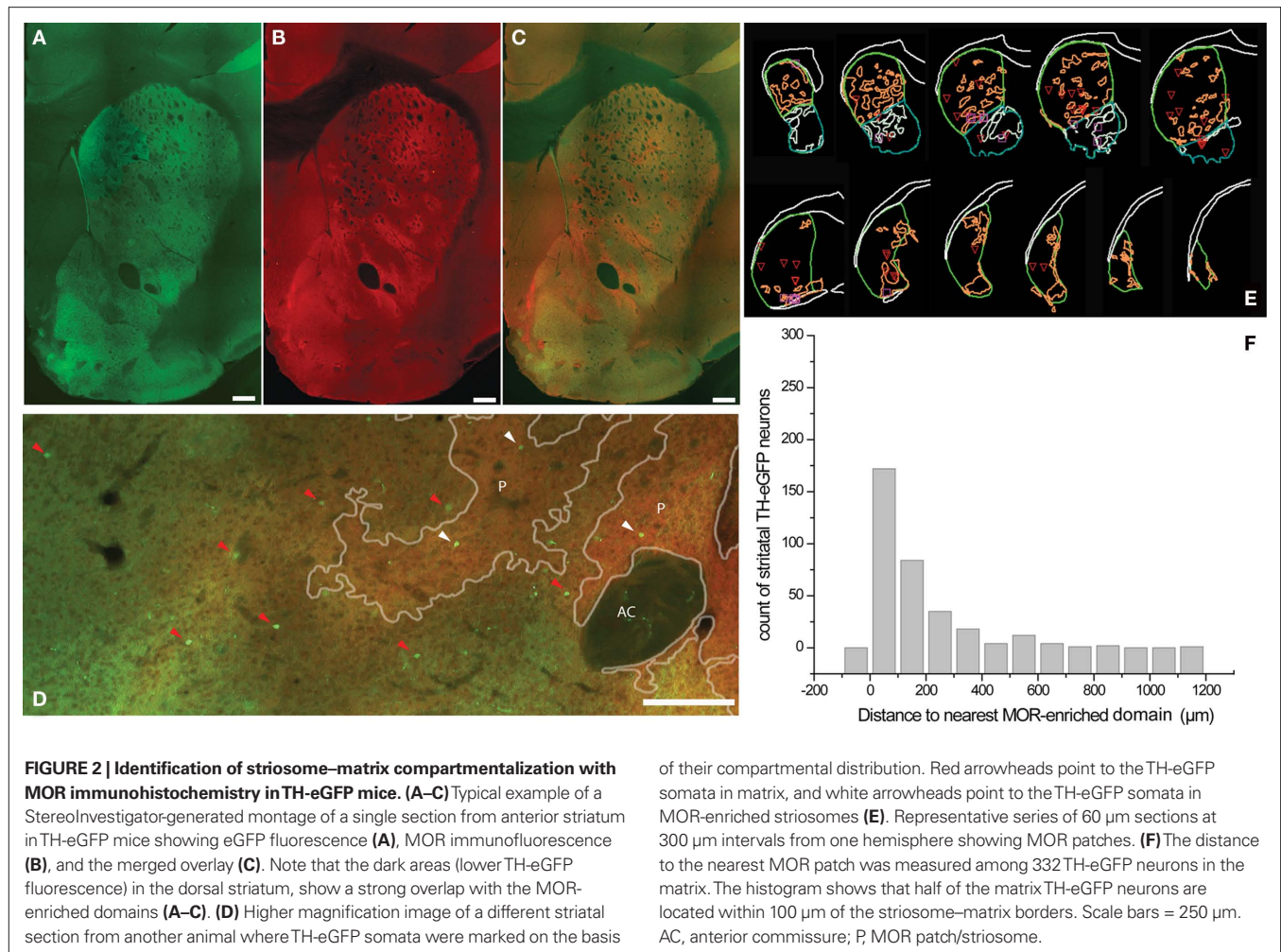


FIGURE 1 | Mapping of electrophysiologically characterized and biocytin-filled TH-eGFP neurons in the striatum. (A) Overlay of all parahorizontal sections ($n = 32$). **(B)** Overlay of all coronal sections ($n = 31$). **(C)** Merged data set after rotating the parahorizontal sections 10° from their long axis and 90° around their short axis.



and ventral striatum [$t(18) = -0.066$, $p = 0.948$] but interestingly in female mice ($n = 4$ hemispheres) it was found that the striatal proportion of MOR-enriched domains in ventral striatum was significantly larger than in male mice [$t(18) = -2.230$, $p = 0.039$]. The stereological data pertaining to MOR-enriched regions are presented in **Tables 1 and 2**.

TH-eGFP LOCATION WITH RESPECT TO TH-rich PATCHES/STRIOSOMES IN YOUNG MICE

Ten TH-eGFP interneurons were recorded from slices taken from young (postnatal day 30–33) TH-eGFP mice where striosome and matrix compartments could be identified under epifluorescent illumination on the basis of a differential TH-fiber density. In young animals, TH-rich “islands” correspond to what will become the dopamine- and TH-poor striosome compartment in adults (Graybiel et al., 1987). Two of these neurons were located on the border between TH-rich dopamine islands and TH-poorer matrix, and both displayed the electrophysiological phenotype of Type IV TH-eGFP interneurons (**Figure 4A**). Interestingly, the remaining eight cells that were recorded within dopamine islands were all found to be Type I TH-eGFP interneurons (**Figure 4B**). The maximum projection images of the neurons in **Figures 4A,B** taken at 5 m intervals indicate that in both cases, there are neurites that

crossover into the neighboring compartments (**Figures 4C,D**). Due to the very limited size of the sample, no statistics were performed on this subset of the data.

DISCUSSION

TH-eGFP INTERNEURONS ARE DIFFERENTIALLY DISTRIBUTED IN DORSAL AND VENTRAL STRIATUM

The current experiments were undertaken to investigate the anatomical distribution of striatal TH-eGFP interneurons. In the first set of experiments, anatomical mapping done with electrophysiologically identified and biocytin-filled TH-eGFP neurons indicated that none of the TH-eGFP subtypes showed a dorsal-ventral or anterior-posterior patterning. In the second set, electrophysiologically unidentified TH-eGFP neurons were stereologically sampled and mapped with respect to the density of MOR immunolabeling in the striatum. The results indicate that there is a non-random distribution of TH-eGFP cells in the MOR-enriched domains in ventral striatum but not in dorsal striatum. TH-eGFP neurons were found in ventral striatal MOR-enriched domains 1.6 times more frequently than what would have expected by chance. The current results do not indicate a regional specialization of the different subtypes of TH-eGFP neurons across the dorsal-ventral divisions of the striatum. However, cortical and local stimulation

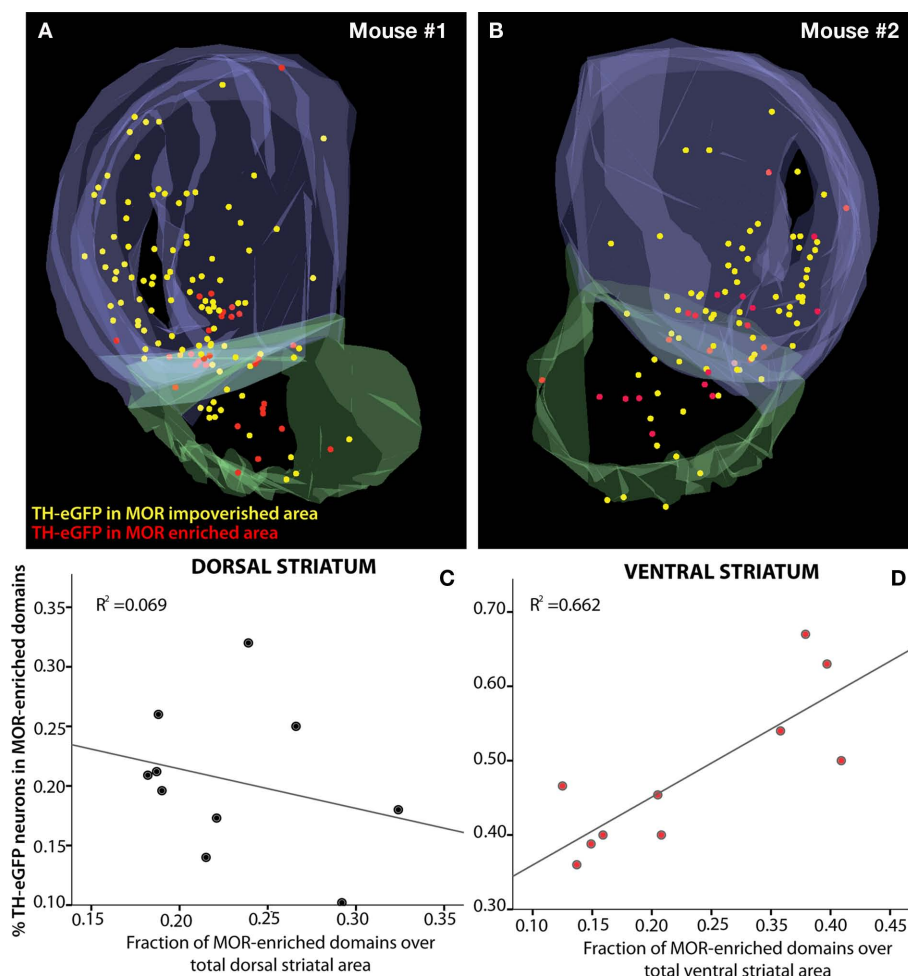


FIGURE 3 | Distribution of TH-eGFP neurons with respect to MOR-enriched areas of the striatum. The raw data ($n = 4$ hemispheres) from stereological cell-counting procedures were aligned and overlaid for 3D visualization after two hemispheres from the same brain were collapsed on each other (**A,B**). Markers show the distribution of systematically random sampled TH-eGFP neurons in MOR-enriched and MOR-impooverished compartments of the

striatum. The plots depict the percent distribution of TH-eGFP neurons in MOR-enriched domains of dorsal and ventral striatum (**C,D**). The relationship between striatal MOR-enriched domains and distribution of TH-eGFP neurons with respect to these domains is significantly different in dorsal (**C**) and ventral (**D**) divisions of the striatum ($p = 0.001$). Note the differences in the scale of y-axes in (**C,D**).

experiments and paired-recordings indicate that TH interneurons are well-integrated elements of striatal circuitry (Ibáñez-Sandoval et al., 2010). Therefore, the disparity in anatomical localization with respect to MOR-enriched domains in the dorsal and ventral striatum suggests that striatal TH interneurons may differentially influence local network dynamics in ventral versus dorsal striatum.

WHY IS THE ANATOMICAL DISTRIBUTION OF TH-eGFP INTERNEURONS DIFFERENT IN THE DORSAL AND VENTRAL STRIATUM?

And further, what is the significance of these differences in anatomical localization? The clues to the answers may lie within the rules that govern the developmental organization of the dorsal and ventral striatal divisions. It has been shown that striatal SPNs and PV-expressing interneurons follow different timelines for embryonic maximal birthrate and postmitotic maturation in dorsal striatum versus nucleus accumbens (Sadikot and Sasseville, 1997). Furthermore, van Vulpén and van der Kooy (1998) found a curious

relationship between birthdates and compartmental localization of cholinergic interneurons: the earliest born cholinergic neurons were more likely to be situated in the striosome compartment whereas later born cholinergic neurons had a higher likelihood to wind up in the matrix. It is possible that ventral striatal TH-eGFP neurons have earlier birthdates than dorsal striatal ones, which may account for different compartmental localization of these neurons across the dorsal–ventral axis of the striatum. Currently, the only available findings from a developmental stance come from the early postnatal maturation of striatal TH interneurons (Busceti et al., 2008). Further experiments are needed to examine the embryonic development and anatomical migratory patterns of TH-eGFP neurons.

Apart from the possibility that there is difference in birthdates, one also must take into account the fact that compartmental organization reflects a complex molecular patterning requiring the orchestrated action of multiple molecules including retinoic

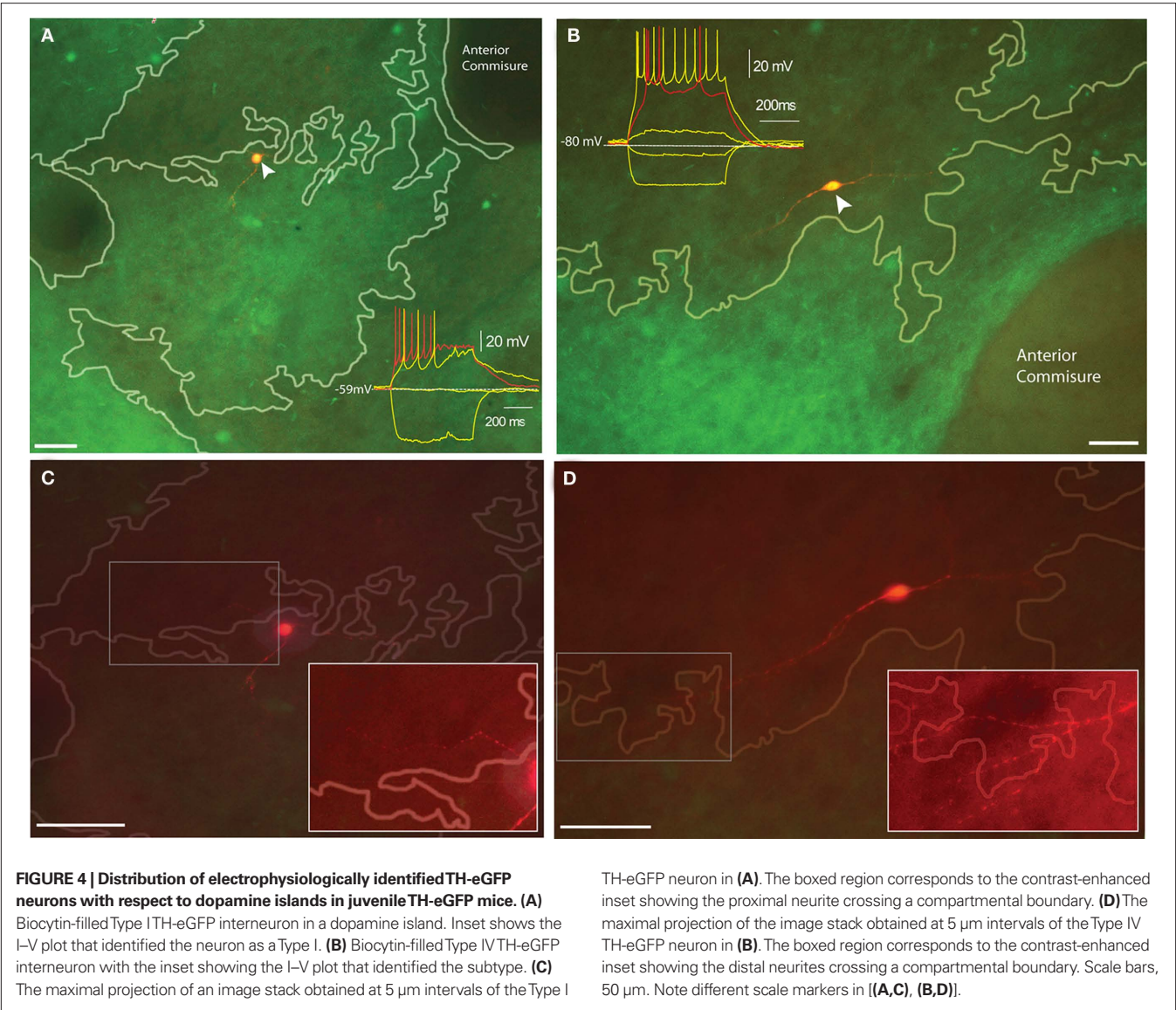


Table 1 | Stereological estimates of the number of TH-eGFP neurons from 60 µm serial sections at 300 µm intervals that were used for stereological counting and mapping of TH-eGFP neurons with respect to MOR-labeling.

	Stereological estimates of striatal TH-eGFP neurons/hemisphere (mean ± SEM)
Total number of striatal TH-eGFP neurons outside MOR-enriched domains	2032.8 ± 226.7
Total number of striatal TH-eGFP neurons inside MOR-enriched domains	723.2 ± 44.9
Total striatal TH-eGFP neurons	2756 ± 192.4
Total number of dorsal striatal TH-eGFP outside MOR-enriched domains	1663.6 ± 115.1
Total number of dorsal striatal TH-eGFP neurons inside MOR-enriched domains	422.1 ± 55.4
Total number of ventral striatal TH-eGFP neurons outside MOR-enriched domains	369.2 ± 47.3
Total number of ventral striatal TH-eGFP neurons inside MOR-enriched domains	301.1 ± 19.5

acid (Liao et al., 2008), notch signaling (Mason et al., 2005), certain transcription factors (Arlotta et al., 2008) cell adhesion (Redies et al., 2002) and guidance molecules (Janis et al., 1999; Hamasaki et al., 2001). Differential sensitivity to these factors in dorsal and ventral striatum may have given rise to the differences in compartmental localization of TH-eGFP interneurons. In particular, it has been shown that the repulsive action of netrins is integral for proper migration of matrix-bound neuronal precursors

Table 2 | Cavalieri estimations of surface area measurements obtained from 60 μm serial sections at 300 μm intervals that were used for stereological counting and mapping of TH-eGFP neurons with respect to MOR-labeling.

Region	Surface area (μm^2)/hemisphere	
	Males ($n = 6$ hemispheres)	Females ($n = 4$ hemispheres)
Total striatal area (A)	39058008	41054280
Total area of MOR-enriched domains (B)	8800958	9404603
(B)/(A)	22.5%	22.9%
Total dorsal striatal area (C)	28785228	29457135
Total area of dorsal MOR-enriched domains (D)	7084028	6145060
(D)/(C)	24.6%	20.9%
Total ventral striatal area (E)	10272779	11597145
Total area of ventral MOR-enriched domains (F)	1716929**	4207880**
(F)/(E)	16.7%**	36.3%**

The independent *t*-test comparisons only indicated a significant difference for MOR-enriched domain estimations in the ventral striatum between the sexes. ** indicates, $p < 0.01$.

(Hamasaki et al., 2001). Subsequently, it was demonstrated that netrin-1 shows a pronounced ventral to dorsal gradient, and that cholinergic interneurons co-expressing netrin-1 largely fall within the ventral striatum (Schatzmler et al., 2008). The same study also found that SOM-expressing GABAergic interneurons co-localized netrin-1 whereas PV and CR-expressing GABAergic interneurons did not. Since PV and CR interneurons do not show compartmental preferences within the striatum (Cowan et al., 1990; Rymar et al., 2004) and cholinergic and NPY-SOM neurons respect compartmental boundaries (Kubota and Kawaguchi, 1993; Martone et al., 1994; Saka et al., 2002), the possibility arises that expression of netrins and/or netrin receptors by TH-eGFP interneurons may be a determining factor of the compartmental localization in the dorsal and ventral striatum.

Although the current results show that there is a disproportionately higher number of TH-eGFP interneurons in MOR-enriched domains of the ventral striatum (~40 versus ~25% in the dorsal striatum), the majority of the TH interneurons reside in MOR-impooverished areas. A closer examination of matrix TH-eGFP neurons indicated that half of the population dwells within 100 μm or less of the striosome-matrix borders. This is consistent with results reported by Busceti et al. (2008) in which the majority of striatal TH neurons clustered near the pioneering nigral dopamine fibers commonly referred as “dopamine islands,” which are destined to form striatal striosomes in the adult (Graybiel et al., 1981; Miura et al., 2007, 2008).

These data suggest that even if they do not reside in striosomes, striatal TH neurons may still participate in intercompartmental communication in a manner similar to that of cholinergic and NPY interneurons (Kawaguchi, 1992; Kubota

and Kawaguchi, 1993; Saka et al., 2002). In order to better understand such a functional role full reconstructions of axonal and dendritic arborization of biocytin-filled TH-eGFP neurons with respect to striosome and matrix compartments in mature mice are necessary.

SUBTYPE-SPECIFIC LOCALIZATION OF TH INTERNEURONS TO TH-eGFP PATCHES/STRIOSOMES IN JUVENILE STRIATUM

In terms of the overall anatomical distribution of electrophysiological subtypes of TH-eGFP interneurons, no preferential regional localization was observed. However, one must bear in mind that there were only a few examples from some electrophysiological subtypes available for anatomical mapping. With an increased number of cases representing each TH-eGFP interneuronal subtype, a clearer picture of any preferential anatomical distribution might be revealed. Still, the preliminary results in this paper in which electrophysiological characterization of TH-eGFP neurons was carried out along with simultaneous compartmental localization based on TH-fiber intensity in young TH-eGFP mice ($n = 10$ neurons) suggest that there is chance that subtypes are localized in different compartments. It is interesting that 8 of 10 such labeled neurons in TH-rich islands displayed characteristics of Type I neurons, the most abundant electrophysiological subtype (>50% of entire recorded population, Ibáñez-Sandoval et al., 2010), whereas the remaining two somata that were located in the TH-poor zones displayed the phenotype of Type IV neurons, the second most prevalent subtype (~25%, Ibáñez-Sandoval et al., 2010). We would have expected to see just the opposite – the more abundant phenotype present in the more abundant striatal matrix compartment – if indeed TH-fiber intense zones correspond to striosomes as suggested (Miura et al., 2007, 2008). The mice from which these recordings and biocytin labeling obtained were aged between PN30–P33, and it is possible that this is a developmental range in which differences in TH-fiber density could be detected but compartments had already started maturation. Thus, TH-fiber rich zones in PN30–33 might correspond to matrix whereas TH-poor(er) zones might have been the striosomes. Indeed, it has been documented in adult cat, monkey and human brains that striosomes show reduced TH immunoreactivity (Graybiel et al., 1987). Indeed, in the MOR-immunolabeled striatal sections from adult TH-eGFP mice (>3 months), we have noticed that the dorsal striatal zones showing an attenuated background TH-eGFP fiber density showed a consistent overlap with the MOR-enriched domains (Figure 2A).

Therefore, it can be argued that depending on the degree of postnatal maturation; TH-fiber-enriched domains in TH-eGFP mice may correspond to patches/striosomes or matrix. However, in either case – juvenile or fully mature-, intensity of the TH-eGFP fiber background can be a distinguishing feature of striatal compartments in these mice. It is interesting to note that at least for Type I and Type IV neurons, striatal TH-eGFP interneurons have processes that cross the boundaries between the TH-enriched regions and the rest of the striatum. To the extent that the TH-enriched regions are in fact the precursors to the adult striosomes, this finding indicates that the axons and dendrites of striatal TH interneurons mediate intercompartment communication.

TH-eGFP INTERNEURONS, THE STRIOSOME–MATRIX MOSAIC AND STRIATAL FUNCTION

Although the exact significance of the mosaic organization of striatum is poorly understood, there is evidence that each compartment may be involved in different aspects of striatal functioning. For instance, the matrix was found to show higher metabolic responses as a result of unrestrained activity, somatosensory stimulation, and brief restraint (Brown et al., 2002). In addition, concurrent dopamine receptor stimulation, cocaine/apomorphine induced stereotypy, and behavioral sensitization lead to differential activation of striatal compartments as measured in terms of early immediate gene responses (Saka et al., 2002). Furthermore, it has been shown by targeted ablation of NPY–SOM⁺ and cholinergic populations using a saporin toxin conjugate against a tachykinin receptor subtype that these interneurons are essential for compartmentally distinct patterns of activation to emerge in the striatum (Saka et al., 2002). Therefore, striatal TH interneurons may be working in parallel with NPY–SOM and cholinergic interneurons in the establishment of regionally different striatal activity patterns. Further anatomical and electrophysiological studies are imperative to determine whether there is a special relationship among these interneurons across striatal compartments.

CONCLUSION

Above all, the current results should motivate further inquiries regarding the precise neurochemical makeup and function of the striatal TH-expressing neurons. There is still controversy concerning the neurochemical heterogeneity in this population. On the one hand, there is strong evidence that they express GABAergic markers and exert GABA-mediated inhibition onto SPNs (Dubach et al., 1987; Cosette et al., 2005b; Mazloom and Smith, 2006; Huot and Parent, 2007; Ibáñez-Sandoval et al., 2010). In addition, there are indications that these cells may possess the cellular components

necessary to synthesize, store, and release dopamine (Tashiro et al., 1989b; Mura et al., 1995, 2000; Betarbet et al., 1997; Lopez-Real et al., 2003; Cosette et al., 2005a; Tande et al., 2006; Busceti et al., 2008). The question, in the light of the current findings, is whether anatomically distinct localized and/or electrophysiologically different TH-eGFP cells are neurochemically the same or dissimilar. The answer is important because it may implicate a role for the TH-eGFP neurons in the observed spatial and temporal heterogeneity of striatal dopamine dynamics (Rodríguez et al., 2006; Wightman et al., 2007).

Finally, the current anatomical results will be essential to interpret commonly reported changes in striatal TH-expressing neuron number following experimentally induced or disease-related loss of striatal dopamine (Dubach et al., 1987; Tashiro et al., 1989a,b; Betarbet et al., 1997; Meredith et al., 1999; Mao et al., 2001; Palfi et al., 2002; Jollivet et al., 2004; Mazloom and Smith, 2006; Tande et al., 2006). Whether the appearance of “novel” TH neurons as a result of dopamine loss follows a distinct anatomical pattern would be very interesting to uncover, as striatal compartments were shown to display separable degrees of susceptibility to toxins and disease-related degeneration (Lawhorn et al., 2008; Sato et al., 2008; Granado et al., 2010). The present findings indicate that TH-eGFP neurons follow a non-random, distinct pattern of distribution across striosome–matrix compartments throughout the dorsal–ventral axis of the striatum. These results provide further impetus for future studies as to whether and how TH-eGFP neurons may affect striatal information processing based their anatomical location.

ACKNOWLEDGMENTS

The authors thank Dr. Laszlo Zaborszky for his critical suggestions on anatomical mapping methodology. This work was supported by NS034865 to James M. Tepper, NS059921 to Elizabeth D. Abercrombie and Rutgers University.

REFERENCES

- Albin, R. L., Young, A. B., and Penney, J. B. (1989). The functional anatomy of basal ganglia disorders. *Trends Neurosci.* 12, 366–375.
- Arlotta, P., Molyneaux, B. J., Jabaudon, D., Yoshida, Y., and Macklis, J. D. (2008). Ctip2 controls the differentiation of medium spiny neurons and the establishment of the cellular architecture of the striatum. *J. Neurosci.* 28, 622–632.
- Berendse, H. W., Voorn, P., te Kortschot, A., and Groenewegen, H. J. (1988). Nuclear origin of thalamic afferents of the ventral striatum determines their relation to patch/matrix configurations in enkephalin-immunoreactivity in the rat. *J. Chem. Neuroanat.* 1, 3–10.
- Bernácer, J., Prensa, L., and Giménez-Amaya, J. M. (2005). Morphological features, distribution and compartmental organization of the nicotinamide adenine dinucleotide phosphate reduced-diaphorase interneurons in the human striatum. *J. Comp. Neurol.* 489, 311–327.
- Bernácer, J., Prensa, L., and Giménez-Amaya, J. M. (2007). Cholinergic interneurons are differentially distributed in the human striatum. *PLoS ONE* 2, e1174. doi: 10.1371/journal.pone.0001174
- Betarbet, R., Turner, R., Chockkan, V., DeLong, M. R., Allers, K. A., Walters, J., Levey, A. I., and Greenamyre, J. T. (1997). Dopaminergic neurons intrinsic to the primate striatum. *J. Neurosci.* 17, 6761–6768.
- Bolam, J. P., Izzo, P. N., and Graybiel, A. M. (1988). Cellular substrate of the histochemically defined striosome/matrix system of the caudate nucleus: a combined Golgi and immunocytochemical study in cat and ferret. *Neuroscience* 24, 853–875.
- Brown, L. L., Feldman, S. M., Smith, D. M., Cavanaugh, J. R., Ackermann, R. F., and Graybiel, A. M. (2002). Differential metabolic activity in the striosome and matrix compartments of the rat striatum during natural behaviors. *J. Neurosci.* 22, 305–314.
- Busceti, C. L., Biagioni, F., Mastroiacovo, F., Bucci, D., Lenzi, P., Pasquali, L., Trabucco, A., Nicoletti, F., and Fornai, F. (2008). High number of striatal dopaminergic neurons during early postnatal development: correlation analysis with dopaminergic fibers. *J. Neural Trans.* 115, 1375–1383.
- Chesselet, M. F., and Graybiel, A. M. (1986). Striatal neurons expressing somatostatin-like immunoreactivity: evidence for a peptidergic interneuronal system in the cat. *Neuroscience* 17, 547–571.
- Cosette, M., Levesque, D., and Parent, A. (2005a). Neurochemical characterization of dopaminergic neurons in the human striatum. *Parkinsonism Relat. Disord.* 11, 277–286.
- Cosette, M., Lecomte, F., and Parent, A. (2005b). Morphology and distribution of dopaminergic neurons intrinsic to the human striatum. *J. Chem. Neuroanat.* 29, 1–11.
- Cowan, R. L., Wilson, C. J., Emson, P. C., and Heizmann, C. W. (1990). Parvalbumin-containing GABAergic interneurons in the rat neostriatum. *J. Comp. Neurol.* 302, 197–205.
- Dubach, M., Schmidt, R., Kunkel, D., Bowden, D. M., Martin, R., and German, D. C. (1987). Primate neostriatal neurons containing tyrosine hydroxylase: immunohistochemical evidence. *Neurosci. Lett.* 75, 205–210.
- Franklin, K. B. J., and Paxinos, G. (2001). *The Mouse Brain in Stereotaxic Coordinates*. San Diego, CA: Academic Press.
- Gerfen, C. R. (1989). The neostriatal mosaic: striatal patch-matrix organization is related to cortical lamination. *Science* 246, 385–388.
- Gerfen, C. R. (1992). The neostriatal mosaic: multiple levels of compartmental organization. *Trends Neurosci.* 15, 133–139.
- Gerfen, C. R., Baimbridge, K. G., and Miller, J. J. (1985). The neostriatal mosaic: compartmental distribution of calcium-binding protein and

- parvalbumin in the basal ganglia of the rat and monkey. *Proc. Natl. Acad. Sci. U.S.A.* 82, 8780–8784.
- Gerfen, C. R., Engber, T. M., Mahan, L. C., Susel, Z., Chase, T. N., Monsma, F. J. Jr., and Sibley, D. R. (1990). D1 and D2 dopamine receptor-regulated gene expression of striatonigral and striatopallidal neurons. *Science* 250, 1429–1432.
- Gerfen, C. R., and Wilson, C. J. (1996). “The basal ganglia,” in *Handbook of Chemical Neuroanatomy*, Vol. 12, *Integrated Systems of the CNS*, Part III, eds L. W. Swanson, A. Björklund, and T. Hökfelt (Amsterdam: Elsevier), 371–468.
- Gong, S., Zheng, C., Doughty, M. L., Losos, K., Didkovsky, N., Schambra, U. B., Nowak, N. J., Joyner, A., Leblanc, G., Hatten, M. E., and Heintz, N. (2003). A gene expression atlas of the central nervous system based on bacterial artificial chromosomes. *Nature* 425, 917–925.
- Granado, N., Ares-Santos, S., O’Shea, E., Vicario-Abejon, C., Colado, M. I., and Moratalla, R. (2010). Selective vulnerability in striosomes and in the nigrostriatal dopaminergic pathway after methamphetamine administration: early loss of TH in striosomes after methamphetamine. *Neurotox. Res.* 18, 48–58.
- Graybiel, A. M., Hirsch, E. C., and Agid, Y. A. (1987). Differences in tyrosine hydroxylase-like immunoreactivity characterize the mesostriatal innervation of striosomes and extrastriosomal matrix at maturity. *Proc. Natl. Acad. Sci. U.S.A.* 84, 303–307.
- Graybiel, A. M., Pickel, V. M., Joh, T. H., Reis, D. J., and Ragsdale, C. W. (1981). Direct demonstration of a correspondence between the dopamine islands and acetylcholinesterase patches in the developing striatum. *Proc. Natl. Acad. Sci. U.S.A.* 78, 5871–5875.
- Hamasaki, T., Goto, S., Nishikawa, S., and Ushio, Y. (2001). A role of netrin-1 in the formation of subcortical structure striatum: repulsive action on the migration of late-born striatal neurons. *J. Neurosci.* 21, 4272–4280.
- Heimer, L., Alheid, G. F., de Olmos, J. S., Groenewegen, H. J., Haber, S. N., Harlan, R. E., and Zahm, D. S. (1997). The accumbens: beyond the core-shell dichotomy. *J. Neuropsychiatry Clin. Neurosci.* 9, 354–381.
- Henny, F., and Jones, B. E. (2008). Projections from basal forebrain to prefrontal cortex comprise cholinergic, GABAergic and glutamatergic inputs to pyramidal cells or interneurons. *Eur. J. Neurosci.* 27, 654–670.
- Herkenham, M., and Pert, C. B. (1981). Mosaic distribution of opiate receptors, parafascicular projections and acetylcholinesterase in the striatum. *Nature* 291, 415–418.
- Holt, D. J., Graybiel, A. M., and Saper, C. B. (1997). Neurochemical architecture of the human striatum. *J. Comp. Neurol.* 384, 1–25.
- Huot, P., Levesque, M., and Parent, A. (2007). The fate of striatal dopaminergic neurons in Parkinson’s disease and Huntington’s chorea. *Brain* 130, 222–232.
- Huot, P., and Parent, A. (2007). Dopaminergic neurons intrinsic to the striatum. *J. Neurochem.* 101, 1441–1447.
- Ibáñez-Sandoval, O., Tecuapetla, F., Unal, B., Shah, F., Koós, T., and Tepper, J. M. (2010). Electrophysiological and morphological characteristics and synaptic connectivity of tyrosine hydroxylase-expressing neurons in adult mouse striatum. *J. Neurosci.* 30, 6999–7016.
- Ikemoto, S. (2007). Dopamine reward-circuitry: two projection systems from the ventral midbrain to the nucleus accumbens-olfactory tubercle complex. *Brain Res. Rev.* 56, 27–78.
- Janis, L. S., Cassidy, R. M., and Kromer, L. F. (1999). Ephrin-A binding and EphA receptor expression delineate the matrix compartment of the striatum. *J. Neurosci.* 19, 4962–4971.
- Jollivet, C., Montero-Menei, C. N., Venier-Julienne, M. C., Sapin, A., Benoit, J. P., and Menei, P. (2004). Striatal tyrosine hydroxylase immunoreactive neurons are induced by L-dihydroxyphenylalanine and nerve growth factor treatment in 6-hydroxydopamine lesioned rats. *Neurosci. Lett.* 362, 79–82.
- Jongen-Relo, A., Groenewegen, H. J., and Voorn, P. (1993). Evidence for multi-compartmental histochemical organization of the nucleus accumbens in the rat. *J. Comp. Neurol.* 337, 267–276.
- Jongen-Relo, A. L., Voorn, P., and Groenewegen, H. J. (1994). Immunohistochemical characterization of the shell and core territories of the nucleus accumbens in the rat. *Eur. J. Neurosci.* 6, 1255–1264.
- Kawaguchi, Y. (1992). Large aspiny cells in the matrix of the rat neostriatum in vitro: physiological identification, relation to the compartments and excitatory postsynaptic currents. *J. Neurophysiol.* 67, 1669–1682.
- Kawaguchi, Y. (1993). Physiological, morphological and histochemical characterization of three classes of interneurons in the neostriatum. *J. Neurosci.* 13, 4908–4923.
- Kawaguchi, Y., Wilson, C. J., Augood, S. J., and Emson, P. C. (1995). Striatal interneurons: chemical, physiological and morphological characterization. *Trends Neurosci.* 18, 527–535.
- Kawaguchi, Y., Wilson, C. J., and Emson, P. C. (1990). Projection subtypes of rat neostriatal matrix cells revealed by intracellular injection of biocytin. *J. Neurosci.* 10, 3421–3438.
- Kita, H. (2001). Neostriatal and globus pallidus stimulation induced inhibitory postsynaptic potentials in entopeduncular neurons in rat brain slice preparations. *Neuroscience* 105, 871–879.
- Kita, H., Chiken, S., Tachibana, Y., and Nambu, A. (2006). Origins of GABA(A) and GABA(B) receptor-mediated responses of the globus pallidus induced after stimulation of the putamen in the monkey. *J. Neurosci.* 26, 6554–6562.
- Kubota, Y., and Kawaguchi, Y. (1993). Spatial distributions of chemically identified intrinsic neurons in relation to patch and matrix compartments of rat neostriatum. *J. Comp. Neurol.* 332, 499–513.
- Lawhorn, C., Smith, D. M., and Brown, L. L. (2008). Striosome-matrix pathology and motor deficits in the YAC 128 mouse model of Huntington’s disease. *Neurobiol. Dis.* 32, 471–478.
- Liao, L., Tsai, H., Wang, H., Chang, J., Lu, K., Wu, H., and Lee, Y. (2008). Modular patterning of structure and function of the striatum by retinoid receptor signaling. *Proc. Natl. Acad. Sci. U.S.A.* 105, 6765–6770.
- Lopez-Real, A., Rodriguez-Pallares, J., Guerra, M. H., and Labandeira-Garcia, J. L. (2003). Localization and functional significance of striatal neurons immunoreactive to aromatic L-amino acid decarboxylase or tyrosine hydroxylase in rat parkinsonian models. *Brain Res.* 969, 135–146.
- Mao, L., Lau, Y. S., Petroske, E., and Wang, J. Q. (2001). Profound astrogenesis in the striatum of adult mice following nigrostriatal dopaminergic lesion by repeated MPTP administration. *Brain Res. Dev. Brain Res.* 131, 57–65.
- Martone, M. E., Young, S. J., Armstrong, D. M., and Groves, P. M. (1994). The distribution of cholinergic perikarya with respect to enkephalin-rich patches in the caudate nucleus of the adult cat. *J. Chem. Neuroanat.* 8, 47–59.
- Mason, H. A., Rakowiecki, S. M., Raftopoulou, M., Nery, S., Huang, Y., Gridley, T., and Fishell, G. (2005). Notch signaling coordinates the pattern of striatal compartments. *Development* 132, 4247–4258.
- Mazloom, M., and Smith, Y. (2006). Synaptic microcircuitry of tyrosine hydroxylase-containing neurons and terminals in the striatum of 1-Methyl-4-Phenyl-1,2,3,6-Tetrahydropyridine treated monkeys. *J. Comp. Neurol.* 495, 453–469.
- Meredith, G. E., Farrell, T., Kellaghan, P., Tan, Y., Zahm, D. S., and Toterdel, S. (1999). Immunocytochemical characterization of catecholaminergic neurons in the rat striatum following dopamine-depleting lesions. *Eur. J. Neurosci.* 11, 3583–3596.
- Mikula, S., Parrish, S. K., Trimmer, J. S., and Jones, E. G. (2009). Complete 3D visualization of primate striosomes by KChIP1 immunostaining. *J. Comp. Neurol.* 514, 507–517.
- Miura, M., Masada, M., and Aosaki, T. (2008). Roles of micro-opioid receptors in GABAergic synaptic transmission in the striosome and matrix compartments of the striatum. *Mol. Neurobiol.* 37, 104–115.
- Miura, M., Saino-Saito, S., Masuda, M., Kobayashi, K., and Aosaki, T. (2007). Compartment-specific modulation of GABAergic synaptic transmission by μ -opioid receptor in the mouse striatum with green fluorescent protein-expressing dopamine islands. *J. Neurosci.* 27, 9721–9728.
- Mura, A., Jackson, D., Manley, M. S., Young, S. J., and Groves, P. M. (1995). Aromatic L-amino acid decarboxylase immunoreactive cells in the rat striatum: a possible site for the conversion of exogenous L-DOPA to dopamine. *Brain Res.* 704, 51–60.
- Mura, A., Linder, J. C., Young, S. J., and Groves, P. M. (2000). Striatal cells containing aromatic L-amino acid decarboxylase: an immunohistochemical comparison with other classes of striatal neurons. *Neuroscience* 98, 501–511.
- Oorschot, D. E. (2010). “Cell types in the different nuclei of the basal ganglia,” in *Handbook of Basal Ganglia Structure and Function*, eds H. Steiner and K. Y. Tseng (San Diego, CA: Academic Press), 63–91.
- Palfi, S., Leventhal, L., Chu, Y., Ma, S. Y., Emborg, M., Bakay, R., Deglon, N., Hantraye, P., Aebischer, P., and Kordower, J. H. (2002). Lentivirally delivered glial cell line-derived neurotrophic factor increases the number of striatal dopaminergic neurons in primate models of nigrostriatal degeneration. *J. Neurosci.* 22, 4942–4954.
- Prasad, K., and Richfield, E. K. (2010). Number and nuclear morphology of TH+ and TH– neurons in the mouse ventral midbrain using epifluorescence stereology. *Exp. Neurol.* 225, 328–340.
- Ragsdale, C. W., and Graybiel, A. M. (1981). The fronto-striatal projection in the cat and monkey and its relationship to inhomogeneities established by acetylcholinesterase

- histochemistry. *Brain Res.* 208, 259–266.
- Redies, C., Kovjanic, D., Heyers, D., Medina, L., Hirano, S., Suzuki, S. T., and Puelles, L. (2002). Patch/matrix patterns of gray matter differentiation in telencephalon of chicken and mouse. *Brain Res. Bull.* 57, 489–493.
- Rivera, A., Cuellar, B., Giron, F. J., Grandy, D. K., de la Calle, A., and Moratalla, R. (2002). Dopamine D4 receptors are heterogeneously distributed in the striosomes/matrix compartments of the striatum. *J. Neurochem.* 80, 219–229.
- Rodriguez, M., Morales, I., Gomez, I., Gonzalez, S., Gonzalez-Hernandez, T., and Gonzalez-Mora, J. L. (2006). Heterogeneous dopamine neurochemistry in the striatum: the fountain-drain matrix. *J. Pharmacol. Exp. Ther.* 19, 31–43.
- Rymar, V. V., Sasseville, R., Luk, K. C., and Sadikot, A. F. (2004). Neurogenesis and stereological morphometry of calretinin immunoreactive GABAergic interneurons of the neostriatum. *J. Comp. Neurol.* 469, 325–339.
- Sadikot, A. F., and Sasseville, R. (1997). Neurogenesis in the mammalian neostriatum and nucleus accumbens: parvalbumin-immunoreactive GABAergic interneurons. *J. Comp. Neurol.* 389, 193–211.
- Saka, E., Iadarola, M., Fitzgerald, D. J., and Graybiel, A. M. (2002). Local circuit neurons in the striatum regulate neural and behavioral responses to dopaminergic stimulation. *Proc. Natl. Acad. Sci. U.S.A.* 99, 9004–9009.
- Sako, W., Morigaki, R., Nagahiro, S., Kaji, R., and Goto, S. (2010). Olfactory type G protein alpha subunit in striosome-matrix dopamine systems in adult mice. *Neuroscience* 170, 497–502.
- Sato, K., Sumi-Ichinose, C., Kaji, R., Ikemoto, K., Nomura, T., Nagatsu, I., Ichinose, H., Ito, M., Sako, W., Nagahiro, S., Graybiel, A. M., and Goto, S. (2008). Differential involvement of striosome and matrix dopamine systems in a transgenic model of dopa-responsive dystonia. *Proc. Natl. Acad. Sci. U.S.A.* 105, 12551–12556.
- Schatzmler, R. A., Goldman, J. S., Simard-Emond, L., Rymar, V., Manitt, C., Sadikot, A. F., and Kennedy, T. E. (2008). Graded expression of netrin-1 by specific neuronal subtypes in the adult mammalian striatum. *Neuroscience* 157, 621–636.
- Tande, D., Hoglinger, G., Debeir, T., Freundlieb, N., Hirsch, E. C., and Francois, C. (2006). New striatal dopamine neurons in MPTP-treated macaques result from a phenotypic shift and not neurogenesis. *Brain* 129, 1194–1200.
- Tashiro, Y., Sugimoto, T., Hattori, T., Uemura, Y., Nagatsu, I., Kikuchi, H., and Mizuno, N. (1989a). Tyrosine hydroxylase-like immunoreactive neurons in the striatum of the rat. *Neurosci. Lett.* 97, 6–10.
- Tashiro, Y., Kaneko, T., Sugimoto, T., Nagatsu, I., Kikuchi, H., and Mizuno, N. (1989b). Striatal neurons with aromatic L-amino acid decarboxylase-like immunoreactivity in the rat. *Neurosci. Lett.* 100, 29–34.
- Tepper, J. M. (2010). “GABAergic interneurons of the striatum,” in *Handbook of Basal Ganglia Structure and Function*, eds H. Steiner and K. Y. Tseng (San Diego, CA: Academic Press), 151–163.
- van Vulpel, E. H., and van der Kooy, D. (1998). Striatal cholinergic interneurons: birthdates predict compartmental localization. *Brain Res. Dev. Brain Res.* 109, 51–58.
- Voorn, P., Gerfen, C. R., and Groenewegen, H. J. (1989). Compartmental organization of the ventral striatum of the rat: immunohistochemical distribution of enkephalin, substance P, dopamine and calcium binding protein. *J. Comp. Neurol.* 289, 189–201.
- Voorn, P., Vanderschuren, L. E., and Groenewegen, H. J. (2004). Putting a spin on the dorsal-ventral divide of the striatum. *Trends Neurosci.* 27, 468–474.
- Wightman, R. M., Heien, M. L., Wassum, K. M., Sombers, L. A., Aragona, B. J., Khan, A. S., Ariansen, J. L., Cheer, J. F., Phillips, P. E., and Carelli, R. M. (2007). Dopamine release is heterogeneous within microenvironments of the rat nucleus accumbens. *Eur. J. Neurosci.* 26, 2046–2054.
- Wu, Y., and Parent, A. (2000). Striatal interneurons expressing calretinin, parvalbumin and NADPH-diaphorase: a comparative study in the rat, monkey and human. *Brain Res.* 863, 182–191.
- Zaborszky, L., Alheid, G. F., Beinfeld, M. C., Eiden, L. E., Heimer, L., and Palkovita, M. (1985). Cholecystokinin innervation of the ventral striatum: a morphological and radioimmunological study. *Neuroscience* 14, 427–453.

Conflict of Interest Statement: The authors declare that the research was conducted in the absence of any commercial or financial relationships that could be construed as a potential conflict of interest.

Received: 10 March 2011; accepted: 24 May 2011; published online: 06 June 2011.

Citation: Ünal B, Ibáñez-Sandoval O, Shah F, Abercrombie ED and Tepper JM (2011) Distribution of tyrosine hydroxylase-expressing interneurons with respect to anatomical organization of the neostriatum. *Front. Syst. Neurosci.* 5:41. doi: 10.3389/fnsys.2011.00041

Copyright © 2011 Ünal, Ibáñez-Sandoval, Shah, Abercrombie and Tepper. This is an open-access article subject to a non-exclusive license between the authors and Frontiers Media SA, which permits use, distribution and reproduction in other forums, provided the original authors and source are credited and other Frontiers conditions are complied with.



An improved BAC transgenic fluorescent reporter line for sensitive and specific identification of striatonigral medium spiny neurons

Kristen K. Ade¹, Yehong Wan¹, Meng Chen¹, Bernd Gloss^{2,3} and Nicole Calakos^{1,3*}

¹ Division of Neurology, Center for Translational Neuroscience, Duke University, Durham, NC, USA

² Neurotransgenic Core Facility, Duke University, Durham, NC, USA

³ Department of Neurobiology, Duke University, Durham, NC, USA

Edited by:

James M. Tepper, Rutgers, The State University of New Jersey, USA

Reviewed by:

David M. Lovinger, National Institutes of Health, USA

Tibor Koos, Rutgers University, USA

*Correspondence:

Nicole Calakos, Center for Translational Neuroscience, Box 2900, Research Dr., Duke University Medical Center, Durham, NC 27710, USA.

e-mail: nicole.calakos@duke.edu

The development of BAC transgenic mice expressing promoter-specific fluorescent reporter proteins has been a great asset for neuroscience by enabling detection of neuronal subsets in live tissue. For the study of basal ganglia physiology, reporters driven by type 1 and 2 dopamine receptors have been particularly useful for distinguishing the two classes of striatal projection neurons – striatonigral and striatopallidal. However, emerging evidence suggests that some of the transgenic reporter lines may have suboptimal features. The ideal transgenic reporter line should (1) express a reporter with high sensitivity and specificity for detecting the cellular subset of interest and that does not otherwise alter the biology of the cells in which it is expressed, and (2) involve a genetic manipulation that does not cause any additional genetic effects other than expression of the reporter. Here we introduce a new BAC transgenic reporter line, *Drd1a*-tdTomato line 6, with features that approximate these ideals, offering substantial benefits over existing lines. In this study, we investigate the integrity of dopamine-sensitive behaviors and test the sensitivity and specificity of tdTomato fluorescence for identifying striatonigral projection neurons in mice. Behaviorally, hemizygous *Drd1a*-tdTomato line 6 mice are similar to littermate controls; while hemizygous *Drd2*-EGFP mice are not. In characterizing the sensitivity and specificity of line 6 mice, we find that both are high. The results of this characterization indicate that line 6 *Drd1a*-tdTomato^{+/−} mice offer a useful alternative approach to identify both striatonigral and striatopallidal neurons in a single transgenic line with a high degree of accuracy.

Keywords: medium spiny neuron, striatum, basal ganglia, direct pathway, striatonigral, BAC, transgenic, tdTomato

INTRODUCTION

The generation of transgenic lines with promoter-specific fluorescent reporter proteins has significantly advanced the field of neurobiological research. By allowing for cell subtype identification and morphological visualization in living tissue, BAC transgenics have greatly facilitated physiological studies of specific neuronal subsets. BAC transgenic mice generated by the Gene Expression Nervous System Atlas (GENSAT) project expressing EGFP fluorescent reporters under the control of the type 1 and 2 dopamine receptor regulatory sequences have been especially useful for discriminating between the two types of striatal projection neurons, striatonigral or direct pathway and striatopallidal or indirect pathway (Gong et al., 2003). These two types of medium spiny neurons (MSNs) have molecular, anatomical, and functional differences, but are not otherwise easily distinguished. Since the introduction of fluorescent reporter transgenic lines to distinguish these cell types in living tissue, they have been used widely to reveal phenotypic differences between these two classes of MSNs as well as evidence for subtype-selective impairment in disease states (Day et al., 2006, 2008; Kreitzer and Malenka, 2007; Shen et al., 2007, 2008; Ade et al., 2008; Cepeda et al., 2008; Gertler et al., 2008; Janssen et al., 2009; Yin et al., 2009; Doig et al., 2010; Flores-Barrera et al., 2010; Gittis et al., 2010; Planert et al., 2010; André et al., 2011).

While the GENSAT *Drd1a*-EGFP and *Drd2*-EGFP transgenic lines have been useful to study the physiology of striatopallidal and striatonigral MSNs, a recent study reports that that introduction of the BAC *Drd2*-EGFP transgene into the mouse genome may alter dopamine D2 receptor surface expression and cause aberrant locomotor behavior (Kramer et al., 2011). These findings raise the need for alternative methodologies to discriminate between these two populations of MSNs.

In a previous study, we evaluated the sensitivity and specificity of using a single transgenic fluorescent reporter to properly identify both populations of striatal projection neurons (Shuen et al., 2008). Fluorescence intensity of a transgenic reporter can vary across lines, limiting the utility of certain lines for identifying all cells expressing the fluorescent reporter, especially when using techniques with relatively low sensitivity such as epifluorescence microscopy commonly found on electrophysiological rigs. The development of the *Drd1a*-tdTomato line 5 (Shuen et al., 2008) was a significant advancement over the existing *Drd1a*-EGFP line as the td-Tomato red fluorescent protein has a higher relative brightness than EGFP (Deliolanis et al., 2008; Drobizhev et al., 2009) as well as a longer excitation wavelength which provides better tissue penetration. However, since its introduction, several characteristics that limit the robustness of the line 5 *Drd1a*-tdTomato transgenic

line have been identified. Breeding experiments demonstrate an X-linked inheritance pattern. In addition, ambiguous mammary glands are more commonly observed on male mice in this line. A putative X-linked transgene also adds another level of care that users of this line need to apply in experimental subject breedings in order to avoid inadvertently studying a biased population of only females in cases where the transgene donor is the father. Lastly, the fertility and litter-size of this transgenic line is severely reduced on a pure C57Bl/6 strain background. Because C57Bl/6 is a commonly used strain in neuroscience, this further limits the utility of this line.

In this study, we characterize a second *Drd1a*-tdTomato BAC transgenic mouse line, line 6. We find that this line has normal fertility in the C57Bl/6 background, an autosomal-inheritance pattern, no obvious morphological or cellular abnormalities, normal behavior in dopamine-sensitive motor tests, and high sensitivity and specificity of the fluorescent reporter for identifying striatonigral MSNs. Altogether, these features overcome significant limitations of existing transgenic lines and provide a useful option for accurate discrimination of both striatonigral and striatopallidal neurons using a single transgenic line.

MATERIALS AND METHODS

MICE

All animal procedures were done humanely to minimize distress and according to protocols approved by the Institutional Animal Care and Use Committee of Duke University. Mice used for behavioral experiments, *Drd1a*-tdTomato (line 6) and GENSAT *Drd2*-EGFP mice (courtesy of Drs. N. Heintz and X. W. Yang; provided to us from the Yang colony in 2006), were backcrossed onto a C57Bl/6 background for a minimum of six generations. In behavioral experiments, transgene-negative littermate controls (−/−) were compared to mice that were hemizygous for the transgene (+/−) of interest. Mice used for imaging experiments had hybrid strain backgrounds (sv129/FVB-1/C57Bl/6). *ChAT*-EGFP mice [B6.Cg-Tg(RP23-268L19-EGFP)2Mik/J] were obtained from The Jackson Laboratory (Bar Harbor, ME, USA). Mice used for electrophysiology experiments were backcrossed onto a C57Bl/6 background. All mice were offspring of breeding pairs in which transgene expression was limited to one parent ensuring that all experimental animals were hemizygous for transgenes of interest. Line 6 *Drd1a*-tdTomato mice are available to the academic research community through The Jackson Laboratory (JAX stock number 16204).

GENOTYPING

Genotyping of *Drd1a*-tdTomato was performed using the following primers: BGH-F (forward primer) 5-CTT CTG AGG CGG AAA GAA CC-3; dDR4 (reverse primer) 5-TTT CTG ATT GAG AGC ATT CG-3. The PCR protocol used is as follows: 1 cycle at 94°C for 2 min, 5 cycles of 94°C for 30 s, 60–55°C touchdown ramp for 30 s and 72°C for 30 s; 25 cycles of 94°C for 30 s, 55°C for 30 s and 72°C for 30 s followed by 1 cycle at 72°C for 5 min. PCR product length is 846 bp. Genotyping of *Drd2*-EGFP was performed using the following primers: D2 (forward) CCC GAA GCT TCT CGA GGC GCG CCC TGT GCG TCA GCA TTT GGA GCA AC; GFPB2 (reverse) TCA GGG TCA GCT TGC CGT AGG5. The PCR protocol used is as follows: 1 cycle at 94°C for 2 min,

5 cycles of 94°C for 30 s, 60–55°C touchdown ramp for 60 s and 72°C for 90 s; 30 cycles of 94°C for 30 s, 55°C for 60 s and 72°C for 90 s followed by 1 cycle at 72°C for 5 min. PCR product length is approximately 800 bp. Genotyping of *ChAT*-EGFP was performed using the following primers: *ChAT* (forward) AGT AAG GCT ATG GGA TTC ATT C; *ChAT* (reverse) AGT TCA CCT TGA TGC CGT TC. The PCR protocol used is as follows: 1 cycle at 94°C for 3 min, 35 cycles of 94°C for 30 s, 52°C for 60 s and 72°C for 60 s and 1 cycle of 72°C for 2 min. PCR product length is approximately 600 bp.

BEHAVIOR

Mice aged 8–11 weeks were tested in the open field (OF) behavioral assay. Animals in their home cages were moved to the room where OF testing was performed at least 12 h prior to the experiment. For testing, animals were placed in OF chambers (21 × 21 × 30 cm) with clear polycarbonate walls. VersaMax Animal Activity Monitor (AccuScan Instruments, Columbus, OH, USA) was used to record behavioral response parameters including horizontal locomotion (distance in cm), counts of vertical movements, and stereotypies (repetitive beam breaks < 1 s apart). Location of mice was mapped and defined as being in either the center or perimeter zones (each 10.5 cm²). Data was recorded in 5-min bins. Time-point values refer to total in each 5-min bin. OF data are reported during basal conditions (first 60 min in chamber) and following an injection of cocaine (20 mg/kg i.p.; minutes 61–180 in chamber). The locomotor response to cocaine was normalized to the mean distance traveled during the 20 min immediately preceding cocaine administration (“baseline locomotion”). The genotype of the experimental subject was not known to the experimenter. Behavioral assays for each genotype were repeated in two separate cohorts. Transgene-positive (+/−) and transgene-negative (−/−) mice for each genotype were compared using 2-way repeated measures ANOVA.

TISSUE FIXATION, IMMUNOSTAINING, AND FLUORESCENCE IMAGING

Three-week-old mice were anesthetized with tribromoethanol (250 mg/kg i.p.) before transcardial perfusion with 4% paraformaldehyde (PFA) in phosphate-buffered saline (PBS), pH 7.4. Brains were extracted and immersed in PFA solution for 24–72 h at 4°C prior to the sectioning of 50 μm slices on a Leica VTS-1000 vibratome (Leica Microsystems, Bannockburn, IL, USA). Slices were transferred to 1X PBS for immunofluorescence staining of free floating sections except for slices prepared from line 6 *Drd1a*-tdTomato^{+/−}/*ChAT*-EGFP^{+/−} mice which were directly mounted with Fluoromount-G mounting medium (Southern Biotech, Birmingham, AL, USA) without additional processing.

Slices were washed in PBS and incubated for 1 h in blocking buffer containing 5% bovine serum albumin, 2% normal goat serum, 0.2% Triton X-100 in 1X PBS prior to immunostaining. Slices were incubated overnight at 4°C with the following primary antibodies and dilutions: parvalbumin (PV) mouse monoclonal (P3088 Sigma, St. Louis, MO, USA) 1:500, somatostatin (SS) rat monoclonal (MAB354 Millipore, Billerica, MA 01821, USA) 1:50–1:100, and DARPP-32 rabbit polyclonal (AB1656 Millipore) 1:500. Secondary antibodies (Alexa Fluor-405 conjugated goat anti-mouse, Alexa Fluor-405 conjugated goat anti-rabbit, and Alexa Fluor-488 conjugated goat anti-mouse; all from Invitrogen, Carlsbad, CA, USA)

were incubated at 1:800 dilutions. Cy5 conjugated donkey anti-rat antibodies were used at 1:200 dilution (Jackson ImmunoResearch Laboratories, Inc., Westgrove, PA, USA). Slices were mounted with Fluoromount-G mounting medium.

Sagittal slices were imaged on a Zeiss Axio Observer Z1 motorized microscope equipped with a 10×/0.30 Plan-NeoFluar Ph1 objective, X-CITE 120XL metal halide fluorescence light source, and Coolsnap ES2 high resolution CCD camera. TdTomato fluorescence was imaged with a red HQ45 filter cube (BP 560/40, FT 585, BP 630/75). The low-magnification sagittal brain view (**Figure 3A**) is a composite image created by stitching together multiple 10× images using MetaMorph 7.6.5 software (Molecular Devices, Sunnyvale, CA, USA). Higher resolution images were acquired using a Zeiss LSM 510 inverted confocal microscope equipped with 405 nm Diode, Argon/2 (458, 477, 488, 514 nm), 561 nm Diode and HeNe 633 nm lasers. Images were acquired using either 10×/0.30 NA (Plan Neo-Fluar) or 20×/0.80 NA (Plan Apochromat) objectives and acquisition software from Zeiss Microimaging (Thornwood, NY, USA). Confocal images were analyzed using ImageJ software (<http://rsbweb.nih.gov/ij/>).

Imaging of 300 μm thick acute coronal cortical–striatal slices was performed on an electrophysiological rig with continuous perfusion of standard artificial cerebrospinal fluid (ACSF). Slices were prepared using the procedure described for electrophysiology recordings. Imaging was performed using a 60× water-immersion objective (LUMPlanFL N, 60×/1.00 NA) under an Olympus BX51WI microscope equipped with phase contrast optics, epifluorescence, an Olympus OLY-150 camera/controller system (Olympus America, Center Valley, PA, USA) and an HR-120 series monochrome video monitor (DAGE-MTI, Michigan City, IN, USA). Cells within the dorsal striatum were first identified by phase-contrast illumination and then checked for fluorescence. Cells that appeared swollen or otherwise necrotic were not included in the analysis.

For both confocal and epifluorescent imaging data, the threshold for a positive signal was an intensity equal to or greater than that of the surrounding neuropil. Cells lacking transgene fluorescence were defined as those in which fluorescence was significantly lower than the surrounding neuropil (characteristic “black hole” appearance). Note: these criteria are different from those used in our previous study to characterize the *Drd1a*-tdTomato line 5 mice, which required fluorescence intensity to be greater than surrounding neuropil to be considered positive (Shuen et al., 2008). To minimize light scattering effects which degrade imaging sensitivity, only cells in the first 60 μm of tissue depth were assessed.

ACUTE SLICE PREPARATION AND ELECTROPHYSIOLOGY

For electrophysiological recordings, acute coronal brain slices (300 μm thick) were prepared from line 6 *Drd1a*-tdTomato^{+/−}/*Drd2*-EGFP^{+/−} transgenic mice and their line 6 *Drd1a*-tdTomato^{−/−}/*Drd2*-EGFP^{+/−} transgenic littermates (P21–27). Mice were anesthetized with tribromoethanol (250 mg/kg i.p.) and transcardially perfused with ice-cold sucrose ACSF oxygenated with 95% O₂ and 5% CO₂ prior to decapitation. Brains were rapidly removed and sectioned in oxygenated, ice-cold sucrose ACSF with a Vibratome 1500 (Vibratome, Bannockburn, IL, USA). Sucrose ACSF contained (in mM): 203 sucrose, 2.5 KCl, 1.2 NaH₂PO₄, 0.5 CaCl₂, 10 MgCl₂, 23 NaHCO₃, and 10 D-(+)-glucose. Slices were maintained in standard ACSF saturated

with 95% O₂ and 5% CO₂ at room temperature (24–25°C) for at least 1 h prior to use. Standard ACSF contained (in mM): 124 NaCl, 2.5 KCl, 1.2 NaH₂PO₄, 2 CaCl₂, 1 MgCl₂, 26 NaHCO₃, and 10 D-(+)-glucose.

Recordings were obtained at room temperature (24–25°C) with continuous perfusion of standard ACSF at a rate of 2–3 ml/min. Whole-cell, patch-clamp recordings from MSNs in the dorsolateral striatum were performed. Cells were visualized with a 40× water-immersion objective (LUMPlanFI, 40×/0.80 w) under an Olympus BX51WI microscope equipped with infrared differential interference contrast optics, epifluorescence and an Olympus OLY-150 camera/controller system (Olympus). Recording pipettes had a resistance of 2–3 M Ω when filled with internal pipette solution containing (in mM): 120 potassium gluconate, 20 KCl, 4 NaCl, 10 HEPES, 0.2 EGTA, 4 MgATP, 0.3 Na₂GTP and 10 sodium phosphocreatine, pH 7.2–7.3 and ~300 mOsm. No compensation was made for the liquid junction potential. Signals were amplified with an Axopatch 200B amplifier (Molecular Devices), digitally converted with a Digidata 1440A analog-to-digital converter (Molecular Devices), and stored on a computer for subsequent off-line analysis.

After establishing whole-cell configuration, cells were voltage clamped at −70 mV to check for series resistance (Rs). Cells with Rs < 20 M Ω were then held in *I* = 0 configuration and were allowed to equilibrate until the resting membrane potential (RMP) stabilized (approximately 3–5 min). The RMP was recorded for 30 s and mean was reported. Current–voltage relationship experiments (to evaluate input resistance and action potential firing rate) were initiated with a membrane potential of −80 mV and consisted of a series of current injections (500 ms duration) between −200 and +400 pA in 25 pA delivered in step-wise increments. All current clamp recordings were sampled at 10 kHz and low-pass filtered at 2 kHz. Electrophysiological traces were analyzed offline using Clampfit 10.0 (Molecular Devices). Rheobase for each cell was defined by the minimal current that evoked action potentials. Graphic presentation and statistical comparison of data were performed using GraphPad Prism software (La Jolla, CA, USA). The mean RMP and the rheobase for each cell were compared statistically across cell types using unpaired Student's *t*-tests. Two-way ANOVA was used to determine group effects of current injection and cell type on number of spikes and on membrane potential. Values are represented as mean \pm SEM.

RESULTS

BEHAVIORAL TESTING

We first investigated the integrity of behaviors that are sensitive to dopamine signaling including general locomotor activity and the acute response to cocaine (Chandler et al., 1990; Karasinska et al., 2005; Bateup et al., 2010). For these experiments, *Drd1a*-tdTomato line 6 mice were backcrossed for six generations to C57Bl/6 mice to minimize behavioral variability due to hybrid strain background. When we compared hemizygous (+/−) mice to transgene-negative littermates (−/−), we found that locomotor activity level was undisturbed in line 6 *Drd1a*-tdTomato^{+/−} mice during OF testing (**Figure 1A**). In response to acute cocaine injection (20 mg/kg i.p.), we observed a greater than three-fold increase in locomotor activity relative to the pre-injection baseline period in mice of both genotypes (**Figure 1B**). No differences in the acute locomotor response to cocaine were observed between line 6 *Drd1a*-tdTomato^{+/−} and their transgene-negative littermate controls (**Figure 1B**).

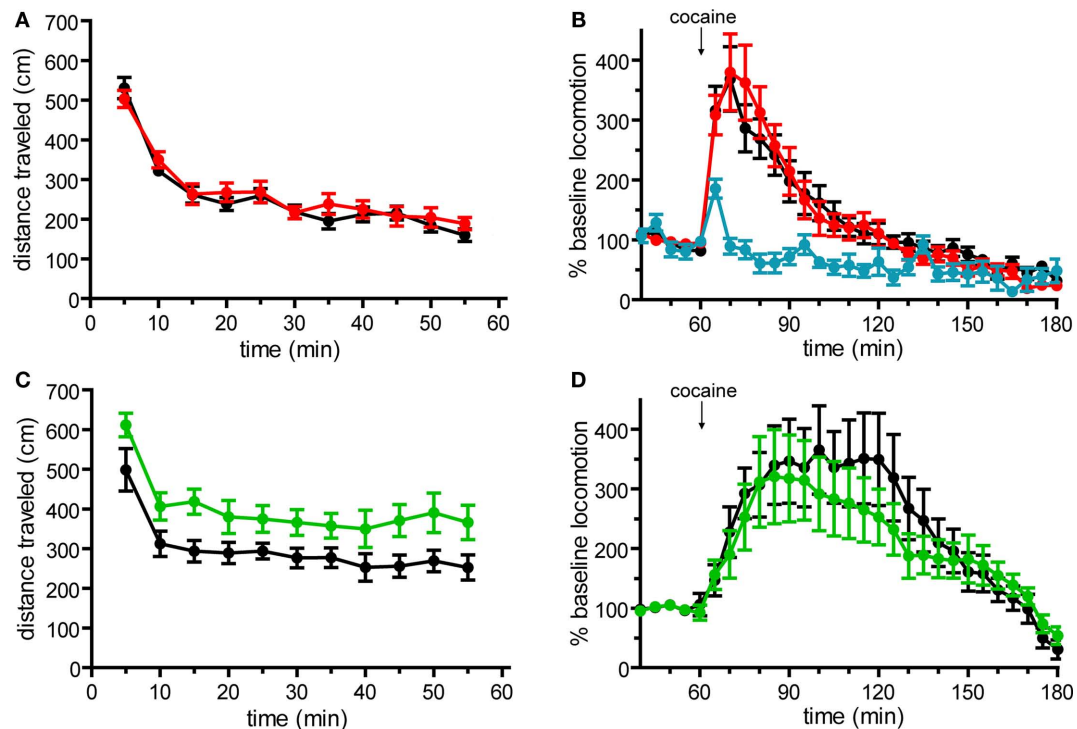


FIGURE 1 | Basal locomotor activity and acute locomotor response to cocaine in *Drd1a*-tdTomato line 6 and *Drd2*-EGFP BAC transgenic mice on C57Bl/6 background. (A) Basal horizontal locomotion of *Drd1a*-tdTomato^{+/−} line 6 mice (red, *n* = 14) is similar to transgene-negative (*Drd1a*-tdTomato^{−/−}) littermates (black, *n* = 15; *p* = 0.515). **(B)** Acute cocaine administration (20 mg/kg i.p.) similarly increases horizontal locomotion in *Drd1a*-tdTomato^{+/−} mice (red, *n* = 14) and *Drd1a*-tdTomato^{−/−} littermates (black, *n* = 15; *p* = 0.945). Blue trace indicates response to vehicle control injection

(*n* = 8 mice, 4 each of *Drd1a*-tdTomato^{+/−} and *Drd1a*-tdTomato^{−/−} mice. Responses were indistinguishable, so data were aggregated.) **(C)** Time course plots of basal horizontal locomotion demonstrate that *Drd2*-EGFP^{+/−} mice (green, *n* = 17) are hyperactive compared to transgene-negative (*Drd2*-EGFP^{−/−}) littermates (black, *n* = 15; *p* = 0.027). **(D)** Acute cocaine administration (20 mg/kg i.p.) induces a similar percent increase in locomotion in *Drd2*-EGFP^{+/−} mice (green, *n* = 17) and *Drd2*-EGFP^{−/−} littermates (black, *n* = 15; *p* = 0.616).

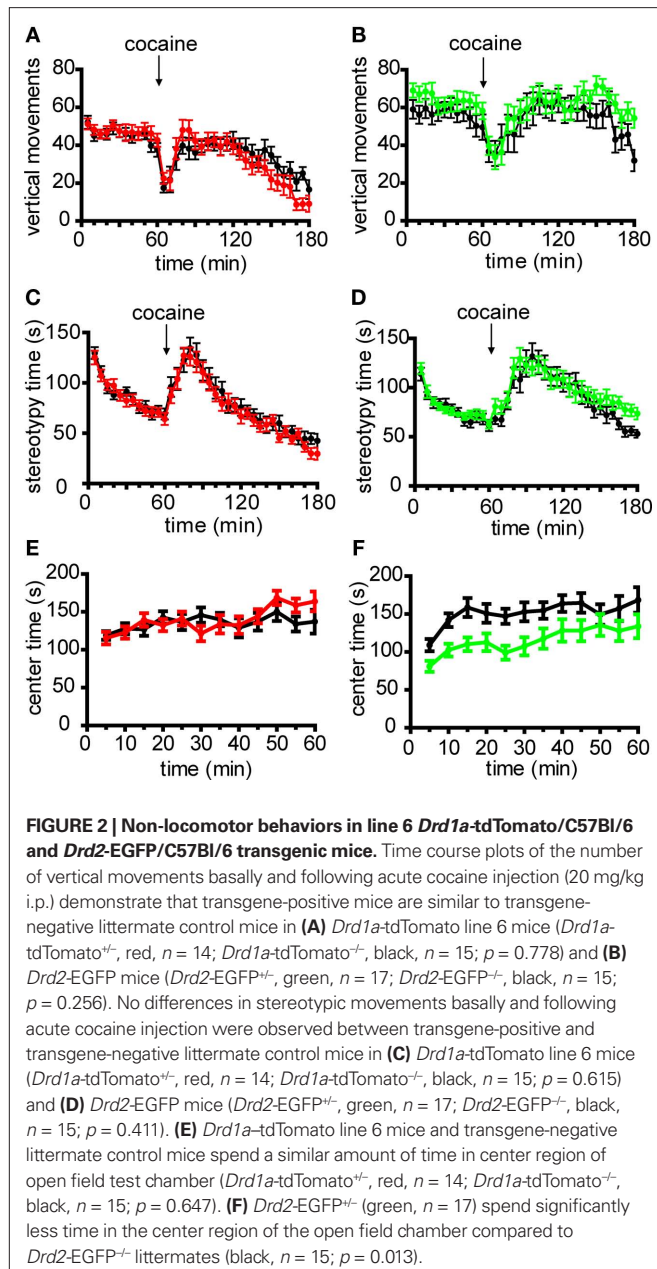
Basal locomotor behavior and acute locomotor response to cocaine were similarly tested in *Drd2*-EGFP transgenic mice. *Drd2*-EGFP mice were first backcrossed to C57Bl/6 mice for six generations. Behavioral testing of *Drd2*-EGFP/ C57Bl/6 served three purposes in these experiments. First, if abnormal, these results would serve as a positive control for our ability to detect abnormalities in these behavioral domains. Second, to our knowledge, these experiments report the locomotor response to acute cocaine in hemizygous *Drd2*-EGFP transgenic mice for the first time. Third, by comparing *Drd2*-EGFP^{+/−} mice in a pure C57Bl/6 background with their transgene-negative littermates, these experiments test for the first time the effects of the transgene on behavior in the absence of confounding variables which arise when using cross-strain behavioral controls. In contrast to line 6 mice, we found that basal locomotor activity during OF testing was significantly higher in hemizygous *Drd2*-EGFP mice as compared to their *Drd2*-EGFP^{−/−} littermates (*p* = 0.027, **Figure 1C**). Although hyperactive, no significant difference in the acute locomotor response to cocaine was observed (**Figure 1D**).

In addition to locomotor activity, other dopamine-dependent behavioral domains including vertical rearing, stereotypies and time spent in the center region of the OF chamber were assessed (Chandler et al., 1990; Tirelli and Witkin, 1994; Pogorelov et al., 2005). Neither

line 6 nor *Drd2*-EGFP mice exhibited significant differences in vertical rearing or time spent performing stereotypic movements, either basally or in response to acute cocaine (**Figures 2A–D**). While line 6 mice showed no differences in the amount of time spent in the center region of the OF chamber (**Figure 2E**), *Drd2*-EGFP mice exhibited a statistically significant decrease in center time during basal activity (*p* = 0.013, **Figure 2F**). Neither line exhibited significant genotypic differences in center time during the response to acute cocaine injection (*p* = 0.187 for line 6 *Drd1a*-tdTomato and *p* = 0.535 for *Drd2*-EGFP, data not shown). Finally, transgene-positive mice were indistinguishable from their transgene-negative littermate controls based on gross morphological features and body weight (*Drd1a*-tdTomato^{+/−} 22.9 ± 1.1 g, *n* = 15; *Drd1a*-tdTomato^{−/−} 22.0 ± 1.0 g, *n* = 14, *p* = 0.601; *Drd2*-EGFP^{+/−} 19.8 ± 0.4 g, *n* = 17; *Drd2*-EGFP^{−/−} 20.3 ± 0.7 g, *n* = 15, *p* = 0.524). In summary, these behavioral data demonstrate normal behavior in line 6 *Drd1a*-tdTomato^{+/−} mice. These data also support the recently reported claim that the *Drd2*-EGFP transgene may induce phenotypic alterations.

SPECIFICITY OF tdTOMATO FLUORESCENCE

Within the dorsal striatum of *Drd1a*-tdTomato line 6 mice, we next investigated the specificity of tdTomato fluorescence for correctly assigning a fluorescent MSN to the striatonigral pathway.



As expected for striatonigral MSNs, a low-magnification view of the brain from a *Drd1a*-tdTomato line 6 mouse demonstrates that fluorescent axonal projections from the striatum bypass the globus pallidus external (GPe) and terminate in the substantia nigra pars reticulata (SNr; **Figure 3A**). At the cellular level, we investigated the extent to which tdTomato expression could be segregated from EGFP expression in *Drd1a*-tdTomato^{+/+}/*Drd2*-EGFP^{+/+} mice. In mice, the vast majority of striatal MSNs send axons through either the striatonigral or striatopallidal pathway, and these two populations of MSN projection neurons can be discriminated by expression of the type 1 and type 2 dopamine receptors, respectively (Gerfen et al., 1990). Thus, if the transgenes reliably identify these two populations, it is predicted that there should not be significant co-expression of the fluorescent reporters among striatal projection

neurons. As predicted, the striatal MSNs identified by DARPP-32 immunolabeling (Anderson and Reiner, 1991; Ouimet et al., 1998) with detectable levels of both EGFP and tdTomato fluorescence were very rare (2.3% of 1095 DARPP-32 positive cells; **Figure 3B**).

Besides MSNs, interneurons of various types collectively represent approximately 5% of striatal neurons (see review by Tepper et al., 2010). Expression of tdTomato was investigated in the three most abundant interneuronal types – fast-spiking interneurons (FSIs), low-threshold spiking interneurons (LTS interneurons), and large tonically active aspiny cholinergic interneurons (TANs). PV immunostaining, to identify FSIs, failed to identify any FSIs with fluorescence from either the *Drd1a*-tdTomato (**Figure 3C**) or *Drd2*-EGFP transgenes (0/52 PV-positive cells). Likewise, somatostatin immunostaining, to identify LTS interneurons, demonstrated that these cells do not contain detectable levels of fluorescence due to either the *Drd1a*-tdTomato (**Figure 3D**) or *Drd2*-EGFP transgenes (0/45 somatostatin-positive cells). TANs were visualized by EGFP fluorescence in *Chat*-EGFP transgenic mice. No overlap was observed between tdTomato and EGFP fluorescence in slices prepared from *Drd1a*-tdTomato^{+/+}/*Chat*-EGFP^{+/+} mice (0/56 EGFP-fluorescent cells, **Figure 3E**). Lastly, astrocytes, as indicated by immunostaining with glial fibrillary acidic protein (GFAP), did not appreciably express tdTomato (0/37 GFAP-positive cells, data not shown). In summary, these studies indicate that tdTomato fluorescence in dorsal striatal cells is highly specific to striatonigral MSNs.

SENSITIVITY OF tdTOMATO FLUORESCENCE

We next investigated whether tdTomato fluorescence also provided adequate sensitivity for detecting the majority of striatonigral MSNs. We addressed this question using two imaging approaches, confocal microscopy of thin fixed brain sections and epifluorescent microscopy of thicker acute brain slices (as commonly prepared for electrophysiological experiments), to define the upper and lower estimates of fluorescence detection sensitivity. In confocal imaging experiments, MSNs were defined by DARPP-32 immunostaining. In mice that were hemizygous for both *Drd1a*-tdTomato and *Drd2*-EGFP transgenes, 8 of 1095 DARPP-32-positive cells (0.7%) did not have detectable fluorescence from either the tdTomato or EGFP reporter proteins (**Figure 3B**). This finding demonstrates that both transgenic reporters have negligible rates of false negativity for identifying MSNs under these imaging conditions (for details see Materials and Methods). We next examined the sensitivity of fluorescence detection in MSNs under imaging conditions commonly used for identification of cells in live tissue during electrophysiological experiments. In acute brain slices (300 μ m thick), medium-sized cells were first identified using phase-contrast illumination and then evaluated for fluorescence. Again, the vast majority of cells were accounted for by detectable fluorescence from the transgenic reporter proteins (518/544 cells; >95%, **Figure 3B**). These findings indicate that tdTomato fluorescence in line 6 mice can be highly sensitive and suitable for identifying all striatonigral MSNs.

INTEGRITY OF tdTOMATO-EXPRESSING MSNs

We considered whether the ectopic expression of tdTomato proteins in MSNs might alter cellular health (Vintersten et al., 2004; Long et al., 2005). We did not find evidence to support a toxic

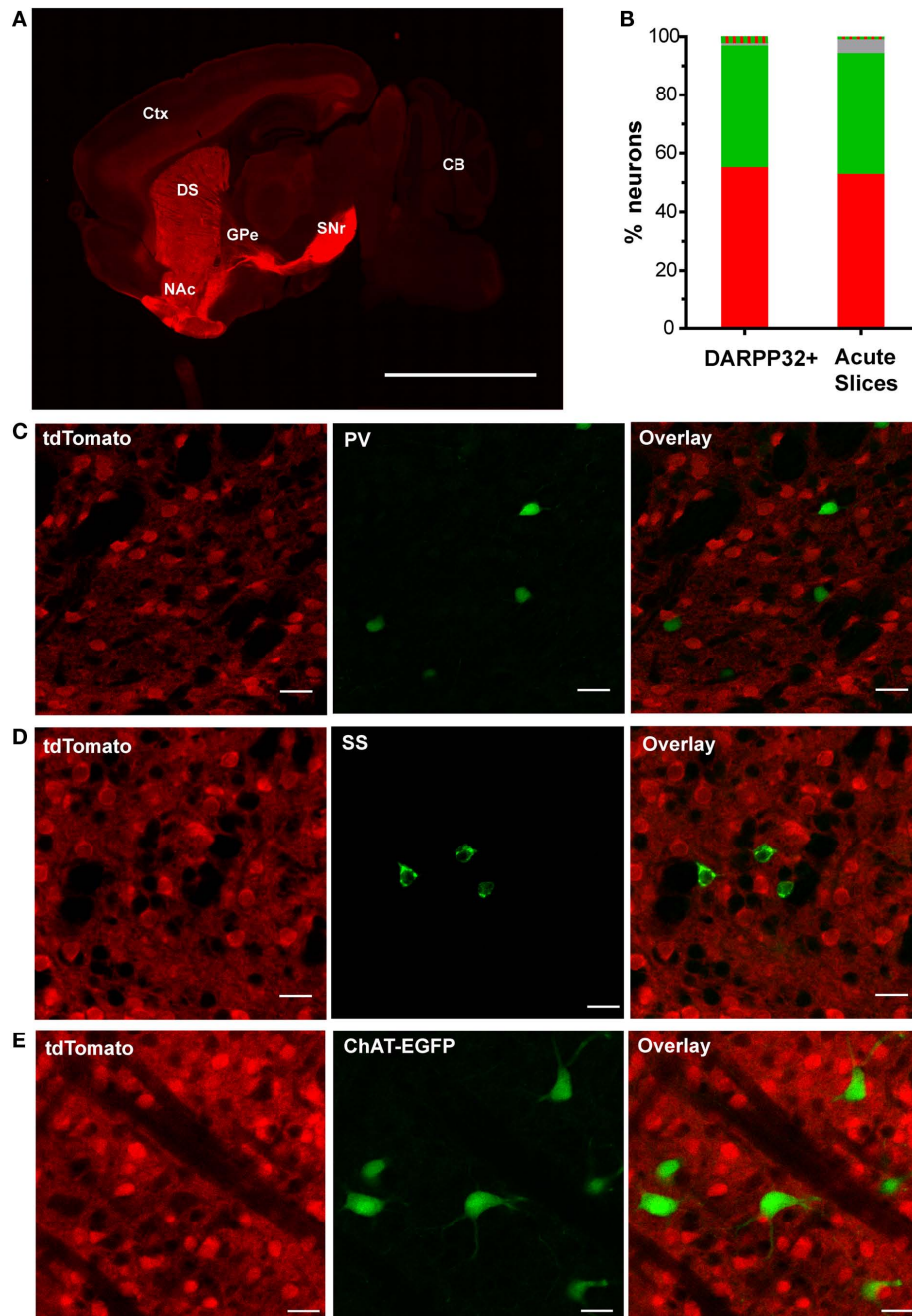


FIGURE 3 | TdTomato fluorescence is sensitive and specific for striatonigral MSNs in the dorsal striatum. (A) A representative low-magnification sagittal

view of tdTomato fluorescence of a brain slice from a hemizygous line 6 *Drd1a*-tdTomato mouse demonstrating strong signal within striatal efferent axons terminating in substantia nigra pars reticulata (SNr) and negligible signal at the globus pallidus external (GPe). Abbreviations: cortex (Ctx), cerebellum (CB), dorsal striatum (DS) and nucleus accumbens (NAc). Scale bar represents 500 μ m. (B) Quantification of fluorescent signal detected in dorsal striatal cells from line 6 *Drd1a*-tdTomato^{+/+}/*Drd2*-EGFP^{+/+} mice. DARPP32+ cells were identified in immunohistochemically stained 50 μ m thick brain sections (n = 605 tdTomato only (red), 457 EGFP only (green), 25 dually labeled (red and green striped), and 8 non-fluorescent (gray) of 1095 total DARPP-32 immunopositive cells). Cells in acute 300 μ m thick slices were identified by phase-contrast illumination. Fluorescent signals were detected using epifluorescence

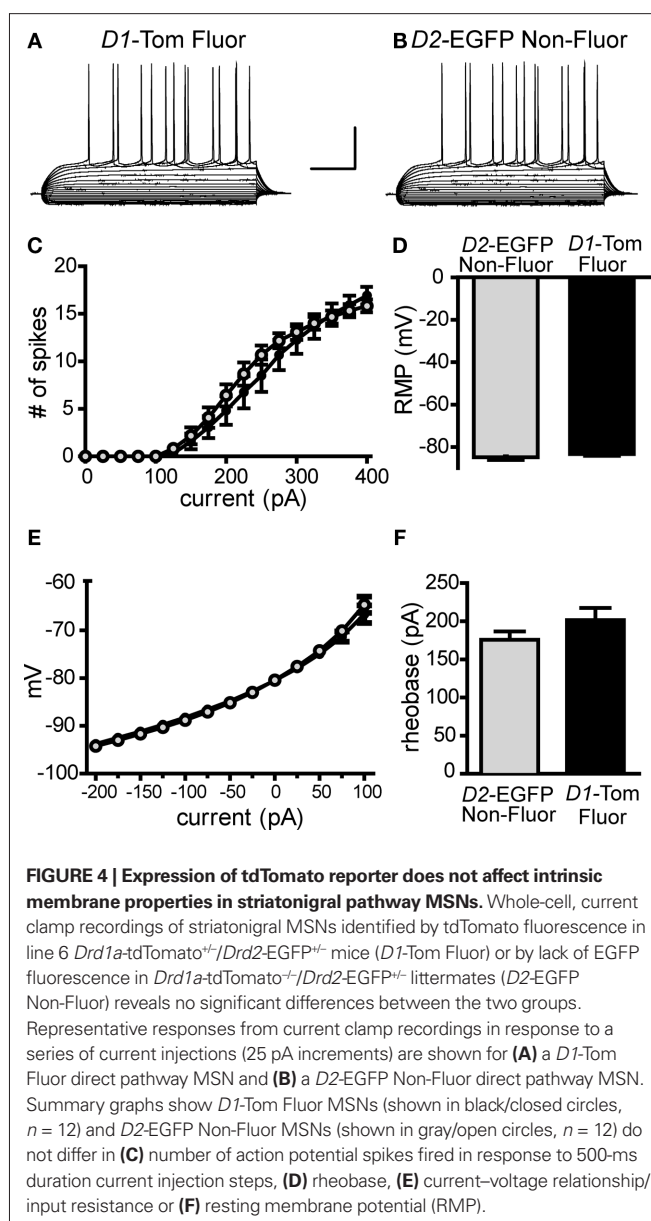
illumination (n = 293 tdTomato only (red), 230 EGFP only (green), 5 dually labeled (red and green striped), and 26 non-fluorescent (gray) of 549 total medium size cells identified by phase contrast illumination). (C) Representative confocal microscopy images demonstrating that cells immunopositive for the fast-spiking GABAergic interneuron marker, parvalbumin (PV), do not express tdTomato (0/52 PV-immunopositive cells). (D) Representative confocal microscopy images demonstrating cells immunopositive for the low-threshold spiking GABAergic interneuron marker, somatostatin (SS), do not express tdTomato (0/45 SS-immunopositive cells). (E) Representative confocal microscopy images demonstrating no overlap between tdTomato and EGFP fluorescence in line 6 *Drd1a*-tdTomato^{+/+}/*ChAT*-EGFP^{+/+} mice (0/56 EGFP-positive cells). For panels (C–E), tdTomato fluorescence (left), interneuron antigen or transgenic reporter fluorescence (middle) and overlay of both signals (right). Scale bars represent 25 μ m.

effect resulting in the loss of striatonigral MSNs because the relative fraction of the total MSNs accounted for by tdTomato-positive neurons (57.9%, **Figure 3B**) was similar to what has been previously reported for striatonigral neurons (Bertran-Gonzalez et al., 2008). To further test cellular integrity, we compared the physiological properties of tdTomato-fluorescent neurons from *Drd1a*-tdTomato^{+/+}/*Drd2*-EGFP^{+/+} mice to non-fluorescent neurons from *Drd1a*-tdTomato^{+/+}/*Drd2*-EGFP^{+/+} littermate control mice. We found no significant differences in RMP, membrane input resistance, rheobase or action potential firing rates (**Figure 4**).

DISCUSSION

In this study, we characterize a new *Drd1a*-tdTomato BAC transgenic mouse line, line 6. Our results show that line 6 mice provide both high specificity and sensitivity for the identification of striatonigral (direct) pathway MSNs and offer several advantages over existing transgenic mouse lines that label striatal projection pathways. Foremost, recent concerns about phenotypic alteration of mice in a commonly used *Drd2*-EGFP transgenic line have raised a need to find alternative means for identifying direct and indirect pathway MSNs. Our results indicate that line 6 mice do not have phenotypic alterations and, if used under experimental conditions similar to those we report here, can be used as a single transgenic line to accurately assign MSNs to both pathways based on the presence or absence of fluorescence. *Drd1a*-tdTomato line 6 mice also offer the advantages that are afforded by (1) the brighter fluorescence of tdTomato in comparison to EGFP (Deliolanis et al., 2008; Drobizhev et al., 2009) and to line 5 *Drd1a*-tdTomato mice (data not shown), (2) an excitation wavelength which provides deeper tissue penetration (reduced scatter) than the excitation wavelength used for EGFP, (3) autosomal inheritance of the transgene, and (4) the ability to easily maintain on a C57Bl/6 background. Although the present study focuses on tdTomato expression in the dorsolateral striatum, representative images of other brain regions that may be of interest are provided (**Figure 5**).

In this study, we first investigated the behavioral integrity of line 6 mice and found no evidence for behavioral abnormalities in activity basally or in response to cocaine during OF testing. These results are similar to those reported for another line of transgenic mice that also contain the upstream regulatory elements for *Drd1a*, GENSAT *Drd1a*-EGFP mice (Kramer et al., 2011). Although the focus of our study was to characterize the new transgenic line, line 6 *Drd1a*-tdTomato, we also provide new evidence that supports the findings by Alvarez and colleagues that *Drd2*-EGFP transgenic mice have altered behavioral phenotypes (Kramer et al., 2011). Both studies demonstrate increased basal locomotion in *Drd2*-EGFP mice, although to differing degrees. In this study, we found that hemizygous mice on a C57Bl/6 background exhibit approximately 130% of littermate control activity levels. In the recent report by Alvarez and colleagues, homozygous mice on a hybrid background exhibited approximately 300% of Swiss Webster control activity levels (Kramer et al., 2011). Following acute cocaine challenge (20 mg/kg i.p.), we observed a robust increase in locomotor activity by hemizygous *Drd2*-EGFP/C57Bl/6 mice that was similar to littermate controls. The degree of acute cocaine-induced locomotor response we observe is consistent with prior observations in C57Bl/6 mice (Schlussman et al., 2003). Testing homozygous



Drd2-EGFP mice, Kramer et al. found that there was no significant locomotor response to acute cocaine when compared to injection with saline. It is presently unclear if the genotype (hemi v. homo), strain background (C57Bl/6 v. hybrid) or other experimental design features are responsible for this difference. However, it is notable that, in the present study, we control for strain background, test only hemizygous mice, and use transgene-negative littermate controls and still find that in two assays (basal levels of locomotion and time spent in center of test chamber) *Drd2*-EGFP transgenic animals have altered behavior. Thus, we provide further evidence that the *Drd2*-EGFP transgenic mouse line has unintended phenotypic disturbances.

Due to concerns about phenotypic abnormalities in the *Drd2*-EGFP line, alternative methods to identify striatopallidal pathway neurons are desirable. The GENSAT A2A-EGFP mice (Gong et al., 2003) provide one such alternative (Warre et al., 2011), although,

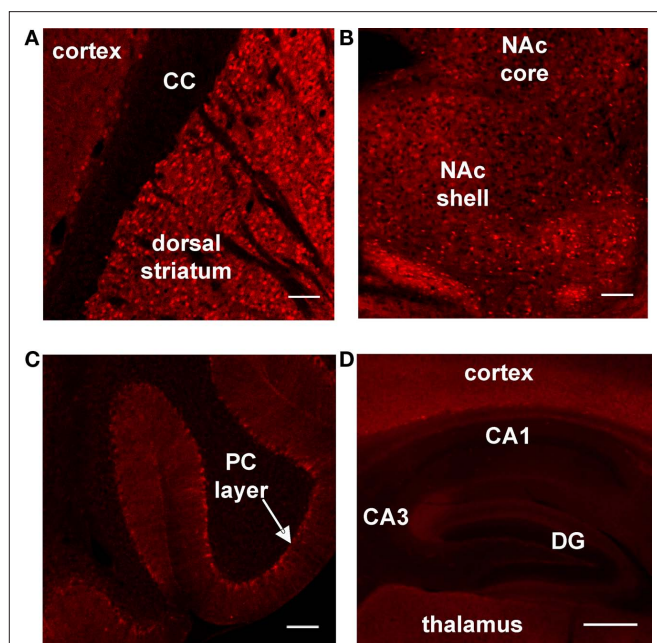


FIGURE 5 | Survey of tdTomato expression in sagittal brain slices prepared from line 6 *Drd1a*-tdTomato^{+/−} mice. Representative confocal images showing tdTomato expression at (A) the border between cortex and striatum (corpus callosum = CC), (B) the nucleus accumbens (NAc) and (C) the cerebellum (Purkinje cell = PC). (D) Representative epifluorescent image showing tdTomato expression in the hippocampus (dentate gyrus = DG). The contrast has been enhanced for each image to highlight tdTomato expression patterns within the subregion. Scale bars for all panels represent 100 μ m.

behavioral characterization of these mice has not yet been reported. Another alternative is to use non-fluorescent cells in a line that reports direct pathway MSNs with high specificity and sensitivity. The results of the present study indicate that assignment of non-fluorescent cells to the indirect pathway can be highly accurate in line 6 mice (Figure 3B). In mice expressing both the *Drd2*-EGFP and *Drd1a*-tdTomato transgenes, greater than 98% of MSNs lacking tdTomato fluorescence had detectable EGFP fluorescence under sensitive confocal imaging conditions. Under less sensitive conditions (epifluorescent imaging and thicker acute brain slices), we still found that, among cells identified by phase contrast illumination, >90% of the cells lacking tdTomato fluorescence had EGFP fluorescence. Therefore, classifying indirect pathway MSNs solely by the absence of tdTomato fluorescence (without taking advantage of additional means to define a cell as a MSN), one can still

expect less than 10% contamination of indirect pathway data sets by type I errors. In reality, soma appearance and electrophysiological characteristics are readily available to the electrophysiologist allowing them to restrict analyses to the subset of cells that are MSNs. We also characterized tdTomato fluorescence in striatal interneurons. Collectively, interneurons comprise approximately 5% of total striatal neurons (Tepper et al., 2010). No tdTomato fluorescence was detected in the three most abundant striatal interneuron subtypes – tonically active cholinergic interneurons, fast-spiking GABAergic interneurons and low-threshold spiking interneurons. Other sparser interneuronal populations, such as calretinin positive GABAergic interneurons and tyrosine hydroxylase positive interneurons were not evaluated, and therefore, may express tdTomato. Finally, among a total of 2373 fluorescent cells from *Drd1a*-tdTomato^{+/−}/*Drd2*-EGFP^{+/−} mice, only 1.6% of cells expressed detectable levels of both fluorophores.

CONCLUSION

In summary, this study characterizes a new transgenic line that expresses tdTomato under the regulatory elements of the *Drd1a* gene. In the experiments reported herein, we found no evidence for changes in behavior or basic cellular properties due to transgene expression in *Drd1a*-tdTomato line 6 mice. Furthermore, the high selectivity and sensitivity of tdTomato fluorescence for reporting striatonigral MSNs in line 6 mice provides a reliable method for classifying both direct and indirect pathway neurons using a single transgenic mouse line.

ACKNOWLEDGMENTS

We would like to acknowledge the following sources for financial support: National Institute of Neurological Disorders and Stroke [T32NS051156 (Kristen Ade), NS064577 (Nicole Calakos), NS064577-S1 (Nicole Calakos), NS054840 (Nicole Calakos)], Klingenstein Foundation (Nicole Calakos), NARSAD (Nicole Calakos) and Duke Institute for Brain Sciences (Nicole Calakos). We would like to thank Samantha Tracy for excellent care and management of mouse colonies; Drs. Jei Deng and Anne West for consultation and reagents used in immunostaining experiments; Dr. Gregg Stanwood for noting the X-linked inheritance pattern of line 5 mice; Drs. Sam Johnson and Yasheng Gao of the Duke University Light Microscopy Core Facility for imaging equipment and consultation; and Drs. William Wetsel and Ramona Rodriguiz and the Neurobehavioral Core Facility for consultation and assistance with behavioral experiments. We thank members of our laboratory and Dr. Jonathan Ting for critical discussion and manuscript comments.

REFERENCES

- Ade, K. K., Janssen, M. J., Ortinski, P. I., and Vicini, S. (2008). Differential tonic GABA conductances in striatal medium spiny neurons. *J. Neurosci.* 28, 1185–1197.
- Anderson, K. D., and Reiner, A. (1991). Immunohistochemical localization of DARPP-32 in striatal projection neurons and striatal interneurons: implications for the localization of D1-like dopamine receptors on different types of striatal neurons. *Brain Res.* 568, 235–243.
- André, V. M., Cepeda, C., Fisher, Y. E., Huynh, M., Bardakjian, N., Singh, S., Yang, X. W., and Levine, M. S. (2011). Differential electrophysiological changes in striatal output neurons in Huntington's disease. *J. Neurosci.* 31, 1170–1182.
- Bateup, H. S., Santini, E., Shen, W., Birnbaum, S., Valjent, E., Surmeier, D. J., Fisone, G., Nestler, E. J., and Greengard, P. (2010). Distinct subclasses of medium spiny neurons differentially regulate striatal motor behaviors. *Proc. Natl. Acad. Sci. U.S.A.* 107, 14845–14850.
- Bertran-Gonzalez, J., Bosch, C., Maroteaux, M., Matamalas, M., Herve, D., Valjent, E., and Girault, J. A. (2008). Opposing patterns of signaling activation in dopamine D1 and D2 receptor-expressing striatal neurons in response to cocaine and haloperidol. *J. Neurosci.* 28, 5671–5685.
- Cepeda, C., André, V. M., Yamazaki, I., Wu, N., Kleiman-Weiner, M., and Levine, M. S. (2008). Differential electrophysiological properties of dopamine D1 and D2 receptor-containing striatal medium-sized spiny neurons. *Eur. J. Neurosci.* 27, 671–682.

- Chandler, C. J., Starr, B. S., and Starr, M. S. (1990). Differential behavioural interactions between the dopamine D-1 antagonist SCH 23390 and the dopamine D-2 antagonists metoclopramide and sulpiride in nonhabituated mice. *Pharmacol. Biochem. Behav.* 35, 285–289.
- Day, M., Wang, Z., Ding, J., An, X., Ingham, C. A., Shering, A. F., Wokosin, D., Ilijic, E., Sun, Z., Sampson, A. R., Mugnaini, E., Deutch, A. Y., Sesack, S. R., Arbuthnott, G. W., and Surmeier, D. J. (2006). Selective elimination of glutamatergic synapses on striatopallidal neurons in Parkinson disease models. *Nat. Neurosci.* 9, 251–259.
- Day, M., Wokosin, D., Plotkin, J. L., Tian, X., and Surmeier, D. J. (2008). Differential excitability and modulation of striatal medium spiny neuron dendrites. *J. Neurosci.* 28, 11603–11614.
- Deliolanis, N. C., Kasmieh, R., Wurdinger, T., Tannous, B. A., Shah, K., and Ntziachristos, V. (2008). Performance of the red-shifted fluorescent proteins in deep-tissue molecular imaging applications. *J. Biomed. Opt.* 13, 044008.
- Doig, N. M., Moss, J., and Bolam, J. P. (2010). Cortical and thalamic innervation of direct and indirect pathway medium-sized spiny neurons in mouse striatum. *J. Neurosci.* 30, 14610–14618.
- Drobizhev, M., Tillo, S., Makarov, N. S., Hughes, T. E., and Rebane, A. (2009). Absolute two-photon absorption spectra and two-photon brightness of orange and red fluorescent proteins. *J. Phys. Chem. B* 113, 855–859.
- Flores-Barrera, E., Vizcarra-Chacon, B. J., Tapia, D., Bargas, J., and Galarraga, E. (2010). Different corticostriatal integration in spiny projection neurons from direct and indirect pathways. *Front. Syst. Neurosci.* 4:15. doi: 10.3389/fnsys.2010.00015
- Gerfen, C. R., Engber, T. M., Mahan, L. C., Susel, Z., Chase, T. N., Monsma, F. J., Jr., and Sibley, D. R. (1990). D1 and D2 dopamine receptor-regulated gene expression of striatonigral and striatopallidal neurons. *Science* 250, 1429–1432.
- Gertler, T. S., Chan, C. S., and Surmeier, D. J. (2008). Dichotomous anatomical properties of adult striatal medium spiny neurons. *J. Neurosci.* 28, 10814–10824.
- Gittis, A. H., Nelson, A. B., Thwin, M. T., Palop, J. J., and Kreitzer, A. C. (2010). Distinct roles of GABAergic interneurons in the regulation of striatal output pathways. *J. Neurosci.* 30, 2223–2234.
- Gong, S., Zheng, C., Doughty, M. L., Losos, K., Didkovsky, N., Schambra, U. B., Nowak, N. J., Joyner, A., Leblanc, G., Hatten, M. E., and Heintz, N. (2003). A gene expression atlas of the central nervous system based on bacterial artificial chromosomes. *Nature* 425, 917–925.
- Janssen, M. J., Ade, K. K., Fu, Z., and Vicini, S. (2009). Dopamine modulation of GABA tonic conductance in striatal output neurons. *J. Neurosci.* 29, 5116–5126.
- Karasinska, J. M., George, S. R., Cheng, R., and O'Dowd, B. F. (2005). Deletion of dopamine D1 and D3 receptors differentially affects spontaneous behaviour and cocaine-induced locomotor activity, reward and CREB phosphorylation. *Eur. J. Neurosci.* 22, 1741–1750.
- Kramer, P. F., Christensen, C. H., Hazelwood, L. A., Dobi, A., Bock, R., Sibley, D. R., Mateo, Y., and Alvarez, V. A. (2011). Dopamine D2 receptor overexpression alters behavior and physiology in Drd2-EGFP mice. *J. Neurosci.* 31, 126–132.
- Kreitzer, A. C., and Malenka, R. C. (2007). Endocannabinoid-mediated rescue of striatal LTD and motor deficits in Parkinson's disease models. *Nature* 445, 643–647.
- Long, J. Z., Lackan, C. S., and Hadjantonakis, A. K. (2005). Genetic and spectrally distinct in vivo imaging: embryonic stem cells and mice with widespread expression of a monomeric red fluorescent protein. *BMC Biotechnol.* 5, 20. doi: 10.1186/1472-6750-5-20
- Ouimet, C. C., Langley-Gullion, K. C., and Greengard, P. (1998). Quantitative immunocytochemistry of DARPP-32-expressing neurons in the rat caudate putamen. *Brain Res.* 808, 8–12.
- Planert, H., Szydlowski, S. N., Hjorth, J. J., Grillner, S., and Silberberg, G. (2010). Dynamics of synaptic transmission between fast-spiking interneurons and striatal projection neurons of the direct and indirect pathways. *J. Neurosci.* 30, 3499–3507.
- Pogorelov, V. M., Rodriguez, R. M., Insko, M. L., Caron, M. G., and Wetsel, W. C. (2005). Novelty seeking and stereotypic activation of behavior in mice with disruption of the Dat1 gene. *Neuropsychopharmacology* 30, 1818–1831.
- Schlussman, S. D., Zhang, Y., Kane, S., Stewart, C. L., Ho, A., and Kreek, M. J. (2003). Locomotion, stereotypy, and dopamine D1 receptors after chronic “binge” cocaine in C57BL/6J and 129/J mice. *Pharmacol. Biochem. Behav.* 75, 123–131.
- Shen, W., Flajolet, M., Greengard, P., and Surmeier, D. J. (2008). Dichotomous dopaminergic control of striatal synaptic plasticity. *Science* 321, 848–851.
- Shen, W., Tian, X., Day, M., Ulrich, S., Tkatch, T., Nathanson, N. M., and Surmeier, D. J. (2007). Cholinergic modulation of Kir2 channels selectively elevates dendritic excitability in striatopallidal neurons. *Nat. Neurosci.* 10, 1458–1466.
- Shuen, J. A., Chen, M., Gloss, B., and Calakos, N. (2008). Drd1a-tdTomato BAC transgenic mice for simultaneous visualization of medium spiny neurons in the direct and indirect pathways of the basal ganglia. *J. Neurosci.* 28, 2681–2685.
- Tepper, J. M., Tecuapetla, F., Koos, T., and Ibanez-Sandoval, O. (2010). Heterogeneity and diversity of striatal GABAergic interneurons. *Front. Neuroanat.* 4:150. doi: 10.3389/fnana.2010.00150
- Tirelli, E., and Witkin, J. M. (1994). Verticalization of behavior elicited by dopaminergic mobilization is qualitatively different between C57BL/6J and DBA/2J mice. *Psychopharmacology (Berl.)* 116, 191–200.
- Vintersten, K., Monetti, C., Gertsenstein, M., Zhang, P., Laszlo, L., Biechele, S., and Nagy, A. (2004). Mouse in red: red fluorescent protein expression in mouse ES cells, embryos, and adult animals. *Genesis* 40, 241–246.
- Warre, R., Thiele, S., Talwar, S., Kamal, M., Johnston, T. H., Wang, S., Lam, D., Lo, C., Khademullah, C. S., Perera, G., Reyes, G., Sun, X. S., Brothie, J. M., and Nash, J. E. (2011). Altered function of glutamatergic cortico-striatal synapses causes output pathway abnormalities in a chronic model of Parkinsonism. *Neurobiol. Dis.* 41, 591–604.
- Yin, H. H., Mulcare, S. P., Hilario, M. R., Clouse, E., Holloway, T., Davis, M. I., Hansson, A. C., Lovinger, D. M., and Costa, R. M. (2009). Dynamic reorganization of striatal circuits during the acquisition and consolidation of a skill. *Nat. Neurosci.* 12, 333–341.

Conflict of Interest Statement: The authors declare that the research was conducted in the absence of any commercial or financial relationships that could be construed as a potential conflict of interest.

Received: 30 March 2011; paper pending published: 13 April 2011; accepted: 09 May 2011; published online: 08 June 2011.

Citation: Ade KK, Wan Y, Chen M, Gloss B and Calakos N (2011) An improved BAC transgenic fluorescent reporter line for sensitive and specific identification of striatonigral medium spiny neurons. *Front. Syst. Neurosci.* 5:32. doi: 10.3389/fnsys.2011.00032

Copyright © 2011 Ade, Wan, Chen, Gloss and Calakos. This is an open-access article subject to a non-exclusive license between the authors and Frontiers Media SA, which permits use, distribution and reproduction in other forums, provided the original authors and source are credited and other Frontiers conditions are complied with.



The corticostriatal and corticosubthalamic pathways: two entries, one target. So what?

Abraham Mathai¹ and Yoland Smith^{1,2*}

¹ Yerkes National Primate Research Center, Emory University, Atlanta, GA, USA

² Department of Neurology, Emory University, Atlanta, GA, USA

Edited by:

Charles J. Wilson, University of Texas at San Antonio, USA

Reviewed by:

Anton Reiner, University of Tennessee Health Science Center, USA

Peter J. Magill, University of Oxford, UK

*Correspondence:

Yoland Smith, Yerkes National Primate Research Center, 954 Gatewood Road NE, Atlanta, GA 30329, USA.
e-mail: ysmi01@emory.edu

The basal ganglia receive cortical inputs through two main stations – the striatum and the subthalamic nucleus (STN). The information flowing along the corticostriatal system is transmitted to the basal ganglia circuitry via the “direct and indirect” striatofugal pathways, while information that flows through the STN is transmitted along the so-called “hyperdirect” pathway. The functional significance of this dual entry system is not clear. Although the corticostriatal system has been thoroughly characterized anatomically and electrophysiologically, such is not the case for the corticosubthalamic system. In order to provide further insights into the intricacy of this complex anatomical organization, this review examines and compares the anatomical and functional organization of the corticostriatal and corticosubthalamic systems, and highlights some key issues that must be addressed to better understand the mechanisms by which these two neural systems may interact to regulate basal ganglia functions and dysfunctions.

Keywords: subthalamic nucleus, striatum, hyperdirect, Parkinson’s disease, basal ganglia, cerebral cortex, monkey, deep brain stimulation

INTRODUCTION

The direct and indirect pathway model of the basal ganglia has traditionally been the most authenticated working basal ganglia model. According to this model, cortical inputs enter the striatum and proceed to the output nuclei of the basal ganglia [internal globus pallidus (GPi) and the substantia nigra pars reticulata (SNr)] via two distinct pathways, enroute to the thalamus which projects back to the cerebral cortex. The “direct pathway” refers to the monosynaptic connection from the striatum to GPi/SNr; whereas the “indirect pathway” is the polysynaptic pathway where the order of connectivity is striatum – external globus pallidus (GPe) – subthalamic nucleus (STN) – GPi/SNr (Albin et al., 1989; DeLong, 1990). Normal basal ganglia functions are achieved when there is a balance between the activities of these two pathways. Movement disorders of basal ganglia origin, both hypokinetic (e.g., Parkinson’s disease) and hyperkinetic (e.g., Huntington’s disease), are thought to result from imbalanced activities between the two pathways; with the polarity of the imbalance determining the kinetics of the disorder (Albin et al., 1989).

In addition to the corticostriatal inputs, the basal ganglia also receive direct cortical information at the level of the STN, which further gets relayed to the GPi/SNr, constituting the “hyperdirect pathway” (Monakow et al., 1978; Nambu et al., 1996; **Figures 1 and 2**). Although the existence of this system has long been recognized, its detailed anatomical organization, integration within the functional circuitry of the basal ganglia and significance in the pathophysiology of the basal ganglia network in movement disorders remains highly hypothetical and poorly understood.

In this review, we compare the anatomical and functional organization of the two main cortical entry systems to the basal ganglia, and critically examine their respective roles in the integration and processing of motor and non-motor information that flows

through the cortico-basal ganglia–thalamocortical loops in normal and pathological conditions. At the end of each section, we highlight some relevant anatomical and functional issues that should be addressed to increase our current knowledge of the complementary roles corticostriatal and corticosubthalamic entry systems to the basal ganglia play in normal and diseased states.

NEURONAL SOURCES AND CONDUCTION VELOCITIES OF CORTICOSTRIATAL VERSUS CORTICOSUBTHALAMIC PROJECTIONS

SOURCES OF THE CORTICOSTRIATAL SYSTEM

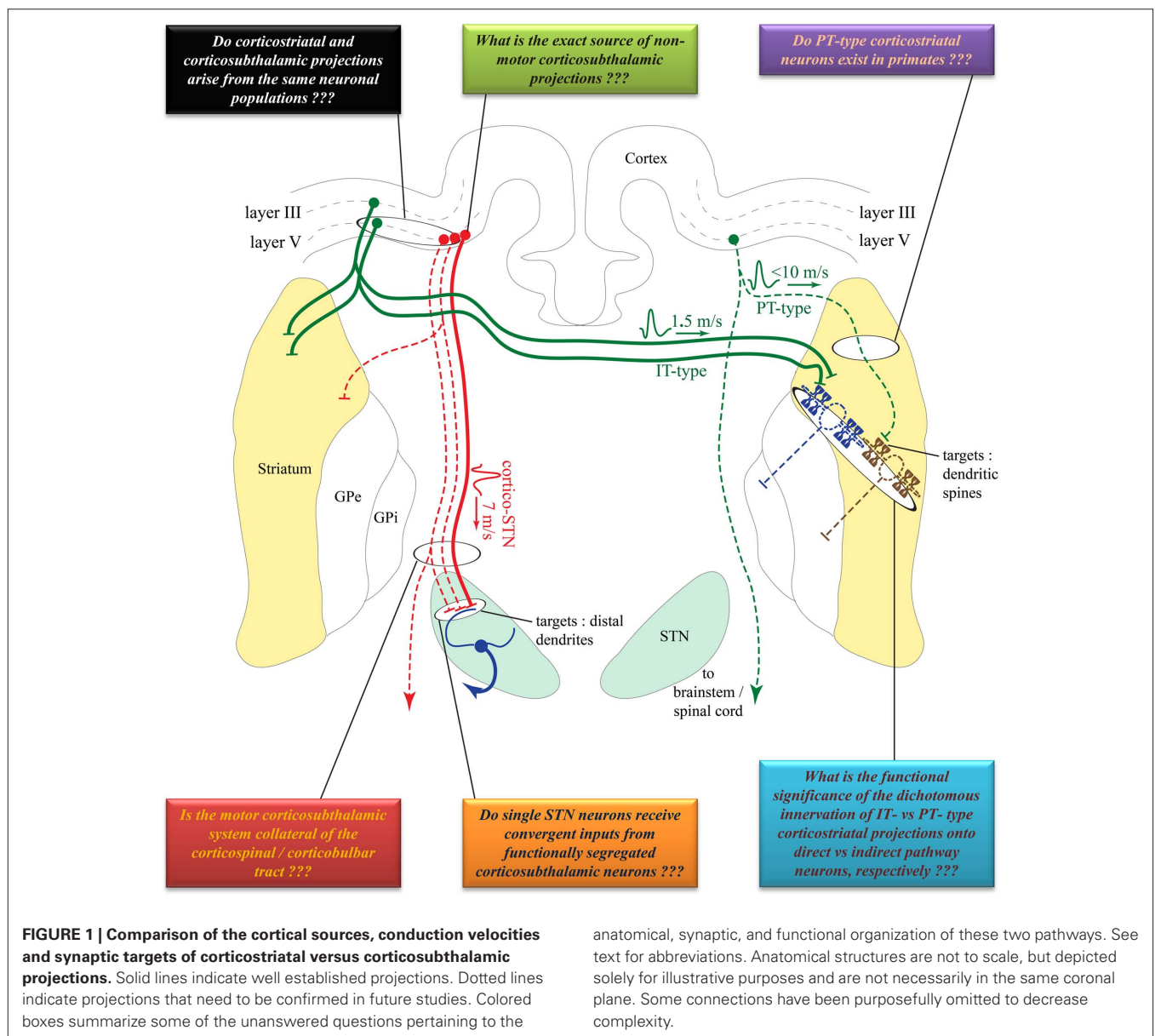
Corticostriatal projections typically arise from small to medium sized layer III and V pyramidal neurons in functionally diverse cortical areas in monkeys, dogs, cats, and rodents (Kemp and Powell, 1970; Kitai et al., 1976; Jones et al., 1977; Oka, 1980; Veening et al., 1980; Royce, 1982; Goldman-Rakic and Selemon, 1986; Tanaka, 1987; McGeorge and Faull, 1989). In rodents, corticostriatal neurons are categorized into two main types: the intratelencephalic (IT) and the pyramidal tract (PT) neurons (Jinnai and Matsuda, 1979; Landry et al., 1984; Wilson, 1987; Cowan and Wilson, 1994; Levesque et al., 1996a,b; Levesque and Parent, 1998; Wright et al., 1999, 2001; Zheng and Wilson, 2002; Reiner et al., 2003; Parent and Parent, 2006). The IT neurons, of which axonal projections are confined to the ipsilateral and contralateral cortex and striatum, are mainly located in layer III and upper layer V of the rat cortex. In contrast, PT neurons are located in the lower layer V, and send long descending axonal projections to the brainstem and spinal cord from which originate thin axon collaterals that innervate the striatum (Reiner et al., 2003; **Figure 1**). A unidirectional pattern of physiological connectivity from IT to PT corticostriatal neurons has been demonstrated in cortical slices (Morishima and Kawaguchi, 2006).

Although single-axon tracing studies have identified distinct populations of corticostriatal projection neurons reminiscent of the rodent IT and PT neurons in monkeys (Parent and Parent, 2006), this dual corticostriatal system is not supported by electrophysiological studies in non-human primates. For instance, stimulation of the motor putamen and the PT does not or very rarely elicit antidromic activation of single neurons in the primary motor cortex (MI) and pre-motor cortices in monkeys (Bauswein et al., 1989; Turner and DeLong, 2000), suggesting that the PT does not give off significant collaterals to the striatum (**Figure 1**). Even in rodents, the functional significance of the dichotomous IT and PT corticostriatal neurons system is not clearly understood. Anatomical evidence suggests that IT-type neurons preferentially innervate direct pathway striato-nigral neurons, whereas PT-type neurons mainly target indirect pathway striato-pallidal neurons (Lei et al., 2004). However, a recent *in vivo* electrophysiology

study could not detect a significant PT-type corticostriatal input onto indirect striatofugal neurons. This study rather showed that IT-type corticostriatal neurons are the main excitatory drive to both direct and indirect striatofugal neurons (Ballion et al., 2008; **Figure 1**).

SOURCES OF THE CORTICOSUBTHALAMIC SYSTEM

The corticosubthalamic projections originate primarily from cortical layer V neurons in rats and monkeys (Rouzaire-Dubois and Scarnati, 1985; Canteras et al., 1990; Nambu et al., 1996). Although overwhelming evidence points to an ipsilateral corticosubthalamic system (Afsharpour, 1985; Feger et al., 1994), one electrophysiological study performed in unilaterally decorticated rats suggests that part of the corticosubthalamic tract may project contralaterally (Rouzaire-Dubois and Scarnati, 1985). However, a subsequent electrophysiological study in rats showed that contralateral cortical



stimulation elicits long latency excitatory responses in the STN which, most likely, rely on oligosynaptic circuits rather than the fast monosynaptic corticosubthalamic connections that mediate ipsilateral effects (Fujimoto and Kita, 1993). Preliminary data suggest that axon collaterals of the corticospinal tract innervate the STN in cats (Iwahori, 1978; Giuffrida et al., 1985). However, this issue must be thoroughly investigated in rats and monkeys using sensitive anatomical and electrophysiological methods. Although part of the corticosubthalamic tract projecting to the motor territory of the STN could, indeed, be axon collaterals of the descending corticospinal and corticobulbar tracts, it is not clear if non-motor projections to the STN originate from axon collaterals of cortical efferents to other cortical or subcortical targets, or from a specific subset of corticosubthalamic neurons (**Figure 1**). In light of recent data suggesting that some of the therapeutic benefits, or side effects, of STN deep brain stimulation could be attributed to antidromic activation of motor (Li et al., 2007) versus non-motor corticosubthalamic systems (Drouot et al., 2004; Temel et al., 2006; Li et al., 2007; Gradinaru et al., 2009), respectively, a detailed knowledge of the exact sources and degree of collateralization of corticosubthalamic axons is essential to a deeper understanding of the mechanisms and anatomical substrates through which STN DBS mediates its wanted and unwanted effects (**Figure 2**).

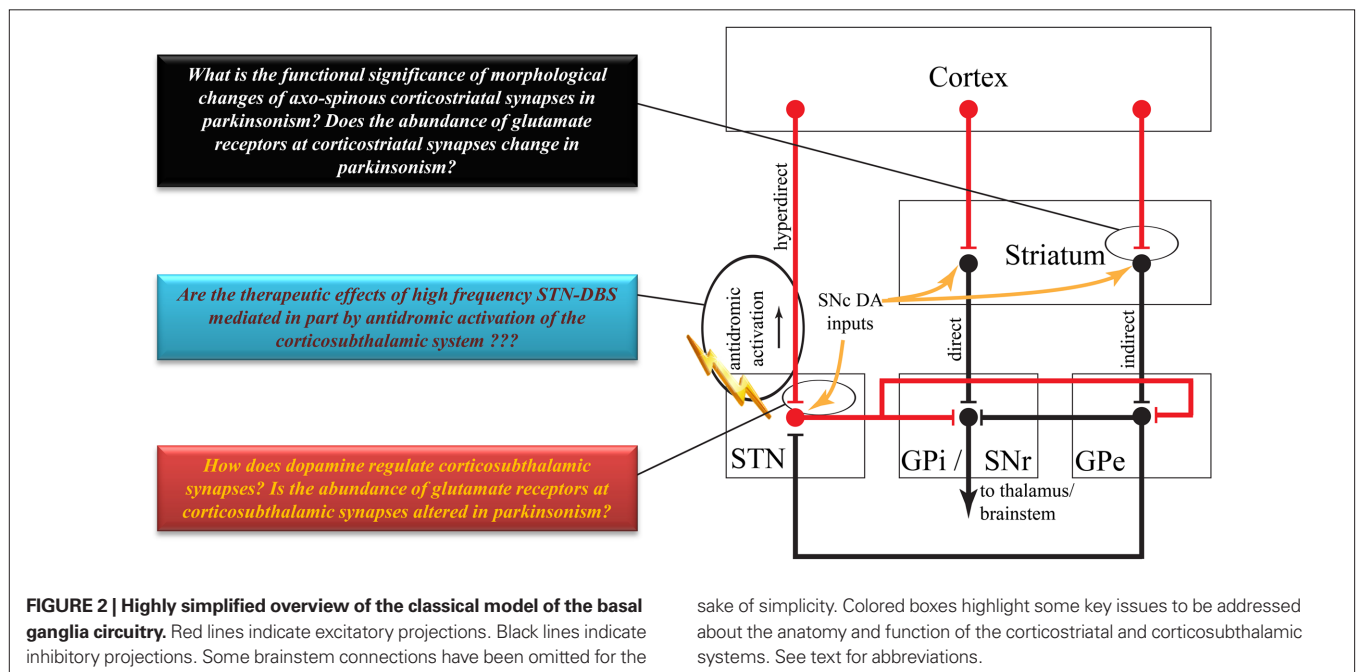
DO THE CORTICOSTRIATAL AND CORTICOSUBTHALAMIC SYSTEMS ORIGINATE FROM SINGLE CORTICAL NEURONS?

In monkeys, striatal stimulation results in monosynaptic short latency spike discharge (10–15 m/s) in the STN (Ohye et al., 1976). Considering that there is no clear evidence for the existence of a striatosubthalamic projection system; some of these short latency responses could possibly be mediated by axons collaterals of single cortical neurons innervating both the striatum and STN. Such short latency responses could also be attributed to activation of fibers of passage leading to the STN. Nevertheless, the extent of

collateralization of single cortical projections to the striatum and the STN is unclear, and must be directly assessed using reliable anatomical approaches (**Figure 1**). In that regard, a recent single-axon tracing study in non-human primates has revealed the existence of corticosubthalamic projections that descend through the cerebral peduncle or the red nucleus, but did not describe any cortical neurons innervating both the striatum and STN (Parent and Parent, 2006). However, a double retrograde labeling study in rats suggested that a subset of individual cortical neurons project to both structures (Feger et al., 1994).

Further evidence for a distinct origin of corticostriatal and corticosubthalamic projection systems is suggested by the different conduction velocities of these axonal projections. In rats, the mean conduction velocity of hyperdirect corticosubthalamic axons (~7 m/s) is much faster than that of the IT-type corticostriatal axons (~1.5 m/s), but is slightly slower than the PT-type corticostriatal axons (<10 m/s; Cowan and Wilson, 1994; Mahon et al., 2001; Slaght et al., 2004; Paz et al., 2005). However, the conduction velocity value of the PT-type corticostriatal axons must be interpreted cautiously because of diameter differences between the rather thin corticostriatal axon collaterals that detach from the large-sized PT main descending axon to the brainstem. Another important aspect to consider is the fact that the speed of conduction of the corticospinal tract (~11.4 m/s in rats, with the fastest reaching ~19 m/s; Mediratta and Nicoll, 1983) is much faster than either corticosubthalamic or corticostriatal axons, thereby suggesting that these projections most likely originate from distinct neuronal populations, though this remains to be demonstrated (**Figure 1**). The functional relevance of these different rates of conduction toward the transmission and integration of information flow through the corticostriatal and corticosubthalamic systems is discussed below.

To better understand the origins and potential sites of cross-talk between corticostriatal and corticosubthalamic neurons, the following critical issues must be addressed (**Figure 1**):



sake of simplicity. Colored boxes highlight some key issues to be addressed about the anatomy and function of the corticostriatal and corticosubthalamic systems. See text for abbreviations.

- (1) Determine the exact sources and innervation patterns of corticosubthalamic projections to motor and non-motor regions of the STN.
- (2) Determine the proportion of motor corticosubthalamic axons that are collaterals of the corticospinal and corticobulbar tracts in primates.
- (3) Determine the degree of collateralization of single corticofugal axons to the striatum and the STN.
- (4) Determine the extent of cross-talk between corticostriatal and corticosubthalamic neurons at the cortical level.

SYNAPTIC MICROCIRCUITRY OF CORTICOSTRIATAL VERSUS CORTICOSUBTHALAMIC SYSTEMS

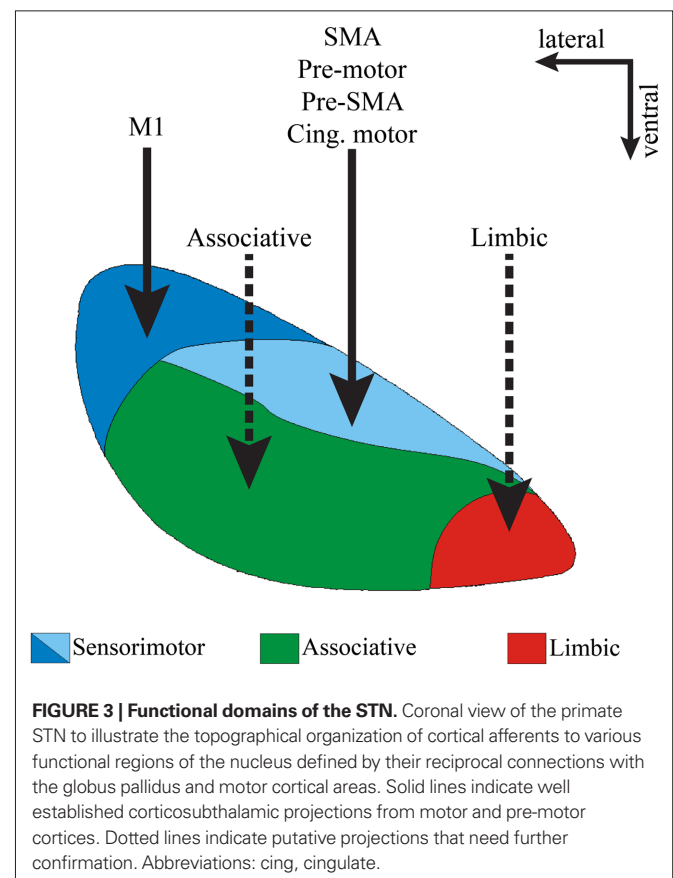
Cortical inputs to the striatum are relatively dense and preferentially target medium spiny neurons (MSNs). In rats, each MSN receives approximately 5000 cortical inputs (Kincaid et al., 1998), that form asymmetric synapses almost exclusively on spine heads (~90%; Kemp and Powell, 1971; Xu et al., 1989; Raju et al., 2006, 2008). It is clear that the corticostriatal system represents, by far, the most massive source of synaptic inputs to striatal projection neurons (Ingham et al., 1998; Raju et al., 2008). In contrast, the corticosubthalamic projection is much less profuse, and gives rise to a rather sparse population of terminals that form asymmetric synapses only with the distal dendrites of STN neurons (Bevan et al., 1995; Mathai et al., 2010). The main source of synaptic inputs to STN neurons is from the GPe, which provides a massive GABAergic innervation that spreads across the whole somatodendritic domain of single STN neurons (Smith et al., 1990, 1998). Despite its relative scarcity and distal location, corticosubthalamic afferents are considered as a major driving force of STN neurons, and a key source of inputs through which motor cortical information reaches basal ganglia output neurons (Nambu et al., 2002; Magill et al., 2004). Complex synaptic mechanisms and membrane properties of STN neurons have been suggested to explain how sparse, distally located cortical inputs could mediate powerful excitatory effects upon STN neurons despite the massive and tonically active inhibitory influences from the GPe (Bevan et al., 2002, 2007).

In addition to the prevalence and distribution of cortical inputs, the abundance, subsynaptic localization, pharmacological properties, and plasticity of postsynaptic glutamate receptors associated with these afferents are other factors that could contribute to the strength of corticostriatal and corticosubthalamic inputs (Figure 2). Striatal projection neurons express a wide variety of AMPA and NMDA receptor subunits and multiple subtypes of metabotropic glutamate receptors (mGluRs). At the electron microscopic level, these receptor proteins are profusely expressed along the plasma membrane of dendritic spines and dendritic shafts where most cortical inputs are located, though most mGluRs and a significant contingent of AMPA and NMDA receptor subunits are also heavily localized extrasynaptically (Paquet and Smith, 2003; Fujiyama et al., 2004; Galvan et al., 2006). Although the functional role of these receptors in corticostriatal transmission and long term plasticity has been demonstrated (Calabresi et al., 2007; Wickens, 2009), the relative abundance of specific receptor subunits at individual cortical synapses remains unknown.

Subthalamic nucleus neurons are also enriched with ionotropic NMDA and AMPA receptor subunits as well as with group I mGluRs (i.e., mGluR1 and mGluR5), located along the plasma

membrane of STN neurons, some of those being in the main body or peri-synaptic to asymmetric glutamatergic synapses (Clarke and Bolam, 1998; Kuwajima et al., 2004). However, there is no detailed study of the expression level of any glutamate receptor subtypes at corticosubthalamic synapses compared with other glutamatergic efferents to the STN (i.e., vesicular glutamate transporter 2 – positive terminals from the thalamus and pedunclopontine nucleus). Thus, to better understand the synaptic mechanisms by which the microcircuitry and relative expression of specific receptor subtypes contribute to the functional effects of corticostriatal versus corticosubthalamic afferents upon their target neurons, a detailed quantitative assessment of the morphological and neurochemical features of these synapses must be achieved (Figure 2). Some of the key information to be gathered include:

- (1) A detailed quantitative analysis of the prevalence and distribution of cortical inputs onto the dendrites of single STN neurons.
- (2) A detailed comparison of the relative abundance of specific glutamate receptor subtypes or subunits at individual corticostriatal versus corticosubthalamic synapses (Figure 3).
- (3) Electrophysiological assessment of the strength, properties and long term plasticity of corticosubthalamic synapses.



FUNCTIONAL SEGREGATION OF CORTICOSTRIATAL VERSUS CORTICOSUBTHALAMIC PATHWAYS

CORTICOSTRIATAL INPUTS ARE FUNCTIONALLY SEGREGATED

Multiple cortical areas project to the striatum in a highly topographic manner creating functionally segregated maps (Alexander et al., 1986). The post-commissural dorsolateral putamen primarily receives sensorimotor cortical afferents, most of the pre-commissural putamen and caudate nucleus receive afferents from associative cortical regions, whereas the limbic and paralimbic cortices, the amygdala and the hippocampus innervate the nucleus accumbens, the ventral caudate, and ventral putamen (Parent and Hazrati, 1995). Although the functional territories in the striatum are largely segregated, somatosensory and motor cortical information representing the same body parts converge onto overlapping regions in the putamen (Flaherty and Graybiel, 1991, 1993). There is no evidence for a similar overlap of somatosensory and motor cortical information in the STN. In fact, there are conflicting data regarding the existence of somatosensory, visual or auditory inputs to the STN from primary sensory cortices (Afsharpour, 1985; Canteras et al., 1988; Kolomiets et al., 2001), but it is worth noting that some sensory modalities can still reach the STN via other routes, such as the tectosubthalamic tract recently described in rodents (Coizet et al., 2009). Complex patterns of overlapping and interdigitation of corticostriatal projections from interconnected associative cortical areas have also been described in the caudate nucleus and ventral striatum of non-human primates (Yeterian and Van Hoesen, 1978; Selemon and Goldman-Rakic, 1985; Parthasarathy et al., 1992), but very little is known about the relative overlap or segregation of associative cortical inputs to the STN.

IS THE CORTICOSUBTHALAMIC SYSTEM FUNCTIONALLY SEGREGATED?

Despite the limited knowledge about the organization of non-motor corticosubthalamic projections compared with the detailed analyses of the corticostriatal systems, the STN is also topographically divided into functional territories, mainly based on its connections with specific functionally segregated regions of the globus pallidus (Figure 3). The dorsolateral and dorsomedial STN primarily processes motor-related information, the ventrolateral STN is the main target of associative-related pallidal inputs, while the ventromedial tip of the STN is primarily connected with limbic pallidal regions including the ventral pallidum (Parent, 1990; Shink et al., 1996; Karachi et al., 2005; Smith, 2011). In primates, cortical inputs from the primary MI innervate the dorsolateral STN, while the supplementary motor area (SMA), pre-motor cortex (PM), and cingulate motor cortex (CM) send projections to the dorsomedial STN (Nambu et al., 1996, 1997; Takada et al., 2001; Figure 3).

However, there is only scarce anatomical evidence of direct cortical projections from associative and limbic cortices to the monkey STN (Monakow et al., 1978). In rodents, lesion studies (Eagle et al., 2008) have suggested that functional connections between the medial prefrontal cortex and the STN are necessary to perform tasks that involve cognitive and reward processing (Dias et al., 1996; Chudasama et al., 2003; Baunez and Gubellini, 2010; Eagle and Baunez, 2010). As of date, the topography and extent of innervation of non-motor cortical inputs to the primate STN

is not known (Figure 1), but recent diffusion-weighted magnetic resonance imaging studies suggest connections between high order associative cortical regions and the STN in humans (Aron et al., 2007). In addition, data from our laboratory indicate that the relative density of cortical terminals in non-motor regions of the monkey STN is as high as that in the motor STN, thereby suggesting significant associative and limbic cortical inputs to the non-human primate STN (Mathai et al., 2010).

DO SINGLE STN NEURONS INTEGRATE FUNCTIONALLY SEGREGATED INFORMATION FLOWING ALONG THE CORTICOSUBTHALAMIC SYSTEM?

Despite the apparent anatomical segregation of motor, associative and limbic cortical inputs to the STN, the small size of the nucleus combined with the large extent of the dendritic tree of single STN neurons, open up the possibility for synaptic convergence of different cortical inputs onto single STN neurons, most particularly those located at the junction between different functional territories (Takada et al., 2001). STN neurons, indeed, harbor long dendrites, which, in primates, can extend as far as 600 μm from their parent cell bodies (Yelnik and Percheron, 1979; Figure 1). It is noteworthy that the extent of the dendritic domain of an individual STN neuron can cover about half, one-fifth, and one-ninth of the STN in the cat, monkey, and human, respectively (Yelnik and Percheron, 1979), thereby indicating that the functional segregation of the STN may increase in an ascending fashion as we compare cats, monkeys, and humans. In rats, some of the corticosubthalamic projections from functionally distinct cortical regions converge onto single STN neurons (Kolomiets et al., 2001), suggesting that the cortico-subthalamic system is, indeed, more functionally convergent than the functionally segregated corticostriatal system, at least in rodents (Kolomiets et al., 2001). In line with this concept, it is worth noting that inputs from functionally segregated regions of the GP converge upon single STN neurons in rats (Bevan et al., 1997; Figure 1). In contrast, albeit extensive, the dendritic tree of striatal MSNs is much more restricted (200–260 μm in diameter in primates) and confined to the close vicinity of parent cell bodies (Graveland et al., 1985). Whether these anatomical differences in the dendritic arborization of striatal MSNs versus subthalamic neurons account for a higher level of convergence of functionally segregated cortical influences upon single STN than striatal neurons remains to be conclusively established, especially in primates (Figure 1).

Another anatomical feature that governs the extent of convergence or divergence of inputs upon their synaptic targets is their respective pattern of axonal arborization inside the target structure. Using single cell filling studies, these features have been studied for the corticostriatal system, but much remains to be done for the corticosubthalamic connections. In the monkey striatum, cortical axons split into about two to five branches upon entering the structure, and later arborize scarcely, but widely (Parent and Parent, 2006), thereby suggesting that each corticostriatal axon could target a large pool of striatal dendrites along its long tortuous course, but form a restricted number of synapses upon each of them. In rodents, PT-type neurons form focal clusters of fine processes and terminals, whereas the axonal projections of IT-type neurons arborize uniformly in the striatum (Wilson, 1987; Cowan and Wilson, 1994; Wright et al., 1999, 2001). As far as the corticosubthalamic

pathway is concerned, very little is known about the extent and pattern of arborization of single cortical axons in the STN (Parent and Parent, 2006).

Thus, in order to assess and compare the degree of convergence between functionally segregated corticostriatal versus corticosubthalamic projections, the following issues must be addressed:

- (1) Determine the sources and pattern of organization of direct sensory inputs to the monkey STN.
- (2) Assess the degree of convergence of motor and somatosensory inputs related to the same body parts into the monkey STN.
- (3) Analyze in detail the topographical organization of non-motor cortical inputs to the STN, especially in the monkey.
- (4) Characterize the course and pattern of arborization of single motor and non-motor corticosubthalamic axons.
- (5) Assess the anatomo-functional convergence of functionally distinct cortical inputs on single STN neurons.

DOPAMINERGIC REGULATION OF GLUTAMATERGIC CORTICOSTRIATAL VERSUS CORTICOSUBTHALAMIC SYSTEMS – IMPLICATIONS FOR PARKINSON'S DISEASE PATHOPHYSIOLOGY

The role of striatal dopamine has been explored in great detail and summarized in comprehensive reviews published over recent decades (Arbuthnott et al., 2000; Nicola et al., 2000; Reynolds and Wickens, 2002; Surmeier et al., 2007, 2009; Kreitzer and Malenka, 2008; Wickens, 2009). In the following account, we will only highlight a few points indicating the importance of dopamine in the regulation of corticostriatal activity so that it can be compared with our current knowledge of the potential effects of dopamine upon the corticosubthalamic system. In the classical models of the basal ganglia, dopamine regulates the balance between the activation of the direct and indirect striatofugal pathways (Wichmann and DeLong, 1996). Striatal dopamine also plays a key role in mediating long term plasticity of glutamatergic corticostriatal synapses (Cragg, 2003; Picconi et al., 2003; Calabresi et al., 2007; Kreitzer and Malenka, 2008; Pawlak and Kerr, 2008). The loss of striatal dopamine in Parkinson's disease leads to a major pruning of dendritic spines on striatal projection neurons (Ingham et al., 1989; Stephens et al., 2005; Zaja-Milatovic et al., 2005; Smith and Villalba, 2008; Villalba et al., 2009; Villalba and Smith, 2010), corresponding with a loss of corticostriatal terminals and a severe dysregulation and imbalance of activity between the direct and indirect striatofugal pathways (DeLong, 1990; Pang et al., 2001; Liang et al., 2008), and a dramatic change in the long term plastic properties of corticostriatal synapses (Calabresi et al., 2007; **Figures 1 and 2**). There is also evidence that dopamine regulates the functional specificity of striatal projection neurons in response to cortical afferents, and that degeneration of the nigrostriatal dopaminergic system in PD underlies some of the pathophysiological patterns of activity striatal and other basal ganglia neurons display in parkinsonian condition (Calabresi et al., 1993, 2000; Florio et al., 1993; Onn and Grace, 1999; Onn et al., 2000; Strafella et al., 2005; **Figure 2**).

Albeit sparser than in the striatum, the STN also receives a dopaminergic innervation from collaterals of the nigrostriatal pathway, and STN neurons express various dopamine receptor subtypes (Lavoie et al., 1989; Hedreen, 1999; Augood et al., 2000;

Francois et al., 2000; Smith and Kieval, 2000; Cragg et al., 2004; Smith and Villalba, 2008; Rommelfanger and Wichmann, 2010). Although there is evidence for physiological dopamine-mediated effects in the STN, functional interactions between the dopamine nigrosubthalamic system and corticosubthalamic afferents remain to be established (**Figure 2**). On the other hand, it is worth noting that the excitatory responses of SNr basal ganglia output neurons in response to cortical stimulation are augmented in 6-hydroxy-dopamine-treated parkinsonian rats compared to control animals (Belluscio et al., 2007). Whether this abnormal increased response of SNr neurons relies on changes in the dopamine-mediated regulation of the corticosubthalamic system in parkinsonism, remains to be established. Preliminary data from our laboratory have demonstrated a significant reduction in the density of vesicular glutamate transporter 1 – positive corticosubthalamic terminals in MPTP-treated parkinsonian monkeys (Mathai et al., 2010), thereby suggesting possible loss of cortical inputs to the STN in the parkinsonian state, as shown in the striatum (see above; **Figure 2**).

To further understand and compare the role played by dopamine in the regulation of the corticosubthalamic versus corticostriatal systems, the following points must be clarified (**Figure 2**):

- (1) Does STN dopamine denervation induce changes in the number, microcircuitry and activity of corticosubthalamic inputs in parkinsonian condition?
- (2) How do dopamine- and dopamine receptor-related drugs affect the strength and plastic properties of corticosubthalamic inputs?
- (3) How do changes in dopaminergic innervation affect sensorimotor properties of STN neurons in response to cortical afferents in the parkinsonian state?
- (4) Does STN dopamine denervation induce downstream regulatory changes in the expression, trafficking, and functional activity of dopamine and glutamate receptors that could influence corticosubthalamic transmission in parkinsonian condition?

FUNCTIONAL INTERACTIONS BETWEEN THE CORTICOSTRIATAL AND CORTICOSUBTHALAMIC SYSTEMS TO REGULATE THE SELECTION OF BASAL GANGLIA MOTOR PROGRAMS IN NORMAL AND PATHOLOGICAL CONDITIONS

Ultimately, the significance of data discussed in this review relies on a better understanding of the functional interactions between information flowing along the corticostriatal and corticosubthalamic systems to mediate basal ganglia functions and dysfunctions in normal and diseased states. In that regard, a functional “center-surround model” of selection of motor programs in the basal ganglia has been proposed based on the temporal activation patterns of the hyperdirect corticosubthalamic pathway, and the direct corticostriatopallidal system (Mink, 1996; Nambu et al., 2000, 2002). According to this model, the cortical information flowing along the hyperdirect pathway is faster, and transmitted in a more diffuse manner than information flowing along the corticostriatal system to the GPi, thereby providing a general excitation over a large pool of basal ganglia output neurons not related to the selected motor act (i.e., the “surround neurons”). In contrast, a corollary signal transmitted along the direct corticostriatofugal pathway is much more focused and conveyed to a restricted pool of GPi neurons (i.e.,

the “center neurons”), that encode and transmit the information related to the desired motor acts to the thalamus and brainstem, thereby inducing focused inhibitory influences upon a pool of basal ganglia output neurons related to the motor act. Finally, a third corollary signal transmitted along the indirect corticostriatofugal pathway inhibits basal ganglia output neurons. Electrophysiological data have, indeed, demonstrated that cortical stimulation evokes a triphasic response in monkey GPi neurons (and rodent GP), including an early excitatory component induced by activation of the STN (Kita, 1992; Maurice et al., 1999; Nambu et al., 2000, 2002), prior to a slower inhibition generated by activation of the direct cortico-striato-GPi system followed by a late excitation most likely due to activation of the indirect cortico-striato-GPe–STN–GPi network (Kita, 1992; Maurice et al., 1999; Nambu et al., 2000, 2002). This attractive working hypothesis serves as an interesting foundation to further understand the possible interactions between the two cortical entry systems to the basal ganglia to control basal ganglia outflow.

However, as for any simplified models, part of it is speculative, and some of the assumptions made rely on anatomical and electrophysiological foundations that deserve some consideration. For instance, although some anatomical studies have proposed the existence of a diffuse subthalamopallidal system (Hazrati and Parent, 1992), as suggested in this model, others have demonstrated that the anatomical relationships between the STN and both pallidal segments are highly specific and topographic (Shink et al., 1996; Smith et al., 1998). In fact, recent single cell filling studies of individual subthalamopallidal and striato-pallidal neurons have revealed a high level of complexity of the axonal arborization of these two systems in the monkey GPi, demonstrating that projections from either systems can terminate in the GPi in a diffuse or focused manner (Parent et al., 1995; Sato et al., 2000). Another issue to be considered is the assumption that the subthalamopallidal system is active before movement onset in order to create the surround excitation proposed in this model. In monkeys, most STN

neurons increase their firing around the time of movement onset or after the action during active step tracking movements (Wichmann et al., 1994; Delong and Wichmann, 2009), thereby reducing the likelihood that the corticosubthalamic projection is involved in the preparation of movements as suggested by the center-surround hypothesis. On the other hand, some human studies have shown that most STN neurons are active before self-paced movements in Parkinson's disease (Paradiso et al., 2003).

To summarize, the functional mechanisms by which corticosubthalamic and corticostriatal projections interact to regulate motor, and possibly non-motor, behavior are complex, and necessitate further investigations.

Some of the key points that must be addressed to increase knowledge in this area:

- (1) The localization and proportion of GPi neurons that display an early STN-mediated excitatory response in normal and parkinsonian state following stimulation of specific cortical areas.
- (2) The changes in the temporal sequences of excitatory and inhibitory responses in GPi neurons following cortical activation in normal and parkinsonian state.

CONCLUSION

In this review, we highlighted some of the main anatomical, neurochemical, and functional features that characterize the two main routes of cortical entry to the basal ganglia circuitry, the corticostriatal, and the corticosubthalamic systems. Despite the large amount of information showing obvious differences in the functional anatomy of these two systems, our basic understanding of the temporal, spatial, and functional relationships through which these neural connections interact to mediate normal basal ganglia function, and their changes thereof in pathological conditions, are paramount in our quest of the mysterious functions of the basal ganglia in normal and diseased states.

REFERENCES

- Afsharpour, S. (1985). Topographical projections of the cerebral cortex to the subthalamic nucleus. *J. Comp. Neurol.* 236, 14–28.
- Albin, R. L., Young, A. B., and Penney, J. B. (1989). The functional anatomy of basal ganglia disorders. *Trends Neurosci.* 12, 366–375.
- Alexander, G. E., Delong, M. R., and Strick, P. L. (1986). Parallel organization of functionally segregated circuits linking basal ganglia and cortex. *Annu. Rev. Neurosci.* 9, 357–381.
- Arbuthnott, G. W., Ingham, C. A., and Wickens, J. R. (2000). Dopamine and synaptic plasticity in the neostriatum. *J. Anat.* 196(Pt 4), 587–596.
- Aron, A. R., Behrens, T. E., Smith, S., Frank, M. J., and Poldrack, R. A. (2007). Triangulating a cognitive control network using diffusion-weighted magnetic resonance imaging (MRI) and functional MRI. *J. Neurosci.* 27, 3743–3752.
- Augood, S. J., Hollingsworth, Z. R., Standaert, D. G., Emson, P. C., and Penney, J. B. Jr. (2000). Localization of dopaminergic markers in the human subthalamic nucleus. *J. Comp. Neurol.* 421, 247–255.
- Ballion, B., Mallet, N., Bezard, E., Lanciego, J. L., and Gonon, F. (2008). Intratelencephalic corticostriatal neurons equally excite striatonigral and striatopallidal neurons and their discharge activity is selectively reduced in experimental parkinsonism. *Eur. J. Neurosci.* 27, 2313–2321.
- Baunez, C., and Gubellini, P. (2010). Effects of GPi and STN inactivation on physiological, motor, cognitive and motivational processes in animal models of Parkinson's disease. *Prog. Brain Res.* 183, 235–258.
- Bauswein, E., Fromm, C., and Preuss, A. (1989). Corticostriatal cells in comparison with pyramidal tract neurons: contrasting properties in the behaving monkey. *Brain Res.* 493, 198–203.
- Belluscio, M. A., Riquelme, L. A., and Murer, M. G. (2007). Striatal dysfunction increases basal ganglia output during motor cortex activation in parkinsonian rats. *Eur. J. Neurosci.* 25, 2791–2804.
- Bevan, M. D., Clarke, N. P., and Bolam, J. P. (1997). Synaptic integration of functionally diverse pallidal information in the entopeduncular nucleus and subthalamic nucleus in the rat. *J. Neurosci.* 17, 308–324.
- Bevan, M. D., Francis, C. M., and Bolam, J. P. (1995). The glutamate-enriched cortical and thalamic input to neurons in the subthalamic nucleus of the rat: convergence with GABA-positive terminals. *J. Comp. Neurol.* 361, 491–511.
- Bevan, M. D., Hallworth, N. E., and Baufreton, J. (2007). GABAergic control of the subthalamic nucleus. *Prog. Brain Res.* 160, 173–188.
- Bevan, M. D., Magill, P. J., Terman, D., Bolam, J. P., and Wilson, C. J. (2002). Move to the rhythm: oscillations in the subthalamic nucleus-external globus pallidus network. *Trends Neurosci.* 25, 525–531.
- Calabresi, P., Centonze, D., and Bernardi, G. (2000). Electrophysiology of dopamine in normal and denervated striatal neurons. *Trends Neurosci.* 23, S57–S63.
- Calabresi, P., Mercuri, N. B., Sancesario, G., and Bernardi, G. (1993). Electrophysiology of dopamine-denervated striatal neurons. Implications for Parkinson's disease. *Brain* 116(Pt 2), 433–452.
- Calabresi, P., Picconi, B., Tozzi, A., and Di Filippo, M. (2007). Dopamine-mediated regulation of corticostriatal synaptic plasticity. *Trends Neurosci.* 30, 211–219.
- Canteras, N. S., Shammah-Lagnado, S. J., Silva, B. A., and Ricardo, J. A. (1988).

- Somatosensory inputs to the subthalamic nucleus: a combined retrograde and anterograde horseradish peroxidase study in the rat. *Brain Res.* 458, 53–64.
- Canteras, N. S., Shammah-Lagnado, S. J., Silva, B. A., and Ricardo, J. A. (1990). Afferent connections of the subthalamic nucleus: a combined retrograde and anterograde horseradish peroxidase study in the rat. *Brain Res.* 513, 43–59.
- Chudasama, Y., Baunez, C., and Robbins, T. W. (2003). Functional disconnection of the medial prefrontal cortex and subthalamic nucleus in attentional performance: evidence for corticostriatal interaction. *J. Neurosci.* 23, 5477–5485.
- Clarke, N. P., and Bolam, J. P. (1998). Distribution of glutamate receptor subunits at neurochemically characterized synapses in the entopeduncular nucleus and subthalamic nucleus of the rat. *J. Comp. Neurol.* 397, 403–420.
- Coizet, V., Graham, J. H., Moss, J., Bolam, J. P., Savasta, M., Mchaffie, J. G., Redgrave, P., and Overton, P. G. (2009). Short-latency visual input to the subthalamic nucleus is provided by the midbrain superior colliculus. *J. Neurosci.* 29, 5701–5709.
- Cowan, R. L., and Wilson, C. J. (1994). Spontaneous firing patterns and axonal projections of single corticostriatal neurons in the rat medial agranular cortex. *J. Neurophysiol.* 71, 17–32.
- Cragg, S. J. (2003). Variable dopamine release probability and short-term plasticity between functional domains of the primate striatum. *J. Neurosci.* 23, 4378–4385.
- Cragg, S. J., Baufreton, J., Xue, Y., Bolam, J. P., and Bevan, M. D. (2004). Synaptic release of dopamine in the subthalamic nucleus. *Eur. J. Neurosci.* 20, 1788–1802.
- DeLong, M., and Wichmann, T. (2009). Update on models of basal ganglia function and dysfunction. *Parkinsonism Relat. Disord.* 15(Suppl. 3), S237–S240.
- DeLong, M. R. (1990). Primate models of movement disorders of basal ganglia origin. *Trends Neurosci.* 13, 281–285.
- Dias, R., Robbins, T. W., and Roberts, A. C. (1996). Dissociation in prefrontal cortex of affective and attentional shifts. *Nature* 380, 69–72.
- Drouot, X., Oshino, S., Jarraya, B., Besret, L., Kishima, H., Remy, P., Dauguet, J., Lefaucheur, J. P., Dolle, F., Conde, E., Bottlaender, M., Peschanski, M., Keravel, Y., Hantraye, P., and Palfi, S. (2004). Functional recovery in a primate model of Parkinson's disease following motor cortex stimulation. *Neuron* 44, 769–778.
- Eagle, D. M., and Baunez, C. (2010). Is there an inhibitory-response-control system in the rat? Evidence from anatomical and pharmacological studies of behavioral inhibition. *Neurosci. Biobehav. Rev.* 34, 50–72.
- Eagle, D. M., Baunez, C., Hutcheson, D. M., Lehmann, O., Shah, A. P., and Robbins, T. W. (2008). Stop-signal reaction-time task performance: role of prefrontal cortex and subthalamic nucleus. *Cereb. Cortex* 18, 178–188.
- Feger, J., Bevan, M., and Crossman, A. R. (1994). The projections from the parafascicular thalamic nucleus to the subthalamic nucleus and the striatum arise from separate neuronal populations: a comparison with the corticostriatal and corticostriatal efferents in a retrograde fluorescent double-labelling study. *Neuroscience* 60, 125–132.
- Flaherty, A. W., and Graybiel, A. M. (1991). Corticostriatal transformations in the primate somatosensory system. Projections from physiologically mapped body-part representations. *J. Neurophysiol.* 66, 1249–1263.
- Flaherty, A. W., and Graybiel, A. M. (1993). Two input systems for body representations in the primate striatal matrix: experimental evidence in the squirrel monkey. *J. Neurosci.* 13, 1120–1137.
- Florio, T., Di Loreto, S., Cerrito, F., and Scarnati, E. (1993). Influence of pre-limbic and sensorimotor cortices on striatal neurons in the rat: electrophysiological evidence for converging inputs and the effects of 6-OHDA-induced degeneration of the substantia nigra. *Brain Res.* 619, 180–188.
- Francois, C., Savy, C., Jan, C., Tande, D., Hirsch, E. C., and Yelnik, J. (2000). Dopaminergic innervation of the subthalamic nucleus in the normal state, in MPTP-treated monkeys, and in Parkinson's disease patients. *J. Comp. Neurol.* 425, 121–129.
- Fujimoto, K., and Kita, H. (1993). Response characteristics of subthalamic neurons to the stimulation of the sensorimotor cortex in the rat. *Brain Res.* 609, 185–192.
- Fujiyama, F., Kuramoto, E., Okamoto, K., Hioki, H., Furuta, T., Zhou, L., Nomura, S., and Kaneko, T. (2004). Presynaptic localization of an AMPA-type glutamate receptor in corticostriatal and thalamostriatal axon terminals. *Eur. J. Neurosci.* 20, 3322–3330.
- Galvan, A., Kuwajima, M., and Smith, Y. (2006). Glutamate and GABA receptors and transporters in the basal ganglia: what does their subsynaptic localization reveal about their function? *Neuroscience* 143, 351–375.
- Giuffrida, R., Li Volsi, G., Maugeri, G., and Perciavalle, V. (1985). Influences of pyramidal tract on the subthalamic nucleus in the cat. *Neurosci. Lett.* 54, 231–235.
- Goldman-Rakic, P. S., and Selemon, L. D. (1986). "Topography of corticostriatal projections in nonhuman primates and implications for functional parcellation of the neostriatum," in *Cerebral Cortex*, eds E. G. Jones and A. Peters (New York: Plenum Press), 447–466.
- Gradinaru, V., Mogri, M., Thompson, K. R., Henderson, J. M., and Deisseroth, K. (2009). Optical deconstruction of parkinsonian neural circuitry. *Science* 324, 354–359.
- Graveland, G. A., Williams, R. S., and Difiglia, M. (1985). A Golgi study of the human neostriatum: neurons and afferent fibers. *J. Comp. Neurol.* 234, 317–333.
- Hazrati, L. N., and Parent, A. (1992). Convergence of subthalamic and striatal efferents at pallidal level in primates: an anterograde double-labeling study with biocytin and PHA-L. *Brain Res.* 569, 336–340.
- Hedreen, J. C. (1999). Tyrosine hydroxylase-immunoreactive elements in the human globus pallidus and subthalamic nucleus. *J. Comp. Neurol.* 409, 400–410.
- Ingham, C. A., Hood, S. H., and Arbutnot, G. W. (1989). Spine density on neostriatal neurones changes with 6-hydroxydopamine lesions and with age. *Brain Res.* 503, 334–338.
- Ingham, C. A., Hood, S. H., Taggart, P., and Arbutnot, G. W. (1998). Plasticity of synapses in the rat neostriatum after unilateral lesion of the nigrostriatal dopaminergic pathway. *J. Neurosci.* 18, 4732–4743.
- Iwahori, N. (1978). A Golgi study on the subthalamic nucleus of the cat. *J. Comp. Neurol.* 182, 383–397.
- Jinnai, K., and Matsuda, Y. (1979). Neurons of the motor cortex projecting commonly on the caudate nucleus and the lower brain stem in the cat. *Neurosci. Lett.* 13, 121–126.
- Jones, E. G., Coulter, J. D., Burton, H., and Porter, R. (1977). Cells of origin and terminal distribution of corticostriatal fibers arising in the sensory-motor cortex of monkeys. *J. Comp. Neurol.* 173, 53–80.
- Karachi, C., Yelnik, J., Tande, D., Tremblay, L., Hirsch, E. C., and Francois, C. (2005). The pallidosubthalamic projection: an anatomical substrate for nonmotor functions of the subthalamic nucleus in primates. *Mov. Disord.* 20, 172–180.
- Kemp, J. M., and Powell, T. P. (1970). The cortico-striate projection in the monkey. *Brain* 93, 525–546.
- Kemp, J. M., and Powell, T. P. (1971). The termination of fibres from the cerebral cortex and thalamus upon dendritic spines in the caudate nucleus: a study with the Golgi method. *Philos. Trans. R. Soc. Lond. B Biol. Sci.* 262, 429–439.
- Kincaid, A. E., Zheng, T., and Wilson, C. J. (1998). Connectivity and convergence of single corticostriatal axons. *J. Neurosci.* 18, 4722–4731.
- Kita, H. (1992). Responses of globus pallidus neurons to cortical stimulation: intracellular study in the rat. *Brain Res.* 589, 84–90.
- Kitai, S. T., Kocsis, J. D., and Wood, J. (1976). Origin and characteristics of the cortico-caudate afferents: an anatomical and electrophysiological study. *Brain Res.* 118, 137–141.
- Kolomiets, B. P., Deniau, J. M., Mailly, P., Menetrey, A., Glowinski, J., and Thierry, A. M. (2001). Segregation and convergence of information flow through the cortico-subthalamic pathways. *J. Neurosci.* 21, 5764–5772.
- Kreitzer, A. C., and Malenka, R. C. (2008). Striatal plasticity and basal ganglia circuit function. *Neuron* 60, 543–554.
- Kuwajima, M., Hall, R. A., Aiba, A., and Smith, Y. (2004). Subcellular and subsynaptic localization of group I metabotropic glutamate receptors in the monkey subthalamic nucleus. *J. Comp. Neurol.* 474, 589–602.
- Landry, P., Wilson, C. J., and Kitai, S. T. (1984). Morphological and electrophysiological characteristics of pyramidal tract neurons in the rat. *Exp. Brain Res.* 57, 177–190.
- Lavoie, B., Smith, Y., and Parent, A. (1989). Dopaminergic innervation of the basal ganglia in the squirrel monkey as revealed by tyrosine hydroxylase immunohistochemistry. *J. Comp. Neurol.* 289, 36–52.
- Lei, W., Jiao, Y., Del Mar, N., and Reiner, A. (2004). Evidence for differential cortical input to direct pathway versus indirect pathway striatal projection neurons in rats. *J. Neurosci.* 24, 8289–8299.
- Levesque, M., Charara, A., Gagnon, S., Parent, A., and Deschenes, M. (1996a). Corticostriatal projections from layer V cells in rat are collaterals of long-range corticofugal axons. *Brain Res.* 709, 311–315.
- Levesque, M., Gagnon, S., Parent, A., and Deschenes, M. (1996b). Axonal arborization of corticostriatal and corticothalamic fibers arising from the second somatosensory area in the rat. *Cereb. Cortex* 6, 759–770.
- Levesque, M., and Parent, A. (1998). Axonal arborization of corticostriatal and corticothalamic fibers arising from prefrontal cortex in the rat. *Cereb. Cortex* 8, 602–613.
- Li, S., Arbutnot, G. W., Jutras, M. J., Goldberg, J. A., and Jaeger, D. (2007). Resonant antidromic cortical circuit activation as a consequence of

- high-frequency subthalamic deep-brain stimulation. *J. Neurophysiol.* 98, 3525–3537.
- Liang, L., Delong, M. R., and Papa, S. M. (2008). Inversion of dopamine responses in striatal medium spiny neurons and involuntary movements. *J. Neurosci.* 28, 7537–7547.
- Magill, P. J., Sharott, A., Bevan, M. D., Brown, P., and Bolam, J. P. (2004). Synchronous unit activity and local field potentials evoked in the subthalamic nucleus by cortical stimulation. *J. Neurophysiol.* 92, 700–714.
- Mahon, S., Deniau, J. M., and Charpier, S. (2001). Relationship between EEG potentials and intracellular activity of striatal and cortico-striatal neurons: an in vivo study under different anesthetics. *Cereb. Cortex* 11, 360–373.
- Mathai, A., Pare, J. F., Jenkins, S., and Smith, Y. (2010). “Glutamatergic inputs to the subthalamic nucleus: a quantitative analysis of the synaptic microcircuitry of vGluT1- and vGluT2-containing terminals in normal and Parkinsonian nonhuman primates,” in *Xth Triennial Meeting of the International Basal Ganglia Society*, Long Branch, NJ.
- Maurice, N., Deniau, J. M., Glowinski, J., and Thierry, A. M. (1999). Relationships between the prefrontal cortex and the basal ganglia in the rat: physiology of the cortico-nigral circuits. *J. Neurosci.* 19, 4674–4681.
- McGeorge, A. J., and Faull, R. L. (1989). The organization of the projection from the cerebral cortex to the striatum in the rat. *Neuroscience* 29, 503–537.
- Mediratta, N. K., and Nicoll, J. A. (1983). Conduction velocities of corticospinal axons in the rat studied by recording cortical antidromic responses. *J. Physiol. (Lond.)* 336, 545–561.
- Mink, J. W. (1996). The basal ganglia: focused selection and inhibition of competing motor programs. *Prog. Neurobiol.* 50, 381–425.
- Monakow, K. H., Akert, K., and Kunzle, H. (1978). Projections of the precentral motor cortex and other cortical areas of the frontal lobe to the subthalamic nucleus in the monkey. *Exp. Brain Res.* 33, 395–403.
- Morishima, M., and Kawaguchi, Y. (2006). Recurrent connection patterns of corticostriatal pyramidal cells in frontal cortex. *J. Neurosci.* 26, 4394–4405.
- Nambu, A., Takada, M., Inase, M., and Tokuno, H. (1996). Dual somatotopical representations in the primate subthalamic nucleus: evidence for ordered but reversed body-map transformations from the primary motor cortex and the supplementary motor area. *J. Neurosci.* 16, 2671–2683.
- Nambu, A., Tokuno, H., Hamada, I., Kita, H., Imanishi, M., Akazawa, T., Ikeuchi, Y., and Hasegawa, N. (2000). Excitatory cortical inputs to pallidal neurons via the subthalamic nucleus in the monkey. *J. Neurophysiol.* 84, 289–300.
- Nambu, A., Tokuno, H., Inase, M., and Takada, M. (1997). Corticostriatal input zones from forelimb representations of the dorsal and ventral divisions of the premotor cortex in the macaque monkey: comparison with the input zones from the primary motor cortex and the supplementary motor area. *Neurosci. Lett.* 239, 13–16.
- Nambu, A., Tokuno, H., and Takada, M. (2002). Functional significance of the cortico-subthalamic-pallidal “hyper-direct” pathway. *Neurosci. Res.* 43, 111–117.
- Nicola, S. M., Surmeier, J., and Malenka, R. C. (2000). Dopaminergic modulation of neuronal excitability in the striatum and nucleus accumbens. *Annu. Rev. Neurosci.* 23, 185–215.
- Ohye, C., Le Gayader, C., and Feger, J. (1976). Responses of subthalamic and pallidal neurons to striatal stimulation: an extracellular study on awake monkeys. *Brain Res.* 111, 241–252.
- Oka, H. (1980). Organization of the cortico-caudate projections. A horseradish peroxidase study in the cat. *Exp. Brain Res.* 40, 203–208.
- Onn, S. P., and Grace, A. A. (1999). Alterations in electrophysiological and dye coupling of striatal spiny and aspiny neurons in dopamine-denervated rat striatum recorded in vivo. *Synapse* 33, 1–15.
- Onn, S. P., West, A. R., and Grace, A. A. (2000). Dopamine-mediated regulation of striatal neuronal and network interactions. *Trends Neurosci.* 23, S48–S56.
- Pang, Z., Ling, G. Y., Gajendiran, M., and Xu, Z. C. (2001). Enhanced excitatory synaptic transmission in spiny neurons of rat striatum after unilateral dopamine denervation. *Neurosci. Lett.* 308, 201–205.
- Paquet, M., and Smith, Y. (2003). Group I metabotropic glutamate receptors in the monkey striatum: subsynaptic association with glutamatergic and dopaminergic afferents. *J. Neurosci.* 23, 7659–7669.
- Paradiso, G., Saint-Cyr, J. A., Lozano, A. M., Lang, A. E., and Chen, R. (2003). Involvement of the human subthalamic nucleus in movement preparation. *Neurology* 61, 1538–1545.
- Parent, A. (1990). Extrinsic connections of the basal ganglia. *Trends Neurosci.* 13, 254–258.
- Parent, A., Charara, A., and Pinault, D. (1995). Single striatofugal axons arborizing in both pallidal segments and in the substantia nigra in primates. *Brain Res.* 698, 280–284.
- Parent, A., and Hazrati, L. N. (1995). Functional anatomy of the basal ganglia. I. The cortico-basal ganglia-thalamo-cortical loop. *Brain Res. Brain Res. Rev.* 20, 91–127.
- Parent, M., and Parent, A. (2006). Single-axon tracing study of corticostriatal projections arising from primary motor cortex in primates. *J. Comp. Neurol.* 496, 202–213.
- Parthasarathy, H. B., Schall, J. D., and Graybiel, A. M. (1992). Distributed but convergent ordering of corticostriatal projections: analysis of the frontal eye field and the supplementary eye field in the macaque monkey. *J. Neurosci.* 12, 4468–4488.
- Pawlak, V., and Kerr, J. N. (2008). Dopamine receptor activation is required for corticostriatal spike-timing-dependent plasticity. *J. Neurosci.* 28, 2435–2446.
- Paz, J. T., Deniau, J. M., and Charpier, S. (2005). Rhythmic bursting in the cortico-subthalamic-pallidal network during spontaneous genetically determined spike and wave discharges. *J. Neurosci.* 25, 2092–2101.
- Picconi, B., Centonze, D., Hakansson, K., Bernardi, G., Greengard, P., Fisone, G., Cenci, M. A., and Calabresi, P. (2003). Loss of bidirectional striatal synaptic plasticity in L-DOPA-induced dyskinesia. *Nat. Neurosci.* 6, 501–506.
- Raju, D. V., Ahern, T. H., Shah, D. J., Wright, T. M., Standaert, D. G., Hall, R. A., and Smith, Y. (2008). Differential synaptic plasticity of the corticostriatal and thalamostriatal systems in an MPTP-treated monkey model of parkinsonism. *Eur. J. Neurosci.* 27, 1647–1658.
- Raju, D. V., Shah, D. J., Wright, T. M., Hall, R. A., and Smith, Y. (2006). Differential synaptology of vGluT2-containing thalamostriatal afferents between the patch and matrix compartments in rats. *J. Comp. Neurol.* 499, 231–243.
- Reiner, A., Jiao, Y., Del Mar, N., Laverghetta, A. V., and Lei, W. L. (2003). Differential morphology of pyramidal tract-type and intratelencephalically projecting-type corticostriatal neurons and their intrastriatal terminals in rats. *J. Comp. Neurol.* 457, 420–440.
- Reynolds, J. N., and Wickens, J. R. (2002). Dopamine-dependent plasticity of corticostriatal synapses. *Neural Netw.* 15, 507–521.
- Rommelfanger, K. S., and Wichmann, T. (2010). Extrastriatal dopaminergic circuits of the basal ganglia. *Front. Neuroanat.* 4:139. doi: 10.3389/fnana.2010.00139
- Rouzaire-Dubois, B., and Scarnati, E. (1985). Bilateral corticostriatal nucleus projections: an electrophysiological study in rats with chronic cerebral lesions. *Neuroscience* 15, 69–79.
- Royce, G. J. (1982). Laminar origin of cortical neurons which project upon the caudate nucleus: a horseradish peroxidase investigation in the cat. *J. Comp. Neurol.* 205, 8–29.
- Sato, F., Parent, M., Levesque, M., and Parent, A. (2000). Axonal branching pattern of neurons of the subthalamic nucleus in primates. *J. Comp. Neurol.* 424, 142–152.
- Selemon, L. D., and Goldman-Rakic, P. S. (1985). Longitudinal topography and interdigitation of corticostriatal projections in the rhesus monkey. *J. Neurosci.* 5, 776–794.
- Shink, E., Bevan, M. D., Bolam, J. P., and Smith, Y. (1996). The subthalamic nucleus and the external pallidum: two tightly interconnected structures that control the output of the basal ganglia in the monkey. *Neuroscience* 73, 335–357.
- Slaght, S. J., Paz, T., Chavez, M., Deniau, J. M., Mahon, S., and Charpier, S. (2004). On the activity of the corticostriatal networks during spike-and-wave discharges in a genetic model of absence epilepsy. *J. Neurosci.* 24, 6816–6825.
- Smith, Y. (2011). “Functional anatomy of the motor and non-motor circuitry of the basal ganglia,” in *Parkinson’s Disease: Non-Motor and Non-Dopaminergic Features*, 1st Edn, eds C. W. Olanow, F. Stocchi, and A. Lang (Oxford: Wiley-Blackwell), 32–55.
- Smith, Y., Bevan, M. D., Shink, E., and Bolam, J. P. (1998). Microcircuitry of the direct and indirect pathways of the basal ganglia. *Neuroscience* 86, 353–387.
- Smith, Y., Bolam, J. P., and Von Krosigk, M. (1990). Topographical and synaptic organization of the GABA-containing pallidum-subthalamic projection in the rat. *Eur. J. Neurosci.* 2, 500–511.
- Smith, Y., and Kievel, J. Z. (2000). Anatomy of the dopamine system in the basal ganglia. *Trends Neurosci.* 23, S28–S33.
- Smith, Y., and Villalba, R. (2008). Striatal and extrastriatal dopamine in the basal ganglia: an overview of its anatomical organization in normal and Parkinsonian brains. *Mov. Disord.* 23(Suppl. 3), S534–S547.
- Stephens, B., Mueller, A. J., Shering, A. F., Hood, S. H., Taggart, P., Arbutnot, G. W., Bell, J. E., Kilford, L., Kingsbury, A. E., Daniel, S. E., and Ingham, C. A. (2005). Evidence of a breakdown of corticostriatal connections in Parkinson’s disease. *Neuroscience* 132, 741–754.
- Strafella, A. P., Ko, J. H., Grant, J., Fraraccio, M., and Monchi, O. (2005). Corticostriatal functional interactions in Parkinson’s disease: a rTMS/[11C]

- raclopride PET study. *Eur. J. Neurosci.* 22, 2946–2952.
- Surmeier, D. J., Ding, J., Day, M., Wang, Z., and Shen, W. (2007). D1 and D2 dopamine-receptor modulation of striatal glutamatergic signaling in striatal medium spiny neurons. *Trends Neurosci.* 30, 228–235.
- Surmeier, D. J., Plotkin, J., and Shen, W. (2009). Dopamine and synaptic plasticity in dorsal striatal circuits controlling action selection. *Curr. Opin. Neurobiol.* 19, 621–628.
- Takada, M., Tokuno, H., Hamada, I., Inase, M., Ito, Y., Imanishi, M., Hasegawa, N., Akazawa, T., Hatanaka, N., and Nambu, A. (2001). Organization of inputs from cingulate motor areas to basal ganglia in macaque monkey. *Eur. J. Neurosci.* 14, 1633–1650.
- Tanaka, D. Jr. (1987). Differential laminar distribution of corticostriatal neurons in the prefrontal and pericruciate gyri of the dog. *J. Neurosci.* 7, 4095–4106.
- Temel, Y., Kessels, A., Tan, S., Topdag, A., Boon, P., and Visser-Vandewalle, V. (2006). Behavioural changes after bilateral subthalamic stimulation in advanced Parkinson disease: a systematic review. *Parkinsonism Relat. Disord.* 12, 265–272.
- Turner, R. S., and DeLong, M. R. (2000). Corticostriatal activity in primary motor cortex of the macaque. *J. Neurosci.* 20, 7096–7108.
- Veening, J. G., Cornelissen, F. M., and Lieven, P. A. (1980). The topical organization of the afferents to the caudatoputamen of the rat. A horseradish peroxidase study. *Neuroscience* 5, 1253–1268.
- Villalba, R. M., Lee, H., and Smith, Y. (2009). Dopaminergic denervation and spine loss in the striatum of MPTP-treated monkeys. *Exp. Neurol.* 215, 220–227.
- Villalba, R. M., and Smith, Y. (2010). Striatal spine plasticity in Parkinson's disease. *Front. Neuroanat.* 4:133. doi: 10.3389/fnana.2010.00133
- Wichmann, T., Bergman, H., and DeLong, M. R. (1994). The primate subthalamic nucleus. I. Functional properties in intact animals. *J. Neurophysiol.* 72, 494–506.
- Wichmann, T., and DeLong, M. R. (1996). Functional and pathophysiological models of the basal ganglia. *Curr. Opin. Neurobiol.* 6, 751–758.
- Wickens, J. R. (2009). Synaptic plasticity in the basal ganglia. *Behav. Brain Res.* 199, 119–128.
- Wilson, C. J. (1987). Morphology and synaptic connections of crossed corticostriatal neurons in the rat. *J. Comp. Neurol.* 263, 567–580.
- Wright, A. K., Norrie, L., Ingham, C. A., Hutton, E. A., and Arbuthnott, G. W. (1999). Double anterograde tracing of outputs from adjacent “barrel columns” of rat somatosensory cortex. Neostriatal projection patterns and terminal ultrastructure. *Neuroscience* 88, 119–133.
- Wright, A. K., Ramanathan, S., and Arbuthnott, G. W. (2001). Identification of the source of the bilateral projection system from cortex to somatosensory neostriatum and an exploration of its physiological actions. *Neuroscience* 103, 87–96.
- Xu, Z. C., Wilson, C. J., and Emson, P. C. (1989). Restoration of the corticostriatal projection in rat neostriatal grafts: electron microscopic analysis. *Neuroscience* 29, 539–550.
- Yelnik, J., and Percheron, G. (1979). Subthalamic neurons in primates: a quantitative and comparative analysis. *Neuroscience* 4, 1717–1743.
- Yeterian, E. H., and Van Hoesen, G. W. (1978). Cortico-striate projections in the rhesus monkey: the organization of certain cortico-caudate connections. *Brain Res.* 139, 43–63.
- Zaja-Milatovic, S., Milatovic, D., Schantz, A. M., Zhang, J., Montine, K. S., Samii, A., Deutch, A. Y., and Montine, T. J. (2005). Dendritic degeneration in neostriatal medium spiny neurons in Parkinson disease. *Neurology* 64, 545–547.
- Zheng, T., and Wilson, C. J. (2002). Corticostriatal combinatorics: the implications of corticostriatal axonal arborizations. *J. Neurophysiol.* 87, 1007–1017.

Conflict of Interest Statement: The authors declare that the research was conducted in the absence of any commercial or financial relationships that could be construed as a potential conflict of interest.

Received: 28 April 2011; paper pending published: 13 June 2011; accepted: 21 July 2011; published online: 01 August 2011.

Citation: Mathai A and Smith Y (2011) The corticostriatal and corticosubthalamic pathways: two entries, one target. So what? *Front. Syst. Neurosci.* 5:64. doi: 10.3389/fnsys.2011.00064

Copyright © 2011 Mathai and Smith. This is an open-access article subject to a non-exclusive license between the authors and Frontiers Media SA, which permits use, distribution and reproduction in other forums, provided the original authors and source are credited and other Frontiers conditions are complied with.



Localization and function of GABA transporters GAT-1 and GAT-3 in the basal ganglia

Xiao-Tao Jin*, Adriana Galvan, Thomas Wichmann and Yoland Smith

Division of Neuroscience, Yerkes National Primate Research Center and Department of Neurology, Emory University, Atlanta, GA, USA

Edited by:

James M. Tepper, Rutgers – The State University of New Jersey, USA

Reviewed by:

Atsushi Nambu, Graduate University for Advanced Studies, Japan
Hitoshi Kita, The University of Tennessee Health Science Center, USA

*Correspondence:

Xiao-Tao Jin, Division of Neuroscience, Yerkes National Primate Research Center and Department of Neurology, Emory University, 954 Gatewood Road NE, Atlanta, GA 30322, USA.
e-mail: jxiaota@emory.edu

GABA transporter type 1 and 3 (GAT-1 and GAT-3, respectively) are the two main subtypes of GATs responsible for the regulation of extracellular GABA levels in the central nervous system. These transporters are widely expressed in neuronal (mainly GAT-1) and glial (mainly GAT-3) elements throughout the brain, but most data obtained so far relate to their role in the regulation of GABA_A receptor-mediated postsynaptic tonic and phasic inhibition in the hippocampus, cerebral cortex and cerebellum. Taking into consideration the key role of GABAergic transmission within basal ganglia networks, and the importance for these systems to be properly balanced to mediate normal basal ganglia function, we analyzed in detail the localization and function of GAT-1 and GAT-3 in the globus pallidus of normal and Parkinsonian animals, in order to further understand the substrate and possible mechanisms by which GABA transporters may regulate basal ganglia outflow, and may become relevant targets for new therapeutic approaches for the treatment of basal ganglia-related disorders. In this review, we describe the general features of GATs in the basal ganglia, and give a detailed account of recent evidence that GAT-1 and GAT-3 regulation can have a major impact on the firing rate and pattern of basal ganglia neurons through pre- and post-synaptic GABA_A- and GABA_B-receptor-mediated effects.

Keywords: GABA transporter, striatum, globus pallidus, substantia nigra, patch clamp recording

INTRODUCTION

GABA is the main neurotransmitter used in the basal ganglia network, and abnormal transmission at specific GABAergic synapses underlies some of the pathophysiological features of various basal ganglia diseases. A tight regulation of GABA homeostasis is essential to mediate normal basal ganglia functions. In this manuscript, we will provide a brief overview of the main characteristics of the different subtypes of GABA transporters in the mammalian CNS, and then discuss some of our recent findings and those from other laboratories about the localization and functions of GABA transporters (GATs) in the basal ganglia. This review does not intend to cover the extensive literature on GATs, but will specifically focus on the distribution and regulatory mechanisms by which these transporters modulate neuronal activity and synaptic transmission in the basal ganglia. Because of the limited amount of data available, this review does not aim at generating integrative concepts about GATs function in the basal ganglia. It is rather focused on the presentation of recent findings that have been gathered about these transporters in specific basal ganglia nuclei, and their potential importance for basal ganglia function and dysfunction. For a more comprehensive account of our current knowledge of GAT function in other brain regions, readers are referred to previous reviews (Borden, 1996; Gadea and Lopez-Colome, 2001; Dalby, 2003; Conti et al., 2004).

GENERAL FEATURES OF GABA TRANSPORTERS

GABA is the main inhibitory neurotransmitter in the mammalian brain. After release from presynaptic terminals, GABA is rapidly removed from the extracellular space by GATs, a regulatory mechanism that terminates inhibitory synaptic transmission (Borden,

1996; Richerson and Wu, 2003), regulates GABA spillover to neighboring synapses (Borden, 1996; Overstreet and Westbrook, 2003), and maintains GABA homeostasis to prevent excessive tonic activation of synaptic and extrasynaptic GABA receptors (Borden, 1996; Semyanov et al., 2004). In addition, the reversal of the GATs function may result in additional GABA release under certain pathological and physiological conditions (Allen et al., 2004; Wu et al., 2007).

GATs CLONING AND PHARMACOLOGY

To date, four different GATs have been described, GAT-1, GAT-2, GAT-3, and the Betain/GABA transporter type 1 (BGT-1). These transporters are members of a large family of 12-transmembrane spanning Na⁺/Cl⁻ coupled transporters (for review, see Borden, 1996). GAT-1 was the first GAT to be cloned (Guastella et al., 1990). The GAT-1 protein sequence in rat (Guastella et al., 1990), mouse (Liu et al., 1993), and human (Nelson et al., 1990) displays a high degree of homology and nearly identical pharmacological properties (Borden, 1996). The GAT-2 and GAT-3, cloned by Borden et al. (1992), display a higher degree of amino acid identity between each other (67% identity), and with the fourth GABA transporter, BGT-1 (68 and 65% identity for GAT-2 and GAT-3, respectively) than with GAT-1 (~52% amino acid identity). The amino acid sequence of GAT-3 in human, rat, and mouse is virtually identical with only a few substitutions (for review, see Borden, 1996). In contrast to other transporters, BGT-1, cloned by Yamauchi et al. (1992), utilizes both GABA and betaine as substrates.

GATs exchange GABA for Na⁺ and Cl⁻. The GABA-transporting function of GATs is particularly dependent on the Na⁺ gradient across the membrane. Although Cl⁻ can significantly enhance the

rate of transport, Cl^- alone does not drive GABA uptake in the absence of Na^+ . The proposed stoichiometry for GAT-1, GAT-2, and GAT-3 is 2 Na^+ :1 Cl^- :1 GABA (Loo et al., 2000; Sacher et al., 2002; Karakossian et al., 2005).

GAT-1 can be pharmacologically isolated from GAT-2, GAT-3, and BGT-1. Various drugs have been identified as highly specific GAT-1 inhibitors (for instance, CI966, SKF 89976A, NO-711, and Tiagabine), while SNAP 5114 is a semiselective blocker of GAT-2 and GAT-3, with a higher affinity for GAT-3 than GAT-2 (IC₅₀ ~5 and 20 μM , respectively). However, because GAT-3 is far more abundant in neurons and glia than GAT-2, SNAP 5114 is commonly used as a GAT-3 blocker in studies of GATs regulation of synaptic transmission in the central nervous system. Microdialysis experiments in rodent hippocampus and thalamus have shown that either local or systemic application of GAT-1 antagonists can increase extracellular GABA concentrations by up to 1.5- to 4-folds the basal levels (Richards and Bowery, 1996; Dalby, 2000). Similarly, application of the GAT-2/GAT-3 blocker, SNAP 5114 (100 μM), increases GABA levels in the thalamus by almost 250%, but has no significant effect on hippocampal GABA concentration (Dalby, 2000).

GATs LOCALIZATION IN THE CNS

The cellular localization of GABA transporters has been studied in the rat brain using both *in situ* hybridization for mRNA (Ratnay and Priestley, 1993; Brecha and Weigmann, 1994; Augood et al., 1995; Durkin et al., 1995; Jursky and Nelson, 1996; Nishimura et al., 1997; Yasumi et al., 1997; Ficková et al., 1999) and immunocytochemistry for transporters protein (Ikegaki et al., 1994; Augood et al., 1995; Minelli et al., 1995; Itouji et al., 1996; Ribak et al., 1996; Conti et al., 1998). The GAT-1 mRNA is expressed throughout the brain, but particularly enriched in the olfactory bulb, basal ganglia, interpeduncular nucleus, cerebellum, and retina (Augood et al., 1995; Durkin et al., 1995; Yasumi et al., 1997). Immunohistochemical studies using antibodies raised against recombinant proteins have shown that GAT-1 is not only expressed in GABAergic neurons, but also in non-GABAergic cells and glia in certain brain regions (for review, see Eulenburg and Gomez, 2010), although their function in these neurons remains poorly understood.

GAT-2 mRNA is weakly expressed throughout the brain, primarily in arachnoid and ependymal cells, and to a much lesser extent, in neurons and astrocytes (Durkin et al., 1995; Conti et al., 1999). GAT-3 mRNA and protein are found predominantly in glial cells (Radian et al., 1990; Ikegaki et al., 1994; Durkin et al., 1995). The strongest GAT-3 expression is found in the glomerular layer of the olfactory bulb, the inner nucleus of the retina, the thalamic paraventricular nucleus, and the globus pallidus (GP; Clark et al., 1992; Ikegaki et al., 1994; Durkin et al., 1995; Minelli et al., 1996). Some of these studies showed that GAT-3 is nearly absent from the neocortex and cerebellar cortex, and very weakly expressed in the hippocampus (Clark et al., 1992; Brecha and Weigmann, 1994; Ikegaki et al., 1994; Durkin et al., 1995), while others provided evidence for significant neocortical expression in rodents (Minelli et al., 1996, 2003; Pow et al., 2005). Finally, low to moderate levels of BGT-1 are expressed in most brain regions (Durkin et al., 1995; Zhou and Ong, 2004).

GATs REGULATION OF SYNAPTIC TRANSMISSION AND PLASTICITY

The effects of GAT-1 modulation on synaptic transmission have been most studied in the CNS. A summary of the main effects of GAT blockade on GABA release and postsynaptic currents in various CNS regions is shown in **Table 1**. GAT-1 inhibitors increase the decay of evoked IPSCs, while not having significant effects on IPSC amplitude in many brain regions (Roepstorff and Lambert, 1992; Thompson and Gähwiler, 1992; Engel et al., 1998; Overstreet and Westbrook, 2003). GAT-1 inhibitors also increase GABA_A receptor-mediated tonic conductances in cerebellar granule cells (Rossi et al., 2003) as well as in granule cells and pyramidal neurons of the hippocampal dentate gyrus (Nusser and Mody, 2002; Semyanov et al., 2003; Sipilä et al., 2007). A recent study also demonstrated that GAT-1 blockade or genetic deletion of GAT-1 specifically impairs long-term potentiation (LTP) induced by theta burst stimulation (Gong et al., 2009) in the CA1 region of mouse hippocampus. While there is compelling evidence that GAT-1 regulates GABAergic transmission in the hippocampus (Thompson and Gähwiler, 1992; Isaacson et al., 1993; Draguhn and Heinemann, 1996; Engel et al., 1998; Nusser and Mody, 2002; Overstreet and Westbrook, 2003; Semyanov et al., 2003), cerebral cortex (Keros and Hablitz, 2005; Bragina et al., 2008; Gonzalez-Burgos et al., 2009), and cerebellum (Rossi et al., 2003), much less is known about the functional role of GAT-1 in the basal ganglia (Rossi et al., 2003; Galvan et al., 2005; Kinney, 2005; Kirmse et al., 2009). Despite its widespread and abundant expression in many brain regions (see Borden, 1996; Eulenburg and Gomez, 2010 for reviews), the role of GAT-3-mediated regulation of GABAergic transmission remains poorly understood compared with GAT-1 functions in most CNS regions, except for the cerebral cortex and some basal ganglia nuclei (**Table 1**).

GAT-1 AND GAT-3 IN THE BASAL GANGLIA

The relative importance of GAT-1 and GAT-3 in the normal and pathological functioning of the basal ganglia, and the possibility that their regulation could be used to achieve beneficial therapeutic responses in basal ganglia disorders remain largely unexplored. In the following sections, we describe the current knowledge of the localization and function of GAT-1 and GAT-3 in various basal ganglia nuclei, and critically discuss their potential relevance as targets for drug therapies of basal ganglia disorders, such as Parkinson's disease.

STRIATUM

GAT-1 AND GAT-3 LOCALIZATION

Most neurons in the striatum, including medium spiny projection neurons and several interneuron subtypes are GABAergic (Kawaguchi et al., 1990). The maintenance of homeostasis in extracellular levels of GABA and GABAergic transmission is, therefore, critical for normal striatal functions. Although the chemical phenotype of most striatal GAT-1-positive cells remains to be determined, it is clear that a significant proportion of the GABAergic neurons in the striatum (including medium spiny neurons and a large proportion of parvalbumin-positive interneurons), express mRNA and immunoreactivity for GAT-1 (Augood et al., 1995; Durkin et al., 1995; Yasumi et al., 1997; Wang and Ong, 1999).

In contrast, the evidence for striatal GAT-3 expression remains controversial. Some of the existing *in situ* hybridization studies have reported negative data (Clark et al., 1992; Durkin et al., 1995),

Table 1 | Summary the effects of GABA transporters blockade on extracellular GABA levels and postsynaptic currents in the CNS

Effects/regions	Hippocampus	Cerebellum	Cortex	Striatum	GP	SNr
Extracellular GABA levels	↑ (Dalby, 2000)	–	–	↑ (Waldeir et al., 1992)	↑ (Galvan et al., 2005) [#]	↑ (Bahena-Trujillo and Arias-Montano, 1999)
eIPSC decay	↑ (Roepstorff and Lambert, 1992; Roepstorff and Lambert, 1994; Thompson and Gahwiler, 1992; Isaacson et al., 1993; Draguhn and Heinemann, 1996; Engel et al., 1998; Overstreet and Westbrook, 2003)	–	↑ (Keros and Hablitz, 2005; Gonzalez-Burgos et al., 2008)	↑ (Kirmse et al., 2008)	↑ (Jin et al., 2011) ↑ (Jin et al., 2011) ^{**}	
eIPSC amplitude	N (Roepstorff and Lambert, 1994; (4) Thompson and Gahwiler, 1992; (5) Isaacson et al., 1993; (6) Draguhn and Heinemann, 1996; (7) Engel et al., 1998; (8) Overstreet and Westbrook, 2003; Lindsly and Frazier, 2010) ↓ (Roepstorff and Lambert, 1992; Overstreet et al., 2000; Safiulina et al., 2009)	–	↓ (Keros and Hablitz, 2005) ↑ (Kinney, 2005) ^{**}	↓ (Kirmse et al., 2008)	N (Jin et al., 2011) ↑ (Jin et al., 2011) ^{**}	
sIPSC decay	N (Jensen et al., 2003) [*]	↑ (Chiu et al., 2005)	↑ (Kinney, 2005) ^{**}	–	↑ (Chen et al., 2003) N (Jin et al., 2011)	
sIPSC amplitude	N (Jensen et al., 2003) [*]	N (Chiu et al., 2005)	↑ (Kinney, 2005) ^{**}	–	N (Chen et al., 2003) ↑ (Jin et al., 2011) ↑ (Jin et al., 2011) ^{**}	
sIPSC frequency	N (Jensen et al., 2003) [*]	–	↑ (Kinney, 2005) ^{**}	–	↓ (Chen et al., 2003) ↑ (Jin et al., 2011) ↑ (Jin et al., 2011) ^{**}	
mIPSC decay	N (Overstreet et al., 2000)	–	–	N (Kirmse et al., 2008)	N (Jin et al., 2011) N (Jin et al., 2011) ^{**}	
mIPSCs amplitude	↓ (Overstreet et al., 2000)	–	–	↓ (Kirmse et al., 2008)	N (Jin et al., 2011) N (Jin et al., 2011) ^{**}	
mIPSC frequency	N (Jensen et al., 2003) [*]	–	–	↓ (Kirmse et al., 2008)	N (Jin et al., 2011) N (Jin et al., 2011) ^{**}	
Tonic currents	↑ (Jensen et al., 2003) [*] ; Nusser and Mody, 2001; Semyanov et al., 2003; Sipla et al., 2007)	↑ (Chiu et al., 2005; Rossi et al., 2003)	↑ (Keros and Hablitz, 2005) ⁺	↑ (Kirmse et al., 2008)	↑ (Jin et al., 2011) ↑ (Jin et al., 2011) ^{**}	
eEPSC amplitude	–	↓ (Gonzalez-Burgos et al., 2008)	–	–	↓ (Jin et al., 2009) ↓ (Jin et al., 2009) ^{**}	

No Symbol (GAT-1 blockers) *GAT-1-deficient mice, # monkeys, ** GAT-3 blocker, ↑ increase, ↓ decrease, N (no change), – (data not available), + GAT-1 plus GAT-3 blockers.

Abbreviations: GP, globus pallidus; Snr, substantia nigra pars reticulata; eIPSC, evoked inhibitory postsynaptic current; sIPSC, spontaneous inhibitory postsynaptic current; mIPSC, miniature inhibitory postsynaptic current.

while others using similar methods or polymerase chain reaction (rt-PCR) techniques have demonstrated a significant level of striatal GAT-3 mRNA expression in the rat caudate-putamen (Yasumi et al., 1997; Ficková et al., 1999). GAT-3 immunoreactivity was also demonstrated in the monkey striatum (Ng et al., 2000). The cellular and chemical phenotypes of GAT-3-positive striatal elements remain poorly characterized in both primates and non-primates.

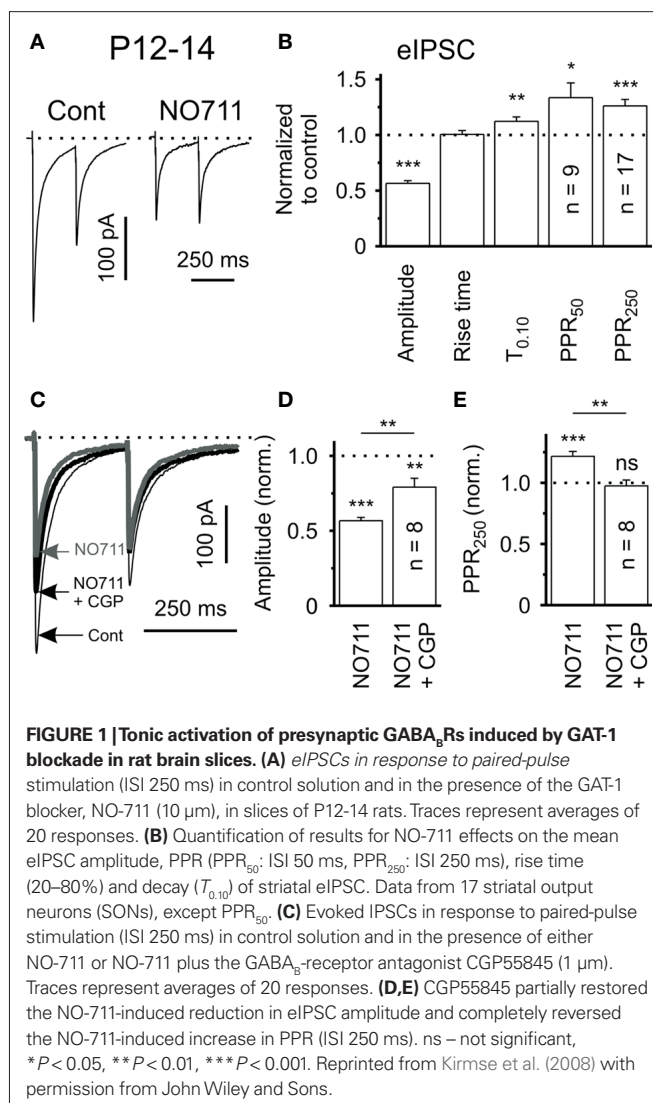
FUNCTIONAL ROLE OF STRIATAL GAT-1

Systemic or local application of the selective GAT-1 inhibitor, SKF 89976A, doubles the extracellular concentration of GABA in the rat striatum (Waldmeier et al., 1992). Consistent with this finding, GAT-1 blockade induces GABA_A receptor-mediated tonic inhibition of striatal neurons (Kirmse et al., 2008), similar to previous reports in the hippocampus (Jensen et al., 2003; Semyanov et al., 2003; Scimemi et al., 2005) and cerebellar Purkinje cells (Chiu et al., 2005). Electrophysiologic brain slice recording studies have demonstrated that bath application of the GAT-1 inhibitors NO-711 prolongs the decay time of IPSCs evoked locally in striatum (Kirmse et al., 2008) and decreases the amplitude of eIPSCs produced by intrastriatal stimulation. The latter effect is most likely caused by a presynaptic mechanism because it was associated with a significant increase of the paired-pulse facilitation ratio (PPR; Figures 1A,B). Interestingly, coapplication of NO-711 and the GABA_B-receptor antagonist CGP55845 only partly restored the GAT-1 blockade-mediated effects on the amplitude of eIPSCs but reduced the PPR to control levels (Figures 1C–E), suggesting that the effects of GAT-1 blockade upon eIPSCs are partially, but not fully mediated by GABA_B receptor-dependent mechanisms (Kirmse et al., 2008). This observation was recently extended to the hippocampus (Safiulina and Cherubini, 2009; Lindsly and Fraxier, 2010). Other mechanisms, including postsynaptic shunting and GABA_A-receptor desensitization due to a persistent activation of GABA_A receptors by high ambient GABA concentration in the presence of NO-711 could also contribute to these effects (Overstreet et al., 2000; Keros and Hablitz, 2005; Kirmse et al., 2008).

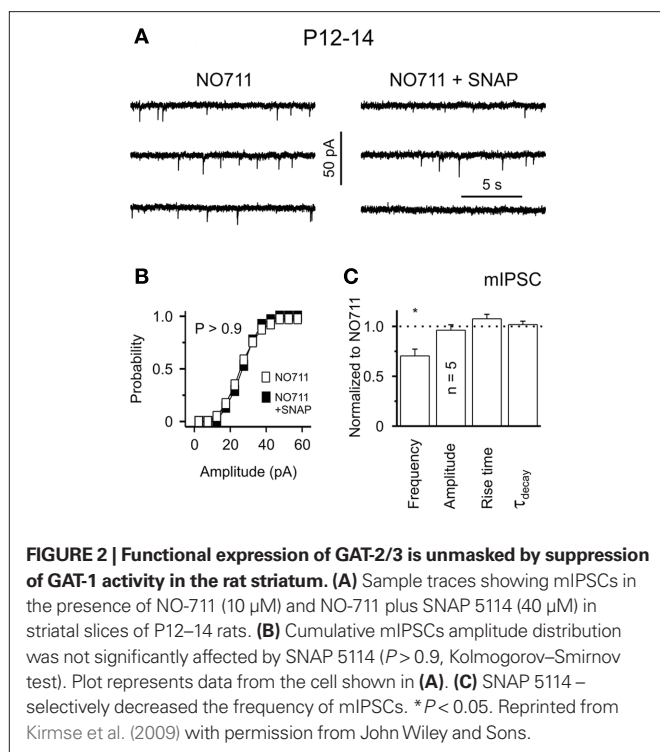
GATs, acting in reverse direction, also contribute to the action potential-independent release of GABA in the rat striatum (Bernath and Zigmond, 1989; Del Arco et al., 1998; Schoffeleer et al., 2000). For instance, microdialysis studies have shown that nipecotic acid, a non-selective GAT blocker, attenuates the amphetamine-induced increase in extracellular concentration of GABA in the striatum of freely moving rats, using a calcium-free microdialysis medium (Del Arco et al., 1998). Nipecotic acid also attenuates glutamate NMDA and dopamine D1-like receptor-mediated [³H]-GABA release from striatal slice and cultured striatal neurons in the presence of the sodium channel blocker tetrodotoxin (Schoffeleer et al., 2000). These results demonstrate that the release of GABA induced by amphetamine or activation of D1-like or NMDA receptors involves a GAT mechanism. This reversal of GAT function may play a role in the behaviorally activating effects of psychostimulant drugs (Schoffeleer et al., 2000).

FUNCTIONAL ROLE OF STRIATAL GAT-3

Although the anatomical evidence for striatal GAT-3 expression is controversial compared with GAT-1 (Clark et al., 1992; Ficková et al., 1999; Ng et al., 2000), there is functional evidence for an active



role of GAT-3 in the rat striatum (Kirmse et al., 2009). Despite the fact that the application of SNAP 5114 alone, a semiselective GAT-3 inhibitor, has no effect on striatal GABAergic transmission, and does not affect GABA_A receptor-mediated tonic currents in striatal projection neurons (Kirmse et al., 2009), the coapplication of SNAP 5114 with the GAT-1 inhibitor NO-711 (10 μM) was shown to reduce the frequency of miniature IPSCs (mIPSCs) without affecting their amplitude or kinetic in striatal neurons (Figures 2A–C). As shown for GAT-1, GAT-3 blockade reduces the mean amplitude of eIPSCs through GABA_B receptor-mediated presynaptic effects in the rat striatum (Kirmse et al., 2009). As the functional effects of GAT-3 blockade on GABAergic transmission may be masked by concomitant GAT-1-mediated effects, it is possible that GAT-3-mediated GABA uptake comes into play only under specific physiological or pathological conditions that result in increases in neuronal activity and GABA release beyond normal levels in the striatum (Kirmse et al., 2009). In other brain regions, it has been shown that that GAT-1 and GAT-3 are largely segregated in pre-terminal neuronal elements and glia, respectively, thus, it



is possible that these transporters might play complementary and synergistic roles towards the regulation of GABAergic transmission in the striatum.

GLOBUS PALLIDUS

GAT-1 AND GAT-3 LOCALIZATION

The rat GP expresses strong mRNA for both GAT-1 and GAT-3 (Durkin et al., 1995; Yasumi et al., 1997). Consistent with these findings, our studies have demonstrated strong GAT-1 and GAT-3 immunoreactivity in the rat and monkey GP (Galvan et al., 2005, 2010; Jin et al., 2009, 2011; **Figure 3**). At the electron microscopic level, GAT-1 is largely expressed in small unmyelinated axons in the rat GP (**Figure 3**), and in both unmyelinated axons and glial processes in the external and internal segments of the GP (GPe and GPi, respectively) in the monkey (**Figure 3**). The pattern of GAT-3 immunoreactivity in the rat and monkey pallidum is strikingly different from that of GAT-1, being almost exclusively expressed in glial cell processes which, in some cases (**Figure 3**) are closely apposed to putative GABAergic terminals forming symmetric synapses or wrapped around axo-dendritic complexes consisting of numerous unlabeled terminals and dendrites of pallidal neurons (**Figure 3**). Despite significant alterations in GAT function, there is no significant change in the general localization pattern of GAT-1 and GAT-3 in the GPe and GPi of MPTP-treated Parkinsonian monkeys (**Figure 3** and below; Galvan et al., 2010).

FUNCTIONAL ROLE OF GAT-1 IN THE GLOBUS PALLIDUS

In normal monkeys, local intrapallidal administration of the GAT-1 antagonist (SKF 89976A) significantly increases the ambient GABA level in GPe, as measured by microdialysis (**Figure 4A**), and reduces the firing rate of GPe and GPi neurons (**Figures 4B1,B2**; Galvan et al.,

2005). We found that the inhibitory effects of GATs blockade on GPI firing are strongly decreased in monkeys rendered Parkinsonians by systemic treatment with the dopaminergic neurotoxin 1-methyl-4-phenyl-1,2,3,6-tetrahydropyridine (MPTP), while the effects on GPe discharge rates remain unaffected (Galvan et al., 2010). In line with our monkey data, systemic administration of tiagabine, a GAT-1 antagonist, increases extracellular levels of GABA by up to threefold in the rat GP (Fink-Jensen et al., 1992). Furthermore, bath application of tiagabine has several significant effects when used in rat brain slice recording experiments: (1) GAT-1 inhibition prolongs the decay time of IPSCs evoked by striatal stimulation, without affecting their amplitude (**Figures 5A,B**). Similar observations have been made in many brain regions, suggesting that it represents a general GAT-1 function in the CNS (Roepstorff and Lambert, 1992; Thompson and Gähwiler, 1992; Engel et al., 1998; Overstreet and Westbrook, 2003; for reviews, see Borden, 1996; Richerson and Wu, 2003). (2) GAT-1 blockade induces GABA_A receptor-mediated tonic currents in rat GP neurons (Jin et al., 2011), another general role reminiscent of GAT-1-mediated effects in other brain regions (for reviews, see Borden, 1996; Richerson and Wu, 2003; Eulenburg and Gomez, 2010). (3) The effects of GAT-1 blockade on spontaneous and miniature IPSCs in rat GP are controversial. On one hand, application of tiagabine prolongs the decay kinetics and reduces the frequency of spontaneous and miniature IPSCs, in part through activation of presynaptic GABA_B autoreceptors (Chen and Yung, 2003). However, we found that the frequency and amplitude of spontaneous, but not miniature, IPSCs is increased following GAT-1 blockade (Jin et al., 2011). The sources of the discrepancy between these different sets of data remain to be established. (4) GAT-1 blockade reduces the frequency, but not the amplitude of mEPSCs (**Figures 5E,G**), most likely through GABA_B receptor-mediated presynaptic inhibitory effects upon glutamatergic transmission (Jin and Smith, 2009). Thus, together with data from the striatum, these findings indicate that GAT-1 regulates striatal and pallidal activity through modulation of persistent synaptic GABA_A receptor-mediated currents (IPSCs), extrasynaptic GABA_A receptor-mediated tonic currents, and presynaptic GABA_B receptors in both GABAergic and glutamatergic terminals (Galvan et al., 2006).

The behavioral effects of GAT-1 blockade in the GP are poorly characterized. Apart from evidence that the unilateral administration of tiagabine in the rat GP induces ipsilateral rotations in rats (Chen and Yung, 2003), very little is known about the influence of GATs on behavior. Given the prominent role of altered GABAergic transmission in parkinsonism (Galvan and Wichmann, 2007), it would be particularly interesting to examine the potential antiparkinsonian effects of GATs. Taking into consideration the physiological effects of GAT-1 blockade on pallidal activity and the proposed pathophysiology of basal ganglia networks in parkinsonism (DeLong, 1990), one could predict that GAT-1 blockade in GPe could induce or exacerbate parkinsonism, due to the increased GABAergic transmission along the indirect pathway, while GAT-1 blockade in GPi could alleviate parkinsonism through increased inhibition of the overactive basal ganglia pallidal outflow to the thalamus and brainstem (DeLong, 1990). However, because we found that the effects of GAT-1 blockers in GPi of Parkinsonian monkeys are altered from normal (Galvan et al., 2010), these speculations are, at best, incomplete with the available data.

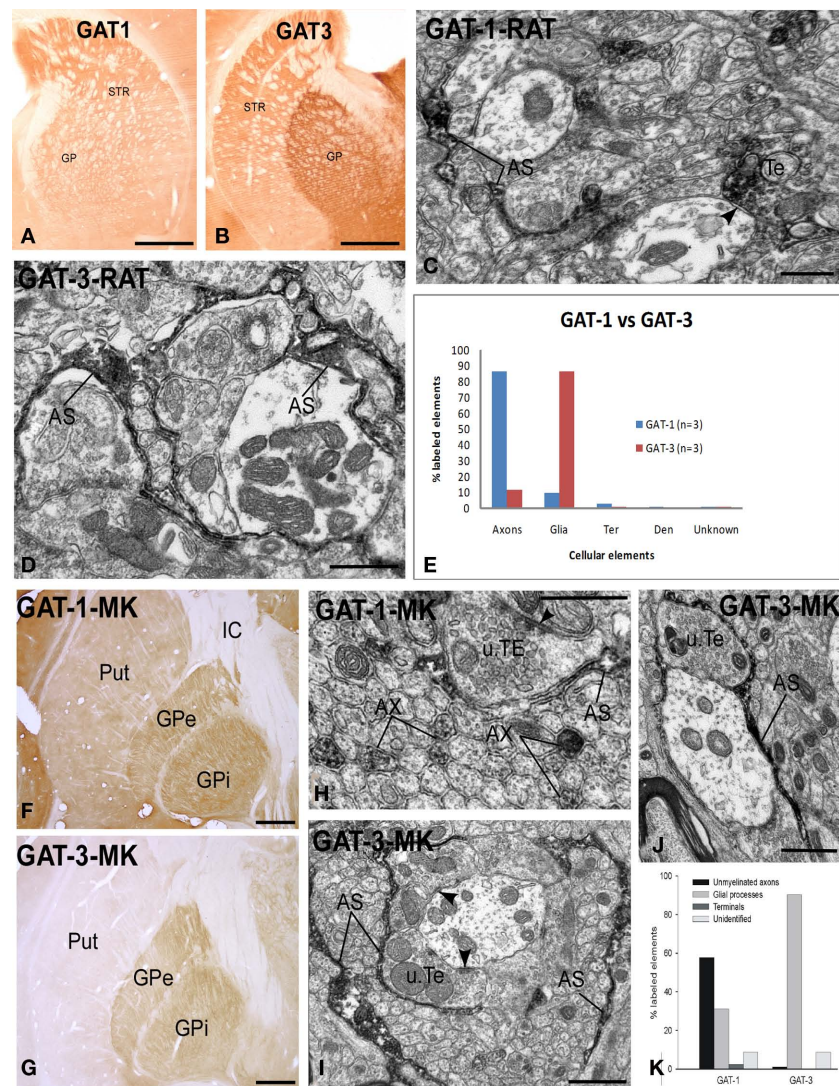


FIGURE 3 | Light and electron micrographs of GAT-1 and GAT-3-immunoreactive elements in the rat and monkey globus pallidus.

(A,B) Light micrographs of GAT-1 and GAT-3 labeling in the rat striatum (STR) and globus pallidus (GP). (C) GAT-1-immunoreactive axon terminal (Te) and astrocytic process (AS) in the rat GP. Note that the labeled terminal forms a symmetric synapse (arrowhead) with an unlabeled dendrite. (D) GAT-3-positive astrocytic processes in close contact with unlabeled terminals and dendrites in the rat GP. (E) Quantification of the percentage of GAT-1- and GAT-3-labeled elements in the rat GP. Note that GAT-1 is predominantly found in unmyelinated axons, whereas GAT-3 is mainly expressed in glial processes. A total of three rats were used in these studies (see Jin et al., 2009, 2011 for details). (F,G) GAT-1 and GAT-3

immunoreactivity in the monkey putamen (Put) and globus pallidus (external and internal segments, GPe, GPi). (H) GAT-1-immunoreactive unmyelinated axons (AX) and astrocytic processes (AS) in the monkey GPe. Note that the labeled AS is in close contact with an unlabeled terminal (u.Te) that forms an axo-dendritic symmetric synapse [arrowhead; (I,J)] GAT-3-positive astrocytes in the monkey GPe (I) and GPi (J). Note the close association between the immunoreactive AS processes and unlabeled axon terminals forming symmetric synapses [arrowheads in (I)]. (K) Quantitative distribution of GAT-1 and GAT-3 across different neuronal and glial elements in the monkey GPe and GPi (see Galvan et al., 2005, 2010 for more details). Scale bars: (A,B,F,G): 1 mm; (C,D,H,I,J): 1 μ m.

FUNCTIONAL ROLE OF GAT-3 IN THE GLOBUS PALLIDUS

The strong expression of GAT-3 in the pallidum of monkeys and rats suggests that this transporter may play an important role in the clearance of extracellular GABA. Supporting this contention, local *in vivo* blockade of GAT-3 increases pallidal GABA levels (Figure 4A), and inhibits the firing rate of pallidal neurons in monkeys (Figures 4C1,C2). In rat brain slice recording studies, GAT-3 blockade increases the decay and amplitude of

evoked IPSCs after striatal stimulation (Figures 5C,D), increases the frequency and amplitude of spontaneous IPSCs, and induces GABA_A receptor-mediated tonic currents in GP neurons (Jin et al., 2011). The mechanisms by which GAT-3, but not GAT-1, blockade increases the amplitude of evoked IPSCs are unknown. One hypothesis put forward in our recent study (Jin et al., 2011) relates to the fact that GAT-3 blockade may result in the activation of a large pool of striatal GABAergic projections neurons and

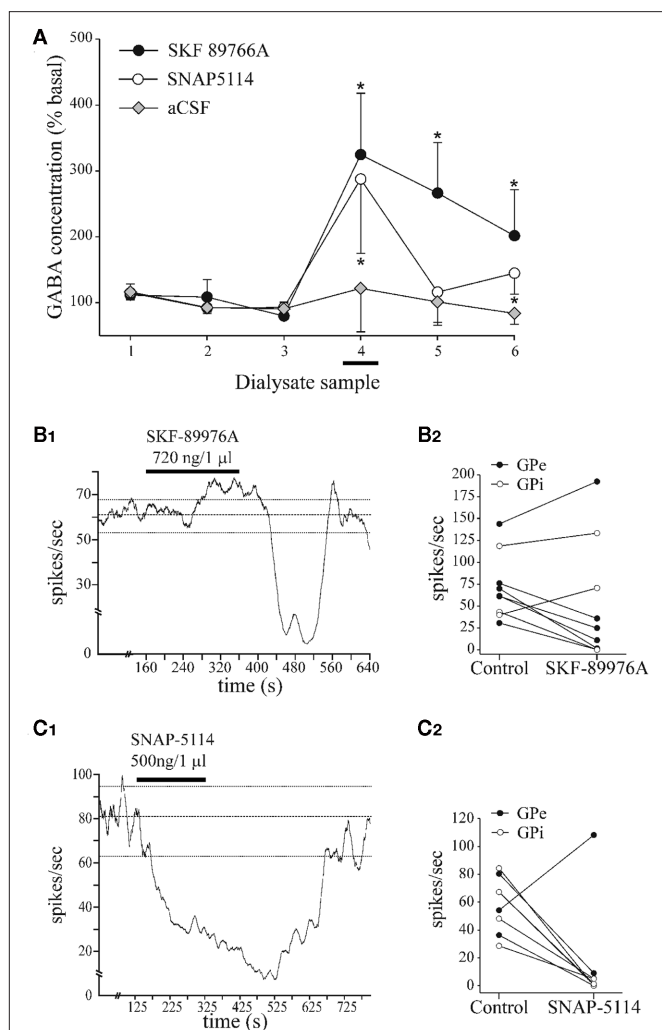


FIGURE 4 | Effects of SKF 89976A and SNAP 5114 on GABA levels in GPe and pallidal discharge rate in monkeys. (A) Dialysate samples were collected every 10 min. SKF 89976A or SNAP 5114 were administered during sample 4 (horizontal bar). Data area means \pm SD from three experiments for each treatment in a single monkey. Difference from ACSF experiments (Mann–Whitney U test): $*P < 0.05$. **(B1)** Example of effect of SKF 89976A on discharge rate of a GPe cell. **(B2)** Discharge rate of GPe and GPI cells during baseline period and at the point of maximal effect of SKF 89976A. **(C1)** The discharge rate of this GPe cell is inhibited after administration of the GAT-3 blocker, SNAP 5114. **(C2)** The discharge rate of GPe and GPI cells during baseline period and at the point of maximal effect of SNAP 5114 injection. In **(B1,C1)**, horizontal bars indicate duration of drug infusions. Dashed lines represent mean discharge rate \pm 2 SD. For more details see Galvan et al. (2005).

interneurons which, under specific conditions, can depolarize other projection neurons, thereby increase GABA release in the GP (Bracci and Panzeri, 2006; Ade et al., 2008).

GAT-3 blockade also reduces glutamatergic transmission, most likely from the subthalamic nucleus, through presynaptic GABA_B-receptor activation (Figures 5F,H). In contrast with the striatum where the effects of GAT-3 blockade alone are fully masked by GAT-1 (Kirmse et al., 2009), the blockade of GAT-3, alone or in the presence of a GAT-1 blocker, produces significant effects on both

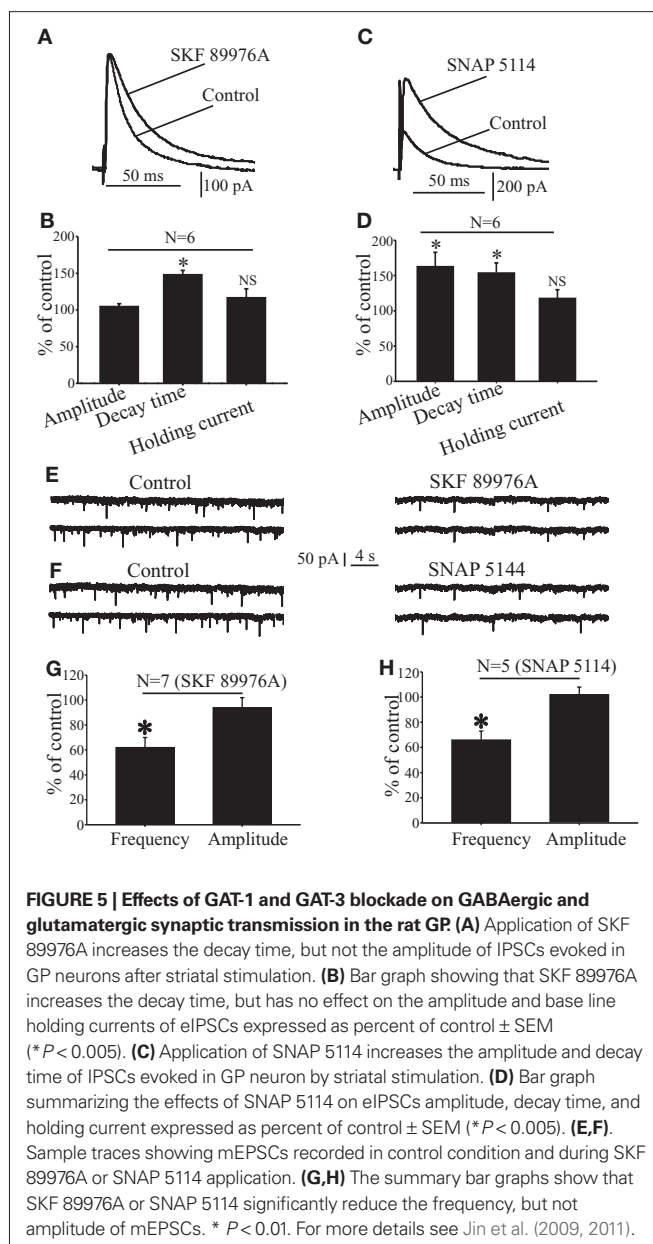


FIGURE 5 | Effects of GAT-1 and GAT-3 blockade on GABAergic and glutamatergic synaptic transmission in the rat GP. (A) Application of SKF 89976A increases the decay time, but not the amplitude of IPSCs evoked in GP neurons after striatal stimulation. **(B)** Bar graph showing that SKF 89976A increases the decay time, but has no effect on the amplitude and base line holding currents of eIPSCs expressed as percent of control \pm SEM ($*P < 0.005$). **(C)** Application of SNAP 5114 increases the amplitude and decay time of IPSCs evoked in GP neuron by striatal stimulation. **(D)** Bar graph summarizing the effects of SNAP 5114 on eIPSCs amplitude, decay time, and holding current expressed as percent of control \pm SEM ($*P < 0.005$). **(E,F)** Sample traces showing mEPSCs recorded in control condition and during SKF 89976A or SNAP 5114 application. **(G,H)** The summary bar graphs show that SKF 89976A or SNAP 5114 significantly reduce the frequency, but not amplitude of mEPSCs. $*P < 0.01$. For more details see Jin et al. (2009, 2011).

GABAergic and glutamatergic transmission in the rat GP (Jin et al., 2009, 2011). These differential effects are consistent with localization studies showing that GAT-3 expression in the striatum is comparatively light, compared with the very strong glial expression in the GP (Figure 3; Clark et al., 1992; Durkin et al., 1995; Yasumi et al., 1997; Ng et al., 2000; Galvan et al., 2005; Jin et al., 2009, 2011). GAT-1 and GAT-3, thus, represent differential target sites through which GABA reuptake may subserve a complementary regulation of GABAergic and glutamatergic transmission in the pallidum.

SUBTHALAMIC NUCLEUS AND SUBSTANTIA NIGRA

Despite their distinct glutamatergic phenotype, rat and human STN neurons, display intense GAT-1 mRNA expression (Yasumi et al., 1997; Augood et al., 1999). There is also evidence from other

brain regions such as cerebral cortex, inferior colliculus, and the deep cerebellar nuclei, that the number of GAT-1 mRNA-containing cells is much larger than that of GABAergic (GAD₆₇ mRNA-) positive cells (Swan et al., 1994; Yasumi et al., 1997), suggesting that GAT-1 expression extends beyond GABAergic neurons in these brain regions (Yasumi et al., 1997). The functional significance of GATs in non-GABAergic neurons remains unknown (Augood et al., 1999). However, it is interesting to note that an ongoing gene transfection clinical trial in PD aims at changing the phenotype of subthalamic neurons into GABAergic cells in order to reduce the overactive glutamatergic outflow from the subthalamic nucleus (Lewitt et al., 2011). The expression of GAT-1 into subthalamic terminals may increase the likelihood of success of this approach. As in other basal ganglia nuclei, GAT-3 immunoreactivity is expressed in astrocytic processes throughout the monkey STN (Ng et al., 2000).

The effects of GAT activity on the neuronal activity in the STN are unknown. Because of the preponderance of GABAergic pallidal terminals in the STN, and because of the fact that extrasynaptic GABA-B receptors appear to play important roles in the modulation of burst firing and the pallidum subthalamic “pacemaker” system (Plenz and Kitai, 1999; Bevan et al., 2002), a better understanding of the mechanisms by which GATs modulate GABAergic STN activity is clearly warranted (for review, see Bevan et al., 2007).

Both GAT-1 and GAT-3 mRNAs are moderately expressed in the rat substantia nigra as a whole. Surprisingly, GAT-1 expression is stronger in dopaminergic pars compacta (SNc) neurons than in the GABAergic pars reticulata (SNr) cells (Durkin et al., 1995; Yasumi et al., 1997), serving as another possible example of GAT-1-mediated function in non-GABAergic neurons. GAT-3 immunoreactivity is also strongly expressed in the monkey SN, where it appears to be preferentially associated with astrocytes (Ng et al., 2000). GAT-1 inhibition significantly reduces [³H] GABA uptake in synaptosomes prepared from the rat SNr (Bahena-Trujillo and Arias-Montano, 1999), and significantly increases extracellular GABA levels in the rat substantia nigra (Fink-Jensen et al., 1992). However, the overall regulatory functions of GATs on synaptic transmission in the SN remain unexplored.

GATs AND PARKINSON'S DISEASE

The data discussed in this review highlight the fact that GAT-1 and GAT-3 represent different target sites through which GABA reuptake may regulate GABAergic and glutamatergic transmission in the

basal ganglia. Although still poorly understood, recent *in vitro* and *in vivo* data from our laboratory and others have demonstrated that GAT-1 and GAT-3 are strongly expressed in the GP, and that their blockade significantly impacts the activity of pallidal neurons under normal and Parkinsonian conditions, by increasing GABA levels and subsequent overactivation of GABA_A- and GABA_B-receptors (Galvan et al., 2005, 2010; Jin et al., 2009, 2011).

Our recent data from primate experiments demonstrate that the impact of GAT-1 and GAT-3 blockade upon neuronal activity is reduced in the GPi of Parkinsonian animals compared with the normal state, despite the fact that the overall pattern of GAT distribution does not change (Galvan et al., 2010). The possible use of drugs that regulate GAT function to treat patients with Parkinson's disease remains speculative. The essential need of tightly regulated GABA homeostasis for normal brain functions reduces the likelihood that systemic administration of GAT blockers could be done without the risk of significant side effects, although such an approach has shown some therapeutic benefits in patients with epilepsy and anxiety (Gadea and Lopez-Colome, 2001; Dalby, 2003; Sarup et al., 2003; Conti et al., 2004; Schwartz and Nihalani, 2006).

Recent evidence suggests that the interaction of GATs with other receptor systems may provide an alternative strategy for the development of Parkinson's disease therapy. For instance, a recent study has demonstrated that adenosine inhibits GAT-1-mediated GABA uptake in the rat GP (Gonzalez et al., 2006). This finding, combined with the fact that A2A-receptor antagonists have significant antiparkinsonian effects (Kanda et al., 2000; Chase et al., 2003), raise the possibility that the antiparkinsonian effects of A2A-receptor antagonists are partly due to presynaptic modulation of GABA release at striatopallidal synapses through disinhibition of GAT-1 function. GABA uptake is also modulated by activation of cannabinoid CB1 receptors in the rat GP (Venderova et al., 2005), providing another mechanism that could be used to regulate the overactive GABAergic striatopallidal transmission in Parkinson's disease (Romero et al., 2002; Brotchie, 2003). These mechanisms of indirect modulation of GAT activity may represent a more promising therapeutic strategy in the treatment of Parkinson's disease than use of primary GAT blockers (for review, see Conti et al., 2004).

ACKNOWLEDGMENTS

This research was supported by NIH grant RO1 NS 0432937 and the Yerkes Primate Center NIH base Grant (RR-00165). Thanks to Jean-Francois Pare and Xing Hu for technical assistance.

REFERENCES

- Ade, K. K., Janssen, M. J., Ortinski, P. I., and Vivini, S. (2008). Differential tonic GABA conductances in striatal medium spiny neurons. *J. Neurosci.* 28, 1185–1197.
- Allen, N. J., Karadottir, R., and Attwell, D. (2004). Reversal or reduction of glutamate and GABA transport in CNS pathology and therapy. *Eur. J. Physiol.* 449, 132–142.
- Augood, S. J., Herbison, A. E., and Emson, P. C. (1995). Localization of GAT-1 GABA transporter mRNA in rat striatum: cellular coexpression with GAD67 mRNA, GAD67 immunoreactivity and parvalbumin mRNA. *J. Neurosci.* 15, 865–874.
- Augood, S. J., Waldvogel, H. J., Munkle, M. C., Faull, R. L. M., and Emson, P. C. (1999). Localization of calcium-binding proteins and GABA transporter (GAT-1) messenger RNA in the human subthalamic nucleus. *Neuroscience* 88, 521–534.
- Bahena-Trujillo, R., and Arias-Montano, J. A. (1999). [³H] gamma-aminobutyric acid transport in rat substantia nigra pars reticulata synaptosomes: pharmacological characterization and phorbol ester-induced inhibition. *Neurosci. Lett.* 274, 119–122.
- Bernath, S., and Zigmond, M. J. (1989). Dopamine may influence striatal GABA release via three separate mechanisms. *Brain Res.* 476, 373–376.
- Bevan, M. D., Hallworth, N. E., and Baufreton, J. (2007). GABAergic control of the subthalamic nucleus. *Prog. Brain Res.* 160, 173–188.
- Bevan, M. D., Magill, P. J., Terman, D., Bolam, J. P., and Wilson, C. J. (2002). Move to the rhythm: oscillations in the subthalamic nucleus-external globus pallidus network. *Trends Neurosci.* 25, 525–531.
- Borden, L. A. (1996). GABA transporter heterogeneity: pharmacology and cellular localization. *Neurochem. Int.* 29, 335–356.
- Borden, L. A., Smith, K. E., Hartig, P. R., Branchek, T. A., and Weinshank, R. L. (1992). Molecular heterogeneity of the gamma-aminobutyric acid (GABA) transport system. *J. Biol. Chem.* 267, 21098–21104.
- Bracci, E., and Panzeri, S. (2006). Excitatory GABAergic effects in striatal projection neurons. *J. Neurophysiol.* 95, 1285–1290.
- Bragina, L., Marchionni, I., Omrani, A., Cozzi, A., Pellegrini-Giampietro, D.

- E., Cherubini, E., and Conti, F. (2008). GAT-1 regulates both tonic and phasic GABAA receptor-mediated inhibition in the cerebral cortex. *J. Neurochem.* 105, 1781–1793.
- Brecha, N. C., and Weigmann, C. (1994). Expression of GAT-1, a high-affinity gamma-aminobutyric acid plasma membrane transporter in the rat retina. *J. Comp. Neurol.* 345, 602–611.
- Brothie, J. M. (2003). CB1 cannabinoid receptor signalling in Parkinson's disease. *Curr. Opin. Pharmacol.* 3, 54–61.
- Chase, T. N., Bibbiani, F., Bara-Jimenez, W., Dimitrova, T., and Oh-Lee, J. D. (2003). Translating A2A antagonist KW6002 from animal models to Parkinsonian patients. *Neurology* 61, S107–S111.
- Chen, L., and Yung, W. H. (2003). Effects of the GABA-uptake inhibitor tiagabine in rat globus pallidus. *Exp. Brain Res.* 152, 263–269.
- Chiu, C. S., Brickley, S., Jensen, K., Spathwell, A., McKinney, S., Candy, S. C., Mody, I., and Laster, H. A. (2005). GABA transporter deficiency causes tremor, ataxia, nervousness, and increased GABA induced tonic conductance in cerebellum. *J. Neurosci.* 25, 3234–3245.
- Clark, J. A., Deutch, A. Y., Gallipoli, P. Z., and Amara, S. G. (1992). Functional expression and CAN distribution of a β -alanine-sensitive neuronal GABA transporter. *Neuron* 9, 337–348.
- Conti, F., Melone, M., De Biasi, S., Minelli, A., Brecha, N. C., and Ducati, A. (1998). Neuronal and glial localization of GAT-1, a high-affinity gamma-aminobutyric acid plasma membrane transporter, in human cerebral cortex: with a note on its distribution in monkey cortex. *J. Comp. Neurol.* 396, 51–63.
- Conti, F., Minelli, A., and Melone, M. (2004). GABA transporters in the mammalian cerebral cortex: localization, development and pathological implications. *Brain Res. Rev.* 45, 196–212.
- Conti, F., Zuccarello, L. V., Barbaresi, P., Minelli, A., Brecha, N. C., and Molone, M. (1999). Neuronal, glial, and epithelial localization of gamma-aminobutyric acid transporter 2, a high-affinity gamma-aminobutyric acid plasma membrane transporter, in the cerebral cortex and neighboring structures. *J. Comp. Neurol.* 409, 482–494.
- Dalby, N. O. (2000). GABA-level increasing and anticonvulsant effects of three different GABA uptake inhibitors. *Neuropharmacology* 39, 2399–2407.
- Dalby, N. O. (2003). Inhibition of gamma-aminobutyric acid uptake: anatomy, physiology and effects against epileptic seizures. *Eur. J. Pharmacol.* 479, 127–137.
- Del Arco, A., Castaneda, T. R., and Mora, F. (1998). Amphetamine releases GABA in the striatum of the freely moving rat: involvement of calcium and high affinity transporter mechanisms. *Neuropharmacology* 37, 199–205.
- DeLong, M. R. (1990). Primate models of movement disorders of basal ganglia origin. *Trends Neurosci.* 13, 281–285.
- Draguhn, A., and Heinemann, U. (1996). Different mechanisms regulate IPSC kinetics in early postnatal and juvenile hippocampal granule cells. *J. Neurophysiol.* 76, 3983–3993.
- Durkin, M. M., Smith, K. E., Borden, L. A., Weinshank, R. L., Branchek, T. A., and Gustafson, E. L. (1995). Localization of messenger RNAs encoding three GABA transporters in rat brain: an in situ hybridization study. *Brain Res. Mol. Brain Res.* 33, 7–21.
- Engel, D., Schmitz, D., Gloveli, T., Frahm, C., Heinemann, U., and Draguhn, A. (1998). Laminar difference in GABA uptake and GAT-1 expression in rat CA1. *J. Physiol.* 512, 643–649.
- Eulenburg, V., and Gomez, J. (2010). Neurotransmitter transporters expressed in glial cells as regulators of synapse function. *Brain Res. Rev.* 63, 103–112.
- Ficková, M., Dahmen, N., Fehr, C., and Hiemke, C. (1999). Quantitation of GABA transporter 3 (GAT3) mRNA in rat brain by competitive RT-PCR. *Brain Res. Protoc.* 4, 341–350.
- Fink-Jensen, A., Suzdak, P. D., Swedberg, M. D. B., Judge, M. E., Hansen, L., and Nielsen, P. G. (1992). The γ -aminobutyric acid (GABA) uptake inhibitor, tiagabine, increases extracellular brain levels of GABA in awake rats. *Eur. J. Pharmacol.* 220, 197–201.
- Gadea, A., and Lopez-Colome, A. M. (2001). Glial transporters for glutamate, glycine, and GABA: GABA transporters. *J. Neurosci. Res.* 63, 461–468.
- Galvan, A., Hu, X., Smith, Y., and Wichmann, T. (2010). Localization and function of GABA transporters in the globus pallidus of Parkinsonian monkeys. *Exp. Neurol.* 223, 505–515.
- Galvan, A., Kuwajima, M., and Smith, Y. (2006). Glutamate and GABA receptors and transporters in the basal ganglia: what does their subsynaptic localization reveal about their function? *Neuroscience* 143, 351–375.
- Galvan, A., Villalba, R. M., West, S. M., Maidment, N. T., Ackerson, L. C., Smith, Y., and Wichmann, T. (2005). GABAergic modulation of the activity of globus pallidus neurons in primates: in vivo analysis of the functions of GABA receptors and GABA transporters. *J. Neurophysiol.* 94, 990–1000.
- Galvan, A., and Wichmann, T. (2007). GABAergic circuits in the basal ganglia and movement disorders. *Prog. Brain Res.* 160, 287–312.
- Gong, N., Li, Y., Cai, G. Q., Niu, R. F., Fang, Q., Wu, K., Chen, Z., Lin, L. N., Xu, L., Fei, J., and Xu, T. L. (2009). GABA transporter-1 activity modulates hippocampal theta oscillation and theta burst stimulation-induced long-term potentiation. *J. Neurosci.* 29, 15836–15845.
- Gonzalez, B., Paz, F., Floran, L., Aceves, J., Erlij, D., and Floran, B. (2006). Adenosine A2A receptor stimulation decrease GAT-1-mediated GABA uptake in the globus pallidus of the rat. *Neuropharmacology* 51, 154–159.
- Gonzalez-Burgos, G., Rotaru, D. C., Zaitsev, A. V., Povysheva, N. V., and Lewis, D. A. (2009). GABA transporter GAT1 prevents spillover at proximal and distal GABA synapses onto primate prefrontal cortex neuron. *J. Neurophysiol.* 101, 533–547.
- Guastella, J., Nelson, N., Nelson, H., Czyzyk, L., Keynan, S., Miedel, M. C., Davidson, N., Lester, H. A., and Kanner, B. I. (1990). Cloning and expression of a rat brain GABA transporter. *Science* 249, 1303–1306.
- Ikegaki, N., Saito, N., Hashima, M., and Tanaka, C. (1994). Production of specific antibodies against GABA transporter subtypes (GAT1, GAT2, GAT3) and their application to immunocytochemistry. *Mol. Brain Res.* 26, 47–54.
- Isaacson, J. S., Solis, J. M., and Nicoll, R. A. (1993). Local and diffuse synaptic actions of GABA in the hippocampus. *Neuron* 10, 165–175.
- Itoji, A., Sakai, N., Tanaka, C., and Saito, N. (1996). Neuronal and glial localization of two GABA transporters (GAT1 and GAT3) in the rat cerebellum. *Mol. Brain Res.* 37, 309–316.
- Jensen, K., Chiu, C. S., Sokolova, I., Lester, H. A., and Mody, I. (2003). GABA transporter-1 (GAT-1)-deficient mice: differential tonic activation of GABAA versus GABAB receptors in the hippocampus. *J. Neurophysiol.* 90, 2690–2701.
- Jin, X.-T., Fare, J.-F., and Smith, Y. (2011). Differential localization and functions of GABA transporters, GAT-1 and GAT-3, in the rat globus pallidus. *Eur. J. Neurosci.* 33, 1504–1518.
- Jin, X.-T., Pare, J.-F., and Smith, Y. (2009). “Blockade of GABA transporter (GAT-1) modulates the GABAergic transmission in the rat globus pallidus,” in *Basal Ganglia IX*, eds H. J. Groenewegen, H. J. Berendse, and P. J. Voorn (New York: Springer Press), 297–307.
- Jin, X.-T., and Smith, Y. (2009). GABA transporters modulate glutamatergic transmission in the rat globus pallidus. *Soc. Neurosci. Abstr.* 134.18.
- Jursky, F., and Nelson, N. (1996). Developmental expression of GABA transporters GAT1 and GAT4 suggests involvement in brain maturation. *J. Neurochem.* 67, 857–867.
- Kanda, T., Jackson, M. J., Smith, L. A., Pearce, R. K., Nakamura, J., Kase, H., Kuwana, Y., and Jenner, P. (2000). Combined use of the adenosine A(2A) antagonist KW-6002 with L-DOPA or with selective D1 or D2 dopamine agonist increases antiparkinsonian activity but not dyskinesia in MPTP-treated monkeys. *Exp. Neurol.* 162, 321–327.
- Karakossian, M. H., Spencer, S. R., Gomez, A. Q., Padilla, O. R., Sacher, A., Loo, D. D., Nelson, N., and Eskandari, S. (2005). Novel properties of a mouse gamma-aminobutyric acid transporter (GAT4). *J. Membr. Biol.* 203, 65–82.
- Kawaguchi, Y., Wilson, C. J., and Emson, P. C. (1990). Projection subtypes of rat neostriatal matrix cells revealed by intracellular injection of biocytin. *J. Neurosci.* 10, 3421–3438.
- Keros, S., and Hablitz, J. J. (2005). Subtype-specific GABA transporter antagonists synergistically modulate phasic and tonic GABAA conductances in rat neocortex. *J. Neurophysiol.* 94, 2073–2085.
- Kinney, G. A. (2005). GAT-3 transporters regulate inhibition in the neocortex. *J. Neurophysiol.* 94, 4533–4537.
- Kirmse, K., Dvorzhak, A., Kirischuk, S., and Grantyn, R. (2008). GABA transporter 1 tunes GABAergic synaptic transmission at output neurons of the mouse neostriatum. *J. Physiol.* 586, 5665–5678.
- Kirmse, K., Kirischuk, S., and Grantyn, R. (2009). Role of GABA transporter 3 in GABAergic synaptic transmission at striatal output neurons. *Synapse* 63, 921–929.
- Lewitt, P. A., Rezaei, A. R., Leehey, M. A., Ojemann, S. G., Flaherty, A. W., Eskandar, E. N., Kostyk, S. K., Thomas, K., Sarkar, A., Siddigui, M. S., Tatter, S. B., Schwab, J. M., Poston, K. L., Henderson, J. M., Kurlan, R. M., Richard, I. H., Van Meter, L., Sapan, C. V., Doring, M. J., Kaplitt, M. G., and Feigin, A. (2011). AAV2-GAD gene therapy for advanced Parkinson's disease: a double-blind, sham-surgery controlled, randomised trial. *Lancet Neurol.* 10, 309–319.
- Lindsley, C., and Fraxier, C. (2010). Two distinct and activity-dependent mechanisms contribute to autoreceptor-mediated inhibition of GABAergic afferents to hilar mossy cells. *J. Physiol.* 588, 2801–2822.
- Liu, Q.-R., Lopez-Cruera, B., Mandiyan, S., Nelson, H., and Nelson, N. (1993). Molecular characterization of four pharmacologically distinct

- y-aminobutyric acid transporters in mouse brain. *J. Biol. Chem.* 268, 2106–2112.
- Loo, D. D., Eskandari, S., Boorer, K. J., Sarkar, H. K., and Wright, E. M. (2000). Role of Cl in electrogenic Na-coupled cotransporters GAT1 and SGLT1. *J. Biol. Chem.* 275, 37414–37422.
- Minelli, A., Barbaresi, P., and Conti, F. (2003). Postnatal development of high-affinity plasma membrane transporters GAT-2 and GAT-3 in the rat cerebral cortex. *Dev. Brain Res.* 142, 7–18.
- Minelli, A., Brecha, N. C., Karschin, C., DeBiasi, S., and Conti, F. (1995). GAT1, a high-affinity GABA plasma membrane transporter, is localized to neurons and astroglia in the cerebral cortex. *J. Neurosci.* 15, 7734–7746.
- Minelli, A., DeBiasi, S., Brecha, N. C., Vitellaro Zuccarello, L., and Conti, F. (1996). GAT-3, a high-affinity GABA plasma membrane transporter, is localized to localized to astrocytic processes, and it is not confined to the vicinity of GABAergic synapses in the cerebral cortex. *J. Neurosci.* 16, 6255–6264.
- Nelson, H., Mandiyan, S., and Nelson, N. (1990). Cloning of the human brain GABA transporter. *FEBS Lett.* 269, 181–184.
- Ng, C. H., Wang, X. S., and Ong, W. Y. (2000). A light and electron microscopic study of the GABA transporter GAT-3 in the monkey basal ganglia and brainstem. *J. Neurocytol.* 29, 595–603.
- Nishimura, M., Sato, K., Mizuno, M., Yoshiya, I., Shimada, S., Saito, N., and Tohyama, M. (1997). Differential expression patterns of GABA transporters (GAT1-3) in the rat olfactory bulb. *Mol. Brain Res.* 45, 268–274.
- Nusser, Z., and Mody, I. (2002). Selective modulation of tonic and phasic inhibitions in dentate gyrus granule cells. *J. Neurophysiol.* 87, 2624–2628.
- Overstreet, L. S., Jones, M. V., and Westbrook, G. L. (2000). Slow desensitization regulates the availability of synaptic GABA(A) receptors. *J. Neurosci.* 20, 7914–7921.
- Overstreet, L. S., and Westbrook, G. L. (2003). Synaptic density regulates independence at unitary inhibitory synapses. *J. Neurosci.* 23, 2618–2626.
- Plenz, D., and Kitai, S. T. (1999). A basal ganglia pacemaker formed by the subthalamic nucleus and external globus pallidus. *Nature* 400, 677–682.
- Pow, D. V., Sullivan, R. K. P., Williams, S. M., Scott, H. L., Dodd, P. R., and Finkelstein, D. (2005). Differential expression of the GABA transporters GAT-1 and GAT-3 in brains of rats, cats, monkeys and humans. *Cell Tissue Res.* 320, 379–392.
- Radian, R., Ottersen, O. P., Storm-Mathisen, J., Castel, M., and Kanner, B. I. (1990). Immunocytochemical localization of the GABA transporter in rat brain. *J. Neurosci.* 10, 1319–1330.
- Rattray, M., and Priestley, J. V. (1993). Differential expression of GABA transporter-1 messenger RNA in subpopulations of GABA neurones. *Neurosci. Lett.* 156, 163–165.
- Ribak, C. E., Tong, W. M., and Brecha, N. C. (1996). GABA plasma membrane transporters, GAT-1 and GAT-3, display different distributions in the rat hippocampus. *J. Comp. Neurol.* 367, 595–606.
- Richards, D. A., and Bowery, N. C. (1996). Comparative effects of the GABA uptake inhibitors, tiagabine and NNC-711, on extracellular GABA levels in the rat ventrolateral thalamus. *Neurochem. Res.* 21, 135–140.
- Richerson, G. B., and Wu, Y. (2003). Dynamic equilibrium of neurotransmitter transporters: not just for reuptake anymore. *J. Neurophysiol.* 90, 1363–1374.
- Roepstorff, A., and Lambert, J. D. (1992). Comparison of the effect of the GABA uptake blockers, tiagabine and nipeotic acid, on inhibitory synaptic efficacy in hippocampal CA1 neurons. *Neurosci. Lett.* 146, 131–134.
- Roepstorff, A., and Lambert, J. D. (1994). Factors contribution to the decay of the stimulus-evoked IPSC in rat hippocampal CA1 neurons. *J. Neurophysiol.* 72, 2911–2926.
- Romero, J., Lastres-Becker, I., de Miguel, R., Berrrendero, F., Ramos, J. A., and Fernandez-Ruiz, J. (2002). The endogenous cannabinoid system and the basal ganglia. Biochemical, pharmacological, and therapeutic aspects. *Pharmacol. Ther.* 95, 137–152.
- Rossi, D. L., Hammann, M., and Attwell, D. (2003). Multiple modes of GABAergic inhibition of rat cerebellar cells. *J. Physiol.* 548, 97–110.
- Sacher, A., Nelson, N., Ogi, J. T., Wright, E. M., Loo, D. D., and Eskandari, S. (2002). Presteady-state and steady-state kinetics and turnover rate of the mouse gamma-aminobutyric acid transporter (mGAT3). *J. Membr. Biol.* 190, 57–73.
- Safulina, V. F., and Cherubini, E. (2009). At immature mossy fibers-CA3 connection, activation of presynaptic GABAB receptors by endogenously released GABA contributes to synapses silencing. *Front. Cell. Neurosci.* 3:1. doi: 10.3389/fnec.2009.001.2009
- Sarup, A., Larsson, O. M., and Schousboe, A. (2003). GABA transporters and GABA-transaminase as drug targets. *Curr. Drug Targets CNS Neurol. Disord.* 2, 369–277.
- Schoffmeier, A. N. M., Vanderschuren, L. J. M. J., Vries, T. J. De., Hogenboom, F., Wardeh, G., and Mulder, A. H. (2000). Synergistically interacting dopamine D1 and NMDA receptors mediate nonvesicular transporter-dependent GABA release from rat striatal medium spiny neurons. *J. Neurosci.* 20, 3496–3505.
- Schwartz, T. L., and Nihalani, N. (2006). Tiagabine in anxiety disorders. *Expert Opin. Pharmacother.* 7, 1977–1987.
- Scimemi, A., Semyanov, A., Sperk, G., Kullmann, D. M., and Walker, M. C. (2005). Multiple and plastic receptors mediate tonic GABAA receptor currents in the hippocampus. *J. Neurosci.* 25, 10016–10024.
- Semyanov, A., Walker, M. C., and Kullmann, D. M. (2003). GABA uptake regulates cortical excitability via cell type-specific tonic inhibition. *Nat. Neurosci.* 6, 484–490.
- Semyanov, A., Walker, M. C., Kullmann, D. M., and Silver, R. A. (2004). Tonically active GABAA receptor: modulating gain and maintaining the tone. *Trends Neurosci.* 27, 262–269.
- Sipilä, S. T., Voipio, J., and Kaila, K. (2007). GAT-1 acts to limit a tonic GABAA current in rat CA3 pyramidal neurons at birth. *Eur. J. Neurosci.* 25, 771–722.
- Swan, M., Najelahim, A., Watson, R. E. B., and Benett, J. P. (1994). Distribution of mRNA for the GABA transporter GAT-1 in the rat brain: evidence that GABA uptake is not limited to presynaptic neurons. *J. Anat.* 185, 315–323.
- Thompson, S. M., and Gähwiler, B. H. (1992). Effects of the GABA uptake inhibitor tiagabine on inhibitory synaptic potentials in rat hippocampal slice cultures. *J. Neurophysiol.* 67, 1698–1701.
- Venderova, K., Brown, T. M., and Brothie, J. M. (2005). Differential effects of endocannabinoids on [3H]-GABA uptake in the rat globus pallidus. *Exp. Neuro.* 194, 284–287.
- Waldmeier, P. C., Stocklin, K., and Feldtrauer, J. J. (1992). Weak effects of local and systemic administration of the GABA uptake inhibitor, SKF 89976A, on extracellular GABA in the rat striatum. *Naunyn-Schmiedeberg Arch. Exp. Pathol. Pharmacol.* 345, 544–547.
- Wang, X. S., and Ong, W. Y. (1999). A light and electron microscopic study of GAT-1 in the monkey basal ganglia. *J. Neurocytol.* 28, 1053–1061.
- Wu, Y., Wang, W., Diez-Sampedro, A., and Richerson, G. B. (2007). Nonvesicular inhibitory neurotransmission via reversal of the GABA transporter GAT-1. *Neuron* 56, 851–865.
- Yamauchi, A., Uchida, S., Kwon, H. M., Preston, A. S., Robey, R. B., Garcia-Perez, A., Burg, M. B., and Handler, J. S. (1992). Cloning of a Na (+)- and Cl (-)-dependent betaine transporter that is regulated by hypertonicity. *J. Biol. Chem.* 267, 649–652.
- Yasumi, M., Sato, K., Shimada, S., Nishimura, M., and Tohyama, M. (1997). Regional distribution of GABA transporter 1 (GAT1) mRNA in the rat brain: comparison with glutamic acid decarboxylase67 (GAD67) mRNA localization. *Brain Res. Mol. Brain Res.* 44, 205–218.
- Zhou, X. M., and Ong, W. Y. (2004). A light and electron microscopic study of betaine/GABA transporter distribution in the monkey cerebral neocortex and hippocampus. *J. Neurocytol.* 33, 233–240.

Conflict of Interest Statement: The authors declare that the research was conducted in the absence of any commercial or financial relationships that could be construed as a potential conflict of interest.

Received: 26 April 2011; paper pending published: 10 May 2011; accepted: 13 July 2011; published online: 28 July 2011.

Citation: Jin X-T, Galvan A, Wichmann T and Smith Y (2011) Localization and function of GABA transporters GAT-1 and GAT-3 in the basal ganglia. *Front. Syst. Neurosci.* 5:63. doi: 10.3389/fnec.2011.00063

Copyright © 2011 Jin, Galvan, Wichmann and Smith. This is an open-access article subject to a non-exclusive license between the authors and Frontiers Media SA, which permits use, distribution and reproduction in other forums, provided the original authors and source are credited and other Frontiers conditions are complied with.



Neuroglial plasticity at striatal glutamatergic synapses in Parkinson's disease

Rosa M. Villalba^{1*} and Yolanda Smith^{1,2}

¹ Division of Neuropharmacology and Neurologic Diseases, Yerkes National Primate Research Center, Emory University, Atlanta, GA, USA

² Department of Neurology, Emory University, Atlanta, GA, USA

Edited by:

James M. Tepper, Rutgers, The State University of New Jersey, USA

Reviewed by:

Jose L. Lanciego, University of Navarra, Spain

Paul Bolam, University of Oxford, UK

*Correspondence:

Rosa M. Villalba, Yerkes National Primate Research Center, Emory University, 954 Gatewood Road NE, Atlanta, GA 30329, USA.
e-mail: rvillal@emory.edu

Striatal dopamine denervation is the pathological hallmark of Parkinson's disease (PD). Another major pathological change described in animal models and PD patients is a significant reduction in the density of dendritic spines on medium spiny striatal projection neurons. Simultaneously, the ultrastructural features of the neuronal synaptic elements at the remaining corticostriatal and thalamostriatal glutamatergic axo-spinous synapses undergo complex ultrastructural remodeling consistent with increased synaptic activity (Villalba and Smith, 2011). The concept of tripartite synapses (TS) was introduced a decade ago, according to which astrocytes process and exchange information with neuronal synaptic elements at glutamatergic synapses (Araque et al., 1999a). Although there has been compelling evidence that astrocytes are integral functional elements of tripartite glutamatergic synaptic complexes in the cerebral cortex and hippocampus, their exact functional role, degree of plasticity and preponderance in other CNS regions remain poorly understood. In this review, we discuss our recent findings showing that neuronal elements at cortical and thalamic glutamatergic synapses undergo significant plastic changes in the striatum of MPTP-treated parkinsonian monkeys. We also present new ultrastructural data that demonstrate a significant expansion of the astrocytic coverage of striatal TS synapses in the parkinsonian state, providing further evidence for ultrastructural compensatory changes that affect both neuronal and glial elements at TS. Together with our limited understanding of the mechanisms by which astrocytes respond to changes in neuronal activity and extracellular transmitter homeostasis, the role of both neuronal and glial components of excitatory synapses must be considered, if one hopes to take advantage of glia-neuronal communication knowledge to better understand the pathophysiology of striatal processing in parkinsonism, and develop new PD therapeutics.

Keywords: glia, MPTP, non-human primates, tripartite synapses, astrocyte, striatum, corticostriatal, thalamostriatal

INTRODUCTION

One of the main neuropathological features of Parkinson's disease (PD) is the degeneration of the nigrostriatal dopaminergic pathway, which induces complex physiological changes within the basal ganglia circuitry, including profound alterations in the activity of the corticostriatal glutamatergic system (Calabresi et al., 1996, 2007; Mallet et al., 2006; Wichmann and Delong, 2007). A major pathological change described in animal models and PD patients is a significant reduction in the density of dendritic spines on striatal medium spiny projection neurons (Ingham et al., 1989; Stephens et al., 2005; Zaja-Milatovic et al., 2005; Day et al., 2006; Deutch et al., 2007; Villalba et al., 2009). Recent evidence from our laboratory demonstrates that the ultrastructural features of pre- and post-synaptic neuronal elements at the remaining corticostriatal and thalamostriatal axo-spinous synapses undergo complex remodeling consistent with increased synaptic activity in the striatum of MPTP-treated parkinsonian monkeys (Villalba and Smith, 2010, 2011). Furthermore, new unpublished findings, recently gathered from these animals demonstrate that perisynaptic astrocytes at cortical and thalamic axo-spinous synapses undergo a significant expansion in parkinsonism. Thus, the goal of this review is to integrate these data, and put forward some

hypotheses about the functional significance of ultrastructural reorganization of striatal glutamatergic synapses in parkinsonian condition.

In contrast to the long term belief that astrocytes were merely providing a passive structural support for neurons, evidence obtained during the past decade has challenged this view indicating that astrocytes actively participate in synaptic transmission and neural communication (Araque et al., 1999a,b; Hirrlinger et al., 2004; Schipke and Kettermann, 2004; Haber et al., 2006; Witcher et al., 2007; Araque, 2008; Fellin, 2009; Perea et al., 2009; Araque and Navarrete, 2010; Paixao and Klein, 2010; Perea and Araque, 2010), which led to the concept of tripartite synapses (TS), suggesting that astrocytes integrate, process, and exchange information with pre- and post-synaptic neuronal synaptic elements (Araque et al., 1999b). It is well established that astrocytes also undergo dynamic structural remodeling in response to physiological or pathological changes in synaptic activity in different areas of the CNS, including the hippocampus, cortex, cerebellum, and hypothalamus (Theodosios and MacVicar, 1996; Ventura and Harris, 1999; Jones and Greenough, 2002; Dervan et al., 2004; Slezak et al., 2006; Todd et al., 2006; Theodosios et al., 2008; Buard et al., 2010; Reichenbach et al., 2010).

In these TS, astrocytes serve as a bridge for non-synaptic communication between neurons, thereby contributing to the processing and integration of synaptic signaling through the formation of complex neuron–glia networks. The use of 3D reconstruction of synaptic complexes at the electron microscopic level has been instrumental in revealing the intimate structural relationships and plasticity of astroglial processes and neuronal elements at synaptic sites. In the hippocampus and mature neocortex, about half of excitatory axo-spinous glutamatergic synapses are covered by astrocytic processes and considered as TS (Spacek, 1985; Ventura and Harris, 1999; Xu-Friedman et al., 2001). In both the sliced and the intact hippocampus, there is evidence that the surface area of the post-synaptic densities (PSDs) are larger when perisynaptic astroglial processes are present, and presumably those synapses are more effective than those without glial ensheathment (Witcher et al., 2007). Furthermore, 3D reconstructions of hippocampal asymmetric axo-spinous synapses have shown that up-regulation of synaptic activity induces a pronounced increase of the glial coverage of both pre- and post-synaptic structures (Lushnikova et al., 2009). Along the same lines, there is a significant increase in the surface area of glial processes wrapped around glutamatergic synapses in the visual cortex of rats raised in a complex environment (Jones and Greenough, 1996), and in the somatosensory cortex of mice subjected to 24 h of whisker stimulation (Genoud et al., 2006). Many other studies have confirmed and extended these observations that perisynaptic astroglia undergo dynamic reorganization correlated with increased synaptic plasticity and neuronal activity in different brain regions (Ventura and Harris, 1999; Genoud et al., 2006; Haber et al., 2006; Todd et al., 2006; Witcher et al., 2007, 2010; Lushnikova et al., 2009; Perea et al., 2009; Reichenbach et al., 2010).

FUNCTIONAL SIGNIFICANCE OF TS IN SYNAPTIC COMMUNICATION AND SYNAPTOGENESIS

As discussed above, the plastic remodeling of glial cells and their active participation in synaptic communication have been demonstrated in different brain regions (Geinisman, 2000; Jourdain et al., 2002; Matsuzaki et al., 2004; Park et al., 2006; Theodosios et al., 2008; Lushnikova et al., 2009; Araque and Navarrete, 2010; Reichenbach et al., 2010). Although the functional significance of these ultrastructural changes remains poorly understood, various mechanisms by which astrocytes could regulate synaptic plasticity have been proposed.

Astrocytes secrete neuroactive substances and actively remove synaptically released neurotransmitters from the synaptic cleft, thereby playing an active role in regulating the spillover of transmitter, most particularly glutamate, across synapses or to extrasynaptic receptors (Paixao and Klein, 2010). Two glial EAAT subtypes (GLAST/EAAT1 and GLT1/EAAT2), distributed on astrocytic membranes in the vicinity of excitatory synapses, indeed, prevent accumulation of extracellular glutamate, overstimulation of glutamate receptors and excitotoxic neuronal death in the CNS (Zhang et al., 2003; Fellin and Carmignoto, 2004). There is evidence for dysregulation of GLT1 expression and increased level of extracellular glutamate in the striatum of MPTP-treated mice (Dervan et al., 2004) and 6-hydroxydopamine-lesioned rats (Chung et al., 2008; Massie et al., 2010; see below). In addition to their transmitter reuptake properties, astrocytes may also be a source of different gliotransmitters, such as glutamate, ATP, GABA, or D-serine, with different potential neuromodulatory roles of synaptic transmission (see Perea et al., 2009).

Astrocytes are also involved in the formation and maintenance of glutamatergic synapses (Witcher et al., 2007; Barres, 2008; Buard et al., 2010; Pfrieger, 2010). Soluble astrocyte-derived signals such as thrombospondins and cholesterol strongly promote both synapse formation and function (Allen and Barres, 2005; Barres, 2008), indicating that interactions between cell surface molecules and the release of various soluble factors by astroglia may be crucially important to mediate the turnover and enlargement of spines observed with synaptic plasticity. Synaptic astroglia are also critical dynamic regulators of the strength and kinetics of synaptic activity. Astrocytes, indeed, respond to neural stimulation or neurochemical changes in the surrounding extracellular space by extending and modifying their processes (Cornell-Bell et al., 1990), especially around active synapses (Oliet et al., 2001; Hirrlinger et al., 2004).

Astrocytes secrete a number of neurotrophic factors that are potent survival factors for various neuronal populations, including nigrostriatal dopaminergic neurons of the substantia nigra pars compacta (SNc), the main targets of neurodegeneration in PD. The glial cell-line-derived neurotrophic factor (GDNF, neurturin), brain-derived neurotrophic factor (BDNF), and mesencephalic astrocyte-derived neurotrophic factor (MANF) indeed, exert strong influences on the growth, development, and neuroprotection of midbrain dopaminergic neurons and their axonal projections in normal and pathological conditions (Lin et al., 1993; Akerud et al., 2001; Cunningham and Su, 2002; Petrova et al., 2003, 2004; Capowski et al., 2007; Sandhu et al., 2009). Interestingly, valproate and 3-hydroxymorphan, both of which being protective of midbrain dopaminergic neurons against MPP⁺-induced neurotoxicity, upregulate the production of neurotrophic factors by astrocytes and reduce reactive microgliosis (Chen et al., 2006).

Together, these findings illustrate a myriad of mechanisms by which astrocytes could actively participate in the development, regulation, protection, and restoration of glutamatergic synapses in the CNS. However, although neuron–glia interactions have been studied in some detail in specific brain regions, very little is known about the substrate and plastic properties of these glio-synaptic networks in the striatum, a basal ganglia structure recognized by its high degree of long term synaptic plasticity and remodeling of glutamatergic synapses in normal and parkinsonian conditions (see below). Thus, as part of an ongoing research program aimed at characterizing the ultrastructural plasticity of cortical and thalamic glutamatergic synapses in the striatum of normal and parkinsonian non-human primates, this review will summarize our recent findings on the synaptic remodeling of axo-spinous synapses in MPTP-treated monkeys (Villalba and Smith, 2010, 2011), and provide new evidence that these morphological changes are accompanied with a significant growth in the extent of glial coverage of striatal glutamatergic synapses in parkinsonian condition.

PLASTICITY OF AXO-SPINOUS STRIATAL GLUTAMATERGIC SYNAPSES IN PARKINSONISM

DENDRITIC SPINES AND AXON TERMINALS

The anatomical substrate and mechanism by which dopamine (DA) regulates striatal glutamatergic activity is complex, activity-dependent and still remains poorly understood (Smith and Bolam, 1990; Bamford et al., 2004; Calabresi et al., 2007; Surmeier et al., 2007; Ballion et al., 2008; Smith and Villalba, 2008; Tian et al., 2010).

The most common targets where dopaminergic and glutamatergic striatal afferent systems functionally interact are the dendritic spines of striatofugal medium spiny neurons (MSNs; Smith and Bolam, 1990). Most, if not all, cortical innervation of MSNs terminates on dendritic spines (Kemp and Powell, 1971; Raju et al., 2006). Although not as extensive as the corticostriatal system, a significant contingent of thalamic glutamatergic afferents also target dendritic spines and display close relationships with dopaminergic terminals in the striatum (Raju et al., 2006; Moss and Bolam, 2008; Smith et al., 2009a,b). In both animal models of parkinsonism (Figures 1A,B) and PD patients, MSNs lose as much as 30–50% dendritic spines which, in rats, is accompanied with a similar decrease in the total number of asymmetric glutamatergic synapses (Ingham et al., 1989, 1998; Stephens et al., 2005; Zaja-Milatovic et al., 2005; Day et al., 2006; Deutch et al., 2007; Neely et al., 2007; Scholz et al., 2008; Schuster et al., 2009; Smith et al., 2009b; Villalba et al., 2009; Garcia et al., 2010; Soderstrom et al., 2010). Despite this significant spine loss, some *in vivo* and *in vitro* electrophysiological studies suggested an increased activity of the corticostriatal system in parkinsonism (Galarraga et al., 1987; Calabresi et al., 1996; Marti et al., 1999), though this issue remains controversial and appears to be more complex than originally thought (Day et al., 2006; Mallet et al., 2006).

Immunocytochemical studies have demonstrated an increased expression of vesicular glutamate transporter 1 (vGluT1) immunoreactivity, a specific marker of corticostriatal terminals, in the striatum of MPTP-treated parkinsonian monkeys (Raju et al., 2008) and postmortem striatal tissue of PD patients (Kashani et al., 2007). In addition, the striatum of DA-depleted rats contains a larger density of perforated asymmetric synapses (Ingham et al., 1998; Meshul et al., 1999, 2000), a form of structural remodeling associated with increased synaptic efficacy in other brain regions (Greenough et al., 1978; Bertoni-Freddari et al., 1993; Harris and Kater, 1994). Therefore, the overactivity of corticostriatal glutamatergic system described by some authors in rodent models of parkinsonism might result from complex structural and neurochemical changes of glutamatergic axo-spinous synapses in DA-depleted striata.

To further address this issue, we used a 3D electron microscopy reconstruction method to perform a rigorous quantitative analysis of the ultrastructural features of spines specifically targeted by thalamic or cortical afferents in the sensorimotor striatum of normal and MPTP-treated parkinsonian monkeys (Figures 1C1–D2); the results of which having been published in several recent reports from our laboratory (see Smith et al., 2009b; Villalba and Smith, 2010, 2011). In summary, the findings presented in these studies demonstrate that thalamostriatal and corticostriatal afferents target different types of striatal spines, and that both systems undergo complex, and partly different, ultrastructural changes indicative of an increased strength of glutamatergic transmission in parkinsonism (Figures 1E–H). These studies revealed three major ultrastructural features of cortical and thalamic glutamatergic axo-spinous synapses in the primate striatum. First, the dendritic spines targeted by vGluT1-containing corticostriatal terminals are significantly larger and harbor a more extensive PSD than those innervated by vesicular glutamate transporter 2 (vGluT2)-positive thalamostriatal boutons. Second, a subset of vGluT2-positive terminals displays a pattern of multisynaptic connectivity. Third, corticostriatal axo-

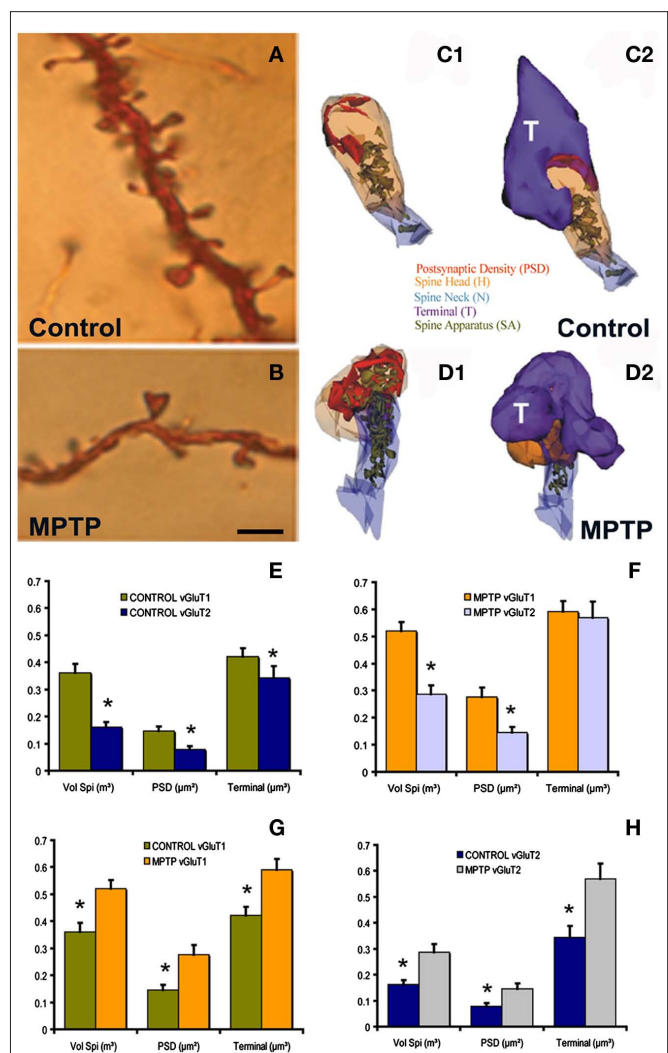


FIGURE 1 | Morphological and ultrastructural changes in striatal MSNs after MPTP treatment. (A,B) Dendrites from Golgi-impregnated MSNs in the caudate nucleus of a control (A) and a MPTP-treated (B) monkey showing the dramatic spine loss (30–50%) after MPTP treatment. (C1–D2) Three-dimensional (3D)-reconstructed images of glutamatergic axo-spinous synapses from a control (C1,C2) and a MPTP-treated (D1,D2) monkeys. The spines are partially transparent to better show and compare the complexity and distribution of the spine apparatus (SA) between control and MPTP-treated monkeys. (E,F) Histograms comparing the morphometric measurements (mean ± SEM; spine volume, PSD area, terminal volume) of structural elements at corticostriatal (vGluT1-positive) and thalamostriatal (vGluT2-positive) glutamatergic synapses using the 3D reconstruction method of serial ultrathin sections collected from 30 axo-spinous synapses in each group from three control and three MPTP-treated animals. The units used for these measurements are indicated in the X-axis within parentheses. In control monkeys (N = 3), the spine volume (Vol. Sp.), the PSD areas, and the size of pre-synaptic terminals at corticostriatal synapses are significantly larger than those at thalamostriatal synapses (*, t-test, $P < 0.001$ for Vol. Sp. and PSD; $P = 0.016$ for terminal (E)). The same is true for MPTP-treated monkeys (N = 3), except for the pre-synaptic terminals that do not show any significant size differences in this condition (F). (G,H) The spine volumes, the PSD areas and the volume of vGluT1- and vGluT2-containing terminals are significantly larger in MPTP-treated parkinsonian monkeys than in controls (*, t-test, $P < 0.001$). Scale bar in (B) [valid for (A)]: 5 μ m. (see Villalba et al., 2009; Villalba and Smith, 2010, 2011 for more detail.)

spinous synapses in the sensorimotor putamen of parkinsonian monkeys undergo complex ultrastructural remodeling consistent with increased synaptic activity (larger spine volume, larger PSDs, increased number of PSD perforations, larger pre-synaptic terminal, larger spine apparatus, increased number and decreased volume of terminal mitochondria; Villalba and Smith, 2011). Although some of these plastic changes also characterize vGluT2-positive axo-spinous synapses (larger spine volume, larger PSDs, increased number of PSD perforations), others are specific to cortical afferents (**Figures 1E–H**). Together with various electrophysiological studies suggesting overactivity of the corticostriatal system in rodent and non-human primate models of parkinsonism (Galarraga et al., 1987; Marti et al., 1999; Gubellini et al., 2002; Liang et al., 2008), these ultrastructural data suggest that striatal MSNs are endowed with a high level of synaptic plasticity that allows, at least early in the disease process, sensorimotor-related information to be properly transmitted and integrated at the striatal level despite a major reduction in the number of corticostriatal synapses (Smith et al., 2009b; Villalba et al., 2009; Villalba and Smith, 2010, 2011).

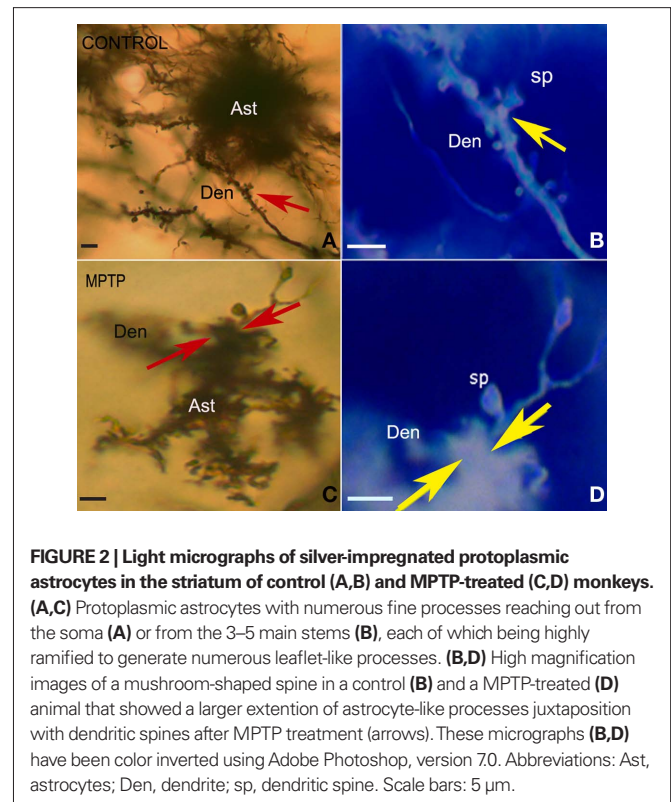
PERISYNAPTIC ASTROCYTES

In light of data summarized above (Smith et al., 2009b; Villalba et al., 2009; Villalba and Smith, 2010, 2011) combined with findings from the hippocampus and other brain regions suggesting tight associations between the growth of perisynaptic astrocytic ensheathment and ultrastructural changes in axo-spinous synaptic elements (see above), we have used 3D electron microscopic reconstruction methods to characterize and compare the extent of astrocytic association with cortical (vGluT1-positive) and thalamic (vGluT2-positive) glutamatergic excitatory axo-spinous synapses in the striatum of normal versus MPTP-treated parkinsonian monkeys. The data obtained in this new analysis are summarized below.

Light and electron microscopic analyses of perisynaptic astrocytes in control and MPTP-treated monkeys

To address this issue, we first used Golgi impregnation and light microscopy (LM) analysis to examine gross relationships between astrocytic processes and dendritic spines on the surface of MSNs in control and MPTP-treated parkinsonian monkeys (**Figure 2**). Then, to perform a deeper analysis of the morphological interactions between axo-spinous synapses and perisynaptic astrocytes, we used electron microscopy (EM) 3D reconstruction to quantify and compare the extent of relationships between astrocytic processes and axo-spinous synapses in control and parkinsonian monkeys (**Figures 3–6**).

LM analysis of astrocytes–dendritic spines relationships. After Golgi impregnation of striatal sections from the post-commissural putamen in three normal and three MPTP-treated parkinsonian monkeys (Vibratome, 60 μm -thickness; for details on animals and Golgi impregnation see Villalba et al., 2009), we found well impregnated astrocytes intermingled with the spiny dendritic trees of MSNs in both control (**Figures 2A,B**) and MPTP-treated (**Figures 2C,D**) animals. The most striking feature of the morphology of protoplasmic astrocytes was the enormous complexity and irregularity of processes arborization, with abundant ramifications often described as bushy or spongiform (**Figures 2A,C**). These glial



cells harbored rich plexuses of fine processes reaching out from the soma (**Figure 2A**), or extended 3–5 primary stems that ramified into a large density of fine processes (**Figure 2C**). At high magnification, some of these processes appeared as thin filopodia- or lamellipodia-like structures, which were insinuated between and around dendritic spines (**Figures 2B,D**).

Ultrastructural analysis of striatal perisynaptic glia. The following analysis was performed on the same material recently used to study striatal axo-spine plasticity in parkinsonian monkeys (Villalba and Smith, 2011). Methodological details related to animal perfusion, tissue preparation, immunocytochemical procedures, and 3D EM reconstruction methods, described extensively in this previous study, will not be repeated here. We will rather focus our brief methodological description on the procedures used to gather new information on perisynaptic astrocytes. In brief, digital images of vGluT1- or vGluT2-immunostained tissue sections used to reconstruct individual axo-spinous synapses in our previous study were re-examined, and those complexes associated with perisynaptic astrocytes in single sections were chosen for this analysis. Following screening of the 60 vGluT1- and 60 vGluT2-axo-spinous complexes analyzed in our previous study (Villalba and Smith, 2011), about one-third was found to display significant perisynaptic astrocytic association, thus chosen for the present analysis. In order to avoid any sampling bias, the observer was blinded to the treatment condition.

In single ultrathin sections, perisynaptic astroglial processes were recognized by their irregular shapes, and “clear” cytoplasm as consequence of their lack of most intracellular organelles (pseudocolored

in blue in **Figures 3A,B and 5B**). Qualitative comparisons of TS between control and MPTP-treated animals in single ultrathin sections revealed that perisynaptic astrocytes exhibit an interdigitated finger-like morphology in control animals (**Figure 3A**), while there is an expansion of astrocytic processes to cover a larger extent of the perimeter of axo-spinous complexes after MPTP treatment (**Figures 3B, 5A,B**).

Three-dimensional reconstructions of striatal tripartite synapses.

Through the analysis and digital collection of material gathered from serial ultrathin sections (20–30 sections per grid), individual TS involving vGluT1- or vGluT2-immunoreactive (IR) terminals in control and MPTP-treated monkeys were reconstructed in 3D using the *Reconstruct* software application (available at: synapses.clm.utexas.edu). A total of eight vGluT1- and vGluT2-positive TS in normal and MPTP-treated states were chosen for this analysis based on the presence of significant perisynaptic astrocytic processes in close apposition with the axo-spinous complexes. To reconstruct perisynaptic astrocytes, thin astroglial processes were traced through serial sections into larger structures to confirm their

identity and quantify their extent in relation to the pre- and post-synaptic neuronal elements at axo-spinous asymmetric synapses. Briefly, serially digitized electron micrographs of the eight TS that involved vGluT1- or vGluT2-IR terminals in control and MPTP-treated monkeys were converted to TIFF format, imported into *Reconstruct*, calibrated, and aligned (see Villalba and Smith, 2011 for details). Finally, the individual contours of the astroglial processes were manually traced in each serial electron micrograph using the *Reconstruct* software. The program calculated the dimensions (surface area and volume) of the perisynaptic astrocytic processes and generated a 3D representation based on the serial sectioning information.

The analysis of these 3D reconstructions allowed us to obtain a detailed knowledge of the relationships between axo-spinous complexes and their perisynaptic astrocytic processes. In both TS formed by vGluT1- or vGluT2-immunoreactive axon terminals (**Figures 4, 5C–F**), highly branched astrocytic processes wrapped themselves around the synapses and formed a non-uniform basket-like structure surrounding the pre- and post-synaptic components of synaptic complexes (**Figures 4, 5C–F**). Some structural differences were noticed when we compared the extent of perisynaptic glial ensheathment of axo-spinous synapses between control and MPTP-treated monkeys. In control animals, the axo-spinous complexes showed numerous astrocyte-free areas (**Figures 4A–C**), whereas in MPTP-treated monkeys, the extent of perisynaptic glia was significantly increased, and the appositions between the axo-spinous complex and the astroglial processes were much tighter and continuous forming an extensive barrier around the synaptic complexes (**Figures 4A'–C', 5C–F**). These differences between the normal and MPTP condition were seen for both vGluT1- and vGluT2-positive glutamatergic synapses (**Figures 4 and 5C–F**).

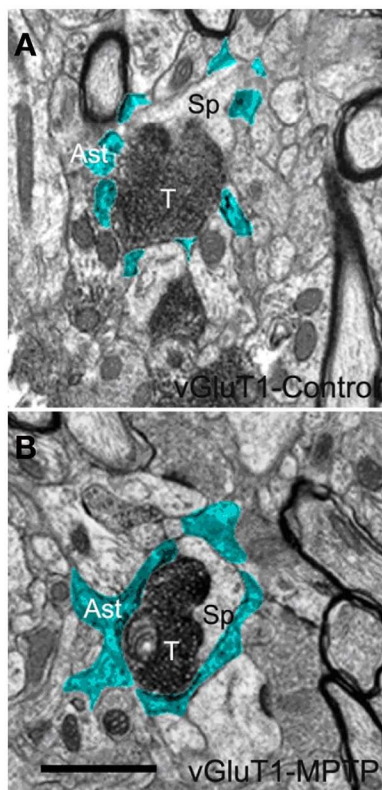


FIGURE 3 | Electron micrographs of a vGluT1-immunoreactive tripartite synapse (TS) in the striatum of a control (A) and a MPTP-treated (B) monkey. Perisynaptic astrocytic processes (Ast) are pseudocolored in blue in (A,B). These single EM images highlight differences in the extension of the astrocyte wrapping of an axo-spinous synapse between control (A) and MPTP (B) treated animals. Pictures were digitally acquired and imported in TIFF format to Adobe Photoshop (version 7.0; Adobe System, San Jose, CA, USA). Abbreviations: Ast, astrocyte; T, axon terminal; Sp, dendritic spine. Scale bar in (B) [valid for (A)]: 1 μ m.

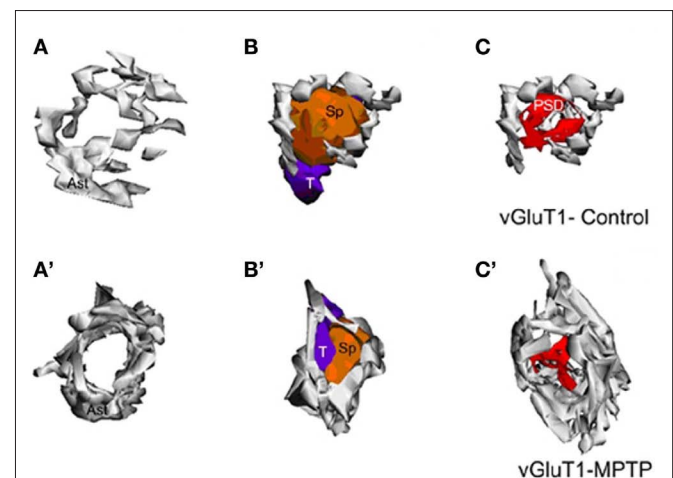


FIGURE 4 | Three-dimensional reconstruction of tripartite synapses (TS) formed by a vGluT1-immunoreactive terminal in the striatum of a control (A–C) and a MPTP-treated (A'–C') monkey. (A–C) In the TS of control animals, the perimeters of the axon-spinous interfaces were only partially surrounded by astroglial processes. **(A'–C')** TS vGluT1-containing synapses in MPTP-treated animals displayed a large increase in astroglial processes ensheathment. Abbreviations: Ast, astrocyte; PSD, post-synaptic density; Sp, dendritic spine; T, axon terminal.

To further substantiate these observations, a comparative quantitative assessment of the total surface area of astrocytic processes in direct contact with the 32 reconstructed vGluT1- or vGluT2-immunoreactive axo-spinous complexes (16 vGluT1-positive; 16

vGluT2-positive) was performed between normal and MPTP-treated monkeys (**Figure 6**; eight TS per group). The statistical analysis (*t*-test; SigmaPlot; version 11.0) showed that the surface of perisynaptic glia associated with vGluT1- and vGluT2-immunoreactive terminals was significantly larger in MPTP-treated than in control monkeys (*, *t*-test, $P = 0.017$ for vGluT1, and $P = 0.006$ for vGluT2; **Figure 6A**). In order to rule out the possibility that this increase in astrocytic surface area was merely due to an increase in the size of the axo-spinous complexes in parkinsonian animals, we calculated the ratio of the volume of the perisynaptic glia over the total volume of the spine and the corresponding axon terminal in each of the 32 TS analyzed (**Figure 6B**), and found that this ratio was significantly larger for vGluT1- and vGluT2-positive TS in MPTP-treated monkeys than in controls ($P = 0.012$), without any significant difference between the two different populations of terminals (*, *t*-test, $P = 0.049$ for vGluT1 and $P = 0.028$ for vGluT2).

CONCLUSION AND FUTURE PERSPECTIVES

Although there is compelling evidence that astrocytes are integral elements of glutamatergic synaptic complexes, and contribute actively to the regulation and processing of synaptic neural communication, their exact functional role and preponderance of these effects in specific CNS regions remain poorly understood. Findings discussed in this review highlight the significant level of structural plasticity cortical and thalamic glutamatergic axo-spinous synapses are endowed with in the primate striatum, and the ultrastructural compensatory changes that affect remaining glutamatergic synapses in the dopamine-denervated striatum of parkinsonian animals. These results, together with various electrophysiological studies suggesting overactivity of the corticostriatal system in rodent and non-human primate models of parkinsonism (Galarraga et al., 1987; Marti et al., 1999; Gubellini et al., 2002; Liang et al., 2008), illustrate the complex level of synaptic plasticity that governs striatal glutamatergic transmission under normal and parkinsonian conditions.

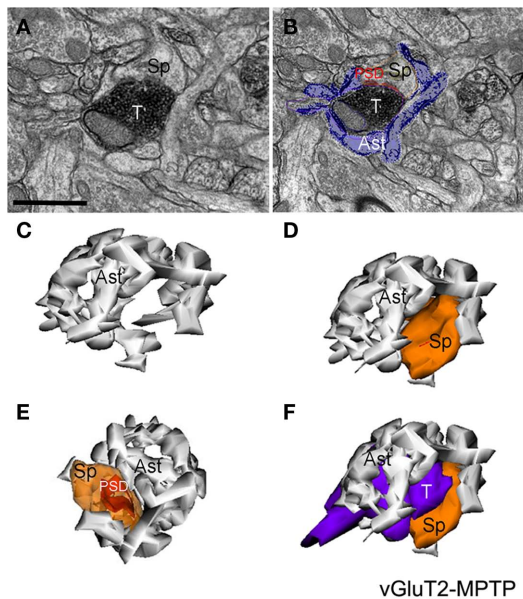


FIGURE 5 | Electron micrographs and three-dimensional (3D)-reconstruction of a tripartite synapse (TS) formed by a vGluT2-immunoreactive terminal in the striatum of a MPTP-treated monkey. (A,B) Electron micrographs of a vGluT2-immunoreactive TS. Note that in (B) the perisynaptic astrocyte was pseudocolored to help identify the glial processes. **(C–F)** 3D-reconstruction of the TS demonstrating the tight interactions between the astroglial processes and the axo-spinous vGluT2-positive complex. Abbreviations: Ast, astrocyte; PSD, post-synaptic density; Sp, dendritic spine; T, axon terminal. Scale bar in (A) [valid for (B)]: 1 μ m.

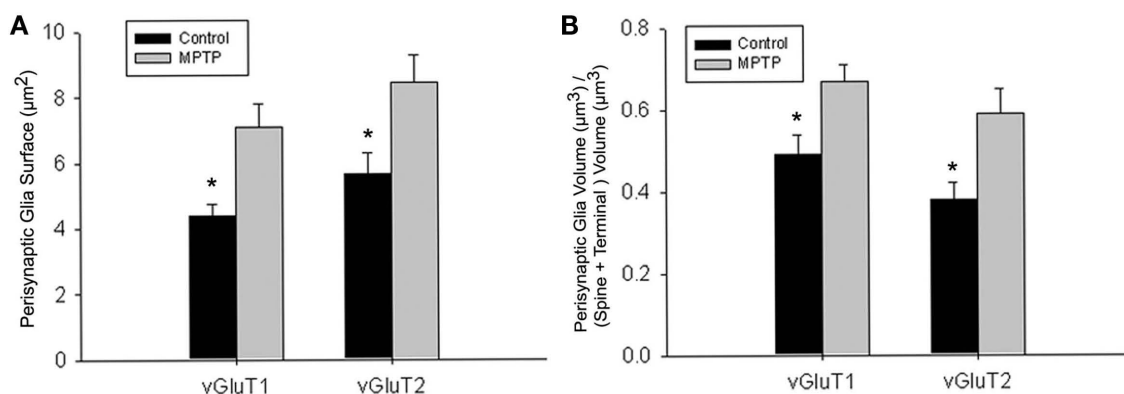


FIGURE 6 | Quantitative analysis of the perisynaptic glia from tripartite synapses (TS) in control and MPTP-treated animals (mean \pm SEM). (A) Histograms comparing the surface area of perisynaptic glia associated with vGluT1- and vGluT2-immunopositive axo-spinous synapses in control ($N = 3$) and MPTP-treated ($N = 3$) monkeys. The surface of the perisynaptic glia was significantly larger (*, *t*-test, $P = 0.017$ for vGluT1 and $P = 0.006$ for vGluT2) in MPTP-parkinsonian monkeys than in control. **(B)** Histograms comparing the ratio

of the volume of the perisynaptic glia over the total volume of the spine and the axon terminals in TS formed by vGluT1- or vGluT2-immunoreactive terminals. This ratio was significantly larger in MPTP than in control condition (*, *t*-test, $P = 0.049$ for vGluT1 and $P = 0.028$ for vGluT2). No significant difference was found between TS formed by vGluT1- or vGluT2-immunoreactive terminals. Total number of reconstructed spines = 32, 8 per group. Statistics were performed by using SigmaPlot (version 11.0).

The increased corticostriatal functions described in MPTP-treated monkeys (Cao et al., 2010) could be the result of a compensatory overactivity of corticostriatal glutamatergic terminals supported by ultrastructural plastic changes described in this and our previous study (Villalba and Smith, 2011). These morphological alterations of axo-spinous cortical and thalamic synapses might underlie the increase in striatal extracellular glutamate concentrations described in rodent models of PD (Lindfors and Ungerstedt, 1990; Meshul et al., 1999; Jonkers et al., 2002; Walker et al., 2009), although these remain controversial (Corsi et al., 2003; Galeffi et al., 2003; Robelet et al., 2004). In addition, the recent *in vitro* and *in vivo* data indicating that striatal spine pruning of MSNs in response to dopamine denervation is significantly attenuated by cortical lesions (Neely et al., 2007; Garcia et al., 2010), suggest that these plastic regulatory changes may indirectly contribute to the loss of some striatal spines in PD through increased release and spillover of extracellular glutamate from overactive glutamatergic synapses. Interestingly, the genetic deletion of cerebellin 1 (*cbln1*), a gene virtually expressed in all neurons of the thalamic parafascicular nucleus (PF), results in an increased density of striatal spines, suggesting that decreased thalamostriatal drive may be able counteract the effects of DA loss on MSN spine loss, and that the loss of thalamostriatal neurons in PD (see Smith et al., 2009a for a review) may be a compensatory response to striatal DA denervation (Kusnoor et al., 2009, 2010). Although speculative, this possibility is further supported by some reports of downregulation of GLT1 and GLAST in rat and mice models of PD (Holmer et al., 2005; Chung et al., 2008; Massie et al., 2010; but see Lievens et al., 2001).

In addition to structural changes in spine heads, PSDs, and pre-synaptic terminals described in our recent studies (Villalba and Smith, 2010, 2011), and summarized in this review, new data presented in this study indicate that perisynaptic astrocytes also undergo complex morphological changes and significant increase of their association with glutamatergic corticostriatal and thalamostriatal axo-spinous synapses in parkinsonian monkeys. These observations are consistent with the idea of an active participation of glial processes in TS structural plasticity, as previously shown in the hypothalamus (Theodosis et al., 2008) and hippocampus (Ventura and Harris, 1999; Witcher et al., 2007, 2010). However, to further understand the functional role such structural changes may have on the plastic reorganization of glutamatergic axo-spinous complexes, changes in extracellular glutamate concentrations, and spine pruning, future studies assessing potential changes in the content of glutamate transporters and growth factors in peri-

synaptic astrocytes between normal and MPTP-treated parkinsonian monkeys are warranted. As discussed in the introduction, perisynaptic astrocytes could regulate synaptic transmission by transmitter uptake or release of glutamate and other transmitter-related neurochemicals. Thus, our findings might underlie a possible change in bi-directional communication between astrocytes and synaptic neuronal elements opening up the possibility for a functional glia–neuronal regulatory loop that could modulate plasticity and efficacy of individual striatal glutamatergic synapses.

In conclusion, the present results add to the growing evidence from other brain regions that both glial and neuronal elements of axo-spinous glutamatergic synapses in the primate striatum are endowed with a high level of structural and, most likely, functional plasticity. However, many unanswered questions remain that must be addressed to better understand the functional role of plastic changes in synaptic glia–neuronal communication in the striatal pathophysiology of parkinsonism. For instance, the prevalence of TS axo-spinous glutamatergic synapses in the striatum in normal and pathological conditions is unknown. Based on data from the hippocampus (Ventura and Harris, 1999; Witcher et al., 2007, 2010), it appears that such a synaptic arrangement is not homogeneous across all excitatory synapses, thereby suggesting that glial influences upon striatal glutamatergic transmission may vary significantly from one synapse to another. This variability in the extent of perisynaptic glia may also make some glutamatergic synapses much more leaky and prone to spill over glutamate in the extracellular medium, thereby activating extrasynaptic receptors, and increase overall striatal activity. Together with our limited understanding of the mechanisms by which astrocytes respond to changes in neuronal activity and extracellular transmitter homeostasis, these issues must be thoroughly investigated if one hopes to take advantage of glia–neuronal communication knowledge to better understand the pathophysiology of striatal processing in parkinsonism, and develop new PD therapeutics that could alter these mechanisms to regulate basal ganglia functions and alleviate disease symptoms.

ACKNOWLEDGMENTS

The authors thank the Yerkes Center Animal Resources Division for help with the care of MPTP-treated monkeys, and Jean-Francois Pare for his technical assistance with serial electron microscopy sections. This work was supported by the NIH grant R01 NS 037948 and by the NCRR Yerkes Primate Center base grant RR00165.

REFERENCES

- Akerud, P., Canals, J. M., Snyder, E. Y., and Arenas, E. (2001). Neuroprotection through delivery of glial cell line-derived neurotrophic factor by neural stem cells in a mouse model of Parkinson's disease. *J. Neurosci.* 21, 8108–8118.
- Allen, N. J., and Barres, B. A. (2005). Signaling between glia and neurons: focus on synaptic plasticity. *Curr. Opin. Neurobiol.* 15, 542–548.
- Araque, A. (2008). Astrocytes process synaptic information. *Neuron Glia Biol.* 4, 3–10.
- Araque, A., and Navarrete, M. (2010). Glial cells in neuronal network function. *Philos. Trans. R. Soc. Lond. B Biol. Sci.* 365, 2375–2381.
- Araque, A., Parpura, V., Sanzgiri, R. P., and Haydon, P. G. (1999a). Tripartite synapses: glia, the unacknowledged partner. *Trends Neurosci.* 22, 208–215.
- Araque, A., Sanzgiri, R. P., Parpura, V., and Haydon, P. G. (1999b). Astrocyte-induced modulation of synaptic transmission. *Can. J. Physiol. Pharmacol.* 77, 699–706.
- Ballion, B., Mallet, N., Bezard, E., Lanciego, J. L., and Gonon, F. (2008). Intratelencephalic corticostriatal neurons equally excite striatonigral and striatopallidal neurons and their discharge activity is selectively reduced in experimental parkinsonism. *Eur. J. Neurosci.* 27, 2313–2321.
- Bamford, N. S., Robinson, S., Palmiter, R. D., Joyce, J. A., Moore, C., and Meshul, C. K. (2004). Dopamine modulates release from corticostriatal terminals. *J. Neurosci.* 24, 9541–9552.
- Barres, B. A. (2008). The mystery and magic of glia: a perspective on their roles in health and disease. *Neuron* 60, 430–440.
- Bertoni-Freddari, C., Fattoretti, P., Casoli, T., Spagna, C., Meier-Ruge, W., and Ulrich, J. (1993). Compensatory enlargement of synaptic size in aging and senile dementia. *Boll. Soc. Ital. Biol. Sper.* 69, 57–63.
- Buard, I., Steinmetz, C. C., Claudepierre, T., and Pfrieger, F. W. (2010). Glial cells promote dendrite formation and the reception of synaptic input

- in Purkinje cells from postnatal mice. *Glia* 58, 538–545.
- Calabresi, P., Picconi, B., Tozzi, A., and Di Filippo, M. (2007). Dopamine-mediated regulation of corticostriatal synaptic plasticity. *Trends Neurosci.* 30, 211–219.
- Calabresi, P., Pisani, A., Mercuri, N. B., and Bernardi, G. (1996). The corticostriatal projection: from synaptic plasticity to dysfunctions of the basal ganglia. *Trends Neurosci.* 19, 19–24.
- Cao, X., Yasuda, T., Uthayathas, W., Watts, R. L., Mouradian, M. M., Mochizuki, H., and Papa, S. M. (2010). Striatal overexpression of DeltaFosB reproduces chronic levodopa-induced involuntary movements. *J. Neurosci.* 30, 7335–7343.
- Capowski, E. E., Schneider, B. L., Ebert, A. D., Seehus, C. R., Szulc, J., Zufferey, R., Aebischer, P., and Svendsen, C. N. (2007). Lentiviral vector-mediated genetic modification of human neural progenitor cells for ex vivo gene therapy. *J. Neurosci. Methods* 163, 338–349.
- Chen, P. S., Peng, G. S., Li, G., Yang, S., Wu, X., Wang, C. C., Wilson, B., Lu, R. B., Gean, P. W., Chuang, D. M., and Hong, J. S. (2006). Valproate protects dopaminergic neurons in midbrain neuron/glia cultures by stimulating the release of neurotrophic factors from astrocytes. *Mol. Psychiatry* 11, 1116–1125.
- Chung, E. K., Chen, L. W., Chan, Y. S., and Yung, K. K. (2008). Downregulation of glial glutamate transporters after dopamine denervation in the striatum of 6-hydroxydopamine-lesioned rats. *J. Comp. Neurol.* 511, 421–437.
- Cornell-Bell, A. H., Thomas, P. G., and Smith, S. J. (1990). The excitatory neurotransmitter glutamate causes filopodia formation in cultured hippocampal astrocytes. *Glia* 3, 322–334.
- Corsi, C., Pinna, A., Gianfriddo, M., Melani, A., Morelli, M., and Pedata, F. (2003). Adenosine A2A receptor antagonism increases striatal glutamate outflow in dopamine-denervated rats. *Eur. J. Pharmacol.* 464, 33–38.
- Cunningham, L. A., and Su, C. (2002). Astrocyte delivery of glial cell line-derived neurotrophic factor in a mouse model of Parkinson's disease. *Exp. Neurol.* 174, 230–242.
- Day, M., Wang, Z., Ding, J., An, X., Ingham, C. A., Shering, A. F., Wokosin, D., Ilijic, E., Sun, Z., Sampson, A. R., Mugnaini, E., Deutch, A. Y., Sesack, S. R., Arbutnot, G. W., and Surmeier, D. J. (2006). Selective elimination of glutamatergic synapses on striatopallidal neurons in Parkinson disease models. *Nat. Neurosci.* 9, 251–259.
- Dervan, A. G., Meshul, C. K., Beales, M., McBean, G. J., Moore, C., Totterdell, S., Snyder, A. K., and Meredith, G. E. (2004). Astroglial plasticity and glutamate function in a chronic mouse model of Parkinson's disease. *Exp. Neurol.* 190, 145–156.
- Deutch, A. Y., Colbran, R. J., and Winder, D. J. (2007). Striatal plasticity and medium spiny neuron dendritic remodeling in parkinsonism. *Parkinsonism Relat. Disord.* 13(Suppl. 3), S251–S258.
- Fellin, T. (2009). Communication between neurons and astrocytes: relevance to the modulation of synaptic and network activity. *J. Neurochem.* 108, 533–544.
- Fellin, T., and Carmignoto, G. (2004). Neurone-to-astrocyte signalling in the brain represents a distinct multifunctional unit. *J. Physiol. (Lond.)* 559, 3–15.
- Galarraga, E., Bargas, J., Martinez-Fong, D., and Aceves, J. (1987). Spontaneous synaptic potentials in dopamine-denervated neostriatal neurons. *Neurosci. Lett.* 81, 351–355.
- Galeffi, F., Bianchi, L., Bolam, J. P., and Della Corte, L. (2003). The effect of 6-hydroxydopamine lesions on the release of amino acids in the direct and indirect pathways of the basal ganglia: a dual microdialysis probe analysis. *Eur. J. Neurosci.* 18, 856–868.
- Garcia, B. G., Neely, M. D., and Deutch, A. Y. (2010). Cortical regulation of striatal medium spiny neuron dendritic remodeling in parkinsonism: modulation of glutamate release reverses dopamine depletion-induced dendritic spine loss. *Cereb. Cortex* 20, 2423–2432.
- Geinisman, Y. (2000). Structural synaptic modifications associated with hippocampal LTP and behavioral learning. *Cereb. Cortex* 10, 952–962.
- Genoud, C., Quairiaux, C., Steiner, P., Hirling, H., Welker, E., and Knott, G. W. (2006). Plasticity of astrocytic coverage and glutamate transporter expression in adult mouse cortex. *PLoS Biol.* 4, e343. doi: 10.1371/journal.pbio.0040343
- Greenough, W. T., West, R. W., and DeVoogd, T. J. (1978). Subsynaptic plate perforations: changes with age and experience in the rat. *Science* 202, 1096–1098.
- Gubellini, P., Picconi, B., Bari, M., Battista, N., Calabresi, P., Centonze, D., Bernardi, G., Finazzi-Agro, A., and Maccarrone, M. (2002). Experimental parkinsonism alters endocannabinoid degradation: implications for striatal glutamatergic transmission. *J. Neurosci.* 22, 6900–6907.
- Haber, M., Zhou, L., and Murai, K. K. (2006). Cooperative astrocyte and dendritic spine dynamics at hippocampal excitatory synapses. *J. Neurosci.* 26, 8881–8891.
- Harris, K. M., and Kater, S. B. (1994). Dendritic spines: cellular specializations imparting both stability and flexibility to synaptic function. *Annu. Rev. Neurosci.* 17, 341–371.
- Hirrlinger, J., Hulsman, S., and Kirchhoff, F. (2004). Astroglial processes show spontaneous motility at active synaptic terminals in situ. *Eur. J. Neurosci.* 20, 2235–2239.
- Holmer, H. K., Keyghobadi, M., Moore, C., and Meshul, C. K. (2005). L-dopa-induced reversal in striatal glutamate following partial depletion of nigrostriatal dopamine with 1-methyl-4-phenyl-1,2,3,6-tetrahydropyridine. *Neuroscience* 136, 333–341.
- Ingham, C. A., Hood, S. H., and Arbutnot, G. W. (1989). Spine density on neostriatal neurones changes with 6-hydroxydopamine lesions and with age. *Brain Res.* 503, 334–338.
- Ingham, C. A., Hood, S. H., Taggart, P., and Arbutnot, G. W. (1998). Plasticity of synapses in the rat neostriatum after unilateral lesion of the nigrostriatal dopaminergic pathway. *J. Neurosci.* 18, 4732–4743.
- Jones, T. A., and Greenough, W. T. (1996). Ultrastructural evidence for increased contact between astrocytes and synapses in rats reared in a complex environment. *Neurobiol. Learn. Mem.* 65, 48–56.
- Jones, T. A., and Greenough, W. T. (2002). "Behavioral experience-dependent plasticity of glial-neuronal interactions," in *The Tripartite Synapse: Glia in Synaptic Transmission*, eds A. Volterra, P. J. Magistretti, and P. G. Haydon (Oxford: Oxford University Press), 248–265.
- Jonkers, N., Sarre, S., Ebinger, G., and Michotte, Y. (2002). MK801 suppresses the L-DOPA-induced increase of glutamate in striatum of hemiparkinson rats. *Brain Res.* 926, 149–155.
- Jourdain, P., Nikonenko, I., Alberi, S., and Muller, D. (2002). Remodeling of hippocampal synaptic networks by a brief anoxia-hypoglycemia. *J. Neurosci.* 22, 3108–3116.
- Kashani, A., Betancur, C., Giros, B., Hirsch, E., and El Mestikawy, S. (2007). Altered expression of vesicular glutamate transporters VGLUT1 and VGLUT2 in Parkinson disease. *Neurobiol. Aging* 28, 568–578.
- Kemp, J. M., and Powell, T. P. (1971). The termination of fibres from the cerebral cortex and thalamus upon dendritic spines in the caudate nucleus: a study with the Golgi method. *Philos. Trans. R. Soc. Lond. B Biol. Sci.* 262, 429–439.
- Kusnoor, S. V., Muly, E. C., Morgan, J. I., and Deutch, A. Y. (2009). Is the loss of thalamostriatal neurons protective in parkinsonism? *Parkinsonism Relat. Disord.* 15(Suppl. 3), S162–S166.
- Kusnoor, S. V., Parris, J., Muly, E. C., Morgan, J. I., and Deutch, A. Y. (2010). Extracerebellar role for *Cerebellin 1*: modulation of dendritic spine density and synapses in striatal medium spiny neurons. *J. Comp. Neurol.* 518, 2525–2537.
- Liang, L., DeLong, M. R., and Papa, S. M. (2008). Inversion of dopamine responses in striatal medium spiny neurons and involuntary movements. *J. Neurosci.* 28, 7537–7547.
- Lievens, J. C., Salin, P., Nieoullon, A., and Kerkerian-Le Goff, L. (2001). Nigrostriatal denervation does not affect glutamate transporter mRNA expression but subsequent levodopa treatment selectively increases GLT1 mRNA and protein expression in the rat striatum. *J. Neurochem.* 79, 893–902.
- Lin, L. F., Doherty, D. H., Lile, J. D., Bektesh, S., and Collins, F. (1993). GDNF: a glial cell line-derived neurotrophic factor for midbrain dopaminergic neurons. *Science* 260, 1130–1132.
- Lindefors, N., and Ungerstedt, U. (1990). Bilateral regulation of glutamate tissue and extracellular levels in caudate-putamen by midbrain dopamine neurons. *Neurosci. Lett.* 115, 248–252.
- Lushnikova, I., Skibo, G., Muller, D., and Nikonenko, I. (2009). Synaptic potentiation induces increased glial coverage of excitatory synapses in CA1 hippocampus. *Hippocampus* 19, 753–762.
- Mallet, N., Ballion, B., Le Moine, C., and Gonon, F. (2006). Cortical inputs and GABA interneurons imbalance projection neurons in the striatum of parkinsonian rats. *J. Neurosci.* 26, 3875–3884.
- Marti, M., Sbrenna, S., Fuxe, K., Bianchi, C., Beani, L., and Morari, M. (1999). In vitro evidence for increased facilitation of striatal acetylcholine release via pre- and postsynaptic NMDA receptors in hemiparkinsonian rats. *J. Neurochem.* 72, 875–878.
- Massie, A., Goursaud, S., Schallier, A., Vermoesen, K., Meshul, C. K., Hermans, E., and Michotte, Y. (2010). Time-dependent changes in GLT-1 functioning in striatum of hemiparkinson rats. *Neurochem. Int.* 57, 572–578.
- Matsuzaki, M., Honkura, N., Ellis-Davies, G. C., and Kasai, H. (2004). Structural basis of long-term potentiation in single dendritic spines. *Nature* 429, 761–766.
- Meshul, C. K., Cogen, J. P., Cheng, H. W., Moore, C., Krentz, L., and McNeill, T. H. (2000). Alterations in rat striatal glutamate synapses following a lesion of the cortico- and/or nigrostriatal pathway. *Exp. Neurol.* 165, 191–206.
- Meshul, C. K., Emre, N., Nakamura, C. M., Allen, C., Donohue, M. K., and

- Buckman, J. F. (1999). Time-dependent changes in striatal glutamate synapses following a 6-hydroxydopamine lesion. *Neuroscience* 88, 1–16.
- Moss, J., and Bolam, J. P. (2008). A dopaminergic axon lattice in the striatum and its relationship with cortical and thalamic terminals. *J. Neurosci.* 28, 11221–11230.
- Neely, M. D., Schmidt, D. E., and Deutch, A. Y. (2007). Cortical regulation of dopamine depletion-induced dendritic spine loss in striatal medium spiny neurons. *Neuroscience* 149, 457–464.
- Oliet, S. H., Piet, R., and Poulain, D. A. (2001). Control of glutamate clearance and synaptic efficacy by glial coverage of neurons. *Science* 292, 923–926.
- Paixao, S., and Klein, R. (2010). Neuron-astrocyte communication and synaptic plasticity. *Curr. Opin. Neurobiol.* 20, 466–473.
- Park, J. B., Skalska, S., and Stern, J. E. (2006). Characterization of a novel tonic gamma-aminobutyric acidA receptor-mediated inhibition in magnocellular neurosecretory neurons and its modulation by glia. *Endocrinology* 147, 3746–3760.
- Perea, G., and Araque, A. (2010). Glia modulates synaptic transmission. *Brain Res. Rev.* 63, 93–102.
- Perea, G., Navarrete, M., and Araque, A. (2009). Tripartite synapses: astrocytes process and control synaptic information. *Trends Neurosci.* 32, 421–431.
- Petrova, P., Raibekas, A., Pevsner, J., Vigo, N., Anafi, M., Moore, M. K., Peaire, A. E., Shridhar, V., Smith, D. I., Kelly, J., Durocher, Y., and Commissong, J. W. (2003). MANF: a new mesencephalic, astrocyte-derived neurotrophic factor with selectivity for dopaminergic neurons. *J. Mol. Neurosci.* 20, 173–188.
- Petrova, P. S., Raibekas, A., Pevsner, J., Vigo, N., Anafi, M., Moore, M. K., Peaire, A. E., Shridhar, V., Smith, D. I., Kelly, J., Durocher, Y., and Commissong, J. W. (2004). Discovering novel phenotype-selective neurotrophic factors to treat neurodegenerative diseases. *Prog. Brain Res.* 146, 168–183.
- Pfriege, F. W. (2010). Role of glial cells in the formation and maintenance of synapses. *Brain Res. Rev.* 63, 39–46.
- Raju, D. V., Ahern, T. H., Shah, D. J., Wright, T. M., Standaert, D. G., Hall, R. A., and Smith, Y. (2008). Differential synaptic plasticity of the corticostriatal and thalamostriatal systems in an MPTP-treated monkey model of parkinsonism. *Eur. J. Neurosci.* 27, 1647–1658.
- Raju, D. V., Shah, D. J., Wright, T. M., Hall, R. A., and Smith, Y. (2006). Differential synaptology of vGluT2-containing thalamostriatal afferents between the patch and matrix compartments in rats. *J. Comp. Neurol.* 499, 231–243.
- Reichenbach, A., Derouiche, A., and Kirchhoff, F. (2010). Morphology and dynamics of perisynaptic glia. *Brain Res. Rev.* 63, 11–25.
- Robelet, S., Melon, C., Guillet, B., Salin, P., and Kerkerian-Le Goff, L. (2004). Chronic L-DOPA treatment increases extracellular glutamate levels and GLT1 expression in the basal ganglia in a rat model of Parkinson's disease. *Eur. J. Neurosci.* 20, 1255–1266.
- Sandhu, J. K., Gardaneh, M., Iwaszow, R., Lanthier, P., Gangaraju, S., Ribecco-Lutkiewicz, M., Tremblay, R., Kiuchi, K., and Sikorska, M. (2009). Astrocyte-secreted GDNF and glutathione antioxidant system protect neurons against 6OHDA cytotoxicity. *Neurobiol. Dis.* 33, 405–414.
- Schipke, C., and Kettenmann, H. (2004). Astrocytes responses to neuronal activity. *Glia* 47, 226–232.
- Scholz, B., Svensson, M., Alm, H., Skold, K., Falth, M., Kultima, K., Guigoni, C., Doudnikoff, E., Li, Q., Crossman, A. R., Bezard, E., and Andren, P. E. (2008). Striatal proteomic analysis suggests that first L-dopa dose equates to chronic exposure. *PLoS ONE* 3, e1589. doi: 10.1371/journal.pone.0001589
- Schuster, S., Doudnikoff, E., Rylander, D., Berthet, A., Aubert, I., Itrich, C., Bloch, B., Cenci, M. A., Surmeier, D. J., Henger, B., and Bezard, E. (2009). Antagonizing L-type Ca²⁺ channel reduces development of abnormal involuntary movement in the rat model of L-3,4-dihydroxyphenylalanine-induced dyskinesia. *Biol. Psychiatry* 65, 518–526.
- Slezak, M., Pfriege, F. W., and Soltys, Z. (2006). Synaptic plasticity, astrocytes and morphological homeostasis. *J. Physiol. Paris* 99, 84–91.
- Smith, A. D., and Bolam, J. P. (1990). The neural network of the basal ganglia as revealed by the study of synaptic connections of identified neurones. *Trends Neurosci.* 13, 259–265.
- Smith, Y., Raju, D., Nanda, B., Pare, J. F., Galvan, A., and Wichmann, T. (2009a). The thalamostriatal systems: anatomical and functional organization in normal and parkinsonian states. *Brain Res. Bull.* 78, 60–68.
- Smith, Y., Villalba, R. M., and Raju, D. V. (2009b). Striatal spine plasticity in Parkinson's disease: pathological or not? *Parkinsonism Relat. Disord.* 15(Suppl. 3), S156–S161.
- Smith, Y., and Villalba, R. (2008). Striatal and extrastriatal dopamine in the basal ganglia: an overview of its anatomical organization in normal and Parkinsonian brains. *Mov. Disord.* 23(Suppl. 3), S534–S547.
- Soderstrom, K. E., O'Malley, J. A., Levine, N. D., Sortwell, C. E., Collier, T. J., and Steece-Collier, K. (2010). Impact of dendritic spine preservation in medium spiny neurons on dopamine graft efficacy and the expression of dyskinesias in parkinsonian rats. *Eur. J. Neurosci.* 31, 478–490.
- Spacek, J. (1985). Three-dimensional analysis of dendritic spines. III. Glial sheath. *Anat. Embryol.* 171, 245–252.
- Stephens, B., Mueller, A. J., Shering, A. F., Hood, S. H., Taggart, P., Arbuthnott, G. W., Bell, J. E., Kilford, L., Kingsbury, A. E., Daniel, S. E., and Ingham, C. A. (2005). Evidence of a breakdown of corticostriatal connections in Parkinson's disease. *Neuroscience* 132, 741–754.
- Surmeier, D. J., Ding, J., Day, M., Wang, Z., and Shen, W. (2007). D1 and D2 dopamine-receptor modulation of striatal glutamatergic signaling in striatal medium spiny neurons. *Trends Neurosci.* 30, 228–235.
- Theodosis, D. T., and MacVicar, B. (1996). Neurone-glia interactions in the hypothalamus and pituitary. *Trends Neurosci.* 19, 363–367.
- Theodosis, D. T., Poulain, D. A., and Oliet, S. H. (2008). Activity-dependent structural and functional plasticity of astrocyte-neuron interactions. *Physiol. Rev.* 88, 983–1008.
- Tian, X., Kai, L., Hockberger, P. E., Wokosin, D. L., and Surmeier, D. J. (2010). MEF-2 regulates activity-dependent spine loss in striatopallidal medium spiny neurons. *Mol. Cell. Neurosci.* 44, 94–108.
- Todd, K. J., Serrano, A., Lacaille, J. C., and Robitaille, R. (2006). Glial cells in synaptic plasticity. *J. Physiol. Paris* 99, 75–83.
- Ventura, R., and Harris, K. M. (1999). Three-dimensional relationships between hippocampal synapses and astrocytes. *J. Neurosci.* 19, 6897–6906.
- Villalba, R. M., Lee, H., and Smith, Y. (2009). Dopaminergic denervation and spine loss in the striatum of MPTP-treated monkeys. *Exp. Neurol.* 215, 220–227.
- Villalba, R. M., and Smith, Y. (2010). Striatal spine plasticity in Parkinson's disease. *Front. Neuroanat.* 4:133. doi: 10.3389/fnana.2010.00133
- Villalba, R. M., and Smith, Y. (2011). Differential structural plasticity of corticostriatal and thalamostriatal axospinous synapses in MPTP-treated parkinsonian monkeys. *J. Comp. Neurol.* 519, 989–1005.
- Walker, R. H., Koch, R. J., Sweeney, J. E., Moore, C., and Meshul, C. K. (2009). Effects of subthalamic nucleus lesions and stimulation upon glutamate levels in the dopamine-depleted rat striatum. *Neuroreport* 20, 770–775.
- Wichmann, T., and DeLong, M. R. (2007). Anatomy and physiology of the basal ganglia: relevance to Parkinson's disease and related disorders. *Handb. Clin. Neurol.* 83, 1–18.
- Witcher, M. R., Kirov, S. A., and Harris, K. M. (2007). Plasticity of perisynaptic astroglia during synaptogenesis in the mature rat hippocampus. *Glia* 55, 13–23.
- Witcher, M. R., Park, Y. D., Lee, M. R., Sharma, S., Harris, K. M., and Kirov, S. A. (2010). Three-dimensional relationships between perisynaptic astroglia and human hippocampal synapses. *Glia* 58, 572–587.
- Xu-Friedman, M. A., Harris, K. M., and Regehr, W. G. (2001). Three-dimensional comparison of ultrastructural characteristics at depressing and facilitating synapses onto cerebellar Purkinje cells. *J. Neurosci.* 21, 6666–6672.
- Zaja-Milatovic, S., Milatovic, D., Schantz, A. M., Zhang, J., Montine, K. S., Samii, A., Deutch, A. Y., and Montine, T. J. (2005). Dendritic degeneration in neostriatal medium spiny neurons in Parkinson disease. *Neurology* 64, 545–547.
- Zhang, J. M., Wang, H. K., Ye, C. Q., Ge, W., Chen, Y., Jiang, Z. L., Wu, C. P., Poo, M. M., and Duan, S. (2003). ATP released by astrocytes mediates glutamatergic activity-dependent heterosynaptic suppression. *Neuron* 40, 971–982.

Conflict of Interest Statement: The authors declare that the research was conducted in the absence of any commercial or financial relationships that could be construed as a potential conflict of interest.

Received: 22 April 2011; paper pending published: 12 May 2011; accepted: 02 August 2011; published online: 23 August 2011.

Citation: Villalba RM and Smith Y (2011) Neuroglial plasticity at striatal glutamatergic synapses in Parkinson's disease. *Front. Syst. Neurosci.* 5:68. doi: 10.3389/fnsys.2011.00068

Copyright © 2011 Villalba and Smith. This is an open-access article subject to a non-exclusive license between the authors and Frontiers Media SA, which permits use, distribution and reproduction in other forums, provided the original authors and source are credited and other Frontiers conditions are complied with.



Dysregulated neuronal activity patterns implicate corticostriatal circuit dysfunction in multiple rodent models of Huntington's disease

Benjamin R. Miller[†], Adam G. Walker[†], Scott J. Barton and George V. Rebec^{*}

Program in Neuroscience and Department of Psychological and Brain Sciences, Indiana University, Bloomington, IN, USA

Edited by:

Elizabeth Abercrombie, Rutgers-Newark: The State University of New Jersey, USA

Reviewed by:

John A. Wolf, University of Pennsylvania, USA
Michael S. Levine, Brain Research Institute, USA

*Correspondence:

George V. Rebec, Program in Neuroscience and Department of Psychological and Brain Sciences, Indiana University, 1101 East 10th Street, Bloomington, IN 47405, USA.
e-mail: rebec@indiana.edu

†Present address:

Benjamin R. Miller, Department of Physiology, University of Texas Southwestern Medical School, 5323 Harry Hines Boulevard, Dallas, TX 75390, USA.
e-mail: benjamin.miller@utsouthwestern.edu;
Adam G. Walker, Department of Pharmacology, Vanderbilt University Medical Center, 1205 Light Hall, Nashville, TN 37232-0697, USA.
e-mail: adam.g.walker@vanderbilt.edu

Huntington's disease (HD) is an autosomal dominant neurodegenerative disorder that targets the corticostriatal system and results in progressive deterioration of cognitive, emotional, and motor skills. Although cortical and striatal neurons are widely studied in animal models of HD, there is little information on neuronal function during expression of the HD behavioral phenotype. To address this knowledge gap, we used chronically implanted micro-wire bundles to record extracellular spikes and local field potentials (LFPs) in truncated (R6/1 and R6/2) and full-length (knock-in, KI) mouse models as well as in transgenic HD rats (tgHD rats) behaving in an open-field arena. Spike activity was recorded in the striatum of all models and in prefrontal cortex (PFC) of R6/2 and KI mice, and in primary motor cortex (M1) of R6/2 mice. We also recorded LFP activity in R6/2 striatum. All HD models exhibited altered neuronal activity relative to wild-type (WT) controls. Although there was no consistent effect on firing rate across models and brain areas, burst firing was reduced in striatum, PFC, and M1 of R6/2 mice, and in striatum of KI mice. Consistent with a decline in bursting, the inter-spike-interval coefficient of variation was reduced in all regions of all models, except PFC of KI mice and striatum of tgHD rats. Among simultaneously recorded neuron pairs, correlated firing was reduced in all brain regions of all models, while coincident bursting, which measures the temporal overlap between bursting pairs, was reduced in striatum of all models as well as in M1 of R6/2s. Preliminary analysis of striatal LFPs revealed aberrant behavior-related oscillations in the delta to theta range and in gamma activity. Collectively, our results indicate that disrupted corticostriatal processing occurs across multiple HD models despite differences in the severity of the behavioral phenotype. Efforts aimed at normalizing corticostriatal activity may hold the key to developing new HD therapeutics.

Keywords: mouse models of Huntington's disease, behavioral electrophysiology, striatal local field potentials, spike synchrony, bursting

INTRODUCTION

The striatum receives input from all areas of cerebral cortex and uses that information to guide behavior. Corticostriatal processing plays a critical role in decision making, habit formation, movement selection, and reward expectancy (Alvarez and Eichenbaum, 2002; Costa et al., 2004; Graybiel, 2008; Israel and Bergman, 2008). In fact, cortical neurons are the primary driver of striatal neuronal activity. Without cortical input, striatal neurons are silent owing to an inwardly rectifying K⁺ current that keeps neuronal membranes hyperpolarized (Wilson and Kawaguchi, 1996). Glutamate released from cortical afferents increases striatal excitability, and when this input is coordinated across large numbers of afferents, the resulting activation of striatal circuits drives downstream processing through the rest of the basal ganglia (Wickens and Wilson, 1998). Thus, the striatum selects and refines the cortical signals that shape behavioral output.

Huntington's disease (HD), an autosomal dominant disorder caused by expansion of a translated CAG (glutamine) repeat in the N-terminal domain of the Huntingtin (HTT) protein (Huntington's Disease Collaborative Research Group, 1993), results

in widespread pathology of the corticostriatal system (Vonsattel and Figlia, 1998). Autopsy of end-stage HD patients reveals substantial degeneration and loss of medium spiny neurons, which account for more than 90% of the striatal neuronal population (Groves, 1983). Medium spiny neurons are the sole output system of the striatum, and they receive massive glutamate input from cortical pyramidal cells, which also undergo substantial degeneration and loss. Although damage occurs in other brain regions, corticostriatal pathology appears to be the primary cause of the cognitive and motor abnormalities that characterize HD (Lawrence et al., 1998).

Various rodent models of HD have been developed with the goal of identifying pathogenic mechanisms that can speed the search for safe and effective treatments. Different approaches have been used to model the HD phenotype. One approach, exemplified by the R6 line of mice, involves expression of the N-terminal fragment consisting of either the first exon or the first 171 amino acids (Mangiarini et al., 1996; Schilling et al., 1999). The result is expression of the truncated mutant HTT protein and an early and robust motor phenotype. The emergence of this phenotype soon after weaning has made the R6/2 model one of the most widely used in

the study of HD (Heng et al., 2008). R6/1 mice also show a robust phenotype but, because of a smaller polyglutamine expansion, onset occurs several weeks later than in R6/2 mice. In these and other truncated models, the polyglutamine expansion occurs independently of its natural genomic and protein context (Ehrnhoefer et al., 2009). An alternative approach is to express the full-length human mutant HTT as exemplified by the knock-in (KI) model, which has the polyglutamine expansion inserted or “knocked in” to the endogenous mouse gene (Shelbourne et al., 1999). In this case, the KI model contains a chimeric mouse–human HD gene, and thus the natural genomic and protein context of the polyglutamine expansion is largely preserved. Relative to the R6 line, KI mice display a less intense and later onset phenotype (Dorner et al., 2007; Menalled et al., 2009). Interestingly, assessments of both truncated and full-length mouse models indicate that the phenotype emerges well before substantial neuronal loss (Hickey et al., 2008). In fact, neuronal loss is not a primary feature of these models, suggesting that neuronal dysfunction, rather than loss *per se*, plays a critical role in the HD behavioral phenotype – an idea supported by clinical evaluations (Gutekunst et al., 2002; Palop et al., 2006).

To determine if functional deficits in corticostriatal neuronal processing is a common feature of HD models, we previously assessed the activity of individual striatal and prefrontal cortical (PFC) neurons in both R6/2 and KI mice (Miller et al., 2008b; Walker et al., 2008) as they behaved in an open-field arena where they could engage in naturally occurring episodes of spontaneous behavior. To assess the generality of our findings, we also recorded open-field striatal firing patterns in a transgenic HD rat (tgHD rat) model (Miller et al., 2010), which expresses a truncated fragment of the HD gene (von Hörsten et al., 2003). Overall, corticostriatal activity patterns are markedly altered in the HD animals relative to wild-type (WT) controls. To extend and update our previous findings to other HD models and other brain regions, we present here preliminary data indicating altered neuronal activity from motor cortex (M1) of R6/2 mice, and striatum of R6/1 mice. We also present early evidence from R6/2 striatum that local field potentials (LFPs), which represent the peri-synaptic activity of a large number of neurons, are altered in HD.

MATERIALS AND METHODS

Detailed methods can be found in Miller et al. (2008b, 2010), and Walker et al. (2008).

ANIMALS

Transgenic R6/1 and R6/2 mice (B6CBA–TgN[HDexon1]62Gpb) contain exon 1 of the human HD gene and are based on the C57BL/6 and CBA background strains (Mangiarini et al., 1996). The R6/2 mouse is characterized by a rapidly progressive phenotype with onset at ~4 weeks and death in ~16 weeks (Mangiarini et al., 1996; Carter et al., 1999; Levine et al., 2004). R6/1 mice are similar to R6/2s, albeit with a shorter repeat length and a later onset phenotype (Mangiarini et al., 1996). Homozygous KI (CAG 140) mice express a chimeric mouse/human exon 1 of the HD gene inserted into the mouse gene via homologous targeting of W9.5 ES cells from a 129sv background strain (Menalled et al., 2003). Homozygous tgHD rat have a Sprague-Dawley background and express a truncated HTT cDNA fragment with 51 CAG (polyglutamine) repeats

under control of the native rat HTT promoter (von Hörsten et al., 2003). Both the KI mouse and tgHD rat express a late onset HD phenotype, relative to R6/1 and R6/2 mice.

All animals, including corresponding WT for each HD model, were housed individually under standard conditions (12-h light/dark cycle with lights on at 07:30 h) with access to food and water *ad libitum*. All housing and animal-use procedures followed NIH guidelines and were approved by the Indiana University Institutional Animal Care and Use Committee.

SURGICAL PROCEDURES

All animals were anesthetized as appropriate (see Miller et al., 2008b, 2010) and mounted in a stereotaxic frame. The scalp was shaved, swabbed with betadine, and after lidocaine (20 mg/ml) was injected subcutaneously, an incision was made at the midline to expose the skull. Trepanations were made over the appropriate brain area according to mouse and rat brain atlases (Paxinos and Watson, 1998; Franklin and Paxinos, 2008). Multi-wire electrode bundles were lowered into each region. Additional holes were drilled for stainless steel anchor screws. Electrode assemblies were permanently attached to the skull with dental acrylic. Antibiotics were applied to the surgical site to prevent infection. Lactated Ringer's solution was administered subcutaneously to counteract dehydration. All animals were allowed 1 week of post-surgical recovery.

IN VIVO ELECTROPHYSIOLOGY

Electrode assemblies were made in-house and consisted of either four or eight, 25–50 μm Formvar-insulated stainless steel recording wires (California Fine Wire Company, Grover Beach, CA, USA) and one, 50 μm uninsulated stainless steel ground wire assembled in a custom fabricated hub. Electrode impedance was consistently ~1 M Ω . The electrode assembly was small, light-weight, and well-tolerated by all animals so that they could behave freely.

All experiments were conducted during the light phase of the diurnal cycle and were 30 min to 1 h in duration. Animals were placed in an open-field arena located in a sound-attenuated and electrically shielded recording chamber. Animals explored freely during the entire recording session. For recording, the electrode assembly was connected to a light-weight flexible harness equipped with field-effect transistors that provide unity-gain current amplification for each of the micro-wires. Extracellular neuronal action potentials and LFPs were routed through preamplifiers with 500 \times gain and 154 Hz to 8.8 kHz band-pass filters for spikes, and 1,000 \times gain and 0.7–170 Hz filters for LFPs. All signals were digitized at 40 kHz and acquired by the Multichannel Acquisition Processor system (Plexon, Dallas, TX, USA). Spikes were sorted online prior to the recording session. Voltage thresholds ≥ 2.5 times background noise were established, and waveform samples (~1,000) were collected to define a template via principal component analysis. The raw signal for each spike was routed to an oscilloscope and audio monitor to facilitate action potential discrimination by matching the analog signal with the digitized template. To maximize the probability that spikes consisted of only one signal (i.e., one neuron source), autocorrelation and inter-spike-interval (ISI) analyses were used to detect the presence of the absolute refractory period. In some cases, Spike 2 software (Cambridge Electronic Design, Cambridge, England) was used to confirm signal isolations offline.

BEHAVIORAL ANALYSIS

Mouse behaviors for all electrophysiological sessions were recorded by videotape and coded by observers who were blind to genotype. We coded open-field behavioral activity (e.g., ambulation, grooming, rearing, sniffing), and quiet rest, which was defined as absence of these and other overt behaviors. Rat behaviors were recorded using an open-field force-plate actometer, which provides a multivariate behavioral sensing arena (Fowler et al., 2001, 2009; Miller et al., 2010).

HISTOLOGY

Electrode placement in each brain area was verified before analysis. Animals were deeply anesthetized and a current pulse (30 μ A for 5 s) was passed through each micro-wire to mark recording sites. Animals were transcardially perfused with saline followed by 10% potassium ferrocyanide [$K_4Fe(CN)_6$] in 10% formalin to produce blue deposits at the site of the recording electrode ("Prussian blue" reaction). Brains were removed and cryoprotected in 30% sucrose dissolved in 10% formalin. The brains were then frozen, and coronal sections (50 μ M) were mounted on gelatin subbed slides to confirm micro-wire location.

DATA ANALYSIS

Neuronal data were analyzed by NeuroExplorer (Nex Technologies, Littleton, MA, USA) and custom written Matlab scripts (Mathworks, Natick, MA, USA). Statistical analyses used GraphPad Prism 5 (GraphPad Software, San Diego, CA, USA) and SigmaPlot 11 (Systat Software, San Jose, CA, USA), and the alpha level of significance was $p < 0.05$. Timestamps of all waveforms obtained from recording sessions were included for analysis. Firing rate was calculated by dividing the spike-trains into 1 s bins (spikes/s). To assess spike-train variability, the coefficient of variation of inter-spike-intervals (CV ISI) was calculated by dividing the SD of all ISIs in a train by the mean ISI of the train. Note that a CV = 1 indicates a Poisson and a CV = 0 is a completely regular spike-train. A CV > 1 indicates a complex spike-train pattern and often indicates bursting activity.

To quantify burst activity in spike-trains, the Poisson surprise algorithm was used (Legendy and Salcman, 1985). We used a minimum burst surprise value of five, which estimates that bursts occur ~150 times ($p < 0.007$) more frequently than would be expected in a Poisson spike-train with the same mean firing rate. The surprise value provides an estimate of the statistical significance of each burst in the spike-train. Therefore, the surprise value is an index of how intense or "surprising" the ISIs of a particular burst is compared with other ISIs in the same train. This method is a rigorous detector of bursts because it is not sensitive to fluctuations in average firing rate and treats each spike-train as an independent source (Legendy and Salcman, 1985). The method, moreover, is well-established for detecting bursts in striatum and cortical structures (Aldridge and Gilman, 1991; Homayoun et al., 2005; Wichmann and Soares, 2006). We used it to measure various indices of bursts (e.g., burst rate, burst duration, ISI in bursts, percent of spikes in the train that participate in burst activity, and the burst surprise value).

Coincident bursts were defined as the number of bursts from two neurons that overlap in time (Lisman, 1997; Miller et al., 2008b, 2010). The mean time that bursts were coincident (coincidence

duration), also was calculated. Coincident bursting and coincidence duration were determined for each pair-wise comparison in each session.

To assess correlated and synchronous firing (coherent firing) between two spike-trains, cross-correlation histograms (CCHs) were constructed for each pair-wise comparison (Parker et al., 1967) in each recording session. All CCHs were constructed based on 1 ms bins and either a ± 1 s (striatum) or ± 0.5 s (cortex) time lag from the zero bin. The CCHs were smoothed using a Gaussian filter with a bin width of three. Significant peaks, which indicate correlated and synchronous firing, were identified using a 95% confidence interval by assuming the null hypothesis that each spike-train is a Poisson process and that firing between neuronal pairs is independent (i.e., flat cross-correlogram; Abeles 1982).

Local field potential oscillations were assessed by analyzing power spectral densities (Fourier transforms) and spectrograms (frequency through time plots) generated in NeuroExplorer. LFP data were collected during discrete behaviors of quiet rest (lack of behavioral activation; see above), rearing and grooming. Each behavioral episode lasted a minimum of 3 s and LFP data were time-locked to the epoch. Power spectral densities were constructed by averaging LFP data for three different mice (three trials per mouse) for each behavior.

RESULTS

SPIKE ELECTROPHYSIOLOGY

Table 1 provides information on all the HD models used in our recording experiments (for comprehensive reviews of various HD rodent models see Levine et al., 2004; Heng et al., 2008). All our electrophysiological data are based on comparisons between HD animals and their respective WTs. All mouse models were recorded at varying stages of the disease from periods of early phenotype expression through later stages. Because of a longer period of phenotype expression, both the R6/1 and KI models are especially useful for this type of analysis, but in all cases, the electrophysiological changes that were evident early on persisted through later stages of disease progression. Thus, data for each model were combined across recording sessions. Assessment of the tgHD rat cohort occurred when animals expressed a mild, but stable phenotype.

Table 2 summarizes our spike electrophysiology results. Neurons were putatively labeled as either medium spiny in striatum or pyramidal in cortex based on well-established waveform and firing properties (see Miller et al., 2008b; Walker et al., 2008, and Discussion for details). We assessed the rate and pattern of spike activity of individual neurons as well as the correlated activity of simultaneously recorded neuronal pairs.

Table 1 | Characteristics of genetic rodent models of HD.

HD model	Repeat length*	Motor phenotype* onset (death)	Ages recorded*
R6/2	130	4 (14) (Mangiarini et al., 1996)	6–13
R6/1	115	12 (32) (Mangiarini et al., 1996)	8–29
KI	125	16 (96) (Menalled et al., 2003)	10–42
tgHD rat	51	40 (96) (von Hörsten et al., 2003)	40–60

*Indicates approximate repeat length.

*Indicates approximate weeks of age.

Changes in rate

Neuronal firing rate provides a metric of the overall level of neuronal activity. Increased levels of firing were found in striatum of both R6 models, but not KI mice or tgHD rats, relative to WT. In fact, rate was decreased in tgHD rats. Increased firing rate also was found in PFC of R6/2, but not KI mice, nor M1 cortex of R6/2s. It appears, therefore, that the R6 truncated mouse models, which show a robust phenotype, are prone to neuronal hyper-activity.

Changes in pattern

Spike pattern, reflected in the CV ISI and burst activity, represents a more detailed aspect of neuronal processing. The CV ISI is commonly used to assess spike-train variability, indicating complex firing patterns of activity (i.e., CV ISI > 1; see Materials and Methods). To quantify individual burst parameters, we used the Poisson burst surprise method to measure the percent of spikes that participate in bursts within each train as well as the burst surprise value (the higher the value the more “surprising” or prominent the burst). All our HD mouse models showed reductions in both CV ISI values and various aspects of bursting relative to WT. The only exceptions were tgHD striatum and the PFC of KI mice. Interestingly, the structure of individual bursts, which includes burst duration and ISI within bursts, was not altered in any model or brain area, suggesting that HD neurons have the capacity to burst, but lack the ability to generate a proper bursting pattern.

Table 2 | Summary of neuronal activity altered in HD models *in vivo*.

	Striatum	Cortex
Firing rate	↑ R6/2 ↑ R6/1 ↔ KI ↓ tgHDrat	↑ R6/2 (PFC, M1) ↔ KI (PFC)
Firing variability (CVISI)	↓ R6/2 ↓ R6/1 ↓ KI ↔ tgHDrat	↓ R6/2 (PFC, M1) ↔ KI (PFC)
Burst firing	↓ R6/2 ↓ R6/1 ↓ 140CAG ↔ tgHDrat	↓ R6/2 (PFC, M1) ↔ KI (PFC)
Coherent firing	↓ R6/2 ↓ R6/1 ↓ KI ↓ tgHDrat	↓ R6/2 (PFC, M1) ↓ KI (PFC)
Coincident* bursts	↓ R6/2 ↓ R6/1 ↓ KI ↓ tgHDrat	↓ R6/2 (M1)

↑ Significantly increased, ↓ significantly decreased, and ↔ no difference relative to WT.

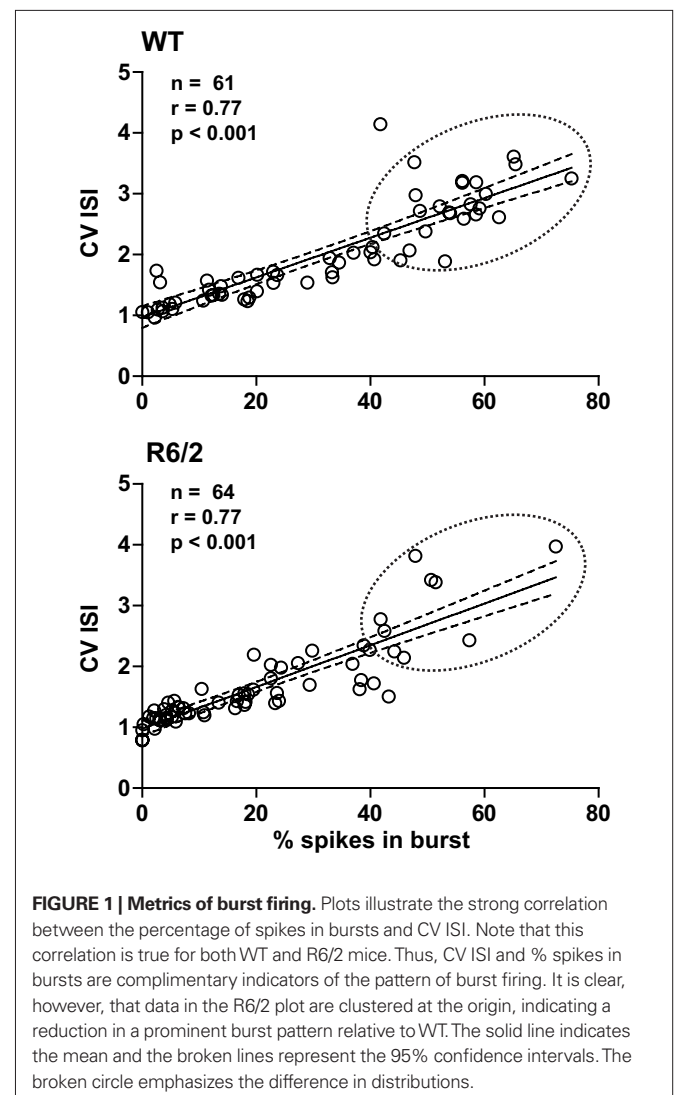
*Coincident bursts were not measured in PFC of R6/2 or KI.

References: R6/2 and KI striatum (Rebec et al., 2006; Miller et al., 2008b); R6/2 and KI PFC (Walker et al., 2008); tgHDrat striatum (Miller et al., 2010); R6/1 striatum and R6/2 M1 cortex data are preliminary and unpublished.

Both the CV ISI and the Poisson surprise methods rely on the deviation of the ISI from a Poisson distribution (Robin et al., 2009). In fact, as shown in **Figure 1**, a strong correlation exists between CV ISI and the percent of spikes in bursts. Note that bursts cluster near the origin in R6/2 mice indicating a reduction in the overall level of burst activity relative to WT.

Reductions in coherent firing among neuron pairs

We also assessed the temporal relationship in spiking between simultaneously recorded pairs of neurons. For this analysis, we constructed cross-correlograms, and in each case, peaks in the histogram that exceeded the confidence interval were defined as significantly coherent neuronal pairs. Interestingly, as shown in **Figure 2**, the temporal dynamics between coherent spiking differs between cortical and striatal neurons. For example, cortical neuron pairs tend to spike in precise temporal or “synchronized” coherence (Sakurai and Takahashi, 2006; Walker et al., 2008), whereas striatal neuron pairs discharge with much broader temporal coherence (Miller et al., 2008b; Ponzi and Wickens, 2010).



In all cases, however, we found a marked reduction in temporally coherent neuronal activity from all brain areas and all HD models recorded.

Reductions in coincident bursts among neuron pairs

We explored the temporal relationship in burst firing between neuron pairs by measuring the number of bursts that overlap in time (Lisman, 1997). Similar to coherent spikes, coincident bursts were

reduced in all brain areas and HD models tested. Moreover, in striatum of R6/2 and KI mice and their respective WT, a higher percentage of coincident bursts occurs in correlated than non-correlated neuronal pairs, suggesting that coherent bursting contributes to coherent spike activity (Miller et al., 2008b).

Figure 3 shows a sample of spike rasters recorded from individual WT and R6/2 mice. Altered firing properties are apparent at the single-neuron level (firing rate, bursts) and at the pair-wise level (coherent firing, coincident bursts). These activity patterns are comparable to what we have reported for striatum and PFC of other HD models (Miller et al., 2008b, 2010; Walker et al., 2008).

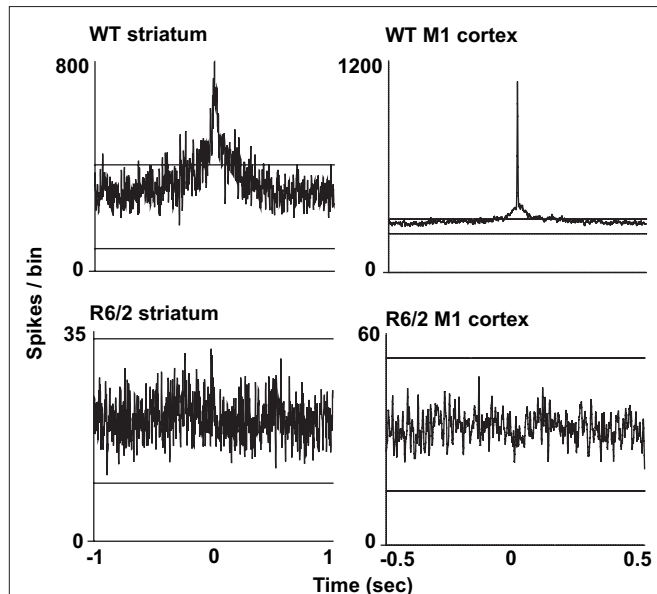


FIGURE 2 | Representative cross-correlograms constructed from a pair of WT and R6/2 striatal neurons (left column) and a pair of WT and R6/2 M1 cortical neurons (right column). The two horizontal lines in each plot indicate the 95% confidence intervals. The two WT peaks exceed the upper confidence interval, indicating significance. Note the different time scales between striatum and cortical cross-correlograms indicating either correlated or synchronous firing, respectively. Striatal and M1 neuron pairs show markedly reduced coherent spike activity (flat and non-significant peak). We note that we have yet to find repetitive peaks and troughs in the cross-correlograms, which indicates oscillatory firing activity between neuronal pairs.

STRIATAL LFPs

We have begun to investigate large ensembles of neurons by recording LFPs, which capture the sum of pre- and post-synaptic neuronal activity. In striatum, ample evidence indicates that LFPs represent a form of local processing, rather than volume conduction from other brain regions (Berke et al., 2004; DeCoteau et al., 2007). To date, we have recorded LFPs from dorsal striatum of three WT and three R6/2 mice during discrete, behaviorally matched epochs (minimum of three epochs per animal) in the open-field. During epochs of quiet rest, striatal LFP oscillations from WT mice were characterized by prominent delta to low theta oscillations (<5–7 Hz); the same was true for R6/2 mice, although a second prominent gamma band (30–40 Hz) oscillation also appeared (Figure 4). Behavioral episodes of rearing, which were strictly defined as upper forelimb rears on the side of the open-field for a minimum of 3 s, revealed delta oscillations in WT and R6/2 mice, but with an additional strong theta band (7–14 Hz) in the R6/2 model. In contrast, episodes of grooming showed no difference in LFP oscillations between R6/2 and WT.

DISCUSSION

Our results indicate that corticostriatal processing is altered in behaving, symptomatic HD rodent models compared to WT controls. This effect is evident in all the models we tested, albeit with some differences that may be related to behavioral phenotype or genetic background of the HD model. At the single-neuron level, for example, firing rate is elevated in strongly symptomatic R6/2

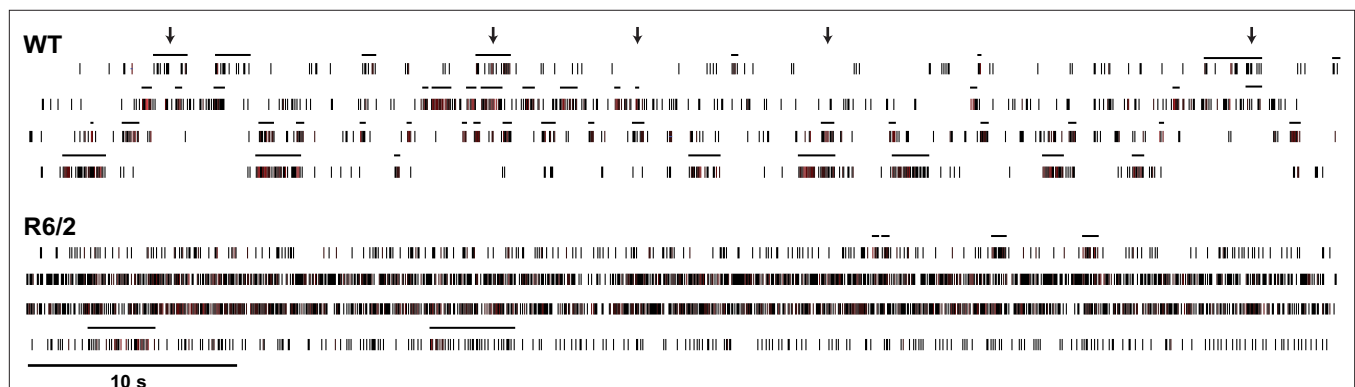


FIGURE 3 | Dysregulated neuronal firing patterns among populations of neurons. Long-timescale (60 s) spike rasters of four simultaneously recorded striatal neurons from WT and R6/2 mice. The horizontal lines above each raster define bursts. Arrows represent representative instances of coincident bursts in the WT raster. It is evident that population activity in WT mice is more phasic (more complex) and bursts are often temporally coherent across neurons relative to R6/2 mice.

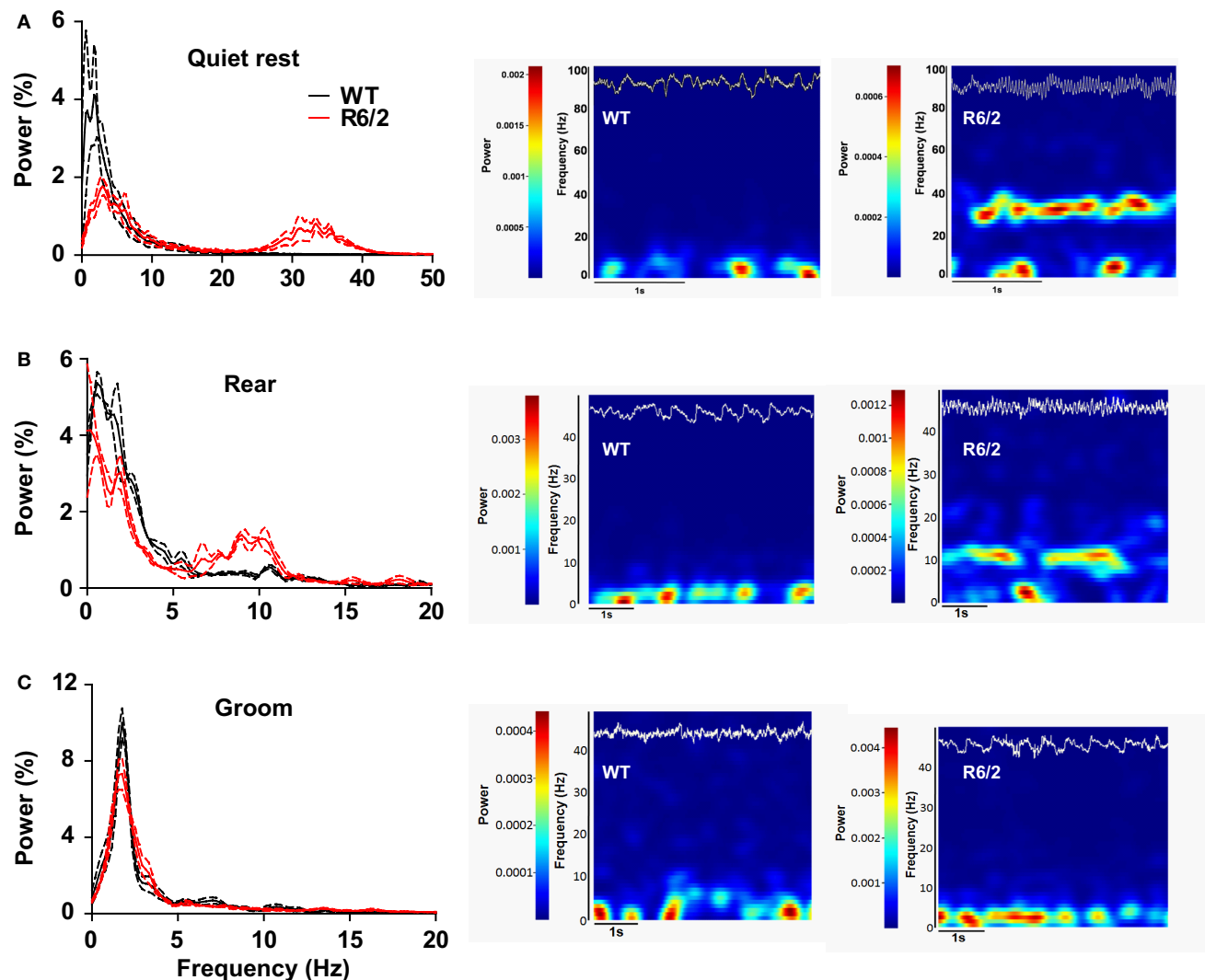


FIGURE 4 | Dysregulated striatal LFP oscillations in R6/2 mice. [(A), left] Power spectral densities of LFPs in striatum during quiet rest. Prominent 30–40 Hz (gamma) oscillations are present in R6/2 and absent in WT. Solid lines represent the mean density and broken lines indicate \pm SEM. [(A), right] Representative spectrograms (frequency through time) of LFP activity during a single epoch of quiet rest from a WT and R6/2 mouse. Frequency and power are

on the y axis; hotter colors represent greater power. The top trace (white) on each spectrogram is the corresponding raw LFP record (to scale). [(B), left and right] Same as (A), but striatal LFPs recorded during rearing. Note the prominent 10 Hz (theta) oscillation in R6/2 and its absence in WT. [(C), left and right] Striatal LFPs during epochs of grooming reveal no difference in LFP oscillations between the genotypes.

mice, but not in mildly symptomatic KI mice. Similarly, PFC burst firing is altered in R6/2s, but not KIs. In striatum, however, burst firing is attenuated in all mouse models. Interestingly, deficits in population-level neuronal processing occur in all brain regions. For example, analysis of cross-correlograms indicates coherent spiking is reduced in all HD models. Coincident bursting (i.e., temporally correlated burst activity between simultaneously recorded neurons) and oscillations of LFPs also show alterations in HD. Thus, neuronal firing patterns and their temporal dynamics are impaired in the HD corticostriatal system during spontaneous open-field behavior.

Our assessments focused on open-field behavior for two reasons. First, open-field testing is conducive to the long-duration (30 min to 1 h) recording sessions typically required for *in vivo* electrophysiology. For example, analysis of bursting, CV ISI, coincident burst-

ing, and construction of reliable cross-correlograms (a measure of coherent firing between neurons; see Materials and Methods) require records of many hundreds of spikes. Without sufficient spike data, the fidelity of these metrics is diminished. Second, coherent spike activity in both cortex (Constantinidis et al., 2002; Putrino et al., 2010) and striatum (Kimura et al., 2003), as well as striatal LFPs (Barnes et al., 2005), have been shown to be differentially driven by task performance, but rodent HD models show robust deficiencies in performing skilled behavioral tasks (Brooks and Dunnett, 2009). Such tasks, moreover, promote synaptic plasticity, which is compromised in cortex (Cummings et al., 2006, 2007) and striatum (Milnerwood et al., 2006) of HD models. In contrast, natural spontaneous open-field behaviors do not require prolonged learning periods and are unlikely to depend on overt changes in

synaptic plasticity. Thus, animals were studied in an open-field arena, which allowed for analysis of multiple, ongoing patterns of neuronal activity.

All HD mouse models showed a progressive behavioral phenotype relative to WT controls (Miller et al., 2008b; Walker et al., 2008). Although tgHD rats lose fine motor skills and develop prominent cognitive deficits at the ages used in our analysis (von Hörsten et al., 2003; Cao et al., 2006; Nguyen, 2006), we found no overt phenotype in the open-field (Miller et al., 2010). In fact, there was no substantial difference in spontaneous behavior (motor activity vs. quiet rest) between the genotypes of each HD model. Thus, it is unlikely that any differences that emerged in our electrophysiological data could be explained simply by differences in behavioral activity in the open-field, but instead are likely to reflect neuronal circuit differences between genotypes (e.g., WT vs. HD). Individual HD models, however, showed some electrophysiological differences (see **Table 2** for summary data; for HD phenotype references see Levine et al., 2004; Heng et al., 2008). These differences could emerge from the genetic background (i.e., strain and species) of each model, which in turn could influence firing activity of corticostriatal circuits. Interestingly, none of the tested models showed a clear trend for corticostriatal activity to worsen through HD progression. This outcome, however, is not entirely unexpected since the disruption in neuronal activity is prominent early on, even in the first recording session. It is likely, therefore, that corticostriatal activity is an early event in HD and persists throughout HD progression. Indeed, similar to our *in vivo* results, *ex vivo* cortical culture networks grown on microelectrode arrays and infected with mutant HTT fragments show reduced spontaneous collective burst firing (Gambazzi et al., 2010). Thus, the mutant HTT protein dramatically changes spontaneous network activity.

In WT striatum, neuronal activity is relatively slow but highly irregular as reflected in a CV ISI > 1 along with prominent episodes of spike bursting. In fact, irregular firing is a common feature of striatal medium spiny neurons (Wilson, 1993). That attenuation of this irregular pattern of activity occurs in most HD models that we have studied to date underscores the point that a simple change in rate (i.e., hyper-excitability) is not the fingerprint of striatal neuropathology. In fact, the change in pattern coupled with reductions in coordinated activity between simultaneously recorded neuronal pairs provides strong evidence for widespread dysfunction in cortical and striatal circuits. Our preliminary LFP data, which represents circuit rather than single-neuron activity, supports this view.

Circuit dysfunction indicates fundamental problems in neuronal communication, and evidence now suggests that a change in the extracellular dynamics of glutamate, an excitatory amino acid that shapes the pattern of both cortical and striatal activity, plays a critical role in HD (Miller and Bezprozvanny, 2010). In striatum, for example, the clearance of extracellular glutamate is significantly decreased in R6/2 relative to WT mice (Miller et al., 2008a). This effect, moreover, is evident early in the progression of the HD behavioral phenotype and can be reversed by increased expression of GLT1 (Miller et al., 2008a), the astroglial glutamate transporter responsible for the uptake of most extracellular glutamate (Danbolt, 2001). Increasing GLT1 expression also ameliorates the HD behavioral phenotype (Miller et al., 2008a). Failure of glutamate uptake likely contributes to the neurodegeneration

that occurs over the course of HD, which is driven in part by activation of extrasynaptic glutamate receptors (Milnerwood et al., 2010). Consistent with this view, deficits in glutamate uptake have been identified in post-mortem striatal tissue obtained from HD patients (Hassel et al., 2008). Dysregulation of glutamate dynamics, therefore, could be a key mechanism underlying our electrophysiological results in HD models. Striatal neurons also receive glutamate input from midline thalamus (Smith and Bolam, 1990), which may comprise another source of glutamate dysfunction in HD (Carroll et al., 2011).

Interneurons also may play a role. In both cortex and striatum, interneurons control the timing and synchrony of spikes generated by output neurons (Hestrin and Galarreta, 2005; Tiesinga et al., 2008). Interestingly, mutant HTT disrupts the mechanism by which receptors for GABA, an inhibitory amino acid released by cortical and striatal interneurons, are trafficked to synapses (Twelvetrees et al., 2010). Thus, loss of GABA-mediated inhibition may interact with deficits in glutamate clearance to disrupt corticostriatal processing in HD.

Striatal medium spiny neurons can be identified apart from other striatal neuron types (e.g., interneurons) by a combination of firing rate and spike waveform shape (Berke et al., 2004; Sharott et al., 2009). But because of the altered firing patterns recorded in a portion of our HD samples, we took a conservative approach and pooled all neurons for analysis. Note, however, that we ensured that all waveform shapes were consistent with putative medium spiny neurons (Berke et al., 2004; Miller et al., 2008b, 2010). It also is relevant that medium spiny neurons comprise >90% of neurons in striatum (Groves, 1983), making other neuron types less likely to be sampled. Moreover, we recognize that medium spiny neurons are not homogeneous. In fact, there is evidence that striato-pallidal neurons, which represent the so-called indirect pathway, degenerate earlier than the striato-nigral or direct pathway in HD patients (Deng et al., 2004; Starr et al., 2008). It is possible, therefore, that medium spiny neurons in our HD mice comprise two distinct populations. Nevertheless, a sizable number of striatal output neurons contribute axon collaterals to both the direct and indirect pathways (Levesque and Parent, 2005), making it difficult to speculate on the implications of possible differences between striato-pallidal and striato-nigral neurons in HD.

Like medium spiny neurons in striatum, cortical neurons can be classified by firing rate and waveform into fast-spiking (>10 spikes/s with narrow after hyperpolarizations, AHPs) and regular-spiking (<10 spikes/s with wide AHPs) neurons, which are thought to correspond to interneurons and pyramidal cells, respectively (McCormick et al., 1985; Connors and Gutnick, 1990; Homayoun and Moghaddam, 2007). In our PFC investigation (Walker et al., 2008), to determine if >10 spikes/s represents a separate class of neurons, we plotted the average of 50 waveforms and measured the AHPs. These data were compared to a random sample of AHPs from those classified as regular-spiking cells based on firing rate. Less than 10% of the cortical neurons (~500) recorded in our PFC investigation could be identified as fast-spiking neurons. Although some of these may be interneurons, our subsequent analysis of AHPs revealed no difference from regular-spiking AHPs, suggesting that our cortical neurons comprise a homogeneous population of presumed pyramidal cells.

Early studies of LFPs suggested that they arose mainly from laminar structures, while detectable oscillations in non-laminar areas (e.g., striatum) were thought to result from simple volume conduction. Ample evidence now argues against this view (Berke et al., 2004; Gatev et al., 2006; DeCoteau et al., 2007; Boraud et al., 2008). For example, entrainment of striatal neurons to LFP oscillations occurs at both beta and theta frequencies (Courtemanche et al., 2003; Berke et al., 2004; DeCoteau et al., 2007). It also is relevant that during periods of quiet rest our WT mice show a prominent LFP oscillation in the theta band (Figure 4), a finding in line with what has been reported in striatum of resting rats (DeCoteau et al., 2007). In fact, data obtained from M1 cortex and striatum indicate that the mechanism underlying LFP oscillations is similar in rat and mouse (Costa et al., 2006). LFPs are key features of behaviorally relevant neuronal processing (Buzsaki, 2006) and thus can make an important contribution to understanding the neural basis of the HD behavioral phenotype, apart from spike pattern analysis. It also appears that LFPs are strongly influenced by glutamate (Buzsaki, 2006), making their assessment in HD models especially appropriate.

Numerous *in vitro* studies of HD models report corticostriatal synaptic dysfunction (for reviews see Cepeda et al., 2007, 2010; Miller and Bezprozvanny, 2010), which may underlie the altered activity patterns observed in our HD animals. Although no one synaptic problem can be pinpointed, it is clear that striatal medium spiny neurons are hyperactive, which is in part due to a progressive increase in input resistance, reduction in cell capacitance, exaggerated glutamate-dependent responses, and increased intracellular calcium levels (see above, and Cepeda et al., 2001; Bezprozvanny and Hayden, 2004). On the other hand, subpopulations of striatal neurons show a decrease in spontaneous excitatory post-synaptic

currents and an increase in spontaneous inhibitory post-synaptic currents (Cummings et al., 2010). Recordings from cortical neurons in multiple HD models has revealed marked changes in synaptic events, including increased frequencies of spontaneous excitatory post-synaptic currents, a higher magnitude of evoked excitatory post-synaptic currents, and biphasic changes in inhibitory post-synaptic currents (Cummings et al., 2009). Interestingly, changes in striatal and cortical synaptic transmission are consistent across various genetic models of HD (Cummings et al., 2009, 2010). Therefore, it will be important to distinguish which facets of synaptic transmission in HD underscore the changes in neuronal activity patterns.

CONCLUSION

Our results point to corticostriatal processing deficits as an underlying feature of the HD behavioral phenotype. Because these deficits are present early in the progression of the disease, they likely set the stage for the increase in symptom severity that emerges later when neuronal degeneration and loss become prominent. Thus, it would be useful to assess HD models even before the behavioral phenotype emerges not only to gauge the onset of neuronal dysfunction but also to establish a target for testing new, more effective therapeutic strategies.

ACKNOWLEDGMENTS

This research was supported by R01 NS 035663, F31 NS 064791, F31 066603, and by the Indiana METACyt Initiative of Indiana University, funded in part through a major grant from the Lilly Endowment, Inc. Jason Ummel, Lauren Walker, Prianka Chilukuri, Wajeeha Hussain, and Desiree Cossyleon assisted with data collection. We also acknowledge the technical support of Paul Langley and the editorial assistance of Faye Caylor.

REFERENCES

- Abeles, M. (1982). Quantification, smoothing, and confidence limits for single-units' histograms. *J. Neurosci. Methods* 5, 317–325.
- Aldridge, J. W., and Gilman, S. (1991). The temporal structure of spike trains in the primate basal ganglia: afferent regulation of bursting demonstrated with precentral cerebral cortical ablation. *Brain Res.* 543, 123–138.
- Alvarez, P., and Eichenbaum, H. (2002). Representations of odors in the rat orbitofrontal cortex change during and after learning. *Behav. Neurosci.* 116, 421–433.
- Barnes, B. W., Liljeholm, M., and Ostlund, S. B. (2005). Activity of striatal neurons reflects dynamic encoding and recoding of procedural memories. *Nature* 437, 1158–1161.
- Berke, J. D., Okatan, M., Skurski, J., and Eichenbaum, H. B. (2004). Oscillatory entrainment of striatal neurons in freely moving rats. *Neuron* 43, 883–896.
- Bezprozvanny, I., and Hayden, M. R. (2004). Deranged calcium signaling and Huntington's disease. *Biochem. Biophys. Res. Commun.* 322, 1310–1317.
- Boraud, T., Brown, P., Goldberg, J. A., Graybiel, A. M., and Magill, P. J. (2008). "Oscillations in the basal ganglia: the good, the bad, and the unexpected," in *The Basal Ganglia VIII*, eds J. P. Bolam, C. A. Ingham, and P. J. Magill (New York: Springer Science and Business Media), 3–22.
- Brooks, S. P., and Dunnett, S. B. (2009). Tests to assess motor phenotype in mice: a user's guide. *Nat. Rev. Neurosci.* 10, 519–529.
- Buzsaki, G. (2006). *Rhythms of the Brain*. New York: Oxford University Press.
- Cao, C., Temel, Y., Blokland, A., Ozen, H., Steinbusch, H. W., Vlamings, R., Nguyen, H. P., von Horsten, S., Schmitz, C., and Visser-Vandewalle, V. (2006). Progressive deterioration of reaction time performance and choreiform symptoms in a new Huntington's disease transgenic rat-model. *Behav. Brain Res.* 170, 257–261.
- Carroll, J. B., Lerch, J. P., Franciosi, S., Spreuw, A., Bissada, N., Henkelman, R. M., and Hayden, M. R. (2011). Natural history of disease in the YAC128 mouse reveals a discrete signature of pathology in Huntington's disease. *Neurobiol. Dis.* PMID: 21458571. [Epub ahead of print].
- Carter, R. J., Lione, L. A., Humby, T., Mangiarini, L., Mahal, A., Bates, G. P., Dunnett, S. B., and Morton, A. J. (1999). Characterization of progressive motor deficits in mice transgenic for the human Huntington's disease mutation. *J. Neurosci.* 19, 3248–3257.
- Cepeda, C., Ariano, M. A., Calvert, C. R., Flores-Hernandez, J., Chandler, S. H., Leavitt, B. R., Hayden, M. R., and Levine, M. S. (2001). NMDA receptor function in mouse models of Huntington disease. *J. Neurosci. Res.* 66, 525–539.
- Cepeda, C., Cummings, D. M., André, V. M., Holley, S. M., and Levine, M. S. (2010). Genetic mouse models of Huntington's disease: focus on electrophysiological mechanisms. *ASN Neuro* 2, e00033.
- Cepeda, C., Wu, N., Andre, V. M., Cummings, D. M., and Levine, M. S. (2007). The corticostriatal pathway in Huntington's disease. *Prog. Neurobiol.* 81, 253–271.
- Connors, B. W., and Gutnick, M. J. (1990). Intrinsic firing patterns of diverse neocortical neurons. *Trends Neurosci.* 13, 99–104.
- Constantinidis, C., Williams, G. V., and Goldman-Rakic, P. S. (2002). A role for inhibition in shaping the temporal flow of information in prefrontal cortex. *Nat. Neurosci.* 5, 175–180.
- Costa, R. M., Cohen, D., and Nicolelis, M. A. (2004). Differential corticostriatal plasticity during fast and slow motor skill learning in mice. *Curr. Biol.* 14, 1124–1134.
- Costa, R. M., Lin, S. C., Sotnikova, T. D., Cyr, M., Gainetdinov, R. R., Caron, M. G., and Nicolelis, M. A. (2006). Rapid alterations in corticostriatal ensemble coordination during acute dopamine-dependent motor dysfunction. *Neuron* 52, 359–369.
- Courtemanche, R., Fujii, N., and Graybiel, A. M. (2003). Synchronous, focally modulated beta-band oscillations characterize local field potential activity in the striatum of awake behaving monkeys. *J. Neurosci.* 23, 11741–11752.
- Cummings, D. M., Andre, V. M., Uzgil, B. O., Gee, S. M., Fisher, Y. E., Cepeda, C.,

- and Levine, M. S. (2009). Alterations in cortical excitation and inhibition in genetic mouse models of Huntington's disease. *J. Neurosci.* 29, 10371–10386.
- Cummings, D. M., Cepeda, C., and Levine, M. S. (2010). Alterations in striatal synaptic transmission are consistent across genetic mouse models of Huntington's disease. *ASN Neuro* 2, e00036.
- Cummings, D. M., Milnerwood, A. J., Dallerac, G. M., Vatsavayi, S. C., Hirst, M. C., and Murphy, K. P. (2007). Abnormal cortical synaptic plasticity in a mouse model of Huntington's disease. *Brain Res. Bull.* 72, 103–107.
- Cummings, D. M., Milnerwood, A. J., Dallerac, G. M., Waights, V., Brown, J. Y., Vatsavayi, S. C., Hirst, M. C., and Murphy, K. P. (2006). Aberrant cortical synaptic plasticity and dopaminergic dysfunction in a mouse model of Huntington's disease. *Hum. Mol. Genet.* 15, 2856–2868.
- Danbolt, N. C. (2001). Glutamate uptake. *Prog. Neurobiol.* 65, 1–105.
- DeCoteau, W. E., Thorn, C., Gibson, D. J., Courtemanche, R., Mitra, P., Kubota, Y., and Graybiel, A. M. (2007). Oscillations of local field potentials in the rat dorsal striatum during spontaneous and instructed behaviors. *J. Neurophysiol.* 97, 3800–3805.
- Deng, Y. P., Albin, R. L., Penney, J. B., Young, A. B., Anderson, K. D., and Reiner, A. (2004). Differential loss of striatal projection systems in Huntington's disease: a quantitative immunohistochemical study. *J. Chem. Neuroanat.* 27, 143–164.
- Dorner, J. L., Miller, B. R., Barton, S. J., Brock, T. J., and Rebec, G. V. (2007). Sex differences in behavior and striatal ascorbate release in the 140 CAG knock-in mouse model of Huntington's disease. *Behav. Brain Res.* 178, 90–97.
- Ehrnhofer, D. E., Butland, S. L., Pouladi, M. A., and Hayden, M. R. (2009). Mouse models of Huntington disease: variations on a theme. *Dis. Model Mech.* 2, 123–129.
- Fowler, S. C., Birkestrand, B. R., Chen, R., Moss, S. J., Vorontsova, E., Wang, G., and Zarcone, T. J. (2001). A force-plate actometer for quantitating rodent behaviors: illustrative data on locomotion, rotation, spatial patterning, stereotypies and tremor. *J. Neurosci. Methods* 107, 107–124.
- Fowler, S. C., Miller, B. R., Gaither, T. W., Johnson, M. A., and Rebec, G. V. (2009). Force-plate quantification of progressive behavioral deficits in the R6/2 mouse model of Huntington's disease. *Behav. Brain Res.* 202, 130–137.
- Franklin, K., and Paxinos, G. (2008). *The Mouse Brain in Stereotaxic Coordinates*, 3rd Edn. New York: Academic Press.
- Gambazzi, L., Gokce, O., Seredenina, T., Katsyuba, E., Runne, H., Markram, H., Giugliano, M., and Luthi-Carter, R. (2010). Factor expression underlies cortical neuron microcircuit hypoconnectivity resulting from exposure to mutant Huntingtin fragments. *J. Pharmacol. Exp. Ther.* 335, 13–22.
- Gatev, P., Darbin, O., and Wichmann, T. (2006). Oscillations in the basal ganglia under normal conditions and in movement disorders. *Mov. Disord.* 21, 1566–1577.
- Graybiel, A. M. (2008). Habits, rituals, and the evaluative brain. *Annu. Rev. Neurosci.* 31, 359–387.
- Groves, P. M. (1983). A theory of the functional organization of the neostriatum and the neostriatal control of voluntary movement. *Brain Res.* 286, 109–132.
- Gutekunst, C.-A., Norflus, F., and Hersch, S. M. (2002). "The neuropathology of Huntington's disease," in *Huntington's Disease*, 3rd Edn, eds G. Bates, P. Harper, and L. Jones (New York: Oxford University Press), 251–275.
- Hassel, B., Tessier, S., Faull, R. L., and Emson, P. C. (2008). Glutamate uptake is reduced in prefrontal cortex in Huntington's disease. *Neurochem. Res.* 33, 232–237.
- Heng, M. Y., Detloff, P. J., and Albin, R. L. (2008). Rodent genetic models of Huntington disease. *Neurobiol. Dis.* 32, 1–9.
- Hestrin, S., and Galarreta, M. (2005). Electrical synapses define networks of neocortical GABAergic neurons. *Trends Neurosci.* 28, 304–309.
- Hickey, M. A., Kosmalska, A., Enayati, J., Cohen, R., Zeitlin, S., Levine, M. S., and Chesselet, M. F. (2008). Extensive early motor and non-motor behavioral deficits are followed by striatal neuronal loss in knock-in Huntington's disease mice. *Neuroscience* 157, 280–295.
- Homayoun, H., Jackson, M. E., and Moghaddam, B. (2005). Activation of metabotropic glutamate 2/3 receptors reverses the effects of NMDA receptor hypofunction on prefrontal cortex unit activity in awake rats. *J. Neurophysiol.* 93, 1989–2001.
- Homayoun, H., and Moghaddam, B. (2007). NMDA receptor hypofunction produces opposite effects on prefrontal cortex interneurons and pyramidal neurons. *J. Neurosci.* 27, 11496–11500.
- Huntington's Disease Collaborative Research Group. (1993). A novel gene containing a trinucleotide repeat that is expanded and unstable on Huntington's disease chromosomes. *Cell* 72, 971–983.
- Israel, Z., and Bergman, H. (2008). Pathophysiology of the basal ganglia and movement disorders: from animal models to human clinical applications. *Neurosci. Biobehav. Rev.* 32, 367–377.
- Kimura, M., Matsumoto, N., Okahashi, K., Ueda, Y., Satoh, T., Minamimoto, T., Sakamoto, M., and Yamada, H. (2003). Goal-directed, serial and synchronous activation of neurons in the primate striatum. *Neuroreport* 14, 799–802.
- Lawrence, A. D., Sahakian, B. J., and Robbins, T. W. (1998). Cognitive functions and corticostriatal circuits: insights from Huntington's disease. *Trends Cogn. Sci.* 2, 379–388.
- Legendy, C. R., and Salzman, M. (1985). Bursts and recurrences of bursts in the spike trains of spontaneously active striate cortex neurons. *J. Neurophysiol.* 53, 926–939.
- Levesque, M., and Parent, A. (2005). The striatofugal fiber system in primates: a reevaluation of its organization based on single-axon tracing studies. *Proc. Natl. Acad. Sci. U.S.A.* 102, 11888–11893.
- Levine, M. S., Cepeda, C., Hickey, M. A., Fleming, S. M., and Chesselet, M. F. (2004). Genetic mouse models of Huntington's and Parkinson's diseases: illuminating but imperfect. *Trends Neurosci.* 27, 691–697.
- Lisman, J. E. (1997). Bursts as a unit of neural information: making unreliable synapses reliable. *Trends Neurosci.* 20, 38–43.
- Mangiarini, L., Sathasivam, K., Seller, M., Cozens, B., Harper, A., Hetherington, C., Lawton, M., Trotter, Y., Leach, H., Davies, S. W., and Bates, G. P. (1996). Exon 1 of the HD gene with an expanded CAG repeat is sufficient to cause a progressive neurological phenotype in transgenic mice. *Cell* 87, 493–506.
- McCormick, D. A., Connors, B. W., Lighthall, J. W., and Prince, D. A. (1985). Comparative electrophysiology of pyramidal and sparsely spiny stellate neurons of the neocortex. *J. Neurophysiol.* 54, 782–806.
- Menalled, L., El-Khodori, B. F., Patry, M., Suárez-Fariñas, M., Orenstein, S. J., Zahasky, B., Leahy, C., Wheeler, V., Yang, X. W., MacDonald, M., Morton, A. J., Bates, G., Leeds, J., Park, L., Howland, D., Signer, E., Tobin, A., and Brunner, D. (2009). Systematic behavioral evaluation of Huntington's disease transgenic and knock-in mouse models. *Neurobiol. Dis.* 35, 319–336.
- Menalled, L. B., Sison, J. D., Dragatsis, I., Zeitlin, S., and Chesselet, M. F. (2003). Time course of early motor and neuropathological anomalies in a knock-in mouse model of Huntington's disease with 140 CAG repeats. *J. Comp. Neurol.* 465, 11–26.
- Miller, B. R., and Bezprozvanny, I. (2010). Corticostriatal circuit dysfunction in Huntington's disease: intersection of glutamate, dopamine and calcium. *Future Neurol.* 5, 735–756.
- Miller, B. R., Dorner, J. L., Shou, M., Sari, Y., Barton, S. J., Sengelaub, D. R., Kennedy, R. T., and Rebec, G. V. (2008a). Up-regulation of GLT1 expression increases glutamate uptake and attenuates the Huntington's disease phenotype in the R6/2 mouse. *Neuroscience* 153, 329–337.
- Miller, B. R., Walker, A. G., Shah, A. S., Barton, S. J., and Rebec, G. V. (2008b). Dysregulated information processing by medium-spiny neurons in striatum of freely behaving mouse models of Huntington's disease. *J. Neurophysiol.* 100, 2205–2216.
- Miller, B. R., Walker, A. G., Fowler, S. C., von Hörsten, S., Riess, O., Johnson, M. A., and Rebec, G. V. (2010). Dysregulation of coordinated neuronal firing patterns in striatum of freely behaving transgenic rats that model Huntington's disease. *Neurobiol. Dis.* 37, 106–113.
- Milnerwood, A. J., Cummings, D. M., Dallerac, G. M., Brown, J. Y., Vatsavayi, S. C., Hirst, M. C., Rezaie, P., and Murphy, K. P. (2006). Early development of aberrant synaptic plasticity in a mouse model of Huntington's disease. *Hum. Mol. Genet.* 15, 1690–1703.
- Milnerwood, A. J., Gladding, C. M., Pouladi, M. A., Kaufman, A. M., Hines, R. M., Boyd, J. D., Ko, R. W., Vasuta, O. C., Graham, R. K., Hayden, M. R., Murphy, T. H., and Raymond, L. A. (2010). Early increase in extrasynaptic nmda receptor signaling and expression contributes to phenotype onset in Huntington's disease mice. *Neuron* 65, 178–190.
- Nguyen, P. V. (2006). Comparative plasticity of brain synapses in inbred mouse strains. *J. Exp. Biol.* 209, 2293–2303.
- Palop, J. J., Chin, J., and Mucke, L. (2006). A network dysfunction perspective on neurodegenerative diseases. *Nature* 443, 768–773.
- Paxinos, G., and Watson, C. (1998). *The Rat Brain in Stereotaxic Coordinates*. New York: Academic Press.
- Perkel, D. H., Gerstein, G. L., and Moore, G. P. (1967). Neuronal spike trains and stochastic point processes. II. Simultaneous spike trains. *Biophys. J.* 7, 419–440.
- Ponzi, A., and Wickens, J. (2010). Sequentially switching cell assemblies in random inhibitory networks of spiking neurons in the striatum. *J. Neurosci.* 30, 5894–5911.
- Putrino, D., Brown, E. N., Mastaglia, F. L., and Ghosh, S. (2010). Differential involvement of excitatory and inhibitory neurons of cat motor cortex in coincident spike activity related to behavioral context. *J. Neurosci.* 30, 8048–8056.

- Rebec, G. V., Conroy, S. K., and Barton, S. J. (2006). Hyperactive striatal neurons in symptomatic Huntington R6/2 mice: variations with behavioral state and repeated ascorbate treatment. *Neuroscience* 137, 327–336.
- Robin, K., Maurice, N., Degos, B., Deniau, J. M., Martinerie, J., and Pezard, L. (2009). Assessment of bursting activity and interspike intervals variability: a case study for methodological comparison. *J. Neurosci. Methods* 179, 142–149.
- Sakurai, Y., and Takahashi, S. (2006). Dynamic synchrony of firing in the monkey prefrontal cortex during working-memory tasks. *J. Neurosci.* 26, 10141–10153.
- Schilling, G., Becher, M. W., Sharp, A. H., Jinnah, H. A., Duan, K., Kotz, J. A., Slunt, H. H., Ratovitski, T., Cooper, J. K., Jenkins, N. A., Copeland, N. G., Price, D. L., Ross, C. A., and Borchelt, D. R. (1999). Intranuclear inclusions and neuritic aggregates in transgenic mice expressing a mutant N-terminal fragment of Huntingtin. *Hum. Mol. Genet.* 8, 397–407.
- Sharott, A., Moll, C. K., Engler, G., Denker, M., Grun, S., and Engel, A. K. (2009). Different subtypes of striatal neurons are selectively modulated by cortical oscillations. *J. Neurosci.* 29, 4571–4585.
- Shelbourne, P. F., Killeen, N., Hevner, R. F., Johnston, H. M., Tecott, L., Lewandoski, M., Ennis, M., Ramirez, L., Li, Z., Iannicola, C., Littman, D. R., and Myers, R. M. (1999). A Huntington's disease CAG expansion at the murine Hdh locus is unstable and associated with behavioural abnormalities in mice. *Hum. Mol. Genet.* 8, 763–774.
- Smith, A. D., and Bolam, J. P. (1990). The neural network of the basal ganglia as revealed by the study of synaptic connections of identified neurones. *Trends Neurosci.* 13, 259–265.
- Starr, P. A., Kang, G. A., Heath, S., Shimamoto, S., and Turner, R. S. (2008). Pallidal neuronal discharge in Huntington's disease: support for selective loss of striatal cells originating the indirect pathway. *Exp. Neurol.* 211, 227–233.
- Tiesinga, P., Fellous, J. M., and Sejnowski, T. J. (2008). Regulation of spike timing in visual cortical circuits. *Nat. Rev. Neurosci.* 9, 97–107.
- Twelveetrees, A. E., Yuen, E. Y., Arancibia-Carcamo, I. L., MacAskill, A. F., Rostaing, P., Lumb, M. J., Humbert, S., Triller, A., Saudou, F., Yan, Z., and Kittler, J. T. (2010). Delivery of GABAARs to synapses is mediated by HAP1-KIF5 and disrupted by mutant Huntingtin. *Neuron* 65, 53–65.
- von Hörsten, S., Schmitt, I., Nguyen, H. P., Holzmann, C., Schmidt, T., Walther, T., Bader, M., Pabst, R., Kobbe, P., Krotova, J., Stiller, D., Kask, A., Vaarmann, A., Rathke-Hartlieb, S., Schulz, J. B., Grasshoff, U., Bauer, I., Vieira-Saecker, A. M., Paul, M., Jones, L., Lindenberg, K. S., Landwehrmeyer, B., Bauer, A., Li, X. J., and Riess, O. (2003). Transgenic rat model of Huntington's disease. *Hum. Mol. Genet.* 12, 617–624.
- Vonsattel, J. P., and Figlia, M. (1998). Huntington disease. *J. Neuropathol. Exp. Neurol.* 57, 360–384.
- Walker, A. G., Miller, B. R., Fritsch, J. N., Barton, S. J., and Rebec, G. V. (2008). Altered information processing in the prefrontal cortex of Huntington's disease mouse models. *J. Neurosci.* 28, 8973–8982.
- Wichmann, T., and Soares, J. (2006). Neuronal firing before and after burst discharges in the monkey basal ganglia is predictably patterned in the normal state and altered in parkinsonism. *J. Neurophysiol.* 95, 2120–2133.
- Wickens, J. R., and Wilson, C. J. (1998). Regulation of action-potential firing in spiny neurons of the rat neostriatum in vivo. *J. Neurophysiol.* 79, 2358–2364.
- Wilson, C. J. (1993). The generation of natural firing patterns in neostriatal neurons. *Prog. Brain Res.* 99, 277–297.
- Wilson, C. J., and Kawaguchi, Y. (1996). The origins of two-state spontaneous membrane potential fluctuations of neostriatal spiny neurons. *J. Neurosci.* 16, 2397–2410.

Conflict of Interest Statement: The authors declare that the research was conducted in the absence of any commercial or financial relationships that could be construed as a potential conflict of interest.

Received: 04 January 2011; accepted: 27 April 2011; published online: 09 May 2011.
Citation: Miller BR, Walker AG, Barton SJ and Rebec GV (2011) Dysregulated neuronal activity patterns implicate corticostriatal circuit dysfunction in multiple rodent models of Huntington's disease. *Front. Syst. Neurosci.* 5:26. doi: 10.3389/fnsys.2011.00026
Copyright © 2011 Miller, Walker, Barton and Rebec. This is an open-access article subject to a non-exclusive license between the authors and Frontiers Media SA, which permits use, distribution and reproduction in other forums, provided the original authors and source are credited and other Frontiers conditions are complied with.



Functional changes in neocortical activity in Huntington's disease model mice: an *in vivo* intracellular study

Edward A. Stern^{1,2*}

¹ Brain Research Center, Bar-Ilan University, Ramat Gan, Israel

² Department of Neurology, MassGeneral Institute for Neurodegenerative Disease, Massachusetts General Hospital, Harvard Medical School, Charlestown, MA, USA

Edited by:

Elizabeth Abercrombie, Rutgers-Newark: The State University of New Jersey, USA

Reviewed by:

Michael S. Levine, Brain Research Institute, USA
George V. Rebec, Indiana University, USA

*Correspondence:

Edward A. Stern, Brain Research Center, Bar-Ilan University, Ramat Gan 52900, Israel.
e-mail: sterned@mail.biu.ac.il

Studies of animal models of Huntington's disease (HD) have revealed that neocortical and neostriatal neurons of these animals *in vitro* exhibit a number of morphological and physiological changes, including increased input resistance and changes in neocortical synaptic inputs. We measured the functional effects of polyglutamate accumulation in neocortical neurons in R6/2 mice (8–14 weeks of age) and their age-matched non-transgenic littermates using *in vivo* intracellular recordings. All neurons showed spontaneous membrane potential fluctuations. The current/voltage and the firing properties of the HD neocortical neurons were significantly altered, especially in the physiologically relevant current range around and below threshold. As a result, membrane potential transitions from the Down state to Up state were evoked with smaller currents in HD neocortical neurons than in controls. The excitation-to-frequency curves of the HD mice were significantly steeper than those of controls, indicating a smaller input–output dynamic range for these neurons. Increased likelihood of Down to Up state transitions could cause pathological recruitment of corticostriatal assemblies by increasing correlated neuronal activity. We measured coherence of the *in vivo* intracellular recordings with simultaneously recorded electrocorticograms. We found that the peak of the coherence at <5 Hz was significantly smaller in the HD animals, indicating that the amount of coherence in the state transitions of single neurons is less correlated with global activity than non-transgenic controls. We propose that decreased correlation of neocortical inputs may be a major physiological cause underlying the errors in sensorimotor pattern generation in HD.

Keywords: Huntington's disease, cortex, striatum, R6/2, intracellular recording, *in vivo*

INTRODUCTION

The corticostriatal pathway is one of the two major inputs to the basal ganglia, containing inputs from virtually every neocortical area. The role of this pathway in sensorimotor and cognitive behavior is only beginning to be unraveled. One key to understanding the corticostriatal neural mechanisms underlying behavior is to study the changes in neocortical activity when it is disrupted by a disease. Huntington's disease (HD) is a neurodegenerative disease primarily affecting the projection neurons in the neocortex and neostriatum (Vonsattel et al., 1985). Symptoms of HD include involuntary movements, but also include sensory and cognitive disruptions, as would be expected when the neuropathology affects large telencephalic areas. HD is characterized by accumulation of abnormal protein (huntingtin) which aggregates in the nucleus and cytoplasm of neocortical pyramidal neurons and neostriatal medium spiny neurons (Davies et al., 1997; DiFiglia et al., 1997). The functional changes in neocortical and neostriatal activity underlying the symptoms of HD begin prior to neurodegeneration, and the mechanisms underlying the changes are poorly understood. Following the discovery of the HD gene (HDCRG, 1993), a number of animal models of the disease have been used to characterize the cellular changes in neocortical neurons and neostriatal neurons prior to degeneration. One of the best known and studied HD transgenic models is the R6/2 line (Mangiarini et al., 1996, 1997; Davies et al., 1997; Bates et al., 1998). In these animals, neocortical

and neostriatal projection neurons develop intranuclear inclusions with a well-established timeline in which all neurons have the inclusions by 8 weeks of age. The animals show behavioral dysfunctions, and die at about 12–14 weeks of age. The relatively short lifespan and fast development of pathology makes these mice ideal for study of pathophysiology, as all of the projection neurons develop inclusions, and no notable neuronal death occurs.

A number of *in vitro* studies have shown altered neurophysiological and neuroanatomical properties of neocortical and neostriatal neurons in the R6/2 mice (Cepeda et al., 2001, 2003a, 2004; Klapstein et al., 2001; Laforet et al., 2001; Levine et al., 2004; Ariano et al., 2005; Andre et al., 2006; Cepeda and Levine, 2006). These studies show significant alterations in neocortical and neostriatal electrophysiological properties including both intrinsic conductances and synaptic properties. Changes in the properties of neostriatal neurons include decreased resting membrane potential, increased input resistance, and pruning of dendritic branching and spine patterns. Physiological changes also include reductions in synaptic currents evoked by stimulation of neocortical white matter (Cepeda et al., 2003a).

The changes in neuronal properties measured *in vitro* are crucial to understanding the effects of the neuropathology on cellular activity. However, in order to understand the changes in the corticostriatal network properties caused by HD pathology, it is necessary to measure the activity of these neurons in the intact animal.

In vivo activity of neocortical neurons has been well characterized in rats (Steriade et al., 1993; Cowan and Wilson, 1994; Timofeev et al., 2000). The membrane potential dynamics of these neurons include spontaneous membrane potential transitions between the quiescent resting membrane potential (Down state) and a depolarized Up state, from which action potential arise. The mechanisms of the spontaneous membrane potential activity in neocortical neurons have been described in detail (Stern et al., 1997; Sachdev et al., 2004). These studies show that the Up states arise from barrages of neocortical synaptic activity interacting with non-linear membrane potential conductances. These barrages of synaptic activity are not present in acute slices, therefore, Up states are not seen in these preparations. To measure the functional effects of HD pathology on the activity of the neocortical network, we measured spontaneous activity and input–output relationships of neocortical neurons in the R6/2 mouse model of HD at time points when all neocortical pyramidal neurons show polyglutamine inclusions, and compared the results to those in age-matched non-transgenic littermates.

MATERIALS AND METHODS

Experiments were approved by the Institutional Animal Care and Use Committees of Massachusetts General Hospital and Bar-Ilan University in accordance with regulations approved by the US National Institutes of Health and the Israeli Ministry of Health.

SURGERY

R6/2 mice and non-transgenic littermate controls were used for this study (Mangiarini et al., 1996, 1997; Davies et al., 1997; Bates et al., 1998). The population had a CAG length of ~160 repeat expansions. The ages of the mice ranged from 8 to 14 weeks. Mice were anesthetized with ketamine/xylazine (150/12 mg/kg) and placed in a custom-built stereotaxic device. Temperature was maintained at 37°C. The scalp was removed and the skull cleaned of tissue. Small holes (1 mm) were drilled for electrocorticogram (ECoG) electrodes over cortex and cerebellum. ECoG electrodes consisted of teflon-insulated silver wire with 1 mm insulation removed placed between dura and skull and cemented in place. ECoG was monitored continuously from the time of electrode placement to monitor depth of anesthesia. A ~4 mm × 4 mm craniotomy was opened over frontal cortex extending caudally to bregma. A cisternal drain was opened to reduce brain pulsations.

RECORDING

Recording electrodes (1.5 mm o.d. glass (A-M Systems); resistance 30–80 MΩ; filled with 1 M potassium acetate (Sigma) were lowered into agranular cortex. Following insertion of the recording electrode, the brain was covered with either 4% agarose or low-temperature melting point wax. Recordings were made under lighter conditions of anesthesia than are commonly used, as the R6/2 line and non-transgenic cohorts are more sensitive to anesthesia than are other mouse lines. The criteria used were evidence of slow-wave activity in the ECoG and lack of response to foot-pinch.

When a neuron was impaled, several minutes of spontaneous activity were recorded using a high-impedance amplifier with active bridge circuitry (IR-283; Cygnus Technology). Data were directly acquired via A/D board (National Instruments) using custom software at 4–10 kHz. For current–voltage and excitation-to-frequency

curves, 200 ms current pulses were injected via the recording electrodes. Data were acquired using Igor Pro (Wavemetrics) or Spike 2/Signal (Cambridge) software. Analysis was performed using Igor Pro, Matlab (MathWorks), and SAS (SAS Institute) software.

RESULTS

All recorded neurons showed spontaneous membrane potential fluctuations. **Figures 1A,B** show representative recordings from non-transgenic littermate and transgenic animals at 11 weeks of age. We found no significant differences in median membrane potential (Down state) values between control and HD neurons ($t = 1.42$; $df = 25$; NS). No significant differences in the median Up state value were found between control and HD neurons ($t = 0.98$; $df = 25$; NS). **Table 1** shows the median and median average deviation of the membrane potential values and input resistances of the neurons measured in this study.

To test if the pattern of fluctuations differed between control and HD neurons, we measured the distribution of durations of the Up and Down states. These distributions are plotted in the average dwell-time histograms shown in **Figure 2** for Up states (**Figure 2A**) and Down states (**Figure 2B**). We found significant differences between the dwell-time distributions of the Down states between control and HD neurons, with the HD neurons having significantly more short down states ($\chi^2 = 25.13$; $df = 15$; $p \leq 0.05$). This result indicates that the R6/2 neurons transition to the Up state more readily than do control neurons. No significant differences between the distributions of the Up state durations were found ($\chi^2 = 41.29$; $df = 51$; NS).

To test for serial dependence in the patterns of state durations, we measured the state durations as a function of the preceding state. Up and Down states were quantified using the method described in

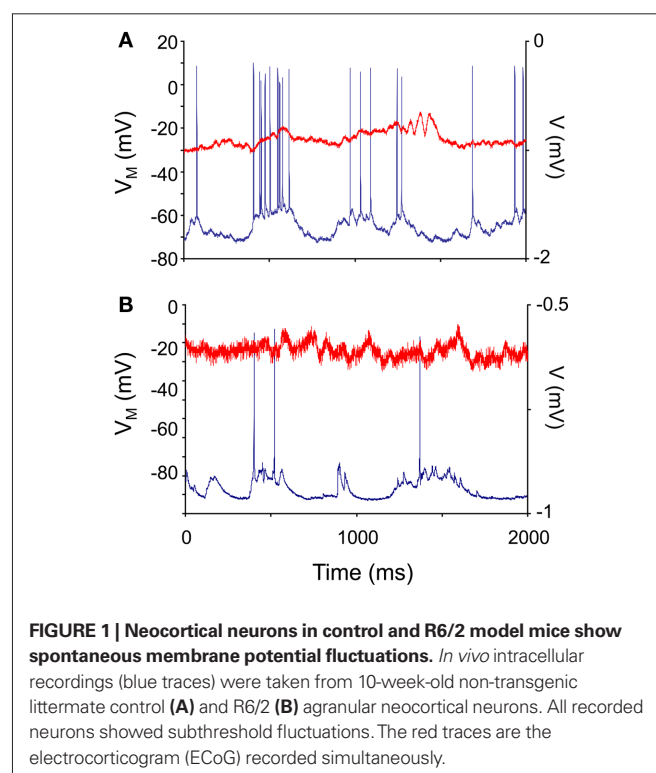


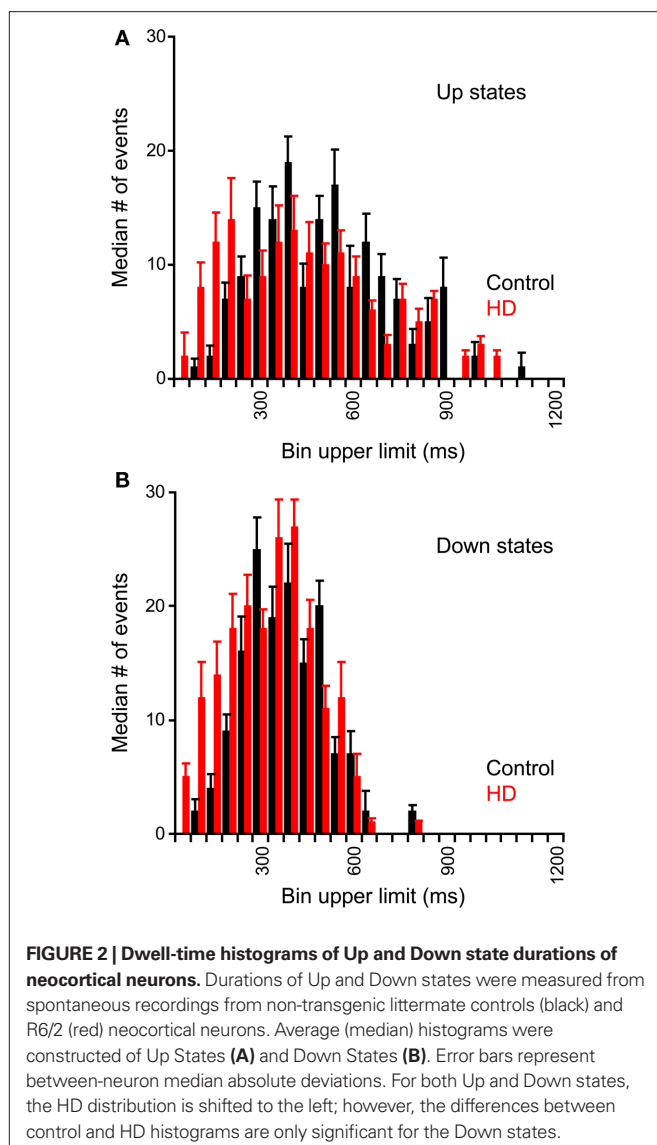
FIGURE 1 | Neocortical neurons in control and R6/2 model mice show spontaneous membrane potential fluctuations. *In vivo* intracellular recordings (blue traces) were taken from 10-week-old non-transgenic littermate control (**A**) and R6/2 (**B**) agranular neocortical neurons. All recorded neurons showed subthreshold fluctuations. The red traces are the electrocorticogram (ECoG) recorded simultaneously.

Stern et al. (1997). Briefly, the all-points histogram of a 10-s sample of the membrane potential was plotted and fitted to a bimodal curve, separated by a single trough. A state transition was calculated as when the membrane voltage passed halfway from the trough to the state modal value. This method eliminates false state transitions. We measured the durations of the Down states as a function of the preceding Up state durations, the Up states as a function of the

Table 1 | Membrane potential and input resistance properties of mouse neocortical neuronal membrane potential and input resistance.

Parameter	Control	R6/2
V_M down	-74 ± 9 mV (13)	-78 ± 12 mV (13)
Up state depolarization	11.5 ± 4.5 mV (13)	13 ± 6.5 mV (13)
R_{in}	89.6 ± 8.4 M Ω (13)	65.1 ± 9.2 M Ω (13)

Numbers denote median \pm median absolute deviation. The numbers in parentheses denote the numbers of neurons in the group.



preceding Down state durations, the Down states as a function of the preceding Down state durations, and the Up states as a function of the preceding Up state durations. Using the serial correlation test for renewal processes to test independence of successive intervals, no significant serial correlations were found between any successive state types of either population of neurons.

A logical place to expect changes in HD neocortical neurons is in the electrical properties of the neurons themselves, as a major neuropathological feature associated with the disease, the polyglutamine inclusions, are intracellular. One of the major changes in R6/2 neostriatal neurons found in acute slice neurons was a significant change in input resistance (Klapstein et al., 2001). We injected current pulses via the intracellular recording electrode to measure the membrane voltage changes and the excitation-to-frequency curves. Taken together, these are a measure of the input-output properties of the neurons. We injected 200 ms duration positive and negative current pulses of up to ± 1 nA, in steps of 100 pA. Each current step was repeated eight times. The average responses to such series are plotted in Figures 3A,B, for a control and HD neuron, respectively.

It can be seen that the responses to current in the HD neurons are larger, indicating higher input resistance overall in these cells. Averages I/V plots for the neurons are shown in Figure 3C. The slopes of the curves are significantly different ($F = 2.63$; $df = 25, 25$; $p \leq 0.05$) indicating that the input resistances of the HD (red) mice are significantly greater than those of the controls (blue). Similar results were found in measurements in acute *in vitro* preparations of R6/2 neostriatal neurons (Klapstein et al., 2001; Ariano et al., 2005). However, because of the large differences in the amount of input between the *in vivo* and *in vitro* preparations, it was necessary to make this comparison in the intact brain to measure the functional consequences of the changes. The average excitation-to-frequency curves for the control (blue) and HD (red) neurons are plotted in Figure 3D. The most noticeable difference between the curves is the increased average responses to current pulses in the lower amplitude range of the HD neurons. In addition, it is clear that the average dynamic range of the neurons is reduced.

Given the hyperexcitability of the HD neocortical neurons shown by the average I/V and f/I plots in Figure 3, we hypothesized that their activity could be less synchronous with that of the neocortical network. The global coherence of the neocortical network is dependent on the envelope of input synchrony, as well as membrane properties of the neurons (Stern et al., 1997, 1998; Timofeev et al., 2000; Leger et al., 2005). We measured the global synchrony of the network by measuring coherence between the membrane potentials and the ECoG, using Hanning windows of 5 s with 50% overlap, following spike removal and downsampling to 1 kHz, giving a resolution of 0.2 Hz. The Hanning window is an amplitude weighting of the time signal with the form $w = 0.5 \times (1 - \cos(2 \times \pi \times (1:M)/(M+1)))$; it is generally used for analysis of continuous signals to reduce the generation of side lobes in the frequency spectrum.

Harmonic means were taken of the coherences in each category. Examples of single 5 s traces are shown in Figures 4A,B for control and HD neurons, respectively. The intracellular traces are plotted in blue, while the ECoG is plotted in red. The coherence averages are shown in Figure 4C for the control (black) and HD (red) neurons.

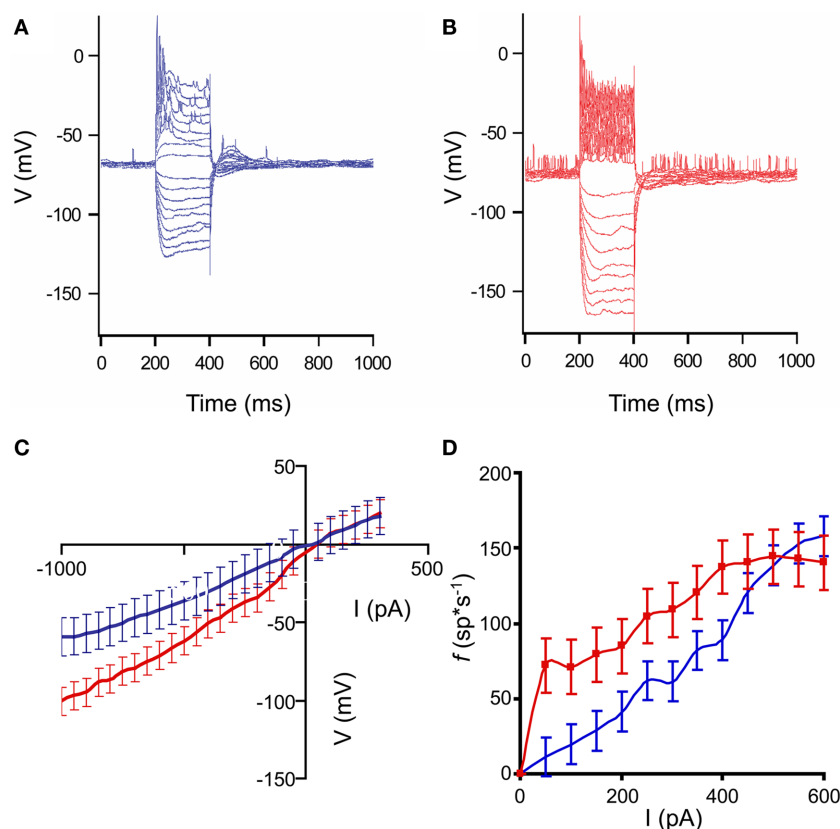


FIGURE 3 | Input-output characteristics of control and HD neurons. (A,B): Representative responses of neocortical neurons to intracellular current pulses. Each trace shown is an average response to eight stimuli. Pulses ranged from ± 100 to 1000 pA in amplitude, and 200 ms duration. **(A):** non-transgenic littermate control neuron; **(B):** R6/2 neuron. In the examples shown, the animals were 9 weeks of age. Note the increased voltage responses in the HD neuron, indicating higher input resistance, as well as the increased spiking, indicating

higher response frequency. **(C):** Average current-voltage plots of control (blue) and HD (red) neurons. Error bars represent between-neuron SD. Note the increased slope of the HD I/V curve. **(D):** Average excitation-to-frequency (f/I) plots for control (blue) and HD (red) neurons. Error bars represent between-neuron SD. The lines are smoothed between the measured points. Note the increase in the f/I slope in the lower part of the range, indicating that the HD neurons have smaller dynamic response ranges, and tend to respond abnormally to relatively weak stimuli.

The overall 95% confidence intervals for the two spectra are shown by dashed lines (Rosenberg et al., 1989; Moran and Bar-Gad, 2010). We tested for differences in coherence in the low-frequency range by comparing the size of the peak at < 5 Hz over neurons between control and HD. This peak includes the energy in the range of the membrane potential state transitions, and was the only peak outside of the confidence intervals. We found that the coherence is significantly reduced in the HD animals (permutation test for independent samples; $t = 2.71$; $df = 17$; $p \leq 0.05$), indicating that the state transitions of these neurons were significantly less correlated with the global activity than those of controls.

DISCUSSION

This study measured the functional properties of neocortical neurons in the R6/2 model of HD at ages when the polyglutamine inclusions are present in all such neurons. Although many *in vitro* studies of the electrophysiological changes of neostriatal and neocortical neurons have been published (Cepeda et al., 2001, 2003b, 2004, 2007; Klapstein et al., 2001; Laforet et al., 2001; Ariano et al., 2005; Andre et al., 2006, 2011; Cepeda and Levine, 2006; Joshi et al.,

2009), the functional changes in the corticostriatal input were not easily extrapolated from these studies, as the functional properties of neocortical neurons *in vivo* are different from those *in vitro*, since the Up state, dependent on large amounts of neocortical input, is not seen in acute reduced preparations.

It is of interest to observe that all neurons showed the subthreshold membrane potential dynamics seen in normal pyramidal neurons. This is also true in other disease models, such as Alzheimer's Disease (Stern et al., 2004). It is as if this type of activity is important enough to the neuron to be maintained as long as the neurons are alive. The principal changes found in the subthreshold membrane potential dynamics of the HD neurons was the increased number of shorter-duration Down states, indicating that the membrane potential of these cells transitioned more easily to the Up state, consistent with the increased input resistance and lower rectification measured in these neurons.

We found that the intrinsic properties of the HD neurons *in vivo* mirrored many of those observed in *in vitro* studies. Consistent with the results observed in neostriatal neurons, we found increased input resistance and reduced rectification properties in the neocortical

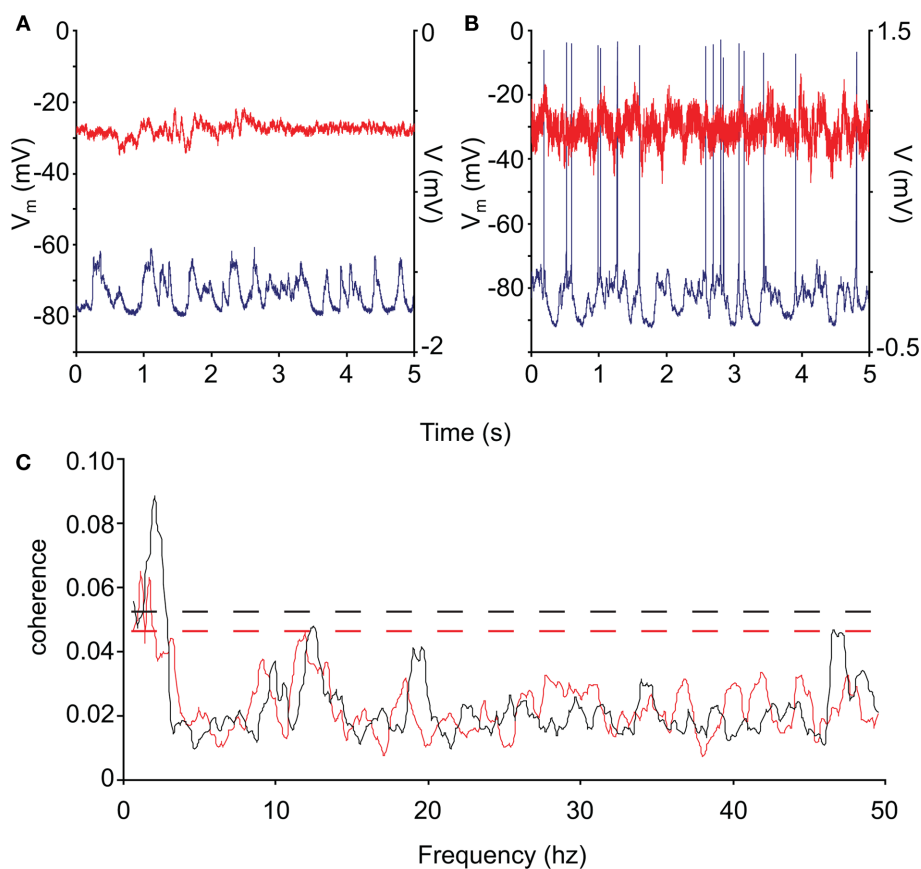


FIGURE 4 | Coherence of control and R6/2 neocortical activity. (A,B) Representative intracellular recordings (blue) and ECoG (red) from control and R6/2 mouse cortex. **(C):** average neuronal/neocortical coherence for the control (black trace) and HD (red trace) neurons. The coherence of the HD membrane

potential with the global activity represented by the ECoG is significantly less than that of the controls in the low-frequency range (<5 Hz), which represents the state transition activity. The dashed lines represent the 95% confidence intervals of the spectra.

neurons. Changes in rectification properties of HD neostriatal neurons (Ariano et al., 2005) and downregulation of potassium channel genes have been observed in previous studies (Zucker et al., 2005). It may be that a principal target of the accumulated polyglutamine is one or more families of potassium channels in the affected neocortical neurons as well, suggesting these channels as a potential therapeutic target.

A major finding of this study is the decreased dynamic range of the f/I curves of the HD neurons. Given the reduced rectification properties of these neurons, it may be that the cells transition to the Up state more readily than do controls. This may give rise to increased activity of these neurons in awake animals (Walker et al., 2008), and may be the cause of the observed changes in corticostriatal post-synaptic currents observed in some studies (Cepeda et al., 2003a). In addition to changing the neocortical inputs, the functional consequences of these changes may be that the number of inputs to these neurons necessary to cause a transition from the Down state to the Up state is reduced, as are the number of inputs necessary to generate an action potential. The reduced membrane potential – ECoG coherence of the HD neurons, shown in Figure 4, is further evidence that the membrane potentials of these neurons can transition for the Down to the Up states more easily than can controls.

The relative difficulty in eliciting the state transitions is a major determinant of neocortical function. Reducing the number of inputs necessary to evoke a state transition could give rise to severe functional abnormalities, such as affecting their ability to participate in coordinated activity within neuronal assemblies. Our results could explain the abnormal correlated activity of neocortical and neostriatal neurons found in awake behaving R6/2 animals in which the synchrony of spikes is significantly reduced (Miller et al., 2008; Walker et al., 2008). In addition, the results observed could underlie some of the behavioral deficits observed in these animals such as reduction of coordinated activity (Carter et al., 1999).

Taken together, the results of this study demonstrate the functional consequences of the neocortical neuronal deficits observed in HD mouse models. While these deficits may underlie some of the changes observed in neostriatal neuronal activity in these models, it remains to be seen how much of those changes are due to the cellular changes resulting from HD pathology, and how much are due to the changes in neocortical input. The changes in neocortical input to neostriatal neurons coupled with differential changes in dopamine transmission (Andre et al., 2011) could explain the

stereotypical behavior observed in these animals. This may be a major neuronal mechanism underlying the sensorimotor and cognitive symptoms of HD.

CONCLUSION

This study demonstrates a possible mechanism of the effect of cellular neuropathology on the properties of the neuronal network as a whole. Taken in conjunction with studies of the cellular effects of HD pathologies in *in vitro* preparations and studies in a wake,

behaving animals, intracellular recordings *in vivo* may provide a vital connection in understanding the effects of the neuropathology in HD on the function of the corticostriatal system.

ACKNOWLEDGMENTS

Supported by the Hereditary Disease Foundation and the Israel Science Foundation. The author Thanks Drs Jang-Ho Cha, Steven Hersch, and Michael Levine and Izhar Bar-Gad for useful suggestions, and Ms. Vered Kellner for help with the analysis.

REFERENCES

- Andre, V. M., Cepeda, C., Fisher, Y. E., Huynh, M., Bardakjian, N., Singh, S., Yang, X. W., and Levine, M. S. (2011). Differential electrophysiological changes in striatal output neurons in Huntington's disease. *J. Neurosci.* 31, 1170–1182.
- Andre, V. M., Cepeda, C., Venegas, A., Gomez, Y., and Levine, M. S. (2006). Altered cortical glutamate receptor function in the R6/2 model of Huntington's disease. *J. Neurophysiol.* 95, 2108–2119.
- Ariano, M. A., Cepeda, C., Calvert, C. R., Flores-Hernandez, J., Hernandez-Echeagaray, E., Klapstein, G. J., Chandler, S. H., Aronin, N., DiFiglia, M., and Levine, M. S. (2005). Striatal potassium channel dysfunction in Huntington's disease transgenic mice. *J. Neurophysiol.* 93, 2565–2574.
- Bates, G. P., Mangiarini, L., Wanker, E. E., and Davies, S. W. (1998). Polyglutamine expansion and Huntington's disease. *Biochem. Soc. Trans.* 26, 471–475.
- Carter, R. J., Lione, L. A., Humby, T., Mangiarini, L., Mahal, A., Bates, G. P., Dunnett, S. B., and Morton, A. J. (1999). Characterization of progressive motor deficits in mice transgenic for the human Huntington's disease mutation. *J. Neurosci.* 19, 3248–3257.
- Cepeda, C., Ariano, M. A., Calvert, C. R., Flores-Hernandez, J., Chandler, S. H., Leavitt, B. R., Hayden, M. R., and Levine, M. S. (2001). NMDA receptor function in mouse models of Huntington disease. *J. Neurosci. Res.* 66, 525–539.
- Cepeda, C., Hurst, R. S., Calvert, C. R., Hernandez-Echeagaray, E., Nguyen, O. K., Jocoy, E., Christian, L. J., Ariano, M. A., and Levine, M. S. (2003a). Transient and progressive electrophysiological alterations in the corticostriatal pathway in a mouse model of Huntington's disease. *J. Neurosci.* 23, 961–969.
- Cepeda, C., Hurst, R. S., Flores-Hernandez, J., Hernandez-Echeagaray, E., Klapstein, G. J., Boylan, M. K., Calvert, C. R., Jocoy, E. L., Nguyen, O. K., Andre, V. M., Vinters, H. V., Ariano, M. A., Levine, M. S., and Mathern, G. W. (2003b). Morphological and electrophysiological characterization of abnormal cell types in pediatric cortical dysplasia. *J. Neurosci. Res.* 72, 472–486.
- Cepeda, C., and Levine, M. S. (2006). Dysfunctional channels are making noise in CAG triplet repeat disorders. *Exp. Neurol.* 202, 267–270.
- Cepeda, C., Starling, A. J., Wu, N., Nguyen, O. K., Uzgil, B., Soda, T., Andre, V. M., Ariano, M. A., and Levine, M. S. (2004). Increased GABAergic function in mouse models of Huntington's disease: reversal by BDNF. *J. Neurosci. Res.* 78, 855–867.
- Cepeda, C., Wu, N., Andre, V. M., Cummings, D. M., and Levine, M. S. (2007). The corticostriatal pathway in Huntington's disease. *Prog. Neurobiol.* 81, 253–271.
- Cowan, R. L., and Wilson, C. J. (1994). Spontaneous firing patterns and axonal projections of single corticostriatal neurons in the rat medial agranular cortex. *J. Neurophysiol.* 71, 17–32.
- Davies, S. W., Turmaine, M., Cozens, B. A., DiFiglia, M., Sharp, A. H., Ross, C. A., Scherzinger, E., Wanker, E. E., Mangiarini, L., and Bates, G. P. (1997). Formation of neuronal intranuclear inclusions underlies the neurological dysfunction in mice transgenic for the HD mutation. *Cell* 90, 537–548.
- DiFiglia, M., Sapp, E., Chase, K. O., Davies, S. W., Bates, G. P., Vonsattel, J. P., and Aronin, N. (1997). Aggregation of huntingtin in neuronal intranuclear inclusions and dystrophic neurites in brain. *Science* 277, 1990–1993.
- HDCRG. (1993). A novel gene containing a trinucleotide repeat that is expanded and unstable on Huntington's disease chromosomes. The Huntington's Disease Collaborative Research Group. *Cell* 72, 971–983.
- Joshi, P. R., Wu, N. P., Andre, V. M., Cummings, D. M., Cepeda, C., Joyce, J. A., Carroll, J. B., Leavitt, B. R., Hayden, M. R., Levine, M. S., and Bamford, N. S. (2009). Age-dependent alterations of corticostriatal activity in the YAC128 mouse model of Huntington disease. *J. Neurosci.* 29, 2414–2427.
- Klapstein, G. J., Fisher, R. S., Zanjani, H., Cepeda, C., Jokel, E. S., Chesselet, M. F., and Levine, M. S. (2001). Electrophysiological and morphological changes in striatal spiny neurons in R6/2 Huntington's disease transgenic mice. *J. Neurophysiol.* 86, 2667–2677.
- Laforet, G. A., Sapp, E., Chase, K., McIntyre, C., Boyce, F. M., Campbell, M., Cadigan, B. A., Warzecki, L., Tagle, D. A., Reddy, P. H., Cepeda, C., Calvert, C. R., Jokel, E. S., Klapstein, G. J., Ariano, M. A., Levine, M. S., DiFiglia, M., and Aronin, N. (2001). Changes in cortical and striatal neurons predict behavioral and electrophysiological abnormalities in a transgenic murine model of Huntington's disease. *J. Neurosci.* 21, 9112–9123.
- Leger, J. F., Stern, E. A., Aertsen, A., and Heck, D. (2005). Synaptic integration in rat frontal cortex shaped by network activity. *J. Neurophysiol.* 93, 281–293.
- Levine, M. S., Cepeda, C., Hickey, M. A., Fleming, S. M., and Chesselet, M. F. (2004). Genetic mouse models of Huntington's and Parkinson's diseases: illuminating but imperfect. *Trends Neurosci.* 27, 691–697.
- Mangiarini, L., Sathasivam, K., Mahal, A., Mott, R., Seller, M., and Bates, G. P. (1997). Instability of highly expanded CAG repeats in mice transgenic for the Huntington's disease mutation. *Nat. Genet.* 15, 197–200.
- Mangiarini, L., Sathasivam, K., Seller, M., Cozens, B., Harper, A., Hetherington, C., Lawton, M., Trotter, Y., Lehrach, H., Davies, S. W., and Bates, G. P. (1996). Exon 1 of the HD gene with an expanded CAG repeat is sufficient to cause a progressive neurological phenotype in transgenic mice. *Cell* 87, 493–506.
- Miller, B. R., Walker, A. G., Shah, A. S., Barton, S. J., and Rebec, G. V. (2008). Dysregulated information processing by medium spiny neurons in striatum of freely behaving mouse models of Huntington's disease. *J. Neurophysiol.* 100, 2205–2216.
- Moran, A., and Bar-Gad, I. (2010). Revealing neuronal functional organization through the relation between multi-scale oscillatory extracellular signals. *J. Neurosci. Methods* 186, 116–129.
- Rosenberg, J. R., Amjad, A. M., Breeze, P., Brillinger, D. R., and Halliday, D. M. (1989). The Fourier approach to the identification of functional coupling between neuronal spike trains. *Prog. Biophys. Mol. Biol.* 53, 1–31.
- Sachdev, R. N., Ebner, F. F., and Wilson, C. J. (2004). Effect of subthreshold up and down states on the whisker-evoked response in somatosensory cortex. *J. Neurophysiol.* 92, 3511–3521.
- Steriade, M., Nunez, A., and Amzica, F. (1993). A novel slow (<1 Hz) oscillation of neocortical neurons in vivo: depolarizing and hyperpolarizing components. *J. Neurosci.* 13, 3252–3265.
- Stern, E. A., Bacskaï, B. J., Hickey, G. A., Attenello, F. J., Lombardo, J. A., and Hyman, B. T. (2004). Cortical synaptic integration in vivo is disrupted by amyloid-beta plaques. *J. Neurosci.* 24, 4535–4540.
- Stern, E. A., Jaeger, D., and Wilson, C. J. (1998). Membrane potential synchrony of simultaneously recorded striatal spiny neurons in vivo. *Nature* 394, 475–478.
- Stern, E. A., Kincaid, A. E., and Wilson, C. J. (1997). Spontaneous subthreshold membrane potential fluctuations and action potential variability of rat corticostriatal and striatal neurons in vivo. *J. Neurophysiol.* 77, 1697–1715.
- Timofeev, I., Grenier, F., and Steriade, M. (2000). Impact of intrinsic properties and synaptic factors on the activity of neocortical networks in vivo. *J. Physiol. Paris* 94, 343–355.
- Vonsattel, J. P., Myers, R. H., Stevens, T. J., Ferrante, R. J., Bird, E. D., and Richardson, E. P. Jr. (1985). Neuropathological classification of Huntington's disease. *J. Neuropathol. Exp. Neurol.* 44, 559–577.
- Walker, A. G., Miller, B. R., Fritsch, J. N., Barton, S. J., and Rebec, G. V. (2008). Altered information processing in the prefrontal cortex of Huntington's disease mouse models. *J. Neurosci.* 28, 8973–8982.

Zucker, B., Luthi-Carter, R., Kama, J. A., Dunah, A. W., Stern, E. A., Fox, J. H., Standaert, D. G., Young, A. B., and Augood, S. J. (2005). Transcriptional dysregulation in striatal projection and interneurons in a mouse model of Huntington's disease: neuronal selectivity and potential neuroprotec-

tive role of HAP1. *Hum. Mol. Genet.* 14, 179–189.

Conflict of Interest Statement: The author declares that the research was conducted in the absence of any commercial or financial relationships that could be construed as a potential conflict of interest.

Received: 01 March 2011; accepted: 03 June 2011; published online: 16 June 2011.

Citation: Stern EA (2011) Functional changes in neocortical activity in Huntington's disease model mice: an in vivo intracellular study. *Front. Syst. Neurosci.* 5:47. doi: 10.3389/fnsys.2011.00047

Copyright © 2011 Stern. This is an open-access article subject to a non-exclusive license between the authors and Frontiers Media SA, which permits use, distribution, and reproduction in other forums, provided the original authors and source are credited and other Frontiers conditions are complied with.



Altered balance of activity in the striatal direct and indirect pathways in mouse models of Huntington's disease

Véronique M. André*, Yvette E. Fisher and Michael S. Levine

Intellectual and Developmental Disabilities Research Center, Department of Psychiatry and Biobehavioral Sciences, David Geffen School of Medicine, Semel Institute, University of California at Los Angeles, Los Angeles, CA, USA

Edited by:

Charles J. Wilson, University of Texas at San Antonio, USA

Reviewed by:

Laurent Venance, Collège de France, France

C. Savio Chan, Northwestern University, USA

*Correspondence:

Véronique M. André, David Geffen School of Medicine, Semel Institute for Neuroscience and Human Behavior, University of California at Los Angeles, 760 Westwood Plaza, NPI 58-258A, Los Angeles, CA 90095, USA.
e-mail: vandre@mednet.ucla.edu

Imbalance in the activity of striatal direct and indirect pathway neurons contributes to motor disturbances in several neurodegenerative diseases. In Huntington's disease (HD), indirect pathway [dopamine (DA) D2 receptor-expressing] medium-sized spiny neurons (MSNs) are believed to show earlier vulnerability than direct pathway MSNs. We examined synaptic activity and DA modulation in MSNs forming the direct and indirect pathways in YAC128 and BACHD mouse models of HD. To visualize the two types of MSNs, we used mice expressing enhanced green fluorescent protein under the control of the promoter for the DA D1 or D2 receptor. Experiments were performed in early symptomatic (1.5 months) and symptomatic (12 months) mice. Behaviorally, early symptomatic mice showed increased stereotypies while symptomatic mice showed decreased motor activity. Electrophysiologically, at the early stage, excitatory and inhibitory transmission onto D1-YAC128 and D1-BACHD MSNs were increased, while there was no change in D2 MSNs. DA modulation of spontaneous excitatory postsynaptic currents (sEPSCs) in slices was absent in YAC128 cells at the early stage, but was restored by treating the slices with the DA depletor tetrabenazine (TBZ). In BACHD mice TBZ restored paired-pulse ratios and a D1 receptor antagonist induced a larger decrease of sEPSCs than in D1-WT cells, suggesting increased DA tone. Finally, TBZ decreased stereotypies in BACHD mice. These results indicate that by reducing DA or antagonizing D1 receptors, increases in inhibitory and excitatory transmission in early phenotypic direct pathway neurons can be normalized. In symptomatic YAC128 mice, excitatory synaptic transmission onto D1 MSNs was decreased, while inhibitory transmission was increased in D2 MSNs. These studies provide evidence for differential and complex imbalances in glutamate and GABA transmission, as well as in DA modulation, in direct and indirect pathway MSNs during HD progression.

Keywords: dopamine, electrophysiology, synaptic activity, glutamate, GABA, postsynaptic currents, Huntington's disease

INTRODUCTION

Huntington's disease (HD) is caused by the mutation of a gene inducing expansion of CAG triplets on the huntingtin (htt) protein (The Huntington's Disease Collaborative Research Group, 1993). In HD, the most obvious neuropathology is observed in the cortex and in the striatum. More specifically, striatal medium-sized spiny neurons (MSNs) expressing enkephalin and dopamine (DA) D2 receptors, forming the indirect pathway, are believed to be the most vulnerable and are preferentially lost in brains of presymptomatic and fully symptomatic patients. In contrast, MSNs expressing substance P and D1 receptors, forming the direct pathway, are believed to be relatively spared early in the progression of the disorder (Vonsattel et al., 1985; Albin et al., 1990).

The earlier vulnerability of indirect pathway MSNs in HD could induce imbalances in striatal output to other basal ganglia nuclei, which will affect the final outflow to the thalamus and contribute to the motor disturbances in the disease. Direct pathway MSNs preferentially project to the substantia nigra pars reticulata and to the internal segment of the globus pallidus (Gerfen, 1992; Bolam et al., 2000) and facilitate movement when activated (Chevalier et al., 1985a,b). In addition, direct pathway MSNs express high levels of DA D1 receptors that enhance synaptic activity when stimulated

by DA. Indirect pathway neurons preferentially project to the external segment of the globus pallidus and inhibit movement when activated (Smith et al., 1998; Kravitz et al., 2010). They express D2 receptors that attenuate synaptic activity when stimulated by DA. Thus, direct and indirect pathways have opposite effects on movement and express DA receptors that have opposite effects on cell excitability.

Medium-sized spiny neurons are driven by two main glutamatergic inputs, those from cortex and thalamus. Intrastriatal inputs from GABAergic interneurons and axon collaterals from other MSNs provide feedforward and feedback inhibition, respectively. DA also exerts control of neurotransmitter release by directly activating presynaptic D2 receptors present on many terminals in the striatum or indirectly by interacting with other endogenous modulators (Malenka and Kocsis, 1988; Lovinger, 2008). In HD, glutamate and DA transmission are altered, which likely produces an imbalance in the activity of the direct and indirect pathways and contributes to the motor, cognitive, and psychiatric symptoms of HD.

Huntington's disease is a neurodegenerative disease characterized by a progression of motor symptoms manifesting as chorea in early stages and as akinesia in later stages (Thompson et al., 1988).

Thus, we hypothesized that alterations in direct and indirect pathway activity would be different at early and late stages of the disease. We examined the YAC128 (yeast artificial chromosome) mouse model of HD at an early symptomatic stage (1.5 months) and a symptomatic stage (12 months). YAC mice with 128 CAG repeats show a biphasic motor phenotype with hyperactivity at 3 months followed by hypoactivity in the open field at 12 months. Modest striatal atrophy occurs at 9 months and a small but significant decrease in striatal neurons is evident at 12 months (Slow et al., 2003). We also examined the BACHD (bacterial artificial chromosome) model at an early symptomatic stage (2 months). BACHD mice express human mutant HTT with 97 CAG repeats and exhibit progressive motor deficits starting at 2 months, followed by late-onset selective neuropathology at 12 months (Gray et al., 2008). BAC and YAC transgenics are used to permit expression of the full-length human mutant HTT, in order to reproduce more faithfully the human condition. BACHD and YAC128 mice develop a more protracted and progressive phenotype than the fragment models such as the R6/2, recapitulating the juvenile form of the disease (Mangiarini et al., 1996; Schilling et al., 1999). Full-length models of HD allow the investigation at an early stage of the disease, when symptoms start to develop while it is more difficult to separate time-dependent changes in fragment models showing rapid and aggressive progression of the disease. They also present more robust motor deficits and neuropathology than the knock-in models (Shelbourne et al., 1999; Wheeler et al., 2000). Although BAC and YAC transgenes allow the expression of large genomic sequence, they display a limited neuronal loss (10–15%) and do not recapitulate a shorter lifespan, as seen in the human condition (Tang et al., 2007).

To assess functional activity of specifically identified neurons, we crossed YAC128 or BACHD mice with mice expressing a reporter gene under the control of the promoter for either DA D1 or D2 receptors. In the double transgenic mice we examined excitatory and inhibitory postsynaptic currents (EPSCs and IPSCs) and DA modulation in direct and indirect pathway MSNs. As tetrabenazine (TBZ) is the only drug providing significant benefit in the treatment of chorea associated with HD, we also tested the effect of this monoamine-depleting agent *in vitro* and *in vivo*. Portions of this study were published previously (André et al., 2011).

MATERIALS AND METHODS

ANIMALS

All experimental procedures were performed in accordance with the United States Public Health Service Guide for Care and Use of Laboratory Animals and were approved by the Institutional Animal Care and Use Committee at the University of California Los Angeles (UCLA). Every effort was made to minimize pain and discomfort. Experiments were conducted in two mouse models of adult-onset HD crossbred to heterozygous FVB/N mice expressing enhanced green fluorescent protein (EGFP) under the control of the promoter for dopamine receptor D1 or D2, obtained from our colony at UCLA. One mouse model carried full-length human mutant HTT, including 128 CAG repeats, on a yeast artificial chromosome (YAC128, line 53; Slow et al., 2003). YAC128 and WT littermates expressing D1- or D2-EGFP were obtained from our colonies at UCLA at 1.5 and 12 months of age. The second mouse

model carried full-length human mutant HHT, including 97 CAG repeats, on a bacterial artificial chromosome (BACHD; Gray et al., 2008). BACHD and WT littermates expressing D1- or D2-EGFP at 2 months of age were also obtained from our colonies.

CELL VISUALIZATION

Enhanced green fluorescent protein-positive cells were visualized in slices using a 40× water immersion lens. The microscope (Olympus BX50WI or Zeiss Axioscope) was equipped with differential interference contrast optics and fluorescence. For infrared videomicroscopy, a halogen lamp and an infrared filter (790 nm, Ealing Optics, Holliston, MA, USA) were used. For fluorescence, ultra-violet light was filtered to obtain 480 nm excitation light. The light source consisted of a mercury lamp (100 W) and fluorescent light was detected with a video camera (QICAM-IR Fast 1394, Burnaby, BC, Canada) optimized to detect EGFP fluorescence and infrared light. Images were digitized and saved using the Q Capture Pro software (version 5, Burnaby, BC, Canada). Once a viable MSN was identified with infrared videomicroscopy, the filter was switched to fluorescence to determine if it was labeled with EGFP. The digitized infrared image was superimposed over the fluorescence image, and electrophysiological recordings proceeded only if the cell identified with infrared light showed a complete overlap with EGFP fluorescence.

EXPERIMENTS IN SLICES

Detailed procedures have been published (Cepeda et al., 1993; André et al., 2010). Briefly, mice were deeply anesthetized with halothane and sacrificed. The brains were dissected and immediately placed in oxygenated ice-cold low- Ca^{2+} artificial cerebrospinal fluid (ACSF) containing (in millimolar): NaCl, 130; KCl, 3; NaH_2PO_4 , 1.25; NaHCO_3 , 26; MgCl_2 , 5; CaCl_2 , 1; and glucose, 10. Coronal slices (350 μm) were cut and transferred to an incubating chamber containing ACSF (with 2 mM CaCl_2 and 2 mM MgCl_2) oxygenated with 95% O_2 -5% CO_2 (pH 7.2–7.4, 290–310 mOsm, $25 \pm 2^\circ\text{C}$). Slices were visualized and EGFP-expressing cells were selected for recordings. The patch pipette contained (in millimolar): Cs-methanesulfonate 130, CsCl 10, NaCl 4, MgCl_2 1, MgATP 5, EGTA 5, HEPES 10, GTP 0.5, phosphocreatine 10, leupeptin 0.1 for voltage clamp recordings. Access resistances were $<20 \text{ M}\Omega$. Spontaneous postsynaptic currents were recorded in standard ACSF at room temperature. Membrane current was filtered at 1 kHz and digitized at 100–200 μs using Clampex 10.2 (gap-free mode). Cells were voltage clamped at -70 mV to determine basic membrane properties and to examine spontaneous glutamate receptor-mediated EPSCs. Bicuculline methiodide (Bic, 10 μM) was applied in order to block GABA_A receptor-mediated currents. For IPSCs, voltage was held at $+10 \text{ mV}$. For experiments examining the modulation of GABA receptor-mediated currents, AMPA and NMDA receptor blockers 2,3-dioxo-6-nitro-1,2,3,4-tetrahydrobenzo[f]quinoxaline-7-sulfonamide (NBQX) and D-(–)-2-amino-5-phosphonopentanoic acid (APV), respectively were added. Baseline activity was recorded for 3–5 min after a 10- to 15-min baseline and another 5–10 min after addition of D1 or D2 receptor agonists (SKF81297 or quinpirole, 5–10 μM). To evoke synaptic currents, a monopolar glass stimulating electrode (patch pipette filled with ACSF, impedance 1.5–1.8 $\text{M}\Omega$) was placed in the corpus callosum, 200–300 μm from the recorded cell.

Test-stimuli (500 μ s duration) were applied every 20 s and averaged over three consecutive trials. Stimulation intensities were set to evoke responses at 30% maximal amplitude. Paired-pulse ratios (PPRs) were used to assess probability of release, and paired-pulses were applied at intervals between 25 and 400 ms.

DRUGS

Stocks of Bic (20 mM, Tocris), D1 receptor agonist SKF81297 (1 mM, Sigma), D2 receptor agonist quinpirole (10 mM, Sigma) were all dissolved in H₂O. TBZ (10 mM, Tocris) was dissolved in 100% DMSO for stock solution and final concentration for electrophysiology was 0.1%. For *in vivo* injections, TBZ (1 mg/ml) was dissolved in a mixture of DMSO/NaCl (50/50). Procedures for determination of the appropriate TBZ dosage *in vivo* have been published (André et al., 2011).

ACUTELY DISSOCIATED NEURONS

Detailed procedures have been published (Flores-Hernandez et al., 2002). Briefly, coronal slices containing the dorsal striatum were dissected, placed in an oxygenated cell-stir chamber (Wheaton, Millville, NJ, USA) and enzymatically treated for 15–20 min with papain (0.5 mg/ml, Calbiochem) at 35°C in a *N*-[2-hydroxyethyl] piperazine-*N*-[2-ethanesulfonic acid] (HEPES)-buffered Hank's balanced salts solution (HBSS, Sigma Chemical) supplemented with (in millimolar) 1 pyruvic acid, 0.005 glutathione, 0.1 NG-nitro-L-arginine, and 1 kynurenic acid. The tissue was rinsed with HEPES-buffered Na-isethionate solution containing (in millimolar) 140 Na isethionate, 2 KCl, 2 MgCl₂, 0.1 CaCl₂, 23 glucose, and 15 HEPES. Striatal slices were mechanically dissociated with fire-polished Pasteur pipettes. The cell suspension was then plated into a 35-mm Petri dish mounted on the stage of an upright fixed-stage microscope containing a HEPES-buffered salt solution. Only fluorescent cells were selected for recordings.

The internal solution consisted of (in millimolar) 175 *N*-methyl-D-glucamine (NMDG), 40 HEPES, 2 MgCl₂, 10 ethylene glycol-bis (β -aminoethyl ether)-*N,N,N',N'*-tetra-acetic acid (EGTA), 12 phosphocreatine, 2 Na₂ATP, 0.2 Na₂GTP, and 0.1 leupeptin (pH 7.25, 265–270 mOsm). The external solution consisted of (in millimolar) 135 NaCl, 20 CsCl, 3 BaCl₂, 2 CaCl₂, 10 glucose, 10 HEPES, and 0.0003 tetrodotoxin (TTX). Drugs were applied through a pressure-driven fast perfusion system using application capillaries positioned a few hundred micrometers from the cell. A DC drive system controlled by a SF-77B perfusion system (Warner Instruments, Hamden, CT, USA) synchronized by pClamp changed solutions by altering the position of the capillary array. NMDA currents (100 μ M, 3 s duration every 10 s) were evoked by applying the agonist while holding the cell at -70 mV. D1 and D2 agonists were applied as previously described (André et al., 2010).

DATA ANALYSIS AND STATISTICS

In the text, values are presented as mean \pm SEM. Data analyses were performed with Origin (Microcal Software, Northampton, MA, USA) and pClamp 10.2. Group means for all measures were compared using Student's *t*-tests (for two group comparisons) using SigmaStat software (SPSS, Chicago, IL, USA). Differences were considered statistically significant when $p < 0.05$. Spontaneous synaptic currents were analyzed offline using the automatic detection

protocol within the Mini Analysis Program (Justin Lee, Synaptosoft, 1999) and subsequently checked manually for accuracy. Event analyses were done blind to genotype. The threshold amplitude for the detection of an excitatory event (5 pA) was set above the root mean square background noise level (1–2 pA at $V_{\text{hold}} = -70$ mV). For inhibitory events, the detection was set at 10 pA because the noise level was higher (2–3 pA at $V_{\text{hold}} = -10$ mV). Amplitude–frequency and cumulative inter-event interval distributions were constructed and compared among the different groups using two-way repeated measures (RM) ANOVAs to compare events at each amplitude and interval, followed by Bonferroni *t*-tests (multiple group comparisons) using SigmaStat software (SPSS, Chicago, IL, USA).

RESULTS

GLUTAMATE TRANSMISSION AND GABA TRANSMISSIONS IN D1-YAC128 CELLS

At 1.5 months, D1-YAC128 cells displayed a higher frequency of spontaneous excitatory postsynaptic currents (sEPSCs) than D1-WT cells ($t_{38} = 2.65$, $p = 0.012$) while at 12 months, this difference was reversed ($t_{29} = 3.24$, $p = 0.003$; **Figures 1A,B**). Cumulative inter-event interval histograms also showed a significantly increased probability of release onto D1-YAC128 cells at the early stage, while at 12 months, they showed a decreased probability of glutamate release onto D1-YAC128 cells (**Figure 1C**).

D1-YAC128 also displayed a higher frequency of sIPSCs at 1.5 months ($t_{47} = 2.36$, $p = 0.022$) while there was no difference at 12 months ($t_{29} = 1.44$, $p = 0.161$, **Figures 1D,E**). Cumulative inter-event interval histograms for IPSCs also showed a significantly increased probability of GABA release onto D1-YAC128 cells at 1.5 months but not at 12 months (**Figure 1F**).

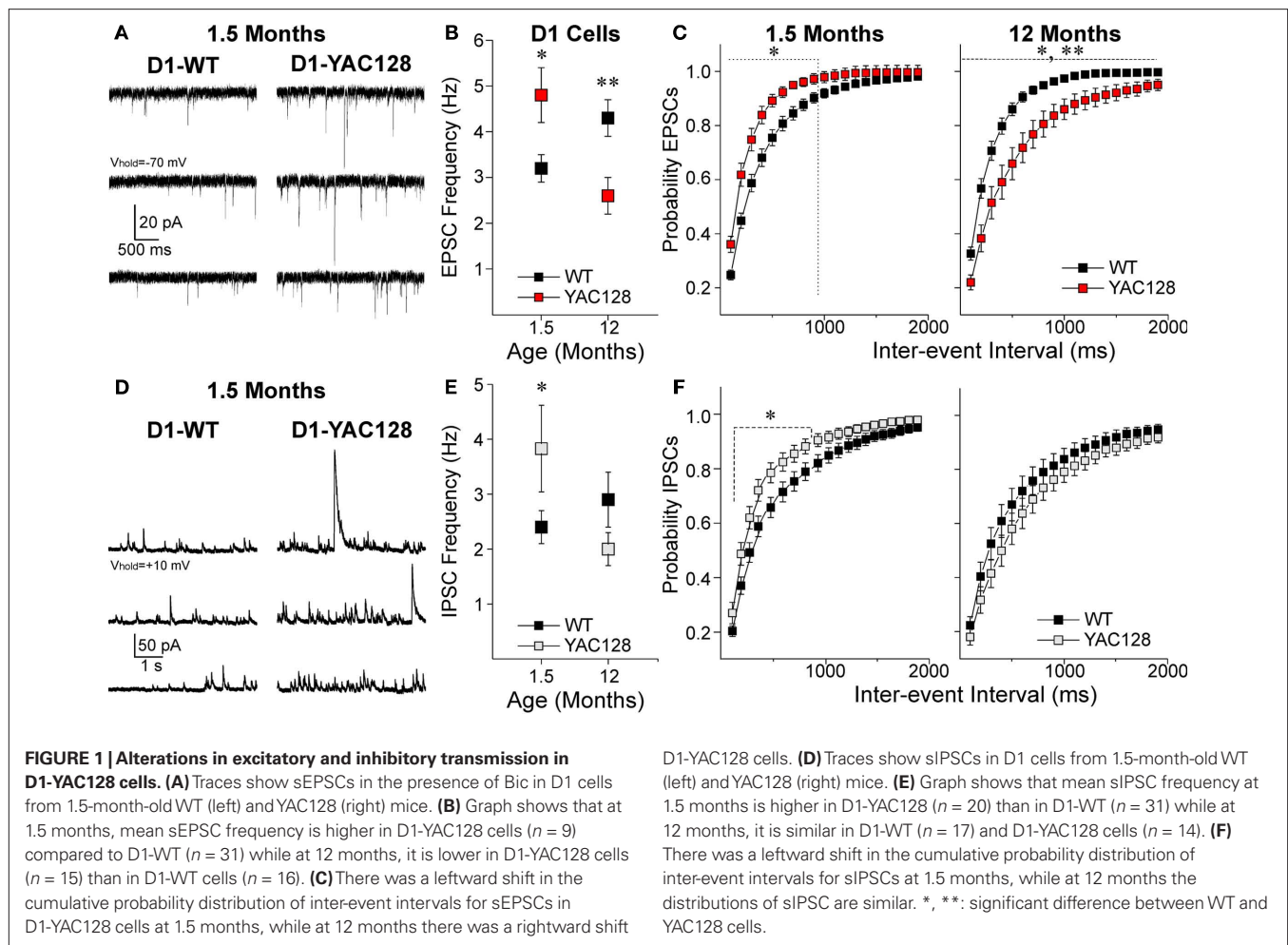
GLUTAMATE TRANSMISSION AND GABA TRANSMISSION IN D2-YAC128 CELLS

In contrast to the D1 cells, D2-YAC128 cells did not show any significant differences in mean sEPSCs at 1.5 ($t_{37} = 0.86$, $p = 0.395$) or at 12 months ($t_{31} = 1.083$, $p = 0.287$, **Figures 2A,B**). Cumulative inter-event interval histograms did not show any differences at 1.5 months but at 12 months, the significant rightward shift suggests a decrease of glutamate release in late stage D2-YAC128 cells (**Figure 2C**).

In 1.5 month D2 cells, there was no difference in the mean IPSC frequency ($t_{40} = 0.693$, $p = 0.492$) or the inter-event interval histogram (**Figures 2D–F**). However, at 12 months, IPSC frequency was increased ($t_{27} = 2.668$, $p = 0.013$) in the D2-YAC128 cells and the cumulative inter-event interval histogram suggested increased probability of GABA release onto D2-YAC128 cells (**Figures 2E,F**).

GLUTAMATE TRANSMISSION AND GABA TRANSMISSION ARE INCREASED IN D1 CELLS IN BACHD MICE AT 2 MONTHS

Similar to D1-YAC128 cells, D1-BACHD cells displayed a higher sEPSC frequency at 2 months ($t_{18} = 2.781$, $p = 0.012$, **Figure 3A**). To provide further evidence that the differences in EPSC frequencies were due to altered glutamate release, we examined responses evoked by stimulation of corticostriatal afferents (eEPSCs) and measured PPRs (André et al., 2011). At 2 months, D1-BACHD cells displayed a significant decrease in PPRs (two-way RM ANOVA $F_{1,89} = 15.6$, $p = 0.001$) at 25 ($t = 3.8$, $p < 0.001$) and 50 ($t = 3.57$,



$p < 0.001$) ms (Figures 3B,C) suggesting an increased probability of glutamate release onto cells of the direct pathway in BACHD mice at an early stage. D2-BACHD cells did not show any difference in PPRs compared to their WT littermates (two-way RM ANOVA $F_{1,83} = 0.19$, $p = 0.662$, Figure 3C), again similar to that finding in D2-YAC128 cells at the early stage.

At this early stage, we found similar increases in frequency of sIPSCs in D1-BACHD as we showed in D1-YAC128 cells with a significant leftward shift in cumulative probability histograms in the D1-BACHD cells suggesting increased probability of GABA release (Figure 3D). However, as the changes in mean sIPSC frequency did not reach significance in D1-BACHD compared to D1-WT cells ($t_{23} = 1.736$, $p = 0.096$, Figure 3D inset), the increase of GABA release might not be of the same amplitude in the BACHD mice as it was in the YAC128 mice, at least at the early stage. D2-BACHD cells did not show any differences in sIPSC mean frequency or in cumulative inter-event interval distribution (Figure 3E).

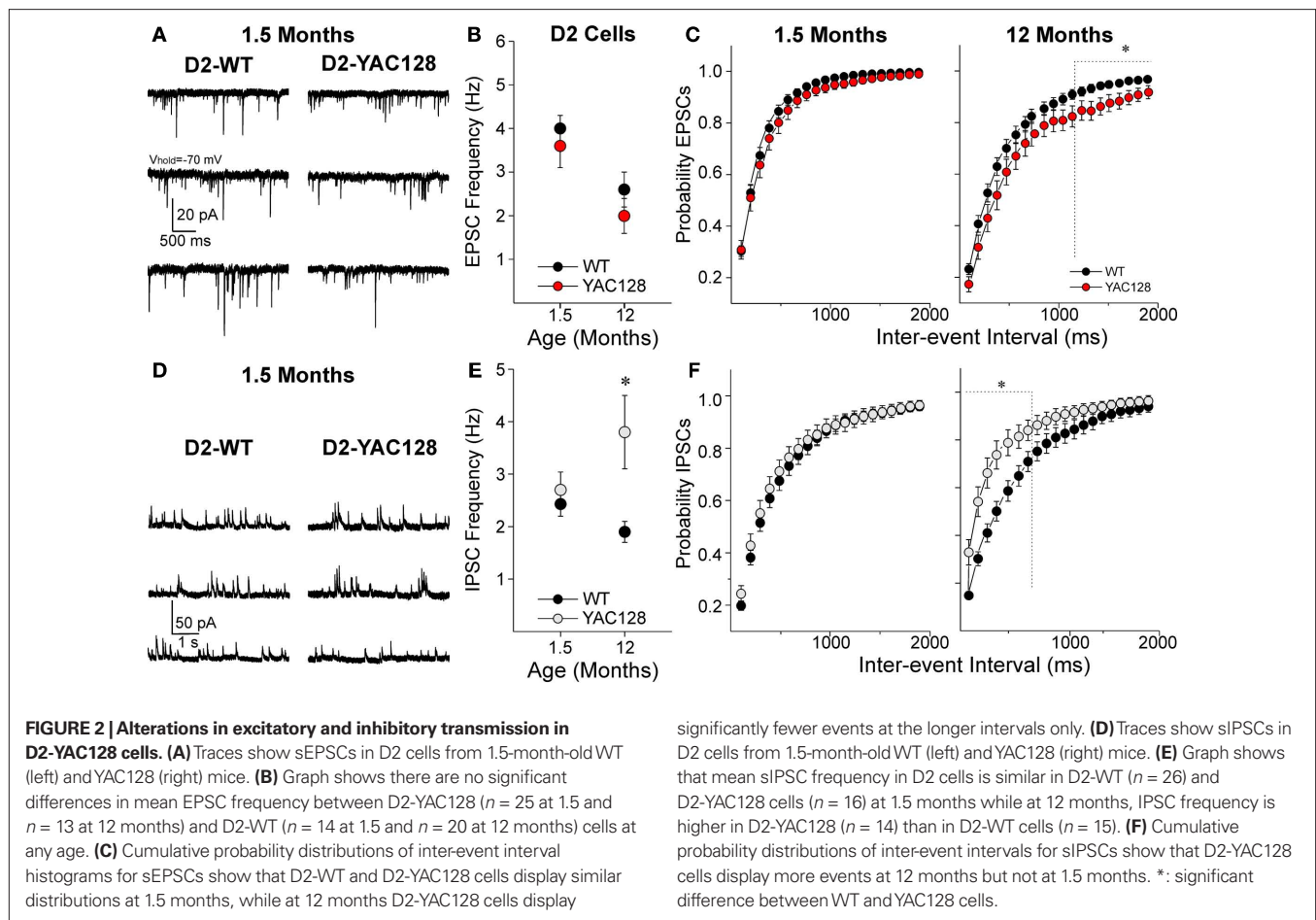
D1 AND D2 RECEPTORS ARE STILL FUNCTIONAL IN YAC128

As EGFP was visible in YAC128 and WT cells and no difference in the intensity of fluorescence was observed (Figure 4A), we hypothesized that DA D1 and D2 receptors are still expressed in

the YAC128 mice. To examine whether D1 and D2 receptors are transported to the surface and functional, we tested the effects of D1 and D2 agonists on postsynaptic NMDA currents in acutely dissociated D1 and D2 MSNs at 1.5 months. It is well known that D1 receptor activation increases NMDA currents while D2 receptor activation decreases them (Cepeda et al., 1993; André et al., 2010). The D1 agonist (SKF81297, 1 μ M) increased NMDA currents in D1 cells similarly in WT (paired t -test, $t_8 = 6.953$, $p < 0.001$) and YAC128 ($t_9 = 2.888$, $p = 0.018$) cells (Figure 4B). The D2 agonist (quinpirole, 10 μ M) similarly decreased NMDA current amplitudes in WT ($t_4 = 3.290$, $p = 0.03$) and YAC128 ($t_4 = 4.103$, $p = 0.015$) cells (Figure 4C).

LOSS OF D1 MODULATION IS REVERSED BY DA BLOCKERS

We examined DA modulation in slices by testing the effect of the D1 agonist SKF81297 on sEPSC frequency at 1.5 months. While in D1-WT cells, SKF81297 increased sEPSC frequency (paired t -test: $t_{20} = 5.867$, $p < 0.001$), the D1 agonist did not have any effect on D1-YAC128 cells ($t_7 = 0.607$, $p = 0.563$; Figures 5A,B). By contrast, at a later stage, the D1 agonist effect was similar in D1-WT and D1-YAC128 cells (André et al., 2011). This early alteration in DA neurotransmission might be induced by abnormal DA concentrations as we show that DA receptors are functional (Figure 4).



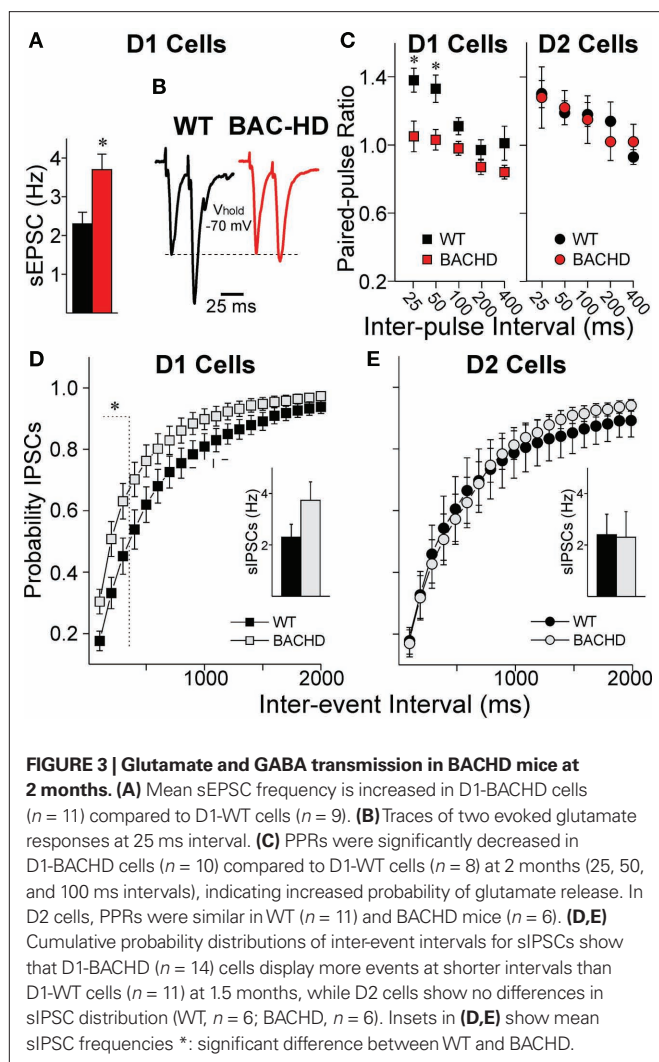
Previous studies showed that elevated striatal DA concentrations decrease DA receptor function (Giros et al., 1996; Dumartin et al., 2000; Wu et al., 2007). In addition, decreasing DA concentrations with TBZ alleviates chorea in HD patients (Huntington Study Group, 2006). TBZ is a monoamine depletor, but it ultimately depletes DA stores (Pettibone et al., 1984), suggesting that decreasing DA might be beneficial for hyperkinetic symptoms. To test whether DA function could be rescued in early HD, we examined the effect of TBZ and D1 antagonists in early HD.

In slices incubated in TBZ (10 μ M) for at least 2 h, SKF81297 significantly increased sEPSC frequency in D1-YAC128 cells ($t_8 = 2.672$, $p = 0.028$), and its effect was similar to that of the D1 agonist in D1-WT cells (Figures 5A,B). In D1-BACHD cells, pre-incubation in TBZ also rescued the decrease in PPRs (Figure 5C). As TBZ was dissolved in DMSO, we tested the effect of DMSO alone on PPR in D1-BACHD cells. In the BACHD cells, DMSO had no effect on PPRs, indicating that the rescue effect was induced by TBZ. PPRs from TBZ-incubated slices in D1-BACHD cells were similar to those of D1-WT cells. To examine whether alterations in glutamate and GABA transmission could be induced by abnormally elevated activation of D1 receptors, we tested the effect of the D1 receptor antagonist SCH23390 (10 μ M) on sEPSC and sIPSC frequency in D1-BACHD cells. SCH23390 was added after a stable baseline of sEPSCs or sIPSCs was established (in different cells), and the

change in frequency was measured after 6–10 min of incubation. In D1-WT cells, SCH23390 (10 and 20 μ M) did not have a significant effect on sEPSC frequency. In contrast 20 μ M SCH23390 significantly decreased sEPSC frequency in D1-BACHD cells ($t_{10} = 2.416$, $p = 0.036$). The D1 antagonist effect was significantly different between WT and BACHD cells ($t_{18} = 2.858$, $p = 0.01$; Figure 5D, inset). SCH23390 (10 μ M) did not significantly decrease sIPSC frequency in D1-WT cells although there was a trend (Figure 5E). In D1-BACHD cells, SCH23390 decreased sIPSC frequency by $-36.3 \pm 11.5\%$ ($t_5 = 3.027$, $p = 0.029$). However, the difference between D1-WT and D1-BACHD cells was not statistically different (Figure 5E, inset).

DISCUSSION

Visualization of direct and indirect pathway MSNs by EGFP expression allowed us to differentiate the two types of MSNs and to uncover alterations in the two pathways that differed with the progression of the disease. The use of mice expressing the reporter protein EGFP through a BAC transgene has proved to alter the expression of the D2 receptor, and induce electrophysiological hypersensitivity to D2 receptor agonists in midbrain DA neurons, as well as hyperactivity, suggesting the need for better tools to visualize D2 receptor-expressing neurons (Kramer et al., 2011). This characterization was mainly performed on homozygote BAC



transgenic mice, and heterozygote mice might display a milder phenotype although the study also found some behavioral changes in heterozygote mice. In our study, we used heterozygote mice and we excluded all D2-EGFP mice for behavioral studies. Although we did not extensively compare EGFP-positive and negative MSNs, we found that the effect of the D2 agonist was decreased in HD mice, and that in early HD, most alterations were present in direct pathway MSNs, validating the use of EGFP to compare WT and HD mice.

GLUTAMATE TRANSMISSION AND GABA TRANSMISSION ARE INCREASED ONTO DIRECT PATHWAY NEURONS AT THE EARLY STAGE OF HD

In both YAC128 and BACHD animal models, we observed an increase in sEPSC and in sIPSC frequency in D1 cells at an early symptomatic age. In addition, there was a decrease in PPRs for evoked glutamate responses (Table 1). Low PPRs at short intervals indicate depletion of neurotransmitter from the presynaptic terminal and an increased probability of release of the immediately releasable store (Zucker, 1989; Choi and Lovinger, 1997). There were also increased frequencies of miniature EPSCs but no change in event amplitude (André et al.,

2011). These results suggest that glutamate release is increased onto direct pathway MSNs. Although we did not perform paired-pulse stimulation to measure PPRs for IPSCs in this particular study, our data on sIPSCs show that the frequency of GABA-mediated events is also higher onto direct pathway MSNs in YAC128 and BACHD mice. Furthermore, we have shown that PPRs of evoked IPSCs are decreased in MSNs in the R6/2 mouse, providing further evidence for the hypothesis of increased GABA release in HD (Rao et al., 2010). Taken together, our results suggest that both glutamate and GABA release are increased on direct pathway MSNs. Previously we demonstrated that the frequency of sIPSCs increases in HD (Cepeda et al., 2004). The present study indicates that the increase is specific to D1-expressing neurons in the early stage.

D1 and D2 receptors are functionally active in acutely dissociated YAC128 cells while D1 and D2 receptors were not responsive in slices. The dissociated preparation isolates neurons from synaptic inputs and from ambient DA, while in slices neurons have active synapses and are exposed to modulators. As striatal neurotransmitter release is modulated by DA receptors located on presynaptic terminals and postsynaptically on the two types of MSNs, we hypothesized that abnormal DA transmission in slices could underlie differential alterations of excitatory and inhibitory transmission onto direct and indirect pathway neurons. Our data show that blocking DA function with a D1 antagonist had larger effects in D1-BACHD cells than in WT cells and that depleting DA with TBZ decreased stereotypies in the BACHD model (André et al., 2011). These findings suggest that at an early stage, DA tone or basal function is increased and might contribute to some of the symptoms in HD by altering neuronal activity in the direct pathway. Our results are in line with observations that DA receptor antagonists and agents that decrease DA reduce chorea and motor symptoms in patients and in animal models while dopaminergic stimulation can exacerbate symptoms (Huntington Study Group, 2006; Tang et al., 2007; Mestre et al., 2009). It is unclear why we did not observe any changes in GABA or glutamate transmission in D2 cells at the early stage. As DA induces reduction of neurotransmitter release onto D2 cells via activation of pre and postsynaptic receptors (Kreitzer and Malenka, 2007; André et al., 2010), a decrease of neurotransmitter release could be expected in D2 cells at an early stage. However, in another study, an increased facilitation of evoked EPSCs was reported in 26-day-old YAC128. The authors suggested this could be interpreted as a decrease in the probability of glutamate release in indirect pathway MSNs (Milnerwood and Raymond, 2007). We could have missed those alterations onto indirect pathway MSNs since we performed our early stage recordings in slightly older mice between 45 and 60 days.

It is also unclear why changes in DA transmission would affect glutamate and GABA synaptic activity in D1 MSNs while having no effects in D2 MSNs, especially if considering that the proportion of high-affinity D2 receptors is much greater than the proportion of high-affinity D1 receptors in the striatum (Richfield et al., 1989). It is important to consider that DA influence also depends on the number of receptors within a sphere of DA spillover (Rice and Cragg, 2008). Although no study evaluated the number of high- and low-affinity DA receptors, it was reported that D1 receptors are in considerable excess of D2 receptors in the striatum (Richfield et al., 1989; Benn et al., 2007). It is therefore possible that in cases

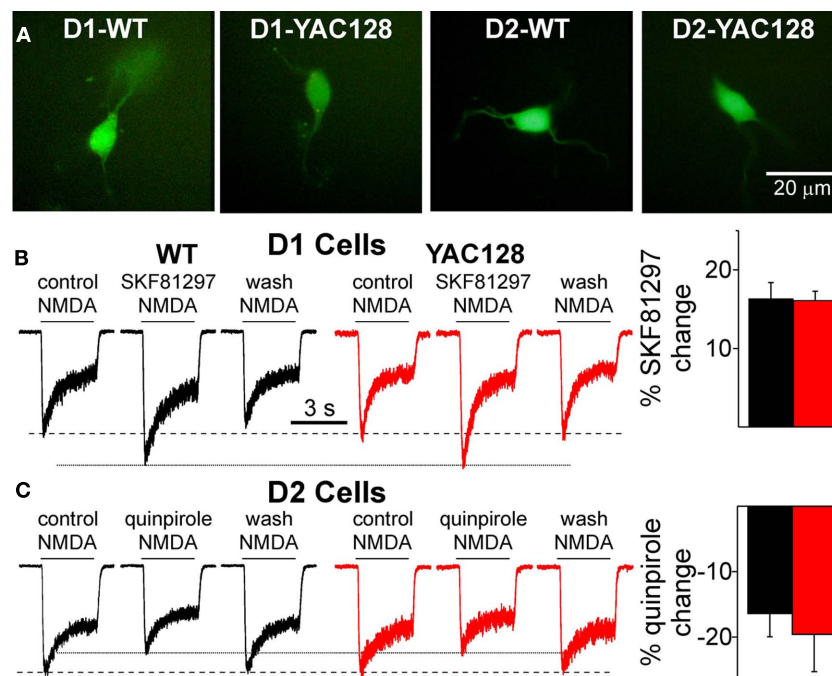


FIGURE 4 | D1 and D2 receptor modulation in acutely dissociated MSNs is similar in WT and YAC128 cells at 1.5 months. (A) Examples of acutely dissociated MSNs in WT and YAC128. **(B)** Traces of NMDA currents (100 μ M) in D1 cells show the D1 agonist SKF81297 (1 μ M) increases the amplitude of NMDA currents in D1-WT ($n = 9$) and D1-YAC128 cells ($n = 10$). Graph shows the

percent potentiation by SKF81297 is similar in D1-WT and D1-YAC128 cells. **(C)** Traces of NMDA currents (100 μ M) in D2 cells show the D2 agonist quinpirole (10 μ M) decreases NMDA currents in D2-WT ($n = 5$) and D2-YAC128 cells ($n = 5$). Graph shows the percent attenuation by quinpirole is similar in D2-WT and D2-YAC128 cells.

of abnormal DA transmission, or DA spillover, D1 receptors are more affected than D2 receptors. Other factors such as differential glutamate cortical and GABAergic striatal inputs formed onto D1 and D2 MSNs (Lei et al., 2004; Kreitzer and Malenka, 2006; Cepeda et al., 2008; Gittis et al., 2010) could also contribute to prominent changes in D1 MSNs in early HD.

GLUTAMATE TRANSMISSION IS DECREASED ONTO ALL MSNs AT A LATE STAGE WHILE GABA TRANSMISSION IS INCREASED ONTO INDIRECT PATHWAY MSNs

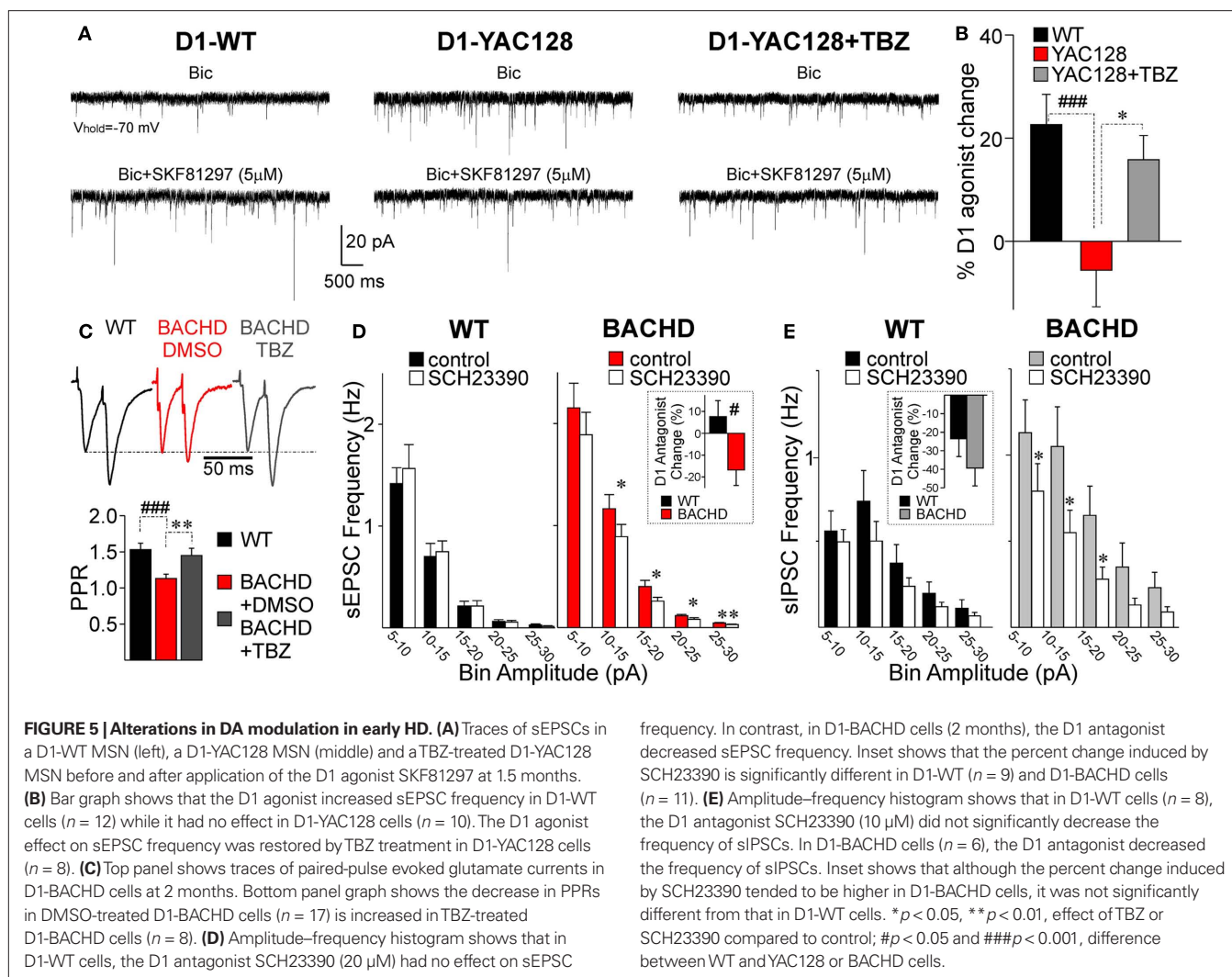
The fact that glutamate transmission is decreased onto both direct and indirect pathway MSNs is consistent with a progressive disconnection between cortex and striatum (Cepeda et al., 2003). However, this effect was more marked onto direct pathway MSNs, showing both decreased sEPSC frequency and increased PPRs, while indirect pathway MSNs showed only a subtle decrease of sEPSCs (Figure 6). In contrast to glutamate transmission, GABA transmission was increased onto indirect pathway MSNs, suggesting that unlike glutamate terminals, GABA terminals might not disconnect in the YAC128 model. In the R6/2 model, we have provided evidence that the increased GABA transmission emanates from GABAergic interneurons that may be hyperexcitable (Rao et al., 2010). The fact that increased inhibition was observed only onto indirect pathway MSNs indicates that cannabinoid signaling might be involved. Cannabinoid type 1 (CB1) receptors are located on striatal GABAergic terminals, inhibiting GABA release when activated (Szabo et al., 1998; Kofalvi et al., 2005). Endogenous ligands for the cannabinoid receptors are released by MSNs via activation of DA D2

receptors located on D2 receptor-expressing MSNs (Giuffrida et al., 1999; Patel et al., 2003). In late HD, a lack of DA or D2 receptors in indirect pathway MSNs could therefore increase GABA release onto indirect pathway MSN via a lack of endocannabinoid release. This effect will not occur in D1 cells, not expressing D2 receptors.

Decreased DA tone or DA function could also contribute to hyperexcitability of interneurons and increased GABA release (Dehorter et al., 2009). Our data showing a lack of effect of a D2 antagonist in D2-YAC128 cells (André et al., 2011) support the hypothesis that DA function is decreased in late HD. In this case, one would also expect an increase of sIPSCs onto direct pathway MSNs, except if direct and indirect pathway MSNs are connected by different types of interneurons as suggested by a recent study (Gittis et al., 2010). In the case of abnormally low DA function, an increase in glutamate release would also be expected since DA D2 receptors are also present on presynaptic glutamate terminals and act to decrease neurotransmitter release when activated by DA (Wang and Pickel, 2002; Bamford et al., 2004). However, sEPSC frequency was not increased in the indirect pathway MSNs, and was even slightly decreased. This might be explained by the loss of corticostriatal inputs at this late stage of the disease.

FUNCTIONAL CONSEQUENCES OF ALTERATIONS IN DIRECT AND INDIRECT PATHWAY MSNs

Increased probability of glutamate release onto D1 cells will shift the balance of direct and indirect pathway activity, disinhibiting output structures such as the colliculus and the thalamus, and increasing



movement (Chevalier and Deniau, 1990). Thus, stereotypies observed in young BACHD and YAC128 mice might be induced by overactivation of D1 cells as has been observed in cases of elevated DA transmission (Usiello et al., 2000; Horvitz et al., 2001). Although hypoactivity in symptomatic HD animals has been reported, there is evidence that hyperactivity and stereotyped behaviors occur in lesion models in rats (Borlongan et al., 1997; Brouillet et al., 1999; Bolivar et al., 2004) and in early stage in transgenic mouse models carrying a short fragment or the full length of the human gene in different strains (Sanberg et al., 1989; Carter et al., 1999; Bolivar et al., 2004; Van Raamsdonk et al., 2005, 2007). Abnormal involuntary movements, dyskinesia and chorea are hallmarks of human pathology at early stages and the hyperkinetic syndrome is progressively replaced by a more hypokinetic syndrome (Thompson et al., 1988). In contrast, a decrease in the activity of direct pathway MSNs could explain the decreased locomotor activity observed in the late symptomatic YAC128 mice.

The resulting effect of increased GABA release could also alter direct and indirect pathway activity. The effect of GABA_A receptor activation on striatal cell excitability depends on the cell membrane potential as the reversal potential for Cl⁻ is ~ -60 mV and the resting membrane potential for MSNs is hyperpolarized (~ -80 to -90 mV).

In vivo, MSN membrane potentials oscillate between hyperpolarized “down” and more depolarized “up” states (Wilson and Kawaguchi, 1996). Therefore, activation of GABA_A receptors depolarizes MSN membrane at rest while it hyperpolarizes membrane potential near the action potential threshold (Mercuri et al., 1991; Koos and Tepper, 1999). Although our results in current-clamp show there are no changes in membrane excitability in YAC128 cells at the early stage (André et al., 2011), more data are needed to determine the consequences of increased GABA on MSN activity.

CONCLUSION

The present findings suggest anomalies in glutamate and GABA transmission in HD might be induced by abnormal DA transmission. Early in the progression of the disease, increased glutamate release onto D1 cells and increased stereotypies are consistent with increased DA tone (Presti et al., 2004). In symptomatic animals, decreased glutamate release onto D1 cells and hypoactive behavior are consistent with decreased DA tone and/or loss of corticostriatal terminals. Our data suggest that modulation of direct pathway neurons with D1 antagonists or agents decreasing DA function in early HD stage might prove useful as a strategy

Table 1 | Summary of changes in spontaneous excitatory and inhibitory currents and dopamine modulation in D1 and D2 cells in early and late stage HD in the YAC128 and BACHD models.

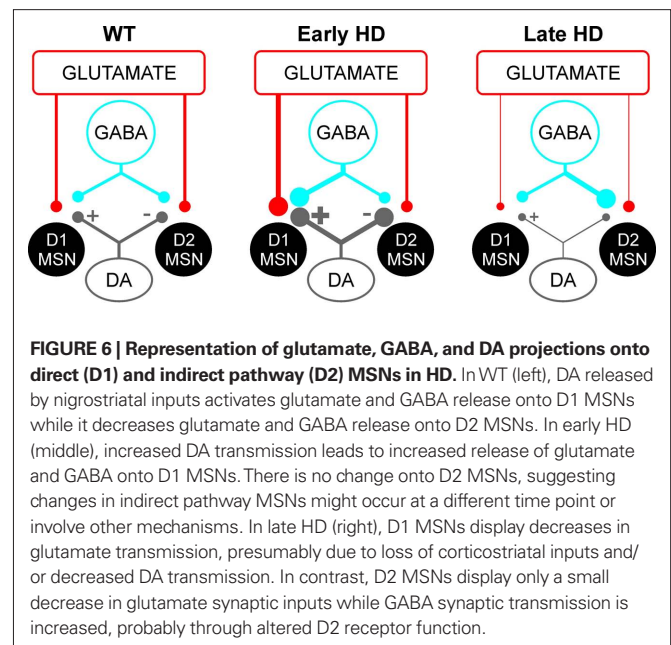
	Early HD		Late HD	
	D1 MSNs	D2 MSNs	D1 MSNs	D2 MSNs
YAC128				
PPR glut	↓	–	↑	–
EPSC frequency	↑	–	↓↓	↓
IPSC frequency	↑	–	–	↑↑
Dopamine modulation of EPSC frequency in slices				
D1 agonist	No effect		Normal	
D2 agonist		No effect		No effect
Dopamine modulation of NMDA currents in isolated neurons				
D1 agonist	Normal		Not tested	
D2 agonist		Normal		
BACHD				
PPR glut	↓	–		
EPSC frequency	↑	–		
IPSC frequency	↑	–		

↓Decrease compared to WT.

↑Increase compared to WT.

–No change compared to WT.

to treat hyperkinetic motor symptoms. In contrast, DA agonists at more advanced stages might prove useful as a strategy to treat hypokinetic motor symptoms. In the future, studies are necessary to understand the consequences of altered GABA and glutamate



transmissions onto basal ganglia output neurons in HD to help direct new therapies and understand the mechanisms underlying the phenotypic changes.

ACKNOWLEDGMENTS

This work was supported by National Institutes of Health Grant NS41574, CHDI, and The Hereditary Disease Foundation.

REFERENCES

- Albin, R. L., Reiner, A., Anderson, K. D., Penney, J. B., and Young, A. B. (1990). Striatal and nigral neuron subpopulations in rigid Huntington's disease: implications for the functional anatomy of chorea and rigidity-akinesia. *Ann. Neurol.* 27, 357–365.
- André, V. M., Cepeda, C., Cummings, D. M., Jocoy, E. L., Fisher, Y. E., Yang, X. W., and Levine, M. S. (2010). Dopamine modulation of excitatory currents in the striatum is dictated by the expression of D1 or D2 receptors and modified by endocannabinoids. *Eur. J. Neurosci.* 31, 14–28.
- André, V. M., Cepeda, C., Fisher, Y. E., Huynh, M., Bardakjian, N., Singh, S., Yang, X. W., and Levine, M. S. (2011). Differential electrophysiological changes in striatal output neurons in Huntington's disease. *J. Neurosci.* 31, 1170–1182.
- Bamford, N. S., Robinson, S., Palmiter, R. D., Joyce, J. A., Moore, C., and Meshul, C. K. (2004). Dopamine modulates release from corticostriatal terminals. *J. Neurosci.* 24, 9541–9552.
- Benn, C. L., Slow, E. J., Farrell, L. A., Graham, R., Deng, Y., Hayden, M. R., and Cha, J. H. (2007). Glutamate receptor abnormalities in the YAC128 transgenic mouse model of Huntington's disease. *Neuroscience* 147, 354–372.
- Bolam, J. P., Hanley, J. J., Booth, P. A., and Bevan, M. D. (2000). Synaptic organisation of the basal ganglia. *J. Anat.* 196(Pt 4), 527–542.
- Bolivar, V. J., Manley, K., and Messer, A. (2004). Early exploratory behavior abnormalities in R6/1 Huntington's disease transgenic mice. *Brain Res.* 1005, 29–35.
- Borlongan, C. V., Koutouzis, T. K., Freeman, T. B., Hauser, R. A., Cahill, D. W., and Sanberg, P. R. (1997). Hyperactivity and hypoactivity in a rat model of Huntington's disease: the systemic 3-nitropropionic acid model. *Brain Res. Brain Res. Protoc.* 1, 253–257.
- Brouillet, E., Conde, F., Beal, M. F., and Hantraye, P. (1999). Replicating Huntington's disease phenotype in experimental animals. *Prog. Neurobiol.* 59, 427–468.
- Carter, R. J., Lione, L. A., Humby, T., Mangiarini, L., Mahal, A., Bates, G. P., Dunnett, S. B., and Morton, A. J. (1999). Characterization of progressive motor deficits in mice transgenic for the human Huntington's disease mutation. *J. Neurosci.* 19, 3248–3257.
- Cepeda, C., André, V. M., Yamazaki, I., Wu, N., Kleiman-Weiner, M., and Levine, M. S. (2008). Differential electrophysiological properties of dopamine D1 and D2 receptor-containing striatal medium-sized spiny neurons. *Eur. J. Neurosci.* 27, 671–682.
- Cepeda, C., Buchwald, N. A., and Levine, M. S. (1993). Neuromodulatory actions of dopamine in the neostriatum are dependent upon the excitatory amino acid receptor subtypes activated. *Proc. Natl. Acad. Sci. U.S.A.* 90, 9576–9580.
- Cepeda, C., Hurst, R. S., Calvert, C. R., Hernández-Echeagaray, E., Nguyen, O. K., Jocoy, E., Christian, L. J., Ariano, M. A., and Levine, M. S. (2003). Transient and progressive electrophysiological alterations in the corticostriatal pathway in a mouse model of Huntington's disease. *J. Neurosci.* 23, 961–969.
- Cepeda, C., Starling, A. J., Wu, N., Nguyen, O. K., Uzgil, B., Soda, T., André, V. M., Ariano, M. A., and Levine, M. S. (2004). Increased GABAergic function in mouse models of Huntington's disease: reversal by BDNF. *J. Neurosci. Res.* 78, 855–867.
- Chevalier, G., and Deniau, J. M. (1990). Disinhibition as a basic process in the expression of striatal functions. *Trends Neurosci.* 13, 277–280.
- Chevalier, G., Vacher, S., Deniau, J. M., and Desban, M. (1985a). Disinhibition as a basic process in the expression of striatal functions. I. The striato-nigral influence on tecto-spinal/tecto-diencephalic neurons. *Brain Res.* 334, 215–226.
- Chevalier, G., Vacher, S., Deniau, J. M., and Desban, M. (1985b). Disinhibition as a basic process in the expression of striatal functions. I. The striato-nigral influence on tecto-spinal/tecto-diencephalic neurons. *Brain Res.* 334, 215–226.
- Choi, S., and Lovinger, D. M. (1997). Decreased probability of neurotransmitter release underlies striatal long-term depression and postnatal development of corticostriatal synapses. *Proc. Natl. Acad. Sci. U.S.A.* 94, 2665–2670.
- Dehorter, N., Guigoni, C., Lopez, C., Hirsch, J., Eusebio, A., Ben-Ari, Y., and Hammond, C. (2009). Dopamine-deprived striatal GABAergic interneurons burst and generate repetitive gigantic IPSCs in medium spiny neurons. *J. Neurosci.* 29, 7776–7787.
- Dumartin, B., Jaber, M., Gonon, F., Caron, M. G., Giros, B., and Bloch, B. (2000).

- Dopamine tone regulates D1 receptor trafficking and delivery in striatal neurons in dopamine transporter-deficient mice. *Proc. Natl. Acad. Sci. U.S.A.* 97, 1879–1884.
- Flores-Hernandez, J., Cepeda, C., Hernandez-Echeagaray, E., Calvert, C. R., Jokel, E. S., Fienberg, A. A., Greengard, P., and Levine, M. S. (2002). Dopamine enhancement of NMDA currents in dissociated medium-sized striatal neurons: role of D1 receptors and DARPP-32. *J. Neurophysiol.* 88, 3010–3020.
- Gerfen, C. R. (1992). The neostriatal mosaic: multiple levels of compartmental organization. *Trends Neurosci.* 15, 133–139.
- Giros, B., Jaber, M., Jones, S. R., Wightman, R. M., and Caron, M. G. (1996). Hyperlocomotion and indifference to cocaine and amphetamine in mice lacking the dopamine transporter. *Nature* 379, 606–612.
- Gittis, A. H., Nelson, A. B., Thwin, M. T., Palop, J. J., and Kreitzer, A. C. (2010). Distinct roles of GABAergic interneurons in the regulation of striatal output pathways. *J. Neurosci.* 30, 2223–2234.
- Giuffrida, A., Parsons, L. H., Kerr, T. M., Rodriguez de Fonseca, F., Navarro, M., and Piomelli, D. (1999). Dopamine activation of endogenous cannabinoid signaling in dorsal striatum. *Nat. Neurosci.* 2, 358–363.
- Gray, M., Shirasaki, D. I., Cepeda, C., Andre, V. M., Wilburn, B., Lu, X. H., Tao, J., Yamazaki, I., Li, S. H., Sun, Y. E., Li, X. J., Levine, M. S., and Yang, X. W. (2008). Full-length human mutant huntingtin with a stable polyglutamine repeat can elicit progressive and selective neuropathogenesis in BACHD mice. *J. Neurosci.* 28, 6182–6195.
- Horvitz, J. C., Williams, G., and Joy, R. (2001). Time-dependent actions of D2 family agonist quinpirole on spontaneous behavior in the rat: dissociation between sniffing and locomotion. *Psychopharmacology (Berl.)* 154, 350–355.
- Huntington Study Group. (2006). Tetrabenazine as antichorea therapy in Huntington disease: a randomized controlled trial. *Neurology* 66, 366–372.
- Kofalvi, A., Rodrigues, R. J., Ledent, C., Mackie, K., Vizi, E. S., Cunha, R. A., and Sperlagh, B. (2005). Involvement of cannabinoid receptors in the regulation of neurotransmitter release in the rodent striatum: a combined immunochemical and pharmacological analysis. *J. Neurosci.* 25, 2874–2884.
- Koos, T., and Tepper, J. M. (1999). Inhibitory control of neostriatal projection neurons by GABAergic interneurons. *Nat. Neurosci.* 2, 467–472.
- Kramer, P. F., Christensen, C. H., Hazelwood, L. A., Dobi, A., Bock, R., Sibley, D. R., Mateo, Y., and Alvarez, V. A. (2011). Dopamine D2 receptor overexpression alters behavior and physiology in Drd2-EGFP mice. *J. Neurosci.* 31, 126–132.
- Kravitz, A. V., Freeze, B. S., Parker, P. R., Kay, K., Thwin, M. T., Deisseroth, K., and Kreitzer, A. C. (2010). Regulation of parkinsonian motor behaviours by optogenetic control of basal ganglia circuitry. *Nature* 466, 622–626.
- Kreitzer, A. C., and Malenka, R. C. (2006). Distinct function and plasticity at striatal direct and indirect pathway synapses. *Abstr. Soc. Neurosci.* 732.20.
- Kreitzer, A. C., and Malenka, R. C. (2007). Endocannabinoid-mediated rescue of striatal LTD and motor deficits in Parkinson's disease models. *Nature* 445, 643–647.
- Lei, W., Jiao, Y., Del Mar, N., and Reiner, A. (2004). Evidence for differential cortical input to direct pathway versus indirect pathway striatal projection neurons in rats. *J. Neurosci.* 24, 8289–8299.
- Lovinger, D. M. (2008). "Presynaptic modulation by endocannabinoids," in *Handbook of Experimental Pharmacology*, eds T. C. Sudhoh and K. Starke (Berlin: Springer-Verlag) 435–477.
- Malenka, R. C., and Kocsis, J. D. (1988). Presynaptic actions of carbachol and adenosine on corticostriatal synaptic transmission studied in vitro. *J. Neurosci.* 8, 3750–3756.
- Mangiarini, L., Sathasivam, K., Siller, M., Cozens, B., Harper, A., Hetherington, C., Lawton, M., Trotter, Y., Leach, H., Davies, S. W., and Bates, G. P. (1996). Exon 1 of the HD gene with an expanded CAG repeat is sufficient to cause a progressive neurological phenotype in transgenic mice. *Cell* 87, 493–506.
- Mercuri, N. B., Calabresi, P., Stefani, A., Stratta, F., and Bernardi, G. (1991). GABA depolarizes neurons in the rat striatum: an in vivo study. *Synapse* 8, 38–40.
- Mestre, T., Ferreira, J., Coelho, M. M., Rosa, M., and Sampaio, C. (2009). Therapeutic interventions for symptomatic treatment in Huntington's disease. *Cochrane Database Syst. Rev.* 3, CD006456.
- Milnerwood, A. J., and Raymond, L. A. (2007). Corticostriatal synaptic function in mouse models of Huntington's disease: early effects of huntingtin repeat length and protein load. *J. Physiol. (Lond.)* 585, 817–831.
- Patel, S., Rademacher, D. J., and Hillard, C. J. (2003). Differential regulation of the endocannabinoids anandamide and 2-arachidonylglycerol within the limbic forebrain by dopamine receptor activity. *J. Pharmacol. Exp. Ther.* 306, 880–888.
- Pettibone, D. J., Totaro, J. A., and Pflueger, A. B. (1984). Tetrabenazine-induced depletion of brain monoamines: characterization and interaction with selected antidepressants. *Eur. J. Pharmacol.* 102, 425–430.
- Presti, M. F., Gibney, B. C., and Lewis, M. H. (2004). Effects of intrastriatal administration of selective dopaminergic ligands on spontaneous stereotypy in mice. *Physiol. Behav.* 80, 433–439.
- Rao, S. R., André, V. M., Cepeda, C., and Levine, M. S. (2010). Altered inhibitory inputs onto striatal medium-sized spiny neurons in the R6/2 mouse model of Huntington's disease. *Abstr. Soc. Neurosci.* 861.16.
- Rice, M. E., and Cragg, S. J. (2008). Dopamine spillover after quantal release: rethinking dopamine transmission in the nigrostriatal pathway. *Brain Res. Rev.* 58, 303–313.
- Richfield, E. K., Penney, J. B., and Young, A. B. (1989). Anatomical and affinity state comparisons between dopamine D1 and D2 receptors in the rat central nervous system. *Neuroscience* 30, 767–777.
- Sanberg, P. R., Calderon, S. F., Giordano, M., Tew, J. M., and Norman, A. B. (1989). The quinolinic acid model of Huntington's disease: locomotor abnormalities. *Exp. Neurol.* 105, 45–53.
- Shilling, G., Becher, M. W., Sharp, A. H., Jinnah, H. A., Duan, K., Kotz, J. A., Slunt, H. H., Ratovitski, T., Cooper, J. K., Jenkins, N. A., Copeland, N. G., Price, D. L., Ross, C. A., and Borchelt, D. R. (1999). Intracellular inclusions and neuritic aggregates in transgenic mice expressing a mutant N-terminal fragment of huntingtin. *Hum. Mol. Genet.* 8, 397–407.
- Shelbourne, P. F., Killeen, N., Hevner, R. F., Johnston, H. M., Tecott, L., Lewandoski, M., Ennis, M., Ramirez, L., Li, Z., Iannicola, C., Littman, D. R., and Myers, R. M. (1999). A Huntington's disease CAG expansion at the murine Hdh locus is unstable and associated with behavioural abnormalities in mice. *Hum. Mol. Genet.* 8, 763–774.
- Slow, E. J., van Raamsdonk, J., Rogers, D., Coleman, S. H., Graham, R. K., Deng, Y., Oh, R., Bissada, N., Hossain, S. M., Yang, Y. Z., Li, X. J., Simpson, E. M., Gutekunst, C. A., Leavitt, B. R., and Hayden, M. R. (2003). Selective striatal neuronal loss in a YAC128 mouse model of Huntington disease. *Hum. Mol. Genet.* 12, 1555–1567.
- Smith, Y., Bevan, M. D., Shink, E., and Bolam, J. P. (1998). Microcircuitry of the direct and indirect pathways of the basal ganglia. *Neuroscience* 86, 353–387.
- Szabo, B., Dorner, L., Pfreundtner, C., Norenberg, W., and Starke, K. (1998). Inhibition of GABAergic inhibitory postsynaptic currents by cannabinoids in rat corpus striatum. *Neuroscience* 85, 395–403.
- Tang, T. S., Chen, X., Liu, J., and Bezprozvanny, I. (2007). Dopaminergic signaling and striatal neurodegeneration in Huntington's disease. *J. Neurosci.* 27, 7899–7910.
- The Huntington's Disease Collaborative Research Group. (1993). A novel gene containing a trinucleotide repeat that is expanded and unstable on Huntington's disease chromosomes. The Huntington's Disease Collaborative Research Group. *Cell* 72, 971–983.
- Thompson, P. D., Berardelli, A., Rothwell, J. C., Day, B. L., Dick, J. P., Benecke, R., and Marsden, C. D. (1988). The coexistence of bradykinesia and chorea in Huntington's disease and its implications for theories of basal ganglia control of movement. *Brain* 111(Pt 2), 223–244.
- Uziel, A., Baik, J. H., Rouge-Pont, F., Picetti, R., Dierich, A., LeMeur, M., Piazza, P. V., and Borrelli, E. (2000). Distinct functions of the two isoforms of dopamine D2 receptors. *Nature* 408, 199–203.
- Van Raamsdonk, J. M., Metzler, M., Slow, E., Pearson, J., Schwab, C., Carroll, J., Graham, R. K., Leavitt, B. R., and Hayden, M. R. (2007). Phenotypic abnormalities in the YAC128 mouse model of Huntington disease are penetrant on multiple genetic backgrounds and modulated by strain. *Neurobiol. Dis.* 26, 189–200.
- Van Raamsdonk, J. M., Pearson, J., Rogers, D. A., Bissada, N., Vogl, A. W., Hayden, M. R., and Leavitt, B. R. (2005). Loss of wild-type huntingtin influences motor dysfunction and survival in the YAC128 mouse model of Huntington disease. *Hum. Mol. Genet.* 14, 1379–1392.
- Vonsattel, J. P., Myers, R. H., Stevens, T. J., Ferrante, R. J., Bird, E. D., and Richardson, E. P. Jr. (1985). Neuropathological classification of Huntington's disease. *J. Neuropathol. Exp. Neurol.* 44, 559–577.

- Wang, H., and Pickel, V. M. (2002). Dopamine D2 receptors are present in prefrontal cortical afferents and their targets in patches of the rat caudate-putamen nucleus. *J. Comp. Neurol.* 442, 392–404.
- Wheeler, V. C., White, J. K., Gutekunst, C. A., Vrbanc, V., Weaver, M., Li, X. J., Li, S. H., Yi, H., Vonsattel, J. P., Gusella, J. F., Hersch, S., Auerbach, W., Joyner, A. L., and MacDonald, M. E. (2000). Long glutamine tracts cause nuclear localization of a novel form of huntingtin in medium spiny striatal neurons in HdhQ92 and HdhQ111 knock-in mice. *Hum. Mol. Genet.* 9, 503–513.
- Wilson, C. J., and Kawaguchi, Y. (1996). The origins of two-state spontaneous membrane potential fluctuations of neostriatal spiny neurons. *J. Neurosci.* 16, 2397–2410.
- Wu, N., Cepeda, C., Zhuang, X., and Levine, M. S. (2007). Altered corticostriatal neurotransmission and modulation in dopamine transporter knock-down mice. *J. Neurophysiol.* 98, 423–432.
- Zucker, R. S. (1989). Short-term synaptic plasticity. *Annu. Rev. Neurosci.* 12, 13–31.
- Conflict of Interest Statement:** The authors declare that the research was conducted in the absence of any commercial or financial relationships that could be construed as a potential conflict of interest.
- Received: 25 February 2011; paper pending published: 20 April 2011; accepted: 03 June 2011; published online: 16 June 2011.
- Citation: André VM, Fisher YE and Levine MS (2011) Altered balance of activity in the striatal direct and indirect pathways in mouse models of Huntington's disease. *Front. Syst. Neurosci.* 5:46. doi: 10.3389/fnsys.2011.00046
- Copyright © 2011 André, Fisher and Levine. This is an open-access article subject to a non-exclusive license between the authors and Frontiers Media SA, which permits use, distribution and reproduction in other forums, provided the original authors and source are credited and other Frontiers conditions are complied with.



In vivo dopamine efflux is decreased in striatum of both fragment (R6/2) and full-length (YAC128) transgenic mouse models of Huntington's disease

Joshua W. Callahan* and Elizabeth D. Abercrombie

Center for Molecular and Behavioral Neuroscience, Rutgers, The State University of New Jersey, Newark, NJ, USA

Edited by:

Jose Vargas, Universidad Nacional Autónoma de México, Mexico

Reviewed by:

Michael S. Levine, Brain Research Institute, USA

John D. Salamone, University of Connecticut, USA

George V. Rebec, Indiana University, USA

*Correspondence:

Joshua W. Callahan, Center for Molecular and Behavioral Neuroscience, Rutgers, The State University of New Jersey, 197 University Avenue, Newark, NJ 07102, USA.
e-mail: joshcall@pegasus.rutgers.edu

Huntington's disease (HD) is characterized by numerous alterations within the corticostriatal circuitry. The striatum is innervated by a dense array of dopaminergic (DA) terminals and these DA synapses are critical to the proper execution of motor functions. As motor disturbances are prevalent in HD we examined DA neurotransmission in the striatum in transgenic (tg) murine models of HD. We used *in vivo* microdialysis to compare extracellular concentrations of striatal DA in both a fragment (R6/2) model, which displays a rapid and severe phenotype, and a full-length (YAC128) model that expresses a more progressive phenotype. Extracellular striatal DA concentrations were significantly reduced in R6/2 mice and decreased concomitantly with age-dependent increasing motor impairments on the rotarod task (7, 9, and 11 weeks). In a sample of 11-week-old R6/2 mice, we also measured tissue concentrations of striatal DA and found that total levels of DA were significantly depleted. However, the loss of total DA content (<50%) was insufficient to account for the full extent of DA depletion in the extracellular fluid (ECF; ~75%). We also observed a significant reduction in extracellular DA concentrations in the striatum of 7-month-old YAC128 mice. In a separate set of experiments, we applied D-amphetamine (AMPH; 10 μ m) locally into the striatum to stimulate the release of intracellular DA into the ECF. The AMPH-induced increase in extracellular DA levels was significantly blunted in 9-week-old R6/2 mice. There also was a decrease in AMPH-stimulated DA efflux in 7-month-old YAC128 mice in comparison to WT controls, although the effect was milder. In the same cohort of 7-month-old YAC128 mice we observed a significant reduction in the total locomotor activity in response to systemic AMPH (2 mg/kg). Our data demonstrate that extracellular DA release is attenuated in both a fragment and full-length tg mouse model of HD and support the concept of DA involvement in aspects of the syndrome.

Keywords: microdialysis, neurodegeneration, dopaminergic, basal ganglia, neostriatum, transgenic, DOPAC, substantia nigra

INTRODUCTION

Huntington's disease (HD) is a genetically inherited neurodegenerative disorder that results in motor, cognitive, and psychiatric disturbances. One out of every 10,000 people is affected with the disorder and an even greater proportion remains at risk. HD is caused by a polyglutamine (CAG) trinucleotide repeat expansion in the IT-15 (*HTT*) gene, located on the short arm of chromosome 4 (The Huntington's Disease Collaborative Research Group, 1993). The mutation is autosomal dominant and onset occurs between 30 and 50 years of age, although in a rare juvenile variant of the disease, symptoms can emerge as early as 5 years old. The severity of symptoms progressively worsens as a function of age and the illness is ultimately fatal (for review see Walker, 2007). No cure exists for HD, however, therapeutics that target the dopamine system have shown promise for managing the motor syndromes that are involved with the disorder (Bonelli and Wenning, 2006; Bonelli and Hofmann, 2007).

Since the discovery of the mutation in the *HTT* gene, several transgenic mouse models expressing the CAG repeat expansion have been developed which recapitulate characteristics of the

disorder, including reductions in total brain volume, mutant huntingtin (mHTT) protein aggregation, transcriptional dysregulation, and neurotransmitter receptor alterations (Davies et al., 1997; Cha et al., 1998; Luthi-Carter et al., 2000; Stack et al., 2005). Critically, these pathological changes are accompanied by progressive motor and cognitive deficits (Menalled and Chesselet, 2002; Levine et al., 2004) that closely mimic the human condition. Transgenic mouse models of HD can be sorted into two broad categories depending on whether they possess a fragment (e.g., exon 1) of the *HTT* gene or the full-length composition. Mouse strains from fragment models express only a truncated mHTT protein fraction and *in vitro* studies have demonstrated that this abbreviated fragment may be more toxic than the full-length protein (Hackam et al., 1998; Lunkes and Mandel, 1998). As such, fragment models typically exhibit an accelerated phenotype in comparison to full-length models that includes motor deficits, altered gait, hypoactivity, and weight loss (Carter et al., 1999). While fragment models display an HD-like phenotype, the obvious weakness is that they lack the natural genomic and protein context of the polyglutamine expansion. This raises the potential

for alterations in protein dynamics and therefore necessitates the use of full-length models to investigate any resulting changes in disease features.

R6 transgenic mice are the most widely used strain derived from the fragment models and were the first established transgenic line in HD research. The most extensively characterized variant of this transgenic strain is the R6/2 line, which express the first of 67 exons and carry a ~160 CAG repeat expansion (Mangiarini et al., 1996). These mice develop an aggressive HD-like phenotype that advances rapidly until the occurrence of spontaneous morbidity by 14–16 weeks of age (Carter et al., 1999). In contrast to the R6 models, the YAC128 transgenic mouse model incorporates the entire HD gene, using a yeast artificial chromosome (YAC) vector system to express the full-length human *HTT* gene with a 128 CAG repeat expansion (Hodgson et al., 1999). The lifespan, as well as the progression of the HD-like phenotype in YAC128 mice is more prolonged than in R6/2 mice, with neuropathological and behavioral abnormalities manifesting at later ages (Slow et al., 2003; Van Raamsdonk et al., 2007).

Evidence implicates abnormal nigrostriatal dopaminergic neurotransmission in HD. In both human cases and animal models, early reductions in the striatal expression of dopamine receptors, attenuated receptor binding, and loss of the dopamine- and cAMP-regulated phosphoprotein (DARPP-32) have been reported (Joyce et al., 1988; Sedvall et al., 1994; Cha et al., 1999; Bibb et al., 2000; Miller and Bezprozvanny, 2010). Reduced dopamine concentrations in striatal tissue and the degeneration of nigrostriatal terminals emerge in late stages of the disorder in both human cases and transgenic models of HD (Kish et al., 1987; Reynolds et al., 1999; Suzuki et al., 2001; Petersén et al., 2002). Additionally, studies utilizing striatal slice preparations have demonstrated that electrically evoked dopamine efflux is reduced in both R6/1 and R6/2 mice (Johnson et al., 2007; Ortiz et al., 2011; respectively), suggesting that dopamine release may be compromised in these models. As of yet, the synaptic release of dopamine has not been studied during awake, behaving conditions in transgenic mouse models of HD.

The goal of the present study was to examine, and compare where possible, nigrostriatal dopamine release dynamics in the fragment R6/2 and the full-length YAC128 mouse models of HD, using *in vivo* microdialysis. Both R6/2 and YAC128 mice develop deficits on the rotarod treadmill task and we measured the levels of striatal dopamine during these periods of motor dysfunction. As analogous neurophysiological abnormalities have been shown to exist across fragment and full-length transgenic models (for review see Cummings et al., 2010), we speculated that neurochemical abnormalities may also be a common feature of such models. Specifically, we hypothesized that extracellular striatal dopamine release would be attenuated in R6/2 and YAC128 mice in awake, behaving conditions concomitant with motor decline and as a function of age. *In vitro* studies have indicated that the intracellular storage of dopamine in nerve terminals may be compromised in HD as well and such a deficiency could contribute to deficits in extracellular dopamine release (Ortiz et al., 2010). In a separate set of experiments, we therefore measured the effects of amphetamine, a dopamine-releasing agent, on local striatal neurochemistry and on locomotor activity in order to investigate the integrity of intracellular dopamine stores in R6/2 and YAC128 mice.

EXPERIMENTAL PROCEDURES

ANIMALS

Transgenic male mice expressing a truncated human *HTT* gene with a 160 ± 10 CAG repeat expansion (R6/2) or a full-length human *HTT* gene with a 128 CAG repeat expansion (YAC128) in exon 1 and their respective wild-type controls were obtained from Jackson Laboratories (Bar Harbor, ME, USA). Animals were housed individually in plastic microisolator cages with food and water available *ad libitum*. Animals were kept under conditions of constant temperature (21°C) and humidity (40%) and maintained on a 12-h light/dark cycle (lights on from 7:00 am to 7:00 pm). All efforts were made to minimize animal suffering and to limit the number of animals utilized for these experiments. Animal procedures were conducted in accordance with the National Institutes of Health *Guide for the Care and Use of Laboratory Animals* and were approved by Rutgers University Institutional Animal Care and Use Committee.

MOTOR PHENOTYPE

Motor coordination was assessed using an Economex rotarod apparatus (Columbus Instruments, Columbus, OH, USA). R6/2 mice and wild-type controls were trained on the rotarod treadmill task at 10 rpm for three consecutive trials (60 s maximum duration) 1 day prior to testing. The following day, mice were tested at five fixed speeds (5, 10, 15, 20, 25 rpm) for two separate trials. Fall latency (s) at each speed was averaged across trials and used for statistical comparison. Testing was carried out at 7, 9, and 11 weeks in separate groups of R6/2 mice and 7 months in YAC128 mice and their respective wild-type controls.

MICRODIALYSIS PROCEDURE

Microdialysis probes were of a vertical, concentric design, similar to that previously described in our laboratory (Cobb and Abercrombie, 2002). Probes were constructed such that the probe inlet consisted of a piece of PE-10 tubing (Clay Adams, Parsippany, NJ, USA) and a piece of fused silica capillary tubing (I.D. 75 μ m and O.D. 150 μ m; Polymicro Technologies, Phoenix, AZ, USA) served as the outlet. A semi-permeable microdialysis membrane (molecular weight cut-off = 13 kD; O.D. = 216 μ m; Spectrum Laboratories, Rancho Dominguez, CA, USA) was placed over the end of the exposed silica tubing, glued to the PE-10 tubing and coated with a thin epoxy layer, leaving a 2-mm long active exchange area at the end of the probe. Probes were continuously perfused with artificial cerebrospinal fluid (aCSF; NaCl 147 mM, KCl 2.5 mM, CaCl₂ 1.3 mM, MgCl₂ 0.9 mM, pH 7.4) using a microliter infusion pump (Harvard Apparatus, Holliston, MA, USA) at a flow rate of 1.5 μ l/min. Prior to implantation, probes were calibrated *in vitro* to determine their relative recovery rates. Only probes with recovery rates between 10 and 15% were used.

R6/2 mice and their wild-type controls were anesthetized with 40–50 mg/kg pentobarbital and 250 mg/kg chloral hydrate (i.p.). YAC128 mice and their wild-type controls were anesthetized with 80–100 mg/kg ketamine and 10 mg/kg xylazine (i.p.). The mice were placed into a stereotaxic frame (David Kopf Instruments, Tujunga, CA, USA) and onto a heating pad to prevent hypothermia. With the skull flat, the microdialysis probe was implanted into the striatum at the following coordinates: AP: +0.5 mm, ML: ± 1.95 mm

relative to bregma and DV: -4.0 mm from dura (Franklin and Paxinos, 2008). Probes were anchored to the skull by two small screws (Small Parts, Miami Lakes, FL, USA) and dental cement. The probe inlet and outlet lines were then fed through a metal tether that attached to the head-post at one end, and to a single-channel fluid swivel (Instech Laboratories, Plymouth Meeting, PA, USA) at the other end. The mice were allowed to recover for at least 18 h before experiments began. Post-operative care consisted of administering lactated Ringer's solution (1.0 – 2.0 ml/30 g body weight, s.c.) and placing the animal under a heat lamp for 1–3 h after surgery. All microdialysis experiments were conducted during the light portion of the diurnal cycle.

DOPAMINE QUANTIFICATION

Microdialysis experiments were conducted in round plastic test chambers (14 cm \times 20 cm) equipped with a counter-balanced arm and a swivel assembly (Instech, Plymouth Meeting, PA, USA). The HPLC–EC system consisted of an injector (Rheodyne, Cotati, CA, USA), a VeloSep RP-18 column (100×3.2 mm; PerkinElmer, Waltham, MA, USA) and a Shimadzu LC-10AD VP solvent delivery pump (Shimadzu Scientific Instruments, Inc., Columbia, MD, USA), that delivered the mobile phase at a flow rate of 0.7 ml/min. The mobile phase was composed of 0.1 M sodium acetate buffer (pH 4.2), 0.1 mM EDTA, 1.2 mM sodium octyl sulfate, and 8% (v/v) methanol. An electrochemical detector (Coulchem II; ESA Inc., Chelmsford, MA, USA) with a flow cell electrode set at an applied potential of $+260$ mV was used. The detector output was connected to a computerized data acquisition system (PowerChrom, Denistone East, NSW, Australia). Dopamine and 3,4-dihydroxyphenylacetic acid (DOPAC) were identified by retention time and quantified based on peak height relative to the peak height of a 10 -nM standard prepared in 0.1 M perchloric acid that was made up fresh daily.

A separate cohort of 11-week-old R6/2 mice and their wild-type controls were sacrificed by decapitation and the striata were rapidly dissected on ice, wrapped in aluminum foil, labeled, and frozen at -80°C until analysis. The weight of each striatum was measured and then tissue was homogenized in 0.1 M perchloric acid containing 100 μM EDTA (20 μl /mg wet tissue weight). Homogenates were centrifuged at $29,200$ g for 25 min at 2 – 8°C . The amount of dopamine in 20 μl samples of the resulting supernatant was quantified by HPLC–EC using the protocol described above for the analysis of dopamine in dialysate samples.

EXPERIMENTAL PROCEDURES

Prior to pharmacological manipulations, baseline dialysate samples were assayed for dopamine until three consecutive samples differed by less than 15% . In experiments involving the local application of D-amphetamine into the striatum via reverse microdialysis, a glass syringe containing a 10 - μM solution of amphetamine dissolved in aCSF was connected to the inlet of the probe following the initial baseline determination. Collection of dialysate samples resumed 15 min later to allow for the fluid to flow through the probe and equilibrate to the drug solution. Samples were collected every 10 min for a 60 -min duration. The effect of local amphetamine on extracellular dopamine was investigated in 9-week-old R6/2 mice, 7-month-old YAC128 mice and

their respective wild-type controls. All experiments involving the local application of amphetamine were conducted 48 h after probe implantation.

In experiments involving systemic administration of D-amphetamine (2 mg/kg, i.p.), the drug was dissolved in sterile 0.9% saline vehicle. The effect of systemic amphetamine on locomotor activity was investigated in 7-month-old YAC128 mice and their wild-type controls. Prior to testing, mice were untethered and the polyethylene tubing emanating from the probes was clipped so that only the acrylic head cap remained. Mice were allowed to habituate in their home cages with this new arrangement for at least 1 week preceding amphetamine treatment. Based on qualitative observations, animals showed no signs of impairment due to either the surgery or the presence of head caps. One day prior to amphetamine administration, mice were habituated to plastic open field chambers (51 cm \times 32 cm \times 20 cm) overnight. Following habituation, mice were administered drug and spontaneous locomotor activity was monitored for 60 min via automated activity chambers equipped with infrared photobeams (Flexfield, San Diego Instruments, Inc., San Diego, CA, USA).

DATA ANALYSIS

Data are presented as mean \pm SEM. Dialysate values represent picograms per 20 μl microdialysis sample. Factorial ANOVA was used to assess main effect in each data set examined. Data then were subdivided according to the interactions found in the global test and separate lower order analyses carried out. Where appropriate, the Bonferroni *post hoc* test was used for multiple comparisons. Differences were considered statistically significant when $p < 0.05$.

HISTOLOGY

Upon completion of each experiment, animals were administered a lethal dose of sodium pentobarbital and were perfused intracardially with 0.9% saline followed by 10% formaldehyde. Brains were extracted and post-fixed in fresh fixative overnight at 4°C and transferred to 30% sucrose in phosphate buffer solution overnight at 4°C for cryoprotection. Coronal sections of 50 μm thickness were obtained from striata and stained with Cresyl Violet to verify probe placement in the striatum. A representative histological section showing a microdialysis probe track in the mouse striatum is shown in **Figure 1**.

MATERIALS

Ketamine was purchased from Phoenix Pharmaceutical Inc. (St. Joseph, MO, USA). Xylazine, chloral hydrate, sodium pentobarbital, and D-amphetamine were purchased from Sigma (St. Louis, MO, USA). All other reagents and chemicals were of the highest purity commercially available (Fisher Scientific, Suwanee, GA, USA).

RESULTS

ROTAROD ASSESSMENT IN R6/2 AND YAC128 MICE

Performance on a fixed speed rotarod paradigm was assessed in R6/2, YAC128 mice and their respective wild-type controls (**Figure 2A**). Mice were placed on an elevated, rotating platform for a maximum of 60 s and the latency that it took for each to fall off was measured at 5 , 10 , 15 , 20 , and 25 rpm. The latency to stay on the rotating platform was significantly reduced

as a function of genotype in 7-week-old [$F(1, 172) = 18.78$; $p < 0.0001$], 9-week-old [$F(1, 104) = 50.84$; $p < 0.0001$], and 11-week-old [$F(1, 72) = 98.22$; $p < 0.0001$] R6/2 mice compared to wild-type controls. *Post hoc* tests revealed that R6/2 mice fell off the rotarod at significantly shorter latencies than wild-type controls at every speed across all ages tested. One-way ANOVA tests showed that the latency to remain on the rotating platform significantly decreased as a function of age in R6/2 mice [$F(2, 39) = 8.074$; $p < 0.01$] but not in wild-type controls [$F(2, 48) = 2.013$; n.s.]. The latency to stay on the rotating platform also was significantly diminished as a function of genotype in

7-month-old YAC128 mice compared to age-matched wild-type controls [$F(1, 56) = 11.88$; $p < 0.01$; **Figure 2B**]. *Post hoc* tests indicated that 7-month-old YAC128 mice fell at significantly shorter latencies than wild-type controls at every speed faster than 5 rpm. Data are only presented in graphical form for 10 and 20 rpm as these speeds are most representative of overall performance in both genotypes.

EXTRACELLULAR STRIATAL DOPAMINE AND DOPAC CONCENTRATIONS R6/2 mice

Extracellular striatal dopamine was significantly attenuated as a function of genotype [$F(1, 34) = 46.96$; $p < 0.0001$; **Figure 3A**]. *Post hoc* tests revealed that there was a significant reduction in extracellular dopamine in R6/2 mice and levels were diminished at 7 weeks (WT: 8.4 ± 0.9 pg/20 μ l; R6/2: 5.6 ± 0.6 pg/20 μ l), 9 weeks (WT: 8.1 ± 1.4 pg/20 μ l; R6/2: 3.3 ± 0.7 pg/20 μ l), and 11 weeks of age (WT: 11.4 ± 1.2 pg/20 μ l; R6/2: 2.7 ± 0.5 pg/20 μ l). One-way ANOVA indicated that extracellular levels of striatal dopamine significantly decreased in R6/2 mice as a function of age [$F(2, 17) = 6.812$; $p < 0.01$]. Specifically, *post hoc* tests demonstrated that extracellular dopamine was significantly reduced in 9- and 11-week old R6/2 mice in comparison to 7-week-old R6/2 mice. There was no change in striatal extracellular dopamine concentrations as a function of age in wild-type controls [$F(2, 17) = 2.303$; n.s.]. Extracellular striatal DOPAC was significantly attenuated as a function of genotype [$F(1, 34) = 50.96$; $p < 0.0001$; **Figure 3B**]. *Post hoc* tests indicated that although extracellular concentrations of striatal DOPAC were not significantly different at 7 weeks (WT: 1569 ± 137 pg/20 μ l; R6/2: 1191 ± 114 pg/20 μ l) they were significantly reduced by 9 weeks (WT: 1589 ± 127 pg/20 μ l; R6/2: 647 ± 122 pg/20 μ l) and 11 weeks of age (WT: 1544 ± 191 pg/20 μ l; R6/2: 503 ± 453 pg/20 μ l) in R6/2 mice in comparison to wild-type controls. A one-way ANOVA revealed that extracellular DOPAC significantly decreased in R6/2 mice as a function of age [$F(2, 17) = 15.32$; $p < 0.001$]. There was no change in extracellular DOPAC amounts as a function of age in wild-type controls [$F(2, 17) = 0.20$; n.s.].

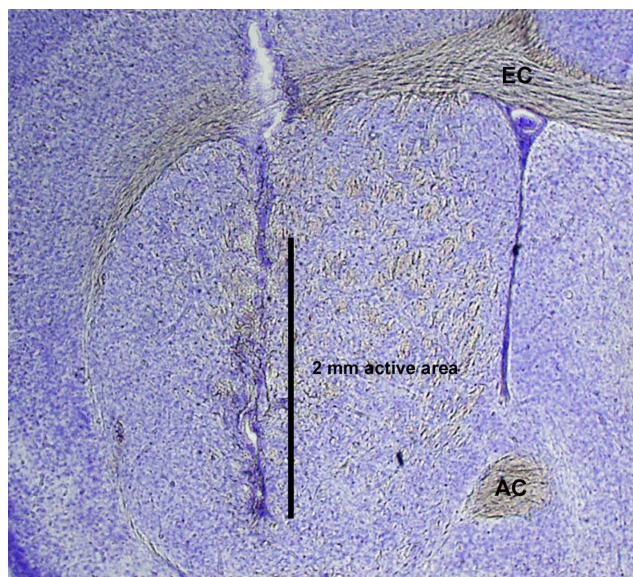


FIGURE 1 | Photomicrograph of Nissl-stained histological section demonstrating representative microdialysis probe placement with a 2-mm active area in mouse striatum. AC, anterior commissure; EC, external capsule.

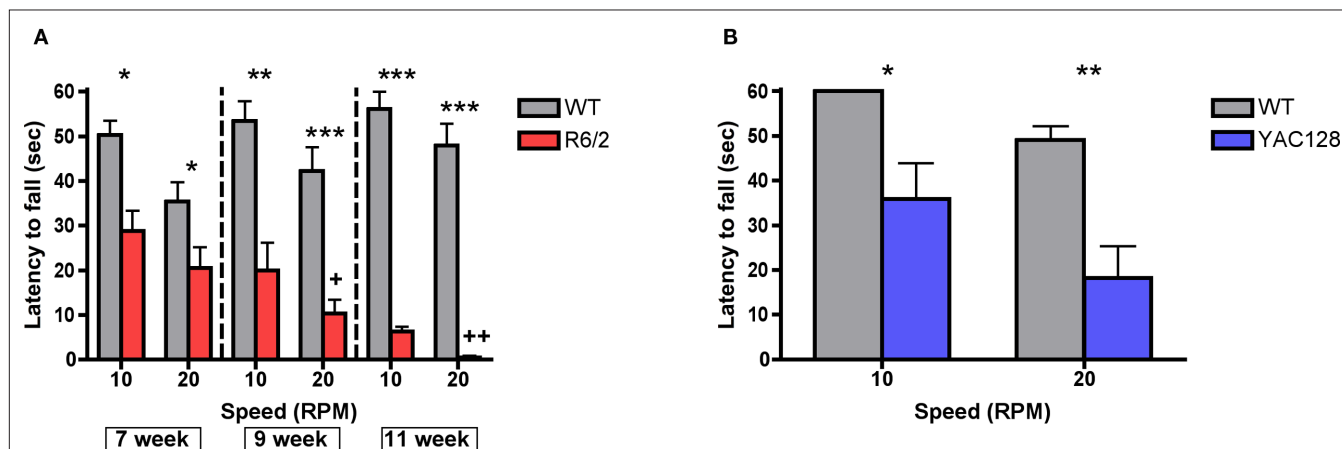


FIGURE 2 | Rotarod performance in (A) R6/2 transgenic mice (7 weeks, $n = 22$ WT, 23 R6/2; 9 weeks, $n = 15$ WT, 13 R6/2; 11 weeks, $n = 14$ WT, 6 R6/2) and (B) 7-month-old YAC128 transgenic mice ($n = 7$ WT, 9 YAC128). All data are mean \pm SEM. * Indicates significantly different from WT, $p < 0.05$; ** indicates $p < 0.001$; *** indicates $p < 0.005$; +, ++ R6/2 week 7 vs. weeks 9 and 11 ($p < 0.05$, 0.01, respectively).

In the 11-week-old cohort, striatal tissue concentrations of dopamine were measured in R6/2 mice and wild-type controls (Figure 4A). R6/2 mice exhibited a significant abatement in striatal tissue dopamine content (5478 ± 487 pg/20 μ l) in comparison to wild-type controls (10680 ± 833 pg/20 μ l) [$t(10) = 5.39$; $p < 0.001$]. The reduction in striatal tissue content of dopamine (47%) was not as dramatic as the reduction in striatal extracellular concentrations of dopamine (76%) in 11-week-old R6/2 mice (Figure 4B).

YAC128 mice

Extracellular dopamine concentrations in 7-month-old YAC128 mice were significantly reduced (5.0 ± 1.4 pg/20 μ l) in comparison to wild-type controls (10.5 ± 1.9 pg/20 μ l) [$t(14) = 2.39$; $p < 0.05$; Figure 5A]. Although extracellular DOPAC levels were slightly lower in 7-month-old YAC128 mice (1834 ± 245 pg/20 μ l), there was no significant difference between wild-type controls (2358 ± 299 pg/20 μ l) [$t(14) = 1.37$; n.s.; Figure 5B].

EFFECT OF LOCAL STRIATAL AMPHETAMINE (10 μ M) APPLICATION ON EXTRACELLULAR DOPAMINE CONCENTRATIONS

R6/2 mice

Local amphetamine induced a significant increase in extracellular dopamine levels across time [$F(6,24) = 75.42$; $p < 0.0001$]. The amphetamine induced increase in dopamine efflux was significantly attenuated as a function of genotype [$F(1,24) = 42.25$; $p < 0.01$; Figure 6A]. *Post hoc* tests indicated that amphetamine induced dopamine release was significantly diminished in 9-week-old R6/2 mice in comparison to wild-type controls at all time intervals measured. The maximum peak response in amphetamine induced dopamine efflux was significantly diminished in 9-week-old R6/2 mice (38.9 ± 7.4 pg/20 μ l) vs. wild-type controls (114.4 ± 10.7 pg/20 μ l) [$t(4) = 5.82$; $p < 0.01$; Figure 6B].

YAC128 mice

Local amphetamine induced a significant increase in extracellular dopamine across time [$F(6,72) = 23.04$; $p < 0.0001$; Figure 7A]. Although amphetamine induced dopamine efflux was diminished

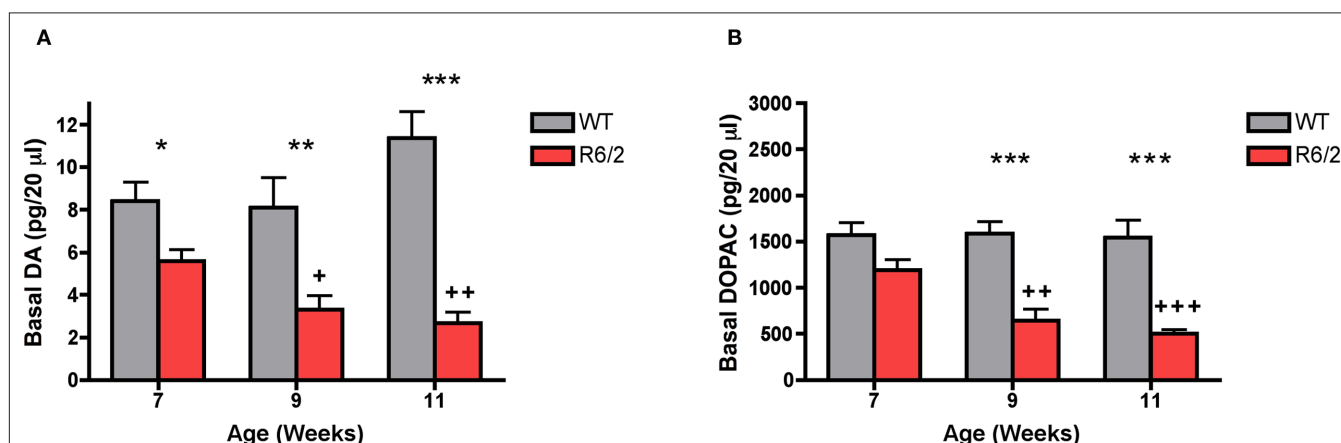


FIGURE 3 | *In vivo* microdialysis measurements of basal levels of extracellular (A) dopamine and (B) DOPAC in striatum of R6/2 transgenic mice (7 weeks, $n = 6$ WT, 6 R6/2; 9 weeks, $n = 6$ WT, 6 R6/2; 11 weeks, $n = 8$ WT, 8 R6/2). Data are picograms per 20 μ l sample. All data are mean \pm SEM. * Indicates significantly different from WT, $p < 0.05$; ** indicates $p < 0.001$; *** indicates $p < 0.005$; +, ++ R6/2 week 7 vs. weeks 9 and 11 ($p < 0.05$, 0.01, respectively).

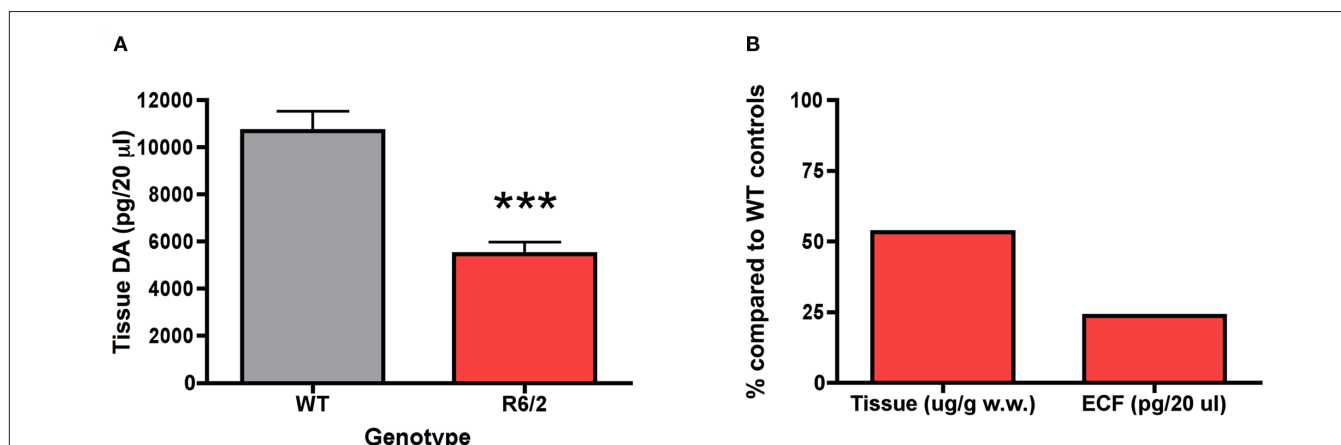
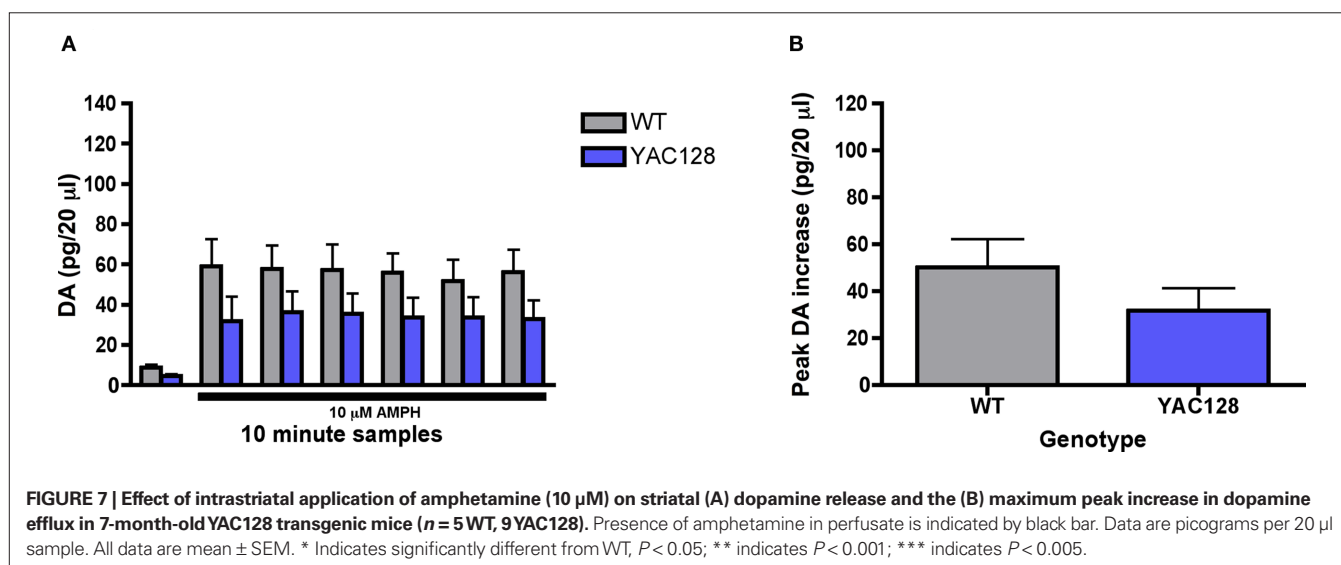
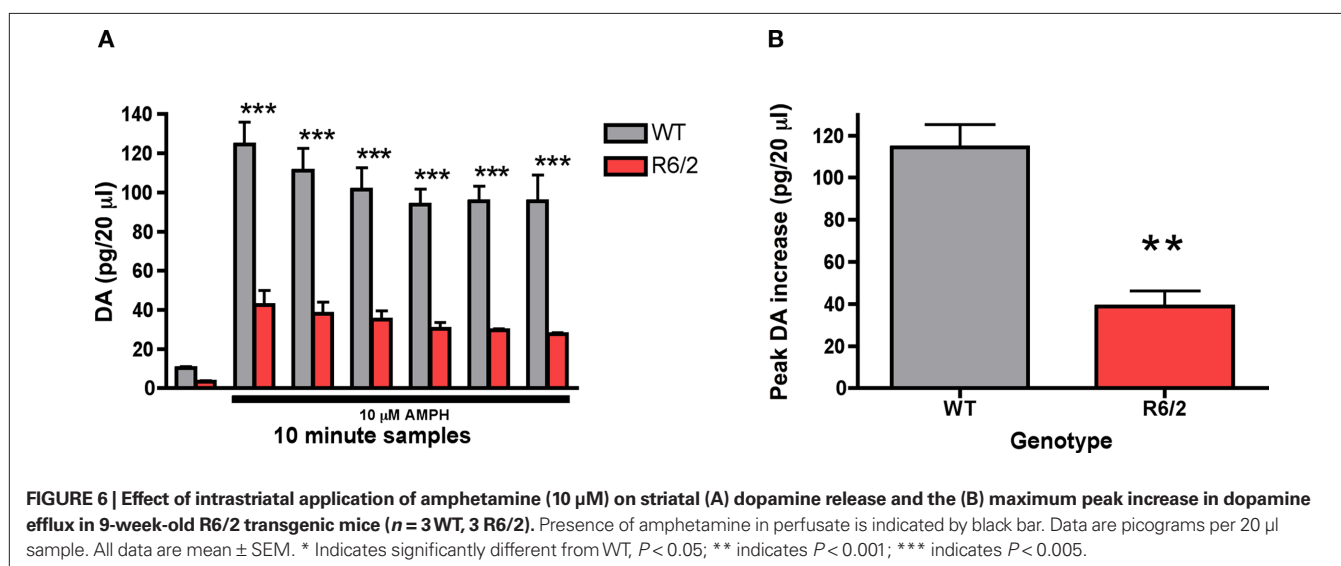
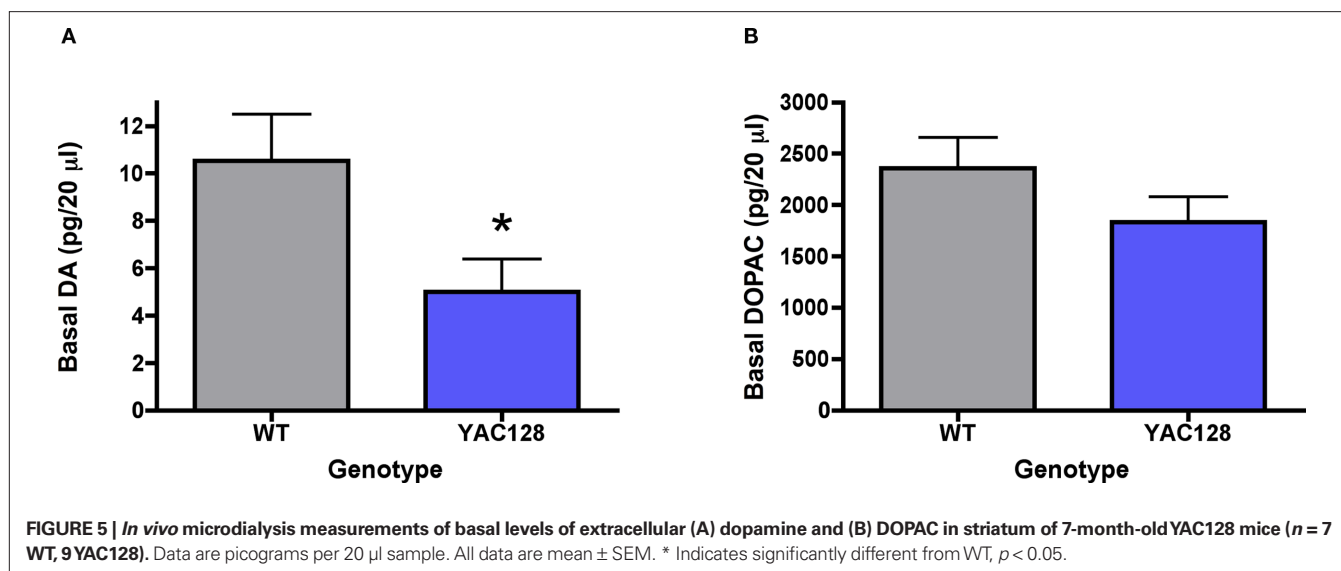


FIGURE 4 | Dopamine content in (A) striatal tissue of 11-week-old R6/2 transgenic mice ($n = 6$ WT, 6 R6/2) and (B) comparison of the percentage of dopamine levels in relation to WT mice in tissue and the extracellular fluid (ECF). Striatal tissue dopamine content data are μ g/g wet weight of tissue and striatal ECF dopamine data are picograms per 20 μ l sample of dialysate. All data are mean \pm SEM. *** Indicates significantly different from WT, $P < 0.005$.



in 7-month-old YAC128 mice in comparison to wild-type controls, there was no significant effect of genotype [$F(1, 72) = 1.93$, n.s.]. Similarly, while the maximum peak response in amphetamine induced dopamine release was diminished in 7-month-old YAC128 mice (31.8 ± 9.6 pg/20 μ l) vs. wild-type controls (50.2 ± 12.0 pg/20 μ l) the effect was not significant [$t(12) = 1.18$; n.s.; **Figure 7B**].

In 7-month-old YAC128 mice, the effect of systemic amphetamine (2 mg/kg, i.p.) on spontaneous locomotor activity was investigated. There was no significant difference in the basal activity counts between genotypes in 7-month-old YAC128 mice and wild-type controls [$t(9) = 0.39$; n.s.; **Figure 8A**]. Amphetamine induced a significant increase in locomotor activity across time [$F(6, 54) = 0.96$; $p < 0.05$]. Although amphetamine induced locomotor activity was diminished in 7-month-old YAC128 mice in comparison to wild-type controls, there was no significant effect of genotype [$F(1, 54) = 3.80$, n.s.]. Collapsing the locomotor counts across all time bins revealed that the total activity in response to amphetamine over 60 min post-drug was significantly attenuated in 7-month-old YAC128 mice vs. wild-type controls [$t(9) = 1.88$; $p < 0.05$; **Figure 8B**].

DISCUSSION

The present studies utilized *in vivo* microdialysis to assess striatal dopamine release dynamics in two transgenic mouse models of HD. We report that the concentrations of extracellular striatal dopamine are reduced in R6/2 and YAC128 transgenic mice relative to their respective wild-type controls. These data are consistent with previous studies demonstrating alterations in nigrostriatal function in both animal models and human cases of HD (e.g., Kish et al., 1987; Petersén et al., 2002; Johnson et al., 2006; Ortiz et al., 2011). Importantly, the present studies extend these findings and represent the first demonstration of attenuated striatal dopamine release across transgenic mouse models of HD constructed using different genetic approaches.

Performance deficits on the rotarod treadmill task are reliably documented across multiple HD transgenic strains, including R6/2 and YAC128 mice (Carter et al., 1999; Slow et al., 2003; Menalled

et al., 2009). In the present studies, significant impairments in the rotarod assay were apparent in R6/2 and YAC128 mice, with rotarod performance being roughly comparable at 7 weeks and 7 months of age, respectively. In both R6/2 and YAC128 mice, decline in motor function were associated with a significant reduction in the levels of extracellular striatal dopamine. Interestingly, while the 7-month age point in YAC128 mice is characterized by motor disturbances, blunt neurodegeneration does not emerge until older ages (Slow et al., 2003) suggesting the presence of alternative pathological alterations. Motor performance and striatal dopamine release were further assessed in R6/2 mice at 9 and 11 weeks of age, with both measures progressively diminishing as a function of group time point. Masuzawa et al. (2003) demonstrated that pentobarbital can attenuate dopamine release and while we used this compound as a general anesthetic during surgical procedures, all experiments took place at least 18 h subsequent to surgery making it unlikely that there was an interaction between anesthesia and extracellular dopamine at the time experiments were conducted. Taken together, these findings lend support to the notion that alterations in synaptic function, including reduced levels of extracellular dopamine, may contribute to the disease phenotype across different transgenic mouse models of HD. Indeed, a wide range of dopamine related abnormalities have been reported, including dopamine receptor sensitization, attenuated striatal dopamine-dependent plasticity and altered dopamine-dependent modulation of corticostriatal currents, that may reflect the attenuated extracellular dopamine concentrations presently reported (Pineda et al., 2005; Cummings et al., 2006; Kung et al., 2007; André et al., 2011).

In addition to extracellular dopamine concentrations, dopamine content in striatal tissue was assessed in 11-week old R6/2 mice. In agreement with previous reports (Reynolds et al., 1999; Mochel et al., 2011), it was found that striatal tissue levels of dopamine were reduced by roughly half, relative to wild-type control animals. Importantly, reductions in tissue concentrations of dopamine were not as severe as the reductions observed in the extracellular fluid (ECF; 45 vs. 75% reduction, respectively), suggesting the presence of an available intracellular pool of dopamine that is not being adequately utilized under spontaneous *in vivo* conditions. This

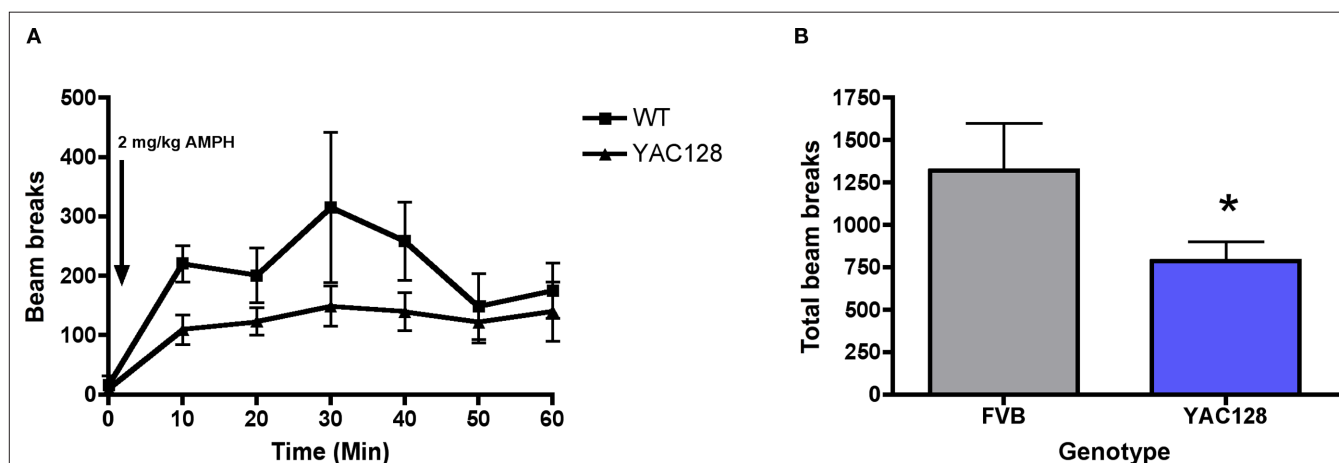


FIGURE 8 | Effect of systemic injection of amphetamine (2 mg/kg; injection indicated by arrow) on (A) 10 min bins of locomotor activity and (B) the total beam break counts during a 60-min period in 7-month-old YAC128 transgenic mice ($n = 5$ WT, 6 YAC128). * Indicates significantly different from WT, $P < 0.05$.

finding is particularly intriguing when viewed in the context of animal models of Parkinson's disease (PD) in which the opposite pattern emerges. In PD models, tissue levels of dopamine must be depleted by greater than 80% in order for deficits in extracellular dopamine release to emerge (Abercrombie et al., 1990). The loss of tissue dopamine content and reductions in the density of postsynaptic dopamine receptors has been reported extensively in HD, however, this finding accentuates the need to account for presynaptic release deficits in HD pathogenesis as well.

There are multiple factors that could contribute to exocytotic release dysfunctions in HD. Several synaptic proteins that are involved in exocytotic processes, including complexin II, snare complex, synaptobrevin 2 and rab3a, have been shown to be abnormal in both transgenic mouse models and human cases of HD (Morton et al., 2001; Freeman and Morton, 2004; Glynn et al., 2007). In line with our results, Morton and Edwardson (2001) demonstrated that there was a progressive decline in complexin II from 7 weeks onward in R6/2 mice. Another potential mechanism may involve alterations in calcium homeostasis and signaling, which could lead to changes in vesicular release probabilities (Bibb et al., 2000; Hansson et al., 2001). Moreover, the mHTT protein also disrupts vesicular transport and such an abnormality could alter vesicular pool sizes (Velier et al., 1998). Indeed, Ortiz et al. (2010) demonstrated that storage vesicles in acute nigrostriatal slices are significantly diminished in R6/2 mice.

Intriguingly, the concentrations of extracellular striatal DOPAC (the main catabolite of dopamine) were significantly decreased in R6/2 mice and showed a tendency to be decreased in YAC128 mice, although this effect was not significant. Extracellular DOPAC derives from, and reflects the metabolism of, newly synthesized dopamine in the cytosol (Zetterström et al., 1988; Yadid et al., 2000). In the present studies, the observation of diminished amounts of striatal DOPAC coupled to the finding that tissue levels of striatal dopamine are reduced lends support to the possibility that cytosolic dopamine pools are depleted as well in transgenic mouse models of HD.

In order to more directly quantify cytosolic dopamine concentrations, we examined the effect of intrastriatal application of amphetamine on striatal dopamine efflux via reverse microdialysis. Amphetamine is a psychostimulant that promotes the release of newly synthesized dopamine from cytosolic pools into the ECF via an impulse-independent, exchange diffusion method and selective inhibition of the dopamine transporter (Fischer and Cho, 1979). Previous work has confirmed the mechanism of action of amphetamine by demonstrating that its stimulant properties are abolished (except at very high doses) with the pretreatment of alpha-methyl-para-tyrosine (AMPT), a compound that inhibits the synthesis of dopamine in the cytosol, but not by reserpine, which depletes dopamine stored in vesicles (Chiueh and Moore, 1974; Niddam et al., 1985; Parker and Cubeddu, 1986; Callaway et al., 1989; Heeringa and Abercrombie, 1995). Alterations in the levels and/or kinetics of the dopamine transporter could obscure the comparisons between genotypes, however, Petersén et al. (2002) demonstrated that the expression patterns of striatal dopamine transporters were comparable and correspondingly Johnson et al. (2006) exhibited that uptake through the dopamine transporter was similar between R6/2 and wild-type controls.

The local application of amphetamine into the striatum produced an increase in extracellular dopamine release in both 9-week-old R6/2 mice and 7-month-old YAC128 mice, as well as in their respective wild-type controls. However, overall dopamine efflux was significantly attenuated across all time points in R6/2 mice and considerably reduced in 7-month-old YAC128 mice, although this effect fell short of significance. Similarly, the maximal effect of amphetamine on dopamine release was attenuated in both R6/2 and YAC128 mice (66 and 37% reductions, respectively). It should be noted that amphetamine-stimulated dopamine levels were considerably lower in the wild-type controls for the YAC128 mice, compared to those for the R6/2 mice. It is plausible that the different background strains and/or the divergent ages of the respective wild-type mice (7 months vs. 9 weeks) may account for the differences in amphetamine-stimulated dopamine release. Alternatively, it is possible that cytosolic pools of dopamine in 7-month-old YAC128 mice are not as depleted as in 9-week-old R6/2 mice. In any case, further experimentation at different age points, both younger and older, is necessary to fully delineate the progression of changes in dopamine release dynamics in the extended phenotype YAC128 mice.

In addition to the effect of local amphetamine on striatal dopamine release, the effect of systemic amphetamine on locomotor activity was assessed in the same cohort of 7-month-old YAC128 mice after a 1-week drug washout period. Phenotype progression is too rapid to challenge the same cohort of R6/2 mice to systemic amphetamine after an extended washout period and as such these experiments were only performed in YAC128 mice. Overall, there was a significant effect of genotype on locomotion, with YAC128 mice showing significantly reduced amphetamine-induced locomotion. This finding is consistent with decreased amphetamine-stimulated dopamine release and parallels a study in which amphetamine-induced locomotor activity was reduced in R6/2 mice (Hickey et al., 2002). These data lend support to the notion that cytosolic dopamine is attenuated in R6/2 and YAC128 mice and may contribute to the deficits in extracellular dopamine concentrations that we report.

Reductions in cytosolic dopamine levels could be caused by either deficits in the production of newly synthesized dopamine or the loss of nigrostriatal terminals. In light of the fact that tyrosine hydroxylase (TH) is the rate-limiting enzyme in the biosynthetic pathway for the production of dopamine, Yohrling et al. (2003) demonstrated a significant reduction in TH activity in the striatum of 12 week-old-R6/2 mice, raising the possibility that deficits in dopamine synthesis may underlie depleted cytosolic concentrations. Alternatively, accumulating evidence indicates that the depletion of dopamine may be the result of nigrostriatal degeneration that manifests in an age-dependent manner. In 16-week-old R6/1 mice there is no difference in the number of nigrostriatal projections or the number of dopamine neurons within the substantia nigra pars compacta (Petersén et al., 2002). By 30 weeks, however, nigrostriatal projections are decreased and the total number of cells within the SNc is reduced (Pineda et al., 2005; Rubio et al., 2009). Interestingly, neurons within the SNc of 16-week-old R6/1 mice were diminished in size and exhibited mHTT aggregate bodies, suggesting that these pathological abnormalities may precede blunt degeneration within this area (Petersén et al., 2002).

Similarly, Ariano et al. (2002) demonstrated that there was a late stage reduction of nigrostriatal terminals in 11–12 week old R6/2 mice. Studies in human cases also indicate that there is a reduction in nigrostriatal terminals and decreased striatal dopamine content in late stages of the disease (Kish et al., 1987; Ginovart et al., 1997; Bohnen et al., 2000).

This is the first report comparing extracellular striatal dopamine release dynamics in a fragment and full-length HD transgenic mouse model under awake behaving conditions and distinctively reveals that extracellular dopamine concentrations are attenuated across models. We speculate that the dysfunctions in dopamine release stems from a multifactorial set of presynaptic abnormalities

that include both impairments in the synaptic machinery required to release dopamine as well as deficits in dopamine production and perhaps dopamine storage. Future research will need to determine with more specificity the nature of such alterations, when they emerge and the extent each contributes to HD symptomatology.

ACKNOWLEDGMENTS

The authors would like to thank Andrew Farrar, Ph.D., for his contributions to the manuscript and Anna Chavez, B.S., for her technical assistance. This research was supported by United States Public Health Service grant NS059921 and the Hereditary Disease Foundation.

REFERENCES

- Abercrombie, E. D., Bonatz, A. E., and Zigmond, M. J. (1990). Effects of L-dopa on extracellular dopamine in striatum of normal and 6 hydroxy-dopamine-treated rats. *Brain Res.* 13, 36–44.
- André, V. M., Cepeda, C., Fisher, Y. E., Huynh, M., Bardakjian, N., Singh, S., Yang, X. W., and Levine, M. S. (2011). Differential electrophysiological changes in striatal output neurons in Huntington's disease. *J. Neurosci.* 31, 1170–1182.
- Ariano, M. A., Aronin, N., Difiglia, M., Tagle, D. A., Sibley, D. R., Leavitt, B. R., Hayden, M. R., and Levine, M. S. (2002). Striatal neurochemical changes in transgenic models of Huntington's disease. *J. Neurosci. Res.* 68, 716–729.
- Bibb, J. A., Yan, Z., Svenningsson, P., Snyder, G. L., Pieribone, V. A., Horiuchi, A., Nairn, A. C., Messer, A., and Greengard, P. (2000). Severe deficiencies in dopamine signaling in presymptomatic Huntington's disease mice. *Proc. Natl. Acad. Sci. U.S.A.* 97, 6809–6814.
- Bohnen, N. I., Koeppe, R. A., Meyer, P., Ficaró, E., Wernette, K., Kilbourn, M. R., Kuhl, D. E., Frey, K. A., and Albin, R. L. (2000). Decreased striatal monoaminergic terminals in Huntington disease. *Neurology* 54, 1753–1759.
- Bonelli, R. M., and Hofmann, P. (2007). A systematic review of the treatment studies in Huntington's disease since 1990. *Expert Opin. Pharmacother.* 8, 141–153.
- Bonelli, R. M., and Wenning, G. K. (2006). Pharmacological management of Huntington's disease: an evidence-based review. *Curr. Pharm. Des.* 12, 2701–2720.
- Callaway, C. W., Kuczenski, R., and Segal, D. S. (1989). Reserpine enhances amphetamine stereotypies without increasing amphetamine-induced changes in striatal dialysate dopamine. *Brain Res.* 505, 83–90.
- Carter, R. J., Lione, L. A., Humby, T., Mangiarini, L., Mahal, A., Bates, G. P., Dunnett, S. B., and Morton, A. J. (1999). Characterization of progressive motor deficits in mice transgenic for the human Huntington's disease mutation. *J. Neurosci.* 8, 3248–3257.
- Cha, J. H., Frey, A. S., Alsdorf, S. A., Kerner, J. A., Kosinski, C. M., Mangiarini, L., Penney, J. B. Jr., Davies, S. W., Bates, G. P., and Young, A. B. (1999). Altered neurotransmitter receptor expression in transgenic mouse models of Huntington's disease. *Philos. Trans. R. Soc. Lond. B Biol. Sci.* 354, 981–989.
- Cha, J. H., Kosinski, C. M., Kerner, J. A., Alsdorf, S. A., Mangiarini, L., Davies, S. W., Penney, J. B., Bates, G. P., and Young, A. B. (1998). Altered brain neurotransmitter receptors in transgenic mice expressing a portion of an abnormal human huntington disease gene. *Proc. Natl. Acad. Sci. U.S.A.* 95, 6480–6485.
- Chiueh, C. C., and Moore, K. E. (1974). Effects of alpha-methyltyrosine on d-amphetamine-induced release of endogenously synthesized and exogenously administered catecholamines from the cat brain in vivo. *J. Pharmacol. Exp. Ther.* 190, 100–108.
- Cobb, W. S., and Abercrombie, E. D. (2002). Distinct roles for nigral GABA and glutamate receptors in the regulation of dendritic dopamine release under normal conditions and in response to systemic haloperidol. *J. Neurosci.* 15, 1407–1413.
- Cummings, D. M., Cepeda, C., and Levine, M. S. (2010). Alterations in striatal synaptic transmission are consistent across genetic mouse models of Huntington's disease. *ASN Neuro* 18, e00036.
- Cummings, D. M., Milnerwood, A. J., Dallérac, G. M., Waights, V., Brown, J. Y., Vatsavayi, S. C., Hirst, M. C., and Murphy, K. P. (2006). Aberrant cortical synaptic plasticity and dopaminergic dysfunction in a mouse model of Huntington's disease. *Hum. Mol. Genet.* 15, 2856–2868.
- Davies, S. W., Turmaine, M., Cozens, B. A., DiFiglia, M., Sharp, A. H., Ross, C. A., Scherzinger, E., Wanker, E. E., Mangiarini, L., and Bates, G. P. (1997). Formation of neuronal intranuclear inclusions underlies the neurological dysfunction in mice transgenic for the HD mutation. *Cell* 90, 537–548.
- Fischer, J. F., and Cho, A. K. (1979). Chemical release of dopamine from striatal homogenates: evidence for an exchange diffusion model. *J. Pharmacol. Exp. Ther.* 208, 203–209.
- Franklin, K., and Paxinos, G. (2008). *The Mouse Brain in Stereotaxic Coordinates*, 3rd Edn. New York, NY: Academic Press.
- Freeman, W., and Morton, A. J. (2004). Regional and progressive changes in brain expression of complexin II in a mouse transgenic for the Huntington's disease mutation. *Brain Res. Bull.* 63, 45–55.
- Ginovart, N., Lundin, A., Farde, L., Halldin, C., Backman, L., Swahn, C. G., Pauli, S., and Sedvall, G. (1997). PET study of the pre- and post-synaptic dopaminergic markers for the neurodegenerative process in Huntington's disease. *Brain* 120, 503–514.
- Glynn, D., Reim, K., Brose, N., and Morton, A. J. (2007). Depletion of complexin II does not affect disease progression in a mouse model of Huntington's disease (HD); support for role for complexin II in behavioural pathology in a mouse model of HD. *Brain Res. Bull.* 72, 108–120.
- Hackam, A. S., Singaraja, R., Wellington, C. L., Metzler, M., McCutcheon, K., Zhang, T., Kalchman, M., and Hayden, M. R. (1998). The influence of huntingtin protein size on nuclear localization and cellular toxicity. *J. Cell Biol.* 141, 1097–1105.
- Hansson, O., Guatteo, E., Mercuri, N. B., Bernardi, G., Li, Y.-J., Castilho, R. F., and Brundin, P. (2001). Resistance to NMDA toxicity correlates with appearance of nuclear inclusions, behavioral deficits and with changes in calcium homeostasis in mice transgenic for exon 1 of the Huntington gene. *Eur. J. Neurosci.* 14, 1494–1504.
- Heeringa, M. J., and Abercrombie, E. D. (1995). Biochemistry of somatodendritic dopamine release in substantia nigra: an in vivo comparison with striatal dopamine release. *J. Neurochem.* 65, 192–200.
- Hickey, M. A., Reynolds, G. P., and Morton, A. J. (2002). The role of dopamine in motor symptoms in the R6/2 transgenic mouse model of Huntington's disease. *J. Neurochem.* 81, 46–59.
- Hodgson, J. G., Agopyan, N., Gutekunst, C. A., Leavitt, B. R., LePiane, F., Singaraja, R., Smith, D. J., Bissada, N., McCutcheon, K., Nasir, J., Jamot, L., Li, X. J., Stevens, M. E., Rosemond, E., Roder, J. C., Phillips, A. G., Rubin, E. M., Hersch, S. M., and Hayden, M. R. (1999). A YAC mouse model for Huntington's disease with full-length mutant huntingtin, cytoplasmic toxicity, and selective striatal neurodegeneration. *Neuron* 23, 181–192.
- Johnson, M. A., Rajan, V., Miller, C. E., and Wightman, R. M. (2006). Dopamine release is severely compromised in the R6/2 mouse model of Huntington's disease. *J. Neurochem.* 97, 737–746.
- Johnson, M. A., Villanueva, M., Haynes, C. L., Seipel, A. T., Buhler, L. A., and Wightman, R. M. (2007). Catecholamine exocytosis is diminished in R6/2 Huntington's disease model mice. *J. Neurochem.* 103, 2102–2110.
- Joyce, J. N., Lexow, N., Bird, E., and Winokur, A. (1988). Organization of dopamine D1 and D2 receptors in human striatum: receptor autoradiographic studies in Huntington's disease and schizophrenia. *Synapse* 2, 546–557.
- Kish, S. J., Shannak, K., and Hornykiewicz, O. (1987). Elevated serotonin and reduced dopamine in subregionally divided Huntington's disease striatum. *Ann. Neurol.* 22, 386–389.
- Kung, V. W., Hassam, R., Morton, A. J., and Jones, S. (2007). Dopamine-dependent long term potentiation in the dorsal striatum is reduced in the R6/2 mouse model of Huntington's disease. *Neuroscience* 146, 1571–1580.
- Levine, M. S., Cepeda, C., Hickey, M. A., Fleming, S. M., and Chesselet, M. F. (2004). Genetic mouse models of

- Huntington's and Parkinson's disease: illuminating but imperfect. *Trends Neurosci.* 27, 691–697.
- Lunkes, A., and Mandel, J. L. (1998). A cellular model that recapitulates major pathogenic steps of Huntington's disease. *Hum. Mol. Genet.* 7, 1355–1361.
- Luthi-Carter, R., Strand, A., Peters, N. L., Solano, S. M., Hollingsworth, Z. R., Menon, A. S., Frey, A. S., Spektor, B. S., Penney, E. B., Schilling, G., Ross, C. A., Borchelt, D. R., Tapscott, S. J., Young, A. B., Cha, J. H., and Olson, J. M. (2000). Decreased expression of striatal signaling genes in a mouse model of Huntington's disease. *Hum. Mol. Genet.* 9, 1259–1271.
- Mangiarini, L., Sathasivam, K., Seller, M., Cozens, B., Harper, A., Hetherington, C., Lawton, M., Trotter, J., Lehrach, H., Davies, S. W., and Bates, G. P. (1996). Exon 1 of the HD gene with an expanded CAG repeat is sufficient to cause a progressive neurological phenotype in transgenic mice. *Cell* 87, 493–506.
- Masuzawa, M., Nakao, S., Miyamoto, E., Yamada, M., Murao, K., Nishi, K., and Shingu, K. (2003). Pentobarbital inhibits ketamine-induced dopamine release in the rat nucleus accumbens: a microdialysis study. *Anesth. Analg.* 96, 148–152.
- Menalled, L. B., and Chesselet, M. F. (2002). Mouse models of Huntington's disease. *Trends Pharmacol. Sci.* 23, 32–39.
- Menalled, L., El-Khodori, B. F., Patry, M., Suárez-Fariñas, M., Orenstein, S. J., Zahasky, B., Leahy, C., Wheeler, V., Yang, X. W., MacDonald, M., Morton, A. J., Bates, G., Leeds, J., Park, L., Howland, D., Signer, E., Tobin, A., and Brunner, D. (2009). Systematic behavioral evaluation of Huntington's disease transgenic and knock-in mouse models. *Neurobiol. Dis.* 35, 319–336.
- Miller, B., and Bezprozvanny, I. (2010). Corticostriatal circuit dysfunction in Huntington's disease: intersection of glutamate, dopamine, and calcium. *Future Neurol.* 5, 735–756.
- Mochel, F., Durant, B., Durr, A., and Schiffmann, R. (2011). Altered dopamine and serotonin metabolism in motorically asymptomatic r6/2 mice. *PLoS ONE* 31, e18336. doi: 10.1371/journal.pone.0018336
- Morton, A. J., and Edwardson, J. M. (2001). Progressive depletion of complexin II in a transgenic mouse model of Huntington's disease. *J. Neurochem.* 76, 166–172.
- Morton, A. J., Faull, R. L., and Edwardson, J. M. (2001). Abnormalities in the synaptic vesicle fusion machinery in Huntington's disease. *Brain Res. Bull.* 56, 111–117.
- Niddam, R., Arbilla, S., Scatton, B., Dennis, T., and Langer, S. Z. (1985). Amphetamine induced release of endogenous dopamine in vitro is not reduced following pretreatment with reserpine. *Naunyn Schmiedeberg Arch. Pharmacol.* 329, 123–127.
- Ortiz, A. N., Kurth, B. J., Osterhaus, G. L., and Johnson, M. A. (2010). Dysregulation of intracellular dopamine stores revealed in the R6/2 mouse striatum. *J. Neurochem.* 112, 755–761.
- Ortiz, A. N., Kurth, B. J., Osterhaus, G. L., and Johnson, M. A. (2011). Impaired dopamine release and uptake in R6/1 Huntington's disease model mice. *Neurosci. Lett.* 492, 11–14.
- Parker, E. M., and Cubeddu, L. X. (1986). Effects of d-amphetamine and dopamine synthesis inhibitors on dopamine and acetylcholine neurotransmission in the striatum. I. Release in the absence of vesicular transmitter stores. *J. Pharmacol. Exp. Ther.* 237, 179–192.
- Petersén, A., Puschban, Z., Lotharius, J., NicNiocaill, B., Wiekop, P., O'Connor, W. T., and Brundin, P. (2002). Evidence for dysfunction of the nigrostriatal pathway in the R6/1 line of transgenic Huntington's disease mice. *Neurobiol. Dis.* 11, 134–146.
- Pineda, J. R., Canals, J. M., Bosch, M., Adell, A., Mengod, G., Artigas, F., Ernfor, P., and Alberch, J. (2005). Brain-derived neurotrophic factor modulates dopaminergic deficits in a transgenic mouse model of Huntington's disease. *J. Neurochem.* 93, 1057–1068.
- Reynolds, G. P., Dalton, C. F., Tillery, C. L., Mangiarini, L., Davies, S. W., and Bates, G. P. (1999). Brain neurotransmitter deficits in mice transgenic for the Huntington's disease mutation. *J. Neurochem.* 72, 1773–1776.
- Rubio, I., Rodríguez-Navarro, J. A., Tomás-Zapico, C., Ruiz, C., Casarejos, M. J., Peruch, J., Gómez, A., Rodal, I., Lucas, J. J., Mena, M. A., and de Yébenes, J. G. (2009). Effects of partial suppression of parkin on huntingtin mutant R6/1 mice. *Brain Res.* 1281, 91–100.
- Sedvall, G., Karlsson, P., Lundin, A., Anvret, M., Suhara, T., Halldin, C., and Farde, L. (1994). Dopamine D1 receptor number – a sensitive PET marker for early brain degeneration in Huntington's disease. *Eur. Arch. Psychiatry Clin. Neurosci.* 243, 249–255.
- Slow, E. J., Van Raamsdonk, J., Rogers, D., Coleman, S. H., Graham, R. K., Deng, Y., Oh, R., Bissada, N., Hossain, S. M., Yang, Y. Z., Li, X. J., Simpson, E. M., Gutekunst, C. A., Leavitt, B. R., and Hayden, M. R. (2003). Selective striatal neuronal loss in a YAC128 mouse model of Huntington disease. *Hum. Mol. Genet.* 12, 1555–1567.
- Stack, E. C., Kubilus, J. K., Smith, K., Cormier, K., Del Signore, S. J., Guelin, E., Ryu, H., Hersch, S. M., and Ferrante, R. J. (2005). Chronology of behavioral symptoms and neuropathological sequel in R6/2 Huntington's disease transgenic mice. *J. Comp. Neurol.* 490, 354–370.
- Suzuki, M., Desmond, T. J., Albin, R. L., and Frey, K. A. (2001). Vesicular neurotransmitter transporters in Huntington's disease: initial observations and comparison with traditional synaptic markers. *Synapse* 15, 329–336.
- The Huntington's Disease Collaborative Research Group. (1993). A novel gene containing a trinucleotide repeat that is expanded and unstable on Huntington's disease chromosomes. *Cell* 72, 971–983.
- Van Raamsdonk, J. M., Warby, S. C., and Hayden, M. R. (2007). Selective degeneration in YAC mouse models of Huntington disease. *Brain Res. Bull.* 72, 124–131.
- Velier, J., Kim, M., Schwarz, C., Kim, T. W., Sapp, E., Chase, K., Aronin, N., and DiFiglia, M. (1998). Wild-type and mutant huntingtins function in vesicle trafficking in the secretory and endocytic pathways. *Exp. Neurol.* 152, 34–40.
- Walker, F. O. (2007). Huntington's disease. *Lancet* 369, 218–228.
- Yadid, G., Harvey-White, J. D., Kopin, I. J., and Goldstein, D. S. (2000). Estimation of striatal dopamine spillover and metabolism in vivo. *Neuroreport* 11, 3367–3373.
- Yohrling, G. J. IV, Jiang, G. C., DeJohn, M. M., Miller, D. W., Young, A. B., Vrana, K. E., and Cha, J. H. (2003). Analysis of cellular, transgenic and human models of Huntington's disease reveals tyrosine hydroxylase alterations and substantia nigra neuropathology. *Brain Res. Mol. Brain Res.* 119, 28–36.
- Zetterström, T., Sharp, T., Collin, A. K., and Ungerstedt, U. (1988). In vivo measurement of extracellular dopamine and DOPAC in rat striatum after various dopamine-releasing drugs; implications for the origin of extracellular DOPAC. *Eur. J. Pharmacol.* 148, 327–334.

Conflict of Interest Statement: The authors declare that the research was conducted in the absence of any commercial or financial relationships that could be construed as a potential conflict of interest.

Received: 02 May 2011; accepted: 01 July 2011; published online: 15 July 2011.

Citation: Callahan JW and Abercrombie ED (2011) In vivo dopamine efflux is decreased in striatum of both fragment (R6/2) and full-length (YAC128) transgenic mouse models of Huntington's disease. *Front. Syst. Neurosci.* 5:61. doi: 10.3389/fnsys.2011.00061

Copyright © 2011 Callahan and Abercrombie. This is an open-access article subject to a non-exclusive license between the authors and Frontiers Media SA, which permits use, distribution and reproduction in other forums, provided the original authors and source are credited and other Frontiers conditions are complied with.



Multi-neuronal recordings in the basal ganglia in normal and dystonic rats

Mark S. Baron^{1*}, Kunal D. Chaniary², Ann C. Rice¹ and Steven M. Shapiro¹

¹ Department of Neurology, Virginia Commonwealth University, Richmond, VA, USA

² Department of Biomedical Engineering, Virginia Commonwealth University, Richmond, VA, USA

Edited by:

Charles J. Wilson, University of Texas at San Antonio, USA

Reviewed by:

Atsushi Nambu, National Institute for Physiological Sciences, Japan
Hitoshi Kita, The University Tennessee Health Science Center, USA

*Correspondence:

Mark S. Baron, Department of Neurology, Virginia Commonwealth University, 6th Floor Sanger Hall, Box 980599, Richmond, VA 23220, USA.
e-mail: mbaron@mcvh-vcu.edu

Classical rate-based pathway models are invaluable for conceptualizing direct/indirect basal ganglia pathways, but cannot account for many aspects of normal and abnormal motor control. To better understand the contribution of patterned basal ganglia signaling to normal and pathological motor control, we simultaneously recorded multi-neuronal and EMG activity in normal and dystonic rats. We used the jaundiced Gunn rat model of kernicterus as our experimental model of dystonia. Stainless steel head fixtures were implanted on the skulls and EMG wires were inserted into antagonistic hip muscles in nine dystonic and nine control rats. Under awake, head-restrained conditions, neuronal activity was collected from up to three microelectrodes inserted in the principal motor regions of the globus pallidus (GP), subthalamic nucleus, and entopeduncular nucleus (EP). In normal animals, most neurons discharged in regular or irregular patterns, without appreciable bursting. In contrast, in dystonic animals, neurons discharged in slow bursty or irregular, less bursty patterns. In normal rats, a subset of neurons showed brief discharge bursts coinciding with individual agonist or antagonist EMG bursts. In contrast, in dystonics, movement related discharges were characterized by more prolonged bursts which persist over multiple dystonic co-contraction epics. The pattern of movement related decreases in discharge activity however did not differ in dystonics compared to controls. In severely dystonic rats, exclusively, simultaneously recorded units often showed abnormally synchronized movement related pauses in GP and bursts in EP. In conclusion, our findings support that slow, abnormally patterned neuronal signaling is a fundamental pathophysiological feature of intrinsic basal ganglia nuclei in dystonia. Moreover, from our findings, we suggest that excessive movement related silencing of neuronal signaling in GP profoundly disinhibits EP and in turn contributes to sustained, unfocused dystonic muscle contractions.

Keywords: dystonia, basal ganglia, globus pallidus, subthalamus, entopeduncular nucleus, microelectrode recording, rats

INTRODUCTION

Dystonia is a devastating condition characterized by ineffective, twisting movements and contorted postures. The prevalence is estimated at 10.7 per 1000 people aged 50–89 years for secondary dystonias due to such causes as Parkinson's disease (PD), cerebral palsy (CP), and strokes (Wenning et al., 2005). Despite being considered the third most common movement disorder (Kernich, 2003), the underlying pathophysiology remains poorly understood. Largely as a result, no current medical or surgical therapies were intentionally designed to treat dystonia.

According to longstanding basal ganglia circuitry models, the striatum is the major site for motor-related inputs into the basal ganglia and the globus pallidus internus (GPi) is the primary output nucleus (Albin et al., 1989; DeLong, 1990). Excitatory inputs to the striatum via the cortex are thought to inhibit GPi neurons along the “direct” monosynaptic pathway. In contrast, cortical activation of the striatum is considered to excite GPi neurons along the “indirect” GP externa (GPe)–subthalamus (STN) pathway by disinhibiting excitatory STN–GPi projections and by inhibiting inhibitory GPe–GPi projections. Ultimately, net reduced inhibitory output from GPi to the ventrolateral (VL) thalamus is thought to release thalamocortical activation. Although the classical basal ganglia circuitry models provide an invaluable framework for conceptualizing

basal ganglia connections, these models have major limitations. Firstly, the models attribute the various hypo- and hyperkinetic movement disorders to opposing alterations in neuronal discharge rates (on the order of seconds to minutes). Yet, overall discharge rates in GPe (Bezard et al., 1999; Raz et al., 2000; Boraud et al., 2001), GPi (Bergman et al., 1994; Bezard et al., 1999; Wichmann and DeLong, 1999), and the thalamus (Pessiglione et al., 2005) are not clearly altered in primate models of PD. Secondly, while such models correctly predict that pallidotomy (GPi ablation) should ameliorate hypokinesia in PD patients (by disinhibiting thalamocortical activity), the models cannot likewise account for comparable surgical benefits of pallidotomy on medication-induced dyskinesias (excessive movements) in these patients (Lozano et al., 1995; Baron et al., 1996). Thirdly, in PD patients undergoing deep brain stimulator (DBS) surgery, intra-operative induction of dyskinesias was associated with alterations in phasic patterned neuronal activity in GPi without corresponding changes in the discharge rates (Lee et al., 2007).

Although many experts in the field are now suggesting that pathological alterations in discharge *patterned* activity hold the key to understanding the various movement disorders, to date, the abnormally patterned discharge activity has not been systematically investigated in animal models of dystonia. To date, the most

extensive neurophysiological recording studies in animals have been conducted in *dt^{cr}* hamsters, which exhibit paroxysmal dystonia only in response to prolonged stress (Loscher et al., 1989; Richter and Loscher, 1993; Bhatia, 2001). Besides this limitation of the model, the neuronal recordings have been collected under general anesthesia, thereby altering the neuronal signals and not reflecting actual dystonic movements. The tottering mutant mice model, which also has paroxysmal dystonia, as well as ataxia, has also been extensively investigated (Scholle et al., 2010), though the basal ganglia physiology has not been explored in this model. Nambu and colleagues (Chiken et al., 2008) have recorded in the basal ganglia in a mouse model of human DTY1 genetic dystonia without the use of sedation. These mice show prominent hyperkinesia with modest evidence of dystonia. Although abnormal neuronal burst and pause patterns were discovered in GP and entopeduncular nucleus (EP) in these animals, the investigators did not monitor for concurrent dystonia during the neuronal recordings.

Toward the present studies, we advanced techniques to record extracellular neuronal discharge activity from basal ganglia nuclei in dystonic rats without the requirement of ear bars and sedation (Chaniary et al., 2011) and developed objective EMG indicators of dystonia (Chaniary et al., 2008). For our animal model, we used the well-established jaundiced Gunn rat model which has clinical and pathological changes closely resembling human kernicterus (Byers et al., 1955; Perlstein, 1960; Volpe, 2008). Gunn rats are genetically deficient of UDP glucuronosyl transferase, the principal liver enzyme responsible for bilirubin clearance. Homozygous recessive (jj) pups appear normal apart from being jaundiced in the first weeks of life. Free unbound bilirubin blood levels are highest at 16–17 days of age when levels of blood albumin, which binds bilirubin and normally keeps it out of brain, are relatively low (Schutta and Johnson, 1969). We create our model by injecting 16-day-old jjs with sulfonamide (sulfa) to competitively displace bilirubin from blood albumin into the brain (Diamond and Schmid, 1966). The rats become prominently dystonic within minutes to hours after injection. Heterozygous non-jaundiced (Nj) rats have about 50% of the normal enzyme activity (Strebel and Odell, 1971) and remain phenotypically normal even after sulfa injection.

MATERIALS AND METHODS

ANIMALS AND BEHAVIORAL RATINGS

Nine jj dystonic and nine Nj control rats were used for the present studies. All jjs were injected with sulfonamide and Njs with saline at day 16 ± 24 h. Post-sulfa administration, the acute bilirubin toxicity often resulted in poor spontaneous hydration and food intake. All animals were carefully monitored each day for loss of body weight. As necessary, the animals were compensated with oral feedings of kitten milk formula and given subcutaneous injections of 5% dextrose in 0.45% NaCl. Animals were assessed clinically on a daily basis and a clinical score (CS) between 0 and 5 was assigned based on the severity of the movement disorder (0 – normal, 1 – slight limb dystonia and gait abnormality, 2 – mild limb dystonia and gait abnormality and impaired righting reflex, 3 – moderate limb dystonia and gait abnormality, with prolonged righting reflex, 4 – severe failure of ambulation, general lack of spontaneous movement with occasional bursts of hyperactivity and no righting reflex, and 5 – moribund, including seizures and agonal respiration; Shaia

and Shapiro, 2002), and 0.5 was added to scores when midway between categories. All experiments were approved and monitored by the Virginia Commonwealth University IRB and performed in accordance with relevant regulatory guidelines.

SURGICAL AND STEREOTAXIC TECHNIQUES

Surgeries were carried out with 2% general isoflurane anesthesia on day 45 ± 24 h. A manufactured stainless steel head holder was secured to the skull with two sets of four screws to thick portions of the parietal bones on each side of the skull. Next, one hindlimb was surgically exposed and fine Teflon coated (50 µm bare, 110 µm coated) stainless steel wires (A-M systems, Carlsborg, WA, USA) were directly implanted with the aid of a 30 gauge needle and sutured into antagonistic hip (gluteus superficialis, gluteus medius) muscle pairs. To assure correct placement of the wires, the wires were stimulated electrically (Grass Technologies, West Warwick, RI, USA) and the expected hindlimb responses verified. The EMG wires were tunneled together subcutaneously and passed through the opening over the skull and then soldered to a micro-circuit board. The board in turn was secured to a removable Teflon cap, which covered the head holder in-between experiments and was secured to the stereotaxic apparatus during the recording sessions. After the initial surgery, the animals were put back in their cages and allowed 24 h for recovery.

On the first day of recordings, the head holder was clamped into a manufactured positioning mechanism via tapered grooves in its walls (Chaniary et al., 2011). The positioner is mounted onto a standard sized, commercial large animal stereotaxic frame. The system contains three control knobs, which permit independent tilting of the head in three directions (yaw, pitch, and roll). A commercial dial test indicator is mounted onto a customized Plexiglas platform, which slides on the arms of the stereotaxic frame. The dial test indicator apparatus was used to achieve flat skull positions along all three directions. The three positioner dials indicated the final placements in each direction. Subsequently, a burr hole was made with a surgical drill to expose the dura for targeting of the hemisphere contralateral to the study hindlimb.

ELECTROPHYSIOLOGICAL RECORDINGS

A five-channel mini-xyz-manipulator (Thomas Recording GmbH, Giessen, Germany) was mounted onto a Kopf stereotaxic arm and up to three quartz glass-insulated platinum/tungsten microelectrodes (100 µm shaft diam.) were individually passed into the brain using a concentric head configuration with 305 µm intra-electrode spacing targeting single nuclei. The globus pallidus (GP, rodent equivalent of GPe), subthalamic nucleus (STN), and (EP, equivalent of GPi) were identified by their characteristic neuronal firing patterns (illustrated in **Figure 1**). These neuronal discharge patterns are readily distinguished from those of surrounding structures in normal and dystonic rats. The optic tract, just below EP, was readily identified by its distinct response to light flashes and provided additional confirmation of the location of the microelectrodes. The posterolateral, presumed motor portions of GP, EP, and the STN were specifically targeted. Successful targeting of the intended motor regions was supported by distinguishing neurons whose discharge activity changed in relation to movement. To curtail damage, the number of microelectrode tracts was restricted in each animal.

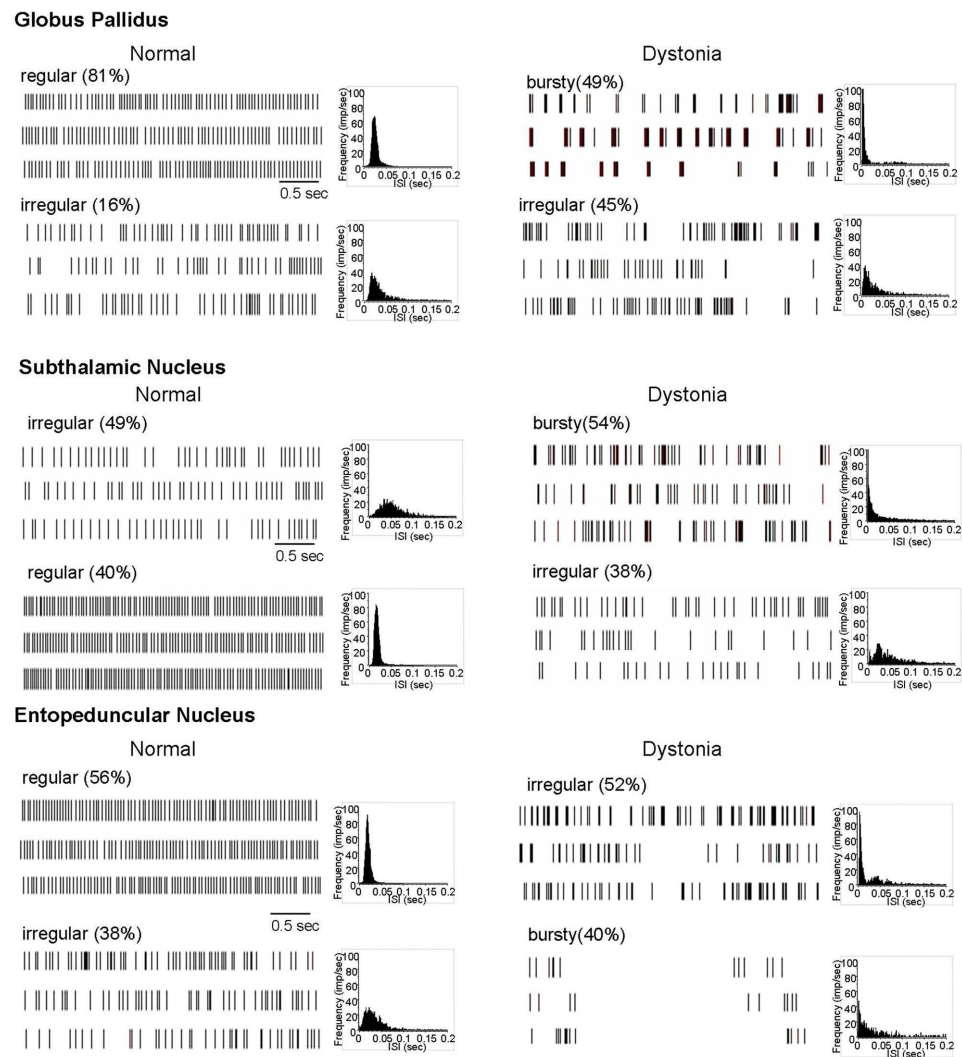


FIGURE 1 | Extracellular neuronal recordings at rest. In normal animals, most neurons in the motor territories of GP, STN, and EP discharged in either a regular or irregular pattern, without appreciable bursting. In contrast, in dystonic

animals, most neurons discharged in either a bursty or highly irregular pattern. Three examples of spike rasters for each of the principal patterns are shown, along with grouped ISI histograms.

During the recording sessions, the animal stood on the Plexiglas platform whose height was adjusted to position the animal to stand comfortably and freely move its limbs, with only the head-restrained. During collection of rest activity, towels were often placed on both sides of the animals' bodies to comfort them and minimize spontaneous movement. Under these conditions, the rats only infrequently displayed overt dystonia. The animals were continuously monitored to assure that they were not moving during collection of rest activity. Towards investigating neuronal correlates of dystonia, neuronal and EMG activity were collected both during spontaneous movements and in response to light touch of the animal's tail by the examiner. The motor activity varied widely from isolated brief to more prolonged movements of individual limbs to more exaggerated whole body movements and the intent of the movements did not appear to differ between dystonic versus normal animals.

Extracellularly recorded action potentials were monitored online using two digital storage oscilloscopes (HAMEG Instruments, Mainhausen, Germany) and collected at a sampling rate of 20 kHz. Quality of neuronal isolation was additionally monitored online on a desktop computer using Sort Client (Plexon Inc., Dallas, TX, USA). Neuronal and EMG activity were collected for a minimum of 120 s at rest in all 18 rats and with movement in 7 of the dystonics and 7 controls. The neuronal data were plotted on graph paper to establish the boundaries of recorded nuclei and transparencies of parasagittal sections from the Paxinos and Watson (1998) atlas were in turn superimposed on these tracks to estimate the precise location in the brain. EMG signals were amplified ($\times 1000$) and filtered (10 Hz–1 kHz) through a differential AC amplifier (A-M Systems, Carlsborg, WA, USA) and digitized through a NI-DAQ card (National Instruments Co., Austin, TX, USA) at a sampling frequency = 4 kHz. The EMG activity was continuously monitored using Sort Client.

DATA ANALYSIS AND STATISTICS

Stored digital data were replayed off-line and individual units were sorted using Off-line Spike Sorter (Plexon Inc.) using a combination of manual (*k*-means clustering, contours and waveform crossing method) and automated sorting techniques (valley-seeking; Lewicki, 1998). This permitted excellent separation of waveforms collected from single or multiple electrodes into distinct clusters. Each separated cluster was carefully examined for loss of neuronal recording and for quality of neuronal isolation. Any obvious artifacts in the signal were removed. Neuronal units were included only if a unit displayed high quality of separation from background noise, the number of recorded potentials exceeded 800, and the activity was recorded for a minimum of 120 s. Also, neuronal units whose location could not be established from the plotted tracks were excluded from all further analysis. Neuronal epics with and without motor activity were considered separately. Neuronal analyses were largely carried out by importing the data into NeuroExplorer software (Nex Technologies, Littleton, MA, USA). For most analyses, neuronal spike data for each nuclei were pooled by treatment groups (jj sulfa, Nj saline).

To define burst periods in a spike train, we initially investigated the Poisson surprise method developed by Legendy and Salcman (1985). This method uses definable levels of “surprise”

to determine the unlikeliness of finding burst interspike intervals (ISIs) in a random stream of ISIs, which are assumed to be Poisson-distributed. Despite its popularity, the Poisson surprise method proved to be unreliable for detecting bursts in dystonic rats. **Figure 2** shows a representative, well-isolated unit from GP with a clear burst pattern in a dystonic Gunn rat (**Figures 2A–C**). Using the Poisson surprise method, at lower surprise values, several adjacent burst epics were wrongly grouped as a single burst, while at progressively higher surprise values, the method failed to detect clear bursts (**Figure 2D**). To overcome these shortcomings of the Poisson surprise method, the interval method was used in which the bursts were identified by individually defining the burst parameters within the algorithm (**Figure 3**). Based on visual inspection of spike trains in dystonic and control rats, various parameters were chosen and subsequently modified until they proved to be highly reliable in detecting and separating out individual bursts in the spike train. The following final parameters were chosen: max. interval to start burst = 6 ms, max. interval to end burst = 9 ms, min. interval between bursts = 20 ms, min. duration of burst = 5 ms, and min. number of spikes in a burst = 3. As can be seen for the representative unit, using these parameters, the interval method provides far superior burst detection compared to the Poisson surprise method in our animals (**Figure 2E**).

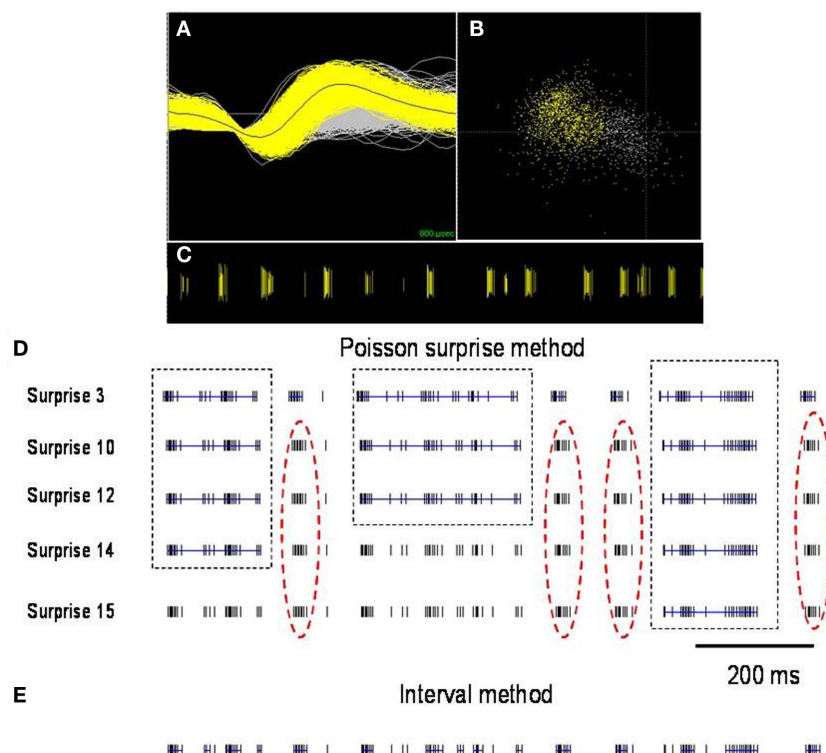


FIGURE 2 | Comparison of burst detection using the Poisson surprise and interval methods. (A) Spike discharge activity (yellow) superimposed on background noise (gray) from a representative neuron in GP of a dystonic rat **(B)**. PCA analysis highlights the neuronal cluster (yellow) from the background (gray). **(C)** Raster display highlights the representative distinct burst clusters. Each vertical line represents an action potential. **(D)** Using lower surprise

values, the Poisson surprise method wrongly classifies adjacent burst periods as one single burst (dashed boxes) and with higher surprise values, obvious bursts are rejected by the algorithm (red dashed oval). **(E)** The interval method provides greater reliability for defining individual burst periods. Blue lines indicate bursts detected in the spike trains using the two illustrated burst detection methods.

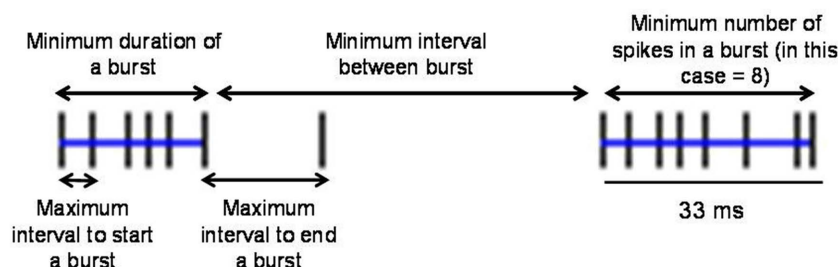


FIGURE 3 | Explanation of parameters used in the interval method to define bursts. The interval method uses the five indicated definable parameters to delineate individual bursts. Blue lines indicate two bursts in the spike train.

Based on inspection of the spike rasters and the shape of the ISI histograms and the results of burst analyses, most neurons in GP, EP, and STN, with the exception of a few outliers, were classified as (1) regular, (2) irregular, or (3) bursty. More specifically, regular firing neurons were characterized by showing tonic discharge activity and symmetrical, sharply peaked, near normally distributed ISI histograms. Irregular firing neurons were characterized by showing tonic discharge activity interrupted by variable length pauses, with flattened, relatively dispersed ISI histograms, with longer pauses reflected by a tail in the ISI histogram. Bursty neurons were characterized by having grouped discharge activity reflected by a leftward peak in the ISI histogram, with significant burstiness using the interval method for burst detection.

Statistically significant relations between neuronal discharge activity and EMG movement epics were detected using peri-event time histogram (PETH) calculations. All segments of the spike train corresponding to EMG movement epics were cut and realigned at the onset of the EMG changes (time = 0) and the histograms plotted for 200 ms before and after the onset of EMG epics. Neurons were considered to show significant movement related responses if four consecutive 10 ms bins differed above or below the baseline mean firing rate (95% confidence limits, $p < 0.001$). Because we did not perform passive examinations and only hip flexor and extensor muscles were recorded, these relations however could not be established with certainty, nor can we exclude the possibility that non-responsive (or responsive) cells were related to different directional movements at the hip.

Statistical analysis was performed using JMP software package (SAS Institute Inc.). Mean \pm SD of the firing rates were determined for each nucleus. Comparisons between the discharge rates, coefficient of variance of ISIs, and burst parameters between groups were made using one-way ANOVA analysis. Multiple comparisons between groups were made using the Tukey–Kramer honestly significant difference (HSD) test. A probability value of <0.05 was considered to be statistically significant for comparisons between groups.

RESULTS

PHENOTYPE OF DYSTONIC GUNN RATS

Within 24 h after sulfa injection, sulfa treated jaundiced animals developed a movement dystonia that closely resembles pure generalized dystonia in humans. While unrestrained (not formally assessed in the present study), the rats regularly showed mild to severe axial

twisting and variable disruptive, prolonged hindlimb extensions with relatively milder forelimb. Of the nine dystonic animals used in this study, six had milder dystonia (CS: ~ 2.0), and three had more severe dystonia (CS: ~ 3.5). At rest, with their heads restrained for the neuronal and EMG recordings, even more severely dystonic animals showed no active signs of dystonia. With self-initiated or provoked movement while restrained, dystonic rats consistently showed variable severities of dystonic extensor posturing of single to multiple limbs mostly without overt truncal involvement. As illustrated by the recordings of antagonistic hip flexor and extensor EMGs (see **Figures 4 and 5**), the dystonic movements were heralded by brief (~ 1 s) to more prolonged antagonistic muscle co-contractions. Refer to our previous publications for further EMG characterization and videos of the animals (Chaniary et al., 2008) and objective assessments of the dystonic gait (Chaniary et al., 2009).

MAJOR ALTERATIONS IN NEURONAL DISCHARGE ACTIVITY IN GP, STN, AND EP IN DYSTONIC RATS AT REST

Neuronal discharge rates in dystonic rats were markedly reduced in GP (62%, $p < 0.0001$) and EP (67%, $p < 0.0001$) and showed a trend toward a reduction in the STN (33%, $p = 0.07$). See **Table 1** for details of discharge rates and patterns and numbers of animals and neurons.

In control animals, neuronal activity in GP, STN, and EP was dominated by (1) regular tonic and (2) irregular discharge patterns, with little burst activity (**Figure 1**). In contrast, in dystonic animals, the patterned activity was dominated by (1) highly irregular and (2) irregular burst activity. During prolonged recordings of up to 5 min, neurons never changed patterns. In distinction from PD and MPTP-treated parkinsonian animals (Hammond et al., 2007), the burst activity was non-oscillatory.

MAJOR ALTERATIONS IN NEURONAL DISCHARGE ACTIVITY IN GP, STN, AND EP IN DYSTONIC RATS DURING MOVEMENT

During voluntary movement epics, hip responsive units in GP, STN, and EP showed phasic increases or decreases in discharge (both $p < 0.001$) in normal and dystonic rats. In GP, there was a significant shift toward more movement related decreases from increases in neuronal discharge activity in dystonic rats compared to controls. The recorded neuronal discharge activity did not change during externally triggered reflexive withdrawal movements. See **Table 2** for details of the movement related neuronal responses, including numbers of animals and neuronal/movement relations.

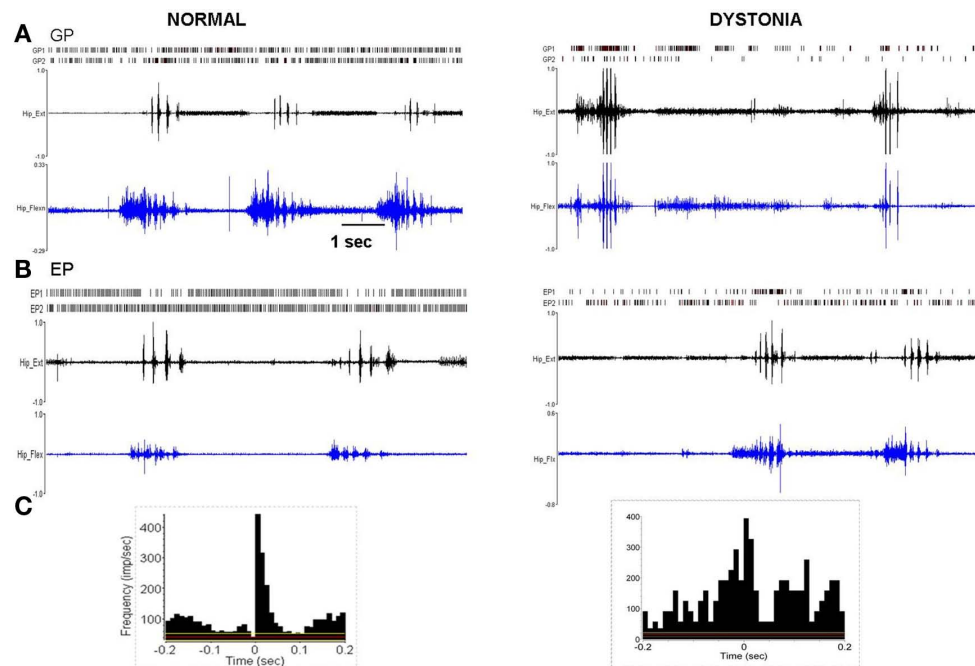


FIGURE 4 | Multi-unit discharge activity during movement in normal and dystonic animals. (A) In normal rats, movement related increases in neuronal discharge activity (illustrated for GP, but also in EP and STN) were dominated by brief bursts which recurred in relation to individual agonist or antagonist EMG epics ($p < 0.001$). In dystonic rats, movement related increases in discharge were characterized by prolonged bursts mostly persisting over multiple dystonic co-contraction epics ($p < 0.001$). **(B)** The pattern of movement related decreases in neuronal discharge activity (illustrated for EP) was similar in normal and dystonic animals. Note that in the illustrated example for a dystonic rat, one neuron shows movement related reduced discharge activity (EP2), while the

second neuron (EP1) shows coincident increased movement related discharge activity (a rare co-occurrence in our sample). **(C)** Peri-event histograms corresponding to the examples in **Figure 4A** confer significant movement related increases in discharge activity. The histograms illustrate collective neuronal discharge activity (y-axis) 200 ms before and after the onset of voluntary movement over multiple movement epics (minimum 15). The voluntary movements were either self-initiated or followed a brief flexor withdrawal response in response to light touch of the animal's tail by the examiner. Red lines indicate the mean firing rate and yellow lines indicate the 95% confidence intervals. Bin size is 10 ms.

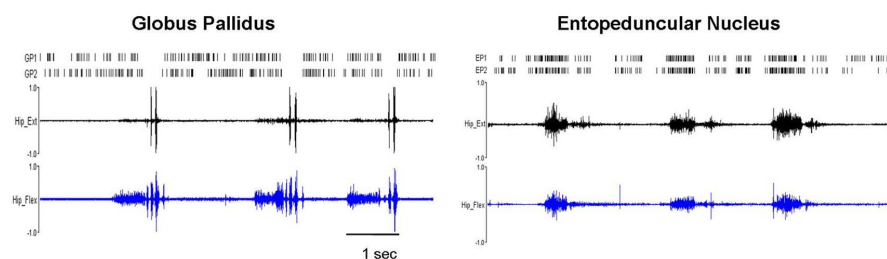


FIGURE 5 | Pathologically synchronized signaling in severely dystonic animals. In more severely dystonic rats ($n = 2$), exclusively, simultaneously recorded units showed abnormally synchronized movement related pauses in GP ($n = 5$ pairs, $p < 0.001$) and bursts in EP ($n = 4$ pairs, $p < 0.001$). In distinction, synchronized discharges were never seen in the STN.

In normal rats, movement related increases were characterized by brief discharge bursts coinciding with either individual agonist or antagonist EMG bursts. In contrast, in dystonic rats, neurons showed prolonged bursts persisting over multiple dystonic co-contraction epics (**Figure 4**). The pattern of movement related decreases in discharge activity however did not differ in dystonics compared to controls. Exclusively in the two severely dystonic rats that were assessed during movement, simultaneously recorded pairs or triplets of neurons separated by an appreciable distance ($\sim 300 \mu\text{m}$) regularly showed abnormally synchronized movement

related discharge activity, without appreciable time lag between neurons (**Figure 5**). The synchronized movement related neuronal discharge activity was specifically confined to pauses in GPe ($n = 5$ pairs) and to bursts in EP ($n = 4$ pairs). Such synchronization was not observed in the STN.

DISCUSSION

We describe for the first time to our knowledge findings from combined EMG and multi-neuronal recordings in the basal ganglia in unsedated rats with active dystonia. In both normal and dystonic

Table 1 | Resting discharge rates and patterned activity in GP, STN, and EP (*n* = 9 dystonic, 9 controls).

Pattern ^a	Rates	Asymmetry index ^b	Burst per minute ^c	% of spikes in burst
GLOBUS PALLIDUS (<i>N</i> = 4 CONTROLS, 4 DYSTONICS)				
Normals (74)	41.2 ± 17.1	0.72 ± 0.22	8.2 ± 13.8	1.4 ± 2.5
Regular (61)	48.3 ± 18.6	0.78 ± 0.16	9.0 ± 13.5	1.5 ± 2.4
Irregular (12)	16.6 ± 6.4	0.36 ± 0.15	0.5 ± 1.4	0.2 ± 0.4
Dystonics (49)	11.3 ± 7.9*	0.07 ± 0.07*	41.3 ± 57.0*	35.0 ± 37.8*
Bursty (24)	13.7 ± 9.9	0.04 ± 0.03	76.5 ± 60.3	65.1 ± 28.3
Irregular (22)	8.2 ± 3.2	0.10 ± 0.10	2.9 ± 4.3	2.1 ± 2.6
SUBTHALAMUS (<i>N</i> = 5 CONTROLS, 4 DYSTONICS)				
Normals (45)	27.3 ± 9.9	0.53 ± 0.30	5.6 ± 8.0	1.4 ± 2.0
Regular (18)	43.0 ± 13.3	0.80 ± 0.20	4.7 ± 5.0	0.7 ± 0.8
Irregular (22)	16.3 ± 8.8	0.40 ± 0.20	6.2 ± 9.6	1.9 ± 2.5
Dystonics (37)	18.1 ± 12.2*	0.23 ± 0.16*	28.7 ± 21.8*	25.5 ± 13.1*
Bursty (20)	21.0 ± 15.6	0.09 ± 0.05	37.2 ± 24.9	32.1 ± 14.9
Irregular (14)	13.4 ± 7.8	0.41 ± 0.20	13.2 ± 16.2	14.2 ± 12.0
ENTOPEDUNCULAR NUCLEUS (<i>N</i> = 4 CONTROLS, 5 DYSTONICS)				
Normals (45)	39.1 ± 14.5	0.59 ± 0.26	9.3 ± 17.9	2.1 ± 2.6
Regular (25)	48.7 ± 19.8	0.74 ± 0.17	10.6 ± 20.3	2.0 ± 4.2
Irregular (17)	19.0 ± 6.9	0.36 ± 0.19	7.4 ± 13.9	2.1 ± 3.7
Dystonics (50)	10.1 ± 6.2*	0.09 ± 0.18*	33.7 ± 41.7*	21.9 ± 22.2*
Bursty (20)	13.2 ± 5.5	0.03 ± 0.01	68.1 ± 42.4	40.4 ± 20.8
Irregular (26)	8.6 ± 6.7	0.13 ± 0.23	7.2 ± 8.7	7.7 ± 8.3

^aSubcategory designations (regular, irregular, bursty) are exclusive of outliers which did not meet criteria for one of the two common types identified for each nucleus for dystonics and controls.

^bAsymmetric index (mode ISI/mean ISI) equals 1 when an ISI histogram fits a Gaussian distribution.

^cBursts were detected using the interval method.

*Indicates significant difference (*p* < 0.05) between normal and dystonic groups.

Table 2 | Neuronal responses during hip movement (*n* = 7 dystonics, 7 controls).

Nuclei	No. of neurons		Type of response of neurons during hip movement					
	Normals	Dystonics	Normals			Dystonics		
			Increase	Decrease	Biphasic	Increase	Decrease	Biphasic
GP	28	25	18	7	3	10	14	1
STN	32	18	27	3	2	13	3	2
EP	36	29	22	12	2	17	11	1

Gunn rats, neurons in motor regions of the basal ganglia commonly increased or decreased discharge firing with movement. In normal rats, movement related increases in neuronal discharge activity were confined to short bursts, which coincided with individual agonist or antagonist EMG bursts. In distinction, in dystonic rats, increases in discharge activity were characterized by prolonged bursts which persisted over multiple co-contraction epics. Also, in more severely affected animals, pairs or triplets of neurons in GP and EP frequently discharged in synchrony. Moreover, with movement, synchronized alternations in discharge activity were limited in GP to practical silencing of discharge and in EP to prominent bursting. While our findings in part support traditional basal ganglia modeling of inhibitory influences of GPe on GPi along the

indirect pathway, they provide novel insight into the contributions of precision multi-neuronal *phasic* basal ganglia signaling to normal and pathological motor control.

At rest, without clinical or EMG evidence for active dystonia, neuronal activity in the basal ganglia of dystonic rats was notable for prominently irregular burst discharge activity with markedly reduced discharge rates in GP and EP, and to a lesser degree in the STN. These background changes in discharge activity are for the most part comparable to reports from humans undergoing DBS surgery for various dystonias. For instance, the discharge rates in GPi in humans with dystonia were mostly reduced compared to rates in normal monkeys (Lenz et al., 1998; Vitek et al., 1999; Sanghera et al., 2003; Merello et al., 2004; Zhuang et al., 2004;

Starr et al., 2005). In contrast to the tonic discharge activity in GPi in normal monkeys, the discharge pattern in dystonic patients was dominated by grouped burst discharges on a particularly silent background. In one investigation of GPe (Vitek et al., 1999), neuronal activity also showed abnormal burst activity, with reduced discharge rates compared to normal monkeys. In contrast, another group (Starr et al., 2005) did not find any definite abnormalities in the neuronal activity in GPe apart from occasional atypical oscillations. However, of potential significance, the motor portion of GPi is specifically targeted during these surgeries using different angular approaches, and therefore, there may be considerable differences between groups with respect to traversing motor versus non-motor territories of GPe. In a single investigation of the STN (Starr et al., 2005), the discharge pattern was dominated by irregular grouped discharges, without clear alterations in the discharge rates.

The presence of highly similar resting neuronal discharge rates and patterned activity in the basal ganglia in dystonic Gunn rats and in humans with various dystonias importantly supports the validity of the Gunn rat animal model. Further, as demonstrated in Gunn rats, patterned discharge activity in GPi (Vitek et al., 1999), STN (Zhuang et al., 2004), and the thalamus (Lenz et al., 1999; Zhuang et al., 2004) was found to correlate with dystonic EMG activity in humans. Moreover, Lenz et al. (1999) showed that the thalamic activity preceded correlated EMG activity. This observation supports that at least for the thalamus, the correlated activity in dystonia is not likely to be epiphenomena. Additionally, because human recording studies have not shown clear differences between various dystonias, our findings should have wide relevance for many forms of dystonia.

In severely dystonic animals, exclusively, two to three simultaneously recorded neurons in GP or EP separated by an appreciable distance (~300 μ m) were often observed to discharge largely in unison without appreciable time lags. From this finding, we hypothesize that in dystonia, abnormally synchronized basal ganglia signaling occurs in lieu of normally highly selective activation of intended and inactivation of unintended muscles during movement and in turn, is responsible for the hallmark overflow of contractions to unintended muscles. Further, we postulate that our findings of exaggerated and synchronized burst activation of neurons in EP which persist throughout repetitive muscle co-contractions contributes to prolonged co-contractions, another hallmark feature of this disorder. Additionally, from prior studies suggesting that inactivation of GP could cause various dystonias and our discovery of excessive and synchronized silencing of neuronal discharge in GP during dystonic movements, we postulate that the etiological source for dystonia in many human forms of dystonia is exaggerated and synchronized movement related silencing of neuronal discharge activity in GP. A surprising finding is the apparently less dramatic alterations in rates and patterned activity in the STN, along with the absence of clear prominent synchronization in dystonia. We reason that in dystonia, excessive and synchronized silencing of GP neurons could lead to a prominent and powerfully influential reduction in GABAergic inhibitory output from GP directly to the proximal dendrites and soma of EP neurons, and, in turn, largely induce prominent synchronized bursting of EP neurons.

Dopamine (DA) concentrations were found to be reduced in a mouse model of DYT1 dystonia, the most common genetic form of human dystonia (Balcioglu et al., 2007; Hewett et al., 2010). DA depletion can be expected to disinhibit DA D2 striatal GABAergic projection neurons and in turn suppress neuronal discharge activity in GPe. Further, in transgenic DYT1 mice, striatal DA D2 receptor function was reported to be impaired and associated with disinhibition of GABAergic transmission (Sciamanna et al., 2009). In humans, Dopa-responsive dystonia has been linked to specific genetic defects which lead to deficiencies in DA production (Ichinose et al., 1994). Using positive emission tomography (PET), Perlmutter et al. (1997a) showed that striatal DA D2 receptor labeling striatum was reduced in patients with focal idiopathic dystonia. These investigators (Perlmutter et al., 1997b) also demonstrated that transiently induced dystonia in MPTP-treated monkeys was temporally correlated with reductions in DA D2-like receptor binding. This background, along with our present findings, leads us to hypothesize that various pathologies along the indirect pathway similarly cause dystonia via exaggerated and synchronized silencing of GPe neurons. This postulate is in part supported by human reports of GP strokes producing dystonia (Ünchau et al., 2000).

Post-mortem studies from human newborns with kernicterus have shown prominent cell loss and gliosis in GPe, GPi, STN, substantia nigra pars reticulata, and less consistently in the cerebellum, hippocampus, and brain stem auditory and oculomotor nuclei (Jew and Sandquist, 1979; Ahdab-Barmada and Moossy, 1984). A number of groups have shown that the pathological changes in jaundiced Gunn rats closely approximate those of human kernicterus (Blanc and Johnson, 1959; Schutta and Johnson, 1967, 1969, 1971; Sturrock and Jew, 1978; Rose and Wisniewski, 1979). Considering the extent of the pathology in kernicterus, the pathogenesis of the dystonia in kernicterus has remained elusive. We initially considered two not necessarily exclusive possibilities: (1) that the dystonia in kernicterus results from a loss of motor-related signaling as a direct result of the loss of cells or (2) that it occurs due to abnormal signaling in surviving cells. The presence of largely movement-induced dystonia in Gunn rats that correlates with phasic changes in signaling of basal ganglia neurons is more supportive of the latter explanation. Studies in torsinA mutant mice have shown that torsinA, the principal protein product of the DYT1 gene is essential to maintain the normal neuronal nuclear membrane structure (Kim et al., 2010). Therefore, mechanisms other than DA dysfunction may play major contributory roles in the development of aberrant signaling in both primary and secondary forms of dystonia.

We acknowledge a number of limitations of the present studies. Firstly, although synchronization was only observed in more severely dystonic animals, we suggest that our small sampling size could have been expected to only uncover profound degrees of synchronization. Secondly, our limited sampling of multi-unit recordings in the STN in dystonic rats was inadequate to exclude comparable synchronization as demonstrated in GP and EP. Thirdly, because we did not perform passive examinations or more extensive EMG recordings over multiple joints, direct relations between the recorded neurons and hip muscle flexor or extensor contractions could not be reliably established. In turn, the temporal relations between the neuronal and EMG events could not be established. Lastly, although the clinical features appear to be highly similar

between primary and secondary forms, the relative shortcomings of DBS and pallidotomy for most secondary dystonias (Holloway et al., 2006) infer limitations in generalizing our findings to other dystonias, in particular to primary forms.

In summary, we have presented novel findings from simultaneously recording from the basal ganglia, along with EMGs from antagonist muscle pairs in unsedated rodents with active dystonia. From our findings, we suggest that in dystonia, dramatic alterations in the underlying discharge activity of basal ganglia neurons, along with a profound loss of independent neuronal signaling, leads to highly pathological signaling during movement. Moreover, we propose that exaggerated and unfocused silencing of GPi neurons during movement results in profound,

highly synchronized movement related burst activity in EP which contributes to the hallmark sustained co-contractions and spread to unintended muscles in dystonia. Why surgical approaches to the GPi do not generally improve such abnormalities in secondary dystonias to a similar degree as seen for primary dystonias remains to be determined. Our methodology could serve to lay the groundwork for pursuing similar comparison studies in other animal models of dystonia.

ACKNOWLEDGMENTS

This research was supported by NIH/NINDS grant R01NS47151 to Steven M. Shapiro and a Thomas F. Kate Miller Jeffress Memorial Trust award to Mark S. Baron.

REFERENCES

- Ahdab-Barmada, M., and Moossy, J. (1984). The neuropathology of kernicterus in the premature neonate: diagnostic problems. *J. Neuropathol. Exp. Neurol.* 43, 45–56.
- Albin, R. L., Young, A. B., and Penney, J. B. (1989). The functional anatomy of basal ganglia disorders. *Trends Neurosci.* 12, 366–375.
- Balcioglu, A., Kim, M. O., Sharma, N., Cha, J. H., Breakefield, X. O., and Standaert, D. G. (2007). Dopamine release is impaired in a mouse model of DYT1 dystonia. *J. Neurochem.* 102, 783–788.
- Baron, M. S., Vitek, J. L., Bakay, R. A., Green, J., Kaneoke, Y., Hashimoto, T., Turner, R. S., Woodard, J. L., Cole, S. A., McDonald, W. M., and DeLong, M. R. (1996). Treatment of advanced Parkinson's disease by posterior GPi pallidotomy, 1-year results of a pilot study. *Ann. Neurol.* 40, 355–366.
- Bergman, H., Wichmann, T., Karmon, B., and DeLong, M. R. (1994). The primate subthalamic nucleus. II. neuronal activity in the MPTP model of parkinsonism. *J. Neurophysiol.* 72, 507–520.
- Bezard, E., Boraud, T., Bioulac, B., and Gross, C. E. (1999). Involvement of the subthalamic nucleus in glutamatergic compensatory mechanisms. *Eur. J. Neurosci.* 11, 2167–2170.
- Bhatia, K. P. (2001). Familial (idiopathic) paroxysmal dyskinesias: an update. *Semin. Neurol.* 21, 69–74.
- Blanc, W. A., and Johnson, L. (1959). Studies on kernicterus; relationship with sulfonamide intoxication, report on kernicterus in rats with glucuronyl transferase deficiency and review of pathogenesis. *J. Neuropathol. Exp. Neurol.* 18, 165–187; discussion 187–189.
- Boraud, T., Bezard, E., Bioulac, B., and Gross, C. E. (2001). Dopamine agonist-induced dyskinesias are correlated to both firing pattern and frequency alterations of pallidal neurones in the MPTP-treated monkey. *Brain* 124, 546–557.
- Byers, R. K., Paine, R. S., and Crothers, B. (1955). Extrapyramidal cerebral palsy with hearing loss following erythroblastosis. *Pediatrics* 15, 248–254.
- Chaniary, K., Baron, M., Rice, A., Wetzel, P., and Shapiro, S. (2008). Electromyographic characterization in an animal model of dystonia. *Mov. Disord.* 23, 1122–1129.
- Chaniary, K. D., Baron, M. S., Rice, A. C., Wetzel, P. A., Ramakrishnan, V., and Shapiro, S. M. (2009). Quantification of gait in dystonic Gunn rats. *J. Neurosci. Methods* 180, 273–277.
- Chaniary, K. D., Baron, M. S., Robinson, P., Rice, A. C., and Shapiro, S. M. (2011). A novel stereotaxic apparatus for neuronal recordings in awake head-restrained rats. *J. Neurosci. Methods* 198, 29–35.
- Chiken, S., Shashidharan, P., and Nambu, A. (2008). Cortically evoked long-lasting inhibition of pallidal neurons in a transgenic mouse model of dystonia. *J. Neurosci.* 28, 13967–13977.
- DeLong, M. R. (1990). Primate models of movement disorders of basal ganglia origin. *Trends Neurosci* 13, 281–285.
- Diamond, I., and Schmid, R. (1966). Experimental bilirubin encephalopathy. the mode of entry of bilirubin-14C into the central nervous system. *J. Clin. Invest.* 45, 678–689.
- Hammond, C., Bergman, H., and Brown, P. (2007). Pathological synchronization in Parkinson's disease: networks, models and treatments. *Trends Neurosci.* 30, 357–364.
- Hewett, J., Johanson, P., Sharma, N., Standaert, D., and Balcioglu, A. (2010). Function of dopamine transporter is compromised in DYT1 transgenic animal model in vivo. *J. Neurochem.* 113, 228–235.
- Holloway, K. L., Baron, M. S., Brown, R., Cifu, D. X., and Ramesh, V. (2006). Deep brain stimulation for dystonia: a meta-analysis. *Neuromodulation* 9, 253–261.
- Ichinose, H., Ohye, T., Takahashi, E., Seki, N., Hori, T., Segawa, M., Nomura, Y., Endo, K., Tanaka, H., Tsuji, S., Fujita, K., and Nagatsu, T. (1994). Hereditary progressive dystonia with marked diurnal fluctuation caused by mutations in the GTP cyclohydrolase I gene. *Nat. Genet.* 8, 236–242.
- Jew, J. Y., and Sandquist, D. (1979). CNS changes in hyperbilirubinemia. Functional implications. *Arch. Neurol.* 36, 149–154.
- Kernich, C. A. (2003). Patient family fact sheet. Dystonia. *Neurologist* 9, 121–122.
- Kim, C. E., Perez, A., Perkins, G., Ellisman, M. H., and Dauer, W. T. (2010). A molecular mechanism underlying the neural-specific defect in torsinA mutant mice. *Proc. Natl. Acad. Sci. U.S.A.* 107, 9861–9866.
- Lee, J. I., Verhagen Metman, L., Ohara, S., Dougherty, P. M., Kim, J. H., and Lenz, F. A. (2007). Internal pallidal neuronal activity during mild drug-related dyskinesias in Parkinson's disease: decreased firing rates and altered firing patterns. *J. Neurophysiol.* 97, 2627–2641.
- Legendy, C. R., and Salzman, M. (1985). Bursts and recurrences of bursts in the spike trains of spontaneously active striate cortex neurons. *J. Neurophysiol.* 53, 926–939.
- Lenz, F. A., Jaeger, C. J., Seike, M. S., Lin, Y. C., Reich, S. G., DeLong, M. R., and Vitek, J. L. (1999). Thalamic single neuron activity in patients with dystonia: dystonia-related activity and somatic sensory reorganization. *J. Neurophysiol.* 82, 2372–2392.
- Lenz, F. A., Suarez, J. I., Metman, L. V., Reich, S. G., Karp, B. I., Hallett, M., Rowland, L. H., and Dougherty, P. M. (1998). Pallidal activity during dystonia: somatosensory reorganization and changes with severity. *J. Neurol. Neurosurg. Psychiatr.* 65, 767–770.
- Lewicki, M. S. (1998). A review of methods for spike sorting: the detection and classification of neural action potentials. *Network* 9, R53–R78.
- Loscher, W., Fisher, J. E. Jr., Schmidt, D., Fredow, G., Honack, D., and Iturrian, W. B. (1989). The sz mutant hamster: a genetic model of epilepsy or of paroxysmal dystonia? *Mov. Disord.* 4, 219–232.
- Lozano, A. M., Lang, A. E., Galvez-Jimenez, N., Miyasaki, J., Duff, J., Hutchinson, W. D., and Dostrovsky, J. O. (1995). Effect of GPi pallidotomy on motor function in Parkinson's disease. *Lancet* 346, 1383–1387.
- Merello, M., Cerquetti, D., Cammarota, A., Tenca, E., Artes, C., Antico, J., Antico, J., and Leiguarda, R. (2004). Neuronal globus pallidus activity in patients with generalised dystonia. *Mov. Disord.* 19, 548–554.
- Paxinos, G., and Watson, W. C. (1998). *The Rat Brain in Stereotaxic Coordinates*. San Diego, CA: Academic Press.
- Perlmuter, J. S., Stambuk, M. K., Markham, J., Black, K. J., McGee-Minnich, L., Jankovic, J., and Moerlein, S. M. (1997a). Decreased [18F]spiperone binding in putamen in idiopathic focal dystonia. *J. Neurosci.* 17, 843–850.
- Perlmuter, J. S., Tempel, L. W., Black, K. J., Parkinson, D., and Todd, R. D. (1997b). MPTP induces dystonia and parkinsonism. Clues to the pathophysiology of dystonia. *Neurology* 49, 1432–1438.
- Perlstein, M. A. (1960). The late clinical syndrome of postictic encephalopathy. *Pediatr. Clin. North Am.* 7, 665–687.
- Pessiglione, M., Guehl, D., Rolland, A. S., Francois, C., Hirsch, E. C., Feger, J., and Tremblay, L. (2005). Thalamic neuronal activity in dopamine-depleted primates: evidence for a loss of functional segregation within basal ganglia circuits. *J. Neurosci.* 25, 1523–1531.
- Raz, A., Vaadia, E., and Bergman, H. (2000). Firing patterns and correlations of spontaneous discharge of pallidal neurons in the normal and the tremulous 1-methyl-4-phenyl-1,2,3,6-tetrahydropyridine vervet

- model of parkinsonism. *J. Neurosci.* 20, 8559–8571.
- Richter, A., and Loscher, W. (1993). Alterations in pharmacological sensitivity of GABAergic but not dopaminergic and glutamatergic systems during ontogenesis in dystonic mutant hamsters. *Eur. J. Pharmacol.* 231, 111–119.
- Rose, A. L., and Wisniewski, H. (1979). Acute bilirubin encephalopathy induced with sulfadimethoxine in Gunn rats. *J. Neuropathol. Exp. Neurol.* 38, 152–164.
- Sanghera, M. K., Grossman, R. G., Kalhorn, C. G., Hamilton, W. J., Ondo, W. G., and Jankovic, J. (2003). Basal ganglia neuronal discharge in primary and secondary dystonia in patients undergoing pallidotomy. *Neurosurgery* 52, 1358–1370.
- Scholle, H. C., Jinnah, H. A., Arnold, D., Biedermann, F. H., Faenger, B., Grassme, R., Hess, E. J., and Schumann, N. P. (2010). Kinematic and electromyographic tools for characterizing movement disorders in mice. *Mov. Disord.* 25, 265–274.
- Schutta, H. S., and Johnson, L. (1967). Bilirubin encephalopathy in the Gunn rat: a fine structure study of the cerebellar cortex. *J. Neuropathol. Exp. Neurol.* 26, 377–396.
- Schutta, H. S., and Johnson, L. (1969). Clinical signs and morphologic abnormalities in Gunn rats treated with sulfadimethoxine. *J. Pediatr.* 75, 1070–1079.
- Schutta, H. S., and Johnson, L. (1971). Electron microscopic observations on acute bilirubin encephalopathy in Gunn rats induced by sulfadimethoxine. *Lab. Invest.* 24, 82–89.
- Sciamanna, G., Bonsi, P., Tassone, A., Cuomo, D., Tschertter, A., Viscomi, M. T., Martella, G., Sharma, N., Bernardi, G., Standaert, D. G., and Pisani, A. (2009). Impaired striatal D2 receptor function leads to enhanced GABA transmission in a mouse model of DYT1 dystonia. *Neurobiol. Dis.* 34, 133–145.
- Shaia, W., and Shapiro, S. M. (2002). Immunohistochemical localization of calcium-binding proteins in the brainstem vestibular nuclei of the jaundiced Gunn rat. *Hear. Res.* 173, 82–90.
- Starr, P. A., Rau, G. M., Davis, V., Marks, W. J. Jr, Ostrem, J. L., Simmons, D., Lindsey, N., and Turner, R. S. (2005). Spontaneous pallidal neuronal activity in human dystonia: comparison with Parkinson's disease and normal macaque. *J. Neurophysiol.* 93, 3165–3176.
- Strebel, L., and Odell, G. B. (1971). Bilirubin uridine disphosphoglucuronyltransferase in rat liver microsomes: genetic variation and maturation. *Pediatr. Res.* 5, 548–559.
- Sturrock, R. R., and Jew, J. Y. (1978). A quantitative histological study of changes in neurons and glia in the Gunn rat brain. *Neuropathol. Appl. Neurobiol.* 4, 209–223.
- Ünchau, A., Mathen, D., Cox, T., Quinn, N. P., Marsden, C. D., and Bhatia, K. P. (2000). Unilateral lesions of the globus pallidus: report of four patients presenting with focal or segmental dystonia. *J. Neurol. Neurosurg. Psychiatr.* 69, 494–498.
- Vitek, J. L., Chockkan, V., Zhang, J. Y., Kaneoke, Y., Evatt, M., DeLong, M. R., Triche, S., Mewes, K., Hashimoto, T., and Bakay, R. A. (1999). Neuronal activity in the basal ganglia in patients with generalized dystonia and hemiballismus. *Ann. Neurol.* 46, 22–35.
- Volpe, J. J. (2008) "Bilirubin and brain injury," in *Neurology of the Newborn*, 5th Edn, ed. J. J. Volpe (Philadelphia, PA: W. B. Saunders), 619.
- Wenning, G. K., Kiechl, S., Seppi, K., Müller, J., Höggl, B., Saletu, M., Rungger, G., Gasperi, A., Willeit, J., and Poewe, W. (2005). Prevalence of movement disorders in men and women aged 50–89 years (Bruneck study cohort): a population-based study. *Lancet Neurol.* 4, 815–820.
- Wichmann, T., and DeLong, M. R. (1999). Oscillations in the basal ganglia. *Nature* 400, 21–22.
- Zhuang, P., Li, Y., and Hallett, M. (2004). Neuronal activity in the basal ganglia and thalamus in patients with dystonia. *Clin. Neurophysiol.* 115, 2542–2557.

Conflict of Interest Statement: The authors declare that the research was conducted in the absence of any commercial or financial relationships that could be construed as a potential conflict of interest.

Received: 23 April 2011; accepted: 01 August 2011; published online: 31 August 2011.
Citation: Baron MS, Chaniary KD, Rice AC and Shapiro SM (2011) Multi-neuronal recordings in the basal ganglia in normal and dystonic rats. *Front. Syst. Neurosci.* 5:67. doi: 10.3389/fnsys.2011.00067
Copyright © 2011 Baron, Chaniary, Rice and Shapiro. This is an open-access article subject to a non-exclusive license between the authors and Frontiers Media SA, which permits use, distribution and reproduction in other forums, provided the original authors and source are credited and other Frontiers conditions are complied with.



Dopaminergic balance between reward maximization and policy complexity

Naama Parush^{1,2*}, Naftali Tishby^{1,3,4} and Hagai Bergman^{1,4,5}

¹ The Interdisciplinary Center for Neural Computation, The Hebrew University, Jerusalem, Israel

² IBM Haifa Research Lab, Haifa, Israel

³ The School of Engineering and Computer Science, The Hebrew University, Jerusalem, Israel

⁴ The Edmond and Lily Safra Center for Brain Sciences, The Hebrew University, Jerusalem, Israel

⁵ Department of Medical Neurobiology (Physiology), Institute of Medical Research Israel-Canada, Hadassah Medical School, The Hebrew University, Jerusalem, Israel

Edited By:

Charles J. Wilson, University of Texas at San Antonio, USA

Reviewed By:

Charles J. Wilson, University of Texas at San Antonio, USA
Thomas Boraud, Université de Bordeaux, France

*Correspondence:

Naama Parush, The Interdisciplinary Center for Neural Computation, The Hebrew University, Jerusalem, Israel.
e-mail: naama.parush@gmail.com

Previous reinforcement-learning models of the basal ganglia network have highlighted the role of dopamine in encoding the mismatch between prediction and reality. Far less attention has been paid to the computational goals and algorithms of the main-axis (actor). Here, we construct a top-down model of the basal ganglia with emphasis on the role of dopamine as both a reinforcement learning signal and as a pseudo-temperature signal controlling the general level of basal ganglia excitability and motor vigilance of the acting agent. We argue that the basal ganglia endow the thalamic-cortical networks with the optimal dynamic tradeoff between two constraints: minimizing the policy complexity (cost) and maximizing the expected future reward (gain). We show that this multi-dimensional optimization processes results in an experience-modulated version of the softmax behavioral policy. Thus, as in classical softmax behavioral policies, probability of actions are selected according to their estimated values and the pseudo-temperature, but in addition also vary according to the frequency of previous choices of these actions. We conclude that the computational goal of the basal ganglia is not to maximize cumulative (positive and negative) reward. Rather, the basal ganglia aim at optimization of independent gain and cost functions. Unlike previously suggested single-variable maximization processes, this multi-dimensional optimization process leads naturally to a softmax-like behavioral policy. We suggest that beyond its role in the modulation of the efficacy of the cortico-striatal synapses, dopamine directly affects striatal excitability and thus provides a pseudo-temperature signal that modulates the tradeoff between gain and cost. The resulting experience and dopamine modulated softmax policy can then serve as a theoretical framework to account for the broad range of behaviors and clinical states governed by the basal ganglia and dopamine systems.

Keywords: basal ganglia, dopamine, softmax, reinforcement-learning

INTRODUCTION

Many studies have characterized basal ganglia (BG) activity in terms of reinforcement learning (RL) algorithms (Barto, 1995; Schultz et al., 1997; Bar-Gad et al., 2003b; Gurney et al., 2004; Balleine et al., 2007). Early physiological works revealed that phasic dopamine activity encodes the mismatch between prediction and reality or the RL temporal difference (TD) error signal (Schultz et al., 1997; Dayan and Balleine, 2002; Fiorillo et al., 2003; Satoh et al., 2003; Morris et al., 2004; Nakahara et al., 2004; Bayer and Glimcher, 2005). In accordance with these RL models of the BG network, dopamine has been shown to modulate the efficacy of cortico-striatal transmission (Reynolds et al., 2001; Surmeier et al., 2007; Kreitzer and Malenka, 2008; Pan et al., 2008; Pawlak and Kerr, 2008; Shen et al., 2008). However most RL models of the BG do not explicitly discuss the issue of BG-driven behavioral policy, or the interactions between the acting agent and the environment.

This work adopts the RL actor/critic framework to model the BG networks. We assume that cortical activity represents the state and modulates the activity of the BG input stages – the striatum. Cortico-striatal synaptic efficacy is adjusted by dopamine

modulated Hebbian rules (Reynolds et al., 2001; Reynolds and Wickens, 2002; McClure et al., 2003; Shen et al., 2008). Striatal activity is further shaped in the downstream BG network (e.g., in the external segment of the globus pallidus, GPe). Finally, the activity of the BG output structures (the internal part of the globus pallidus and the substantia nigra pars reticulata; GPi and SNr respectively) modulate activity in the brainstem motor nuclei and thalamo-frontal cortex networks that control ongoing and future actions (Deniau and Chevalier, 1985; Mink, 1996; Hikosaka, 2007). It is assumed that the mapping of the BG activity and action does not change along the BG main axis (from the striatum to the BG output stages) or in the BG target structures. Therefore, the specific or the distributed activity of the striatal neurons and the neurons in the downstream BG structures represents the desired action. Moreover, the excitatory cortical input to the striatum as dictated by the cortical activity and the efficacy of the cortico-striatal synapses represents the specific state-action pair Q-value.

To simplify our BG model, we modeled the BG main axis as the connections from the D2 containing projection neurons of the striatum, through the GPe, to the BG output structures. We

neglected (at this stage) many of the other critical features of the BG networks such as the BG direct pathway structures (direct connections between D1 dopamine receptors containing striatal cells and the GPi/SNr), the subthalamic nucleus (STN) and the reciprocal connections between the GPe and the striatum and the STN. We further assumed that the activity of the BG output structures inhibits their target structures – the thalamus and brainstem motor nuclei (Hikosaka and Wurtz, 1983; Deniau and Chevalier, 1985; Parush et al., 2008); thus the action probability is considered to be inversely proportional to the BG output distributed activity.

Most previous RL models of the BG network assume that the computational goal of the BG is to maximize the (discounted) cumulative sum of a single variable – the reward (pleasure) prediction error. Thus, the omission of reward and aversive events are considered events with negative reward values as compared to the positive values of food/water predicting cues and delivery. However, in many cases the cost of an action is different from a negative gain. We therefore suggest that the emotional dimensions of behavior in animals and humans must be represented by more than a single axis. In the following sections we present a behavioral policy that seeks the optimal tradeoff between maximization of cumulative expected reward and minimization of cost. Here we use policy complexity as the representative of a cost. We assume that agents pay a price for a more complicated behavioral policy, and therefore try to minimize the complexity of their behavioral policy. We simulate the behavior of an agent aiming at multi-dimensional optimization of its behavior while engaged in a decision task similar to the multi-armed bandit problem (Vulkan, 2000; Morris et al., 2006).

Although we used two axes (gain and cost), we obviously do not claim that there are no other, or better, axes that span the emotional space of the animal. For example, arousal, novelty, and minimization of pain could all be functions that the BG network attempts to optimize. Nevertheless, we believe that the demonstration of the much richer repertoire of behavioral policy enabled by the multi-dimensional optimization processes sheds light on the goals and algorithms of the BG network. Future research should enable us to determine the actual computational aim and algorithms of the BG networks.

“MINIMAL COMPLEXITY – MAXIMAL REWARD” BEHAVIORAL POLICY

When an agent is faced with the task of selecting and executing an action, it needs to perform a transformation from a state representing the present and past (internal and external) environment to an action. However, at least two competitive principles guide the agent. On the one hand, it aims to maximize the valuable outcome (cumulative future-discounted reward) of the selected action. On the other hand, the agent is interested in minimizing the cost of its action, for example to act according to a policy with minimal complexity.

The transition from state to action requires knowledge of the state identity. A state identity representation can be thought of as a long vector of letters describing the size, shape, color, smell, and other variables of the objects in the current environment. The longer the vector representing the state, the better is our knowledge of that state. The complexity of the state representation required by a policy reflects the complexity of the policy. Therefore we define policy complexity as the length of the state representation required by that policy. We can estimate the length of the representation of the state identity required by a policy by observing the length of the state that can be extracted on average given the chosen actions. This definition therefore classifies policies that require detailed representations of the state as complex. On the other hand, a policy that does not commit to a specific pair of actions and states, and therefore does not require a lengthy state representation, has low complexity. Formally, we can therefore define the state–action mutual information – $MI(S; A)$ (for a brief review of the concepts of entropy and mutual information – see Box 1) as a measure of policy complexity (see formal details in Appendix 1).

The following example can serve to better understand the notion of representation length and policy complexity. Assume an agent is facing one of four possible states S_1, S_2, S_3, S_4 with equal probability, and using policy A, B, or C chooses one of two possible actions A_1, A_2 . Policy A determines that action A_1 is chosen for all states, policy B chooses the action randomly for all states, and policy C determines that action A_1 is chosen for states S_1, S_2 , and action A_2 is chosen for states S_3, S_4 . In policies A and B determining the action does not require knowledge of the state (and the state can not be extracted given the chosen action), and therefore

BOX 1 | Entropy, mutual information, and uncertainty

The entropy function quantifies in bits the amount of “randomness” or “uncertainty” of a distribution. If $|X| = n$, $x \in X$ is a variable with distribution $p(x)$ ($\sum_{x \in X} p(x) = 1$), then the entropy is defined by: $H(X) = -\sum_{x \in X} p(x) \log_2(p(x))$ (Cover and Thomas, 1991).

The entropy values range from 0 to $\log_2(n)$.

The situation where $H(X) = 0$ is obtained when there is no randomness associated with the variable; i.e., the identity of x is known with full certainty. For example: $p(x = c) = 1$, $p(x \neq c) = 0$.

The situation where $H(X) = \log_2(n)$ is obtained when x is totally random: $p(x) = 1/n$ for all values of x . Intermediate values correspond to intermediate levels of uncertainty.

Entropy quantifies the amount of “uncertainty” when dealing with two variables.

$H(X|Y)$ denotes the entropy of variable $x \in X$ given variable $y \in Y$; i.e., $H(X|Y) = -\sum_{x \in X, y \in Y} p(x, y) \log_2(p(x|y))$. The entropy of a pair of variables is given by $H(X, Y) = H(X) + H(Y|X)$.

The mutual information between two variables can be defined as the number of bits of “uncertainty” of one of the variables reduced by knowledge of the other variable (on average): $MI(X; Y) = H(X) - H(X|Y)$.

The mutual information between two variables can also be defined by the Kullback–Leibler divergence (Dkl) between the actual probability of the pair $X, Y [p(x, y)]$ and the expected probability if the variables were independent [$p(x)p(y)$] (Cover and Thomas, 1991):

$$MI(X; Y) = D_{kl}(p(x, y) || p(x)p(y)) = \sum_{x, y} p(x, y) \log_2 \left(\frac{p(x, y)}{p(x)p(y)} \right).$$

there is no required state representation, and the representation length and policy complexity is 0. By contrast in policy C determining the action does not require full knowledge of the state but only whether the state is S_1, S_2 or S_3, S_4 . Therefore the required state representation only needs to differentiate between two possibilities. This could be done using a codeword of one bit (for example 0 representing S_1, S_2 and 1 representing S_3, S_4). Hence the representation length and policy complexity is 1 bit. As expected, it can be shown that for policies A and B $MI(S; A) = 0$, and for policy C $MI(S; A) = 1$.

The policy complexity is a measure of the policy commitment to the future action given the state (see formal details in Appendix 1). Higher MI values make it possible to classify the action (given a state) with higher resolution. In the extreme high case, the specific action is determined from the state, $MI(S; A) = \log_2$ (number of possible actions), and all the entropy (uncertainty) of the action is eliminated. In the extreme low case $MI(S; A) = 0$, and the chosen action is completely unpredictable from the state.

Combining both expected reward and policy complexity factors produces an optimization problem that aims at minimal commitment to state–action mapping (maximal exploration) while maximizing the future reward. A similar optimization can be found in (Klyubin et al., 2007; Tishby and Polani, 2010). Below we show that the optimization problem introduces a tradeoff parameter β that balances the two optimization goals. Setting a high β value will bias the optimization problem toward maximizing the future reward, while setting a low β value will bias the optimization problem toward minimizing the cost, i.e., the policy complexity.

We solve the optimization problem of minimum complexity – maximum reward by a generalization of the Blahut–Arimoto algorithm for rate distortion problems (Blahut, 1972; Cover and Thomas, 1991, and see Appendix 2 for details). This results in the following equation:

$$\begin{aligned} p(als) &= \frac{p(a)}{Z(s)} e^{\beta Q(s,a)} \\ p(a) &= \sum_s p(als) p(s) \\ Z(s) &= \sum_a p(a) e^{\beta Q(s,a)} \end{aligned} \quad (1)$$

where $p(als)$ is the probability of action a given a state s , or the behavioral policy, $p(a)$ is the overall probability of action a , averaged over all possible states. $Q(s,a)$ is the value of the state–action pairs, and β is the inverse of the pseudo-temperature parameter, or the tradeoff parameter that balances the two optimization goals. Finally, $Z(s)$ is a normalization factor (summed over all possible actions) that limits $p(als)$ to the range of 0–1.

In the RL framework the state–action Q-value is updated as a function of the discrepancy between the predicted Q value and the actual outcome. Thus, when choosing the next step, the behavioral policy influences which of the state–action pairs is updated. In the more general case of an agent interacting with a stochastic environment, the behavioral policy changes the state–action Q-value (expected reward of a state–action pair), which in turn may change

the policy. Thus, another equation concerning the expected reward ($Q(s,a)$ values) should be associated with the previous equations (convergence of value and policy iterations, Sutton and Barto, 1998). However, in our simplified BG model, the policy and Q-value are not changed simultaneously since the Q-value is modified by the cortico-striatal synaptic plasticity, and the policy is modified by the level of dopamine. These two specific modifications may occur through different molecular mechanisms, e.g., D1 activation that affects synaptic plasticity and D2 activation that affects post synaptic excitability (Kerr and Wickens, 2001; Pawlak and Kerr, 2008; but see Shen et al., 2008) and at different timescales (Schultz, 1998; Goto et al., 2007). At this stage of our model, we therefore do not require simultaneous convergence of the expected reward values with the policy.

The behavioral policy $p(a|s) = \frac{p(a)}{Z(s)} e^{\beta Q(s,a)}$ that optimizes the reward/complexity tradeoff resembles the classical RL softmax distribution where the probability of choosing an action is exponentially dependent on the action's expected reward and β – the inverse of the pseudo-temperature parameter (Sutton and Barto, 1998). Here, the probability of choosing an action given a specific state $p(als)$ is exponentially dependent on the state–action Q-value multiplied by the prior probability of choosing the specific action independently of the state – $p(a)$. This prior probability gives the advantage to actions that are chosen more often, and for this reason was dubbed the “experience-modulated softmax policy” here. This is in line with preservation behavior, where selected actions are influenced by the pattern of the agent's past choices (Slovic et al., 1999; Lau and Glimcher, 2005; Rutledge et al., 2009). In cases where the a-priori probability of all actions is equal, the experience-modulated softmax policy is equivalent to the classical softmax policy. Finally, in single state scenarios (i.e., an agent is facing only one state, but still has more than one possible action) where $p(als) = p(a)$, the policy maximizes the expected reward without minimizing the state–action MI. Therefore, $p(a) = 1$ for the action with the highest Q-value.

THE DUAL ROLE OF DOPAMINE IN THE MODEL

Many studies have indicated that dopamine influences BG firing rate properties directly and not only by modulating cortico-striatal synaptic plasticity. Apomorphine (an ultrafast-acting D2 dopamine agonist) has an immediate (<1 min) effect on Parkinsonian patients and on the discharge rate of BG neurons (Stefani et al., 1997; Levy et al., 2001; Nevet et al., 2004). There is no consensus regarding the effect of dopamine on the excitability of striatal neurons (Nicola et al., 2000; Onn et al., 2000; Day et al., 2008), probably since the *in vivo* effect of dopamine on striatal excitability is confounded by the many closed loops inside the striatum (Tepper et al., 2008), and the reciprocal connections with the GPe and the STN. Nevertheless, most researchers concur that high tonic dopamine levels decrease the discharge rate of BG output structures, whereas low levels of tonic dopamine increase the activity of BG output (in rodents: Ruskin et al., 1998; in primates: Fillion et al., 1991; Boraud et al., 1998, 2001; Papa et al., 1999; Heimer et al., 2002; Nevet et al., 2004; and in human patients: Merello et al., 1999; Levy et al., 2001). These findings strongly indicate that tonic dopamine plays a significant role in

shaping behavioral policy beyond a modulation of the efficacy of the cortico-striatal synapses. We suggest that dopamine serves as the inverse of β ; i.e., as the pseudo-temperature, or the tradeoff parameter between policy complexity and expected reward (Eq. 1).

In our model, dopamine thus plays a dual role in the striatum. First, dopamine has a role in updating the Q-values by modulating the efficacy of the cortico-striatal connections, and second, in setting β (the inverse of the pseudo temperature). However, since changing the excitability is faster than modulating synaptic plasticity, dopamine acts at different timescales and the effects of lack or excess of dopamine may appear more rapidly as changes in the softmax pseudo-temperature parameter of the behavioral policy than in the changes in the Q-values.

The following description can provide a possible characterization of the influence of dopamine on the computational physiology of the BG. The baseline activity of the striatal neurons, and by extension of the BG output neurons that represent all actions, is modulated by the tonic levels of striatal dopamine. In addition, striatal neural activity is modulated by the specific state–action value (Q-value), and in turn determines the activity of the BG output neurons which encode a specific probability for each action. High dopamine levels decrease the dynamic range of the Q-value's influence (the baseline activity of the striatal neurons decreases, and consequently the dynamic range of the additional decrease in their discharge is reduced). Therefore different Q-values will result in similar BG output activity, and consequently the action probability will be more uniform. On the other hand, low dopamine levels result in a large dynamic range of striatal discharge, producing a probability distribution that is more closely related to the cortical Q-values preferring higher values. At moderate or normal dopamine levels the probability distribution of future action is dependent on the Q-values.

This behavior is also captured in the specifics of our model. A high amount of dopamine is equivalent to low β values (or a high pseudo temperature), yielding a low state–action MI. This policy resembles gambling, where the probability of choosing an action is not dependent on the state and therefore is not correlated with the outcome prospects. Lowering the amount of dopamine, increasing β , causes an increase in the MI. In this case, the action probability is specifically related to the state–action Q-value preferring higher reward prospects. In the extreme and most conservative case, the policy chooses deterministically the action with the highest reward prospect (greedy behavior).

SIMULATING A PROBABILISTIC TWO-CHOICE TASK

We simulated the behavior of the experience modulated softmax model in a probabilistic two-choice task similar to one used previously in our group (Morris et al., 2006). We only simulated the portion of the task in which there are multiple states in which the subject is expected to choose one of two actions (either move left or right). Intermingled with the trials on the binary decision task are forced choice trials (not discussed here). The different states are characterized by their different (action dependent) reward prospects. Actions can lead to a reward with one of the following probabilities: 25, 50, 75, or 100%. The task states consist of all combinations of the different reward probabilities. The states are distributed uniformly (i.e., all 16 states have equal probability). Note

that since both sides are symmetrically balanced between high and low probabilities, there should be no prior preference for either of the actions (the trials on the forced choice task are also symmetrically balanced). Therefore, there is equal probability of choosing either of the sides ($p(\text{left})=p(\text{right})=0.5$), and the experience-modulated softmax behaves like the regular softmax policy.

Figures 1–4 illustrate the simulation results. **Figure 1** illustrates the expected reward as a function of the state–action MI for different dopamine levels. Since in our model dopamine acts as $1/\beta$, decreasing the dopamine level causes both the state–action MI (complexity of the policy, cost) and the average expected reward (gain) to increase until they reach a plateau. On the other hand, increasing the dopamine level leads to conditions with close to 0 complexity and reward (“no pain, no gain” state).

Figure 2 illustrates, for different dopamine levels, the probability of choosing an action as a function of the expected reward relative to the total sum of expected rewards. At low dopamine levels the expected reward is maximized, and therefore the action with a higher expected reward is always chosen (greedy behavioral policy). At moderate dopamine levels (i.e., simulating normal dopamine conditions) the probability of choosing an action is proportional to its relative expected reward. This is very similar to the results seen in (Morris et al., 2006), and in line with a probability matching action selection policy (Vulkan, 2000) where the probability of choosing an action is proportional to the action's relative expected reward. High dopamine levels yield a random policy, where the probability of choosing an action is not dependent on its expected reward.

A unique feature of the multi-dimensional optimization policy (Eq. 1) is the effect of an *a priori* probability for action (modulation by experience). **Figure 3** illustrates the behavioral policy of an

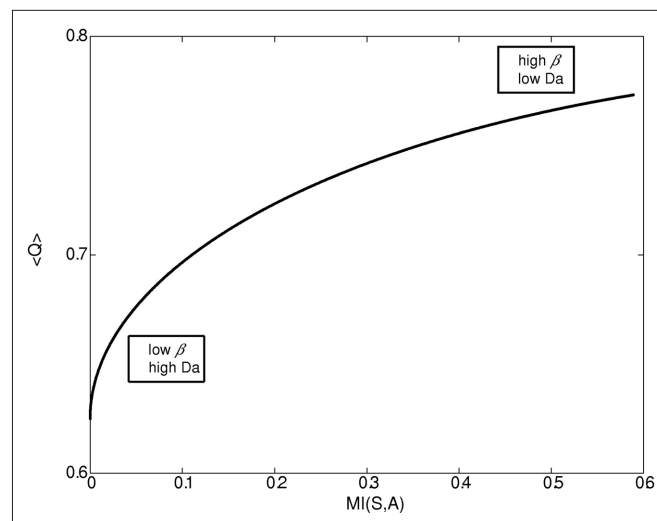


FIGURE 1 | Expected reward as a function of the complexity of the behavioral policy for different β /dopamine levels. High dopamine (Da) or low β (inverse of the softmax pseudo-temperature variable) lead to a simple reward policy, e.g., a random policy with low state–action mutual information ($MI(s,a)$), and low expected reward $\langle Q \rangle$. On the other hand, a low dopamine level leads to a complex (deterministic) policy with high MI and high expected reward. In general, both state–action MI and expected reward $\langle Q \rangle$ increase with beta (though when beta is close to 0, the increase in MI is very slow).

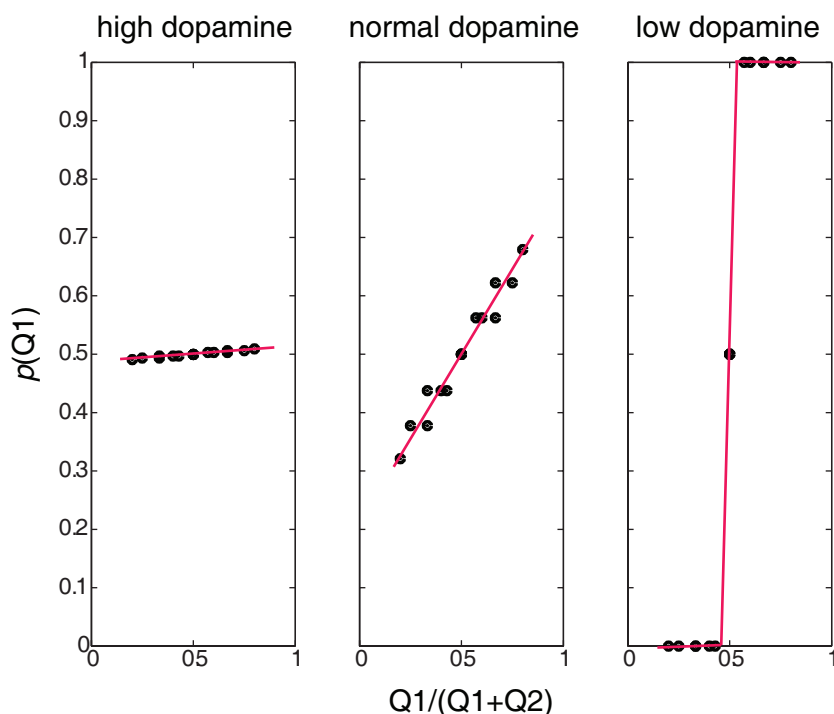


FIGURE 2 | Behavioral policies at different β /dopamine levels.

Probability of choosing Q1 as a function of the ratio between Q1 and (Q1+Q2): high dopamine (low β) – random policy, not dependent on the Q-value, normal (moderate dopamine and β) – policy dependent on the

Q-value (preferring higher values), low dopamine (high β) – deterministic (greedy) policy – choosing the higher Q-values, and the dots represent values calculated in the simulation, and the lines are linear curve fittings of these points.

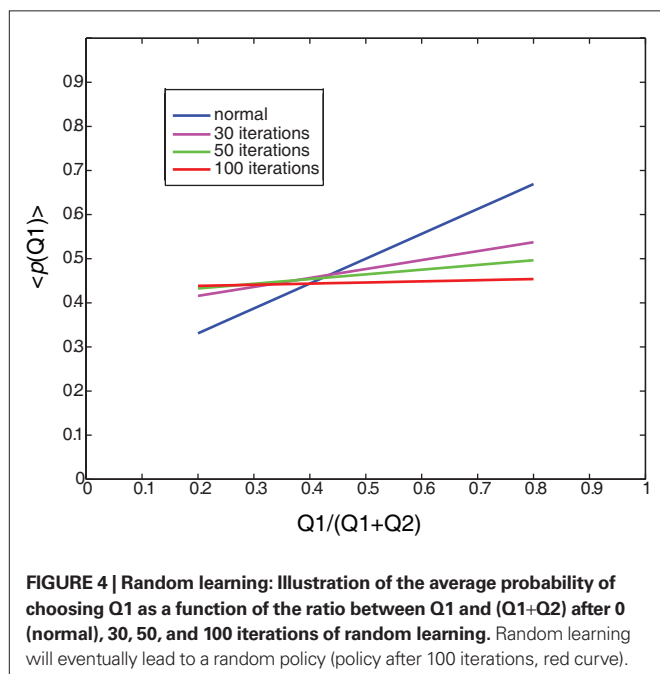
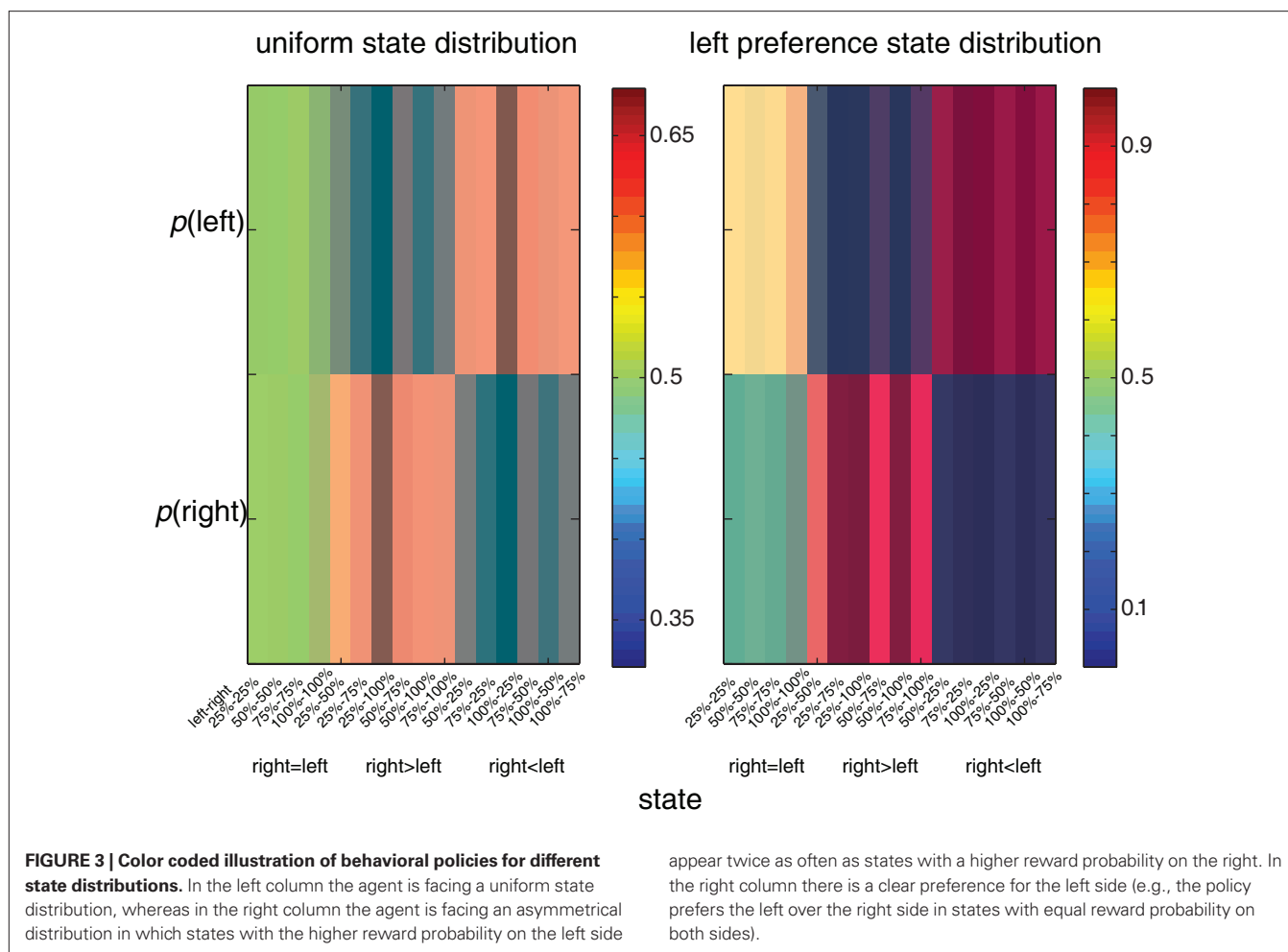
agent with moderate dopamine levels in two scenarios. In the first scenario the agent is facing a uniform state distribution, whereas in the second scenario the agent is facing an asymmetrical distribution in which states with a higher reward probability on the left side appear twice as often as states with a higher reward probability on the right. In the latter distribution there is clear preference for the left side (e.g., the policy prefers the left over the right in states with equal reward probability on both sides). Thus, the history or the prior probability to perform an action influences the action selection policy. **Figure 4** illustrates the expected reward as a function of the state–action MI for both the experience-modulated softmax and the regular softmax policies. As expected, since the experience-modulated softmax policy is driven by minimizing the state–action MI while maximizing the reward, the experience-modulated softmax policy will result in higher expected reward values.

MODELING DOPAMINE RELATED MOVEMENT DISORDERS

Our simulations depict a maximization (greedy) action selection policy for low dopamine levels. However, in practice, an extreme lack of dopamine causes Parkinsonian patients to exhibit akinesia – a lack of movement. Severe akinesia cannot be explained mathematically by our model. The normalization of the softmax equation ensures that the sum of $p(a|s)$ over all a is 1, and for this reason there cannot be a condition where all $p(a|s)$, for all a and all s , are close to 0. We suggest that in these extreme cases the BG neural network does not unequivocally implement the experience-

modulated softmax algorithm. Since the activity of the BG output structures inhibits their target structures, and a lack of dopamine increases the BG output activity, extremely low dopamine levels can result in complete inhibition and therefore total blockage of activity, i.e., akinesia. In these cases an extraordinary high Q-value may momentarily overcome the inhibition and cause paradoxical kinesia (Keefe et al., 1989; Schlesinger et al., 2007; Bonanni et al., 2010).

Another dopamine related movement disorder is levo-3,4-dihydroxyphenylalanine (L-DOPA) induced dyskinesia. Dopamine replacement therapy (DRT) by either L-DOPA or dopamine agonists is the most effective pharmacological treatment for Parkinson's disease. However, almost all patients treated with long term DRT develop dyskinesia – severely disabling involuntary movements. Once these involuntary movements have been established, they will occur on every administration of DRT. Our model provides two possible computational explanations for L-DOPA induced dyskinesia. First, the high levels of dopamine force the system to act according to a random or gambling policy. The second possible cause of dyskinesia is related to the classical role of dopamine in modulating synaptic plasticity and reshaping the cortico-striatal connectivity (Surmeier et al., 2007; Kreitzer and Malenka, 2008; Russo et al., 2010). Thus high (but not appropriate) dopamine levels randomly reinforce state–action pairs. We define this type of random reinforcement as random learning. **Figure 5** illustrates the average action policy caused by random learning over time. Thus, dyskinesia may be avoided



by dopaminergic treatments that do not modulate the cortico-striatal synaptic efficacy (less D1 activation) while maintaining all other D2 therapeutic benefits.

DISCUSSION

In contrast to previous BG models that have concentrated on either explaining pathological behavior (e.g., Albin et al., 1989) or on learning paradigms and action selection (e.g., Schultz et al., 1997; Cohen and Frank, 2009; Wiecki and Frank, 2010), here we attempt to integrate both the phasic and tonic effects of dopamine to account for both normal and pathological behaviors in the same model. We presented a BG related top-down model in which the tonic dopamine level balances maximizing the expected reward and reducing the policy complexity. Our agent aims to maximize the expected reward while minimizing the complexity of the state description, i.e., by preserving the minimal information for reward maximization. This approach is also related to the information bottleneck method (Tishby et al., 1999), where dimensionality reduction aims to reduce the MI between the input and output layers while maximizing the MI between the output layer and a third variable. Hence, the transition from input to output preserves only relevant information. In the current model, the dimension-

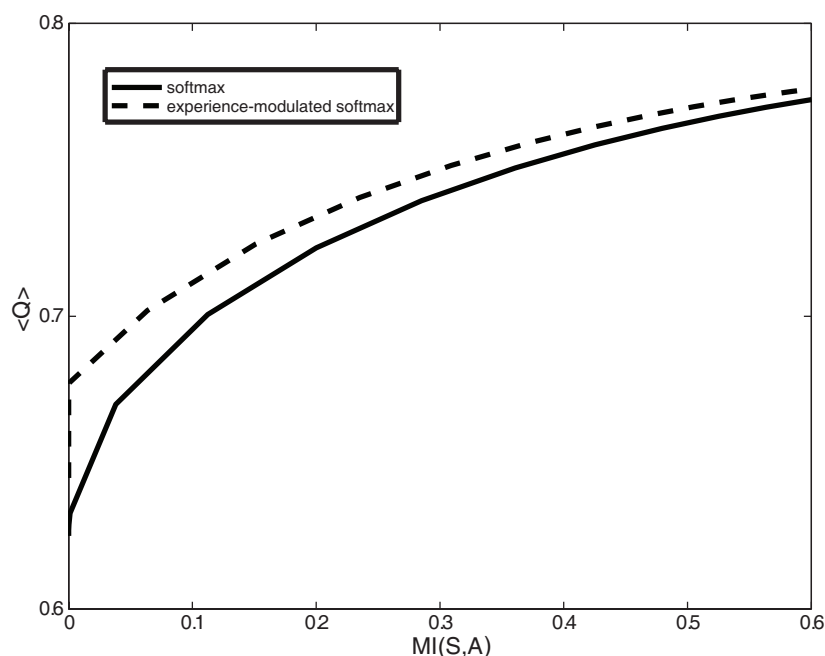


FIGURE 5 | Expected reward ($\langle Q \rangle$) as a function of the complexity of the behavioral policy ($MI(S,A)$) for both the experience-modulated softmax and the regular softmax policies in the case of asymmetrical distribution of states. The agent is facing an asymmetrical distribution in which states with the

higher reward probability on the left side appear twice as often as states with a higher reward probability on the right. In this scenario, for given complexity values, the experience-modulated softmax policy yields a higher expected reward value.

ality reduction from state to action, or at the network level from cortex to BG (Bar-Gad et al., 2003b), preserves relevant information on reward prospects. This dimensionality reduction can also account for the de-correlation issues associated with the BG pathway (Bar-Gad et al., 2003a,b). In addition, the complexity of the representation of the states can be considered as the “cost” of the internal representation of these states. Hence the model solves a minimum cost vs. maximum reward variation problem. This is the first BG model to show that a softmax like policy is not arbitrary selected, but rather is the outcome of the optimization problem solved by the BG.

Like the softmax policy (Sutton and Barto, 1998), our model experience-modulated softmax policy is exponentially dependent on the expected reward. However in this history-modulated distribution, the probability of an action a , given a state s , is also dependent on the prior action probability. In cases where the prior probability uniformly distributes over the different actions, the experience-modulated softmax policy behaves like the regular softmax. Therefore our model can account for softmax and probability matching action selection policies seen in previous studies (Vulkan, 2000; Morris et al., 2006). Furthermore, it would be interesting to confirm these predictions by replicating these or similar experiments while manipulating the prior action statistics (for example as seen in Figure 3).

Changing the dopamine level from low to high shifts the action policy from a conservative (greedy) policy that chooses the highest outcome to a policy that probabilistically chooses the action according to the outcome (probability matching). Eventually, with a very high level of dopamine, the policy will turn into a random

(gambling) policy where the probability of choosing an action is independent of its outcome. This shift in behavioral policy can result from normal or pathological transitions. High dopamine levels can be associated with situations that involve excitement or where the outcome provides high motivation (Satoh et al., 2003; Niv et al., 2006). Pathological lacks or excesses of dopamine also change the policy as is seen in akinetic and dyskinetic states typical of Parkinson’s disease. We suggest that blocking the dopamine treatment effects leading to random learning while preserving the pseudo-temperature effects of the treatment may lead to amelioration of akinesia while avoiding L-DOPA induced dyskinesia.

To conclude, the experience-modulated softmax model provides a new conceptual framework that casts dopamine in the role of setting the action policy on a scale of risky to conservative and normal to pathological behaviors. This model introduces additional dimensions to the problem of optimal behavioral policy. The organism not only aims to satisfy reward maximization but also other objectives. This pattern has been observed in many experiments where behavior is not in line with merely maximizing task return (Talmi et al., 2009). In the future, other objectives can be added to the model as well as other balancing substances. These additional dimensions will introduce richer behavior to the BG model that will more closely resemble real life decisions and perhaps account for other pathological cases as well.

ACKNOWLEDGMENTS

This study was partly supported by the FP7 Select and Act grant (Hagai Bergman) and by the Gatsby Charitable Foundation (Naftali Tishby).

REFERENCES

- Albin, R. L., Young, A. B., and Penney, J. B. (1989). The functional anatomy of basal ganglia disorders. *Trends Neurosci.* 12, 366–375.
- Balleine, B. W., Delgado, M. R., and Hikosaka, O. (2007). The role of the dorsal striatum in reward and decision-making. *J. Neurosci.* 27, 8161–8165.
- Bar-Gad, I., Heimer, G., Ritov, Y., and Bergman, H. (2003a). Functional correlations between neighboring neurons in the primate globus pallidus are weak or nonexistent. *J. Neurosci.* 23, 4012–4016.
- Bar-Gad, I., Morris, G., and Bergman, H. (2003b). Information processing, dimensionality reduction and reinforcement learning in the basal ganglia. *Prog. Neurobiol.* 71, 439–473.
- Barto, A. G. (1995). “Adaptive critics and the basal ganglia,” in *Models of Information Processing in the Basal Ganglia*, eds J. C. Houk, J. L. Davis, and D. G. Beiser (Cambridge: The MIT Press), 215–232.
- Bayer, H. M., and Glimcher, P. W. (2005). Midbrain dopamine neurons encode a quantitative reward prediction error signal. *Neuron* 47, 129–141.
- Blahut, R. E. (1972). Computation of channel capacity and rate distortion function. *IEEE Trans. Inform. Theory* IT 18, 460–473.
- Bonanni, L., Thomas, A., Anzellotti, F., Monaco, D., Cicciocioppo, F., Varanese, S., Bifulchetti, S., D’Amico, M. C., Di Iorio, A., and Onofri, M. (2010). Protracted benefit from paradoxical kinesia in typical and atypical parkinsonisms. *Neurol. Sci.* 31, 751–756.
- Boraud, T., Bezard, E., Bioulac, B., and Gross, C. E. (2001). Dopamine agonist-induced dyskinesias are correlated to both firing pattern and frequency alterations of pallidal neurones in the MPTP-treated monkey. *Brain* 124, 546–557.
- Boraud, T., Bezard, E., Guehl, D., Bioulac, B., and Gross, C. (1998). Effects of L-DOPA on neuronal activity of the globus pallidus externus (GPe) and globus pallidus internus (GPi) in the MPTP-treated monkey. *Brain Res.* 787, 157–160.
- Cohen, M. X., and Frank, M. J. (2009). Neurocomputational models of basal ganglia function in learning, memory and choice. *Behav. Brain Res.* 199, 141–156.
- Cover, T. M., and Thomas, J. A. (1991). *Elements of Information Theory*. Wiley, New York.
- Day, M., Wokosin, D., Plotkin, J. L., Tian, X., and Surmeier, D. J. (2008). Differential excitability and modulation of striatal medium spiny neuron dendrites. *J. Neurosci.* 28, 11603–11614.
- Dayan, P., and Balleine, B. W. (2002). Reward, motivation, and reinforcement learning. *Neuron* 36, 285–298.
- Deniau, J. M., and Chevalier, G. (1985). Disinhibition as a basic process in the expression of striatal functions. II. The striato-nigral influence on thalamo-cortical cells of the ventromedial thalamic nucleus. *Brain Res.* 334, 227–233.
- Filion, M., Tremblay, L., and Bedard, P. J. (1991). Effects of dopamine agonists on the spontaneous activity of globus pallidus neurons in monkeys with MPTP-induced parkinsonism. *Brain Res.* 547, 152–161.
- Fiorillo, C. D., Tobler, P. N., and Schultz, W. (2003). Discrete coding of reward probability and uncertainty by dopamine neurons. *Science* 299, 1898–1902.
- Goto, Y., Otani, S., and Grace, A. A. (2007). The Yin and Yang of dopamine release: a new perspective. *Neuropharmacology* 53, 583–587.
- Gurney, K., Prescott, T. J., Wickens, J. R., and Redgrave, P. (2004). Computational models of the basal ganglia: from robots to membranes. *Trends Neurosci.* 27, 453–459.
- Heimer, G., Bar-Gad, I., Goldberg, J. A., and Bergman, H. (2002). Dopamine replacement therapy reverses abnormal synchronization of pallidal neurons in the 1-methyl-4-phenyl-1,2,3,6-tetrahydropyridine primate model of parkinsonism. *J. Neurosci.* 22, 7850–7855.
- Hikosaka, O. (2007). GABAergic output of the basal ganglia. *Prog. Brain Res.* 160, 209–226.
- Hikosaka, O., and Wurtz, R. H. (1983). Visual and oculomotor functions of monkey substantia nigra pars reticulata. IV. Relation of substantia nigra to superior colliculus. *J. Neurophysiol.* 49, 1285–1301.
- Keefe, K. A., Salamone, J. D., Zigmond, M. J., and Stricker, E. M. (1989). Paradoxical kinesia in parkinsonism is not caused by dopamine release. *Studies animal model. Arch. Neurol.* 46, 1070–1075.
- Kerr, J. N., and Wickens, J. R. (2001). Dopamine D-1/D-5 receptor activation is required for long-term potentiation in the rat neostriatum in vitro. *J. Neurophysiol.* 85, 117–124.
- Klyubin, A. S., Polani, D., and Nehaniv, C. L. (2007). Representations of space and time in the maximization of information flow in the perception-action loop. *Neural Comput.* 19, 2387–2432.
- Kreitzer, A. C., and Malenka, R. C. (2008). Striatal plasticity and basal ganglia circuit function. *Neuron* 60, 543–554.
- Lau, B., and Glimcher, P. W. (2005). Dynamic response-by-response models of matching behavior in rhesus monkeys. *J. Exp. Anal. Behav.* 84, 555–579.
- Levy, R., Dostrovsky, J. O., Lang, A. E., Sime, E., Hutchison, W. D., and Lozano, A. M. (2001). Effects of apomorphine on subthalamic nucleus and globus pallidus internus neurons in patients with Parkinson’s disease. *J. Neurophysiol.* 86, 249–260.
- McClure, S. M., Daw, N. D., and Montague, P. R. (2003). A computational substrate for incentive salience. *Trends Neurosci.* 26, 423–428.
- Merello, M., Balej, J., Delfino, M., Cammarota, A., Betti, O., and Leiguarda, R. (1999). Apomorphine induces changes in GPi spontaneous outflow in patients with Parkinson’s disease. *Mov. Disord.* 14, 45–49.
- Mink, J. W. (1996). The basal ganglia: focused selection and inhibition of competing motor programs. *Prog. Neurobiol.* 50, 381–425.
- Morris, G., Arkadir, D., Nevet, A., Vaadia, E., and Bergman, H. (2004). Coincident but distinct messages of midbrain dopamine and striatal tonically active neurons. *Neuron* 43, 133–143.
- Morris, G., Nevet, A., Arkadir, D., Vaadia, E., and Bergman, H. (2006). Midbrain dopamine neurons encode decisions for future action. *Nat. Neurosci.* 9, 1057–1063.
- Nakahara, H., Itoh, H., Kawagoe, R., Takikawa, Y., and Hikosaka, O. (2004). Dopamine neurons can represent context-dependent prediction error. *Neuron* 41, 269–280.
- Nevet, A., Morris, G., Saban, G., Feinstein, N., and Bergman, H. (2004). Rate of substantia nigra pars reticulata neurons is reduced in non-parkinsonian monkeys with apomorphine-induced orofacial dyskinesia. *J. Neurophysiol.* 92, 1973–1981.
- Nicola, S. M., Surmeier, J., and Malenka, R. C. (2000). Dopaminergic modulation of neuronal excitability in the striatum and nucleus accumbens. *Annu. Rev. Neurosci.* 23, 185–215.
- Niv, Y., Joel, D., and Dayan, P. (2006). A normative perspective on motivation. *Trends Cogn. Sci.* 10, 375–381.
- Onn, S. P., West, A. R., and Grace, A. A. (2000). Dopamine-mediated regulation of striatal neuronal and network interactions. *Trends Neurosci.* 23, S48–S56.
- Pan, W. X., Schmidt, R., Wickens, J. R., and Hyland, B. I. (2008). Tripartite mechanism of extinction suggested by dopamine neuron activity and temporal difference model. *J. Neurosci.* 28, 9619–9631.
- Papa, S. M., DeSimone, R., Fiorani, M., and Oldfield, E. H. (1999). Internal globus pallidus discharge is nearly suppressed during levodopa-induced dyskinesias. *Ann. Neurol.* 46, 732–738.
- Parush, N., Arkadir, D., Nevet, A., Morris, G., Tishby, N., Nelken, I., and Bergman, H. (2008). Encoding by response duration in the basal ganglia. *J. Neurophysiol.* 100, 3244–3252.
- Pawlak, V., and Kerr, J. N. (2008). Dopamine receptor activation is required for corticostriatal spike-timing-dependent plasticity. *J. Neurosci.* 28, 2435–2446.
- Reynolds, J. N., Hyland, B. I., and Wickens, J. R. (2001). A cellular mechanism of reward-related learning. *Nature* 413, 67–70.
- Reynolds, J. N., and Wickens, J. R. (2002). Dopamine-dependent plasticity of corticostriatal synapses. *Neural Netw.* 15, 507–521.
- Ruskin, D. N., Rawji, S. S., and Walters, J. R. (1998). Effects of full D1 dopamine receptor agonists on firing rates in the globus pallidus and substantia nigra pars compacta in vivo: tests for D1 receptor selectivity and comparisons to the partial agonist SKF 38393. *J. Pharmacol. Exp. Ther.* 286, 272–281.
- Russo, S. J., Dietz, D. M., Dumitriu, D., Morrison, J. H., Malenka, R. C., and Nestler, E. J. (2010). The addicted synapse: mechanisms of synaptic and structural plasticity in nucleus accumbens. *Trends Neurosci.* 33, 267–276.
- Rutledge, R. B., Lazzaro, S. C., Lau, B., Myers, C. E., Gluck, M. A., and Glimcher, P. W. (2009). Dopaminergic drugs modulate learning rates and perseveration in Parkinson’s patients in a dynamic foraging task. *J. Neurosci.* 29, 15104–15114.
- Satoh, T., Nakai, S., Sato, T., and Kimura, M. (2003). Correlated coding of motivation and outcome of decision by dopamine neurons. *J. Neurosci.* 23, 9913–9923.
- Schlesinger, I., Erikk, I., and Yarnitsky, D. (2007). Paradoxical kinesia at war. *Mov. Disord.* 22, 2394–2397.
- Schultz, W. (1998). The phasic reward signal of primate dopamine neurons. *Adv. Pharmacol.* 42, 686–690.
- Schultz, W., Dayan, P., and Montague, P. R. (1997). A neural substrate of prediction and reward. *Science* 275, 1593–1599.
- Shannon, C. E. (1959). Coding theorems for a discrete source with a fidelity criterion. *IRE Nat. Conv. Rec.* 4, 142–163.
- Shen, W., Flajolet, M., Greengard, P., and Surmeier, D. J. (2008). Dichotomous dopaminergic control of striatal synaptic plasticity. *Science* 321, 848–851.
- Slovin, H., Abeles, M., Vaadia, E., Haalman, I., Prut, Y., and Bergman, H. (1999).

- Frontal cognitive impairments and saccadic deficits in low-dose MPTP-treated monkeys. *J. Neurophysiol.* 81, 858–874.
- Stefani, A., Stanzione, P., Bassi, A., Mazzone, P., Vangelista, T., and Bernardi, G. (1997). Effects of increasing doses of apomorphine during stereotaxic neurosurgery in Parkinson's disease: clinical score and internal globus pallidus activity. Short communication. *J. Neural. Transm.* 104, 895–904.
- Surmeier, D. J., Ding, J., Day, M., Wang, Z., and Shen, W. (2007). D1 and D2 dopamine-receptor modulation of striatal glutamatergic signaling in striatal medium spiny neurons. *Trends Neurosci.* 30, 228–235.
- Sutton, R. S., and Barto, A. G. (1998). *Reinforcement Learning – An Introduction*. Cambridge, MA: The MIT Press.
- Talmi, D., Dayan, P., Kiebel, S. J., Frith, C. D., and Dolan, R. J. (2009). How humans integrate the prospects of pain and reward during choice. *J. Neurosci.* 29, 14617–14626.
- Tepper, J. M., Wilson, C. J., and Koos, T. (2008). Feedforward and feedback inhibition in neostriatal GABAergic spiny neurons. *Brain Res. Rev.* 58, 272–281.
- Tishby, N., Pereira, F., and Bialek, W. (1999). “The information bottleneck method 9-9-1999,” in *The 37th Annual Allerton Conference on Communication, Control, and Computing*, Allerton.
- Tishby, N., and Polani, D. (2010). “Information theory of decisions and actions,” in *Perception-Reason-Action Cycle: Models, Algorithms and Systems*, eds C. Vassilis, D. Polani, A. Hussain, N. Tishby, and J. G. Taylor (New York: Springer), 601–636.
- Vulkan, N. (2000). An economist's perspective on probability matching. *J. Econ. Surv.* 14, 101–118.
- Wiecki, T. V., and Frank, M. J. (2010). Neurocomputational models of motor and cognitive deficits in Parkinson's disease. *Prog. Brain Res.* 183, 275–297.
- Conflict of Interest Statement:** The authors declare that the research was conducted in the absence of any commercial or financial relationships that could be construed as a potential conflict of interest.

Received: 31 December 2010; paper pending published: 14 February 2011; accepted: 20 April 2011; published online: 09 May 2011.
Citation: Parush N, Tishby N and Bergman H (2011) Dopaminergic balance between reward maximization and policy complexity. *Front. Syst. Neurosci.* 5:22. doi: 10.3389/fnys.2011.00022

Copyright © 2011 Parush, Tishby and Bergman. This is an open-access article subject to a non-exclusive license between the authors and Frontiers Media SA, which permits use, distribution and reproduction in other forums, provided the original authors and source are credited and other Frontiers conditions are complied with.

APPENDIX

FORMAL QUANTIFICATION OF POLICY COMPLEXITY

In this paper policy complexity is defined as the length of the state representation required by the policy; i.e., the length of the representation of the state identity that can be extracted given the chosen action.

A state representation is a codeword that encodes the state, and the representation length is the codeword length. The term “length” refers to the number of letters in the codeword that can uniquely represent the state (distinguish it from all other possible states). Since the codeword should be decoded in a unique way, its length is bounded from below by the minimal uniquely decodable encoding of the state identity that can be extracted from the chosen action. In order to quantify the minimal length we turn to the Kraft–McMillan inequality: source symbols (x) from an alphabet of size d can be encoded into a uniquely decodable code if the codeword lengths $l(x)$ obtain $\sum_{\{x\}} d^{-l(x)} \leq 1$ (Cover and Thomas, 1991).

We denote the average codeword by $L(C) = \sum_{\{x\}} p(x)l(x)$, where $p(x)$ is the probability of source word x , and the entropy of the source is $H_d(X) = -\sum_{\{x\}} p(x)\log_d(p(x))$.

$$\begin{aligned} L(C) - H_d(X) &= \sum_{\{x\}} p(x)l(x) + \sum_{\{x\}} p(x)\log_d(p(x)) \\ &= -\sum_{\{x\}} p(x)\log_d(d^{-l(x)}) + \sum_{\{x\}} p(x)\log_d(p(x)) \\ &= \sum_{\{x\}} p(x)\log_d\left(\frac{p(x)}{d^{-l(x)}}\right) \\ &= \sum_{\{x\}} p(x)\log_d\left(\frac{p(x)/\sum_{\{x'\}} d^{-l(x')}}{d^{-l(x)}/\sum_{\{x'\}} d^{-l(x')}}\right) \\ &= \sum_{\{x\}} p(x)\log_d\left(\frac{p(x)}{d^{-l(x)}/\sum_{\{x'\}} d^{-l(x')}}\right) \\ &\quad - \sum_{\{x\}} p(x)\log_d\left(\sum_{\{x'\}} d^{-l(x')}\right) \\ &= \sum_{\{x\}} p(x)\log_d\left(\frac{p(x)}{d^{-l(x)}/\sum_{\{x'\}} d^{-l(x')}}\right) - \log_d\left(\sum_{\{x'\}} d^{-l(x')}\right) \end{aligned}$$

Let's denote: $c = \sum_{\{x'\}} d^{-l(x')}$, $q(x) = \frac{d^{-l(x)}}{c}$

$$\begin{aligned} L(C) - H_d(X) &= \sum_{\{x\}} p(x)\log_d\left(\frac{p(x)}{q(x)}\right) - \log_d(c) \\ &= D_{kl}(p \parallel q) - \log_d(c) \end{aligned}$$

$D_{kl}(p \parallel q) \geq 0$ (Cover and Thomas, 1991), and $c \leq 1, \log_d(c) \leq 0$ (Kraft McMillan inequality).

Therefore:

$$\begin{aligned} D_{kl}(p \parallel q) - \log_d(c) &\geq 0 \\ L(C) &\geq H_d(X) \end{aligned}$$

Hence the average codeword length is equal or larger than the entropy of the source $H_d(X)$.

The source entropy corresponds to the amount of uncertainty in the distribution of source words X . This uncertainty is resolved once the identity of the source word is known. In our settings the source word is the state representation that can be extracted given the chosen action, and the relevant source entropy is the amount of uncertainty on the state identity that is resolved by knowing the chosen action. $H(S)$ is the original state uncertainty, and $H(S|A)$ is the uncertainty remaining even when the action is given. The difference between these terms is the state uncertainty that is resolved given the chosen action. Therefore in our case the relevant source entropy is $H(S) - H(S|A)$. This term is also known as the state action mutual information $MI(S; A) = H(S) - H(S|A)$. In other words $MI(S; A)$ is a lower bound of the policy state representation length. Consequently minimizing $MI(S; A)$ is equivalent to minimizing the policy state representation length, i.e., minimizing the policy complexity.

In addition we can measure the commitment to the future directly by the mutual information between the current state (denoted by s_t) and the following series of actions and states [denoted by $(a_t, s_{t+1}, \dots, a_{n-1}, s_n)$]:

$$\begin{aligned} MI(s_t; a_t, s_{t+1}, \dots, a_{n-1}, s_n) &= MI(s_t; a_t) + MI(s_t; s_{t+1} | a_t) \\ &\quad + MI(s_t; a_{t+1} | a_t, s_{t+1}) \\ &\quad + \dots + MI(s_t; s_n | a_t, s_{t+1}, \dots, s_{n-1}, a_{n-1}) \end{aligned}$$

[according to the chain rule of information (Cover and Thomas, 1991)]. However, due to the first order Markov property of the series, the transition from state to state depends only on the action chosen according to the previous state. In other words, it is independent of states that are more than one step backward or the order of the states:

$$\begin{aligned} MI(s_t; a_{k-1} | a_t, s_{t+1}, \dots, s_{k-1}) &= MI(s_t; s_k | a_t, s_{t+1}, \dots, a_{k-1}) \\ &= 0, k \neq t+1 \\ &= MI(s_t; A)MI(s_t; a_1, s_2, \dots, a_{n-1}, s_n) \\ &= MI(S; A) + MI(s_t; s_{t+1} | a_t) \end{aligned}$$

where $MI(s_t; s_{t+1} | a_t)$ denotes the mutual information between two adjacent states (state at step t and state at step $t+1$) given the action that generated the transformation between the states. Since this measure is dependent solely on $p(s_t; s_{t+1} | a_t)$, and in our setting is independent of the agent's policy, minimizing $MI(s_t; a_1, s_2, \dots, a_{n-1}, s_n)$ is equivalent to minimizing $MI(S; A)$. Therefore, $MI(S; A)$ (state-action MI) can be used as a measure of policy complexity.

COMBINING MAXIMUM REWARD AND MINIMUM COMPLEXITY GOALS

The optimal tradeoff of achieving the two goals of maximum reward and minimum complexity can be achieved by solving a variation problem similar to rate distortion theory (RDT; Shannon, 1959). In the framework of communication theory, RDT characterizes the tradeoff between the rate, or signal representation size, and the average distortion of the reconstructed signal. It determines the level of the expected distortion, given the desired information rate.

Here we characterize the tradeoff between the state representation size and a function (state action value) dependent on the original state (similar formalizations can be found in (Klyubin et al., 2007; Tishby and Polani, 2010):

$$\min_{p(a|s)} \left\{ \text{MI}(S, A) - \beta \langle Q \rangle + \sum_s \lambda(s) \left(\sum_a p(a|s) - 1 \right) \right\},$$

$$\text{where } \text{MI}(S, A) = \sum_{s,a} p(a|s) p(s) \log_2 \left(\frac{p(a|s)}{p(a)} \right),$$

$$\langle Q \rangle = \sum_{s,a} p(a|s) p(s) Q(s, a),$$

β is the tradeoff parameter (the Lagrange multiplier), and $Q(s, a)$ (the state-action Q-value) denotes the expected reward when performing action a in state s .

The third part of the equation $\sum_s \lambda(s) \left(\sum_a p(a|s) - 1 \right)$ adds the normalization constraint on the total of the distribution of each state to be 1 ($\lambda(s)$ are the normalization Lagrange multipliers for each state s).

The probability of choosing an action a independent of the state is given by:

$$P(a) = \sum_s p(a|s) p(s).$$

The solution to the variation problem:

$$\frac{\partial \left[\text{MI}(S, A) - \beta f(A, S) + \sum_s \lambda(s) \left(\sum_a p(a|s) - 1 \right) \right]}{\partial p(a|s)} = 0$$

$$\begin{aligned} 1. \quad \frac{\partial \text{MI}(S, A)}{\partial p(a|s)} &= \frac{\sum_{s,a} p(a|s) p(s) \log_2 \left(\frac{p(a|s)}{p(a)} \right)}{\partial p(a|s)} \\ &= p(s) \log_2 \left(\frac{p(a|s)}{p(a)} \right) + p(a|s) p(s) \\ &\quad \times \frac{p(a)}{p(a|s)} \frac{p(a) - p(s)p(a|s)}{p(a)^2} \\ &\quad - \sum_{s' \neq s} p(a|s') p(s') \frac{p(a)}{p(a|s')} \frac{(-) p(a|s') p(s)}{p(a)^2} \\ &= p(s) \left[\log_2 \left(\frac{p(a|s)}{p(a)} \right) + 1 - \frac{p(s)p(a|s)}{p(a)} \right. \\ &\quad \left. - \frac{\sum_{s'} p(s') p(a|s')}{p(a)} \right] \\ &= p(s) \left[\log_2 \left(\frac{p(a|s)}{p(a)} \right) + 1 - \frac{\sum_s p(s) p(a|s)}{p(a)} \right] \\ &= p(s) \left[\log_2 \left(\frac{p(a|s)}{p(a)} \right) + 1 - \frac{p(a)}{p(a)} \right] \\ &= p(s) \log_2 \left(\frac{p(a|s)}{p(a)} \right) \end{aligned}$$

$$2. \quad \frac{\partial f(S, A)}{\partial p(a|s)} = \frac{\partial \sum_{s,a} p(a|s) p(s) Q(s, a)}{\partial p(a|s)} = p(s) Q(s, a)$$

$$3. \quad \frac{\partial \sum_s \lambda(s) \left(\sum_a p(a|s) - 1 \right)}{\partial p(a|s)} = \lambda(s)$$

$$4. \quad \frac{\partial \left[\text{MI}(S, A) - \beta f(A, S) + \sum_s \lambda(s) \left(\sum_a p(a|s) - 1 \right) \right]}{\partial p(a|s)} = 0 \Rightarrow$$

$$p(s) \left[\log_2 \left(\frac{p(a|s)}{p(a)} \right) - \beta Q(s, a) + \frac{\lambda(s)}{p(s)} \right] = 0 \Rightarrow$$

$$p(a|s) = p(a) e^{\beta Q(s, a) - \frac{\lambda(s)}{p(s)}}, \sum_a p(a|s) = 1 \Rightarrow$$

$$\sum_a p(a) e^{\beta Q(s, a) - \frac{\lambda(s)}{p(s)}} = 1 \Rightarrow$$

$$e^{-\frac{\lambda(s)}{p(s)}} = \frac{1}{\sum_a p(a) e^{\beta Q(s, a)}} \Rightarrow$$

$$p(a|s) = \frac{p(a) e^{\beta Q(s, a)}}{\sum_{a'} p(a') e^{\beta Q(s, a')}}.$$

The solution can be obtained by a generalization of the Blahut-Arimoto algorithm for rate distortion problems (Blahut, 1972; Cover and Thomas, 1991); namely alternately iterating between the following equations until they converge:

$$p(a|s) = \frac{p(a)}{Z(s)} e^{\beta Q(s, a)}$$

$$p(a) = \sum_s p(a|s) p(s)$$

$$Z(s) = \sum_a p(a) e^{\beta Q(s, a)}$$

Note that using the state expected reward values $V(s)$ instead of the state-action pair expected reward values $Q(s, a)$ yields similar results:

$p(a|s) = \frac{p(a)}{Z(s)} e^{\beta V(s')}$ where s' is the state that follows state s given action a .



Reduced GABA content in the motor thalamus during effective deep brain stimulation of the subthalamic nucleus

Alessandro Stefani^{1,2*}, Ernesto Fedele^{3,4}, Mariangela Pierantozzi², Salvatore Galati⁵, Francesco Marzetti², Antonella Peppe¹, Francesco Saverio Pastore², Giorgio Bernardi^{1,2} and Paolo Stanzione^{1,2}

¹ Istituto di Ricovero e Cura a Carattere Scientifico, Fondazione S. Lucia, Roma, Italy

² Dip. Neuroscienze, Università di Roma Tor Vergata, Roma, Italy

³ Dip. Medicina Sperimentale, Sezione di Farmacologia e Tossicologia, Università degli Studi di Genova, Genoa, Italy

⁴ Centro di Eccellenza per la Ricerca Biomedica, Università degli Studi di Genova, Genoa, Italy

⁵ Neurocenter (EOC) of Southern Switzerland, Lugano, Switzerland

Edited by:

Jose Bargas, National Autonomous University of Mexico, Mexico

Reviewed by:

Gordon Arbuthnott, Okinawa Institute of Science and Technology, Japan
William Hutchison, University Health Network, Canada

*Correspondence:

Alessandro Stefani, Dip Neuroscienze, Univ Tor Vergata, V.le Montpellier, 1 00133 Rome, Italy.
e-mail: stefani@uniroma2.it

Deep brain stimulation (DBS) of the subthalamic nucleus (STN), in Parkinson's disease (PD) patients, is a well established therapeutic option, but its mechanisms of action are only partially known. In our previous study, the clinical transitions from OFF- to ON-state were not correlated with significant changes of GABA content inside GPi or substantia nigra reticulata. Here, biochemical effects of STN-DBS have been assessed in putamen (PUT), internal pallidus (GPi), and inside the antero-ventral thalamus (VA), the key station receiving pallidothalamic fibers. In 10 advanced PD patients undergoing surgery, microdialysis samples were collected before and during STN-DBS. cGMP, an index of glutamatergic transmission, was measured in GPi and PUT by radioimmunoassay, whereas GABA from VA was measured by HPLC. During clinically effective STN-DBS, we found a significant decrease in GABA extracellular concentrations in VA (–30%). Simultaneously, cGMP extracellular concentrations were enhanced in PUT (+200%) and GPi (+481%). These findings support a thalamic dis-inhibition, in turn re-establishing a more physiological corticostriatal transmission, as the source of motor improvement. They indirectly confirm the relevance of patterning (instead of mere changes of excitability) and suggest that a rigid interpretation of the standard model, at least when it indicates the hyperactive indirect pathway as key feature of hypokinetic signs, is unlikely to be correct. Finally, given the demonstration of a key role of VA in inducing clinical relief, locally administration of drugs modulating GABA transmission in thalamic nuclei could become an innovative therapeutic strategy.

Keywords: stereotactic neurosurgery, subthalamus, globus pallidus, antero-ventral thalamus, GABA, glutamate, cGMP, UPDRS

INTRODUCTION

In early 2000s, it was proposed, besides from the traditional neurosurgery performed on a single target for severe Parkinson's disease (PD) patients (commonly the subthalamic nucleus – STN – or the globus pallidus pars interna – GPi) the so-called “multi-target strategy,” consisting of simultaneous and bilateral implantation of multiple basal ganglia (BG) nuclei (Peppe et al., 2004; Stefani et al., 2009). In principle, our genuine purpose was to improve treatment of specific signs of clinical Parkinsonism, for example ensuring a more efficient control of involuntary movements. With this goal in mind, in a cohort of advanced PD patients afflicted by rather disabling dyskinesias, both STN and GPi were implanted bilaterally. As a consequence, it was possible to conclude that GPi-DBS provided efficacious recovery from hypokinesia that was not significantly worse than STN-DBS (Peppe et al., 2004), years before recent comparative investigations (Follett et al., 2010).

However, the simultaneous switch-ON of both targets did not produce higher benefits than each target alone, neither on dyskinesia nor in the management of axial signs. Rather, the clinical indication for that sort of invasive – and costly – “double-targeting” approach tended to become less in time.

Nevertheless, that research line allowed us to study biochemical changes occurring, simultaneously, in GPi as well as in the ventral anterior thalamus (VA), the crucial structure conveying pallidofugal information to cortex, and in putamen (PUT). Indeed, it was possible to measure endogenous amino acids, collectible from extracellular space intra-GPi, intra-VA, and intra-PUT, before and during an efficacious DBS delivery (Fedele et al., 2001; Stefani et al., 2005, 2006; Galati et al., 2006).

At first, at odd with traditional views, the administration of the dopamine agonist apomorphine, although clinically efficacious, failed to modify GABA and glutamate content in GPi. Also 30–40 min STN-DBS (with clinically relevant parameters) barely affected GABA, taurine, aspartate, and glutamate concentrations (Fedele et al., 2001). On the other hand, STN-DBS had promoted the augmentation of the GPi [and substantia nigra pars reticulata (SNr)] cGMP levels (Stefani et al., 2005; Galati et al., 2006). The implicit interpretation of these unexpected findings was that, instead of silencing STN-mediated transmission, DBS might dictate a clustered and increased discharge pattern in SNr. Those data were initially considered paradoxical, since in conflict, at least in part, with findings collected in rodent's disease model. For instance, some

rat studies showed the prevalent inhibition of SNr during STN-DBS (Windels et al., 2003, 2005). These inconsistencies may reveal that the abrupt dopamine depletion by 6-OHDA, possibly for the overwhelming role of fast occurring compensatory mechanisms, is not fit to investigate properly the electrophysiological and chemical features that PD imposes.

If we consider the cGMP increase as an indirect estimation of neuronal activity in GPi during STN-DBS (Fedele and Raiteri, 1999), our findings were in theoretical accord with the STN-DBS-mediated excitation and clustering of the GPi firing pattern as observed in MPTP primates (Hashimoto et al., 2003).

Yet, the relevance of the cGMP finding, *per se*, was uncertain; after all, it depends on an acute change of the NMDA-NO endogenous transmission (notoriously impaired in extrapyramidal disorders, but not exactly a routine therapeutic target!).

Is it feasible that similar changes in cGMP levels are really correlated with consistent clinical amelioration in every PD patient?

How could we further deepen our knowledge on the biochemical counterparts of the OFF–ON behavioral transitions?

Do the observed changes in the first output stations (GPi/SNr) affect the motor thalamus, the crucial structure conveying motor information to cortex?

How STN-DBS influence intra thalamic GABA and, in turn, corticostriatal transmission?

Therefore, we investigated the extracellular GABA concentration in VA during the first delivery of STN-DBS ($n = 10$), at clinically relevant or null voltage. Simultaneously, in the same PD patients, the cGMP level was measured in GPi ($n = 10$) and PUT ($n = 6$).

In synthesis, our results will show that DBS reversibly reduces (–30%) VA GABA levels, increases cGMP levels in GPi and also significantly increases cGMP concentration in PUT, as far as the clinical transition to ON-state takes place.

Our findings sound in accord with the growing body of evidence refreshing and reforming the standard model of BG circuitry. The dogma about an hyperactive indirect pathway as a crucial hallmark of Parkinsonian hypokinetic signs, for instance, has been revisited since the relief from akinesia and rigidity occurs in the absence of reduced GPi excitability and changes of GPi GABA levels. However, clinical “ON-state” requires a rapid change in thalamic GABA content, as here described. Therefore, these results confirm, in line with older models, that VA is the core clinical player in determining thalamocortical transmission.

PATIENTS AND METHODS

Ten advanced PD patients (mean age = 57.6 ± 9.2 years; mean UPDRS score in OFF = 47.7 ± 8.1 ; mean disease duration = 11 ± 3.1 years) were included in this study according to selection criteria previously reported (Fedele et al., 2001; Stefani et al., 2006). Stimulating permanent electrodes were implanted in both the STN and the GPi, bilaterally. For trajectory details, and implantation procedures, see Figure 1 legend and References (Fedele et al., 2001; Stefani et al., 2005, 2006). Written, informed consent was obtained from each patient. The Local Ethics Committee approved the protocol and consent form describing the risks and potential benefits of the study. At time for surgery, every patient was under washout (at least overnight withdrawal from L-DOPA and 3-day suspension of dopamine-agonists).

Probes were infused with sterile PBS (5 $\mu\text{L}/\text{min}$) for stabilization (90 min). Then, basal microdialysis samples (50 μL each) and clinical data were collected for 50 min. Afterward, STN-DBS was switched on for 60 min ($n = 10$ patients, Table 1 and Figure 2). Stimulation parameters were: 90 μs , 130 Hz and mean 2.4 V (but see Figure 1 legend). After 60 min DBS, 60 min of recovery were performed. All procedures were without additional risks for the patient, since guide tubes for micro-recordings were already placed in each target (STN and GPi).

Clinical changes were assessed utilizing selected items of UPDRS (rigidity 0–4, finger tapping 0–4, hand movement 0–4; total = 0 corresponds to “normal,” 12 maximum score) by a neurologist blind to the stimulus intensity between 0 and 3 V. GABA and cGMP were determined by HPLC and by RIA, respectively.

Significance of GABA and cGMP changes was assessed by comparing the mean of the concentrations obtained in the single fractions under basal conditions with those during STN-DBS and during recovery conditions. Mean values were compared by ANOVA two way (first main factor: treatment with three levels: basal, treatment, recovery; second main factor: time with six levels) corrected by Greenhouse–Geisser correction and followed by *post hoc* Scheffé test to assess the significance of the differences between single fractions. Given the not demonstrated normality of biochemical data the results were also confirmed by non-parametric Friedman ANOVA followed by Wilcoxon as *post hoc* test. Clinical scores were compared using similar non-parametric methods. Correlation were studied between the maximal changes induced by DBS in the GABA and cGMP concentrations (Pearson parametric correlations) and clinical score (non-parametric Spearman correlations). The changes were evaluated as the maximum change of each of these parameters in comparison to their mean basal score.

RESULTS

CLINICAL EFFECT OF DBS

For all the fore-coming biochemical results during STN-DBS, consider that they correlate with a significant change of UPDRS (at least 30% amelioration of main examined motor features). To note, *post hoc* Wilcoxon test showed a significant UPDRS score amelioration from the first 10 min of DBS in comparison to all the basal score. Only in case of PUT cGMP, the statistical data comparing biochemical and clinical scores did not reach significance (but because of the small sample).

GPi cGMP

Deep brain stimulation produced a clear cut increase of cGMP levels (Table 1, Figure 2; average +606.2%, ANOVA main effect $df = 2/18$; $\epsilon = 0.515$; $df = 1.03/9.28$; $F = 20.56$, $p = 0.00002$). *Post hoc* Scheffé test showed: basal vs DBS $p = 0.000047$; DBS vs recovery $p = 0.000489$. Friedman ANOVA followed by Wilcoxon confirmed these significances.

To note, the quantification of intra-GPi GABA, in this series of patients, was not performed since already investigated in our seminal paper (Fedele et al., 2001); to mention, no significant change of GPi GABA was observed even following prolonged and clinically effective stimulation periods.

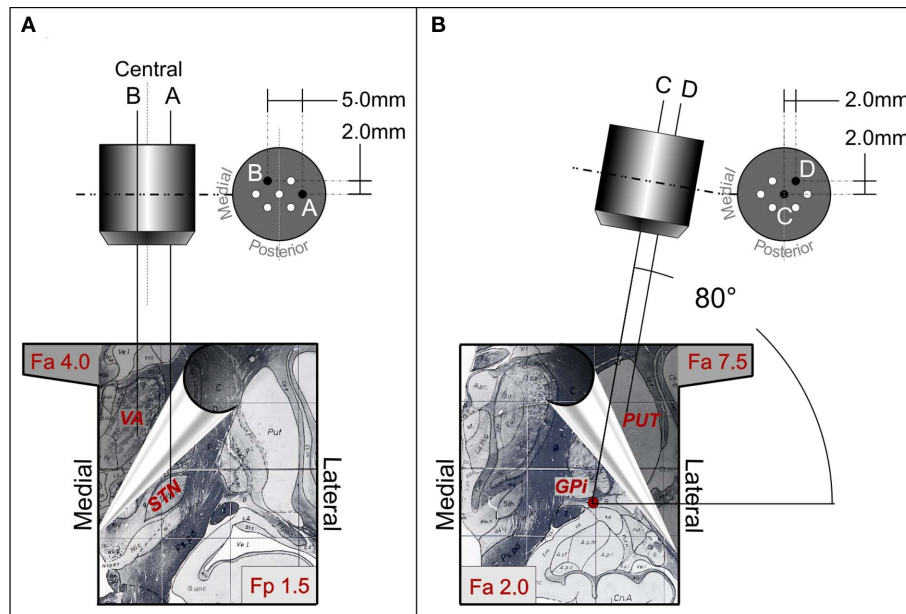


FIGURE 1 | Trajectories of the multi-electrodes-probes holders aimed at the STN-VA (A) and at the PUT-GPI (B). Each section shows representative diagrams of the utilized multi-electrode holder (top) and, at the bottom, two different partially superimposed sections of atlas (note the hand leaving the superior section). The left bottom panel shows coronal atlas section at 1.5 mm posterior to the inter-commissural midline (Fp 1.5, STN target) and at 4 mm anterior to the inter-commissural midline (Fa 4.0 VA target). The right bottom panel illustrates coronal atlas section at 2 mm anterior to the inter-commissural midline (Fa 2.0 GPI target) and at 7.5 mm anterior to the inter-commissural midline (Fa 7.5 PUT target). To reach STN passing through the VA, the central electrode of the multi-electrode holder (A) was aimed at a target at 8.5 mm of laterality, -4 mm with respect to the AC-PC line, and at the mid point of the AC-PC line. The trajectory had an angle of 70° – 75° in sagittal plane and of 85° – 90° in the coronal plane. The more lateral electrode of the multi-electrode holder [electrode A in (A)] was at 3.5 mm of laterality from the central one. This laterality allowed to reach a target at 12.0 mm of laterality from the mid line, which is the usual location of the STN target. On the contrary, the electrode B

trajectory was 1.5 mm more medial than the central one and 2 mm more anterior. The probe membrane (4 mm length) was positioned between 11.0 and 7.0 mm above the target ($+7$ to $+3$ mm above the inter-commissural plane), along the trajectory of electrode B. Given the angle in the sagittal planes (70° – 75°), the trajectory had a laterality of 7.0 mm and, at the level of $+7$ to $+3$ mm above the inter-commissural plane, its antero-posterior position was between $+6.0$ and $+4.0$ mm with respect to the midpoint of the inter-commissural line, corresponding to the center of VA. After electrophysiological identification of the targets, the recording electrode in the GPI was replaced by a microdialysis probe [trajectory C in (B)]. A second probe was positioned in trajectory D, at the level of PUT [D in (B)], utilizing the antero-lateral hole of the multi-electrode holder according to the coronal angle used. Probe membrane was positioned at a laterality between 22.5 and 25.0 mm, a depth of $+9.0$ with respect to the inter-commissural plane, and between $+4.8$ and $+7.5$ mm anterior to the midpoint of the inter-commissural line. Probes and stimulating electrode real positions were verified during surgery by X-ray in antero-posterior and latero-lateral projection.

MOTOR THALAMUS GABA

STN-DBS produced a significant decrease in GABA level during stimulation (Table 1, Figure 2; average -31.1% ; ANOVA main effect $df = 2/18$; $\epsilon = 0.784$; $df = 1.56/14.11$, $F = 11.83$, $p = 0.000523$; 0.0016 Greenhouse–Geisser correction). *Post hoc* Scheffé test showed: basal vs DBS $p = 0.000783$; DBS vs recovery $p = 0.00413$. Friedman ANOVA followed by Wilcoxon confirmed these levels of significance.

PUTAMEN cGMP

DBS produced a clear cut increase of PUT cGMP ($n = 6$), as already partially described (Stefani et al., 2006). The average increase was 220%; the mean value was significantly higher (Wilcoxon test, $Z = 2.52$, $p < 0.05$) than the mean basal and recovery. In each patient, the rise of PUT cGMP was clear from the section following DBS-ON (Figure 2).

DISCUSSION

In the classical BG model (Albin et al., 1989; DeLong, 1990), PD akinesia results from an imbalance between indirect and direct pathways and correlates with an overactivity of the STN and the GPI.

Since the early nineties, the similar efficacy promoted by STN-DBS and subthalamotomy suggested that high-frequency stimulation acted through a sort of functional ablation. The so-called “suppression hypothesis” (Benazzouz et al., 2000; Filali et al., 2004) insisted on firing silencing as the major DBS mechanism of action. Whilst such hypothesis gained credit *inside* STN (Filali et al., 2004), since each stimulus was in fact followed by a no-spiking time window, it was abundantly challenged by evidence collected in target stations (GPI/SNr) in primates and humans (see later).

To further complicate this issue, studies performed in rodent’s models of PD have shown quite conflicting data. Some groups have described a prevalent inhibition of SNr during STN-DBS, through GABA release eventually from GP, utilizing stimulation period abundantly sufficient to induce behavioral changes (up to 1 h, Windels et al., 2003, 2005). Others, by means of multi-channel recordings in freely moving rats described the prevalence of a mixed response (“nearly equal numbers of excitatory and inhibitory responses were found in the GP and SNr”) and a relevant decrease of burst firing (Shi et al., 2006).

Table 1 | The table synthesizes the more relevant data detected by microdialysis samples during efficacious STN-DBS.

	Basal	STN-DBS	Recovery
cGMP-GPi (fmol/50 μ L, $n = 10$)			
Mean	1.6	9.7	3.1
SD	0.5	5.7	1.6
GABA-VA (pmol/50 μ L, $n = 6$)			
Mean	4.5	3.1	4.2
SD	0.5	0.8	0.9
cGMP-PUT (fmol/50 μ L, $n = 6$)			
Mean	1.45	3.2	1.8
SD	0.1	1.3	0.3
UPDRS section III (selected items)			
Mean	8.4	5.5	8.2
SD	1.0	1.4	0.9

In humans and non-human primates (NHP), we and others have documented that the clinical benefit may parallel an increased – and not decreased – GPi and SNr discharge rate and, more importantly, a dramatic modulation of their pattern of activity (Hashimoto et al., 2003; Galati et al., 2006). Accordingly, as detailed since our pioneering papers in the GPi of PD patients, DBS failed to affect amino acids levels (no GABA decrease, in particular, Fedele et al., 2001) but caused a large increment of the cGMP title (Stefani et al., 2005).

Whereas the negligible modification of glutamate could be attributable to lack of sensitivity of the technique, the lack of GABA concentration change suggests that a strong dampening of excitability (in GPi/SNr) is not likely to occur during clinically relevant STN-DBS (whilst it is the rule under apomorphine! i.e., Stefani et al., 1997, 1999).

Investigations performed in MPTP-treated primates sound more in agreement with our central hypotheses. The GPi neuronal activity recorded during efficacious STN-DBS is indeed more regular, being time locked to the stimulus pulse, and had less bursting activity (Hashimoto et al., 2003; Hahn et al., 2008).

The mismatch between 6-OHDA rodents and humans is puzzling but highlights once more that the abrupt dopamine denervation induced by standard 6-OHDA intoxication – weeks/months, in rats – is not fully appropriate for human PD. This may reflect the overwhelming role played by some compensatory mechanisms in the non-human models, at replicating most changes of the progressively developing disease in humans. By taking into account data collected in human and non-human primates, it is reasonable to speculate that some features of the standard model, if centered on the putative hyperactivity of GPi/SNr as key factor underlying Parkinsonian OFF-state, are wrong.

At least three recent observations modify further our perception of BG functional circuitry. First, Brown and colleagues showed abundant evidence for the behavioral role of specific band frequencies (i.e., alpha rhythms for attention, beta for motor performance) linking cortex, STN and GPi. Even “acute” dopamine denervation (our TTX-mediated inactivation of the medial fore-brain bundle, Galati et al., 2009, 2010) potentiated a synchronized low frequency discharge coupling STN-GPi to cortex. This pathological synergy between cortex and BG, in our hands, was

suppressed by direct modulation of STN firing discharge by the gabamimetic muscimol and replicated by intra-GP injection of the D2-antagonist haloperidol. Overall, these findings reinforce the idea that fast motor commands are transferred through the hyper-direct pathway, alongside or in combination with changes of striatofugal networks.

Second, experiments performed with optogenetics supported the relevant role sub-served by cortico-STN pathway, if, as Gradinaru suggested, behaviorally effective high-frequency DBS was associated with a clear activation of axons impinging STN neurons.

Third, a renewed interest in non-cortical excitatory inputs to striatum (that is, thalamic outputs impinging on cholinergic interneurons) forces us to consider the possibility that the thalamo-putaminal-pallidal loop plays a relevant role, as far as salient stimuli may perturb motor planning.

Overall, these considerations suggest that over-emphasis on fine details of circuitry may obscure a bigger picture.

The decrease of GABA concentration inside the motor thalamus (VA), during effective STN-DBS, reconciles with some aspects of the old model of BG function (Albin et al., 1989; DeLong, 1990). The GABA levels’ reduction, in VA, would dis-inhibit VA firing activity and possibly influence its patterning; reduced bursting and/or suppressed oscillatory activity are the most likely results, as already inferred (Guo et al., 2008). The precise firing properties of human VA/VL during effective STN-DBS are unknown (but see Kempf et al., 2009) and we did not perform multiple recording traces in human PD VA on ethical grounds, since the latter is not a target of stimulation in PD (whilst appropriate in some pharmaco-resistant epileptic patients, Hodaie et al., 2006). However, previous studies may help the interpretation.

On one hand, GPi-DBS reduced VA/VL firing activity in *normal monkeys* (Anderson et al., 2003); on the other, Vitek described a mixed response in MPTP-intoxicated primates. Although the “lack of a significant reduction in the mean rate of discharge” was attributed to the early DBS-induced brisk excitation peak, there is no doubt that the “the most relevant changes due to effective DBS-STN was a dramatic modification of the PSTH, hence of patterning,” characterized by “reduced bursting and more regular spike trains in thalamus” (Xu et al., 2008). Similarly, the Rubin and Terman (2004) model emphasized that STN-DBS, in order to be beneficial, induced clustered firing patterns in GPi, whose clear consequence is a regularization of VA discharge (more tonic, no pausing; see **Figure 3**).

As pointed out by Guo, STN-DBS altered Parkinsonian GPi activity in a way that may improve thalamocortical relay fidelity (Rubin and Terman, 2004; Guo et al., 2008). In this context, the reduced GABA levels that we observed would impede prolonged post-spiking after hyper-polarization, and favors a more regular pattern of neuronal activity (in striking contrast with the GABAergic and dopaminergic modulation of delta waves in reticular nuclei, i.e., Urbano et al., 2009).

The VA/VL nuclei complex represents the crucial link between BG outputs and specific cortical areas (Blandini et al., 2000; Obeso et al., 2008). Therefore, once VA-VL is modulated by STN-DBS (as a consequence of reduced GABA release), immediate changes in thalamocortical transmission would occur. Imaging studies have demonstrated a re-activation of fronto-temporo-parietal cortex at

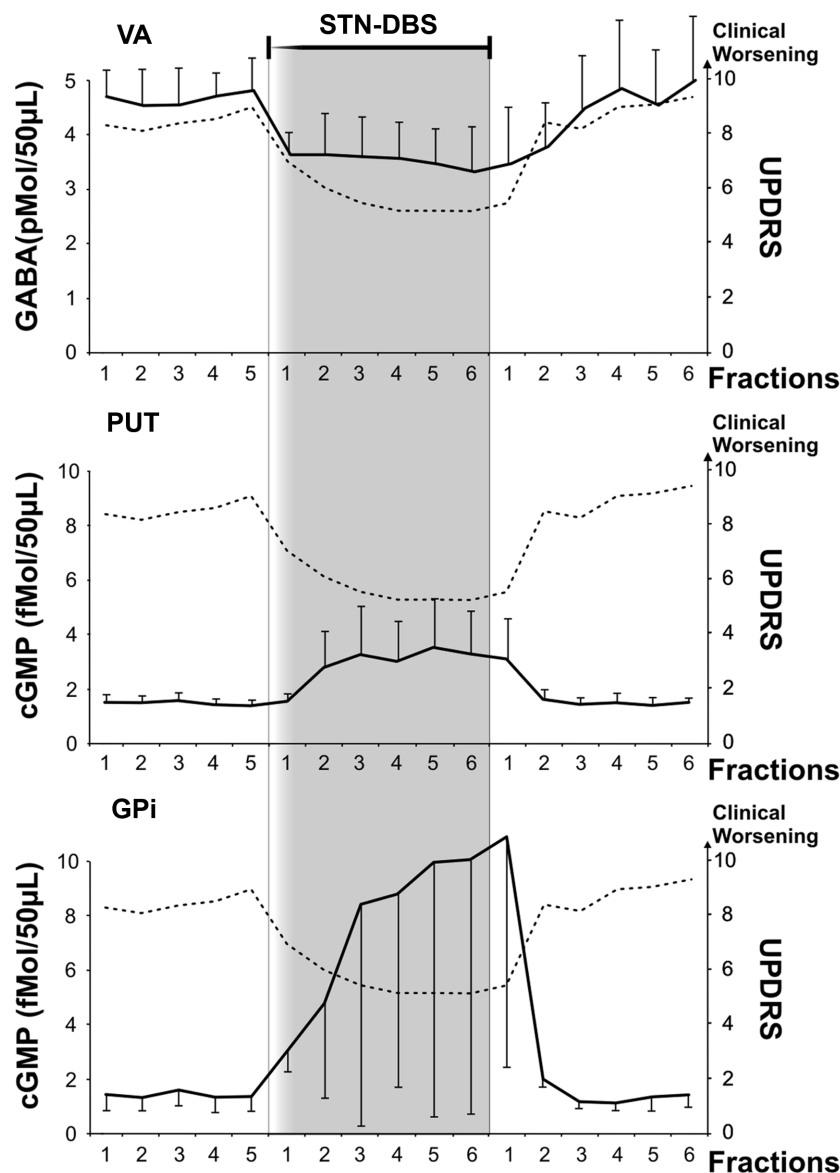
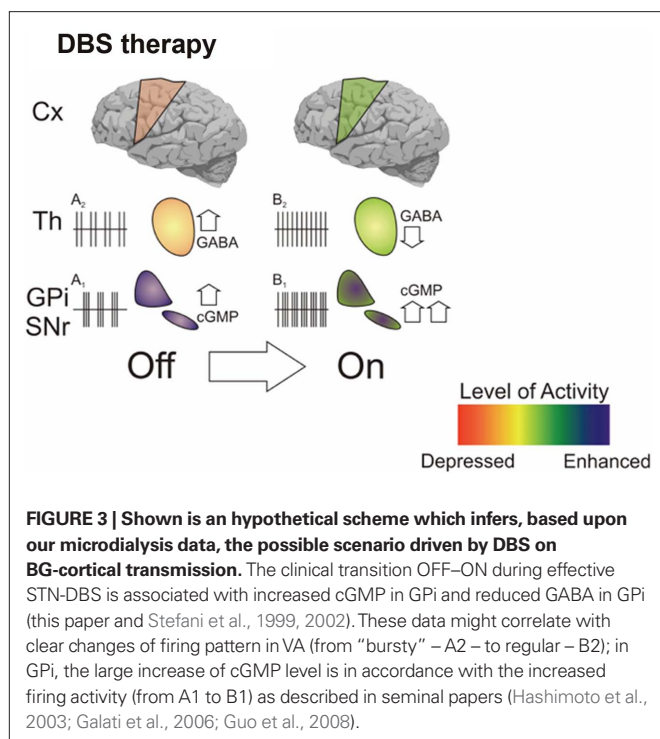


FIGURE 2 | Microdialysis data from VA, PUT and GPi and clinical evaluation before, during and after STN-DBS. Microdialysis probes were infused (5 µl/min) for stabilization (90 min). During stabilization, the permanent stimulating electrode (Medtronic mod 3389) was implanted in ipsilateral STN. Following STN electrode insertion and probe stabilization, collection of 10-min fraction samples (50 µl each) started. The first five fractions of each probe were utilized for basal evaluation either for GABA (VA probe, scale on the left y axis in pMol/50 µl) or for cGMP (PUT and GPi probes, scale on the left y axis in fMol/50 µl). Basal values are in the white area at the left of the shaded area. Values represent mean \pm SD. After Medtronic mod 3389 electrode implantation, monopolar STN-DBS was then switched on by a Medtronic external device Model 3625 at a rate between 130 and 160 Hz, anodal pulse of 60–90 µs, and voltage progressively increased by steps of 0.1 V up to the appearance of side effects (paresthesia or dystonia or myoclonus). Voltage was never above 3.0 V. Voltage stimulation was then decreased by 10% or more to obtain disappearance of clinical side effects.

Clinical assessment started with microdialysis basal fraction collection. Clinical changes, contra lateral upper limb rigidity and akinesia were continuously assessed by an expert neurologist utilizing selected items of UPDRS (rigidity 0–4, finger tapping 0–4, hand movement 0–4; total = 0 corresponds to “normal,” 12 maximum score; scale on the right y axis in each frame), while remaining blind to the stimulus intensity between 0 and 3 V. The patient was unaware of the time of stimulus ON. In all the reported patients, an improvement of the sum of rigidity and akinesia of the upper contralateral arm of more than 30% was achieved without side effects within the first 10 min of stimulation at an intensity ranging between 2 and 3 V, while the first fraction during stimulation was collected. STN-DBS intensity was kept constant thereafter and 10-min fractions were collected during 1 h of stimulation while clinical efficacy was continuously monitored to ensure persistence of the clinical effects. Clinical scores and biochemical parameters are reported every 10 min. After 1 h, STN-DBS was discontinued and 10-min fractions were collected for one additional hour.

rest after effective STN-DBS (Hilker et al., 2004, but see Hershey et al., 2003). Even in case STN-DBS apparently decreased rCBF in the motor cortex at rest – implying a reduction of abnormal

overactivity in the motor system – this allowed selective cortical re-activation during active movement (Limousin et al., 1997; Payoux et al., 2004).



The two main effects induced by STN-DBS, as here described (increased cGMP in GPi and lower GABA in VA) seem in conflict each other, but do not necessarily correlate. STN-DBS indeed reverberate on multiple sites, including VTA and PPN extended area (Stefani et al., 2007), which in turn affect ascending pathways toward thalamus. In other words, the proteiform response to DBS on distant structures might overcome the strict boundaries of the direct/indirect pathway scheme.

Besides, the data concerning the DBS-mediated increase, inside PUT, of cGMP appear, in this context, as a further confirmation of the reinstalled physiological BG-cortex and cortico-BG transmission (otherwise impaired by PD OFF-state).

FUNCTIONAL IMPLICATIONS

We are showing a consistent, DBS-mediated GABA decline in the motor thalamus, which may associate with simultaneous increase of GPi and PUT cGMP.

A number of investigations from multiple disciplines are supporting the hypothesis that stimulation-induced modulation of pathological network activity represents the most likely mechanism of DBS (Brown, 2003). However, successful theories founded on the rebalancing of beta/gamma band frequencies should not discard, in agreement with recent conclusions by Johnson, Vitek, and McIntyre (“DBS improves Parkinsonian motor symptoms by inducing global changes in firing pattern and rate along the pallidothalamocortical sensorimotor circuit,” Johnson et al., 2009), the central result of this report, that the motor thalamus is the critical station where efficacious re-modulation (electrical or chemical) of pathological outputs promotes good therapeutic outcomes.

So far, several considerations have limited the utilization of microdialysis in the surgery room; it represents a time-consuming approach, and ethical observations demand not to stress any patient if an immediate benefit is not perceived. Second, the “double-target” strategy has lost many fans, nowadays, making unlikely the simultaneous insertion of multiple electrodes in different BG stations. In other words, very few groups are still advocating these methods (but see Kilpatrick et al., 2010).

Yet, as we have tried to present in this paper, microdialysis had the profound merit to clarify the limitations of a dogmatic box and arrow cartoon scheme on BG circuitry, if merely intended as a simplistic balancing between overactive structures of the indirect pathway and facilitating structures governing the direct pathway. In this content, **Figure 3** aims at presenting, albeit speculatively, findings derived from our last decade studies, again illustrating the importance to match functional recordings with alterations of endogenous transmitters.

In the next future, it is likely that newly developing approaches, centered on functional biochemistry, will be applied to PD patients. In particular, new electrochemical techniques, including fast-scan cyclic voltammetry (FSCV; Agnesi et al., 2009), should allow to detect changes that are happening on a second-to-second time scale (also feasible for chronically used implanted recordings, as would be required for DBS feedback).

As a matter of fact, the Wireless Instantaneous Neurochemical Concentration Sensor (WINCS) is currently a research device, whose resolution was established on pig brain, but it is designed for human use and is capable of *in vivo* FSCV plus amperometry, sampling at sub-second time resolution (Agnesi et al., 2009; Van Gompel et al., 2010). It promises, for instance, to assess if and to what extent effective STN-DBS is actually changing the tonic/phasic release of endogenous dopamine in human caudate/putamen (Covey and Garriss, 2009; Van Gompel et al., 2010).

Overall, the implementation of these techniques will represent a real upgrade of our understanding of STN-DBS mechanisms of actions and, more critically, of our knowledge around the acute processes which rule clinical transitions in different extrapyramidal disorders.

CONCLUSION

Much recent literature has attempted to explain the mechanisms of action of DBS. Using optogenetic techniques, Gradinaru et al. (2009) have suggested that the more critical behaviorally related change promoted by high-frequency STN stimulation, in 6-OHDA rodents, is the direct activation of cortical axons to STN. This may stimulate new interest into DBS-mediated modulation of corticofugal pathways (i.e., the increase of putaminal cGMP that we have described), as inferred in early 2000s (Ashby et al., 2001).

On the other hand, in a brain slice preparation thalamostriatal axons exerted a marked modulation of firing in striatal cholinergic interneurons (in response to salient stimuli; Ding et al., 2010). This pathway would affect cortical input to medium spiny neuron (MSN), enhancing the postsynaptic responsiveness of striatopallidal MSNs, which strongly influence motor programming. This suggests that interpretation of the BG circuitry in terms of

strict boundaries between direct and indirect pathways (limited to local, STN–pallidal interactions) is obsolete and must include a re-evaluation of thalamostriatal inputs.

That said, immediate transfer to the clinical practice is not easy. Cortical stimulation still retains some devotees, but is questionable as a first-line choice for treating movement disorders. Thalamic DBS regained interest through our small patient's series (Stefani et al., 2009), but is far from a consolidated target.

Overall, these considerations highlight once more the gap between rodent modeling and human disease. In humans, adaptive and compensatory mechanisms are far from well established, hence not easily replicable.

The microdialysis study presented here brings us back to solid data. We demonstrate that, whatever is the final modulation in cortex (1) GABA decline in the motor thalamus is central for the

clinical amelioration but (2) that the latter may associate (under DBS) or not (under LD, Stefani et al., 2011) with changes of GPI cGMP (a marker of STN–pallidal excitability). In other words, the modulation of VA GABA, clearly relevant for clinical score, occurs despite on-going changes of pallidal discharge.

As a parsimonious explanation, during LD-mediated clinical amelioration, pathways other than the pallidothalamic, but still affecting VA, indeed contribute to the rebalancing of the thalamocortical output. During STN-DBS, the reduction in VA GABA content derives from complex mechanisms, including selective activation of small pallidothalamic fibers or direct modulation of pallidal neuropil.

ACKNOWLEDGMENTS

This work has been supported by Ministero della Salute Grants to Paolo Stanzione and Alessandro Stefani.

REFERENCES

- Agnesi, F., Tye, S. J., Bledsoe, J. M., Griessenauer, C. J., Kimble, C. J., Sieck, G. C., Bennet, K. E., Garris, P. A., Blaha, C. D., and Lee, K. H. (2009). Wireless instantaneous neurotransmitter concentration system-based amperometric detection of dopamine, adenosine, and glutamate for intraoperative neurochemical monitoring. *J. Neurosurg.* 111, 701–711.
- Albin, R. L., Young, A. B., and Penney, J. B. (1989). The functional anatomy of basal ganglia disorders. *Trends Neurosci.* 5, 366–375.
- Anderson, M. E., Postupna, N., and Ruffo, M. (2003). Effects of high-frequency stimulation in the internal globus pallidus on the activity of thalamic neurons in the awake monkey. *J. Neurophysiol.* 89, 1150–1160.
- Ashby, P., Paradiso, G., Saint-Cyr, J. A., Chen, R., Lang, A. E., and Lozano, A. M. (2001). Potentials recorded at the scalp by stimulation near the human subthalamic nucleus. *Clin. Neurophysiol.* 112, 431–437.
- Benazzouz, A., Gao, D. M., Ni, Z. G., Piallat, B., Bouali-Benazzouz, R., and Benabid, A. L. (2000). Effect of high-frequency stimulation of the subthalamic nucleus on the neuronal activities of the substantia nigra pars reticulata and ventrolateral nucleus of the thalamus in the rat. *Neuroscience* 99, 289–295.
- Blandini, F., Nappi, G., Tassorelli, C., and Martignoni, E. (2000). Functional changes of the basal ganglia circuitry in Parkinson's disease. *Prog. Neurobiol.* 62, 63–88.
- Brown, P. (2003). Oscillatory nature of human basal ganglia activity: relationship to the pathophysiology of Parkinson's disease. *Mov. Disord.* 18, 357–363.
- Covey, D. P., and Garris, P. A. (2009). Using fast-scan cyclic voltammetry to evaluate striatal dopamine release elicited by subthalamic nucleus stimulation. *Conf. Proc. IEEE Eng. Med. Biol. Soc.* 3306–3309.
- DeLong, M. R. (1990). Primate models of movement disorders of basal ganglia origin. *Trends Neurosci.* 13, 281–285.
- Ding, J. B., Guzman, J. N., Peterson, J. D., Goldberg, J. A., and Surmeier, D. J. (2010). Thalamic gating of corticostriatal signaling by cholinergic interneurons. *Neuron* 67, 294–307.
- Fedele, E., Mazzone, P., and Stefani, A. (2001). Microdialysis in Parkinsonian patient basal ganglia: acute apomorphine-induced clinical and electrophysiological effects not paralleled by changes in the release of neuroactive amino acids. *Exp. Neurol.* 167, 356–365.
- Fedele, E., and Raiteri, M. (1999). *In vivo* studies of the cerebral glutamate receptor/NO/cGMP pathway. *Prog. Neurobiol.* 58, 89–120.
- Filali, M., Hutchison, W. D., Palter, V. N., Lozano, A. M., and Dostrovsky, J. O. (2004). Stimulation-induced inhibition of neuronal firing in human subthalamic nucleus. *Exp. Brain Res.* 156, 274–281.
- Follett, K. A., Weaver, F. M., Stern, M., Hur, K., Harris, C. L., Luo, P., Marks, W. J., Rothlind, J., Sager, O., Moy, C., Pahwa, R., Burchiel, K., Hogarth, P., Lai, E. C., Duda, J. E., Holloway, K., Samii, A., Horn, S., Bronstein, J. M., Stoner, G., Starr, P. A., Simpson, R., Baltuch, G., De Salles, A., Huang, G. D., and Reda, D. J. (2010). Pallidal versus subthalamic deep-brain stimulation for Parkinson's disease. *N. Engl. J. Med.* 362, 2077–2091.
- Galati, S., D'Angelo, V., Olivola, E., Marzetti, F., Di Giovanni, G., Stanzione, P., and Stefani, A. (2010). Acute inactivation of the medial forebrain bundle imposes oscillations in the SNr: a challenge for the 6-OHDA model? *Exp. Neurol.* 225, 294–301.
- Galati, S., Mazzone, P., Fedele, E., Pisani, A., Peppe, A., and Pierantozzi, M. (2006). Biochemical and electrophysiological changes of substantia nigra pars reticulata driven by subthalamic stimulation in patients with Parkinson's disease. *Eur. J. Neurosci.* 23, 2923–2928.
- Galati, S., Stanzione, P., D'Angelo, V., Fedele, E., Marzetti, F., Sancesario, G., Procopio, T., and Stefani, A. (2009). The pharmacological blockade of medial forebrain bundle induces an acute pathological synchronization of the cortico-subthalamic nucleus-globus pallidus pathway. *J. Physiol.* 587, 4405–4423.
- Gradinaru, V., Mogri, M., Thompson, K. R., Henderson, J. M., and Deisseroth, K. (2009). Optical deconstruction of Parkinsonian neural circuitry. *Science* 324, 354–359.
- Guo, Y., Rubin, J. E., McIntyre, C. C., Vietk, J. L., and Terman, D. (2008). Thalamocortical relay fidelity varies across subthalamic nucleus deep brain stimulation protocols in a data-driven computational model. *J. Neurophysiol.* 99, 1477–1492.
- Hahn, P. J., Russo, G. S., Hashimoto, T., Miocinovic, S., Xu, W., McIntyre, C. C., and Vitek, J. L. (2008). Pallidal burst activity during therapeutic deep brain stimulation. *Exp. Neurol.* 211, 243–251.
- Hashimoto, T., Elder, C. M., Okun, M. S., Patrick, S. K., and Vitek, J. L. (2003). Stimulation of the subthalamic nucleus changes the firing pattern of pallidal neurons. *J. Neurosci.* 23, 1916–1923.
- Hershey, T., Revilla, F. J., Wernle, A. R., McGee-Minnich, L., Antenor, J. V., and Videen, T. O. (2003). Cortical and subcortical blood flow effects of subthalamic nucleus stimulation in PD. *Neurology* 61, 816–821.
- Hilker, R., Voges, J., Weisenbach, S., Kalbe, E., Burghaus, L., and Ghaemi, M. (2004). Subthalamic nucleus stimulation restores glucose metabolism in associative and limbic cortices and in cerebellum: evidence from a FDG–PET study in advanced Parkinson's disease. *J. Cereb. Blood Flow Metab.* 24, 7–16.
- Hodaie, M., Cordella, R., Lozano, A. M., Wennberg, R., and Dostrovsky, J. O. (2006). Bursting activity of neurons in the human anterior thalamic nucleus. *Brain Res.* 1115, 1–8.
- Johnson, M. D., Vitek, J. L., and McIntyre, C. C. (2009). Pallidal stimulation that improves Parkinsonian motor symptoms also modulates neuronal firing patterns in primary motor cortex in the MPTP-treated monkey. *Exp. Neurol.* 219, 359–362.
- Kempf, F., Brücke, C., Salih, E., Trottenberg, T., Kupsch, A., and Schneider, G. H. (2009). Gamma activity and reactivity in human thalamic local field potentials. *Eur. J. Neurosci.* 29, 943–953.
- Kilpatrick, M., Church, E., Danish, S., Stiefel, M., Jaggi, J., and Halpern, C. (2010). Intracerebral microdialysis during deep brain stimulation surgery. *J. Neurosci. Methods* 190, 106–111.
- Limousin, P., Greene, J., Pollak, P., Rothwell, J., Benabid, A. L., and Frackowiak, R. (1997). Changes in cerebral activity pattern due to subthalamic nucleus or internal pallidum stimulation in Parkinson's disease. *Ann. Neurol.* 42, 283–291.
- Obeso, J. A., Rodríguez-Oroz, M. C., Benitez-Temino, B., Blesa, F. J., Guridi, J., and Marin, C. (2008). Functional organization of the basal ganglia: therapeutic implications for Parkinson's disease. *Mov. Disord.* 23, S548–S559.
- Payoux, P., Remy, P., Damier, P., Miloudi, M., Loubinoux, I., Pidoux, B., Gaura, V., Rascol, O., Samson, Y., and Agid, Y. (2004). Subthalamic nucleus stimulation reduces abnormal motor cortical overactivity in Parkinson disease. *Arch. Neurol.* 61, 1307–1313.

- Peppe, A., Pierantozzi, M., Bassi, A., Altibrandi, M. G., Brusa, L., Stefani, A., Stanzione, P., and Mazzone, P. (2004). Stimulation of the subthalamic nucleus compared with the globus pallidus internus in patients with Parkinson disease. *J. Neurosurg.* 101, 195–200.
- Rubin, J. E., and Terman, D. (2004). High-frequency stimulation of the subthalamic nucleus eliminates pathological thalamic rhythmicity in a computational model. *J. Comput. Neurosci.* 16, 211–235.
- Shi, L. H., Luo, F., Woodward, D. J., and Chang, J. Y. (2006). Basal ganglia neural responses during behaviorally effective deep brain stimulation of the subthalamic nucleus in rats performing a treadmill locomotion test. *Synapse* 59, 445–457.
- Stefani, A., Bassi, A., Mazzone, P., Pierantozzi, M., Gattoni, G., Altibrandi, M. G., Giacomini, P., Peppe, A., Bernardi, G., and Stanzione, P. (2002). Subdyskinetic apomorphine responses in globus pallidus and subthalamus of Parkinsonian patients: lack of clear evidence for the 'indirect pathway'. *Clin. Neurophysiol.* 113, 91–100.
- Stefani, A., Fedele, E., Galati, S., Pepicelli, O., Frasca, S., and Pierantozzi, M. (2005). Subthalamic stimulation activates internal pallidus: evidence from cGMP microdialysis in PD patients. *Ann. Neurol.* 57, 448–452.
- Stefani, A., Fedele, E., Galati, S., Raiteri, M., Pepicelli, O., and Brusa, L. (2006). Deep brain stimulation in Parkinson's disease patients: biochemical evidence. *J. Neural Transm.* 70, S401–S408.
- Stefani, A., Fedele, E., Vitek, J., Pierantozzi, M., Galati, S., Marzetti, F., Peppe, A., Bernardi, G., and Stanzione, P. (2011). The clinical efficacy of L-dopa and STN-DBS share a common marker: reduced GABA content in the motor thalamus. *Cell Death Dis.* (in press).
- Stefani, A., Lozano, A. M., Peppe, A., Stanzione, P., Galati, S., and Tropepi, D. (2007). Bilateral deep brain stimulation of the pedunculopontine and subthalamic nuclei in severe Parkinson's disease. *Brain* 130, 1596–1607.
- Stefani, A., Mazzone, P., Bassi, A., Bernardi, G., Altibrandi, M. G., Peppe, A., Pierantozzi, M., and Stanzione, P. (1999). Electrophysiological and clinical desensitization to apomorphine administration in Parkinsonian patients undergoing stereotaxic neurosurgery. *Exp. Neurol.* 156, 209–213.
- Stefani, A., Peppe, A., Pierantozzi, M., Galati, S., Moschella, V., and Stanzione, P. (2009). Multi-target strategy for Parkinsonian patients: the role of deep brain stimulation in the centromedian-parafascicular complex. *Brain Res. Bull.* 78, 113–118.
- Stefani, A., Stanzione, P., Bassi, A., Mazzone, P., Vangelista, T., and Bernardi, G. (1997). Effects of increasing doses of apomorphine during stereotaxic neurosurgery in Parkinson's disease: clinical score and internal globus pallidus activity. *J. Neural Transm.* 104, 895–904.
- Urbano, F. J., Bisagno, V., Wikinski, S. I., Uchitel, O. D., and Llinás, R. R. (2009). Cocaine acute "binge" administration results in altered thalamocortical interactions in mice. *Biol. Psychiatry* 66, 769–776.
- Van Gompel, J. J., Chang, S. Y., Goerss, S. J., Kim, I. Y., Kimble, C., Bennet, K. E., and Lee, K. H. (2010). Development of intraoperative electrochemical detection: wireless instantaneous neurochemical concentration sensor for deep brain stimulation feedback. *Neurosurg. Focus* 29, E6.
- Windels, F., Bruet, N., Poupard, A., Feuerstein, C., Bertrand, A., and Savasta, M. (2003). Influence of the frequency parameter on extracellular glutamate and gamma-aminobutyric acid in substantia nigra and globus pallidus during electrical stimulation of subthalamic nucleus in rats. *J. Neurosci. Res.* 72, 259–267.
- Windels, F., Carcenac, C., Poupard, A., and Savasta, M. (2005). Pallidal origin of GABA release within the substantia nigra pars reticulata during high-frequency stimulation of the subthalamic nucleus. *J. Neurosci.* 25, 5079–5086.
- Xu, W., Russo, G. S., Hashimoto, T., Zhang, J., and Vitek, J. L. (2008). Subthalamic nucleus stimulation modulates thalamic neuronal activity. *J. Neurosci.* 28, 11916–11924.

Conflict of Interest Statement: The authors declare that the research was conducted in the absence of any commercial or financial relationships that could be construed as a potential conflict of interest.

Received: 30 December 2010; paper pending published: 02 February 2011; accepted: 22 March 2011; published online: 05 April 2011.

Citation: Stefani A, Fedele E, Pierantozzi M, Galati S, Marzetti F, Peppe A, Pastore FS, Bernardi G and Stanzione P (2011) Reduced GABA content in the motor thalamus during effective deep brain stimulation of the subthalamic nucleus. *Front. Syst. Neurosci.* 5:17. doi: 10.3389/fnsys.2011.00017

Copyright © 2011 Stefani, Fedele, Pierantozzi, Galati, Marzetti, Peppe, Pastore, Bernardi and Stanzione. This is an open-access article subject to a non-exclusive license between the authors and Frontiers Media SA, which permits use, distribution and reproduction in other forums, provided the original authors and source are credited and other Frontiers conditions are complied with.



Dynamic stereotypic responses of basal ganglia neurons to subthalamic nucleus high-frequency stimulation in the parkinsonian primate

Anan Moran^{1†}, Edward Stein^{1†}, Hadass Tischler¹, Katya Belevovsky¹ and Izhar Bar-Gad^{1,2*}

¹ The Leslie and Susan Gonda Brain Research Center, Bar-Ilan University, Ramat-Gan, Israel

² The Goodman Faculty of Life Sciences, Bar-Ilan University, Ramat-Gan, Israel

Edited by:

James M. Tepper, Rutgers, The State University of New Jersey, USA

Reviewed by:

Thomas Boraud, Université de Bordeaux, France

Thomas Wichmann, Emory University, USA

*Correspondence:

Izhar Bar-Gad, Gonda Brain Research Center, Bar-Ilan University, Ramat-Gan 52900, Israel.

e-mail: bargadi@mail.biu.ac.il

[†]A. Moran and E. Stein have contributed equally to this work.

Deep brain stimulation (DBS) in the subthalamic nucleus (STN) is a well-established therapy for patients with severe Parkinson's disease (PD); however, its mechanism of action is still unclear. In this study we explored static and dynamic activation patterns in the basal ganglia (BG) during high-frequency macro-stimulation of the STN. Extracellular multi-electrode recordings were performed in primates rendered parkinsonian using 1-methyl-4-phenyl-1,2,3,6-tetrahydropyridine. Recordings were performed simultaneously in the STN and the globus pallidus externus and internus. Single units were recorded preceding and during the stimulation. During the stimulation, STN mean firing rate dropped significantly, while pallidal mean firing rates did not change significantly. The vast majority of neurons across all three nuclei displayed stimulation driven modulations, which were stereotypic within each nucleus but differed across nuclei. The predominant response pattern of STN neurons was somatic inhibition. However, most pallidal neurons demonstrated synaptic activation patterns. A minority of neurons across all nuclei displayed axonal activation. Temporal dynamics were observed in the response to stimulation over the first 10 seconds in the STN and over the first 30 seconds in the pallidum. In both pallidal segments, the synaptic activation response patterns underwent delay and decay of the magnitude of the peak response due to short term synaptic depression. We suggest that during STN macro-stimulation the STN goes through a functional ablation as its upper bound on information transmission drops significantly. This notion is further supported by the evident dissociation between the stimulation driven pre-synaptic STN somatic inhibition and the post-synaptic axonal activation of its downstream targets. Thus, BG output maintains its firing rate while losing the deleterious effect of the STN. This may be a part of the mechanism leading to the beneficial effect of DBS in PD.

Keywords: deep brain stimulation, Parkinson's disease, non-human primate, 1-methyl-4-phenyl-1,2,3,6-tetrahydropyridine, globus pallidus, subthalamic nucleus, short term plasticity, basal ganglia

INTRODUCTION

The basal ganglia (BG) are a group of interconnected subcortical nuclei that are involved in motor, limbic, and associative tasks (Alexander et al., 1986). Parkinson's disease (PD) is characterized by a degeneration of midbrain dopaminergic neurons (Bernheimer et al., 1973) that project to multiple targets in the BG, primarily the striatum (Anden et al., 1964). High-frequency deep brain stimulation (DBS) of some of the BG nuclei such as the subthalamic nucleus (STN) or the globus pallidus internus (GPi) has been found to ameliorate motor symptoms in severe cases of PD in humans (Siefried and Lippitz, 1994; Limousin et al., 1995) as well as in primates rendered parkinsonian using 1-methyl-4-phenyl-1,2,3,6-tetrahydropyridine (MPTP; Benazzouz et al., 1993).

Modulation of the neuronal activity in the cortico-BG loop during high-frequency DBS has been studied for more than a decade (Benazzouz et al., 1993, 2000; Hashimoto et al., 2003; Bar-Gad et al., 2004; Brown et al., 2004; Meissner et al., 2005; Kuhn et al., 2006; Dorval et al., 2008; McCairn and Turner, 2009), but the mechanism underlying the ameliorating effect is still unclear. Studies of

the stimulated nucleus have yielded contradictory evidence: most direct studies demonstrate an inhibition during STN (Benazzouz et al., 2000; Tai et al., 2003; Filali et al., 2004; Welter et al., 2004) and GPi (Dostrovsky et al., 2000; Wu et al., 2001; Montgomery Jr., 2006) stimulation. Studies in slices report similar observations (Beurrier et al., 2001; Magarinos-Ascone et al., 2002). Notably, few human (Carlson et al., 2010) and *in vitro* (Garcia et al., 2003) studies point out that the STN is not silenced during the stimulation. Studies of brain areas downstream to the STN (Hashimoto et al., 2003; Maurice et al., 2003) and GPi (Anderson et al., 2003) reveal activation patterns which are inconsistent with the somatic silencing in the stimulated nucleus.

Analysis of globus pallidus (GP) discharge patterns during STN and GPi stimulations has revealed stereotypic discharge patterns synchronized to the stimulation pulses that are thought to be driven synaptically by the stimulated nucleus (Hashimoto et al., 2003; Bar-Gad et al., 2004; Kita et al., 2005; Stefani et al., 2005; Erez et al., 2009; McCairn and Turner, 2009). These synaptic activation patterns displayed dynamics over the stimulation period which

led to the suggestion of a short term reversible synaptic depression (Erez et al., 2009; Prescott et al., 2009). *In vitro* observations are consistent with this notion and have described a short synaptic facilitation followed by a longer depression (Hanson and Jaeger, 2002; Rav-Acha et al., 2005).

Despite the vast and elaborated experimental work, as well as modeling studies (McIntyre et al., 2004a; Rubin and Terman, 2004; Leblois et al., 2006), a single coherent theory consistent with all the current observations has yet to be formulated. Modeling studies have revealed a clear difference between somatic and axonal activity in the stimulated area resulting in the dissociation of the stimulated nucleus from its targets. This principle was demonstrated first on thalamocortical cells undergoing suprathreshold DBS which caused suppression of intrinsic firing in the soma, but generated efferent output at the stimulus frequency in the axon (McIntyre et al., 2004a). This study was followed by an additional modeling work which predicted axonal activation of STN neurons and GPi fibers during STN DBS (Miocinovic et al., 2006).

In the current study we examined the single neuron activation patterns throughout the BG and their dynamics, during the application of STN high-frequency macro-stimulation to behaving primates treated with MPTP. In addition, we examined the dissociation hypothesis stating that the stimulated STN goes through a somatic inhibition while its downstream pallidal targets are activated by STN efferents. To that end, multi-electrode extracellular recordings were performed in the STN and GP during high-frequency stimulation of the STN.

MATERIALS AND METHODS

ANIMALS

Two cynomolgus (*Macaca fascicularis*) male monkeys were used (N: 3.8 kg; P: 4.5 kg). The monkeys' water and food consumption and weight were followed daily, and their health was monitored by a veterinarian. All procedures were in accordance with the National Institutes of Health Guide for the Care and Use of Laboratory Animals and Bar-Ilan University Guidelines for the Use and Care of Laboratory Animals in Research and were approved and supervised by the Institutional Animal Care and Use Committee.

SURGERY AND INDUCTION OF PARKINSONISM

The monkeys underwent a surgical procedure to attach two 27 mm square Cilux recording chambers (Alpha Omega Engineering, Nazareth, Israel) to the skull allowing bilateral access to the BG. In this study we used recordings only from the chamber over the left hemisphere in monkey N and the chamber over the right hemisphere in monkey P. The chambers were tilted at 35° for N and 40° for P in the sagittal plane, with their center targeted at stereotaxic coordinates A4-L8-H1 (Szabo and Cowan, 1984) of the left hemisphere for monkey N, and A5-L6-H2 of the right hemisphere for monkey P. The surgical procedure was performed under general anesthesia induced by intramuscular ketamine-HCl (10 mg/kg) and Domitor (0.1 mg/kg) and maintained by isoflurane and N₂O ventilation. Parkinsonism was induced by five intramuscular injections of 0.4 mg/kg MPTP-HCl (Sigma) neurotoxin. MPTP injections were given under intramuscular ketamine-HCl (10 mg/kg) anesthesia and over a period of 4 days, after which the monkeys developed severe and stable parkinsonism. The monkeys'

parkinsonian state was assessed daily using the Schneider scale (Schneider et al., 2003) and was severe and stable throughout the recording period [monkey N: 43.9 ± 3.8 , monkey P: 44.0 ± 2.7 mean \pm SD, on a scale of 0 (asymptomatic) to 53 (maximal symptoms)]. The symptoms included all the major parkinsonian symptoms except for rest tremor, which is typically not exhibited by this species. Additionally, both monkeys had dystonia, primarily in the lower limbs. Recordings were resumed 5 days following the last MPTP injection for both monkeys.

RECORDING AND STIMULATION

The monkeys were seated in a primate chair and their head was fixed during the recording sessions. Using a cylindrical guide, multiple glass-coated tungsten recording microelectrodes (impedance 0.2–0.7 M Ω at 1 kHz) and one stimulation concentric macro-electrode (Narylene coated tungsten microelectrode inside a Narylene coated stainless steel cannula, impedance 2–3 K Ω at 1 kHz; We Sense, Nazareth, Israel) were advanced separately (EPS 4.10, Alpha-Omega Engineering) into the STN and GP. The two electrode towers allowed different trajectories to the GP (eight microelectrodes) and STN (three microelectrodes and one concentric electrode) with 10° between the towers. The distinction between the pallidal segments was determined online based on characteristics of neuronal activity, and the existence of border cells and white matter fibers between the two segments. All GPe neurons used in this study were high-frequency pausers. STN trajectories were performed through the internal capsule, until reaching the STN which was identified by large and highly oscillating background activity, and isolated single units with 20–30 spikes/s. Stimulation location within the STN relied both on recording STN activity with the concentric inner recording microelectrode and by leveling the concentric outer macro-contact to other recording electrodes. All stimulation locations were at least 0.5 mm ventral to the STN dorsal border. The electrode signal was continuously sampled at 40 kHz (Alphamap 10.10, Alpha-Omega Engineering), amplified ($\times 1000$) and wide band-pass filtered (2–8000 Hz four-pole Butterworth filter; MCP-Plus 4.10, Alpha-Omega Engineering). High-frequency monophasic cathodal constant voltage stimulation pulses (2 V, 60 μ s, resulting maximal current ~ 1 mA) were delivered via the macro-electrode using an optically isolated stimulator (STG-2008, Multichannel Systems, Reutlingen, Germany). These Stimulating parameters were chosen as the ones usually used in human surgeries. The voltage was chosen to be below a voltage which produced motor contractions. The interval between consecutive pulses was 8 ms, leading to a stimulation frequency of 125 Hz. Recording sessions consisted of 60 s of baseline activity followed by ~ 125 s (15600 stimuli) of stimulation.

HISTOLOGY

Following completion of the experiment, the animals were anesthetized using ketamine-HCl (10 mg/kg) and stereotactic marking micro-lesions (DC current, 60 μ A for 30 s) were made. The animals were then deeply anesthetized using sodium pentobarbital (50 mg/kg) and transcardially perfused with 1 L of physiological saline, followed by 1 L of 4% paraformaldehyde. The whole brain was removed and buffered in graded sucrose solution 10–30% over

7 days. The brain was then frozen at -25°C and cut in the coronal plane using a cryostat (Leica Microsystems). Each section was digitized using a 10-MPixel digital camera and sections of interest were mounted onto glass slides and Nissl stained.

DATA PREPROCESSING

The digitized continuous signal of each electrode was preprocessed to remove the stimulation pulse artifacts using the Stimulus Artifact Removal Graphical Environment – SARGE (Erez et al., 2010; Figure 1). Following artifact removal, the signal was off-line sorted (OFS-2.8.4, Plexon, Dallas, TX, USA) to generate one or more spike trains. The spike train quality and stability were assessed according to the following criteria: (1) P[inter-spike interval (ISI) shorter than 1 ms] $<0.1\%$; (2) normalized signal-to-noise ratio (SNR) >4 ; (3) spike shape was not significantly altered throughout the session. The normalized SNR was defined as the ratio of the peak to trough amplitude of the mean spike shape to the standard deviation of the recorded signal. The spike shape stability was assessed by comparison of the mean spike shape in the early (pre-stimulation) part of the recording with the late part (during stimulation) of the recording and the verification that they appear in a single cluster during the off-line sorting. All further data analysis was performed using custom written code (MATLAB 2009A, Mathworks, Natick, MA, USA).

FIRING RATE

Firing rate was calculated prior to and during the stimulation. The mean firing rate over the last 60 s preceding the stimulation was termed the “baseline rate.” The mean firing rate during the last 60 s of the stimulation was termed “during rate.” The calculation of firing rate during the stimulation included compensation for the stimulation period in which the spikes were not identifiable [termed non-usable period (NP)] due to the artifact of the electric pulse (Erez et al., 2010). If we denote the firing rate compensated for the NP as FR_{NP} for a neuron stimulated at a stimulation interval τ_i with a NP of τ_{NP} and the recorded firing rate of FR_{rec} $\text{FR}_{\text{NP}} = \text{FR}_{\text{rec}} \cdot \frac{\tau_i}{\tau_i - \tau_{\text{NP}}}$.

RESPONSE TYPE CLASSIFICATION

The rate normalized peri-stimulus time histogram (PSTHs) aligned to stimulation pulses (bin size 0.1 ms) were classified into one of the following groups:

- 1 *Axonal activation*: neurons undergoing axonal activation are characterized by a high probability to fire following the stimulation with a short and fixed latency (a very low jitter). We introduced an automated classification algorithm which is similar to the one used manually in previous studies (Kita and Kitai, 1991; Hashimoto et al., 2003). We defined the activation delay (τ_{peak}) as the delay of the bin with the maximal firing rate (FR_{peak}) across the rate normalized PSTH. Let us define FR_{Mean} as the mean firing rate across the PSTH and $\text{FR}_{\text{Threshold}} = \text{FR}_{\text{Mean}} + 0.66 (\text{FR}_{\text{peak}} - \text{FR}_{\text{Mean}})$. The jitter around τ_{peak} was defined as the cumulative width of consecutive bins surrounding τ_{peak} whose firing rate was higher than $\text{FR}_{\text{Threshold}}$. A neuron's probability to fire following a stimulation pulse was defined as the cumulative probability to fire over all jitter bins. A neuron was classified as undergoing axonal activation if: $\tau_{\text{peak}} < 2$ ms (Kita and

Kitai, 1991), jitter <0.5 ms (Iremonger et al., 2006), and its probability to fire following a stimulation pulse >0.1 (Iremonger et al., 2006).

- 2 *Inhibition*: Firing rate of neurons in this group dropped by more than 80% during the stimulation period relative to their baseline firing rate.
- 3 *Synaptic activation*: The PSTH of neurons undergoing synaptic activation displayed several typical patterns which were all characterized by a large variability in the FR and displayed a single, double, or even triple clear peaks at different but stereotypic times. On the other hand, neurons which did not respond to the stimulation were characterized by a stable FR relative to the stimulation. The coefficient of variation (CV) method detects these variations while taking into account the mean firing rate and is thus a natural candidate for classifying the neurons into synaptic activated and non-responding neurons. Let us denote FR_{PSTH} as the rate normalized PSTH. The rate coefficient of variation (CV_{Rate}) criterion was defined as $\text{CV}_{\text{Rate}} = \frac{\text{std}(\text{FR}_{\text{PSTH}})}{E[\text{FR}_{\text{PSTH}}]}$ where $\text{mean}[\text{FR}_{\text{PSTH}}] = \frac{1}{N} \sum_{i=1}^N \text{FR}_{\text{PSTH}}(t_i)$ and $\text{std}(\text{FR}_{\text{PSTH}}) = \sqrt{\frac{1}{N} \sum_{i=1}^N (\text{FR}_{\text{PSTH}}(t_i) - \text{mean}[\text{FR}_{\text{PSTH}}])^2}$, where $\text{FR}_{\text{PSTH}}(t_i)$ is the firing rate of the i -th bin in the normalized PSTH. Neurons with $\text{CV}_{\text{Rate}} > 0.15$ during the stimulation that did not display an axonal activation or an inhibitory response were classified as neurons undergoing synaptic activation.
- 4 No response: neurons which did not display any of the above response types.

RESPONSE DYNAMICS

Two partial PSTHs normalized to rate were generated for every neuron displaying a synaptic response. The *early response PSTH* was calculated over the first 30 s of stimulation whereas the *late response PSTH* was calculated over the last 30 s of stimulation. The peaks of the early and late PSTHs in the range of 2–7 ms were compared. Comparison included differences in the peak latency and maximal rate. The peak magnitude was defined as the difference between the peak rate and the PSTH mean firing rate. The peak jitter was defined as the width at the top 33% of the peak magnitude. Outliers (PSTHs with an unclear peak or multiple close peaks) were not included in this analysis.

INFORMATION TRANSFER

A neuron's entropy is upper bounded by the entropy of the ISI distribution (Stevens and Zador, 1996) $H = -\sum_{p(\text{ISI})} p(\text{ISI}) \cdot \log_2(p(\text{ISI}))$ where $p(\text{ISI})$ denotes the probability of the appearance of a specific ISI using bins of 0.1 ms. The upper limit on a neuron's capability to transfer information is the entropy per ISI multiplied by the rate. The nuclei's upper bound on information transfer was calculated by averaging over the neuronal upper bound of the nuclei population.

RESULTS

ANATOMY

Recordings were performed in the STN, GPe, and GPi. 70 neurons from the GPe, 49 neurons from the GPi and 36 neurons from the STN were recorded in 29 sessions. The neurons were distributed

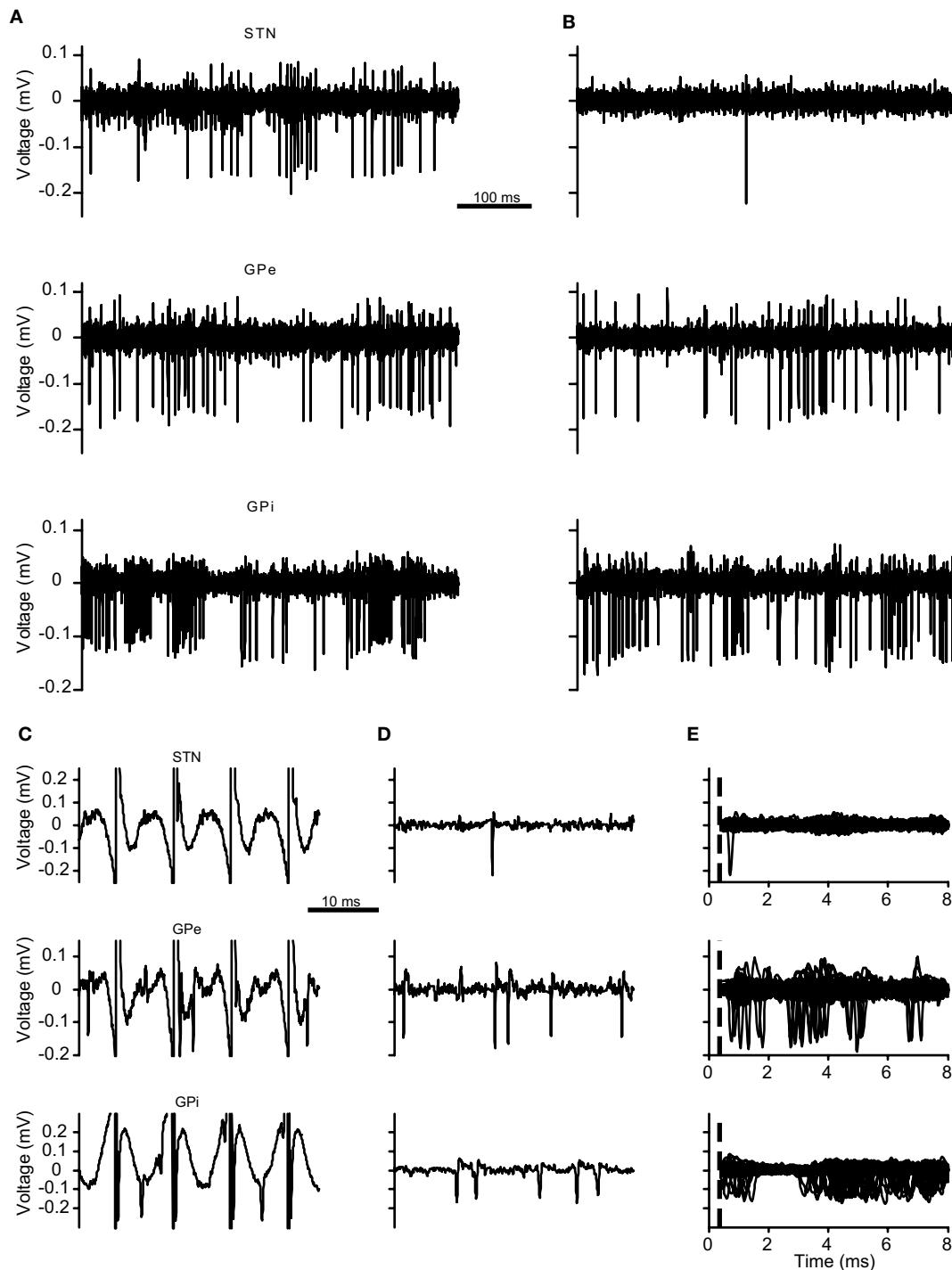


FIGURE 1 | STN, GPe, and GPi recording traces. (A–E) The neuronal activity of recorded electrodes located in the (top) STN, (middle) GPe, and (bottom) GPi across different sessions. **(A)** Trace prior to the stimulation. **(B)** Trace during the stimulation period following stimulation artifact removal. **(C,D)** Short traces

demonstrating artifact removal results. **(C)** Traces with stimulation artifacts. **(D)** Same traces following stimulation artifact removal. **(E)** Peri-stimulus trace of 100 consecutive stimulation pulses. The dotted line marks the end of the non-usable period (NP).

almost equally between the two primates (GPe N-44 P-26, GPi N-25 P-24, and STN N-19 P-17). The recording sites from both monkeys were overlaid on the postmortem anatomical reconstruction of the right hemisphere of monkey P (**Figure 2**).

FIRING RATE

The firing rate during the last 60 s of the stimulation was calculated and compared to the baseline firing rate over an equivalent period prior to the stimulation. During the stimulation the STN firing rate

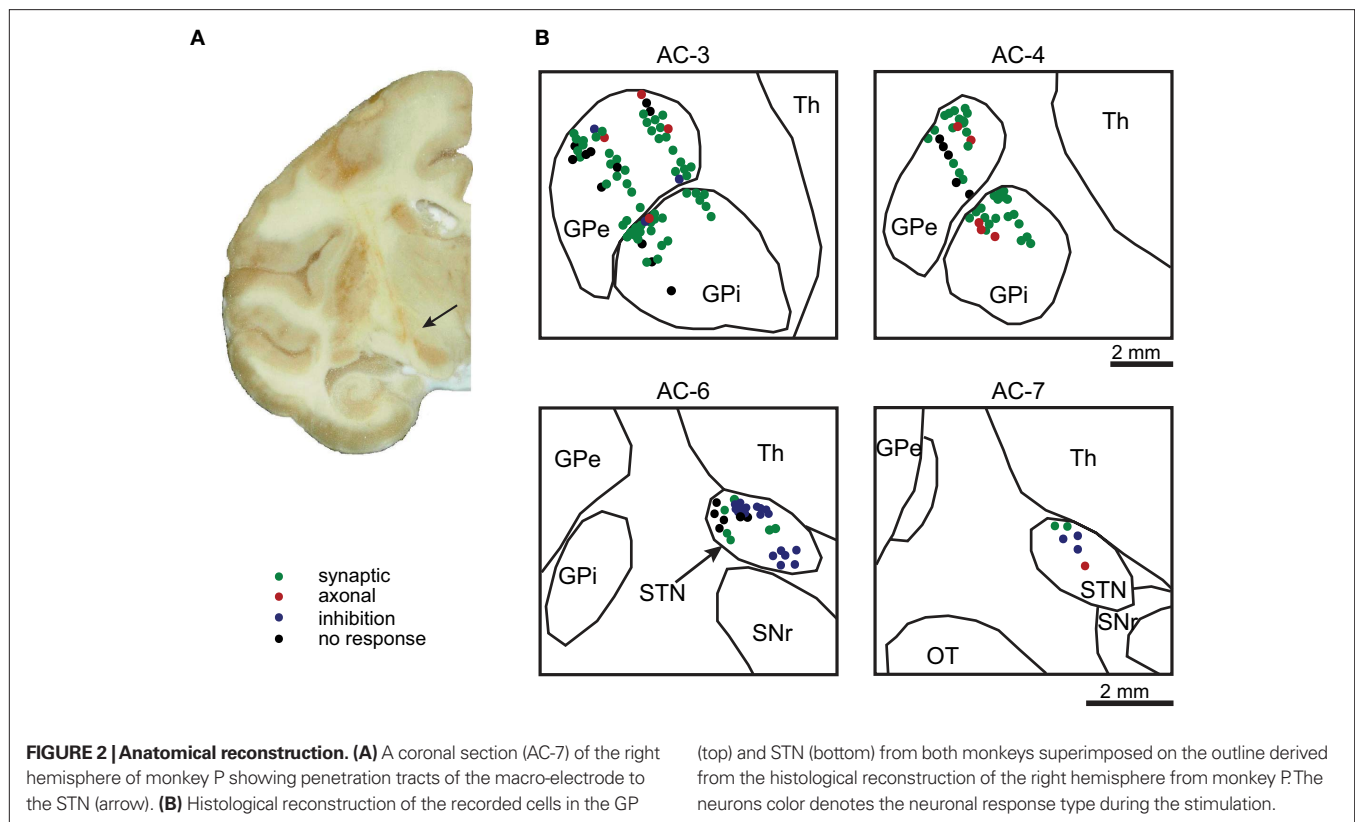


FIGURE 2 | Anatomical reconstruction. (A) A coronal section (AC-7) of the right hemisphere of monkey P showing penetration tracts of the macro-electrode to the STN (arrow). **(B)** Histological reconstruction of the recorded cells in the GP

(top) and STN (bottom) from both monkeys superimposed on the outline derived from the histological reconstruction of the right hemisphere from monkey P. The neurons color denotes the neuronal response type during the stimulation.

decreased significantly (31.2 ± 2.2 spikes/s before, 12.3 ± 2.9 during, mean \pm SEM, Wilcoxon signed rank test, $p < 0.01$). However, the GPi and GPe firing rates did not change significantly (76.4 ± 5.2 before, 72.1 ± 6.2 during and 59.1 ± 3.4 before, 57.3 ± 4.4 during respectively, Wilcoxon signed rank test, $p > 0.05$). Firing rate analysis performed animal wise, resulted in similar results: STN rate dropped significantly in both primates while GPe and GPi rate did not change significantly in either animal. Calculations of firing rates during the stimulation were compensated for the NP, which was equal to 0.75 ms in the current dataset (Figure 3A).

The normalized (and NP compensated) rate functions were calculated over the whole stimulation period using 100 ms bin size and smoothed by a (600 ms STD) Gaussian filter. The normalized rate displayed temporal dynamics in all three nuclei. The STN displayed the largest changes over the first 10 s of stimulation and stabilized at a rate which was substantially smaller than the baseline rate ($-61.6 \pm 0.1\%$ during the last 60 s of stimulation, mean \pm SEM). Both pallidal segments displayed smaller rate changes over the first 30 s and stabilized at a rate which was very close to the baseline rate (GPe $-3.2 \pm 0.1\%$, GPi $-5.1 \pm 0.0\%$, Figure 3B).

RESPONSE TYPES

Most neurons displayed stereotypic responses to stimulation pulses. The responses were classified based on their PSTH into several categories (Figure 4A):

- 1 **Axonal activation:** Neurons displaying high entrainment to the stimulation; i.e., the neurons fired following each stimulation pulse with a high probability ($53.3 \pm 12.1\%$, $n = 10$;

mean \pm SEM), at short latencies (< 2 ms) following the stimulation (Total 1.1 ± 0.1 ms, $n = 10$; STN 0.7 ms, $n = 1$; GPe 1.2 ± 0.2 ms, $n = 5$; GPi 1.1 ± 0.3 ms, $n = 4$; mean \pm SEM) with a very low jitter (0.3 ± 0.0 ms, $n = 10$; mean \pm SEM). This type of activation cannot be explained by the slower and highly variable synaptic transmission.

- 2 **Inhibition:** Neurons whose firing rate during the stimulation decreased by more than 80% relative to their baseline firing rate ($-96.3 \pm 0.9\%$, $n = 24$; mean \pm SEM). This response was the predominant response in the STN, where 58% of the neurons displayed inhibition during the stimulation (Figure 4B).
- 3 **Synaptic activation:** Neurons displaying stereotypic response patterns with a high CV_{Rate} (0.03 ± 0.00 before, 0.45 ± 0.02 during, $n = 99$; mean \pm SEM). This response was the predominant response in both segments of the GP (71% in the GPe and 84% in the GPi; Figure 4B).
- 4 **No response:** Neurons displaying a low CV_{Rate} during the stimulation (0.03 ± 0.00 before, 0.10 ± 0.01 during, $n = 22$; mean \pm SEM).

RESPONSE DYNAMICS

Neurons with a synaptic response displayed temporal dynamics in their response over the stimulation period (Figure 5A). The changes were characterized by an increased latency (0.4 ± 0.1 ms in both segments of the GP with GPe $n = 37$ and GPi $n = 30$; mean \pm SEM) and a decreased peak amplitude ($33.1 \pm 4.8\%$ in the GPe and $27.4 \pm 4.6\%$ in the GPi; mean \pm SEM) of the locked response (Figure 5B). These response pattern dynamics complemented the firing rate dynamics

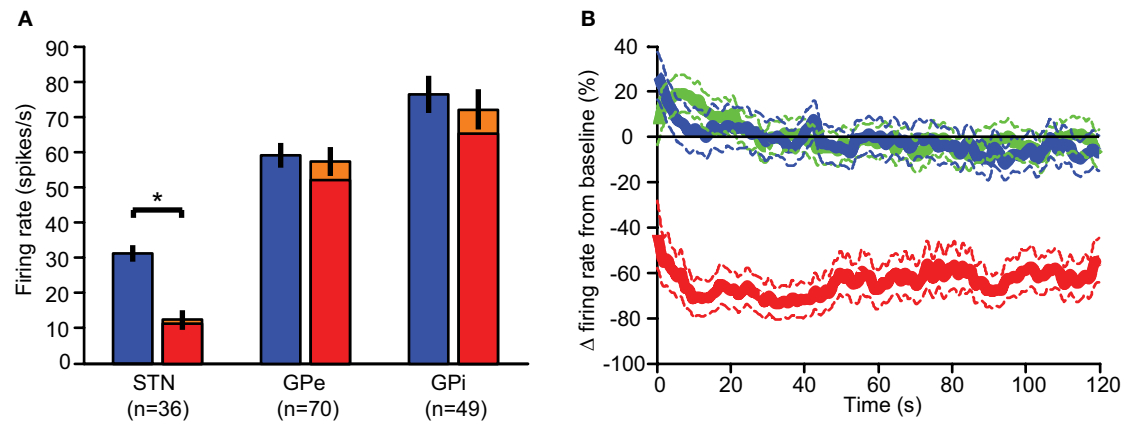


FIGURE 3 | Neuronal firing rate. (A) The mean firing rates for the periods prior to stimulation (blue), during stimulation (red), and NP compensated (orange) in the STN, GPe, and GPi. Error bars represent SEM (* $p < 0.01$). (B) The firing rate dynamics during the stimulation relative to the baseline rate of the STN (red), GPe (green), and GPi (blue); dashed lines represent the SEM.

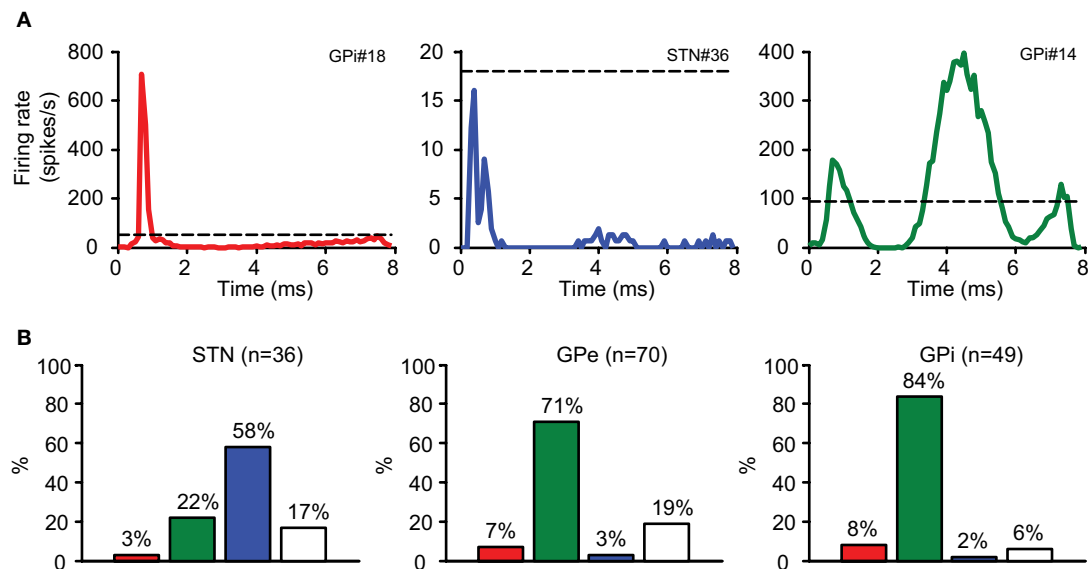


FIGURE 4 | Stimulation response types. (A) The PSTH demonstrates typical response types: axonal activation (red), inhibition (blue), and synaptic response (green). Dashed line represents baseline rate prior to stimulation. (B) The distribution of response types in the recorded nuclei.

in both segments of the GP over the first 30 s of the stimulation (**Figure 5B**). In the STN, firing rate dynamics were observed over the first 10 s of the stimulation but no response pattern dynamics were observed at population level.

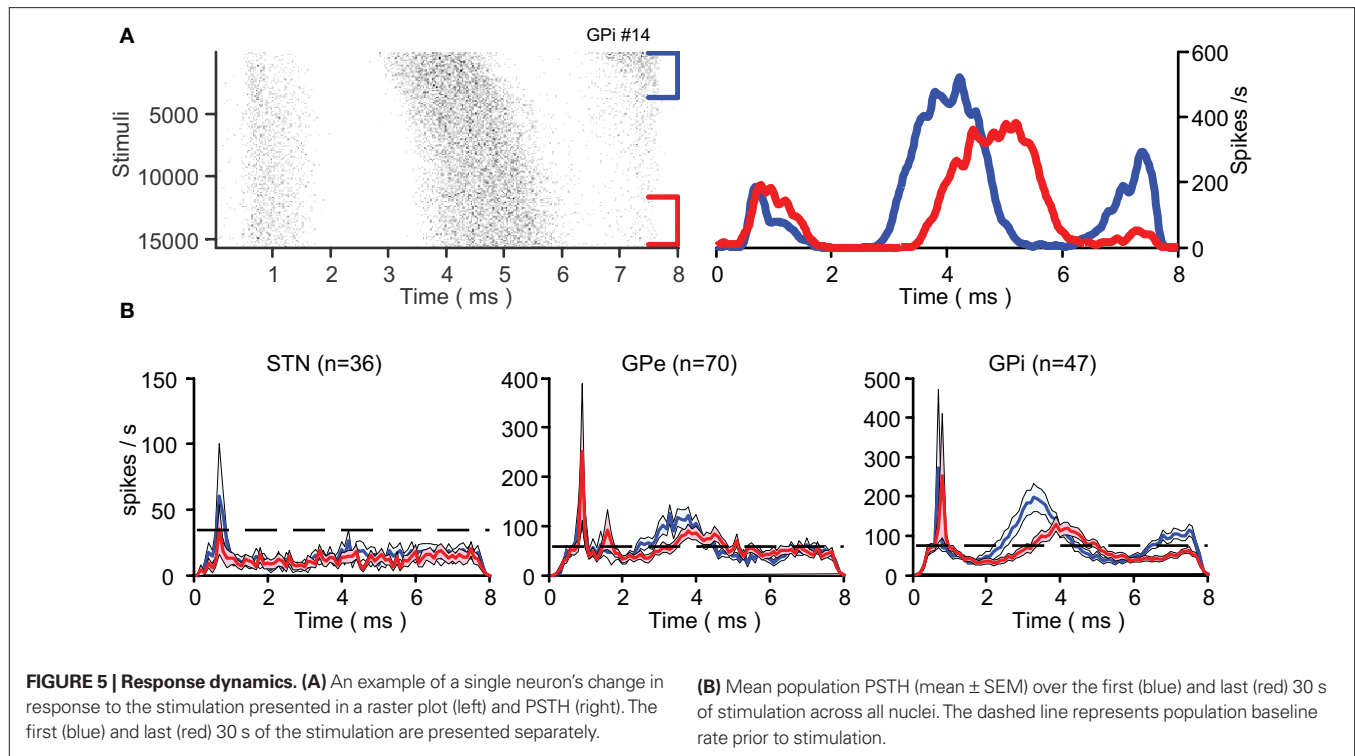
TRANSMISSION SCHEME

Axonal (antidromic) and synaptic transmission delays between the stimulated nucleus and target neurons in the STN, GPe, and GPi were calculated. The delay and jitter were based on the mean latency of the peak and its standard deviation respectively. Antidromic delays were similar across nuclei (~1 ms) with a very low jitter (0.3 ms). Synaptic transmission delays were slightly larger

in the GPi than in the GPe. The synaptic delay (~3.9 ms) and jitter (~1.3 ms) were substantially larger than the axonal delay and jitter (**Table 1**).

ENTROPY

The neurons' upper bound on information transfer was calculated prior and during the stimulation. The upper bound is the outcome of multiplying the entropy per ISI by the neuronal firing rate. The STN capability to transmit information dropped significantly from 176.1 ± 10.8 bit/s (mean \pm SEM) prior to the stimulation, to 71.8 ± 14.6 bit/s during the stimulation (Wilcoxon signed rank test $p < 0.01$). The upper bound of transmission capability in the GPe



did not display a major reduction (GPe 293.7 ± 12.5 bit/s before, 276.4 ± 14.2 bit/s during Wilcoxon signed rank test $p > 0.05$) and the upper bound in the GPI was reduced significantly but to a lesser extent than the STN reduction (348.1 ± 16.5 bit/s before, 308.3 ± 20.1 bit/s during, Wilcoxon signed rank test $p < 0.01$; Figure 6).

DISCUSSION

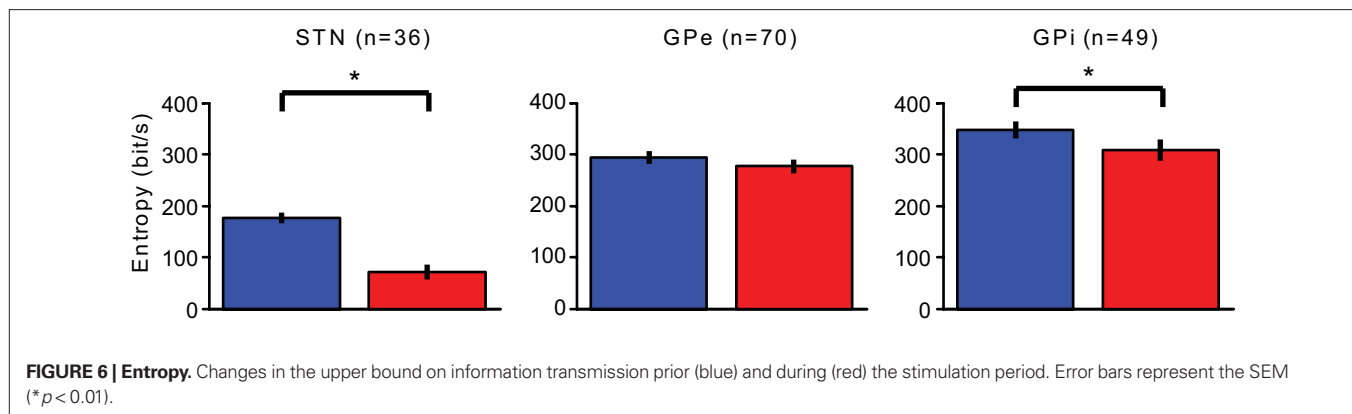
The present study examined the neuronal response within the BG to STN macro-stimulation in primates rendered parkinsonian using MPTP. Recordings were performed simultaneously in the STN, GPe, and GPI during the stimulation and were compared to recordings of the same neurons prior to the stimulation. The firing rate in the STN decreased significantly during the stimulation. In contrast, GPe and GPI firing rates did not change significantly. The firing patterns following each stimulation pulse demonstrated stereotypic firing patterns that were classified into a few basic response categories. In the STN the predominant response was an overall reduction in the activity (inhibitory response). In contrast, the predominant responses in both segments of the GP were synaptic activation patterns. A minority of the neurons in all of these targets displayed axonal activation or no response at all. The neurons which displayed a synaptic response demonstrated temporal dynamics in their response pattern. The predominant part of the dynamics took place over the first 10 s of stimulation in the STN and the first 30 s in the GP. Derivation of the upper bound on information transmission in the three nuclei showed a major decrease in the STN's ability to transfer information while the GPI displayed only a minor reduction in its upper bound on information transmission.

Table 1 | Transmission scheme.

Target	Transmission type	Transmission delay (mean \pm SEM, ms)	Jitter (mean \pm SEM, ms)	n
GPe	Synaptic	3.8 ± 0.1	1.2 ± 0.1	50
GPI	Synaptic	4.0 ± 0.1	1.4 ± 0.1	40
STN	Axonal	0.7 ± 0.0	0.4 ± 0.0	1
GPe	Axonal	1.2 ± 0.2	0.3 ± 0.0	5
GPI	Axonal	1.1 ± 0.3	0.3 ± 0.0	4

The applied stimulation parameters were similar to those applied successfully in humans (Kuhn et al., 2008) and other animal studies trying to replicate the clinical environment (Hashimoto et al., 2003). The stimulation amplitude (2 V) was chosen to be strong enough to elicit neural responses, but without generating motor constrictions caused by stimulation of descending internal capsule fibers. The chosen parameter values and the choice of constant voltage pulses were done to comply with these clinical studies although most scientific studies of electric stimulation use constant current pulses as this provides a more direct measure of affecting the neurons (Lemon, 1984). In this study we have no direct measures of the clinical change in the parkinsonian symptoms and therefore we make no claims regarding the therapeutic value of the stimulation.

The recordings in the STN were almost exclusively in the dorsal motor domain (Wichmann et al., 1994), while recordings in both pallidal segments were more distributed throughout the functional domains although many were in the classical motor domain (Parent and Hazrati, 1995). Neuronal response in both segments of the GP to STN stimulation did not display spatial differences. This lack of



evident organization of the responses is shown in relation to the anatomical reconstruction (Figure 2). The responses of neurons within territories classically defined as belonging to different functional domains did not display different properties. However, as we have limited coverage of the GP we cannot rule out such a spatial organization.

The firing rate of most STN neurons (58%) decreased significantly during the stimulation, with many of them undergoing complete cessation of firing. This is consistent with previous studies demonstrating STN inhibition during DBS (Benazzouz et al., 2000; Filali et al., 2004; Welter et al., 2004; Meissner et al., 2005; but see Carlson et al., 2010 for conflicting results). The reason for the discrepancy between these studies may be due to the different stimulations setups where the predominant parameter is probably the current intensity. We make this assumption based on observations in our data of STN neurons that displayed a minor or no response to low stimulation intensities (stimulation at 500 mV, data not shown) and displayed the typical inhibitory response at high stimulation intensities. This observation is consistent with the hypothesis that current intensity is the predominant factor in activation of neural elements (Ranck Jr., 1975; Butson and McIntyre, 2006; Miocinovic et al., 2009; Carlson et al., 2010).

The rate of the simultaneously recorded GPe and GPi neurons did not change significantly during the stimulation despite the major change in STN activity. This observation is surprising in light of the “box and arrow” models (Albin et al., 1989; DeLong, 1990) that view the STN projections to the GP as the main glutamatergic excitatory afferents (Smith and Parent, 1988; Robledo and Feger, 1990; Shink and Smith, 1995). The findings are nevertheless consistent with previous works which have failed to report a reduction in GP firing rate during STN stimulation (Hashimoto et al., 2003; Stefani et al., 2005). The fact that recordings during the stimulation period were performed simultaneously in the STN and both segments of the GP directly highlights the dissociation between the STN’s pre-synaptic somatic inhibition and the post-synaptic GP activation which does not comply with this inhibition. This dissociation phenomenon is consistent with previous modeling studies (McIntyre et al., 2004a; Miocinovic et al., 2006).

The recorded neurons displayed stereotypic response patterns to each stimulation pulse.

1 *Axonal activation:* This response type was characterized by a high entrainment to the stimulation; i.e., the neuron fired following stimulation at short constant delays with a high

probability. This high fidelity of the neuronal firing was complemented by a minimal jitter in the firing latency relative to the pulse time. This type of activation presumably results from the antidromic activation of the neuron by the stimulation via its axon (Kita and Kitai, 1991; Hashimoto et al., 2003). The delays and jitter were consistent with previous results demonstrating axonal activation (Kita and Kitai, 1991; Nambu et al., 2000; Hashimoto et al., 2003). The rapid response and low jitter cannot be explained by synaptic activation (Nambu et al., 2000). Some previous studies of neuronal activation following DBS did not observe this type of response (Meissner et al., 2005). This difference in the apparent observations may be due to the very short NP masked by the stimulation which was typically 0.75 ms in our study which prevented the masking of this fast response by the stimulation artifact. The antidromic GPi response is inconsistent with anatomical findings which are not aware of GPi efferent projections to the STN. Thus, GPi’s antidromic response may be an outcome of the stimulating electrode affecting the lenticular fasciculus which is a GPi efferent tract connected to the thalamus. This phenomenon is consistent with a previous computational study (Miocinovic et al., 2006). Neurons displaying axonal activation were activated following 53% of the stimulation. These results are also consistent with *in vitro* studies (Iremonger et al., 2006) which found that when stimulating the rat’s internal capsule at 125 Hz and recording in the primary motor cortex (M1), only about 50% of the stimulation pulses resulted in an antidromic activations.

2 *Inhibition:* This response type was characterized by a significant reduction in the firing rate throughout the stimulation relative to the baseline firing rate. This type of response was observed mainly in the STN and is consistent with previous work (Benazzouz et al., 2000; Filali et al., 2004; Meissner et al., 2005). In general the stimulated nucleus displayed a predominant inhibitory response either in GPi stimulation (Boraud et al., 1996; Dostrovsky et al., 2000) or STN stimulation. It is plausible that neurons classified as displaying an inhibitory response actually displayed an axonal response that was obscured by the non-usable period. This may also explain the dissociation mentioned above.

3 *Synaptic activation:* This response type was characterized by excitatory and inhibitory activation patterns. Excitatory activation patterns displayed an excitation (3–5 ms following the

stimulation pulse). In some cases, double or even triple excitatory modulations were observed (i.e., when additional excitations were observed at 0.7–2 and/or 6.5–7.3 ms). That was the predominant response in both segments of the GP. This result is consistent with previous studies of STN and GP stimulation (Nambu et al., 2000; Hashimoto et al., 2003; Bar-Gad et al., 2004; Erez et al., 2009). The latencies of the synaptic effects are congruent with previously described synaptic transmission delays (Nambu et al., 2000; Hashimoto et al., 2003; Erez et al., 2009). The second activation pattern was characterized by an inhibitory modulation (2–4 ms following the stimulation pulse). This response was displayed by a minority of the neurons. These inhibitory effects were probably a result of GABAergic synaptic input released from the pallidal collaterals of excited GP axons.

A predominant part of GPe neurons undergoing synaptic activation displayed an excitatory activation about 3 ms following STN stimulation, consistent with STN GPe synaptic transmission delay (Kita and Kitai, 1991; Hashimoto et al., 2003). Examination of GPi stimulation induced activity reveals reduced activity 5–6 ms following the stimulation. The expected 3 ms delay from the STN to the GPe combined with the 3-ms delay from the GPe to GPi (Kita, 2001) is expected to yield such an inhibitory effect roughly 6 ms after the stimulation pulses. However, additional GPe indirect effects such as reduced overall GPi rate due to the longer duration effect of IPSPs were not observed.

During the stimulation, temporal dynamics were observed in both firing rate and pattern. Firing rate dynamics were observed in both segments of the GP over the first 30 s of stimulation, when the firing rate changed and finally stabilized around baseline. STN firing rate dynamics was observed only over the first 10 s of the stimulation when the firing rate stabilized at ~40% of the baseline rate. The stimulation locked response displayed evolution both in decay of the firing rate and delay in the response to stimulation in both segments of the GP. No dynamics was observed in the STN although we assume that STN neurons with a synaptic response did display temporal dynamics over the stimulation. This dynamic process was probably obscured by a combination of a short integration period due to fast STN dynamics over the first 10 s of stimulation on one hand and the STN's low baseline firing rate on the other. The combination of these factors resulted in a noisy PSTH in which the fine temporal dynamics could not be extracted with confidence.

One of the principal findings of this study is the GP short term plasticity mechanism during STN macro-stimulation. This finding is consistent with a similar mechanism observed during GP

stimulation (Erez et al., 2009). We assume that fast recurrent axonal activation results in neurotransmitter depletion in the synapses, leading to a slower buildup of the post-stimulus response (Zucker and Regehr, 2002). We suggest that the two temporal dynamics observed are actually the outcome of a single process. As the GP firing rate increases upon stimulation onset, a gradual process of synapse depletion begins. This process results in a normalization of the firing rate and at the same time a delay and decay of the excitatory peak (See supplementary information Erez et al., 2009). We refer to the observed dynamics as short term plasticity since the neurons rapidly return to baseline.

The changes in information transmission within the BG during STN stimulation are key components in understanding the effect of STN stimulation at the system level. In addition, STN stimulation provided a unique opportunity to toggle the BG between two pathological states over a very short interval and compare the system level flow of information in those states. During the stimulation, STN entropy dropped significantly. This was attributed primarily to the change in the firing rate. At the same time GP entropy displayed changes to a much lesser extent. According to classical information theory, the entropy is the upper bound on the channel capacity. As a result we may infer that major changes in entropy eventually result in a change in the flow of information. Hence we assume that during the stimulation the STN went through a functional ablation. This fits the perception of the “functional ablation” during the stimulation which was suggested earlier (Benabid et al., 2002; McIntyre et al., 2004b).

We suggest that during STN macro-stimulation, the STN goes through a functional ablation and its upper bound on information transmission to downstream nuclei drops significantly. This is further supported by the evident dissociation between the pre-synaptic somatic inhibition and the post-synaptic axonal activation of its downstream targets and the reduction in the STN-pallidal synaptic efficacy. At the same time downstream GP segments display normal firing rates and are not affected by the deleterious effect of the STN. This mechanism may potentially be one of the key components leading to the alleviating effect of DBS in PD.

ACKNOWLEDGMENTS

We thank A. Korngreen for helpful discussions and K. McCairn, M. Dror, and P. Malmud for their help in animal treatment. This work was supported by grants from the Ministry of Health (MOH), the Israeli Science Foundation (ISF), and the Legacy Heritage Biomedical Program of the ISF.

REFERENCES

- Albin, R. L., Young, A. B., and Penney, J. B. (1989). The functional anatomy of basal ganglia disorders. *Trends Neurosci.* 12, 366–375.
- Alexander, G. E., DeLong, M. R., and Strick, P. L. (1986). Parallel organization of functionally segregated circuits linking basal ganglia and cortex. *Annu. Rev. Neurosci.* 9, 357–381.
- Anden, N. E., Carlsson, A., Dahlstroem, A., Fuxe, K., Hillarp, N. A., and Larsson, K. (1964). Demonstration and mapping out of nigro-neostriatal dopamine neurons. *Life Sci.* 3, 523–530.
- Anderson, M. E., Postupna, N., and Ruffo, M. (2003). Effects of high-frequency stimulation in the internal globus pallidus on the activity of thalamic neurons in the awake monkey. *J. Neurophysiol.* 89, 1150–1160.
- Bar-Gad, I., Elias, S., Vaadia, E., and Bergman, H. (2004). Complex locking rather than complete cessation of neuronal activity in the globus pallidus of a 1-methyl-4-phenyl-1,2,3,6-tetrahydropyridine-treated primate in response to pallidal microstimulation. *J. Neurosci.* 24, 9410–9419.
- Benabid, A. L., Benazzous, A., and Pollak, P. (2002). Mechanisms of deep brain stimulation. *Mov. Disord.* 17(Suppl. 3), S73–S74.
- Benazzous, A., Gao, D. M., Ni, Z. G., Piallat, B., Bouali, B. R., and Benabid, A. L. (2000). Effect of high-frequency stimulation of the subthalamic nucleus on the neuronal activities of the substantia nigra pars reticulata and ventrolateral nucleus of the thalamus in the rat. *Neuroscience* 99, 289–295.
- Benazzous, A., Gross, C., Feger, J., Boraud, T., and Bioulac, B. (1993). Reversal of rigidity and improvement in motor performance by subthalamic high-frequency stimulation in MPTP-treated monkeys. *Eur. J. Neurosci.* 5, 382–389.

- Bernheimer, H., Birkmayer, W., Hornykiewicz, O., Jellinger, K., and Seitelberger, F. (1973). Brain dopamine and the syndromes of Parkinson and Huntington. Clinical, morphological and neurochemical correlations. *J. Neurol. Sci.* 20, 415–455.
- Beurrier, C., Bioulac, B., Audin, J., and Hammond, C. (2001). High-frequency stimulation produces a transient blockade of voltage-gated currents in subthalamic neurons. *J. Neurophysiol.* 85, 1351–1356.
- Boraud, T., Bezard, E., Bioulac, B., and Gross, C. (1996). High frequency stimulation of the internal globus pallidus (GPi) simultaneously improves parkinsonian symptoms and reduces the firing frequency of GPi neurons in the MPTP-treated monkey. *Neurosci. Lett.* 215, 17–20.
- Brown, P., Mazzone, P., Oliviero, A., Altibrandi, M. G., Pilato, F., Tonali, P. A., and Di Lazzaro, V. (2004). Effects of stimulation of the subthalamic area on oscillatory pallidal activity in Parkinson's disease. *Exp. Neurol.* 188, 480–490.
- Butson, C. R., and McIntyre, C. C. (2006). Role of electrode design on the volume of tissue activated during deep brain stimulation. *J. Neural Eng.* 3, 1–8.
- Carlson, J. D., Cleary, D. R., Cetas, J. S., Heinricher, M. M., and Burchiel, K. D. (2010). Deep brain stimulation (DBS) does not silence neurons in subthalamic nucleus in Parkinson's patients. *J. Neurophysiol.* 103, 962–967.
- DeLong, M. R. (1990). Primate models of movement disorders of basal ganglia origin. *Trends Neurosci.* 13, 281–285.
- Dorval, A. D., Russo, G. S., Hashimoto, T., Xu, W., Grill, W. M., and Vitek, J. L. (2008). Deep brain stimulation reduces neuronal entropy in the MPTP-primate model of Parkinson's disease. *J. Neurophysiol.* 100, 2807–2818.
- Dostrovsky, J. O., Levy, R., Wu, J. P., Hutchison, W. D., Tasker, R. R., and Lozano, A. M. (2000). Microstimulation-induced inhibition of neuronal firing in human globus pallidus. *J. Neurophysiol.* 84, 570–574.
- Erez, Y., Czitron, H., McCairn, K., Bebelovsky, K., and Bar-Gad, I. (2009). Short-term depression of synaptic transmission during stimulation in the globus pallidus of 1-methyl-4-phenyl-1,2,3,6-tetrahydropyridine-treated primates. *J. Neurosci.* 29, 7797–7802.
- Erez, Y., Tischler, H., Moran, A., and Bar-Gad, I. (2010). Generalized framework for stimulus artifact removal. *J. Neurosci. Methods* 191, 45–59.
- Filali, M., Hutchison, W. D., Palter, V. N., Lozano, A. M., and Dostrovsky, J. O. (2004). Stimulation-induced inhibition of neuronal firing in human subthalamic nucleus. *Exp. Brain Res.* 156, 274–281.
- Garcia, L., Audin, J., D'Alessandro, G., Bioulac, B., and Hammond, C. (2003). Dual effect of high-frequency stimulation on subthalamic neuron activity. *J. Neurosci.* 23, 8743–8751.
- Hanson, J. E., and Jaeger, D. (2002). Short-term plasticity shapes the response to simulated normal and parkinsonian input patterns in the globus pallidus. *J. Neurosci.* 22, 5164–5172.
- Hashimoto, T., Elder, C. M., Okun, M. S., Patrick, S. K., and Vitek, J. L. (2003). Stimulation of the subthalamic nucleus changes the firing pattern of pallidal neurons. *J. Neurosci.* 23, 1916–1923.
- Remonger, K. J., Anderson, T. R., Hu, B., and Kiss, Z. H. (2006). Cellular mechanisms preventing sustained activation of cortex during subcortical high-frequency stimulation. *J. Neurophysiol.* 96, 613–621.
- Kita, H. (2001). Neostriatal and globus pallidus stimulation induced inhibitory postsynaptic potentials in entopeduncular neurons in rat brain slice preparations. *Neuroscience* 105, 871–879.
- Kita, H., and Kitai, S. T. (1991). Intracellular study of rat globus-pallidus neurons – membrane-properties and responses to neostriatal, subthalamic and nigral stimulation. *Brain Res.* 564, 296–305.
- Kita, H., Tachibana, Y., Nambu, A., and Chiken, S. (2005). Balance of mono-synaptic excitatory and disynaptic inhibitory responses of the globus pallidus induced after stimulation of the subthalamic nucleus in the monkey. *J. Neurosci.* 25, 8611–8619.
- Kuhn, A. A., Kempf, F., Brucke, C., Gaynor, D. L., Martinez-Torres, I., Pogossyan, A., Trottenberg, T., Kupsch, A., Schneider, G. H., Hariz, M. I., Vandenberghe, W., Nuttin, B., and Brown, P. (2008). High-frequency stimulation of the subthalamic nucleus suppresses oscillatory beta activity in patients with Parkinson's disease in parallel with improvement in motor performance. *J. Neurosci.* 28, 6165–6173.
- Kuhn, A. A., Kupsch, A., Schneider, G. H., and Brown, P. (2006). Reduction in subthalamic 8–35 Hz oscillatory activity correlates with clinical improvement in Parkinson's disease. *Eur. J. Neurosci.* 23, 1956–1960.
- Leblois, A., Boraud, T., Meissner, W., Bergman, H., and Hansel, D. (2006). Competition between feedback loops underlies normal and pathological dynamics in the basal ganglia. *J. Neurosci.* 26, 3567–3583.
- Lemon, R. N. (1984). *Methods for Neuronal Recording in Conscious Animals*. New York: Wiley.
- Limousin, P., Pollak, P., Benazzouz, A., Hoffmann, D., Broussolle, E., Perret, J. E., and Benabid, A. L. (1995). Bilateral subthalamic nucleus stimulation for severe Parkinson's disease. *Mov. Disord.* 10, 672–674.
- Magarinos-Ascone, C., Pazo, J. H., Macadar, O., and Buno, W. (2002). High-frequency stimulation of the subthalamic nucleus silences subthalamic neurons: a possible cellular mechanism in Parkinson's disease. *Neuroscience* 115, 1109–1117.
- Maurice, N., Thierry, A. M., Glowinski, J., and Deniau, J. M. (2003). Spontaneous and evoked activity of substantia nigra pars reticulata neurons during high-frequency stimulation of the subthalamic nucleus. *J. Neurosci.* 23, 9929–9936.
- McCairn, K. W., and Turner, R. S. (2009). Deep brain stimulation of the globus pallidus internus in the parkinsonian primate: local entrainment and suppression of low-frequency oscillations. *J. Neurophysiol.* 101, 1941–1960.
- McIntyre, C. C., Grill, W. M., Sherman, D. L., and Thakor, N. V. (2004a). Cellular effects of deep brain stimulation: model-based analysis of activation and inhibition. *J. Neurophysiol.* 91, 1457–1469.
- McIntyre, C. C., Mori, S., Sherman, D. L., Thakor, N. V., and Vitek, J. L. (2004b). Electric field and stimulating influence generated by deep brain stimulation of the subthalamic nucleus. *Clin. Neurophysiol.* 115, 589–595.
- Meissner, W., Leblois, A., Hansel, D., Bioulac, B., Gross, C. E., Benazzouz, A., and Boraud, T. (2005). Subthalamic high frequency stimulation resets subthalamic firing and reduces abnormal oscillations. *Brain* 128, 2372–2382.
- Miocinovic, S., Lempka, S. F., Russo, G. S., Maks, C. B., Butson, C. R., Sakaie, K. E., Vitek, J. L., and McIntyre, C. C. (2009). Experimental and theoretical characterization of the voltage distribution generated by deep brain stimulation. *Exp. Neurol.* 216, 166–176.
- Miocinovic, S., Parent, M., Butson, C. R., Hahn, P. J., Russo, G. S., Vitek, J. L., and McIntyre, C. C. (2006). Computational analysis of subthalamic nucleus and lenticular fasciculus activation during therapeutic deep brain stimulation. *J. Neurophysiol.* 96, 1569–1580.
- Montgomery, E. B. Jr. (2006). Effects of GPi stimulation on human thalamic neuronal activity. *Clin. Neurophysiol.* 117, 2691–2702.
- Nambu, A., Tokuno, H., Hamada, I., Kita, H., Imanishi, M., Akazawa, T., Ikeuchi, Y., and Hasegawa, N. (2000). Excitatory cortical inputs to pallidal neurons via the subthalamic nucleus in the monkey. *J. Neurophysiol.* 84, 289–300.
- Parent, A., and Hazrati, L. N. (1995). Functional anatomy of the basal ganglia. I. The cortico-basal ganglia-thalamo-cortical loop. *Brain Res. Brain Res. Rev.* 20, 91–127.
- Prescott, I. A., Dostrovsky, J. O., Moro, E., Hodaie, M., Lozano, A. M., and Hutchison, W. D. (2009). Levodopa enhances synaptic plasticity in the substantia nigra pars reticulata of Parkinson's disease patients. *Brain* 132, 309–318.
- Ranck, J. B. Jr. (1975). Which elements are excited in electrical stimulation of mammalian central nervous system: a review. *Brain Res.* 98, 417–440.
- Rav-Acha, M., Sagiv, N., Segev, I., Bergman, H., and Yarom, Y. (2005). Dynamic and spatial features of the inhibitory pallidal GABAergic synapses. *Neuroscience* 135, 791–802.
- Robledo, P., and Feger, J. (1990). Excitatory influence of rat subthalamic nucleus to substantia nigra pars reticulata and the pallidal complex: electrophysiological data. *Brain Res.* 518, 47–54.
- Rubin, J. E., and Terman, D. (2004). High frequency stimulation of the subthalamic nucleus eliminates pathological thalamic rhythmicity in a computational model. *J. Comput. Neurosci.* 16, 211–235.
- Schneider, J. S., Goncz, H., and Decamp, E. (2003). Development of levodopa-induced dyskinesias in parkinsonian monkeys may depend upon rate of symptom onset and/or duration of symptoms. *Brain Res.* 990, 38–44.
- Shink, E., and Smith, Y. (1995). Differential synaptic innervation of neurons in the internal and external segments of the globus pallidus by the. *J. Comp. Neurol.* 358, 119–141.
- Siegfried, J., and Lippitz, B. (1994). Bilateral chronic electrostimulation of ventroposterolateral pallidum: a new therapeutic approach for alleviating all parkinsonian symptoms. *Neurosurgery* 35, 1126–1129.
- Smith, Y., and Parent, A. (1988). Neurons of the subthalamic nucleus in primates display glutamate but not GABA immunoreactivity. *Brain Res.* 453, 353–356.
- Stefani, A., Fede, E., Galati, S., Pepicelli, O., Frasca, S., Pierantozzi, M., Peppe, A., Brusa, L., Orlacchio, A., Hainsworth, A. H., Gattoni, G., Stanzione, P., Bernardi, G., Raiteri, M., and Mazzone, P. (2005). Subthalamic stimulation activates internal pallidus: evidence from

- cGMP microdialysis in PD patients. *Ann. Neurol.* 57, 448–452.
- Stevens, C. F., and Zador, A. (1996). “Information through a spiking neuron,” in *Advances in Neural Information Processing Systems*, Vol. 8, eds D. S. Touretzky, M. Mozer, and M. E. Hasselmo (Cambridge, MA: MIT Press), 75–81.
- Szabo, J., and Cowan, W. M. (1984). A stereotaxic atlas of the brain of the cynomolgus monkey (*Macaca fascicularis*). *J. Comp. Neurol.* 222, 265–300.
- Tai, C. H., Boraud, T., Bezard, E., Bioulac, B., Gross, C., and Benazzouz, A. (2003). Electrophysiological and metabolic evidence that high-frequency stimulation of the subthalamic nucleus bridges neuronal activity in the subthalamic nucleus and the substantia nigra reticulata. *FASEB J.* 17, 1820–1830.
- Welter, M. L., Houeto, J. L., Bonnet, A. M., Bejjani, P. B., Mesnage, V., Dormont, D., Navarro, S., Cornu, P., Agid, Y., and Pidoux, B. (2004). Effects of high-frequency stimulation on subthalamic neuronal activity in parkinsonian patients. *Arch. Neurol.* 61, 89–96.
- Wichmann, T., Bergman, H., and DeLong, M. R. (1994). The primate subthalamic nucleus. I. Functional properties in intact animals. *J. Neurophysiol.* 72, 494–506.
- Wu, Y. R., Levy, R., Ashby, P., Tasker, R. R., and Dostrovsky, J. O. (2001). Does stimulation of the GPI control dyskinesia by activating inhibitory axons? *Mov. Disord.* 16, 208–216.
- Zucker, R. S., and Regehr, W. G. (2002). Short-term synaptic plasticity. *Annu. Rev. Physiol.* 64, 355–405.
- Conflict of Interest Statement:** The authors declare that the research was conducted in the absence of any commercial or financial relationships that could be construed as a potential conflict of interest.
- Received: 31 December 2010; accepted: 08 April 2011; published online: 26 April 2011.
Citation: Moran A, Stein E, Tischler H, Bebelovsky K and Bar-Gad I (2011) Dynamic stereotypic responses of basal ganglia neurons to subthalamic nucleus high-frequency stimulation in the parkinsonian primate. *Front. Syst. Neurosci.* 5:21. doi: 10.3389/fnsys.2011.00021
Copyright © 2011 Moran, Stein, Tischler, Bebelovsky and Bar-Gad. This is an open-access article subject to a non-exclusive license between the authors and Frontiers Media SA, which permits use, distribution and reproduction in other forums, provided the original authors and source are credited and other Frontiers conditions are complied with.



Neighboring pallidal neurons do not exhibit more synchronous oscillations than remote ones in the MPTP primate model of Parkinson's disease

Rea Mitelman^{1,2*}, Boris Rosin^{1†}, Hila Zadka^{1,3}, Maya Slovik¹, Gali Heimer⁴, Ya'akov Ritov^{2,5}, Hagai Bergman^{1,2,6} and Shlomo Elias^{1,7}

¹ Department of Medical Neurobiology, Institute of Medical Research Israel-Canada, The Hebrew University – Hadassah Medical School, Jerusalem, Israel

² The Interdisciplinary Center for Neural Computation, The Hebrew University, Jerusalem, Israel

³ Department of Psychology, The Hebrew University, Jerusalem, Israel

⁴ Pediatric Neurology Unit, The Edmond and Lily Safra Children's Hospital, Sheba Medical Center, Tel Hashomer, Israel

⁵ Department of Statistics, The Hebrew University, Jerusalem, Israel

⁶ Edmond and Lily Safra Center for Brain Sciences, The Hebrew University, Jerusalem, Israel

⁷ Department of Medicine, Hadassah University Hospital, Jerusalem, Israel

Edited by:

Charles J. Wilson, University of Texas at San Antonio, USA

Reviewed by:

Robert S. Turner, University of Pittsburgh, USA

Hitoshi Kita, The University Tennessee Health Science Center, USA

*Correspondence:

Rea Mitelman, Department of Medical Neurobiology (Physiology), Institute of Medical Research Israel-Canada, The Hebrew University – Hadassah Medical School, POB 12272, Jerusalem 91120, Israel.

e-mail: rea.mitelman@mail.huji.ac.il

[†]Rea Mitelman and Boris Rosin have contributed equally to this work.

In the healthy primate, neurons of the external and internal segments of the globus pallidus (GP) present a primarily irregular firing pattern, and a negligible level of synchrony is observed between pairs of neurons. This holds even for neighboring cells, despite their higher probability to receive common inputs and to innervate each other via lateral connectivity. In the Parkinsonian primate, this changes drastically, and many pairs of GP cells show synchronous oscillations. To address the relation between distance and synchrony in the Parkinsonian state, we compared the synchrony of discharge of close pairs of neurons, recorded by the same electrode, with remote pairs, recorded by different ones. However, spike trains of neighboring cells recorded by the same extracellular electrode exhibit the shadowing effect; i.e., lack of detection of spikes that occur within a few milliseconds of each other. Here, we demonstrate that the shadowing artifact can both induce apparent correlations between non-correlated neurons, as well as conceal existing correlations between neighboring ones. We therefore introduced artificial shadowing in the remote pairs, similar to the effect we observed in the close ones. After the artificial shadowing, neighboring cells did not show a higher tendency to oscillate synchronously than remote ones. On the contrary, the average percentage (over all sessions) of artificially shadowed remote pairs exhibiting synchronous oscillations was 35.4% compared to 17.2% in the close ones. Similar trend was found when the unshadowed remote pairs were separated according to the estimated distance between electrode tips: 29.9% of pairs at approximate distance of less than 750 μm were significantly synchronized, in comparison with 28.5% of the pairs whose distance was more than 750 μm . We conclude that the synchronous oscillations in the GP of MPTP treated primates are homogeneously distributed.

Keywords: primate, basal ganglia, spike trains, synchronization, MPTP, oscillations, globus pallidus

INTRODUCTION

The basal ganglia are a set of subcortical nuclei which play an important role in the control of behavior. This can be seen in both normal physiology, as well as in several movement disorders, the most prominent being Parkinson's disease (PD). The basal ganglia receive inputs from cortical and thalamic areas, and in a mostly feed-forward manner innervate the brainstem motor nuclei and the motor thalamic nuclei which close the loop back to the motor cortices (Haber and Gdowski, 2004). Anatomically, there is a high level of convergence of inputs from the cortex to the input nuclei of the basal ganglia, the striatum and the subthalamic nucleus. Further convergence exists in the next stages of the basal ganglia, which consist of both segments of the globus pallidus (GP) as well as the substantia nigra pars reticulata (SNr). The external segment of the globus pallidus (GPe) is an internal nucleus within the basal ganglia network, whereas the internal segment of the globus pallidus (GPi)

and the SNr form the network's output nuclei. Both the GPe and the GPi are relatively small nuclei, and have approximately two orders of magnitude fewer neurons than their major input – the striatum (Percheron et al., 1987; Bar-Gad et al., 2003b).

In the healthy primate, the firing pattern of most GP neurons is irregular (DeLong, 1971). Despite the high level of convergence of input innervations (Percheron et al., 1984) and inhibitory collaterals (Kita and Kita, 1994; Sato et al., 2000), GP neurons exhibit negligible synchrony (Nini et al., 1995; Raz et al., 2000). This is the case even between neighboring cells (Bar-Gad et al., 2003a), despite their high probability of sharing at least some of the input and/or having anatomical lateral connections.

In both human PD patients and monkeys treated with the neurotoxin 1-methyl-4-phenyl-1,2,3,6-tetrahydropyridine (MPTP), these properties change drastically. Synchrony appears between pairs of GP neurons, and the firing of many of them is dominated

by episodes of periodic bursts. Typically, these periodic oscillations occur within two narrow frequency bands, approximately the tremor frequency (around 5–7 Hz) and double-tremor frequencies (Nini et al., 1995; Raz et al., 2000; Levy et al., 2002). In the rodents unilaterally injected with 6-hydroxy-dopamine (6-OHDA), the level of synchrony was found to moderately decrease with the distance (Mallet et al., 2008). However, no similar study has apparently been conducted in Parkinsonian primates.

Traditional studies of single neuron activity in awake behaving animals involve extracellular electrophysiological recordings which are subjected to detection and sorting of action potential (spike) waveforms (Abeles and Goldstein, 1977; Lewicki, 1998). However, the detection of spikes of neighboring neurons recorded by the same electrode, is affected by the shadowing effect (Bar-Gad et al., 2001); namely, when two neurons fire approximately together, the sorting process fails to identify both action potentials (Figure 1A). Although stereo-recording (e.g., by tetrode) might reduce the shadowing effect, they don't completely eradicate it (Harris et al., 2000). The shadowing effect distorts the spike to spike cross-correlation function of the two neurons, and may lead to false appearance of synchronization (Bar-Gad et al., 2001).

Bar-Gad et al. (2003a) developed a method to estimate the cross-correlogram of an unsynchronized pair of neighboring neurons (with shadowing effect), assuming the autocorrelation functions are known (Bar-Gad et al., 2001). They concluded that cross-correlograms which are significantly different from the expected function are therefore synchronous. However, in the Parkinsonian state, the autocorrelation functions might be severely affected by the shadowing effects, and therefore the real (i.e., unshadowed) autocorrelation functions are unknown. We cannot assume that the autocorrelation functions are flat (as done in the normal state) because of the known pathological oscillatory firing. Therefore a different approach is required.

Here we confirm that the shadowing effect can create false synchronization, as reported by Bar-Gad et al. (2001). However, we also show that in other cases, this undesired alteration in data can also conceal existing synchrony. Therefore, one cannot assume that the extent of correlation found under the shadowing effect represents an upper bound for the real correlations. We thus present a new method which enables a balanced comparison of close and remote pairs by artificially shadowing the remote pairs. This method creates two populations of pairs, which differ only in the distance between the cells, but not in the shadowing effect. Thereby, we can compare them and estimate the spatial distribution of the synchrony in the GP of the MPTP treated primate. Understanding the spatiotemporal pattern of the pallidal synchrony in the Parkinsonian primate can shed new light on the basal ganglia functional connectivity. Furthermore, these patterns may help clarify what role these pathological oscillations play downstream to the basal ganglia.

MATERIALS AND METHODS

RECORDING PROCEDURES AND MPTP INJECTIONS

The experiments were carried out on two vervet monkeys (Cu and S, *Cercopithecus aethiops aethiops*, females, weighing 3.8 and 3.6 kg, respectively). Primates' care and surgical procedures were in accordance with the *NIH Guide for the Care and Use of Laboratory Animals*

(1996) and the Hebrew University Guidelines for the Use and Care of Laboratory Animals in Research, supervised by the Institutional Committee for Animal Care and Use.

Both monkeys were trained to sit in a monkey chair; monkey Cu was also trained to perform a self-initiated button-pressing task to obtain a liquid reward. After training, a recording chamber was attached to the monkey's skull under surgical procedure. Details of the surgery and data recording of monkey Cu methods were given previously (Heimer et al., 2002, 2006; Bar-Gad et al., 2003a; Elias et al., 2007). Surgery and data recording details of monkey S were identical to those performed on monkey Cu, unless stated otherwise. Briefly, a Cilux recording chamber (Cu – 18 mm round base; S – 27 mm square base) was tilted 50° laterally in the coronal plane and was positioned by a stereotactic device to cover most of the pallidal area (Contreras et al., 1981; Szabo and Cowan, 1984; Martin and Bowden, 2000).

The exact position of the chamber was verified using an MRI scan and electrophysiological mapping.

On each recording day, glass-coated tungsten electrodes (127 µm diameter tungsten rods coated with a layer of approximately 100 µm glass, yielding a total diameter of ~350 µm for a length of 8–10 cm), confined to a concentric guide tube, were inserted into the brain. The electrodes' relative and absolute location was a consequence of the chamber's tilted angle. Therefore, distances on the plane tangent to the chamber (and therefore the cranium) are defined "horizontal", and distances perpendicular to the cranium are defined "vertical".

The horizontal distance between the different electrodes was defined by the spatial arrangement of the electrodes within the guide: for monkey S the four electrodes were confined in a 570-µm inner diameter guide (i.e., 2 × 2 square with a 410-µm side). For monkey Cu the eight electrodes were confined in a 1420-µm inner diameter guide (i.e., one central electrode with a distance of 505 µm from each of the seven surrounding ones). Layout design can be found at: http://www.alphaomega-eng.com/pr_site/mt_layout/mt_designs.htm.

A mechanical micro-drive (EPS – Electrode Positioning System 1.28, Alpha-Omega Engineering, Nazareth, Israel) was used to lower each electrode individually through the dura into the brain while tracking its depth. Inside the recording target, we manipulated the electrode depth until an optimal and stable signal to noise ratio of spiking activity had been achieved. Vertical distances between the electrodes were therefore variable and typically ranged between 0 and 2000 µm. Distance between electrodes tips was estimated based on depth and horizontal distances. However, it should be stressed that this depth is subject to inaccuracies resulting mainly from the electrodes flexibility. This might be more pronounced in our settings, in which long (8–10 cm), and thin (350 µm diameter) electrodes were used, in order to minimize the spatial spread of the recording tips of the microelectrodes.

After recordings in the normal state, the monkeys were rendered Parkinsonian by five intramuscular injections of 0.4 mg/kg of MPTP-HCl dissolved in ~0.5 ml of normal saline (Cu: Aldrich, Milwaukee, WI, USA; S: Sigma, Israel) over a period of 4 days. The monkeys were clinically assessed on a regular basis using a modified primate clinical staging scale (Benazzouz et al., 1995; Imbert et al., 2000). The monkeys developed severe Parkinsonism 5 days after initiation of MPTP treatment, and received an average score

of 30.0/36 (Cu) and 20.0/25 (S). Recordings were resumed 4 days after the last MPTP injection. In monkey Cu, recordings were also conducted after treatment with dopamine replacement therapy (these data are not included in this report).

Pallidal neurons were identified according to their stereotactic coordinates (based on the MRI and the primate atlas data) and their real-time physiological properties (typical spike shape, firing rate, and pattern), which are considerably different from striatal neurons located above (DeLong, 1971). Differentiation into GPe and GPi neurons was determined by the depth of the electrode and other anatomical/physiological structures identified along the electrode trajectory (e.g., border cells). Pallidal cells which could not be classified as GPe or GPi neurons were considered GP neurons.

RECORDING AND SPIKE SORTING

The electrode output was sorted and classified in real time by a template-matching algorithm (Cu: MSD, S: ASD; Alpha-Omega Engineering, Nazareth, Israel). In addition, the electrode output was also bandpass filtered (Cu: 300–6000 Hz, S: 250–5000, MCP-plus; Alpha-Omega Engineering) and continuously sampled (Cu: 24 kHz, S: 40 kHz, AlphaMap; Alpha-Omega Engineering). The continuous sampling of the electrode output of monkey Cu was also subjected to an offline spike-sorting procedure (AlphaSort; Alpha-Omega Engineering) based on principal-component analysis of the spike patterns (Abeles and Goldstein, 1977). We applied two sets of principal components (PCs), a default based on cortical recordings (Abeles and Goldstein, 1977) and a set of PCs that were created by a library of 131 waveforms of well isolated pallidal spikes recorded by the same setup (Bar-Gad et al., 2003a). Offline sorting was performed using both cortical and pallidal PCs, and the best result was taken for each pair.

Both offline (monkey Cu) and online (monkey S) sorting was verified by the existence of a refractory period in the inter-spike interval histogram (cells in which more than 2% of the total inter-spike intervals were less than 2 ms were excluded) and by the stability of the firing rate of the cells (inspected by human observer). In the stability analysis, the instantaneous firing rate of the neurons as a function of time was displayed for the entire period of recording, and the largest segment of stable data was selected for additional analysis. Spike times were saved at the sampling rate of the analog data (Cu: 24 kHz; S: 40 kHz).

DATA ANALYSIS

All data analysis was done on custom software using *Matlab* (The MathWorks). Only pairs of neurons which were recorded simultaneously and fulfilled the isolation criteria (refractory period and stability of discharge rate) for at least 150 s were included. For analysis of the shadowing effect, which is a phenomenon at the sub-millisecond order, we used the original sampling rate. For the inspection of synchronous oscillations, we down sampled the data to a sampling rate of 1 kHz.

We used auto and cross-correlation functions for time domain analyses. The cross correlation of all pairs of cells recorded by the same electrode showed a clear shadowing effect (Figure 1A). We used a global shuffling method for the frequency domain analysis (Rivlin-Etzion et al., 2006), which reflects this domain more reliably than standard spectrum or coherence functions by compensating

for the effect of the refractory period. This method is especially useful for bursting oscillations, which are typical at the Parkinsonian pallidum. Similar to previous work (Heimer et al., 2006), we used a frequency resolution of 0.25 Hz; shuffling was repeated 20 times; the confidence interval was set based on the flat high frequency range (270–300 Hz); and the range of interest for significant oscillations was 4.5–30 Hz. Since we used shadowed spike trains, which rendered noisy spectrograms especially in the low frequencies, we defined a higher threshold than described previously (Rivlin-Etzion et al., 2006). To define a significant oscillation in this study, a segment of three consecutive samples were required to cross a confidence level of $p = 10^{-5}$. Furthermore, we required that the local maximum of an interval which crossed the confidence level would be within the range of interest (4.5–30 Hz).

Single neurons were defined “oscillatory” if they had at least one segment in their auto-spectrum function which fulfilled the criteria detailed above. Similarly, close pairs of neurons were defined “synchronized” if they had at least one segment in their cross-spectrum which fulfilled these criteria. Remote pairs of neurons were graded between 0 and 1 (synchronization index), according to their probability of being detected as “synchronized” had they been affected by the shadowing effect (see below). For further analysis, a non-synchronization index was also defined, such that it completed the synchronization index to 1 (i.e., their probability of not being detected as synchronized had they been affected by shadowing). For a synchronized pair, the oscillation frequency was defined as the frequency of the maximal peak in the cross-spectrum (within the range of interest).

ESTIMATING THE SHADOWING EFFECT

In order to mimic the shadowing effect on remote cells, we first estimated the shadowing effect of the close pairs (see details in the Appendix). Briefly, we used previously derived mathematical equations (Eqs 1 and 2 in the Appendix) which estimate the recorded cross-correlation function and recorded firing rate, given the probability to miss a spike in each time sample (termed “shadowing vector”) and the original – “true” firing rates of the two cells (Bar-Gad et al., 2001). Based on the same formula we estimated the shadowing vector (as well as the original firing rates), given the recorded firing rate and cross correlation. This can be done under several assumptions, which are necessary for mathematically extracting the shadowing vector (see details in the Appendix). First, we assume that the shadowing effect is shorter than the refractory period. Second, the shadowing vectors of a pair of neurons are symmetric; i.e., the shadowing vector of the first cell at time t equals the shadowing vector of the second cell at time minus t . Finally, we assume that during complete shadowing (i.e., at time samples in which the shadowing vector, or the lost spike probability, equals 1), no spike was detected at either of the cells. This process yielded one shadowing vector per close pair.

To test the shadowing effect estimation method, we used data recorded from the two monkeys, where spikes are detected and sorted with different methods. Offline sorting (monkey Cu) yielded a longer shadowing period than online sorting (monkey S), apparently reflecting the longer “dead time” required by the offline sorting algorithm. The averaged shadowing vectors of monkeys Cu and

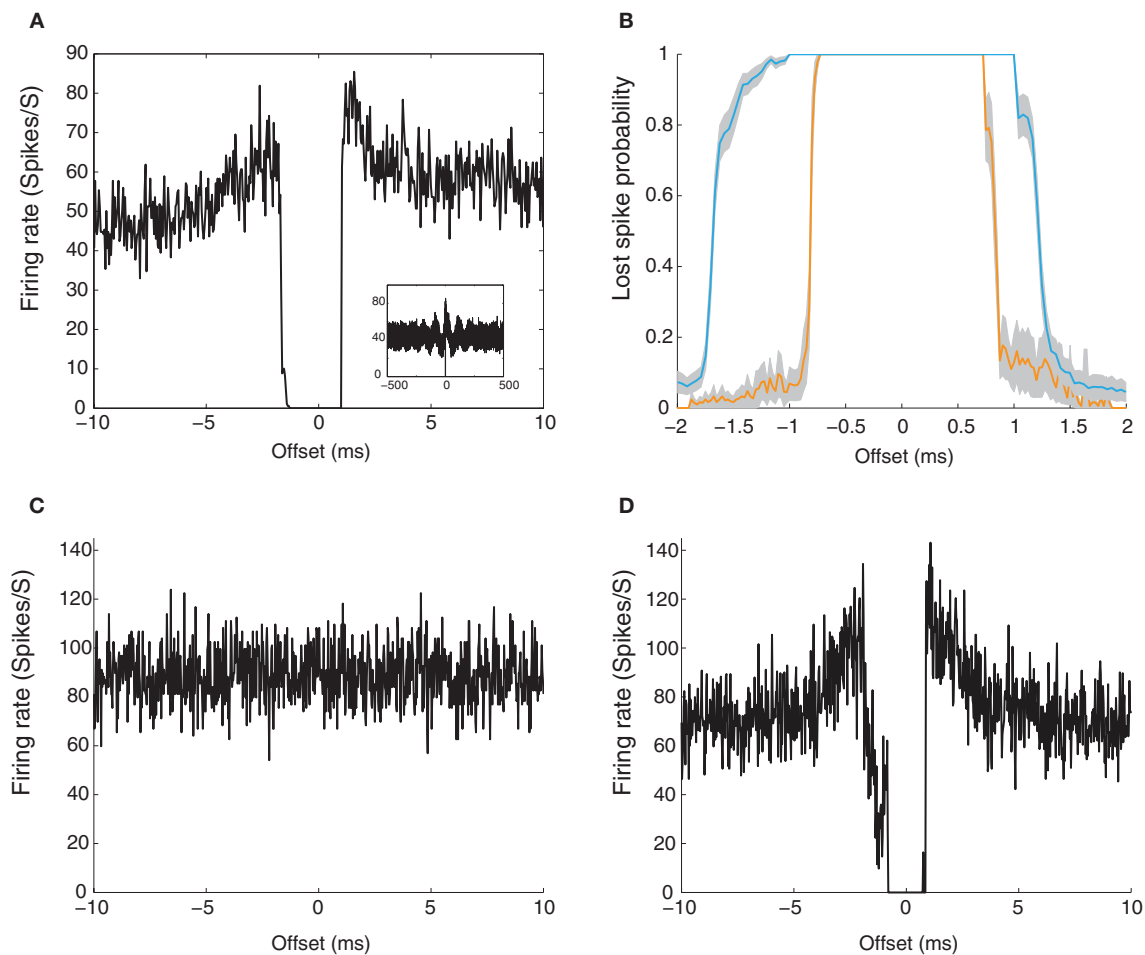


FIGURE 1 | The shadowing effect – demonstration, quantification, and artificial shadowing. (A) Cross correlation function of a pair of neighboring pallidal neurons (i.e., extracellularly recorded by the same electrode, Monkey Cu). The shadowing effect is approximately within 1 ms offset. This pair also exhibits synchronous oscillations, as can be seen in the larger time scale (± 500 ms) cross correlation histogram in the inset. **(B)** Mean shadowing effect, as estimated from

the close pairs sorted offline (monkey Cu, $n = 24$ pairs, in blue) and online (monkey S, $n = 15$ pairs, in orange). Gray shading marks the SEM. The shadowing effect for the online sorting is shorter than that of the offline sorting. **(C)** Example of cross correlation of a pallidal remote pair (i.e., recorded by different electrodes) from monkey S. **(D)** Cross correlation of the pair shown in (C), after artificial shadowing by one of the five representative shadowing vectors.

S are shown in **Figure 1B**. During the analysis of the remote pairs of each monkey, we used the shadowing vectors derived from the close pairs of the same monkey.

MIMICKING THE SHADOWING EFFECT

Artificial shadowing of a pair of spike trains recorded by different electrodes, by a given shadowing vector, was done by dropping spikes from these spike trains with the probability derived from the shadowing vector. A simplified approach would have been to take the average shadowing vector and use it to shadow the remote pairs. However, this would not have fully represented the diversity of the different shadowing vectors. Ideally, we should have artificially shadowed each remote pair with all possible shadowing vectors (as calculated for all the close pairs of a particular monkey). However, repeating the artificial shadowing and all further analyses with all shadowing vectors for all remote pairs was computationally heavy. Therefore, we chose five representative shadowing vectors (per monkey in this study), and applied them to the remote pairs.

The representative vectors were chosen in the following way: all the shadowing vectors were pooled together, and for each time sample, five values were chosen such that they divided the amplitude of the shadowing vector at each time sample into six evenly spaced shares. This approach (known as six-quantiles), is a natural extension of the median concept (achieved by dividing the data into two equal shares), and still provides a good representation of the population diversity. As stated above, this was done separately for each monkey.

Since shadowing is stochastic in nature (there are points in which the probability of missing a spike lies between 0 and 1), we repeated the artificial shadowing with a given shadowing vector five times and averaged the resulting time and frequency correlation functions. This yielded a single correlation function per shadowing vector. All in all, we had five cross-spectrum functions for any given pair of remote neurons, one from each representative shadowing vector. The relative part out of these five functions which was considered synchronous (according to the parameters

mentioned above), was defined as synchronization index of that pair. This index represents the probability ($p = 0, 0.2, 0.4, \dots, 1$) of a remote pair to be detected as synchronized, had it been affected by the shadowing effect. A complementary non-synchronization index was also defined, such that it completes the synchronization index to 1. Close pairs were classified as either synchronized or non-synchronized (which is equivalent to a synchronization index of 1 or 0 respectively). **Figures 1C,D** illustrates the artificial shadowing of a remote pair by one of the five shadowing vectors (for simplified visualization). Applying the shadowing vectors yielded the short term artifacts observed in the close pairs, as planned.

STATISTICAL COMPARISON OF CLOSE AND REMOTE PAIRS

Comparison of two populations (close vs. remote pairs) divided into two categories (synchronized vs. non-synchronized) is typically done by 2×2 contingency table. This method was easily expanded in our continuous case by replacing the discrete number of synchronized pairs by the sum of the synchronization index, which could be a fraction. Similarly, the number of non-synchronized pairs was replaced by the sum of the non-synchronization index. This yielded a continuous 2×2 contingency table per recording session.

For each pallidal population, we obtained an $N \times 2 \times 2$ hypermatrix, where N represents the number of recording sessions ($N = 16$ and 33 recording sessions for monkey Cu and S respectively). First, we summed the results over the N sessions. This yielded, for each population (GPe, GPi, GP-pooled), a 2×2 continuous version of the contingency table previously described. To test the hypothesis that both close and remote pairs originate from the same distribution, we used a two-tailed statistical Fisher's exact test, with the null hypothesis that close pairs are as synchronized as remote ones (the χ^2 test was not suitable because of the relative small N for the GPi population).

However, since the pallidal oscillations in the Parkinsonian monkey are episodic in nature, this analysis method might distort the results. For example, if during oscillatory episodes more remote pairs were recorded, this might create the impression that they have a higher probability for synchronous oscillations. Furthermore, in an analysis of three or more simultaneously recorded neurons, not all comparisons are independent (e.g., if there is synchrony between the neuron pair A–B and B–C, one would probably find a synchrony between the A–C pair). Therefore, counting correlated pairs might again bias the results.

To overcome this, we used additionally a different statistical method. We averaged the synchronization index of the close and remote populations, over all N sessions. This method yielded the average synchrony percentage per recording session (for close and remote pairs separately), rather than the total percentage of synchronized pairs. Here, we used a statistical two-tailed Student's t -test, comparing the session's synchronicity. As before, our null hypothesis was that in an average session, the fraction of synchronized pairs of close neurons was identical to that of the remote pairs.

RESULTS

SHADOWING EFFECT IN THE TIME AND FREQUENCY DOMAIN

Previous studies (Bar-Gad et al., 2001) have revealed that the shadowing effect can induce apparent synchrony between neurons recorded simultaneously from the same electrode. These effects are

visible in the time domain, but are clearer in the frequency domain. **Figure 2A** presents the temporal (first row) and frequency (second row) correlation of a remote pallidal pair. The insets present the autocorrelation and auto-spectrum of the two cells. In both domains, the pair shows no significant synchronous oscillations (although one of the cells does show oscillations). The effect of artificial shadowing on the correlation and the cross-spectrum functions of this pair is shown in **Figure 2B**. Both functions (in the time and frequency domains) present clear and statistically significant (here calculated only for the frequency domain) synchronous oscillations at approximately 10 Hz.

Here we show that the shadowing effect can also have the opposite effect and mask existing synchrony. This opposite phenomenon is presented in **Figure 3**. Here, a remote pair displays significant synchronous oscillations (**Figure 3A**). However, after artificial shadowing by one of the five possible shadowing vectors (**Figure 3B**), the peak in the cross-spectrum function is smoothed and the cross-spectrum does not meet the significance criteria. Thus, the artificial shadowing by this shadowing vector results in no-detection of synchronous oscillations of this pair of neurons. Application of the other four representative shadowing vectors here also masked the synchrony and yielded a synchronization index of 0.

Thus, the net effect of the shadowing on the detection of neuronal synchronous oscillations is not unidirectional and two error types are possible. First, there are false positive errors; i.e., detection of significant synchronous oscillations in the shadowed pair which were not there in the original spike trains. Second, there are false negative errors; i.e., synchronous oscillations that were missed because of the shadowing effect. The fraction of the two errors was found to differ between the two monkeys, probably because of the difference in sorting method of the close pairs and the resulting shadowing vectors (**Figure 1B**). For monkey S ($n = 91$ pairs, sorted online, and ~ 2 ms duration shadowing effect), P (false positive) = 0.074, and P (false negative) = 0.171, whereas for monkey Cu ($n = 349$ pairs, sorted offline, and ~ 3.5 ms shadowing effect), P (false positive) = 0.27, and P (false negative) = 0.309. Apparently, the longer duration of the shadowing vector originating from the offline sorting process led to the higher error values in this case.

Next, we wanted to further understand the connection between these types of errors and the firing properties of each of the neurons in a given pair. To do so, we calculated the probabilities of having zero, one, or two of the cells significantly oscillatory in each of the pairs. This was done given the probability of having one of the possible types of errors, as well as the two correct possibilities (correct detection and rejection of synchronous oscillations). These results are summed at **Table 1**. The most striking result is that all cases in which the shadowing effect created apparent synchrony occurred when only one of the cells in the pair was significantly oscillatory. On the other hand, about half of the cases in which synchrony was concealed by the shadowing effect occurred when none of the cells in the pair was considered oscillatory.

Thus overall, the shadowing effect on neighboring neurons is not one-sided, and it induces both false detection of synchronous oscillations, as well as misses of existing synchronous oscillations. Therefore, a proper comparison of the close pairs to the remote ones should balance this effect.

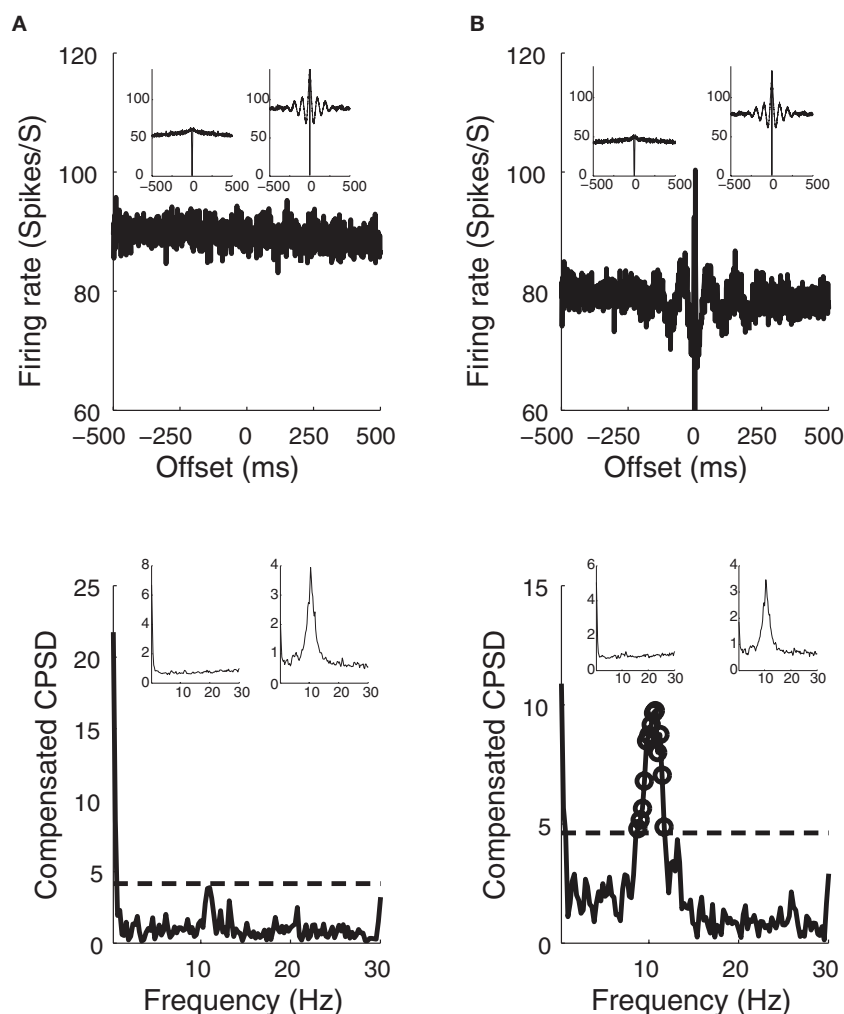


FIGURE 2 | Shadowing effect induces artificial synchronous oscillations. (A) A remote pair (same pair as in Figures 1C,D) which does not exhibit significant synchronous oscillations. First row – cross-correlation function (inset: auto correlation functions); second row – cross power spectral density (CPSD, inset: auto-spectral densities). Note that one of the cells is oscillatory whereas the other one is not. **(B)** The same pair as in A, after artificial shadowing by one of the

representative shadowing vectors. At the time domain (first row) we can see the large deflection around $t = 0$ which is caused by the shadowing effect. Both time domain and frequency domain (second row) demonstrate synchronous oscillations (insets show auto correlations and auto-spectrum after shadowing). Confidence levels in the frequency domain are marked with a broken line. Significant samples (at least three continuous) are marked with a circle.

SYNCHRONY IN THE DIFFERENT PALLIDAL POPULATIONS

We divided the pallidal cell population into three groups – GPe, GPi, and GP (i.e., unclassified cells within the GP). We analyzed separately the GPe pairs, and the GPi pairs, and then pooled all three pallidal populations together (“GP-pooled”).

We used two different statistical approaches in the comparison of close and remote pairs (see details in the Materials and Methods). The results of the contingency table analysis, which pools all pairs and ignores the sessions in which they were recorded, are summarized in **Table 2**. In the pooled data (as in most sub-groups), the fraction of synchrony in the close pairs (20.5%) was slightly higher than in the remote one without shadowing (17.7%). After application of the shadowing effects to the remote pairs (to balance this effect on the close pairs) we found that the fraction of synchrony in the close pairs (20.5%) was actually lower than that in

the remote ones (32.2%). Thus, to our surprise, we failed to reject the null hypothesis that the fraction of synchrony in the close pairs is equal to that found at the remote ones (after artificial shadowing).

Similar trend was achieved in the second analysis method of averaging the synchrony over the recording sessions. This method has the advantage of compensating the episodic nature of the oscillations (see Materials and Methods). These results are summarized in **Table 3**. In the pooled data, the average synchrony of the close pairs (17.2%) was smaller than that of the remote ones, both before and after artificial shadowing (29.2 and 35.4%, respectively).

Both analysis methods yielded similar results. After artificial shadowing, the remote pairs tend to be more synchronized than the close ones. This was the case for both monkeys, in both the GPe and the GP-pooled population. In the GPi we observed opposite trends in the two monkeys, but the number of close pairs in our

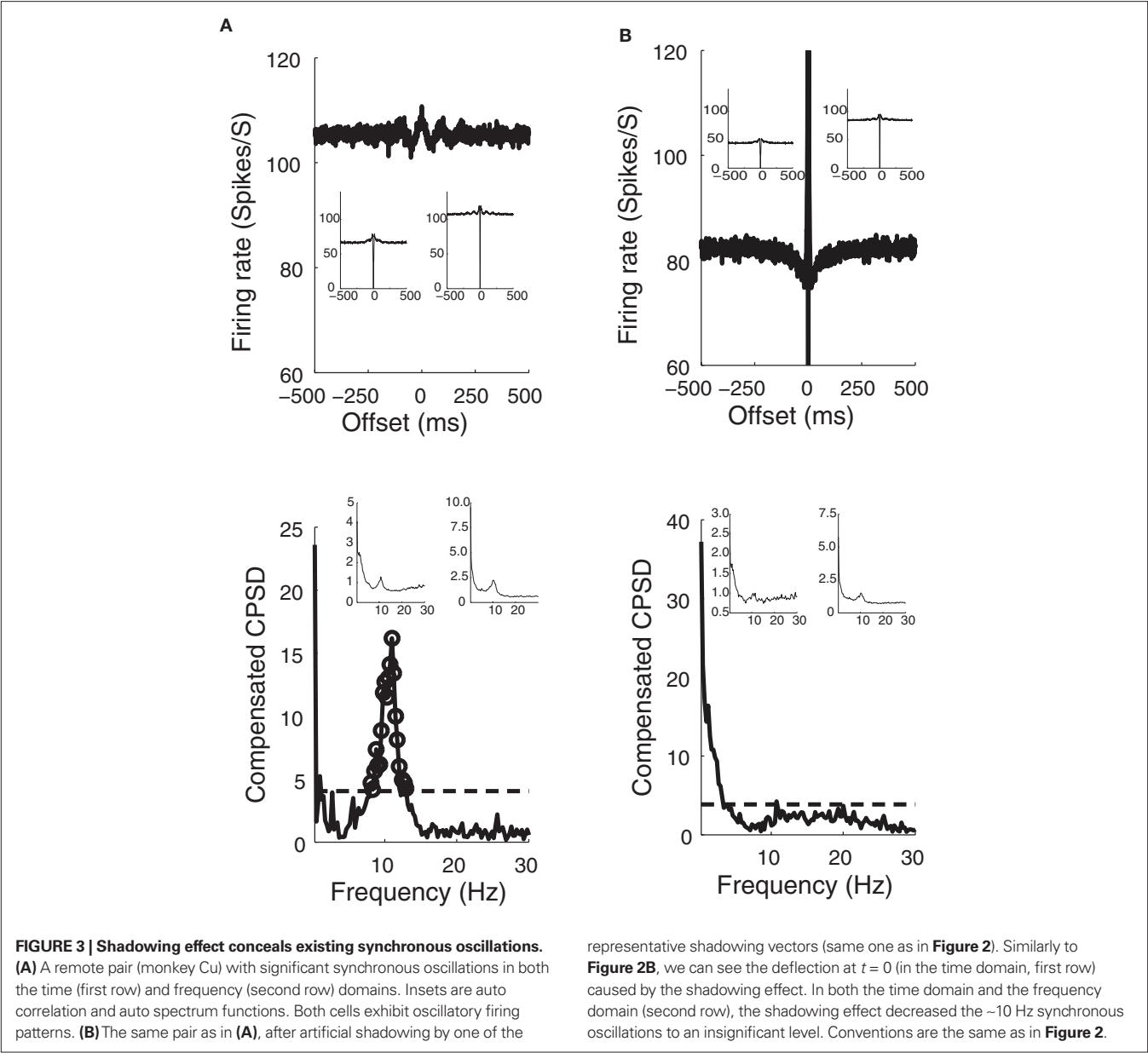


Table 1 | The shadowing effect and oscillatory activity of the single cells.

Number of significantly oscillating cells in the pair	Synchronous oscillations before and after artificial shadowing ("hit") (%)	Artificial shadowing concealed existing synchronous oscillations ("miss") (%)	Shadowing created apparent synchronous oscillations ("false alarm") (%)	No synchronous oscillations before and after artificial shadowing ("correct rejection") (%)
None	1.7	52.1	0.0	89.1
Only one	36.0	38.1	100.0	10.0
Both	62.3	9.8	0.0	0.9

Relationships between firing properties of each of the single neurons in a given pair, and the outcome of the shadowing effect. The left column gives the number of cells within a pair that were defined as oscillatory. Each of the next columns addresses one of the four possibilities of detection of synchronous oscillations given the shadowing effect (signal detection theory). That is, synchronous oscillations were detected before and after shadowing ("hit"); synchronous oscillations were concealed by the shadowing ("miss"); shadowing created apparent synchronous oscillations ("false alarm"); or there were no synchronous oscillations both before and after shadowing ("correct rejection"). We present here the probability of having none, one, or both oscillatory cells within the pair, given each one of the four possibilities (so that each column is summed to 100%). We can see that all "false alarms" occurred when only one of the cells in the pair was oscillatory. On the other hand, about half of the "misses" occurred when none of the cells in the pair were significantly oscillatory.

Table 2 | Ratio of synchronous oscillating pairs out of total population of pairs: comparison between neighboring and remote cells.

Monkey		Ratio of synchronous oscillating pairs out of total population of pairs				Fisher's exact test
		Close		Remote shadowed (unshadowed in parentheses)		p-value (unshadowed in parentheses)
		Ratio	%	Ratio	%	
GPe	Cu	3/19	15.8	29.4 (7)/118	24.9 (5.9)	0.562 (0.144)
	S	2/13	15.4	2.8 (4)/53	5.3 (7.5)	0.253 (0.337)
	Both	5/32	15.6	32.2 (11)/171	18.8 (6.4)	0.806 (0.142)
GPi	Cu	3/3	100	15.0 (22)/23	65.2 (95.7)	0.529 (1)
	S	0/2	0	10.8 (10)/14	77.1 (71.4)	0.083 (0.125)
	Both	3/5	60	25.8 (32)/37	69.7 (86.5)	0.637 (0.188)
GP-pooled	Cu	6/24	25	119.2 (57)/349	34.2 (16.3)	0.503 (0.265)
	S	2/15	13.3	22.6 (21)/91	24.8 (23.1)	0.513 (0.515)
	Both	8/39	20.5	141.8 (78)/440	32.2 (17.7)	0.151 (0.664)

Ratio of synchronous oscillating pairs out of total population of pairs in the different nuclei. Each artificially shadowed pair was scored between 0 and 1 based on the synchronization index. The sum of this score for the whole population represents the number of pairs which were significantly oscillatory. For the remote pairs we also present, in parentheses, the results of the original, unshadowed pairs. A two-tailed Fisher's exact test was performed under the null hypothesis of an identical fraction of synchrony in the close and the remote pairs.

Table 3 | Average percentage of synchronous oscillating pairs per session: comparison between neighboring and remote cells.

Monkey		Number of sessions		Average percentage of synchronous oscillating pairs per session		t-Test p-value (unshadowed in parentheses)
		Close	Remote	Close	Remote shadowed (unshadowed in parentheses)	
GPe	Cu	10	10	10.0	23.5 (6.5)	0.179 (0.674)
	S	13	20	15.4	6.9 (12.0)	0.477 (0.790)
	Both	23	30	13.0	12.5 (10.2)	0.941 (0.725)
GPi	Cu	2	3	100.0	67.6 (97.4)	0.108 (0.423)
	S	2	10	0.0	79.3 (70.0)	0.0002 (0.001)
	Both	4	13	50.0	76.6 (76.3)	0.437 (0.446)
GP-pooled	Cu	14	16	21.4	39.0 (20.3)	0.141 (0.932)
	S	15	33	13.3	33.6 (33.5)	0.098 (0.105)
	Both	29	49	17.2	35.4 (29.2)	0.040 (0.188)

Percentage of synchronous oscillating pairs in an average session in the different nuclei (regardless of the number of pairs recorded in it). The percentage of significantly synchronous oscillating pairs per session is presented in the second and third columns from the right. For the remote pairs, the percentage of pairs after artificial shadowing is presented, with the percentage of original, unshadowed pairs in parentheses. Similar to **Table 1**, the two-tailed t-test hypothesis is that close pairs have the same percentage of synchrony as remote ones.

database was very small (three and two close pairs in monkeys Cu and S, respectively). We conclude that in the MPTP treated primate, close pairs of GP neurons have a similar tendency for synchronous oscillations as remote pairs.

To further validate our results, we divided the remote pairs' population into two subpopulations. This was done according to the estimated distance between the electrode tips, with a cutoff between categories at 750 μm . We preferred to use two categories, rather than continuous spectrum, since this distance estimation suffers a certain noise, resulting from the electrodes flexibility. Since both subpopulations were recorded by different electrodes, we compared the synchrony of the original, unshadowed signal.

Similarly to the previously described comparisons of close and remote pairs, we first compared the ratio of synchronous pairs (**Table 4**). For the GPe, GPi, and GP-pooled populations the closer (i.e., less than 750 μm apart) pairs were slightly but insignificantly less synchronized than the further distant ones (15.8% and 20.0% of the GP-pooled pairs, respectively). Finally, we compared the average percentage of synchrony per recording session (**Table 5**). Again, no significant difference was found between closer and further distant pairs in GPe, GPi, and GP-pooled populations (for GP-pooled population, average synchrony of 29.9% in the closer pairs, in comparison with 28.5% in those further distant).

FREQUENCY DISTRIBUTION OF SYNCHRONOUS OSCILLATIONS

Next, we compared the frequency of the synchronous oscillations in the two populations (close and remote pairs). As previously mentioned, most oscillations appeared in two frequency bands: approximately 5–7.5 and 10–12.5 Hz, which are roughly the tremor frequency and its double. Again, for the artificially shadowed remote pairs, we calculated the oscillation frequency under each of the representative shadowing vectors, and weighted them accordingly.

Figure 4 shows the distribution of peak frequency in the oscillatory pairs in the close and the artificially shadowed remote population. Since the population of close pairs which showed significant synchronous oscillations was relatively small, we pooled

the results of both monkeys. This was done in the GP-pooled population, GPe and GPi (in which only monkey Cu had close pairs oscillating synchronously). It can clearly be seen that in all three areas the frequency distribution of neighboring and remote cells was very similar (though the small population of GPi neurons makes it more difficult to substantiate it thoroughly). Increased power over 20 Hz is likely an artifact of the shadowing, as it was not seen in the unshadowed remote pairs. We therefore conclude that synchronous oscillations in the Parkinsonian GP are distributed homogeneously, and there is no preference for different frequencies of synchronous oscillations by close vs. remote pairs of GP neurons.

Table 4 | Ratio of synchronous oscillating remote pairs in two distance categories.

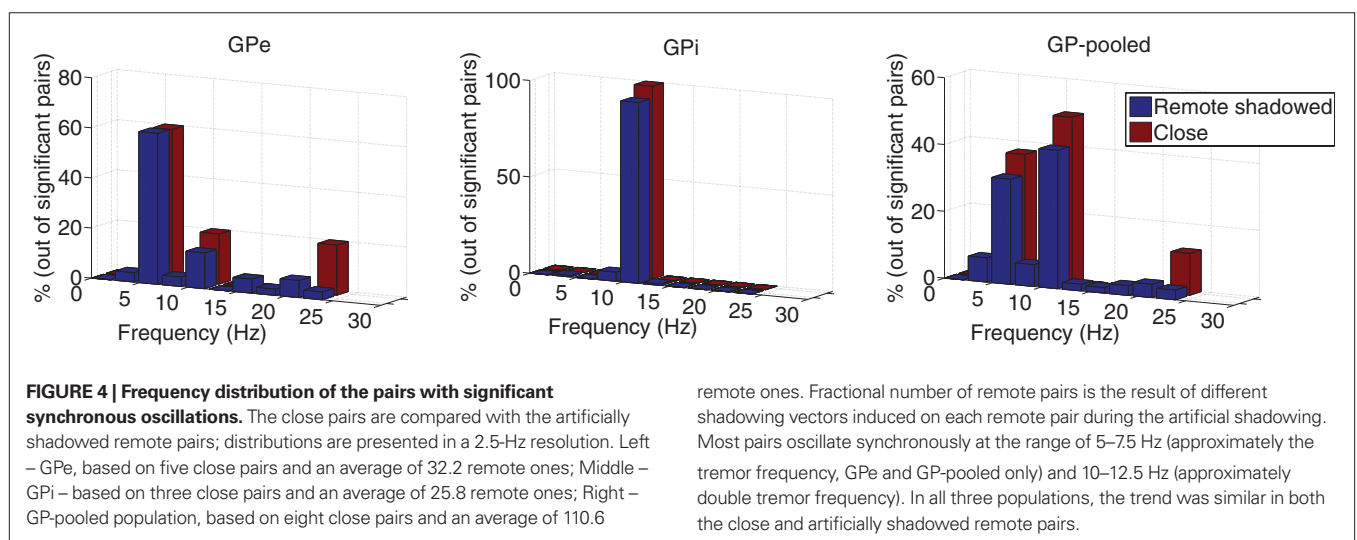
Monkey		Ratio of synchronous oscillating pairs out of total population of pairs				Fisher's exact test p -value
		<750 μm		>750 μm		
		Ratio	%	Ratio	%	
GPe	Cu	5/69	7.2	2/49	4.1	0.38
	S	2/40	5.0	2/13	15.4	0.25
	Both	7/109	6.4	4/62	6.5	0.61
GPi	Cu	5/5	100.0	17/18	94.4	1.00
	S	9/12	75.0	1/2	50.0	0.51
	Both	14/17	82.4	18/20	90.0	0.42
GP-pooled	Cu	25/180	13.9	32/169	18.9	0.13
	S	13/60	21.7	8/31	25.8	0.42
	Both	38/240	15.8	40/200	20.0	0.16

Ratio of synchronous oscillating pairs out of the entire remote pairs population in the different nuclei. Similarly to **Table 2**, a two-tailed Fisher's exact test was performed under the null hypothesis of an identical fraction of synchrony in the two distance categories. Distances were estimated according to the assumed three dimensional locations of the electrode tips, when these were available.

Table 5 | Average percentage of synchronous oscillating pairs per session in two distance categories.

	Monkey	Number of sessions	Average percentage of synchronous oscillating pairs per session				t-Test <i>p</i> -value
			<750 μm		>750 μm		
			<750 μm	>750 μm	<750 μm	>750 μm	
GPe	Cu	9	8	3.3	8.3	0.55	
	S	14	8	2.9	25.0	0.10	
	Both	23	16	3.0	16.7	0.09	
GPi	Cu	2	3	100.0	97.2	0.50	
	S	9	2	77.8	50.0	0.48	
	Both	11	5	81.8	78.3	0.88	
GP-pooled	Cu	15	13	21.0	19.1	0.88	
	S	27	15	34.8	36.7	0.90	
	Both	42	28	29.9	28.5	0.90	

Percentage of synchronous oscillating pairs in an average session in the different nuclei (regardless of the number of pairs recorded in it, similar to **Table 3**). The percentage of significantly synchronous oscillating pairs per session is presented in the second and third columns from the right. As before, the two-tailed t-test hypothesis is that pairs in the two distance categories have the same percentage of synchrony.



DISCUSSION

We analyzed correlations of close pairs of GP neurons recorded by the same electrode and compared their synchrony to that of pairs recorded by different electrodes (200–2000 μm apart) in the Parkinsonian MPTP treated primates. In addition we compared intermediate distant pairs (less than 750 μm) to further distant ones (over 750 μm). Our results indicate that pathological synchronization of pallidal activity in the MPTP treated monkeys does not fall off across a few millimeters of tissue. Furthermore, the frequency distribution of the significant synchronous oscillations of close and remote pairs was found to be similar. These findings are in line with our previous report of emergence of synchronous oscillations between striatal cholinergic interneurons (TANs) and pallidal neurons after MPTP treatment. In the normal state TANs have no correlation with pallidal activity. The high level of oscillatory correlated activity between random pairs of TAN and GP neuron suggests that coherent, homogeneous oscillations of the whole basal ganglia circuitry underlie the clinical features of the MPTP primate model of PD (Raz et al., 2001).

Along the line of previous work in the rodent 6-OHDA model of PD (Mallet et al., 2008), our results suggest that the pallidal synchrony spans most of these nuclei. However, Mallet et al. found that synchronization decreases with distance. One possible explanation for this discrepancy is the delicate method of multi-contact silicone probes which was used in that study. These probes cover a range of distances from a hundred of microns to a few millimeters, whereas our methods divide the population of neuron pairs in a binary fashion. Furthermore, the close pairs which were recorded in our study by the same electrode were probably within less than a 100- μm apart (Abeles, 1974; Gray et al., 1995). On the other hand, the primate pallidum is larger than the rodent pallidum, and therefore our “remote” units, even those in the subcategory of over 750 μm , might still be in the closer pallidal territories than the remote rodent ones. This difference in scales may underlie the discrepancy between the studies.

Alternatively, the discrepancy could be the result of differences in the model of PD. First, our recordings were made on awake animals, whereas Mallet et al. used urethane anesthetized animals. Next, our dopamine depletion model was systemic and therefore bilateral, whereas the 6-OHDA model was unilateral. Finally, MPTP treated vervet monkeys demonstrate all major Parkinsonian motor symptoms, including rigidity and Parkinsonian tremor. Unilaterally injected 6-OHDA rodents, on the other hand, mainly display motor asymmetry, which is manifested in an increased tendency for turning (Ungerstedt, 1968). The homogeneous level of synchronous oscillations found in the MPTP primate model could cause a broad effect of synchronous oscillations downstream to the basal ganglia; e.g., in the motor thalamus and motor cortex. This, in turn, could lead to a more pronounced clinical effect in the Parkinsonian vervets in comparison to rodents (Beal, 2001).

The homogeneous spatial pattern of pathological GP synchrony may assist in finding the origin of the phenomenon. We might conjecture that if the synchronous oscillations emerge within the GP (rather than upstream in the basal ganglia), there

would be higher synchrony between close pairs than between remote ones. However, it was theoretically shown (DeLiang, 1995) that local interactions can cause global, homogeneous synchrony. Therefore, we believe that the attempt to derive the origin of the synchronous oscillations from our results requires a separate theoretical analysis. Such theoretical approach should take into consideration the specific properties of the GP, including its high firing rate and its predominantly inhibitory innervation.

We therefore suggest that future research should focus on two directions. First, in order to minimize the shadowing effect and maximize the separation quality of the different units, tetrodes, rather than single electrodes, should be used (Harris et al., 2000; Ecker et al., 2010). This is especially important since we cannot rule out the possibility that artificial shadowing have a different effect than the “natural” shadowing. It should be mentioned, though, that the shadowing effect still exists on tetrodes recordings. Hence, for a complete suppression of the shadowing effect one should use more than four contacts and/or a more advanced sorting algorithm (Takahashi and Sakurai, 2009; Franke et al., 2010). Second, to complete the comparison between rodent’s and primate’s spatial distribution of pallidal pathological synchronous oscillations, recordings within verified distances inside the primate and human (during DBS surgeries) pallidum should be performed (e.g., by multi-contact silicone probes).

Our work focused on the second order level of synchronous neural activity, i.e., pair wise correlations. At this level, no difference was found between close and remote pairs in the primate GP. However, this does not rule out the possibility that higher orders of synchrony differ between close and remote populations of neurons. Indeed, such a result was recently found in the primate visual cortex (Ohiorhenuan et al., 2010). Such an analysis with our data is not possible since recording of more than two neurons by a single electrode is extremely rare in the primate GP.

To conclude, our findings strongly imply that the pathological synchronous oscillations in the Parkinsonian MPTP treated primate have a homogeneous spatial pattern. This pattern probably contributes to the robust effect of the pallidal oscillations on their target downstream to the basal ganglia. This robust effect can underlie the severe motor abnormalities in PD.

ACKNOWLEDGMENTS

We thank G. Goelman for MRI, V. Sharkansky, S. Freeman, and A. Shaposhnikov for technical assistance, Y. Ben Shaul, M. Joshua, and Y. Prut for suggestions on early stages of this work and E. Singer for language editing. This study was partly supported by the Hebrew University Netherlands Association (HUNA) “Fighting against Parkinson” and the Vorst family foundation grant (HB), the Dekker foundation fellowship (BR); the Foulkes Foundation fellowship, and a fellowship from MYERS-JDC-BROOKDALE Institute of Gerontology and Human Development and ESHEL, the Association for the Planning and Development of Services for the Aged in Israel (SE); the Israel Science Foundation grant (YR) and by the “Hoffman Leadership and Responsibility” fellowship program at the Hebrew University (RM).

REFERENCES

- Abeles, M. (1974). "A journey into the brain," in *Signal Analysis and Pattern Recognition in Biomedical Engineering*, ed. G. F. Inbar (New York: Wiley), 41–59.
- Abeles, M., and Goldstein, M. H. (1977). Multispike train analysis. *Proc. IEEE* 65, 762–773.
- Bar-Gad, I., Heimer, G., Ritov, Y., and Bergman, H. (2003a). Functional correlations between neighboring neurons in the primate globus pallidus are weak or nonexistent. *J. Neurosci.* 23, 4012–4016.
- Bar-Gad, I., Morris, G., and Bergman, H. (2003b). Information processing, dimensionality reduction and reinforcement learning in the basal ganglia. *Prog. Neurobiol.* 71, 439–473.
- Bar-Gad, I., Ritov, Y., Vaadia, E., and Bergman, H. (2001). Failure in identification of overlapping spikes from multiple neuron activity causes artificial correlations. *J. Neurosci. Methods* 107, 1–13.
- Beal, M. F. (2001). Experimental models of Parkinson's disease. *Nat. Rev. Neurosci.* 2, 325–334.
- Benazzouz, A., Boraud, T., Dubqdat, P., Boireau, A., Stutzmann, J. M., and Gross, C. (1995). Riluzole prevents MPTP-induced Parkinsonism in the rhesus monkey: a pilot study. *Eur. J. Pharmacol.* 284, 299–307.
- Contreras, C. M., Mexicano, G., and Guzman-Flores, C. A. (1981). Stereotaxic brain atlas of the green monkey (*Cercopithecus aethiops aethiops*). *Bol. Estud. Med. Biol.* 31, 383–428.
- DeLiang, W. (1995). Emergent synchrony in locally coupled neural oscillators. *IEEE Trans. Neural Netw.* 6, 941–948.
- DeLong, M. R. (1971). Activity of pallidal neurons during movement. *J. Neurophysiol.* 34, 414–427.
- Ecker, A. S., Berens, P., Keliris, G. A., Bethge, M., Logothetis, N. K., and Tolias, A. S. (2010). Decorrelated neuronal firing in cortical microcircuits. *Science* 327, 584–587.
- Elias, S., Joshua, M., Goldberg, J. A., Heimer, G., Arkadir, D., Morris, G., and Bergman, H. (2007). Statistical properties of pauses of the high-frequency discharge neurons in the external segment of the globus pallidus. *J. Neurosci.* 27, 2525–2538.
- Franke, F., Natora, M., Boucsein, C., Munk, M., and Obermayer, K. (2010). An online spike detection and spike classification algorithm capable of instantaneous resolution of overlapping spikes. *J. Comput. Neurosci.* 29, 127–148.
- Gray, C. M., Maldonado, P. E., Wilson, M., and McNaughton, B. (1995). Tetrodes markedly improve the reliability and yield of multiple single-unit isolation from multi-unit recordings in cat striate cortex. *J. Neurosci. Methods* 63, 43–54.
- Haber, S. N., and Gdowski, M. J. (2004). "The basal ganglia," in *The Human Nervous System*, eds G. Paxinos and J. K. Mai (New York, NY: Elsevier Academic Press), 676–738.
- Harris, K. D., Henze, D. A., Csicsvari, J., Hirase, H., and Buzsaki, G. (2000). Accuracy of tetrode spike separation as determined by simultaneous intracellular and extracellular measurements. *J. Neurophysiol.* 84, 401–414.
- Heimer, G., Bar-Gad, I., Goldberg, J. A., and Bergman, H. (2002). Dopamine replacement therapy reverses abnormal synchronization of pallidal neurons in the 1-methyl-4-phenyl-1,2,3,6-tetrahydropyridine primate model of Parkinsonism. *J. Neurosci.* 22, 7850–7855.
- Heimer, G., Rivlin-Etzion, M., Bar-Gad, I., Goldberg, J. A., Haber, S. N., and Bergman, H. (2006). Dopamine replacement therapy does not restore the full spectrum of normal pallidal activity in the 1-methyl-4-phenyl-1,2,3,6-tetra-hydropyridine primate model of Parkinsonism. *J. Neurosci.* 26, 8101–8114.
- Imbert, C., Bezaud, E., Guitraud, S., Boraud, T., and Gross, C. E. (2000). Comparison of eight clinical rating scales used for the assessment of MPTP-induced Parkinsonism in the Macaque monkey. *J. Neurosci. Methods* 96, 71–76.
- Kita, H., and Kita, S. T. (1994). The morphology of globus pallidus projection neurons in the rat: an intracellular staining study. *Brain Res.* 636, 308–319.
- Levy, R., Hutchison, W. D., Lozano, A. M., and Dostrovsky, J. O. (2002). Synchronized neuronal discharge in the basal ganglia of Parkinsonian patients is limited to oscillatory activity. *J. Neurosci.* 22, 2855–2861.
- Lewicki, M. S. (1998). A review of methods for spike sorting: the detection and classification of neural action potentials. *Network* 9, R53–R78.
- Mallet, N., Pogossyan, A., Marton, L. F., Bolam, J. P., Brown, P., and Magill, P. J. (2008). Parkinsonian beta oscillations in the external globus pallidus and their relationship with subthalamic nucleus activity. *J. Neurosci.* 28, 14245–14258.
- Martin, R. F., and Bowden, D. M. (2000). *Primate Brain Maps: Structure of the Macaque Brain*. Amsterdam: Elsevier Science.
- Nini, A., Feingold, A., Slovov, H., and Bergman, H. (1995). Neurons in the globus pallidus do not show correlated activity in the normal monkey, but phase-locked oscillations appear in the MPTP model of Parkinsonism. *J. Neurophysiol.* 74, 1800–1805.
- Ohiorehuan, I. E., Mechler, F., Purpura, K. P., Schmid, A. M., Hu, Q., and Victor, J. D. (2010). Sparse coding and high-order correlations in fine-scale cortical networks. *Nature* 466, 617–621.
- Percheron, G., Francois, C., and Yelnik, J. (1987). "Spatial organization and information processing in the core of the basal ganglia," in *The Basal Ganglia*, eds M. B. Carpenter and A. Jayaraman (New York: Plenum Press), 205–226.
- Percheron, G., Yelnik, J., and Francois, C. (1984). A Golgi analysis of the primate globus pallidus. III. Spatial organization of the striato-pallidal complex. *J. Comp. Neurol.* 227, 214–227.
- Raz, A., Frechter-Mazar, V., Feingold, A., Abeles, M., Vaadia, E., and Bergman, H. (2001). Activity of pallidal and striatal tonically active neurons is correlated in MPTP-treated monkeys but not in normal monkeys. *J. Neurosci.* 21, RC128.
- Raz, A., Vaadia, E., and Bergman, H. (2000). Firing patterns and correlations of spontaneous discharge of pallidal neurons in the normal and the tremulous 1-methyl-4-phenyl-1,2,3,6-tetrahydro pyridine vervet model of Parkinsonism. *J. Neurosci.* 20, 8559–8571.
- Rivlin-Etzion, M., Ritov, Y., Heimer, G., Bergman, H., and Bar-Gad, I. (2006). Local shuffling of spike trains boosts the accuracy of spike train spectral analysis. *J. Neurophysiol.* 95, 3245–3256.
- Sato, F., Lavallee, P., Levesque, M., and Parent, A. (2000). Single-axon tracing study of neurons of the external segment of the globus pallidus in primate. *J. Comp. Neurol.* 417, 17–31.
- Szabo, J., and Cowan, W. M. (1984). A stereotaxic atlas of the brain of the cynomolgus monkey (*Macaca fascicularis*). *J. Comp. Neurol.* 222, 265–300.
- Takahashi, S., and Sakurai, Y. (2009). Sub-millisecond firing synchrony of closely neighboring pyramidal neurons in hippocampal CA1 of rats during delayed non-matching to sample task. *Front. Neural Circuits* 3:9. doi: 10.3389/neuro.04.009.2009.
- Ungerstedt, U. (1968). 6-Hydroxydopamine induced degeneration of central monoamine neurons. *Eur. J. Pharmacol.* 5, 107–110.

Conflict of Interest Statement: The authors declare that the research was conducted in the absence of any commercial or financial relationships that could be construed as a potential conflict of interest.

Received: 31 December 2010; paper pending published: 14 February 2011; accepted: 13 June 2011; published online: 30 June 2011.
 Citation: Mitelman R, Rosin B, Zadka H, Slovov M, Heimer G, Ritov Y, Bergman H and Elias S (2011) Neighboring pallidal neurons do not exhibit more synchronous oscillations than remote ones in the MPTP primate model of Parkinson's disease. *Front. Syst. Neurosci.* 5:54. doi: 10.3389/fnsys.2011.00054
 Copyright © 2011 Mitelman, Rosin, Zadka, Slovov, Heimer, Ritov, Bergman and Elias. This is an open-access article subject to a non-exclusive license between the authors and Frontiers Media SA, which permits use, distribution and reproduction in other forums, provided the original authors and source are credited and other Frontiers conditions are complied with.

APPENDIX

THE MATHEMATICS OF ARTIFICIAL SHADOWING

Extracellular recording of spiking activity is based on detection of instantaneous events (spikes) in the high pass filtered analog signal and sorting them according to their pattern. This process is known as “spike sorting.” The underlying assumption is that different cells, recorded by the same electrode (neighboring cells), can be detected according to their different shape. However, spikes occurring within a few milliseconds cannot be detected, because of their shape overlap. This phenomenon was termed the “shadowing effect” by Bar-Gad et al. (2001).

The probability to miss a spike within a given spike train, as a function of the spike’s lag from a spike in the neighboring spike train, was termed the “shadowing vector.” Given the actual firing rate (p), the shadowing vector ($S_{n,m}$) and the shadowing duration (α) the observed firing rate (p^*), can be calculated as follows (Bar-Gad et al., 2001):

$$p_m^* = p_m \left(1 - p_n \sum_{\tau=-\alpha}^{\alpha} S_{n,m}(\tau) \right) \quad (1)$$

Furthermore, given the neurons’ actual firing rate (P_n, P_m), their autocorrelation (a), and the shadowing vector (S) – the cross-correlation function ($c_{n,m}^*$) of two uncorrelated spike trains recorded by the same electrode can be calculated as follows (Bar-Gad et al., 2001, Eq. 5):

$$c_{n,m}^*(t) = \frac{P_n}{1 - p_n \sum_{\tau=-\alpha}^{\alpha} S_{n,m}(\tau)} \left(1 - \sum_{\tau=-\alpha}^{\alpha} S_{n,m}(\tau) a_n(t+\tau) \right) \left(1 - \sum_{\tau=-\alpha}^{\alpha} S_{m,n}(\tau) a_m(t-\tau) \right) \quad (2)$$

We assume that the refractory period of the neurons is longer than the shadowing period, similar to Bar-Gad et al. (2003a). This means that the autocorrelation equals 1 at $t = 0$, and 0 for the rest of the shadowing period. This assumption further simplifies the cross-correlation estimation to:

$$c_{n,m}^*(t) = \frac{P_n}{P_m} (1 - S_{n,m}(-t)) (1 - S_{m,n}(t)) \quad (3)$$

We further assume that the shadowing period is symmetric, i.e., that $S_{m,n}(t) = S_{n,m}(-t) \equiv S(t)$, and then get Eq. (4):

$$c_{n,m}^*(t) = \frac{P_n P_m}{P_m^*} (1 - S(t))^2 \quad (4)$$

The shadowing vector $S(t)$ can be calculated from Eq. 4. Since $S(t)$ is a probability vector, its values are limited to the interval $[0, 1]$, hence we get a single solution:

$$S(t) = 1 - \sqrt{\frac{P_m^* c_{n,m}^*(t)}{P_n P_m}} \quad (5)$$

This allows an approximated solution, if $P_m^* \approx P_m$ and $P_n^* \approx P_n$ as follows:

$$S(t) \approx 1 - \sqrt{\frac{c_{n,m}^*(t)}{P_n}} \quad (6)$$

Furthermore, we have a satisfied set of second degree equations. We have the following empirical data: P_n^*, P_m^* , and $c_{n,m}^*(t)$ for $-\alpha \leq t \leq \alpha$, whereas we are interested in $S(t)$ for $-\alpha \leq t \leq \alpha$, as well as p_n and p_m . This yields $2\alpha + 1$ equations (Eq. 5) for $-\alpha \leq t \leq \alpha$, and two more equations (Eq. 1) for p_n and p_m – altogether $2\alpha + 3$ equations for $2\alpha + 3$ variables.

A set of equations of the second degree does not necessarily have an algebraic solution. Therefore, we used two numerical approaches. First, we used an iterative solution, which initiated in the approximated solution (Eq. 6), and iteratively used Eq. 5 to improve the solution. Second, we used the Matlab *fsolve* function for the solution of the equation. Both methods yielded similar solutions.

This solution assumes independence between the two spike trains. However, this term might be violated in our data. Therefore, we verified this method by estimating a shadowing vector from an artificially shadowed cross-correlogram. Different shadowing vectors were applied on all 349 pairs recorded by different electrodes (i.e., not originally distorted by the shadowing effect) from monkey Cu. Then we used the above method to estimate the shadowing vector, and calculated the error between known and estimated shadowing vectors. The absolute error per index in the vector was 0.017 ± 0.036 (average \pm SD, values representing the probability of missing a spike, hence they vary between 0 and 1). Thus, the estimation of the shadowing effects is satisfactory for our purposes despite the possible violation of the assumption of independent spike train.



Reduced pallidal output causes dystonia

Atsushi Nambu^{1*}, Satomi Chiken¹, Pullanipally Shashidharan², Hiroki Nishibayashi³, Mitsuhiro Ogura³, Koji Kakishita³, Satoshi Tanaka³, Yoshihisa Tachibana¹, Hitoshi Kita⁴ and Toru Itakura³

¹ Division of System Neurophysiology, National Institute for Physiological Sciences and Department of Physiological Sciences, Graduate University for Advanced Studies, Okazaki, Japan

² Department of Neurology, Mount Sinai School of Medicine, New York, NY, USA

³ Department of Neurological Surgery, Wakayama Medical University, Wakayama, Japan

⁴ Department of Anatomy and Neurobiology, College of Medicine, University of Tennessee Health Science Center, Memphis, TN, USA

Edited by:

Charles J. Wilson, University of Texas at San Antonio, USA

Reviewed by:

Thomas Wichmann, Emory University, USA

Jose Obeso, Universidad de Navarra, Spain

*Correspondence:

Atsushi Nambu, Division of System Neurophysiology, National Institute for Physiological Sciences, 38 Nishigonaka, Myodaiji, Okazaki 444-8585, Japan.
e-mail: nambu@nips.ac.jp

Dystonia is a neurological disorder characterized by sustained or repetitive involuntary muscle contractions and abnormal postures. In the present article, we will introduce our recent electrophysiological studies in hyperkinetic transgenic mice generated as a model of DYT1 dystonia and in a human cervical dystonia patient, and discuss the pathophysiology of dystonia on the basis of these electrophysiological findings. Recording of neuronal activity in the awake state of DYT1 dystonia model mice revealed reduced spontaneous activity with bursts and pauses in both internal (GPi) and external (GPe) segments of the globus pallidus. Electrical stimulation of the primary motor cortex evoked responses composed of excitation and subsequent long-lasting inhibition, the latter of which was never observed in normal mice. In addition, somatotopic arrangements were disorganized in the GPi and GPe of dystonia model mice. In a human cervical dystonia patient, electrical stimulation of the primary motor cortex evoked similar long-lasting inhibition in the GPi and GPe. Thus, reduced GPi output may cause increased thalamic and cortical activity, resulting in the involuntary movements observed in dystonia.

Keywords: dystonia, globus pallidus, extracellular recording, stereotactic surgery, movement disorders

INTRODUCTION

Dystonia is a neurological disorder characterized by sustained or repetitive involuntary muscle contractions and abnormal postures. The pathophysiology of dystonia is poorly understood. No consistent neuropathological or biochemical changes have been detected yet. On the other hand, abnormal neuronal activity in the basal ganglia has been reported during stereotactic surgery for deep brain stimulation (DBS) in dystonia patients (Vitek et al., 1999; Zhuang et al., 2004; Starr et al., 2005; Tang et al., 2007).

In the present article, we will introduce our recent electrophysiological studies in hyperkinetic transgenic mice generated as a model of DYT1 dystonia (Chiken et al., 2008) and in a human cervical dystonia patient (Nishibayashi et al., 2011), and discuss the pathophysiology of dystonia on the basis of these electrophysiological findings. Firstly, we investigated the neuronal activity in the entopeduncular nucleus and globus pallidus in transgenic model mice of DYT1 dystonia (Chiken et al., 2008), the most common type of human primary generalized dystonia. Secondly, we also had a chance to record neuronal activity in the internal (GPi) and external (GPe) segments of the globus pallidus of a human cervical dystonia patient during stereotactic surgery (Nishibayashi et al., 2011). The entopeduncular nucleus and globus pallidus in rodents correspond to the GPi and GPe in primates, respectively, and thus, we will call these nuclei GPi and GPe hereafter. The GPi and GPe are two important nuclei in the basal ganglia circuitry, and their abnormal neuronal activity has been reported in movement disorders. We paid special attention to the responses of GPi and GPe neurons evoked by cortical stimulation. In voluntary movements,

activity originating in the cortex is transmitted through the basal ganglia circuitry and finally reaches the output station of the basal ganglia, i.e., the GPi. Cortical stimulation can mimic information processing through the basal ganglia circuitry (Nambu et al., 2002; Tachibana et al., 2008). Motor cortical stimulation typically induces triphasic responses composed of early excitation, inhibition, and late excitation in GPi and GPe neurons of normal monkeys and rodents (Yoshida et al., 1993; Nambu et al., 2000; Chiken and Tokuno, 2003). The origin of each component has been identified, with the amplitudes and durations reflecting neuronal activity of the corresponding basal ganglia pathways and nuclei. In the studies by Chiken et al. (2008) and Nishibayashi et al. (2011), long-lasting inhibition was evoked in the GPi and GPe of both DYT1 dystonia model mice and a human cervical dystonia patient.

MATERIALS AND METHODS

ANIMAL STUDY

The DYT1 gene on chromosome 9q34 codes the torsinA protein (Ozelius et al., 1997). A three-base pair (GAG) deletion in the DYT1 gene, resulting in the loss of a glutamic acid residue (ΔE) in the torsinA protein (Ozelius et al., 1997), causes human DYT1 dystonia. Recently, Shashidharan et al. (2005) generated a transgenic mouse model by overexpression of human ΔE -torsinA. These transgenic mice developed hyperkinesia and rapid bidirectional circling. They also exhibited abnormal involuntary movements with dystonic-appearing self-clasping of limbs and head-shaking.

In the study by Chiken et al. (2008), six DYT1 dystonia model (5–28 weeks old, both male and female) and six age-matched normal mice were used. The experimental protocols were approved by the Animal Care and Use Committees of the Mount Sinai School of Medicine and the National Institutes of Natural Sciences, and all experiments were conducted according to the guidelines of the National Institutes of Health Guide for the Care and Use of Laboratory Animals. Each mouse was anesthetized with ketamine hydrochloride (100 mg/kg body weight, i.p.) and xylazine hydrochloride (4–5 mg/kg, i.p.), and fixed in a conventional stereotaxic apparatus. The skull was widely exposed. The exposed skull was completely covered with transparent acrylic resin, and then a small U-frame made of acetal resin for head fixation was mounted and fixed on the head of the mouse.

After recovery from the first surgery (2 or 3 days later), the mouse was positioned in a stereotaxic apparatus with its head restrained using the U-frame head holder under light anesthesia with ketamine hydrochloride (30–50 mg/kg, i.p.). A part of the skull in one hemisphere was removed to access the motor cortex, GPi, and GPe. Two pairs of bipolar stimulating electrodes (tip distance, 300–400 μm) made of 50- μm -diameter Teflon-coated tungsten wires were inserted into the primary motor cortex, one into the caudal forelimb region and the other into the orofacial region. These regions were confirmed by observing movements evoked by intracortical microstimulation. Stimulating electrodes were then fixed therein using acrylic resin.

After full recovery from the second surgery, the mouse was positioned in a stereotaxic apparatus with its head restrained painlessly using the U-frame head holder. The mouse lay down quietly in the awake state. For single unit recording of GPi and GPe neurons, a glass-coated Elgiloy-alloy microelectrode (0.8–1.5 M Ω at 1 kHz) was inserted vertically into the brain through the dura mater using a hydraulic microdrive. Signals from the electrode were amplified, converted to digital pulses using a window discriminator, and sampled using a computer. Spontaneous discharges were recorded, and spontaneous discharge rates and autocorrelograms (bin width of 0.5 ms) of the neurons were calculated from continuous digitized recordings for 30 s. Electrical stimulation of the primary motor cortex (200 μs duration single pulse, 20–50 μA strength), which induced muscle twitches in the corresponding body parts, was delivered. Similar intensities were used for dystonia model and normal mice. Responses to cortical stimulation were examined by constructing peristimulus time histograms (PSTHs; bin width of 1 ms) for 100 stimulus trials.

HUMAN STUDY

In the study by Nishibayashi et al. (2011), one cervical dystonia patient received stereotactic surgery for DBS electrode implantation into the bilateral GPi. The patient was 62-year-old female, and had a disease duration of 32 months, and a Toronto western spasmodic torticollis rating scale (TWSTRS) score of 54. Microelectrode recordings were performed to identify the targets. In addition, 10 Parkinson's disease patients [eight male and two female; mean age, 61.9 years; mean disease duration, 126 months; mean levodopa dosage, 460 mg/day; preoperative unified Parkinson's disease rating scale (UPDRS), 25.3 (best)–66.6 (worst)] were also investigated for comparison. Medications were withdrawn

18 h before operation in most patients. This study was approved by the ethical committee of Wakayama Medical University and followed its guidelines.

Surgery including microelectrode recordings was performed under local anesthesia. Burr holes were made bilaterally on the coronal suture about 30 mm lateral from the midline. After dural incision, a strip electrode with four platinum discs (5-mm-diameter) spaced 10 mm apart (Unique Medical, Tokyo, Japan) was inserted into the subdural space in the posterolateral direction, and placed on the upper limb region of the primary motor cortex ipsilateral to the target GPi. Electrical stimulation (1.0 ms duration single pulse, 1–20 mA strength at 1 Hz) was delivered through two of the four discs. A pair of discs inducing muscle twitches in the contralateral upper limb at the lowest intensity was selected. In the following recordings, stimulation was delivered through this pair at an intensity inducing clear muscle twitches (4–16 mA) at 1 Hz. A microelectrode (FC1002, Medtronic, Minneapolis, MN, USA) was inserted through the same burr hole targeting the tentative target in the posteroventral GPi, which was determined on the basis of magnetic resonance imaging (MRI). Neuronal activity was amplified, displayed (Leadpoint 9033A0315, Medtronic), and fed to a computer for online analysis. The responses induced by electrical stimulation of the cortex were assessed by constructing PSTHs (bin width of 1 ms) for 20–120 stimulus trials. Spontaneous discharge rates and patterns were analyzed from autocorrelograms (bin width of 0.5 ms) constructed from continuous digitized recordings for 50 s. On the basis of the microelectrode recordings, DBS electrodes (Model 3387, Medtronic) were implanted bilaterally into the GPi.

RESULTS

SPONTANEOUS ACTIVITY OF GPi AND GPe NEURONS IN DYT1 DYSTONIA MODEL MICE

GPi (50.6 ± 15.7 Hz, mean \pm SD, $n = 94$; **Figure 1A**) and GPe (54.5 ± 16.3 Hz, $n = 70$) neurons in normal mice fired continuously at a high discharge rate. Traces of digitized spikes and autocorrelograms indicated that GPi (**Figures 1A,B**) and GPe neurons fired irregularly in normal mice. On the other hand, the firing frequency of GPi (27.8 ± 19.1 Hz, $n = 90$; **Figure 1C**) and GPe (35.4 ± 19.0 Hz, $n = 204$) neurons in DYT1 dystonia model mice was significantly lower than that in normal mice (**Figure 1E**; $p < 0.001$, Mann–Whitney U test). Discharge patterns also differed in dystonia model mice (**Figures 1C,D**). Bursts and pauses were frequently observed in GPi (thick black lines and thick white lines in **Figure 1C**) and GPe neurons of dystonia model mice.

RESPONSES OF GPi AND GPe NEURONS TO CORTICAL STIMULATION IN DYT1 DYSTONIA MODEL MICE

Cortical stimulation typically evoked a triphasic response composed of early excitation, followed by inhibition, and late excitation in GPi (**Figure 2A**) and GPe neurons of normal mice. On the other hand, the most common response pattern of GPi (56%) and GPe (41%) neurons in dystonia model mice was short-latency monophasic or biphasic excitation followed by long-lasting inhibition (**Figure 2B**), a pattern never observed in normal mice. The duration of the long-lasting inhibition was 73.7 ± 29.4 ms in the GPi ($n = 29$) and 66.7 ± 31.3 ms in the GPe ($n = 46$).

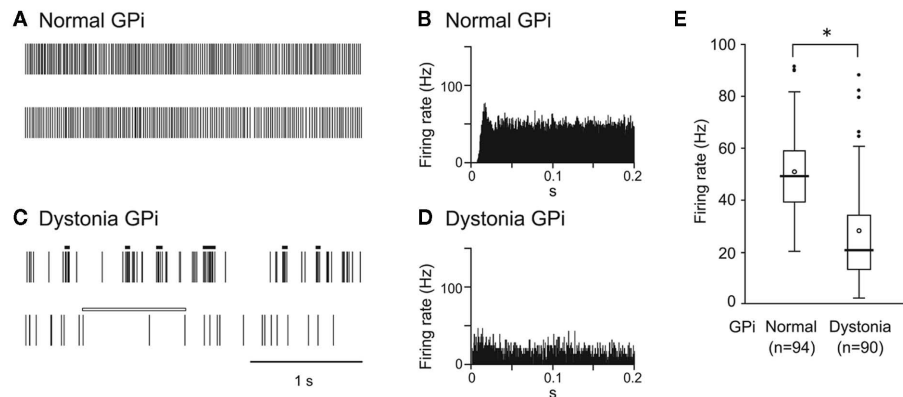


FIGURE 1 | Spontaneous activity of neurons in the internal segment of the globus pallidus (GPI) in DYT1 dystonia model mice. (A,C) Spikes are shown as digital signals in normal (A) and dystonia model (C) mice. Bursts and pauses in the digital signals are indicated by horizontal black thick lines and horizontal white thick lines, respectively. **(B,D)** Auto-correlograms are shown in normal (B) and dystonia model (D) mice. **(E)** Box plots of firing rates in normal (left) and dystonia model (right) mice. The

boxes are constructed with the top line bounding the upper quartile and the bottom line bounding the lower quartile. The median and mean excluding outliers are indicated by a thick horizontal line and an open circle in the box, respectively. The short horizontal lines show the largest and smallest values that are not outliers. Outliers are shown as small closed circles. *, significantly different ($p < 0.001$, Mann-Whitney U test). Modified from Chiken et al. (2008).

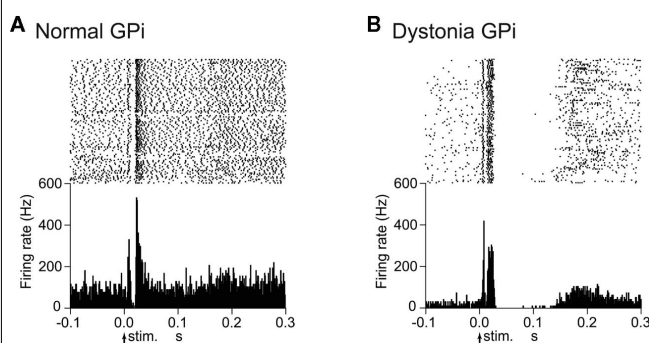


FIGURE 2 | Responses of GPI neurons to cortical stimulation in DYT1 dystonia model mice. (A) Raster and peristimulus time histograms (PSTHs) for normal mice. Cortical stimuli were delivered at time 0 (arrows) for 100 trials. **(B)** Raster and PSTHs for dystonia model mice. Abnormal responses with long-lasting inhibition were observed. Modified from Chiken et al. (2008).

SOMATOTOPIC ORGANIZATION OF THE GPI AND GPe IN DYT1 DYSTONIA MODEL MICE

Stimulation of both forelimb and orofacial regions of the motor cortex was performed. By observing cortically evoked responses, cortical regions projecting to each GPI neuron could be identified. In normal mice, many neurons responded to stimulation of the forelimb region, and a small number of neurons responded to stimulation of the orofacial region (Figure 3A). The number of neurons with convergent inputs from both forelimb and orofacial regions was small (7%). On the other hand, the number of GPI neurons with convergent inputs was increased in dystonia model mice (28%).

The locations of recorded GPI neurons are plotted on the basis of cortical inputs in Figure 3B. In the GPI of normal mice, the neurons with forelimb inputs were distributed over a wide area

of the GPI, although not in its most medial portion (Figure 3B top). A few neurons with orofacial inputs were found in the lateral portion of the GPI. In dystonia model mice, however, such a segregation disappeared. The number of GPI neurons with orofacial inputs and those with convergent inputs was increased, and they intruded into the central portion of the GPI, although the most medial portion remained unresponsive (Figure 3B bottom). Similar changes were also observed in the GPe. These observations suggest that somatotopic arrangements are disorganized in the GPI and GPe of dystonia model mice.

ACTIVITY OF GPI AND GPe NEURONS IN A HUMAN CERVICAL DYSTONIA PATIENT

Neurons were recorded mostly in motor territories of the GPI and GPe. The firing rates of GPI (62.3 ± 12.1 Hz, $n = 9$) and GPe (45.8 ± 17.6 Hz, $n = 11$) neurons in a cervical dystonia patient were significantly lower than those of GPI (92.7 ± 40.1 Hz, $n = 34$) and GPe (81.0 ± 52.5 Hz, $n = 17$) neurons in Parkinsonian patients ($p < 0.05$, t -test). Most GPI and GPe neurons of a cervical dystonia patient showed burst (6/9 GPI and 5/11 GPe) or oscillatory (1–4 Hz) burst (1/9 GPI and 6/11 GPe) activity (Figure 4A). More than one-third of recorded neurons (6/13 GPI and 4/11 GPe in a cervical dystonia patient and 21/68 GPI and 18/45 GPe in Parkinsonian patients) showed responses to cortical stimulation. These GPI and GPe neurons were considered to be located in the upper limb regions of the GPI and GPe, because these neurons often responded to sensory stimulation of the upper limb. In Parkinsonian patients, response patterns to cortical stimulation were combinations of early excitation, inhibition, and late excitation (data not shown). On the other hand, in a cervical dystonia patient, long-lasting inhibition preceded by excitation (Figure 4B) and long-lasting monophasic inhibition (Figure 4C) were the typical response patterns. These response patterns are very similar to those observed in dystonia model mice (compare Figures 4B,C with Figure 2B).

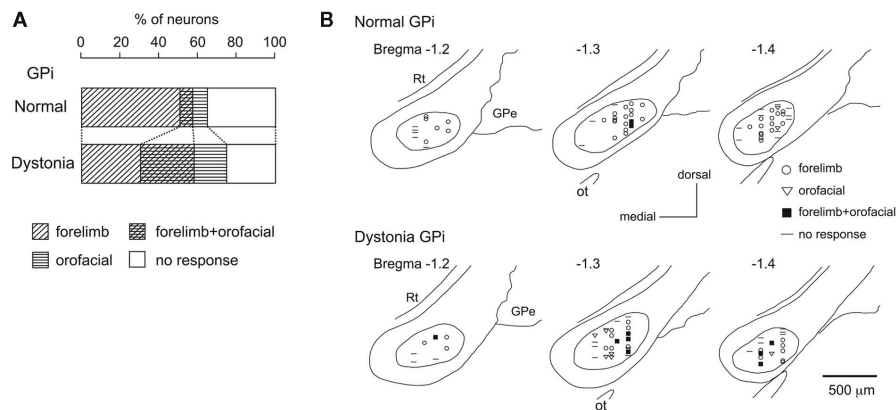


FIGURE 3 | Somatotopic organization in the GPi of DYT1 dystonia model mice. (A) Proportions of neurons classified on the basis of cortical inputs in normal (top) and dystonia model (bottom) mice. (B) Distribution of recorded GPi neurons indicated by symbols on the basis of cortical inputs. Data from

normal (top) and dystonia model (bottom) mice are shown in frontal sections. Figures in the left upper corner represent distance from bregma. GPe, external segment of the globus pallidus; Rt, reticular thalamic nucleus; Ot, optic tract. Modified from Chiken et al. (2008).

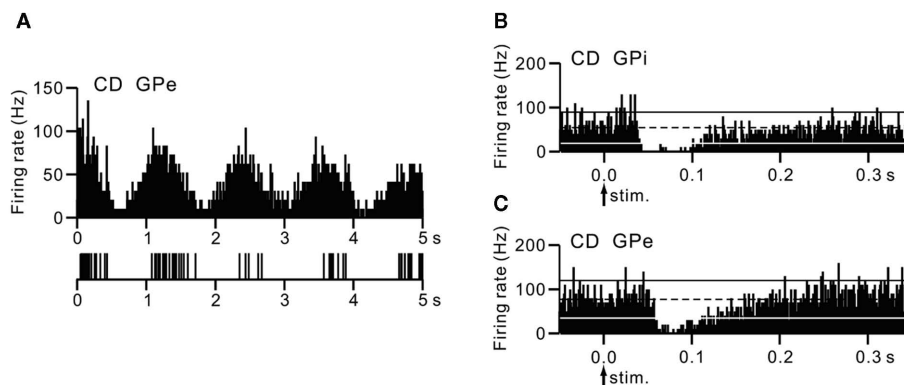


FIGURE 4 | Activity of GPi and GPe neurons in a human cervical dystonia patient. (A) Autocorrelograms and slow traces of digitized spikes of GPe neurons recorded from a cervical dystonia (CD) patient. (B,C) PSTHs (bin width of 1 ms) showing the responses of GPi (B) and GPe (C) neurons evoked by stimulation of the upper limb region of the primary motor cortex in a cervical dystonia patient. Cortical stimuli

were delivered at time 0 (arrows) for 100 trials. The mean firing rate is indicated by black dotted lines. The statistical levels of $p < 0.05$ (one-tailed t -test) calculated from the firing rate during 100 ms preceding the onset of stimulation are indicated by black and white solid lines (upper and lower limits of $p < 0.05$). Modified from Nishibayashi et al. (2011).

DISCUSSION

The first part of the present article characterized the electrophysiological properties of transgenic mice developed to express human ΔE -torsinA as a model of DYT1 dystonia. These mice exhibited: (1) decreased GPi and GPe activity with bursts and pauses, (2) cortically evoked long-lasting inhibition in the GPi and GPe, and (3) somatotopic disorganization in the GPi and GPe. In the second part, similar activity changes, such as decreased activity with bursts and cortically evoked long-lasting inhibition, were also observed in the GPi and GPe of a human cervical dystonia patient. These neuronal abnormalities may be responsible for the symptoms observed in dystonia.

DECREASED GPi AND GPe ACTIVITY IN DYSTONIA

In the present article, reduction of the spontaneous firing rates of GPi and GPe neurons was observed in dystonia model mice and

a human cervical dystonia patient. Alteration of firing patterns was also observed in both of them, including bursting discharges and pauses. Decreased discharge rates and irregularly grouped discharges with intermittent pauses in GPi and GPe neurons were also reported in patients with generalized dystonia (Vitek et al., 1999; Zhuang et al., 2004; Starr et al., 2005) and cervical dystonia (Tang et al., 2007). Dystonic hamsters with paroxysmal generalized dystonia also exhibited reduced and bursting GPi activity (Gernert et al., 2002). The correlation between abnormal neuronal activity and abnormal movements was not investigated in the present mice study, because it was difficult to observe abnormal movements under head fixation. The mechanisms responsible for decreased firing rates may include: (1) alteration of membrane properties of GPi and GPe neurons, (2) increased inhibitory inputs to the GPi and GPe, such as GABAergic inputs from the striatum, and/or (3) decreased excitatory inputs to the GPi and

GPe, such as glutamatergic inputs from the subthalamic nucleus (STN). Inhibitory inputs from the striatum to the GPi and GPe were increased in dystonia model mice as discussed in the next section.

CORTICALLY EVOKED LONG-LASTING INHIBITION IN GPi AND GPe NEURONS OF DYSTONIA

In normal mice, cortical stimulation typically induced triphasic responses composed of early excitation, inhibition, and late excitation in GPi and GPe neurons. Similar triphasic responses were also observed in the GPi and GPe of rats and monkeys. The origin of each component has been intensively studied (Ryan and Clark, 1991; Maurice et al., 1998, 1999; Nambu et al., 2000; Kita et al., 2004; Tachibana et al., 2008). Early excitation is mediated by the cortico-STN-GPe/GPi pathway, while inhibition and late excitation are mediated by the cortico-striato-GPe/GPi and cortico-striato-GPe-STN-GPe/GPi pathways, respectively.

On the other hand, in dystonia model mice we examined, cortical stimulation induced early excitation followed by late long-lasting inhibition in GPi and GPe neurons. Similar response patterns were induced in GPi and GPe neurons of a human cervical dystonia patient. These abnormal patterns of responses may be generated through the cortico-basal ganglia pathways. The early excitation seems to be mediated, at least in its early phase, by the cortico-STN-GPe/GPi pathway, as in normal mice, since the latency of the early excitation in dystonia model mice was short and similar to that in normal mice. The origin of the late long-lasting inhibition may be (1) increased inhibitory input via the striato-GPe/GPi pathway, or (2) decreased excitatory input via the STN-GPe/GPi pathway. The latter explanation seems less likely to be correct, since our preliminary observation indicates that the spontaneous activity of STN neurons is unchanged in dystonia model mice. Thus, increased activity through both cortico-striato-GPi *direct* and cortico-striato-GPe *indirect* pathways is considered to be the fundamental change in dystonia. The above observations also suggest that spontaneous excitation in the cortex that is transmitted to the GPi and GPe through the cortico-basal ganglia pathways could also induce short-latency excitation and long-lasting inhibition, which might be the origins of bursts and pauses, respectively.

SOMATOTOPIC DISORGANIZATION IN THE GPi AND GPe OF DYSTONIA

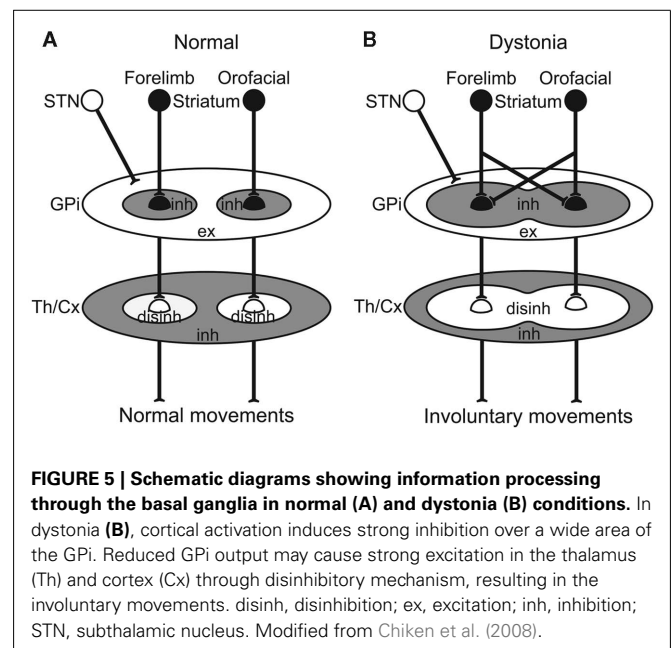
The somatotopic organization in the GPi and GPe was observed in normal mice as well as monkeys (DeLong et al., 1985; Yoshida et al., 1993). On the other hand, in dystonia model mice, somatotopic arrangements were disorganized, and many GPi and GPe neurons received convergent inputs from both forelimb and orofacial regions. Widened somatosensory receptive fields in pallidal neurons were reported in patients with generalized (Vitek et al., 1999) and focal (Lenz et al., 1998; Sanger et al., 2001) dystonia. Interference of information processing may occur through the cortico-basal ganglia pathways. One explanation for this could be that each single GPi or GPe neuron receives inputs from more striatal neurons in dystonia model mice than in normal mice. Such an explanation agrees well with the hypothesis that in dystonia, inhibition in the GPi/GPe is increased through the striato-GPe/GPi pathways as described in the previous section.

PATHOPHYSIOLOGY OF DYSTONIA

The GPi, the output nucleus of the basal ganglia, is composed of GABAergic inhibitory neurons and fires at high frequency in normal states. Its target structures, such as the thalamus and frontal cortex, are thus continuously inhibited. Striatal inputs reduce GPi activity in a temporal fashion, excite thalamic and cortical neurons through disinhibitory mechanism, and finally release appropriate movements with appropriate timing (Figure 5A; Nambu et al., 2000, 2002). On the other hand, in dystonia model mice and a human cervical dystonia patient, cortical excitation induced long-lasting inhibition in the GPi (Figure 5B). This suggests that even tiny amounts of spontaneous or voluntary neuronal activity originating in the cortex are transmitted through the cortico-basal ganglia pathways to induce strong, long-lasting inhibition in the GPi. Moreover, somatotopic disorganization was noted in the GPi of dystonia, and cortical activation could induce inhibition over a wide area of the GPi. Reduced GPi output may activate wide areas of the thalamus and cortex in an uncontrollable fashion, resulting in the involuntary movements observed in dystonia. In a similar manner, the cortical areas controlling agonist and antagonist muscles are concurrently activated, and co-contraction of agonist and antagonist muscles could be induced. This may also explain the “motor overflow” that is unintentional muscle contraction during voluntary movements in dystonia. Activation of the upper limb region in the motor cortex, for example, may inhibit large areas of the GPi and finally induce involuntary movements of multiple body parts (Figure 5B).

CONCLUSION

The activity of GPi and GPe neurons in DYT1 dystonia model mice and a human cervical dystonia patient was investigated. Both of them showed similar activity changes, such as decreased spontaneous activity with bursts and long-lasting inhibition evoked by cortical stimulation, indicating increased activity through



the cortico-striato-GPi *direct* and cortico-striato-GPe *indirect* pathways. Such a mechanism may explain the pathophysiology of dystonia: Neuronal activity originating in the cortex is transmitted through the cortico-basal ganglia pathways to induce strong, long-lasting inhibition in the GPi. Reduced GPi output may cause increased thalamic and cortical activity, resulting in the involuntary movements.

ACKNOWLEDGMENTS

The animal study was supported by a Grants-in-Aid for Exploratory Research (18650089) and a Grants-in-Aid for Scientific Research (B) (18300135) from the Ministry of Education,

Culture, Sports, Science, and Technology of Japan (MEXT), The Uehara Memorial Foundation, Takeda Science Foundation, and United States–Japan Brain Research Cooperative Program (Atsushi Nambu); a Grants-in-Aid for Scientific Research (C) (19500354) from MEXT (Satomi Chiken); and National Institute of Neurological Disorders and Stroke–National Institutes of Health Grant (NS-043038) (Pullanipally Shashidharan). The human study was supported by Wakayama Foundation for the Promotion of Medicine (Toru Itakura), a Grants-in-Aid for Scientific Research (B) (18300135) from MEXT and the Uehara Memorial Foundation (Atsushi Nambu), and NIH grants (NS-47085 and NS-57236) (Hitoshi Kita).

REFERENCES

- Chiken, S., Shashidharan, P., and Nambu, A. (2008). Cortically evoked long-lasting inhibition of pallidal neurons in a transgenic mouse model of dystonia. *J. Neurosci.* 28, 13967–13977.
- Chiken, S., and Tokuno, H. (2003). Ablation of striatal interneurons influences activities of entopeduncular neurons. *Neuroreport* 14, 675–678.
- DeLong, M. R., Crutcher, M. D., and Georgopoulos, A. P. (1985). Primate globus pallidus and subthalamic nucleus: functional organization. *J. Neurophysiol.* 53, 530–543.
- Gernert, M., Bennay, M., Fedrowitz, M., Rehders, J. H., and Richter, A. (2002). Altered discharge pattern of basal ganglia output neurons in an animal model of idiopathic dystonia. *J. Neurosci.* 22, 7244–7253.
- Kita, H., Nambu, A., Kaneda, K., Tachibana, Y., and Takada, M. (2004). Role of ionotropic glutamatergic and GABAergic inputs on the firing activity of neurons in the external pallidum in awake monkeys. *J. Neurophysiol.* 92, 3069–3084.
- Lenz, F. A., Suarez, J. I., Metman, L. V., Reich, S. G., Karp, B. I., Hallett, M., Rowland, L. H., and Dougherty, P. M. (1998). Pallidal activity during dystonia: somatosensory reorganization and changes with severity. *J. Neurol. Neurosurg. Psychiatr.* 65, 767–770.
- Maurice, N., Deniau, J. M., Glowinski, J., and Thierry, A. M. (1998). Relationships between the prefrontal cortex and the basal ganglia in the rat: physiology of the corticosubthalamic circuits. *J. Neurosci.* 18, 9539–9546.
- Maurice, N., Deniau, J. M., Glowinski, J., and Thierry, A. M. (1999). Relationships between the prefrontal cortex and the basal ganglia in the rat: physiology of the cortico-nigral circuits. *J. Neurosci.* 19, 4674–4681.
- Nambu, A., Tokuno, H., Hamada, I., Kita, H., Imanishi, M., Akazawa, T., Ikeuchi, Y., and Hasegawa, N. (2000). Excitatory cortical inputs to pallidal neurons via the subthalamic nucleus in the monkey. *J. Neurophysiol.* 84, 289–300.
- Nambu, A., Tokuno, H., and Takada, M. (2002). Functional significance of the cortico-subthalamo-pallidal ‘hyperdirect’ pathway. *Neurosci. Res.* 43, 111–117.
- Nishibayashi, H., Ogura, M., Kakishita, K., Tanaka, S., Tachibana, Y., Nambu, A., Kita, H., and Itakura, T. (2011). Cortically evoked responses of human pallidal neurons recorded during stereotactic neurosurgery. *Mov. Disord.* 26, 469–476.
- Ozelius, L. J., Hewett, J. W., Page, C. E., Bressman, S. B., Kramer, P. L., Shalish, C., de Leon, D., Brin, M. F., Raymond, D., Corey, D. P., Fahn, S., Risch, N. J., Buckler, A. J., Gusella, J. F., and Breakefield, X. O. (1997). The early-onset torsion dystonia gene (DYT1) encodes an ATP-binding protein. *Nat. Genet.* 17, 40–48.
- Ryan, L. J., and Clark, K. B. (1991). The role of the subthalamic nucleus in the response of globus pallidus neurons to stimulation of the prelimbic and agranular frontal cortices in rats. *Exp. Brain Res.* 86, 641–651.
- Sanger, T. D., Tarsy, D., and Pascual-Leone, A. (2001). Abnormalities of spatial and temporal sensory discrimination in writer’s cramp. *Mov. Disord.* 16, 94–99.
- Shashidharan, P., Sandu, D., Potla, U., Armata, I. A., Walker, R. H., McNaught, K. S., Weisz, D., Sreenath, T., Brin, M. F., and Olanow, C. W. (2005). Transgenic mouse model of early-onset DYT1 dystonia. *Hum. Mol. Genet.* 14, 125–133.
- Starr, P. A., Rau, G. M., Davis, V., Marks, W. J. Jr., Ostrem, J. L., Simmons, D., Lindsey, N., and Turner, R. S. (2005). Spontaneous pallidal neuronal activity in human dystonia: comparison with Parkinson’s disease and normal macaque. *J. Neurophysiol.* 93, 3165–3176.
- Tachibana, Y., Kita, H., Chiken, S., Takada, M., and Nambu, A. (2008). Motor cortical control of internal pallidal activity through glutamatergic and GABAergic inputs in awake monkeys. *Eur. J. Neurosci.* 27, 238–253.
- Tang, J. K., Moro, E., Mahant, N., Hutchison, W. D., Lang, A. E., Lozano, A. M., and Dostrovsky, J. O. (2007). Neuronal firing rates and patterns in the globus pallidus internus of patients with cervical dystonia differ from those with Parkinson’s disease. *J. Neurophysiol.* 98, 720–729.
- Vitek, J. L., Chockkan, V., Zhang, J. Y., Kaneoke, Y., Evatt, M., DeLong, M. R., Triche, S., Mewes, K., Hashimoto, T., and Bakay, R. A. E. (1999). Neuronal activity in the basal ganglia in patients with generalized dystonia and hemiballismus. *Ann. Neurol.* 46, 22–35.
- Yoshida, S., Nambu, A., and Jinnai, K. (1993). The distribution of the globus pallidus neurons with input from various cortical areas in the monkeys. *Brain Res.* 611, 170–174.
- Zhuang, P., Li, Y., and Hallett, M. (2004). Neuronal activity in the basal ganglia and thalamus in patients with dystonia. *Clin. Neurophysiol.* 115, 2542–2557.

Conflict of Interest Statement: The authors declare that the research was conducted in the absence of any commercial or financial relationships that could be construed as a potential conflict of interest.

Received: 21 April 2011; accepted: 18 October 2011; published online: 28 November 2011.

Citation: Nambu A, Chiken S, Shashidharan P, Nishibayashi H, Ogura M, Kakishita K, Tanaka S, Tachibana Y, Kita H and Itakura T (2011) Reduced pallidal output causes dystonia. *Front. Syst. Neurosci.* 5:89. doi: 10.3389/fnsys.2011.00089

Copyright © 2011 Nambu, Chiken, Shashidharan, Nishibayashi, Ogura, Kakishita, Tanaka, Tachibana, Kita and Itakura. This is an open-access article subject to a non-exclusive license between the authors and Frontiers Media SA, which permits use, distribution and reproduction in other forums, provided the original authors and source are credited and other Frontiers conditions are complied with.



Inter-hemispheric asymmetry of nigrostriatal dopaminergic lesion: a possible compensatory mechanism in Parkinson's disease

Javier Blesa^{1,2*}, Carlos Juri^{1,3}, Miguel Á. García-Cabezas^{4,5}, Rebeca Adánez^{1,2}, Miguel Á. Sánchez-González^{4,5}, Carmen Cavada^{4,5} and José A. Obeso^{1,2}

¹ Laboratorio de Trastornos del Movimiento, Neurociencias, Centro de Investigación Médica Aplicada, Departamento de Neurología y Neurocirugía, Clínica Universidad de Navarra, Pamplona, Spain

² Centro de Investigación Biomédica en Red sobre Enfermedades Neurodegenerativas, Instituto Carlos III, Ministerio de Ciencia e Innovación, Madrid, Spain

³ Departamento de Neurología, Pontificia Universidad Católica de Chile, Santiago, Chile

⁴ Departamento de Anatomía, Histología y Neurociencia, Facultad de Medicina, Universidad Autónoma de Madrid, Madrid, Spain

⁵ Instituto de Investigación Sanitaria IdiPAZ, Madrid, Spain

Edited by:

Jose Vargas, Universidad Nacional Autónoma de México, Mexico

Reviewed by:

Alessandro Stefani, University of Rome, Italy

M. Gustavo Murer, Universidad de Buenos Aires, Argentina

*Correspondence:

Javier Blesa, Centro de Investigación Médica Aplicada-Neurociencias, Universidad de Navarra, Pío XII 35, Pamplona 31008, Spain.
e-mail: jblesa@unav.es

The onset of Parkinson's disease (PD) is characterized by focal motor features in one body part, which are usually correlated with greater dopaminergic depletion in the contralateral posterior putamen. The role of dopamine (DA) hemispheric differences in the onset and progression of motor symptoms of PD, however, remains undefined. Previous studies have demonstrated that unilateral manipulations of one nigrostriatal system affect contralateral DA turnover, indicating a functional and compensatory inter-dependence of the two nigrostriatal systems. In preliminary data obtained by our group from asymmetric PD patients, a higher asymmetry index as measured by 6-[¹⁸F] fluoro-L-dopa (¹⁸F-DOPA) positron emission tomography (PET) was associated with a higher threshold (i.e., greater dopaminergic loss) for the onset of motor symptoms in the less-affected side. To further elucidate the underlying basis for this, we carried out a complementary study in monkeys using PET to assess and correlate the degree of dopaminergic striatal depletion with motor activity. Control and 1-methyl-4-phenyl-1,2,3,6-tetrahydropyridine (MPTP)-intoxicated monkeys with symmetrical lesions were characterized behaviorally and with ¹⁸F-DOPA PET. In parallel, an acute lesion was inflicted in the nigrostriatal projection unilaterally in one monkey, generating a 30% dopaminergic depletion in the ipsilateral striatum, which was not associated with any noticeable parkinsonian feature or deficit. The monkey remained asymptomatic for several months. Subsequently, this monkey received systemic MPTP, following which motor behavior and PET were repeatedly evaluated during progression of parkinsonian signs. The brains of all monkeys were processed using immunohistochemical methods. Our results suggest that the onset of motor signs is related to and influenced by the dopaminergic status of the less-affected, contralateral striatum. Although this work is still preliminary, the study agrees with our general hypothesis of hemispheric inter-dependence in the compensation of striatal DA deficit in PD.

Keywords: MPTP, Parkinson's disease, PET, dopaminergic, ¹⁸F-DOPA, compensatory mechanisms

INTRODUCTION

Parkinson's disease (PD) is a neurodegenerative disorder characterized mainly by neuronal cell loss predominantly affecting the nigrostriatal dopaminergic pathway (Dickson et al., 2009). However, disease progression is also associated with neuronal loss in the serotonergic, cholinergic, and noradrenergic neurotransmitter systems and with widespread synuclein pathology (Halliday et al., 2008).

The loss of dopaminergic striatal innervation in PD progresses over a period of years before classical motor features arise (Nandhagopal et al., 2009). Accordingly, very powerful compensatory mechanisms must therefore be activated in order to maintain motor activity within normal clinical limits during

this pre-symptomatic stage, now recognized to last for a significant period of time (mean 7 years). Indeed, initial motor manifestations typically appear when about 70–80% of striatal nerve terminals and 50–60% of substantia nigra pars compacta (SNc) neurons have been lost (Bernheimer et al., 1973; Fearnley and Lees, 1990, 1991). Remarkably, such a large reduction is associated with very mild clinical manifestations confined to a body segment, i.e., slowness of one hand, tremor of the foot, shoulder rigidity, etc., which is paralleled by unequal striatal innervation and asymmetric dopaminergic neuronal loss (Fearnley and Lees, 1991).

One essential feature of PD at onset is the focal and asymmetrical distribution of motor signs, the cause of which remains

elusive (Djaldetti et al., 2006). Animal models generally produce generalized bilateral deficits (Beal, 2010), which preclude analysis of this essential early asymmetric characteristic. Indeed, the basal ganglia model and its variants that have been developed since the mid-1980s have been unable to address the role and functional significance of inter-hemispheric connectivity. Thus, basal ganglia pathophysiology has been discussed and elaborated without including bilateral, inter-hemispheric connectivity, and possible physiological influences. Accordingly, the role of dopamine (DA) hemispheric differences in the onset and progression of motor features of PD remains by and large undefined (Djaldetti et al., 2006). Previous studies in animal models provoking acute or chronic unilateral lesion of the dopaminergic nigrostriatal system have shown a reciprocal interaction between the intact and DA-depleted striatum (Nieoullon et al., 1977; Andersson et al., 1980; Van Camp et al., 2010). Some previous reports studying the effects of unilateral and bilateral partial lesions of the nigrostriatal system in 6-hydroxydopamine (6-OHDA) rats suggested an inter-dependent regulation of the two nigrostriatal systems, which could provide some compensatory support for the lesioned hemisphere (Rodriguez et al., 1990; Castellano et al., 1993; Roedter et al., 2001).

In earlier 6- ^{18}F fluoro-L-dopa (^{18}F -DOPA) positron emission tomography (PET) studies on PD patients, we obtained data which strongly suggest that complete or partial indemnity of striatal DA in one hemisphere increases significantly the capacity of the primarily damaged striatum to compensate for DA depletion (Juri et al., 2009). Here we compared the features of 1-methyl-4-phenyl-1,2,3,6-tetrahydropyridine (MPTP)-treated monkeys of different symptom severity with those observed in one monkey with a surgical lesion of the nigrostriatal system followed up with progressive systemic MPTP administration to induce an asymmetrical parkinsonism. This represents a preliminary case-study regarding an asymmetrical model where the onset of motor features and striatal DA depletion has been monitored *in vivo* by using ^{18}F -DOPA PET. We realize the limitations of an ($n = 1$) observation. Nevertheless, this is a model which mimics more closely the onset and evolution of motor features in PD patients, and it is therefore potentially very useful to ascertain newer therapeutic agents.

MATERIALS AND METHODS

ANIMALS

Seventeen monkeys (*Macaca fascicularis*; 4.7 ± 1.1 years old) from RC Hartelust (Tilburg, The Netherlands), weighing 3.6 ± 1.02 kg, were included in this study. Animals were housed in an animal room under standard conditions of air exchange (16 l/min), humidity (50%), and light/dark cycles (8 a.m. to 8 p.m.) and were fed fresh fruit and commercial pellets, with free access to water. All procedures were performed according to the European Council Directive 86/609/EEC and in accordance with the Society for Neuroscience Policy on the Use of Animals in Neuroscience Research. The University of Navarra Ethics Committee for Animal Testing and state authorities approved the experimental design.

Bilateral symmetric parkinsonism

Parkinsonism was induced as previously reported (Blesa et al., 2010) by systemic administration (i.v.) of MPTP using a low-dose

regimen (0.5 mg/kg every 2 weeks) to obtain partial, slowly progressive and *bilateral* degeneration of the nigrostriatal dopaminergic system. In order to classify the motor status, a validated motor score (Kurlan scale; Kurlan et al., 1991) was used. Four animals were included in each group and classified as: (1) *Control*, normal, intact monkeys ($n = 4$); (2) *Asymptomatic*, animals that received MPTP but never showed any evidence of motor impairment ($n = 4$); (3) *Initial Parkinsonian*, this group consisted of four monkeys that developed mild motor features for several weeks. Subsequently, without further intoxication they showed minimal residual parkinsonian features or complete motor recovery. Accordingly, they were considered to be at the threshold between the asymptomatic and symptomatic stages; (4) *Stable Parkinsonian*, were those monkeys that exhibited parkinsonian features after MPTP and remained affected thereafter ($n = 4$). Each animal had to remain stable for at least 1 month in the corresponding motor state to be classified in a given group.

To generate the model, motor behavior was analyzed weekly after MPTP injection. Inter-subject sensitivity to MPTP leads to variable outcomes during the initial intoxication period (first two doses). A monkey that was free of motor manifestations after the second injection was considered to be *Asymptomatic* and received no further MPTP. All other monkeys developed parkinsonian features after the initial MPTP doses. Four of these animals with initial motor symptoms were left to improve until they exhibited only minimal or no motor (*Initial Parkinsonian*) features without further intoxication, while others continued to receive MPTP until a stable parkinsonian state was obtained (*Stable Parkinsonian*). The latter showed bilateral and symmetric motor deficits which persisted unchanged until the end of the study.

Bilateral asymmetric parkinsonism (case-study monkey)

One monkey (*M. fascicularis*; 4 years old, weight 2.5 kg) was used in this preliminary study. First, a unilateral lesion of the right nigrostriatal pathway was made. Following anesthesia (ketamine/midazolam) the monkey was fixed to a stereotactic device and a trepanus was performed following the right subthalamic nucleus (STN) coordinates (6 mm posterior and 4 mm lateral to anterior commissure and 27.5 mm ventral to the dura). The STN was localized by neuronal extracellular recordings. A mechanical lesion was made ventromedial to STN without affecting it.

Subsequently, several months after establishing the initial focal lesion which interrupted the nigrostriatal projection unilaterally, the same monkey received systemic administration (i.v.) of MPTP using a low-dose regimen of 0.25 mg/kg every 2 weeks on four occasions which resulted in early and mild unilateral parkinsonian features contralateral to the previously lesioned side. Then, 0.5 mg/kg was given every 2 weeks until the development of bilateral motor features consistent with stable parkinsonism. This allowed the severity and evolution of motor features to be separated and for each hemibody to be designated according to the *Primary Affected Side* (the right side of the body) or *Secondary Affected Side* (the left side of the body).

MOTOR BEHAVIOR

Peanuts test

This manual motor task test measured the time taken for the monkey to reach out and retrieve four peanuts that had been placed in front of it. The test was performed with the monkey comfortably seated in a cage specifically prepared for this purpose, with a methacrylate front panel and two symmetrical holes with a diameter of 5 cm. Each hole corresponded to the positioning of each of the hands. Peanuts were placed within circles (2 cm in diameter) in a tray directly in line with the panel holes. The examiner recorded the time taken for the monkey to perform the test five times with each hand alternately.

PET STUDIES

Positron emission tomography studies were conducted using the radioligand ^{18}F -DOPA in a dedicated small animal Philips Mosaic tomograph (Cleveland, OH, USA). The radiotracer was intravenously injected through the saphenous vein simultaneously to the beginning of a list mode study. To block peripheral decarboxylation of ^{18}F -DOPA, 50 mg of carbidopa was given orally 1 h prior to the scans and anesthesia. Anesthesia was initially induced by intramuscular injections of ketamine (10 mg/kg) and midazolam (1 mg/kg) to allow preparation and handling of the monkeys. Anesthesia was maintained during the scans with a mixture of ketamine (5 mg/kg) and midazolam (0.5 mg/kg).

Studies were conducted using baseline conditions and after stabilization in the different motor states in the bilaterally lesioned animals. Regarding the case-study monkey with unilateral lesion of the nigrostriatal pathway and subsequent MPTP intoxication, the assessments were conducted following the mechanical lesion, and then 2 weeks after the second MPTP dose when the monkey was still asymptomatic, after the onset of unilateral parkinsonism, and when bilateral parkinsonian features had developed. A stabilization period was also allowed after the onset of unilateral and bilateral parkinsonism before conducting the studies. PET data acquisitions and analyses were performed using the standard protocol described previously by our group (Collantes et al., 2009; Blesa et al., 2010).

HISTOLOGICAL ANALYSIS

Animals were perfused with saline, followed by 4% paraformaldehyde in phosphate buffer (PB, 0.1 M, pH 7.4) and a series of PB sucrose solutions (5–20%). Brains were removed from the skull, cut into 40 μm thick coronal sections and stored for immunohistochemical procedures (Cavada et al., 1995). Tyrosine hydroxylase (TH) positive cells in the mesencephalon were counted by stereological analysis. Dopaminergic innervation was studied by immunostaining of TH in the striatum. All analyses were performed on the right hemisphere.

IMMUNOHISTOCHEMICAL PROCEDURES

Immunoreactivity for TH was localized using the protocol outlined in Sanchez-Gonzalez et al. (2005). Briefly, sections were incubated with mouse anti-TH antibody (1/1000 dilution: MAB5280 Chemicon International, Temecula, CA, USA), followed by a secondary biotinylated antibody (1/400 dilution: AP160B; 1:400;

Chemicon International, Temecula, CA, USA). Visualization was carried out using Avidin/Biotin complex (ABC) Vectastain Elite[®] (Vector Labs, Burlingame, CA, USA) and diaminobenzidine (DAB; Sigma).

QUANTIFICATION METHODS

Estimates of the number of TH-immunoreactive(-ir) neuronal bodies in the mesencephalon were quantified according to stereological principles. Eight coronal sections, regularly spaced at intervals of 1200 μm , from the caudal edges of the mammillary bodies rostrally to the decussation of the superior cerebellar peduncle caudally, were analyzed for each animal. The stereology system consisted of a Zeiss Axioskop optical microscope (Oberkochen, Germany) equipped with a digital camera (Axio-Cam HRC, Zeiss, Germany) and StereoInvestigator software (version 8.0, MicroBrightField, Williston, VT, USA). The camera settings were maintained throughout the duration of the experiment. We traced arbitrary landmarks based on external references with the StereoInvestigator software to delineate the SNc (A9) and ventral tegmental area (A10) in each region of interest.

The relative density of TH-ir fibers in the caudate and putamen was quantified by measuring the optical density (OD) of immunostaining using Image J (1.41o, NIH, USA) software. A total of seven rostro-caudal sections for each monkey – three anterior and four posterior to the anatomical references – regularly spaced at intervals of 2400 μm were examined.

STATISTICS

All statistics were performed with SPSS software (version 16.0 software for Windows; SPSS Inc., Chicago, IL, USA). Two-sided *p* values of less than 0.05 and 0.01 were considered significant.

Differences in continuous and normally distributed variables of ^{18}F -DOPA Ki, numbers of TH-ir cells, and optical densities were analyzed using two-way repeated measures analyses of variance (ANOVA), followed by the Bonferroni *post hoc* test. Normality was checked by the Kolmogorov–Smirnov test.

RESULTS

MOTOR BEHAVIOR

Monkeys that received systemic MPTP could be categorized as *Asymptomatic*, *Initial Parkinsonian*, and *Stable Parkinsonian* at the time of analysis (9 weeks after last MPTP dose). The group of monkeys labeled as *Initial Parkinsonian* developed moderate parkinsonism (Kurlan scale score of ~ 5) after initial MPTP doses and were subsequently left to stabilize (Kurlan scale ~ 2). *Stable Parkinsonian* monkeys developed relatively severe bilateral motor deficits during the intoxication phase (Kurlan scale scores of ~ 17), but some recovery took place during the stabilization period, so that by the end of the experiment they showed moderate parkinsonian features (Kurlan scale score of ~ 11).

The case-study monkey showed no motor abnormality initially, as evidenced by the results of the motor scale and peanuts test, despite relatively significant dopaminergic depletion of the right striatum (see below). Subsequently, MPTP administration induced progressive bradykinesia, which manifested on the left

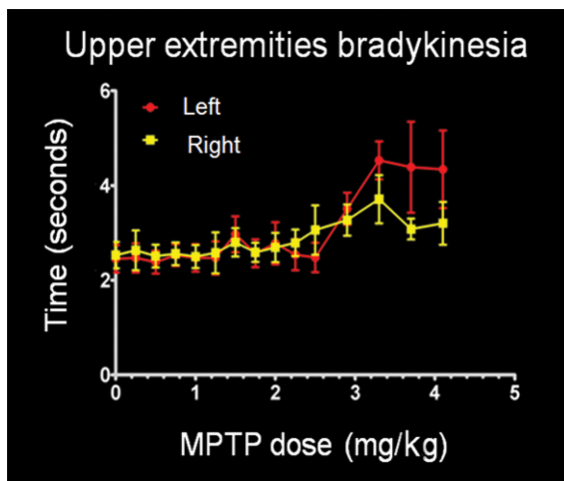


FIGURE 1 | Motor behavior. Evolution of hand bradykinesia using the peanuts test in the case-study monkey with asymmetric involvement of the nigrostriatal dopaminergic system. The left hand (contralateral to the *Primary Affected Side*) exhibits a progressive increase in time taken to complete the test in parallel with increased 1-methyl-4-phenyl-1,2,3,6-tetrahydropyridine (MPTP) total dose, while the right hand shows modest involvement.

side as clearly shown by the motor scale and the asymmetric loss of motor ability, contralateral to the *Primary Affected Side* in the peanuts test (Figure 1). As the effect of MPTP progressed, parkinsonian features became more severe and generalized. This monkey

thus exhibited bilateral, albeit asymmetrical, parkinsonism by the end of the intoxication period.

PET STUDY

The ^{18}F -DOPA PET showed a linear reduction of uptake in the monkey groups receiving parenteral MPTP (Figure 2). Such a pattern of uptake reduction correlated very significantly with the Kurlan motor score ($p = 0.00$; $R = 0.77$), SNc cell loss ($p = 0.00$; $R = 0.93$), and decline of striatal TH immunolabeling ($p = 0.00$; $R = 0.91$).

In the monkey with the unilateral lesion, ^{18}F -DOPA PET uptake was reduced in the *Primary Affected Side* by 30% with respect to the contralateral side and continued to decrease bilaterally once MPTP was given. Importantly, the initial asymmetry in ^{18}F -DOPA uptake was maintained during MPTP intoxication until the last stage, when the monkey had developed bilateral motor features (Figure 2). For this one monkey, it was noticeable that the magnitude of dopaminergic depletion associated with the onset of motor manifestations in the lesioned side (*Primary Affected Side*) was much higher than that observed in the model of symmetric parkinsonisms induced by systemic MPTP administration.

HISTOLOGY

Tyrosine hydroxylase innervation of the striatum

For the case-study monkey, TH immunoreactivity reduction was, as expected, greater in the *Primary Affected Side* (Figure 3). In monkeys with MPTP-induced bilateral deficit, a progressive

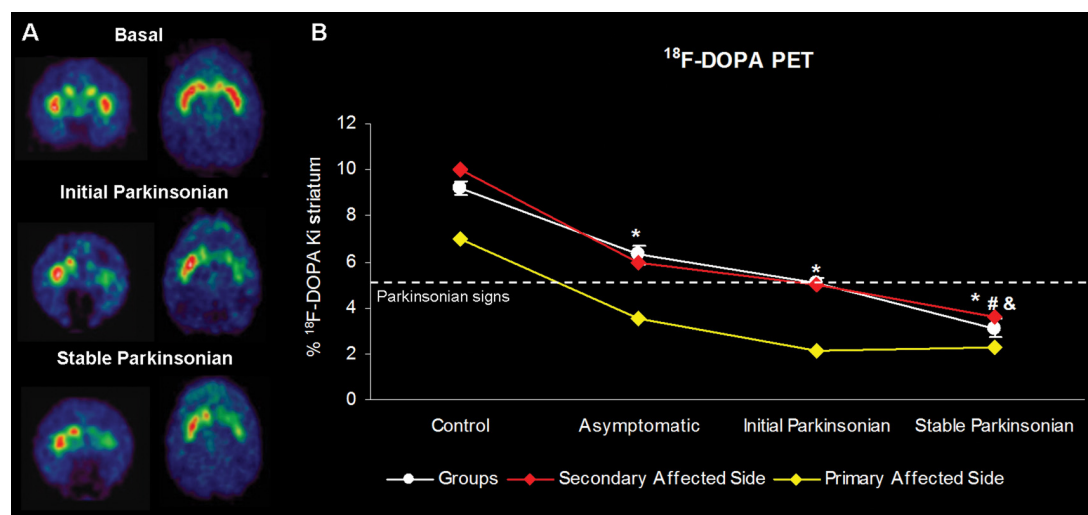
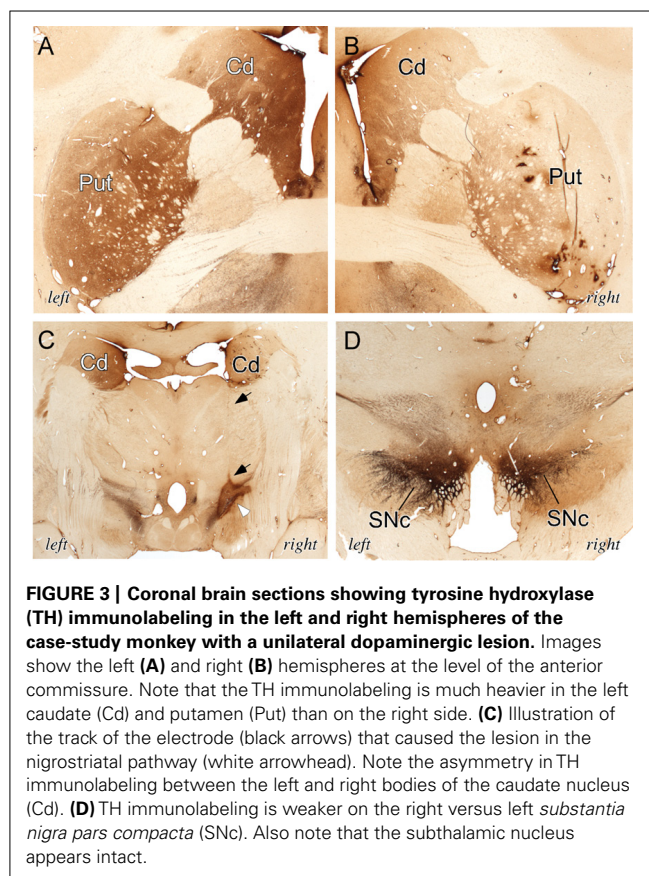


FIGURE 2 | (A) Representative 6-[^{18}F] fluoro-L-dopa (^{18}F -DOPA) positron emission tomography (PET) brain images of the asymmetrically affected (case-study) monkey in coronal and transversal orientation at baseline, after 1-methyl-4-phenyl-1,2,3,6-tetrahydropyridine (MPTP) treatment (~Initial Parkinsonian), and after the final MPTP administration (~Stable Parkinsonian). **(B)** Comparison of ^{18}F -DOPA uptake in control and MPTP-treated monkeys ($n = 16$; white line), and dopaminergic uptake of the *Primary Affected Side* (yellow line) and *Secondary Affected Side* (red line) in the case-study monkey with asymmetric dopamine depletion. In this

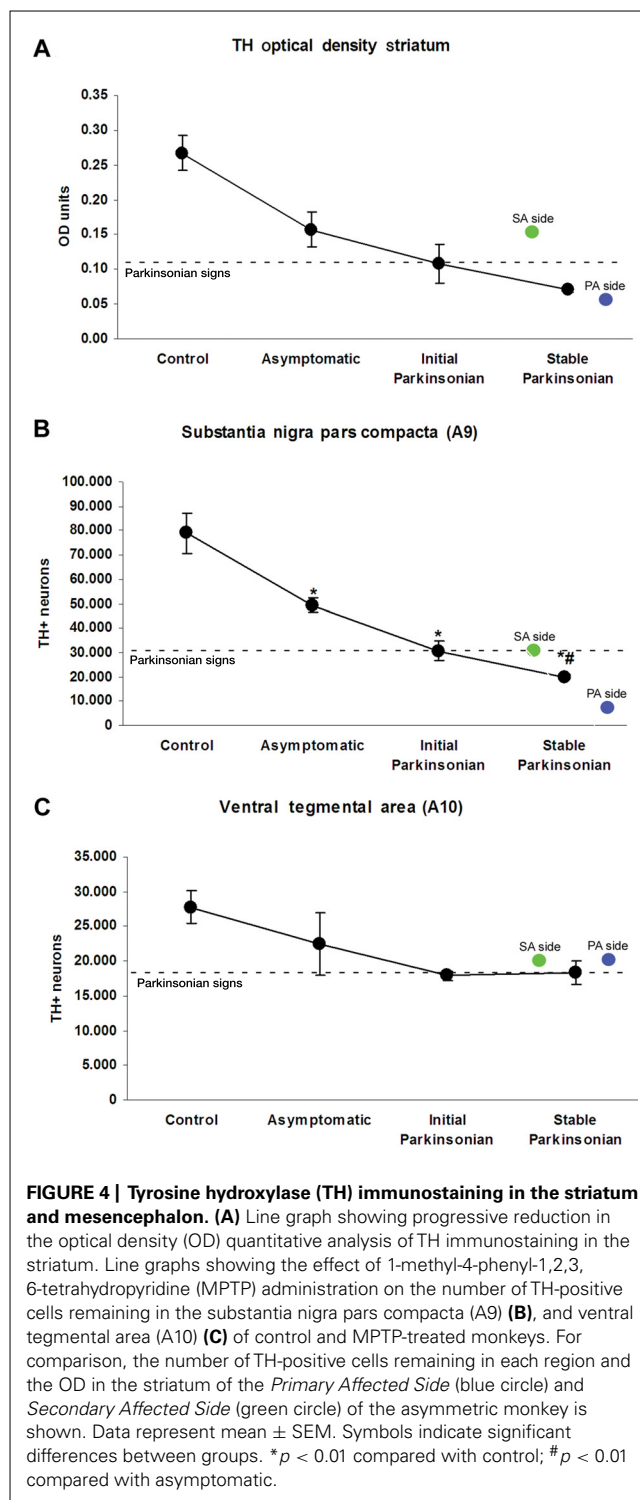
last-mentioned monkey with the asymmetric lesion, a constant asymmetry between both striata is observed after the unilateral lesion, which remained more or less stable after MPTP administration. Note that the observed depletion at the beginning of parkinsonism in the *Primary Affected Side* is greater than expected based on the general model. Data represent mean \pm SEM. Symbols indicate significant differences between groups. * $p < 0.01$ compared with control; # $p < 0.01$ compared with asymptomatic; & $p < 0.05$ compared with recovered group.



reduction in the level of immunoreactivity for TH was observed in the striatum (Figure 4A), which correlated with the severity of parkinsonism for the different groups. The magnitude of the reduction in the case-study monkey TH immunoreactivity was close to that (i.e., greatest loss) for the *Stable Parkinsonian* group (Figure 4A).

Dopaminergic cells in the mesencephalon

For monkeys receiving MPTP parenterally, the number of TH-ir neurons in A9 declined in parallel with the increased severity of motor deficits (Figure 4B). The minimal cell loss was a 37% reduction with respect to controls in the *Asymptomatic* group; this is in comparison to the *Stable Parkinsonian* group which showed a 75% reduction. For the case-study monkey, cell counts of TH-ir neuronal cell bodies in the mesencephalon showed bilateral loss of these neurons in the SNc (A9), which was greater in the *Primary Affected Side* (Figure 4B) than in the *Secondary Affected Side*. Moreover, the values fit well with the degree of motor deficit, so that the most severe parkinsonian features in the *Primary Affected Side* corresponded with a lower cell count than the less severe *Secondary Affected Side*. Importantly, cell loss in the SNc of the *Primary Affected Side* was greater even than that of monkeys with *Stable Parkinsonism*. Cell loss in A10 (ventral tegmental area) was similar to that observed in monkeys with parkinsonism induced by systemic MPTP administration (Figure 4C).



DISCUSSION

The manner by which the brain compensates for progressive striatal DA depletion over the course of many years before clinical motor features of PD are manifested is yet to be elucidated. The main recognized compensatory mechanisms include increased dopaminergic pre-synaptic turnover, down-regulation

of pre-synaptic dopaminergic auto-receptors and DA transporter, and up-regulation of post-synaptic dopaminergic receptors (Hornykiewicz and Kish, 1987; Zigmond et al., 1989; Zigmond, 1997; Brotchie and Fitzer-Attas, 2009). Undoubtedly, the more classic and reputedly compensatory mechanism of striatal depletion in PD consists of an increased DA striatal turnover, as established in the 6-OHDA-lesioned rat model (Zigmond et al., 1990) and in human PD patients (Hornykiewicz, 1975; Zigmond et al., 1990; Pifl and Hornykiewicz, 2006). More recently, some studies have challenged the fundamental role attributed to striatal DA turnover in compensating for PD. Thus, substantia nigra (SN) firing was not found to be significantly increased in the unilateral 6-OHDA rat model (Rodriguez and Gonzalez-Hernandez, 1999), and the changes in striatal DA turnover in the MPTP monkey model were observed too late in the evolution of the process to account for the pre-symptomatic period (Bezard et al., 2001). This led to the suggestion that other compensatory mechanisms beyond the striatum may be more relevant or important in the early phase of PD (Bezard et al., 2003). These may include increased glutamatergic and serotonergic striatal input (Boulet et al., 2008) and modulation of basal ganglia output circuits and beyond (Obeso et al., 2004; Tang et al., 2011).

A possible role of the inter-hemispheric influence of basal ganglia function and compensation of the dopaminergic deficit has been suggested but has received little attention. To this extent, crossed afferents to the striatum from the contralateral SN and ventral tegmental area were observed in the rat, which persisted after corpus callosotomy (Fass and Butcher, 1981). Nieoullon et al. (1977) showed in cats that infusion of DA in the SNc (resulting in a decreased DA concentration in the striatum) was associated with an increase in the liberation of DA in the contralateral striatum and the opposite effect when the DA infusion was stopped (Nieoullon et al., 1977). In rats with an ibotenic acid-induced striatal lesion, Narang et al. (1993) demonstrated increased striatal D2 receptor mRNA expression contralaterally. Neurophysiologic changes have also been demonstrated contralaterally to unilateral lesions; for example, a decrease in the rate of neuronal discharge in the contralateral STN (Perier et al., 2000) or an increase in the firing rate of contralateral SN GABAergic neurons (Gonzalez-Hernandez et al., 2004). With specific relevance to our current approach, a study comparing the effect of unilateral versus bilateral striatal 6-OHDA lesions in rats showed a marked aggravation of locomotor and exploratory behavior and the use of the forelimbs, suggesting a functional compensatory inter-dependence of the two nigrostriatal systems (Roedter et al., 2001). Finally, we have obtained preliminary findings in PD patients suggesting that the absence of clinically evident signs in early unilateral PD is related not only with the dopaminergic depletion of the less-affected striatum but also to the degree of putamen Ki asymmetry between sides (Juri et al., 2009).

We report here for the first time a direct comparison between symmetrical and asymmetrical dopaminergic depletion in the MPTP monkey model. We readily acknowledge that the results are very preliminary as only one monkey with an asymmetrical lesion has been studied and some un-controlled variables could potentially undermine these preliminary results. For instance, the lesion could have impinged upon the STN or its efferent connections to

the globus pallidus pars interna, which would have had an anti-parkinsonian effect. However we believe that such a possibility is unlikely anatomically as well as in terms of the putative impact on motor behavior. Thus, the focal lesion was medio-ventral to the STN and the efferent fibers projecting from the motor STN to the motor globus pallidus pars interna and externa are dorso-lateral, and therefore, quite remote from the lesion site. These motor fibers arising from the dorso-lateral STN are well recognized to be responsible for conveying excessive glutamatergic activity, which gives rise to the parkinsonian state. Thus, we have no doubt the motor STN was completely spared in this monkey. In the symmetrical monkeys there was a very powerful correlation between motor behavior and degree of dopaminergic lesion as evaluated by PET *in vivo* and post-mortem. The case-study monkey with asymmetric lesion did not fit into such a general pattern, showing a higher reduction in ^{18}F -DOPA uptake in the PET studies and greater SNc cell loss than expected for the degree of motor deficit. In other words, the asymmetric monkey tolerated a more severe dopaminergic lesion before becoming fully parkinsonian.

These findings support the hypothesis that the contralateral dopaminergic activity of the less-affected hemisphere plays a role in compensating for dopaminergic depletion of the most affected hemisphere in PD. To our knowledge this is the first concerted attempt to analyze using PET the role of inter-hemispheric asymmetry in DA depletion.

Asymmetry in the onset of the motor manifestations is a characteristic feature of PD. The cause of this asymmetry is not known (Djaldetti et al., 2006), but it could reflect a different vulnerability of the SNc to the factor(s) involved in the genesis of the disorder. Data from PD patients have suggested that those with higher asymmetry could evolve slower than those with a more symmetrical motor involvement (Poewe, 2006), particularly when tremor is the predominant motor manifestation (Djaldetti et al., 2006).

CONCLUSION

The data presented here indicate that asymmetry of dopaminergic depletion is probably involved in the clinical manifestations of the primarily affected body side in PD patients. The precise mechanisms of such inter-hemispheric influence and inter-dependence are not well understood and warrant further investigation. Our findings open a new experimental approach to study PD and may be highly relevant when considering the early treatment of PD in general, and the application of neuroprotective therapies in particular.

ACKNOWLEDGMENTS

This work was supported in part by the Plan Nacional de Investigación (SAF2005-08416; SAF2008-04276), Ministerio de Ciencia e Innovación, and by the UTE-CIMA agreement with the Universidad de Navarra. Carlos Juri was supported by the ALBAN Programme, the European Union Programme of High Level Scholarships for Latin America, scholarship No. E07D403507CL. Monkeys were housed and cared for at the CIFA (Centro de Investigación de Farmacología Aplicada) Primate Unit at the University of Navarra.

REFERENCES

- Andersson, K., Schwarcz, R., and Fuxe, K. (1980). Compensatory bilateral changes in dopamine turnover after striatal kainate lesion. *Nature* 283, 94–96.
- Beal, M. F. (2010). Parkinson's disease: a model dilemma. *Nature* 466, S8–S10.
- Bernheimer, H., Birkmayer, W., Hornykiewicz, O., Jellinger, K., and Seitelberger, F. (1973). Brain dopamine and the syndromes of Parkinson and Huntington. Clinical, morphological and neurochemical correlations. *J. Neurol. Sci.* 20, 415–455.
- Bezard, E., Dovero, S., Prunier, C., Ravenscroft, P., Chalon, S., Guilleloteau, D., Crossman, A. R., Bioulac, B., Brochie, J. M., and Gross, C. E. (2001). Relationship between the appearance of symptoms and the level of nigrostriatal degeneration in a progressive 1-methyl-4-phenyl-1,2,3,6-tetrahydropyridine-lesioned macaque model of Parkinson's disease. *J. Neurosci.* 21, 6853–6861.
- Bezard, E., Gross, C. E., and Brochie, J. M. (2003). Presymptomatic compensation in Parkinson's disease is not dopamine-mediated. *Trends Neurosci.* 26, 215–221.
- Blesa, J., Juri, C., Collantes, M., Penuelas, I., Prieto, E., Iglesias, E., Marti-Climent, J., Arbizu, J., Zubieta, J. L., Rodriguez-Oroz, M. C., Garcia-Garcia, D., Richter, J. A., Cavada, C., and Obeso, J. A. (2010). Progression of dopaminergic depletion in a model of MPTP-induced Parkinsonism in non-human primates. An (18F)-DOPA and (11C)-DTBZ PET study. *Neurobiol. Dis.* 38, 456–463.
- Boulet, S., Mounayar, S., Poupard, A., Bertrand, A., Jan, C., Pessiglione, M., Hirsch, E. C., Feuerstein, C., Francois, C., Feger, J., Savasta, M., and Tremblay, L. (2008). Behavioral recovery in MPTP-treated monkeys: neurochemical mechanisms studied by intrastriatal microdialysis. *J. Neurosci.* 28, 9575–9584.
- Brochie, J., and Fitzer-Attas, C. (2009). Mechanisms compensating for dopamine loss in early Parkinson disease. *Neurology* 72, S32–S38.
- Castellano, M. A., Rivero, F. L., and Rodriguez, M. (1993). Spontaneous firing of nigrostriatal dopaminergic neurons in split-brain rats. *Neurosci. Lett.* 162, 1–4.
- Cavada, C., Company, T., Hernandez-Gonzalez, A., and Reinoso-Suarez, F. (1995). Acetylcholinesterase histochemistry in the macaque thalamus reveals territories selectively connected to frontal, parietal and temporal association cortices. *J. Chem. Neuroanat.* 8, 245–257.
- Collantes, M., Prieto, E., Penuelas, I., Blesa, J., Juri, C., Marti-Climent, J. M., Quincoces, G., Arbizu, J., Riverol, M., Zubieta, J. L., Rodriguez-Oroz, M. C., Luquin, M. R., Richter, J. A., and Obeso, J. A. (2009). New MRI, 18F-DOPA and 11C-(+)-alpha-dihydrotetraabenazine templates for *Macaca fascicularis* neuroimaging: advantages to improve PET quantification. *Neuroimage* 47, 533–539.
- Dickson, D., Braak, H., Duda, J., Duyckaerts, C., Gasser, T., Halliday, G., Hardy, J., Leverenz, J., Del Tredici, K., Wszolek, Z., and Litvan, I. (2009). Neuropathological assessment of Parkinson's disease: refining the diagnostic criteria. *Lancet Neurol.* 8, 1150–1157.
- Djaldetti, R., Ziv, I., and Melamed, E. (2006). The mystery of motor asymmetry in Parkinson's disease. *Lancet Neurol.* 5, 796–802.
- Fass, B., and Butcher, L. L. (1981). Evidence for a crossed nigrostriatal pathway in rats. *Neurosci. Lett.* 22, 109–113.
- Fearnley, J., and Lees, A. (1991). Ageing and Parkinson's disease: substantia nigra regional selectivity. *Brain* 114(Pt 5), 2283–2301.
- Fearnley, J. M., and Lees, A. J. (1990). Striatonigral degeneration. A clinicopathological study. *Brain* 113(Pt 6), 1823–1842.
- Gonzalez-Hernandez, T., Barroso-Chinea, P., and Rodriguez, M. (2004). Response of the GABAergic and dopaminergic mesostriatal projections to the lesion of the contralateral dopaminergic mesostriatal pathway in the rat. *Mov. Disord.* 19, 1029–1042.
- Halliday, G., Hely, M., Reid, W., and Morris, J. (2008). The progression of pathology in longitudinally followed patients with Parkinson's disease. *Acta Neuropathol.* 115, 409–415.
- Hornykiewicz, O. (1975). Brain monoamines and parkinsonism. *Psychopharmacol. Bull.* 11, 34–35.
- Hornykiewicz, O., and Kish, S. J. (1987). Biochemical pathophysiology of Parkinson's disease. *Adv. Neurol.* 45, 19–34.
- Juri, C., Arbizu, J., Blesa, J., Rodriguez-Oroz, M. C., Prieto, E., Iglesias, E., Collantes, M., Richter, J. A., Penuelas, I., and Obeso, J. A. (2009). *Reciprocal Relationship Between the Striatum Bilaterally and Compensation of Dopaminergic Depletion in Early Parkinson's Disease. An 18F-FDOPA PET Study. Program 52024/J34 2009 Neuroscience Meeting Planner*. Chicago, IL: Society for Neuroscience.
- Kurlan, R., Kim, M., and Gash, D. (1991). Oral levodopa dose-response study in MPTP-induced hemiparkinsonian monkeys: assessment with a new rating scale for monkey parkinsonism. *Mov. Disord.* 6, 111–118.
- Nandhagopal, R., Kuramoto, L., Schulzer, M., Mak, E., Cragg, J., Lee, C., McKenzie, J., McCormick, S., Samii, A., Troiano, A., Ruth, T., Sossi, V., de la Fuente-Fernandez, R., Calne, D., and Stoessl, A. (2009). Longitudinal progression of sporadic Parkinson's disease: a multi-tracer positron emission tomography study. *Brain* 132, 2970–2979.
- Narang, N., Hunt, M., Pundt, L., Alburges, M., and Wamsley, J. (1993). Unilateral ibotenic acid lesion of the caudate putamen results in D2 receptor alterations on the contralateral side. *Exp. Neurol.* 121, 40–47.
- Nieouillon, A., Cheramy, A., and Glowinski, J. (1977). Interdependence of the nigrostriatal dopaminergic systems on the two sides of the brain in the cat. *Science* 198, 416–418.
- Obeso, J. A., Rodriguez-Oroz, M. C., Lanciego, J. L., and Rodriguez Diaz, M. (2004). How does Parkinson's disease begin? The role of compensatory mechanisms. *Trends Neurosci.* 27, 125–127; author reply 127–128.
- Perier, C., Agid, Y., Hirsch, E. C., and Feger, J. (2000). Ipsilateral and contralateral subthalamic activity after unilateral dopaminergic lesion. *Neuroreport* 11, 3275–3278.
- Pifl, C., and Hornykiewicz, O. (2006). Dopamine turnover is upregulated in the caudate/putamen of asymptomatic MPTP-treated rhesus monkeys. *Neurochem. Int.* 49, 519–524.
- Poewe, W. (2006). The natural history of Parkinson's disease. *J. Neurol.* 253(Suppl. 7), VII2–VII6.
- Rodriguez, M., Castellano, M. A., and Palarea, M. D. (1990). Inter-hemispheric regulation of dopaminergic ascending systems. *Life Sci.* 47, 377–384.
- Rodriguez, M., and Gonzalez-Hernandez, T. (1999). Electrophysiological and morphological evidence for a GABAergic nigrostriatal pathway. *J. Neurosci.* 19, 4682–4694.
- Roedter, A., Winkler, C., Samii, M., Walter, G. F., Brandis, A., and Nikkhah, G. (2001). Comparison of unilateral and bilateral intrastriatal 6-hydroxydopamine-induced axon terminal lesions: evidence for inter-hemispheric functional coupling of the two nigrostriatal pathways. *J. Comp. Neurol.* 432, 217–229.
- Sanchez-Gonzalez, M. A., Garcia-Cabezas, M. A., Rico, B., and Cavada, C. (2005). The primate thalamus is a key target for brain dopamine. *J. Neurosci.* 25, 6076–6083.
- Tang, C. C., Poston, K. L., Dhawan, V., and Eidelberg, D. (2011). Abnormalities in metabolic network activity precede the onset of motor symptoms in Parkinson's disease. *J. Neurosci.* 30, 1049–1056.
- Van Camp, N., Vreys, R., Van Laere, K., Lauwers, E., Beque, D., Verhoye, M., Casteels, C., Verbruggen, A., Debys, Z., Mortelmans, L., Sijbers, J., Nuyts, J., Baekelandt, V., and Van der Linden, A. (2010). Morphologic and functional changes in the unilateral 6-hydroxydopamine lesion rat model for Parkinson's disease discerned with muSPECT and quantitative MRI. *MAGMA* 23, 65–75.
- Zigmond, M. J. (1997). Do compensatory processes underlie the preclinical phase of neurodegenerative disease? Insights from an animal model of parkinsonism. *Neurobiol. Dis.* 4, 247–253.
- Zigmond, M. J., Abercrombie, E. D., Berger, T. W., Grace, A. A., and Stricker, E. M. (1990). Compensations after lesions of central dopaminergic neurons: some clinical and basic implications. *Trends Neurosci.* 13, 290–296.
- Zigmond, M. J., Berger, T. W., Grace, A. A., and Stricker, E. M. (1989). Compensatory responses to nigrostriatal bundle injury. Studies with 6-hydroxydopamine in an animal model of parkinsonism. *Mol. Chem. Neuropathol.* 10, 185–200.

Conflict of Interest Statement: The authors declare that the research was conducted in the absence of any commercial or financial relationships that could be construed as a potential conflict of interest.

Received: 21 April 2011; accepted: 25 October 2011; published online: 24 November 2011.

Citation: Blesa J, Juri C, García-Cabezas MÁ, Adánez R, Sánchez-González MÁ, Cavada C and Obeso JA (2011) Inter-hemispheric asymmetry of nigrostriatal dopaminergic lesion: a possible compensatory mechanism in Parkinson's disease. *Front. Syst. Neurosci.* 5:92. doi: 10.3389/fnsys.2011.00092

Copyright © 2011 Blesa, Juri, García-Cabezas, Adánez, Sánchez-González, Cavada and Obeso. This is an open-access article subject to a non-exclusive license between the authors and Frontiers Media SA, which permits use, distribution and reproduction in other forums, provided the original authors and source are credited and other Frontiers conditions are complied with.



Loss of specificity in basal ganglia related movement disorders

Maya Bronfeld¹ and Izhar Bar-Gad^{1,2*}

¹ The Leslie and Susan Gonda (Goldschmied) Multidisciplinary Brain Research Center, Bar-Ilan University, Ramat-Gan, Israel

² The Mina and Everard Goodman Faculty of Life Sciences, Bar-Ilan University, Ramat-Gan, Israel

Edited by:

Charles J. Wilson, University of Texas at San Antonio, USA

Reviewed by:

Peter Redgrave, University of Sheffield, UK

Thomas Wichmann, Emory University, USA

*Correspondence:

Izhar Bar-Gad, Gonda Brain Research Center, Bar-Ilan University, Ramat-Gan 52900, Israel.

e-mail: izhar.bar-gad@biu.ac.il

The basal ganglia (BG) are a group of interconnected nuclei which play a pivotal part in limbic, associative, and motor functions. This role is mirrored by the wide range of motor and behavioral abnormalities directly resulting from dysfunction of the BG. Studies of normal behavior have found that BG neurons tend to phasically modulate their activity in relation to different behavioral events. In the normal BG, this modulation is highly specific, with each neuron related only to a small subset of behavioral events depending on specific combinations of movement parameters and context. In many pathological conditions involving BG dysfunction and motor abnormalities, this neuronal specificity is lost. Loss of specificity (LOS) manifests in neuronal activity related to a larger spectrum of events and consequently a large overlap of movement-related activation patterns between different neurons. We review the existing evidence for LOS in BG-related movement disorders, the possible neural mechanisms underlying LOS, its effects on frequently used measures of neuronal activity and its relation to theoretical models of the BG. The prevalence of LOS in many BG-related disorders suggests that neuronal specificity may represent a key feature of normal information processing in the BG system. Thus, the concept of neuronal specificity may underlie a unifying conceptual framework for the BG role in normal and abnormal motor control.

Keywords: basal ganglia, information encoding, movement, Parkinson's disease, dystonia, dyskinesia, Tourette syndrome

THE BASAL GANGLIA

The basal ganglia (BG) are a group of interconnected nuclei which are reciprocally connected with the cortex and some brainstem nuclei to form partially closed loops (Joel and Weiner, 1994; Haber et al., 2000), and thus have an important role in normal motor, associative, and limbic function (Alexander et al., 1986; Alexander and Crutcher, 1990a). Information is sent from multiple parts of the cortex and thalamus to the BG input structures: the striatum and the subthalamic nucleus (STN). This input is integrated and processed via multiple pathways within the BG until reaching the output structures: the globus pallidus internus (GPI) and the substantia nigra pars reticulata (SNr; Albin et al., 1989; DeLong, 1990). The output of the BG is conveyed to the thalamus and to multiple brainstem structures. The loops through the BG are closed by projections from the thalamic nuclei receiving BG innervation to frontal cortical areas and by projections from the brainstem nuclei to thalamic nuclei projecting back to BG input structures (Carpenter et al., 1976; Kim et al., 1976; Nambu et al., 1988; McHaffie et al., 2005). Anatomical studies have found that the information going through the BG is segregated into partially overlapping motor, associative, and limbic loops, defined by the cortical area from which the BG input arises and the type of information it processes (Alexander et al., 1986; Haber et al., 2000). The motor BG domain is the most studied to date and will be the main focus of this review.

The role of the BG in behavioral modulation has historically been inferred using two complementary methods: the activity of BG neurons during normal behavior (Mink, 1996), and behavioral abnormalities associated with BG dysfunction (Crossman, 1987).

NORMAL BASAL GANGLIA MOVEMENT-RELATED ACTIVITY

Early animal studies found that neurons in the BG phasically change their activity in close temporal relation to different movements, primarily of the contralateral limbs (DeLong, 1971, 1972, 1973). Detailed examinations revealed that the activity of BG neurons was related to different parameters of movements such as direction, velocity, amplitude, muscular load, and force (Georgopoulos et al., 1983; Crutcher and DeLong, 1984; Brotchie et al., 1991a; Mink and Thach, 1991a; Turner and Anderson, 1997). Later studies found that some BG neurons also encode non-motor aspects of the behavior, such as external and internal cues and triggers, type of reinforcement and movement context (Alexander and Crutcher, 1990b; Brotchie et al., 1991b; Mushiake and Strick, 1995; Turner and Anderson, 2005). Notably, the activity of many BG neurons was found to be related not to a single movement parameter, but rather to combinations of motor and contextual features (Mink and Thach, 1991b; Arkadir et al., 2004). Overall, BG neuronal encoding of most of these behavioral parameters is not spatially organized, i.e., neurons encoding the same parameter do not tend to cluster together, and similarly, closely located neurons often encode different behavioral parameters (DeLong et al., 1985; Mink and Thach, 1991a). The only exception to this rule is the somatotopic organization that can be found in the BG. Neurons related to movements of the leg, arm, or face tend to be clustered together in their respective somatotopic territories (Alexander and DeLong, 1985; DeLong et al., 1985; Wichmann et al., 1994). This highly specific and mostly spatially diffuse nature of BG movement-related neuronal activity is likely the cause for

the relatively small number of movement-related neurons found in intact animals (DeLong, 1971). Indeed, the relative fraction of task-related neurons and the observed patterns of neuronal selectivity are highly dependent on the exact motor and associative parameters of the experimental motor tasks (DeLong, 1973; Mink and Thach, 1987).

Highly specific movement-related activity modulations have been found in all processing levels of the BG, but their expression differs depending on the basic firing characteristics of the neurons in each structure. The projection neurons of the striatum (BG input stage) are quiescent most of the time, and fire a short burst of activity in response to preferred events (DeLong, 1973; Liles, 1985). In contrast, neurons in the globus pallidus externus (GPe, BG internal stage) and internus (BG output stage) are tonically active with a high-frequency baseline firing rate, and their movement-related activity is either a decrease or an increase in firing rate, with increases more common in intact animals (DeLong, 1971; Turner and Anderson, 1997).

BASAL GANGLIA DYSFUNCTION

The importance of the BG system is evidenced by the severe behavioral abnormalities associated with both experimentally induced and naturally occurring BG dysfunction. Selective anatomical and functional abnormalities in the cortico-BG system have been observed in patients suffering from disorders such as Parkinson's disease (Agid, 1991), Huntington's chorea (Glass et al., 2000; Deng et al., 2004), dystonia (Marsden et al., 1985), and motor tics (Singer and Minzer, 2003), which were therefore considered "BG-related movement disorders." Animal models and anecdotal findings in human patients confirmed that localized dysfunctions (inactivation or disinhibition) of different parts of the BG could directly induce behavioral abnormalities similar to the symptoms observed in these disorders (Martin and Alcock, 1934; Crossman et al., 1988; Hamada

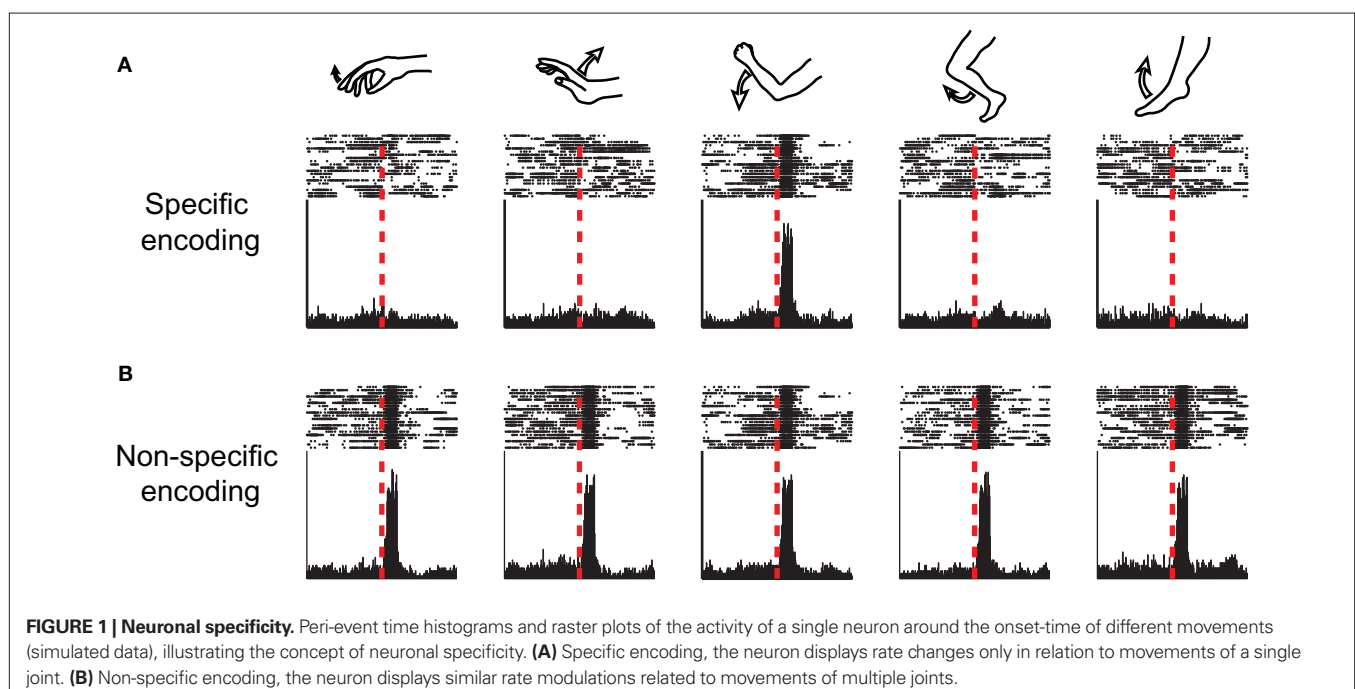
and DeLong, 1992; Grabli et al., 2004; Desmurget and Turner, 2008; McCairn et al., 2009; Bronfeld et al., 2010). The exact nature of the abnormal symptoms has been related to the type and location of the BG dysfunction.

NEURONAL LOSS OF SPECIFICITY

Different BG-related disorders are associated with a wide variety of clinical manifestations and physiological abnormalities. Despite these differences, one physiological phenomenon is common to many BG-related disorders: neuronal loss of specificity (LOS). In many of these pathological conditions, individual BG neurons lose their characteristic selective movement-related activity profiles and instead display similar activity modulations related to a broader range of behavioral events (**Figure 1**). In this section we review evidence for BG LOS in human patients and in animal models of the major BG-related diseases.

PARKINSON'S DISEASE

Parkinson disease (PD) is the most extensively studied BG-related disorder, and has inspired many of the current models of the BG. PD is a neurodegenerative movement disorder characterized by hypokinesia (immobility, slowed and small movements), muscle rigidity and tremor (Parkinson, 1817; Agid, 1991). Loss of dopaminergic innervation to the BG was identified as the basic pathology underlying many of the motor symptoms of PD (Hornykiewicz, 1966), which can be replicated in the non-human primate model of PD. Administration of 1-methyl-4-phenyl-1,2,3,6-tetrahydropyridine (MPTP) to monkeys leads to selective death of dopaminergic neurons and mimics many clinical symptoms of the disorder (Burns et al., 1983). This model has enabled extensive study of the neurophysiological changes associated with PD (Jenner, 2003). Recording of neuronal activity from the BG of human PD patients has recently become possible due to the use of



stereotactic neurosurgical intervention procedures targeting the GPi or the STN to ameliorate PD symptoms (Anderson et al., 2005; Rodriguez-Oroz et al., 2005). While this type of research is limited by the lack of control data from healthy subjects, it is often compared to observations made in non-human primates. Studies of BG movement-related activity have revealed both direct and indirect evidence of neuronal LOS in PD. The relative number of pallidal neurons displaying movement-related activity is substantially larger in MPTP-treated monkeys and in human PD patients compared with normal monkeys (Filion et al., 1988; Williams et al., 2005; Baker et al., 2010; Erez et al., 2011). Studies also found that in these parkinsonian states a large fraction of neurons display activity modulations related to movements of more than a single body part (**Figure 1**), including activity modulations related to movements of both the arm and the leg, movements of multiple joints and movements of the ipsilateral limbs (Filion et al., 1988; Taha et al., 1996; Boraud et al., 2000; Levy et al., 2001; Baker et al., 2010). However, some level of somatotopic organization is still preserved in the parkinsonian state, despite the formation of a larger somatotopic overlap (Rodriguez-Oroz et al., 2001; Theodosopoulos et al., 2003; Baker et al., 2010). PD-related LOS was also observed in the activity of thalamic neurons receiving BG output (Pessiglione et al., 2005).

DYSTONIA

Dystonia is a movement disorder characterized by intermittent and sustained muscle contractions, often involving co-contraction of agonist and antagonist muscles, which leads to involuntary abnormal movements and postures (Fahn and Eldridge, 1976). Dystonia may appear in a variety of pathological conditions, but is most often associated with a lesion or dysfunction of the cortico-BG system (Marsden et al., 1985; Guehl et al., 2009). Evidence for LOS in some types of focal dystonia were found in human patients using non-invasive techniques: transcranial magnetic stimulation (TMS) and functional magnetic resonance imaging (fMRI). These studies found abnormal alterations in the somatotopic organization of the cortico-striatal circuits, mainly in the form of increased overlap between areas, suggesting reduced specificity of the neural representation (Tamburin et al., 2002; Delmaire et al., 2005; Quartarone et al., 2008).

Recordings of neurophysiological activity in non-human primate models of more severe or generalized types of dystonia found that dystonia was associated with a systematic increase in the sensorimotor responsiveness of BG neurons with increased multi-joint, multi-limb, and multi-directional movement-related activity (Guehl et al., 2009). Similar activity patterns were observed in recordings of neuronal activity in the GPi of dystonia patients (Lenz et al., 1998; Vitek et al., 1999; Chang et al., 2007), obtained during neurosurgical interventions for the treatment of severe dystonia (Coubes et al., 2000). Studies also found that the gross somatotopic organization, such as the separation between “arm” and “leg” areas, was maintained in the pallidum of dystonia patients (Chang et al., 2007), but the more subtle somatotopic organization that can be detected in sensorimotor cortical and thalamic areas, such as the spatially separated representations of different digits, was disturbed (Bara-Jimenez et al., 1998; Lenz et al., 1999).

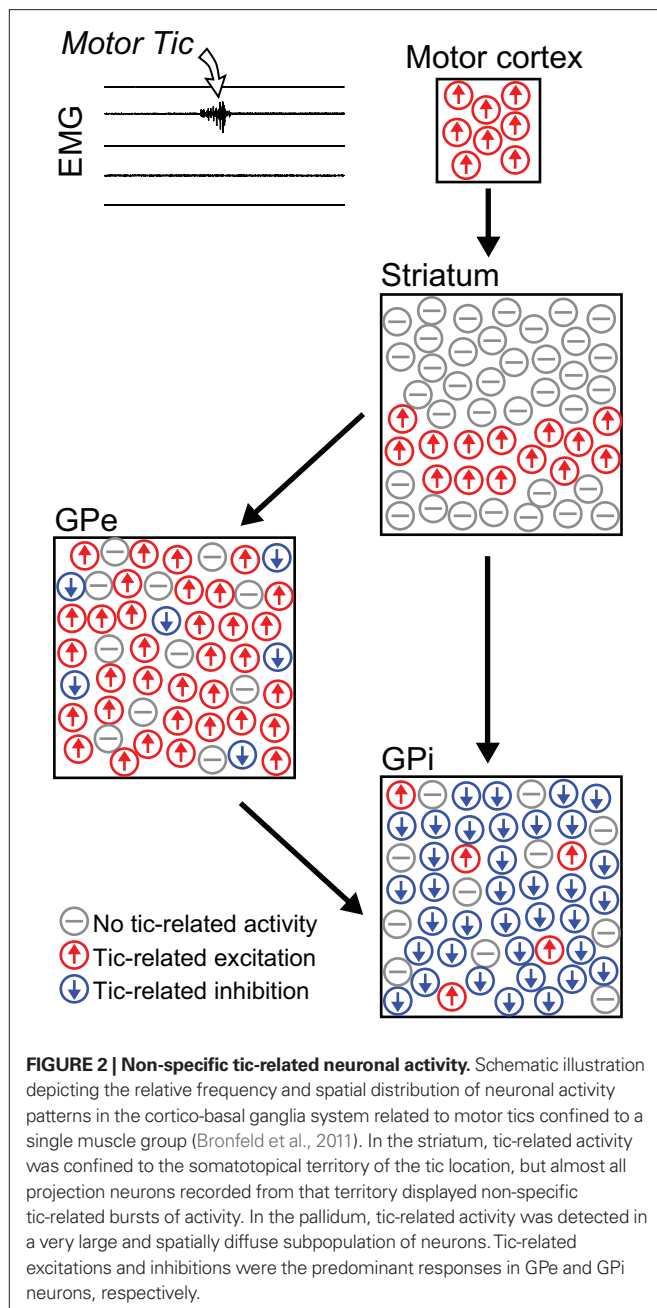
Notably, some degree of dystonia often appears as a comorbid symptom both in human PD patients and in MPTP-treated primates (Tabbal et al., 2006; Del and Albanese, 2008; Wickremaratchi et al., 2009). The relative contribution of each comorbid disorder to the observed LOS in such cases is currently unknown.

TICS

Motor tics are repetitive involuntary brief muscle contractions that can appear either as the primary or a secondary symptom in several human movement disorders, most notably Tourette syndrome (TS; Kurlan, 2004). Tics are primarily associated with dysfunction of the BG input structure – the striatum (Singer and Minzer, 2003). Our studies (McCairn et al., 2009; Bronfeld et al., 2011) of BG neuronal activity in a non-human primate model of motor tics suggested that tics were also associated with BG LOS (**Figure 2**). In the striatum, tic-related activity was somatotopically organized, but almost all neurons recorded from the tic-related somatotopic territory displayed non-specific tic-related activity (Bronfeld et al., 2011). In the GPe and GPi, a larger than normal fraction of recorded neurons (over 70%) demonstrated strong activity modulations related to tic-movements, even though tics were confined to one or a few muscles (McCairn et al., 2009). Similar findings were observed in the GPi of TS patients undergoing neurosurgery (Zhuang et al., 2009). Tic-related neurons were diffusely distributed within GPe and GPi, with no spatial organization of neurons expressing similar types of tic-related activity (**Figure 2**), suggesting a loss of the somatotopic organization in these structures (McCairn et al., 2009; Zhuang et al., 2009).

CHOREA

Chorea is a hyperkinetic symptom characterized by involuntary and irregular continuous movements (Wild and Tabrizi, 2007), which appears in several BG-related disorders (Crossman, 1987) such as Huntington's disease (HD; Marshall, 2004), L-dopa-induced dyskinesia in PD patients (Bezard et al., 2001), and hemiballism (Martin and Alcock, 1934). The heterogeneity of the background conditions associated with chorea makes it difficult to characterize the abnormal neuronal activity specifically related to chorea, rather than to the accompanying motor dysfunctions. One study of pallidal movement-related activity in HD patients reported that the proportion of movement-related GPi cells was similar in their samples of HD and PD patients, but lower than reported for parkinsonian primates, and multi-joint responses were not found in HD (Starr et al., 2008). Unfortunately, the results of this study are severely confounded by the small sample size (only one HD patient). Two other studies of choreic movements induced in non-human primates by either systemic administration of a dopaminergic agonist (Nevet et al., 2004) or local GPe microinjections of a GABA-A antagonist (Bronfeld et al., 2010) reported no increase of correlated pallidal activity which might have suggested movement-related LOS. However, our work on experimentally induced chorea in non-human primates suggests that during a choreic state some pallidal neurons may demonstrate phasic activity modulations related to a wider than expected range of behavioral events associated with a sensorimotor task, but these data remain anecdotal (Bronfeld et al., 2010). Thus, additional studies both in human patients and in animal models are required to establish the degree of LOS in chorea.



BEHAVIORAL DISORDERS

While most studies of BG function and dysfunction have focused on their role in motor control, there is increasing interest in the involvement of the BG in associative and limbic functions, particularly in the context of BG-related behavioral disorders. Dysfunction of the cortico-BG system have been consistently found in disorders of behavioral regulation such as obsessive-compulsive disorder (OCD) and attention-deficit-hyperactivity disorder (ADHD; Swanson et al., 1998; Graybiel and Rauch, 2000; Whiteside et al., 2004; di Michele et al., 2005). Moreover, these disorders show high comorbidity rates with other BG-related movement disorders (Swanson et al., 1998; Murphy et al., 2000; Anderson et al., 2001; Peterson et al., 2001). Animal studies have found that the same local

BG pharmacological manipulation that induces abnormal movements can induce complex abnormal behaviors such as stereotypy and hyperactivity/attention-deficit reminiscent of OCD and ADHD respectively, depending on the site and type of innervation within the BG (Yoshida et al., 1991; Grabli et al., 2004; Worbe et al., 2008). Taken together, this suggests that a similar BG neurophysiological dysfunction may underlie both motor and behavioral disorders, with the different manifestations determined by the identity of the affected functional territory and extent of the pathology (Joel, 2001). It is still unknown whether LOS is a feature of BG-related behavioral disorders, but there is a strong possibility given the similar neuronal substrates of the motor, limbic, and associative BG circuits.

MECHANISMS UNDERLYING NEURONAL SPECIFICITY

Patterns of event-related neuronal activity are determined by spatial and temporal integrations of inputs to the neuron. Neurons of the BG integrate both “external” inputs from the thalamus and cortex as well as “internal” inputs from other neurons within the BG. Thus, LOS at the output stage of the BG may be attributed either to LOS of the inputs to the system (cortical or thalamic LOS), or to alterations in the internal processing of the information within the BG system. As described in Section “Neuronal Loss of Specificity,” LOS of BG neurons can be observed following local inactivation or disinhibition restricted to the BG, without a direct disturbance of the inputs to the system. This suggests that LOS may, in some cases, be primarily driven by dysfunctions of intrinsic BG information processing. In this section we present possible mechanisms of LOS generated or maintained internally by the BG system. Internal processing within the BG system leading to neuronal specificity may be performed either by “intra-nucleus” computation using inhibitory collaterals or interneurons (**Figure 3A**) or by “inter-nuclei” computation utilizing the integration of projections from multiple upstream nuclei (**Figure 3B**).

SPECIFICITY RELATED TO INTRA-NUCLEUS PROCESSING

Specificity generated by computation within a nucleus may be mediated by local inhibitory axon collaterals and/or by inhibitory or modulatory interneurons. The most elaborate local network with such properties can be found in the striatum. The striatum contains a single type of GABAergic projection neurons (medium spiny neurons, MSNs) whose activity is modulated by multiple types of GABAergic, cholinergic, and dopaminergic interneurons, as well as by collateral connections from other MSNs (Calabresi et al., 2000; Tepper et al., 2004; Ibanez-Sandoval et al., 2010). The converging effect of these connections modulates the activity of striatal neurons receiving common excitatory cortical/thalamic inputs (**Figure 3A**; Wilson, 2007). This modulation may thus generate a selective movement-related activity profile, as neighboring neurons tend to inhibit other MSNs either directly through their collaterals or indirectly via the GABAergic interneurons (Tepper et al., 2004; Wilson, 2007). Disruption of the activity of this intrinsic striatal network could alter the pattern of inhibitory inputs to the neurons and lead to neuronal LOS. Support for this hypothesis can be found in our recent study which showed that local application of the GABA-A antagonist bicuculline in the striatum, which

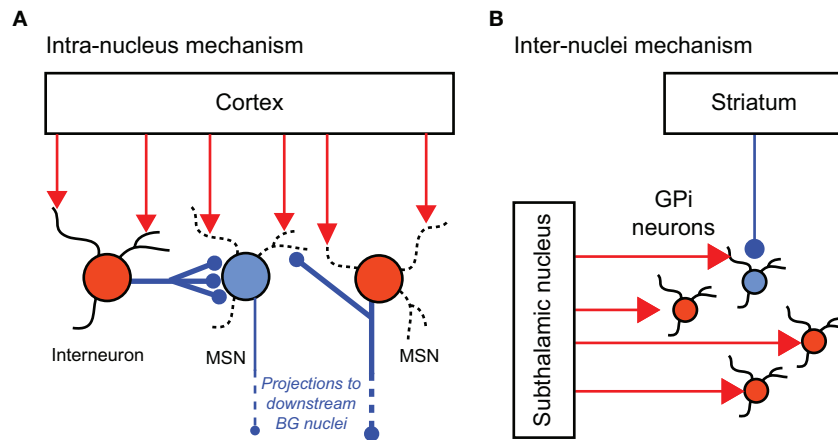


FIGURE 3 | Neural mechanisms underlying neuronal specificity.

Schematic illustrations of intra-nucleus (A) and inter-nuclei (B) mechanisms underlying neuronal specificity. Red and blue filled circles represent excited and inhibited neurons, respectively. (A) In the striatum, inhibitory projections from GABAergic interneurons and collaterals from neighboring projection neurons (MSNs) enable selective activation of some MSNs while

inhibiting others, in response to common excitatory cortical inputs (Based on: Tepper et al., 2004). (B) In the GPi, the combined effects of spatially focused inhibitory projections from the striatum, and spatially diffused excitatory projections from the subthalamic nucleus enable selective movement-related excitation/inhibition activity patterns (Based on: Mink, 1996).

affects only the intrinsic inhibitory network without affecting the excitatory striatal afferents, induces LOS in the striatum and in its downstream targets (Bronfeld et al., 2011).

The significance of lateral processing is reduced in downstream nuclei of the BG system. The GPe does not contain interneurons, but its projection neurons send local axon collaterals (Kita and Kitai, 1994; Sadek et al., 2007). While this suggests that some level of internal processing may be performed within the GPe, the functional significance of these lateral connections has never been examined. The GPi does not contain interneurons either, and moreover, its projection neurons have no significant local axon collaterals (Parent et al., 2001). The STN, which is excitatory in nature, is unsuited for performing internal processing to increase the specificity of its neurons. Thus, the movement-related activity profiles of the pallidal and subthalamic neurons are most likely governed by the input patterns they receive.

SPECIFICITY RELATED TO INTER-NUCLEI PROCESSING

The GPi integrates excitatory and inhibitory information from multiple BG nuclei, conveyed via several pathways (Albin et al., 1989; DeLong, 1990; Nambu et al., 2002). Inhibitory information from the “direct” pathway is sent from the striatum. The “indirect” and “hyper-direct” pathways involve inhibitory projections from the GPe and excitatory projections from the STN, respectively (Figure 3B). BG output is further modulated by reciprocal connections between the GPe and GPi (Hazrati et al., 1990) and between STN and GPe (Shink et al., 1996), and by dopaminergic innervation (Rommelfanger and Wichmann, 2010). Several models of the BG suggest that the combined effects of inputs from the different pathways can generate “center-surround” patterns of activity (Figure 3B) that lead to neuronal selectivity (Mink, 1996; Nambu et al., 2002; see also “Action Selection” section). Disruption of the normal balance between the different pathways was suggested to underlie many BG-related movement disorders (Crossman et al.,

1988; Albin et al., 1989; DeLong, 1990; Deng et al., 2004; Maia and Frank, 2011) and some evidence suggests it may also be involved in neuronal LOS observed in these disorders.

In the striatum, neurons belonging to the direct or indirect pathways express different subtypes of dopamine receptors (D1 or D2, respectively) that are modulated in opposing manners by dopamine (neuronal excitation or inhibition, respectively; Gerfen et al., 1990). Selective activation of D1 or D2 receptors in the striatum differentially influence the movement-related activity of striatal neurons during performance of a sensorimotor task (Inase et al., 1997), suggesting that this mechanism could contribute to striatal neuronal specificity. We have shown that during the expression of motor tics, LOS was accompanied by an altered increase/decrease ratio of GPi movement-related activity compared to this ratio in intact animals, with phasic rate decreases becoming more frequent (McCairn et al., 2009). This shifted excitation–inhibitions balance suggests that LOS in this case may be associated with an imbalance of the different input pathways to the GPi.

EFFECTS OF LOSS OF SPECIFICITY ON PROPERTIES OF NEURONAL ACTIVITY

Loss of specificity is defined as an increase in the type and number of behavioral events eliciting similar activity modulations in a neuron, leading to a reduction in the selectivity of the encoding of events. In the extreme case, a complete loss of selectivity results in an equivalent representation of all events. Neuronal LOS may have a major effect on other properties of neurophysiological activity, especially at the population level. In this section we discuss some commonly studied neuronal characteristics and their relation to LOS.

NUMBER OF MOVEMENT-RELATED NEURONS

A widely accepted indicator of LOS is an increase in the fraction of movement-related neurons out of the whole neuronal population. This is based on the premise that in the normal state many neurons

which appear to be unrelated to behavior are in fact movement-related, but have a highly selective activity profile, and are therefore unrelated to the specific combination of kinematic and contextual properties of the applied behavioral paradigm (**Figure 4A**, left). LOS will increase the number of events that each neuron encodes (**Figure 4A**, right), encompassing a wider range of motor parameters and behavioral paradigms. Under these circumstances neurons that were previously deemed “unrelated” might now demonstrate movement-related activity. This inevitably leads to an increase in the overall number of neurons whose activity is related to any behavioral task (**Figure 4B**). This measure of LOS has been widely reported in studies of BG-related disorders (see “Neuronal Loss of Specificity” section and Filion et al., 1988; Lenz et al., 1998; Williams et al., 2005; Baker et al., 2010; Erez et al., 2011), but several confounding factors must be taken into account when evaluating its reliability as an indicator of neuronal LOS.

One limitation is that studies of movement encoding in the BG of human patients suffering from different BG-related disorders can only compare their results to findings obtained from non-human primates. This is due to the fact that recordings from healthy normal people are not available using current technologies. However,

the validity of such direct inter-species comparisons is uncertain. In addition, studies of human patients often utilize a variety of methods of motor examination, which may differ from methods used in potentially comparable human and animal studies (Sterio et al., 1994; Taha et al., 1996; Hutchison et al., 2003; Starr et al., 2005; Chang et al., 2007). This may cause a problem as the fraction of movement-related neurons has been shown to be highly dependent on the exact features of the performed motor task (DeLong, 1973; Mink and Thach, 1987), and might even be affected by its cognitive demands and by the subject’s emotional state (Alexander and Crutcher, 1990b; Brotchie et al., 1991b; Arkadir et al., 2004). This implies that differences in task and setup should be taken into account when evaluating the fraction of movement-related neurons observed in different studies, and optimally only data obtained from experiments in which a similar motor task was used should be compared.

Another limitation arises from the fact that the relative number of movement-related neurons varies significantly between different functional territories within the same nucleus. For example, the prevalence of movement-related neurons may seem larger when recording at the motor compared to the associative functional territories (DeLong, 1971; Alexander and DeLong, 1985; Wichmann

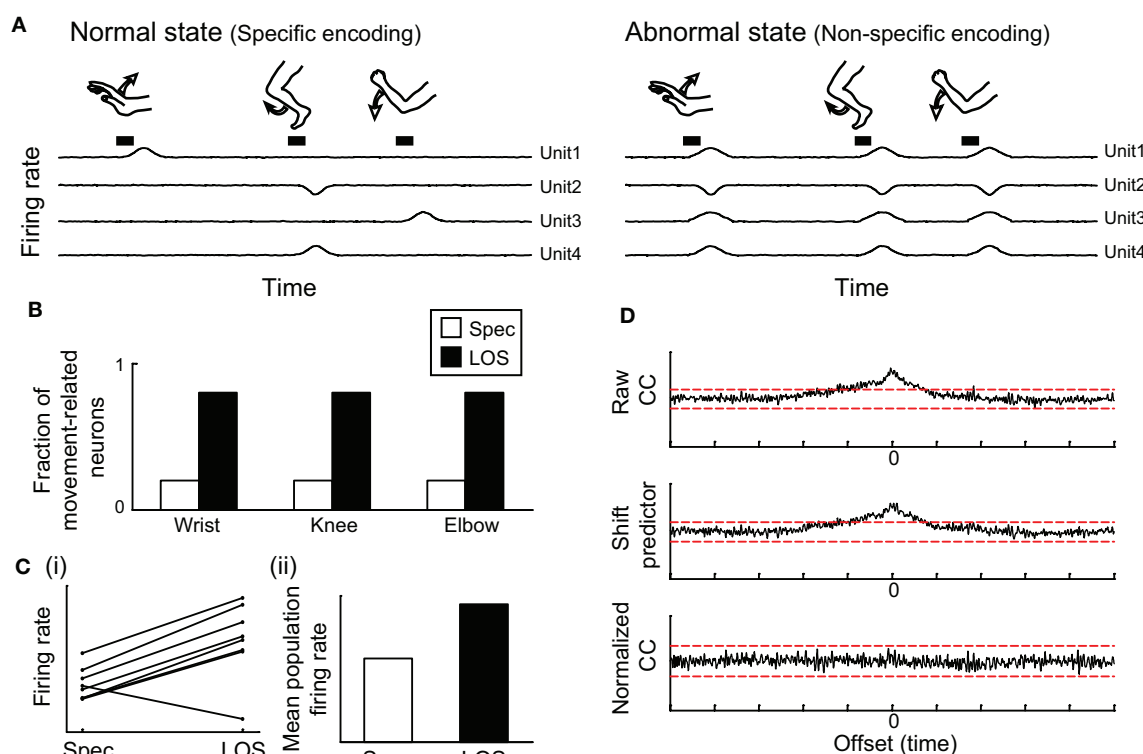


FIGURE 4 | Effect of loss of specificity on properties of neuronal activity.

(A) Illustration of firing rate fluctuations of multiple neurons, depicting rate modulations related to different movements, in a neuronal population for which rate increases are the predominant pattern of movement-related activity. *Left:* Specific encoding, each neuron modulates its firing rate in response to a single type of movement. *Right:* Loss of specificity (LOS); each neuron displays similar movement-related rate modulations in response to a larger range of movements. **(B)** Following LOS, the fraction of movement-related neurons is increased. **(C)** The number of movements eliciting rate modulations in each

neuron increases, resulting in an increased effect of movements on the overall average firing rate of each neuron (i). For a population in which most neurons have a dominant non-specific response pattern (such as firing rate increase), LOS has an effect on the overall average firing rate of the population (ii). **(D)** Non-specific encoding of movements generates correlations between pairs of neurons (top panel). These correlations represent only the common rate modulations attributed to the commonly encoded movements, and following subtraction of these effects (middle panel, the shift predictor), the normalized correlation function shows no correlation between the neurons (bottom panel).

et al., 1994; Jaeger et al., 1995). As many studies of human patients often specifically target the motor territory of the BG they may be inherently biased toward a higher prevalence of movement-related neurons. Furthermore, considering that in the STN and GP the distance between one territory or another may be only 1–2 mm with no clear physiological borders between territories (DeLong, 1971; Wichmann et al., 1994), the sampling distribution of two neuronal populations might easily be inadvertently skewed toward one of the functional domains and thus influence the fraction of movement-related neurons. Even within the motor territory, the somatotopic organization of the BG means that the number of recorded neurons might be affected by the interaction between recording location and the body part involved in the motor task.

These confounding features might partially account for the substantial differences in the fraction of movement-related neurons reported in different studies, especially experiments comparing results from human patients and non-human primates (Filion et al., 1988; Taha et al., 1996; Williams et al., 2005; Leblois et al., 2006; Chang et al., 2007; Guehl et al., 2009). Despite the aforementioned limitations, the fraction of movement-related neurons should not be excluded as a measure of LOS. When comparing normal and abnormal states of subjects performing the same motor task and controlling for the location of recorded neurons, it may serve as a robust measure of LOS.

RATE CHANGES

In some circumstances, LOS may lead to an apparent global change in the overall activation level of the neurons. Consider for example a neuronal population in which each neuron responds selectively to different behavioral events, but event-related neuronal rate modulations are always or predominantly of the same type (either firing rate increases or decreases). In the normal state, neuronal specificity will lead to rate modulations in only a small fraction of the neurons at any given time, resulting in a minor effect on the overall firing rate of the population. However, LOS will lead to more neurons displaying activity modulations related to any behavioral event, and their combined effect may result in an apparent change in the mean firing rate of the population, whose direction (increase or decrease of the rate) depends on the predominant modulation of the neurons (**Figure 4C**). This description could be applicable to both the striatum, in which all projection neurons increase their firing rate in relation to preferred events (DeLong, 1973), and to the globus pallidus, in which firing rate increases are predominant in the normal state (Mitchell et al., 1987; Mink and Thach, 1991b; Turner and Anderson, 1997) and decreases in some abnormal states (McCairn et al., 2009).

However, global firing rate changes are certainly not always related to LOS. First, LOS might only account for firing rate changes observed in behaving subjects, and not in subjects during periods of passive immobility. Second, global rate changes are often attributed to tonic changes in activation, rather than phasic event-related changes. Examination of firing patterns and rate modulations over time could help differentiate between global and event-related rate modulations. Thus, the possibility of neuronal LOS should be addressed in cases of observed population rate changes in moving/behaving subjects.

CORRELATED ACTIVITY

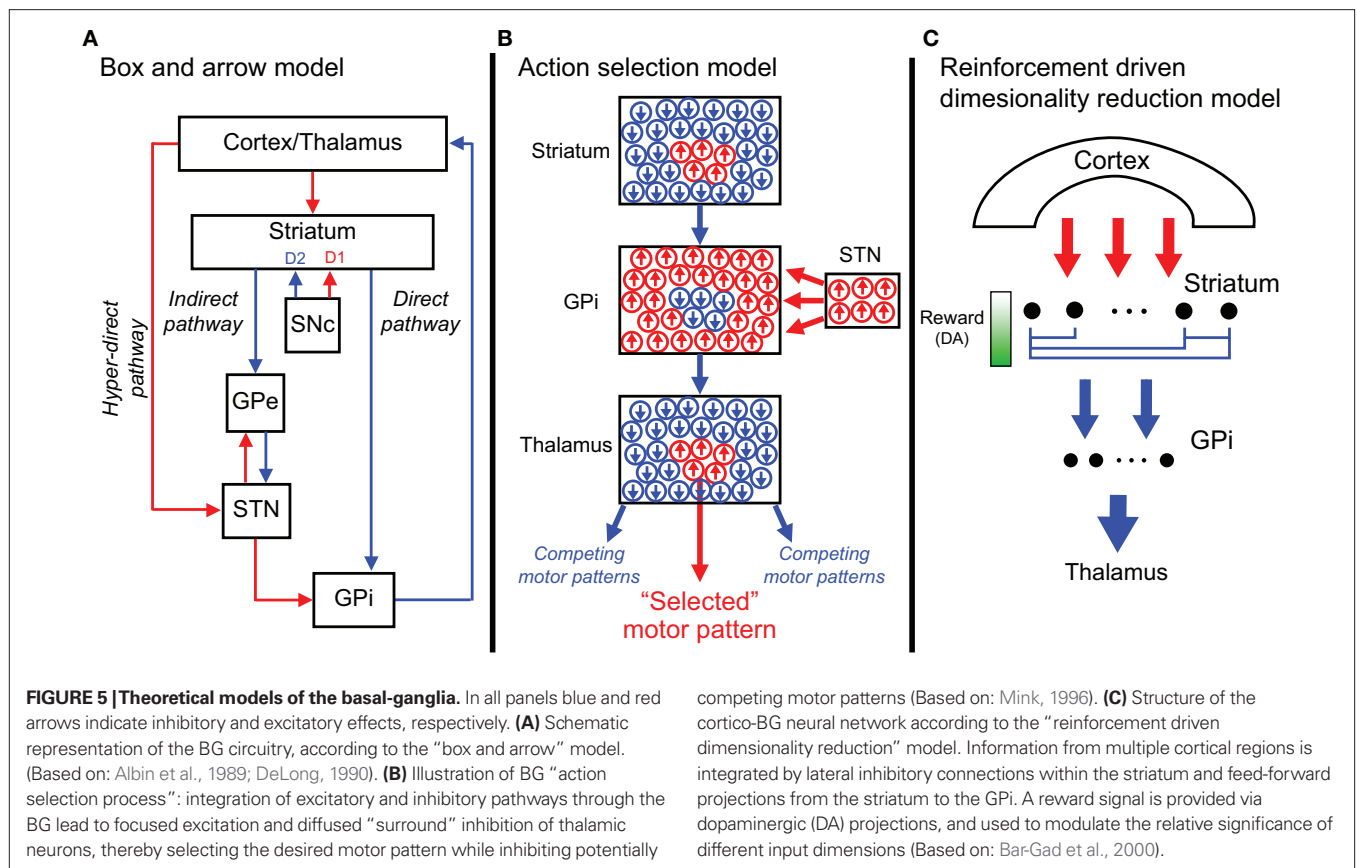
Another potential epiphenomenon of neuronal LOS is an increase in the level of temporally correlated activity across a neuronal population. The most widely used measure of correlated activity is the cross-correlation function, which describes the temporal correlation between spiking activities of pairs of neurons (Perkel et al., 1967). Whenever two neurons encode the same behavioral event, they will both phasically change their activity around occurrences of that event, resulting in periods of temporally related rate modulations. For a population of neurons with highly selective movement-related activity profiles, commonly encoded events will be rare and thus the firing rate of each neuron will fluctuate in a temporally independent way (**Figure 4A**). As neurons become less specific, they are more likely to encode the same events, and thus display more periods of common rate modulations. In this case, a change in the spiking probability of one neuron, resulting from the commonly encoded behavioral event, will be accompanied by a change in spiking probability of other neurons encoding the same event. As a result, the cross-correlation function of the neurons will be more likely to demonstrate a significant correlation between them (**Figure 4D**; Nevet et al., 2007). This is regarded as an “artificial” correlation, as it may occur despite the lack of a direct neural pathway connecting the neurons (Stevens and Gerstein, 1976).

An increase in the level of correlated activity in the BG was reported in BG-related movement disorders (Raz et al., 2000). The LOS that is also observed in these disorders stresses the importance of controlling for commonly encoded events when evaluating the true level of correlations in the system. Several statistical methods have been developed for removing the effects of commonly encoded events from cross-correlation functions, such as the shift predictor (**Figure 4D**; Moore et al., 1966; Stevens and Gerstein, 1976), joint peri-event time histograms (Gochin et al., 1990), and signal and noise correlations (Gawne and Richmond, 1993).

However, while LOS might affect the level of correlation, there are several parameters mediating its effect. A recent study emphasized that the likelihood of correlation modulation by commonly encoded events depends on the number of events and the magnitude of the event-related rate modulations (Nevet et al., 2007). This implies that a lack of correlation cannot be used to exclude the possibility of LOS in the system. Additionally, there are other factors which may contribute to an increased level of correlation unrelated to LOS, such as global brain activation states or population wide oscillatory activity patterns (Nini et al., 1995; Urbain et al., 2000).

THEORETICAL MODELS OF BG FUNCTION AND DYSFUNCTION

Theoretical models have tried to conceptualize the accumulating data of the BG system into a unified model explaining its role in normal behavior and in different pathological states (**Figure 5**). The early “box and arrow” model relied primarily on the anatomical connectivity of the BG, and described different normal and pathological states as deriving from global changes in the overall firing rate in different nuclei within the pathway. Later models addressed more detailed spatial and temporal patterns of the BG output, and how changes in these patterns may lead to abnormal states. This section reviews these models and the extent to which they address the phenomena of LOS in different BG-related disorders.



THE BOX AND ARROW MODEL

The “box and arrow” model described the BG as part of a feedback loop influencing the level of cortical excitability (Albin et al., 1989; DeLong, 1990). Each BG nucleus was described as a single unit (“box”) whose activity exerts either excitation or inhibition (positive or negative “arrows”) on its downstream targets (Figure 5A). An increase or a decrease in the level of activity of the BG output structure (the GPi for most movement-related information) was considered to inhibit or facilitate (disinhibit) cortical activity, respectively, via the thalamus.

Neuronal specificity is not accounted for at all by this model, as it treats each nucleus as a single entity, while disregarding the complex and unique movement-related firing patterns of different neurons within the same nucleus. Thus, the model assumes that specificity is not a significant feature of either the normal or pathological states, since multiple neurons are expected to be activated simultaneously and in a similar manner as an underlying definition of the model. Accordingly, LOS cannot be explained in the context of the box and arrow model.

ACTION SELECTION

A model that tried to account for the dynamic intra-nucleus and inter-nuclei effects of BG neuronal activity, and offer a network-level model of the BG was the “action selection” model. This model depicted the BG as instructing the cortex on which action should be selected for performance out of a multitude of potential actions (Mink, 1996). According to this model, each possible motor pattern (action) is represented by a small group of neurons in the BG

output structure. Selective inhibition of one such group of neurons, while facilitating the activity of all the others, leads to facilitation of the cortical neurons encoding the selected action while inhibiting other competing actions (Figure 5B; Chevalier and Deniau, 1990).

The selection process was proposed to be mediated by intra-nucleus connections, inter-nuclei connections, or a combination of both (see also “Mechanisms Underlying Neuronal Specificity”). Intra-nucleus models derived originally from the lateral inhibitory connections between projection neurons in the striatum, which suggested that activation of one neuron can lead to inhibition of others (Wickens, 1993). It was later suggested that the same outcome could also be achieved by the local striatal network of inhibitory GABAergic interneurons (Koos and Tepper, 1999). According to inter-nuclei models, the selection process utilizes the excitatory and inhibitory projections reaching the GPi via different BG pathways (Mink, 1996; Nambu et al., 2002). These models rely on the different spatial distribution of afferents originating from the different pathways. Thus, the direct pathway from the striatum generates focused inhibition in a subpopulation of GPi neurons, while projections from the STN and GPe (through the hyper-direct and indirect pathways) exert diffuse GPi excitation. The combined effect of inputs from these pathways generates a focused center of GPi inhibition surrounded by diffused excitation, forming the “Mexican hat” activation pattern (Figure 5B).

Neuronal specificity in the normal BG and the observed pallidal movement-related activity may be explained in terms of the action selection model. The underlying assumption of the model,

that each small neuronal group in the GPi encodes a particular motor pattern, entails selective activity profiles of these neurons. According to the model, the pallidal neurons whose activity is related to a particular motor task are the neurons encoding for the task-specific motor patterns, and any potentially competing patterns. These two neuronal populations should display opposing patterns of movement-related rate modulations, which account for the observed movement-related rate increases and decreases (DeLong, 1971). The smaller subpopulation of neurons displaying movement-related inhibition is composed of neurons whose activity facilitates the selection of the desired appropriate motor pattern. The larger population of neurons excited around movement-time includes neurons whose movement-related activity generates increased inhibition (suppression) of the competing motor patterns (Mink, 1996).

According to the action selection model, LOS may be explained as a failure to select a single motor pattern, and/or by a failure to inhibit competing patterns. However, certain predictions of the action selection model regarding patterns of neuronal specificity in BG-related movement disorders have recently been contested by experimental data. Action selection models suggest that hypokinetic symptoms of PD are related to an inability to remove excessive inhibition from the cortical neurons related to the desired motor pattern (Mink, 1996). However, the GPi neuronal population in PD still displays a mixture of movement-related firing rate increases and decreases, in proportions comparable to the normal state, suggesting that the potential for cortical disinhibition is maintained (Bergman et al., 1994; Taha et al., 1996; Williams et al., 2005). An action selection model of motor tics hypothesized that tics are associated with an abnormal inhibition of a restricted subset of pallidal neurons, whose activity encodes the tic-related motor pattern (Mink, 2001; Albin and Mink, 2006). However, our results from a non-human primate model of motor tics indicated that a vast majority, rather than a restricted subpopulation of GPi neurons were inhibited around tic-times (**Figure 2**; McCairn et al., 2009). According to the action selection hypothesis such an activity pattern should have led to the simultaneous activation of multiple motor patterns. Instead, the only expressed movement was the localized motor tic (McCairn et al., 2009; Bronfeld et al., 2011).

REINFORCEMENT DRIVEN DIMENSIONALITY REDUCTION

The reinforcement driven dimensionality reduction (RDDR) model provides a conceptual representation of the BG and their role in neural information processing within the central nervous system (Bar-Gad et al., 2003). The BG are depicted as receiving high-dimensionality input and generating a compressed lower-dimensionality representation of it, while maintaining maximal information regarding the original input (**Figure 5C**). Thus, the BG serve as an integrator of the vast information available to the organism which is represented by the distributed activity of multiple brain regions. This information is integrated and compressed within the BG and conveyed to other brain structures (such as the frontal cortex, or subcortical structures), which can use it to optimally direct the organism's behavior. The RDDR model differs from the action selection model by the type of information conveyed by the BG and the way it is represented. In the RDDR

model, the decision of which action should be performed is not taken by the BG, but rather at the level of their downstream targets (e.g., the frontal cortex). The activity of each pallidal neuron does not represent one specific motor pattern. Instead, specific combinations of inputs, representing different states or properties of the organism, the behavior and the environment, are represented by the combined activity of pallidal neurons. In the RDDR model, the role of reinforcement is to modulate the relative "importance" of the different input dimensions. Reward-related dimensions receive more detailed representations, while unrewarded dimensions are poorly represented in the output of the BG.

Neuronal specificity is directly derived from maximizing the amount of transferred information in the RDDR model. The activity of each pallidal neuron represents a unique subspace of inputs; for example, inputs relevant to a specific motor task. Several neurons can be related to the same task (encode a similar set of inputs) as long as their activity encodes different features of it. This selective representation increases the efficiency of the network by enabling a small number of neurons to transfer larger (maximal) amounts of information (Bar-Gad et al., 2000). The RDDR model can also account for the importance of LOS as a key feature of BG-related disorders. LOS reduces the information capacity of each neuron, as it uniformly encodes many different input states (Bar-Gad et al., 2000). This degrades the overall amount of information conveyed by the BG, making its output signal unreliable for accurate reconstruction of the original input space. The degraded information conveyed to the cortical neurons may lead to the choice of inappropriate courses of action, which will manifest as abnormal behavioral patterns.

MULTIPLE FUNCTIONS

While different theoretical models disagree on the very basic question of what is the role of the BG signal, the complex and multi-functional nature of the system suggests that it may serve multiple roles. For example, BG event-related activity displays a wide temporal distribution relative to the observed event. In the motor domain, some movement-related activity can be detected well before movement onset while some occurs after movement initiation (Georgopoulos et al., 1983; Hikosaka and Wurtz, 1983; Brothie et al., 1991a; Gardiner and Nelson, 1992; Jaeger et al., 1995; Turner and Anderson, 1997). These temporally distinct signals may contribute to different computational processes performed by the BG system. These may include activation of motor planning or selection mechanisms mediated by early BG signals and sensorimotor feedback or learning mechanisms mediated by the late signals (Turner and Desmurget, 2010). Furthermore, it is possible that signals processed within the limbic, cognitive, or motor loops going through the BG (Alexander et al., 1986; Haber et al., 2000) may serve separate roles when conveyed to their downstream targets. If this is the case than perhaps any one theoretical model captures only one aspect of BG functionality, and multiple models may co-exist as attaining to different computational tasks performed by the BG system (Joel and Weiner, 1994; Maia and Frank, 2011).

One implication of this hypothesis is that different functional pathways may be differentially affected in BG-related disorders. If this is the case we might expect to observe unique patterns of LOS in different pathological conditions. This may be reflected by LOS

occurring in some aspects of a behavior but not in others. For example, we might observe LOS of the motor responses to a behavior but not to the cognitive aspects of it, or vice versa. Such selective dysfunction may also be reflected by changes in the temporal distribution of event-related neuronal activity, which was reported in one study of MPTP-treated monkeys (Leblois et al., 2006).

ROLE OF BASAL-GANGLIA LOSS OF SPECIFICITY

Loss of neuronal specificity is a feature of the abnormal neuronal activity associated with many BG-related movement disorders. Its prevalence suggests that it may be a key factor of the BG pathophysiology leading to abnormal motor or behavioral symptoms. However, since LOS is a common feature of multiple hypokinetic and hyperkinetic disorders, what might account for their unique and diverse clinical manifestations? Based on existing data, we speculate that different symptoms may be related to the location and type of BG dysfunction and to the level of dopaminergic modulation.

Computational models of the cortico-BG system often regard the BG as a multilayer feed-forward neural network, in which each layer contains different patterns of both external and internal connectivity (Bar-Gad et al., 2003; Gurney et al., 2004). Selective changes to any one of these parameters were shown to have different effects on the network output, depending on their type and location (Prescott et al., 2006). While no direct models for LOS were examined, arguably this may apply to network selectivity profiles as well. Thus, while the loss of selectivity may be a common feature, the exact nature or pattern of information that is lost following its processing within a dysfunctional BG system may account for the nature of the observed motor or behavioral abnormalities.

Another parameter that may affect the pattern of BG output is dopamine, which is often regarded as a reinforcement signal indicating the relative saliency or importance of various inputs (Schultz, 2007; Joshua et al., 2009a; Zhang et al., 2009). Anatomical and physiological evidence suggest that the dopaminergic signal in the striatum is largely diffused rather than spatially selective, affecting multiple synaptic connections simultaneously (Schultz, 1998; Moss and Bolam, 2008; Joshua et al., 2009b). Thus, the dopaminergic signal by itself is probably not responsible for the specificity observed in BG neurons. Rather, fluctuations in the levels of dopamine in

the system can induce dynamic changes in network connectivity by weakening or strengthening synaptic connections (Wickens et al., 1996; Kerr and Wickens, 2001). These internal connections within the BG system may in turn be responsible for the observed patterns of neuronal specificity (see section “Mechanisms Underlying Neuronal Specificity”). In the normal state, fluctuations in dopamine levels are expected to be related to events in the organism’s environment and thus lead to adaptive changes in the BG network and in the organism’s behavior. In many BG-related disorders there is a dysregulation of the dopaminergic system (Hassler, 1939; Hesse et al., 2005; Gil and Rego, 2008; Steeves and Fox, 2008; Wichmann, 2008; Wong et al., 2008; Tripp and Wickens, 2009), which may result both in a breakdown of the relation between dopamine levels and the relative saliency or reward value of the inputs to the system, and in maladaptive changes in the BG network connectivity. This could lead to both a loss of specificity of the neuronal encoding and to degradation of the information conveyed by the BG and thus induce the input-inappropriate expression of abnormal movements and behaviors (Bar-Gad et al., 2000; Gurney et al., 2001).

SUMMARY

Neuronal specificity emerges as a key feature of information processing in the normal BG. BG specificity has a multi-dimensional nature, with neurons showing selective activity patterns related to different combinations of motor, associative, and limbic properties of state and behavior. This highlights the special role of the BG in integrating and processing information from multiple modalities to influence behavior. Accordingly, loss of specificity of neuronal encoding is a main feature in BG dysfunction. Evidence for LOS have been observed in many BG-related disorders, both in human patients and in animal models of the disorder. The appearance of LOS following localized BG dysfunction with intact patterns of input to the system, suggests that LOS is primarily a direct result of changes in the internal processing within the BG. This prevalence of LOS implies that neuronal specificity reflects a basic computational role of the BG, and its loss may be the major underlying pathology driving the appearance of abnormal motor symptoms. Future computational and theoretical models of BG function should address its multi-modality neuronal specificity and explore changes in specificity related to different BG dysfunctions.

REFERENCES

- Agid, Y. (1991). Parkinson’s disease: pathophysiology. *Lancet* 337, 1321–1324.
- Albin, R. L., and Mink, J. W. (2006). Recent advances in Tourette syndrome research. *Trends Neurosci.* 29, 175–182.
- Albin, R. L., Young, A. B., and Penney, J. B. (1989). The functional anatomy of basal ganglia disorders. *Trends Neurosci.* 12, 366–375.
- Alexander, G. E., and Crutcher, M. D. (1990a). Functional architecture of basal ganglia circuits: neural substrates of parallel processing. *Trends Neurosci.* 13, 266–271.
- Alexander, G. E., and Crutcher, M. D. (1990b). Neural representations of the target (goal) of visually guided arm movements in three motor areas of the monkey. *J. Neurophysiol.* 64, 164–178.
- Alexander, G. E., and DeLong, M. R. (1985). Microstimulation of the primate neostriatum. II. Somatotopic organization of striatal microexcitable zones and their relation to neuronal response properties. *J. Neurophysiol.* 53, 1417–1430.
- Alexander, G. E., DeLong, M. R., and Strick, P. L. (1986). Parallel organization of functionally segregated circuits linking basal ganglia and cortex. *Annu. Rev. Neurosci.* 9, 357–381.
- Anderson, K. E., Louis, E. D., Stern, Y., and Marder, K. S. (2001). Cognitive correlates of obsessive and compulsive symptoms in Huntington’s disease. *Am. J. Psychiatry* 158, 799–801.
- Anderson, V. C., Burchiel, K. J., Hogarth, P., Favre, J., and Hammerstad, J. P. (2005). Pallidal vs subthalamic nucleus deep brain stimulation in Parkinson disease. *Arch. Neurol.* 62, 554–560.
- Arkadir, D., Morris, G., Vaadia, E., and Bergman, H. (2004). Independent coding of movement direction and reward prediction by single pallidal neurons. *J. Neurosci.* 24, 10047–10056.
- Baker, K. B., Lee, J. Y., Mavinkurve, G., Russo, G., Walter, B., DeLong, M. R., Bakay, R. A., and Vitek, J. L. (2010). Somatotopic organization in the internal segment of the globus pallidus in Parkinson’s disease. *Exp. Neurol.* 222, 219–225.
- Bar-Gad, I., Havazelet-Heimer, G., Goldberg, J. A., Ruppert, E., and Bergman, H. (2000). Reinforcement-driven dimensionality reduction – a model for information processing in the basal ganglia. *J. Basic Clin. Physiol. Pharmacol.* 11, 305–320.
- Bar-Gad, I., Morris, G., and Bergman, H. (2003). Information processing, dimensionality reduction and reinforcement learning in the basal ganglia. *Prog. Neurobiol.* 71, 439–473.
- Bara-Jimenez, W., Catalan, M. J., Hallett, M., and Gerloff, C. (1998). Abnormal somatosensory homunculus in dystonia of the hand. *Ann. Neurol.* 44, 828–831.
- Bergman, H., Wichmann, T., Karmon, B., and DeLong, M. R. (1994). The primate subthalamic nucleus. II. Neuronal activity in the MPTP model

- of parkinsonism. *J. Neurophysiol.* 72, 507–520.
- Bezard, E., Brotchie, J. M., and Gross, C. E. (2001). Pathophysiology of levodopa-induced dyskinesia: potential for new therapies. *Nat. Rev. Neurosci.* 2, 577–588.
- Boraud, T., Bezard, E., Bioulac, B., and Gross, C. E. (2000). Ratio of inhibited-to-activated pallidal neurons decreases dramatically during passive limb movement in the MPTP-treated monkey. *J. Neurophysiol.* 83, 1760–1763.
- Bronfeld, M., Belevovsky, K., and Bar-Gad, I. (2011). Spatial and temporal properties of tic-related neuronal activity in the cortico-basal ganglia loop. *J. Neurosci.* (in press).
- Bronfeld, M., Belevovsky, K., Erez, Y., Bugaysen, J., Korngreen, A., and Bar-Gad, I. (2010). Bicuculline induced chorea manifests in focal rather than globalized abnormalities in the activation of the external and internal globus pallidus. *J. Neurophysiol.* 104, 3261–3275.
- Brotchie, P., Iansek, R., and Horne, M. K. (1991a). Motor function of the monkey globus pallidus. 1. Neuronal discharge and parameters of movement. *Brain* 114(Pt 4), 1667–1683.
- Brotchie, P., Iansek, R., and Horne, M. K. (1991b). Motor function of the monkey globus pallidus. 2. Cognitive aspects of movement and phasic neuronal activity. *Brain* 114(Pt 4), 1685–1702.
- Burns, R. S., Chiu, C. C., Markey, S. P., Ebert, M. H., Jacobowitz, D. M., and Kopin, I. J. (1983). A primate model of parkinsonism: selective destruction of dopaminergic neurons in the pars compacta of the substantia nigra by *N*-methyl-4-phenyl-1,2,3,6-tetrahydropyridine. *Proc. Natl. Acad. Sci. U.S.A.* 80, 4546–4550.
- Calabresi, P., Centonze, D., Gubellini, P., Pisani, A., and Bernardi, G. (2000). Acetylcholine-mediated modulation of striatal function. *Trends Neurosci.* 23, 120–126.
- Carpenter, M. B., Nakano, K., and Kim, R. (1976). Nigrothalamic projections in the monkey demonstrated by autoradiographic techniques. *J. Comp. Neurol.* 165, 401–415.
- Chang, E. F., Turner, R. S., Ostrem, J. L., Davis, V. R., and Starr, P. A. (2007). Neuronal responses to passive movement in the globus pallidus internus in primary dystonia. *J. Neurophysiol.* 98, 3696–3707.
- Chevalier, G., and Deniau, J. M. (1990). Disinhibition as a basic process in the expression of striatal functions. *Trends Neurosci.* 13, 277–280.
- Coubes, P., Roubertie, A., Vayssiere, N., Hemm, S., and Echenne, B. (2000). Treatment of DYT1-generalised dystonia by stimulation of the internal globus pallidus. *Lancet* 355, 2220–2221.
- Crossman, A. R. (1987). Primate models of dyskinesia: the experimental approach to the study of basal ganglia-related involuntary movement disorders. *Neuroscience* 21, 1–40.
- Crossman, A. R., Mitchell, I. J., Sambrook, M. A., and Jackson, A. (1988). Chorea and myoclonus in the monkey induced by gamma-aminobutyric acid antagonism in the lentiform complex. The site of drug action and a hypothesis for the neural mechanisms of chorea. *Brain* 111(Pt 5), 1211–1233.
- Crutcher, M. D., and DeLong, M. R. (1984). Single cell studies of the primate putamen. II. Relations to direction of movement and pattern of muscular activity. *Exp. Brain Res.* 53, 244–258.
- Del, S. F., and Albanese, A. (2008). Levodopa-induced dyskinesias and their management. *J. Neurol.* 255(Suppl. 4), 32–41.
- Delmaire, C., Krainik, A., Tezenas du, M. S., Gerardin, E., Meunier, S., Mangin, J. F., Sangla, S., Garner, L., Vidailhet, M., and Lehericy, S. (2005). Disorganized somatotopy in the putamen of patients with focal hand dystonia. *Neurology* 64, 1391–1396.
- DeLong, M. R. (1971). Activity of pallidal neurons during movement. *J. Neurophysiol.* 34, 414–427.
- DeLong, M. R. (1972). Activity of basal ganglia neurons during movement. *Brain Res.* 40, 127–135.
- DeLong, M. R. (1973). Putamen: activity of single units during slow and rapid arm movements. *Science* 179, 1240–1242.
- DeLong, M. R. (1990). Primate models of movement disorders of basal ganglia origin. *Trends Neurosci.* 13, 281–285.
- DeLong, M. R., Crutcher, M. D., and Georgopoulos, A. P. (1985). Primate globus pallidus and subthalamic nucleus: functional organization. *J. Neurophysiol.* 53, 530–543.
- Deng, Y. P., Albin, R. L., Penney, J. B., Young, A. B., Anderson, K. D., and Reiner, A. (2004). Differential loss of striatal projection systems in Huntington's disease: a quantitative immunohistochemical study. *J. Chem. Neuroanat.* 27, 143–164.
- Desmurget, M., and Turner, R. S. (2008). Testing basal ganglia motor functions through reversible inactivations in the posterior internal globus pallidus. *J. Neurophysiol.* 99, 1057–1076.
- di Michele, F., Prichep, L., John, E. R., and Chabot, R. J. (2005). The neurophysiology of attention-deficit/hyperactivity disorder. *Int. J. Psychophysiol.* 58, 81–93.
- Erez, Y., Tischler, H., Belevovsky, K., and Bar-Gad, I. (2011). Dispersed activity during passive movement in the globus pallidus of the 1-methyl-4-phenyl-1,2,3,6-tetrahydropyridine (MPTP)-treated primate. *PLoS ONE* 6, e16293. doi: 10.1371/journal.pone.0016293
- Fahn, S., and Eldridge, R. (1976). Definition of dystonia and classification of the dystonic states. *Adv. Neurol.* 14, 1–5.
- Filion, M., Tremblay, L., and Bedard, P. J. (1988). Abnormal influences of passive limb movement on the activity of globus pallidus neurons in parkinsonian monkeys. *Brain Res.* 444, 165–176.
- Gardiner, T. W., and Nelson, R. J. (1992). Striatal neuronal activity during the initiation and execution of hand movements made in response to visual and vibratory cues. *Exp. Brain Res.* 92, 15–26.
- Gawne, T. J., and Richmond, B. J. (1993). How independent are the messages carried by adjacent inferior temporal cortical neurons? *J. Neurosci.* 13, 2758–2771.
- Georgopoulos, A. P., DeLong, M. R., and Crutcher, M. D. (1983). Relations between parameters of step-tracking movements and single cell discharge in the globus pallidus and subthalamic nucleus of the behaving monkey. *J. Neurosci.* 3, 1586–1598.
- Gerfen, C. R., Engber, T. M., Mahan, L. C., Susel, Z., Chase, T. N., Monsma, F. J. Jr., and Sibley, D. R. (1990). D1 and D2 dopamine receptor-regulated gene expression of striatonigral and striatopallidal neurons. *Science* 250, 1429–1432.
- Gil, J. M., and Rego, A. C. (2008). Mechanisms of neurodegeneration in Huntington's disease. *Eur. J. Neurosci.* 27, 2803–2820.
- Glass, M., Dragunow, M., and Faull, R. L. (2000). The pattern of neurodegeneration in Huntington's disease: a comparative study of cannabinoid, dopamine, adenosine and GABA(A) receptor alterations in the human basal ganglia in Huntington's disease. *Neuroscience* 97, 505–519.
- Gochin, P. M., Gerstein, G. L., and Kaltenbach, J. A. (1990). Dynamic temporal properties of effective connections in rat dorsal cochlear nucleus. *Brain Res.* 510, 195–202.
- Grabli, D., McCairn, K., Hirsch, E. C., Agid, Y., Feger, J., Francois, C., and Tremblay, L. (2004). Behavioural disorders induced by external globus pallidus dysfunction in primates: I. Behavioural study. *Brain* 127, 2039–2054.
- Graybiel, A. M., and Rauch, S. L. (2000). Toward a neurobiology of obsessive-compulsive disorder. *Neuron* 28, 343–347.
- Guehl, D., Cuny, E., Ghorayeb, I., Michelet, T., Bioulac, B., and Burbaud, P. (2009). Primate models of dystonia. *Prog. Neurobiol.* 87, 118–131.
- Gurney, K., Prescott, T. J., and Redgrave, P. (2001). A computational model of action selection in the basal ganglia. II. Analysis and simulation of behaviour. *Biol. Cybern.* 84, 411–423.
- Gurney, K., Prescott, T. J., Wickens, J. R., and Redgrave, P. (2004). Computational models of the basal ganglia: from robots to membranes. *Trends Neurosci.* 27, 453–459.
- Haber, S. N., Fudge, J. L., and McFarland, N. R. (2000). Striatonigrostriatal pathways in primates form an ascending spiral from the shell to the dorsolateral striatum. *J. Neurosci.* 20, 2369–2382.
- Hamada, I., and DeLong, M. R. (1992). Excitotoxic acid lesions of the primate subthalamic nucleus result in transient dyskinesias of the contralateral limbs. *J. Neurophysiol.* 68, 1850–1858.
- Hassler, R. (1939). Zur pathologischen anatomie des senilen und des parkinsonistischen tremor. *J. Psychol. Neurol.* 43, 193–230.
- Hazrati, L. N., Parent, A., Mitchell, S., and Haber, S. N. (1990). Evidence for interconnections between the two segments of the globus pallidus in primates: a PHA-L anterograde tracing study. *Brain Res.* 533, 171–175.
- Hesse, S., Muller, U., Lincke, T., Barthel, H., Villmann, T., Angermeyer, M. C., Sabri, O., and Stengler-Wenzke, K. (2005). Serotonin and dopamine transporter imaging in patients with obsessive-compulsive disorder. *Psychiatry Res.* 140, 63–72.
- Hikosaka, O., and Wurtz, R. H. (1983). Visual and oculomotor functions of monkey substantia nigra pars reticulata. III. Memory-contingent visual and saccade responses. *J. Neurophysiol.* 49, 1268–1284.
- Hornykiewicz, O. (1966). Dopamine (3-hydroxytyramine) and brain function. *Pharmacol. Rev.* 18, 925–964.
- Hutchinson, W. D., Lang, A. E., Dostrovsky, J. O., and Lozano, A. M. (2003). Pallidal neuronal activity: implications for models of dystonia. *Ann. Neurol.* 53, 480–488.
- Ibanez-Sandoval, O., Tecuapetla, F., Unal, B., Shah, F., Koos, T., and Tepper, J. M. (2010). Electrophysiological and morphological characteristics and synaptic connectivity of tyrosine hydroxylase-expressing neurons in adult mouse striatum. *J. Neurosci.* 30, 6999–7016.
- Inase, M., Li, B. M., and Tanji, J. (1997). Dopaminergic modulation of neuronal activity in the monkey putamen through D1 and D2 receptors during a delayed Go/Nogo task. *Exp. Brain Res.* 117, 207–218.

- Jaeger, D., Gilman, S., and Aldridge, J. W. (1995). Neuronal-activity in the striatum and pallidum of primates related to the execution of externally cued reaching movements. *Brain Res.* 694, 111–127.
- Jenner, P. (2003). The contribution of the MPTP-treated primate model to the development of new treatment strategies for Parkinson's disease. *Parkinsonism Relat. Disord.* 9, 131–137.
- Joel, D. (2001). Open interconnected model of basal ganglia-thalamocortical circuitry and its relevance to the clinical syndrome of Huntington's disease. *Mov. Disord.* 16, 407–423.
- Joel, D., and Weiner, I. (1994). The organization of the basal ganglia-thalamocortical circuits: open interconnected rather than closed segregated. *Neuroscience* 63, 363–379.
- Joshua, M., Adler, A., and Bergman, H. (2009a). The dynamics of dopamine in control of motor behavior. *Curr. Opin. Neurobiol.* 19, 615–620.
- Joshua, M., Adler, A., Prut, Y., Vaadia, E., Wickens, J. R., and Bergman, H. (2009b). Synchronization of midbrain dopaminergic neurons is enhanced by rewarding events. *Neuron* 62, 695–704.
- Kerr, J. N., and Wickens, J. R. (2001). Dopamine D-1/D-5 receptor activation is required for long-term potentiation in the rat neostriatum in vitro. *J. Neurophysiol.* 85, 117–124.
- Kim, R., Nakano, K., Jayaraman, A., and Carpenter, M. B. (1976). Projections of the globus pallidus and adjacent structures: an autoradiographic study in the monkey. *J. Comp. Neurol.* 169, 263–290.
- Kita, H., and Kitai, S. T. (1994). The morphology of globus pallidus projection neurons in the rat: an intracellular staining study. *Brain Res.* 636, 308–319.
- Koos, T., and Tepper, J. M. (1999). Inhibitory control of neostriatal projection neurons by GABAergic interneurons. *Nat. Neurosci.* 2, 467–472.
- Kurlan, R. (2004). "Tourette's syndrome," in *Movement Disorders: Neurologic Principles and Practice*, eds R. L. Watts and C. K. Williams (New York: McGraw-Hill Medical Publishing), 685–692.
- Leblois, A., Meissner, W., Bezard, E., Bioulac, B., Gross, C. E., and Boraud, T. (2006). Temporal and spatial alterations in GPi neuronal encoding might contribute to slow down movement in Parkinsonian monkeys. *Eur. J. Neurosci.* 24, 1201–1208.
- Lenz, F. A., Jaeger, C. J., Seike, M. S., Lin, Y. C., Reich, S. G., DeLong, M. R., and Vitek, J. L. (1999). Thalamic single neuron activity in patients with dystonia: dystonia-related activity and somatic sensory reorganization. *J. Neurophysiol.* 82, 2372–2392.
- Lenz, F. A., Suarez, J. I., Metman, L. V., Reich, S. G., Karp, B. I., Hallett, M., Rowland, L. H., and Dougherty, P. M. (1998). Pallidal activity during dystonia: somatosensory reorganization and changes with severity. *J. Neurol. Neurosurg. Psychiatry* 65, 767–770.
- Levy, R., Dostrovsky, J. O., Lang, A. E., Sime, E., Hutchison, W. D., and Lozano, A. M. (2001). Effects of apomorphine on subthalamic nucleus and globus pallidus internus neurons in patients with Parkinson's disease. *J. Neurophysiol.* 86, 249–260.
- Liles, S. L. (1985). Activity of neurons in putamen during active and passive movements of wrist. *J. Neurophysiol.* 53, 217–236.
- Maia, T. V., and Frank, M. J. (2011). From reinforcement learning models to psychiatric and neurological disorders. *Nat. Neurosci.* 14, 154–162.
- Marsden, C. D., Obeso, J. A., Zarranz, J. J., and Lang, A. E. (1985). The anatomical basis of symptomatic hemidystonia. *Brain* 108(Pt 2), 463–483.
- Marshall, F. J. (2004). "Clinical features and treatment of Huntington's disease," in *Movement Disorders: Neurologic Principles and Practice*, eds R. L. Watts and W. C. Koller (New York: The McGraw-Hill Companies), 589–601.
- Martin, J. P., and Alcock, N. S. (1934). Hemichorea associated with a lesion of the corpus luyssii. *Brain* 57, 504–516.
- McCaig, K. W., Bronfeld, M., Belevsky, K., and Bar-Gad, I. (2009). The neurophysiological correlates of motor tics following focal striatal disinhibition. *Brain* 132, 2125–2138.
- McHaffie, J. G., Stanford, T. R., Stein, B. E., Coizet, V., and Redgrave, P. (2005). Subcortical loops through the basal ganglia. *Trends Neurosci.* 28, 401–407.
- Mink, J. W. (1996). The basal ganglia: focused selection and inhibition of competing motor programs. *Prog. Neurobiol.* 50, 381–425.
- Mink, J. W. (2001). Basal ganglia dysfunction in Tourette's syndrome: a new hypothesis. *Pediatr. Neurol.* 25, 190–198.
- Mink, J. W., and Thach, W. T. (1987). Preferential relation of pallidal neurons to ballistic movements. *Brain Res.* 417, 393–398.
- Mink, J. W., and Thach, W. T. (1991a). Basal ganglia motor control. I. Nonexclusive relation of pallidal discharge to five movement modes. *J. Neurophysiol.* 65, 273–300.
- Mink, J. W., and Thach, W. T. (1991b). Basal ganglia motor control. II. Late pallidal timing relative to movement onset and inconsistent pallidal coding of movement parameters. *J. Neurophysiol.* 65, 301–329.
- Mitchell, S. J., Richardson, R. T., Baker, F. H., and DeLong, M. R. (1987). The primate globus pallidus: neuronal activity related to direction of movement. *Exp. Brain Res.* 68, 491–505.
- Moore, G. P., Perkel, D. H., and Segundo, J. P. (1966). Statistical analysis and functional interpretation of neuronal spike data. *Annu. Rev. Physiol.* 28, 493–522.
- Moss, J., and Bolam, J. P. (2008). A dopaminergic axon lattice in the striatum and its relationship with cortical and thalamic terminals. *J. Neurosci.* 28, 11221–11230.
- Murphy, T. K., Goodman, W. K., Ayoub, E. M., and Voeller, K. K. (2000). On defining Sydenham's chorea: where do we draw the line? *Biol. Psychiatry* 47, 851–857.
- Mushiake, H., and Strick, P. L. (1995). Pallidal neuron activity during sequential arm movements. *J. Neurophysiol.* 74, 2754–2758.
- Nambu, A., Tokuno, H., and Takada, M. (2002). Functional significance of the cortico-subthalamo-pallidal 'hyperdirect' pathway. *Neurosci. Res.* 43, 111–117.
- Nambu, A., Yoshida, S., and Jinnai, K. (1988). Projection on the motor cortex of thalamic neurons with pallidal input in the monkey. *Exp. Brain Res.* 71, 658–662.
- Nevet, A., Morris, G., Saban, G., Arkadir, D., and Bergman, H. (2007). Lack of spike-count and spike-time correlations in the substantia nigra reticulata despite overlap of neural responses. *J. Neurophysiol.* 98, 2232–2243.
- Nevet, A., Morris, G., Saban, G., Fainstein, N., and Bergman, H. (2004). Discharge rate of substantia nigra pars reticulata neurons is reduced in non-parkinsonian monkeys with apomorphine-induced orofacial dyskinesia. *J. Neurophysiol.* 92, 1973–1981.
- Nini, A., Feingold, A., Sloviter, H., and Bergman, H. (1995). Neurons in the globus pallidus do not show correlated activity in the normal monkey, but phase-locked oscillations appear in the MPTP model of parkinsonism. *J. Neurophysiol.* 74, 1800–1805.
- Parent, A., Levesque, M., and Parent, M. (2001). A re-evaluation of the current model of the basal ganglia. *Parkinsonism Relat. Disord.* 7, 193–198.
- Parkinson, J. (1817). *An Essay on the Shaking Palsy*. London: Sherwood, Neely and Jones.
- Perkel, D. H., Gerstein, G. L., and Moore, G. P. (1967). Neuronal spike trains and stochastic point processes. II. Simultaneous spike trains. *Biophys. J.* 7, 419–440.
- Pessiglione, M., Guehl, D., Rolland, A. S., Francois, C., Hirsch, E. C., Feger, J., and Tremblay, L. (2005). Thalamic neuronal activity in dopamine-depleted primates: evidence for a loss of functional segregation within basal ganglia circuits. *J. Neurosci.* 25, 1523–1531.
- Peterson, B. S., Pine, D. S., Cohen, P., and Brook, J. S. (2001). Prospective, longitudinal study of tic, obsessive-compulsive, and attention-deficit/hyperactivity disorders in an epidemiological sample. *J. Am. Acad. Child Adolesc. Psychiatry* 40, 685–695.
- Prescott, T. J., Montes Gonzalez, F. M., Gurney, K., Humphries, M. D., and Redgrave, P. (2006). A robot model of the basal ganglia: behavior and intrinsic processing. *Neural Netw.* 19, 31–61.
- Quartarone, A., Morgante, E., Sant'angelo, A., Rizzo, V., Bagnato, S., Terranova, C., Siebner, H. R., Berardelli, A., and Girlanda, P. (2008). Abnormal plasticity of sensorimotor circuits extends beyond the affected body part in focal dystonia. *J. Neurol. Neurosurg. Psychiatry* 79, 985–990.
- Raz, A., Vaadia, E., and Bergman, H. (2000). Firing patterns and correlations of spontaneous discharge of pallidal neurons in the normal and the tremulous 1-methyl-4-phenyl-1,2,3,6-tetrahydropyridine vervet model of parkinsonism. *J. Neurosci.* 20, 8559–8571.
- Rodriguez-Oroz, M. C., Obeso, J. A., Lang, A. E., Houeto, J. L., Pollak, P., Rehncrona, S., Kulisevsky, J., Albanese, A., Volkmann, J., Hariz, M. I., Quinn, N. P., Speelman, J. D., Guridi, J., Zamarril, L., Gironell, A., Molet, J., Pascual-Sedano, B., Pidoux, B., Bonnet, A. M., Agid, Y., Xie, J., Benabid, A. L., Lozano, A. M., Saint-Cyr, J., Romito, L., Contarino, M. F., Scerrati, M., Fraix, V., and Van Blercom, N. (2005). Bilateral deep brain stimulation in Parkinson's disease: a multi-centre study with 4 years follow-up. *Brain* 128, 2240–2249.
- Rodriguez-Oroz, M. C., Rodriguez, M., Guridi, J., Mewes, K., Chockman, V., Vitek, J., DeLong, M. R., and Obeso, J. A. (2001). The subthalamic nucleus in Parkinson's disease: somatotopic organization and physiological characteristics. *Brain* 124, 1777–1790.
- Rommelfanger, K. S., and Wichmann, T. (2010). Extrastriatal dopaminergic circuits of the basal ganglia. *Front. Neuroanat.* 4:139. doi: 10.3389/fnana.2010.00139
- Sadek, A. R., Magill, P. J., and Bolam, J. P. (2007). A single-cell analysis of intrinsic connectivity in the rat globus pallidus. *J. Neurosci.* 27, 6352–6362.

- Schultz, W. (1998). Predictive reward signal of dopamine neurons. *J. Neurophysiol.* 80, 1–27.
- Schultz, W. (2007). Multiple dopamine functions at different time courses. *Annu. Rev. Neurosci.* 30, 259–288.
- Shink, E., Bevan, M. D., Bolam, J. P., and Smith, Y. (1996). The subthalamic nucleus and the external pallidum: two tightly interconnected structures that control the output of the basal ganglia in the monkey. *Neuroscience* 73, 335–357.
- Singer, H. S., and Minzer, K. (2003). Neurobiology of Tourette's syndrome: concepts of neuroanatomic localization and neurochemical abnormalities. *Brain Dev.* 25(Suppl. 1), S70–S84.
- Starr, P. A., Kang, G. A., Heath, S., Shimamoto, S., and Turner, R. S. (2008). Pallidal neuronal discharge in Huntington's disease: support for selective loss of striatal cells originating the indirect pathway. *Exp. Neurol.* 211, 227–233.
- Starr, P. A., Rau, G. M., Davis, V., Marks, W. J. Jr., Ostrem, J. L., Simmons, D., Lindsey, N., and Turner, R. S. (2005). Spontaneous pallidal neuronal activity in human dystonia: comparison with Parkinson's disease and normal macaque. *J. Neurophysiol.* 93, 3165–3176.
- Steeves, T. D., and Fox, S. H. (2008). Neurobiological basis of serotonin-dopamine antagonists in the treatment of Gilles de la Tourette syndrome. *Prog. Brain Res.* 172, 495–513.
- Sterio, D., Beric, A., Dogali, M., Fazzini, E., Alfaro, G., and Devinsky, O. (1994). Neurophysiological properties of pallidal neurons in Parkinson's disease. *Ann. Neurol.* 35, 586–591.
- Stevens, J. K., and Gerstein, G. L. (1976). Interactions between cat lateral geniculate neurons. *J. Neurophysiol.* 39, 239–256.
- Swanson, J., Castellanos, F. X., Murias, M., LaHoste, G., and Kennedy, J. (1998). Cognitive neuroscience of attention deficit hyperactivity disorder and hyperkinetic disorder. *Curr. Opin. Neurobiol.* 8, 263–271.
- Tabbal, S. D., Mink, J. W., Antenor, J. A., Carl, J. L., Moerlein, S. M., and Perlmuter, J. S. (2006). 1-Methyl-4-phenyl-1,2,3,6-tetrahydropyridine-induced acute transient dystonia in monkeys associated with low striatal dopamine. *Neuroscience* 141, 1281–1287.
- Taha, J. M., Favre, J., Baumann, T. K., and Burchiel, K. J. (1996). Characteristics and somatotopic organization of kinesthetic cells in the globus pallidus of patients with Parkinson's disease. *J. Neurosurg.* 85, 1005–1012.
- Tamburin, S., Manganotti, P., Marzi, C. A., Fiaschi, A., and Zanette, G. (2002). Abnormal somatotopic arrangement of sensorimotor interactions in dystonic patients. *Brain* 125, 2719–2730.
- Tepper, J. M., Koos, T., and Wilson, C. J. (2004). GABAergic microcircuits in the neostriatum. *Trends Neurosci.* 27, 662–669.
- Theodosopoulos, P. V., Marks, W. J. Jr., Christine, C., and Starr, P. A. (2003). Locations of movement-related cells in the human subthalamic nucleus in Parkinson's disease. *Mov. Disord.* 18, 791–798.
- Tripp, G., and Wickens, J. R. (2009). Neurobiology of ADHD. *Neuropharmacology* 57, 579–589.
- Turner, R. S., and Anderson, M. E. (1997). Pallidal discharge related to the kinematics of reaching movements in two dimensions. *J. Neurophysiol.* 77, 1051–1074.
- Turner, R. S., and Anderson, M. E. (2005). Context-dependent modulation of movement-related discharge in the primate globus pallidus. *J. Neurosci.* 25, 2965–2976.
- Turner, R. S., and Desmurget, M. (2010). Basal ganglia contributions to motor control: a vigorous tutor. *Curr. Opin. Neurobiol.* 20, 704–716.
- Urbain, N., Gervasoni, D., Souliere, F., Lobo, L., Rentero, N., Windels, F., Astier, B., Savasta, M., Fort, P., Renaud, B., Luppi, P. H., and Chouvet, G. (2000). Unrelated output of subthalamic nucleus and globus pallidus neuronal activities across vigilance states in the rat. *Eur. J. Neurosci.* 12, 3361–3374.
- Vitek, J. L., Chockkan, V., Zhang, J. Y., Kaneoke, Y., Evatt, M., DeLong, M. R., Triche, S., Mewes, K., Hashimoto, T., and Bakay, R. A. (1999). Neuronal activity in the basal ganglia in patients with generalized dystonia and hemiballismus. *Ann. Neurol.* 46, 22–35.
- Whiteside, S. P., Port, J. D., and Abramowitz, J. S. (2004). A meta-analysis of functional neuroimaging in obsessive-compulsive disorder. *Psychiatry Res* 132, 69–79.
- Wichmann, T. (2008). Commentary: dopaminergic dysfunction in DYT1 dystonia. *Exp. Neurol.* 212, 242–246.
- Wichmann, T., Bergman, H., and DeLong, M. R. (1994). The primate subthalamic nucleus. I. Functional properties in intact animals. *J. Neurophysiol.* 72, 494–506.
- Wickens, J. (1993). *A Theory of the Striatum*. Oxford: Pergamon Press.
- Wickens, J. R., Begg, A. J., and Arbutnot, G. W. (1996). Dopamine reverses the depression of rat corticostriatal synapses which normally follows high-frequency stimulation of cortex in vitro. *Neuroscience* 70, 1–5.
- Wickremaratne, M. M., Ben-Shlomo, Y., and Morris, H. R. (2009). The effect of onset age on the clinical features of Parkinson's disease. *Eur. J. Neurol.* 16, 450–456.
- Wild, E. J., and Tabrizi, S. J. (2007). The differential diagnosis of chorea. *Pract. Neurol.* 7, 360–373.
- Williams, Z. M., Neimat, J. S., Cosgrove, G. R., and Eskandar, E. N. (2005). Timing and direction selectivity of subthalamic and pallidal neurons in patients with Parkinson disease. *Exp. Brain Res.* 162, 407–416.
- Wilson, C. J. (2007). "GABAergic inhibition in the neostriatum," in *Progress in Brain Research GABA and the Basal Ganglia – From Molecules to Systems*, ed. J. M. Tepper (Amsterdam: Elsevier), 91–110.
- Wong, D. F., Brasic, J. R., Singer, H. S., Schretlen, D. J., Kuwabara, H., Zhou, Y., Nandi, A., Maris, M. A., Alexander, M., Ye, W., Rousset, O., Kumar, A., Szabo, Z., Gjedde, A., and Grace, A. A. (2008). Mechanisms of dopaminergic and serotonergic neurotransmission in Tourette syndrome: clues from an in vivo neurochemistry study with PET. *Neuropsychopharmacology* 33, 1239–1251.
- Worbe, Y., Baup, N., Grabli, D., Chaigneau, M., Mounayar, S., McCairn, K., Feger, J., and Tremblay, L. (2008). Behavioral and movement disorders induced by local inhibitory dysfunction in primate striatum. *Cereb. Cortex* 19, 1844–1856.
- Yoshida, M., Nagatsuka, Y., Muramatsu, S., and Nijima, K. (1991). Differential roles of the caudate nucleus and putamen in motor behavior of the cat as investigated by local injection of GABA antagonists. *Neurosci. Res.* 10, 34–51.
- Zhang, J., Berridge, K. C., Tindell, A. J., Smith, K. S., and Aldridge, J. W. (2009). A neural computational model of incentive salience. *PLoS Comput. Biol.* 5, e1000437. doi: 10.1371/journal.pcbi.1000437
- Zhuang, P., Hallett, M., Zhang, X., Li, J., Zhang, Y., and Li, Y. (2009). Neuronal activity in the globus pallidus internus in patients with tics. *J. Neurol. Neurosurg. Psychiatry* 80, 1075–1081.

Conflict of Interest Statement: The authors declare that the research was conducted in the absence of any commercial or financial relationships that could be construed as a potential conflict of interest.

Received: 31 January 2011; accepted: 20 May 2011; published online: 03 June 2011.
Citation: Bronfeld M and Bar-Gad I (2011) Loss of specificity in basal ganglia related movement disorders. *Front. Syst. Neurosci.* 5:38. doi: 10.3389/fnsys.2011.00038
Copyright © 2011 Bronfeld and Bar-Gad. This is an open-access article subject to a non-exclusive license between the authors and Frontiers Media SA, which permits use, distribution and reproduction in other forums, provided the original authors and source are credited and other Frontiers conditions are complied with.



Frontal cortex-like functions of the subthalamic nucleus

Christelle Baunez^{1,2*} and Sylvie Lardeux^{1,2†}

¹ Laboratoire de Neurobiologie de la Cognition, UMR6155 CNRS, Université de Provence Marseille, Marseille, France

² Pôle3C, UMR6155, Université de Provence, Marseille, France

Edited by:

Elizabeth Abercrombie,
Rutgers–Newark: The State University
of New Jersey, USA

Reviewed by:

Andrew M. Farrar, University at
Buffalo, The State University of New
York, USA

Verity Brown, University of St.
Andrews, UK

*Correspondence:

Christelle Baunez, Laboratoire de
Neurobiologie de la Cognition,
UMR6155 CNRS, Aix-Marseille
Université, Marseille, France.
e-mail: christelle.
baunez@univ-provence.fr

†Present address:

Sylvie Lardeux, Department of
Psychiatry, Albert Einstein College of
Medicine, Bronx, NY, USA.

The subthalamic nucleus (STN) has been considered a motor structure for a long time. Over the last 20 years, anatomical and behavioral data have highlighted the position of the STN within a prefrontal-associative and a limbic loops, suggesting that the STN should play a critical role in frontal functions such as attention, inhibitory control (including impulsive action, compulsivity, impulsive choice), and motivation. Here we will review the work highlighting these functions of the STN.

Keywords: basal ganglia, subthalamic nucleus, deep brain stimulation, attention, motivation, impulsivity, compulsion, behavioral inhibition

INTRODUCTION

When studying the basal ganglia, many researchers focus their experiments on the so-called motor loop, one of the five loops described by Alexander et al. (1986). In this motor loop, the subthalamic nucleus (STN) belongs to the indirect pathway, positioned as a relay between the external and the internal globus pallidus (GPe and GPi respectively). Its dysregulation in the case of parkinsonism lead to the suggestion of STN inactivation as an alternative strategy to dopaminergic treatments. STN high frequency stimulation (HFS) was therefore introduced (Limousin et al., 1995) and is currently very successful in treating the motor symptoms of Parkinson's disease (PD). More recently, the STN has also been described as a possible input structure to the basal ganglia since it receives a direct projection from the cortex, a pathway now called the "hyperdirect pathway" (Nambu et al., 2002). When looking at the classical diagrams of the five parallel loops, the STN is traditionally drawn only on the motor loop, but anatomical data indicate that it should not be omitted from the other loops, including the associative and limbic circuits. Indeed, the STN receives and sends projections from/to the ventral pallidum (VP) and also receives inputs from the prefrontal cortex (Groenewegen and Berendse, 1990; Groenewegen et al., 1993; Maurice et al., 1998a,b, 1999). Given these connections, it is expected that its

functional involvement should not be limited to motor functions, but should also include "frontal functions," like attention, inhibition control, and motivation. Some aspects of them have been partially reviewed (Temel et al., 2005), but there are now more experimental and clinical sets of data supporting this involvement of STN in frontal-like functions, and especially on motivation.

STN IN ATTENTION AND IMPULSIVITY

STN IN ATTENTION

The role of the STN in arousal, wakefulness, and alertness was first suggested in the late 1960s based on studies carried out in the cat (Naquet et al., 1966; Lindsley et al., 1970). This line of research was abandoned until the resurgence of interest in the STN as a therapeutic target for the treatment of PD in the 1990s (Bergman et al., 1990; Benazzouz et al., 1993).

In a study assessing the effects of STN lesions on the performance of a simple reaction time (RT) task, we have shown that STN lesions induce a dramatic increase in the number of premature responses (i.e., early withdrawal of the paw from a lever, before the onset of the visual trigger stimulus). This deficit was hypothesized to result from either an attentional deficit or disinhibition (Baunez et al., 1995).

In order to further assess attentional functions in rats, we have then used the "5-choice serial RT task" (5-CSRTT) in which the animals are trained to wait and detect a brief visual stimulus that is randomly presented in five possible different locations. The animals have to divide their attention between these five possible choices and then respond by making a nose-poke in the appropriate location in order to obtain a food reward. The

Abbreviations: 5-CSRTT, 5-choice serial reaction time task; CS, conditioned stimulus; DBS, deep brain stimulation; FR1, fixed ratio 1; GPe/i, external/internal segment of the globus pallidus; HFS, high frequency stimulation; OCD, obsessive compulsive disorder; OFC, orbito-frontal cortex; PD, Parkinson's disease; PET, positron emission tomography; RT, reaction time; STN, subthalamic nucleus; US, unconditioned stimulus; VP, ventral pallidum.

measure of accuracy is considered as an index of attentional performance (Robbins, 2002). In this specific visual attentional task, we have shown that bilateral excitotoxic lesions of the STN seriously impaired accuracy, thus suggesting an attentional deficit (Baunez and Robbins, 1997). These results were the first to highlight the involvement of STN in cognitive functions. Decreased accuracy in the same task was also observed after pharmacological inactivation of the STN induced by stimulation of GABA receptors with muscimol (Baunez and Robbins, 1999). Interestingly enough, bilateral STN HFS did not reproduce the severe deficit on accuracy in the 5-CSRTT, but only induced a transient deficit (Baunez et al., 2007). This difference between STN lesion and HFS suggests that HFS does not truly mimic an inactivation of the structure, as suggested by human imaging data (for example (Hershey et al., 2003)).

We provided the first evidence of a functional role for the hyperdirect pathway in the attentional deficits observed in this behavioral task by disconnecting the medial prefrontal cortex and the STN, through lesioning the prefrontal cortex on one side and the STN on the contralateral side. Indeed, the disconnection induced similar deficits to those observed after bilateral STN lesions (Chudasama et al., 2003).

From our rat data, the STN therefore appears to be involved in attentional processes, possibly via the hyperdirect pathway. Clinical studies assessing the cognitive functions of PD patients who underwent STN deep brain stimulation (DBS) showed contrasting results. Some of those also report some attentional decline (Saint-Cyr et al., 2000; Mallet et al., 2007; York et al., 2008), while others report improvements (Fimm et al., 2009), or no further decline (Ardouin et al., 1999; Brusa et al., 2001). Unfortunately, these studies rarely used tasks specifically designed to assess attention. Furthermore, it is important to note that human data are mostly provided by clinical studies in PD patients, therefore depleted in DA. The effects of STN manipulation in a DA depleted brain may therefore not always match animal studies carried out in intact subjects. However, when STN HFS was applied in DA depleted rats performing the attentional task, there was no detrimental effect of STN HFS on the measure of visual attention (i.e., accuracy; Baunez et al., 2007).

STN AND INHIBITION CONTROL

The control of inhibition is commonly associated with impulsivity and compulsive behavior. Impulsivity itself can be dissociated into various aspects: impulsive action and impulsive choice (Eagle and Baunez, 2010). The effects of STN manipulations have been studied on these various forms by means of different behavioral procedures.

Impulsive action

As previously mentioned, we have observed increased premature responding after STN lesions in a simple RT task. This deficit may reflect a lack of inhibitory control (Baunez et al., 1995). This result has been replicated after a unilateral STN lesion (Phillips and Brown, 1999).

Premature responses can also be measured in the visual attentional task, the 5-CSRTT, when the animals are unable to wait for the brief visual stimulus, but respond in any hole before the onset of the light. In this task, we have shown that bilateral

lesions of STN increase premature responses (Baunez and Robbins, 1997). Reversible inactivation of the STN by intra-STN muscimol injections induced the same effect (Baunez and Robbins, 1999). Surprisingly, here again, although HFS is supposed to mimic an inactivation of the stimulated target, bilateral STN HFS did not increase the number of premature responses (Baunez et al., 2007), a measure that has been shown to be amplitude and frequency dependent in rats performing a RT task (Desbonnet et al., 2004). This latter observation confirms that STN HFS may not inactivate the STN in the same manner as the lesion or muscimol injections do. However STN HFS applied in PD patients was shown to impair response inhibition in a go/no go task (Ballanger et al., 2009), in line with our lesion studies and in line with the computational model suggesting that the STN could play a critical role in “holding a response” (Frank et al., 2007). A more recent study confirmed this effect of STN HFS on go–no go performance but provided further details, showing that the limbic territory of STN (i.e., ventral) was more responsible for the control of inhibition than the motor territory (i.e., dorsal; Hershey et al., 2010). Although the functional territories are clearly identified and have been functionally dissociated in humans (Mallet et al., 2007), it is difficult to address this issue in the rodents and all the studies currently available in the rat do not allow discussion of the functions of the STN in terms of anatomical territories.

Many manipulations have been tested in the 5-CSRTT and reviewing these numerous studies (Eagle and Baunez, 2010) lead to the generation of a schematic diagram illustrated in **Figure 1**, in which each lesion that induces increased premature responding are highlighted. These structures include the infra-limbic cortex, orbito-frontal cortex (OFC), dorso-medial striatum, and the STN. We have also added the cingulate cortex, the nucleus accumbens (core and shell), as pharmacological treatment or manipulation of the task can also increase premature responding in animals with damage to these regions.

The premature responses measured in RT and 5-CSRT tasks, or incorrect responses in a go/no go task reflect the inability to inhibit the initiation of a response, including the selection of the action to perform and waiting for the trigger signal. In contrast, impulse control is often studied in human subjects using a stop task. However, it is becoming clear that the stop task, by measuring the speed to stop an ongoing action, involves different inhibitory processes which depend on different neural mechanisms (Rubia et al., 2001; Eagle et al., 2008a).

Using this task, it was indeed shown in human subjects that STN activation was correlated with faster stopping abilities (Aron and Poldrack, 2006). In line with this observation, using a stop-signal RT task in the rat, we have shown that STN lesions impair animals' ability to stop an action once it has been initiated (Eagle et al., 2008b). Again, we have synthesized the data obtained in the rat on the schematic diagram illustrated in **Figure 1**. This figure highlights again an interesting set of cerebral structures: the OFC, the dorso-medial striatum, as well as the STN.

Perseverative behavior–compulsivity

Another form of deficit in response inhibition relates to repetition of a response, even if it might be an inappropriate response. This is also called compulsive behavior and is often linked with

addiction when the drug consumption switches from recreational use to compulsive use. When testing the effects of bilateral STN lesions in the 5-CSRTT, we have observed an increased level of perseverative responses toward the response locations and toward the magazine where the animals collect the food reward. These results suggest a deficit in response control and an increased level of motivation for the reward (discussed in the next paragraph; Baunez and Robbins, 1997). Interestingly, the perseverative responses on both response location and reward magazine were also observed after bilateral STN HFS (Baunez et al., 2007) and after pharmacological inactivation of the STN (Baunez and Robbins, 1999). Increased perseverative responses in the 5-CSRTT have been also observed after lesion of the pre-limbic cortex, the OFC, the dorso-medial striatum, and the nucleus accumbens core (after failed trials; Eagle and Baunez, 2010), as shown in **Figure 2**.

Impulsive choice

Impulsive choice is traditionally assessed using the delay-discounting task. In this task, the animals are given the choice between a small but immediate reward and a large but delayed reward. When tested in this procedure, the STN-lesioned animals were surprisingly able to overcome their impulsivity and wait for a bigger reward (Winstanley et al., 2005), in line with the enhanced incentive motivation observed after STN lesions (Baunez et al., 2002). This result suggests that when impulsivity competes with motivation, motivation for a bigger reward wins in STN-lesioned

rats. This dissociation between impulsive action enhanced by STN lesions and decreased impulsive choice was confirmed by another study (Uslaner and Robinson, 2006). These results suggest a specific role of STN in the control of inhibition that can be under the influence of the motivation for the outcome (Eagle and Baunez, 2010).

Again, although there are discrepant results regarding the effects of OFC, **Figure 3** illustrates commonalities of effects between the OFC, the dorso-medial striatum, and the STN.

Conclusion

Taken together these deficits reported on various forms of inhibitory control highlight a potential role for the STN in impulse control disorders. In line with this hypothesis, STN HFS has been shown to have beneficial effects in patients suffering from obsessive compulsive disorder (OCD; Mallet et al., 2008). The network involving the OFC, the dorso-medial striatum, and the STN highlighted in **Figure 3** seems to be critical for certain forms of impulsivity/compulsivity. Interestingly, a recent study using PET imaging suggests that the therapeutic effect of STN HFS in OCD patients is related to a decrease in prefrontal cortex metabolism (Le Jeune et al., 2010).

STN IN MOTIVATIONAL PROCESSES

The first observation that the STN may be involved in motivational processes comes from behavioral studies of STN lesions in

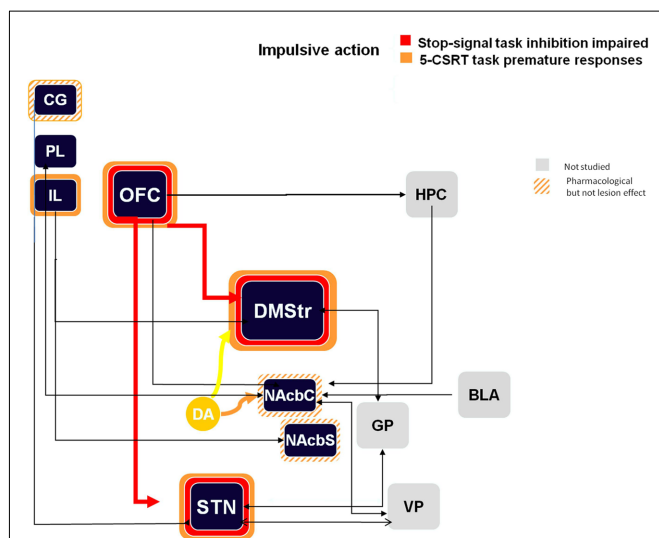


FIGURE 1 | Schematic representation of the impulsive action processes in the stop task and the 5-CSRTT (premature responses) from lesion and pharmacological manipulations. Colored bands surrounding each structure highlight the impulsive-like effect of the lesion of the given structure. Hatched-shaded bands indicate no effect of excitotoxic lesion, but an effect under pharmacological manipulation or other conditions). Gray structures indicate that no information is available. Arrows materialize anatomical connections between regions. CG, cingulate cortex; PL, pre-limbic cortex; IL, infra-limbic cortex; OFC, orbito-frontal cortex; HPC, hippocampus; DMStr, dorso-medial striatum; NAcB, nucleus accumbens core; NAcS, nucleus accumbens shell; GP, globus pallidus; BLA, basolateral amygdala; STN, subthalamic nucleus; VP, ventral pallidum.

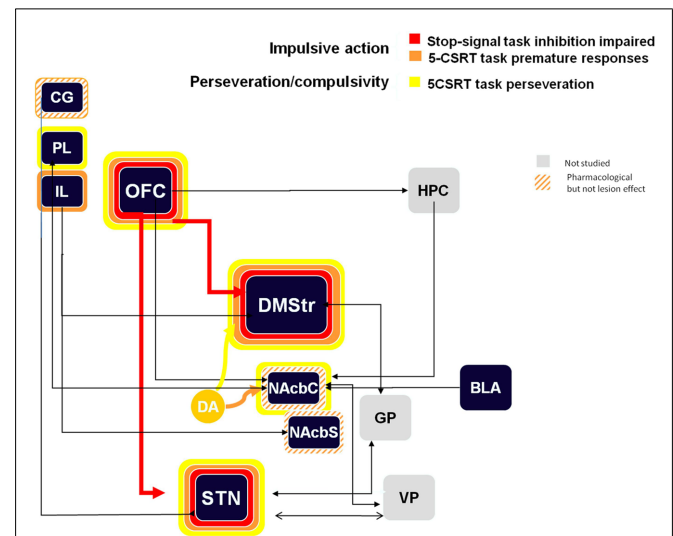
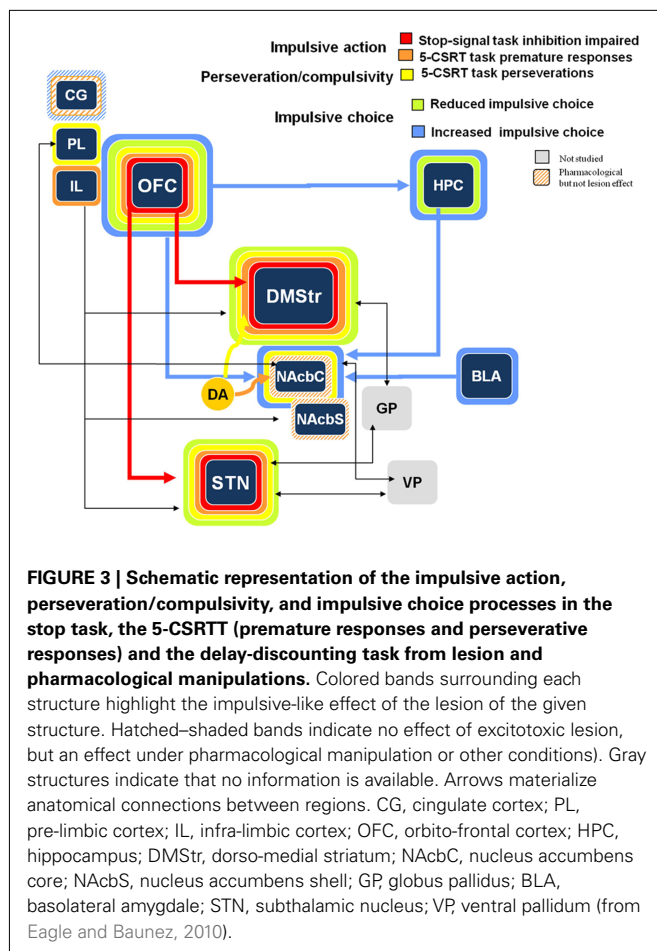


FIGURE 2 | Schematic representation of the impulsive action and perseveration/compulsivity processes in the stop task and the 5-CSRTT (premature responses and perseverative responses) from lesion and pharmacological manipulations. Colored bands surrounding each structure highlight the impulsive-like effect of the lesion of the given structure. Hatched-shaded bands indicate no effect of excitotoxic lesion, but an effect under pharmacological manipulation or other conditions). Gray structures indicate that no information is available. Arrows materialize anatomical connections between regions. CG, cingulate cortex; PL, pre-limbic cortex; IL, infra-limbic cortex; OFC, orbito-frontal cortex; HPC, hippocampus; DMStr, dorso-medial striatum; NAcB, nucleus accumbens core; NAcS, nucleus accumbens shell; GP, globus pallidus; BLA, basolateral amygdala; STN, subthalamic nucleus; VP, ventral pallidum.



rats. Indeed, in the 5-CSRTT, bilateral lesions of the STN dramatically increases the number of perseverative responses made at the food receptacle (Baunez and Robbins, 1997). This deficit may indicate an increase in motivation for the reward. In addition, clinical reports showed that an infarct or tumor in the STN could lead to pathology such as hyperphagia, hypersexuality, and mood exaltation (Trillet et al., 1995; Absher et al., 2000; Barutca et al., 2003). Taken together, these data suggest that the STN may be implicated in motivation.

We thus decided to assess directly the role of the STN in motivational processes by studying its involvement in motivation for food (Baunez et al., 2002). In this study, we first showed that bilateral lesions of the STN did not affect primary motivational processes as assessed by measures of food consumption during 2 or 24 h. On the other hand, STN lesions increased motivation for stimuli associated with food as assessed in several behavioral tasks. The conditioned locomotor activity procedure allows measurement of locomotor activity when animals anticipate food delivery. After conditioning, rats with STN lesions had a higher locomotor activity during the waiting period that indicates a higher level of expectation for the food. Furthermore, in a conditioned reinforcement task, in which a lever is associated with a conditioned stimulus (CS, i.e., a light previously paired with food), when compared to control rats performance, STN lesions increased the number of responses on the lever associated with the CS. These

results show that STN lesions do not affect the association between the CS and the unconditioned stimulus (US, i.e., the food), but that it increases the motivation for the reward. Further studies looking at the role of the STN in food motivation confirmed these results using other behavioral tasks. Indeed, in a conditioned place preference task, STN lesions increased the time spent in the compartment associated with food (Baunez et al., 2005). In this paradigm, animals learn to associate a particular environment with a particular reward, while another environment serves as control. After conditioning, in the absence of the reward, an increase in the time spent in the environment associated with the reward indicates an increase in the incentive motivation for it. In addition, in an autoshaping or a sign tracking task, in which a visual stimulus or a lever is presented as a CS when the reward is delivered, STN lesions increased the number of approaches to the stimulus or lever presses on the lever associated with reward delivery and not on the control lever (Winstanley et al., 2005; Uslaner et al., 2008), thus confirming the increased motivation for stimuli associated with food after STN lesion (Baunez et al., 2002). Finally, although the food consumption measured in a continuous schedule of reinforcement (fixed ratio 1, FR1), in which one lever press leads to the delivery of one sucrose pellet, is not affected by STN lesion (Baunez et al., 2002), the willingness to work for food was increased by STN lesions as shown in the progressive ratio task where the lesion increases the last ratio completed (Baunez et al., 2005). In this task, the number of lever presses required to receive the same reward increases within the session until the animal stops responding for the reward, thereby reaching its breaking point (or last ratio completed). This paradigm allows direct measurement of the motivation to exert effort to obtain a particular reward. It is possible that the STN lesion impaired the perception of the “cost of the reward” as observed after excitotoxic lesion of the nucleus accumbens (Bowman and Brown, 1998). However, this could hardly explain the results observed in the conditioned place preference since this task does not involve any effort or cost.

Taken together these results show that the STN is implicated in incentive motivation for food since lesions to this nucleus increase responses to stimuli associated with food. In contrast, the STN is not involved in food consumption, ruling out the possibility that STN lesions might simply increase hunger.

Interestingly, further studies have shown that STN lesions do not affect cocaine or alcohol consumption either, as measured in a FR1 task (Baunez et al., 2005; Lardeux and Baunez, 2008). The lesion does not change alcohol consumption in the home cage, whatever the alcohol concentration tested or the type of alcohol [ethanol or aniseed-flavored alcohol (i.e., pastis); Lardeux and Baunez, 2008]. These results show that whatever the reward tested, the lesion of the STN does not affect reward consumption, which rules out a possible accidental lesion of the lateral hypothalamus that is in close vicinity with the STN. The STN is thus not involved in primary reward processes.

Interestingly, as for food, STN lesions affect motivational processes for cocaine and alcohol, but in different ways. Indeed, a striking result shows that STN lesions decrease motivation for cocaine, having an opposite effect than for food (Baunez et al., 2005). In fact, STN lesions decrease the willingness to work for self-administered cocaine, as assessed in the progressive ratio task.

It is to be noted that another study showed the opposite results (Uslaner et al., 2005), but number of reward the rats received per session is so low that one may wonder whether or not the animals had acquired the self-administration behavior. Furthermore, in the conditioned place preference task, lesions of the STN decreased the time spent in the compartment associated with cocaine. These unexpected results highlight a possible role for the STN in modulating the reactivity of the reward system with regard to the nature of the reward involved, and open a new and interesting research strategy for treatment of cocaine addiction. Indeed, the STN could be an interesting target where motivation for the drug could be decreased, while other forms of motivation would not be altered, and even a resumption of interest in some activities would occur. To explore this possibility further, we then tried to replicate these results using DBS of the STN instead of a lesion. Interestingly, as for the lesion and shown in **Figure 4**, STN HFS decreases the motivation for cocaine while increasing the motivation for food (Rouaud et al., 2010). These results, while obtained in intact rats, are in line with some clinical observations in PD patients, reporting craving for sweet food in some cases, or decreased addictive behavior toward their dopaminergic treatment after STN DBS (Witjas et al., 2005; Ardouin et al., 2006; Knobel et al., 2008; Lim et al., 2009). These results suggest that STN HFS could thus represent an interesting strategy for the treatment of cocaine addiction.

When testing the effects of bilateral STN lesions on motivation for alcohol, we have shown that it could also affect motivation in an opposite manner depending on the animals' initial preference for the reward (Lardeux and Baunez, 2008). In this study, rats were separated into two groups, High and Low Drinkers depending on their alcohol preference. After STN lesions, High Drinker rats showed an increase of their motivation for alcohol, while Low Drinker rats showed a decrease in their motivation, as assessed by both the progressive ratio task and the conditioned place preference task (Lardeux and Baunez, 2008).

Taken together, these behavioral results show that STN lesions affect incentive motivation depending on the nature of the reward, but also on the initial level of preference for the reward. This latter observation highlights how critical pre-surgery assessment of the patients can be, in order to prevent or better anticipate some of the possible side-effects of STN DBS in PD patients (for example, in a patient with history of alcoholism, STN DBS could lead to relapse).

The first motivational neuronal correlates in the STN have been observed in the monkey (Matsumura et al., 1992). They recorded STN neurons that were activated only when the target presentation was followed by reward delivery. A more recent monkey study showed that STN neurons respond during the reward anticipation phase or after the reward delivery (Darbaky et al., 2005). In the rat, neuronal responses to the stimulus predicting the reward and to the reward delivery have also been shown (Teagarden and Rebec, 2007). We have recently performed electrophysiological recording of STN neurons in rats revealing that they can encode the value of the reward (Lardeux et al., 2009). We designed a task where the rat had to press and hold a lever down for 1 s. Halfway through the holding period, a stimulus predicting which one of the two possible rewards will

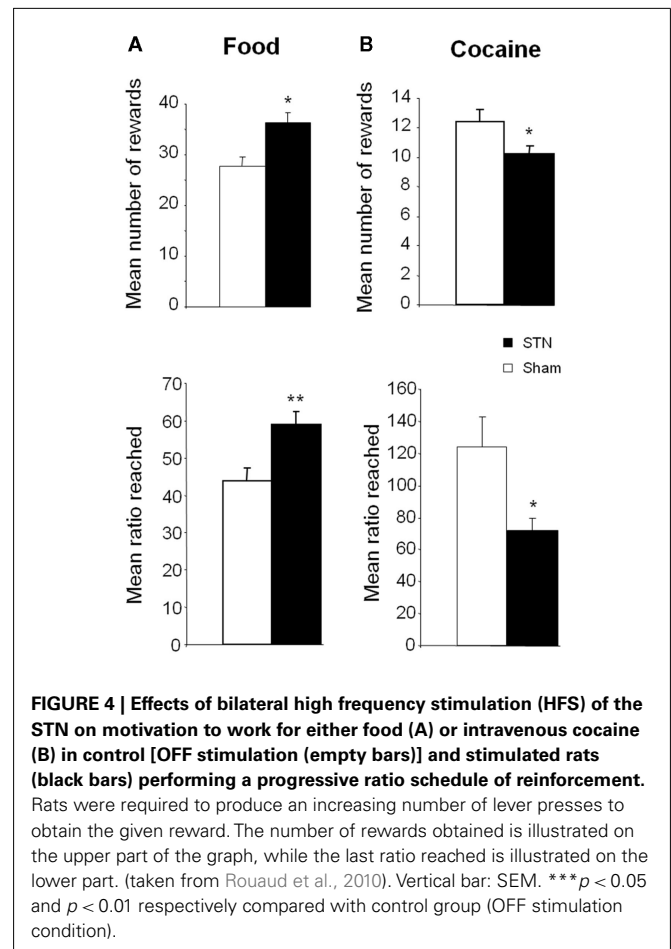


FIGURE 4 | Effects of bilateral high frequency stimulation (HFS) of the STN on motivation to work for either food (A) or intravenous cocaine (B) in control [OFF stimulation (empty bars)] and stimulated rats (black bars) performing a progressive ratio schedule of reinforcement. Rats were required to produce an increasing number of lever presses to obtain the given reward. The number of rewards obtained is illustrated on the upper part of the graph, while the last ratio reached is illustrated on the lower part. (taken from Rouaud et al., 2010). Vertical bar: SEM. *** $p < 0.05$ and $p < 0.01$ respectively compared with control group (OFF stimulation condition).

be delivered at the end of the trial was briefly presented. We have shown that STN neurons could be categorized into sub-populations responding differently to the various rewards. One sub-population responded exclusively to the cue predicting a 4% sucrose solution, but did not respond to the cue predicting the other reward (32% sucrose solution). The other sub-population responded to the cue predicting 32% sucrose, but not to the cue predicting 4% (Lardeux et al., 2009). In another study, we further showed that this dissociation is also observed when the two rewards are sucrose and cocaine (Lardeux et al., 2008). These studies showed that the STN encodes the reinforcing properties of a reward. We have also shown that some STN neurons, that we called “oops” neurons, encode behavioral error depending on the expected reward.

These electrophysiological results showing a differential encoding depending on the nature and on the preference for a reward are in line with the behavioral results suggesting a role of STN in motivation with regards to the nature of the reward, its valence and also to the preference for it. Since the encoding of the relative preference for a reward has been observed in the OFC of the monkey (Tremblay and Schultz, 1999), it might well be possible that this role of STN is under the control of the OFC via the so-called “hyperdirect pathway.” The direct cortical influence on STN activity may also explain the existence of “oops neurons” that

share properties with anterior cingulate neurons recorded in the monkey (Amiez et al., 2005).

GENERAL CONCLUSION

By reviewing the wide-range of data available regarding the involvement of the STN in frontal-like functions, it is now obvious that this small region of the brain plays a critical role in far more than motor functions. Not only can inactivation of the STN affect attentional processes, it can induce a loss of inhibitory control, in line with the proposition that an intact STN could help “holding your horses” (Frank et al., 2007) and affect motivational processes. These possible dysfunctions caused by STN inactivation could be important when considering that the current strategy for the treatment of parkinsonism is STN DBS. Whether STN DBS mimics strictly an inactivation is still under debate, but several lines of evidence indicate that it might not be truly the case (see for review Gubellini et al., 2009).

For many years the STN has been considered as a relay structure of the striatal information on the so-called “indirect pathway.” The network we have highlighted involving the dorso-medial striatum supports this view. However, it also seems obvious from various points raised in this review that the hyperdirect pathway, especially that involving the OFC, contributes a lot to some of

the behavioral responses observed after STN manipulation. To what extent and how the STN integrates both direct cortical and indirect striatal informations remains to be elucidated, but the STN may be at a critical juncture to operate as a “gate-control” for action selection under the influence of the most valuable reward.

Despite its relatively small size, the STN appears to be not only important and valuable for the treatment of PD, but its involvement in frontal functions suggests that it could be an interesting structure to target for the treatment of psychiatric disorders such as OCD (Mallet et al., 2008) and possibly addiction (Krack et al., 2010; Rouaud et al., 2010).

ACKNOWLEDGMENTS

This work has been supported by grants from the “Centre National de la Recherche Scientifique” (CNRS), the “Université de Provence,” the “Agence Nationale pour la Recherche” (ANR-05-JC05_48262 and ANR-09-MNPS-028-01 to Christelle Baunez), the MILDT-InCa-INSERM grant to Christelle Baunez, the Fondation pour la Recherche sur le Cerveau to Christelle Baunez and the Ministry for Higher Education and Research to Sylvie Lardeux. The authors thank Dr. L. Mallet for helpful suggestions on the manuscript and Dr. C. Winstanley for improving the english.

REFERENCES

- Absher, J. R., Vogt, B. A., Clark, D. G., Flowers, D. L., Gorman, D. G., Keyes, J. W., and Wood, F. B. (2000). Hypersexuality and hemiballism due to subthalamic infarction. *Neuropsychiatry Neuropsychol. Behav. Neurol.* 13, 220–229.
- Alexander, G. E., DeLong, M. R., and Strick, P. L. (1986). Parallel organization of functionally segregated circuits linking basal ganglia and cortex. *Annu. Rev. Neurosci.* 9, 357–381.
- Amiez, C., Joseph, J. P., and Procyk, E. (2005). Anterior cingulate error-related activity is modulated by predicted reward. *Eur. J. Neurosci.* 21, 3447–3452.
- Arduin, C., Pillon, B., Peiffer, E., Bejjani, P., Limousin, P., Damier, P., Arnulf, I., Benabid, A. L., Agid, Y., and Pollak, P. (1999). Bilateral subthalamic or pallidal stimulation for Parkinson's disease affects neither memory nor executive functions: a consecutive series of 62 patients. *Ann. Neurol.* 46, 217–223.
- Arduin, C., Voon, V., Worbe, Y., Abouazar, N., Czernecki, V., Hossaini, H., Pelissolo, A., Moro, E., Lhommee, E., Lang, A. E., Agid, Y., Benabid, A. L., Pollak, P., Mallet, L., and Krack, P. (2006). Pathological gambling in Parkinson's disease improves on chronic subthalamic nucleus stimulation. *Mov. Disord.* 21, 1941–1946.
- Aron, A. R., and Poldrack, R. A. (2006). Cortical and subcortical contributions to stop signal response inhibition: role of the subthalamic nucleus. *J. Neurosci.* 26, 2424–2433.
- Ballanger, B., van, E. T., Moro, E., Lozano, A. M., Hamani, C., Boulinguez, P., Pellecchia, G., Houle, S., Poon, Y. Y., Lang, A. E., and Strafella, A. P. (2009). Stimulation of the subthalamic nucleus and impulsivity: release your horses. *Ann. Neurol.* 66, 817–824.
- Barutca, S., Turgut, M., Meydan, N., and Ozsunar, Y. (2003). Subthalamic nucleus tumor causing hyperphagia – case report. *Neurol. Med. Chir. (Tokyo)* 43, 457–460.
- Baunez, C., Amalric, M., and Robbins, T. W. (2002). Enhanced food-related motivation after bilateral lesions of the subthalamic nucleus. *J. Neurosci.* 22, 562–568.
- Baunez, C., Christakou, A., Chudasama, Y., Forni, C., and Robbins, T. W. (2007). Bilateral high-frequency stimulation of the subthalamic nucleus on attentional performance: transient deleterious effects and enhanced motivation in both intact and parkinsonian rats. *Eur. J. Neurosci.* 25, 1187–1194.
- Baunez, C., Dias, C., Cador, M., and Amalric, M. (2005). The subthalamic nucleus exerts opposite control on cocaine and “natural” rewards. *Nat. Neurosci.* 8, 484–489.
- Baunez, C., Nieoullon, A., and Amalric, M. (1995). In a rat model of parkinsonism, lesions of the subthalamic nucleus reverse increases of reaction time but induce a dramatic premature responding deficit. *J. Neurosci.* 15, 6531–6541.
- Baunez, C., and Robbins, T. W. (1997). Bilateral lesions of the subthalamic nucleus induce multiple deficits in an attentional task in rats. *Eur. J. Neurosci.* 9, 2086–2099.
- Baunez, C., and Robbins, T. W. (1999). Effects of transient inactivation of the subthalamic nucleus by local muscimol and APV infusions on performance on the five-choice serial reaction time task in rats. *Psychopharmacology (Berl.)* 141, 57–65.
- Benazzouz, A., Gross, C., Feger, J., Boraud, T., and Bioulac, B. (1993). Reversal of rigidity and improvement in motor performance by subthalamic high-frequency stimulation in MPTP-treated monkeys. *Eur. J. Neurosci.* 5, 382–389.
- Bergman, H., Wichmann, T., and DeLong, M. R. (1990). Reversal of experimental parkinsonism by lesions of the subthalamic nucleus. *Science* 249, 1436–1438.
- Bowman, E. M., and Brown, V. J. (1998). Effects of excitotoxic lesions of the rat ventral striatum on the perception of reward cost. *Exp. Brain Res.* 123, 439–448.
- Brusa, L., Pierantozzi, M., Peppe, A., Altibrandi, M. G., Giacomini, P., Mazzone, P., and Stanzione, P. (2001). Deep brain stimulation (DBS) attentional effects parallel those of l-dopa treatment. *J. Neural Transm.* 108, 1021–1027.
- Chudasama, Y., Baunez, C., and Robbins, T. W. (2003). Functional disconnection of the medial prefrontal cortex and subthalamic nucleus in attentional performance: evidence for corticostriatal interaction. *J. Neurosci.* 23, 5477–5485.
- Darbaky, Y., Baunez, C., Arecchi, P., Legallet, E., and Apicella, P. (2005). Reward-related neuronal activity in the subthalamic nucleus of the monkey. *Neuroreport* 16, 1241–1244.
- Desbonnet, L., Temel, Y., Visser-Vandewalle, V., Blokland, A., Hornikx, V., and Steinbusch, H. W. (2004). Premature responding following bilateral stimulation of the rat subthalamic nucleus is amplitude and frequency dependent. *Brain Res.* 1008, 198–204.
- Eagle, D. M., Bari, A., and Robbins, T. W. (2008a). The neuropsychopharmacology of action inhibition: cross-species translation of the stop-signal and go/no-go tasks. *Psychopharmacology (Berl.)* 199, 439–456.
- Eagle, D. M., Baunez, C., Hutcheson, D. M., Lehmann, O., Shah, A. P., and Robbins, T. W. (2008b). Stop-signal reaction-time task performance: role of prefrontal cortex and subthalamic nucleus. *Cereb. Cortex* 18, 178–188.

- Eagle, D. M., and Baunez, C. (2010). Is there an inhibitory-response-control system in the rat? Evidence from anatomical and pharmacological studies of behavioral inhibition. *Neurosci. Biobehav. Rev.* 34, 50–72.
- Fimm, B., Heber, I. A., Coenen, V. A., Fromm, C., Noth, J., and Kronenburger, M. (2009). Deep brain stimulation of the subthalamic nucleus improves intrinsic alertness in Parkinson's disease. *Mov. Disord.* 24, 1613–1620.
- Frank, M. J., Samanta, J., Moustafa, A. A., and Sherman, S. J. (2007). Hold your horses: impulsivity, deep brain stimulation, and medication in parkinsonism. *Science* 318, 1309–1312.
- Groenewegen, H. J., and Berendse, H. W. (1990). Connections of the subthalamic nucleus with ventral striatopallidal parts of the basal ganglia in the rat. *J. Comp. Neurol.* 294, 607–622.
- Groenewegen, H. J., Berendse, H. W., and Haber, S. N. (1993). Organization of the output of the ventral striatopallidal system in the rat: ventral pallidal efferents. *Neuroscience* 57, 113–142.
- Gubellini, P., Salin, P., Kerkerian-LeGoff, L., and Baunez, C. (2009). Deep brain stimulation in neurological diseases and experimental models: from molecule to complex behavior. *Prog. Neurobiol.* 89, 79–123.
- Hershey, T., Campbell, M. C., Videen, T. O., Lugar, H. M., Weaver, P. M., Hartlein, J., Karimi, M., Tabbal, S. D., and Perlmuter, J. S. (2010). Mapping Go-No-Go performance within the subthalamic nucleus region. *Brain* 133, 3625–3634.
- Hershey, T., Revilla, F. J., Wernle, A. R., Gee-Minnich, L., Antenor, J. V., Videen, T. O., Dowling, J. L., Mink, J. W., and Perlmuter, J. S. (2003). Cortical and subcortical blood flow effects of subthalamic nucleus stimulation in PD. *Neurology* 61, 816–821.
- Knobel, D., Aybek, S., Pollo, C., Vingerhoets, F. J., and Berney, A. (2008). Rapid resolution of dopamine dysregulation syndrome (DDS) after subthalamic DBS for Parkinson disease (PD): a case report. *Cogn. Behav. Neurol.* 21, 187–189.
- Krack, P., Hariz, M. I., Baunez, C., Guridi, J., and Obeso, J. A. (2010). Deep brain stimulation: from neurology to psychiatry? 1. *Trends Neurosci.* 33, 474–484.
- Lardeux, S., and Baunez, C. (2008). Alcohol preference influences the subthalamic nucleus control on motivation for alcohol in rats. *Neuropsychopharmacology* 33, 634–642.
- Lardeux, S., Palleressompoulle, D., Pernaud, R., Cador, M., and Baunez, C. (2008). Selective encoding of natural reward versus cocaine by subthalamic nucleus neurons. *Abstr. Soc. Neurosci.* 34, 88.4.
- Lardeux, S., Pernaud, R., Palleressompoulle, D., and Baunez, C. (2009). Beyond the reward pathway: coding reward magnitude and error in the rat subthalamic nucleus. *J. Neurophysiol.* 102, 2526–2537.
- Le Jeune, F., Verin, M., N'Diaye, K., Drapier, D., Leray, E., du Montcel, S. T., Baup, N., Pelissolo, A., Polosan, M., Mallet, L., Yelnik, J., Devaux, B., Fontaine, D., Chereau, I., Bourguignon, A., Peron, J., Sauleau, P., Raoul, S., Garin, E., Krebs, M. O., Jaafari, N., and Millet, B. (2010). Decrease of prefrontal metabolism after subthalamic stimulation in obsessive-compulsive disorder: a positron emission tomography study. *Biol. Psychiatry* 68, 1016–1022.
- Lim, S. Y., O'Sullivan, S. S., Kotschet, K., Gallagher, D. A., Lacey, C., Lawrence, A. D., Lees, A. J., O'Sullivan, D. J., Peppard, R. F., Rodrigues, J. P., Schrag, A., Silberstein, P., Tisch, S., and Evans, A. H. (2009). Dopamine dysregulation syndrome, impulse control disorders and punting after deep brain stimulation surgery for Parkinson's disease. *J. Clin. Neurosci.* 16, 1148–1152.
- Limousin, P., Pollak, P., Benazzouz, A., Hoffmann, D., Le Bas, J. F., Broussole, E., Perret, J. E., and Benabid, A. L. (1995). Effect of parkinsonian signs and symptoms of bilateral subthalamic nucleus stimulation. *Lancet* 345, 91–95.
- Lindsley, D. F., Barton, R. J., and Atkins, R. J. (1970). Effects of subthalamic lesions on peripheral and central arousal thresholds in cats. *Exp. Neurol.* 26, 109–119.
- Mallet, L., Polosan, M., Jaafari, N., Baup, N., Welter, M. L., Fontaine, D., du Montcel, S. T., Yelnik, J., Chereau, I., Arbus, C., Raoul, S., Aouizerate, B., Damier, P., Chabardes, S., Czernecki, V., Ardouin, C., Krebs, M. O., Bardinet, E., Chaynes, P., Burbaud, P., Cornu, P., Derost, P., Bougerol, T., Bataille, B., Mattei, V., Dormont, D., Devaux, B., Verin, M., Houeto, J. L., Pollak, P., Benabid, A. L., Agid, Y., Krack, P., Millet, B., and Pelissolo, A. (2008). Subthalamic nucleus stimulation in severe obsessive-compulsive disorder. *N. Engl. J. Med.* 359, 2121–2134.
- Mallet, L., Schupbach, M., N'Diaye, K., Remy, P., Bardinet, E., Czernecki, V., Welter, M. L., Pelissolo, A., Ruberg, M., Agid, Y., and Yelnik, J. (2007). Stimulation of subterritories of the subthalamic nucleus reveals its role in the integration of the emotional and motor aspects of behavior. *Proc. Natl. Acad. Sci. U.S.A.* 104, 10661–10666.
- Matsumura, M., Kojima, J., Gardiner, T. W., and Hikosaka, O. (1992). Visual and oculomotor functions of monkey subthalamic nucleus. *J. Neurophysiol.* 67, 1615–1632.
- Maurice, N., Deniau, J. M., Glowinski, J., and Thierry, A. M. (1998a). Relationships between the prefrontal cortex and the basal ganglia in the rat: physiology of the corticostriatal circuits. *J. Neurosci.* 18, 9539–9546.
- Maurice, N., Deniau, J. M., Ménétreay, A., Glowinski, J., and Thierry, A. M. (1998b). Prefrontal cortex-basal ganglia circuits in the rat: involvement of ventral pallidum and subthalamic nucleus. *Synapse* 29, 363–370.
- Maurice, N., Deniau, J. M., Glowinski, J., and Thierry, A. M. (1999). Relationships between the prefrontal cortex and the basal ganglia in the rat: physiology of the corticostriatal circuits. *J. Neurosci.* 19, 4674–4681.
- Nambu, A., Tokuno, H., and Takada, M. (2002). Functional significance of the cortico-subthalamo-pallidal “hyperdirect” pathway. *Neurosci. Res.* 43, 111–117.
- Naquet, R., Denavit, M., and de Fessard, D. (1966). Comparison between the role of the subthalamus and that of the different bulbomesencephalic structures in the maintenance of wakefulness. *Electroencephalogr. Clin. Neurophysiol.* 20, 149–164.
- Phillips, J. M., and Brown, V. J. (1999). Reaction time performance following unilateral striatal dopamine depletion and lesions of the subthalamic nucleus in the rat. *Eur. J. Neurosci.* 11, 1003–1010.
- Robbins, T. W. (2002). The 5-choice serial reaction time task: behavioural pharmacology and functional neurochemistry. *Psychopharmacology (Berl.)* 163, 362–380.
- Rouaud, T., Lardeux, S., Panayotis, N., Palleressompoulle, D., Cador, M., and Baunez, C. (2010). Reducing the desire for cocaine with subthalamic nucleus deep brain stimulation. *Proc. Natl. Acad. Sci. U.S.A.* 107, 1196–1200.
- Rubia, K., Russell, T., Overmeyer, S., Brammer, M. J., Bullmore, E. T., Sharma, T., Simmons, A., Williams, S. C., Giampietro, V., Andrew, C. M., and Taylor, E. (2001). Mapping motor inhibition: conjunctive brain activations across different versions of go/no-go and stop tasks. *Neuroimage* 13, 250–261.
- Saint-Cyr, J. A., Trepanier, L. L., Kumar, R., Lozano, A. M., and Lang, A. E. (2000). Neuropsychological consequences of chronic bilateral stimulation of the subthalamic nucleus in Parkinson's disease. *Brain* 123(Pt 10), 2091–2108.
- Teagarden, M. A., and Rebec, G. V. (2007). Subthalamic and striatal neurons concurrently process motor, limbic, and associative information in rats performing an operant task. *J. Neurophysiol.* 97, 2042–2058.
- Temel, Y., Blokland, A., Steinbusch, H. W., and Visser-Vandewalle, V. (2005). The functional role of the subthalamic nucleus in cognitive and limbic circuits 2. *Prog. Neurobiol.* 76, 393–413.
- Tremblay, L., and Schultz, W. (1999). Relative reward preference in primate orbitofrontal cortex. *Nature* 398, 704–708.
- Trillet, M., Vighetto, A., Croisile, B., Charles, N., and Aimard, G. (1995). Hemiballismus with logorrhea and thymoaffective disinhibition caused by hematoma of the left subthalamic nucleus. *Rev. Neurol. (Paris)* 151, 416–419.
- Uslaner, J. M., Dell'Orco, J. M., Pevzner, A., and Robinson, T. E. (2008). The influence of subthalamic nucleus lesions on sign-tracking to stimuli paired with food and drug rewards: facilitation of incentive salience attribution? *Neuropsychopharmacology* 33, 2352–2361.
- Uslaner, J. M., and Robinson, T. E. (2006). Subthalamic nucleus lesions increase impulsive action and decrease impulsive choice – mediation by enhanced incentive motivation? *Eur. J. Neurosci.* 24, 2345–2354.
- Uslaner, J. M., Yang, P., and Robinson, T. E. (2005). Subthalamic nucleus lesions enhance the psychomotor-activating, incentive motivational, and neurobiological effects of cocaine 1. *J. Neurosci.* 25, 8407–8415.
- Winstanley, C. A., Baunez, C., Theobald, D. E., and Robbins, T. W. (2005). Lesions to the subthalamic nucleus decrease impulsive choice but impair autoshaping in rats: the importance of the basal ganglia in Pavlovian conditioning and impulse control. *Eur. J. Neurosci.* 21, 3107–3116.

- Witjas, T., Baunez, C., Henry, J. M., Delfini, M., Regis, J., Cherif, A. A., Peragut, J. C., and Azulay, J. P. (2005). Addiction in Parkinson's disease: impact of subthalamic nucleus deep brain stimulation. *Mov. Disord.* 20, 1052–1055.
- York, M. K., Dulay, M., Macias, A., Levin, H. S., Grossman, R., Simpson, R., and Jankovic, J. (2008). Cognitive declines following bilateral subthalamic nucleus deep brain stimulation for the treatment of Parkinson's disease. *J. Neurol. Neurosurg. Psychiatr.* 79, 789–795.
- Conflict of Interest Statement:** The authors declare that the research was conducted in the absence of any commercial or financial relationships that could be construed as a potential conflict of interest.
- Received: 22 April 2011; paper pending published: 25 July 2011; accepted: 21 September 2011; published online: 11 October 2011.
- Citation: Baunez C and Lardeux S (2011) Frontal cortex-like functions of the subthalamic nucleus. *Front. Syst. Neurosci.* 5:83. doi: 10.3389/fnsys.2011.00083
- Copyright © 2011 Baunez and Lardeux. This is an open-access article subject to a non-exclusive license between the authors and Frontiers Media SA, which permits use, distribution and reproduction in other forums, provided the original authors and source are credited and other Frontiers conditions are complied with.



Noradrenaline and Parkinson's disease

Claire Delaville^{1,2}, Philippe De Deurwaerdère^{1,2} and Abdelhamid Benazzouz^{1,2,3*}

¹ UMR5293, Institut des Maladies Neurodégénératives, Université de Bordeaux, Bordeaux, France

² UMR5293, Institut des Maladies Neurodégénératives, Centre National de la Recherche Scientifique, Bordeaux, France

³ Centre Hospitalier Universitaire, Bordeaux, France

Edited by:

Elizabeth Abercrombie, Rutgers-Newark: The State University of New Jersey, USA

Reviewed by:

Christine E. Collins, Vanderbilt University, USA
Alessandro Stefani, University of Rome, Italy

*Correspondence:

Abdelhamid Benazzouz, Institut des Maladies Neurodégénératives, Université Bordeaux Segalen, 146, rue Léo-Saignat, 33076 Bordeaux Cedex, France.
e-mail: abdelhamid.benazzouz@u-bordeaux2.fr

Parkinson's disease (PD) is characterized by the degeneration of dopamine (DA) neurons in the substantia nigra *pars compacta*, and motor symptoms including bradykinesia, rigidity, and tremor at rest. These symptoms are exhibited when striatal dopamine concentration has decreased by around 70%. In addition to motor deficits, PD is also characterized by the non-motor symptoms. However, depletion of DA alone in animal models has failed to simultaneously elicit both the motor and non-motor deficits of PD, possibly because the disease is a multi-system disorder that features a profound loss in other neurotransmitter systems. There is growing evidence that additional loss of noradrenaline (NA) neurons of the locus coeruleus, the principal source of NA in the brain, could be involved in the clinical expression of motor as well as in non-motor deficits. In the present review, we analyze the latest evidence for the implication of NA in the pathophysiology of PD obtained from animal models of parkinsonism and from parkinsonian patients. Recent studies have shown that NA depletion alone, or combined with DA depletion, results in motor as well as in non-motor dysfunctions. In addition, by using selective agonists and antagonists of noradrenaline alpha receptors we, and others, have shown that $\alpha 2$ receptors are implicated in the control of motor activity and that $\alpha 2$ receptor antagonists can improve PD motor symptoms as well as L-Dopa-induced dyskinesia. In this review we argue that the loss of NA neurons in PD has an impact on all PD symptoms and that the addition of NAergic agents to dopaminergic medication could be beneficial in the treatment of the disease.

Keywords: Parkinson's disease, motor and non-motor symptoms, noradrenaline, dopamine, locus coeruleus

INTRODUCTION

Parkinson's disease (PD) is a degenerative disorder of the central nervous system that impairs motor skills, cognitive processes, and other functions. Motor symptoms are characterized by tremor, rigidity, bradykinesia, and postural instability. Among non-motor symptoms are autonomic dysfunction, sensory and sleep difficulties, cognitive, and neurobehavioral problems, including dementia and depression. For example, depression occurs in approximately 45% of all PD patients and reduces patient's quality of life independently from motor symptoms (Lemke et al., 2004). These non-motor symptoms are common in the advanced stages of the disease.

Parkinson's disease is a non-hereditary disease of unknown etiology that usually appears after the age of 50 and affects both sexes equally (Jankovic and Talosa, 1988). It is well-known to be characterized by a progressive degeneration of dopaminergic (DAergic) neurons (70–75%) in the substantia nigra *pars compacta* (SNc), which results in a dopamine (DA) depletion in the striatum (Ehringer and Hornykiewicz, 1960). However, it is misleading to reduce PD to a malady of the SNc. Indeed, it has been repeatedly shown over the last 50 years that noradrenergic (NAergic) cells from the locus coeruleus (LC) also degenerate in the disease (Greenfield and Bosanquet, 1953; Ehringer and Hornykiewicz, 1960; German et al., 1992; Bertrand et al., 1997; Tohogi et al., 1997; Ehringer and Hornykiewicz, 1998). The neuronal loss in the LC is greater (83%) than in the SNc (78%; Zarow et al., 2003). This is in agreement with the Braak's theory (Braak and Del Tredici, 2008) that proposed a progressive caudo-rostral alteration of monoaminergic centers in

the symptomatology of PD with a degeneration of LC NAergic neurons occurring before that of SNc DAergic neurons. Several studies revealed the existence of a correlation between the severity of DA and noradrenaline (NA) depletions with the severity of PD neurological symptoms (Marie et al., 1995; Selikhova et al., 2002). While the DAergic system is the main target of the pharmacological approaches to PD, corrections of the NA alterations inherent to the disease could improve the efficacy of current therapies. In this review we focus on the implication of the LC NA system in the pathophysiology of PD and on the different therapeutic approaches using NAergic agents.

NORADRENERGIC SYSTEMS IN THE CENTRAL NERVOUS SYSTEM

THE NORADRENERGIC SYSTEM

Two main NAergic systems can be distinguished: one is composed of neurons belonging to the medulla oblongata (A1/C1 nucleus), whereas the other is more rostral (A2/C2 nucleus) and is located in the pons (Gaspar, 1994). The caudal NAergic system corresponds to diffuse groups of cells in the lower brainstem. The rostral NAergic system corresponds mainly to the locus coeruleus (LC, A6) located in the pons.

Noradrenaline release exerts potent neuromodulatory effects on synaptic transmission, changing the membrane potential, excitability of neurons and synaptic plasticity *via* adrenergic receptors (ARs). Two subtypes of ARs have been described: alpha ARs ($\alpha 1$ and $\alpha 2$) and beta ARs ($\beta 1$, $\beta 2$, and $\beta 3$). These ARs are found throughout

the brain including the striatum and substantia nigra. Different subtypes are coupled to different G proteins. In general, excitatory effects are mediated by $\alpha 1$ and β postsynaptic ARs (McCormick and Wang, 1991; McCormick et al., 1991; Arcos et al., 2003) and inhibitory effects by $\alpha 2$ presynaptic ARs (Belujon et al., 2007; Benarroch, 2009; Table 1).

THE LOCUS COERULEUS

The LC nucleus is present in all mammalian species and represents the main source of NA for the central nervous system (Mann, 1983; Aston-Jones, 2004). Synaptic inputs from several sources influence the activity of LC neurons. The LC NAergic system, via its widespread projections, modulates cortical, subcortical, and brainstem circuits. Due to the very small size of the LC, biochemical studies are unable to differentiate LC nucleus vs surrounding areas. A lot of

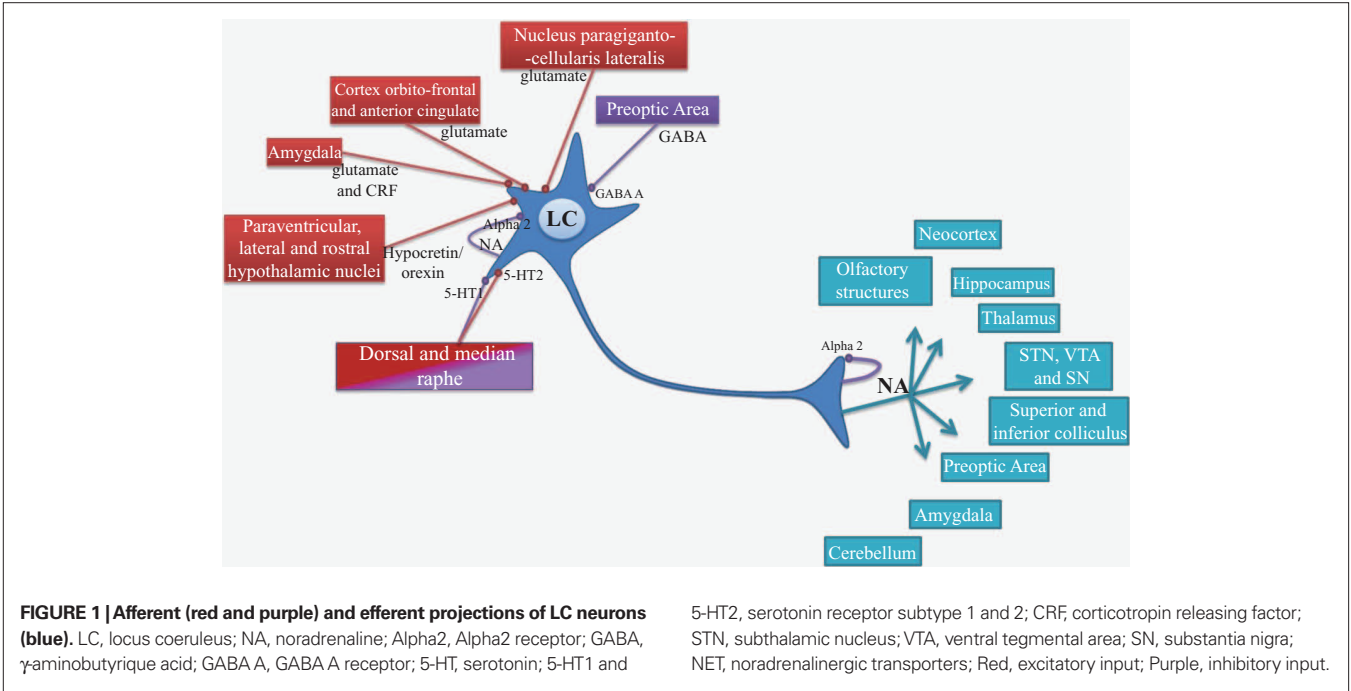
retrograde and anterograde tract tracing studies over the years, that have been well recapitulated by Aston-Jones (2004) and Benarroch (2009), have demonstrated the numerous afferent and efferent connections of LC neurons. These reviews document that the orbitofrontal and anterior cingulate cortices provide the main source of glutamatergic afferent drive to the LC. LC modulates a variety of central functions through the release of NA into several brain areas including neocortex, hippocampus, thalamus, subthalamic nucleus, and substantia nigra. These projections are only sparse in striatum and spinal cord. Figure 1 summarizes the major afferent and efferent projections of the LC.

The biochemistry of NA neurons has relevance to PD. Because L-Dopa, the metabolic precursor of DA, given to patients to enhance DA synthesis, is also a metabolic precursor of NA. In the normal condition, tyrosine hydroxylase (TH) catalyzes the conversion of

Table 1 | Adrenergic receptor characteristics.

Receptor subtypes	G protein	Distribution	Effects
Alpha 1	Gq	Postsynaptic throughout brain (including cortex, thalamus, STN, Striatum...)	↑ Excitability
Alpha 2	Gi/o	Presynaptic on NAergic and non-NAergic terminals	↓ Spontaneous firing and excitability; ↓ Neurotransmitter release
Beta 1	Gs	Postsynaptic in cerebral cortex, mainly expressed in the heart and the kidney	Adenylate cyclase activation; diffuse cellular response
Beta 2	Gs/Gi	Postsynaptic in cerebellum and cerebral cortex, hippocampus, midbrain..., mainly expressed in peripheral nervous system	Adenylate cyclase activation, resulting in an increase of cAMP; LTP facilitation
Beta 3	Gs	Adipose tissue	Adenylate cyclase activation; regulation of body weight

STN, subthalamic nucleus; LTP, long-term potentiation; cAMP, cyclic adenosine monophosphate.



the amino acid tyrosine to L-Dopa. Both normally produced and administered L-Dopa are catalyzed to DA by L-aromatic amino acid decarboxylase (AADC). DA beta-hydroxylase (DBH) synthesizes NA from DA in the cytosol and either the vesicular monoamine transporter (VMAT) moves the NA into vesicles ready for exocytotic release or monoamine oxidase A degrades the NA. Once released into the extracellular space, reuptake of NA is performed by the plasmalemmal noradrenaline transporter (Rascol et al., 2001), while extracellular NA also limits its own release through the stimulation of auto-inhibitory α_2 ARs (Figure 1). Of note, as reported in the cortex (Tanda et al., 1997), NET can also transport extracellular DA inside NAergic neurons.

The LC NAergic system contributes to long-term synaptic plasticity, pain modulation, energy homeostasis and control of local blood flow (McCormick, 1992). LC neurons fire in two distinct modes, tonic and phasic (Aston-Jones and Cohen, 2005a,b). Tonic activity is characterized by a sustained and highly regular pattern of discharge that is highest during wakefulness and decreases during slow-wave sleep. This tonic activity plays a central role in the sleep–waking cycle anticipating the fluctuations of electroencephalographic activity and promoting a state of vigilance. It is indeed well known that the stimulation of central NAergic receptors leads to changes in the state of vigilance. There is also a sustained increase in tonic discharge rate in response to environmental stimuli that elicit behavioral arousal and exploratory behavior. During focused attention and accurate task performance, LC neurons reduce their tonic firing to a moderate rate and respond phasically to task-relevant stimuli. The phasic bursts of LC activity are closely associated with highly accurate behavioral responses. Thus the LC nucleus has a major role in arousal, attention and stress response (Berridge and Waterhouse, 2003; Aston-Jones and Cohen, 2005a).

Alteration of the LC NAergic system has been implicated in many pathologies such as sleep and arousal disorders, attention deficit, hyperactivity disorder, post-traumatic stress disorder and psychiatric disorders, including anxiety, depression, schizophrenia, and mechanisms of opioid addiction (Benarroch, 2009). It constitutes a target for pharmacological treatment of these conditions (Aston-Jones, 2004; Rommelfanger and Weinshenker, 2007; Benarroch, 2009).

THE LOCUS COERULEUS NORADRENERGIC SYSTEM IN PD

Locus coeruleus is often severely affected in neurodegenerative diseases (Saper et al., 1991) and a growing number of anatomical and biochemical data has stressed this point in PD. In line with the drastic decrease in NAergic cell bodies (Chan-Palay and Asan, 1989), significant depletions (>80%) of NA concentration have also been reported in the PD brain (Taquet et al., 1982; Jenner et al., 1983; Gaspar et al., 1991). Consistently, Positron emission tomography (Dailly et al., 2006) studies have reported that [11 C] RTI-32, an *in vivo* marker of both DA transporter (DAT) and NET binding, was reduced in several regions including those poorly innervated by DAergic fibers (Marie et al., 1995; Remy et al., 2005). It has also been shown that NAergic synapses change size and shape of the pre- and postsynaptic components, polymorphism of the synaptic vesicles and marked morphological alterations of the mitochondria (Chan-Palay and Asan, 1989; Baloyannis et al., 2006). Cash et al. (1984, 1986) have reported an increase in

the density of α_1 and β_1 ARs in synaptosomal and microsomal fractions in the 6-hydroxydopamine (6-OHDA) rat model of PD (see below) as well as in the pre-frontal cortex of parkinsonian patients. The studies in animal models and PD patients suggest that the impairment of LC NAergic function could contribute to the motor and non-motor symptoms of PD.

THE LOCUS COERULEUS NORADRENERGIC SYSTEM IN ANIMAL MODELS OF PD

A variety of models have been developed over the years with the increase in understanding of PD. Most, if not all, animal models have focused on DA depletion because PD symptoms typically occur in humans when approximately 70–80% of DA tissue content in the striatum has been lost (Bezard et al., 2001; McNamara and Durso, 2006). The impairment of the NAergic system, also typical of the human disease, has been neglected for several years to the point that most rat models of the disease, generated by administration of the catecholaminergic neurotoxin 6-OHDA, incorporate the concomitant protection of NAergic neurons with the NET blocker desipramine (see below). The reasons that have led to ignoring the role of NAergic neurons in the disease could be related to the demonstration that NAergic neurons are not directly responsible for the behavioral effects of L-Dopa in animal models. Also, the striatum has been the main target of the anti-parkinsonian treatments, a brain region that is poorly innervated by NAergic fibers. Nonetheless, NAergic mechanisms may participate in the therapeutic outcome of L-Dopa (Fox et al., 2001) and NA may act in brain regions that may profoundly impact on the control of motor behaviors, including the subthalamic nucleus (Belujon et al., 2007). The few data available regarding the various animal models of PD support a non-negligible role of NA in the aberrant motor output consequent to DA depletion.

Non-human primate models of the disease have been developed after the discovery of a specific neurotoxin 1-methyl-4-phenyl-1,2,3,6-tetrahydropyridine (MPTP) able to induce parkinsonism in humans (Langston and Ballard, 1983). MPTP has been shown to produce parkinsonian motor deficits in the non-human primate that are similar to PD (Langston and Ballard, 1984). This model has been essential in the understanding of the pathophysiology of PD (Fox and Brotchie, 2010) and the development of new therapeutic approaches, such as the lesion or high frequency stimulation of the subthalamic nucleus (Bergman et al., 1990; Benazzouz et al., 1993, 1996). MPTP-treated rhesus monkeys mimicked the DAergic cell degeneration in the SNc and profound striatal DA depletion. However, the inter-regional pattern of striatal DA loss typically encountered in the idiopathic PD, i.e., a significantly greater depletion of DA in the putamen compared to the caudate nucleus, is not reproduced in this model (Pifl et al., 1991). It was originally reported that MPTP did not cause LC cell death in non-human primates. However, it has become clear that MPTP also causes a distinct and often severe cell loss in the LC and/or NE depletion in terminal fields (Javitch et al., 1984; Mitchell et al., 1985; Di Paolo et al., 1986; Forno et al., 1986; Miyoshi et al., 1988; Pifl et al., 1991). MPTP-treated monkeys developed typical parkinsonian signs of bradykinesia, tremor, and hypokinesia. Behavioral symptoms of PD could involve the concomitant loss of DAergic and NAergic neurons, rather than DAergic neurons alone.

1-Methyl-4-phenyl-1,2,3,6-tetrahydropyridine has been also used in mice. MPTP-treated mice with 80% loss of DA do not exhibit profound motor impairments (German et al., 1992; Marien et al., 2004; Archer and Fredriksson, 2006). The fact that MPTP treatment in mice has little to no effect on LC neurons or NA tissue content may explain the lack of motor deficits. In support of a role of NA in motor symptoms in PD, DBH^{-/-} mice display motor impairments associated with a hypodopaminergic state. These mice synthesize normal amounts of DA, but, in the absence of NA, the release of DA seems to be decreased (Rommelfanger and Weinshenker, 2007). This is consistent with data reporting the excitatory influence exerted by NA on DAergic neuron function (see below interaction between DA and NA). One important note is that DBH^{-/-} mice are supplemented with NA agonists and NA itself during development as DBH is necessary for development (Thomas et al., 1995). Taken together, these data suggest that the behavioral symptoms of PD appear to be correlated with a concomitant loss of DA and NA.

The reserpinized rat model (Colpaert, 1987) and the VMAT KO mice (VMAT^{-/-} mice; Taylor et al., 2009) also support an interaction between DAergic and NAergic systems in PD motor symptoms. Reserpine blocks the VMAT, leading to a rapid decrease in the release of monoamines. The cardinal signs of the disease including tremor, rigidity, and hypokinesia are induced by reserpine in rats. The order of occurrence and time course of these signs appear to resemble the natural history of the human disease (Colpaert, 1987; Taylor et al., 2009). Surprisingly, drugs that increase post-synaptic ARs activation or NA availability, but not DA modulation, are effective in reducing parkinsonian signs in reserpinized rats (Colpaert, 1987). These observations led to the proposal that adrenergic mechanisms in the brain may play an important role in modifying motor and non-motor signs. As VMAT is impaired in both the reserpinized rats and the VMAT^{-/-} mice models, the involvement of serotonin (5-HT) in these mechanisms cannot be excluded because VMAT is also involved in the reuptake of serotonin. Reserpine treatments and VMAT^{-/-} mice do not only result in SNc DAergic and LC NAergic systems depletions, they also induce an almost total depletion of DA and NA from the other catecholaminergic nuclei as well as 5-HT originating from the raphe nuclei. In PD, it is estimated that 40–60% of 5-HT neurons degenerate in some cases (Kish, 2003; Kish et al., 2008; Politis et al., 2010).

The 6-OHDA rat is probably the most popular model of PD. Different 6-OHDA models of PD have been developed in which the toxin has been injected into different parts of the nigrostriatal pathway to cause DAergic cell loss in the SNc, resulting in DA depletion in the striatum (Deumens et al., 2002). 6-OHDA can be injected directly into the SNc, the medial forebrain bundle (MFB) or the striatum. The first two modes of injection are used to develop severe lesions of DAergic neurons corresponding to an advanced stage of the disease, while striatal injection of 6-OHDA is used to produce partial DA cell loss corresponding to the early stage of the disease (Kirik et al., 1998; Yuan et al., 2005; Breit et al., 2007). Such models exhibit some motor disabilities related to sensorimotor degradation though freezing, hypokinesia and tremor are not present. In addition, the non-motor symptoms are not evident (Amalric et al., 1995; Olsson et al., 1995; Branchi et al., 2008). It is noteworthy that 6-OHDA lesion of DAergic neurons causes LC NAergic

neurons to be overactive with an irregular pattern of discharge (Wang et al., 2009), suggesting that their influence is magnified in DA-lesioned rats.

Noradrenaline depletion in the rodent by *N*-(2-chloroethyl)-*N*-ethyl-2-bromobenzylamine (DSP-4) is an approach commonly used to model human neuropsychiatric disorders in rodents. Even though the efficacy of DSP-4 in destroying NA fibers is region- and species-dependent (Dailly et al., 2006), convincing evidence indicates that DSP-4 is a neurotoxin that lesions NAergic terminals arising selectively from the LC (Fritschy and Grzanna, 1989; Grzanna et al., 1989; Fritschy and Grzanna, 1991). Concomitant to the data obtained in non-human primates and genetic mice models of PD (Pifl et al., 1991; Rommelfanger and Weinshenker, 2007), we have recently found that NA depletion alone induces severe motor deficits similar to those reported after 6-OHDA lesion (Delaville et al., 2010). In contrast to a 6-OHDA lesion (Deumens et al., 2002), the motor impairments consequent to NA depletion were not related to DAergic cell loss. Furthermore, the motor deficits reported in 6-OHDA-lesioned rats were not aggravated by the additional depletion of NA (Delaville et al., 2010). Another study has reported that denervation of LC NAergic terminals potentiated the 6-OHDA-induced partial DAergic neurodegeneration and akinesia only in rats treated with a D2 receptor antagonist, haloperidol (Srinivasan and Schmidt, 2003). Only a few studies have specifically addressed the non-motor symptoms of PD in animal models. Our recent data (Delaville et al., 2010) show that additional NA depletion in 6-OHDA-lesioned rats induced anxiety and fear behavior in the elevated plus maze, both being non-motor symptoms of PD. Recently, it has been reported that additional NA depletion impaired working memory in a manner similar to that observed after bilateral inactivation of LC suggesting that the NAergic system of the LC may play an important role in acquisition of spatial memory (Khakpour-Taleghani et al., 2009). Nevertheless, it has been reported that the deficits of spatial information processing in PD are solely a consequence of the striatal DAergic dysfunction (De Leonibus et al., 2007).

In conclusion, most animal models have focused on the motor symptoms related to the nigrostriatal DAergic system. A thorough examination of the data suggests that NAergic neuron dysfunction plays a non-negligible role in the motor and non-motor symptoms. The link between non-motor symptoms and the impairment of NAergic system has been also noted in humans.

INVOLVEMENT OF NA IN PD SYMPTOMS

Although it is relatively common to describe a variety of significant biochemical alterations in PD patients, it is more difficult to demonstrate for each neurotransmitter a specific role in the pathophysiology of the disease. This point could be addressed by careful post-mortem studies which should correlate a specific biochemical pattern observed in a given patient with his detailed clinical history. PET imaging studies demonstrate that it is possible to assess *in vivo* the neocortical monoamine terminal loss (including NA), and to elucidate its potential role in the complex cognitive and affective impairment in PD (Marie et al., 1995). This part of the review is focused on the most relevant studies investigating the role of NA depletion in specific motor and non-motor symptoms related to PD in human patients and associated with the above-mentioned animal models (Table 2).

Table 2 | Involvement of the LC in specific motor and non-motor symptoms of PD and their reference studies.

	Symptoms	References
Motor symptoms	Akinesia	Hornykiewicz (1975) ^H , Narabayashi et al. (1991) ^H , Bezard et al. (1999) ^M
	Freezing	Tohgi et al. (1990) ^H , Mizuno et al., (1994) ^H , Sandyk (1996) ^H , Ringendahl and Sierla (1997) ^H , Devos et al. (2010) ^H
	Locomotor activity	Narabayashi et al. (1991) ^H , Nishi et al. (1991) ^R , Hill and Brotchie (1999) ^R
	“On–off” phenomenon	Sandyk (1996) ^H
	Postural instability	Narabayashi et al. (1991) ^H , Grimbergen et al. (2009) ^H
	Tremor	Colpaert (1987) ^R , Wilbur et al. (1988) ^H , Yamazaki et al. (1979) ^R
Non-motor symptoms	Anxiety	Stein et al. (1990) ^H , Lauterbach et al. (2003) ^H
	Attention and vigilance	Stern et al. (1984) ^H , Mayeux et al. (1987) ^H , Bédard et al. (1998) ^H , Riekkinen et al. (1998) ^H
	Dementia	Mann and Yates (1983) ^H , Cash et al. (1987) ^H , Mayeux et al. (1987) ^H , Chan-Palay and Asan (1989) ^H
	Depression	Mayeux et al. (1986) ^H , Cummings (1992) ^H , Dooneief et al. (1992) ^H , Bader and Hell (1998) ^H , Kasper et al. (2000) ^H , Oertel et al. (2001) ^H , Schrag et al. (2001) ^H , Lemke (2002) ^H , Selikhova et al. (2002) ^H , Lemke et al. (2004) ^H , Yamamoto (2004) ^H , Remy et al. (2005) ^H

H, human studies; *M*, Monkey studies; *R*, Rat studies.

(a) Motor symptoms

Parkinson's disease presents a wider spectrum of motor symptoms when both DA and NA deficiency are combined (Narabayashi et al., 1991). α 2ARs agonism potentiates the anti-parkinsonian action of L-Dopa treatment (Hill and Brotchie, 1999). It is also suggested that alpha-adrenergic mechanisms and in particular α 2ARs, may be involved in reserpine-induced tremor and rigidity (Colpaert, 1987). In human, akathisia and pseudo-parkinsonian tremor are modulated by a NAergic pathway that projects from the LC to the limbic system (Wilbur et al., 1988); these symptoms are improved by an α 2ARs agonist or a β ARs antagonist (Wilbur et al., 1988). Several studies have also reported the involvement of the LC NA pathway in freezing (Mizuno et al., 1994; Sandyk, 1996; Ringendahl and Sierla, 1997; Devos et al., 2010), the “on–off” phenomenon (Sandyk, 1996), postural instability (Narabayashi et al., 1991), and akinesia (Hornykiewicz, 1975; Narabayashi et al., 1991).

(b) Non-motor symptoms

Improvements in medication to treat the motor symptoms have highlighted the non-motor symptoms, which represent one of the main concerns of preclinical and clinical studies (Chaudhuri and Odin, 2010). The non-motor symptoms may appear many years before the onset of the motor complications in PD (Lemke et al., 2004). Whilst we focus on potential DAergic sources of mental dysfunction in PD, the potential role of NAergic systems should be kept in mind as well. Indeed, specific loss of DAergic and NAergic innervation of the limbic system is associated with cognitive and neurobehavioral problems, including dementia (Cash et al., 1987), depression (Cummings, 1992; Remy et al., 2005), anxiety (Stein et al., 1990; Lauterbach et al., 2003), and attention deficits (Riekkinen et al., 1998).

In a rat model of early stage PD, striatal DAergic degeneration and NAergic alterations in prefrontal cortex may have caused emotional reactivity and anxiety (Tadaiesky et al., 2008). These findings

are consistent with data showing that, in naive rats, NAergic function regulates the responsiveness to environmental cues and anxiety behavior (Lapiz et al., 2001). In humans, it is also thought that the enhanced anxiety found in elderly people may be related to the loss of DAergic and NAergic innervations (Gareri et al., 2002).

One of the most devastating non-motor symptoms in PD is depression (Cummings, 1992; Bader and Hell, 1998; Oertel et al., 2001; Schrag et al., 2001; Lemke, 2002; Yamamoto, 2004; Remy et al., 2005). The incidence of depression is currently high in PD, reaching a prevalence of 40% in some studies (Mayeux et al., 1986; Dooneief et al., 1992). The reason for the high frequency of depression in PD is poorly understood but, even if in some patients a dopamine agonist (pramipexole) can improve this symptom (Bxarone et al., 2010), the combined depletion of the three monoaminergic systems may be an explanation. In the unilateral rat model of PD, we have found that the DA depletion combined with NA depletion induced by DSP-4 and 5-HT depletion induced by the tryptophane hydroxylase inhibitor parachlorophenylalanine reduced the sucrose consumption and enhanced the time of immobility in the Porsolt test (Delaville et al., 2010). Importantly, only the combined depletions of all three monoamine systems resulted in a depressive-like behavior. It has been reported in humans that the binding of [¹¹C]RTI-32 in the LC and in several regions of the limbic system including the anterior cingulate cortex, the amygdala, and the ventral striatum was inversely correlated with the degree of apathy and the intensity of depression in the patients (Remy et al., 2005). [¹¹C] RTI-32 is a ligand displaying similar affinities to DAT and NET but with far lower affinity for the 5-HTergic transporter (Carroll et al., 1995). Thus, it seems that the DAergic and NAergic innervations are involved in PD depression and might specifically play a role in apathy, which is a major feature of depression. A histological study has shown that LC neuron morphology is more severely altered in PD with depression than in PD without depression (Chan-Palay and Asan, 1989).

It has also been shown that LC cell loss correlates significantly with performance on reaction time tasks and continuous performance tasks that measure attention and vigilance (Stern et al., 1984;

Mayeux et al., 1987; Bedard et al., 1998; Riekkinen et al., 1998; McNamara and Durso, 2006). LC damage results in severe loss of cortical and limbic NAergic innervation with a 40–78% decrease in NA, its metabolites and related enzymes in PD. These changes are more marked in patients with dementia than in those without dementia (Cash et al., 1987; Mayeux et al., 1987).

EVIDENCE FOR THE INTERACTION BETWEEN NA AND DA IN PD

The concomitant loss of NA and DA could therefore promote aberrant motor and non-motor symptoms, suggesting that the two systems could interact in the brain. Only a few studies demonstrate the role of DA in NAergic modulation in PD. In addition to the increase in firing rate of LC NA neurons (Wang et al., 2009), an increase in the density of β ARs in the cerebral cortex, the forebrain, thalamic nuclei, the midbrain, the hippocampus, and the cerebellum has been reported in 6-OHDA rats with a selective DAergic neuron lesion (Johnson et al., 1989). In general, a decrease in DAergic neuron function seems to enhance NAergic system activity.

Although anatomical evidence for innervation of DA containing brain regions by NAergic fibers in the rat is scarce, functional studies suggest the existence of NAergic inputs that facilitate DAergic transmission (Jenner et al., 1983). Indeed, Ponzio et al. (1981) demonstrated that NAergic nerve terminals originating from the LC may be involved in regulating the functional activity of the DAergic nerve terminals both in the cerebral cortex and the striatum. This regulation appears to be excitatory in nature and is present early in development. These data are confirmed by pharmacological studies showing that α 1ARs antagonism may reduce the sensitivity of the mesolimbic DAergic system to pharmacological or environmental challenge (Davis et al., 1985; Snoddy and Tessel, 1985; Auclair et al., 2002). Since most antipsychotic drugs exhibit both D2 receptor and α 1ARs antagonist properties, they may alleviate psychosis not only through blockade of postsynaptic DAergic receptors, but also presynaptically on the mesolimbic DAergic system, through their α 1ARs antagonistic action (Mathe et al., 1996). Conversely, stimulation of α 2ARs and β 1ARs elevates DA extracellular levels in the striatum by acting at sites downstream of the DAergic neurons themselves (Chopin et al., 1999; Hudson et al., 1999). More specifically, β 1ARs and α 2ARs regulate the phosphorylation of DARPP-32, a phosphoprotein regulated by DAergic transmission, in neostriatal neurons. Gi protein activation by α 2ARs antagonizes Gs/PKA signaling mediated by D1 receptors and α 2ARs in striatonigral and striatopallidal neurons respectively, thereby enhancing D2 receptor/Gi signaling in striatopallidal neurons (Hara et al., 2010). Reches and Meiner (1992) did not report any change in striatal DA synthesis and release after lesions of the dorsal NA bundle (DNEB). It is therefore suggested that any possible effect of the LC on DA transmission in the striatum is not mediated by the DNEB.

In parallel, the LC NAergic system is thought to exert a neuroprotective influence on SNc DAergic neurons. The first hints that NA promotes DAergic neuron survival came from MPTP studies in non-human primates and mice (Mavridis et al., 1991; Fornai et al., 1996). These studies reported that the damage to nigrostriatal DAergic neurons induced by MPTP was potentiated by pre-treatment with DSP4. Rommelfanger et al. (2004) subsequently showed that either pharmacological or genetic blockade

of NET, which increases extracellular NA, also protects DAergic neurons from MPTP damage in mice. The mechanisms underlying the neuroprotective influence of NA are not clearly determined (Rommelfanger and Weinshenker, 2007).

THERAPEUTIC APPROACHES TARGETING THE NAERGIC SYSTEM

EFFECTS OF L-THREO-DOPS ON MOTOR AND NON-MOTOR SYMPTOMS

Treatment of PD has focused on supplementing DA levels indirectly through L-Dopa administration or on stimulating directly DAergic receptors with DA agonists. Despite the success of these therapies, certain features of PD fail to respond to treatment and even worsen with DA replacement therapy. Among these incapacitating refractory symptoms are apathy, depression, memory loss, akathisia, postural instability, and sudden transient freezing. Clinical and experimental evidence suggests that NA deficiency may be responsible for some of these PD symptoms (see above).

The DA replacement therapy with L-Dopa probably alters the activity of NAergic neurons. Indeed, L-Dopa may enter NAergic neurons to be decarboxylated to DA. Nishi et al. (1991) but not Hollister et al. (1979), have suggested that central NAergic terminals play a significant role in the increase of locomotor activity induced by L-Dopa administration in rats with striatal DA deficiency. Nevertheless, NAergic neurons do not release DA synthesized from L-Dopa as it has been reported that the total destruction of 5-HTergic neurons abolished the releasing effect of L-Dopa (Tanaka et al., 1999), even in brain regions receiving substantial amount of NAergic fibers (Navailles et al., 2010a,b). On the other hand, NAergic neurons could participate in the clearance of extracellular DA. Indeed, because NET is able to transport DA, NAergic fibers could modify the pattern of L-Dopa-induced DA release depending on the relative innervation of brain regions by NAergic neurons. Thus, in the striatum, it has been reported that desipramine enhanced L-Dopa-induced DA release (Arai et al., 2008), suggesting that the clearance could be higher in brain regions more densely innervated. Finally, one could expect an increase in NA tissue content and/or an increase in NA release induced by L-Dopa. The finding that the α 2AR antagonist idazoxan is efficient in reducing the dyskinesia induced by L-Dopa but not by the DA agonist apomorphine (Fox et al., 2001) in MPTP-treated monkeys supports a change in NAergic neuron function induced by L-Dopa.

L-Threo-dihydroxyphenylserine (L-threo-DOPS), an non-natural NAergic precursor, has been shown to be effective in relieving motor and non-motor symptoms of PD (Kuno, 1997). Indeed, in the rat, the duration of harmaline induced tremor was significantly reduced by intraventricular administration of L-threo-DOPS (Yamazaki et al., 1979). In PD patients, Ogawa et al. (1984, 1985) have shown that 10 days treatment with L-threo-DOPS substantially improved patient's freezing episodes, rigidity, and dysarthria. Narabayashi et al. (1991) have reported that treatment with L-threo-DOPS, in combination with a peripheral AADC inhibitor, may have profound effects on freezing phenomena in patients with PD (Tohgi et al., 1990; Tohgi et al., 1993). Other aspects of akinesia also improved considerably in a majority of these patients (Yamamoto et al., 1986), although rigidity and tremor were barely affected (Jenner et al., 1983). When L-threo-DOPS

treatment was stopped, the freezing returned to almost the former level, even though the patients continued to receive L-Dopa and benserazide. This could be explained by the fact that L-Dopa measurably affects NA content in the cerebrospinal fluid compared to L-threo-DOPS treatment (Maruyama et al., 1996). In addition to the improvement of motor symptoms, psychological symptoms have also been improved by L-threo-DOPS (Suzuki et al., 1984; Azuma et al., 1991).

EFFECTS OF NAERGIC RECEPTOR MODULATION ON MOTOR AND NON-MOTOR SYMPTOMS

α 2ARs are distributed widely within the basal ganglia, including the substantia nigra (Schapira, 2005). Mavridis et al. (1991) have suggested that the activation of α 1ARs, which results in an increase in NAergic tone, facilitates locomotor activity, and inversely, α 2ARs activation, by decreasing NAergic tone, inhibits locomotor activity. In PD, hypoactivation of NAergic tone may be involved in the manifestation of tremor and rigidity. In the reserpine rat, yohimbine, an α 2ARs antagonist blocked tremor and improved rigidity but not hypokinesia (Colpaert, 1987).

In the 6-OHDA rat and MPTP monkey models of PD, blockade of α 2ARs by idazoxan improved motor disabilities (Bezard et al., 1999; Belujon et al., 2007) in a manner comparable to that induced by a minimal dose of L-Dopa (Bezard et al., 1999). Although these findings provide support for the therapeutic potential of α 2ARs in the treatment of PD, idazoxan as a monotherapy in PD patients did not display anti-parkinsonian actions (Henry et al., 1999; Rascol et al., 2001; Colosimo and Craus, 2003). However, co-administration of idazoxan with L-Dopa can provide an anti-parkinsonian action lasting more than twice the duration obtained with L-Dopa alone. Interestingly, the α 2AR agonist clonidine and β ARs blockers like propranolol are effective in treating akathisia and tardive dyskinesia (Wilbur et al., 1988). However, clonidine is more often used to treat attention deficit in PD. Attention accuracy was not affected by withdrawal of DAergic drugs in mild or severe PD patients. Clonidine retarded accuracy of performance in a difficult attention test in PD patients (Riekkinen et al., 1998). It seems that the NAergic system via α 2AR may act differentially on the manifestation of motor and non-motor symptoms in PD. α 2AR antagonism would lead to motor amelioration whereas α 2ARs agonism would have non-motor benefits.

Non-motor symptoms are also improved by the use of selective α 1AR agonists. For example, naphthoxazine may improve performance in some cognitive tests of "frontal functions," including the Stroop and the odd-man-out tests, which have been previously found to be affected in PD (Bedard et al., 1998). This drug reduced the percentage of errors and restored the lateralization of N100 during the shifting reaction time task, suggesting that it may act on the processes underlying the shifting deficit in these patients (Bedard et al., 1998). NAergic compounds could also be efficient in depression in PD. Reboxetine, a specific NET inhibitor, significantly improved depression scores (Lemke, 2002). This agent did not significantly change parkinsonian motor symptoms or dosage of L-Dopa. Reboxetine was effective and well tolerated in PD patients receiving 4 weeks of treatment of moderate-to-severe depression. Recently, however, the other NET inhibitor atomoxetine failed to reduce depression in PD patients (Weintraub et al., 2010).

The use of selective NET inhibitors may be critically dependent on the status of NA neurons which, as mentioned above, can be severely damaged.

There are good theoretical and clinical reasons, including pharmacological specificity of effects and low incidence of side effects, to consider reboxetine, idazoxan, clonidine, or naphthoxazine for the treatment of different symptoms in different cases of PD. The efficacy of some of these drugs including the selective NET inhibitors would, however, be critically dependent on the status of LC NAergic fibers. Finally, the wide spectrum of pathophysiological conditions found in the human disease is still not directly addressed in animal models. The predictive efficacy of NAergic compounds in the treatment of non-motor symptoms in PD may require the development of better behavioral tests in animal models.

EFFECTS OF NAERGIC AGENTS ON L-DOPA INDUCED DYSKINESIA

The side effects associated with long-term L-Dopa treatment today constitute an important cause of functional disability. Side effects such as abnormal involuntary movements and psychiatric disorders remain difficult to manage without causing an increase in parkinsonian immobility. Moreover, management of the phenomenon of the "off" period is limited by these same side effects. The causes of L-Dopa-induced dyskinesia are unclear. It probably involves non-physiological pulsatile stimulation of DAergic receptors or non-physiological release of DA (e.g., from 5-HTergic nerve terminals) in the striatum (Tanaka et al., 1999; Carta et al., 2007; Navailles et al., 2010b). Treatments targeting non-DAergic neurotransmitter systems including glutamate, GABA, NA, acetylcholine, 5-HT, adenosine, and cholecystokinin have been studied (Colosimo and Craus, 2003). It has been recently proposed that lesion of the LC is correlated with the onset of L-Dopa-induced dyskinesia (Fornai et al., 2007). In the 6-OHDA rat model, lesioned rats showed a sensitization-desensitization turning response, whereas in 6-OHDA rats with an additional NAergic degeneration induced by DSP-4, the turning activity was maximal throughout the test. Double-lesioned rats exhibited a lower percentage of dose failure episodes during treatment. NAergic denervation appears to be associated with prolonged long-term DAergic sensitization.

This type of response appears to be comparable to that reported in the clinical setting with intermittent L-Dopa administration where no desensitization occurs once the abnormal response is established (Ruckert et al., 1997; Perez et al., 2009a,b). Fulceri et al. (2007) also demonstrated that unilateral damage to the NAergic system precedes the onset of dyskinesia and worsens the severity of L-Dopa-induced contralateral abnormal involuntary movements in hemi-parkinsonian rats. Furthermore, increases in locomotor activity after L-Dopa administration were markedly suppressed in DA and NA deficient groups. This may suggest that additional NAergic denervation selectively decreases the motor response to L-Dopa treatment (Nishi et al., 1991; Mizuno et al., 1994; Perez et al., 2007).

In view of these results, NAergic modulation has been considered to decrease L-Dopa side effects. In 6-OHDA rats, the α 2AR antagonist atipamezole and the α 2AR agonist dexmedetomidine increased and decreased contralateral circling evoked by L-Dopa respectively. Atipamezole also prolonged the duration of action of L-Dopa. The α 1AR antagonist prazosin partially antagonized

the effect of L-Dopa and had a strong inhibitory effect on the atipamezole-induced potentiation of the L-Dopa response (Haapalinna et al., 2003; Yavich et al., 2003). This suggests that atipamezole can modulate motor function indirectly, by stimulating the release of NA and directly, by blocking postsynaptic α 2ARs in neurons other than NAergic ones.

In MPTP-treated monkeys, blockade of α 2ARs by idazoxan in combination with L-Dopa did not impair the anti-parkinsonian response but significantly reduced dyskinesias and delayed their onset, so that the "on" state without dyskinesias was prolonged. The antidyskinetic effect of idazoxan was maintained when repeatedly administered for 10 days and the locomotor response to L-Dopa was significantly increased by chronic administration of idazoxan (Henry et al., 1999; Grondin et al., 2000; Fox et al., 2001). The same antidyskinetic effect has been shown with the α 2ARs antagonists yohimbine, rauwolscine, and fipamezole (Gomez-Mancilla and Bedard, 1993; Henry et al., 1999; Grondin et al., 2000; Savola et al., 2003; Fox and Brotchie, 2010). In the case of idazoxan and fipamezole, an extension of the duration of action of levodopa was also observed. All these antagonists had no effect on their own on DA overflow (Yavich et al., 2003). On the other hand, the α 2ARs agonist clonidine and the β ARs antagonist propranolol markedly reduced the dyskinetic movements induced by L-Dopa at the cost of a return to parkinsonism (Gomez-Mancilla and Bedard, 1993). Another study in the MPTP-lesioned primate has shown that idazoxan significantly reduced L-Dopa-induced dyskinesia, suggesting that α 2ARs stimulation may be involved in the generation of L-Dopa-induced dyskinesia (Fox et al., 2001; Bara-Jimenez et al., 2004).

In humans, however, neither idazoxan nor fipamezole had any effect on duration of on time. These drugs have shown variable benefits in clinical trials (Rascol et al., 1994). The poor efficacy could be explained by the dose used in the different studies. In the MPTP primate model, a significant effect of idazoxan on dyskinesia was

observed over a range of doses from 1 to 10 mg/kg whereas much lower doses were used in human studies (approximately 0.25–1.0 mg/kg). Similarly, the maximal efficacy of fipamezole in reducing L-Dopa-induced dyskinesia in humans was low compared to that reported in the monkey. It is not clear whether the doses and routes employed of either drug might provide equivalent plasma or brain drug levels across the two species. Side effects with α 2ARs antagonists used in human studies included hypertension, facial flushing, and headache which could be inherent to α 2ARs blockade. These side effects were dose-dependent and doses higher than 20 mg were not well tolerated (Fox and Brotchie, 2010). However, other α 2ARs antagonists could be developed. For example, it has been shown in rats that atipamezole had no effect on blood pressure (Haapalinna et al., 2003). Further studies are warranted to confirm the potential benefit of α 2ARs antagonists in L-Dopa-induced dyskinesia.

CONCLUDING REMARKS

Studies in a variety of models and species indicate that NAergic cell loss in the LC could be a conditioning factor for the natural history of PD. LC NA exerts an excitatory drive on the nigrostriatal DAergic system. The use of therapeutic strategies leading to an increase in NA in the brain of PD patients may have a specific place in the treatment of the disease. Pharmacological modulation of the NAergic system, specifically with α 2-AR antagonists, perhaps by inhibiting autoreceptor function, could be important in the treatment of different symptoms of PD and of L-Dopa-induced dyskinesia.

ACKNOWLEDGMENTS

Claire Delaville was supported by a fellowship from the Ministère de l'Éducation Nationale, de la Recherche et de la Technologie (MENRT). The University Bordeaux Segalen and the Centre National de la Recherche Scientifique (CNRS) funded this study. We wish to thank Dr. Martin Guthrie for English reading of the manuscript.

REFERENCES

- Amalric, M., Moukhles, H., Nieoullon, A., and Daszuta, A. (1995). Complex deficits on reaction time performance following bilateral intrastriatal 6-OHDA infusion in the rat. *Eur. J. Neurosci.* 7, 972–980.
- Arai, A., Tomiyama, M., Kannari, K., Kimura, T., Suzuki, C., Watanabe, M., Kawarabayashi, T., Shen, H., and Shoji, M. (2008). Reuptake of L-DOPA-derived extracellular DA in the striatum of a rodent model of Parkinson's disease via norepinephrine transporter. *Synapse* 62, 632–635.
- Archer, T., and Fredriksson, A. (2006). Influence of noradrenaline denervation on MPTP-induced deficits in mice. *J. Neural Transm.* 113, 1119–1129.
- Arcos, D., Sierra, A., Nunez, A., Flores, G., Aceves, J., and Arias-Montano, J. A. (2003). Noradrenaline increases the firing rate of a subpopulation of rat subthalamic neurones through the activation of alpha 1-adrenoceptors. *Neuropharmacology* 45, 1070–1079.
- Aston-Jones, G. (2004). "Locus coeruleus, A5 and A7 noradrenergic cell groups," in *The Rat Nervous System*, 3rd Edn, ed G. Paxinos (New York: Elsevier), 259–284.
- Aston-Jones, G., and Cohen, J. D. (2005a). Adaptive gain and the role of the locus coeruleus-norepinephrine system in optimal performance. *J. Comp. Neurol.* 493, 99–110.
- Aston-Jones, G., and Cohen, J. D. (2005b). An integrative theory of locus coeruleus-norepinephrine function: adaptive gain and optimal performance. *Annu. Rev. Neurosci.* 28, 403–450.
- Auclair, A., Cotecchia, S., Glowinski, J., and Tassin, J. P. (2002). D-amphetamine fails to increase extracellular dopamine levels in mice lacking alpha 1b-adrenergic receptors: relationship between functional and nonfunctional dopamine release. *J. Neurosci.* 22, 9150–9154.
- Azuma, T., Suzuki, T., Sakoda, S., Mizuno, R., Tsujino, S., Kobayashi, T., Kishimoto, S., Hiraga, T., Matsubara, T., Yoshida, S., and Tone, K. (1991). Effect of long-term L-threo-3, 4-dihydroxyphenylserine administration on alpha 2-adrenergic receptors in platelet membranes in neurologic disorders. *Acta Neurol. Scand.* 84, 46–50.
- Bader, J. P., and Hell, D. (1998). [Parkinson syndrome and depression]. *Fortschr. Neurol. Psychiatr.* 66, 303–312.
- Baloyannis, S. J., Costa, V., and Baloyannis, I. S. (2006). Morphological alterations of the synapses in the locus coeruleus in Parkinson's disease. *J. Neurol. Sci.* 248, 35–41.
- Bara-Jimenez, W., Dimitrova, T., Sherzai, A., Favit, A., Mouradian, M. M., and Chase, T. N. (2004). Effect of monoamine reuptake inhibitor NS 2330 in advanced Parkinson's disease. *Mov. Disord.* 19, 1183–1186.
- Bedard, M. A., el Massioui, F., Malapani, C., Dubois, B., Pillon, B., Renault, B., and Agid, Y. (1998). Attentional deficits in Parkinson's disease: partial reversibility with naphthoxazine (SDZ NVI-085), a selective noradrenergic alpha 1 agonist. *Clin. Neuropharmacol.* 21, 108–117.
- Belujon, P., Bezard, E., Taupignon, A., Bioulac, B., and Benazzouz, A. (2007). Noradrenergic modulation of subthalamic nucleus activity: behavioral and electrophysiological evidence in intact and 6-hydroxy-dopamine-lesioned rats. *J. Neurosci.* 27, 9595–9606.
- Benarroch, E. E. (2009). The locus ceruleus norepinephrine system: functional organization and potential clinical significance. *Neurology* 73, 1699–1704.
- Benazzouz, A., Boraud, T., Feger, J., Burbard, P., Bioulac, B., and Gross, C. (1996). Alleviation of experimental hemiparkinsonism by high-frequency stimulation of the subthalamic nucleus in primates: a comparison with L-Dopa treatment. *Mov. Disord.* 11, 627–632.

- Benazzouz, A., Gross, C., Feger, J., Boraud, T., and Bioulac, B. (1993). Reversal of rigidity and improvement in motor performance by subthalamic high-frequency stimulation in MPTP-treated monkeys. *Eur. J. Neurosci.* 5, 382–389.
- Bergman, H., Wichmann, T., and DeLong, M. R. (1990). Reversal of experimental parkinsonism by lesions of the subthalamic nucleus. *Science* 249, 1436–1438.
- Berridge, C. W., and Waterhouse, B. D. (2003). The locus coeruleus-noradrenergic system: modulation of behavioral state and state-dependent cognitive processes. *Brain Res. Brain Res. Rev.* 42, 33–84.
- Bertrand, E., Lechowicz, W., Szpak, G. M., and Dymecki, J. (1997). Qualitative and quantitative analysis of locus coeruleus neurons in Parkinson's disease. *Folia Neuropathol.* 35, 80–86.
- Bezard, E., Brefel, C., Tison, F., Peyro-Saint-Paul, H., Ladure, P., Rascol, O., and Gross, C. E. (1999). Effect of the alpha 2 adrenoceptor antagonist, idazoxan, on motor disabilities in MPTP-treated monkey. *Prog. Neuropsychopharmacol. Biol. Psychiatry* 23, 1237–1246.
- Bezard, E., Dovero, S., Prunier, C., Ravenscroft, P., Chalou, S., Guilleateau, D., Crossman, A. R., Bioulac, B., Brochie, J. M., and Gross, C. E. (2001). Relationship between the appearance of symptoms and the level of nigrostriatal degeneration in a progressive 1-methyl-4-phenyl-1,2,3,6-tetrahydropyridine-lesioned macaque model of Parkinson's disease. *J. Neurosci.* 21, 6853–6861.
- Braak, H., and Del Tredici, K. (2008). Invited article: nervous system pathology in sporadic Parkinson disease. *Neurology* 70, 1916–1925.
- Branchi, I., D'Andrea, I., Armida, M., Cassano, T., Pezzola, A., Potenza, R. L., Morgese, M. G., Popoli, P., and Alleva, E. (2008). Nonmotor symptoms in Parkinson's disease: investigating early-phase onset of behavioral dysfunction in the 6-hydroxydopamine-lesioned rat model. *J. Neurosci. Res.* 86, 2050–2061.
- Breit, S., Bouali-Benazzouz, R., Popa, R. C., Gasser, T., Benabid, A. L., and Benazzouz, A. (2007). Effects of 6-hydroxydopamine-induced severe or partial lesion of the nigrostriatal pathway on the neuronal activity of pallido-subthalamic network in the rat. *Exp. Neurol.* 205, 36–47.
- Bxarone, P., Poewe, W., Albrecht, S., Debieuvre, C., Massey, D., Rascol, O., Tolosa, E., and Weintraub, D. (2010). Pramipexole for the treatment of depressive symptoms in patients with Parkinson's disease: a randomised, double-blind, placebo-controlled trial. *Lancet Neurol.* 9, 573–580.
- Carroll, F. I., Scheffel, U., Dannals, R. F., Boja, J. W., and Kuhar, M. J. (1995). Development of imaging agents for the dopamine transporter. *Med. Res. Rev.* 15, 419–444.
- Carta, M., Carlsson, T., Kirik, D., and Bjorklund, A. (2007). Dopamine released from 5-HT terminals is the cause of L-DOPA-induced dyskinesia in parkinsonian rats. *Brain* 130, 1819–1833.
- Cash, R., Dennis, T., L'Heureux, R., Raisman, R., Javoy-Agid, F., and Scatton, B. (1987). Parkinson's disease and dementia: norepinephrine and dopamine in locus coeruleus. *Neurology* 37, 42–46.
- Cash, R., Raisman, R., Lanfumey, L., Ploska, A., and Agid, Y. (1986). Cellular localization of adrenergic receptors in rat and human brain. *Brain Res.* 370, 127–135.
- Cash, R., Ruberg, M., Raisman, R., and Agid, Y. (1984). Adrenergic receptors in Parkinson's disease. *Brain Res.* 322, 269–275.
- Chan-Palay, V., and Asan, E. (1989). Alterations in catecholamine neurons of the locus coeruleus in senile dementia of the Alzheimer type and in Parkinson's disease with and without dementia and depression. *J. Comp. Neurol.* 287, 373–392.
- Chaudhuri, K. R., and Odin, P. (2010). The challenge of non-motor symptoms in Parkinson's disease. *Prog. Brain Res.* 184, 325–341.
- Chopin, P., Colpaert, F. C., and Marien, M. (1999). Effects of alpha-2 adrenoceptor agonists and antagonists on circling behavior in rats with unilateral 6-hydroxydopamine lesions of the nigrostriatal pathway. *J. Pharmacol. Exp. Ther.* 288, 798–804.
- Colosimo, C., and Craus, A. (2003). Noradrenergic drugs for levodopa-induced dyskinesia. *Clin. Neuropharmacol.* 26, 299–305.
- Colpaert, F. C. (1987). Pharmacological characteristics of tremor, rigidity and hypokinesia induced by reserpine in rat. *Neuropharmacology* 26, 1431–1440.
- Cummings, J. L. (1992). Depression and Parkinson's disease: a review. *Am. J. Psychiatry* 149, 443–454.
- Dailly, E., Chenu, F., Petit-Demouliere, B., and Bourin, M. (2006). Specificity and efficacy of noradrenaline, serotonin depletion in discrete brain areas of Swiss mice by neurotoxins. *J. Neurosci. Methods* 150, 111–115.
- Davis, M., Kehne, J. H., and Commissaris, R. L. (1985). Antagonism of apomorphine-enhanced startle by alpha 1-adrenergic antagonists. *Eur. J. Pharmacol.* 108, 233–241.
- Delaville, C., Chetrit, J., Abdallah, K., Morin, S., Cardoit, L., De Deurwaerdere, P., and Benazzouz, A. (2010). Involvement of monoamine deficiency in motor and nonmotor disabilities of Parkinson's disease: behavioural, biochemical and electrophysiological studies (Int. Basal Ganglia Soc. Abstr.).
- De Leonibus, E., Pascucci, T., Lopez, S., Oliverio, A., Amalric, M., and Mele, A. (2007). Spatial deficits in a mouse model of Parkinson disease. *Psychopharmacology (Berl.)* 194, 517–525.
- Deumens, R., Blokland, A., and Prickaerts, J. (2002). Modeling Parkinson's disease in rats: an evaluation of 6-OHDA lesions of the nigrostriatal pathway. *Exp. Neurol.* 175, 303–317.
- Devos, D., Defebvre, L., and Bordet, R. (2010). Dopaminergic and non-dopaminergic pharmacological hypotheses for gait disorders in Parkinson's disease. *Fundam. Clin. Pharmacol.* 24, 407–421.
- Di Paolo, T., Bedard, P., Daigle, M., and Boucher, R. (1986). Long-term effects of MPTP on central and peripheral catecholamine and indoleamine concentrations in monkeys. *Brain Res.* 379, 286–293.
- Dooneief, G., Mirabello, E., Bell, K., Marder, K., Stern, Y., and Mayeux, R. (1992). An estimate of the incidence of depression in idiopathic Parkinson's disease. *Arch. Neurol.* 49, 305–307.
- Ehringer, H., and Hornykiewicz, O. (1960). [Distribution of noradrenaline and dopamine (3-hydroxytyramine) in the human brain and their behavior in diseases of the extrapyramidal system]. *Klin. Wochenschr.* 38, 1236–1239.
- Ehringer, H., and Hornykiewicz, O. (1998). Distribution of noradrenaline and dopamine (3-hydroxytyramine) in the human brain and their behavior in diseases of the extrapyramidal system. *Parkinsonism Relat. Disord.* 4, 53–57.
- Fornai, F., di Poggio, A. B., Pellegrini, A., Ruggieri, S., and Paparelli, A. (2007). Noradrenaline in Parkinson's disease: from disease progression to current therapeutics. *Curr. Med. Chem.* 14, 2330–2334.
- Fornai, F., Vaglini, F., Maggio, R., Bonuccelli, U., and Corsini, G. U. (1996). Excitatory amino acids and MPTP toxicity. *Adv. Neurol.* 69, 167–176.
- Forno, L. S., Langston, J. W., DeLanney, L. E., Irwin, I., and Ricaurte, G. A. (1986). Locus coeruleus lesions and eosinophilic inclusions in MPTP-treated monkeys. *Ann. Neurol.* 20, 449–455.
- Fox, S. H., and Brochie, J. M. (2010). The MPTP-lesioned non-human primate models of Parkinson's disease. Past, present, and future. *Prog. Brain Res.* 184, 133–157.
- Fox, S. H., Henry, B., Hill, M. P., Peggs, D., Crossman, A. R., and Brochie, J. M. (2001). Neural mechanisms underlying peak-dose dyskinesia induced by levodopa and apomorphine are distinct: evidence from the effects of the alpha(2) adrenoceptor antagonist idazoxan. *Mov. Disord.* 16, 642–650.
- Fritschy, J. M., and Grzanna, R. (1989). Immunohistochemical analysis of the neurotoxic effects of DSP-4 identifies two populations of noradrenergic axon terminals. *Neuroscience* 30, 181–197.
- Fritschy, J. M., and Grzanna, R. (1991). Selective effects of DSP-4 on locus coeruleus axons: are there pharmacologically different types of noradrenergic axons in the central nervous system? *Prog. Brain Res.* 88, 257–268.
- Fulceri, F., Biagioni, F., Ferrucci, M., Lazzeri, G., Bartalucci, A., Galli, V., Ruggieri, S., Paparelli, A., and Fornai, F. (2007). Abnormal involuntary movements (AIMs) following pulsatile dopaminergic stimulation: severe deterioration and morphological correlates following the loss of locus coeruleus neurons. *Brain Res.* 1135, 219–229.
- Gareri, P., De Fazio, P., and De Sarro, G. (2002). Neuropharmacology of depression in aging and age-related diseases. *Ageing Res. Rev.* 1, 113–134.
- Gaspar, P. (1994). *Anatomy of the Noradrenergic Pathways in the Primate Brain Alteration in Parkinson's Disease*. Boca Raton: CRC Press, 73–88.
- Gaspar, P., Duyckaerts, C., Alvarez, C., Javoy-Agid, F., and Berger, B. (1991). Alterations of dopaminergic and noradrenergic innervations in motor cortex in Parkinson's disease. *Ann. Neurol.* 30, 365–374.
- German, D. C., Manaye, K. F., White, C. L. III, Woodward, D. J., McIntire, D. D., Smith, W. K., Kalaria, R. N., and Mann, D. M. (1992). Disease-specific patterns of locus coeruleus cell loss. *Ann. Neurol.* 32, 667–676.
- Gomez-Mancilla, B., and Bedard, P. J. (1993). Effect of nondopaminergic drugs on L-dopa-induced dyskinesias in MPTP-treated monkeys. *Clin. Neuropharmacol.* 16, 418–427.
- Greenfield, J. G., and Bosanquet, F. D. (1953). The brain-stem lesions in Parkinsonism. *J. Neurol. Neurosurg. Psychiatr.* 16, 213–226.
- Grimbergen, Y. A., Langston, J. W., Roos, R. A., and Bloem, B. R. (2009). Postural instability in Parkinson's disease: the adrenergic hypothesis and the locus coeruleus. *Expert Rev. Neurother.* 9, 279–290.
- Grondin, R., Hadj Tahar, A., Doan, V. D., Ladure, P., and Bedard, P. J. (2000). Noradrenoceptor antagonism

- with idazoxan improves L-dopa-induced dyskinesias in MPTP monkeys. *Naunyn Schmiedeberg's Arch. Pharmacol.* 361, 181–186.
- Grzanna, R., Berger, U., Fritschy, J. M., and Geffard, M. (1989). Acute action of DSP-4 on central norepinephrine axons: biochemical and immunohistochemical evidence for differential effects. *J. Histochem. Cytochem.* 37, 1435–1442.
- Haapalinna, A., Leino, T., and Heinonen, E. (2003). The alpha 2-adrenoceptor antagonist atipamezole potentiates anti-Parkinsonian effects and can reduce the adverse cardiovascular effects of dopaminergic drugs in rats. *Naunyn Schmiedeberg's Arch. Pharmacol.* 368, 342–351.
- Hara, M., Fukui, R., Hieda, E., Kuroiwa, M., Bateup, H. S., Kano, T., Greengard, P., and Nishi, A. (2010). Role of adrenoceptors in the regulation of dopamine/DARPP-32 signaling in neostriatal neurons. *J. Neurochem.* 113, 1046–1059.
- Henry, B., Fox, S. H., Peggs, D., Crossman, A. R., and Brotchie, J. M. (1999). The alpha2-adrenergic receptor antagonist idazoxan reduces dyskinesia and enhances anti-parkinsonian actions of L-dopa in the MPTP-lesioned primate model of Parkinson's disease. *Mov. Disord.* 14, 744–753.
- Hill, M. P., and Brotchie, J. M. (1999). The adrenergic receptor agonist, clonidine, potentiates the anti-parkinsonian action of the selective kappa-opioid receptor agonist, enadoline, in the monoamine-depleted rat. *Br. J. Pharmacol.* 128, 1577–1585.
- Hollister, A. S., Breese, G. R., and Mueller, R. A. (1979). Role of monoamine neural systems in L-dihydroxyphenylalanine-stimulated activity. *J. Pharmacol. Exp. Ther.* 208, 37–43.
- Hornykiewicz, O. (1975). Brain monoamines and parkinsonism. *Natl. Inst. Drug Abuse Res. Monogr. Ser.* 11, 13–21.
- Hudson, A. L., Robinson, E. S., Lallies, M. D., Tyacke, R. J., Jackson, H. C., and Nutt, D. J. (1999). In vitro and in vivo approaches to the characterization of the alpha2-adrenoceptor. *J. Auton. Pharmacol.* 19, 311–320.
- Jankovic, J., and Talosa, E. (1988). *Parkinson's Disease and Movement Disorders*, 5th Edn. Baltimore: Lippincott William and Wilkins.
- Javitch, J. A., Uhl, G. R., and Snyder, S. H. (1984). Parkinsonism-inducing neurotoxin, N-methyl-4-phenyl-1,2,3,6-tetrahydropyridine: characterization and localization of receptor binding sites in rat and human brain. *Proc. Natl. Acad. Sci. U.S.A.* 81, 4591–4595.
- Jenner, P., Sheehy, M., and Marsden, C. D. (1983). Noradrenaline and 5-hydroxytryptamine modulation of brain dopamine function: implications for the treatment of Parkinson's disease. *Br. J. Clin. Pharmacol.* 15(Suppl. 2), 277S–289S.
- Johnson, E. W., Wolfe, B. B., and Molinoff, P. B. (1989). Regulation of subtypes of beta-adrenergic receptors in rat brain following treatment with 6-hydroxydopamine. *J. Neurosci.* 9, 2297–2305.
- Kasper, S., el Giamal, N., and Hilger, E. (2000). Reboxetine: the first selective noradrenaline re-uptake inhibitor. *Expert Opin. Pharmacother.* 1, 771–782.
- Khakpour-Taleghani, B., Lashgari, R., Motamedi, F., and Naghdi, N. (2009). Effect of reversible inactivation of locus ceruleus on spatial reference and working memory. *Neuroscience* 158, 1284–1291.
- Kirik, D., Rosenblad, C., and Bjorklund, A. (1998). Characterization of behavioral and neurodegenerative changes following partial lesions of the nigrostriatal dopamine system induced by intrastriatal 6-hydroxydopamine in the rat. *Exp. Neurol.* 152, 259–277.
- Kish, S. J. (2003). Biochemistry of Parkinson's disease: is a brain serotonergic deficiency a characteristic of idiopathic Parkinson's disease? *Adv. Neurol.* 91, 39–49.
- Kish, S. J., Tong, J., Hornykiewicz, O., Rajput, A., Chang, L. J., Guttman, M., and Furukawa, Y. (2008). Preferential loss of serotonin markers in caudate versus putamen in Parkinson's disease. *Brain* 131, 120–131.
- Kuno, S. (1997). [Treatment of Parkinson's disease with multiple drugs]. *Nippon Rinsho* 55, 59–64.
- Langston, J. W., and Ballard, P. (1984). Parkinsonism induced by 1-methyl-4-phenyl-1,2,3,6-tetrahydropyridine (MPTP): implications for treatment and the pathogenesis of Parkinson's disease. *Can. J. Neurol. Sci.* 11, 160–165.
- Langston, J. W., and Ballard, P. A. Jr. (1983). Parkinson's disease in a chemist working with 1-methyl-4-phenyl-1,2,5,6-tetrahydropyridine. *N. Engl. J. Med.* 309, 310.
- Lapiz, M. D., Mateo, Y., Durkin, S., Parker, T., and Marsden, C. A. (2001). Effects of central noradrenaline depletion by the selective neurotoxin DSP-4 on the behaviour of the isolated rat in the elevated plus maze and water maze. *Psychopharmacology (Berl.)* 155, 251–259.
- Lauterbach, E. C., Freeman, A., and Vogel, R. L. (2003). Correlates of generalized anxiety and panic attacks in dystonia and Parkinson disease. *Cogn. Behav. Neurol.* 16, 225–233.
- Lemke, M. R. (2002). Effect of reboxetine on depression in Parkinson's disease patients. *J. Clin. Psychiatry* 63, 300–304.
- Lemke, M. R., Fuchs, G., Gemende, I., Herting, B., Oehlwein, C., Reichmann, H., Rieke, J., and Volkmann, J. (2004). Depression and Parkinson's disease. *J. Neurol.* 251(Suppl. 6), 24–27.
- Mann, D. M. (1983). The locus coeruleus and its possible role in ageing and degenerative disease of the human central nervous system. *Mech. Ageing Dev.* 23, 73–94.
- Mann, D. M., and Yates, P. O. (1983). Pathological basis for neurotransmitter changes in Parkinson's disease. *Neuropathol. Appl. Neurobiol.* 9, 3–19.
- Marie, R. M., Barre, L., Rioux, P., Allain, P., Lechevalier, B., and Baron, J. C. (1995). PET imaging of neocortical monoaminergic terminals in Parkinson's disease. *J. Neural Transm. Park. Dis. Dement. Sect.* 9, 55–71.
- Marien, M. R., Colpaert, F. C., and Rosenquist, A. C. (2004). Noradrenergic mechanisms in neurodegenerative diseases: a theory. *Brain Res. Brain Res. Rev.* 45, 38–78.
- Maruyama, W., Naoi, M., and Narabayashi, H. (1996). The metabolism of L-DOPA and L-threo-3,4-dihydroxyphenylserine and their effects on monoamines in the human brain: analysis of the intraventricular fluid from parkinsonian patients. *J. Neurol. Sci.* 139, 141–148.
- Mathe, J. M., Nomikos, G. G., Hildebrand, B. E., Hertel, P., and Svensson, T. H. (1996). Prazosin inhibits MK-801-induced hyperlocomotion and dopamine release in the nucleus accumbens. *Eur. J. Pharmacol.* 309, 1–11.
- Mavridis, M., Degryse, A. D., Lategan, A. J., Marien, M. R., and Colpaert, F. C. (1991). Effects of locus coeruleus lesions on parkinsonian signs, striatal dopamine and substantia nigra cell loss after 1-methyl-4-phenyl-1,2,3,6-tetrahydropyridine in monkeys: a possible role for the locus coeruleus in the progression of Parkinson's disease. *Neuroscience* 41, 507–523.
- Mayeux, R., Stern, Y., Sano, M., Cote, L., and Williams, J. B. (1987). Clinical and biochemical correlates of bradyphrenia in Parkinson's disease. *Neurology* 37, 1130–1134.
- Mayeux, R., Stern, Y., Williams, J. B., Cote, L., Frantz, A., and Dyrenfurth, I. (1986). Clinical and biochemical features of depression in Parkinson's disease. *Am. J. Psychiatry* 143, 756–759.
- McCormick, D. A. (1992). Neurotransmitter actions in the thalamus and cerebral cortex. *J. Clin. Neurophysiol.* 9, 212–223.
- McCormick, D. A., Pape, H. C., and Williamson, A. (1991). Actions of norepinephrine in the cerebral cortex and thalamus: implications for function of the central noradrenergic system. *Prog. Brain Res.* 88, 293–305.
- McCormick, D. A., and Wang, Z. (1991). Serotonin and noradrenaline excite GABAergic neurones of the guinea-pig and cat nucleus reticularis thalami. *J. Physiol.* 442, 235–255.
- McNamara, P., and Durso, R. (2006). Neuropharmacological treatment of mental dysfunction in Parkinson's disease. *Behav. Neurol.* 17, 43–51.
- Mitchell, I. J., Cross, A. J., Sambrook, M. A., and Crossman, A. R. (1985). Sites of the neurotoxic action of 1-methyl-4-phenyl-1,2,3,6-tetrahydropyridine in the macaque monkey include the ventral tegmental area and the locus coeruleus. *Neurosci. Lett.* 61, 195–200.
- Miyoshi, R., Kito, S., Ishida, H., and Katayama, S. (1988). Alterations of the central noradrenergic system in MPTP-induced monkey parkinsonism. *Res. Commun. Chem. Pathol. Pharmacol.* 62, 93–102.
- Mizuno, Y., Kondo, T., and Mori, H. (1994). Various aspects of motor fluctuations and their management in Parkinson's disease. *Neurology* 44, S29–S34.
- Narabayashi, H., Yokochi, F., Ogawa, T., and Igakura, T. (1991). [Analysis of L-threo-3, 4-dihydroxyphenylserine effect on motor and psychological symptoms in Parkinson's disease]. *No To Shinkei* 43, 263–268.
- Navailles, S., Bioulac, B., Gross, C., and De Duerwaerdere, P. (2010a). Chronic L-DOPA therapy alters central serotonergic function and L-DOPA-induced dopamine release in a region-dependent manner in a rat model of Parkinson's disease. *Neurobiol. Dis.* 41, 585–590.
- Navailles, S., Bioulac, B., Gross, C., and De Duerwaerdere, P. (2010b). Serotonergic neurons mediate ectopic release of dopamine induced by L-DOPA in a rat model of Parkinson's disease. *Neurobiol. Dis.* 38, 136–143.
- Nishi, K., Kondo, T., and Narabayashi, H. (1991). Destruction of norepinephrine terminals in 1-methyl-4-phenyl-1,2,3,6-tetrahydropyridine (MPTP)-treated mice reduces locomotor activity induced by L-dopa. *Neurosci. Lett.* 123, 244–247.
- Oertel, W. H., Hoglinger, G. U., Caraceni, T., Girotti, F., Eichhorn, T., Spottke, A. E., Krieg, J. C., and Poewe, W. (2001). Depression in Parkinson's disease. An update. *Adv. Neurol.* 86, 373–383.
- Ogawa, N., Kuroda, H., Yamamoto, M., Nukina, I., and Ota, Z. (1984). Improvement in freezing phenomenon of Parkinson's disease after

- DL-threo-3, 4-dihydroxyphenylserine. *Acta Med. Okayama* 38, 301–304.
- Ogawa, N., Yamamoto, M., and Takayama, H. (1985). L-threo-3,4-dihydroxyphenylserine treatment of Parkinson's disease. *J. Med.* 16, 525–534.
- Olsson, M., Nikkha, G., Bentlage, C., and Bjorklund, A. (1995). Forelimb akinesia in the rat Parkinson model: differential effects of dopamine agonists and nigral transplants as assessed by a new stepping test. *J. Neurosci.* 15, 3863–3875.
- Perez, V., Marin, C., Rubio, A., Aguilar, E., Barbanoj, M., and Kulisevsky, J. (2009a). Effect of the additional noradrenergic neurodegeneration to 6-OHDA-lesioned rats in levodopa-induced dyskinesias and in cognitive disturbances. *J. Neural Transm.* 116, 1257–1266.
- Perez, V., Sosti, V., Rubio, A., Barbanoj, M., Gich, I., Rodriguez-Alvarez, J., and Kulisevsky, J. (2009b). Noradrenergic modulation of the motor response induced by long-term levodopa administration in Parkinsonian rats. *J. Neural Transm.* 116, 867–874.
- Perez, V., Sosti, V., Rubio, A., Barbanoj, M., Rodriguez-Alvarez, J., and Kulisevsky, J. (2007). Modulation of the motor response to dopaminergic drugs in a parkinsonian model of combined dopaminergic and noradrenergic degeneration. *Eur. J. Pharmacol.* 576, 83–90.
- Pifl, C., Schingnitz, G., and Hornykiewicz, O. (1991). Effect of 1-methyl-4-phenyl-1,2,3,6-tetrahydropyridine on the regional distribution of brain monoamines in the rhesus monkey. *Neuroscience* 44, 591–605.
- Politis, M., Wu, K., Loane, C., Kiferle, L., Molloy, S., Brooks, D. J., and Piccini, P. (2010). Staging of serotonergic dysfunction in Parkinson's disease: an in vivo 11C-DASB PET study. *Neurobiol. Dis.* 40, 216–221.
- Ponzio, F., Hallman, H., and Jonsson, G. (1981). Noradrenaline and dopamine interaction in rat brain during development. *Med. Biol.* 59, 161–169.
- Rascol, O., Arnulf, I., Peyro-Saint Paul, H., Brefel-Courbon, C., Vidailhet, M., Thalamas, C., Bonnet, A. M., Descombes, S., Bejjani, B., Fabre, N., Montastruc, J. L., and Agid, Y. (2001). Idazoxan, an alpha-2 antagonist, and L-DOPA-induced dyskinesias in patients with Parkinson's disease. *Mov. Disord.* 16, 708–713.
- Rascol, O., Fabre, N., Blin, O., Poulik, J., Sabatini, U., Senard, J. M., Ane, M., Montastruc, J. L., and Rascol, A. (1994). Naltrexone, an opiate antagonist, fails to modify motor symptoms in patients with Parkinson's disease. *Mov. Disord.* 9, 437–440.
- Reches, A., and Meiner, Z. (1992). The locus coeruleus and dopaminergic function in rat brain: implications to parkinsonism. *Brain Res. Bull.* 28, 663–666.
- Remy, P., Doder, M., Lees, A., Turjanski, N., and Brooks, D. (2005). Depression in Parkinson's disease: loss of dopamine and noradrenaline innervation in the limbic system. *Brain* 128, 1314–1322.
- Riekkinen, M., Kejonen, K., Jakala, P., Soinen, H., and Riekkinen, P. Jr. (1998). Reduction of noradrenaline impairs attention and dopamine depletion slows responses in Parkinson's disease. *Eur. J. Neurosci.* 10, 1429–1435.
- Ringdahl, H., and Sierla, T. (1997). [Freezing phenomenon in Parkinson disease]. *Fortschr. Neurol. Psychiatr.* 65, 435–445.
- Rommelfanger, K. S., and Weinshenker, D. (2007). Norepinephrine: the redheaded stepchild of Parkinson's disease. *Biochem. Pharmacol.* 74, 177–190.
- Rommelfanger, K. S., Weinshenker, D., and Miller, G. W. (2004). Reduced MPTP toxicity in noradrenaline transporter knockout mice. *J. Neurochem.* 91, 1116–1124.
- Ruckert, N., Bubser, M., and Schmidt, W. J. (1997). 6-Hydroxydopamine lesion of locus coeruleus and the antiparkinsonian potential of NMDA-receptor antagonists in rats. *J. Neural Transm.* 104, 363–377.
- Sandyk, R. (1996). Freezing of gait in Parkinson's disease is improved by treatment with weak electromagnetic fields. *Int. J. Neurosci.* 85, 111–124.
- Saper, C. B., Sorrentino, D. M., German, D. C., and de Lacalle, S. (1991). Medullary catecholaminergic neurons in the normal human brain and in Parkinson's disease. *Ann. Neurol.* 29, 577–584.
- Savola, J. M., Hill, M., Engstrom, M., Merivuori, H., Wurster, S., McGuire, S. G., Fox, S. H., Crossman, A. R., and Brotchie, J. M. (2003). Fipamezole (JP-1730) is a potent alpha2 adrenergic receptor antagonist that reduces levodopa-induced dyskinesia in the MPTP-lesioned primate model of Parkinson's disease. *Mov. Disord.* 18, 872–883.
- Schapira, A. H. (2005). Present and future drug treatment for Parkinson's disease. *J. Neurol. Neurosurg. Psychiatr.* 76, 1472–1478.
- Schrag, A., Jahanshahi, M., and Quinn, N. P. (2001). What contributes to depression in Parkinson's disease? *Psychol. Med.* 31, 65–73.
- Selikhova, M. V., Kogan, B. M., Serkin, G. V., and Gusev, E. I. (2002). [Catecholamine metabolism in different forms of Parkinson's disease]. *Zh. Nevrol. Psikiatr. Im. S. S. Korsakova.* 102, 37–40.
- Snoddy, A. M., and Tessel, R. E. (1985). Prazosin: effect on psychomotor-stimulant cues and locomotor activity in mice. *Eur. J. Pharmacol.* 116, 221–228.
- Srinivasan, J., and Schmidt, W. J. (2003). Potentiation of parkinsonian symptoms by depletion of locus coeruleus noradrenaline in 6-hydroxydopamine-induced partial degeneration of substantia nigra in rats. *Eur. J. Neurosci.* 17, 2586–2592.
- Stein, M. B., Heuser, I. J., Juncos, J. L., and Uhde, T. W. (1990). Anxiety disorders in patients with Parkinson's disease. *Am. J. Psychiatry* 147, 217–220.
- Stern, Y., Mayeux, R., and Cote, L. (1984). Reaction time and vigilance in Parkinson's disease. Possible role of altered norepinephrine metabolism. *Arch. Neurol.* 41, 1086–1089.
- Suzuki, T., Sakoda, S., Ueki, M., Kishimoto, S., Hayashi, A., Kondo, T., and Narabayashi, H. (1984). Treatment of parkinsonism with L-threo-3,4-dihydroxyphenylserine: a pharmacokinetic study. *Neurology* 34, 1446–1450.
- Tadaiesky, M. T., Dombrowski, P. A., Figueiredo, C. P., Cargnin-Ferreira, E., Da Cunha, C., and Takahashi, R. N. (2008). Emotional, cognitive and neurochemical alterations in a premotor stage model of Parkinson's disease. *Neuroscience* 156, 830–840.
- Tanaka, H., Kannari, K., Maeda, T., Tomiyama, M., Suda, T., and Matsunaga, M. (1999). Role of serotonergic neurons in L-DOPA-derived extracellular dopamine in the striatum of 6-OHDA-lesioned rats. *Neuroreport* 10, 631–634.
- Tanda, G., Pontieri, F. E., Frau, R., and Di Chiara, G. (1997). Contribution of blockade of the noradrenaline carrier to the increase of extracellular dopamine in the rat prefrontal cortex by amphetamine and cocaine. *Eur. J. Neurosci.* 9, 2077–2085.
- Taquet, H., Javoy-Agid, F., Cesselin, F., Hamon, M., Legrand, J. C., and Agid, Y. (1982). Microtopography of methionine-enkephalin, dopamine and noradrenaline in the ventral mesencephalon of human control and Parkinsonian brains. *Brain Res.* 235, 303–314.
- Taylor, T. N., Caudle, W. M., Shepherd, K. R., Noorian, A., Jackson, C. R., Iuvone, P. M., Weinshenker, D., Greene, J. G., and Miller, G. W. (2009). Nonmotor symptoms of Parkinson's disease revealed in an animal model with reduced monoamine storage capacity. *J. Neurosci.* 29, 8103–8113.
- Thomas, S. A., Matsumoto, A. M., and Palmiter, R. D. (1995). Noradrenaline is essential for mouse fetal development. *Nature* 374, 643–646.
- Tohgi, H., Abe, T., Saheki, M., Yamazaki, K., and Murata, T. (1997). Concentration of catecholamines and indoleamines in the cerebrospinal fluid of patients with vascular parkinsonism compared to Parkinson's disease patients. *J. Neural Transm.* 104, 441–449.
- Tohgi, H., Abe, T., and Takahashi, S. (1993). The effects of L-threo-3,4-dihydroxyphenylserine on the total norepinephrine and dopamine concentrations in the cerebrospinal fluid and freezing gait in parkinsonian patients. *J. Neural Transm. Park. Dis. Dement. Sect. 5*, 27–34.
- Tohgi, H., Abe, T., Takahashi, S., Takahashi, J., Ueno, M., and Nozaki, Y. (1990). Effect of a synthetic norepinephrine precursor, L-threo-3,4-dihydroxyphenylserine on the total norepinephrine concentration in the cerebrospinal fluid of parkinsonian patients. *Neurosci. Lett.* 116, 194–197.
- Wang, T., Zhang, Q. J., Liu, J., Wu, Z. H., and Wang, S. (2009). Firing activity of locus coeruleus noradrenergic neurons increases in a rodent model of Parkinsonism. *Neurosci. Bull.* 25, 15–20.
- Weintraub, D., Mavandadi, S., Mamikonyan, E., Siderowf, A. D., Duda, J. E., Hurtig, H. I., Colcher, A., Horn, S. S., Nazem, S., Ten Have, T. R., and Stern, M. B. (2010). Atomoxetine for depression and other neuropsychiatric symptoms in Parkinson disease. *Neurology* 75, 448–455.
- Wilbur, R., Kulik, F. A., and Kulik, A. V. (1988). Noradrenergic effects in tardive dyskinesia, akathisia and pseudoparkinsonism via the limbic system and basal ganglia. *Prog. Neuropsychopharmacol. Biol. Psychiatry* 12, 849–864.
- Yamamoto, M. (2004). [Depression in Parkinson's disease]. *Nippon Rinsho* 62, 1661–1666.
- Yamamoto, M., Ogawa, N., and Ujike, H. (1986). Effect of L-threo-3,4-dihydroxyphenylserine chronic administration on cerebrospinal fluid and plasma free 3-methoxy-4-hydroxy-phenylglycol concentration in patients with Parkinson's disease. *J. Neurol. Sci.* 73, 39–44.
- Yamazaki, M., Tanaka, C., and Takaori, S. (1979). Significance of central noradrenergic system on harmaline induced tremor. *Pharmacol. Biochem. Behav.* 10, 421–427.
- Yavich, L., Sirvio, J., Haapalinna, A., Ylinen, A., and Mannisto, P. T. (2003).

- Atipamezole, an α_2 -adrenoceptor antagonist, augments the effects of L-DOPA on evoked dopamine release in rat striatum. *Eur. J. Pharmacol.* 462, 83–89.
- Yuan, H., Sarre, S., Ebinger, G., and Michotte, Y. (2005). Histological, behavioural and neurochemical evaluation of medial forebrain bundle and striatal 6-OHDA lesions as rat models of Parkinson's disease. *J. Neurosci. Methods* 144, 35–45.
- Zarow, C., Lyness, S. A., Mortimer, J. A., and Chui, H. C. (2003). Neuronal loss is greater in the locus coeruleus than nucleus basalis and substantia nigra in Alzheimer and Parkinson diseases. *Arch. Neurol.* 60, 337–341.
- Conflict of Interest Statement:** The authors declare that the research was conducted in the absence of any commercial or financial relationships that could be construed as a potential conflict of interest.
- Received: 02 February 2011; paper pending published: 27 March 2011; accepted: 04 May 2011; published online: 18 May 2011.
- Citation: Delaville C, De Deurwaerdère P and Benazzouz A (2011) Noradrenaline and Parkinson's disease. *Front. Syst. Neurosci.* 5:31. doi: 10.3389/fnsys.2011.00031
- Copyright © 2011 Delaville, De Deurwaerdère and Benazzouz. This is an open-access article subject to a non-exclusive license between the authors and Frontiers Media SA, which permits use, distribution and reproduction in other forums, provided the original authors and source are credited and other Frontiers conditions are complied with.



Pharmacological and physiological characterization of the tremulous jaw movement model of parkinsonian tremor: Potential insights into the pathophysiology of tremor

Lyndsey E. Collins-Praino¹, Nicholas E. Paul¹, Kristen L. Rychalsky¹, James R. Hinman¹, James J. Chrobak¹, Patrick B. Senatus² and John D. Salamone^{1*}

¹ Behavioral Neuroscience Division, Department of Psychology, University of Connecticut, Storrs, CT, USA

² Department of Surgery, University of Connecticut Health Center, Farmington, CT, USA

Edited by:

Elizabeth Abercrombie, Rutgers-Newark: The State University of New Jersey, USA

Reviewed by:

Gregor Rainer, University of Fribourg, Switzerland
Constance Hammond, Université de la Méditerranée, France

*Correspondence:

John D. Salamone, Division of Behavioral Neuroscience, Department of Psychology, University of Connecticut, Storrs, CT 06269-1020, USA.
e-mail: john.salamone@uconn.edu

Tremor is a cardinal symptom of parkinsonism, occurring early on in the disease course and affecting more than 70% of patients. Parkinsonian resting tremor occurs in a frequency range of 3–7 Hz and can be resistant to available pharmacotherapy. Despite its prevalence, and the significant decrease in quality of life associated with it, the pathophysiology of parkinsonian tremor is poorly understood. The tremulous jaw movement (TJM) model is an extensively validated rodent model of tremor. TJMs are induced by conditions that also lead to parkinsonism in humans (i.e., striatal DA depletion, DA antagonism, and cholinomimetic activity) and reversed by several antiparkinsonian drugs (i.e., DA precursors, DA agonists, anticholinergics, and adenosine A_{2A} antagonists). TJMs occur in the same 3–7 Hz frequency range seen in parkinsonian resting tremor, a range distinct from that of dyskinesia (1–2 Hz), and postural tremor (8–14 Hz). Overall, these drug-induced TJMs share many characteristics with human parkinsonian tremor, but do not closely resemble tardive dyskinesia. The current review discusses recent advances in the validation of the TJM model, and illustrates how this model is being used to develop novel therapeutic strategies, both surgical and pharmacological, for the treatment of parkinsonian resting tremor.

Keywords: dopamine, adenosine A_{2A}, acetylcholine, muscarinic, basal ganglia, caudate putamen, neostriatum, subthalamic nucleus

PARKINSONIAN RESTING TREMOR

Idiopathic Parkinson's disease is just one member of a broader family of motor disorders known as parkinsonism (Alvarez et al., 2007), a group that also includes encephalitic, pugilistic, and drug-induced parkinsonism. Regardless of subtype, all forms of parkinsonism share in common four core symptoms: bradykinesia, postural instability, rigidity, and tremor (Hoehn and Yahr, 1967). Tremor, defined as “a rhythmic and involuntary oscillation of a body part, caused by reciprocal innervations of a muscle, which leads to repetitive, stereotyped contractions with regular frequency and amplitude,” is sometimes considered to be the cardinal symptom of parkinsonism (Deuschl et al., 2000; Mansur et al., 2007). This tremor, present predominantly at rest, appears early on in the disease course and causes a significant amount of life distress (Mansur et al., 2007). It presents in up to 75% of individuals with PD, and has been shown to occur in a frequency range of 3–7 Hz, a range distinct from that seen in dyskinesias (1–2 Hz), essential tremor (8 Hz), and postural tremors (8–12 Hz; Findley et al., 1981; Findley and Capildeo, 1984; Marsden, 1984; Elbe and Koller, 1990; Hunker and Abbs, 1990; Deuschl et al., 1996, 2000; Spieker et al., 1997).

Usually beginning unilaterally in the distal segments of the extremities, parkinsonian tremor frequently spreads bilaterally, often affecting both upper and lower limbs, as well as facial muscles, as the disease progresses (Adams and Victor, 1993; Koster

et al., 1997; Salamone et al., 1998; Deuschl et al., 2000; Morrison et al., 2008). While the most common form of parkinsonian resting tremor in humans is a “pill rolling” tremor of the hands, tremulous “up-and-down” movements of the jaw in parkinsonian patients have also been well documented (Barbeau, 1986; Selby, 1986; Young, 1986; Hunker and Abbs, 1990; Adams and Victor, 1993; Ben-Pazi et al., 2001; Schneider et al., 2006; Sheffield and Jankovic, 2007; Leventoglu and Baysal, 2008; Jankovic, 2009). Oral tremor also is induced by long-term administration of DA antagonists, a condition known as “rabbit syndrome” and defined as “rhythmic jaw tremor” (Weiss et al., 1980). This type of tremor is alleviated by common antiparkinsonian drugs, but exacerbated by cholinomimetic administration (Sovner and Dimascio, 1977; Weiss et al., 1980; Yassa and Lal, 1986). Thus, it is considered to be a form of drug-induced parkinsonian tremor (Sovner and Dimascio, 1977; Weiss et al., 1980; Tarsy, 1983).

The neural network thought to underlie parkinsonian tremor is complex, consisting of changes to the open and closed loop connections between neocortex, basal ganglia, and thalamus. According to current models of basal ganglia function, reductions of the DA input from substantia nigra pars compacta (particularly from the retrorubral area A8 portion of the SNc in tremor-dominant PD) to the striatum leads to an increase in output from the subthalamic nucleus (STN), a nucleus consisting of neurons and circuits that are

particularly correlated with tremor (Reck et al., 2009). This, in turn, produces an overstimulation of GABAergic neurons in substantia nigra pars reticulata (SNr) and globus pallidus internal (GPi), and a subsequent inhibition of the ventral lateral and ventral anterior nuclei of the thalamus, leading ultimately to the reduced output of the sensorimotor cortex and the motor impairments observed in parkinsonism. Most recently, hypotheses of parkinsonism have focused not just on these changes in firing rates, but also on alterations in firing patterns (see Obeso et al., 2000, 2008; Bevan et al., 2002; Brown, 2003 for review). Specifically, increases in the activity of subthalamic and internal globus pallidus neurons are thought to cause these nuclei to enter a regime of rhythmic firing, resulting in an excessive synchrony (particularly in the Beta band; Bergman et al., 1998; Obeso et al., 2000, 2008; Brown et al., 2001; Levy et al., 2002). This excessive synchrony may be particularly important for the generation and maintenance of parkinsonian tremor.

The neurochemical cascade thought to underlie parkinsonian tremor is similarly multifaceted, with multiple neurotransmitters, including GABA, serotonin, adenosine, and acetylcholine (ACh), interacting with DA in the regulation of basal ganglia motor functions related to parkinsonism (Hornykiewicz, 1972, 1973; DeLong, 1990; Young and Penney, 1993; McSwain and Forman, 1995; Finn et al., 1997b; Hauber et al., 1998; Salamone et al., 1998; Mayorga et al., 1999a; Wichmann et al., 2001; Trevitt et al., 2002; Carlson et al., 2003a,b; Ishiwari et al., 2004; Obeso et al., 2008; Vanover et al., 2008). Interestingly, these other neurotransmitters offer additional avenues for therapeutic intervention. In addition to DAergic treatments for parkinsonism, muscarinic antagonists often are used as antiparkinsonian agents, and they have been shown in clinical studies to suppress tremor (McEvoy, 1983; Schrag et al., 1999; Milanov, 2001; Koller, 2002). More recently, antagonists of adenosine A_{2A} receptors have been shown to produce antitremor effects in animal models (Correa et al., 2004; Salamone et al., 2008a,b) and in human patients with Parkinson's disease (Bara-Jimenez et al., 2003; Pinna, 2009).

The study of parkinsonian tremor has proven to be something of an enigma in the field. Although tremor is considered to be the most specific marker of parkinsonism, with estimates of 95% probability that the presence of classical resting tremor indicates idiopathic PD, tremor severity has not been shown to parallel disease progression (Deuschl et al., 2000). Additionally, the system dynamics of parkinsonian tremor have shown that, despite the nearly uniform frequencies associated with tremor-related oscillations (i.e., 3–7 Hz; Hunker and Abbs, 1990), these oscillations occur independently of one another, with electromyographic (EMG) activity of tremor in one limb being uncorrelated to the EMG activity of another limb exhibiting tremor (O'Suilleabhain and Matsumoto, 1998; Hurtado et al., 2000, 2004; Raethjen et al., 2000, 2009; Ben-Pazi et al., 2001). Even within the tremor circuitry itself, tremors have not been shown to be tightly correlated with tremor-related neural activity in the nuclei of the basal ganglia and thalamus: tremor-related neural activity may wax and wane while limb tremor persists; conversely, tremor-related oscillations may exist in the neurocircuitry while no limb tremor is apparent (Hurtado et al., 2004). These seemingly paradoxical findings have led to a variety of questions about the pathophysiology underlying tremorogenesis in parkinsonism. Yet despite these lingering questions, relatively few clinical studies have specifically emphasized

the pharmacology of tremor (e.g., Schrag et al., 2002; Navan et al., 2003, 2005; Sung et al., 2008; Binder et al., 2009) and there is considerable uncertainty about the neurochemical mechanisms that underlie the pathophysiology of parkinsonian tremor (Wilms et al., 1999; Deuschl et al., 2000, 2001; Bergman and Deuschl, 2002; Sung et al., 2008). While parkinsonian tremor seems to result from oscillating activity in the central nervous system (and not due to reflexes in the periphery; see Hunker and Abbs, 1990 for review), it appears to be generated by multiple oscillators, and it is unclear where these oscillators are located (though the basal ganglia loops are a likely candidate, oscillators in the thalamus have also been proposed) or by what mechanism these oscillators produce tremor (O'Suilleabhain and Matsumoto, 1998; Deuschl et al., 2000). Given the uncertainty surrounding this cardinal symptom of parkinsonism, studies employing animal models of parkinsonian resting tremor are imperative (Muthuraman et al., 2008). Basic research using animal models of drug-induced tremor enables researchers to investigate the neurochemical mechanisms that regulate tremor and to study the development of oscillatory patterns of activity in the brain that are thought to underlie tremorogenesis. Eventually, this research could lead to the development of novel treatments.

THE TREMULOUS JAW MOVEMENT MODEL IN RODENTS: DEVELOPMENT AND VALIDATION

While a variety of animal models of parkinsonian tremor exist, most of these are models of postural or action tremors, and not of resting tremor (see Wilms et al., 1999). Although a few models of resting tremor have been produced, these have mainly been in primates and have involved the destruction of multiple nuclei or pathways, a paradigm that is expensive and impractical for most preclinical pharmaceutical testing (Wilms et al., 1999). The tremulous jaw movement (TJM) model may provide a resolution for many of these difficulties. TJMs, defined as rapid vertical deflections of the lower jaw that are not directed at any stimulus, are a rodent model of parkinsonian resting tremor (for reviews, see Salamone et al., 1998, 2001, 2005; see also Rodriguez Diaz et al., 2001; Cenci et al., 2002). TJMs generally occur in phasic bursts of repetitive jaw movement activity, with multiple movements within each burst. Willner (1990) cautions that animal models should undergo an evaluation for their validity using criteria similar to those used in the rigorous validation of psychological tests. Thus, a great deal of effort has been expended in the analysis of the pharmacological, temporal, and anatomical characteristics of the TJM model in order to evaluate whether these tremulous movements in rats are sufficiently similar to human parkinsonian tremor to allow for their validation as an animal model of tremor. TJMs have been shown to possess many of the neurochemical, anatomical, and pharmacological characteristics of parkinsonism, and thus meet a reasonable set of validation criteria for use as an animal model of parkinsonian tremor (Salamone et al., 1998; Cenci et al., 2002). Animal models in psychopharmacology are evaluated for their validity based upon a number of criteria (Willner, 1990). These including face validity (the phenomenological similarity between the model and the disorder, including etiology and symptomatology), construct validity (the degree of similarity between the identified variable (e.g., tremor), and the behavior being studied in the model), and predictive validity (primarily, the positive response to therapeutic

drugs). As described below, the TJM model of parkinsonism is one of the few models of experimental tremor that meets these validation criteria.

VALIDATION OF THE TREMULOUS JAW MOVEMENT MODEL: TJMs ARE INDUCED BY THE SAME NEUROCHEMICAL AND PHARMACOLOGICAL CONDITIONS THAT LEAD TO PARKINSONISM IN HUMANS

Tremulous jaw movements are induced by a number of conditions that parallel the neurochemistry of idiopathic and drug-induced parkinsonism. For example, several DAergic conditions that are associated with parkinsonism in humans have been shown to induce TJMs (**Table 1**). Depletions of striatal dopamine by the neurotoxic agent 6-OHDA (Jicha and Salamone, 1991; Finn et al., 1997b; Rodriguez-Diaz et al., 2001) or acute administration of reserpine (Baskin and Salamone, 1993; Steinpreis and Salamone, 1993; Salamone and Baskin, 1996; Salamone et al., 2008b) have been shown to induce TJM activity in rats. Several studies have demonstrated that TJMs are also induced by acute or sub-chronic administration of “typical” antipsychotic drugs that act as DA antagonists (Glassman and Glassman, 1980; Rupniak et al., 1985, 1986; Jicha and Salamone, 1991; Steinpreis and Salamone, 1993; Steinpreis et al., 1993; Egan et al., 1996; Trevitt et al., 1998; Wisniecki et al., 2003; Ishiwari et al., 2005; Betz et al., 2007, 2009; Collins et al., 2010a). In contrast, “atypical” antipsychotic drugs, such as clozapine, olanzapine, and quetiapine, which are less likely to induce motor side effects in humans, do not induce TJMs (Trevitt et al., 1998, 1999; Betz et al., 2005, 2009).

Cholinomimetic drugs acting on central muscarinic receptors, which can produce or exacerbate parkinsonian symptoms in humans (Duvoisin, 1967; Aquilonius, 1980; Ott and Lannon, 1992; Kao et al., 1993; Song et al., 2008), also produce robust bursts of TJM activity in rats (Rupniak et al., 1983, 1985; Salamone et al., 1986, 2005; **Table 1**). Muscarinic agonists, such as pilocarpine, have been repeatedly demonstrated to induce TJMs (Rupniak et al., 1983, 1985; Salamone et al., 1986, 1990; Stewart et al., 1987, 1988; Baskin et al., 1994; Finn et al., 1997a,b; Collins et al., 2010a). Similar findings have been reported with the administration of various anticholinesterases, including physostigmine and tacrine (Kelley et al., 1989; Mayorga et al., 1997; Simola et al., 2004; Tronci et al., 2007; Kasture et al., 2009; Pinna et al., 2010). Most recently, galantamine, a “new generation” anticholinesterase, was demonstrated to induce TJMs (Collins et al., 2011; **Figure 1**). This is consistent with data from clinical patient populations, which suggest that the “new generation” anticholinesterases donepezil, rivastigmine, and galantamine also induce tremor (Bourke and Drukenbrod, 1998; Shea et al., 1998; Arai, 2000; Aarsland et al., 2003; Gurevich et al., 2006; McCain et al., 2007; Litvinenko et al., 2008; Song et al., 2008). Donepezil, for example, has been reported to induce jaw tremor as a side effect (Song et al., 2008). Given the increasing numbers of people receiving anticholinesterases for the treatment of Alzheimer’s disease, this is particularly concerning, and suggests that a new population of people may be at risk for developing drug-induced tremor. These observations indicate that research on the pathogenesis of tremor needs to include anticholinesterase-induced tremor as well as DAergic conditions.

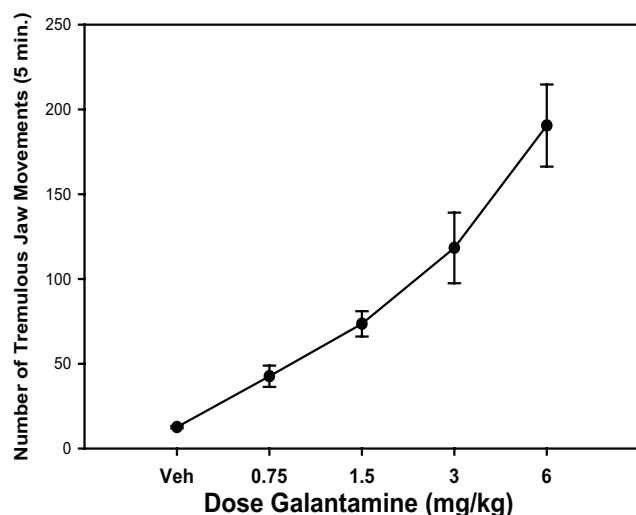


FIGURE 1 | Effects of different IP doses of the anticholinesterase galantamine on tremulous jaw movements (Collins et al., 2011).

Mean (\pm SEM) number of jaw movements (per 5 min) in rats ($n = 8$) treated with either saline vehicle (Veh) or galantamine. Using a within-groups design, all rats received all drug treatments in a randomly varied order (one treatment per week). Rats were observed in three 5-min periods 10–25 min after injection. Repeated measures ANOVA revealed that galantamine produced a significant increase in tremulous jaw movement activity [$F(4,28) = 25.8$; $p < 0.001$].

*Significant difference from vehicle control ($p < 0.05$).

VALIDATION OF THE TREMULOUS JAW MOVEMENT MODEL: TJMs OCCUR IN THE SAME LOCAL FREQUENCY RANGE AS PARKINSONIAN TREMOR

Parkinsonian resting tremor in humans is generally reported to occur within a peak frequency range of 3–7 Hz (Adams and Victor, 1993; Staude et al., 1995). This range is distinct from that seen in dyskinesias (1–2 Hz), essential tremor (8 Hz), and postural tremors (8–12 Hz) (Findley et al., 1981; Findley and Gresty 1981, 1988; Findley and Capildeo, 1984; Marsden, 1984; Findley, 1988; Elbe and Koller, 1990; Hunker and Abbs, 1990; Deuschl et al., 1996, 2000; Spieker et al., 1997). Strikingly, the tremulous oral movements that are induced by interference with DA transmission and by cholinomimetics have also been found to occur within the 3 to 7-Hz range, consistent with the frequency of parkinsonian resting tremor in humans (See and Chapman, 1991; Salamone and Baskin, 1996; Finn et al., 1997b; Mayorga et al., 1997; Cousins et al., 1998; Salamone et al., 1998; Ishiwari et al., 2005; Collins et al., 2010a; Galtieri et al., 2010).

Studies employing slow-motion videotaping methods have demonstrated that the majority of TJMs induced either by interference with striatal dopamine (either through DA depletion or antagonism; Salamone and Baskin, 1996; Finn et al., 1997b; Ishiwari et al., 2005) or cholinomimetic stimulation (Finn et al., 1997b; Mayorga et al., 1997; Collins et al., 2011) occur in “bursts” with a local frequency range of 3–7 Hz (based on an analysis of the inter-movement time, whereby local frequency was equal to the inverse of the inter-movement time). EMG recording methods also have been used to characterize the local frequency of TJMs. Cousins et al. (1998) found that the lateral temporalis muscle is the

jaw closing muscle most strongly correlated with tacrine-induced TJMs in rats; examination of 1 s raw EMG traces demonstrated that the local frequency of these TJMs was in the 3 to 7-Hz frequency (Cousins et al., 1998). Furthermore, this study indicated that the variability in the jaw movement frequency distribution obtained was comparable to the variability in tremor frequencies shown by parkinsonian patients (see Staude et al., 1995). A more recent study demonstrated that the frequency range of TJMs induced by the muscarinic agonist pilocarpine were in the 3 to 7-Hz frequency range after both a high (4.0 mg/kg) and low (0.5 mg/kg) dose (Collins et al., 2010a).

Currently, improvements in the frequency characterization of TJMs are being conducted using time series analysis of EMG data. Since the physiological events underlying tremor can be considered as a continuously varying waveform, the use of these continuous time series techniques (as opposed to discrete stochastic point process techniques) is appropriate for the analysis of the EMG data obtained from rats displaying TJMs (Halliday et al., 1995). More specifically, because tremor has been described as a second order linear stochastic process, spectral analysis techniques based on the Fourier transform can be used (Timmer et al., 1998a,b). The employment of these techniques provides for a systematic, quantitative temporal analysis of EMG data recorded during drug-induced TJMs. A recent study employed these techniques to perform a frequency analysis of the jaw movements induced by both DA antagonism and cholinomimetic administration (Collins et al., 2010c). Rats were implanted with tungsten wire electrodes bilaterally in the lateral temporalis muscle. Following a sufficient recovery period, rats received either an acute injection of the muscarinic agonist pilocarpine, the anticholinesterase galanthamine, or a sub-chronic injection of the DA D2 antagonist pimozide. Rats were then connected to a Cheetah 16 Neuralynx recording system (Neuralynx, Bozeman, MT, USA) via a multiwire cable and recordings of EMG activity during TJM observation were performed. Representative traces were examined using the Neuraview program (Neuralynx, Bozeman, MT, USA) to identify appropriate epochs of tremor and non-tremor activity and then imported into Matlab 7.4 (Mathworks Inc., Natick, MA, USA). A spectrum of each epoch was then calculated using the multi-taper spectral estimation method. Spectral analysis revealed that, during periods of tremor activity, a distinct peak was consistently present between 4 and 7 Hz. This was true for tremor activity induced by both DA antagonism and cholinomimetic administration. Conversely, during periods of quiescence (i.e., when no tremor activity was occurring in the jaw), no distinct peak was present in the spectral analysis. Example traces and spectral analyses are presented in **Figure 2**. These results with time series analysis demonstrate that drug-induced TJMs are accompanied by EMG activity that is occurring in the parkinsonian tremor frequency range, and serve to provide further validation of the TJM model of parkinsonian resting tremor.

VALIDATION OF THE TREMULOUS JAW MOVEMENT MODEL: TJMs ARE REVERSED BY WELL CHARACTERIZED AND PUTATIVE ANTIPARKINSONIAN DRUGS

In addition to being produced by many of the same neurochemical conditions that induce parkinsonism in humans, TJMs in rats also can also be reduced by both clinically utilized and putative

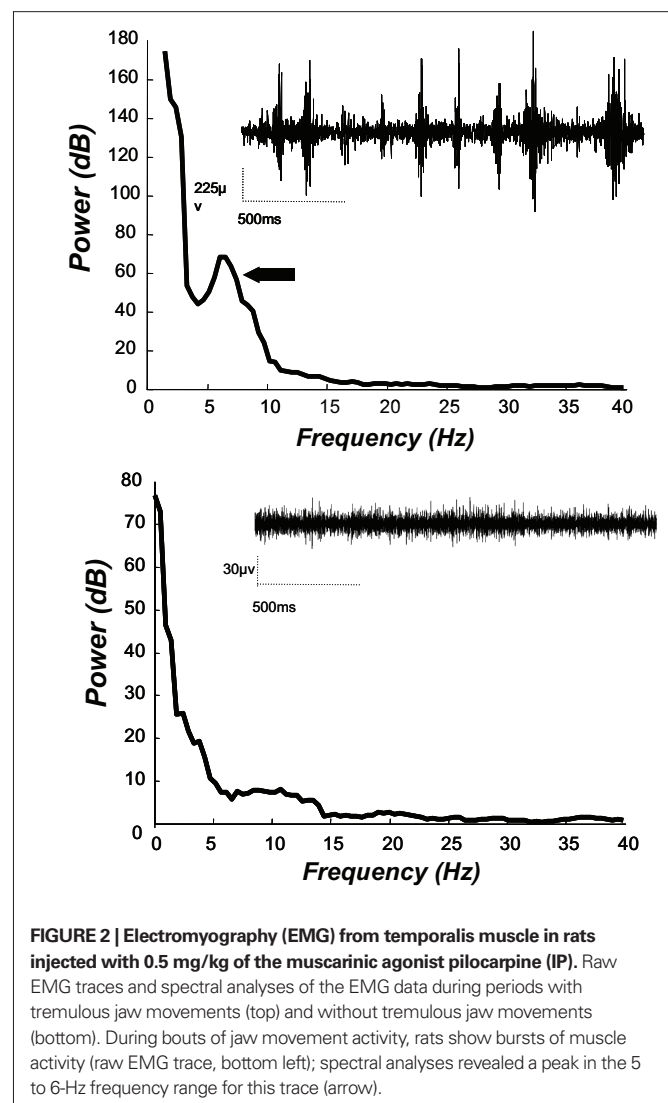


FIGURE 2 | Electromyography (EMG) from temporalis muscle in rats injected with 0.5 mg/kg of the muscarinic agonist pilocarpine (IP). Raw EMG traces and spectral analyses of the EMG data during periods with tremulous jaw movements (top) and without tremulous jaw movements (bottom). During bouts of jaw movement activity, rats show bursts of muscle activity (raw EMG trace, bottom left); spectral analyses revealed a peak in the 5 to 6-Hz frequency range for this trace (arrow).

antiparkinsonian drugs from many drug classes (**Table 2**). Administration of L-DOPA, currently the gold standard for the treatment of parkinsonian motor impairment, led to a significant reduction of TJMs (Cousins and Salamone, 1996; Cousins et al., 1997). Similarly, several DA agonists, including apomorphine, pergolide, bromocriptine, ropinirole and CY 208-243, have been shown to reduce TJMs (Baskin and Salamone, 1993; Cousins et al., 1997; Salamone et al., 2005). The potency of DAergic drugs for suppressing TJMs is highly correlated with the clinical potency of these drugs for reducing parkinsonian tremor in humans (Salamone et al., 2005). For example, the weak partial D1 agonist SKF 38393, which is not antiparkinsonian in humans or primates (Braun et al., 1987; Boyce et al., 1990; Close et al., 1990), did not decrease cholinomimetic-induced jaw movements (Cousins et al., 1997). Conversely, the full DA D1 receptor agonists SKF 82958 and dihydrexidine, which have been shown to have antiparkinsonian actions in MPTP-treated primates (Taylor et al., 1991; Akai et al., 1995a,b; Gnanalingham et al., 1995), are capable of producing a robust suppression of cholinomimetic-induced TJMs (Mayorga et al., 1999a).

Antiparkinsonian anticholinergics, such as the muscarinic antagonists benztropine, scopolamine, and atropine, also reliably suppress TJM activity (Rupniak et al., 1983; Salamone et al., 1986, 1990; Steinpreis et al., 1993; Salamone and Baskin, 1996; Cousins et al., 1997; Mayorga et al., 1997; Betz et al., 2007, 2009; **Table 2**). Taken together with studies showing that cholinomimetics can induce TJMs, these findings reinforce the idea that the striatal DA and ACh systems interact in a complex way to regulate motor function and dysfunction (Aquiloni, 1980; Zigmond et al., 1987; Olanas et al., 1996; Salamone et al., 1998, 2001; Olanas and Onali, 1999; Calabresi et al., 2000, 2006; Pisani et al., 2003, 2007; Zhou et al., 2003; Morris et al., 2004; Cragg, 2006; Threlfell et al., 2010). The striatum contains large aspiny cholinergic neurons, and is rich in muscarinic receptors, with M1 and M4 subtypes being the predominant postsynaptic receptors (Hersch et al., 1994; Santiago and Potter, 2001). The M4 subtype of muscarinic receptor in particular has been implicated in the regulation of TJM activity (Mayorga et al., 1999c; Salamone et al., 2001; Betz et al., 2007, 2009).

Most recently, the ability of adenosine A_{2A} antagonists to reverse TJMs has been extensively studied (**Table 2**). Adenosine A_{2A} receptors are highly expressed in neostriatum, and A_{2A} antagonists exert motor effects in rodents and primates that are consistent with antiparkinsonian actions (Ferré et al., 1997, 2004; Rosin et al., 1998; Chen et al., 2001; Morelli and Pinna, 2001; Morelli et al., 2007; Salamone et al., 2008b; Collins et al., 2010a,b). Human clinical reports have indicated that the adenosine A_{2A} antagonists istradefylline (KW 6002), preladenant (SCH 420814), ST-1535, and BIIB014 significantly improve motor deficits, reduce OFF time, and increase ON time in parkinsonian patients, suggesting that members of this drug class may be efficacious as antiparkinsonian agents (Hauser et al., 2003, 2008; Jenner, 2005; LeWitt et al., 2008; Stacy et al., 2008; Gillespie et al., 2009; Pinna, 2009; Factor et al., 2010; Fernandez et al., 2010; Mizuno et al., 2010; Salamone, 2010; Knebel et al., 2011). The adenosine A_{2A} antagonists KF 17837, istradefylline, SCH 58261, ST 1535, ANR94, AA47070, MSX-3, and MSX-4 have all been shown to significantly reverse the TJMs induced by DA depletion, DA antagonism, and cholinomimetic administration (Correa et al., 2004; Simola et al., 2004; Tronci et al., 2007; Salamone et al., 2008a; Betz et al., 2009; Collins et al., 2010a; Pinna et al., 2010; Collins et al., 2011; Collins-Praino et al., 2011b). The ability of TJMs to be reversed by several classes of commonly used as well as experimental antiparkinsonian drugs provides support for the predictive validity of the TJM model as a rodent model of parkinsonian tremor.

VALIDATION OF THE TREMULOUS JAW MOVEMENT MODEL: ANATOMICAL CHARACTERISTICS OF THE TJMs IN RATS ARE SIMILAR TO THOSE OF HUMAN PARKINSONIAN TREMOR

Multiple studies have demonstrated that TJMs induced by interference with DA transmission and by cholinomimetic administration are dependent upon striatal mechanisms, particularly upon the ventrolateral striatum (VLS). The VLS, thought to be a rodent homolog of the primate ventral putamen, is somatotopically organized (Pisa, 1988; Jicha and Salamone, 1991; Salamone et al., 1993a,b) and receives input from sensory and motor cortices related to head, orofacial, and forepaw areas (McGeorge and Faull, 1989; Salamone et al., 1998). Since the VLS is considered to be the homolog of the primate ventral putamen, it is interesting to note that the putamen

is the striatal subregion within which DA depletions are most highly correlated with the presence of tremor in human parkinsonian patients (Bernheimer et al., 1973). Overall, the VLS is considered to be a critical striatal subregion at which DA, ACh, and adenosine receptor mechanisms interact to regulate TJMs (Salamone et al., 1998, 2008b; see VLS section in **Figure 3**).

Depletions of DA in the VLS by local injections of 6-OHDA were shown to induce TJMs, while injections in other striatal regions were ineffective (Jicha and Salamone, 1991; Finn et al., 1997a). A similar pattern has been reported using manipulations of the cholinergic system (Kelley et al., 1989; Salamone et al., 1990; Kikuchi de Beltran et al., 1992). Microdialysis methods demonstrated that increases in extracellular levels of ACh in VLS were correlated with the jaw movements induced by tacrine and physostigmine (Cousins et al., 1999). Cholinomimetic-induced TJMs were suppressed by local injections of muscarinic antagonists into the VLS but not into the medial striatum (Kelley et al., 1989; Salamone et al., 1990; Kikuchi de Beltran et al., 1992; Mayorga et al., 1997). Hemicholinium, which reduces ACh synthesis by blocking high affinity choline uptake, suppressed tacrine-induced jaw movements when injected into the VLS, but not into overlying cortex (Cousins et al., 1999). The suppression of pilocarpine-induced jaw movements that was produced by the DA D1 agonist SKF 82958 was reversed by injections of the D1 antagonist SCH 23390 into VLS, but not overlying cortex (Mayorga et al., 1999a). In addition, injections of the c-AMP analog 8-bromo-c-AMP into the VLS suppressed pilocarpine-induced jaw movements, while injections into cortex were ineffective (Mayorga et al., 1999b).

Most recently, it has been hypothesized that the VLS is the neostriatal subregion within which adenosine A_{2A} antagonists can suppress TJM activity. Recent studies demonstrated that injections of the adenosine A_{2A} antagonist MSX-3 directly into the VLS suppressed the TJMs induced by the DA antagonist pimozide

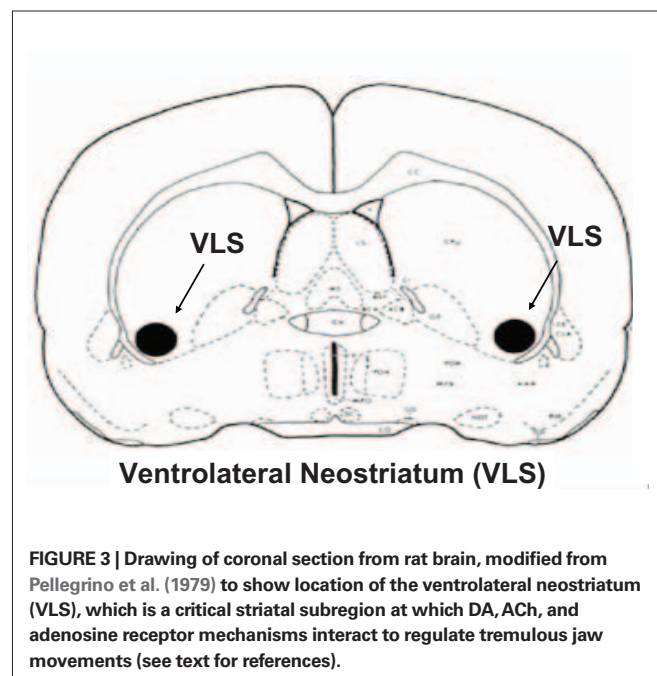


FIGURE 3 | Drawing of coronal section from rat brain, modified from Pellegrino et al. (1979) to show location of the ventrolateral neostriatum (VLS), which is a critical striatal subregion at which DA, ACh, and adenosine receptor mechanisms interact to regulate tremulous jaw movements (see text for references).

(Salamone et al., 2008a). In addition, the adenosine A_{2A} antagonist istradefylline reversed pimozide-induced c-Fos expression in the VLS at a dose that also suppressed pimozide-induced TJMs (Betz et al., 2009).

TREMULOUS JAW MOVEMENTS ARE NOT A MODEL OF TARDIVE DYSKINESIA

Since oral movements in rats have been observed to result from chronic administration of DA antagonists, it could be suggested that TJMs represent an animal model of tardive dyskinesia (Ellison et al., 1987; Ellison and See, 1989; Creed et al., 2010). However, several lines of evidence conflict with this view. First, the fact that a tremor is orofacial does not make it a model of tardive dyskinesia, *per se*. As reviewed above, parkinsonian tremors can include up-and-down movements of the jaw (Barbeau, 1986; Hunker and Abbs, 1990), and “rabbit syndrome” is a drug-induced parkinsonian tremor that is characterized by chewing-like movements (Sovner and Dimascio, 1977; Weiss et al., 1980; Tarsy, 1983). Differences between rodents and humans in the relative prevalence of hand versus jaw tremor may simply be due to species differences in motor system anatomy and physiology (i.e., the relative proportion of the motor system dedicated to orofacial versus limb control in rodents and humans; Salamone et al., 1998).

By definition, tardive dyskinesia is produced by *chronic* administration of DA antagonists. In contrast, TJMs in rats can be produced by acute or sub-chronic administration of DA antagonists (Glassman and Glassman, 1980; Rupniak et al., 1985, 1986; Jicha and Salamone, 1991; Steinpreis and Salamone, 1993; Steinpreis et al., 1993; Egan et al., 1996; Ishiwari et al., 2005; Salamone et al., 2008a; Collins et al., 2010a; Galtieri et al., 2010) or by acute DA depletion with reserpine (Baskin and Salamone, 1993; Steinpreis and Salamone, 1993; Salamone et al., 2008b). Furthermore, while muscarinic ACh antagonists reduce both parkinsonian symptoms in humans and TJMs in rats (Betz et al., 2007; Collins et al., 2011), they worsen tardive dyskinesia (Fahn et al., 1974; Burnett et al., 1980; Noring et al., 1984). Similarly, while L-DOPA reduces TJMs (Cousins et al., 1997), it is well known to induce dyskinesias. Finally, as described earlier, the jaw movements induced by DA depletion or cholinomimetics have frequency characteristics that are quite different from tardive dyskinesia. While TJMs show maximal activity in the 3 to 7-Hz frequency range (See and Chapman, 1991; Salamone and Baskin, 1996; Finn et al., 1997b; Mayorga et al., 1997; Cousins et al., 1998; Salamone et al., 1998; Ishiwari et al., 2005; Collins et al., 2010a; Galtieri et al., 2010), tardive dyskinesia is typically in the range of 1–2 Hz (Alpert et al., 1976; Wirshing et al., 1989a,b).

THE UTILITY OF THE TREMULOUS JAW MOVEMENT MODEL FOR ASSESSING NOVEL TREATMENT STRATEGIES FOR TREMOR: RECENT DEVELOPMENTS

As described above, basal ganglia regulation of motor function involves interactions between a wide array of transmitters and neuromodulators, including DA, ACh, adenosine, 5-HT, GLU, and GABA, as well as circuits that interconnect striatal and non-striatal regions. The complexity of these interactions provides a daunting challenge to the investigator, but it also provides a framework for understanding how a symptom such as tremor

can be induced or ameliorated by a variety of different conditions. Moreover, it provides avenues for the development of novel treatments for tremor.

In view of the continued uncertainty about the pathophysiology of parkinsonian tremor (Deuschl et al., 2000; Sung et al., 2008), it is important to identify the physiological conditions that are correlated with the generation of tremulous movements in animal models. As described above, pharmacological evidence links the VLS subregion of the neostriatum to the production of TJMs. In a recent preliminary study, increased tremor-related oscillatory activity in local field potential (LFP) signals was observed within the VLS subregion of the neostriatum during the occurrence of pilocarpine-induced TJMs (Collins et al., 2010c). During tremor activity, there was a sharp increase in LFP power in the VLS in the 5 to 8-Hz band (**Figure 4**). This increase in power was noticeably absent in VLS when tremor activity was not occurring. This is consistent with findings from the spectral analyses of EMG traces recorded from the temporalis muscle during tremor and non-tremor epochs (see above). Furthermore, during periods of tremor activity, there was a broad increase in beta band (15–30 Hz) activity (**Figure 4**). This increase in beta band power was not present during periods without TJM activity. These findings are consistent with studies obtained from parkinsonian patients. Both single-unit and LFP recordings in patients with Parkinson’s disease have shown evidence of tremor-related frequencies (~4–8 Hz) and increased “beta” (~8–30 Hz) frequency activity in basal ganglia structures, typically globus pallidus, and STN (Hutchison et al., 1997; Weinberger et al., 2006; see also Hutchison et al., 2004 or Hammond et al., 2007 for reviews). Additionally, increases at both ~6 Hz (tremor frequency) and ~20 Hz (beta frequency) can be observed in LFP signals in globus pallidus and STN of Parkinson’s disease patients off L-DOPA, while after L-DOPA treatment is reinstated, both the tremor and beta frequency LFPs diminish (Brown et al., 2001). The relationship between a specific neurophysiological phenomenon (e.g., altered output in specific structures and changes in the frequency of output) and particular Parkinsonian symptoms is unclear, although some evidence suggests that the low frequency increase at 4–8 Hz is related to tremor, while the increase in “beta” (15–30 Hz) interferes with the initiation and maintenance of movements (Levy et al., 2002; see however Weinberger et al., 2006). It has been proposed that the focal (spatially-limited) occurrence of gamma (~40–80 Hz) is associated with movement initiation (Courtenance et al., 2003; Masimore et al., 2005) and that changes in striatal neurochemistry that lead to parkinsonism transform basal ganglia circuits from participating in focal (spatially limited) gamma ensembles toward more global beta oscillations (e.g., Pessiglione et al., 2005). In light of this, the findings of increases in VLS LFP power at 4–8 Hz and in the beta band during TJMs may provide important information about the physiological mechanisms underlying tremorogenesis.

Tremulous jaw movements have also been examined in relation to hippocampal theta and epileptiform activity. Doses of the cholinergic agonist pilocarpine can induce increases in theta (6–10 Hz) during awake-immobility in the rat, but there was no obvious temporal relationship between theta and the presence/absence of TJMs (Collins et al., 2010c; **Figure 5**). In addition, although very

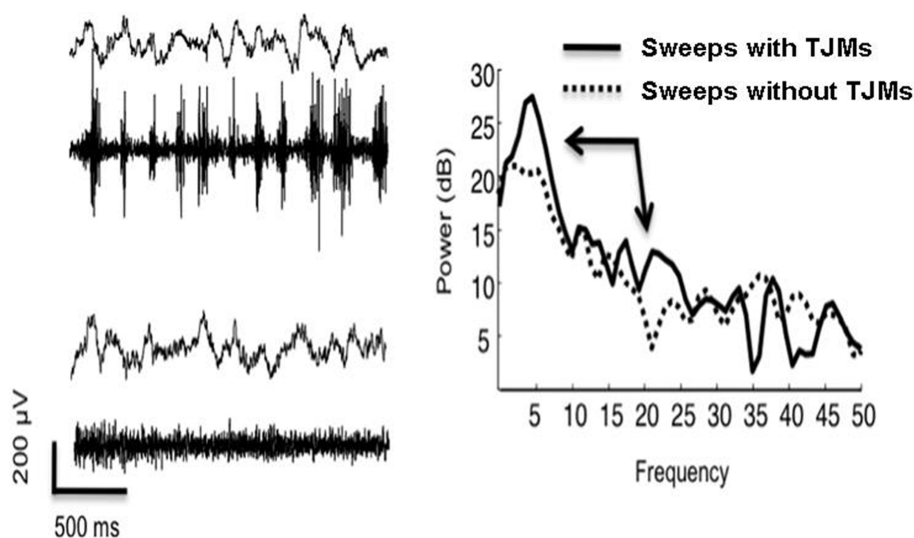


FIGURE 4 | Ventrolateral neostriatal LFP signal (Left: top trace in each pair) and EMG (Left: bottom trace in each pair) with and without rhythmic EMG activity (temporalis muscle) in behaving-rat following 0.5 mg pilocarpine. Traces were recording 10–15 min following treatment. Power spectral density (right) of 2-s traces

indicate prominent increase in power in 5–8 Hz band as well as a broad increase in beta band “15–30” Hz activity (see arrows). Note increased frequency and regularity of ~5 Hz signal in traces with rhythmic EMG activity as compared to slower and less regular LFP traces in absence of rhythmic EMG activity.

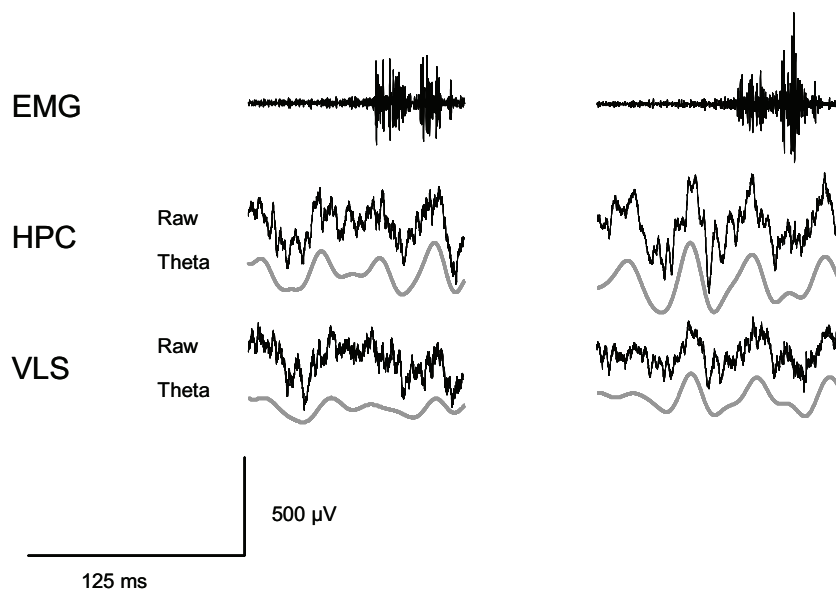


FIGURE 5 | Electromyographic (EMG) activity indicates the presence of jaw movement activity (upper left trace). Concurrently recorded hippocampal LFP indicates the absence of hippocampal theta (middle left). In another trace, EMG indicates a jaw movement burst (upper right trace) occurring in the presence of hippocampal theta (middle right). The two

phenomena occur independently of each other and are not correlated. Additionally, no epileptiform activity is present during the occurrence of either jaw movement burst at the dose of 0.5 mg/kg pilocarpine. Epileptiform activity only becomes apparent at a much higher dose of pilocarpine (i.e., 50 mg/kg pilocarpine, data not shown).

high doses of pilocarpine such as 50.0–100 mg/kg IP can produce epileptiform activity, no epileptiform activity is seen under pharmacological conditions that produce TJMs (data not shown). In conjunction with the earlier findings presented, these recent data provide further evidence that TJMs are being induced via actions within the VLS itself and not being driven by other factors, such as hippocampal theta or epileptiform activity.

Tremulous jaw movements have become a useful model for experimental assessment of diverse tremorogenic and tremorolytic conditions. As reviewed above, adenosine A_{2A} antagonists can suppress TJMs; consistent with this observation, we recently found that systemic administration of non-sedative doses of the A_{2A} agonist CGS 21680 can induce TJMs (Figure 6). Moreover, TJMs have been shown to be attenuated by several serotonergic

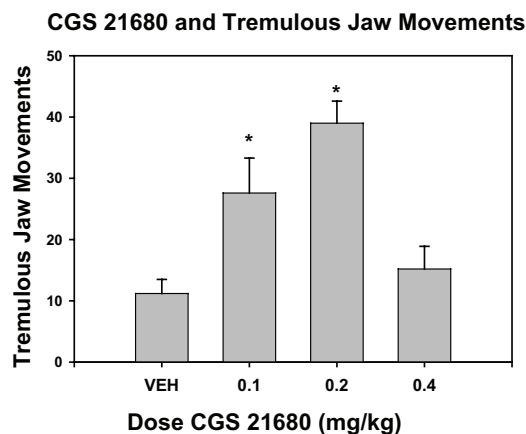


FIGURE 6 | Effect of the adenosine A_{2A} agonist CGS 21680 on the induction of tremulous jaw movements. One group of rats was used; all animals received IP injections of the following doses: saline vehicle, 0.1 mg/kg, 0.2 mg/kg, and 0.4 mg/kg ($n = 8$). Using a within-groups design, all rats received all drug treatments in a randomly varied order (one treatment per week). Injections were given 5 min before the animals were placed in a TJM observation chamber. All animals were allowed to habituate in the chamber for 10 min, and were subsequently observed for tremulous jaw movements for 15 min. Data are shown as mean (\pm SEM) number of individual jaw movements (per 15 min observation period). Systemic injections of CGS 21680 induced tremulous jaw movements overall [$F(3,21) = 9.15$, $p < 0.001$]. Planned comparisons indicated that there were significant differences between vehicle and 0.1 mg/kg CGS 21680 and 0.2 mg/kg ($*p < 0.05$). At the 0.4-mg/kg dose of CGS 21680, rats showed profound sedation, and were either drowsy or asleep during the observation period. (Data are from the Pharm D. honors thesis of Dr. K. L. Rychalsky, University of Connecticut).

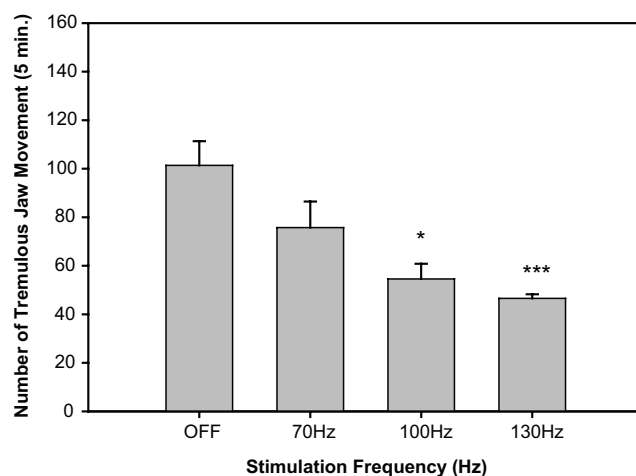


FIGURE 7 | Effect of subthalamic nucleus deep brain stimulation on the tremulous jaw movements induced by 3.0 mg/kg of the anticholinesterase galantamine (IP; data are from Collins-Praino et al., 2011a). All rats were implanted with unilateral subthalamic nucleus stimulating electrodes. After injection of galantamine, rats had alternating 5-min periods of stimulation off, followed by stimulation on; stimulation frequency was varied across the session. This curve shows the frequency-dependence of the effect of deep brain stimulation on tremulous jaw movements; there was an overall suppressive effect of brain stimulation on jaw movement activity [$F(3,50) = 4.6$, $p < 0.01$]. $*p = 0.05$; $***p < 0.001$.

drugs, including the serotonin 5-HT₂ family antagonist mianserin (Carlson et al., 2003b), the 5-HT_{2A} receptor inverse agonist, ACP-103 (Vanover et al., 2008), and the 5-HT(1A) agonists 8-OH-DPAT, buspirone, and F-97013-GD (Zazpe et al., 2006). The TJM model also has been incorporated into methods used to discriminate between the effects of typical antipsychotics and later-generation compounds such as clozapine, olanzapine, and quetiapine (Chesler and Salamone, 1996; Trevitt et al., 1998, 1999; Betz et al., 2005). Tacrine-induced TJMs also were shown to be suppressed by the T-type calcium channel blocker zonisamide (Miwa et al., 2008, 2009, 2011), which has anticonvulsant and tremorolytic effects in humans. Furthermore, stimulation of GABA transmission in SNr, either by local injection the GABA_A agonist muscimol (Finn et al., 1997a) or by nigral transplantation of engineered GABA-producing cells (Carlson et al., 2003a) reduced cholinomimetic-induced TJMs.

In recent years, high frequency stimulation of the STN has become a standard treatment of tremor used by neurosurgeons (Ashkan et al., 2004). In MPTP-treated primates, high frequency stimulation of the STN has been shown to improve rigidity and motor scores (Benazzouz et al., 1993, 1996; Ashkan et al., 2004). In 1993, the first bilateral STN electrodes were implanted in human patients, and high frequency STN stimulation improved rigidity, tremor, akinesia, postural/gait instabilities, independence, and quality of life, as well as reducing drug-induced dyskinesias (Benabid et al., 1994; Limousin et al., 1995, 1998; Ashkan et al.,

2004). Despite its efficacy as a therapeutic measure, however, a clear consensus on the mechanism of action of DBS has yet to be reached, and several competing hypotheses have been put forward. Animal models of tremor could be useful for investigating potential mechanisms of action of DBS. In a recent study by Collins-Praino et al. (2011a), TJMs were induced by a DA D1 antagonist (SCH 39166), a DA D2 antagonist (pimozide), a muscarinic agonist (pilocarpine), and an anticholinesterase (galantamine). Unilateral high frequency stimulation (130 Hz) of the STN, but not of a striatal control site, was shown to be effective at reversing the TJMs induced by all four pharmacological agents (Figure 7). Stimulation at lower frequencies or intensities failed to decrease TJMs compared to baseline “OFF” epochs, indicating that this response is not only dependent upon the brain area stimulated but also upon the frequency and intensity parameters used. When the adenosine A_{2A} antagonist MSX-3 was co-administered with high frequency stimulation of the STN, both the frequency and intensity parameters necessary to produce a suppression of galantamine-induced TJMs were drastically reduced (Figure 7). These results serve to provide a further validation of the TJM model, and also may have critical significance for the selection of parameters used during deep brain stimulation in parkinsonian patients undergoing this procedure for the treatment of medically refractory tremor. Based on the results of this study, it is possible that the prescription of an adenosine A_{2A} antagonist to these patients may result in a significant reduction in the frequency and/or intensity parameters needed for therapeutic efficacy and, thereby, a near doubling of the therapeutic window for these parkinsonian patients.

Table 1 | Neurochemical and pharmacological conditions that induce TJMs.

DA depletion using 6-OHDA	Rodriguez-Diaz et al. (2001), Jicha and Salamone (1991), Finn et al. (1997b)
DA depletion using reserpine	Steinpreis and Salamone (1993), Baskin and Salamone (1993), Salamone and Baskin (1996), Salamone et al. (2008)
DA antagonism using "typical" antipsychotic drugs	Glassman and Glassman (1980), Rupniak et al. (1985, 1986), Jicha and Salamone (1991), Steinpreis et al. (1993), Steinpreis and Salamone (1993), Egan et al. (1996), Trevitt et al. (1998), Wisniecki et al. (2003), Ishiwari et al. (2005), Betz et al. (2007, 2009), Collins et al. (2010a)
Muscarinic agonists	Rupniak et al. (1983, 1985), Salamone et al. (1986, 1990), Stewart et al. (1987, 1988), Baskin et al. (1994), Finn et al. (1997a,b), Collins et al. (2010a)
Anticholinesterases	Kelley et al. (1989), Mayorga et al. (1997), Simola et al. (2004), Tronci et al. (2007), Kasture et al. (2009), Pinna et al. (2010), Collins-Praino et al. (2011b)

Table 2 | Antiparkinsonian drugs that reverse tremulous jaw movements.

DA Precursors (L-DOPA)	Cousins and Salamone (1996), Cousins et al. (1997)
DA Agonists	Baskin and Salamone (1993), Cousins et al. (1997), Mayorga et al. (1999a), Salamone et al. (2005)
Amantadine	Cousins et al. (1997)
Diphenhydramine	Carlson et al. (2000)
Muscarinic antagonists	Rupniak et al. (1983), Salamone et al. (1986, 1990), Steinpreis et al. (1993), Salamone and Baskin (1996), Cousins et al. (1997), Mayorga et al. (1997), Betz et al. (2007, 2009)
Adenosine A _{2A} antagonists	Correa et al. (2004), Simola et al. (2004), Tronci et al. (2007), Salamone et al. (2008a), Betz et al. (2009), Collins et al. (2010a), Pinna et al. (2010), Collins-Praino et al. (2011b)

CONCLUSION

In conclusion, the TJM model shares many of the pharmacological, temporal, and anatomical characteristics of human parkinsonian tremor. Thus, it can be viewed as meeting a reasonable set of validation criteria as a rodent model of parkinsonian resting tremor. The validation of this model represents a significant advance forward in the scientific study of parkinsonian resting tremor, which still has a great deal of uncertainty surrounding its pathophysiology. The TJM model allows for

basic research into the neurochemical mechanisms that regulate tremor, and the development of oscillatory patterns of activity in the brain that are thought to underlie tremorogenesis. Eventually, this research may lead to the development of novel treatments for tremor.

ACKNOWLEDGMENT

This work was supported by grants to John D. Salamone from the University of Connecticut Research Foundation.

REFERENCES

- Aarsland, D., Hutchison, M., and Larsen, J. P. (2003). Cognitive, psychiatric and motor response to galantamine in Parkinson's disease with dementia. *Int. J. Geriatr. Psychiatry* 18, 937–941.
- Adams, R. D., and Victor M. (1993). "Tremors, myoclonus, spasms and tics," in eds R. D. Adams, and M. Victor. *Principles of Neurology* 5th edition (New York: McGraw Hill), 69–79.
- Akai, T., Ozawa, M., Yamaguchi, M., Mizuta, E., and Kuno, S. (1995a). Combination treatment of the partial D2 agonist terguride with the D1 agonist SKF 82958 in 1-methyl-4-phenyl-1,2,3,6-tetrahydropyridine-lesioned parkinsonian cynomolgus monkeys. *J. Pharmacol. Exp. Ther.* 273, 309–314.
- Akai, T., Ozawa, M., Yamaguchi, M., Mizuta, E., and Kuno, S. (1995b). Behavioral involvement of central dopamine D1 and D2 receptors in 1-methyl-4-phenyl-1,2,3,6-tetrahydropyridine (MPTP)-lesioned parkinsonian cynomolgus monkeys. *Jpn. J. Pharmacol.* 67, 117–124.
- Alpert, M., Diamond, F., and Friedhoff, A. J. (1976). Tremorographic studies in tardive dyskinesia. *Psychopharmacol. Bull.* 12, 5–7.
- Alvarez, M. V., Evidente, V. G., and Driver-Dunkley, E. D. (2007). Differentiating Parkinson's disease from other parkinsonian disorders. *Semin. Neurol.* 27, 356–362.
- Aquilonius, S. M. (1980). "Cholinergic mechanisms in the CNS related to Parkinson's disease," in *Parkinson's Disease-Current Progress, Problems and Management*, eds U. K. Rinne, M. Klinger, and Stamm, G. (North Holland: Elsevier), 17–27.
- Arai, M. (2000). Parkinsonism onset in a patient concurrently using tiapride and donepezil. *Intern. Med.* 39, 863.
- Ashkan, K., Wallace, B., Bell, B. A., and Benabid, A. L. (2004). Deep brain stimulation of the subthalamic nucleus in Parkinson's Disease 1993–2003: where are we 10 years on? *Br. J. Neurosurg.* 18, 19–34.
- Bara-Jimenez, W., Sherzai, A., Dimitrova, T., Favit, A., Bibbiani, F., Gillespie, M., Morris, M. J., Mouradian, M. M., and Chase, T. N. (2003). Adenosine A(2A) receptor antagonist treatment of Parkinson's disease. *Neurology* 61, 293–296.
- Barbeau, A. (1986). "Parkinson's disease: clinical features and etiopathology," in *Handbook of Clinical Neurology*, Vol. 5 *Extrapyramidal Disorders*, eds P. J. Vinken, G. W. Bruyn, and I. Klawans, II (North Holland: Elsevier), 87–152.
- Baskin, P., Gianutsos, G., and Salamone, J. D. (1994). Repeated scopolamine injections sensitize rats to pilocarpine-induced vacuous jaw movements and enhance striatal muscarinic receptor binding. *Pharmacol. Biochem. Behav.* 49, 437–442.
- Baskin, P., and Salamone, J. D. (1993). Vacuous jaw movements in rats induced by acute reserpine administration: interactions with different doses of apomorphine. *Pharmacol. Biochem. Behav.* 46, 793–797.
- Benabid, A. L., Pollak, P., Gross, C., Hoffmann, D., Benazzouz, A., Gao, D. M., Laurent, A., Gentil, M., and Perret, J. (1994). Acute and long-term effects of subthalamic nucleus stimulation in Parkinson's disease. *Stereotact. Funct. Neurosurg.* 62, 76–84.
- Benazzouz, A., Boraud, T., Feger, J., Boraud, P., Bioulac, B., and Gross, C. (1996). Alleviation of experimental hemiparkinsonism by high-frequency stimulation of the subthalamic nucleus in primates: a comparison with L-DOPA treatment. *Mov. Disord.* 11, 627–632.
- Benazzouz, A., Gross, C., Feger, J., Boraud, T., and Bioulac, B. (1993). Reversal of

- rigidity and improvement in motor performance by subthalamic high-frequency stimulation in MPTP-treated monkeys. *Eur. J. Neurosci.* 5, 382–389.
- Ben-Pazi, H., Bergman, H., Goldberg, J. A., Giladi, N., Hansel, D., Reches, A., and Simon, E. S. (2001). Synchrony of rest tremor in multiple limbs in Parkinson's disease: evidence for multiple oscillators. *J. Neural Transm.* 108, 287–296.
- Bergman, H., and Deuschl, G. (2002). Pathophysiology of Parkinson's disease: from clinical neurology to basic neuroscience and back. *Mov. Disord.* 17(Suppl. 3), s28–s40.
- Bergman, H., Feingold, A., Nini, A., Raz, A., Slovlin, H., Abeles, M., and Vaadia, E. (1998). Physiological aspects of information processing in the basal ganglia of normal and parkinsonian patients. *Trends Neurosci.* 21, 32–38.
- Bernheimer, H., Birkmayer, W., Hornykiewicz, O., Jellinger, K., and Seitelberger, F. (1973). Brain dopamine and the syndromes of Parkinson and Huntington: clinical, morphological and neurochemical correlations. *J. Neurol. Sci.* 20, 415–455.
- Betz, A., Ishiwari, K., Wisniecki, A., Huyn, N., and Salamone, J. D. (2005). Quetiapine (Seroquel) shows a pattern of behavioral effects similar to the atypical antipsychotics clozapine and olanzapine: studies with tremulous jaw movements in rats. *Psychopharmacology (Berl.)* 179, 383–392.
- Betz, A. J., McLaughlin, P. J., Burgos, M., Weber, S. M., and Salamone, J. D. (2007). The muscarinic receptor antagonist tropicamide suppresses tremulous jaw movements in a rodent model of parkinsonian tremor: possible role of M4 receptors. *Psychopharmacology (Berl.)* 194, 347–359.
- Betz, A. J., Vontell, R., Valenta, J., Worden, L., Sink, K. S., Font, L., Correa, M., Sager, T. N., and Salamone, J. D. (2009). Effects of the adenosine A2A antagonist KW-6002 (istradefylline) on pimoide-induced oral tremor and striatal c-Fos expression: comparisons with the muscarinic antagonist tropicamide. *Neuroscience* 163, 97–108.
- Bevan, M. D., Magill, P. J., Terman, D., Bolam, J. P., and Wilson, C. J. (2002). Move to the rhythm: oscillations in the subthalamic nucleus-external globus pallidus network. *Trends Neurosci.* 25, 525–531.
- Binder, S., Deuschl, G., and Volkmann, J. (2009). Effect of cabergoline on parkinsonian tremor assessed by long-term actigraphy. *Eur. Neurol.* 61, 149–153.
- Bourke, D., and Drukenbrod, R. W. (1998). Possible association between donepezil and worsening Parkinson's disease. *Ann. Pharmacother.* 32, 610–611.
- Boyce, S., Rupniak, N. M., Steventon, M. J., and Iversen, S. D. (1990). Differential effects of D1 and D2 agonists in MPTP-treated primates: functional implications for Parkinson's disease. *Neurology* 40, 927–933.
- Braun, A., Fabbrini, G., Mouradian, M. M., Serrati, C., Barone, P., and Chase, T. (1987). Selective D-1 dopamine receptor agonist treatment of Parkinson's disease. *J. Neural Transm.* 68, 41–50.
- Brown, P. (2003). Oscillatory nature of human basal ganglia activity: relationship to the pathophysiology of Parkinson's disease. *Mov. Disord.* 18, 357–363.
- Brown, P., Oliviero, A., Mazzone, P., Insola, A., Ttonali, P., and Di Lazzaro, V. (2001). Dopamine dependency of oscillations between subthalamic nucleus and pallidum in Parkinson's disease. *J. Neurosci.* 21, 1033–1038.
- Burnett, G. B., Prange, A. J., Wilson, I. C., Jolli, L. A., Creese, I. C., and Snyder, S. H. (1980). Adverse effects of anticholinergic antiparkinsonian drugs in tardive dyskinesia. *Neuropsychobiology* 6, 109–120.
- Calabresi, P., Centonze, D., Gubellini, P., Pisani, A., and Bernardi, G. (2000). Acetylcholine-mediated modulation of striatal function. *Trends Neurosci.* 23, 120–126.
- Calabresi, P., Picconi, B., Parnetti, L., and Di Filippo, M. (2006). A convergent model for cognitive dysfunctions in Parkinson's disease: the critical dopamine-acetylcholine synaptic balance. *Lancet Neurol.* 5, 974–983.
- Carlson, B. B., Behrstock, S., Tobin, A. J., and Salamone, J. D. (2003a). Brain implantations of engineered GABA-releasing cells suppress tremor in an animal model of parkinsonism. *Neuroscience* 119, 927–932.
- Carlson, B. B., Wisniecki, A., and Salamone, J. D. (2003b). Local injections of the 5-hydroxytryptamine antagonist mianserin into substantia nigra pars reticulara block tremulous jaw movements in rats: studies with a putative model of parkinsonian tremor. *Psychopharmacology (Berl.)* 165, 229–237.
- Carlson, B. B., Trevitt, J. T., and Salamone, J. D. (2000). Effects of H1 antagonists on cholinomimetic-induced tremulous jaw movements: studies of diphenhydramine, doxepin, and mepyramine. *Pharmacol. Biochem. Behav.* 65, 683–689.
- Cenci, M. A., Whishaw, I. Q., and Schallert, T. (2002). Animal models of neurological deficits: how relevant is the rat? *Nat. Rev. Neurosci.* 3, 574–579.
- Chen, J. F., Moratalla, R., Impagnatiello, F., Grandy, D. K., Cuellar, B., Rubinstein, M., Beilstein, M. A., Hackett, E., Fink, J. S., Low, M. J., Ongini, E., and Schwarzschild, M. A. (2001). The role of the D2 dopamine receptor (D2R) in A2A adenosine-receptor (A2AR) mediated behavioral and cellular responses as revealed by A2A and D2 receptor knockout mice. *Proc. Natl. Acad. Sci. U.S.A.* 98, 1970–1975.
- Chesler, E., and Salamone, J. (1996). Effects of acute and repeated clozapine injections on cholinomimetic-induced vacuuous jaw movements. *Pharmacol. Biochem. Behav.* 54, 619–624.
- Close, S. P., Elliott, P. J., Hayes, A. G., and Marriott, A. S. (1990). Effects of classical and novel agents in a MPTP-induced reversible model of Parkinson's disease. *Psychopharmacology (Berl.)* 102, 295–300.
- Collins, L. E., Galtieri, D. J., Brennum, L. T., Sager, T. N., Hockemeyer, J., Müller, C. E., Hinman, J. R., Chrobak, J. J., and Salamone, J. D. (2010a). Cholinomimetic-induced tremulous jaw movements are suppressed by the adenosine A2A antagonists MSX-3 and SCH58261, but not the adenosine A1 antagonist DPCPX: possible relevance for drug-induced parkinsonism. *Pharmacol. Biochem. Behav.* 94, 561–569.
- Collins, L. E., Galtieri, D. J., Collins, P., Jones, S. K., Port, R. G., Paul, N. E., Hockemeyer, J., Muller, C. E., and Salamone, J. D. (2010b). Interactions between adenosine and dopamine receptor antagonists with different selectivity profiles: effects on locomotor activity. *Behav. Brain Res.* 211, 148–155.
- Collins, L. E., Chrobak, J. J., and Salamone, J. D. (2010c). The characterization of electromyographic and EEG activity in the tremulous jaw movement model: the use of time series analysis to investigate the pathophysiology of parkinsonian resting tremor. *Society for Neuroscience Annual Meeting Abstract Locator*, San Diego, CA.
- Collins, L. E., Paul, N. E., Abbas, S. F., Leser, C. E., Galtieri, D. J., Chrobak, J. J., Baqi, Y., Muller, C. E., and Salamone, J. D. (2011). Oral tremor induced by galantamine in rats: a model of the parkinsonian side effects of cholinomimetics used to treat Alzheimer's disease. *Pharmacol. Biochem. Behav.* 99, 414–422.
- Collins-Praino, L. E., Paul, N. E., Ledgard, F., Podurgiel, S., Kovner, R., Satzer, D., McPherson, M., Rhodes, C., Hussain, N., Huber, M., Salamone, J. D., and Senatus, P. B. (2011a). Effect of subthalamic nucleus deep brain stimulation on drug-induced tremulous jaw movements. (In preparation).
- Collins-Praino, L. E., Pennarolla, A., Port, R. G., Sager, T. N., and Salamone, J. D. (2011b). The novel adenosine antagonist Lu AA47070 reverses the motor and motivational effects produced by dopamine D2 receptor blockade. (Submitted).
- Correa, M., Wisniecki, A., Betz, A., Dobson, D. R., O'Neill, M. F., O'Neill, M. J., and Salamone, J. D. (2004). The adenosine A2A antagonist KF 17837 reverses the locomotor suppression and tremulous jaw movements induced by haloperidol in rats: possible relevance to parkinsonism. *Behav. Brain Res.* 148, 47–54.
- Courtenance, R., Fujii, N., and Graybiel, A. M. (2003). Synchronous, focally modulated beta-band oscillations characterize local field potential activity in the striatum of awake behaving monkeys. *J. Neurosci.* 23, 11741–11752.
- Cousins, M. S., Atherton, A., and Salamone, J. D. (1998). Behavioral and electromyographic characterization of the local frequency of tacrine-induced tremulous jaw movements. *Physiol. Behav.* 64, 153–158.
- Cousins, M. S., Carriero, D. L., and Salamone, J. D. (1997). Tremulous jaw movements induced by the acetylcholinesterase inhibitor tacrine: effects of antiparkinsonian drugs. *Eur. J. Pharmacol.* 322, 137–145.
- Cousins, M. S., Finn, M., Trevitt, J., Carriero, D. L., Conlan, A., and Salamone, J. D. (1999). The role of ventrolateral striatal acetylcholine in the production of tacrine-induced jaw movements. *Pharmacol. Biochem. Behav.* 62, 439–447.
- Cousins, M. S., and Salamone, J. D. (1996). Involvement of ventrolateral striatal dopamine in movement initiation and execution: a microdialysis and behavioral investigation. *Neuroscience* 70, 849–859.
- Cragg, S. J. (2006). Meaningful silences: how dopamine listens to the Ach pause. *Trends Neurosci.* 29, 125–131.
- Creed, M., Hamani, C., and Nobrega, J. N. (2010). Deep brain stimulation of the subthalamic or entopeduncular nucleus attenuates vacuuous chewing movements in a rodent model of tardive dyskinesia. *Eur. Neuropsychopharmacol.* 21, 393–400.
- DeLong, M. R. (1990). Primate model of movement disorders of basal ganglia origin. *Trends Neurosci.* 13, 281–285.
- Deuschl, G., Krack, P., Lauk, M., and Timmer, J. (1996). Clinical neurophys-

- iology of tremor. *J. Clin. Neurophysiol.* 13, 110–121.
- Deuschl, G., Raethjen, J., Baron, R., Lindemann, M., Wilms, H., and Krack, P. (2000). The pathophysiology of parkinsonian tremor: a review. *J. Neurol.* 247(Suppl. 5), V/33–V/48.
- Deuschl, G., Raethjen, J., Lindemann, M., and Krack, P. (2001). The pathophysiology of tremor. A review. *Muscle Nerve* 24, 716–735.
- Duvoisin, R. C. (1967). Cholinergic-anticholinergic antagonism in parkinsonism. *Arch. Neurol.* 17, 124–136.
- Egan, M. F., Hurd, Y., Ferguson, J., Bachus, S. E., Hamid, E. H., and Hyde, T. M. (1996). Pharmacological and neurochemical differences between acute and tardive vacuous chewing movements induced by haloperidol. *Psychopharmacology (Berl.)* 127, 337–345.
- Elbe, R. J., and Koller, W. C. (1990). *Tremor*. Baltimore, MD: Johns Hopkins University Press.
- Ellison, G., and See, R. (1989). Rats administered chronic neuroleptics develop oral movements which are similar in form to those in humans with tardive dyskinesia. *Psychopharmacology (Berl.)* 98, 564–566.
- Ellison, G., See, R., Levin, E., and Kinney, J. (1987). Tremorous mouth movements in rats administered chronic neuroleptics. *Psychopharmacology* 92, 122–126.
- Factor, S., Mark, M. H., Watts, R., Struck, L., Mori, A., Ballerini, R., Sussman, N. M., and Istradefylline 6002-US-007 Study Group. (2010). A long-term study of istradefylline in subjects with fluctuating Parkinson's disease. *Parkinsonism Relat. Disord.* 16, 423–426.
- Fahn, W. E., Lake, C. R., and Gerber, C. J. (1974). Cholinergic suppression of tardive dyskinesia. *Psychopharmacology (Berl.)* 42, 135–137.
- Fernandez, H. H., Greeley, D. R., Zweig, R. M., Wojcieszek, J., Mori, A., and Sussman, N. M. (2010). Istradefylline as monotherapy for Parkinson disease: results of the 6002-US-051 trial. *Parkinsonism Relat. Disord.* 16, 16–20.
- Ferré, S., Ciruela, F., Canals, M., Marcellino, D., Burgueno, J., Casado, V., Hillion, J., Torvinen, M., Fanelli, F., Benedetti, P. D., Goldberg, S. R., Bouvier, M., Fuxe, K., Agnati, L. F., Lluis, C., Franco, R., and Woods, A. (2004). Adenosine A2A-dopamine D2 receptor-receptor heteromers. Targets for neuro-psychiatric disorders. *Parkinsonism Relat. Disord.* 10, 265–271.
- Ferré, S., Freidholm, B. B., Morelli, M., Popoli, P., and Fuxe, K. (1997). Adenosine-dopamine receptor-receptor interactions as an integrative mechanism in the basal ganglia. *Trends Neurosci.* 20, 482–487.
- Findley, L. J. (1988). "Tremors: differential diagnosis and pharmacology," in *Parkinson's Disease and Movement Disorders*, eds J. Jankovic and E. Tolosa (Baltimore: Urban and Schwarzenberg), 243–262.
- Findley, L. J., and Capildeo, R. (1984). *Movement Disorders: Tremor*. Oxford: Oxford University Press.
- Findley, L. J., and Gresty, M. A. (1981). Tremor. *Br. J. Hosp. Med.* 26, 16–32.
- Findley, L. J., and Gresty, M. A. (1988). Head, facial, and voice tremor. *Adv. Neurol.* 49, 239–253.
- Findley, L. J., Gresty, M. A., and Halmagyi, G. M. (1981). Tremor, the cogwheel phenomenon and clonus in Parkinson's disease. *J. Neurol. Neurosurg. Psychiatry* 44, 534–546.
- Finn, M., Mayorga, A. J., Conlan, A., and Salamone, J. D. (1997a). Involvement of pallidal and nigral GABA mechanisms in the generation of tremulous jaw movements in rats. *Neuroscience* 80, 532–544.
- Finn, M., Jassen, A., Baskin, P., and Salamone, J. D. (1997b). Tremulous characteristic of vacuous jaw movements induced by pilocarpine and ventrolateral striatal dopamine depletions. *Pharmacol. Biochem. Behav.* 57, 243–249.
- Galtieri, D. J., Collins, L. E., Paul, N. E., and Salamone, J. D. (2010). Subchronic administration of the dopamine D1 antagonist SCH 39166 (ecopipam) induces parkinsonian motor impairment in a rodent model of parkinsonism: potential role of the direct pathway. *Society for Neuroscience Annual Meeting Abstract Locator*, San Diego, CA.
- Gillespie, R. J., Bamford, S. J., Gaur, S., Jordan, A. M., Lerpiniere, J., Mansell, H. L., and Stratton, G. C. (2009). Antagonists of the human A(2A) receptor. Part 5: highly bio-available pyrimidine-4-carboxamides. *Bioorg. Med. Chem. Lett.* 19, 2664–2667.
- Glassman, R. B., and Glassman, H. N. (1980). Oral dyskinesia in brain-damaged rats withdrawn from neuroleptics: implication for models of tardive dyskinesia. *Psychopharmacology (Berl.)* 69, 19–25.
- Gnanalingham, K. K., Erol, D. D., Hunter, A. J., Smith, L. A., Jenner, P., and Marsden, C. D. (1995). Differential anti-parkinsonian effects of benzazepine D1 dopamine agonists with varying efficacies co-administered with quinpirole in primate and rodent models of Parkinson's disease. *Psychopharmacology (Berl.)* 117, 287–297.
- Gurevich, T. Y., Shabtai, H., Korczyn, A. D., Simon, E. S., and Giladi, N. (2006). Effect of rivastigmine on tremor in patients with Parkinson's disease and dementia. *Mov. Disord.* 21, 1663–1666.
- Halliday, D. M., Rosenberg, J. R., Amjad, A. M., Breeze, B., Conway, B. A., and Farmer, S. F. (1995). A framework for the analysis of mixed time series/point process data-theory and application to the study of physiological tremor, single motor unit discharges, and electromyograms. *Prog. Biophys. Mo. Biol.* 64, 237–278.
- Hammond, C., Bergman, H., and Brown, P. (2007). Pathological synchronization in Parkinson's disease: networks, models and treatments. *Trends Neurosci.* 30, 357–364.
- Hauber, W., Nagel, J., Sauer, R., and Muller, C. E. (1998). Motor effects induced by a blockade of adenosine A2A receptors in the caudate-putamen. *Neuroreport* 9, 1803–1806.
- Hauser, R. A., Hubble, J. P., Truong, D. D., and Istradefylline US-001 Study Group. (2003). Randomized trial of the adenosine A(2A) receptor antagonist istradefylline in advanced PD. *Neurology* 61, 297–303.
- Hauser, R. A., Shulman, L. M., Trugman, J. M., Roberts, J. W., Mori, A., Ballerini, R., Sussman, N. M., and Istradefylline 6002-US-013 Study Group. (2008). Study of istradefylline in patients with Parkinson's disease on levodopa with motor fluctuations. *Mov. Disord.* 23, 2177–2185.
- Hersch, S. M., Gutekunst, C. A., Rees, H. D., Heilman, C. J., and Levey, A. I. (1994). Distribution of m1-m4 muscarinic receptor proteins in the rat striatum: light and electron microscopic immunocytochemistry using subtype-specific antibodies. *J. Neurosci.* 14, 3351–3363.
- Hoehn, M. M., and Yahr, M. D. (1967). Parkinsonism: onset, progression, and mortality. *Neurology* 17, 427–442.
- Hornykiewicz, O. (1972). "Dopamine and its physiological significance in brain function," in *The Structure and Function of Nervous Tissue*, ed. G. H. Browne (New York: Academic Press), 367–414.
- Hornykiewicz, O. (1973). Dopamine in the basal ganglia. *Br. Med. Bull.* 29, 172–178.
- Hunker, C. J., and Abbs, J. H. (1990). Uniform frequency of parkinsonian resting tremor in the lips, jaw, tongue and index finger. *Mov. Disord.* 5, 71–77.
- Hurtado, J. M., Lachaux, J. P., Beckley, D. J., Gray, C. M., and Sigvardt, K. A. (2000). Inter- and intralimb oscillator coupling in parkinsonian tremor. *Mov. Disord.* 15, 683–691.
- Hurtado, J. M., Rubchinsky, L. L., Sigvardt, K. A., Wheelock, V. L., and Pappas, C. T. E. (2004). Temporal evolution of oscillations and synchrony in GPI/muscle pairs in Parkinson's disease. *J. Neurophysiol.* 93, 1569–1584.
- Hutchison, W. D., Dostrovsky, J. O., Walters, J. R., Courtemanche, R., Boraid, T., Goldberg, J., and Brown, P. (2004). Neuronal oscillations in the basal ganglia and movement disorders: evidence from whole animal and human recordings. *J. Neurosci.* 24, 9240–9243.
- Hutchison, W. D., Lozano, A. M., Tasker, R. R., Lang, A. E., and Dostrovsky, J. O. (1997). Identification and characterization of neurons with tremor-frequency activity in human globus pallidus. *Exp. Brain Res.* 113, 557–563.
- Ishiwari, K., Betz, A., Weber, S., Felsted, J., and Salamone, J. D. (2005). Validation of the tremulous jaw movement model for assessment of the motor effects of typical and atypical antipsychotics: effects of pimozide (Orap) in rats. *Pharmacol. Biochem. Behav.* 80, 351–362.
- Ishiwari, K., Mingote, S., Correa, M., Trevitt, J. T., Carlson, B. B., and Salamone, J. D. (2004). The GABA uptake inhibitor beta-alanine reduces pilocarpine-induced tremor and increases extracellular GABA in substantia nigra pars reticulata as measured by microdialysis. *J. Neurosci. Methods* 140, 39–46.
- Jankovic, J. (2009). Disease oriented approach to botulinum toxin use. *Toxicon* 54, 614–623.
- Jenner, P. (2005). Istradefylline, a novel adenosine A2A receptor antagonist, for the treatment of Parkinson's disease. *Expert Opin. Investig. Drugs* 14, 729–738.
- Jicha, G., and Salamone, J. D. (1991). Vacuous jaw movements and feeding deficits in rats with ventrolateral striatal dopamine depletions: possible model of parkinsonian symptoms. *J. Neurosci.* 11, 3822–3829.
- Kao, K. P., Kwan, S. Y., Lin, K. P., and Chang, Y. C. (1993). Coexistence of Parkinson's disease and myasthenia gravis: a case report. *Clin. Neurol. Neurosurg.* 95, 137–139.
- Kasture, S., Pontis, S., Pinna, A., Schintu, N., Spina, L., Longoni, R., Simola, N., Ballero, M., and Morelli, M. (2009). Assessment of symptomatic and neuroprotective efficacy of Mucuna pruriens seed extract in rodent model of Parkinson's disease. *Neurotox. Res.* 15, 111–122.
- Kelley, A. E., Bakshi, V. P., Delfs, J. M., and Lang, C. G. (1989). Cholinergic stimulation of the ventrolateral striatum elicits mouth movements in rats:

- pharmacological and regional specificity. *Psychopharmacology (Berl.)* 99, 542–549.
- Kikuchi de Beltran, K., Koshikawa, N., Saigusa, T., Watanabe, K., Koshida, Y., and Kobayashi, M. (1992). Cholinergic/dopaminergic interaction in the rat striatum assessed from drug-induced repetitive oral movements. *Eur. J. Pharmacol.* 214, 181–189.
- Knebel, W., Rao, N., Uchimura, T., Mori, A., Fisher, J., Gastonguay, M. R., and Chaikin, P. (2011). Population pharmacokinetic analysis of istradefylline in healthy subjects and in patients with Parkinson's disease. *J. Clin. Pharmacol.* 51, 40–52.
- Koller, W. C. (2002). Treatment of early Parkinson's disease. *Neurology* 58, S79–S86.
- Koster, B., Lauk, M., Timmer, J., and Lucking, C. H. (1997). Side to side correlation of pathological tremors. *Electroencephalogr. Clin. Neurophysiol.* 103, 211–220.
- Leventoglu, A., and Baysal, A. I. (2008). Benign tremulous Parkinson's disease. *Acta Neurol. Belg.* 108, 48–52.
- Levy, R., Ashby, P., Hutchison, W. D., Lang, A. E., Lozano, A. M., and Dostrovsky, J. O. (2002). Dependence of subthalamic nucleus oscillation on movement and dopamine in Parkinson's disease. *Brain* 125, 1196–1209.
- LeWitt, P. A., Guttman, M., Tetrud, J. W., Tuite, P. J., Mori, A., Chaikin, P., Sussman, N. M., and 6002-US-005 Study Group. (2008). Adenosine A2A receptor antagonist istradefylline (KW-6002) reduces “off” time in Parkinson's disease: a double-blind, randomized, multicenter clinical trial (6002-US-005). *Ann. Neurol.* 63, 295–302.
- Limousin, P., Krack, P., Pollak, P., Benazzouz, A., Ardouin, C., Hoffmann, D., and Benabid, A. L. (1998). Electrical stimulation of the subthalamic nucleus in advanced Parkinson's disease. *N. Engl. J. Med.* 339, 1105–1111.
- Limousin, P., Pollak, P., Benazzouz, A., Hoffmann, D., Le Bas, J. F., Broussolle, E., Perret, J. E., and Benabid, A. L. (1995). Effect of Parkinsonian signs and symptoms of bilateral subthalamic nucleus stimulation. *Lancet* 345, 91–95.
- Litvinenko, I. V., Odinak, M. M., Mogilnaya, V. I., and Emelin, A. Y. (2008). Efficacy and safety of galantamine (remnilyl) for dementia in patients with Parkinson's disease (an open controlled trial). *Neurosci. Behav. Physiol.* 38, 937–945.
- Mansur, P. H. G., Cury, L. K. P., Andrade, A. O., Pereira, A. A., Miotto, G. A., Soares, A. B., and Naves, E. L. (2007). A review of techniques for tremor recording and quantification. *Crit. Rev. Biomed. Eng.* 35, 343–362.
- Marsden, C. (1984). “Origins of normal and pathological tremor,” in *Movement Disorders: Tremor*, eds L. Findley and R. Capildeo (London: Butterworth), 37–84.
- Masimore, B., Schmitzer-Torbert, N. C., Kakalios, J., and Redish, A. D. (2005). Transient striatal gamma local field potentials signal movement initiation in rats. *Neuroreport* 16, 2021–2024.
- Mayorga, A. J., Carriero, D. L., Cousins, M. S., Gianutsos, G., and Salamone, J. D. (1997). Tremulous jaw movements produced by acute tacrine administration: possible relation to parkinsonian side effects. *Pharmacol. Biochem. Behav.* 56, 273–279.
- Mayorga, A. J., Trevitt, J. T., Conlan, A., Ginutsos, G., and Salamone, J. D. (1999a). Striatal and nigral D1 mechanisms involved in the antiparkinsonian effects of SKF 82958 (APB): studies of tremulous jaw movements in rats. *Psychopharmacology* 143, 72–81.
- Mayorga, A. J., Gianutsos, G., and Salamone, J. D. (1999b). Effects of striatal injections of 8-bromo-cyclic AMP on pilocarpine-induced tremulous jaw movements in rats. *Brain Res.* 829, 180–184.
- Mayorga, A. J., Cousins, M. S., Conlan, A., Gianutsos, G., and Salamone, J. D. (1999c). Characterization of the muscarinic receptor subtype mediating pilocarpine-induced tremulous jaw movements in rats. *Eur. J. Pharmacol.* 364, 7–11.
- McCain, K. R., Sawyer, T. S., and Spiller, H. A. (2007). Evaluation of centrally acting cholinesterase inhibitor exposures in adults. *Ann. Pharmacother.* 41, 1632–1637.
- McEvoy, J. P. (1983). The clinical use of anticholinergic drugs as treatments for extrapyramidal side effects of neuroleptic drugs. *J. Clin. Psychopharmacol.* 3, 288–302.
- McGeorge, A. J., and Faull, R. L. M. (1989). Organization of the projection from the cerebral cortex to the striatum in the rat. *Neuroscience* 29, 503–537.
- McSwain, M. L., and Forman, L. M. (1995). Severe parkinsonian symptom development on combination treatment with tacrine and haloperidol. *J. Clin. Psychopharmacol.* 15, 284.
- Milanov, I. (2001). Electromyographic differentiation of tremors. *Clin. Neurophysiol.* 112, 1626–1632.
- Miwa, H., Hama, K., Kajimoto, Y., and Kondo, T. (2008). Effects of zonisamide on experimental tremors in rats. *Parkinsonism Relat. Disord.* 14, 33–36.
- Miwa, H., Koh, J., Kajimoto, Y., and Kondo, T. (2011). Effects of T-type calcium channel blockers on a parkinsonian tremor model in rats. *Pharmacol. Biochem. Behav.* 97, 656–659.
- Miwa, H., Kubo, T., Suzuki, A., and Kondo, T. (2009). Effects of zonisamide on c-Fos expression under conditions of tacrine-induced tremulous jaw movements in rats: a potential mechanism underlying its anti-parkinsonian tremor effect. *Parkinsonism Relat. Disord.* 15, 30–35.
- Mizuno, Y., Hasegawa, K., Kondo, T., Kuno, S., and Yamamoto, M. (2010). Clinical efficacy of istradefylline (KW-6002) in Parkinson's disease: a randomized, controlled study. *Mov. Disord.* 25, 1437–1443.
- Morelli, M., Di Paolo, T., Wardas, J., Calon, F., Xiao, D., and Schwarzschild, M. A. (2007). Role of adenosine A2A receptors in parkinsonian motor impairment and L-DOPA-induced motor complications. *Prog. Neurobiol.* 83, 293–309.
- Morelli, M., and Pinna, A. (2001). Interaction between dopamine and adenosine A2A receptors as a basis for the treatment of Parkinson's disease. *Neurol. Sci.* 22, 71–72.
- Morris, G., Arkadir, D., Nevet, A., Vaadia, E., and Bergman, H. (2004). Coincident but distinct messages of midbrain dopamine and striatal tonically active neurons. *Neuron* 43, 133–143.
- Morrison, S., Kerr, G., and Silburn, P. (2008). Bilateral tremor relations in Parkinson's disease: effects of mechanical coupling and medication. *Parkinsonism Relat. Disord.* 14, 298–308.
- Muthuraman, M., Govindan, R. B., Deuschl, G., Heute, U., and Raethjen, J. (2008). Differentiating phase shift and delay in narrow band coherent signals. *Clin. Neurophysiol.* 119, 1062–1070.
- Navan, P., Findley, L. J., Jeffs, J. A., Pearce, R. K., and Bain, P. G. (2003). Randomized, double-blind, 3-month parallel study of the effects of pramipexole, pergolide, and placebo on parkinsonian tremor. *Mov. Disord.* 18, 1324–1331.
- Navan, P., Findley, L. J., Undy, M. B., Pearce, R. K., and Bain, P. G. (2005). A randomly assigned double-blind cross-over study examining the relative anti-parkinsonian tremor effects of pramipexole and pergolide. *Eur. J. Neurol.* 12, 1–8.
- Noring, U., Povleson, U. J., Casey, D. E., and Gerlach, J. (1984). Effect of a cholinomimetic drug (RS 86) in tardive dyskinesia and drug-related parkinsonism. *Psychopharmacology* 84, 569–571.
- Obeso, J. A., Rodríguez-Oroz, M. C., Benitez-Temino, B., Blesa, F. J., Guridi, J., Marin, C., and Rodríguez, M. (2008). Functional organization of the basal ganglia: therapeutic implications for Parkinson's disease. *Mov. Disord.* 23, S548–S559.
- Obeso, J. A., Rodríguez-Oroz, M. C., Rodríguez, M., Lanciego, J. L., Artieda, J., Gonzalo, N., and Olanow, C. W. (2000). Pathophysiology of the basal ganglia in Parkinson's disease. *Trends Neurosci.* 23, S8–S19.
- Olianas, M. C., Adem, A., Karlsson, E., and Onali, P. (1996). Rat striatal muscarinic receptors coupled to the inhibition of adenylyl cyclase activity: potent block by the selective m4 ligand muscarinic toxin 3 (MT3). *Br. J. Pharmacol.* 118, 283–288.
- Olianas, M. C., and Onali, P. (1999). PD 102807, a novel muscarinic M4 receptor antagonist, discriminates between striatal and cortical muscarinic receptors coupled to cyclic AMP. *Life Sci.* 65, 2233–2240.
- O'Suilleabhain, P. E., and Matsumoto, J. Y. (1998). Time-frequency analysis of tremors. *Brain* 121, 2127–2134.
- Ott, B. R., and Lannon, M. C. (1992). Exacerbation of Parkinsonism by tacrine. *Clin. Neuropharmacol.* 15, 322–325.
- Pellegrino, L. J., Pellegrino, A. S., and Cushman, A. J. (1979). *A Stereotaxic Atlas of the Rat Brain*. New York: Plenum.
- Pessiglione, M., Guehl, D., Rolland, A. S., Francios, C., Hirsch, E. C., Feger, J., and Tremblay, L. (2005). Thalamic neuronal activity in dopamine-depleted primates: evidence for a loss of functional segregation within basal ganglia circuits. *J. Neurosci.* 25, 1523–1531.
- Pinna, A. (2009). Novel investigational adenosine A2A receptor antagonists for Parkinson's disease. *Expert Opin. Investig. Drugs* 18, 1619–1631.
- Pinna, A., Schintu, N., Simola, N., Volpini, R., Pontis, S., Cristalli, G., and Morelli, M. (2010). A new ethyladenine antagonist of adenosine A(2A) receptors: behavioral and biochemical characterization as an antiparkinsonian drug. *Neuropharmacology* 58, 613–623.
- Pisa, M. (1988). Motor somatotopy in the striatum of rat: manipulation, biting and gait. *Behav. Brain Res.* 27, 21–35.
- Pisani, A., Bernardi, G., Ding, J., and Surmeier, D. J. (2007). Re-emergence of striatal cholinergic interneurons in movement disorders. *Trends Neurosci.* 30, 545–553.
- Pisani, A., Bonsi, P., Centonze, D., Gubellini, P., Bernardi, G., and

- Calabresi, P. (2003). Targeting striatal cholinergic interneurons in Parkinson's disease: focus on metabotropic glutamate receptors. *Neuropharmacology* 45, 45–56.
- Raethjen, J., Govindan, R. B., Muthuraman, M., Kopper, F., Volkmann, J., and Deuschl, G. (2009). Cortical correlates of the basic and first harmonic frequency of Parkinsonian tremor. *Clin. Neurophysiol.* 120, 1866–1872.
- Raethjen, J., Lindemann, M., Schmaljohann, H., Wenzelburger, R., Pfister, G., and Deuschl, G. (2000). Multiple oscillators are causing parkinsonian and essential tremor. *Mov. Disord.* 15, 84–94.
- Reck, C., Florin, E., Wojtecki, L., Krause, H., Groiss, S., Voges, J., Maarouf, M., Sturm, V., Schnitzler, A., and Timmermann, L. (2009). Characterization of tremor-associated local field potentials in the subthalamic nucleus in Parkinson's disease. *Eur. J. Neurosci.* 29, 599–612.
- Rodriguez Diaz, M., Abdala, P., Barroso-Chinea, P., Obeso, J., and Gonzalez-Hernandez, T. (2001). Motor behavioural changes after intracerebroventricular injection of 6-hydroxy-dopamine in the rat: an animal model of Parkinson's disease. *Behav. Brain Res.* 122, 79–92.
- Rosin, D. L., Robeva, A., Woodard, R. L., Guyenet, P. G., and Linden, J. (1998). Immunohistochemical localization of adenosine A2A receptors in the rat central nervous system. *J. Comp. Neurol.* 401, 163–186.
- Rupniak, N. M., Jenner, P., and Marsden, C. D. (1986). Acute dystonia induced by neuroleptic drugs. *Psychopharmacology* 88, 403–419.
- Rupniak, N. M., Jenner, P., and Marsden, C. D. (1983). Cholinergic modulation of perioral behavior induced by chronic neuroleptic administration to rats. *Psychopharmacology (Berl.)* 79, 226–230.
- Rupniak, N. M., Jenner, P., and Marsden, C. D. (1985). Pharmacological characterization of spontaneous or drug-induced purposeless chewing movements in rats. *Psychopharmacology (Berl.)* 85, 71–79.
- Salamone, J. D. (2010). Preladenant, a novel adenosine A(2A) receptor antagonist for the potential treatment of parkinsonism and other disorders. *Idrugs* 13, 723–731.
- Salamone, J. D., and Baskin, P. (1996). Vacuous jaw movements induced by acute reserpine and low-dose apomorphine: possible model of parkinsonian tremor. *Pharmacol. Biochem. Behav.* 53, 179–183.
- Salamone, J. D., Betz, A. J., Ishiwari, K., Felsted, J., Madson, L., Mirante, B., Clark, K., Font, L., Korbey, S., Sager, T. N., Hockemeyer, J., and Muller, C. E. (2008a). Tremorolytic effects of adenosine A2A antagonists: implications for parkinsonism. *Front. Biosci.* 13, 3594–3605.
- Salamone, J. D., Ishiwari, K., Betz, A. J., Farrar, A. M., Mingote, S. M., Font, L., Hockemeyer, J., Müller, C. E., and Correa, M. (2008b). Dopamine/adenosine interactions related to locomotion and tremor in animal models: possible relevance to parkinsonism. *Parkinsonism Relat. Disord.* 14, S130–S134.
- Salamone, J. D., Carlson, B. B., Rios, C., Lentini, E., Correa, M., Wisniewski, A., and Betz, A. (2005). Dopamine agonists suppress cholinomimetic-induced tremulous jaw movements in an animal model of Parkinsonism: tremorolytic effects of pergolide, ropinirole and CY 208-243. *Behav. Brain Res.* 156, 173–179.
- Salamone, J. D., Correa, M., Carlson, B., Wisniewski, A., Mayorga, A., Nisenbaum, E., Nisenbaum, L., and Felder, C. (2001). Neostriatal muscarinic receptor subtypes involved in the generation of tremulous jaw movements in rodents. Implications for cholinergic involvement in parkinsonism. *Life Sci.* 68, 2579–2584.
- Salamone, J. D., Johnson, C. J., McCullough, L. D., and Steinpreis, R. E. (1990). Lateral striatal cholinergic mechanisms involved in oral motor activities in the rat. *Psychopharmacology* 102, 529–534.
- Salamone, J. D., Kurth, P. A., McCullough, L. D., Sokolowski, J. D., and Cousins, M. S. (1993a). The role of brain dopamine in response initiation: effects of haloperidol and regionally-specific dopamine depletions on the local rate of instrumental responding. *Brain Res.* 628, 218–226.
- Salamone, J. D., Mahan, K., and Rogers, S. (1993b). Ventrolateral striatal dopamine depletions impair feeding and food handling in rats. *Pharmacol. Biochem. Behav.* 44, 605–610.
- Salamone, J. D., Lalies, M. D., Channell, S. L., and Iversen, S. D. (1986). Behavioural and pharmacological characterization of the mouth movements induced by muscarinic agonists in the rat. *Psychopharmacology* 88, 467–471.
- Salamone, J. D., Mayorga, A. J., Trevitt, J. T., Cousins, M. S., Conlan, A., and Nawab, A. (1998). Tremulous jaw movements in rats: a model of parkinsonian tremor. *Prog. Neurobiol.* 56, 591–611.
- Santiago, M. P., and Potter, L. T. (2001). Biotinylated m4-toxin demonstrates more M4 muscarinic receptor protein on direct than indirect striatal projection neurons. *Brain Res.* 894, 12–20.
- Schneider, S. A., Edwards, M. J., Cordvari, C., Macleod, W. N., and Bhatia, K. P. (2006). Botulinum toxin A may be efficacious as treatment for jaw tremor in Parkinson's disease. *Mov. Disord.* 21, 1722–1724.
- Schrag, A., Keens, J., Warner, J., and Ropinirole Study Group. (2002). Ropinirole for the treatment of tremor in early Parkinson's disease. *Eur. J. Neurol.* 9, 253–257.
- Schrag, A., Schelosky, L., Scholz, U., and Poewe, W. (1999). Reduction of Parkinsonian signs in patients with Parkinson's disease by dopaminergic versus anticholinergic single-dose challenges. *Mov. Disord.* 14, 252–255.
- See, R., and Chapman, M. (1991). Cholinergic modulation of oral activity in drug-naïve and chronic haloperidol-treated rats. *Pharmacol. Biochem. Behav.* 39, 49–54.
- Selby, G. (1986). "Parkinson's disease," in *Handbook of Clinical Neurology*, eds P. Vinken and G. W. Bruyn (New York: Wiley), 173–211.
- Shea, C., MacKnight, C., and Rockwood, K. (1998). Donepezil for treatment of dementia with Lewy bodies: a case series of nine patients. *Int. Psychogeriatr.* 10, 229–238.
- Sheffield, J. K., and Jankovic, J. (2007). Botulinum toxin in the treatment of tremors, dystonias, sialorrhea and other symptoms associated with Parkinson's disease. *Expert Rev. Neurother.* 7, 637–647.
- Simola, N., Fenu, S., Baraldi, P. G., Tabrizi, M. A., and Morelli, M. (2004). Blockade of adenosine A2A receptors antagonizes parkinsonian tremor in the rat tacrine model by an action on specific striatal regions. *Exp. Neurol.* 189, 182–188.
- Song, I. U., Kim, J. S., Ryu, S. B., An, J. Y., and Lee, K. S. (2008). Donepezil-induced jaw tremor. *Parkinsonism. Relat. Disord.* 14, 584–585.
- Sovner, R., and Dimascio, A. (1977). The effect of benzotropine mesylate in the rabbit syndrome and tardive dyskinesia. *Am. J. Psychiatry* 134, 1301–1302.
- Spieker, S., Strole, V., Sailer, A., Boose, A., and Dichgans, J. (1997). Validity of long-term electromyography in the quantification of tremor. *Mov. Disord.* 12, 985–991.
- Stacy, M., Silver, D., Mendis, T., Sutton, J., Mori, A., Chaikin, P., and Sussman, N. M. (2008). A 12-week, placebo-controlled study (6002-US-006) of istradefylline in Parkinson disease. *Neurology* 70, 2233–2240.
- Stade, G., Wolf, W., Ott, M., Oertel, W. H., and Dengler, R. (1995). Tremor as a factor in prolonged reaction times of parkinsonian patients. *Mov. Disord.* 10, 153–162.
- Steinpreis, R. E., Baskin, P., and Salamone, J. D. (1993). Vacuous jaw movements induced by sub-chronic administration of haloperidol: interactions with scopolamine. *Psychopharmacology* 111, 99–105.
- Steinpreis, R. E., and Salamone, J. D. (1993). Effects of acute haloperidol and reserpine administration on vacuous jaw movements in three different age groups of rats. *Pharmacol. Biochem. Behav.* 46, 405–409.
- Stewart, B. R., Jenner, P., and Marsden, C. D. (1988). The pharmacological characterization of pilocarpine-induced chewing in the rat. *Psychopharmacology (Berl.)* 97, 228–234.
- Stewart, B. R., Rose, S., Jenner, P., and Marsden, C. D. (1987). Pilocarpine-induced purposeless chewing behaviour in rats is dependent on intact central stores of 5-HT. *Eur. J. Pharmacol.* 142, 173–176.
- Sung, Y. H., Chung, S. J., Kim, S. R., and Lee, M. C. (2008). Factors predicting response to dopaminergic treatments for resting tremor of Parkinson's disease. *Mov. Disord.* 23, 137–140.
- Tarsy, D. (1983). Neuroleptic-induced extrapyramidal reactions: classification, description and diagnosis. *Clin. Neuropharmacol.* 6, s9–s26.
- Taylor, J. R., Lawrence, D. E., Redmond, J. D., Elsworth, J. D., Roth, R. H., Nichols, D. E., and Mailman, R. B. (1991). Dihydropyridine, a full dopamine D1 agonist, reduces MPTP-induced parkinsonism in monkeys. *Eur. J. Pharmacol.* 199, 389–392.
- Threlfell, S., Clements, M. A., Khodai, T., Pienaar, I. S., Exley, R., Wess, J., and Cragg, S. J. (2010). Striatal muscarinic receptors promote activity dependence of dopamine transmission via distinct receptor subtypes on cholinergic interneurons in ventral versus dorsal striatum. *J. Neurosci.* 30, 3398–3408.
- Timmer, J., Lauk, M., Pflieger, W., and Deuschl, G. (1998a). Cross-spectral analysis of physiological tremor and muscle activity. I. Theory and application to unsynchronized electromyogram. *Biol. Cybern.* 78, 349–357.
- Timmer, J., Lauk, M., Pflieger, W., and Deuschl, G. (1998b). Cross-spectral analysis of physiological tremor and muscle activity. II. Application to synchronized electromyogram. *Biol. Cybern.* 78, 359–368.
- Trevitt, J. T., Atherton, A., Aberman, J., and Salamone, J. D. (1998). Effects of subchronic administration of

- clozapine, thioridazine and haloperidol on tests related to extrapyramidal motor function in the rat. *Psychopharmacology* 137, 61–66.
- Trevitt, J. T., Carlson, B. B., Correa, M., Keene, A., Morales, M., and Salamone, J. D. (2002). Interactions between dopamine D1 receptors and GABA mechanisms in substantia nigra pars reticulata: neurochemical and behavioral studies. *Psychopharmacology (Berl.)* 159, 229–237.
- Trevitt, J. T., Carlson, B. B., and Salamone, J. D. (1999). Behavioral assessment of atypical antipsychotics in rats: studies of the effects of olanzapine (Zyprexa). *Psychopharmacology (Berl.)* 145, 309–316.
- Tronci, E., Simola, N., Borsini, F., Schintu, N., Frau, L., Carminati, P., and Morelli, M. (2007). Characterization of the antiparkinsonian effects of the new adenosine A2A receptor antagonist ST1535: acute and subchronic studies in rats. *Eur. J. Pharmacol.* 566, 94–102.
- Vanover, K. E., Betz, A. J., Weber, S. M., Bibbiani, F., Kielaite, A., Weiner, D. M., Davis, R. E., Chase, T. N., and Salamone, J. D. (2008). A 5-HT_{2A} receptor inverse agonist, ACP-103, reduces tremor in a rat model and levodopa-induced dyskinesias in a monkey model. *Pharmacol. Biochem. Behav.* 90, 540–544.
- Weinberger, M., Mahant, N., Hutchison, W. D., Lozano, A. M., Moro, E., Hodaie, M., Lang, A. E., and Dostrovsky, J. O. (2006). Beta oscillatory activity in the subthalamic nucleus and its relation to dopaminergic response in Parkinson's disease. *J. Neurophysiol.* 96, 3248–3256.
- Weiss, K. J., Ciraulo, D. A., and Shader, R. I. (1980). Physostigmine test in the rabbit syndrome and tardive dyskinesia. *Am. J. Psychiatry* 137, 627–628.
- Wichmann, T., Kliem, M. A., and DeLong, M. R. (2001). Antiparkinsonian and behavioral effects of inactivation of the substantia nigra pars reticulata in hemiparkinsonian primates. *Exp. Neurol.* 167, 410–424.
- Willner, P. (1990). "Behavioural models in psychopharmacology," in *Behavioral Models in Psychopharmacology*, ed. P. Willner (Cambridge: Cambridge University Press), 3–18.
- Wilms, H., Sievers, J., and Deuschl, G. (1999). Animal models of tremor. *Mov. Disord.* 14, 557–571.
- Wirshing, W. C., Cummings, J. L., Dencker, S. J., and May, P. R. (1989a). Electromechanical characteristics of tardive dyskinesia. *J. Neuropsychiatry Clin. Neurosci.* 3, 10–17.
- Wirshing, W. C., Friedenberg, D. L., Cummings, J. L., and Bartzokis, G. (1989b). Effects of anticholinergic agents on patients with tardive dyskinesia and concomitant drug-induced parkinsonism. *J. Clin. Psychopharmacol.* 9, 407–411.
- Wisniecki, A., Correa, M., Arizzi, M. N., Ishiwari, K., and Salamone, J. D. (2003). Motor effects of GABA (A) antagonism in globus pallidus: studies of locomotion and tremulous jaw movements in rats. *Psychopharmacology (Berl.)* 170, 140–149.
- Yassa, R., and Lal, S. (1986). Prevalence of the rabbit syndrome. *Am. J. Psychiatry* 143, 656–657.
- Young, A., and Penney, J. (1993). Biochemical and functional organization of the basal ganglia, in *Parkinson's Disease and Movement Disorders*, eds J. Jankovic and E. Tolosa (Baltimore: Williams & Wilkins), 1–12.
- Young, R. P. (1986). "Tremor," in *Diseases of the Nervous System*, eds A. K. Asbury, G. M. McKinn, and M. I. McDonald (Philadelphia: W.B. Saunders), 435–451.
- Zazpe, A., Artaiz, I., Innerarity, A., Del Olmo, E., Castro, E., Labeaga, L., Pazos, A., and Orjales, A. (2006). In vitro and in vivo characterization of F-97013-GD, a partial 5-HT_{1A} agonist with antipsychotic- and antiparkinsonian-like properties. *Neuropharmacology* 51, 129–140.
- Zhou, F. M., Wilson, C. J., and Dani, J. A. (2003). Muscarinic and nicotinic cholinergic mechanisms in the mesostriatal dopamine systems. *Neuroscientist* 9, 23–36.
- Zigmond, M. J., Stricker, E. M., and Berger, T. W. (1987). "Parkinsonism: insights from animal models utilizing neurotoxic agents," in *Animal Models of Dementia*, ed. J. T. Coyle (New York: John Wiley and Sons, Inc.), 1–38.

Conflict of Interest Statement: The authors declare that, except for income received from my primary employer, no financial support or compensation has been received from any individual or corporate entity over the past three years for research or professional service and there are no personal financial holdings that could be perceived as constituting a potential conflict of interest.

Received: 01 February 2011; paper pending published: 27 March 2011; accepted: 03 June 2011; published online: 04 July 2011.

Citation: Collins-Praino LE, Paul NE, Rychalsky KL, Hinman JR, Chrobak JJ, Senatus PB and Salamone JD (2011) Pharmacological and physiological characterization of the tremulous jaw movement model of parkinsonian tremor: Potential insights into the pathophysiology of tremor. *Front. Syst. Neurosci.* 5:49. doi: 10.3389/fnsys.2011.00049

Copyright © 2011 Collins-Praino, Paul, Rychalsky, Hinman, Chrobak, Senatus and Salamone. This is an open-access article subject to a non-exclusive license between the authors and Frontiers Media SA, which permits use, distribution and reproduction in other forums, provided the original authors and source are credited and other Frontiers conditions are complied with.



Putative cholinergic interneurons in the ventral and dorsal regions of the striatum have distinct roles in a two choice alternative association task

Orli Yarom¹ and Dana Cohen^{1,2*}

¹ Gonda Interdisciplinary Brain Research Center, Bar Ilan University, Ramat-Gan, Israel

² The Goodman Faculty of Life Sciences, Bar Ilan University, Ramat-Gan, Israel

Edited by:

James M. Tepper, Rutgers, The State University of New Jersey, USA

Reviewed by:

Joshua D. Berke, University of Michigan, USA

Mandar Shrikrishna Jog, University of Western Ontario, Canada

*Correspondence:

Dana Cohen, The Gonda Interdisciplinary Brain Research Center, Bar Ilan University, Ramat Gan 52900, Israel.

e-mail: danacoh@gmail.com

The striatum consists of GABAergic projection neurons and various types of interneurons. Despite their relative scarcity, these interneurons play a key role in information processing in the striatum. One such class of interneurons is the cholinergic tonically active neurons (TANs). In the dorsal striatum, TANs are traditionally considered to be responsive to events of motivational significance. However, in recent years, studies have suggested that TANs are not exclusively related to reward and reward-predicting stimuli, but may contribute to other processes, including responses to aversive stimuli, detecting the spatial location of stimuli and generating movement. Currently there is little data concerning TAN activity in the ventral striatum (VS) of behaving animals. Here, we simultaneously recorded neurons in the ventral and the dorsolateral (DLS) regions of the striatum while animals performed a two choice alternative association task. Our data show that a large percentage of the putative TANs in both regions responded around movement initiation and execution. The majority of these neurons exhibited directional selectivity which was stronger in DLS relative to VS. In addition, the preferred directions in VS were mostly contralateral to the recording site whereas the observed preferred directions in DLS were equally distributed contralaterally and ipsilaterally to the recording site. The most interesting difference between DLS and VS was that DLS TANs maintained activity alterations throughout the movement whereas TANs in VS exhibited short-lasting phasic activity alterations that were maintained throughout the movement by different neurons. Our findings suggest that coding of movement by TANs in both regions overlaps to some degree, yet the differences in response patterns support the notion that the TANs in DLS participate in the motor loop whereas TANs in VS convey event-related information such as movement initiation, movement direction, and end of movement.

Keywords: cholinergic interneurons, dorsal striatum, ventral striatum, motor control, chronic recording, movement coding

INTRODUCTION

The striatum, which is the main input structure of the basal ganglia, has been implicated in a variety of functions essential to shaping behavior such as goal-directed actions, action selection, habit formation, reward evaluation, flexible shifting of responses, and motor skill learning (Jog et al., 1999; Ragozzino, 2003; Costa et al., 2004; Yin et al., 2004, 2005; Lau and Glimcher, 2007; Gan et al., 2010). The striatum receives projections originating from wide portions of cortical areas (Parent and Hazrati, 1995) providing it with the information required for performing such diverse functions. Based on its input topography, the striatum has been divided into three functionally distinct regions: the dorsolateral striatum (DLS) which integrates sensorimotor information, the dorsomedial striatum (DMS), which integrates associative information and the ventral striatum (VS) which integrates limbic information (Joel and Weiner, 1994; Yin and Knowlton, 2006; Graybiel, 2008; Humphries and Prescott, 2010). The striatum consists of a relatively small number of cell types: the GABAergic projection neurons and a few types of interneurons. The projection neurons, comprising about 95% of striatal population, are the

medium spiny neurons (MSNs; Gerfen, 1988). The interneurons comprise the remaining 5% and include the GABAergic fast spiking interneurons (FSIs), the tonically active neurons (TANs), and other interneurons, which have been the subject of very few studies. Despite their scarcity the FSIs and the TANs can effectively alter the activity of the projection neurons (Tepper and Bolam, 2004; Ding et al., 2010). Specifically, the TANs, presumably cholinergic interneurons (Wilson et al., 1990; Bennett and Wilson, 1999), have been studied extensively in behaving monkeys and shown to respond to events of motivational significance such as reward and stimuli predictive of reward (Kimura et al., 1984; Apicella et al., 1991, 1997; Aosaki et al., 1994; Morris et al., 2004). In recent years, studies suggest that the TANs' role may not be confined to reward and motivation but to a broader range of processes such as detection of aversive stimuli (Blazquez et al., 2002; Ravel et al., 2003; Yamada et al., 2004), recognition of the context in which motivationally significant stimuli are presented (Shimo and Hikosaka, 2001; Yamada et al., 2004; Lee et al., 2006; Ravel et al., 2006) and detection of spatial locations of stimuli (Shimo and Hikosaka, 2001; Ravel et al., 2006). A few studies have shown that TANs are

also involved in movement control (Lee et al., 2006; Ravel et al., 2006). The vast majority of studies examining TAN activity in behaving monkeys have been conducted in the dorsal striatum, and mostly report similar responses in the caudate and putamen which are homologous to the rat DLS and DMS, respectively (but see, Yamada et al., 2004). Unlike the TANs in the DLS and the DMS, information about TAN activity in the VS is still lacking.

We addressed the role of TANs in the DLS and the VS by simultaneously recording activity of neuronal ensembles in these regions while rats performed a two choice alternative association task. We compared the nature of the TANs' response patterns observed in the two regions during movement execution to test to what extent their activations in the different regions overlap in order to decipher their specific contribution to task performance.

MATERIALS AND METHODS

All procedures were approved by Bar Ilan University institutional animal care and use committee and were performed in accordance with the National Institutes of Health guidelines.

BEHAVIORAL PARADIGM

The training procedure has previously been described in detail (Cohen and Nicolelis, 2004). Briefly, adult male Long-Evans rats were pretrained to nose poke a hole and wait for a tone (12 kHz) to receive 50 μ l of water. The time delay to the tone was gradually increased until rats consistently waited for 550–700 ms during 85% of the trials. Upon reaching criterion rats were removed from the water deprivation protocol and underwent surgery. After about 7–10 days of recovery, animals started training on the two choice alternative association task. In this stage, after nose poking the center hole for 550–700 ms, either a high (18 kHz) or a low (7 kHz) tone was played and two side doors covering holes located left and right to the center hole opened. Depending on the tone played, rats had to nose poke either the left hole (18 kHz) or the right hole (7 kHz). After each correct trial, rats received 50 μ l of water as a reward in the poked hole. An error trial occurred when a rat nose poked the wrong side hole. In this case, the rat was forced to repeat the trial until performed correctly to prevent the development of a side preference. The intertrial interval changed randomly, ranging between 14 and 24 s. An infrared source-detector system was installed behind each door, to detect the entrance and retraction of the rat's snout into and from the hole. Each session continued until at least 35 correct responses were made in each direction (70 correct trials). For 2 weeks rats trained one session a day during which a criterion of above 80% correct responses was reached. Although recordings were made throughout training, we report here only on the best day of training, when performance was above criterion.

SURGICAL PROCEDURE

The surgical procedure has previously been described in detail (Nicolelis et al., 1997; Jacobson et al., 2009). In brief, adult male Long-Evans rats weighing 350–450 g (Harlan and Taconic) were initially sedated by 5% isoflurane and then injected i.m. with ketamine HCl and xylazine HCl (100 and 10 mg/kg, respectively). Supplementary injections of ketamine and xylazine were given as required. The rat's head was fixed in a stereotaxic frame

(Kopf Instruments, USA). An incision was made to expose the skull surface, connective tissue was removed and the skull surface cleaned. Two craniotomies, slightly larger than the electrode arrays, were made bilaterally above the dorsolateral (AP = 0.5; ML = 3.9; Depth = 3.9) and ventral striatum (nucleus accumbens; AP = -1.5; ML = 1.8; Depth = 6.9). 4 \times 4 or 4 \times 8 electrode arrays made with isonel coated tungsten wires (diameters of 35 or 50 microns) were slowly lowered into the brain. Electrodes were fixed in place using dental cement, leaving only the connectors exposed.

Electrode placement was confirmed histologically after performing electrolytic lesions, perfusion with 4% formalin, and brain fixation with 20% sucrose, formalin, cryostat sectioning with 60 μ m slice thickness, and cresyl violet staining.

DATA COLLECTION

Neural activity was amplified, band-pass filtered at 150–8000 Hz, and sampled at 40 kHz using a multichannel acquisition processor system (MAP system; Plexon Inc, Dallas, TX, USA). The activity was initially sorted online; however, all waveforms exceeding a selected threshold were saved for later analysis. Offline sorting was done on all recorded units to ensure that only single units were used in this study.

NEURONAL CLASSIFICATION

Neurons were classified using three parameters: firing rate, coefficient of variation (cv), and valley to amplitude ratio (VAR). Firing rate was calculated as number of recorded spikes divided by session duration. The cv was calculated by dividing the standard deviation of the inter spike intervals (ISIs) by their mean. The VAR was calculated as the absolute value of the first valley in the waveform divided by the difference between its minimum value and the following maximum (see inset in **Figure 2A**).

The percent of time with ISIs > 2 s was calculated as in (Schmitzer-Torbert and Redish, 2008; Gage et al., 2010) by summing over ISIs longer than 2 s and dividing the sum by the total recording time.

DATA ANALYSIS

Movement-related neurons

Neurons were considered movement related only if the following two conditions were met: (1) their firing rate during left or right movements was significantly different from their baseline firing rate measured two seconds prior to trial initiation; and (2) their firing rate during left or right movements was significantly different from their firing rate during the waiting period in which rats nose poked the center hole and waited to hear the played tone without moving. Firing rates were compared using the Wilcoxon signed rank test, with a criterion of $p < 0.01$.

Direction selective units

Movements were divided into three phases: beginning, middle, and end. Movement-related neurons were tested for directional selectivity by testing for significant differences in their firing rate during left and right movements during each of these phases using the Wilcoxon rank sum test with a criterion of $p < 0.01$. If a significant difference was found in one or more phases, the unit was considered to be direction selective.

The normalized average direction selective neuron

The preferred direction of a neuron was determined by comparing its firing rates calculated throughout the movements in each direction and averaged over trials. The direction in which the neuron exhibited a higher firing rate was termed the preferred direction. The other direction was termed the non-preferred direction. Each movement within a trial was divided into nine equal bins and the firing rate was calculated for all neurons in each of the nine bins. The firing rate in each bin was then averaged per neuron over the entire session during trials in the preferred and non-preferred directions separately. In order to examine population activity, each neuron's activity was normalized according to the bin with the highest rate. Then the firing rate of the entire population of neurons during each bin was averaged in the two directions separately.

Selectivity index (SI)

The SI of a neuron was defined by the following equation:

$$SI = \text{abs} \left(\frac{FR_L - FR_R}{FR_L + FR_R} \right)$$

FR_L and FR_R are the average firing rates of each neuron during left and right trials, respectively. The firing rates in all trials were calculated in 100 ms bins taken at the beginning, middle, and end of the movement. The final SI of a neuron was the SI averaged over the three movement phases.

Trial classification

Spike counts in 100 ms bins at the beginning, middle, and end of movement were calculated for all trials. Spike count histograms were constructed and normalized to generate probability distributions of spike counts for left and right movements. The probabilities of drawing a given spike count during a trial were calculated for the left and right separately, and the movement direction in that trial was determined by the larger probability of the two.

RESULTS

RECORDING NEURAL ACTIVITY DURING THE PERFORMANCE OF AN ASSOCIATION TASK

The performance of association tasks has been linked to activation of both the dorsal and the ventral regions of the striatum (Atallah et al., 2007) making this task ideal for studying the similarities and differences in DLS and VS ensemble activation. In the present study rats were trained on a two choice alternative association task in which they had to associate movement to the left and to the right with a high and a low pitch tone, respectively (see Materials and Methods). 12 Long-Evans male rats were trained on the task for 2 weeks during which a criterion of above 80% correct responses was met. On average, rats reached criterion after 8 days of training. The average reaction time (the time period from playing the tone until movement onset) and movement duration in the best performed session were 0.16 ± 0.05 s and 0.32 ± 0.06 s, respectively. In this report, we include data collected during the best performed session of each rat.

We recorded neural activity in both DLS and VS using electrode arrays of 32 and 16 tungsten wires with diameters of 35 and 50 microns. An example of electrode positioning in DLS and in VS is

shown in **Figures 1A,B**, respectively. Although the electrode tips were positioned ± 100 μm above and below the presented planar sections, recording sites of all animals were projected and plotted on the sections with the largest number of recording sites (**Figure 1C**; DLS: Bregma = -3.86 ; and VS: Bregma = -6.82). Reconstruction of electrode positioning showed that the recording electrodes were confined to the DLS and VS (**Figure 1C**). A total of 88 and 80 well-isolated neurons were recorded during the best performed session in DLS and VS, respectively. Firing properties such as firing rate, cv, relative quiescence periods and waveform properties such as duration, valley to peak amplitude (VPA) and VAR of the recorded neurons were closely examined. Several of these properties enabled classification of the neurons into three well-separated clusters. The best separation was obtained when the firing rates, the cvs, and the VARs were used (**Figure 2A**). These parameters enabled classification of the recorded neurons into three groups: putative medium spiny neurons (pMSNs), putative tonically active neurons (pTANs), and putative fast spiking interneurons (pFSIs). Firing rate better isolated the pFSIs which typically exhibit high firing rates. The cv better isolated the pMSNs which typically exhibit high values because of their phasic firing pattern. The VAR better isolated the pTANs because their long duration spikes are cut at the end of the

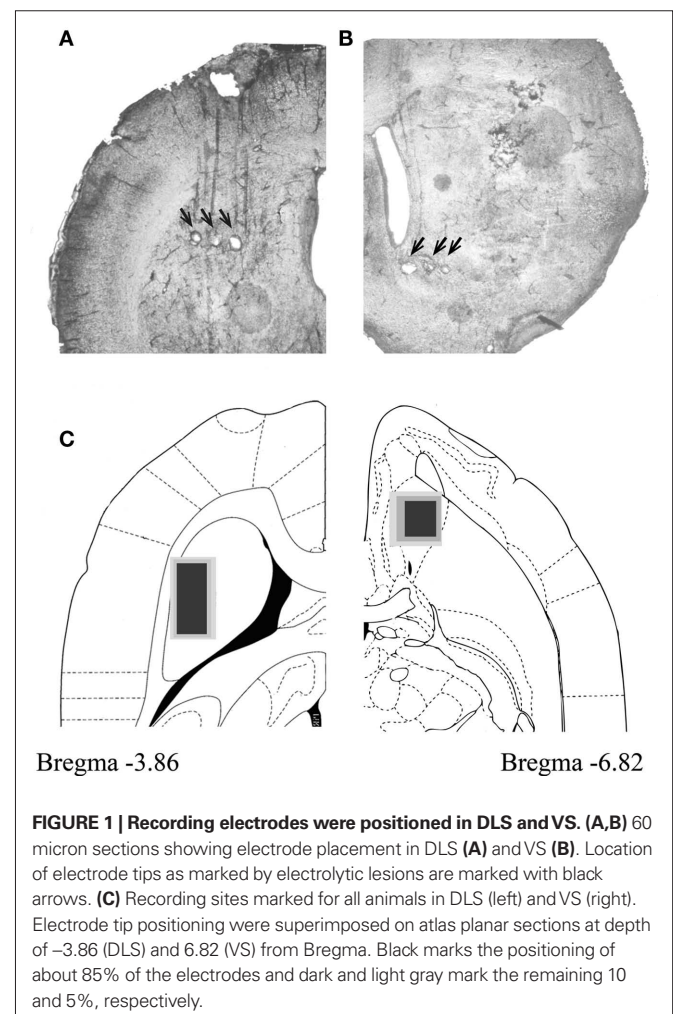
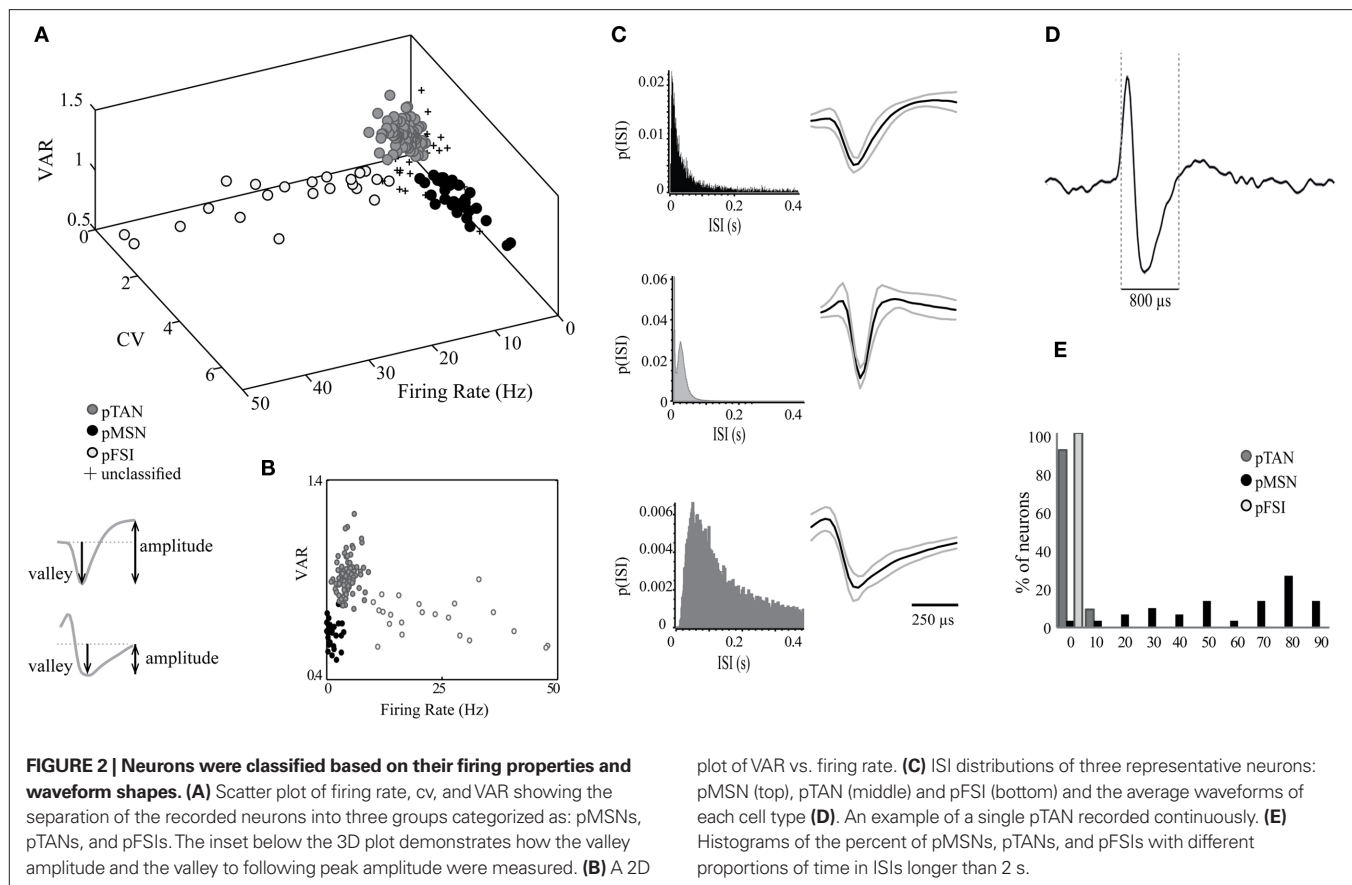


FIGURE 1 | Recording electrodes were positioned in DLS and VS. (A,B) 60 micron sections showing electrode placement in DLS (**A**) and VS (**B**). Location of electrode tips as marked by electrolytic lesions are marked with black arrows. (**C**) Recording sites marked for all animals in DLS (left) and VS (right). Electrode tip positioning were superimposed on atlas planar sections at depth of -3.86 (DLS) and 6.82 (VS) from Bregma. Black marks the positioning of about 85% of the electrodes and dark and light gray mark the remaining 10 and 5%, respectively.



sampled segment (**Figure 2D**) making the valley to following peak values smaller relative to valley amplitude and consequently isolates the TANs from waveforms which are fully captured like the FSIs and the MSNs. The contribution of the VAR to the isolation of the pTANs is shown in the 2D plot in **Figure 2B**.

To minimize the likelihood of falsely assigning a neuron to a specific group, a set of parameters was defined for each of the groups such that if a neuron exhibited a clear separation on two of the parameters but deviated on the third, it was excluded from the analysis. Application of this strict rule excluded about 10% of the neurons. The excluded neurons are marked by a + sign in **Figure 2A**. The ISI probability histograms of neurons representative of the three groups and the average waveforms of all neurons within these groups are shown in **Figure 2C**. The pMSNs exhibited both short and long ISIs whereas the FSIs rarely exhibited ISIs longer than 200 ms. In addition, the pTANs exhibited prolonged refractory periods and tonic firing with random ISIs. The final verification of the classification was based on the calculation of the percentage of time with ISIs longer than 2 s (see Materials and Methods). As expected, the vast majority of pTANs and pFSIs did not show any long pauses in firing. This contrasts with the pMSNs which were quiescent for the greater part of the recording sessions (**Figure 2E**).

Overall we recorded 39 and 49 pTANs in DLS and VS, respectively. The pTANs in both striatal regions exhibited similar properties. For example their firing rates were 4.87 ± 1.63 Hz in DLS and 4.33 ± 1.64 Hz in VS; their cvs were 1.06 ± 0.19 in DLS and 0.97 ± 0.24 in VS; their VARs were 0.92 ± 0.07 in DLS and

plot of VAR vs. firing rate. **(C)** ISI distributions of three representative neurons: pMSN (top), pTAN (middle) and pFSI (bottom) and the average waveforms of each cell type **(D)**. An example of a single pTAN recorded continuously. **(E)** Histograms of the percent of pMSNs, pTANs, and pFSIs with different proportions of time in ISIs longer than 2 s.

0.92 ± 0.10 in VS; and the fractions of time in ISIs longer than 2 s were 0.02 ± 0.03 in DLS and 0.03 ± 0.04 in VS. The group of identified pTANs exhibit firing rates of about five spikes per second, cv values representing tonic firing with random distribution of long ISIs and long duration waveforms. These values are similar to those reported in primate and in rodent studies (Alexander and DeLong, 1985; Hikosaka et al., 1989; Aosaki et al., 1994; Raz et al., 1996; Joshua et al., 2008; Schmitzer-Torbert and Redish, 2008; Inokawa et al., 2010).

THE pTANs IN DLS AND IN VS EXHIBIT DIFFERENTIAL DIRECTION SELECTIVITY DURING MOVEMENT

Throughout our recordings, we observed that many of the pTANs changed their firing rates during several behavioral events compared to their basal firing rate. The neurons increased or decreased their firing rate during different parts of a trial. For example, the raster plots and peri-event time histograms (PETHs) shown in **Figure 3A** belong to a pTAN that increased its firing rate prior to trial initiation and during movement to the left (**Figure 3A**; top panel) and then decreased its firing rate during reward receipt and consumption (**Figure 3A**; bottom panel). It should be noted that this type of reward-related activity was more frequent in VS. We also observed that the pTANs could respond differentially during movements to the left and to the right. The pTAN in the example did not change its firing rate during movement to the right (**Figure 3A**; middle panel). Quantitatively, we considered a neuron to be movement related if its firing rate during movement was significantly

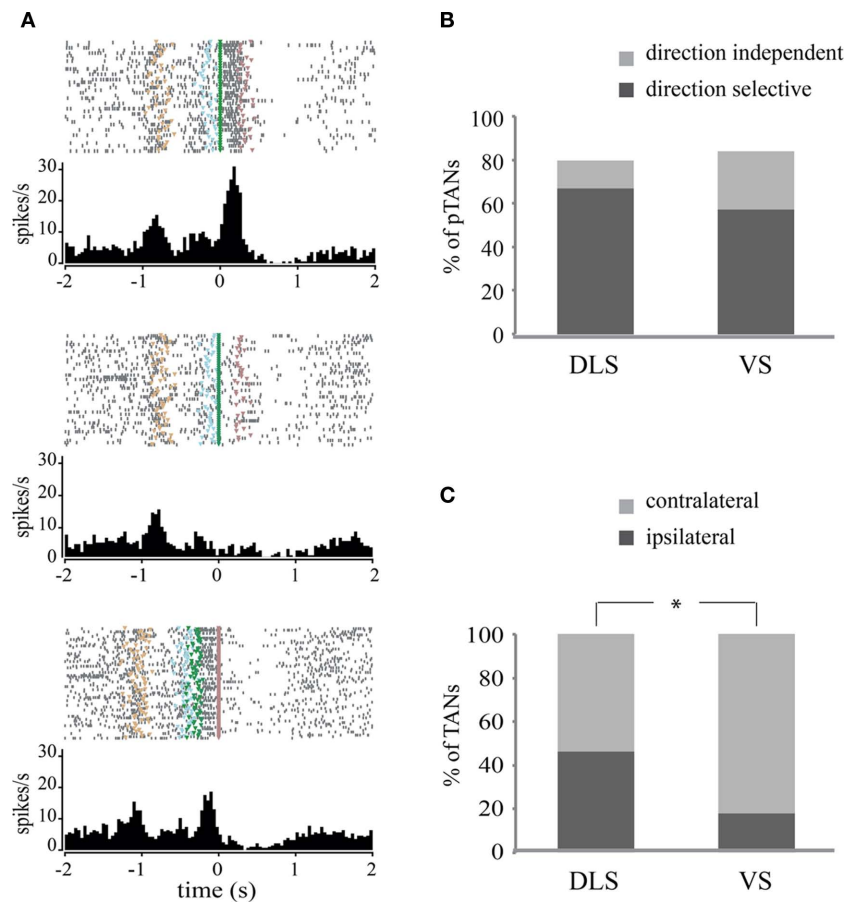


FIGURE 3 | Putative tonically active neurons in DLS and in VS exhibit movement-related activity. (A) Raster plots and their corresponding peri-event time histograms (PETHs) of a direction selective pTAN recorded in VS. Trials are presented top to bottom as they were presented during the session. Entering the center hole is marked in tan; beginning of the tone is marked in light blue; movement initiation is marked in green; and reward is

marked in violet. Top panel: plot is aligned to the beginning of movement toward the left side; middle: plot is aligned to beginning of movement to the right side; bottom: plot is aligned to reward. **(B)** Percent of movement related and direction selective pTANs in DLS and VS. **(C)** Percent of direction selective pTANs in which the preferred direction was contralateral or ipsilateral to the recording site.

different ($p < 0.01$) from its firing rate during the intertrial interval and while nose poking the center hole (the waiting period) regardless of movement direction (see Materials and Methods). On the basis of these criteria, the vast majority of the recorded pTANs were found to be movement related (**Figure 3B**). The percentages of movement-related neurons were similar in DLS (31 out of 39; 79%) and in VS (41 out of 49; 84% $p > 0.5$).

To test whether the pTANs are direction selective we compared the activity of movement-related neurons during left and right movements (see Materials and Methods). We observed that the majority of the pTANs were selective for movement direction (**Figure 3B**) and usually increased their firing rate during movement in the preferred direction while maintaining basal firing rates in the other direction or slightly decreasing it (**Figure 3A**; top and middle panels). The percentages of direction selective neurons were higher in the DLS (26 out of 31; 84%) compared to VS (28 out of 41; 68%) but the difference was not significant ($p = 0.13$).

We then tested whether direction selective neurons have preferred laterality; that is, we examined whether neurons recorded in the left hemisphere responded more strongly when the animal

performed a movement to the left (ipsilateral preference) or to the right (contralateral preference). Surprisingly, neurons in VS exhibited a significant preference for the contralateral direction (82% contralateral vs. 18% ipsilateral) whereas neurons in DLS did not exhibit a preferred laterality (54% contralateral vs. 46% ipsilateral; $p < 0.05$, Chi-square test, **Figure 3C**).

Overall, our recordings clearly show that pTANs in DLS and in VS exhibit significant movement-related activations with strong directional selectivity that cannot be distinguished based on the size of the responding population. However, the pTANs in VS had a strong preference for movements in directions contralateral to the recording site whereas the pTANs in DLS responded to movement in both directions regardless of recording site, which is suggestive of their different functions.

DIRECTION SELECTIVE pTANs EXHIBIT DIFFERENTIAL PHASIC ACTIVATION IN DLS AND VS

We next investigated whether the patterns of responses in DLS and VS are similar or distinct. We first examined the representative neurons in each of these regions by averaging the normalized firing

rate of each neuron over all direction selective neurons. Despite the fact that the number of direction selective pTANs in the two striatal regions was similar, the firing patterns of the average neurons in these regions were different. In DLS the average firing rate in the preferred direction resembled a bell shape while in VS the average firing rate was concave with a slight increase toward the end of the movement (**Figure 4A**; top and bottom, respectively).

To pinpoint the source of this difference we calculated the number of neurons contributing selectively to the normalized response during different phases of the movement and also calculated the magnitude of the difference in firing rates during left and right movements. Based on the firing pattern of the normalized average neuron we divided the movement duration per trial into three parts: beginning, middle, and end. We compared the activity during left and right movements and tested in each part whether the firing rates in the two directions were significantly different. This allowed us to map the response of each pTAN to one of seven optional patterns depicted in **Figure 4B**. The observed distributions of pTAN activity patterns in DLS and VS were significantly different. Neurons in VS tended to exhibit sharp phasic responses

lasting only a fraction of the movement whereas neurons in DLS tended to exhibit prolonged responses typically lasting two consecutive parts and even throughout the movement. The percent of pTANs exhibiting selectivity during a single phase was significantly higher in VS (83%) compared to DLS (33%; $p < 0.01$). To verify this result we calculated the overlap in the neuronal population during 2 consecutive phases of movement. Indeed, the overlap in neuronal activation during the beginning and middle parts of the movement was higher in DLS (9/23; 39%) compared to VS (3/21; 14%) and reached significance when comparing the middle and end parts of the movements (DLS: 17/25; 68%; VS: 5/25; 20%; $p < 0.01$). The observed activation patterns indicate that VS pTANs exhibit short-lasting phasic responses during different parts of the movement whereas DLS pTANs contribute throughout the movement.

To differentiate the contributions of population size and modulation strength to the normalized average neuron in both regions, we calculated selectivity indices for each of the pTAN populations. Selectivity indices averaged over DLS pTANs were significantly higher than the pTANs of VS (**Figure 4C**; DLS: SI = 0.57; $n = 10$; and VS: SI = 0.30; $n = 7$, Wilcoxon rank sum test, $p < 0.01$). The

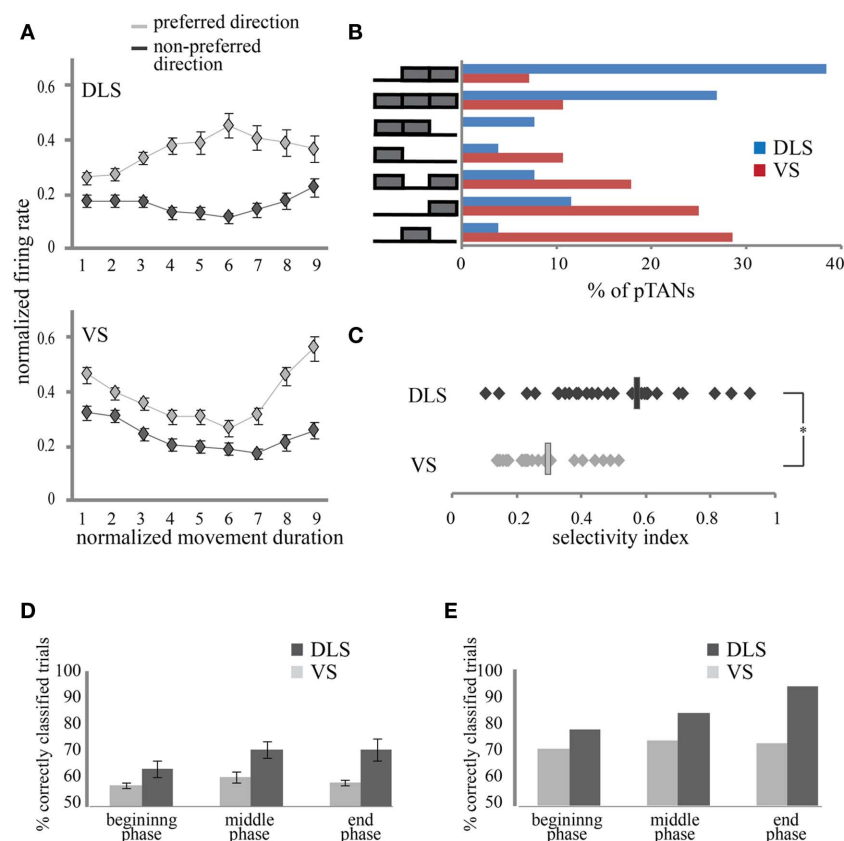


FIGURE 4 | Firing patterns characteristics of pTANs in DLS and in VS.

(A) Average, normalized population activity of direction selective DLS (top) and VS (bottom) pTANs during movement, separated into preferred and non-preferred directions. Error bars are standard error of means. (B) pTANs in DLS and in VS exhibit distinct direction selectivity patterns. On the left: selectivity patterns marking movement phases with significant difference between left and right activation. For example, the top row includes neurons which exhibited significant

left and right firing differences during the middle and end of movement but not after movement initiation. On the right: the percent of pTANs in DLS (blue) and VS (red) assigned to each of the patterns. (C) Selectivity indices of direction selective pTANs in DLS and VS. Average values of SI are marked by rectangles. (D) Percent of trials in which movement direction was correctly predicted from the activity of single neurons, averaged over animals. Error bars are standard error of the means. (E) Percent of trials predicted correctly by the best neurons in each striatal region.

differences in selectivity indices calculated for DLS and VS during the three movement phases were not significant (DLS: 0.49, 0.59, and 0.63; VS: 0.23, 0.39, and 0.29, $p > 0.1$). In DLS, the percent of direction selective neurons during the middle (77%) and end (85%) of movement was almost twice as high as that at the beginning (46%) of the movement whereas in VS these differences were moderate (39, 46, and 61%; at the beginning, middle, and end of movement, respectively; **Figure 4B**). It seems that the modulation strength and the population size are synergistic in action and therefore contribute together to the observed modulation in the response of the normalized average neuron (**Figure 4A**). The difference in selectivity indices and population size between the two regions indicates that pTANs in DLS exhibit more pronounced activation when animals move in the preferred direction compared to pTANs in VS.

In order to further elucidate the differences in neuronal activation between DLS and VS we tested how well we could predict the movement direction of any given trial from the neuronal firing. For each neuron, the firing histograms during left and right movements were calculated and normalized. A trial was classified as a left or a right movement trial if the number of spikes released during this trial was more likely to be drawn from the normalized firing histogram of that direction excluding the trial itself (see methods). The percent of correctly classified trials was calculated for all neurons in both regions during the three movement phases. As expected from the selectivity indices, the activity of pTANs in DLS enabled a more reliable classification of the trials into left and right movements than that of pTANs in VS (DLS: $n = 10$; 64, 71, and 71%; VS: $n = 7$; 58, 61, and 59%; for beginning, middle, and end of movement, respectively; $p < 0.01$; **Figure 4D**). The classification quality was similar during the different movement phases in both regions ($p > 0.5$) and in both regions, it was significantly better than chance level ($p < 0.01$). Importantly, in both regions there were neurons that were much better than the average in predicting movement direction (DLS: 80, 89, and 95%; and VS: 71, 72, and 72%; **Figure 4E**) suggesting that this information is readily available in both regions.

We conclude that the difference in pTANs' activation in the two striatal regions results from two sources: the first is that pTANs in DLS tend to show more pronounced directional selectivity by exhibiting a stronger firing rate during movements in the preferred relative to the non-preferred direction. Secondly, the responses of pTANs in DLS are prolonged relative to those of pTANs in VS which exhibit short-lasting phasic responses. This kind of firing pattern is expected to flatten the average normalized firing because different neurons contribute during different parts of the movement, each with a smaller SI. Consequently, both regions enable extraction of information regarding movement direction that is significantly better than chance level, yet DLS provided more reliable information than VS.

DISCUSSION

In this study we simultaneously measured the neural activity of pTANs in DLS and VS while rats performed an associative task. Our data show without a doubt that the majority of the recorded pTANs in both striatal regions are movement related, and that most of them are also direction selective. In both regions, we observed

similar proportions of movement related and direction selective pTANs. Nevertheless, the firing patterns of pTANs in both regions were quite different at the single cell level and the population. First, the preferred direction of pTANs in VS was typically contralateral to the recording site whereas in DLS the preferred direction of different pTANs was equally distributed ipsilaterally and contralaterally. In addition, pTANs in DLS tended to be selective throughout the movement while pTANs in VS mostly showed transient selectivity during different parts of the movement. Finally, pTANs in the DLS exhibited higher values of selectivity indices compared to pTANs in VS and consequently were better at providing information regarding movement direction at the single trial level.

The significant movement-related TAN activity we observed in our study challenges traditional assumptions concerning the role of TANs in reward and motivation. A few studies have reported TAN responses related to movement that seem to concur with our results (Lee et al., 2006; Ravel et al., 2006). In Lee et al. (2006) the percent of TANs that responded to movement reached 74% when movement was self timed by the animal, compared to less than 40% when movement was cued. The majority of studies in non-human primates have used behavioral paradigms which require a "go" cue for movement initiation which may reduce the likelihood of identifying movement-related TAN activation. Ravel et al. (2006) found that one-quarter of striatal TANs responded to the direction of movement and one-quarter responded to the context in which the stimulus–movement combination occurred. In our paradigm these two conditions cannot be distinguished because the number of error trials performed by the well trained animals was too low to enable reliable analysis of neuronal activity, suggesting that it is possible that some of the TANs we identified as movement-related code for movement in a specific context. Another possible explanation is the different movement requirements from behaving monkeys and behaving rats. In most studies that examine TAN activity in behaving monkeys, the subjects are restrained in their seat, their head is fixed, and the movements required of them are minimal. In our task, as in most behaving rat experiments, the rat is not restrained and is required to perform a complex movement which strongly activates the motor cortex (Cohen and Nicolelis, 2004) and likely the thalamus, and as a result the striatum.

The MSNs in the striatum have been shown to respond strongly during motor skill learning and assuming some similarity in the afferents of different striatal cell types supports the ability of TANs in dorsal striatum to exhibit motor responses. Indeed, Nambu et al. (2002) showed that stimulation of the primary motor cortex and the supplementary motor area caused excitation in both MSNs and TANs. In addition, about 60% of TANs were activated during passive or active movement of the forelimb. Thus, it is likely that in addition to other aspects of behavior, TANs in the rat DLS, which is the homologue of the monkey putamen, is involved in passive and active movements.

Even though movement-related activity is expected in the DLS, it is quite intriguing to see such activity in VS, a structure associated mainly with reward and motivation. However, this type of activity is in line with the hypothesized role of VS as a "limbic-motor interface" as proposed by Mogenson et al. (1980). Contrary to activity in the DLS, TANs in the VS show short-lasting, phasic direction selectivity. These TANs may provide an informative signal that a

movement was initiated and to which direction, rather than taking part directly in movement control as is the case for the DLS TANs. The primary output region of the VS is the ventral pallidum, which is considered to be a central convergence point for many structures related to reward including the orbitofrontal, prefrontal and infralimbic cortices, the amygdala, lateral hypothalamus, ventral tegmental area, etc. (Smith et al., 2009). It is possible that after an action has been selected and initiated VS conveys the information regarding the action to ventral pallidum, where integration with the action outcome occurs.

As part of the theoretically segregated limbic loop, it is still unclear how VS receives information regarding motor responses. One possibility is that this information is conveyed by the pedunculo-pontine nucleus (PPn) in the brainstem. The PPn plays a role in the production and control of movement (reviewed in Jenkinson et al., 2009) and has been shown to respond to sensory and motor task events (Matsumura et al., 1997; Pan and Hyland, 2005). On the other hand, the PPn also receives inputs from many reward-related structures, including the ventral pallidum (Semba and Fibiger, 1992; Mena-Segovia et al., 2004; Winn, 2006) and provides one of the strongest excitatory inputs to the ventral tegmental area and substantia nigra pars compacta in the midbrain (Scarnati et al., 1984; Blaha and Winn, 1993; Pan and Hyland, 2005; Mena-Segovia et al., 2008). It is possible that the PPn conveys task-event information to the dopamine neurons of the midbrain, and this information is in turn conveyed to the VS. Further studies are required to clarify whether the information processed by TANs in VS is motor in nature or rather specific information essential for task performance such as movement direction, movement onset etc., and to locate the circuits transferring this information to the VS.

An important issue to address is why our neuronal sampling was skewed toward TANs rather than the neurons prevalent in striatum – the MSNs. Other studies in rats that have recorded activity in the striatum using tetrodes report that the majority of the

recorded neurons were MSNs as expected from their prevalence in the striatum. Although the source of this misrepresentation is not clear, it is possible that the wire diameter used in our recording electrodes may have been a contributing factor. The 50 micron wires enable a larger detection volume which increases the likelihood of detecting large currents generated by distant large neurons like the TANs while losing the sensitivity required for detecting small currents generated by small cells like the MSNs and the FSI. On the other hand, when recording neural activity in mice using microwires of 35 and 50 microns in diameter, the misrepresentation observed in rats disappear (unpublished data and see also Costa et al., 2006; Yin et al., 2009). Further studies have to be performed in order to clarify this issue.

CONCLUSION

The differences we observed in the firing patterns of TANs in DLS and in VS support a distinct role for this type of interneuron in each striatal region. TANs in the DLS mostly exhibited directional selectivity that continued throughout the movement duration, peaking around halfway, reminiscent of movement kinematics for ballistic movements. It is possible, therefore, that these interneurons participate in the motor loop and are involved in real-time control of movements. The pTANs in VS, on the other hand, showed short-lasting transient directional selectivity that was maintained throughout the movement by different neurons. Consequently, these neurons better fit to provide information regarding different movement-related events such as movement direction, movement initiation and expectation of movement ending. Our study calls for reassessment of the TANs' role in motor processing using a variety of behavioral paradigms.

ACKNOWLEDGMENTS

This study was supported by the Israel Science Foundation (ISF) grant # 861/06.

REFERENCES

- Alexander, G. E., and DeLong, M. R. (1985). Microstimulation of the primate neostriatum. II. Somatotopic organization of striatal microexcitable zones and their relation to neuronal response properties. *J. Neurophysiol.* 53, 1417–1430.
- Aosaki, T., Tsubokawa, H., Ishida, A., Watanabe, K., Graybiel, A. M., and Kimura, M. (1994). Responses of tonically active neurons in the primates striatum undergo systematic changes during behavioral sensorimotor conditioning. *J. Neurosci.* 14, 3969–3984.
- Apicella, P., Legallet, E., and Trouche, E. (1997). Responses of tonically discharging neurons in the monkey striatum to primary rewards delivered during different behavioral states. *Exp. Brain Res.* 116, 456–466.
- Apicella, P., Ljungberg, T., Scarnati, E., and Schultz, W. (1991). Responses to reward in monkey dorsal and ventral striatum. *Exp. Brain Res.* 85, 491–500.
- Atallah, H. E., Lopez-Paniagua, D., Rudy, J. W., and O'Reilly, R. C. (2007). Separate neural substrates for skill learning and performance in the ventral and dorsal striatum. *Nat. Neurosci.* 10, 126–131.
- Bennett, B. D., and Wilson, C. J. (1999). Spontaneous activity of neostriatal cholinergic interneurons in vitro. *J. Neurosci.* 19, 5586–5596.
- Blaha, C. D., and Winn, P. (1993). Modulation of dopamine efflux in the striatum following cholinergic stimulation of the substantia nigra in intact and pedunculo-pontine tegmental nucleus-lesioned rats. *J. Neurosci.* 13, 1035–1044.
- Blazquez, P. M., Fujii, N., Kojima, J., and Graybiel, A. M. (2002). A0 network representation of response probability in the striatum. *Neuron* 33, 973–982.
- Cohen, D., and Nicolelis, M. A. (2004). Reduction of single-neuron firing uncertainty by cortical ensembles during motor skill learning. *J. Neurosci.* 24, 3574–3582.
- Costa, R. M., Cohen, D., and Nicolelis, M. A. (2004). Differential corticostriatal plasticity during fast and slow motor skill learning in mice. *Curr. Biol.* 14, 1124–1134.
- Costa, R. M., Lin, S. C., Sotnikova, T. D., Cyr, M., Gainetdinov, R. R., Caron, M. G., and Nicolelis, M. A. (2006). Rapid alterations in corticostriatal ensemble coordination during acute dopamine-dependent motor dysfunction. *Neuron* 52, 359–369.
- Ding, J. B., Guzman, J. N., Peterson, J. D., Goldberg, J. A., and Surmeier, D. J. (2010). Thalamic gating of corticostriatal signaling by cholinergic interneurons. *Neuron* 67, 294–307.
- Gage, G. J., Stoetznner, C. R., Wiltschko, A. B., and Berke, J. D. (2010). Selective activation of striatal fast-spiking interneurons during choice execution. *Neuron* 67, 466–479.
- Gan, J. O., Walton, M. E., and Phillips, P. E. (2010). Dissociable cost and benefit encoding of future rewards by mesolimbic dopamine. *Nat. Neurosci.* 13, 25–27.
- Gerfen, C. R. (1988). Synaptic organization of the striatum. *J. Electron Microsc. Tech.* 10, 265–281.
- Graybiel, A. M. (2008). Habits, rituals, and the evaluative brain. *Annu. Rev. Neurosci.* 31, 359–387.
- Hikosaka, O., Sakamoto, M., and Usui, S. (1989). Functional properties of monkey caudate neurons. I. Activities related to saccadic eye movements. *J. Neurophysiol.* 61, 780–798.
- Humphries, M. D., and Prescott, T. J. (2010). The ventral basal ganglia, a selection mechanism at the crossroads of space, strategy, and reward. *Prog. Neurobiol.* 90, 385–417.
- Inokawa, H., Yamada, H., Matsumoto, N., Muranishi, M., and Kimura, M. (2010). Juxtacellular labeling of tonically active neurons and phasically active neurons in the rat striatum. *Neuroscience* 168, 395–404.

- Jacobson, G. A., Lev, I., Yarom, Y., and Cohen, D. (2009). Invariant phase structure of olivo-cerebellar oscillations and its putative role in temporal pattern generation. *Proc. Natl. Acad. Sci. U.S.A.* 106, 3579–3584.
- Jenkinson, N., Nandi, D., Muthusamy, K., Ray, N. J., Gregory, R., Stein, J. E., and Aziz, T. Z. (2009). Anatomy, physiology, and pathophysiology of the pedunculopontine nucleus. *Mov. Disord.* 24, 319–328.
- Joel, D., and Weiner, I. (1994). The organization of the basal ganglia-thalamo-cortical circuits: open interconnected rather than closed segregated. *Neuroscience* 63, 363–379.
- Jog, M. S., Kubota, Y., Connolly, C. I., Hillegaart, V., and Graybiel, A. M. (1999). Building neural representations of habits. *Science* 286, 1745–1749.
- Joshua, M., Adler, A., Mitelman, R., Vaadia, E., and Bergman, H. (2008). Midbrain dopaminergic neurons and striatal cholinergic interneurons encode the difference between reward and aversive events at different epochs of probabilistic classical conditioning trials. *J. Neurosci.* 28, 11673–11684.
- Kimura, M., Rajkowski, J., and Everts, E. (1984). Tonicly discharging putamen neurons exhibit set-dependent responses. *Proc. Natl. Acad. Sci. U.S.A.* 81, 4998–5001.
- Lau, B., and Glimcher, P. W. (2007). Action and outcome encoding in the primate caudate nucleus. *J. Neurosci.* 27, 14502–14514.
- Lee, I. H., Seitz, A. R., and Assad, J. A. (2006). Activity of tonically active neurons in the monkey putamen during initiation and withholding of movement. *J. Neurophysiol.* 95, 2391–2403.
- Matsumura, M., Watanabe, K., and Ohye, C. (1997). Single-unit activity in the primate nucleus tegmenti pedunculopontinus related to voluntary arm movement. *Neurosci. Res.* 28, 155–165.
- Mena-Segovia, J., Bolam, J. P., and Magill, P. J. (2004). Pedunculopontine nucleus and basal ganglia: distant relatives or part of the same family? *Trends Neurosci.* 27, 585–588.
- Mena-Segovia, J., Winn, P., and Bolam, J. P. (2008). Cholinergic modulation of midbrain dopaminergic systems. *Brain Res. Rev.* 58, 265–271.
- Mogenson, G. J., Jones, D. L., and Yim, C. Y. (1980). From motivation to action: functional interface between the limbic system and the motor system. *Prog. Neurobiol.* 14, 69–97.
- Morris, G., Arkadir, D., Nevet, A., Vaadia, E., and Bergman, H. (2004). Coincident but distinct messages of midbrain dopamine and striatal tonically active neurons. *Neuron* 43, 133–143.
- Nambu, A., Kaneda, K., Tokuno, H., and Takada, M. (2002). Organization of corticostriatal motor inputs in monkey putamen. *J. Neurophysiol.* 88, 1830–1842.
- Nicolelis, M. A., Ghazizadeh, A. A., Faggin, B. M., Votaw, S., and Oliveira, L. M. (1997). Reconstructing the engram: simultaneous, multisite, many single neuron recordings. *Neuron* 18, 529–537.
- Pan, W. X., and Hyland, B. I. (2005). Pedunculopontine tegmental nucleus controls conditioned responses of midbrain dopamine neurons in behaving rats. *J. Neurosci.* 25, 4725–4732.
- Parent, A., and Hazrati, L. N. (1995). Functional anatomy of the basal ganglia. I. The cortico-basal ganglia-thalamo-cortical loop. *Brain Res. Brain Res. Rev.* 20, 91–127.
- Ragozzino, M. E. (2003). Acetylcholine actions in the dorsomedial striatum support the flexible shifting of response patterns. *Neurobiol. Learn. Mem.* 80, 257–267.
- Ravel, S., Legallet, E., and Apicella, P. (2003). Responses of tonically active neurons in the monkey striatum discriminate between motivationally opposing stimuli. *J. Neurosci.* 23, 8489–8497.
- Ravel, S., Sardo, P., Legallet, E., and Apicella, P. (2006). Influence of spatial information on responses of tonically active neurons in the monkey striatum. *J. Neurophysiol.* 95, 2975–2986.
- Raz, A., Feingold, A., Zelanskaya, V., Vaadia, E., and Bergman, H. (1996). Neuronal synchronization of tonically active neurons in the striatum of normal and parkinsonian primates. *J. Neurophysiol.* 76, 2083–2088.
- Scarnati, E., Campana, E., and Pacitti, C. (1984). Pedunculopontine-evoked excitation of substantia nigra neurons in the rat. *Brain Res.* 304, 351–361.
- Schmitzer-Torbert, N. C., and Redish, A. D. (2008). Task-dependent encoding of space and events by striatal neurons is dependent on neural subtype. *Neuroscience* 153, 349–360.
- Semba, K., and Fibiger, H. C. (1992). Afferent connections of the laterodorsal and the pedunculopontine tegmental nuclei in the rat: a retro- and antero-grade transport and immunohistochemical study. *J. Comp. Neurol.* 323, 387–410.
- Shimo, Y., and Hikosaka, O. (2001). Role of tonically active neurons in primate caudate in reward-oriented saccadic eye movement. *J. Neurosci.* 21, 7804–7814.
- Smith, K. S., Tindell, A. J., Aldridge, J. W., and Berridge, K. C. (2009). Ventral pallidum roles in reward and motivation. *Behav. Brain Res.* 196, 155–167.
- Tepper, J. M., and Bolam, J. P. (2004). Functional diversity and specificity of neostriatal interneurons. *Curr. Opin. Neurobiol.* 14, 685–692.
- Wilson, C. J., Chang, H. T., and Kitai, S. T. (1990). Firing patterns and synaptic potentials of identified giant aspiny interneurons in the rat neostriatum. *J. Neurosci.* 10, 508–519.
- Winn, P. (2006). How best to consider the structure and function of the pedunculopontine tegmental nucleus: evidence from animal studies. *J. Neurol. Sci.* 248, 234–250.
- Yamada, H., Matsumoto, N., and Kimura, M. (2004). Tonicly active neurons in the primate caudate nucleus and putamen differentially encode instructed motivational outcomes of action. *J. Neurosci.* 24, 3500–3510.
- Yin, H. H., and Knowlton, B. J. (2006). The role of the basal ganglia in habit formation. *Nat. Rev. Neurosci.* 7, 464–476.
- Yin, H. H., Knowlton, B. J., and Balleine, B. W. (2004). Lesions of dorsolateral striatum preserve outcome expectancy but disrupt habit formation in instrumental learning. *Eur. J. Neurosci.* 19, 181–189.
- Yin, H. H., Mulcare, S. P., Hilario, M. R., Clouse, E., Holloway, T., Davis, M. I., Hansson, A. C., Lovinger, D. M., and Costa, R. M. (2009). Dynamic reorganization of striatal circuits during the acquisition and consolidation of a skill. *Nat. Neurosci.* 12, 333–341.
- Yin, H. H., Ostlund, S. B., Knowlton, B. J., and Balleine, B. W. (2005). The role of the dorsomedial striatum in instrumental conditioning. *Eur. J. Neurosci.* 22, 513–523.

Conflict of Interest Statement: The authors declare that the research was conducted in the absence of any commercial or financial relationships that could be construed as a potential conflict of interest.

Received: 31 January 2011; accepted: 18 May 2011; published online: 31 May 2011.
 Citation: Yarom O and Cohen D (2011) Putative cholinergic interneurons in the ventral and dorsal regions of the striatum have distinct roles in a two choice alternative association task. *Front. Syst. Neurosci.* 5:36. doi: 10.3389/fnys.2011.00036
 Copyright © 2011 Yarom and Cohen. This is an open-access article subject to a non-exclusive license between the authors and Frontiers Media SA, which permits use, distribution and reproduction in other forums, provided the original authors and source are credited and other Frontiers conditions are complied with.



A critical review of habit learning and the basal ganglia

Carol A. Seger* and Brian J. Spiering

Department of Psychology, Colorado State University, Fort Collins, CO, USA

Edited by:

Elizabeth Abercrombie,
Rutgers-Newark: The State University
of New Jersey, USA

Reviewed by:

Christopher I. Petkov,
Newcastle University, UK
Heiko J. Luhmann, Institut für
Physiologie und Pathophysiologie,
Germany

***Correspondence:**

Carol A. Seger, Department of
Psychology, 1876 Campus Delivery,
Colorado State University, Fort Collins,
CO 80523, USA.
e-mail: carol.seger@colostate.edu

The current paper briefly outlines the historical development of the concept of habit learning and discusses its relationship to the basal ganglia. Habit learning has been studied in many different fields of neuroscience using different species, tasks, and methodologies, and as a result it has taken on a wide range of definitions from these various perspectives. We identify five common, but not universal, definitional features of habit learning: that it is inflexible, slow or incremental, unconscious, automatic, and insensitive to reinforcer devaluation. We critically evaluate for each of these how it has been defined, its utility for research in both humans and non-human animals, and the evidence that it serves as an accurate description of basal ganglia function. In conclusion, we propose a multi-faceted approach to habit learning and its relationship to the basal ganglia, emphasizing the need for formal definitions that will provide directions for future research.

Keywords: basal ganglia, habit learning, automaticity, reward

INTRODUCTION

The concept of habit learning has developed through the fruitful interaction of researchers in several intellectual domains, including animal learning, cognitive psychology, cognitive neuropsychology, and behavioral neuroscience. As a result, habit learning has taken on a variety of proposed definitions. In this paper, we will first describe the historical evolution of habit learning as a concept. We will then briefly describe the anatomical and functional roles of the basal ganglia that may underlie learning in general and habit learning in particular. Finally, we will revisit the defining features of habit learning and assess how well they characterize learning in the basal ganglia.

HISTORICAL EVOLUTION OF THE HABIT LEARNING CONCEPT

The term habit was used, but not explicitly defined, by William James in the seminal *Principles of Psychology* (James, 1890). It was used on occasion by early researchers studying animal learning, in particular Hull (1934a,b) and Lashley (1930, 1950). “Habit” roughly corresponded to the resulting motor behavior (e.g., Lashley referred to the “maze running habit”), and habit learning to acquisition of these behaviors in an instrumental learning context.

HIPPOCAMPAL RESEARCH: EARLY DEFINITIONS OF HABIT LEARNING

The earliest use of “habit learning” to refer to a specific form of learning came from researchers studying the effects of hippocampal damage in human and non-human animals. By the late 1960s it was clear that hippocampal damage affected learning on many, but not all, tasks. Hirsh (1974) first used the term “habit learning” to describe a particular type of memory or learning system. He defined the habit system as that “responsible for the learning of which hippocampally ablated animals are capable” (1974, p 421). Thus, from the beginning habit learning was defined negatively, in terms of what it was not (i.e., hippocampally based), rather than what it was. To Hirsh, the primary feature of hippocampal-based learning was contextual encoding (e.g., of the particular spatial and

temporal context at encoding) and retrieval of information that was contextually sensitive. He argued in contrast that habit learning was similar to the stimulus–response (S–R) learning processes proposed by earlier learning researchers, and that these S–R associations were specifically insensitive to context.

Miskin et al. (1984) extended Hirsh’s concept of habit learning. Following Hirsh, they identified features of habit learning as the opposite those of hippocampally-based learning. One set of features was “rapid” versus “slow” learning. Rapid learning was defined as one-trial learning, which required the hippocampus, whereas slow learning required repeated trials and was preserved in amnesia. They immediately related the “rapid”–“slow” distinction to the distinction posed by Hirsh, which they referred to as flexible (contextually sensitive in Hirsh) versus inflexible learning. They proposed that there is “a trade-off between short-term flexibility afforded by the memory system and long-term reliability afforded by the habit system” (p. 73). Finally, they argued that habits were a relatively primitive form of learning that should therefore appear earlier in ontogeny as well as phylogeny, which they supported with developmental evidence from their lab.

Mishkin and colleagues were also the first to propose a crucial role for the basal ganglia in habit learning. The basis for their argument, which they termed “admittedly speculative” was the early development of the basal ganglia both in phylogeny and ontogeny, and the presence of widespread anatomical projections to the striatum from cortex that “provide a mechanism through which cortically processed sensory inputs could become associated with motor outputs generated in the pallidum and so yield the stimulus–response bonds that constitute habits” (p. 74).

COGNITIVE PSYCHOLOGY: HABIT AS IMPLICIT AND AUTOMATIC

The field of cognitive psychology did not use the term habit learning, but from the late 1960s through the 1980s several concepts were developed in this field that later were incorporated into theories of habit learning. These distinctions included unconscious,

or implicit, learning and memory (in contrast with conscious or explicit learning and memory), and automatic processing (in contrast with controlled processing). Both of these distinctions fall broadly within “dual process” theories of cognition that see one type of cognitive process as relatively unconscious, automatic, evolutionarily early, and similar across individuals, in contrast with a second type of cognitive process that is conscious, controlled, evolutionarily more recent, and subject to significant individual differences (see Evans, 2008 for a review).

Reber (1967) coined the term “implicit learning”; the concept was extended to “implicit memory” by Graf and Schacter (1985). The focus in both areas of research was on consciousness: identifying what could or could not be learned and/or retrieved without awareness. Implicit memory was defined as “when previous experiences facilitate performance on a task that does not require conscious or intentional recollection of those experiences” (Schacter, 1987, p. 501). Implicit memory tasks typically used priming paradigms in which improvement in accuracy and/or processing time was observed for repeated stimuli; priming was later divided into perceptual (repeated visual stimulus processing) and conceptual (repeated semantic processing) forms (Keane et al., 1991).

Seger (1994, p. 164) outlined three guidelines for implicit learning: (1) “the knowledge gained in implicit learning is not fully accessible to consciousness, in that subjects cannot provide a full ... verbal account of what they have learned,” (2) “information [learned] ... is more complex than a single simple association or frequency count,” and (3) “implicit learning does not involve processes of conscious hypothesis testing but is an incidental consequence of the type and amount of cognitive processing performed on the stimuli.” Implicit learning was studied using several different tasks, most often the serial reaction time task (which measures improvement in reaction time when responding to stimuli when presented in a repeating sequence in comparison with stimuli presented in random order), and the artificial grammar task (which measures the ability of subjects to discriminate letter strings that follow a complex sequential pattern determined by a finite state automaton, or artificial grammar, from those that violate the pattern).

Another influential concept from cognitive psychology was that of automaticity, originally developed by Shiffrin and Schneider (1977) to account for different forms of attentional scanning. The concepts of automatic and controlled processing were widely adopted across various domains within cognitive psychology. Shiffrin and Schneider (1977) gave multiple criteria for considering a process to be automatic, including (1) automatic processes are not constrained by short-term memory capacity limitations and do not require attention; (2) automatic processes are generally performed too quickly to be consciously accessible and once initiated are completed regardless of subjects’ intentions; (3) automatic processes require significant training, undergoing a gradual shift from controlled to automatic through the course of practice; and (4) automatic processes, once acquired, are difficult to modify. Criterion 1 led to an operational definition of automaticity as primary task performance not negatively affected by a parallel, short-term memory demanding task.

Through development of the process dissociation procedure, Jacoby (1991) related automaticity to implicit learning and memory. He argued that participants should be able to exert strategic

control over conscious knowledge, and theorized that they should be able to control the behavioral expression of this knowledge in accordance with task instructions. Conversely, he argued that participants should be unable exert strategic control over unconscious knowledge and theorized that they might have difficulty controlling the behavioral expression of this knowledge. The critical feature of the process dissociation procedure is that participants are asked to demonstrate knowledge via both “inclusion” and “exclusion” instructions. Inclusion instructions demand that participants produce behavior in accordance with a learned structure, while exclusion instructions demand that participants produce discordant behavior. This approach led to a different operational definition of automaticity. Automatic processing is measured by calculating the intrusion of the previously learned material into the exclusion condition (false positives); controlled processing is defined as the difference between performance in the inclusion condition and the automatic processing measure.

COGNITIVE NEUROPSYCHOLOGY: HABIT AS A TYPE OF “NON-DECLARATIVE” MEMORY

Larry Squire and colleagues integrated the approaches taken by researchers examining hippocampal lesions in non-human animals, researchers in cognitive psychology, and researchers studying human patients with amnesia. Their theory developed across time. Cohen and Squire (1980) initially defined procedural learning as “operations governed by rules or procedures” in contrast to hippocampally based learning, which they characterized as “operations that depend on specific, declarative, data-based material.” The term “procedural” was adapted from artificial intelligence research (Winograd, 1972; Anderson, 1982). Anderson’s (1982) view was that all cognitive knowledge started by being represented declaratively, as individual “propositions,” and procedural knowledge was formed by the compilation of groups of propositions into procedures. Procedural knowledge accounted well for the tasks known to be preserved in amnesia at that time, including pursuit rotor (Corkin, 1968), mirror drawing (Milner, 1962), and mirror reading (Cohen and Squire, 1980).

During the 1980s and early 1990s amnesic subjects were shown to have intact learning across a large number of novel tasks, primarily drawn from the implicit memory and learning literatures. These included perceptual priming (Graf and Schacter, 1985), the serial reaction time task (Nissen and Bullemer, 1987), artificial grammar learning (Knowlton et al., 1992), category learning using the Posner dot pattern task (Knowlton and Squire, 1993), and some aspects of learning on the Tower of Hanoi task (Cohen, 1984). It soon became clear that the term “procedural” was insufficient to characterize all the different types of non-hippocampal learning and memory. Squire and Zola-Morgan (1988) created the term “non-declarative” and defined it as “a heterogeneous collection of abilities: motor skills, perceptual skills, and cognitive skills (these abilities and perhaps others are examples of procedural memory); as well as simple classical conditioning, adaptation level effects, priming, and other instances where experience alters performance independently of providing a basis for the conscious recollection of past events” (p. 171). Non-declarative memory thus incorporated the cognitive psychology distinction between implicit and explicit memory with the result that hippocampal-based declarative

learning was now identified as memory that was accessible to consciousness, and the heterogeneous non-declarative memory systems as unconscious.

Squire and Zola-Morgan (1988, 1991) developed what was to become an often reprinted figure illustrating the types and subtypes of declarative and non-declarative memory (the 1991 version is shown in **Figure 1**). In Squire and Zola-Morgan (1988) the term “habit” isn’t used; instead, several different “skills” are described including motor skills (pursuit motor, Corkin, 1968; serial reaction time, Nissen and Bullemer, 1987; mirror drawing Milner, 1962), perceptual skills (mirror reading; Cohen and Squire, 1980), and cognitive skills (Tower of Hanoi; Cohen, 1984. Hebb digits task; Brooks and Baddeley, 1976). By 1991, Squire and colleagues referred to this type of non-declarative memory as “skills and habits,” as shown in **Figure 1**. They noted the basal ganglia as one potential neural system involved in habits and skills, along with the cerebellum.

ANIMAL LEARNING: HABIT LEARNING AS ONE FORM OF INSTRUMENTAL CONDITIONING

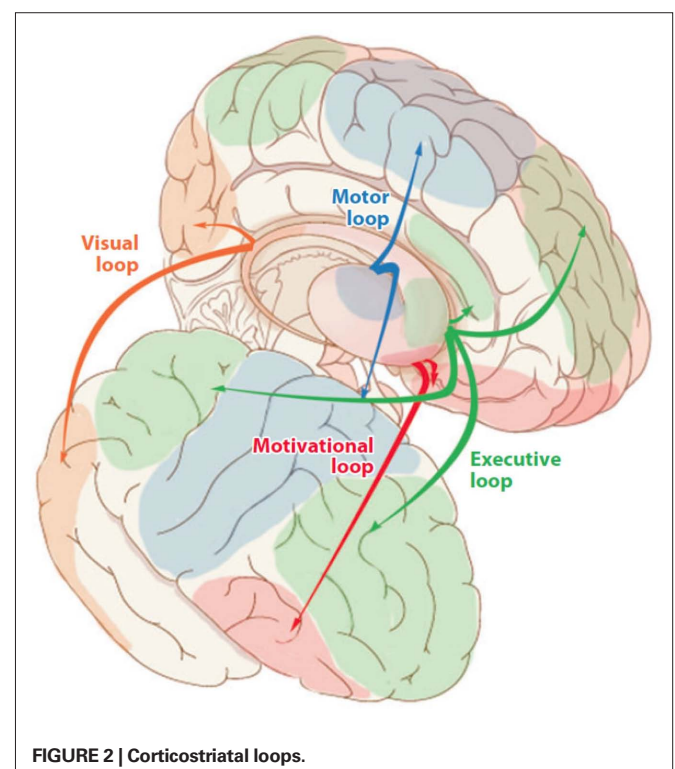
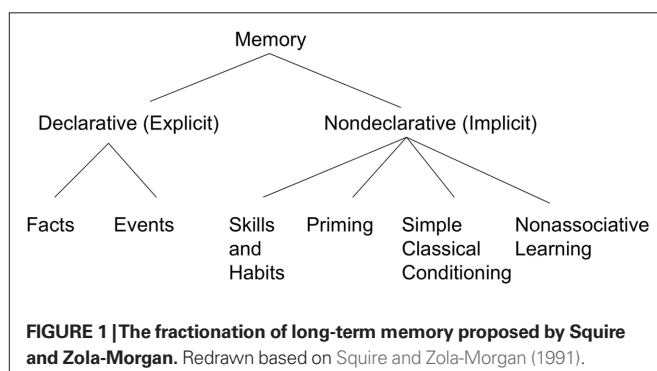
In the 1980s, Dickinson (1985) proposed separate “goal-directed behavior” and “habit” instrumental learning systems, based on whether execution of the learned behavior is sensitive to the value of the reward or not, respectively. One typical manipulation is to devalue the reinforcer by satiating the animal before testing; the value of a food reward is greater when the animal is hungry than when it has recently fed. An animal will perform a habitual act to obtain food even when it has eaten to satiation. He contrasted habit with goal-directed behavior, which is sensitive to the motivational state of the animal. Subsequent neuroscience studies (Yin and Knowlton, 2006; Packard, 2009) found that the distinction between goal-directed and habitual learning corresponded with reliance on different parts of the basal ganglia: the dorsomedial rodent striatum (homologous to the primate anterior caudate nucleus), and the dorsolateral striatum (homologous to the primate posterior putamen) respectively.

Graybiel (2008) recently offered a broad definition of habit learning. “First, habits (mannerisms, customs, rituals) are largely learned; in current terminology, they are acquired via experience-dependent plasticity. Second, habitual behaviors occur repeatedly over the course of days or years, and they can become remarkably fixed. Third, fully acquired habits are performed almost automatically, virtually non-consciously, allowing attention to be focused elsewhere. Fourth, habits tend to involve an ordered, structured action sequence that is prone to being elicited by a particular context or stimulus. And finally, habits can comprise cognitive expressions

of routine (habits of thought) as well as motor expressions of routine” (Graybiel, 2008, p. 361). Like Squire’s approach to non-declarative memory, Graybiel’s definition brings together several features from previous work, including that habits are relatively automatic, and unconscious, and that habits can be inflexible and rigid (particularly well learned habits). Graybiel emphasizes two additional features of habit: first, that motor habits are sequential behaviors with complex structure, going beyond a simple concept of a “response,” and second, that habits can extend beyond motor behaviors to include cognitive processes.

THE BASAL GANGLIA AND LEARNING

The basal ganglia are a group of subcortical nuclei, including the striatum, globus pallidus, substantia nigra, and subthalamic nucleus in humans. The basal ganglia interact with cerebral cortex via corticostriatal loops, in which information projects from cortex to the striatum, to the basal ganglia output nuclei, to the thalamus, and from there back to cortex (Alexander et al., 1986; Seger, 2008). The functions of the basal ganglia are supported by three pathways from the striatum to the thalamus, termed the “direct,” “indirect,” and “hyperdirect” pathways (Frank, 2005; Cohen and Frank, 2009). Broadly, the three pathways together implement a balance between regulating tonic inhibition in cortex as well as selective activation or gating of particular representations. The representations that the basal ganglia act upon is determined by the region of cortex within each corticostriatal loop. Although projections are continuous and there are no firm dividing lines between loops, it is useful for practical purposes to identify functionally different loops. Our approach includes four distinct loops (Seger and Cincotta, 2005; Seger, 2008) and is illustrated in **Figure 2**. They are the motor loop,



which connects motor and premotor cortexes with the putamen; the executive loop, which connects lateral and medial prefrontal regions with the anterior caudate; the visual loop, which connects inferior temporal regions with the posterior caudate, and the motivational loop, which connects ventromedial prefrontal regions with the ventral striatum (including the nucleus accumbens and ventral caudate and putamen). Given the broad patterns of cortical projections to the basal ganglia, it is not surprising that the basal ganglia are associated with a large variety of functions, including motor control (Redgrave et al., 2010), cognitive coordination (Stocco et al., 2010), and emotional functions (Nakano et al., 2000).

The basal ganglia are involved in learning through a variety of inherent plasticity mechanisms. The best studied is N-Methyl-D-aspartate (NMDA) modulated long-term potentiation (LTP) at the corticostriatal synapse. Corticostriatal synapses also receive dopaminergic input and LTP is highly sensitive to the presence of dopamine (Pawlak and Kerr, 2008). Dopamine projections come from the midbrain, including the ventral tegmental area and portions of the substantia nigra. Some dopamine neuron activity is sensitive to reward expectation and is computationally well-described by reward prediction error (Schultz, 2002; Bromberg-Martin et al., 2010). This dopamine signal is well-suited to serve as a learning signal indicating the presence of unexpected rewards, thus the organism is more likely to repeat the behavior leading to the reward in the future.

The basal ganglia are particularly important in learning the relationship between sensory information and motor responses on the basis of trial by trial feedback (Seger, 2008; Shohamy et al., 2008). Computational models of dopamine-mediated plasticity within the direct pathway (Ashby and Ennis, 2006), and across pathways (Frank, 2005; Cohen and Frank, 2009) do an excellent job of accounting for learning in this type of task. Convergent evidence from a variety of species and techniques supports the view that the basal ganglia are critical for learning in these tasks (Yin and Knowlton, 2006; Graybiel, 2008; Balleine et al., 2009; Packard, 2009; Seger, 2009). Most habit learning tasks follow the same stimulus–response–reward/feedback task structure (Seeger, 2009), and thus it is reasonable to propose that the basal ganglia should be important in habit learning.

REASSESSMENT OF HABIT LEARNING'S DEFINING CHARACTERISTICS

As the concept of habit learning developed, a number of different defining features were proposed. The following features were most commonly cited: inflexible, slow, unconscious, automatic, and insensitive to reinforcer devaluation. Here we revisit each of these defining criteria, asking the following questions about each: Why was it proposed? How precisely is it defined, and are there different definitions in use in different research areas? How accurately does this feature describe basal ganglia related learning? And, if relevant, how practical is the criterion for use with both human and non-human animals?

INFLEXIBLE

The characterization of habit learning as “inflexible” comes from Hirsh (1974), in contrast with flexible, context-dependent learning that was subserved by the hippocampus. Miskin et al. (1984) also included inflexible in their definition of habit learning, as

did Squire and colleagues in their development of the concept of non-declarative memory. Habit learning was independently characterized as inflexible by Dickinson (1985), who defined inflexibility in contrast to goal oriented behaviors, later shown to rely on prefrontal and dorsomedial striatal systems (Yin and Knowlton, 2006).

Flexible or inflexible has not been formally defined. The working definitions of these terms differ depending on whether habit learning is contrast with the hippocampal or prefrontal system. Within the hippocampal system, flexibility is often thought to be a consequence of individual memories formed by the hippocampus that can be applied to new situations. A commonly task thought to require hippocampally mediated flexibility is transitive inference, in which subjects are taught a set of ordinal relations, e.g., $A > B$, $B > C$, and then tested on whether they can infer that $A > C$ (Eichenbaum and Fortin, 2009). Some researchers have argued that the basal ganglia are limited to learning the individual ordinal relations and cannot support transitive inference or related phenomena (Myers et al., 2003; Shohamy et al., 2006). However, other research has found an opposite pattern of results, in which transitive inference relies on corticostriatal dopaminergic systems and is actually enhanced when the hippocampus is inhibited (Frank et al., 2003). Similar findings of hippocampal independence on other tasks thought to reflect flexibility (e.g., novelty transfer, Driscoll et al., 2004) indicate that this concept needs to be reassessed. Research is currently underway in a number of labs to better characterize what specific computational roles are played in inference tasks (Moustafa et al., 2010; Shohamy and Adcock, 2010).

Habit learning “inflexibility” is also defined in contrast with the sorts of flexibility enabled by executive functions subserved by the prefrontal cortex. In fact, executive functions were originally defined in clinical neuroscience as the ability to deal with novel or non-routine situations (Shallice, 1982). Prefrontal cortex enables flexible behavior through a variety of mechanisms involved in planning (setting goals, hypothesis formation, and testing), working memory (holding information online for several seconds), and cognitive control (the ability to execute plans in the face of distractions or other forms of interference; O'Reilly et al., 2010). Some have argued that the basal ganglia implement an inflexible learning process limited to past experience which then interacts with the flexible representations in prefrontal cortex.

Daw et al. (2005) argue that the basal ganglia select behaviors on the basis of the previous history of reinforcement, whereas the prefrontal cortex enables “model-based” control based on theories or strategies. Activity in the basal ganglia can be predicted by measures taken from reinforcement-learning modeling, specifically reward prediction (the estimate of the expected reward associated with choosing a particular behavior in the current state) and reward prediction error (the difference between the predicted and actually received reward). In this sense, the basal ganglia is inflexible because it is constrained to act in accordance with past reinforcement history. However, some studies have found patterns of basal ganglia activity that cannot be completely accounted for by reinforcement-learning models (Lopez-Paniagua and Seger, 2011).

One limitation of reinforcement-learning models is that they model the environment as a finite set of repeating states. In reality, organisms face situations that vary continuously, and need

to be able to generalize to similar but not identical situations. The basal ganglia are active in categorization tasks that require generalization to related, but novel, stimuli, indicating at least some flexibility (for review of some possible mechanisms, see Seger, 2008). It is unclear what the limits are to generalization in habit learning, and what role the basal ganglia may play in generalization.

SLOW OR INCREMENTAL

Habit learning was first characterized as slow or incremental by Miskin et al. (1984). As with “inflexible,” this criterion was defined on the basis of learning in hippocampally ablated animals, in which learning required multiple trials. In contrast, animals with an intact hippocampus can show one-trial learning. The terms “slow” and “incremental” are often interpreted as requiring hundreds or thousands of trials, but this is not well established. Standard approaches from cognitive psychology involve examining learning curves for accuracy and reaction time, and potentially then habit learning can be thought to be complete when asymptote is achieved (see **Figure 3**, bottom section). Attempts to formalize learning rates come from reinforcement learning and state space modeling approaches. Reinforcement-learning approaches result in two common measures: reward prediction error, which is the measure of how unexpected the received reward is, and value, which is the expected reward associated with the current stimulus and associated action. When learning is the fastest, RPE is the highest and value rapidly changes. As a task is learned, RPE reduces to zero and value asymptotes toward its maximum (**Figure 3**, middle section).

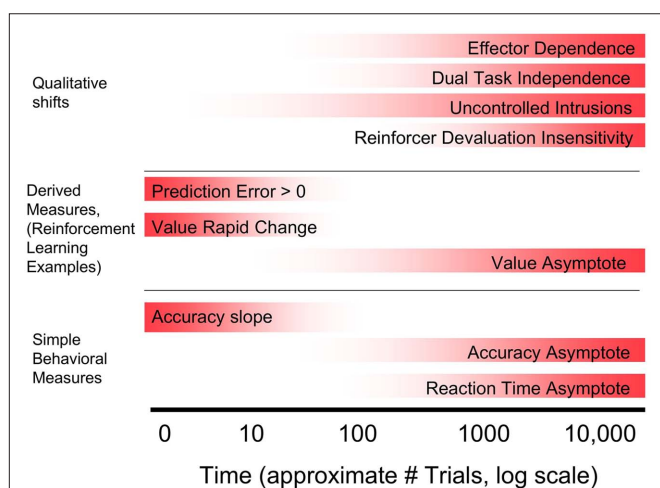


FIGURE 3 | Comparison of various possible criteria for habit learning that develop across learning on the basis of approximate point in training at which learning becomes habitual. Note that only criteria that can develop across training are included; criteria that are required across the entire time course of learning (unconscious, inflexible) are not. Top section: Qualitative criteria including two operational definitions of automaticity, and reinforcer devaluation. Middle and Bottom section: possible operational definitions of slow or incremental. Middle: Criteria based on computational modeling. This approach is illustrated using reinforcement-learning measures (reward prediction error, and value, or reward prediction) although other approaches can also be used. Bottom: Commonly used simple behavioral measures of learning.

Determining whether basal ganglia dependent learning is slow will depend on the operational definition of slow. However, it should be noted that basal ganglia dependent learning tasks vary greatly in how many trials it takes for subjects to reach maximal performance. Cromer et al. (2011) found that activity in the head of the caudate reached asymptote after five trials in a rule-learning paradigm. Delgado et al. (2005) found greatest caudate activity in an fMRI study during early learning (the first 8 repetitions of each stimulus) in comparison with later learning. Notably, these results are all from the caudate nucleus. Some researchers argue that the putamen should primarily subserve habitual learning. Studies that examine putamen activity during learning often find slower increases than in the caudate. However, activity levels in the putamen often follow behavior: activity reaches its maximum as behavioral accuracy reaches asymptote (Brasted and Wise, 2004; Williams and Eskandar, 2006), or as reinforcement-learning measures of learning, e.g., reward prediction, reach their maximum (Seger et al., 2010). Regional differences in learning speed are discussed further in the Conclusion.

If habit learning is acquired gradually, then when is performance fully habitual? Some people have argued that habits continue to develop even beyond the point at which behavioral measures cease to change, e.g., accuracy and reaction time reach their asymptotes. Grol et al. (2006) found continued practice related change in basal ganglia activity during these time points. Helie et al. (2010) and Waldschmidt and Ashby (2011) examined learning related changes long past the point at which accuracy reached asymptote, and found that basal ganglia activity continued to change and ultimately decreased to baseline levels. A more formal computational approach to measuring learning rates would be particularly helpful in this regard, as well as theories that can account for different levels of expertise and their neural correlates.

UNCONSCIOUS

Unconsciousness, as a defining feature of habit learning, stems from the inclusion of habit learning as a subtype of non-declarative memory by Squire and Zola-Morgan (1988, 1991). In their theory, declarative memory was accessible to consciousness, whereas non-declarative memory was not.

Consciousness can be difficult to define both on a practical and theoretical level. It is difficult to assess the degree of conscious access to knowledge in non-human animals, and impossible to assess verbalizable knowledge. Even with humans, there is debate about which measures of awareness are best for assessing whether there is conscious access to knowledge or not (Seth et al., 2008). Assessing awareness during task performance can affect the subject's strategic approach to the task, whereas assessing awareness after a task can easily miss information that might have been accessible to awareness during performance. On a more theoretical level, it is not always clear whether the relationship between awareness and learning is a necessary one; one logical possibility is that awareness is epiphenomenal and does not play a causal role in learning.

Recent research has found that the basal ganglia are involved in a wide variety of learning tasks, both ones in which learning is inaccessible to consciousness (Pessiglione et al., 2008), and in tasks in which subjects are aware of what they have learned, such as rule-learning tasks, arbitrary visuomotor learning tasks, and simple unstructured categorization tasks (Seger et al., 2011). Basal ganglia

recruitment is similar for relatively simple categorization tasks associated with high levels of verbalizable knowledge and more complex tasks associated with little verbalizable knowledge (Seger, 2008). Thus, basal ganglia do not seem to be exclusively associated with either conscious or unconscious learning. Furthermore, in recent research consciousness has proved to be a less reliable sign of hippocampal involvement in memory. The hippocampus has been shown to be required in several implicit learning tasks. These include contextual cuing, in which subjects become faster at searching repeated stimulus arrays (Greene et al., 2007), and some sequential relationships in the serial reaction time task (Schendan et al., 2003; Ergorul and Eichenbaum, 2006; Wilkinson et al., 2009).

AUTOMATIC

The concept of automaticity was developed in cognitive psychology by Shiffrin and Schneider (1977). It is itself a complex concept with four main characteristics. Three of these characteristics have already been discussed as potential defining features of habit learning: that automatic performance is unconscious, that the knowledge applied automatically is rigid or inflexible, and that automatic processes are acquired slowly and incrementally. The remaining characteristic is that automatic processes do not require the limited capacity cognitive mechanisms involved in short-term memory and selective attention. This leads to an operational definition that automatic tasks should be able to be performed in a dual task situation along with a demanding task that requires short-term memory and selective attention processes.

Although this definition is on the surface clear, in practice it is hard to know whether a particular dual task actually monopolizes appropriate limited capacity cognitive mechanisms. Recently, the concept of controlled processing has undergone extensive revision; there is no longer support for a simple modal model of memory, with a single limited capacity short-term memory store, though evidence suggests there are some general purpose or shared resources (Lavie, 2010). The modern view of short-term, or working, memory, and executive function includes qualitatively different short-term stores for different materials (Linden, 2007), and instead of a single attentional mechanism it includes a wide variety of cognitive control mechanisms (Banich et al., 2009; Braver et al., 2009). Learning in basal ganglia dependent tasks is often less affected by dual tasks than comparison tasks (Zeithamova and Maddox, 2006).

Dual task independence is also problematic when considering whether the basal ganglia are involved in habit learning, because the basal ganglia are in addition important for executive functions involved in task switching and selection. Thus, in a dual task situation any basal ganglia activity could be due to demands on the basal ganglia for coordinating the dual tasks, rather than for either of the tasks individually (Poldrack et al., 2005). Nevertheless, some researchers have used dual task methodologies successfully, such as Foerde et al. (2006) who found greater reliance on the basal ganglia for classification learning during dual task conditions in comparison with single task conditions. Interestingly, they found greater reliance on the putamen during dual task learning, which raises the possibility that dual tasks may load some corticostriatal networks more than others.

An alternative operational definition was proposed by Jacoby: that an automatic process will be performed regardless of a person's intentions, and thus will affect performance on a task even when the subject is attempting to not be affected (an exclusion task in Jacoby's terminology). This operational definition has not often been used in examining the basal ganglia in habit learning, though some researchers studying motor sequence learning have found that the striatum is recruited during automatic performance and is affected by prefrontal cortical mechanisms when subjects attempt to suppress the automatic performance (Destrebecqz et al., 2005).

REINFORCER REVALUATION INSENSITIVITY

The requirement that habit learning be insensitive to reinforcer revaluation comes from the field of animal learning. It has the advantage of being well defined, and it is clear how to apply this criterion experimentally, at least with non-human animal subjects. It is also clear how this criterion relates to learning in basal ganglia dependent tasks. This criterion dissociates the dorsomedial from dorsolateral striatum, with only the latter involved in habitual action.

The criterion does have some practical disadvantages. It requires two manipulations: first, the subject's value for the reinforcer must be changed (typically via feeding to satiation), and second, the behavior must be tested under conditions of extinction. It is unclear how effectively this procedure can be used with human subjects, who are more likely to notice that they are no longer being rewarded and change their behavior strategically (though some studies with humans have been published; Valentin et al., 2007). Second, it is unclear how the shift to reinforcer value independence corresponds to other meaningful transitions in the development of expertise, such as reaching asymptotic behavioral performance, or the emergence of dual task independence (Ashby et al., 2010; see also Figure 3).

CONCLUSION

As surveyed above, no single defining feature completely captures all the commonly-held beliefs about habit learning. Furthermore, the combination of these features are not always compatible. For example, the criterion of reinforcer devaluation and dual task independence each imply that learning should be considered habitual at a different point in training. We draw three main conclusions from our examination of habit learning and the basal ganglia. First, we provide a taxonomy of criteria for habit learning and divide them into two primary classes. Second, we examine patterns within the different corticostriatal loops and argue that the loops differ in the degree to which they meet criteria for habit learning, with the motor loop qualifying on more criteria than the executive loop. Third, we argue that the basal ganglia and corticostriatal systems interact with other neural systems and therefore that habit learning should not be assumed to exclusively require the basal ganglia, and describe some ways that these systems may interact.

The criteria for habit learning discussed above fall into two types. One type are criteria that can apply at any stage of learning, early or late. In particular, the criteria that learning is unconscious and inflexible were traditionally meant to characterize learning at all stages. Another type of criteria is based on the view

that habit learning develops across time and emerges as learning progresses. There have been various behavioral hallmarks of learning that have been proposed. **Figure 3** illustrates these hallmarks and indicates approximate points in time across training that they may be achieved. Broadly, behavioral landmarks can be divided into three subtypes. First, those based on simple analyses of behavior such as accuracy and reaction time, in which learning is defined as habitual when the measure reaches asymptote, or when the task is “overlearned” via continued training past the point of asymptote. Second, those that apply computational modeling techniques to extract latent parameters thought to characterize learning. The most commonly used approach is from reinforcement learning, in which there are two relevant parameters: reward prediction error and value, or reward prediction itself. Learning can be considered habitual when prediction error approaches zero, and reward prediction approaches asymptote. Both simple behavioral and model-based approaches provide potential operational definitions for the criterion of “slow or incremental.” Third, qualitative criteria that are achieved at some point in learning. These include reinforcer devaluation insensitivity, automaticity defined as dual task insensitivity, and automaticity defined as inability to consciously control habitual knowledge. In addition, the field of motor learning suggests an additional possible criterion: the emergence of motor effector specificity. Across training, motor learning begins with relatively abstract representations that are accessible to multiple motor effectors, but learning become specific to the motor effector across training (Abrahamse et al., 2010).

The multiplicity, and at times incommensurability, of the different criteria for habit learning reinforces our belief that the field would benefit by moving towards more precise definitions of the various habit learning features. Formal mathematical or computational models will clarify exactly what is meant by slow and fast, flexible and inflexible learning and will allow for clear testable predictions. Formal models also have the advantage that they provide insight into potential underlying neural mechanisms; for example, reinforcement-learning modeling is particularly useful because it can be related to the firing patterns of dopaminergic neurons and the effects of dopamine on synaptic plasticity in the basal ganglia (Cohen and Frank, 2009; Moustafa and Gluck, 2011).

Another important lesson is that the basal ganglia is not a single unitary structure that is limited to a single cognitive domain. As described above, the basal ganglia and cortex interact in corticostriatal loops that implement different cognitive functions depending on the cortical regions involved. In **Table 1** we summarize evidence for whether each corticostriatal loop meets criteria for being habitual. Broadly, regions participating in the motor loop (putamen and motor cortex) meet most criteria for habit learning, whereas regions participating in the visual loop are not well studied, and regions participating in the executive loop have a mixed pattern of results, meeting criteria for habit learning on some dimensions, but missing it on many more. The results summarized in **Table 1** broadly support arguments made by researchers studying rodents who argue that the putamen (rodent dorsolateral striatum) is the neural substrate for habit learning and that the caudate (dorsomedial striatum) is involved in non-habitual goal-directed learning.

Table 1 | Habit learning criteria within dorsal corticostriatal loops.

Criterion	Executive	Visual	Motor
QUALITATIVE DIFFERENCES			
Inflexible defined as reinforcement based ¹	Mixed	?	Yes
Unconscious ²	Mixed	?	Mixed
Automatic: dual task independent ³	No	?	Yes
Automatic: PDP exclusion intrusions ⁴	No	?	Yes
Reinforcer devaluation ⁵	No	?	Yes
SLOW OR INCREMENTAL: COMPUTATIONAL MEASURES⁶			
Reward prediction error	Strong	Weak	Weak
Value	Weak	Strong	Strong
SLOW OR INCREMENTAL: SIMPLE BEHAVIORAL MEASURES			
Learning rate (slope) ⁷	Strong	Weak	Weak
Learning asymptote	Weak	Strong	Strong
Changes beyond asymptote ⁸	Mixed	?	Yes

¹Daw et al. (2005) and Lopez-Paniagua and Seger (2011).

²Seger et al. (2011) and Pessiglione et al. (2008).

³Poldrack et al. (2005), Foerde et al. (2006), and Waldmann and Ashby (2011).

⁴Destrebecqz et al. (2005).

⁵Balleine et al. (2009) and Yin and Knowlton (2006).

⁶Haruno and Kawato (2006) and Seger et al. (2010).

⁷Brasted and Wise, 2004, Williams and Eskandar (2006), and Seger et al. (2010).

⁸Grol et al. (2006), Helie et al. (2010), and Waldschmidt and Ashby (2011).

Finally, it is important to avoid equating the behaviorally-defined habit learning system with the neurally-defined basal ganglia system. Given the complexity of habit learning, it likely recruits a number of neural systems in healthy, intact organisms. Neuroimaging studies of skill and habit learning tasks typically find learning related plasticity in several neural systems (Poldrack and Gabrieli, 2001; Poldrack et al., 2005). Probably the most studied system is the medial temporal lobe. However, other neural systems such as the cerebellum have an effect on learning and interact with basal ganglia system (Doyon et al., 2009). Exactly how these systems interact during habit learning is an open area of research. One approach is to postulate that habit learning and other systems learn independently and in parallel; the system that ultimately controls behavior is determined by competitive interactions between the systems (Ashby et al., 1998; Poldrack and Packard, 2003; Packard, 2009). Another approach assumes that initial learning is accomplished by a non-habit learning system, but that knowledge is transferred to the habit system across training (Ashby et al., 2010). When the basal ganglia and hippocampus systems are examined, some experimental results find antagonism, some cooperation, and some complete independence (see Seger and Miller, 2010, for a review). Among researchers studying human learning, an emerging view is that the hippocampus is recruited the first time a stimulus is seen in order to set up a memory representation of that stimulus, and that the basal ganglia can then utilize this representation when learning relations between the stimulus and the response (Meeter et al., 2008; Shohamy et al., 2008; Seger et al., 2011). Between the basal ganglia and prefrontal systems, the traditional view that the basal ganglia subserves habit learning led initially to arguments that cortical activity should precede activity in the basal ganglia. However,

more recent theories argue that the basal ganglia are active primarily during learning, and that well established habits are represented cortically (Pasupathy and Miller, 2005; Seger and Cincotta, 2006; Ashby et al., 2007, 2010).

REFERENCES

- Abrahamse, E. L., Jiménez, L., Verwey, W. B., and Clegg, B. A. (2010). Representing serial action and perception. *Psychon. Bull. Rev.* 17, 603–623.
- Alexander, G. E., DeLong, M. R., and Strick, P. L. (1986). Parallel organization of functionally segregated circuits linking basal ganglia and cortex. *Annu. Rev. Neurosci.* 9, 357–381.
- Anderson, J. R. (1982). Acquisition of cognitive skill. *Psychol. Rev.* 89, 369–406.
- Ashby, F. G., Alfonso-Reese, L. A., Turken, A. U., and Waldron, E. M. (1998). A neuropsychological theory of multiple systems in category learning. *Psychol. Rev.* 105, 442–481.
- Ashby, F. G., Ennis, D. M., and Spiering, B. J. (2007). A neurobiological theory of automaticity in perceptual categorization. *Psychol. Rev.* 114, 632–656.
- Ashby, F. G., and Ennis, J. M. (2006). The role of the basal ganglia in category learning. *Psychol. Learn. Mem.* 1–36.
- Ashby, F. G., Turner, B. O., and Horvitz, J. C. (2010). Cortical and basal ganglia contributions to habit learning and automaticity. *Trends Cogn. Sci. (Regul. Ed.)* 14, 191–232.
- Balleine, B. W., Lijeholm, M., and Ostlund, S. B. (2009). The integrative function of the basal ganglia in instrumental conditioning. *Behav. Brain Res.* 199, 43–52.
- Banich, M. T., Mackiewicz, K. L., Depue, B. E., Whitmer, A. J., Miller, G. A., and Heller, W. (2009). Cognitive control mechanisms, emotion and memory: a neural perspective with implications for psychopathology. *Neurosci. Biobehav. Rev.* 33, 613–630.
- Brasted, P. J., and Wise, S. P. (2004). Comparison of learning-related neuronal activity in the dorsal premotor cortex and striatum. *Eur. J. Neurosci.* 19, 721–740.
- Braver, T. S., Paxton, J. L., Locke, H. S., and Barch, D. M. (2009). Flexible neural mechanisms of cognitive control within human prefrontal cortex. *Proc. Natl. Acad. Sci. U.S.A.* 106, 7351–7356.
- Bromberg-Martin, E. S., Matsumoto, M., and Hikosaka, O. (2010). Dopamine in motivational control: rewarding, aversive, and alerting. *Neuron* 68, 815–834.
- Brooks, D. N., and Baddeley, A. D. (1976). What can amnesic patients learn? *Neuropsychologia* 14, 111–122.
- Cohen, M. X., and Frank, M. J. (2009). Neurocomputational models of basal ganglia function in learning, memory and choice. *Behav. Brain Res.* 199, 141–156.
- Cohen, N. J. (1984). “Preserved learning capacity in amnesia: evidence for multiple memory systems,” in *The Neuropsychology of Memory*, eds. N. Butters and L. Squire (New York: Guilford), 83–103.
- Cohen, N. J., and Squire, L. R. (1980). Preserved learning and retention of pattern-analyzing skill in amnesia: dissociation of knowing how and knowing that. *Science* 210, 207–210.
- Corkin, S. (1968). Acquisition of motor skill after bilateral medial temporal-lobe excision. *Neuropsychologia* 6, 255–265.
- Cromer, J. A., Machon, M., and Miller, E. K. (2011). Rapid association learning in the primate prefrontal cortex in the absence of behavioral reversals. *J. Cogn. Neurosci.* 23, 1823–1828.
- Daw, N. D., Niv, Y., and Dayan, P. (2005). Uncertainty-based competition between prefrontal and dorsolateral striatal systems for behavioral control. *Nat. Neurosci.* 8, 1704–1711.
- Delgado, M. R., Miller, M. M., Inati, S., and Phelps, E. A. (2005). An fMRI study of reward-related probability learning. *Neuroimage* 24, 862–873.
- Destrebecqz, A., Peigneux, P., Laureys, S., Degueldre, C., Del Fiore, G., Aerts, J., Luxen, A., Van Der Linden, M., Cleeremans, A., and Maquet, P. (2005). The neural correlates of implicit and explicit sequence learning: interacting networks revealed by the process dissociation procedure. *Learn. Mem.* 12, 480–490.
- Dickinson, A. (1985). Actions and habits: the development of behavioural autonomy. *Philos. Trans. R. Soc. Lond. B Biol. Sci.* 308, 67–78.
- Doyon, J., Bellec, P., Amsel, R., Penhune, V., Monchi, O., Carrier, J., LeHéricy, S., and Benali, H. (2009). Contributions of the basal ganglia and functionally related brain structures to motor learning. *Behav. Brain Res.* 199, 61–75.
- Driscoll, I., and Sutherland, R. J., Prusky, G. T., and Rudy, J. W. (2004). Damage to the hippocampal formation does not disrupt representational flexibility as measured by a novelty transfer test. *Behav. Neurosci.* 118, 1427–1432.
- Eichenbaum, H., and Fortin, N. J. (2009). The neurobiology of memory based predictions. *Philos. Trans. R. Soc. Lond. B Biol. Sci.* 364, 1183–1191.
- Ergorul, C., and Eichenbaum, H. (2006). Essential role of the hippocampal formation in rapid learning of higher-order sequential associations. *J. Neurosci.* 26, 4111–4117.
- Evans, J. S. (2008). Dual-processing accounts of reasoning, judgment, and social cognition. *Annu. Rev. Psychol.* 59, 255–278.
- Foerde, K., Knowlton, B. J., and Poldrack, R. A. (2006). Modulation of competing memory systems by distraction. *Proc. Natl. Acad. Sci. U.S.A.* 103, 11778–11783.
- Frank, M. J. (2005). Dynamic dopamine modulation in the basal ganglia: a neurocomputational account of cognitive deficits in medicated and non-medicated Parkinsonism. *J. Cogn. Neurosci.* 17, 51–72.
- Frank, M. J., Rudy, J. W., and O'Reilly, R. C. (2003). Transitivity, flexibility, conjunctive representations, and the hippocampus. II. A computational analysis. *Hippocampus* 13, 341–354.
- Graf, P., and Schacter, D. L. (1985). Implicit and explicit memory for new associations in normal and amnesic subjects. *J. Exp. Psychol. Learn. Mem. Cogn.* 11, 501–518.
- Graybiel, A. M. (2008). Habits, rituals, and the evaluative brain. *Annu. Rev. Neurosci.* 31, 359–387.
- Greene, A. J., Gross, W. L., Elsinger, C. L., and Rao, S. M. (2007). Hippocampal differentiation without recognition: an fMRI analysis of the contextual cueing task. *Learn. Mem.* 14, 548–553.
- Grol, M. J., de Lange, F. P., Verstraten, F. A., Passingham, R. E., and Toni, I. (2006). Cerebral changes during performance of overlearned arbitrary visuomotor associations. *J. Neurosci.* 26, 117–125.
- Haruno, M., and Kawato, M. (2006). Different neural correlates of reward expectation and reward expectation error in the putamen and caudate nucleus during stimulus-action-reward association learning. *J. Neurophysiol.* 95, 948–959.
- Helie, S., Roeder, J. L., and Ashby, F. G. (2010). Evidence for cortical automaticity in rule-based categorization. *J. Neurosci.* 30, 14225–14234.
- Hirsh, J. (1974). The hippocampus and contextual retrieval of information from memory: a theory. *Behav. Biol.* 12, 421–444.
- Hull, C. L. (1934a). The concept of the habit-family hierarchy and maze learning: part I. *Psychol. Rev.* 41, 33–54.
- Hull, C. L. (1934b). The concept of the habit-family hierarchy and maze learning: part II. *Psychol. Rev.* 41, 134–152.
- Jacoby, L. L. (1991). A process dissociation framework: separating automatic from intentional uses of memory. *J. Mem. Lang.* 30, 513–541.
- James, W. (1890). *Principles of Psychology*. New York: Henry Holt.
- Keane, M. M., Gabrieli, J. D., Fennema, A. C., Growdon, J. H., and Corkin, S. (1991). Evidence for a dissociation between perceptual and conceptual priming in Alzheimer's disease. *Behav. Neurosci.* 105, 326–342.
- Knowlton, B. J., Ramus, S., and Squire, L. R. (1992). Intact artificial grammar learning in amnesia: dissociation of classification learning and explicit memory for specific instances. *Psychol. Sci.* 3, 172–179.
- Knowlton, B. J., and Squire, L. R. (1993). The learning of categories: parallel brain systems for item memory and category knowledge. *Science* 262, 1747–1749.
- Lashley, K. S. (1930). Basic neural mechanisms in behavior. *Psychol. Rev.* 37, 1–24.
- Lashley, K. S. (1950). “In search of the engram,” in *Society of Experimental Biology Symposium*, Vol. 4 (Cambridge: Cambridge University Press), 454–480.
- Lavie, N. (2010). Attention, distraction, and cognitive control under load. *Curr. Dir. Psychol. Sci.* 19, 143–148.
- Linden, D. E. (2007). The working memory networks of the human brain. *Neuroscientist* 13, 257–267.
- Lopez-Panigagua, D., and Seger, C. A. (2011). Interactions within and between corticostriatal loops during component processes of category learning. *J. Cogn. Neurosci.* 23, 3068–3083.
- Meeter, M., Radics, G., Myers, C. E., Gluck, M. A., and Hopkins, R. O. (2008). Probabilistic categorization: how do normal participants and amnesic patients do it? *Neurosci. Biobehav. Rev.* 32, 237–248.
- Milner, B. (1962). “Les troubles de la mémoire accompagnant des lésions hippocampiques bilatérales,” in *Physiologie de l'Hippocampe* (Paris: Centre National de la Recherche Scientifique), 257–272.
- Miskin, M., Malamut, B., and Bachevalier, J. (1984). “Memories and habits: two neural systems,” in *Neurobiology of Learning and Memory*, eds. G. Lynch, J. L. McGaugh, and N. M. Weinberger (New York: Guilford), 65–67.
- Moustafa, A. A., and Gluck, M. A. (2011). A neurocomputational model of dopamine and prefrontal-striatal interactions during multicue category

- learning by Parkinson patients. *J. Cogn. Neurosci.* 23, 151–167.
- Moustafa, A. A., Keri, S., Herzallah, M. M., Myers, C. E., and Gluck, M. A. (2010). A neural model of hippocampal-striatal interactions in associative learning and transfer generalization in various neurological and psychiatric patients. *Brain Cogn.* 74, 132–144.
- Myers, C. E., Shohamy, D., Gluck, M. A., Grossman, S., Kluger, A., Ferris, S., Golomb, J., Schnirman, G., and Schwartz, R. (2003). Dissociating hippocampal versus basal ganglia contributions to learning and transfer. *J. Cogn. Neurosci.* 15, 185–193.
- Nakano, K., Kayahara, T., Tsutsumi, T., and Ushiro, H. (2000). Neural circuits and functional organization of the striatum. *J. Neurol.* 247, V1–V15.
- Nissen, M. J., and Bullemer, P. (1987). Attentional requirements of learning: evidence from performance measures. *Cogn. Psychol.* 19, 1–32.
- O'Reilly, R. C., Herd, S. A., and Pauli, W. M. (2010). Computational models of cognitive control. *Curr. Opin. Neurobiol.* 20, 257–261.
- Packard, M. G. (2009). Exhumed from thought: basal ganglia and response learning in the plus-maze. *Behav. Brain Res.* 199, 24–31.
- Pasupathy, A., and Miller, E. K. (2005). Different time courses of learning-related activity in the prefrontal cortex and striatum. *Nature* 433, 873–876.
- Pawlak, V., and Kerr, J. N. (2008). Dopamine receptor activation is required for corticostriatal spike-timing-dependent plasticity. *J. Neurosci.* 28, 2435–2446.
- Pessiglione, M., Petrovic, P., Daunizeau, J., Palminteri, S., Dolan, R. J., and Frith, C. D. (2008). Subliminal instrumental conditioning demonstrated in the human brain. *Neuron* 59, 561–567.
- Poldrack, R. A., and Gabrieli, J. D. (2001). Characterizing the neural mechanisms of skill learning and repetition priming: evidence from mirror reading. *Brain* 124, 67–82.
- Poldrack, R. A., and Packard, M. G. (2003). Competition among multiple memory systems: converging evidence from animal and human brain studies. *Neuropsychologia* 41, 245–251.
- Poldrack, R. A., Sabb, F. W., Foerde, K., Tom, S. M., Asarnow, R. F., Bookheimer, S. Y., and Knowlton, B. J. (2005). The neural correlates of motor skill automaticity. *J. Neurosci.* 25, 5356–5364.
- Reber, A. S. (1967). Implicit learning of artificial grammars. *J. Mem. Lang.* 6, 855–863.
- Redgrave, P., Rodriguez, M., Smith, Y., Rodriguez-Oroz, M. C., Lehericy, S., Bergman, H., Agid, Y., DeLong, M. R., and Obeso, J. A. (2010). Goal-directed and habitual control in the basal ganglia: implications for Parkinson's disease. *Nat. Rev. Neurosci.* 11, 760–772.
- Schacter, D. L. (1987). Implicit memory: history and current status. *J. Exp. Psychol. Learn. Mem. Cogn.* 13, 501–518.
- Schendan, H. E., Searl, M. M., Melrose, R. J., and Stern, C. E. (2003). An fMRI study of the role of the medial temporal lobe in implicit and explicit sequence learning. *Neuron* 37, 1013–1025.
- Schultz, W. (2002). Getting formal with dopamine and reward. *Neuron* 36, 241–263.
- Seiger, C. A. (1994). Implicit learning. *Psychol. Bull.* 115, 163–196.
- Seiger, C. A. (2008). How do the basal ganglia contribute to categorization? Their roles in generalization, response selection, and learning via feedback. *Neurosci. Biobehav. Rev.* 32, 265–278.
- Seiger, C. A. (2009). “The involvement of corticostriatal loops in learning across tasks, species, and methodologies,” in *The Basal Ganglia IX*, eds H. J. Groenewegen, P. Voorn, H. W. Berendse, A. B. Mulder, and A. R. Cools (New York: Springer-Verlag), 25–39.
- Seiger, C. A., and Cincotta, C. M. (2005). The roles of the caudate nucleus in human classification learning. *J. Neurosci.* 25, 2941–2951.
- Seiger, C. A., and Cincotta, C. M. (2006). Dynamics of frontal, striatal, and hippocampal systems during rule learning. *Cereb. Cortex* 16, 1546–1555.
- Seiger, C. A., Dennison, C. S., Lopez-Paniagua, D., Peterson, E. J., and Roark, A. A. (2011). Dissociating hippocampal and basal ganglia contributions to category learning using stimulus novelty and subjective judgments. *Neuroimage* 55, 1739–1753.
- Seiger, C. A., and Miller, E. K. (2010). Category learning in the brain. *Annu. Rev. Neurosci.* 33, 203–219.
- Seiger, C. A., Peterson, E. J., Cincotta, C. M., Lopez-Paniagua, D., and Anderson, C. W. (2010). Dissociating the contributions of independent corticostriatal systems to visual categorization learning through the use of reinforcement learning modeling and Granger causality modeling. *Neuroimage* 50, 644–656.
- Seth, A. K., Dienes, Z., Cleeremans, A., Overgaard, M., and Pessoa, L. (2008). Measuring consciousness: relating behavioural and neurophysiological approaches. *Trends Cogn. Sci. (Regul. Ed.)* 12, 314–321.
- Shallice, T. (1982). Specific impairments of planning. *Philos. Trans. R. Soc. Lond. B Biol. Sci.* 298, 199–209.
- Shiffrin, W., and Schneider, R. M. (1977). Controlled and automatic human information processing: 1. Detection, search, and attention. *Psychol. Rev.* 84, 1–66.
- Shohamy, D., and Adcock, R. A. (2010). Dopamine and adaptive memory. *Trends Cogn. Sci. (Regul. Ed.)* 14, 464–472.
- Shohamy, D., Myers, C. E., Geghman, K. D., Sage, J., and Gluck, M. A. (2006). L-dopa impairs learning, but spares generalization, in Parkinson's disease. *Neuropsychologia* 44, 774–784.
- Shohamy, D., Myers, C. E., Kalanithi, J., and Gluck, M. A. (2008). Basal ganglia and dopamine contributions to probabilistic category learning. *Neurosci. Biobehav. Rev.* 32, 219–236.
- Squire, L. R., and Zola-Morgan, S. (1988). Memory: brain systems and behavior. *Trends Neurosci.* 11, 170–175.
- Squire, L. R., and Zola-Morgan, S. (1991). The medial temporal lobe memory system. *Science* 253, 1380–1386.
- Stocco, A., Lebiere, C., and Anderson, J. R. (2010). Conditional routing of information to the cortex: a model of the basal ganglia's role in cognitive coordination. *Psychol. Rev.* 117, 541–574.
- Valentin, V. V., Dickinson, A., and O'Doherty, J. P. (2007). Determining the neural substrates of goal-directed learning in the human brain. *J. Neurosci.* 27, 4019–4026.
- Waldschmidt, J. G., and Ashby, F. G. (2011). Cortical and striatal contributions to automaticity in information-integration categorization. *Neuroimage* 56, 1791–1802.
- Wilkinson, L., Khan, Z., and Jahanshahi, M. (2009). The role of the basal ganglia and its cortical connections in sequence learning: evidence from implicit and explicit sequence learning in Parkinson's disease. *Neuropsychologia* 47, 2564–2573.
- Williams, Z. M., and Eskandar, E. N. (2006). Selective enhancement of associative learning by microstimulation of the anterior caudate. *Nat. Neurosci.* 9, 562–568.
- Winograd, T. (1972). Understanding natural language. *Cogn. Psychol.* 3, 1–191.
- Yin, H. H., and Knowlton, B. J. (2006). The role of the basal ganglia in habit formation. *Nat. Rev. Neurosci.* 7, 464–476.
- Zeithamova, D., and Maddox, W. T. (2006). Dual-task interference in perceptual category learning. *Mem. Cognit.* 34, 387.

Conflict of Interest Statement: The authors declare that the research was conducted in the absence of any commercial or financial relationships that could be construed as a potential conflict of interest.

Received: 01 February 2011; paper pending published: 27 March 2011; accepted: 01 August 2011; published online: 30 August 2011.
Citation: Seiger CA and Spiering BJ (2011) A critical review of habit learning and the basal ganglia. *Front. Syst. Neurosci.* 5:66. doi: 10.3389/fnsys.2011.00066
Copyright © 2011 Seiger and Spiering. This is an open-access article subject to a non-exclusive license between the authors and Frontiers Media SA, which permits use, distribution and reproduction in other forums, provided the original authors and source are credited and other Frontiers conditions are complied with.



Basal ganglia preferentially encode context dependent choice in a two-armed bandit task

André Garenne^{1,2†}, Benjamin Pasquereau^{1,2†}, Martin Guthrie^{1,2}, Bernard Bioulac^{1,2,3} and Thomas Boraud^{1,2*}

¹ Université de Bordeaux, UMR 5293, Institut des Maladies Neurodégénératives, Bordeaux, France

² CNRS, UMR 5293, Institut des Maladies Neurodégénératives, Bordeaux, France

³ Centre Hospitalier Universitaire de Bordeaux, Bordeaux Cedex, France

Edited by:

James M. Tepper, Rutgers, The State University of New Jersey, USA

Reviewed by:

Izhar Bar-Gad, Bar-Ilan University, Israel
Brian Hyland, University of Otago, New Zealand

*Correspondence:

Thomas Boraud, UMR Centre National de la Recherche Scientifique 5293, 146, rue Leo Saignat, 33 076 Bordeaux Cedex, France.
e-mail: tboraud@u-bordeaux2.fr

[†]Both authors had equal contribution to this work.

Decision is a self-generated phenomenon, which is hard to track with standard time averaging methods, such as peri-event time histograms (PETHs), used in behaving animals. Reasons include variability in duration of events within a task and uneven reaction time of animals. We have developed a temporal normalization method where PETHs were juxtaposed all along task events and compared between neurons. We applied this method to neurons recorded in striatum and GPi of behaving monkeys involved in a choice task. We observed a significantly higher homogeneity of neuron activity profile distributions in GPi than in striatum. Focusing on the period of the task during which the decision was taken, we showed that approximately one quarter of all recorded neurons exhibited tuning functions. These so-called coding neurons had average firing rates that varied as a function of the value of both presented cues, a combination here referred to as context, and/or value of the chosen cue. The tuning functions were used to build a simple maximum likelihood estimation model, which revealed that (i) GPi neurons are more efficient at encoding both choice and context than striatal neurons and (ii) context prediction rates were higher than those for choice. Furthermore, the mutual information between choice or context values and decision period average firing rate was higher in GPi than in striatum. Considered together, these results suggest a convergence process of the global information flow between striatum and GPi, preferentially involving context encoding, which could be used by the network to perform decision-making.

Keywords: decision making, electrophysiology, striatum, globus pallidus, primate

INTRODUCTION

In a visually guided motor task, decision-making is a distributed neural process that involves the basal ganglia (BG) interacting with the frontal and prefrontal cortical areas as well as with the dopaminergic system (Opris and Bruce, 2005; Schultz, 2006; Daw, 2007; Samejima and Doya, 2007; Kable and Glimcher, 2009). In a recent electrophysiological study in behaving monkeys, using a multiple choice task, we showed that the encoding of the movement direction by the neurons of the striatum (the main input of the BG) and the internal globus pallidus (GPi, the main output of the BG) is modulated by the incentive value of the action (Pasquereau et al., 2007). This could provide a mechanism by which motor program selection could be learned under dopamine control (Samejima and Doya, 2007).

However, the selection process, is only partially accessible using classical electrophysiological analysis methods, such as PETHs. This is because, even when a cue is presented at a known time and the time of the locomotor action to implement the decision is known, the actual moment of decision-making cannot be observed and so its temporal relationship to the cue and other events cannot be precisely known. Moreover, experimental protocols for decision-making assessments (including those used in our own studies) assign a randomly variable duration between task events in order to decorrelate all the steps from one another. This means that the time between events varies for each trial. This,

along with the fact that cognitive processing time varies from trial to trial for each animal, prevents the direct comparison of the time course of the neuronal activity profiles. Despite the intrinsic limitation that PETH computation does not by itself provide a framework for statistical inference (Czanner et al., 2008), it remains a widely used tool that provides meaningful insights and whose efficiency has been improved (Endres and Oram, 2010). To solve this conundrum, we developed a simple method to normalize time durations in each trial and thus to build a normalized inter-event time histogram (NIETH) for individual neurons. This normalization method was applied to the whole trial duration because BG activity is notoriously variable and may have dynamic encoding capacities (Arkadir et al., 2004). Using this method, we analyzed data previously recorded in the GPi and the striatum of two monkeys during a reward probability-based, free-choice motor task (Figure 1, see Pasquereau et al., 2007 for details). We then focused our analysis on a possible correlation between the neuronal activity in striatum and GPi and the animal behavior during the crucial period between the appearance of the cue and the go signal, the decision period (DP). To link neuronal activity to behavior, we investigated neuronal coding of behavioral events as a possible basis for a computational predictive model and their mutual information to quantify their interdependence. We thus addressed the questions of how and where information flows were processed in the BG system.

MATERIALS AND METHODS

The reader is invited to refer to the first paper dealing with these data (Pasquereau et al., 2007) for an exhaustive description of materials and methods involved with the data acquisition. Here we provide a summary including only the details necessary to explain the additional analyses and results.

ANIMAL TRAINING AND SURGERY

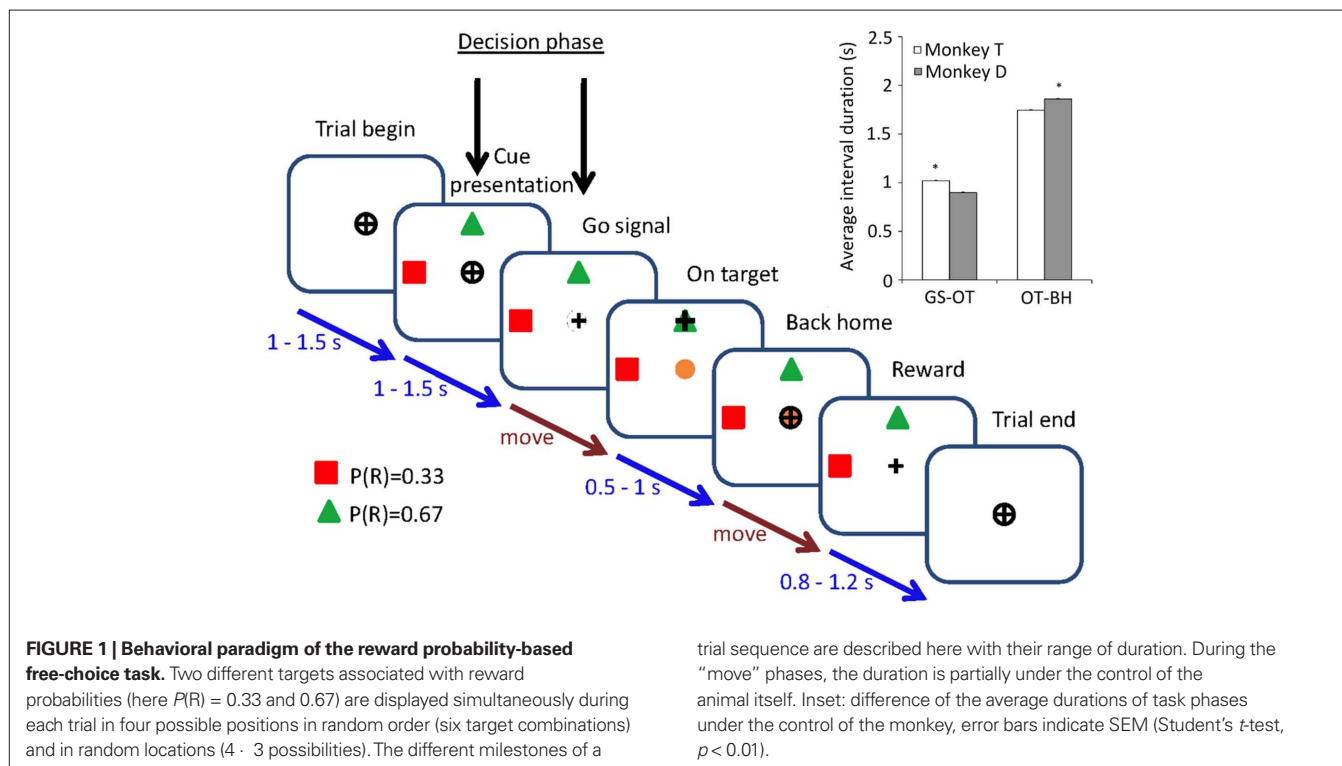
The study was conducted on two female rhesus monkeys (*Macaca mulatta*, weighing 5.6 and 4 kg). The primates were kept under water restriction to increase their motivation during the task training. A veterinarian skilled in the healthcare and maintenance of non-human primates supervised all aspects of animal care. Surgical and experimental procedures were performed in accordance with the Council Directive of 24 November 1986 (86/609/EEC) of the European Community and the National Institute of Health Guide for the Care and Use of Laboratory Animals. In the task, monkeys were trained to move a custom-made manipulandum in a horizontal plane with their right hand. The manipulandum moved a cursor on a computer screen placed 50 cm in front of the monkey. In each trial of a session, two different cue targets (randomly chosen from a set of four targets, each with a different reward probability ($P(R) = [0, 0.33, 0.67, \text{and } 1]$)) were displayed simultaneously on the screen. Each cue appeared randomly in one of four possible directions ($0^\circ, 90^\circ, 180^\circ, 270^\circ$). In order to induce a situation in which there was always an optimal choice, a single trial could not include two identical cues or two targets in the same location. After a random period (1–1.5 s), the “go” signal was given and the monkey had to initiate a movement toward one of the two targets. Once this position was reached the animal had to hold the cursor on the target for a random period (0.5–1 s) after which the cursor had

to be moved back to the central position. The reward was then delivered (fruit juice) according to the probability associated with the chosen target. For each successful trial, if the monkey chose the target associated with the highest probability of receiving a reward, their choice was defined as optimal. If not, they would still receive reward with a probability equal to that for the chosen target. A recording chamber was then implanted on the skull of each animal. The surgical procedure for attaching the recording chamber has been extensively described in previous publications (Bezard et al., 2001; Boraud et al., 2001).

For purposes of analysis of the relationship between external sensory cues and the neuronal firing activity, we consider that the context in which the animal was making the decision was the combination of the two targets that were visible during a trial. Thus, with two targets selected from four, there are six possible combinations and therefore six distinct contexts within which the animal makes a decision on which target to choose. Due to the animals being over-trained, they never choose a target associated with a 0 reward probability. Consequently, they are considered to have only three possible choices associated with the remaining 0.33, 0.67, and 1 reward probabilities.

RECORDING AND DATA ACQUISITION

Neuronal recordings were performed in the dorsolateral striatum and the GPi. Data acquisition, spike sorting, and storage are described elsewhere (Pasquereau et al., 2007). The following behavioral events were recorded and stored simultaneously with the electrophysiological recordings: trial begin (TB), cue presentation (CP), go signal (GS), on target (OT), back home (BH), reward/no reward (RW/NRW), and finally trial end (TE). This is described in Figure 1.



DATA ANALYSIS

The analyses were performed with custom-made Matlab (MathWorks, Natick, MA, USA) and NeuroExplorer tools and scripts (Nex Technologies, Littleton, MA, USA), and C# libraries (Microsoft, Seattle, WA, USA).

NIETH ANALYSIS

NIETHS EXTRACTION AND NORMALIZATION

To have an overall view of the neuronal dynamics associated with the choice task and to compare both striatal and pallidal activity profiles, we investigated the temporal outline of NIETHs across all the steps of the task. Therefore, we have implemented an algorithm that can automatically identify event sequences of interest within the NIETHs and extract the spike trains related to these events. In a first step, the algorithm, extracted all the recorded sequences where the monkey completed every event through the course of the trial (here the event sequence: TB–CP–GS–OT–BH–RW–TE) and discarded sequences where any event was not completed (e.g., where the monkey failed to return the cursor to home). Because recording continues until and after reward delivery, we were able to note that the firing profile in cases where reward was obtained and those where no reward was obtained were different. Therefore, all trials in which no reward was gained were also discarded. In summary, in the presented results only successfully completed trials where a reward was obtained are shown in order to minimize variation in neuronal activity due to inter-trial variation in behavioral profile. The algorithm then computes the NIETHs using each occurrence of the complete event sequence. Duration of the inter-event intervals (IEI) is either random or behaviorally dependent as shown on **Figure 1** and this adds variability to the NIETH length and thus makes inter-neuron activity profile comparisons difficult. In a second step, an additional procedure of time normalization of the NIETH is implemented to solve this problem. The first IEI between TB and CP is always split into the same number of time bins in every trial and for every neuron. This means that the duration of a bin in one trial is not equal to that in another trial but that the number of bins for a given TB–CP interval is the same for every trial. In our study, the first IEI (TB–CP) was always split into 100 bins in order to obtain a bin size close to 10 ms (Zhang and Reid, 2005). Because the duration of this event can vary from 1 to 1.5 s, the length of a bin can thus vary from 10 to 15 ms, but the average length of bin duration can be calculated. This average bin duration is then used for all subsequent IEIs (CP–GS, GS–OT). Because the average duration of each subsequent event differs, the number of bins allocated for each event also changes. Thus, for example if the average duration of the TB–CP event was 1.2 s and for the CP–GS event was 1.8 s, the CP–GS event would be divided into $100 \cdot 1.8/1.2 = 150$ bins. This rescaling prevents time normalization biases by maintaining IEI durations close to the original. Due to the similar IEI average durations between different neurons (most of the random durations are generated by the software itself), this normalization technique finally allows NIETHs alignment in time and thus their comparison. At the same time, amplitude normalization (Burkhardt and Whittle, 1973; Gage et al., 2010) is applied to the NIETH based on the maximum number of spikes observed at any point in time over the

whole time course of a trial. This amplitude normalization allows averaging of the profile of activation of many neurons across an event, whatever the maximal firing rate of individual neurons, by considering only their deviation from their baseline level. Without the amplitude normalization, neurons with a high maximal firing rate would have a disproportionate effect on the profile and, assuming that the information within the system is transmitted by population encoding, would distort the representation of the information across the course of an event.

Monkey data have been separately processed and not pooled because of a non-negligible level of variability related to their individual behavior. Indeed, the analysis of the distribution of the two inter-events intervals which are under the control of the animal (GS–OT and OT–BH) exhibited significant differences as shown in **Figure 1** inset. Using this method, we have performed new analyses of the data of a previous publication by our team (Pasquereau et al., 2007).

NIETHS STUDY AND COMPARISON

We compared NIETH distributions between striatum and GPi. Our first goal here was to find whether salient activity profile features emerged in the neuronal activity of the two structures. To achieve this, two complementary approaches were explored, applied separately to each monkey. The first approach consisted in computing correlation coefficient matrices between every neuron NIETH. The second relied on the computation of NIETH entropies to estimate the variability within their population. The Shannon (1948) entropy computation (and its derived methods) is now often used as a non-linear analysis tool providing information on neuronal activity temporal organization (Borst and Theunissen, 1999; Lim et al., 2010) or complexity characterization (Haslinger et al., 2010). Here, we used it to quantify the activity variability throughout the task in parallel for every neuron. If the activity profiles are similar, successive entropy values will be low and vice versa. Both approaches were performed on all the NIETHs. The Shannon entropy H (here in bits) of a discrete variable X with n possible values is given by:

$$H(X) = \sum_{i=1}^n p(x_i) I(x_i) = - \sum_{i=1}^n p(x_i) \log_2(p(x_i))$$

where $p(x_i)$ is the probability associated with (x_i) . Due to the high dimensionality of NIETHs, a preliminary discretization procedure is applied before entropy calculation. NIETH amplitudes vary between 0 and 1 and we arbitrarily chose to linearly distribute their values into a 10 interval alphabet ranging from 1 to 10 (i.e., a 0.527 or a 0.596 amplitude value will provide a 5 and a 0.758 will provide a 7). These computations were performed with a dedicated Matlab toolbox (Peng et al., 2005) which was also used for further mutual information calculations. These analyses were performed separately on the two monkeys and on striatum and GPi.

EXTRACTION OF “CODING NEURONS”

The monkey's decision is made between the CP and the movement initiation triggered by the GS. This period of time includes the decision process phase itself, but it may also include an amount of time during which the monkey has already made its decision and

just waits for the GS. Because it is not easy to differentiate between the decision period and the waiting period (Leblois et al., 2006a), we computed averaged firing rates for each neuron during this decision period (DPAFR) for each different context presented to the monkey and for each of its actual choices. We first extracted the neurons for which significant variations in DPAFR were related to any of the six different context values or to any of the three choice reward probabilities by applying a one-way ANOVA. We thus designated any neuron that had a significant variation in DPAFR to at least one context or one choice as a coding neuron. When the ANOVA was positive we applied *post hoc* methods based on the Tukey's least significant difference procedure. We thus obtained tuning functions for each neuron which associated preferential coding context or choice values with a peak in the firing rate. These tuning functions were then applied to basic modeling studies. These analyses were performed with the Matlab Statistical toolbox and applied separately both to the two monkeys and to striatum and GPi.

FIRING RATE CARRIED INFORMATION ANALYSIS

We computed mutual information between the DPAFRs and the context value, for coding neurons. The mutual information I between two discrete random variables X and Y is expressed in bits and is given by:

$$I(X, Y) = \sum_{y \in Y} \sum_{x \in X} p(x, y) \cdot \log \left(\frac{p(x, y)}{p(x) \cdot p(y)} \right)$$

where $p(x, y)$ is the joint probability distribution function of X and Y , $p(x)$, and $p(y)$ are the marginal probability distribution functions of X and Y respectively. The results were used to investigate the respective involvements of the GPi and of the striatum in the processing of information of choice and context encoding in BG.

TUNING FUNCTION MODEL PREDICTION

The tuning functions derived in the "coding neurons" section were then used as a simple reverse model to assess how good the tuning function was at predicting a direction given the average firing rate in the decision period as an input. For every coding neuron in both structures, the tuning function exhibited a preferential context/choice value encoding (e.g., one neuron can have its highest DPAFR when the animal is presented with a given context or choice number). For each previously extracted coding neuron, our predictive model thus associated the six different reference DPAFRs of the tuning function with each of the six different context values (and respectively the three DPAFRs associated with each of the three choice values). The model was then used as follows: DPAFRs were computed for each trial of a given coding neuron. For every trial, the experimental DPAFR was applied as an input to the tuning function (core of the model) which returned the most likely context or choice theoretical value (i.e., that for which reference DPAFR was closest to the experimental DPAFR). When this theoretical value was the same as the actual, the trial model prediction was considered as successful. Success rates were then computed for context and choice encoding in both monkeys and in both striatum and GPi.

The prediction quality of the model was then compared to random choices based on context and choice chance based rates (respectively 16.67 and 33.33% to obtain the actual value with a random draw). The significance of the model retrieval rates was compared to the chance based rates using a Kolmogorov–Smirnov test. A Wilcoxon rank signed test was then applied on success rates to compare the power of the model concerning context and choice prediction in order to conclude which was most efficiently encoded in the recorded structures.

RESULTS

NIETHS EXTRACTION

The software successfully extracted and normalized, both in time and amplitude, the global NIETHs from all recorded neurons and according to the previously defined sequence of events. The present study is based on 111 striatal cells (53 in monkey T and 58 in monkey D) and 107 pallidal cells (51 in monkey T and 56 in monkey D). The normalized NIETH distributions among striatal and pallidal neurons in both monkeys are presented in **Figure 2**. Several automatic clustering of neuronal subpopulations algorithms, based on principal component analysis of the NIETHs profiles, have been tested here without success. This failure is consistent with the time axis position distribution of the NIETH amplitude peak, as shown in **Figure 2**. This position is here used as a NIETH sorting parameter and it clearly appears as continuously distributed from one neuron to another all along the time axis.

THE POPULATION ACTIVITY SYNCHRONIZATION DIFFERS BETWEEN STRIATAL AND PALLIDAL NEURONS

A two-way ANOVA was applied to the average correlation coefficient (ACC) values to investigate possible monkey and structure combination (GPi–striatum, GPi–GPi, and striatum–striatum) effects. The resulting p -values were significant ($p < 0.01$) and provide evidence for interactions between monkey, structure combination and ACC. NIETH correlation coefficient matrices were then processed and compared separately for both monkeys and for striatal and GPi neurons. As was expected after a visual control of **Figure 2**, differences were revealed between the two regions regarding the neuronal dynamics, as shown in **Figures 3A,B**. The NIETHs correlation coefficient values were higher between GPi neurons than striatum neurons in both monkeys. This demonstrates that there is less dynamic variability between GPi neurons and this was confirmed by the estimate of their ACC values according to structure. As shown in **Figure 3C**, these latter differed significantly between the two regions. This emphasizes a higher temporal synchronization of GPi neuronal spike trains compared to striatum. Moreover, the lowest absolute value of correlation coefficient occurred in both monkeys when computing the ACC value between GPi and striatum, which is another argument in favor of a possible functional dissociation between the two structures. These results were similar in both monkeys.

The measure of the Shannon entropy between striatum and GPi added consistent results to this first outcome (respectively 3.11 and 1.25 for monkey T and 2.79 and 1.19 for monkey D). Indeed, Shannon entropy can be considered as a measure of the variability

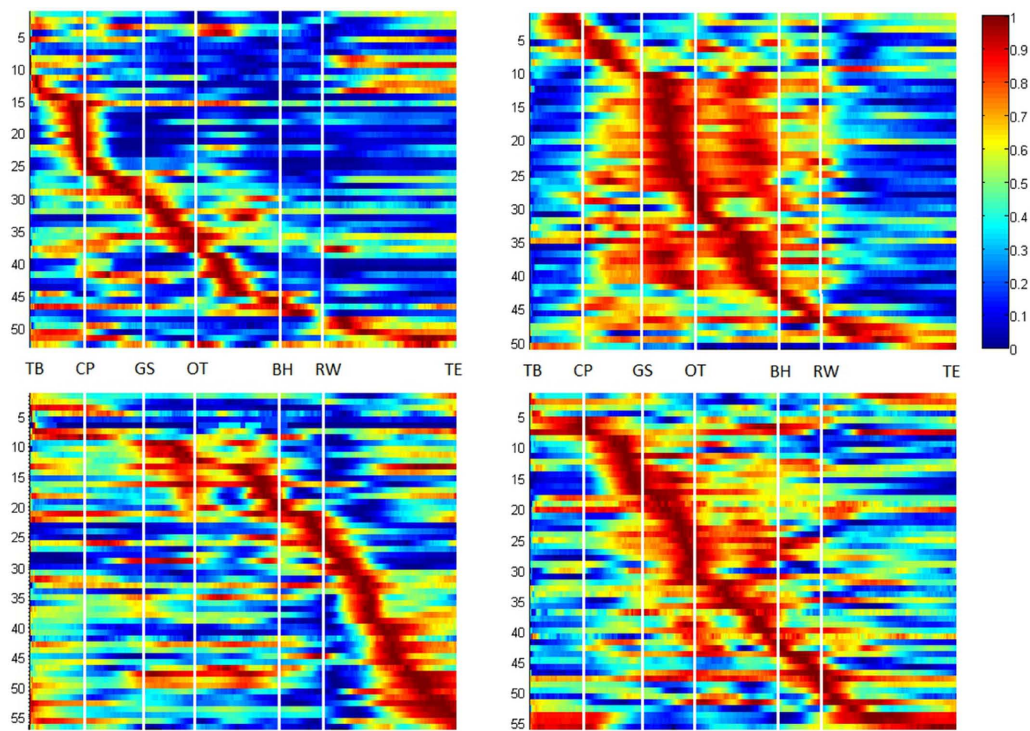


FIGURE 2 | NIETH plots from the striatum (left) and GPi (right) of monkey T (top) and monkey D (bottom), aligned on each event. The neurons were sorted using the curve peak time value. The color bar indicates the normalized amplitude value for each neuron.

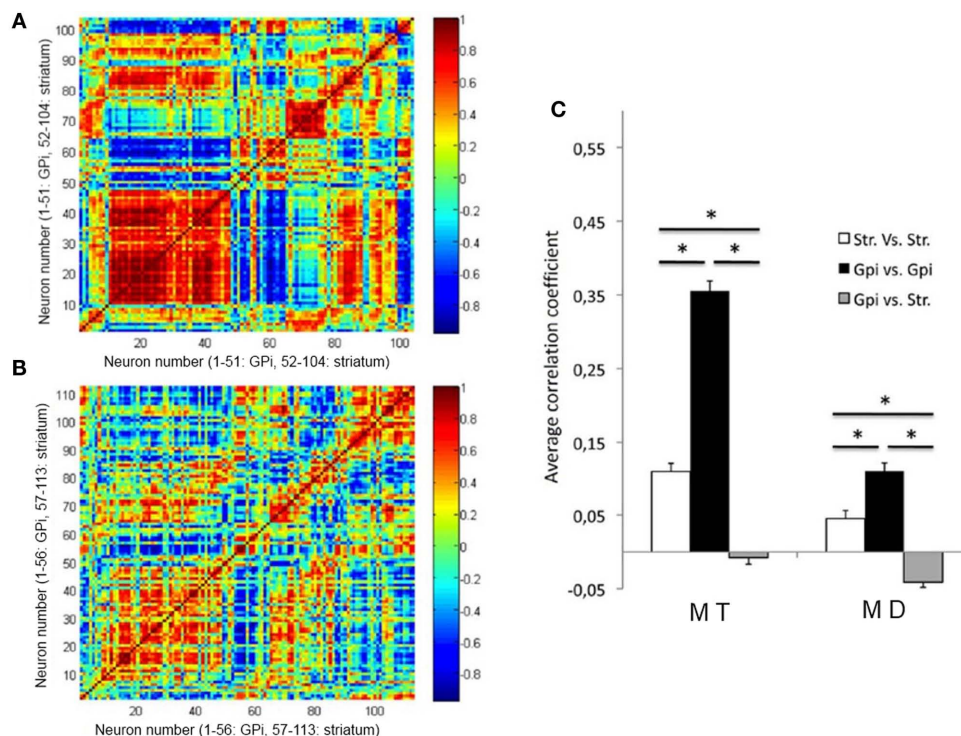
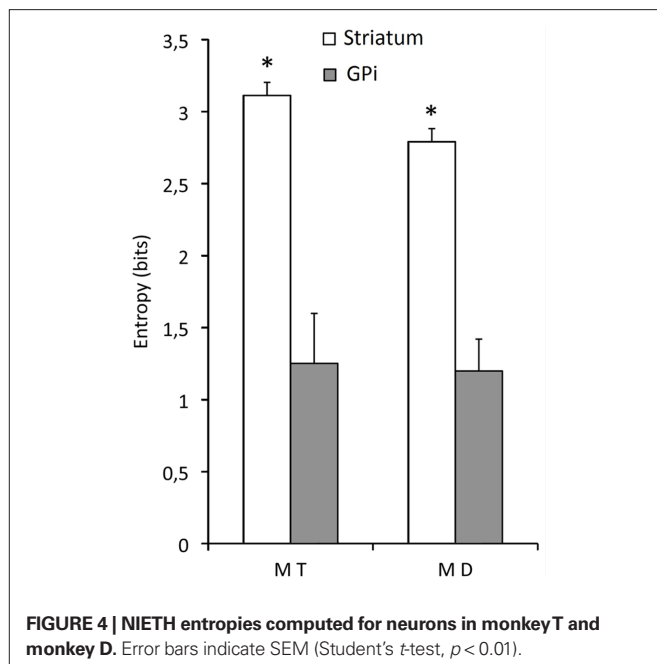


FIGURE 3 | Cross-correlation matrices of all the neuron NIETHs for monkey T (A) and monkey D (B). (C) Histograms of average correlation coefficient values of the neuron NIETHs. Color bar: correlation coefficient value, error bars indicate SEM (one-way ANOVA, $p < 0.01$, *post hoc*: Tukey's least significant difference procedure).



of the signals emitted by a source (here the NIETHs shapes) and we noticed that, in both monkeys, the value was lower in GPi than in striatum, as shown in **Figure 4**.

These two results suggest that, considering a given behavioral event expected value such as a choice or a context encoding, the information carried by striatum seems condensed in GPi.

CODING NEURONS ACTIVITY ANALYSIS

Only neurons that showed an average DPAFR that was dependent on the context or choice were used for analysis of the coding (one-way ANOVA, $p < 0.01$). For monkey T, 33.96% of the striatal ($n = 53$) and 21.57% of the GPi neurons ($n = 51$) and for monkey D, respectively 17.24% ($n = 58$) and 14.29% ($n = 56$) displayed such a property (**Figure 5A**). Tuning function curves were extracted for each coding neuron by computing the DPAFR for every context and choice for that neuron. Some tuning function samples are shown here that exhibit either preferential context (**Figure 5B**) or choice coding values (**Figure 5C**).

Mutual information between DPAFRs and both context and choice values were computed and the results expressed in bits. The resulting amount of mutual information carried by striatal neurons was less than that carried by GPi neurons both in context (0.20 vs. 0.73 for monkey T and 0.28 vs. 0.72 for monkey D) and in choice encoding (0.11 vs. 0.29 for monkey T and 0.10 vs. 0.34 for monkey D, Mann–Whitney test, $p < 0.01$) as shown in **Figures 6A,B**. GPi neurons appear as more reliable encoders because the DPAFRs of GPi neurons yielded more information on both the context and the choice values than those of striatal neurons in both monkeys. This implies that the context and/or the choice information are refined between the striatum and the pallidal processing stages and therefore suggests an information convergence mechanism from one structure to another in the sense of a dimensionality reduction (Bar-Gad et al., 2003). On average, one GPi neuron provides as much information as 2.9 striatum neurons in context encoding

(and respectively 2.5 in choice encoding). In other words, sampling of fewer neurons in GPi is required to obtain a similar amount of information about both context and choice.

PERFORMANCE OF REVERSE TUNING CURVE MODEL

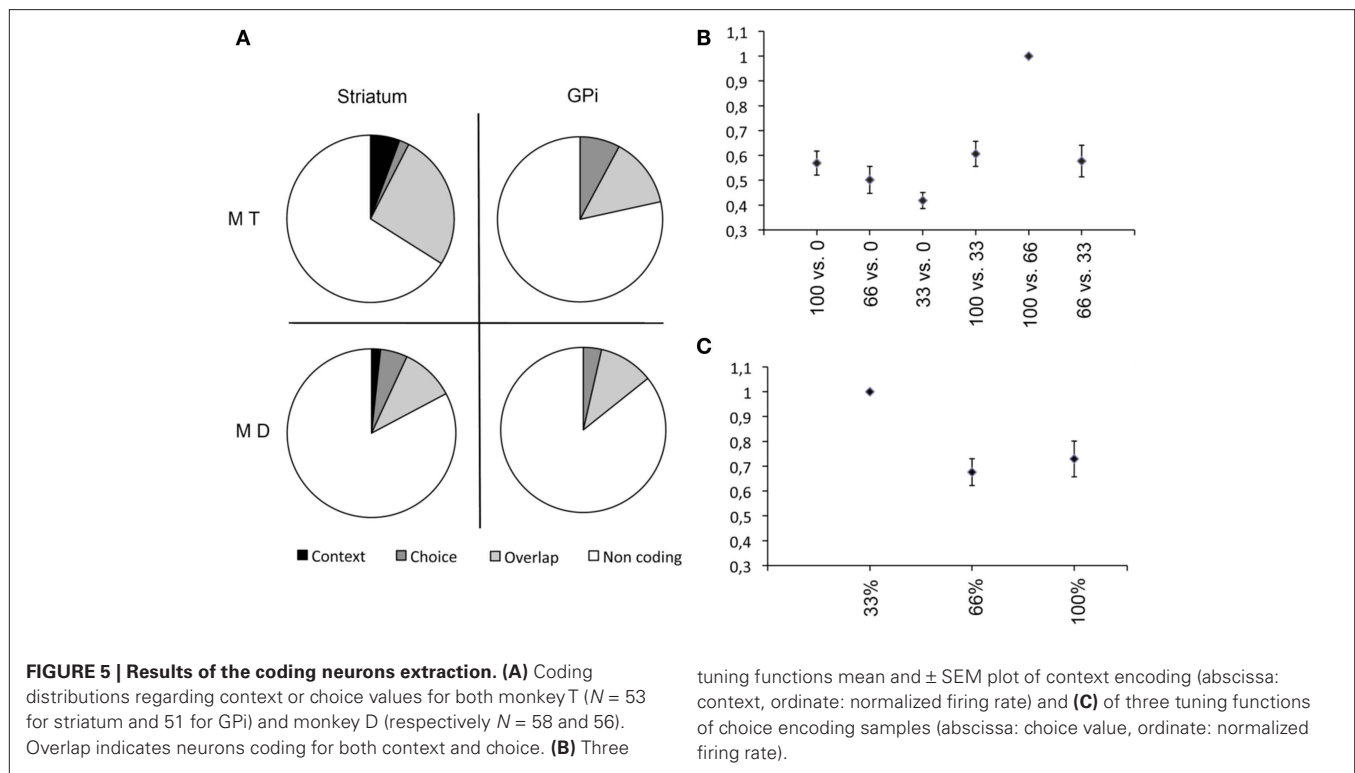
The previously constructed tuning curves were then used as a model to assess their capability of predicting a context or choice given a DPAFR as input. When the output of the model was the same context or choice that had generated the DPAFR, the model was considered to have made a successful selection. This allowed us to estimate the efficiency of the model in reconstructing the original choice and context values. **Figures 6C,D** summarize these computations. Our empirical method provided information on the ability of the model to reconstruct a significant part of the original data and thus on its retrieval capability. This allowed us to compare the predictive power of the two neuronal subpopulations. Considering the context or choice prediction rates, we observed a significant higher success rate for GPi neurons compared to striatal neurons. This corroborates the previous mutual information outcomes and confirms a greater involvement of the GPi compared to striatum in both context value and choice encoding and thus an information convergence process. The second result was obtained by comparing the averaged level of context and choice encoding success rates, relative to chance, giving an unbiased respective retrieval success rate. As shown in **Figure 6C,D**, the success rate profiles of context and choice encoding were similar for the two monkeys. In a first step we compared the actual success rates of the model to the success rates due to chance, which can be described by a binomial distribution with a success base probability value of 16.67% for context and 33.33% for choice. Kolmogorov–Smirnov tests applied for both monkeys for both striatum and GPi vs. chance give p -values of $p < 1\%$ for both context and choice. This confirmed that the model predicted both context and choice at a level far greater than chance. In the second step we subtracted the success base chance rate from the actual model results to remove bias and compared the predictive power of the model in context and choice encoding (Bernard and Lapointe, 1987). A Mann–Whitney test was then applied to the unbiased data using an alternative hypothesis of “less” for the choice prediction. For both monkeys and both anatomical structures $p < 0.01$ were obtained. This suggests that, during the decision period, the average value of the firing rates of the GPi and striatal neurons preferentially encodes the context rather than the choice value.

DISCUSSION

This study presents a novel attempt to shed light on the correlation between BG neuron spike train dynamics and behavioral decision-making tasks. It provides evidence that encoding neurons show at least two remarkable properties: (i) the firing activity of GPi neurons during the DP carries more information on the context and on the choice values than the striatal neurons and (ii) both structures preferentially encode the context rather than the choice.

THE BG ENCODED INFORMATION AS A CONTINUUM DURING THE TASK

We have presented in this paper, several original approaches to improve analysis of time-dynamic neuronal activity as well as of the information flows in the striatum and the GPi of an animal involved in a sensory-motor probabilistic decision-task. These



approaches rely on normalized NIETH profiles (PETH computed on all the events of the task) analysis. This approach clearly showed that neurons of both structures cannot be classified into different clusters. Instead, they encoded the various parameters of the task as a continuum of responses (Figure 2). It also brings out that NIETH profile variability was higher in the striatum than in the GPi.

DIFFERENT LEVELS OF SYNCHRONIZATION IN THE STRIATUM AND THE GPi

The higher level of synchronization inside the GPi than in the striatum was then analyzed using two different methods: correlation coefficient analysis (Figure 3) and the computation of entropy (Figure 4). This confirmed our previous work (Pasquereau et al., 2007) where we showed that, during the executive part of a choice task, the GPi activity is strongly related to the action performed (encoding mainly movement parameters and action value), while the striatum stays more variable, encoding different parameters (chosen target value, non-chosen target value, motor parameters, action value, etc) in roughly equal proportions of neurons. This study shows that this focus on the action to perform in the output structure of the BG is associated with a high correlation level between GPi neurons. Experiments have shown that only 10–15% of GPi neurons responded to a specific task (Pasquereau et al., 2007) and moreover it makes sense that such simple behavior does not recruit the whole BG system. These data may seem at variance with another study showing decorrelation between GP neurons in a discrimination task (Joshua et al., 2009). However, this study used a non-instrumental task (the animal had no action to perform in response to the cues) while, in our task, the action consequent upon the choice between two options is an essential

aspect of the task. Considering different populations of neurons coding different tuning functions, their differential activation related to one specific trial will allow the selection of one specific action as a result of competitive mechanisms (Mink, 1996; Gurney et al., 2001; Nambu, 2004; Leblois et al., 2006b). Comparing these two studies reinforces the hypothesis that the very significant and transient synchronized response in the GPi neural population reflects the decision-making and action selection processes occurring in the cortico-BG loop.

BASAL GANGLIA ENCODE CONTEXTS AND CHOICES

In our experiments monkeys were over-trained and maximized their payoff by choosing the target with the higher reward value (for details see Pasquereau et al., 2007). This implies that the encoding strategies for the BG may vary between two boundaries: either it may solely encode the chosen target or its activity may be related to the context dependent choice (Mink and Thach, 1991). We have therefore focused our analysis on the decision period and used two methods to assess the relationship between the neural activity of the BG and the choices performed by the animals (Figure 6). Our model study reveals a better correlation for the encoding of the context than for the encoding of the choice and both (model and mutual information measure) show that the GPi is a better predictor than the striatum for both parameters. These data imply that, during the critical phase, when the animal decides which action to perform, the BG are deeply involved in the computation process which leads to the decision. The fact that there is a robust transformation (as shown by the higher correlation between GPi neurons) of the cortical input information as it passes from the input structure (the striatum) to the output

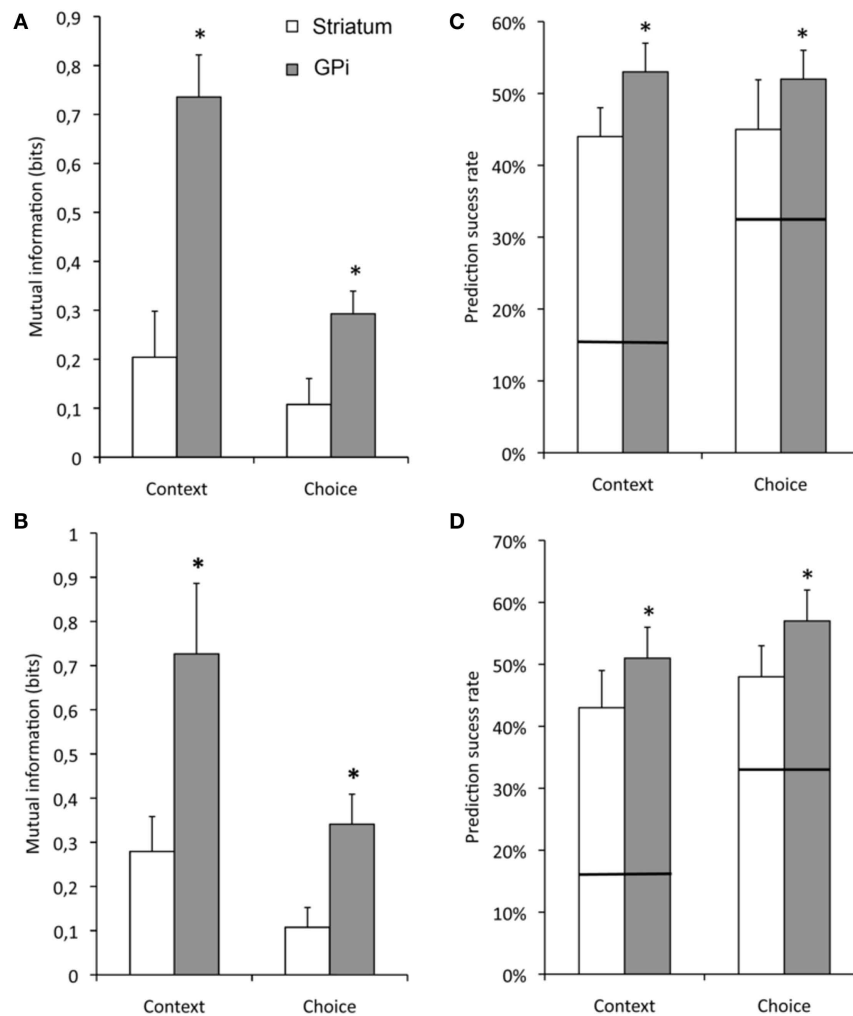


FIGURE 6 | Mutual information between DPAFR and context and choice values (A) for monkey T and (B) for monkey D. Prediction model success rates: (C) for monkey T and (D) for monkey D. Horizontal bars on (C,D)

histograms indicate the respective success base chance to predict the correct values (respectively 1/6 for context and 1/3 for choice). Error bars indicate SEM (Mann–Whitney test, $p < 0.01$).

stage (the GPi) is a further confirmation of the importance of the BG in the decision-making process. Two hypotheses can explain why the correlation is higher for the context than for the choice: (i) the BG preferentially encoded the context or (ii) the BG takes into account the context in order to perform a choice. The latter hypothesis has already been proposed by other teams (Morris et al., 2006; Niv et al., 2006) and supports the hypothesis that the cortex BG loop acts as a SARSA learning system and encodes the combination of choice made and context within which the choice is made. Unfortunately, as the monkeys optimized their behavior in our task, thus maximizing their gains, it is impossible to rule out either of these hypotheses.

CONCLUSION

This work is a first attempt to analyze comprehensively the process of neural computation occurring in the BG during the full duration of a trial of a behavioral task. The high variability of BG

neural population firing rate and the impossibility to define clear cut categories of neurons, especially in the output stage, makes this approach more appropriate than the classical PETH which reduces the richness of the time course of the neural responses. The normalization approach we adopted allowed us to visualize and analyze the decision period and allowed us to demonstrate the crucial role played by this structure on the decision-making process. Our model based approach to the coding neuron tuning functions led us to deduce that the context was comparatively better encoded than the choice. The fact that the GPi encodes the context more than the choice itself can also be related to the fact that the different aspects of the context converge from the striatum to the GPi (Mink, 1996). Taken together with our previous data (Pasquereau et al., 2007) and theoretical approach (Leblois et al., 2006a) we infer that this contextual information is used to shape the tuning functions allowing decision to occur by competition mechanisms in the cortex BG loop.

REFERENCES

- Arkadir, D., Morris, G., Vaadia, E., and Bergman, H. (2004). Independent coding of movement direction and reward prediction by single pallidal neurons. *J. Neurosci.* 24, 10047–10056.
- Bar-Gad, I., Morris, G., and Bergman, H. (2003). Information processing, dimensionality reduction and reinforcement learning in the basal ganglia. *Prog. Neurobiol.* 71, 439–473.
- Bernard, P.-M., and Lapointe, C. (1987). *Mesures statistiques en épidémiologie*. Québec: Presses de l'Université du Québec.
- Bezard, E., Boraud, T., Chalon, S., Brothier, J. M., Guilloteau, D., and Gross, C. E. (2001). Pallidal border cells: an anatomical and electrophysiological study in the MPTP-treated monkey. *Neuroscience* 103, 119–125.
- Boraud, T., Bezard, E., Bioulac, B., and Gross, C. (2001). Dopamine agonist-induced dyskinesias are correlated to both firing pattern and frequency alteration of pallidal neurons in the MPTP-treated monkey. *Brain* 124, 546–557.
- Borst, A., and Theunissen, F. E. (1999). Information theory and neural coding. *Nat. Neurosci.* 2, 947–957.
- Burkhardt, D. A., and Whittle, P. (1973). Intensity coding in the frog retina. Quantitative relations between impulse and graded activity. *J. Gen. Physiol.* 61, 305–322.
- Czanner, G., Eden, U. T., Wirth, S., Yanike, M., Suzuki, W. A., and Brown, E. N. (2008). Analysis of between-trial and within-trial neural spiking dynamics. *J. Neurophysiol.* 99, 2672–2693.
- Daw, N. D. (2007). Dopamine: at the intersection of reward and action. *Nat. Neurosci.* 10, 1505–1507.
- Endres, D., and Oram, M. (2010). Feature extraction from spike trains with Bayesian binning: 'latency is where the signal starts'. *J. Comput. Neurosci.* 29, 149–169.
- Gage, G. J., Stoetznner, C. R., Wiltschko, A. B., and Berke, J. D. (2010). Selective activation of striatal fast-spiking interneurons during choice execution. *Neuron* 67, 466–479.
- Gurney, K., Prescott, T. J., and Redgrave, P. (2001). A computational model of action selection in the basal ganglia. I. A new functional anatomy. *Biol. Cybern.* 84, 401–410.
- Haslinger, R., Klinkner, K. L., and Shalizi, C. R. (2010). The computational structure of spike trains. *Neural Comput.* 22, 121–157.
- Joshua, M., Adler, A., Rosin, B., Vaadia, E., and Bergman, H. (2009). Encoding of probabilistic rewarding and aversive events by pallidal and nigral neurons. *J. Neurophysiol.* 101, 758–772.
- Kable, J. W., and Glimcher, P. W. (2009). The neurobiology of decision: consensus and controversy. *Neuron* 63, 733–745.
- Leblois, A., Boraud, T., Meissner, W., Bergman, H., and Hansel, D. (2006a). Competition between feedback loops underlies normal and pathological dynamics in the basal ganglia. *J. Neurosci.* 26, 3567–3583.
- Leblois, A., Meissner, W., Bezard, E., Bioulac, B., Gross, C. E., and Boraud, T. (2006b). Temporal and spatial alterations in GPi neuronal encoding might contribute to slow down movement in Parkinsonian monkeys. *Eur. J. Neurosci.* 24, 1201–1208.
- Lim, J., Sanghera, M. K., Darbin, O., Stewart, R. M., Jankovic, J., and Simpson, R. (2010). Nonlinear temporal organization of neuronal discharge in the basal ganglia of Parkinson's disease patients. *Exp. Neurol.* 224, 542–544.
- Mink, J. W. (1996). The basal ganglia: focused selection and inhibition of competing motor programs. *Prog. Neurobiol.* 50, 381–425.
- Mink, J. W., and Thach, W. T. (1991). Basal ganglia motor control. II. Late pallidal timing relative to movement onset and inconsistent pallidal coding of movement parameters. *J. Neurophysiol.* 65, 301–329.
- Morris, G., Nevet, A., Arkadir, D., Vaadia, E., and Bergman, H. (2006). Midbrain dopamine neurons encode decisions for future action. *Nat. Neurosci.* 9, 1057–1063.
- Nambu, A. (2004). A new dynamic model of the cortico-basal ganglia loop. *Prog. Brain Res.* 143, 461–466.
- Niv, Y., Daw, N. D., and Dayan, P. (2006). Choice values. *Nat. Neurosci.* 9, 987–988.
- Opris, I., and Bruce, C. J. (2005). Neural circuitry of judgment and decision mechanisms. *Brain Res. Brain Res. Rev.* 48, 509–526.
- Pasquereau, B., Nadjar, A., Arkadir, D., Bezard, E., Goillandeau, M., Bioulac, B., Gross, C. E., and Boraud, T. (2007). Shaping of motor responses by incentive values through the basal ganglia. *J. Neurosci.* 27, 1176–1183.
- Peng, H., Long, F., and Ding, C. (2005). Feature selection based on mutual information: criteria of max-dependency, max-relevance, and min-redundancy. *IEEE Trans. Pattern Anal. Mach. Intell.* 27, 1226–1238.
- Samejima, K., and Doya, K. (2007). Multiple representations of belief states and action values in corticobasal ganglia loops. *Ann. N. Y. Acad. Sci.* 1104, 213–228.
- Schultz, W. (2006). Behavioral theories and the neurophysiology of reward. *Annu. Rev. Psychol.* 57, 87–115.
- Shannon, C. E. (1948). The mathematical theory of communication. *Bell Syst. Tech. J.* 27:379–423.
- Zhang, Y., and Reid, R. C. (2005). Single-neuron responses and neuronal decisions in a vernier task. *Proc. Natl. Acad. Sci. U.S.A.* 102, 3507–3512.

Conflict of Interest Statement: The authors declare that the research was conducted in the absence of any commercial or financial relationships that could be construed as a potential conflict of interest.

Received: 01 February 2011; paper pending published: 25 February 2011; accepted: 20 April 2011; published online: 09 May 2011.
 Citation: Garenne A, Pasquereau B, Guthrie M, Bioulac B and Boraud T (2011) Basal ganglia preferentially encode context dependent choice in a two-armed bandit task. *Front. Syst. Neurosci.* 5:23. doi: 10.3389/fnsys.2011.00023
 Copyright © 2011 Garenne, Pasquereau, Guthrie, Bioulac and Boraud. This is an open-access article subject to a non-exclusive license between the authors and Frontiers Media SA, which permits use, distribution and reproduction in other forums, provided the original authors and source are credited and other Frontiers conditions are complied with.



Input dependent cell assembly dynamics in a model of the striatal medium spiny neuron network

Adam Ponzi* and Jeff Wickens

Neurobiology Research Unit, Okinawa Institute of Science and Technology, Okinawa, Japan

Edited by:

Charles J. Wilson, University of Texas at San Antonio, USA

Reviewed by:

Joshua D. Berke, University of Michigan, USA

Mark D. Humphries, Group for Neural Theory, LNC, DEC, ENS, France

*Correspondence:

Adam Ponzi, Okinawa Institute of Science and Technology, 12-22 Suzaki, Uruma-shi, Okinawa, Japan.
e-mail: adamp@oist.jp

The striatal medium spiny neuron (MSN) network is sparsely connected with fairly weak GABAergic collaterals receiving an excitatory glutamatergic cortical projection. Peri-stimulus time histograms (PSTH) of MSN population response investigated in various experimental studies display strong firing rate modulations distributed throughout behavioral task epochs. In previous work we have shown by numerical simulation that sparse random networks of inhibitory spiking neurons with characteristics appropriate for UP state MSNs form cell assemblies which fire together coherently in sequences on long behaviorally relevant timescales when the network receives a fixed pattern of constant input excitation. Here we first extend that model to the case where cortical excitation is composed of many independent noisy Poisson processes and demonstrate that cell assembly dynamics is still observed when the input is sufficiently weak. However if cortical excitation strength is increased more regularly firing and completely quiescent cells are found, which depend on the cortical stimulation. Subsequently we further extend previous work to consider what happens when the excitatory input varies as it would when the animal is engaged in behavior. We investigate how sudden switches in excitation interact with network generated patterned activity. We show that sequences of cell assembly activations can be locked to the excitatory input sequence and outline the range of parameters where this behavior is shown. Model cell population PSTH display both stimulus and temporal specificity, with large population firing rate modulations locked to elapsed time from task events. Thus the random network can generate a large diversity of temporally evolving stimulus dependent responses even though the input is fixed between switches. We suggest the MSN network is well suited to the generation of such slow coherent task dependent response which could be utilized by the animal in behavior.

Keywords: striatum, computational modeling, inhibition, medium spiny neuron, cell assembly, population dynamics, spiking network

1. INTRODUCTION

Experimentally testing theoretical work on the dynamics of brain networks requires measurement of key predictions of models. With existing technologies it is in general not possible to obtain a complete record of the activity of entire populations of cells embedded within networks in intact, behaving animals. Most data is obtained by recording small groups or single neurons during behavioral tasks, frequently reported as peri-stimulus time histograms (PSTH). Such studies of neural response to behavioral task events and sensory stimuli throughout the brain demonstrate large firing rate fluctuations on slow behaviorally relevant timescales in both single cells and cell populations. These large slow firing rate modulations in PSTH do not simply occur at stimulus offset and onset but tend to be broadly distributed throughout the trial period (Jin et al., 2009). The different responses of a sample of cells from a network may provide a signature of network dynamical activity.

The striatal medium spiny neuron (MSN) network is one neural network which shows strong modulations in PSTH during behavioral tasks. MSNs are GABAergic and comprise more

than 90% of the cells of the striatum which forms the main input structure to the basal ganglia (BG) (McGeorge and Faull, 1989; Oorschot, 1996; Wickens et al., 2007). Since the MSN network is composed of sparse, random, and weak connections (Czubayko and Plenz, 2002; Tunstall et al., 2002; Koos et al., 2004; Taverna et al., 2004), its function has been puzzling and inconsistent with its often supposed winner-take-all role (Groves, 1983; Wickens et al., 1991; Beiser and Houk, 1998; Suri and Schultz, 1999; Bar-Gad and Bergman, 2001). Recent experimental observations of striatal slices show that MSN cell assemblies display episodes of spontaneous and recurrent bursting activity (Carrillo-Reid et al., 2008) while *in vivo* behavioral studies show that coherent bursting activity in cortico-BG microcircuits is important in the encoding of movement (DeLong, 1973; Hikosaka et al., 1989, 2000, 2006; Jaeger et al., 1995; Kasanetz et al., 2006; Miller et al., 2008) and the execution of learned motor programs and sequence learning (Kimura, 1990; West et al., 1990; Brothie et al., 1991; Gardiner and Kitai, 1992; Kimura et al., 1992; Kermadi and Joseph, 1995; Mushiake and Strick, 1996; Aldridge and Berridge, 1998; Jog et al., 1999; Doya, 2000; Barnes et al., 2005; Kubota et al., 2009). A recent

study (Jin et al., 2009) found that populations of striatal neurons display a variety of response profiles during tasks. Firing rates were strongly modulated in various epochs of the task and individual cells responded with activity peaks that were distributed at different temporal delays after individual task events. The authors suggested the neurons could have encoded time as a population.

Other BG inhibitory networks also exhibit firing rate modulations that are time locked to behavioral tasks. PSTH of pallidal cells in song bird Area X display rate increases and decreases significantly correlated with song temporal structure (Goldberg et al., 2010) and pallidal cells also exhibit a broad range of firing rates during motor tasks (Joshua et al., 2009). However cells also generally exhibit strong trial-to-trial variability in the timing of their activity during motor tasks (Tomko and Crapper, 1974; Goldberg et al., 2010).

It is *a priori* surprising that large slow modulations in PSTH exist since the cells generating these responses receive inputs from very many cells (~ 10000). Indeed, according to the law of large numbers, a reduction in fluctuation size is to be expected when many independent inputs to a cell are combined. On the other hand if the excitatory inputs to an MSN covary on slow timescales then the MSN activity can be expected to show large modulations on similar time scales. Even if pairwise correlations between inputs are themselves weak (Schneidman et al., 2006; Yim et al., 2011) their cumulative effect may be strong. Such strongly covarying inputs might translate into large fluctuations in PSTH when the stimuli are repeatedly presented.

However the MSN response is also determined by the activity generated within the striatum through feedback inhibition among MSNs and feedforward inhibition from fast spiking interneurons in particular. Indeed in recent modeling work on the striatal MSN network (Ponzi and Wickens, 2008a,b, 2010a) we have shown that coherent cell assembly population dynamics on slow behaviorally relevant timescales can be generated simply by the MSN network in isolation, even when excitatory input is constant and unvarying. We showed that such activity occurs if the network has the sparse random striatally relevant connectivity of around 10–30% and cortical excitation is appropriate so that cells are excited just above firing threshold. In this “balanced” situation even small changes in network generated inhibition or cortical excitation can cause cells to switch between firing and quiescent states. We demonstrated that under these circumstances individual cells displayed broadly distributed firing rates and that the network generated complex spatio-temporal dynamics (Usher et al., 1994, 1995; Ermentrout, 1998; Huerta and Rabinovich, 2004) while spiking itself was highly irregular (Tomko and Crapper, 1974; Softky and Koch, 1993; Holt et al., 1996; Shadlen and Newsome, 1998; Compte et al., 2003; Miura et al., 2007; Renart et al., 2007; Barbieri and Brunel, 2008). Networks with balanced excitation and inhibition (van Vreeswijk and Sompolinsky, 1996; Amit and Brunel, 1997) generically produce irregular chaotic spiking with broad rate distributions.

Here we wish to understand how the large amplitude firing rate fluctuations on slow time scales generated by the MSN network are modulated when excitatory input varies as it would in a behavioral task. Thus we investigate how the MSN network transforms cortical driving activity. On the one hand MSN network generated

activity may be suppressed so that PSTH simply reflect the variations in cortical driving. Alternatively MSN activity may evolve chaotically independent of the cortical activity. In this case we would expect MSN PSTH to be structureless after many stimulus presentations are averaged. Or finally interaction between cortical driving and MSN network generated activity may occur, thus generating complex patterns in PSTH.

First we extend our previous study of MSN network dynamics and show that similar dynamical activity occurs when the excitatory input to cells is composed of many independent Poisson spike trains. We also investigate how network dynamics depends on cortical excitation strength (Ponzi and Wickens, 2009) and on the time scale of inhibitory neurotransmitter. Next we show that the MSN network can generate coherent repeatable responses to variations in cortical driving input. Cell assemblies display large firing rate modulations over a broad range of temporal delays up to many hundreds of milliseconds after particular task events (Ponzi and Wickens, 2010b) resulting in strongly modulated stimulus and temporally specific PSTH. Finally we investigate how the stimulus locked fluctuations in PSTH depend on connectivity and input strength.

These network generated behaviors may be relevant in reinforcement learning tasks where the animal shows a transition from exploratory to exploitative behavior (for example (Barnes et al., 2005)). Moreover the dual encoding of stimulus identity and elapsed time in a single spiking network (Buonomano and Merzenich, 1995; Maass et al., 2002; Jaeger and Hass, 2004; Karmarkar and Buonomano, 2007; Buonomano and Maass, 2009) may be relevant in the temporal credit assignment tasks which are thought to deeply involve the striatum and dopaminergic systems.

2. MODEL

The network is composed of model MSNs with parameters set so they are in the vicinity of a bifurcation from a stable fixed point to spiking limit cycle dynamical behavior (Ponzi and Wickens, 2010a). This models the dynamics in the UP state when the cells are all receiving excitatory drive to firing threshold levels of depolarization. To describe the cells we use the $I_{Na,p} + I_k$ model described in (Izhikevich, 2005) which is two-dimensional and given by,

$$\begin{aligned} C \frac{dV_i}{dt} &= I_i(t) - g_L (V_i - E_L) - g_{Na} m_\infty (V_i) (V_i - E_{Na}) \\ &\quad - g_k n_i (V_i - E_k) \\ \frac{dn_i}{dt} &= (n_\infty - n_i) / \tau_n \end{aligned} \quad (1)$$

having leak current I_L , persistent Na^+ current $I_{Na,p}$ with instantaneous activation kinetic and a relatively slower persistent K^+ current I_k . $V_i(t)$ is the membrane potential of the i^{th} cell, C the membrane capacitance, $E_{L,Na,k}$ are the channel reversal potentials, and $g_{L,Na,k}$ are the maximal conductances. $n_i(t)$ is K^+ channel activation variable of the i^{th} cell. The steady state activation curves m_∞ and n_∞ are both described by, $x_\infty(V) = 1 / (1 + \exp\{(V_\infty^x - V) / k_\infty^x\})$ where x denotes m or n and V_∞^x and k_∞^x are fixed parameters. τ_n is the fixed timescale of the K^+ activation variable. The term $I_i(t)$ is the input current to the i^{th} cell.

The parameters are chosen so that the cell is the vicinity of a *saddle-node on invariant circle* (SNIC) bifurcation, characterizing a Type 1 neuron model. As the current $I_i(t)$ in equation (1) increases through the bifurcation point the stable node fixed point and the unstable saddle fixed point annihilate each other and a limit cycle having zero frequency is formed (Izhikevich, 2005). Increasing current further increases the frequency of the limit cycle. This is an appropriate model to use for an MSN in the UP state, since its dynamics are in qualitative agreement with several aspects of MSN firing (Wilson, 1993; Wilson and Nisenbaum, 1995; Wilson and Kawaguchi, 1996; Wickens and Wilson, 1998). Firstly the SNIC bifurcation allows firing at arbitrarily low frequencies (Izhikevich, 2005) which is important since MSNs are known to fire with very low frequencies (Wilson, 1993). Secondly MSNs do not show subthreshold oscillations (Wilson and Nisenbaum, 1995; Wilson and Kawaguchi, 1996; under normal circumstances, but see McCarthy et al., 2011). Finally the SNIC bifurcation does not allow bistability between a spiking state and a quiescent state (Izhikevich, 2005) in agreement with studies of MSNs (Wilson and Nisenbaum, 1995; Wilson and Kawaguchi, 1996; Wickens and Wilson, 1998). However detailed channel properties such as the interaction of L-type Ca^{2+} and slowly inactivating K^{+} channels in the MSN have not been included in the model.

The input current $I_i(t) = I_i^C(t) + I_i^M(t)$ in equation (1) is composed of two parts. One component $I_i^M(t)$ comes from the MSN inhibitory network and the other component $I_i^C(t)$ represents the current from excitatory sources, the cortex and the thalamus. We describe the excitatory component first.

We model the excitatory part as a stochastic process. In general the excitatory component will be given by Rall-type synapses (Rall, 1967; Destexhe et al., 1998) $I_i^C(t) = (V_C - V_i(t))X_i(t)$ where $X_i(t) = \sum_l b_{il}^C a_{il}(t)$. V_C is the excitatory reversal potential, set here to the realistic value 0.0 mV. The MSN cells are considered to be contacted by many excitatory inputs l which are non-overlapping between the MSN cells i . Indeed while a given corticostriatal axon will often be providing input to a substantial number of cells (about 800 on average) within the volume of the arborization zone of a typical corticostriatal axon there are about 68000 striatal spiny neurons, making the average common input about 1.2% or less (Zheng and Wilson, 2002). Our assumption of zero common input is not, however, supposed to be a statement of biological fact. We wish to investigate how much correlated activity arises from local interactions among MSNs, rather than via common input. b_{il}^C are fixed channel parameters from the l^{th} excitatory cortical or thalamic input to the i^{th} MSN cell, described below. The $a_{il}(t)$ are the quantities of postsynaptically bound neurotransmitter from the l^{th} excitatory input to the i^{th} MSN cell. They are given by $\tau_a \frac{da_{il}}{dt} = \sum_m \delta(t - t_{ilm}) - a_{il}$ where the Dirac delta function $\delta()$ part represents a series of spikes from the l^{th} input to the i^{th} cell at times t_{ilm} and τ_a is a time scale which we set to the realistic value of 10 ms. The term $X_i(t)$ is then described by,

$$\tau_a dX_i = \sum_l b_{il}^C \left(\sum_m \delta(t - t_{ilm}) \right) dt - X_i dt. \quad (2)$$

We assume the input spikes follow independent Poisson processes with varying rates $r_{il}^C(t)$. This is a simple and compact way to describe the input activity in the simulation and is not supposed to be necessarily perfectly biologically realistic. This model is an attempt to understand how the MSN network behaves under the simplest assumptions, which do not include correlation between inputs. The contribution provided by many such independent Poisson processes is approximately Gaussian and we can replace the spike series by a term given by the mean rate plus a fluctuation proportional to the SD, $r_{il}^C(t)dt + \epsilon_{il}(t)\sqrt{r_{il}^C(t)dt}$ where $\epsilon_{il}(t)$ is a standard normally distributed random variable (mean zero, std unity) (Brunel and Hakim, 1999). Assuming that spikes are independent across i and l , the term $\sum_l \epsilon_{il}(t)b_{il}^C\sqrt{r_{il}^C(t)dt}$ which arises can also be replaced by its expectation and fluctuation $0 + \epsilon_i(t)\sqrt{dt\sum_l (b_{il}^C)^2 r_{il}^C(t)}$ where $\epsilon_i(t)$ is standard normal noise term independent in i and t and we have used $\langle \epsilon_{il}(t) \rangle = 0$ and $\langle \epsilon_{il}(t)\epsilon_{ik}(t) \rangle = 0$, ($l \neq k$) and $\langle \epsilon_{il}(t)\epsilon_{ik}(t) \rangle = 1$, ($l = k$). Therefore we calculate $X_i(t)$ using,

$$\tau_a dX_i = \left(\sum_l^{N_C} b_{il}^C r_{il}^C(t) - X_i \right) dt + \epsilon_i(t) \left[dt \sum_l^{N_C} (b_{il}^C)^2 r_{il}^C(t) \right]^{1/2}. \quad (3)$$

MSN cells are each contacted by around 10000 cortical and thalamic cells and we therefore set $N_C = 10000$. For each given cortical stimulus we draw the 10000 rates r_{il}^C for each MSN i independently from a certain fixed distribution, here a normalized Pareto distribution (see below). The normalized Pareto distribution with power-law tail parameter α and expectation r^C is chosen so that even though there are many, 10000, inputs to the cell the mean input strength can still show large fluctuations across cells when the tail parameter α is small enough. Sums of power-law distributed variables (with finite variance, $\alpha > 1$) do still converge to the Gaussian distribution, but the convergence rate is very slow. If instead the r_{il}^C are chosen from a narrow distribution, for example the Gaussian, when many inputs are averaged all the cells will have approximately the same input strength and stimulus specificity will not be possible. Variation of the tail parameter α controls the size in fluctuations in input strength across cells and therefore the amount of input specificity. Input specificity here is defined as 1 minus the normalized scalar product between the mean input vectors $\langle X_i \rangle = \sum_l^{N_C} b_{il}^C r_{il}^C$ for two different cortical stimuli. When $\alpha < 2$ stimuli will have specificity which increases as α decreases toward unity. As α increases past 2 however the limit distribution is a Gaussian and stimuli lose specificity when many inputs (here 10000) are summed over.

We have chosen to use the Pareto distribution as a device to produce a large variation in excitation strength across MSN cells as only the simplest of several possibilities. There are others which may be biologically plausible or possible. For example correlation in inputs to a single cell may also produce similar effects (Yim et al., 2011). Since all the afferents to a cell are combined into a single stochastic equation (3), and interactions between them are

not addressed, which method is used is not central to the modeling described here.

The b_{ij}^C are also fixed in our simulations reported here, although in reality they may vary with short term facilitation and suppression as well as by *LTP* and *LTD*. We choose the b_{ij}^C independently from a uniform distribution on $[0, 2b^C]$.

The inhibitory current part is provided by the GABAergic collaterals of the striatal network and given by $I_i^M(t) = (V_i(t) - V_M) \sum_j -k_{ij}^M g_j(t)$. These synapses are also described by Rall-type synapses (Rall, 1967) contributing to $I_i(t)$ where the current into postsynaptic neuron i is summed over all inhibitory presynaptic neurons j and V_M and k_{ij}^M are channel parameters. $g_j(t)$ is the quantity of postsynaptically bound neurotransmitter given by, $\tau_g \frac{dg_j}{dt} = \Theta(V_j(t) - V_{th}) - g_j$ for the j^{th} presynaptic cell. Here $V_{th} = -40$ mV is a threshold, and $\Theta(x)$ is the Heaviside function. g_j is a low-pass filter of presynaptic firing.

The timescale τ_g should be set relatively large so that the postsynaptic conductance follows the exponentially decaying time average of multiple preceding presynaptic high frequency spikes. In simulations here we use two values for $\tau_g = 20, 50$, for comparison, so that postsynaptically bound transmitter exponentially decays to half its value in time $\tau_g \ln(2) \approx 14, 34$ ms. In our network model what we are reproducing with the synapses is the time course of recovery of the membrane potential to firing threshold after a spike from another MSN. The time scales in the model have been adjusted so that the IPSP decay time scale is near that observed in experimental studies. The choice of $\tau_g \ln(2) \approx 34$ was motivated by (Janssen et al., 2009) which shows a time course of MSN IPSP with a half life of recovery of about 30–40 ms, although a fairly large range of values has been found in various studies depending on experimental conditions as well as on cell type (D1 or D2), and also dependent on facilitating and depressing properties (Tunstall et al., 2002; Koos et al., 2004; Tecuapetla et al., 2004; Taverna et al., 2008; Planert et al., 2010).

The network structure is described by the parameters $k_{ij}^M = (k^M/\rho) \epsilon_{ij} Z_{ij}$ where ϵ_{ij} is another uniform quenched random variable on $[0.8, 1.2]$ independent in i and j . $Z_{ij} = 1$ if cells i and j are connected and zero otherwise. In the simulations reported here we use random networks where cells i and j are connected with probability ρ , producing binomial degree distributions, and there are no self-connections, $Z_{ii} = 0$. k^M is a parameter which is rescaled by the connection probability ρ so that when the network connectivity is varied the average total inhibition on each cell is constant independent of ρ . k^M is set so that IPSPs are around $200 \mu V$, very similar to real striatal IPSPs, at connectivities of around $\rho = 0.1$ when the postsynaptic cell is just above firing threshold.

Striatal MSNs are likely to contact (and be contacted by) about 500 other MSNs (Plenz, 2003; Koos et al., 2004; Tepper et al., 2004; Wickens et al., 2007). Furthermore the probability of a connection is estimated to be fairly low, $\rho = 0.05$ – 0.3 . To simulate a striatal network which respects these two figures would require, say, a network of around $500/0.2 = 2500$ cells. However this neglects the fact that not all cells are cortically excited into the UP state (Wickens and Wilson, 1998) and such never firing cells can be left out of network simulations. We suppose that only about 10–30% of MSNs are cortically excited at any

time, and perform simulations of 500 UP state MSNs with sparse connectivities.

All simulations were carried out with the stochastic weak second order Runge-Kutta integrator described in (Burrage and Platen, 1994) with integration time step 0.1 ms, except for the calculation of Lyapunov exponent which was performed with a deterministic fourth order Runge-Kutta with time step 0.01 ms.

3. METHODS

3.1. K-MEANS ALGORITHM

Here we explain how the k-means algorithm is used in this paper. The number of clusters k is chosen to be $N/k = 15$ where N is the number of cells used in the simulation. The cross-correlation matrix of cells' firing rates is calculated based on a 2 s moving window. Each cell i has a vector of cross-correlation coefficients \vec{c}_i . Each cluster centroid's initial location $\vec{d}_j, j = 1, \dots, k$ is chosen randomly as one on the cells' vector of cross-correlation coefficients \vec{c}_i . All cells i are assigned to be in the cluster j whose centroid is nearest to their cross-correlation coefficient vector, $\text{argmin}_j (|\vec{c}_i - \vec{d}_j|)$ where $|\vec{x}|$ is length of \vec{x} . Any empty clusters are removed. New cluster centroid vectors are calculated as the mean vector of cells assigned to the cluster $\vec{d}_j = \langle \vec{c}_i \rangle_{\text{cells } i \in \text{cluster } j}$. The process is repeated until there are no cells which change their assigned clusters. Notice the final amount of clusters may be (and usually is) less than the original k . For all statistical calculations (except example single clusterings) the clustering is performed several (10) times and the results averaged since final clusters are not unique but depend on the initial random placing of cluster centroids. Finally results are compared with a null hypothesis where the cells are randomly shuffled between clusters. The difference between the k-means clustering results and the random clustering results demonstrates that k-means clusters are significant.

3.2. LYAPUNOV EXPONENT CALCULATION

The Lyapunov exponent calculation is performed on the deterministic system where inputs do not fluctuate and uses all $3 \times 500 = 1500$ dynamical variables in the 500 cell system. First a perturbed 1500 dimensional orbit $r_p(\vec{0})$ near the system orbit, $r(\vec{0})$ is selected by random perturbation $\vec{d}_0 = r_p(\vec{0}) - r(\vec{0})$ of size $D_0 = \sqrt{\vec{d}_0 \cdot \vec{d}_0} = 10^{-12}$. After both orbits are iterated once (0.01 ms) the new separation vector is calculated $\vec{d}_1 = r_p(\vec{1}) - r(\vec{1})$ with length D_1 . The maximal Lyapunov exponent is calculated as $\gamma_1 = \ln(D_1/D_0)$. The perturbed orbit is rescaled in the direction of maximal separation, $r_p(\vec{1}) \leftarrow r(\vec{1}) + (r_p(\vec{1}) - r(\vec{1}))(D_0/D_1)$. This process is repeated for many iterations and many values $\gamma_i = \ln(D_i/D_0)$ of the Lyapunov exponent are calculated. The running average is calculated through $(1/t) \sum_{i=1}^t \gamma_i$ and plotted versus $0.01t$ after discarding a transient of 30000 ms.

3.3. NORMALIZED PARETO DISTRIBUTION

The pdf is given by,

$$f_{\gamma, \alpha}(x) = \gamma \alpha / (1 + \gamma x)^{1+\alpha} \quad (4)$$

with tail parameter α and expectation $1/(\gamma(\alpha - 1))$.

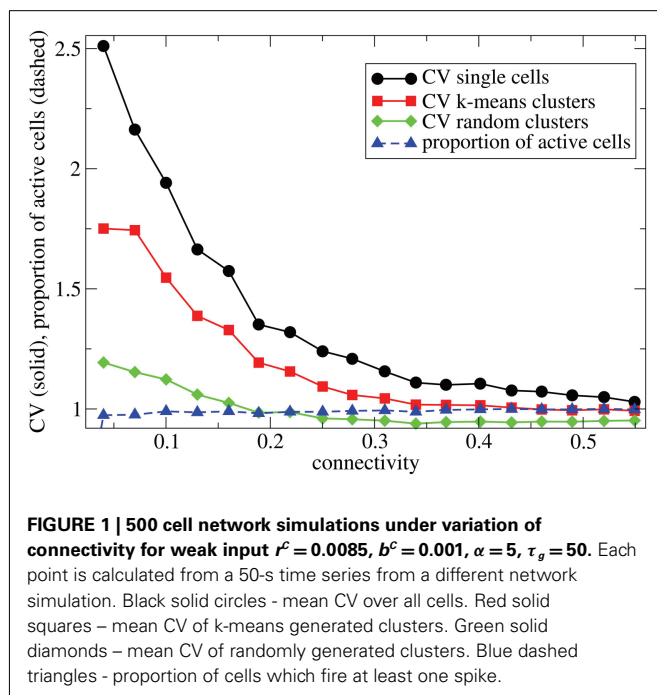
4. RESULTS

We first investigate how the network behaves under parameter variation. We vary connectivity, input strength, and inhibitory neurotransmitter timescale using excitatory input which is almost uniform across cells, $\alpha = 5$. Subsequently we investigate stimulus switching with lower values of $\alpha = 1.5$ to generate stimulus specific variations in excitation across cells in the network.

4.1. NETWORK PARAMETER VARIATION UNDER UNIFORMLY DISTRIBUTED INPUT

In **Figure 1** we describe how the spiking activity of 500 cell networks depends on connectivity ρ at low input rates $r^C \sim 10$ Hz and uniform input distribution $\alpha = 5$. Throughout the whole connectivity range the proportion of active cells (which fire at least one spike during the simulation period) is usually 100% (**Figure 1**, blue dashed triangles) and cells firing completely regularly with constant inter-spike-interval (ISI) are absent. The whole network is therefore engaged in dynamical activity. To investigate the structure of this dynamical activity we use the coefficient of variation (CV) of the cells' ISI distributions (Tomko and Crapper, 1974). This defined to be the ISI standard deviation divided by the ISI mean for each cell, then averaged over all active cells. A high value, larger than unity, indicates spiking which is burstier (more clustered) than Poisson, while as the CV approaches zero firing becomes more regular. As connectivity increases the coefficient of variation (**Figure 1**, black solid circles) decreases from a high value near 2.5 to a value near 1. This means that at low connectivity many cells are firing in a bursty way with episodes of high frequency spiking separated by long silent periods, while at high connectivity most cells are firing in a Poisson like way without high frequency bursts and pauses.

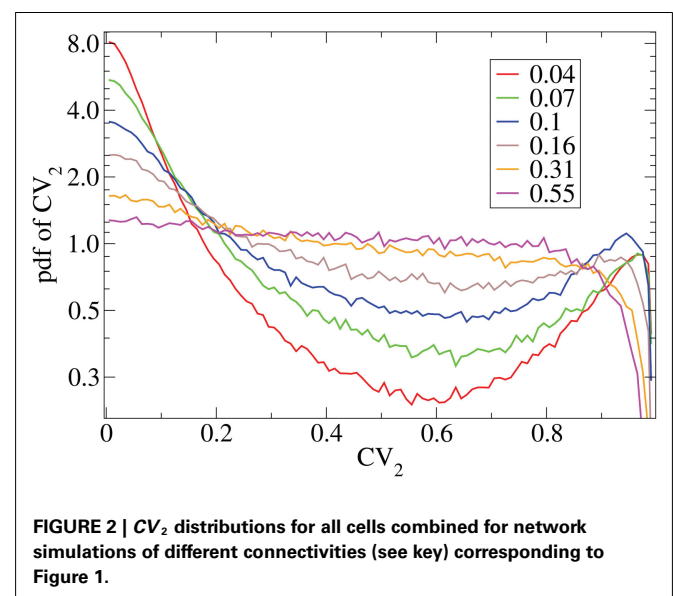
The coefficient of variation provides a useful single value to understand how burstiness varies under variation of network

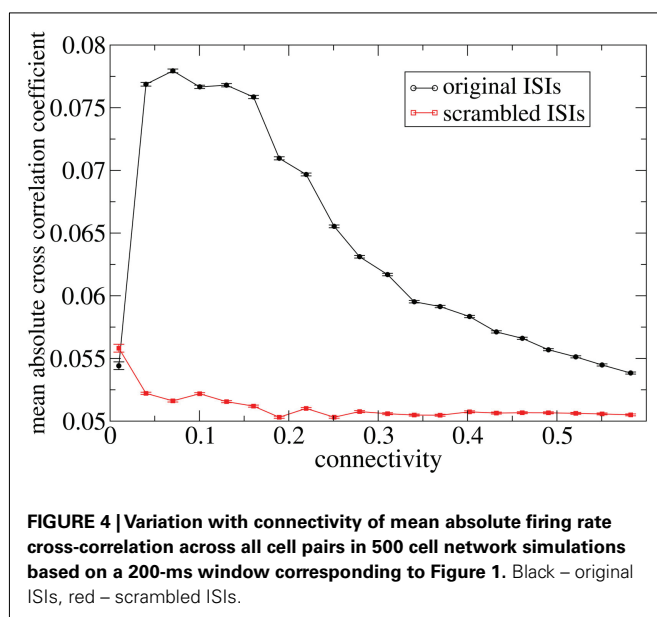
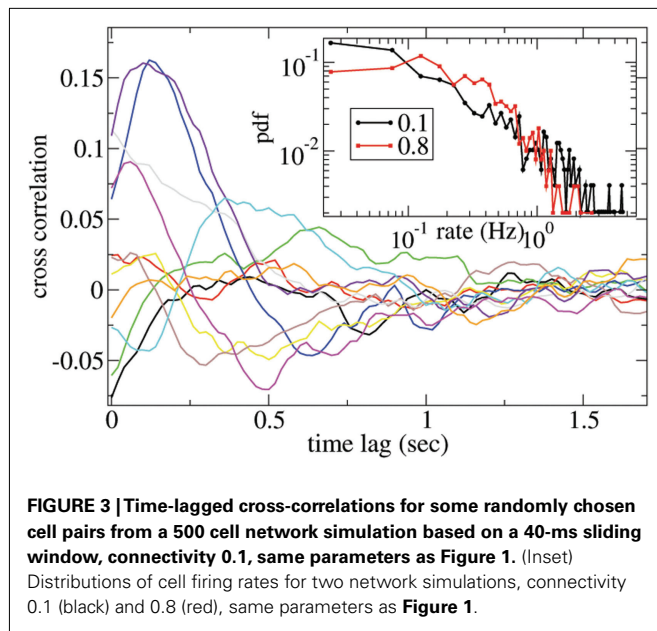


parameters. More detail however can be discerned from the distribution of the localized coefficients of variation, defined by $CV_n^i = |ISI_{n+1}^i - ISI_n^i| / (ISI_{n+1}^i + ISI_n^i)$, where ISI_n^i denotes the n^{th} spike of cell i . Each differently colored distribution, denoted CV_2 , shown in **Figure 2** is a different network simulation where all the CV_n^i across all i and n are combined in each distribution. The bimodal behavior at low connectivity, with peak near zero and near unity, characteristic of bursty activity changes over to a flat distribution with depletion near unity characteristic of Poisson processes with absolute refractory period at high connectivity.

We have demonstrated that cells fire spikes in a clustered bursty way at low connectivity even when cortical excitation is composed of many independent Poisson processes. Next we investigate whether they fire these bursts coherently or independently. To investigate this we calculate cross-correlation matrices of cell firing rates. We generate cell firing rate time series for all cells by counting the spikes of each cell in a moving window. We use a time window sufficiently long so that irregular fluctuations in precise spike timing do not affect the results.

Figure 3 shows some time-lagged cross-correlation coefficients between randomly selected cell pairs in a 500 cell network simulation. As can be seen, even when cortical input is highly noisy large variations in cross-correlation are present up to time lags of many hundreds of milliseconds. Peaks in cross-correlation do not generally occur at zero time-lag but may be hundreds of milliseconds later. This may express causal relationships between cell firing which exist even on this long timescale, much longer than any of the timescales prescribed by the model parameters. In **Figure 4** the mean of the absolute value of the simultaneous (time-lag zero) cross-correlation coefficient of all cell pairs is plotted versus connectivity for many 500 cell network simulations. To make this plot we use a 200-ms time window, reflecting cross-correlation between cells in the window from -100 to $+100$ ms of the time-lagged cross-correlation. We then take its absolute value and average across all cells. The black line in **Figure 4** shows that at





low connectivities, precisely where the cells display episodic burst firing, cross-correlations have large absolute magnitude while at higher connectivities this decays. The red line shows the result of the same calculation but where each cell's ISI time series is initially scrambled. This acts as a control measure removing most of the correlation. At high connectivity the unscrambled ISI result (black line) approaches this control but at low connectivity they are significantly different.

In fact at low connectivities cells do not fire in bursts individually but in slowly varying episodically firing cell assemblies, even in this case of Poisson cortical excitation. To demonstrate this explicitly we apply a clustering algorithm (k-means) to the cross-correlation matrix of cell firing rates to divide the cells into

clusters (see Methods). Then we generate *cluster spike time series* by merging the spikes of each cluster member cell, preserving each spike's timing, and measure the mean CV of the resultant spike sequences. Since clusters are not unique (see Methods) this procedure is repeated 10 times and the results averaged. This quantity (Figure 1, red solid squares) also decreases with increasing connectivity. The large value it takes at low connectivities indicates cells fire in assemblies together in episodes and are quiescent together in episodes. This quantity is significantly higher at low connectivities than the control measure we also show in Figure 1 (green solid diamonds). The make the control measure clusters are again generated by the clustering algorithm but the cells are then randomly shuffled between the clusters before their spike time series are merged.

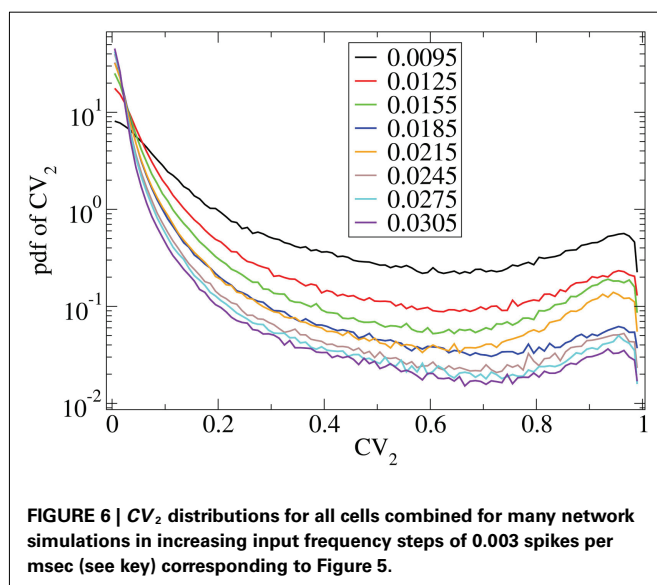
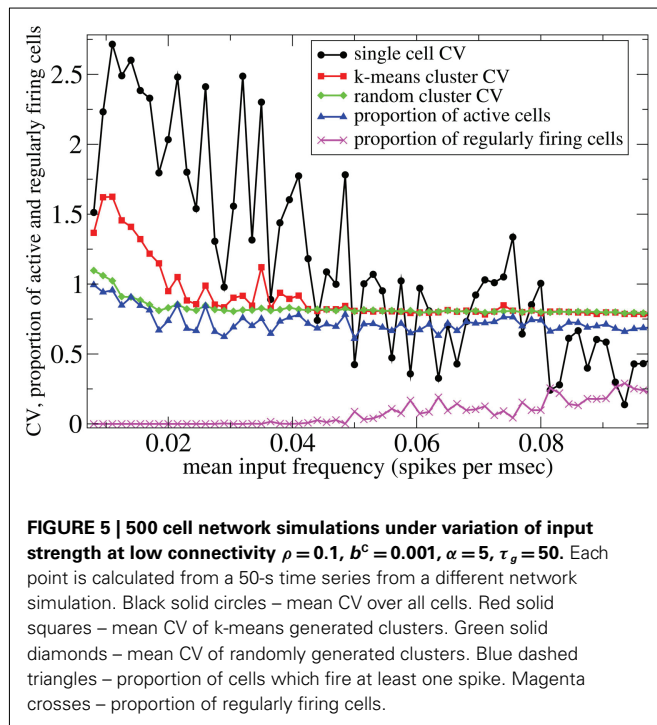
We did not attempt to *optimize* clustering (Humphries, 2011). However we do show that the (sub-optimal) algorithm produces a result which is significantly different to the null hypothesis where the cells are randomly assigned to clusters. Therefore the (non-random) clustering is meaningful. We thus provide objective demonstration that cell assemblies exist. Indeed the clusters are strongly determined by the network connectivity (Ponzi and Wickens, 2010a). In future work it may be useful to employ more optimal clustering methodologies (Humphries, 2011).

Cell firing rate distributions also vary dependent on connectivity (Figure 3(Inset)). At low connectivity the distribution of cell firing rates (black, connectivity $\rho = 0.1$) is approximately consistent with a power-law with many cells firing very slowly and a few firing very fast. On the other hand at high connectivity (red, $\rho = 0.8$) the distribution is narrower and peaks at an intermediate value. Broad firing rate distributions are observed in many brain regions (Lee et al., 1998; Nevet et al., 2007) and in modeling studies of balanced random networks (van Vreeswijk and Sompolinsky, 1996; Amit and Brunel, 1997). They may be relevant for the generation of large firing rate fluctuations representing different stimuli.

These results show that at the sparse connectivities characteristic of many real brain networks, including the MSN network of the striatum, cells show very broadly distributed firing rates and form cell assemblies whose members fire highly irregularly in slow coherent bursty episodes separated by pauses (Ponzi and Wickens, 2010a). Here we demonstrate this occurs even when cortical input is noisy and biologically plausibly composed of many Poisson spike trains.

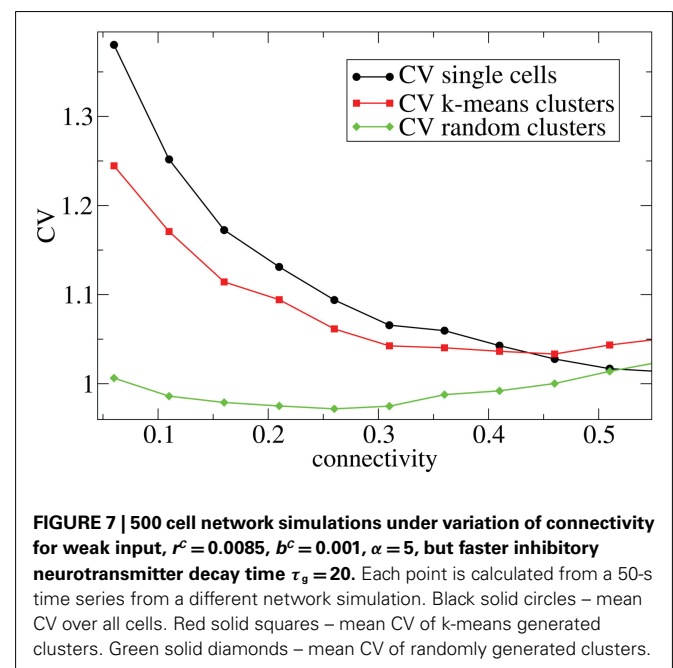
However Figure 5, which shows how spiking in sparsely connected networks ($\rho = 0.1$) driven by excitation uniform across cells ($\alpha = 5$) depends on excitatory input rate, r^C , C demonstrates that this interesting dynamical behavior also depends strongly on the strength of cortical excitation (Ponzi and Wickens, 2009). As mean excitatory input, r^C , increases the proportion of active cells (Figure 5, blue dashed triangles) decreases from 100% to a value around 75% and simultaneously the single cell CV (Figure 5, black solid circles) decreases to a value below unity (~ 0.75). Similarly our measure of the quantity of episodically firing cell assemblies (Figure 5, red solid squares) decreases to below zero and becomes equal to the control measure (Figure 5, green solid diamonds). CV values below one and near zero imply more regularly (periodically) firing cells are present. This is confirmed by direct calculation of

the proportion of regularly firing cells, (magenta crosses) (which are cells whose ISI variance is zero or less than a small threshold determined by the numerical integration time step). As can be seen the quantity of regularly firing cells increases at higher input strengths. This is also demonstrated by the CV_2 distributions (Figure 6) which show an increasing accumulation near zero as input strength increases, indicating the presence of more regularly firing cells. In fact (although detailed behavior does depend on other parameters) as input strength increases the network becomes locked into states where fewer cells are firing with higher rates which permanently suppress other cells, while a remaining



portion of the cells continue to display bursting behavior. The reduction in the quantity of active inhibitory connections this brings about allows some cells to fire nearly periodically under the cortical excitation. Which cells fire and which are quiescent depends on the details of the network structure and also on the distribution of input rates across cells.

Other network parameters also affect results. The above calculations were all performed with the half life of inhibitory neurotransmitter decay set to $\tau_g \ln(2) \approx 34$ ms. In Figures 7–10 we show that when this is reduced to $\tau_g \ln(2) \approx 14$ similar variations with connectivity and input strength are observed but the measured values of episodic burstiness, as quantified by the CV value and CV_2 distribution, are somewhat reduced. The reduction in burstiness occurs because IPSP decay times are reduced which reduces the periods of time where cells remain quiescent. However in the absence of inhibition cells still fire roughly regularly at a constant rate due to their fixed mean excitation levels. These two effects produce ISI distributions which are more regular and reduce the CVs. In close correspondence with the longer time scale results shown in Figure 1, as connectivity increases single cell CV (Figure 7, black circles) decreases while k-means cluster CV (Figure 7 red squares) also decreases but remains strongly above its control (Figure 7 green diamonds). CV_2 distributions (Figure 8) appear very similar to their longer time scale counterparts, (Figure 2), displaying a cross-over from a bimodal profile at low connectivity to flatter profile at higher connectivity. Similarly the variation with input strength is not strongly affected by reducing τ_g . Figure 9 shows that single cell CV, k-means cluster CV and random cluster CV for network simulations with $\tau_g \ln(2) \approx 14$ ms display very similar variations under input strength variation as their longer time scale counterparts, Figure 5. Similar corresponding CV_2 profiles (Figure 10) show the same change over from a bimodal profile to a peaked near zero profile as input



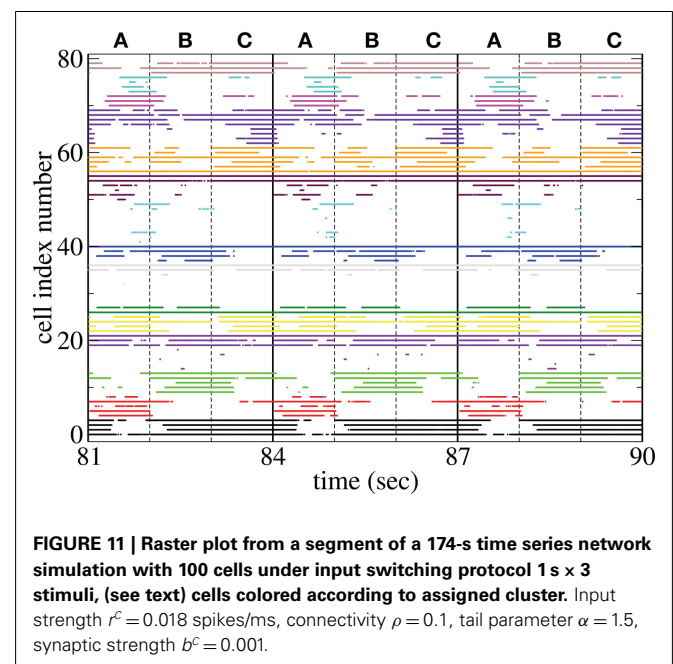
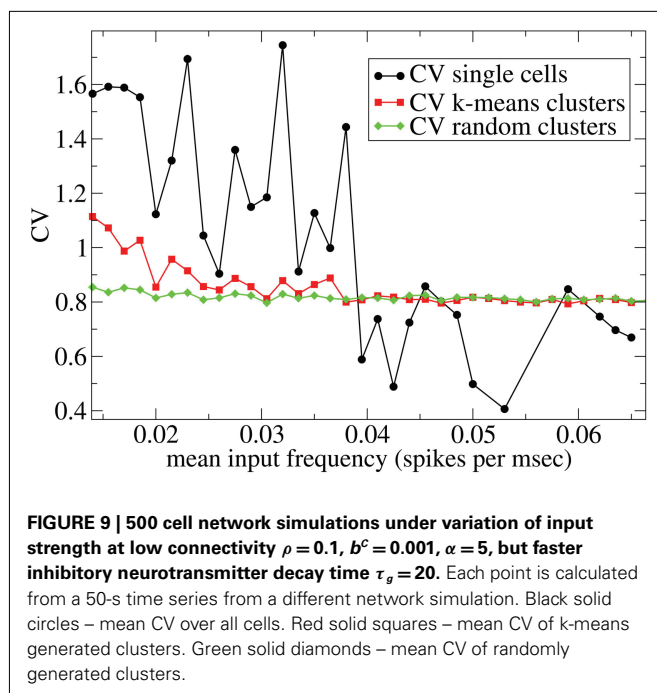
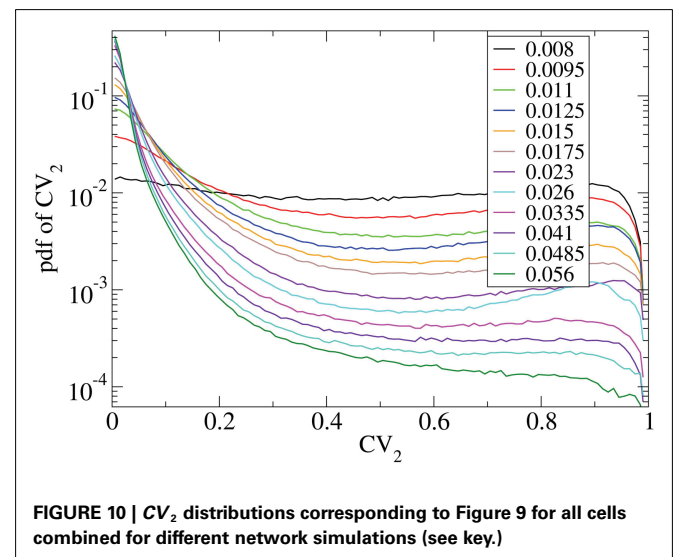
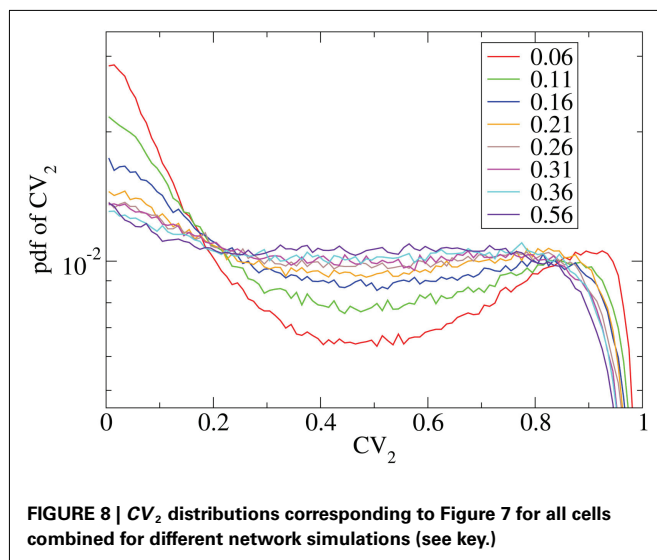
strength increases. Indeed simulations show that this time scale can be reduced further but not so far that the membrane potential IPSPs do not act as a slow-pass filter for several presynaptic spikes.

4.2. NETWORK DYNAMICS UNDER INPUT SWITCHING

What could be the use of the slowly varying cell assembly dynamics generated by the MSN network? To address this question we investigate how the network responds to stimuli. Here we set the input specificity parameter α to a lower value $\alpha = 1.5$ to generate stimulus specific activities.

Figure 11 shows a segment of a raster plot of all the active cells from a 100 cell network simulation under an stimulus switching

protocol. Three different inputs A , B , and C , each of which consists of a set of $i = 100 \times l = 10000$ firing rates, r_{il}^A , r_{il}^B , and r_{il}^C are applied for 1 s, each alternately and repetitively. All the rates in the matrices r_{il} are drawn independently randomly and then fixed for the duration of the 174 s simulation. The cells in **Figure 11** have been ordered by the clustering algorithm with 15 clusters and colored according to their assigned clusters. Vertical lines denote the input switching times. **Figure 12** shows the corresponding *cluster PSTH* locked to stimulus onset time. To construct this Figure the spikes of cells in a given cluster are merged and binned at given time lags from the onset of one of the stimuli, then the number of spikes in a bin is divided by the bin size (10 ms) and the number of cells in the cluster to give PSTH rates per second per cell.



Figures 11 and 12 demonstrate that different stimuli evoke different sets of cells. This is shown by the very different cluster firing rates in the two stimuli in **Figure 12** for any given cluster. However the activation of cells is not simply determined by the input strengths. If this were the case (roughly speaking) the most strongly excited cells in any particular stimulus would remain active throughout that stimulus period while the least strongly activated would remain quiescent throughout the stimulus. In fact the network activity provides cells with a large diversity of responses to a given stimulus, rather than a static state of active and quiescent cells. Individual cells fire in specific temporal patterns *locked to stimulus onset*, (Ponzi and Wickens, 2010b), as can be seen by the repetitive nature of some of the cell spike rasters in **Figure 11**. For example cell number 74 (colored cyan) fires only during the latter half of stimulus A “in anticipation” of stimulus B while cell number 17 (colored purple) fires a sharp peak near the onset of stimulus C. Furthermore cell assemblies composed of large numbers of cells can also fire in specific stimulus onset locked temporal patterns. For example the green cluster of cells, numbered around 10–15 fires strongly as a coherent assembly for over a second, but only during the latter half of stimulus B and first half of stimulus C. This is also clearly demonstrated by the PSTH in **Figure 12** where certain clusters develop large fluctuations in firing rate up to many hundreds of milliseconds after a given stimulus onset. For example the magenta cluster fires strongly during the latter half of stimulus A and more weakly during the first half of stimulus C.

These observations are not trivial since the network can display chaotic temporal evolution (Ponzi and Wickens, 2010a) and each stimulus presentation can occur in a different network state or context, depending on the history of the network. Therefore there are differences in the responses to repeated presentations of the same stimulus and one might expect the firing rate fluctuations of many cells to average themselves out over many presentations. However large fluctuations in cluster PSTH are possible because the strength of the network generated instability is weak (see below).

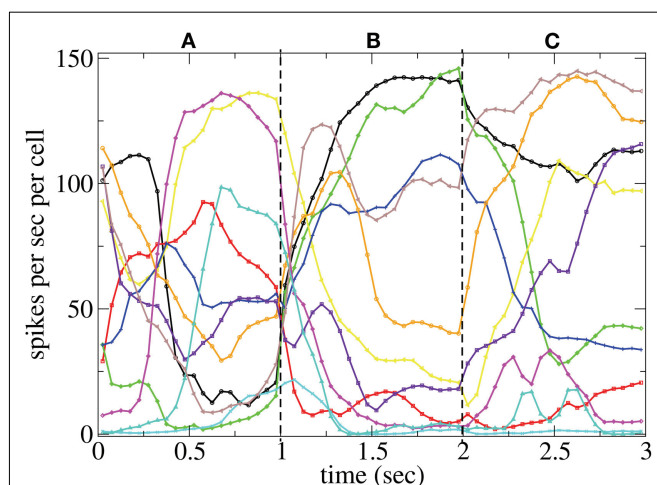


FIGURE 12 | PSTH of clusters corresponding to Figure 11 and colored the same way in spikes per second per cell.

Large stimulus locked fluctuations occur hundreds of milliseconds after stimulus switching even though input firing rates are fixed for the duration of each stimulus on all excitatory input synapses and each input describes a noisy Poisson spike process. The fluctuations occur on behaviorally relevant timescales. Since the clusters are composed of many cells they may provide a powerful force to drive or modulate downstream motor targets by inhibition when cluster firing rates are high or disinhibition during pauses in cluster firing at specific times after stimulus onset.

The appearance of stimulus locked temporally structured dynamics strongly depends on the system parameters however. At higher input strength, as shown in the spike raster plot in **Figure 13** active cells fire at higher rates and more regularly and there are more completely silent cells. Many cells, such as those numbered #1 and #2 (colored black) fire regularly across all stimuli. Thus stimulus specificity is weakened while temporally specific stimulus locking is lost. At higher connectivity, as shown by the spike raster plot in **Figure 14**, stimulus specificity is strong since many cells fire during only one stimulus (for example the brown colored cells #39–47 fire only during stimulus C) however temporal specificity is weak since cells fire continuously throughout a particular stimulus. Indeed at higher connectivity, cell dynamics approaches a more “winners-take-all” type behavior (Fukai and Tanaka, 1997).

4.3. LYAPUNOV EXPONENT

Network simulations can display complex cell assembly dynamics locked to stimulus onset times. How can such behavior occur?

In **Figure 15** we show the maximal Lyapunov exponent γ (Gluckenheimer and Holmes, 1983) calculated for a single deterministic network simulation [here the noise term in equation (3) has been set to zero; see Methods]. The inset shows $\gamma(t) = (1/\Delta t) \log(D(t + \Delta t)/D(t))$ where $\Delta t = 0.01$ ms is the time increment and $D(t)$ is the distance between two nearby deterministic trajectories at time t . $\gamma(t)$ measures the rate of separation

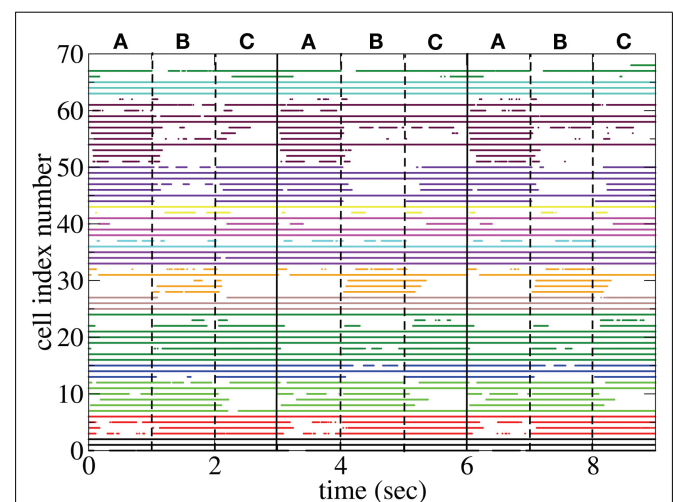
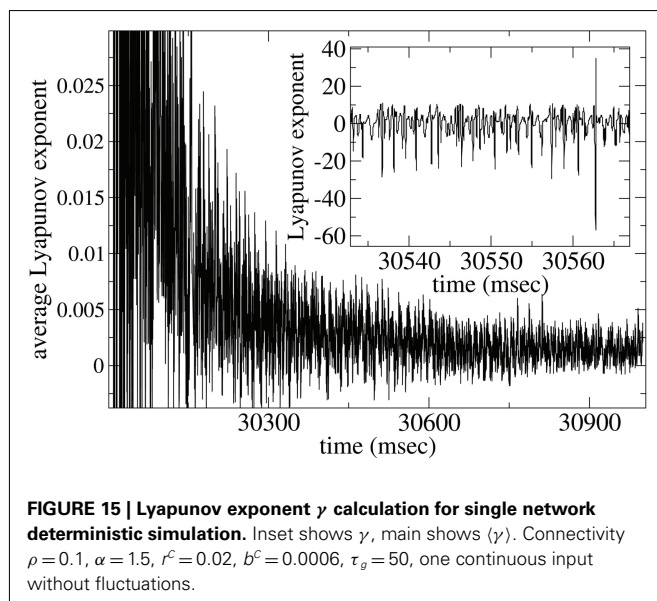
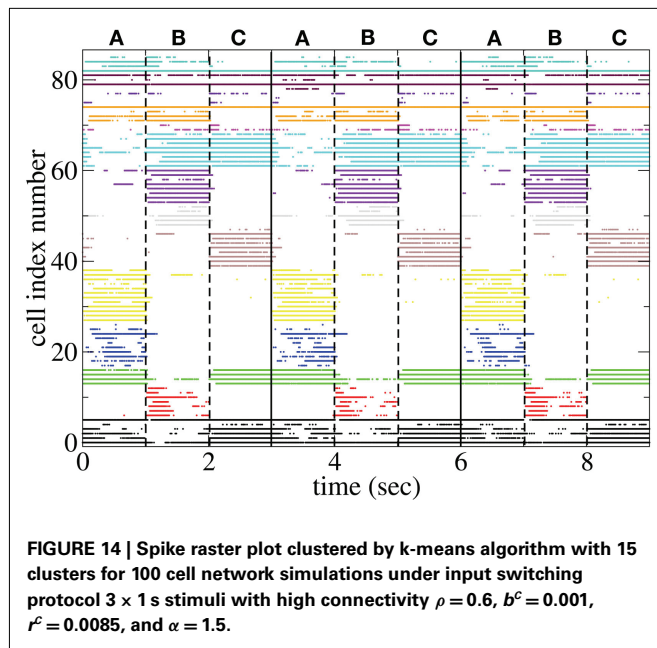


FIGURE 13 | Spike raster plot clustered by k-means algorithm with 15 clusters for 100 cell network simulations under input switching protocol 3×1 s stimuli with high input strength $\rho = 0.1$, $b^c = 0.001$, $r^c = 0.025$, and $\alpha = 1.5$.



of the two trajectories, when negative the trajectories converge exponentially, when positive they diverge. The former indicates a stable periodic (or fixed point) state while the latter indicates the presence of unstable dynamics and chaos.

The $\gamma(t)$ points (Figure 15 inset) show large fluctuations, sometimes apparently unstable (positive) but often stable (negative). These fluctuations may be caused by the dynamical system remaining close to a meta-stable attractor state for some time before randomly switching between such meta-stable attractors (Kaneko and Tsuda, 2003; Tsuda et al., 2004). The average Lyapunov exponent $\gamma^{AV}(t) = \langle \gamma(\tau) \rangle_\tau$, where $\langle \dots \rangle_\tau$ denotes time averaging from $\tau = 0$ to t , shown in Figure 15(main), appears

to approach a low positive value close to zero. Thus the system may be in a marginally stable very long “transient” state before reaching a permanent attractor state. Network dynamics may be consistent with the paradigm of “weak chaos” (Zillmer et al., 2009) or the “edge of chaos” (Langton, 1990; Bertchinger and Natschläger, 1995), since the Lyapunov exponent is close to zero, “between” a chaotic and a stable state (Ponzi and Wickens, 2010a). A transient state can also be observed in the paradigm of winner-less-competition based on heteroclinic channels (Rabinovich et al., 2000, 2001, 2008a,b; Nowotny and Rabinovich, 2007). Thus long dynamical transient states which are initiated when stimuli suddenly change may be responsible for the temporally locked cell firing observed in simulations of appropriate connectivity and input characteristics. In such a state the system does not either fall to a fixed point attractor state too rapidly nor does the system find a strongly unstable state where strong random fluctuations would be incompatible with large modulations in PSTH after many presentations are averaged.

5. DISCUSSION

In this paper we have extended a model of an MSN network (Ponzi and Wickens, 2010a) to the case where excitatory input to each cell is composed of many independent Poisson processes. We show that in spite of this noisy input at low connectivities with weak excitation cells form assemblies which fire highly irregularly but in coherent episodes on long behaviorally relevant timescales and firing rates are very broadly distributed. However when excitation is increased cells fire more regularly and a permanently quiescent component appears.

When excitatory inputs have a power-law distribution ($\alpha < 2$) so that cells receive a broad distribution of net excitations, MSN cell population PSTH are both stimulus and temporally specific. Temporal modulations occur for many hundreds of milliseconds after excitatory input rates are suddenly changed even though the inputs are fixed during this period. These time scales are much longer than any that exist in the system parameters. Such modulations are often observed in studies of behavioral tasks at distinct epochs during task events.

We suggest that the low connectivity observed in the striatum is necessary to generate strong firing rate modulations in PSTH. Using two time series examples we demonstrate that stimulus specific PSTH do not occur at high connectivity or high input strength and therefore this activity is not a trivial result which can be generated by any network under any conditions. At high connectivity cells either fire fairly regularly throughout a particular stimulus or are quiescent throughout. Cell activity is stimulus specific but does not display large rate variations locked to stimulus onset. On the other hand at high levels of cortical excitation many cells fire throughout all stimuli and thus stimulus specificity does not occur.

We suggest the MSN network facilitates the generation of marginally stable dynamical transients initiated at sudden stimulus switches. This may also possibly be true for the other sparse networks ubiquitous throughout the brain. Thus the network adds temporal specificity on long behaviorally relevant timescales to stimulus specificity. The dynamics generated by the network is not strongly unstable and therefore cell firing rates have low variability across repeat presentations of the same stimulus. However

the dynamics does not rapidly enter a periodic or fixed point state either and therefore a large diversity of temporally varying cell responses can be generated in spite of the fixed excitatory input. We have also shown (Ponzi and Wickens, 2011) that the reduction in variability after stimulus switching characterized by repeatable temporal evolution is equivalent to a reduction in Fano factor across repeated stimulus presentations in qualitative agreement with several experimental studies of neural activity (Churchland et al., 2006, 2010; Mitchell et al., 2007). Thus we offer the prediction that this phenomenon, so far observed only in cortex, should also be observed in MSN activity.

The response of chaotic firing rate networks of excitatory and inhibitory neurons to periodically varying inputs has also been recently studied in (Rajan et al., 2010). The model presented here extends this work to investigate the interaction of network generated chaos with excitatory drive in a purely inhibitory network of conductance based spiking cells with parameters chosen to resemble the striatal MSN network. In other possibly related work (Pehlevan and Sompolinsky, 2011; van Vreeswijk and Hansel, 2011) have shown that a random network operating in the regime where excitation and inhibition are balanced can generate cells with various realistic static tuning curves. The balanced network amplifies small variations in input drive. Although we have not varied the stimulus discriminability parameter α here systematically we observe (data not shown) that strong network responses can occur even under very subtle changes in excitation. Here the amplification is simply a result of the competitive selective behavior of this purely inhibitory asymmetrically connected network (at relatively sparse striatal connectivities.) Since cells are close to firing threshold switching a driving activation from one cell to another can cause a large change in the distribution (and temporal evolution) of activity across the network.

This model could be experimentally tested by simultaneously recording from striatal cell populations while manipulating the corticostriatal input. This is feasible using calcium imaging in brain slices and optogenetic activation of the cortical inputs. The model presented here provides a framework for the analysis of data from such an experiment. Experimental manipulation of connectivity is more difficult, and may require cell cultures. The properties of PSTH predicted by the model, for which some data is already available, provide a means for experimental testing in awake animals.

The crucial test of the model is blocking the lateral inhibition of MSNs. If blocking lateral inhibition does not change MSN PSTH time courses, and also does not change cortical activity patterns, then the model is falsified. If it does change MSN PSTH, the model is supported. The possibility exists, in the latter case, that the changed MSN network dynamics would, by feedback via the cortex, produce further changes in MSN PSTH. To exclude this possibility it would be necessary to block the outputs of the MSNs as well. In practice, it may be possible to do this using optogenetic methods to block lateral inhibition by MSNs. In the future we hope to address in more detail exactly how to test these models.

Large temporally specific fluctuations may be utilized in the time delayed reinforcement learning tasks (Sutton and Barto, 1998) known to recruit the striatum. For example to provide fluctuations at specific times necessary to facilitate exploration of both

sensory input and motor response (Doya and Sejnowski, 1996; Kao et al., 2005; Olveczky et al., 2005; Andalman and Fee, 2009) or simply to drive temporally delayed motor response. As learning proceeds the large fluctuations may be reduced and the network “locked” when excitatory input strength is increased (Levi et al., 2004). Related experimental studies show that learning to perform procedural tasks alters neural firing patterns in the sensorimotor striatum as behavior becomes more stereotyped (Barnes et al., 2005) with the task related activity of some cells strongly enhanced and others strongly suppressed. Such activity is reminiscent of the regularly firing and permanently suppressed cell populations which appear when input strength is increased as described above. Excitatory input strength and specificity may be varied through the action of dopamine or other neuromodulators during learning.

There are several good models of the striatum, for example (Beiser and Houk, 1998; Brown et al., 1999; Gurney et al., 2001; Bar-Gad et al., 2003; Humphries et al., 2006, 2009; McCarthy et al., 2011; Yim et al., 2011). The model we present here is not intended to be a complete model of the striatum. It is simply a model of MSN network activity which we hope complements other more complete modeling approaches. The striatum itself is vastly more intricate, including many different types of feedforward and feedback interneurons, different MSN cell types (D1 and D2), facilitating and depressing inhibitory synapses, patch, and matrix connectivity structure, correlations in excitatory input, feedback from thalamo-cortical loops, etc. We do not claim that these striatal components will not alter the network activity we present here. Rather the strategy we adopt is to start with one component, in this case the MSN network, and try to understand its behavior in isolation. In future work we will try to understand how other components, such as the feedforward interneurons, may modify or control the complex MSN network generated dynamical activity which we demonstrate here is possible. In fact we demonstrate that this behavior itself, before other striatal components are included, is nearly as complex as observed in many experimental recording studies in behavioral tasks. This is also the approach taken in (McCarthy et al., 2011) which also investigates the dynamics of the MSN network in isolation. The use of a different type of MSN cell model (including intrinsic oscillations in relation to pathological Parkinsonism) illustrates how useful minimal models may be for making different predictions about (some aspects of) network dynamics which can be easily traced back to differences in the basic behavior of the elements of the model. We hope the appreciation of the complex activity that can be generated by the MSN network will be valuable to provide insight into the roles of the various other striatal components and thus the role of the striatum in behavior and cognition.

6. CONCLUSION

We previously showed that the MSN network could produce sequences of cell assembly activations when the network receives a fixed pattern of constant input excitation. We here extend this work to consider what happens when the input varies as it would in the more realistic situation of an animal engaged in behavior. We show that the sequence of cell assembly activations can be locked to the input sequence and we outline the range of parameters where this property arises.

REFERENCES

- Aldridge, J. W., and Berridge, K. C. (1998). Coding of serial order by neostriatal neurons: a natural action approach to movement sequence. *J. Neurosci.* 18, 2777–2787.
- Amit, D. J., and Brunel, N. (1997). Dynamics of a recurrent network of spiking neurons before and following learning. *Network* 8, 373–404.
- Andalman, A. S., and Fee, M. S. (2009). A basal ganglia-forebrain circuit in the songbird biases motor output to avoid vocal errors. *Proc. Natl. Acad. Sci. U.S.A.* 106, 12518–12523.
- Barbieri, F., and Brunel, N. (2008). Can attractor network models account for the statistics of firing during persistent activity in prefrontal cortex? *Front. Neurosci.* 2:115. doi:10.3389/neuro.01.003.2008
- Bar-Gad, I., and Bergman, H. (2001). Stepping out of the box: information processing in the neural networks of the basal ganglia. *Curr. Opin. Neurobiol.* 11, 689–695.
- Bar-Gad, I., Morris, G., and Bergman, H. (2003). Information processing, dimensionality reduction and reinforcement learning in the basal ganglia. *Prog. Neurobiol.* 71, 439–473.
- Barnes, T. D., Kubota, Y., Hu, D., Jin, D. Z., and Graybiel, A. M. (2005). Activity of striatal neurons reflects dynamic encoding and recoding of procedural memories. *Nature* 437, 1158–1161.
- Beiser, D. G., and Houk, J. C. (1998). Model of cortical-basal ganglionic processing: encoding the serial order of sensory events. *J. Neurophysiol.* 79, 3168–3188.
- Bertchinger, N., and Natschläger, T. (1995). Real-time computation at the edge of chaos in recurrent neural networks. *Neural Comput.* 16, 1413–1436.
- Brothie, P., Iansek, R., and Horne, M. K. (1991). Motor functions of the monkey globus pallidus. II. Cognitive aspects of movement and phasic neuronal activity. *Brain* 114, 1685–1702.
- Brown, J., Bullock, D., and Grossberg, S. (1999). How the basal ganglia use parallel excitatory and inhibitory learning pathways to selectively respond to unexpected rewarding cues. *J. Neurosci.* 19, 10502–10511.
- Brunel, N., and Hakim, V. (1999). Fast global oscillations in networks of integrate-and-fire neurons with low firing rates. *Neural Comput.* 11, 1621–1671.
- Buonomano, D. V., and Maass, W. (2009). State-dependent computations: spatiotemporal processing in cortical networks. *Nat. Rev. Neurosci.* 10, 113–125.
- Buonomano, D. V., and Merzenich, M. M. (1995). Temporal information transformed into a spatial code by a neural network with realistic properties. *Science* 267, 1028–1030.
- Burrage, K., and Platen, E. (1994). Runge-Kutta methods for stochastic differential equations. *Ann. Numer. Math.* 1, 63–78.
- Carrillo-Reid, L., Tecuapetla, F., Tapia, D., Hernandez-Cruz, A., Galarra, E., Drucker-Colin, R., and Bargas, J. (2008). Encoding network states by striatal cell assemblies. *J. Neurophysiol.* 99, 1435.
- Churchland, M. M., Yu, B. M., Cunningham, J. P., Sugrue, L. P., Cohen, M. R., Corrado, G. S., Newsome, W. T., Clark, A. M., Hosseini, P., Scott, B. B., Bradley, D. C., Smith, M. A., Kohn, A., Movshon, J. A., Armstrong, K. M., Moore, T., Chang, S. W., Snyder, L. H., Ryu, S. I., Santhanam, G., Sahani, M., and Shenoy, K. V. (2010). Stimulus onset quenches neural variability: a widespread cortical phenomenon. *Nat. Neurosci.* 13, 369–378.
- Churchland, M. M., Yu, B. M., Ryu, S. I., Santhanam, G., and Shenoy, K. V. (2006). Neural variability in pre-motor cortex provides a signature of motor preparation. *J. Neurosci.* 26, 3697–3712.
- Compte, A., Constantinidis, C., Tegnaer, J., Raghavachari, S., Chafee, M. V., Goldman-Rakic, P. S., and Wang, X.-J. (2003). Temporally irregular mnemonic persistent activity in prefrontal neurons of monkeys during a delayed response task. *J. Neurophysiol.* 90, 3441–3454.
- Czubayko, U. Å., and Plenz, D. (2002). Fast synaptic transmission between striatal spiny projection neurons. *Proc. Natl. Acad. Sci. U.S.A.* 99, 15764–15769.
- DeLong, M. R. (1973). Putamen: activity of single units during slow and rapid arm movements. *Science* 179, 1240–1242.
- Destexhe, A., Mainen, Z. F., and Sejnowski, T. J. (1998). “Kinetic models of synaptic transmission,” in *Methods in Neuronal Modeling*, 2nd Edn, eds C. Koch and I. Segev (Cambridge, MA: MIT Press), 1–26.
- Doya, K. (2000). Complementary roles of the basal ganglia and cerebellum in learning and motor control. *Curr. Opin. Neurobiol.* 10, 732–739.
- Doya, K., and Sejnowski, T. J. (1996). “A novel reinforcement model of birdsong vocalization learning,” in *Advances in Neural Information Processing 7*, eds G. Tesauero, D. S. Touretzky, T. K. Leen (Cambridge, MA: MIT Press), 101–108.
- Ermentrout, G. B. (1998). Neural networks as spatio-temporal pattern-forming systems. *Rep. Prog. Phys.* 61, 353–430.
- Fukai, T., and Tanaka, S. (1997). A simple neural network exhibiting selective activation of neuronal ensembles: from winner-take-all to winners-share-all. *Neural Comput.* 9, 77–97.
- Gardiner, T. W., and Kitai, S. T. (1992). Single-unit activity in the globus pallidus and neostriatum of the rat during performance of a trained head movement. *Exp. Brain Res.* 88, 517–530.
- Gluckheimer, J., and Holmes, P. (1983). *Non-linear Oscillations, Dynamical Systems and Bifurcations of Vector Fields*. Berlin: Springer, 1983.
- Goldberg, J. H., Adler, A., Bergman, H., and Fee, M. S. (2010). Singing-related neural activity distinguishes two putative pallidal cell types in the songbird basal ganglia: comparison to the primate internal and external pallidal segments. *J. Neurosci.* 30, 7088–7098.
- Groves, P. M. (1983). A theory of the functional organization of the neostriatum and the neostriatal control of voluntary movement. *Brain Res.* 286, 109–132.
- Gurney, K., Prescott, T. J., and Redgrave, P. (2001). A computational model of action selection in the basal ganglia II: analysis and simulation of behaviour. *Biol. Cybern.* 85, 411–423.
- Hikosaka, O., Nakamura, K., and Nakhara, H. (2006). Basal ganglia orient eyes to reward. *J. Neurophysiol.* 95, 567–584.
- Hikosaka, O., Sakamoto, M., and Usui, S. (1989). Functional properties of monkey caudate neurons I. Activities related to saccadic eye movements. *J. Neurophysiol.* 61, 780–798.
- Hikosaka, O., Takikawa, Y., and Kawagoe, R. (2000). Role of the basal ganglia in the control of purposive saccadic eye movements. *Physiol. Rev.* 80, 953–978.
- Holt, G. R., Softky, W. R., Koch, C., and Douglas, R. J. (1996). Comparison of discharge variability in vitro and in vivo in cat visual cortex neurons. *J. Neurophysiol.* 75, 1806–1814.
- Huerta, R., and Rabinovich, M. I. (2004). Reproducible sequence generation in random neural ensembles. *Phys. Rev. Lett.* 93, 238104.
- Humphries, M. D. (2011). Spike-train communities: finding groups of similar spike trains. *J. Neurosci.* 31, 2321–2336.
- Humphries, M. D., Stewart, R. D., and Gurney, K. N. (2006). A physiologically plausible model of action selection and oscillatory activity in the basal ganglia. *J. Neurosci.* 26, 12921–12942.
- Humphries, M. D., Wood, R. D., and Gurney, K. N. (2009). Dopamine-modulated dynamic cell assemblies generated by the GABAergic striatal microcircuit. *Neural Netw.* 22, 1174–1188.
- Izhikevich, E. M. (2005). *Dynamical Systems in Neuroscience: The Geometry of Excitability and Bursting*. Cambridge, MA: MIT press.
- Jaeger, D., Gilman, S., and Aldridge, J. W. (1995). Neuronal activity in the striatum and pallidum of primates related to the execution of externally cued reaching movements. *Brain Res.* 694, 111–127.
- Jaeger, H., and Hass, H. (2004). Harnessing Nonlinearity: predicting chaotic systems and saving energy in wireless communication. *Science* 304, 78.
- Janssen, M. J., Ade, K. K., Fu, Z., and Vicini, S. (2009). Dopamine modulation of GABA tonic conductance in striatal output neurons. *J. Neurosci.* 29, 5116–5126.
- Jin, D. Z., Fujii, N., and Graybiel, A. M. (2009). Neural representation of time in cortico-basal ganglia circuits. *Proc. Natl. Acad. Sci. U.S.A.* 106, 19156–19161.
- Jog, M. S., Kubota, Y., Connolly, C. I., Hillegaart, V., and Graybiel, A. M. (1999). Building neural representations of habits. *Science* 286, 1745–1749.
- Joshua, M., Adler, A., Rosin, B., Vaadia, E., and Bergman, H. (2009). Encoding of probabilistic rewarding and aversive events by pallidal and nigral neurons. *J. Neurophysiol.* 101, 758–772.
- Kaneko, K., and Tsuda, I. (2003). Chaotic itinerancy. *Chaos* 13, 926–936.
- Kao, M. H., Doupe, A. J., and Brainard, M. S. (2005). Contributions of an avian basal ganglia-forebrain circuit to real-time modulation of song. *Nature* 433, 638–643.
- Karmarkar, U. R., and Buonomano, D. V. (2007). Timing in the absence of clocks: encoding time in neural network states. *Neuron* 53, 427–438.
- Kasanez, F., Riquelme, L. A., O'Donnell, P., and Murer, M. G. (2006). Turning off cortical ensembles stops striatal

- up states and elicits phase perturbations in cortical and striatal slow oscillations in rat in vivo. *J. Physiol. (Lond.)* 577, 97–113.
- Kermadi, I., and Joseph, J. P. (1995). Activity in the caudate nucleus of monkey during spatial sequencing. *J. Neurophysiol.* 74, 911–933.
- Kimura, M. (1990). Behaviorally contingent property of movement-related activity of the primate putamen. *J. Neurophysiol.* 63, 1277–1296.
- Kimura, M., Aosaki, T., Hu, Y., Ishida, A., and Watanabe, K. (1992). Activity of primate putamen neurons is selective to a mode of voluntary movement: visually guided, self-initiated or memory-guided. *Exp. Brain Res.* 89, 473–477.
- Koos, T., Tepper, J. M., and Wilson, C. J. (2004). Comparison of IPSCs evoked by spiny and fast-spiking neurons in the neostriatum. *J. Neurosci.* 24, 7916–7922.
- Kubota, Y., Liu, J., Hu, D., DeCoteau, W. E., Eden, U. T., Smith, A. C., and Graybiel, A. M. (2009). Stable encoding of task structure coexists with flexible coding of task events in sensorimotor striatum. *J. Neurophysiol.* 102, 2142–2160.
- Langton, C. G. (1990). Computation at the edge of chaos. *Physica D* 42, 12–37.
- Lee, D., Port, N. L., Kruse, W., and Georgopoulos, A. P. (1998). Variability and correlated noise in the discharge of neurons in motor and parietal areas of the primate cortex. *J. Neurosci.* 18, 1161–1170.
- Levi, R., Varona, P., Arshavsky, Y. I., Rabinovich, M. I., and Selverston, A. I. (2004). Dual sensory-motor function for a molluscan statocyst network. *J. Neurophysiol.* 91, 336–345.
- Maass, W., Natschlager, T., and Markram, H. (2002). Real-time computing without stable states: a new framework for neural computation based on perturbations. *Neural Comput.* 14, 2531–2560.
- McCarthy, M. M., Moore-Kochlacs, C., Gu, X., Boyden, E. S., Han, X., and Kopell, N. (2011). Striatal origin of the pathologic beta oscillations in Parkinsons disease. *Proc. Natl. Acad. Sci. U.S.A.* 108, 11620–11625.
- McGeorge, A. J., and Faull, R. L. (1989). The organization of the projection from the cerebral cortex to the striatum in the rat. *Neuroscience* 29, 503–537.
- Miller, B. R., Walker, A. G., Shah, A. S., Barton, S. J., and Rebec, G. V. (2008). Dysregulated information processing by medium spiny neurons in striatum of freely behaving mouse models of Huntingtons disease. *J. Neurophysiol.* 100, 2205–2216.
- Mitchell, J. F., Sundberg, K. A., and Reynolds, J. J. (2007). Differential attention dependent response modulation across cell classes in macaque visual area V4. *Neuron* 55, 131–41.
- Miura, K., Tsubo, Y., Okada, M., and Fukai, T. (2007). Balanced excitatory and inhibitory inputs to cortical neurons decouple firing irregularity from rate modulations. *J. Neurosci.* 27, 13802–13812.
- Mushiake, H., and Strick, P. L. (1996). Pallidal neuron activity during sequential arm movements. *J. Neurophysiol.* 74, 2754–2758.
- Nevet, A., Morris, G., Saban, G., Arkadir, D., and Bergman, H. (2007). Lack of spike-count and spike-time correlations in the substantia nigra reticulata despite overlap of neural responses. *J. Neurophysiol.* 98, 2232–2243.
- Nowotny, T., and Rabinovich, M. I. (2007). Dynamical origin of independent spiking and bursting activity in neural microcircuits. *Phys. Rev. Lett.* 98, 128106.
- Olczyk, B. P., Andalman, A. S., and Fee, M. S. (2005). Vocal experimentation in the juvenile songbird requires a basal ganglia circuit. *PLoS Biol.* 3, e153. doi:10.1371/journal.pbio.0030153
- Oorschot, D. E. (1996). Total number of neurons in the neostriatal, pallidal, subthalamic, and substantia nigral nuclei of the rat basal ganglia. *J. Comp. Neurol.* 366, 580–599.
- Pehlevan, C., and Sompolinsky, H. (2011). *Sensory selectivity in random cortical circuits*. Program No. 624.09, 2011 Neuroscience Meeting Planner. Washington, DC: Society for Neuroscience.
- Planert, H., Szydlowski, S. N., Hjorth, J. J., Grillner, S., and Silberberg, G. (2010). Dynamics of synaptic transmission between fast-spiking interneurons and striatal projection neurons of the direct and indirect pathways. *J. Neurosci.* 30, 3499–3507.
- Plenz, D. (2003). When inhibition goes incognito: feedback interaction between spiny projection neurons in striatal function. *Trends Neurosci.* 26, 436–443.
- Ponzi, A., and Wickens, J. (2008a). *Multiscale switching cell assembly clusters naturally emerge in simulations of random inhibitory networks of Hodgkin Huxley neurons*. Program No. 670.9, 2008 Neuroscience Meeting Planner. Washington, DC: Society for Neuroscience, Online.
- Ponzi, A., and Wickens, J. (2008b). Cell assemblies in large sparse inhibitory networks of biologically realistic spiking neurons advances. *NIPS* 21, 1273–1281.
- Ponzi, A., and Wickens, J. (2009). *A balanced striatal network model*. Program No. 845.21, 2009 Neuroscience Meeting Planner. Chicago, IL: Society for Neuroscience, Online.
- Ponzi, A., and Wickens, J. (2010a). Sequentially switching cell assemblies in random inhibitory networks of spiking neurons in the striatum. *J. Neurosci.* 30, 5894–5911.
- Ponzi, A., and Wickens, J. (2010b). *Input dependent cell assembly dynamics in an inhibitory spiking network model*. Program No. 380.19, 2010 Neuroscience Meeting Planner. San Diego, CA: Society for Neuroscience, Online.
- Ponzi, A., and Wickens, J. (2011). “Input dependent variability in a model of the striatal medium spiny neuron network,” in *Proceedings of ICCN, The Third International Conference on Cognitive Neurodynamics*, Hokkaido.
- Rabinovich, M., Huerta, R., and Laurent, G. (2008a). Transient dynamics for neural processing. *Science* 321, 48–50.
- Rabinovich, M. I., Huerta, R., Varona, P., and Afraimovich, V. S. (2008b). Transient cognitive dynamics, metastability, and decision making. *PLoS Comput. Biol.* 4, e1000072. doi:10.1371/journal.pcbi.1000072
- Rabinovich, M., Volkovskii, A., Lecanda, P., Huerta, R., Abarbanel, H. D. I., and Laurent, G. (2001). Dynamical encoding by networks of competing neuron groups: winnerless competition. *Phys. Rev. Lett.* 87, U149–U151.
- Rabinovich, M. I., Huerta, R., Volkovskii, A., Abarbanel, H. D. I., Stopfer, M., and Laurent, G. (2000). Dynamical coding of sensory information with competitive networks. *J. Physiol. Paris* 94, 465.
- Rajan, K., Abbott, L. F., and Sompolinsky, H. (2010). Stimulus-dependent suppression of chaos in recurrent neural networks. *Phys. Rev. E Stat. Nonlin. Soft Matter Phys.* 82, 011903.
- Rall, W. (1967). Distinguishing theoretical synaptic potentials computed for different soma-dendritic distributions of synaptic input. *J. Neurophysiol.* 30, 1138–1168.
- Renart, A., Moreno-Bote, R., Wang, X.-J., and Parga, N. (2007). Mean-driven and fluctuation-driven persistent activity in recurrent networks. *Neural Comput.* 19, 1–46.
- Schneidman, E., Berry, M. J., Segev, R., and Bialek, W. (2006). Weak pairwise correlations imply strongly correlated network states in a neural population. *Nature* 440, 1007–1012.
- Shadlen, M. N., and Newsome, W. T. (1998). The variable discharge of cortical neurons: implications for connectivity, computation, and information coding. *J. Neurosci.* 18, 3870–3896.
- Softky, W. R., and Koch, C. (1993). The highly irregular firing of cortical cells is inconsistent with temporal integration of random EPSPs. *J. Neurosci.* 13, 334–350.
- Suri, R. E., and Schultz, W. (1999). A neural network model with dopamine-like reinforcement signal that learns a spatial delayed response task. *Neuroscience* 91, 871–890.
- Sutton, R. S., and Barto, A. G. (1998). *Reinforcement Learning: An Introduction*. Cambridge: MIT Press.
- Taverna, S., Ilijic, E., and Surmeier, D. J. (2008). Recurrent collateral connections of striatal medium spiny neurons are disrupted in models of Parkinsons disease. *J. Neurosci.* 28, 5504–5512.
- Taverna, S., van Dongen, Y. C., Groenewegen, H. J., and Pennartz, C. M. A. (2004). Direct physiological evidence for synaptic connectivity between medium-sized spiny neurons in rat nucleus accumbens in situ. *J. Neurophysiol.* 91, 1111–1121.
- Tecuapetla, F., Koos, T., Tepper, J. M., Kabbani, N., and Yeckel, M. F. (2004). Differential dopaminergic modulation of neostriatal synaptic connections of striatopallidal axon collaterals. *J. Neurosci.* 29, 8977–8990.
- Tepper, J. M., Koos, T., and Wilson, C. J. (2004). GABAergic microcircuits in the neostriatum. *Trends Neurosci.* 27, 662–669.
- Tomko, G., and Crapper, D. (1974). Neuronal variability: non-stationary responses to identical visual stimuli. *Brain Res.* 79, 405–418.
- Tsuda, I., Fujii, H., Tadokoro, S., Yasuoka, T., and Yamaguti, Y. (2004). Chaotic itinerancy as a mechanism of irregular changes between synchronization and desynchronization in a neural network. *J. Integr. Neurosci.* 3, 159–182.
- Tunstall, M. J., Oorschot, D. E., Keen, A., and Wickens, J. R. (2002). Inhibitory interactions between spiny projection neurons in the rat striatum. *J. Neurophysiol.* 88, 1263–1269.
- Usher, M., Stemmler, M., Koch, C., and Olami, Z. (1994). Network amplification of local fluctuations causes high spike rate variability, fractal firing patterns and oscillatory local

- field potentials. *Neural Comput.* 6, 795–836.
- Usher, M., Stemmler, M., and Olami, Z. (1995). Dynamic pattern formation leads to $1/f$ noise in neural populations. *Phys. Rev. Lett.* 74, 326.
- van Vreeswijk, C., and Hansel, D. (2011). *Balanced network model of orientation selectivity in primary visual cortex without orientation map*. Program No. 175.12, 2011 Neuroscience Meeting Planner. Washington, DC: Society for Neuroscience, Online.
- van Vreeswijk, C., and Sompolinsky, H. (1996). Chaos in neuronal networks with balanced excitatory and inhibitory activity. *Science* 274, 6.
- West, M. O., Carelli, R. M., Pomerantz, M., Cohen, S. M., Gardnet, J. P., Chapin, J. K., and Woodward, D. J. (1990). A region in the dorsolateral striatum of the rat exhibiting single-unit correlations with specific locomotor limb movements. *J. Neurophysiol.* 64, 1233–1246.
- Wickens, J. R., Alexander, M. E., and Miller, R. (1991). Two dynamic modes of striatal function under dopaminergic-cholinergic control: simulation and analysis of a model. *Synapse* 8, 1–12.
- Wickens, J. R., Arbuthnott, G., and Shindou, T. (2007). Simulation of GABA function in the basal ganglia: computational models of GABAergic mechanisms in basal ganglia function. *Prog. Brain Res.* 160, 316.
- Wickens, J. R., and Wilson, C. J. (1998). Regulation of action-potential firing in spiny neurons of the rat neostriatum in vivo. *J. Neurophysiol.* 79, 2358–2364.
- Wilson, C. J. (1993). The generation of natural firing patterns in neostriatal neurons. *Prog. Brain Res.* 99, 277.
- Wilson, C. J., and Kawaguchi, Y. (1996). The origins of two-state spontaneous membrane potential fluctuations of neostriatal spiny neurons. *J. Neurosci.* 16, 2397–2410.
- Wilson, C. J., and Nisenbaum, E. S. (1995). Potassium currents responsible for inward and outward rectification in rat neostriatal spiny projection neurons. *J. Neurosci.* 15, 4449–4463.
- Yim, M. Y., Aertsen, A., and Kumar, A. (2011). Significance of input correlations in striatal function. *PLoS Comput. Biol.* 7, e1002254. doi:10.1371/journal.pcbi.1002254
- Zheng, T., and Wilson, C. J. (2002). Corticostriatal combinatorics: the implications of corticostriatal axonal arborizations. *J. Neurophysiol.* 87, 1007–1017.
- Zillmer, R., Brunel, N., and Hansel, D. (2009). Very long transients, irregular firing, and chaotic dynamics in networks of randomly connected inhibitory integrate-and-fire neurons. *Phys. Rev. E Stat. Nonlin. Soft Matter Phys.* 79, 031909.

Conflict of Interest Statement: The authors declare that the research was conducted in the absence of any commercial or financial relationships that could be construed as a potential conflict of interest.

Received: 20 April 2011; accepted: 04 February 2012; published online: 27 March 2012.

Citation: Ponzi A and Wickens J (2012) Input dependent cell assembly dynamics in a model of the striatal medium spiny neuron network. *Front. Syst. Neurosci.* 6:6. doi: 10.3389/fnsys.2012.00006

Copyright © 2012 Ponzi and Wickens. This is an open-access article distributed under the terms of the Creative Commons Attribution Non Commercial License, which permits non-commercial use, distribution, and reproduction in other forums, provided the original authors and source are credited.



Creation of computerized 3D MRI-integrated atlases of the human basal ganglia and thalamus

Abbas F. Sadikot^{1*}, M. Mallar Chakravarty², Gilles Bertrand¹, Vladimir V. Rymer¹, Fahd Al-Subaie¹ and D. Louis Collins²

¹ Cone Laboratory for Research in Neurosurgery, Montreal Neurological Institute, McGill University, Montreal, QC, Canada

² The McConnell Brain Imaging Center, Montreal Neurological Institute, McGill University, Montreal, QC, Canada

Edited by:

James M. Tepper, Rutgers, The State University of New Jersey, USA

Reviewed by:

Christine E. Collins, Vanderbilt University, USA

Yoland Smith, Emory University, USA

*Correspondence:

Abbas F. Sadikot, Cone Laboratory, Montreal Neurological Institute, 3801 University Street, Montreal, QC, Canada H3A2B4.

e-mail: abbas.sadikot@mcgill.ca

Functional brain imaging and neurosurgery in subcortical areas often requires visualization of brain nuclei beyond the resolution of current magnetic resonance imaging (MRI) methods. We present techniques used to create: (1) a lower resolution 3D atlas, based on the Schaltenbrand and Wahren print atlas, which was integrated into a stereotactic neurosurgery planning and visualization platform (VIPER); and (2) a higher resolution 3D atlas derived from a single set of manually segmented histological slices containing nuclei of the basal ganglia, thalamus, basal forebrain, and medial temporal lobe. Both atlases were integrated to a canonical MRI (Colin27) from a young male participant by manually identifying homologous landmarks. The lower resolution atlas was then warped to fit the MRI based on the identified landmarks. A pseudo-MRI representation of the high-resolution atlas was created, and a non-linear transformation was calculated in order to match the atlas to the template MRI. The atlas can then be warped to match the anatomy of Parkinson's disease surgical candidates by using 3D automated non-linear deformation methods. By way of functional validation of the atlas, the location of the sensory thalamus was correlated with stereotactic intraoperative physiological data. The position of subthalamic electrode positions in patients with Parkinson's disease was also evaluated in the atlas-integrated MRI space. Finally, probabilistic maps of subthalamic stimulation electrodes were developed, in order to allow group analysis of the location of contacts associated with the best motor outcomes. We have therefore developed, and are continuing to validate, a high-resolution computerized MRI-integrated 3D histological atlas, which is useful in functional neurosurgery, and for functional and anatomical studies of the human basal ganglia, thalamus, and basal forebrain.

Keywords: brain atlas, Parkinson's disease, stereotactic neurosurgery, image guidance

INTRODUCTION

Despite impressive gains in medical imaging during the last two decades, significant challenges remain when visualizing the structure of the living brain. The resolution and contrast of standard *in vivo* magnetic resonance imaging (MRI) is well below that required to visualize subnuclei and fiber tracts of the basal ganglia, thalamus, and brainstem. Since image-guided neurosurgery for Parkinson's disease often targets subnuclei of the thalamus, subthalamic area, basal ganglia, and brainstem, reliable targeting needs to be supplemented with invasive neurophysiological methods. Furthermore, advances in functional brain imaging have allowed increasing visualization of activation in subcortical brain areas, but only low-resolution atlases are available for interpretation of these changes. Most available print atlases of the human brain delineate subcortical nuclei in tissue sectioned in three planes, derived from different hemispheres using multiple brains (Olszewski and Baxter, 1954; Talairach, 1957; Schaltenbrand and Bailey, 1959; Van Buren and Maccubbin, 1962; Andrew et al., 1969; Van Buren and Borke, 1972; Schaltenbrand and Wahren, 1977; Afshar et al., 1978; Talairach and Tournoux, 1988). Bertrand and Thompson published the first computerized digitized atlas, which was derived from the Schaltenbrand print atlas. This atlas could be mapped

to stereotactic ventriculograms using constrained affine transformations (Bertrand et al., 1973). The atlas was used in stereotactic neurosurgery of the thalamus and basal ganglia, and also served as the basis for functional atlases of deep brain stimulation responses (Hardy et al., 1979a,b,c, 1981). A variety of digital atlases have since been created from original print versions (Yoshida, 1987; Kazarnovskaya et al., 1991; Hardy et al., 1992; Niemann et al., 1994; Nowinski et al., 1997; Sramka et al., 1997; Yeo and Nowinski, 1997; Niemann and van Nieuwenhofen, 1999; Yelnik et al., 2000; Berks et al., 2001).

Challenges faced when creating computerized 3D digital atlases from print atlases include: (1) Print atlases often have low inter-slice resolution and variable inter-slice distances. Reconstructed nuclei data may be fractured, reducing atlas utility. Furthermore, minor errors in photographic representations in stereotactic space can result in a shift between reconstructed slices, making image integration difficult in 3D space. Robust reconstruction algorithms that account for slice-to-slice variability, and anatomical differences between the atlas and patient data, can help enhance the quality of 3D visualization and atlas integration (St-Jean et al., 1998; Chakravarty et al., 2006a, 2008). (2) Differences in stereotactic location of nuclear structures may be noted when comparing data derived in different planes from

different hemispheres. Simple representation of the three planes of a print atlas is therefore not useful in computerized atlas aided analysis of neurosurgical plans, since the data sets do not match in all planes. (St-Jean et al., 1998; Niemann and van Nieuwenhofen, 1999; Nowinski et al., 2005, 2008; Chakravarty et al., 2006a,b, 2008, 2009; Sather and Patil, 2007; Yelnik et al., 2007). Multiplanar reconstruction from a unique histological data set is more useful (St-Jean et al., 1998) although only low resolution is obtained in most cases due to lack of detail in the source data. (3) Histological artifacts related to different stains (e.g., myelin, Nissl) can be problematic, especially in large sections, limiting proper identification of outlines of nuclei and tracts. Furthermore, thalamic nuclear nomenclature is highly complex, making it difficult to provide reliable outlines in multiplanar 3D mode on the basis of an initially low-resolution data set. (4) Tissue inhomogeneity can occur due to shear stress on sectioning, and artifacts can result from histological processing and slice mounting, further reducing the ability to interpret the underlying anatomy. For this reason, it is necessary to apply computerized reconstruction methods to minimize slice-to-slice variations in tissue morphology and staining intensity. (5) Classical atlases such as that of Schaltenbrand are based largely on detailed histological delineations using Hassler's nomenclature (Hassler et al., 1965; Schaltenbrand and Wahren, 1977). This terminology, which includes a distinct parcellation of the thalamus, has proved useful for neurosurgeons, and classical anatomists. Correspondence in 3D atlas space of Hassler's terminology with more commonly used thalamic nomenclature based on work in human and non-human primates would be desirable (Hirai and Jones, 1989b).

Here, we summarize our recent work on the creation and implementation of two digitized 3D atlases of subcortical structures. We first created a lower resolution atlas based on axial slices derived from the Schaltenbrand and Wahren print atlas (St-Jean et al., 1998; Atkinson et al., 2002; Strafella et al., 2004; Duval et al., 2006; Tyvaert et al., 2009). More recently, we created a higher resolution atlas derived from a new set of coronal histological slices, with delineation of thalamic and basal forebrain nuclei based on multiple terminologies (Chakravarty et al., 2006a,b, 2009; Duval et al., 2006). We concurrently developed novel tools for the creation of volumetric voxel-based 3D atlases from histological data sets, and methods for effective integration of the digitized atlases with canonical high-resolution MRI scans, or individual participant or patient MRIs. Availability of high-resolution digitized deformable atlases of subcortical nuclei will greatly aid in image-guided neurosurgery in subcortical areas, and in interpretation of structural and functional brain imaging data.

MATERIALS AND METHODS

Two computerized 3D atlases were created. The first atlas was created using the Schaltenbrand and Wahren print atlas. Details of image processing used for atlas development are presented in the Section "Results." This atlas was integrated into VIPER, a stereotactic visual integration platform for enhanced reality (St-Jean et al., 1998). VIPER allows visualization of stereotactic tools, electrodes, and virtual lesions in the 3D atlas space. The second atlas was created using the post-mortem brain of a middle-aged man who died of a non-neurological cause. The brain was fixed in 10% buffered formalin, hemi-sectioned in the mid-sagittal plane, and blocked to obtain the thalamus, basal

ganglia, basal forebrain, and temporal lobe of the left hemisphere. The brain was then embedded in paraffin, and sectioned in the coronal plane, perpendicular to the AP-PC plane (Chakravarty et al., 2006a). Pairs of 15 μ m thick slices were sampled from this data set at 0.70 mm intervals, yielding a total of 86 pairs of slices across the block. For each pair of slices, one was stained with Luxol Fast Blue for myelin, while the other was stained with a Nissl stain for neurons and glia. Subsequent image processing for atlas development is presented in the Section "Results." Computerized software used for image analysis included Adobe Photoshop 7, and MINC image analysis tools developed at the McConnell Brain Imaging Centre at the MNI (available at: <http://www.bic.mni.mcgill.ca/ServicesSoftware>).

RESULTS

INITIAL CREATION OF A 3D DIGITIZED ATLAS WITH A SURGICAL PLANNING PLATFORM

We initially created a digitized computerized 3D version of the atlas of Schaltenbrand and Wahren (St-Jean et al., 1998). The digital atlas was created from an axial data set with varying slice thickness of 0.5–3 mm due to the slice-to-slice distance variations in the original photographic plates (Schaltenbrand and Wahren, 1977). The 2D contour data was extracted into a vector format. Hermite polynomials were applied in order to interpolate the 2D contour data to achieve a 0.5-mm isotropic voxel resolution in the reconstructed 3D data set.

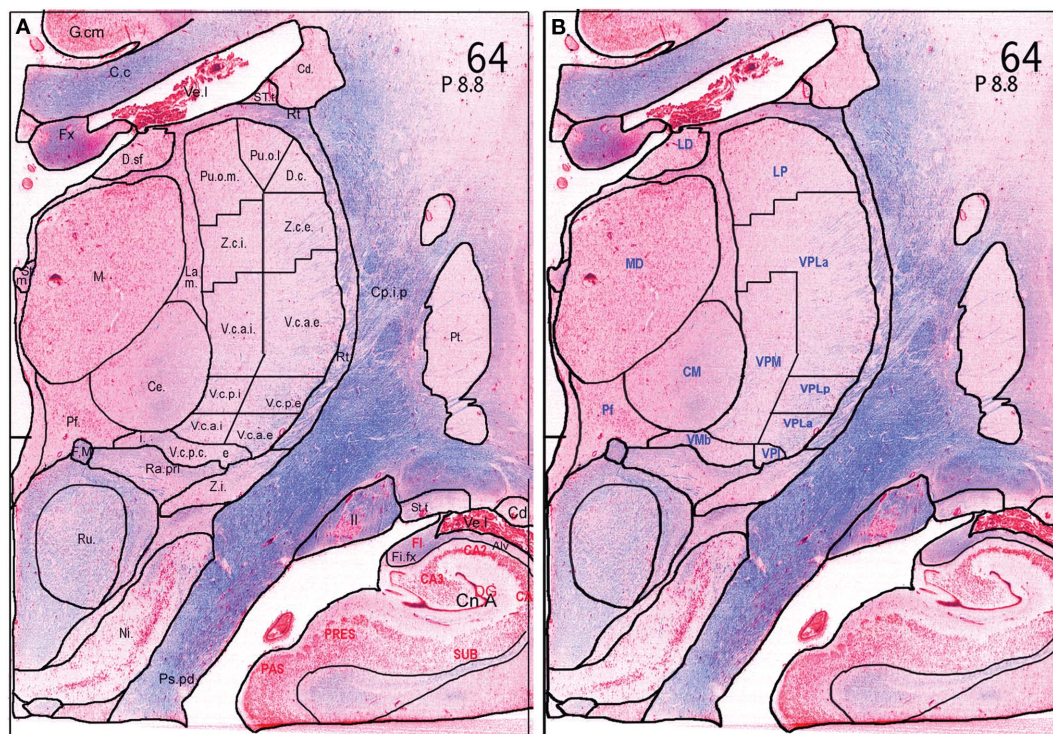
A methodology was then developed to create a customized version of the Schaltenbrand and Wahren atlas which can be automatically integrated to a patient's MRI scan on a routine basis. The reconstructed 3D digital atlas was first warped to fit Colin27, a widely used high resolution, high signal-to-noise canonical reference MRI volume, which is derived by averaging 27 T1-weighted MRI scans of the same participant (Collins et al., 1995; Holmes et al., 1998). Two hundred fifty homologous point-pairs of landmarks were manually identified on both the digitized atlas and the canonical volume using REGISTER (Macdonald et al., 1994). The volumetric version of the Schaltenbrand atlas was then warped to the reference MRI using Bookstein's 3D thin-plate-spline interpolation approach (Bookstein, 1989). The result of this initial labor-intensive step is a 3D volumetric MRI-integrated reference atlas of the basal ganglia and thalamus.

The MRI-integrated reference digital atlas may then be integrated to individual patient MRI scans using a non-labor-intensive automated process. An automated non-linear intensity matching algorithm, ANIMAL (Collins et al., 1995), is applied to generate a transform which matches a patient's MRI to the Colin27 MRI average. Application of the inverse of this transformation allows integration of the 3D digital atlas into the patient's MRI reference space. The MRI-integrated atlas can also be used in the VIPER stereotactic platform, which allows visualization of stereotactic targets, neurosurgical instruments (deep brain stimulation leads, leukotomes, retractable searching electrodes), and lesions in the atlas and MRI spaces (St-Jean et al., 1998).

DEVELOPMENT OF A HIGHER RESOLUTION 3D DIGITIZED ATLAS WITH INCORPORATION OF MULTIPLE NOMENCLATURES OF NUCLEI OF THE THALAMUS, BASAL GANGLIA, AND BASAL FOREBRAIN

While the previously described 3D atlas proved very useful (St-Jean et al., 1998; Atkinson et al., 2002; Strafella et al., 2004; Duval et al., 2006; Van Der Werf et al., 2006; Tyvaert et al., 2009;

In order to develop a tool for visualization and understanding of the 3D relationships of the basal ganglia, thalamus, and basal forebrain, two atlas data sets were derived from the contours manually defined on the original histological data. The first, a voxel-based atlas, was created with labels assigned to each voxel of the reconstructed histological volume, facilitating investigation of the nuclear boundaries when navigating through the transverse, sagittal, or coronal slices of the volume (**Figures 2A–D**). The second is a geometric atlas which extracts structures using a marching cubes algorithm (Cline et al., 1987), and enables visualization of the 3D relationship of subcortical nuclei and tracts. The result is a volumetric 3D atlas with 105 separately labeled structures including the basal ganglia, thalamus, subthalamic area, basal forebrain, and temporal lobe (**Figure 2I**).



September 2011 | Volume 5 | Article 71 | 439

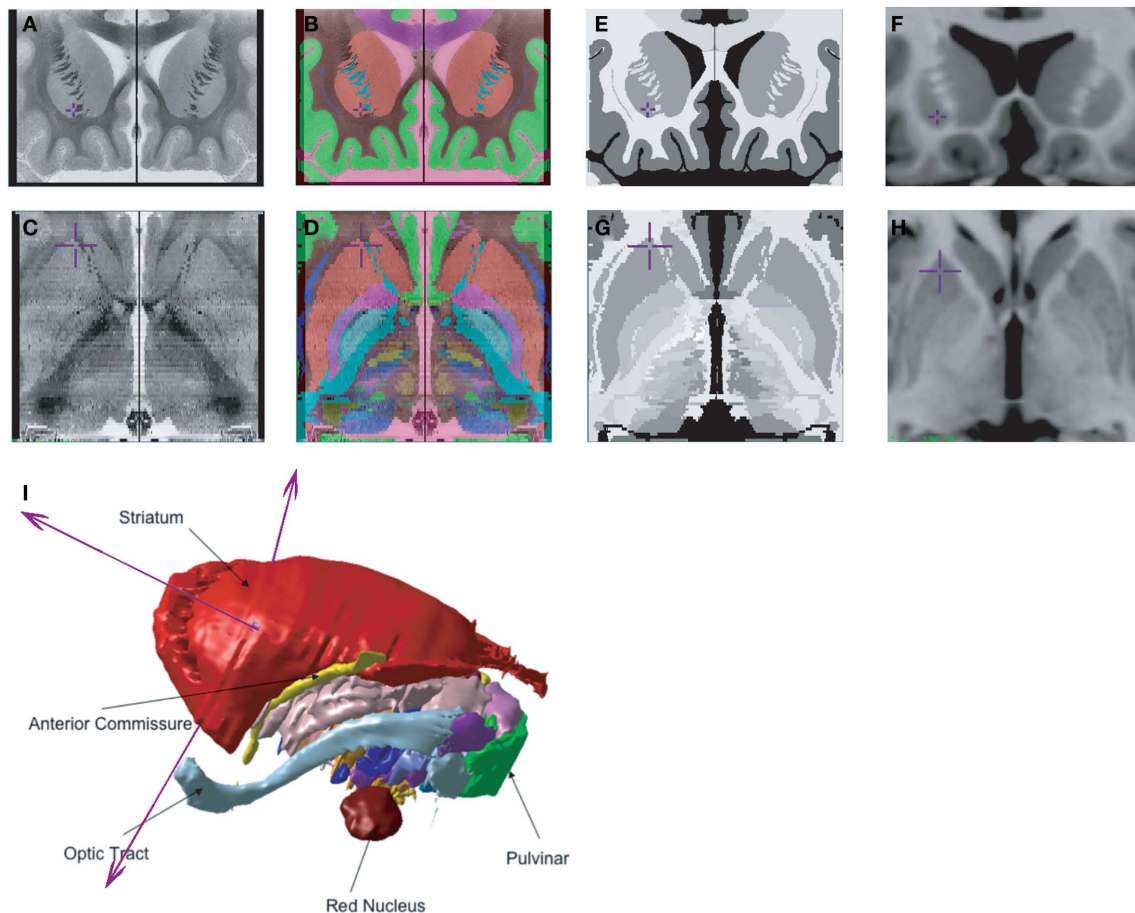


FIGURE 2 | Different 3D atlas representations and integration with a high-contrast, high-resolution MRI (Colin27) (A). Histological volume created from the original coronal data (C). Axial reconstruction of the histological volume created from the original coronal brain slices (B). Coronal voxel-label atlas created from the contours identified on the histological atlas (D). Reformatted axial views created from the 3D voxel-label atlas (E,G). Pseudo-MRI from original coronal

data (E), with a reformatted axial view (G). The pseudo-MRI is created by modifying the intensity of the labels in the voxel-label atlas (B) to a high-contrast, high-resolution MRI templates (F,H). The pseudo-MRI is then used to estimate a non-linear transformation which matches the atlas to a high-resolution template MRI volume, or directly to a patient or participant's MRI (I). 3D geometric atlas created from the 3D surface rendering of labels in the voxel-label atlas (B).

Once the 3D voxel-based atlas was completed, two separate methods were used to integrate the atlas to a patient or participant MRI (Holmes et al., 1998; Chakravarty et al., 2008). In the first strategy, also used in our initial atlas (St-Jean et al., 1998), multiple homologous points were identified in the atlas and on the Colin27 MRI. An affine transformation was then used to fit the atlas to the Colin27 MRI. ANIMAL can then be used to aid in atlas integration with the patient or participant MRI. In a second strategy, a novel pseudo-MRI (Figures 2E,G) was created by matching the intensity of basal ganglia nuclei, thalamus, and internal capsule in the voxel-label atlas (Figures 2B,D) to the corresponding structures on Colin27 MRI (Figures 2F,H). The pseudo-MRI atlas is then warped to the Colin27 brain using ANIMAL. The same transform is then applied to the voxel-based atlas, resulting in integration of the atlas with the Colin27 template. The resulting atlas-integrated Colin27 MRI can then be warped to the target patient MRI using standard MRI-to-MRI non-linear registration techniques such as the ANIMAL

algorithm. As an alternative, the pseudo-MRI can be directly integrated with the patient MRI, with comparable results (St-Jean et al., 1998; Chakravarty et al., 2008).

APPLICATIONS OF THE ATLASES

The two atlases have been adapted to a number of applications in human, including incorporation with a surgical planning platform (St-Jean et al., 1998), analysis of microelectrode responses in the subthalamic nucleus during cortical transcranial magnetic stimulation (Strafella et al., 2004), analysis of fMRI–EEG data in patients with epilepsy (Tyvaert et al., 2009), confirming the stereotactic position of the sensory thalamus (Figures 3A–F) by correlating the atlas with stimulation induced sensory responses (Chakravarty et al., 2005, 2008). The atlases have also been used to clarify the location of effective thalamic lesions for medically intractable tremor, and in determining the position of deep brain stimulation electrodes (Atkinson et al., 2002). Display of lesions, or active electrode contacts from multiple patients, in a common probabilistic

atlas-integrated space, allows for statistical analysis of differences in clinical outcome. For example, our recent analysis of (Chakravarty et al., 2006b) motor outcome after subthalamic stimulation indicates that the most effective electrodes for relief of appendicular manifestations of Parkinson's disease (**Figures 4A–C**) are located in the posterior and lateral part of the subthalamic nucleus, and dorsal to the nucleus, in the region of the zona incerta and ventral thalamus (Chakravarty et al., 2006b; Sadikot et al., 2006).

In addition to surgical targeting, the VIPER platform provides a useful method for virtual *in vivo* “histological” analysis of effective and less effective lesions or DBS lead positions for tremor (Atkinson et al., 2002). The MRI-integrated reference atlas was also used to display electrophysiological responses from the internal capsule or the subthalamic nucleus in a common reference space (Strafella et al., 2004; Duerden et al., 2011). Finally, the atlases are also used in analysis of subcortical functional activation in multiple modalities, including PET and fMRI. For example, the atlas was recently used to demonstrate that activation of intralaminar nuclei occurs prior to anterior thalamic nuclei in patients with generalized spike and wave epilepsy studied by fMRI–EEG (Tyvaert et al., 2009).

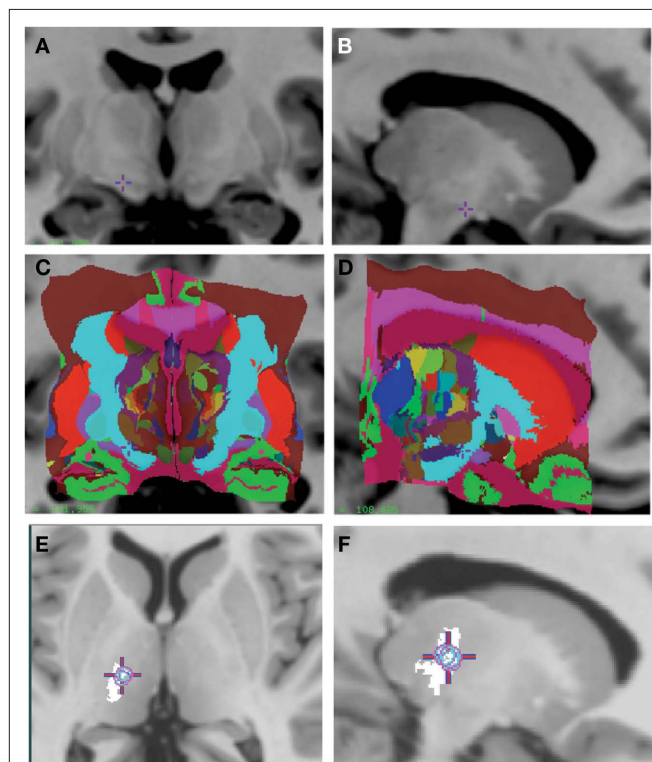


FIGURE 3 | (A–D) Voxel-label atlas of the basal ganglia and thalamus integrated into a high-contrast high-resolution MRI (Colin27). **(E,F)** The sensory thalamus is isolated in the atlas and represented on coronal and sagittal views. The average stereotactic position of the somatosensory responses obtained during stereotactic neurosurgery in the thalamus from nine patients is integrated into the same MRI. The somatosensory responses were obtained using a curved retractable stimulator, and the position of hand/arm area responses from multiple patients was analyzed in the atlas-integrated reference space. The circle represents the 90% probability map of somatosensory responses, which map to the rostral portion of the ventral posterior somatosensory nucleus of the thalamus.

DISCUSSION

When digital atlases were first used for integration with patient's stereotactic ventriculograms, CT scans, or MRI scans, linear transformations mapping the atlas to patient data were estimated to register an atlas to an individual patient scan (Bertrand et al., 1973; Hardy et al., 1980a,b, 1981; Yoshida, 1987; Yeo and Nowinski, 1997). Atlas integration by simple linear scaling of axial, sagittal, or coronal data sets is limited by the fact that the three planes are necessarily derived from different hemispheres of different individuals. This results in variations of the position of structures in stereotaxic space (Niemann and van Nieuwenhofen, 1999; Nowinski, 2004; Nowinski et al., 2007), which is especially important to note when attempting to scale the three representations of nuclear structures into the triplanar MRI space of a patient or individual participant. Attempts at creating 3D atlas versions from histological data are limited by the quality, triplanar anatomical correspondence, and resolution of the initial data set. We have developed methods for partially correcting for artifacts resulting from variations in staining intensity, shear, and inter-slice distance variations, allowing creation of a lower resolution 3D data set based on the Schaltenbrand and Wahren Atlas. The

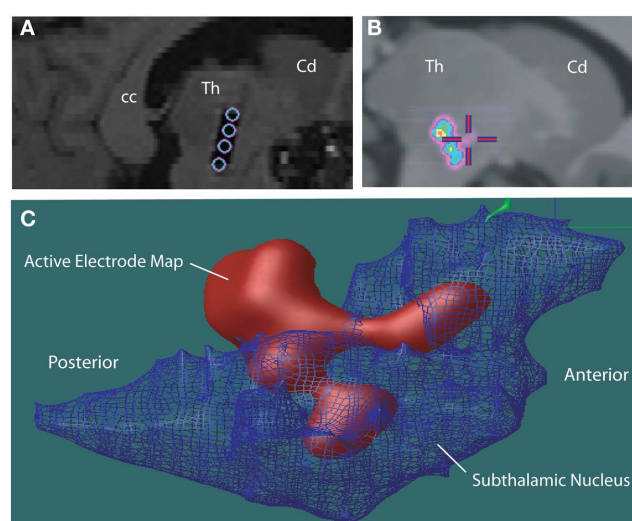


FIGURE 4 | (A) Post-operative sagittal T1-weighted MRI scan of a patient who underwent insertion of subthalamic stimulators for Parkinson's disease. The hypointense signal artifact shows the four electrode contacts (Medtronic 3387) that traverse the subthalamic nucleus, identified during surgery using an array of five microelectrodes (“Ben’s Gun” array). The electrode contacts are within, and dorsal to the subthalamic nucleus. Abbreviations: cc, corpus callosum; Cd, caudate; Th, thalamus. **(B)** The automatic non-linear image matching and automatic labeling (ANIMAL) algorithm was used to integrate each patient's MRI scan with the canonical high-resolution MRI (Colin27), resulting in a common space for evaluation of electrode positions from different patients. A probabilistic average map of active contacts of subthalamic stimulators associated with the best outcome for motor symptoms of the contralateral side is shown. **(C)** The voxel-labeled 3D atlas was integrated with the probabilistic volume map of the most effective active electrode contacts in patients with Parkinson's disease with subthalamic stimulator implants. The subthalamic nucleus is represented as a net. A 90% probability map of most effective electrode positions shows they are localized in the dorsolateral subthalamic nucleus, and areas dorsal and posterior to the subthalamic nucleus, including the zona incerta, Forel's fields, and ventral thalamus.

missing inter-slice data in the original data set was accounted for using Hermite cubic polynomials allowed for creation of smooth 3D structures. The lower resolution 3D atlas was integrated to a stereotactic platform that allows surgical tool representation and creation of virtual lesions in atlas space. The utility of computerized 3D atlases can be limited by the accuracy of the method used for integration into patient or participant target imaging. In order to overcome the limitations of linear scaling methods used for atlas integration into patient data, our group was one of the first to apply non-linear transformations which warp a digital atlas to fit pre-operative or post-operative patient MRI data, accounting for local variations in the anatomy (St-Jean et al., 1998; Atkinson et al., 2002).

To improve atlas resolution, we created a new high-resolution 3D data set from histological data from a middle-aged man who died from a non-neurological cause. Thalamic atlases, especially those created for stereotactic neurosurgery, mainly use Hassler's detailed parcellation of the thalamus. More recent work has emphasized homologies between parcellations in non-human primates and humans (Jones, 2007). In the work of Hirai and Jones, cytoarchitecture and tract-tracing data based on connections of the monkey thalamus, were harmonized with that of human thalamic parcellation based on myelo-architecture and histochemical stains (Walker, 1938; Hirai and Jones, 1989b; Jones, 2007). In creating our higher resolution 3D atlas, we therefore undertook to present nomenclature using both commonly applied terminologies, allowing precise 2D and 3D homology between the nomenclature used by the Hassler school and that of Jones and Hirai. We also compared terminologies for basal forebrain and amygdala nuclei used in the Schaltenbrand atlas (Schaltenbrand and Wahren, 1977), with the more recent atlas of Paxinos and Mai (Mai et al., 2008), and the work of Brockhaus (Gloor, 1997). To date, our atlas boundaries are derived from myelin and Nissl stains. Other authors have provided important additional data sets based on chemical anatomy, particularly the calcium binding proteins, which provide useful additional information compared to traditional cytoarchitectonic and histochemical parcellations (Morel et al., 1997; Mai et al., 2004, 2008; Yelnik et al., 2007; Bhattacharjee et al., 2008; Bardinet et al., 2009; Krauth et al., 2010).

Many groups use template based procedures to warp atlases to pre-operative patient data. Once the atlas has been customized to an MRI, a non-linear transformation can be estimated to match the anatomy between the atlas and the template. Essentially, the atlas matching problem is then simplified to the standard MRI-to-MRI non-linear registration problem (Chakravarty et al., 2009). For example, D'Haese et al. developed a combined anatomical and electrophysiological atlas (D'Haese et al., 2005; Pallavaram et al., 2010) which integrated subcortical delineations and electrophysiological intraoperative recordings from the subthalamic nucleus registered to a template created from the average of pre-operative data. This group noted that the choice of template was crucial for the accuracy of subsequent atlas customization due to the dif-

fering underlying anatomies between populations suffering from neurodegenerative diseases and the template. Other groups have suggested that non-linear transformations should be used with caution in the atlas customization procedure as they may abnormally deform the morphology of the subcortical neuroanatomy (Yelnik et al., 2007; Bardinet et al., 2009). Their work uses histological and MRI data prospectively acquired from a single subject, and they demonstrate impressive target-localization accuracy using only affine transformations. The work of these authors has been validated using intraoperative recordings and post-operative electrode location.

Work from our group argues that non-linear transformations alone may be suboptimal for pre-operative atlas-based target identification (Chakravarty et al., 2009). Pre-operative planning is limited by the accuracy of the warping techniques used. Validation of non-linear registration algorithms is a notoriously difficult problem given the lack of a universally accepted "gold-standard" (Chakravarty et al., 2009; Klein et al., 2009). Many groups simply use anatomical correspondence between intraoperative recordings and post-operative electrode locations to validate their findings. However, we propose it is important to borrow heavily from the medical image processing community where several methods have been proposed for the validation of non-linear registration algorithms (Hellier et al., 2003; Robbins et al., 2004; Chakravarty et al., 2009; Klein et al., 2009).

We have applied our atlases to a wide variety of applications, including use in a stereotactic planning platform (St-Jean et al., 1998), probabilistic analysis of thalamic lesions used for alleviation of tremor (Atkinson et al., 2002), analysis of the stereotactic location of the human sensory thalamus using information obtained during intraoperative stimulation (Figures 3E,F) or following activation visualized by functional brain imaging (Chakravarty et al., 2008), probabilistic analysis of the topography and location of motor fibers of the posterior limb of the internal capsule obtained using intraoperative stimulation (Duerden et al., 2011), and probabilistic analysis of the location of effective and less effective subthalamic nucleus stimulation electrodes (Chakravarty et al., 2006b; Sadikot et al., 2006). Ongoing work includes further application of the atlas to functional neurosurgery, analysis of positions of subcortical lesions or electrodes, interpretation of subcortical functional activation data, and use with *in vivo* tractography. Future work by our group and many others, will involve creation of additional computerized atlases based on diverse chemical anatomy data, and atlas integration with functional data obtained using functional brain imaging, physiological responses obtained during neurosurgery, or with anatomical tractography information.

ACKNOWLEDGMENTS

This work was supported by grants to Abbas F. Sadikot and D. Louis Collins from the CIHR and NSERC.

REFERENCES

- Afshar, F., Watkins, E. S., and Yap, J. C. (1978). *Stereotaxic Atlas of the Human Brainstem and Cerebellar Nuclei: A Variability Study*. New York: Raven Press.
- Andrew, J., Tomlinson, J. D. W., and Watkins, E. S. (1969). *A Stereotaxic Atlas of the Human Thalamus and Adjacent Structures: A Variability Study*. Baltimore: Williams & Wilkins.
- Atkinson, J. D., Collins, D. L., Bertrand, G., Peters, T. M., Pike, G. B., and Sadikot, A. F. (2002). Optimal location of thalamotomy lesions for tremor associated with Parkinson disease: a probabilistic analysis based on postoperative magnetic resonance imaging and an integrated digital atlas. *J. Neurosurg.* 96, 854–866.
- Bardinet, E., Bhattacharjee, M., Dormont, D., Pidoux, B., Malandain, G.,

- Schupbach, M., Ayache, N., Cornu, P., Agid, Y., and Yelnik, J. (2009). A three-dimensional histological atlas of the human basal ganglia. II. Atlas deformation strategy and evaluation in deep brain stimulation for Parkinson disease. *J. Neurosurg.* 110, 208–219.
- Berks, G., Pohl, G., and Keyserlingk, D. G. (2001). 3D-VIEWER: an atlas-based system for individual and statistical investigations of the human brain. *Methods Inf. Med.* 40, 170–177.
- Bertrand, G., Oliver, A., and Thompson, C. J. (1973). The computerized brain atlas: its use in stereotaxic surgery. *Trans. Am. Neurol. Assoc.* 98, 233.
- Bhattacharjee, M., Pitiot, A., Roche, A., Dormont, D., and Bardin, E. (2008). Anatomy-preserving nonlinear registration of deep brain ROIs using confidence-based block-matching. *Med. Image Comput. Assist. Interv.* 11, 956–963.
- Bookstein, F. L. (1989). Principal warps – thin-plate splines and the decomposition of deformations. *IEEE Trans. Pattern Anal. Mach. Intell.* 11, 567–585.
- Chakravarty, M. M., Bertrand, G., Hodge, C. P., Sadikot, A. F., and Collins, D. L. (2006a). The creation of a brain atlas for image guided neurosurgery using serial histological data. *Neuroimage* 30, 359–376.
- Chakravarty, M. M., Sadikot, A. F., Mongia, S., Bertrand, G., and Collins, D. L. (2006b). Towards a multi-modal atlas for neurosurgical planning. *Med. Image Comput. Assist. Interv.* 9, 389–396.
- Chakravarty, M. M., Sadikot, A. F., Germann, J., Bertrand, G., and Collins, D. L. (2005). Anatomical and electrophysiological validation of an atlas for neurosurgical planning. *Med. Image Comput. Assist. Interv.* 8, 394–401.
- Chakravarty, M. M., Sadikot, A. F., Germann, J., Bertrand, G., and Collins, D. L. (2008). Towards a validation of atlas warping techniques. *Med. Image Anal.* 12, 713–726.
- Chakravarty, M. M., Sadikot, A. F., Germann, J., Hellier, P., Bertrand, G., and Collins, D. L. (2009). Comparison of piece-wise linear, linear, and non-linear atlas-to-patient warping techniques: analysis of the labeling of subcortical nuclei for functional neurosurgical applications. *Hum. Brain Mapp.* 30, 3574–3595.
- Cline, H. E., Dumoulin, C. L., Hart, H. R. Jr., Lorensen, W. E., and Ludke, S. (1987). 3D reconstruction of the brain from magnetic resonance images using a connectivity algorithm. *Magn. Reson. Imaging* 5, 345–352.
- Collins, D. L., Evans, A. C., Holmes, C., and Peters, T. M. (1995). Automatic 3D segmentation of neuro-anatomical structures from MRI. *Inf. Process. Med. Imaging* 3, 139–152.
- D'Haese, P. F., Cetinkaya, E., Konrad, P. E., Kao, C., and Dawant, B. M. (2005). Computer-aided placement of deep brain stimulators: from planning to intraoperative guidance. *IEEE Trans. Med. Imaging* 24, 1469–1478.
- Duerden, E. G., Finniss, K. W., Peters, T. M., and Sadikot, A. F. (2011). Three-dimensional somatotopic organization and probabilistic mapping of motor responses from the human internal capsule. *J. Neurosurg.* 114, 1706–1714.
- Duval, C., Panisset, M., Strafella, A. P., and Sadikot, A. F. (2006). The impact of ventrolateral thalamotomy on tremor and voluntary motor behavior in patients with Parkinson's disease. *Exp. Brain Res.* 170, 160–171.
- Gloor, P. (1997). *The Temporal Lobe and Limbic System*. New York: Oxford University Press.
- Hardy, T. L., Bertrand, G., and Thompson, C. J. (1979a). The position and organization of motor fibers in the internal capsule found during stereotactic surgery. *Appl. Neurophysiol.* 42, 160–170.
- Hardy, T. L., Bertrand, G., and Thompson, C. J. (1979b). Thalamic recordings during stereotactic surgery. I. Surgery topography of evoked and nonevoked rhythmic cellular activity. *Appl. Neurophysiol.* 42, 185–197.
- Hardy, T. L., Bertrand, G., and Thompson, C. J. (1979c). Thalamic recordings during stereotactic surgery. II. Location of quick-adapting touch-evoked (novelty) cellular responses. *Appl. Neurophysiol.* 42, 198–202.
- Hardy, T. L., Bertrand, G., and Thompson, C. J. (1980a). Organization and topography of sensory responses in the internal capsule and nucleus ventralis caudalis found during stereotactic surgery. *Appl. Neurophysiol.* 42, 335–351.
- Hardy, T. L., Bertrand, G., and Thompson, C. J. (1980b). Position and organization of thalamic cellular activity during diencephalic recording. I. Pressure-evoked activity. *Appl. Neurophysiol.* 43, 18–27.
- Hardy, T. L., Bertrand, G., and Thompson, C. J. (1981). Touch-evoked thalamic cellular activity. The variable position of the anterior border of somesthetic SI thalamus and somatotopy. *Appl. Neurophysiol.* 44, 302–313.
- Hardy, T. L., Smith, J. R., Brynildson, L. R., Flanagan, H. F., Gray, J. G., and Spurlock, D. (1992). Magnetic resonance imaging and anatomic atlas mapping for thalamotomy. *Stereotact. Funct. Neurosurg.* 58, 30–32.
- Hassler, R., Mundinger, F., and Riechert, T. (1965). Correlations between clinical and autaptic findings in stereotaxic operations of parkinsonism. *Confin. Neurol.* 26, 282–290.
- Heimer, L., Harlan, R. E., Alheid, G. F., Garcia, M. M., and de Olmos, J. (1997). Substantia innominata: a notion which impedes clinical-anatomical correlations in neuropsychiatric disorders. *Neuroscience* 76, 957–1006.
- Hellier, P., Barillot, C., Corouge, I., Gibaud, B., Le Goualher, G., Collins, D. L., Evans, A., Malandain, G., Ayache, N., Christensen, G. E., and Johnson, H. J. (2003). Retrospective evaluation of intersubject brain registration. *IEEE Trans. Med. Imaging* 22, 1120–1130.
- Hirai, T., and Jones, E. G. (1989a). Distribution of tachykinin- and enkephalin-immunoreactive fibers in the human thalamus. *Brain Res. Brain Res. Rev.* 14, 35–52.
- Hirai, T., and Jones, E. G. (1989b). A new parcellation of the human thalamus on the basis of histochemical staining. *Brain Res. Brain Res. Rev.* 14, 1–34.
- Holmes, C. J., Hoge, R., Collins, L., Woods, R., Toga, A. W., and Evans, A. C. (1998). Enhancement of MR images using registration for signal averaging. *J. Comput. Assist. Tomogr.* 22, 324–333.
- Jones, E. G. (2007). *The Thalamus*. Cambridge, NY: Cambridge University Press.
- Kazarnovskaya, M. I., Borodkin, S. M., Shabalov, V. A., Krivosheina, V. Y., and Golanov, A. V. (1991). 3-D computer model of subcortical structures of human brain. *Comput. Biol. Med.* 21, 451–417.
- Klein, A., Andersson, J., Ardekani, B. A., Ashburner, J., Avants, B., Chiang, M. C., Christensen, G. E., Collins, D. L., Gee, J., Hellier, P., Song, J. H., Jenkinson, M., Lepage, C., Rueckert, D., Thompson, P., Vercauteren, T., Woods, R. P., Mann, J. J., and Parsey, R. V. (2009). Evaluation of 14 nonlinear deformation algorithms applied to human brain MRI registration. *Neuroimage* 46, 786–802.
- Krauth, A., Blanc, R., Poveda, A., Jeanmonod, D., Morel, A., and Szekely, G. (2010). A mean three-dimensional atlas of the human thalamus: generation from multiple histological data. *Neuroimage* 49, 2053–2062.
- Macdonald, D., Avis, D., and Evans, A. C. (1994). Multiple surface identification and matching in magnetic-resonance images. *Vis. Biomed. Comput.* 2359, 160–169.
- Mai, J. K., Assheuer, J., and Paxinos, G. (1994). *Atlas of the Human Brain*. Amsterdam: Elsevier Academic Press.
- Mai, J. K., Voss, T., and Paxinos, G. (2008). *Atlas of the Human Brain*. Amsterdam: Elsevier Academic Press.
- Malandain, G., Bardin, E., Nelissen, K., and Vanduffel, W. (2004). Fusion of autoradiographs with an MR volume using 2-D and 3-D linear transformations. *Neuroimage* 23, 111–127.
- Morel, A., Magnin, M., and Jeanmonod, D. (1997). Multiarchitectonic and stereotactic atlas of the human thalamus. *J. Comp. Neurol.* 387, 588–630.
- Niemann, K., Naujokat, C., Pohl, G., Wollner, C., and von Keyserlingk, D. (1994). Verification of the Schaltenbrand and Wahren stereotactic atlas. *Acta Neurochir. (Wien)* 129, 72–81.
- Niemann, K., and van Nieuwenhofen, I. (1999). One atlas – three anatomies: relationships of the Schaltenbrand and Wahren microscopic data. *Acta Neurochir. (Wien)* 141, 1025–1038.
- Nowinski, W. L. (2004). Co-registration of the Schaltenbrand-Wahren microseries with the probabilistic functional atlas. *Stereotact. Funct. Neurosurg.* 82, 142–146.
- Nowinski, W. L., Belov, D., Thirunavukarasu, A., and Benabid, A. L. (2005). A probabilistic functional atlas of the VIM nucleus constructed from pre-, intra- and postoperative electrophysiological and neuroimaging data acquired during the surgical treatment of Parkinson's disease patients. *Stereotact. Funct. Neurosurg.* 83, 190–196.
- Nowinski, W. L., Fang, A., Nguyen, B. T., Raphael, J. K., Jagannathan, L., Raghavan, R., Bryan, R. N., and Miller, G. A. (1997). Multiple brain atlas database and atlas-based neuroimaging system. *Comput. Aided Surg.* 2, 42–66.
- Nowinski, W. L., Liu, J., and Thirunavukarasu, A. (2008). Quantification and visualization of three-dimensional inconsistency of the ventrointermediate nucleus of the thalamus in the Schaltenbrand-Wahren brain atlas. *Acta Neurochir.* 150, 647–653; discussion 653.
- Nowinski, W. L., Thirunavukarasu, A., Liu, J., and Benabid, A. L. (2007). Correlation between the anatomical and functional human subthalamic nucleus. *Stereotact. Funct. Neurosurg.* 85, 88–93.
- Olszewski, J., and Baxter, D. W. (1954). *Cytoarchitecture of the Human Brain Stem*. Philadelphia: Lippincott.
- Pallavaram, S., Dawant, B. M., Remple, M. S., Neimat, J. S., Kao, C., Konrad, P. E., and D'Haese, P. F. (2010). Effect of brain shift on the creation of functional atlases for deep brain stimulation surgery. *Int. J. Comput. Assist. Radiol. Surg.* 5, 221–228.
- Robbins, S., Evans, A. C., Collins, D. L., and Whitesides, S. (2004). Tuning and comparing spatial normalization methods. *Med. Image Anal.* 8, 311–323.

- Sadikot, A., Mongia, S., Chakravarty, M., Panisset, M., and Collins, D. (2006). *A Novel Probabilistic Analysis of Electrode Positions in the Subthalamic Nucleus Related to Clinical Outcome*. San Francisco: American Association of Neurological Surgeons.
- Sather, M. D., and Patil, A. A. (2007). Direct anatomical localization of the subthalamic nucleus on CT with comparison to Schaltenbrand-Wahren atlas. *Stereotact. Funct. Neurosurg.* 85, 1–5.
- Schaltenbrand, G., and Bailey, P. (1959). *Einführung in die Stereotaktischen Operationen, mit einem Atlas des menschlichen Gehirns. Introduction to Stereotaxis, with an Atlas of the Human Brain*. Stuttgart: Thieme.
- Schaltenbrand, G., and Wahren, W. (1977). *Atlas for Stereotaxy of the Human Brain*. Chicago: Year Book Medical Publishers.
- Sramka, M., Ruzicky, E., and Novotny, M. (1997). Computerized brain atlas in functional neurosurgery. *Stereotact. Funct. Neurosurg.* 69, 93–8.
- St-Jean, P., Sadikot, A. F., Collins, L., Clonda, D., Kasrai, R., Evans, A. C., and Peters, T. M. (1998). Automated atlas integration and interactive three-dimensional visualization tools for planning and guidance in functional neurosurgery. *IEEE Trans. Med. Imaging* 17, 672–680.
- Strafella, A. P., Vanderwerf, Y., and Sadikot, A. F. (2004). Transcranial magnetic stimulation of the human motor cortex influences the neuronal activity of subthalamic nucleus. *Eur. J. Neurosci.* 20, 2245–2249.
- Talairach, J. (1957). *Atlas d'anatomie stéréotaxique: repérage radiologique indirect des noyaux gris centraux des régions mésencéphalo-sous-optique et hypothalamique de l'homme*. Paris: Masson.
- Talairach, J., and Tournoux, P. (1988). *Co-Planar Stereotaxic Atlas of the Human Brain: 3-Dimensional Proportional System: An Approach to Cerebral Imaging*. Stuttgart: G. Thieme; New York: Thieme Medical Publishers.
- Tyvaert, L., Chassagnon, S., Sadikot, A., Levan, P., Dubeau, F., and Gotman, J. (2009). Thalamic nuclei activity in idiopathic generalized epilepsy: an EEG-fMRI study. *Neurology* 73, 2018–2022.
- Van Buren, J. M., and Borke, R. C. (1972). *Variations and Connections of the Human Thalamus*. Berlin, NY: Springer-Verlag.
- Van Buren, J. M., and Maccubbin, D. A. (1962). An outline atlas of the human basal ganglia with estimation of anatomical variants. *J. Neurosurg.* 19, 811–839.
- Van Der Werf, Y. D., Sadikot, A. F., Strafella, A. P., and Paus, T. (2006). The neural response to transcranial magnetic stimulation of the human motor cortex. II. Thalamocortical contributions. *Exp Brain Res.* 175, 246–255.
- Walker, A. E. (1938). *The Primate Thalamus*. Chicago, IL: The University Press.
- Yelnik, J., Bardin, E., Dormont, D., Malandain, G., Ourselin, S., Tande, D., Karachi, C., Ayache, N., Cornu, P., and Agid, Y. (2007). A three-dimensional, histological and deformable atlas of the human basal ganglia. I. Atlas construction based on immunohistochemical and MRI data. *Neuroimage* 34, 618–638.
- Yelnik, J., Damier, P., Bejjani, B. P., Francois, C., Gervais, D., Dormont, D., Arnulf, I., Bonnet, M. A., Cornu, P., Pidoux, B., and Agid, Y. (2000). Functional mapping of the human globus pallidus: contrasting effect of stimulation in the internal and external pallidum in Parkinson's disease. *Neuroscience* 101, 77–87.
- Yeo, T. T., and Nowinski, W. L. (1997). Functional neurosurgery aided by use of an electronic brain atlas. *Acta Neurochir. Suppl.* 68, 93–99.
- Yoshida, M. (1987). Creation of a three-dimensional atlas by interpolation from Schaltenbrand-Bailey's atlas. *Appl. Neurophysiol.* 50, 45–48.

Conflict of Interest Statement: The authors declare that the research was conducted in the absence of any commercial or financial relationships that could be construed as a potential conflict of interest.

Received: 13 May 2011; paper pending published: 05 June 2011; accepted: 08 August 2011; published online: 06 September 2011.
Citation: Sadikot AF, Chakravarty MM, Bertrand G, Rymar VV, Al-Subaie F and Collins DL (2011) Creation of computerized 3D MRI-integrated atlases of the human basal ganglia and thalamus. *Front. Syst. Neurosci.* 5:71. doi: 10.3389/fnsys.2011.00071
Copyright © 2011 Sadikot, Chakravarty, Bertrand, Rymar, Al-Subaie and Collins. This is an open-access article subject to a non-exclusive license between the authors and Frontiers Media SA, which permits use, distribution and reproduction in other forums, provided the original authors and source are credited and other Frontiers conditions are complied with.



Chaotic desynchronization as the therapeutic mechanism of deep brain stimulation

Charles J. Wilson^{1*}, Bryce Beverlin II² and Theoden Netoff³

¹ Department of Biology, University of Texas at San Antonio, San Antonio, TX, USA

² School of Physics and Astronomy, University of Minnesota, Minneapolis, MN, USA

³ Department of Biomedical Engineering, University of Minnesota, Minneapolis, MN, USA

Edited by:

James M. Tepper, Rutgers, The State University of New Jersey, USA

Reviewed by:

Thomas Wichman, Emory University, USA

Robert S. Turner, University of Pittsburgh, USA

*Correspondence:

Charles J. Wilson, Department of Biology, University of Texas at San Antonio, One UTSA Circle, San Antonio, TX 78249, USA.

e-mail: charles.wilson@utsa.edu

High frequency deep-brain stimulation of the subthalamic nucleus (deep brain stimulation, DBS) relieves many of the symptoms of Parkinson's disease in humans and animal models. Although the treatment has seen widespread use, its therapeutic mechanism remains paradoxical. The subthalamic nucleus is excitatory, so its stimulation at rates higher than its normal firing rate should worsen the disease by increasing subthalamic excitation of the globus pallidus. The therapeutic effectiveness of DBS is also frequency and intensity sensitive, and the stimulation must be periodic; aperiodic stimulation at the same mean rate is ineffective. These requirements are not adequately explained by existing models, whether based on firing rate changes or on reduced bursting. Here we report modeling studies suggesting that high frequency periodic excitation of the subthalamic nucleus may act by desynchronizing the firing of neurons in the globus pallidus, rather than by changing the firing rate or pattern of individual cells. Globus pallidus neurons are normally desynchronized, but their activity becomes correlated in Parkinson's disease. Periodic stimulation may induce chaotic desynchronization by interacting with the intrinsic oscillatory mechanism of globus pallidus neurons. Our modeling results suggest a mechanism of action of DBS and a pathophysiology of Parkinsonism in which synchrony, rather than firing rate, is the critical pathological feature.

Keywords: basal ganglia, deep brain stimulation, Parkinson's disease

INTRODUCTION

The motor symptoms of Parkinson's disease have long been attributed to increased firing rates of neurons in the globus pallidus, which then are thought to inhibit thalamic neurons relaying signals to the motor cortex (for reviews see Albin et al., 1989; Wichmann and DeLong, 1996). An alternative explanation is based on the observation that pallidal and subthalamic neurons in animal models of the disease exhibit low frequency rhythmic bursting not normally present (e.g., Bergman et al., 1994; Raz et al., 2000). Bursting occurs near the tremor frequency (7–10 Hz), and the normally uncorrelated firing across cells becomes synchronized at about twice that frequency (Nini et al., 1995). Local field potentials show a large increase in power in the beta band (the frequency of synchrony; Dostrovsky and Bergman, 2004; Gatev et al., 2006; Brown, 2007). If the change in firing pattern, and not rate, causes the symptoms of Parkinson's disease, then the beneficial effects (e.g., Wichmann and DeLong, 2006) of deep brain stimulation (DBS) may act by disrupting the pathological pattern, either the low frequency bursting, or the synchronous firing, or both (Rubin and Terman, 2004; Guo et al., 2008; Dorval et al., 2010; Schiff, 2010). A computational model has been proposed for the oscillations and the therapeutic mechanism of DBS (Rubin and Terman, 2004; Guo et al., 2008). It assumes that DBS entrains the globus pallidus cells, increasing synchrony but abolishing beta oscillations. This is thought to regularize pallidothalamic inhibition and allow blocked signals to traverse the thalamus to the motor cortex. In this model, any stimulus that can entrain the globus pallidus at rates faster than the burst frequency, and thereby suppress the low frequency oscillations that engage the

intrinsic resonance of the thalamus, should abolish the symptoms. It does not directly address the mechanism of frequency specificity of the stimulus. Furthermore, it has recently been shown that the effectiveness of DBS depends on the periodicity of the stimulation (Dorval et al., 2010); Poisson patterns of stimulation at the same mean frequency were much less effective. This suggests that the effectiveness of DBS may depend on some dynamic process unique to periodically driven systems.

Here we present an alternative hypothesis, that DBS does not entrain the neurons but instead disrupts population synchrony. Basal ganglia output neurons are autonomous oscillators that fire rhythmically when isolated from synaptic inputs (Atherton and Bevan, 2005; Kita et al., 2005). Periodically driven oscillators, including neurons, exhibit several different patterns of synchrony depending on stimulus intensity and frequency: phase-shifting, phase locking, and chaos (e.g., Glass and Mackey, 1988; Elbert et al., 1994; Kaplan et al., 1996). During stimulus driven phase locking, the trajectories of cells that are out of phase with each other will converge, and synchrony of the network will increase. However, when the periodic stimulus evokes a chaotic response, nearby trajectories diverge, and the oscillators are actively desynchronized.

MATERIALS AND METHODS

CONSTRUCTION OF DETERMINISTIC PHASE MAPS

When a periodically firing neuron is perturbed by an injected (or synaptic) current, it may alter the neuron's phase, making it fire earlier or later than it would have otherwise. The degree to which a stimulus may alter the timing of the next action

potential depends upon the phase in the cell's oscillation at which it is applied. By stimulating the neuron at different phases and measuring the resulting change in spike timing, a phase-resetting curve (PRC) can be calculated (for review see Gutkin et al., 2005). For a neuron firing with period T_c and being stimulated by a periodic stimulus with period T_s the relative timing between the stimulus and the neuron's action potential ts_{i+1} , can be calculated from the timing of the previous stimulus ts_i using a map. Notation used is indicated in **Figure 1**. The change in interspike interval (ISI) Δt caused by the stimulus is determined by the cell's PRC. By dividing the time of the stimulus relative to the previous action potential by the cell's period we can determine its phase. The stimulus phase on the next cycle can be calculated as:

$$\frac{ts_{i+1}}{T_c} = \frac{ts_i}{T_c} + m_s * \text{PRC}\left[\frac{ts_i}{T_c}\right] - 1 + \frac{T_s}{T_c},$$

in which the PRC is scaled by the size and sign of the stimulus, m_s . For our purposes, all phases were defined relative to the cell's period T_c . By substituting $\phi_i = ts_i/T_c$ the map of stimulus phase relative to action potential firing can be rewritten as:

$$\phi_{i+1} = \phi_i + m_s * \text{PRC}[\phi_i] - 1 + \frac{T_s}{T_c}.$$

A similar approach is taken when we need to calculate the timing of action potentials relative to the stimulus, for example in calculating the peristimulus histogram.

$$\frac{tr_{i+1}}{T_c} = \frac{tr_i}{T_c} + m_s * \text{PRC}\left[1 - \frac{tr_i}{T_c}\right] + 1 - \frac{T_s}{T_c}$$

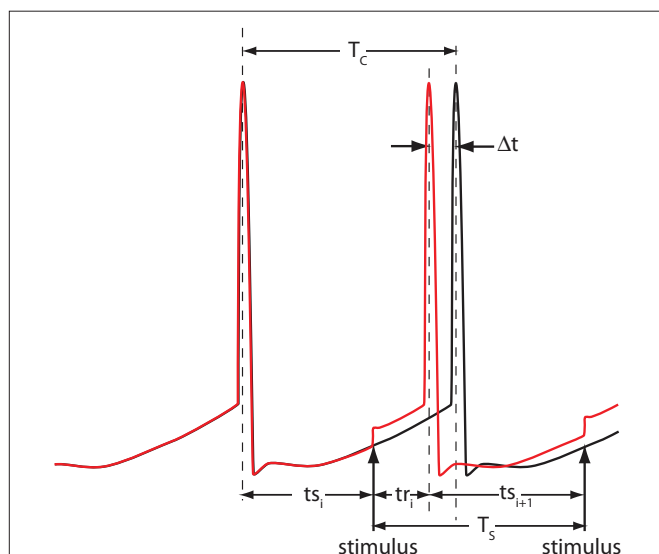


FIGURE 1 | Notation. Two trajectories of a spontaneously active neuron firing with period T_c are shown, one unperturbed (black) and one perturbed by the stimulus presented at period T_s . The phase-dependent change in the period caused by the stimulus is Δt . Stimulation latencies relative to cell firing are indicated by ts , and response latencies relative to the stimulus are labeled tr .

We used a PRC shape measured from a simplified conductance-based model of the basal ganglia output cells that we based on data from Atherton and Bevan (2005). It consisted of a low threshold persistent sodium current, a fast sodium action potential current, a high-threshold spike repolarization potassium current, a high-threshold calcium current, calcium pump, and a calcium-dependent potassium current. The model is not an accurate representation of all the firing patterns reported for the substantia nigra pars reticulata neuron, but did reproduce the basic pattern of spontaneous activity. Its PRC was similar to that reported for a more complex model of the cells of the external segment of globus pallidus (whose firing patterns are similar) by Schultheiss et al. (2010). The specific PRC used was:

$$\begin{aligned} \text{PRC}[\Phi] = & (0.325 - 0.299 * \cos[2\pi\Phi] - 0.013 * \cos[2\pi2 * \Phi] \\ & - 0.005 * \cos[2\pi3 * \Phi] \\ & - 0.003 * \cos[2\pi4 * \Phi] - 0.129 * \sin[2\pi\Phi] \\ & + 0.017 * \sin[2\pi2 * \Phi] \\ & + 0.006 * \sin[2\pi3 * \Phi] + 0.003 * \sin[2\pi4 * \Phi]). \end{aligned}$$

At high stimulus intensities, the PRC approaches a causal limit, corresponding to immediate firing in response to the stimulus. This limit, the resetting line, has a slope of -1 . For large stimuli, the PRC is partly absorbed into the phase resetting line. This was incorporated into the definition of the PRC used here.

The behavior of the neuron in response to periodic inputs can take on three different forms, entrainment, quasiperiodicity, or chaos. When entrained to the stimulus, cells receiving the stimulus will converge in phase. In quasiperiodicity, their patterns of activity are complex but two neurons starting at nearly the same phase will on average retain their phase difference. Chaotic activity is aperiodic and two neurons starting at nearly the same phase will rapidly diverge in the timing of their firing. To characterize the three patterns of response, we calculated the Lyapunov exponent of the response. This was done by calculating the phases repeatedly from an arbitrary starting point. After 500 initial iterations, the map was iterated an additional 10,000 times. At each of these, the slope of the map was calculated at the new phase point, and the log of the absolute value of the slope at visited phase points was averaged across the 10,000 cycles.

CONSTRUCTION OF THE STOCHASTIC PHASE MAP

The PRC represents an idealized version of the response of a repetitively firing neuron to stimulation. The most significant simplification is that it ignores the variability in the cell's ISI. The neuron's spike times can vary from interval to interval due to unaccounted-for external inputs or intrinsic noise in the neuron's membrane. Noise produces many small phase perturbations during each ISI. When a neuron receives multiple stimuli during a single ISI, the phase is shifted after each one, causing phase to become decoupled from time. This "latent phase" (Winfree, 2000) can only be realized when the neuron fires an action potential.

The distribution of latent phases of stimulation caused by noise can be inferred from the distribution of ISIs observed in the absence of stimulation. The effect of this uncertainty in the latent phase of the stimulus on the PRC has been described by

Ermentrout et al. (2011), who also describe an approximation to the variance of the PRC as a function of mean latent phase of the stimulus. Using this approach, we represented each point in the PRC as a probability distribution of the phase change caused by an input. This probabilistic PRC was used to make a stochastic phase map that takes as input the probability distribution of neuron phases for the i th stimulus and calculates the distribution for the $(i + 1)$ th iteration. The mean value at each phase corresponds to the deterministic phase map and the variance is altered according to the variance of the PRC at that mean phase. Phase (as a proportion of the ISI) was divided into 200 increments, and the stochastic map was instantiated as a 200×200 stochastic matrix. Each row in the matrix was a normal distribution with a mean equal to the mean value of the PRC at that phase, and with variance calculated as in Ermentrout et al. (2011).

The steady-state probability distribution of the stimulus phases of the neurons to periodic stimulation can be determined from the stochastic map matrix by taking the largest eigenvector, λ corresponding to the largest eigenvalue. The Lyapunov exponent is the log of the average slope of the map and can be calculated as:

$$LE = \int_0^1 \lambda(\phi) \log[1 + m_s * PRC'(\phi)] d\phi,$$

in which the slope of the PRC at each phase $[PRC'(\phi)]$ is weighted by the probability density of neurons at that phase in the steady state.

NETWORK SIMULATIONS

We simulated a network of neurons subjected to periodic stimulation. Each neuron was modeled as a periodic oscillator whose phase was updated according to the input amplitude and the neuron's PRC. Each cell received input from three sources: (1) an independent noise source, (2) a common noise source, and (3) DBS stimulus. The neurons in this simulation were uncoupled from each other. The phase of each cell i was calculated as follows:

$$\frac{d\phi_i(t)}{dt} = \Omega + \zeta_i(t) + \eta(t)$$

$$\zeta_i(t) = A_i \text{Var}(\phi_i) N_i(0,1) \sqrt{\Delta t}$$

$$\eta(t) = B \text{Var}(\phi_i) N(0,1) \sqrt{\Delta t}$$

Here, ϕ_i is the phase of cell i at time t , Ω is the natural period of the neuron (set to 1 for all cells in this simulation), $\zeta_i(t)$ is the random (independent) stochastic input, and $\eta(t)$ is the common stochastic input, which are dependent on the square root of the time step, Δt . The coefficients A_i and B scale the noise inputs, which are multiplied by $N(0, 1)$, a zero-mean random variable with SD 1. $\text{Var}(\phi_i)$ is the variance of each stochastic input for unitary noise, calculated as the integral of the square of the PRCs up to the time of stimulus as:

$$\text{Var}(\phi) = \int_{\phi_1}^{\phi_2} \text{PRC}^2(s) ds$$

We modeled a population of uncoupled cells receiving common stochastic input $\eta(t)$ from an external brain region. The other stochastic input, $\zeta(t)$, represents independent noise inputs to the cells, including intrinsic noise and unshared synaptic inputs from nearby cells or other brain areas. The shared input was adjusted to impose a substantial correlation but not perfect synchrony among the cells in the absence of DBS stimulation. This was done so that both synchronizing and desynchronizing effects of the DBS stimulus could be readily observed. When a cell received a DBS input, we used the PRC to determine a cell's phase shift to external inputs as:

$$\phi_i^+(t) = \phi_i^- - m_s * \text{PRC}(\text{mod}(\phi_i^-, 1)),$$

in which the phase immediately after the stimulus $\phi_i^+(t)$ is equal to the phase immediately before the stimulus $\phi_i^-(t)$ minus the cell's response to the input, $\text{PRC}(\phi_i^-)$. Changes in the stimulus amplitude were simulated by scaling the coefficient m_s . The phase-update from periodic stimulation only occurred when time t equaled the stimulus time t_s . We also kept track of the resetting of each cell's oscillation to ensure that no cell's phase was advanced to a point prior to the stimulus time – only an immediate spike is possible in that case.

MEASUREMENT OF SYNCHRONY

We simulated 100 uncoupled cells starting with randomly distributed initial phases normalized between 0 and 1. A periodic stimulus was delivered throughout the simulation, the frequency, and strength of which was varied to examine the effect on network dynamics. The network had no spatial distribution, meaning that we stimulated all cells with equal amplitude. The frequency of stimulation ranged from 1 to 2 times the natural frequency of the cell. The relative strength of stimulation ranged from -1 to 1 (negative strengths indicating inhibition), with a peak advance of 30% of the phase at the largest stimulation strength. To determine population entrainment from the DBS, we calculated the entropy (as phase distribution) of the population as:

$$\text{Entropy} = - \sum_{j=1}^B p(\phi_j) \ln(p(\phi_j))$$

in which $p(\phi_j)$ is the probability of a cell being in bin j of B total bins. A high value of entropy indicates a population of cells that are evenly distributed in phase, or “splay phase,” while a low value of entropy indicates synchrony. The theoretical maximum entropy for 100 bins is approximately 4.6. We found that entropy more accurately represented the network's synchrony than a Kuramoto order parameter (Kuramoto, 1984) because at certain stimulus frequencies the population was entrained into two clusters of neurons at exactly opposite phases. This configuration resulted in zero-synchrony measured using the Kuramoto order parameter yet a low value for entropy.

COMPOUND SYNAPTIC PHASE-RESETTING CURVE FOR ISOLATED STIMULI

When stimulating a neuron at high rates, multiple stimulus inputs may occur within one ISI. While it is straightforward to predict the phase advance cause by a single input, the response to the second input must be calculated recursively. The presentation of a stimulus

causes a change in the phase of the neuron that is not revealed until the neuron fires its next action potential. Therefore we refer to the phase of the neuron at the time of the second stimulus as the latent phase, as in the case of ongoing noise. Because a synaptic stimulus, unlike noise, cannot be assumed to average to zero, a statistical approach cannot be used. The cumulative phase advance must be calculated by determining the latent phase and stimulus amplitude at each time point, and summing the phase advances to all the stimuli. To implement this, we discretized time and decomposed the synaptic current into a series of discrete impulses occurring at each point in time. The latent phase assigned to each stimulus impulse was calculated from the phase of the previous stimulus and the change in latent phase it produced (Netoff et al., 2005). The resulting phase evolution was given as:

$$\phi_{i+1} = \frac{\Delta t * i}{T_c} + \phi_i * m_s[\Delta t * i] * \text{PRC}[\phi_i],$$

in which ϕ_i is latent phase of the cell at the time of the i th stimulus, m_s is the stimulus magnitude and Δt is the time increment. Thus the effect of a temporally extended synaptic current arising from any sequence of synaptic inputs could be approximated by setting m_s accordingly for each time point. At each time $i * \Delta t$ a new latent phase value was calculated, and this was repeated until the latent phase achieved a value of 1 (indicating that the cell fired). The resolution of the measurement of phase changes was set by Δt , for which we used $T_c/5000$. We calculated the compound (PRC_{syn}) by applying a stimulus sequence $m_s[t]$ starting at various time delays after the onset of an action potential. This represents the experiment in which a stimulus is presented very rarely, so that the effect of a prior stimulus is completely dissipated before the next stimulus is presented. These are the conditions used for calculating the post-stimulus histogram. The response to a single input may not accurately reflect the neuron's response to a periodic stimulus, for which the effects of stimuli from previous cycles may accumulate. Therefore, we calculate two synaptic PRCs, one for singular stimuli and one for stimuli presented periodically.

MODELING RESPONSE OF THE SYNAPTIC RESPONSE TO DBS

We modeled the direct subthalamo-pallidal pathway using an excitatory synaptic current with a latency of 1 ms, an instantaneous rise, and a decay time constant of 2.5 ms, which is typical of AMPA excitation. The direct inhibitory effect of antidromic activation of globus pallidus external (GPe) segmentaxons in the subthalamic nucleus was modeled as a smaller but longer-lasting hyperpolarizing current, with a latency of 1.5 ms, and a decay time constant of 5 ms (based on the measurement by Sims et al., 2008). We selected -0.6 as the ratio of inhibition to excitation, as this produced a small net inhibitory effect at low frequencies and intensities, as described by Kita et al. (2005).

For a periodically firing neuron and a stimulus given at intervals much longer than the cell period, the relationship between the PRC and the post-stimulus histogram has been described by Gutkin et al. (2005). Their analysis requires that the stimulus does not insert extra action potentials, meaning that any one trial in the post-stimulus histogram has no more than one action potential during one firing period after the stimulus. Thus the histograms

are measured for the period T , during which the cell fires once. The post-stimulus histogram is effectively a firing latency histogram. Because neurons in the subthalamo-pallidal pathway do not burst in response to single stimuli (Kita et al., 2005), it is possible to estimate the post-stimulus histogram directly from the PRC.

We treated the entire stimulus sequence starting at time t_s as a single impulse stimulus for calculation of the PRC_{syn} . Because the stimulus is absent for times before t_s , the distinction between phase and time need not be made for that period. This stimulus time measured from the most recent action potential t_s and response latency t_r would sum to the ISI T_c in the absence of an effective stimulus. Stimulation may change the response latency by an amount dependent on the stimulus time as calculated by the PRC_{syn} . We constructed the post-stimulus histogram by uniformly sampling stimulus phase ϕ_s , and plotting the probability of obtaining a value of ϕ_r .

COMPOUND SYNAPTIC PHASE-RESETTING CURVE FOR PERIODIC STIMULI

During high frequency stimulation, the next stimulus may arrive before the effects of previous ones have completely dissipated. When the neuron's response to a periodic stimulus has reached steady state, the influence of stimulus history is absorbed into a constant component. The steady-state stimulus current for an exponentially decaying input as we have used for each of the monosynaptic effects of subthalamic stimulation is given by:

$$m_s[t - t_0] = \delta * \frac{e^{-(t-t_0)/\tau}}{1 - e^{1/(F*\tau)}},$$

in which t_0 is the time of the most recent stimulus, τ is the decay time constant of synaptic current, δ is the increment of the current on each stimulus, and F is stimulus frequency. Synaptic currents for both excitatory and inhibitory inputs (each with its own δ and τ) were calculated using this equation, and summed. The resulting periodic input waveform was used to calculate the compound synaptic PRC. At steady state, there is a frequency-dependent constant current associated with each synaptic component, whose sum may create a constant offset in the compound PRC, equivalent to a change in the cell's unperturbed firing rate.

Because of its longer time constant, the constant component of the current at most stimulus intensities was dominated by inhibition. This periodic form of the compound synaptic PRC was used to make a phase map. To make a stochastic map, the effect of background current noise must be incorporated. That noise acts through the cells intrinsic PRC, not the synaptic PRC.

For purposes of calculating the variance of the cyclic synaptic PRC, we assumed that the greatest phase shift produced by the stimulus occurred at the time of stimulus presentation. With this simplification, we calculate the variance of that curve in the same way as the discrete stimulation (Ermentrout et al., 2011). During the part of the ISI before the onset of the stimulus the latent phase is dispersed by the accumulation of phase shifts induced by a Gaussian noise current. The variance of the latent phase distribution at the moment just preceding the stimulus (t_s) is given by

$$\text{var}[t_s^-] = \eta^2 \int_0^{t_s} \text{PRC}^2[s] ds,$$

in which η is the SD of the current noise, and PRC is the *cellular* PRC. At the time of the stimulus, the variance is altered because trajectories at different latent phases at the moment of stimulation are shifted by different amounts. The variance immediately after the stimulus is:

$$\text{var}[ts^+] = \text{var}[ts^-] * (1 - \text{PRC}'_{\text{syn}}[ts])^2,$$

in which PRC'_{syn} is the derivative of the cyclic *synaptic* PRC. During the remaining part of the ISI, additional phase dispersion is caused by background current noise. This component of the variance is decreased by phase advances, and increased by phase delays. The total variance for the PRC_{syn} is:

$$\text{var}[\phi] = \eta^2 \int_0^{\phi} \text{PRC}^2[s] ds * (1 - \text{PRC}'_{\text{syn}}[\phi])^2 + \eta^2 \int_{\phi + \text{PRC}_{\text{syn}}[\phi]}^1 \text{PRC}^2[s] ds.$$

The stochastic map was then calculated as described previously.

CALCULATING THE FIRING RATE DURING STIMULATION

During repetitive stimulation, stimuli shift the phase of cell firing in a phase-dependent manner and the effect of each stimulus on the rate of firing is determined by the phase at which the stimulus occurs relative to the previous action potential. The probability distribution of such phases is given by the stationary distribution of stimulus phases. The firing rate for each stimulation rate and intensity was calculated from the product of that distribution and the compound synaptic PRC, which was summed to calculate the average phase change expected from each stimulus. The reciprocal of that sum is the average fractional change in rate. Baseline firing rate was 60 Hz.

RESULTS

The desynchronizing effect of high frequency stimulation on identical noise-free model neurons is shown in **Figures 2A,B**. Two conductance-based simple one-compartment model neurons that show spontaneous oscillations near the rate of globus pallidus output neurons are shown in **Figure 2A**. They had identical periods, and so maintained their relative phase relationship at the start of the simulation. When they were both stimulated with the same periodic high frequency train of current pulses, they did not respond identically. Because the first stimulus fell at slightly different phases of their ongoing oscillation, each cell's phase was changed in a slightly different way. These changes were, on average, amplified over subsequent cycles of stimulation. Both cells fired irregularly during the stimulation and their phase relationship varied erratically as shown in **Figure 2B**. Analysis of this effect is complicated by the multidimensional nature of the conductance model and the oscillatory mechanism. A simplified representation of this model neuron can be obtained by measuring its PRC, shown in **Figure 2C**. In this graph the change of the cell's ISI in response to a single brief current injection is plotted as a function of the time of stimulation after the preceding action potential. Both the change in ISI and the time of the stimulus are normalized by the unperturbed ISI to be in units of phase. Advances in phase, meaning decreases in ISI caused by the stimulus, are shown as positive. The response to a depolarizing pulse is shown. The PRC scales with

stimulus strength (over a range of small stimulus intensities), and is inverted when the current pulses are hyperpolarizing. The PRC can be readily converted to a phase map, as shown in **Figures 2D,E** (blue line). This gives the phase of the $(i+1)$ th stimulus relative to the preceding action potential, as a function of the phase of the i th stimulus. It is calculated by adding the PRC to the identity line (in red), and shifting it up or down respectively according to whether the cell is firing more rapidly or more slowly than the stimulus is presented. In **Figure 2D**, the stimulation rate is 20% higher than the cell's natural firing rate, so the map is shifted down, resulting in two equilibria, which are the crossings with the identity line. The stability of equilibria can be determined by the slope of the map; equilibria at crossings with negative slopes are stable. Only one of the equilibria in **Figure 2D** is stable, as indicated by the black dot, and so regardless of the phase of the stimulus at the start of stimulation, the cell will speed up slightly and become phase locked to the stimulus at a phase corresponding to that equilibrium. Trajectories from all starting phases will converge to this phase and become phase locked to the stimulus. The negative value of the Lyapunov exponent is indicative of entrainment to the stimulus and synchrony among stimulated neurons. In the chaotic example in **Figure 2E**, the stimulation rate is faster and the amplitude is not changed. There are no equilibria because the PRC does not cross the line of identity, and trajectories are complicated and do not repeat. However, some regions on the phase map are never visited by the trajectories, and some are visited often. The Lyapunov exponent measured in this case is positive, indicating that the phase relationship between two cells starting near each other in phase will diverge exponentially in time. This phase difference between the two neurons over the stimulated cycles is shown in **Figure 2F**. The neurons start at almost the same phase (nearly zero phase difference) and within 10 cycles, the phase difference has grown exponentially to large value indicating the neurons are no longer synchronized. For very small amplitude stimulation and non-zero difference between the frequency of the cell and stimulus, there are also no equilibria on the map, but the effect of stimulation on phases of neurons is very small, and the Lyapunov exponent is nearly zero, indicating that the cells will maintain their phase relationships on average (not shown). The effect of stimulus intensity and frequency of current pulses on synchrony as measured by the Lyapunov exponent is shown in **Figure 2G**. For depolarizing (excitatory) stimuli, chaotic desynchronization occurs at intermediate stimulus intensities, large enough to produce effects on cell phase but too small to entrain cells completely, and at frequencies of stimulation greater than 50% faster than the cells' spontaneous firing rate. Hyperpolarizing (inhibitory) stimuli produce chaotic desynchronization of model neurons over a wider range of stimulus frequencies and intensities. In both cases, small changes in either frequency or intensity of the stimulation can cause a switch between synchronization (in blue) and desynchronization (in red).

EFFECTS OF CELLULAR VARIABILITY

Some features of the effects of stimulation shown in **Figure 2** are caused by the idealized nature of the cells' oscillation in the stochastic map. Globus pallidus neurons are not perfect oscillators; their period varies due to intrinsic noise and irregular synaptic inputs. We incorporated irregularity of the cell's firing using a stochastic

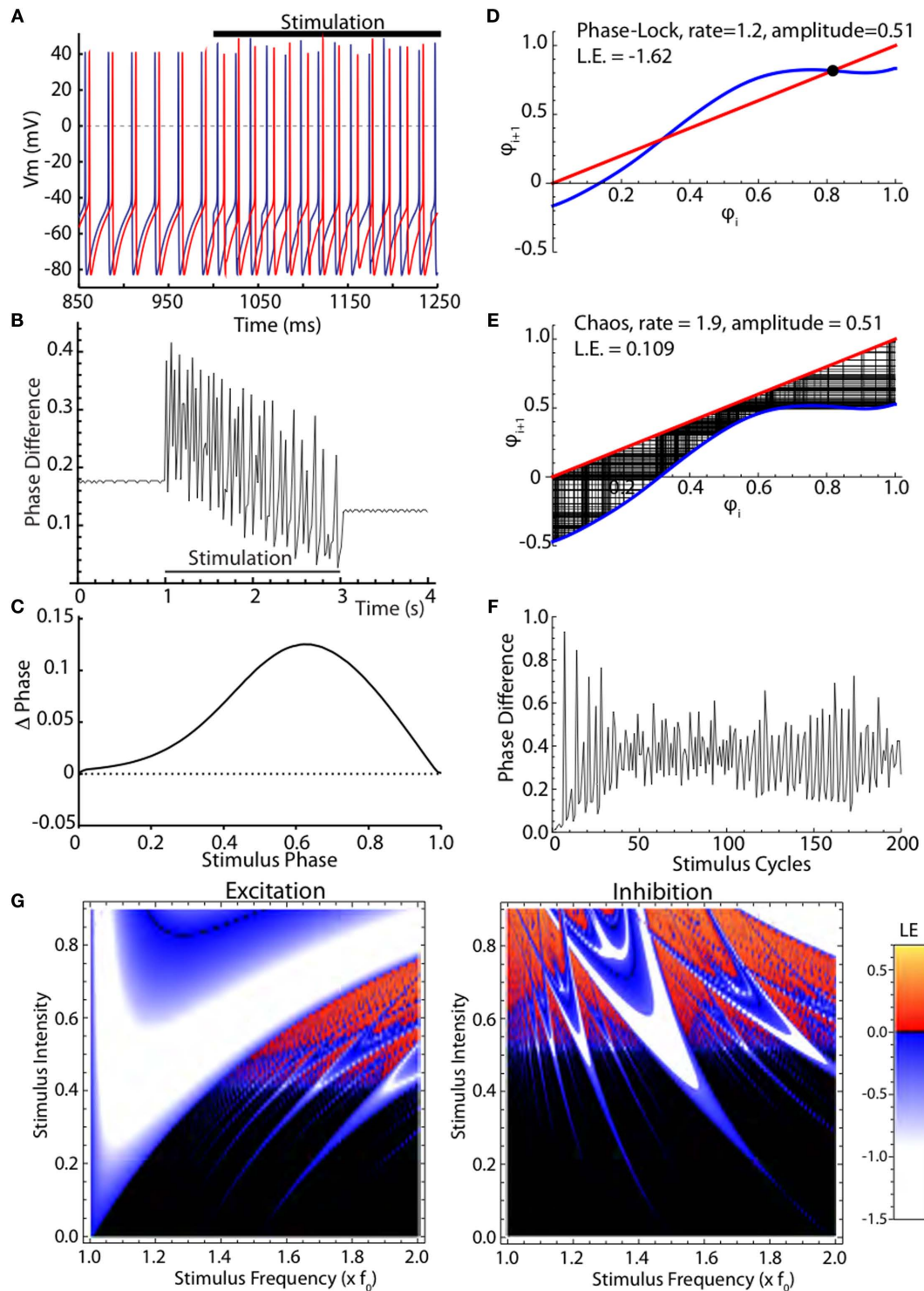


FIGURE 2 | Chaotic desynchronization in a model neuron. (A) Two uncoupled conductance-based simulated neurons before and during stimulation with high frequency current pulses. **(B)** The neurons' phase relationship is disturbed during the stimulation. **(C)** The phase-resetting curve (PRC), a simplification of the neuron model consisting of a phase-dependent phase shift by a current pulse. **(D)** Iterative phase map. The phase of the stimulus for the next stimulation is calculated from its PRC and its phase on the previous cycle. **(E)** Phase map for chaotic desynchronization, leading to a non-repeating non-random sequence of

phases. **(F)** Phase differences for two initially nearby trajectories in the chaotic map. **(G)** Map of stimulus strength and frequency dependence of firing patterns using the Lyapunov exponent. Negative Lyapunov exponents (white to blue) indicate phase convergence and synchrony. Positive Lyapunov exponents (red to orange) indicate chaotic phase divergence. Lyapunov exponents near zero, indicating neither active synchronization nor desynchronization, are shown black. Inhibitory current pulses also produce chaotic firing and divergence of trajectories, but over a different range of rates.

phase map, as shown in **Figure 3**. The variance of the PRC can be approximated from an estimate of the average variability in the absence of stimuli, and from the shape of the PRC (Ermentrout et al., 2011). An example stochastic-PRC, showing the mean effect of a current pulse on firing phase and the variance of that effect, is shown in **Figure 3A**. The map constructed from the stochastic PRC calculates a probability distribution of stimulus phase on the $(i + 1)$ th stimulus presentation given a probability distribution of phase of the i th stimulus. Examples of stochastic phase maps for stimulation at the same frequency as the neuron's spontaneous rate, or at twice that frequency are shown in **Figure 3B**. The steady-state probability distribution obtained after many iterations of the stochastic map can be used to calculate the Lyapunov exponent, and to determine whether the stimulus will actively synchronize the cells, desynchronize them, or have no effect on synchrony. The relationship between stimulus frequency, amplitude, and Lyapunov exponent for the stochastic model neuron is shown in **Figure 3C**. The result is similar to that obtained in the deterministic case, except that the fine fractal mosaic of synchronization and desynchronization is smoothed by cellular irregularity. In the region that gives rise to chaotic desynchronization, the fine dependency on tiny changes in stimulus parameters is not seen. This occurs because irregularity in the firing pattern ensures that the trajectories visit regions of the map associated with expansion and folding of trajectories required for chaotic desynchronization.

Simulations of a population of neurons synchronized by common noise input confirmed the results obtained using the Lyapunov exponents. We simulated a group of 100 neurons, each oscillating at the same unperturbed rate and having the same PRC, but receiving noisy current perturbations from two sources. One of the noise sources was common to all the cells, and so tended to synchronize them, whereas the other was independent for each neuron. In the absence of high frequency stimulation the cells stabilized with a moderate amount of synchrony, corresponding to an entropy measure of about 2.5. These models were stimulated with depolarizing or hyperpolarizing current pulses over the same range of stimulus intensities and frequencies used in **Figure 3C**. The steady-state effect of stimulation on synchrony was assessed using a measure of population entropy (see Materials and Methods). The results for depolarizing pulses are shown in **Figure 3D**. Stimulus frequencies and intensities that yielded positive Lyapunov exponents desynchronized the neurons (increased entropy), whereas those yielding negative Lyapunov exponents caused synchronization. Examples of two stimulus parameter sets are shown in **Figures 3E,F**.

In this model network, it was also possible to measure the importance of periodicity for the desynchronizing effect of high frequency stimulation. We varied the periodicity of the high frequency stimulation, making it increasingly less regular but maintaining its average frequency. As reported for the clinical effectiveness of DBS (Dorval et al., 2010), randomization of the high frequency current pulses caused a rapid decline in the desynchronization effect of the stimulus, as shown in **Figure 3G**.

SYNAPTIC STIMULATION

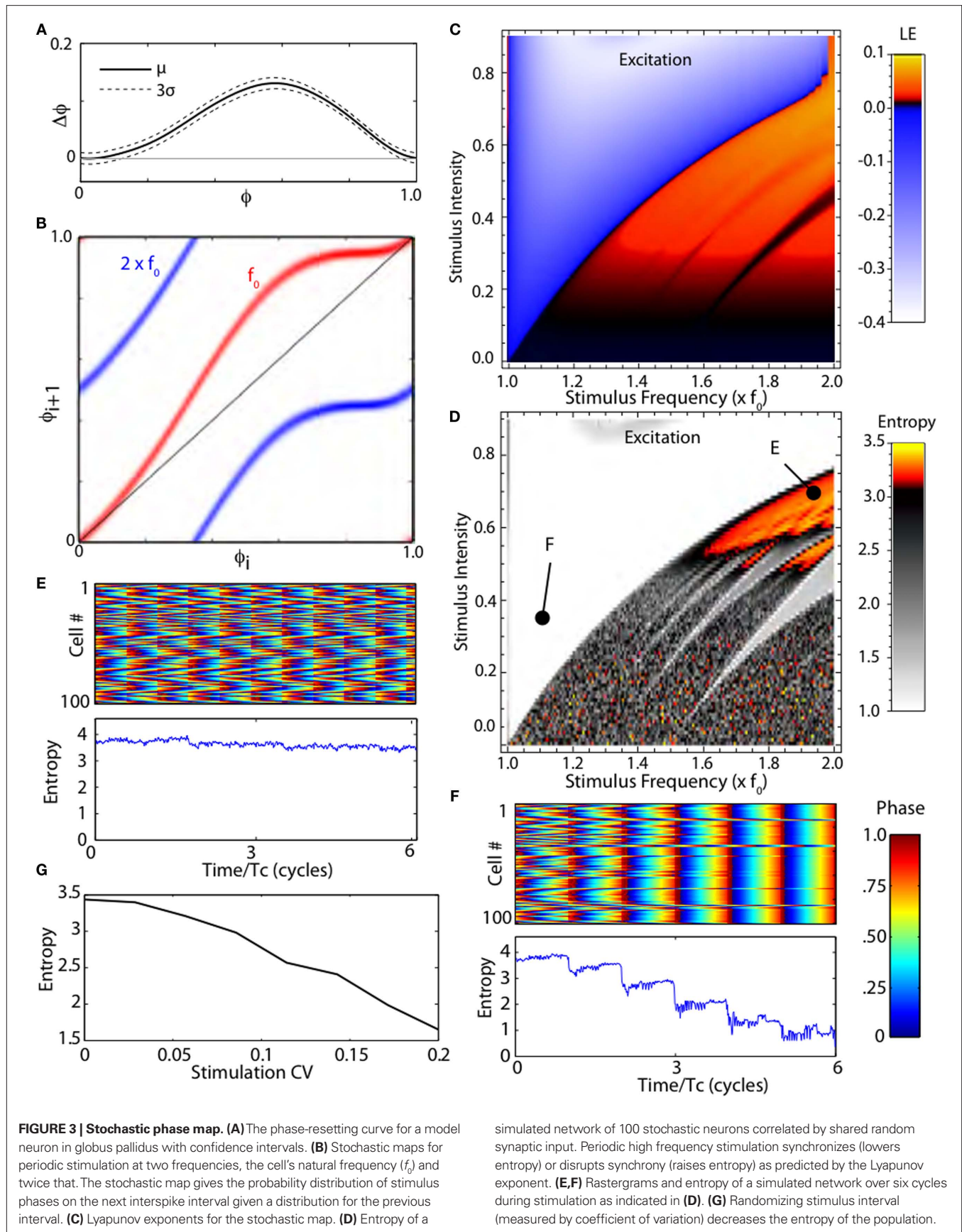
Subthalamic nucleus stimulation monosynaptically excites neurons in the internal segment of the globus pallidus (Kita and Kitai, 1991; Nakanishi et al., 1991) but it also recruits inhibitory connections

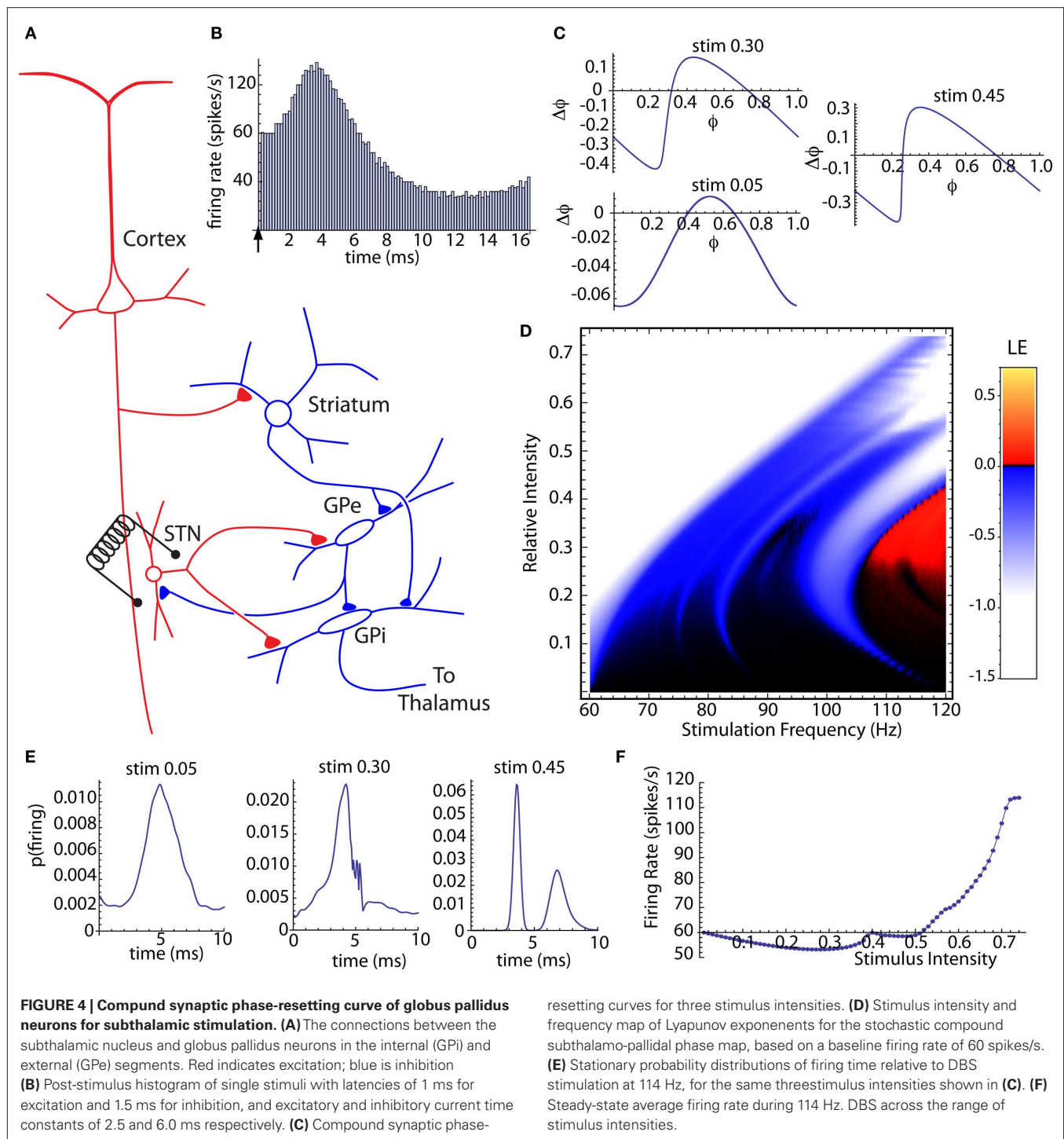
between the pallidal segments (e.g., Kita, 1994; Kita et al., 2005). The most direct pathways recruited by subthalamic stimulation are shown in **Figure 4A**. Note that most of the same pathways are present and may be stimulated by electrodes in either the GPe or GPi. There are a variety of indirect pathways that may be recruited, and it is not certain which pathways are most essential for DBS (e.g., Gradinaru et al., 2009; Xu et al., 2011). The presence of both excitatory and inhibitory effects of STN stimulation are reflected in the post-stimulus changes in firing observed after single stimuli (Nambu et al., 2000; Kita et al., 2005) and during DBS (Hashimoto et al., 2003; Kita et al., 2005; McCairn and Turner, 2009). We constructed a compound synaptic current generated in the GPi neuron by the stimulus, composed of a subthalamo-pallidal EPSC with a latency of 1 ms and a pallido-pallidal IPSC evoked by the axon reflex antidromically activated from the subthalamic nucleus and inhibiting the GPi via the GPe-GPi collateral of the same axons. The inhibitory pathway had a latency of 1.5 ms. The EPSC component decayed exponentially with a time constant of 2.5 ms, and the IPSC component had a decay time constant of 5 ms (Sims et al., 2008). The IPSC had an amplitude 0.6 that of the EPSC. This ratio of inhibition to excitation was selected to produce a post-stimulus time histogram similar to that recorded by Kita et al. (2005). A typical post-stimulus time histogram for this stimulus is shown in **Figure 4B**.

We calculated the compound synaptic PRCs generated by this synaptic stimulus. Unlike the idealized PRCs in **Figures 2 and 3**, these included temporally extended responses to both excitatory and inhibitory components, and so both the shape and size of the PRC depended on stimulus strength. They also depended on the unperturbed firing rate of the cell, which was fixed at 60 Hz. Examples of the synaptic PRCs obtained at three different stimulus intensities are shown in **Figure 4C**. The curves are shifted in the downward (phase-retarding) direction by the influence of the inhibitory component of the synaptic stimulus, especially at low stimulus intensities. Because of its longer duration, the inhibitory synaptic current accumulated over multiple stimulation presentations. The compound synaptic PRC is a periodic function (see Materials and Methods) for repeated stimulation, and includes the cumulative effect of the steady-state periodic train of synaptic stimuli.

We then constructed a family of stochastic phase maps for the compound synaptic PRCs, and used them to calculate Lyapunov exponents over a range of stimulation intensities and frequencies as shown in **Figure 4D**. As before, stimulation frequencies were varied starting from the baseline firing rate of the cell and extending to twice that rate (60–120 Hz). This revealed a frequency-sensitivity for stimulus-induced desynchronization similar to that of clinically effective DBS (Rizzone et al., 2001; Chen et al., 2008). A stochastic map was also constructed for the probability of neuronal firing at various times after a DBS stimulus. The stationary distribution obtained from the map is the steady-state post-stimulus firing probability, and so should predict the post-stimulus histogram that would be obtained during DBS. These were sensitive to changes in stimulus intensity and frequency. Three examples, corresponding to the same three synaptic PRCs shown in **Figure 4C**, but for a stimulation frequency of 114 Hz, are shown in **Figure 4E**.

To examine the relationship between phase locking, chaos, and firing rate, we calculated the firing rate for the same series of intensities at 114 Hz. We did this by multiplying the stationary





distribution of stimulus arrival times with the PRC, to get an average phase shift that could be converted to an average frequency change. The effect of stimulus intensity on firing rate during DBS is shown in **Figure 4F**. At low intensities, accumulation of the longer-lasting inhibitory synaptic current dominated, and DBS produced a decrease in firing rate, similar to that reported by Kita et al. (2005). At higher intensities, increased entrainment of the cell by the stimulus caused an increase in firing rate, as in Hashimoto et al. (2003).

Our results indicate that maximal desynchronization should occur at lower intensities, even ones causing a slowing of firing rate, and not showing strong phase locking to the stimulus.

DISCUSSION

Our model is very abstract, and does not address some of the practical aspects of DBS. For example, we do not address the shape or size of the electric field generated by the DBS stimulus, and the resulting

differences in stimulation that occur across the population of STN neurons (Miocinovic et al., 2009). We also consider only the effects of the stimulus on STN and GPe cells and their processes, and not the host of other cell types whose axons are in or near the region of the stimulus (Xu et al., 2011) and may contribute to the effect of the stimulus. We have also not included rate heterogeneity of GPi neurons. Neurons with different natural frequencies would have corresponding shifts in the frequency specificity of their response to periodic stimulation. In our simulations, we used shared input as a way of creating correlated activity in basal ganglia output neurons. The true cause of correlations between output neurons in parkinsonism is not known. If their correlations were caused by synaptic coupling rather than shared input, they might be less sensitive to the desynchronizing effect of periodic stimulation. This last simplification is common to nearly all models of DBS.

The beneficial effects of DBS on the symptoms of Parkinson's disease may not be attributable to its effects on firing rate, but rather to disruption of low frequency bursting, synchrony of firing, or both (Hashimoto et al., 2003; McCairn and Turner, 2009). Previous theoretical studies have assumed that DBS synchronizes firing in basal ganglia output neurons, emphasizing its effects on low frequency oscillations (Rubin and Terman, 2004; Guo et al., 2008). Our results do not directly address the importance of the slow oscillatory bursting, but rather the correlations among neurons. These two mechanisms of DBS are not mutually exclusive, and may be acting simultaneously. To the extent that entrained activity in the globus pallidus can prevent bursting in the thalamus, as in the Rubin and Terman (2004) model, it should still do so when the cells are not entrained, but activated asynchronously. Chaotic desynchronization might also act indirectly to disrupt bursting and other structured activity in pallidal neurons by decorrelating activity in their inputs. This mechanism may have even contributed but gone unrecognized in the simulations with the conductance-based neuron models by Rubin and Terman and others.

It is also possible that bursting could continue during DBS, but become desynchronized among neurons, as observed by McCairn and Turner (2009). Whether bursting is suppressed or only decorrelated by DBS, increased entropy across the GPi neuronal population should distribute pallidothalamic inhibition in time. This more constant pallidothalamic synaptic barrage would be less likely to engage the low frequency resonance in thalamic neurons which in the Rubin and Terman model is considered to be responsible for the parkinsonian symptoms.

If the desynchronizing effects of DBS were critical to its effectiveness, it would explain the periodicity requirement and frequency-sensitivity of DBS. Our model further predicts that increasing stimulus intensity beyond the therapeutically effective range will entrain the population and degrade effectiveness of DBS. It also explains the observations that basal ganglia output cells are not precisely entrained, but rather fire irregularly ($CV \sim 1$) during DBS (Hahn et al., 2008), and that spike-wise correlations of activity in basal ganglia output neurons are suppressed rather than enhanced during DBS (Degos et al., 2005). Of course, if cells were entrained to the stimulus, their firing would be highly correlated. Our model also explains why randomization of the stimulus interval degrades clinical effectiveness (Dorval et al., 2010).

Our results suggest that inhibitory, as well as excitatory inputs, may contribute to DBS effectiveness. We suggest that effectiveness in disrupting the correlations between nearby basal ganglia output neurons may determine the effectiveness of DBS stimulation sites, intensities, and frequencies. A similar mechanism may underlie the beneficial effects of DBS on other neurological and psychiatric conditions.

ACKNOWLEDGMENTS

Supported by NIH grant NS047085 (Charles J. Wilson), NSF CAREER 0954797 (Theoden I. Netoff), and U. Minnesota Grant-in-Aid (Bryce Beverlin II).

REFERENCES

- Albin, R. L., Young, A. B., and Penney, J. B. (1989). The functional anatomy of basal ganglia disorders. *Trends Neurosci.* 12, 366–375.
- Atherton, J. F., and Bevan, M. D. (2005). Ionic mechanisms underlying autonomous action potential generation in the somata and dendrites of GABAergic substantia nigra pars reticulata neurons in vitro. *J. Neurosci.* 25, 8722–8781.
- Bergman, H., Wichmann, T., Karmon, B., and DeLong, M. R. (1994). The primate subthalamic nucleus. II. Neuronal activity in the MPTP model of parkinsonism. *J. Neurophysiol.* 72, 507–520.
- Brown, P. (2007). Abnormal oscillatory synchronization in the motor system leads to impaired movement. *Curr. Opin. Neurobiol.* 17, 656–664.
- Chen, C. C., Litvak, V., Gilbertson, T., Kühn, A., Lu, C. S., Lee, S. T., Tsai, C. H., Tisch, S., Limousin, P., Hariz, M., and Brown, P. (2008). Excessive synchronization of basal ganglia neurons at 20 Hz slows movement in Parkinson's disease. *Exp. Neurol.* 205, 214–221.
- Degos, B., Deniau, J.-M., Thierry, A.-M., Glowinski, J., Pezard, L., and Maurice, N. (2005). Neuroleptic-induced catalepsy: electrophysiological mechanisms of functional recovery induced by high-frequency stimulation of the subthalamic nucleus. *J. Neurosci.* 25, 7687–7696.
- Dorval, A. D., Kuncel, A. M., Birdno, M. J., Turner, D. A., and Grill, W. M. (2010). Deep brain stimulation alleviates parkinsonian bradykinesia by regularizing pallidal activity. *J. Neurophysiol.* 104, 911–921.
- Dostrovsky, J., and Bergman, H. (2004). Oscillatory activity in the basal ganglia—relationship to normal physiology and pathophysiology. *Brain* 127, 721–722.
- Elbert, T., Ray, W. J., Kowalik, Z. J., Skinner, J. E., Graff, K. E., and Birbaumer, N. (1994). Chaos and physiology: deterministic chaos in excitable cell assemblies. *Physiol. Rev.* 74, 1–47.
- Ermentrout, G. B., Beverlin, B. II, Troyer, T., and Netoff, T. I. (2011). The variance of phase-resetting curves. *J. Comput. Neurosci.* doi: 10.1007/s10827-010-0305-9. [Epub ahead of print].
- Gatev, P., Darbin, O., and Wichmann, T. (2006). Oscillations in the basal ganglia under normal conditions and in movement disorders. *Mov. Disord.* 21, 1566–1577.
- Glass, L., and Mackey, M. C. (1988). *From Clocks to Chaos*. Princeton: Princeton University Press, 248.
- Gradinaru, V., Mogri, M., Thompson, K. R., Henderson, J. M., and Deisseroth, K. (2009). Optical deconstruction of parkinsonian neural circuitry. *Science* 324, 354–359.
- Guo, Y., Rubin, J. E., McIntyre, C. C., Vitek, J. L., and Terman, D. (2008). Thalamocortical relay fidelity varies across subthalamic nucleus deep brain stimulation protocols in a data-driven computational model. *J. Neurophysiol.* 99, 1477–1492.
- Gutkin, B. S., Ermentrout, G. B., and Reyes, A. D. (2005). Phase-response curves give the responses of neurons to transient inputs. *J. Neurophysiol.* 94, 1623–1635.
- Hahn, P. J., Russo, G. S., Hashimoto, T., Miocinovic, S., Xu, W., McIntyre, C. C., and Vitek, J. L. (2008). Pallidal burst activity during therapeutic deep brain stimulation. *Exp. Neurol.* 211, 243–251.
- Hashimoto, T., Elder, C. M., Okun, M. S., Patrick, S. K., and Vitek, J. L. (2003). Stimulation of the subthalamic nucleus changes the firing pattern of pallidal neurons. *J. Neurosci.* 23, 1916–1923.
- Kaplan, D. T., Clay, J. R., Manning, T., Glass, L., Guevara, M. R., and Shrier, A. (1996). Subthreshold dynamics in periodically stimulated squid giant axons. *Phys. Rev. Lett.* 76, 4074–4077.
- Kita, H. (1994). "Physiology of two disinaptic pathways from the sensorimotor cortex to the basal ganglia output nuclei," in *The Basal Ganglia IV: New Ideas and Data on Structure*

- and Function, eds G. Percheron, J. S. McKenzie, and J. Féger (New York: Springer), 263–276.
- Kita, H., and Kitai, S. T. (1991). Intracellular study of rat globus pallidus neurons: membrane properties and responses to neostriatal, subthalamic and nigral stimulation. *Brain Res.* 564, 296–305.
- Kita, H., Tachibana, Y., Nambu, A., and Chiken, S. (2005). Balance of mono-synaptic excitatory and disynaptic inhibitory responses of the globus pallidus induced after stimulation of the subthalamic nucleus in the monkey. *J. Neurosci.* 25, 8611–8619.
- Kuramoto, Y. (1984). *Chemical Oscillations, Waves, and Turbulence*. Berlin: Springer-Verlag.
- McCairn, K., and Turner, R. S. (2009). Deep brain stimulation of the globus pallidus internus in the parkinsonian primate: local entrainment and suppression of low-frequency oscillations. *J. Neurophysiol.* 101, 1941–1960.
- Miocinovic, S., Lempka, S. F., Russo, G. S., Maks, C. B., Butson, C. R., Sakale, K. E., Vitek, J. L., and McIntyre, C. C. (2009). Experimental and theoretical characterization of the voltage distribution generated by deep brain stimulation. *Exp. Neurol.* 216, 166–176.
- Nakanishi, H., Kita, H., and Kitai, S. T. (1991). Intracellular study of rat entopeduncular nucleus neurons in an in vitro slice preparation: response to subthalamic stimulation. *Brain Res.* 549, 285–291.
- Nambu, A., Tokuno, H., Hamada, I., Kita, H., Imanishi, M., Akazawa, T., Ikeuchi, Y., and Hasegawa, N. (2000). Excitatory cortical inputs to pallidal neurons via the subthalamic nucleus in the monkey. *J. Neurophysiol.* 84, 289–300.
- Netoff, T. I., Aker, C. D., Bettencourt, J. C., and White, J. A. (2005). Beyond two-cell networks: experimental measurement of neuronal responses to multiple synaptic inputs. *J. Comput. Neurosci.* 18, 287–295.
- Nini, A., Feingold, A., Slovlin, H., Bergman, H. (1995). Neurons in the globus pallidus do not show correlated activity in the normal monkey, but phase-locked oscillations appear in the MPTP model of parkinsonism. *J. Neurophysiol.* 74, 1800–1805.
- Raz, A., Vaadia, E., and Bergman, H. (2000). Firing patterns and correlations of spontaneous discharge of pallidal neurons in the normal and the tremulous 1-methyl-4-phenyl-1,2,3,6-tetrahydropyridine vervet model of parkinsonism. *J. Neurosci.* 20, 8559–8571.
- Rizzone, M., Lanotte, M., Bergamasco, B., Tavella, A., Torre, E., Faccani, G., Melcarne, A., and Lopiano, L. (2001). Deep brain stimulation of the subthalamic nucleus in Parkinson's disease: effects of variation in stimulus parameters. *J. Neurol. Neurosurg. Psychiatr.* 71, 215–219.
- Rubin, J. E., and Terman, D. (2004). High frequency stimulation of the subthalamic nucleus eliminates pathological thalamic rhythmicity in a computational model. *J. Comput. Neurosci.* 16, 211–235.
- Schiff, S. J. (2010). Towards model-based control of Parkinson's disease. *Philos. Transact. A Math. Phys. Eng. Sci.* 368, 2269–1308.
- Schultheiss, N. W., Edgerton, J. R., and Jaeger, D. (2010). Phase response curve analysis of a full morphological globus pallidus neuron model reveals distinct perisomatic and dendritic modes of synaptic integration. *J. Neurosci.* 30, 2767–2782.
- Sims, R. E., Woodhall, G. L., Wilson, C. L., and Stanford, I. M. (2008). Functional characterization of GABAergic pallidopallidal and striatopallidal synapses in the rat globus pallidus in vitro. *Eur. J. Neurosci.* 28, 2401–2408.
- Wichmann, T., and DeLong, M. R. (1996). Functional and pathophysiological models of the basal ganglia. *Curr. Opin. Neurobiol.* 6, 751–758.
- Wichmann, T., and DeLong, M. R. (2006). Deep brain stimulation for neurologic and neuropsychiatric disorders. *Neuron* 52, 197–204.
- Winfrey, A. T. (2000). *The Geometry of Biological Time*, 2nd Edn. New York: Springer-Verlag.
- Xu, W., Miocinovic, S., Zhang, J., Baker, K. B., McIntyre, C. C., and Vitek, J. L. (2011). Dissociation of motor symptoms during deep brain stimulation of the subthalamic nucleus in the region of the internal capsule. *Exp. Neurol.* 288, 294–297.

Conflict of Interest Statement: The authors declare that the research was conducted in the absence of any commercial or financial relationships that could be construed as a potential conflict of interest.

Received: 22 April 2011; paper pending published: 23 May 2011; accepted: 05 June 2011; published online 21 June 2011.

Citation: Wilson CJ, Beverlin B II and Netoff T (2011) Chaotic desynchronization as the therapeutic mechanism of deep brain stimulation. *Front. Syst. Neurosci.* 5:50. doi: 10.3389/fnsys.2011.00050

Copyright © 2011 Wilson, Beverlin II and Netoff. This is an open-access article subject to a non-exclusive license between the authors and Frontiers Media SA, which permits use, distribution and reproduction in other forums, provided the original authors and source are credited and other Frontiers conditions are complied with.